

C–H and C–F Activation by Manganese, Nickel and Ruthenium Catalysis

Dissertation

for the award of the degree

“Doctor rerum naturalium”

of the Georg-August-University of Göttingen



within the doctoral program of chemistry

of the Georg-August-University School of Science (GAUSS)

submitted by

Valentin Müller

from Northeim

Göttingen, 2021

Thesis Committee

Prof. Dr. Lutz Ackermann, Institute of Organic and Biomolecular Chemistry, University of Göttingen

Prof. Dr. Shoubhik Das, ORSY Division, Department of Chemistry, University of Antwerp

Members of the Examination Board

Reviewer: Prof. Dr. Lutz Ackermann, Institute of Organic and Biomolecular Chemistry, University of Göttingen

Second Reviewer: Prof. Dr. Shoubhik Das, ORSY Division, Department of Chemistry, University of Antwerp

Further Members of the Examination Board

Prof. Dr. Konrad Koszinowski, Institute of Organic and Biomolecular Chemistry, University of Göttingen

Prof. Dr. Dietmar Stalke, Institute of Inorganic Chemistry, University of Göttingen

Jun.-Prof. Dr. Johannes Walker, Institute of Organic and Biomolecular Chemistry, University of Göttingen

Dr. Holm Frauendorf, Institute of Organic and Biomolecular Chemistry, University of Göttingen

Date of the Oral Examination: 29.03.2021

Acknowledgment

An erster Stelle möchte ich mich ganz herzlich bei meinem Doktorvater Prof. Dr. Lutz Ackermann bedanken, dass er mir die Möglichkeit gegeben hat in seinem Team unter exzellenten Bedingungen zu forschen. Die hervorragende Ausstattung, die internationale Diversität sowie der wissenschaftliche Output machen diesen Arbeitskreis einzigartig. Weiterhin bin ich dankbar für die Möglichkeit an hochrangigen internationalen Konferenzen teilgenommen haben zu dürfen und an regelmäßigen H-CCAT Treffen agile Forschung zu erleben.

Bei Prof. Dr. Shoubhik Das möchte ich mich für die Übernahme des Korreferats und die hilfreichen Anregungen bedanken. Ebenso viel Dank gilt den weiteren Mitgliedern der Prüfungskommission Prof. Dr. Konrad Koszinowski, Prof. Dr. Dietmar Stalke, Jun.-Prof. Dr. Johannes Walker und Dr. Holm Frauendorf.

Bei Dr. Volker Derdau und Remo Weck möchte ich mich für die schöne Zeit und die Hilfe während meines Aufenthalts bei Sanofi-Aventis in Frankfurt bedanken.

Ebenso möchte ich mich bei allen analytischen Abteilungen im Hause für das gewissenhafte und schnelle Messen jeglicher Arten von Substanzen herzlich bedanken. Im Besonderen gilt dies der NMR-Abteilung und der Massenspektrometrie, die mir durch kompetente Ratschläge bei Problemen jeglicher Art geholfen haben.

Natürlich gebührt ein großer Dank auch den vielen Mitarbeitern und ehemaligen Mitarbeitern die diesen Arbeitskreis über die Jahre bereichert haben. Ein großer Dank geht dabei an Daniel, Uttam, Nikos, Lorena und Nate mit denen ich immer viel Spaß hatte auch wenn es manchmal „horrible“ zugging. Weiterhin möchte ich Dr. Antonis Messinis und Dr. Debasish Ghorai für die zahlreichen Hilfen, wenn es um Kristallstrukturen ging, danken. Ein besonderer Dank gilt Joachim und Isaac, mit denen ich zusammen aufregende Projekte bewältigen durfte was immens viel Spaß gemacht hat.

Für alle administrativen und organisatorischen Fragen möchte ich Gabriele Keil-Knepel und Bianca Spitalieri danken. Weiterhin gilt mein Dank auch Karsten Rauch, Ralf Gerke und Stefan Beußhausen für ihre mühevollen und wichtigen Beiträge die Laborarbeit deutlich effizienter zu gestalten.

Ein Besonderer Dank geht auch an Ralf, Torben, Julia und Lina für die unterhaltsamen Kaffeepausen und die exzellente Verpflegung.

Für den wöchentlichen interdisziplinären Austausch und den gemeinsamen Aktivitäten nach Feierabend möchte ich mich auch bei Mike, Jerome und Marcus bedanken.

Für das gewissenhafte and akribische Korrekturlesen dieser Arbeit möchte ich mich bei Dr. Torben Rogge, Nikolaos Kaplaneris, Uttam Dhawa, Dr. Korkit Korvorapun, Isaac Choi, Adelina Kopp, Leonardo Massignan und Julia Struwe ganz herzlich bedanke.

Ein großer Dank gebührt meinen Eltern, die mir das Studium überhaupt erst ermöglichen haben und mich bei allen Entscheidungen unterstützt haben. Mein letzter und größter Dank gebührt Merle, du warst trotz vieler Strapazen immer für mich da und ich weiß, dass ich manchmal wenig Zeit für dich hatte, dennoch waren die gemeinsamen Momente unendlich aufmunternd und zauberhaft.

Valentin Müller

Table of Contents

1. Introduction.....	1
1.1. Transition Metal-Catalyzed C–H Activation	1
1.2. Secondary Phosphine Oxides.....	6
1.3. Nickel-Catalyzed C–F bond Activation.....	7
1.4. Nickel-Catalyzed C–H Activation for Alkene Hydroarylations	13
1.5. Enantioselective Nickel-Catalyzed C–H Activation.....	18
1.6. Ruthenium-Catalyzed C–H Activation	21
1.7. Ruthenium-Catalyzed Hydrogen Isotope Exchange	23
1.8. Remote C–H Activation by Ruthenium Catalysis	26
1.8.1. Stoichiometric Remote C–H functionalization of Ruthenium Complexes	27
1.8.2. <i>meta</i> C–H Alkylation under Ruthenium Catalysis	29
1.9. Heterogeneous C–H Functionalization	36
2. Objectives.....	40
3. Results and Discussion.....	43
3.1. SPO-Nickel Catalysts for C–F Alkylations	43
3.1.1. Optimization Studies for Primary Alkylmagnesium Reagents	44
3.1.2. Scope of the C–F Alkylation using Primary Alkylmagnesium Reagents	48
3.1.3. Optimization Studies for Secondary Alkylmagnesium Reagents	52
3.1.4. Scope of the C–F Alkylation using Secondary Alkylmagnesium Reagents ..	56
3.2. Manganese-Catalyzed Allylative and Alkenylative C–H/C–F Functionalization..	61
3.2.1. Optimization Studies for the Alkenylative C–H/C–F Functionalization	61
3.2.2. Scope of the Allylative and Alkenylative C–H/C–F Functionalizations.....	63
3.2.3. Experiment with Cyclometalated Complex 204	67
3.3. Asymmetric Nickel-Catalyzed Hydroarylations by C–H Activation	68
3.3.1. Optimization Studies for Enantioselective Intramolecular Nickel-Catalyzed Hydroarylations by C–H Activation.....	69
3.3.2. Scope of the Enantioselective Nickel-Catalyzed <i>endo</i> -Hydroarylation	71
3.3.3. Mechanistic Studies.....	76
3.3.4. Proposed Catalytic Cycle	81

3.4. Hydrogen Isotope Exchange by Ruthenium-Catalyzed C–H Activation	84
3.4.1. Optimization Studies for Ruthenium(II)-Catalyzed Hydrogen Isotope Exchange	85
3.4.2. Scope of the Ruthenium(II)-Catalyzed Hydrogen Isotope Exchange	89
3.4.3. Mechanistic Studies	95
3.4.4. Proposed Catalytic Cycle	97
3.4.5. Tritiation of Pharmaceuticals	98
3.5. Recyclable Ruthenium Catalysts for remote C–H Alkylations	99
3.5.1. Optimization Studies of <i>meta</i> C–H Alkylations by Recyclable Ruthenium Catalyst	100
3.5.2. Test of Heterogeneity for <i>meta</i> C–H Alkylations by Recyclable Ruthenium Catalyst	102
3.5.3. Scope of <i>meta</i> C–H Alkylations by Recyclable Ruthenium Catalyst	105
3.5.4. Mechanistic Studies of <i>meta</i> C–H Alkylations by Recyclable Ruthenium Catalyst	117
3.5.5. Proposed Catalytic Cycle	119
3.5.6. Optimization Studies of Photo-induced <i>meta</i> C–H Alkylation by Recyclable Ruthenium Catalyst	121
3.5.7. Scope of Photo-induced <i>meta</i> C–H Alkylation by Recyclable Ruthenium Catalyst	122
4. Summary and Outlook	124
5. Experimental Part.....	129
5.1. General Remarks.....	129
5.2. General Procedures	134
5.2.1. General Procedure A: SPO-Nickel Catalysis with Linear Grignard Reagents	134
5.2.2. General Procedure B: SPO-Nickel Catalysis with Branched Grignard Reagents	134
5.2.3. General Procedure C: Manganese(I)-Catalyzed Allylative C–H/C–F Functionalization	134
5.2.4. General Procedure D: Manganese(I)-Catalyzed Allylative or Alkenylative C–H/C–F Functionalization	135
5.2.5. General Procedure E: Nickel-Catalyzed Enantioselective Intramolecular Hydroarylation.....	135
5.2.6. General Procedure F: Nickel-Catalyzed Racemic Intramolecular Hydroarylation.....	136

5.2.7. General Procedure G: HIE of Benzoic Acids and Bioactive Compounds ...	136
5.2.8. General Procedure H: Recyclable Ruthenium Catalyst for <i>meta</i> C–H Activation	136
5.2.9. General Procedure I: Recyclable Ruthenium Catalyst for C4/C6 Dialkylation C–H Activation.....	137
5.2.10. General Procedure J: Recyclable Ruthenium Catalyst for <i>meta</i> C–H Activation under Photo-induced Conditions	137
5.3. SPO-Nickel Catalyst for C–F Alkylations	138
5.3.1. Characterization Data	138
5.3.2. Synthesis of 194 and 195	163
5.4. Manganese(I)-Catalyzed Allylative and Alkenylative C–H/C–F Functionalization.....	166
5.4.1. Characterization Data	166
5.4.2. Experiments with Cyclometalated Complex 204	177
5.5. Asymmetric Nickel-Catalyzed Hydroarylations by C–H Activation	178
5.5.1. Characterization Data	178
5.5.2. Mechanistic Studies.....	187
5.6. Hydrogen Isotope Exchange by Ruthenium-Catalyzed C–H Activation	195
5.6.1. Characterization Data	195
5.6.2. Mechanistic Studies.....	211
5.7. Recyclable Ruthenium Catalyst for remote C–H Activation.....	214
5.7.1. Synthesis of Hybrid Ruthenium catalysts 221a and 221b	214
5.7.2. Test of Heterogeneity for <i>meta</i> C–H Alkylations by Recyclable Ruthenium Catalyst	215
5.7.3. Characterization Data	217
5.7.4. Mechanistic Studies.....	245
5.8. Crystallographic Data	249
6. References	263
7. Appendix: NMR-Spectra and HPLC Chromatograms.....	303

List of Abbreviations

Å	Ångström
Ac	acetyl
acac	acetyl acetonate
$[\alpha]_D$	specific rotation at 589 nm
Ad	adamantyl
ADME	absorption, distribution, metabolism, and excretion
Alk	alkyl
Am	amyl
AMLA	ambiphilic metal ligand activation
API	active pharmaceutical ingredient
Ar	aryl
atm	atmospheric pressure
ATR	attenuated total reflection
<i>b</i>	branched
BDE	bond dissociation energy
BHT	2,6-di- <i>tert</i> -butyl-4-methylphenol
BIES	base-assisted internal electrophilic substitution
Bn	benzyl
Bu	butyl
br	broad
C	Celsius
<i>c</i>	concentration (in g / 100 mL)
calc.	calculated
<i>cat.</i>	catalytic
CMD	concerted metalation deprotonation
cod	1,5-cyclooctadiene
Cp	cyclopentadienyl
Cp*	pentamethylcyclopentadienyl
CPME	cyclopentyl methyl ether

C _q	quaternary carbon
Cy	cyclohexyl
δ	chemical shift (NMR)
d	doublet
DCE	1,2-dichloroethane
DFT	density functional theory
DG	directing group
DMF	<i>N,N</i> -dimethylformamide
DMSO	dimethyl sulfoxide
DoM	directed <i>ortho</i> -metalation
dppe	1,3-bis(diphenylphosphino)ethane
dppf	1,1'-bis(diphenylphosphino)ferrocene
dppp	1,3-bis(diphenylphosphino)propane
d.r.	diastereomeric ratio
<i>ee</i>	enantiomeric excess
EI	electron ionization
equiv	equivalents
e.r.	enantiomeric ratio
ESI	electrospray ionization
Et	ethyl
EWG	electron-withdrawing group
g	gram
GC	gas chromatography
<i>gem</i>	geminal
h	hour
HASPO	heteroatom-substituted secondary phosphine
Hept	heptyl
hept	heptet
Het	heteroaryl or heteroatom
HIE	Hydrogen isotope exchange

HMPA	hexamethylphosphoramide
HPLC	high-performance liquid chromatography
HR-MS	high resolution mass spectrometry
Hz	hertz
<i>i</i>	<i>iso</i>
ICP-OES	inductively coupled plasma optical emission spectrometry
IR	infrared
<i>J</i>	coupling constant
K	Kelvin
<i>k</i>	reaction rate constant
kcal	kilocalorie
KIE	kinetic isotope effect
L	liter or (pre-)ligand
<i>l</i>	linear
LED	light-emitting diode
LLHT	ligand-to-ligand hydrogen transfer
M	metal or molar
<i>m</i>	<i>meta</i>
m	Multiplet or meter
M. p.	melting point
<i>m/z</i>	mass-to-charge ratio
MAD	methylaluminium bis(2,6-di- <i>tert</i> -butyl-4-methylphenoxide)
Me	methyl
Mes	mesityl
mg	milligram
MHz	megahertz
min	minutes
mm	millimeter
mmol	millimole
MPAA	mono- <i>N</i> -protected amino acid

MS	mass spectrometry or molecular sieves
Ms	methanesulfonyl (mesyl)
NDC	nitrogen-doped carbon
Np	naphthyl
NBS	<i>N</i> -bromosuccinimide
NHC	N-heterocyclic carbene
NMP	<i>N</i> -methylpyrrolidinone
NMR	nuclear magnetic resonance
n.r.	no reaction
<i>o</i>	<i>ortho</i>
p	pentet
<i>p</i>	<i>para</i>
Pent	pentyl
Ph	phenyl
Piv	pivaloyl (trimethylacetyl)
PMP	<i>para</i> -methoxyphenyl
Poly	copolymer of styrene and divinylbenzene
ppm	parts-per-million
Pr	propyl
py	pyridyl
pym	pyrimidyl
q	quartet
R	(organic) rest
<i>rac</i>	racemic
<i>r</i> DG	removable directing group
rel. int.	relative intensity
rt	room temperature
σ -CAM	σ -complex-assisted metathesis
s	singlet or second
sat.	saturated

SET	single electron transfer
SPO	secondary phosphine oxide
SPS	solvent purification system
ssNMR	solid-state nuclear magnetic resonance
<i>T</i>	temperature
<i>t</i>	triplet or time
<i>t</i>	tert
TADDOL	$\alpha,\alpha,\alpha',\alpha'$ -tetraaryl-2,2-disubstituted 1,3-dioxolane-4,5-dimethanol
TEM-EDX	transmission electron microscopy linked with energy-dispersive X-ray spectroscopy
TEMPO	2,2,6,6-tetramethylpiperidine- <i>N</i> -oxide
TFA	trifluoroacetic acid
TFE	2,2,2-trifluoroethanol
THF	tetrahydrofuran
TLC	thin layer chromatography
TM	transition metal
Tol	tolyl
Ts	<i>para</i> -toluenesulfonyl (tosyl)
<i>t_r</i>	retention time
UV	ultraviolet
X	(pseudo)halide
XPS	X-ray photoelectron spectroscopy

1. Introduction

During the last century, organic synthesis faced major challenges in the development of novel compounds. Within areas of high importance like pharmacy, agricultural economics, material science and others, the improvement of synthetic methods, and therefore the larger number of innovative compounds, affected the life of billions of people. Although these developments constitute a tremendous benefit for society, such as an increasing number of amenities, the consequences in terms of pollution show the importance for more ecological methods.^[1]

In 1998, Anastas and Warner declared catalysis as one of the key principles within the *12 Principles of Green Chemistry*,^[2] since catalytic rather than stoichiometric amounts of reagents can be used and readily available chemicals can be functionalized without the need of pre-functionalization. Considering these aspects, catalysis is an important and powerful technique to reduce energy consumption, minimizing the generation of waste and use alternative chemicals apart from toxic agents.^[3]

1.1. Transition Metal-Catalyzed C–H Activation

Transformations in organic synthesis, including catalytic reactions, to form C–C and C–Het bonds have long been dominated by modifications of functional groups and therefore typically require elements for pre-functionalization. Since a pre-functionalization increases the overall number of necessary synthetic steps, a direct coupling improves the overall atom economy.^[4] In this context, major advances during the last five decades were achieved by metal-catalyzed cross-coupling reactions to form carbon–carbon (C–C) and carbon–heteroatom (C–Het) bonds.^[5] Even though the first examples were already reported in the late 19th century by Glaser^[6] and Ullmann^[7] using stoichiometric or catalytic amounts of copper, their application was limited due to harsh reaction conditions, low selectivities and moderate yields. It was not until the discovery of palladium-catalyzed cross-coupling reactions almost 70 years later, that these transformations found considerable use in organic synthesis. Especially in the field of C–C bond formation, a wide variety of different organometallic coupling partners were established, resulting in a range of well-known named reactions, such as the Suzuki-Miyaura,^[8] Negishi,^[9] Mizoroki-Heck,^[10] Kumada-Corriu,^[11] Hiyama,^[12] Stille^[13] and

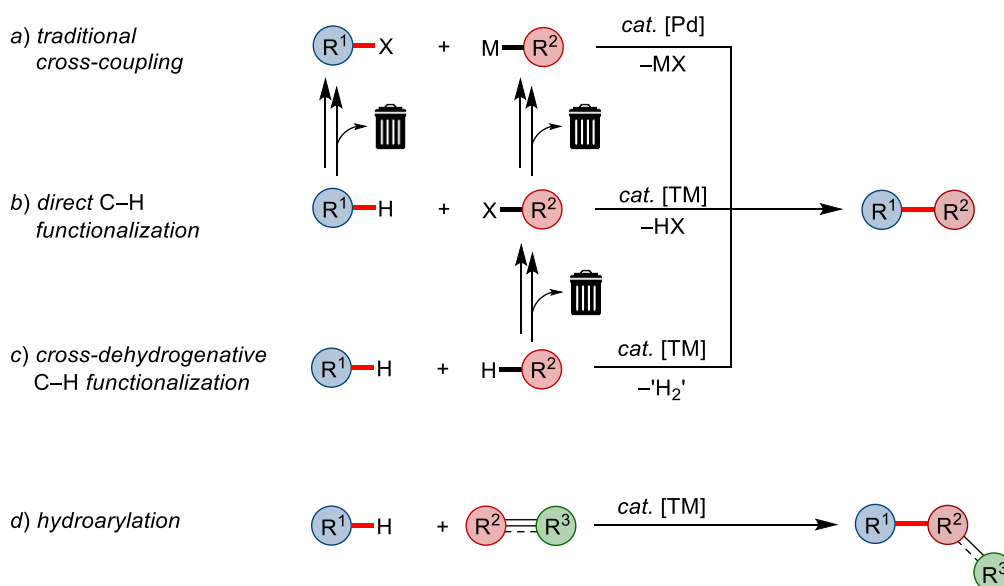
Sonogashira-Hagihara^[14] cross-coupling reactions. All these milestones have found widespread applications ranging from material sciences to the late-stage diversification of biologically active compounds and are nowadays a routine tool in organic synthesis.^[15] Consequently, these significant innovations culminated in the award of the Nobel Prize for Chemistry in 2010 for R. F. Heck, E.-i. Negishi and A. Suzuki.^[16]

Despite recent efforts to render cross-coupling chemistry more environmentally-friendly and cost effective by avoiding rare noble transition metals,^[17] toxic solvents,^[18] non-reusable reagents^[19] and high catalyst loadings,^[20] the main issues, namely the required pre-functionalization of organic nucleophiles and the intrinsic generation of stoichiometric amounts of waste are nevertheless unavoidable. In addition to the costly pre-functionalization, the employed nucleophiles are in most cases either not stable under ambient conditions (e.g. RMgX, RZnX) or toxic (e.g. (Alkyl)₃SnR, RZnX) and are therefore less attractive for applications (Scheme 1.1a).^[21]

To overcome these limitations, the selective functionalization of omnipresent C–H bonds is a highly desirable alternative to conventional cross-couplings in terms of atom- and step-economy.^[4] The importance of sustainable alternatives resulted in a tremendous development of catalytic methods using the concept of C–H bond activation/functionalization as an efficient alternative,^[22] with applications to pharmaceutical industries^[23] and material sciences.^[24] The major advantage compared to classical cross-coupling chemistry is the replacement of an organometallic reagent by a simple C–H bond. However, pre-functionalization of one coupling partner is still needed, resulting byproduct formation (Scheme 1.1b).

In addition, cross-dehydrogenative C–H activations^[25] are a highly atom-economical approach, because formally only molecular hydrogen is generated as the byproduct (Scheme 1.1c). However, those reactions usually require stoichiometric amounts of expensive and toxic chemical oxidants, such as silver(I) and copper(II). Recent developments showed the substitution of commonly used chemical oxidants by electricity to facilitate more sustainable transformations.^[26]

A special arena within the C–H activation regime are the redox neutral hydroarylations of alkenes and alkynes.^[27] Due to the nature of an addition reaction, a perfect atom- as well as step-economy is possible without the need for pre-functionalizations (Scheme 1.1d).



Scheme 1.1. Comparison between traditional cross-coupling chemistry and C–H activation.

While direct C–H functionalizations, in theory, overcome the drawbacks of classical cross-coupling approaches in terms of sustainability, other challenges must be faced. One challenge is the absence of pre-functionalization within one coupling partner. Whereas in cross-coupling reactions the selectivity is determined by the substitution pattern of the electrophile and the nucleophile, most organic molecules contain several C–H bonds with similar dissociation energies,^[28] thus rendering the selective transformation of a specific C–H bond a task of key importance.^[29] Throughout the years, various approaches to address this issue were developed and are mainly based on catalyst control or substrate control. While approaches based on catalyst control are mainly characterized by a tunable catalyst that achieves a predictable site-selectivity independent of the inherent properties of the substrate,^[30] strategies that are based on substrate control can be divided into three subsets: (ii) inherent electronic bias, where one C–H bond has a higher acidity compared to all others,^[31] (iii) steric control *via* shielding of C–H bonds^[32] and (iv) the use of a LEWIS-basic group, that pre-coordinates the transition metal and directs the C–H activation at a predetermined position (Figure 1.1a).^[33] While these concepts allow a selective C–H activation to occur, the major drawbacks are the availability of suitable catalysts for catalyst-controlled selectivity (i) and the dependence on the nature of the substrate (ii & iii), resulting in a rather narrow substrate scope. In contrast, the introduction of a directing group (DG), allows the use of a broad variety of substrates. Although the incorporation of a DG (iv) results in additional synthetic effort, the use of

weakly coordinating,^[34] removable^[35] or transient^[36] directing groups expanded the range of applications considerably (Figure 1.1b).

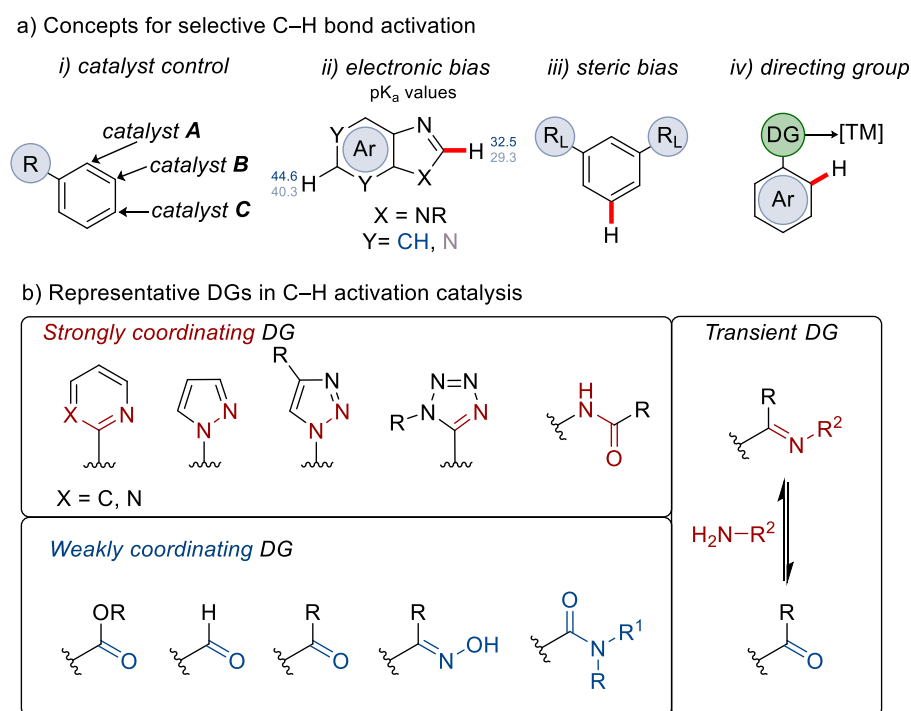
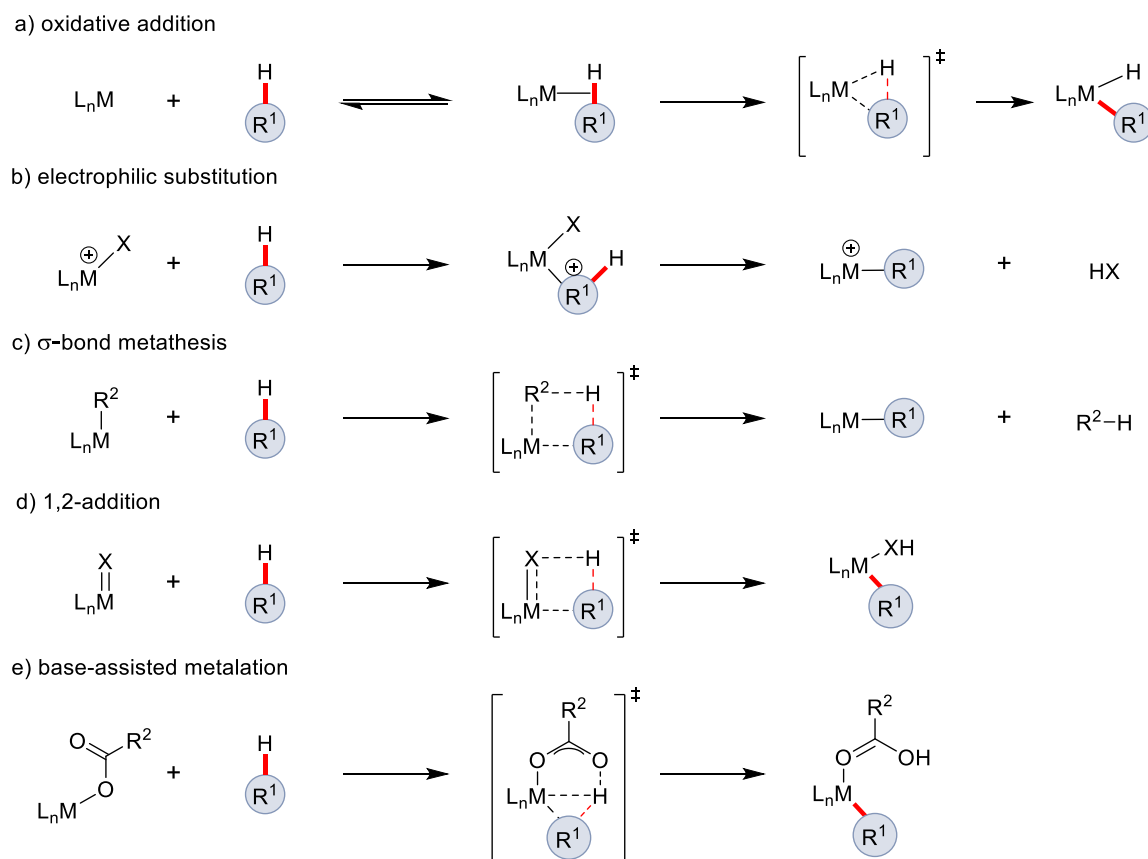


Figure 1.1. a) Methods for positional selectivity in C–H activation. b) Commonly used DGs in C–H activation catalysis.

To develop novel and efficient metal-catalyzed C–H functionalizations, a detailed mechanistic understanding of their modes of action is required. As a result, the mechanism of the key C–H cleavage step was and is still studied extensively. Excluding outer-sphere/radical-type mechanisms,^[37] the key C–H bond activation step can occur through five distinct mechanistic pathways, which are dependent on the electronic nature and the coordination environment of the metal center (Scheme 1.2).^[38] An oxidative addition pathway is typically observed for electron-rich late transition metals in low oxidation states, such as rhenium, ruthenium, osmium, iridium, platinum.^[38a] The main feature of this pathway is a stabilizing agostic interaction between the C–H bond and the metal center during the activation process (Scheme 1.2a). A C–H activation *via* electrophilic substitution is most prominent with late transition metals or post-transition metals in high oxidation states, such as palladium(II), platinum(II-IV), or mercury(II).^[38d] The electron-deficient character of the metal, is often stabilized by highly polar reaction media, allowing an electrophilic attack of the metal center on the carbon atom, resulting in the substitution of one proton by the metal (Scheme 1.2b). In contrast, early transition metals, especially in a d⁰ configuration, as well as lanthanides and actinides, tend to favor

a σ -bond metathesis pathway,^[38b] which involves the concerted formation and breaking of C–H and C–M bonds in the transition state (Scheme 1.2c). Another pathway observed predominantly with early transition metals is the 1,2-addition of the C–H bond onto a M=X bond.^[38b] This pathway mainly features metal-ligand multiple bonds, e.g. alkylidene or imido ligands, and C–H activation occurs *via* a $[2_\sigma+2_\pi]$ reaction, where the X group serves as the formal hydrogen acceptor (Scheme 1.2d). Another category of C–H cleavage processes is the base-assisted C–H activation. This rather recently developed pathway is mainly observed for complexes bearing a carboxylate ligand.^[38a] Within this mechanistic manifold, C–H cleavage occurs simultaneously to the formation of a new R–M bond; meanwhile the proton is transferred to the coordinated base (Scheme 1.2e).



Scheme 1.2. Different pathways for organometallic C–H activation.

Depending on the exact transition state structure and the involved accumulation of partial charges,^[39] the base-assisted metalation pathway can be further categorized (Figure 1.2). While Fagnou and Gorelsky have coined the term CMD (*concerted metalation deprotonation*) based on a deprotonative transition state with electron-poor arenes,^[40] computational studies by Macgregor and Davies revealed an agostic interaction between the transition metal and the C–H bond,^[41] being rationalized by the term *ambiphilic*

metal-ligand activation (AMLA). Notably, when the base is bound to the metal centre AMLA and CMD are essentially the same process.^[41a] Experimental characteristic of CMD-type C–H functionalizations is often a clear preference for electron-poor arenes with acidic C–H bonds.^[42] Recently, *base-assisted internal electrophilic substitution* (BIES) was introduced by Ackermann to explain the preferred activation of electron-rich substrates compared to kinetic acidic C–H bonds.^[43]

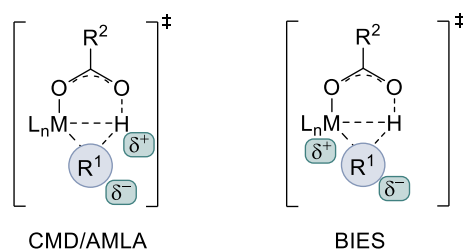
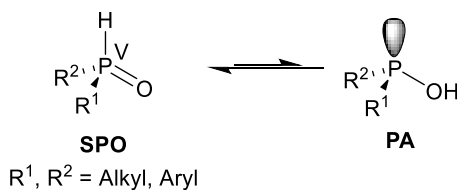


Figure 1.2. Proposed transition states for base-assisted C–H metalations.

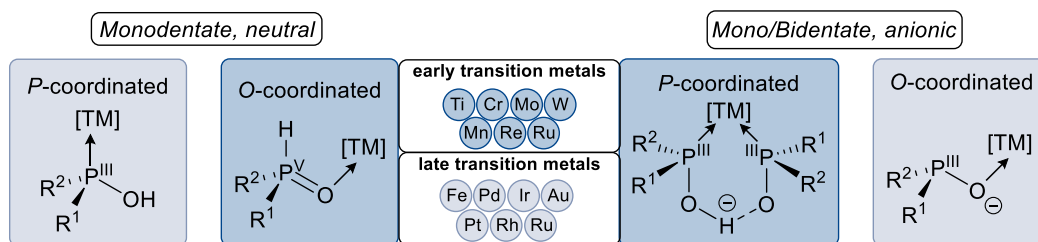
1.2. Secondary Phosphine Oxides

The design of suitable ligands for metal-catalyzed transformations is crucial for efficient and selective processes and is reflected by the enormous amount of developed phosphine ligands^[44] among others.^[45] In this context, electron-rich phosphines are difficult to handle, due to their air- and moisture-sensitivity and require multistep syntheses.^[46] In contrast, secondary phosphine oxides (SPOs) show an excellent stability against air and moisture, even with alkyl substituents, and have a tunable donating nature. Since their first catalytic application in 1986 by van Leeuwen,^[47] SPOs became an important class of ligands with applications in cross-coupling chemistry^[48] and asymmetric catalysis^[49] among others.^[50] While most ligand conformations are pre-defined, SPOs have the unique ability to alter their electronic structure between the stable pentavalent phosphorus ($\sigma^4\lambda^5$) configuration and the potentially strongly *P*-donor ligand with a trivalent phosphinous acid (PA) type structure ($\sigma^3\lambda^3$). While most SPOs exist in the pentavalent form, a shift in equilibria can be facilitated by strongly electron-withdrawing substituents, silylating agents or in the presence of transition metals (Scheme 1.3).^[51]



Scheme 1.3. Conversion of SPOs to PAs.

Owing to the increased synthetic utility, a variety of synthetic pathways to prepare achiral aryl,^[52] alkyl^[53] and ferrocenyl^[54] SPOs as well as chiral (*R,R*)-TADDOL,^[55] (*S,R_p*)-DIAPHOX,^[56] JoSPOphos^[57] and *P*-stereogenic^[58] SPOs were developed. Depending on the affinity of the metal center towards the soft phosphorus or the hard oxygen atom, a number of different coordination modes can be observed.^[59] In general, early transition metals coordinate through the hard oxygen atom and late transition metals prefer the soft phosphorus atom (Scheme 1.4).^[60] In addition, metals with both types of coordination have also been reported.^[61]



Scheme 1.4. Main coordination modes of SPOs and PAs.

1.3. Nickel-Catalyzed C–F bond Activation

While many cross-couplings rely on palladium catalysts, earth abundant 3d metals or main group elements are in terms of costs and availability more attractive.^[22b, 62] Especially nickel, as the “impoverished younger sibling of palladium” shows important features,^[63] such as highly reactive organometallic species and a variety of accessible oxidation states, within synthetically useful reaction conditions (Figure 1.3). Based on this, nickel is considered as an excellent candidate for reactions involving unreactive electrophiles and reactions involving single electron transfers.^[64] As a result, numerous applications in synthetic and green chemistry were developed involving the activation of even unreactive C(aryl)–O and C(aryl)–F bonds.^[65]



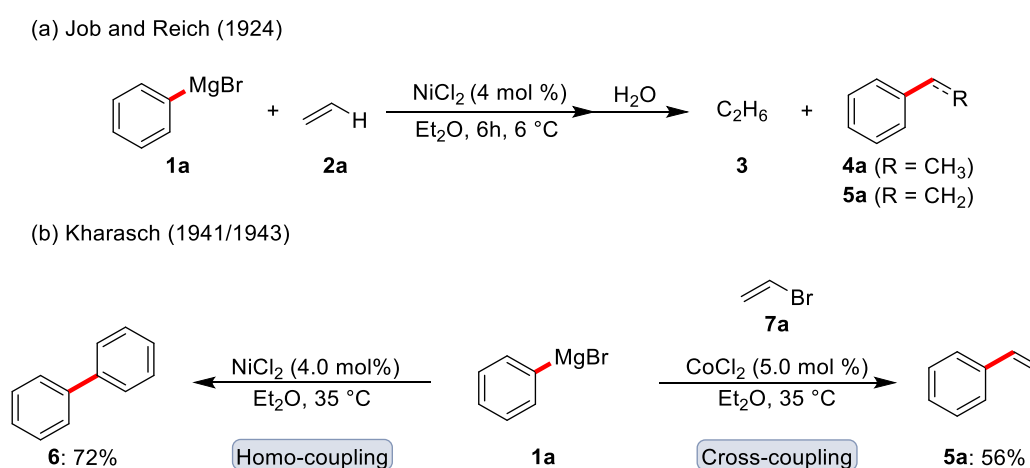
	<p>-1 0 +1 +2 +3 +4</p> <p>Smaller atomic radius</p> <p>Harder</p> <p>Facile oxidative addition</p> <p>Facile β-migratory insertion</p>	<p>0 +1 +2 +3 +4</p> <p>Larger atomic radius</p> <p>Softer</p> <p>Facile reductive elimination</p> <p>Facile β-hydride elimination</p>	
-----------------------------------------------------------------------------------	----------------------------------------------------------------------------------------------------------------------------------------------------------	---------------------------------------------------------------------------------------------------------------------------------------------------------	-------------------------------------------------------------------------------------

Figure 1.3. Properties of nickel and palladium in cross-coupling chemistry.

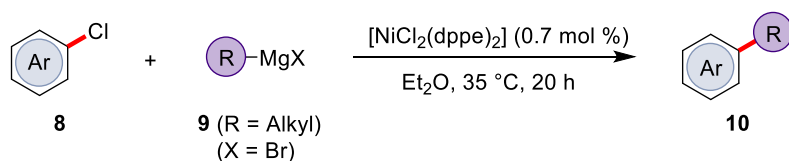
Inspired by the Barbier reaction,^[66] Victor Grignard discovered in 1900 the formation of organomagnesium halides,^[67] extremely valuable and important synthetic tools,^[68] that set the stage for one of the first successful combinations of organometallic reagents within catalysis by using NiCl_2 in 1924 (Scheme 1.5a).^[69] Following these discoveries, Kharsash developed in 1941 the metal-catalyzed homo-coupling of organomagnesium reagents.^[70] Interestingly, the study was focused on earth-abundant 3d metals, such as CoCl_2 , MnCl_2 , FeCl_2 and NiCl_2 , and showed already the first reported catalytic cross-coupling, by using vinyl bromide and phenylmagnesium bromide (Scheme 1.5b).^[71]



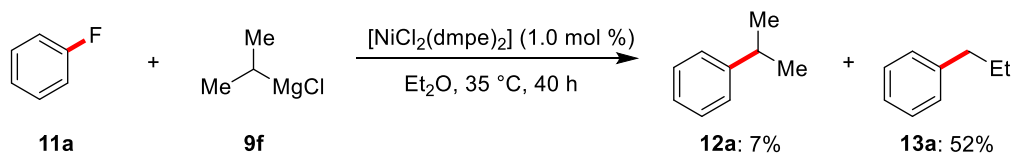
Scheme 1.5. Early studies in nickel-catalyzed coupling reactions.

Studies by Kumada^[11a] and Corriu^[11b] resulted in the nickel-catalyzed cross-coupling reaction of Grignard reagents with aryl halides, currently known as the Kumada-Corriu reaction, and showed the important effect of additional phosphine ligands within the catalysis (Scheme 1.6a).^[72] As an extension, Kumada achieved the C–F activation under nickel catalysis, using $\text{NiCl}_2(\text{dmpe})$, fluorobenzene **11a** and isopropylmagnesium chloride.^[73] Unfortunately the facile β -hydride elimination resulted in a predominant isomerization of the secondary alkyl group (Scheme 1.6b). Even though the development of functional group tolerant nucleophiles and the use of (pseudo)halides marked a great milestone in cross-coupling reactions,^[15] it took almost 25 years until the unique reactivity of nickel towards inert C–F bonds was fully addressed.

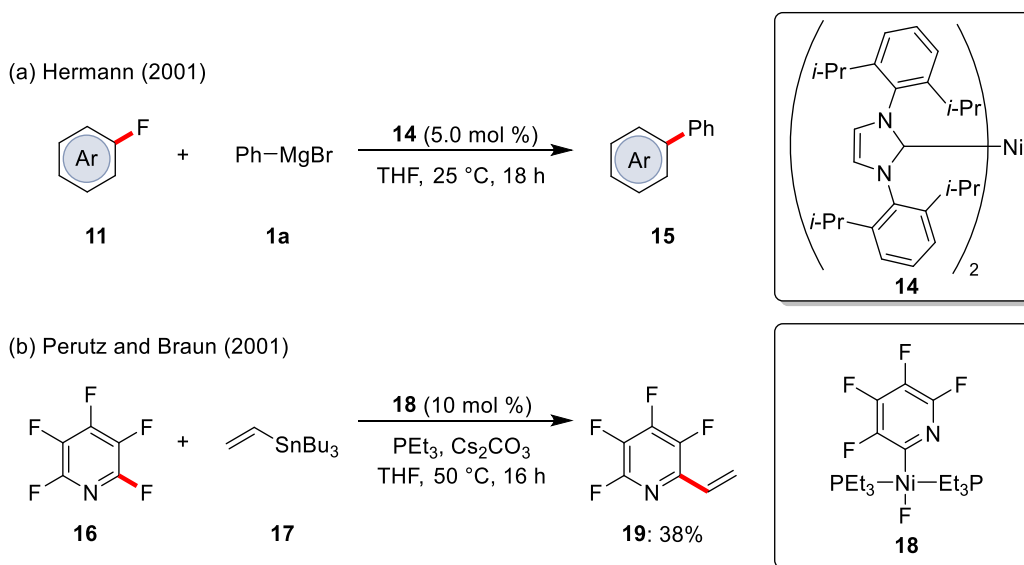
(a) Kumada and Tamao (1972)



(b) Kumada (1973)

**Scheme 1.6.** Pioneering studies in nickel-catalyzed cross-couplings using alkyl magnesium halides **9**.

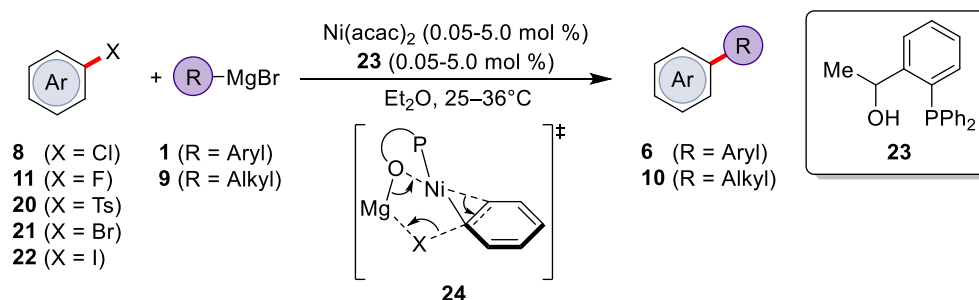
In 2001, the group of Herrmann showed that the nickel NHC complex **14** catalyzed the reaction between aryl fluorides **11** and Grignard reagent **1a** to generate biaryls (Scheme 1.7a).^[74] The catalytically active species is thought to be a nickel(0) species coordinated by a sole NHC ligand. During the same time, Perutz and Braun reported the first catalytic cross-coupling reaction of polyfluorinated arenes (Scheme 1.7b).^[75] Using a pre-formed nickel(II)-fluoro-phosphine complex **18**, a Stille-type coupling was achieved.

**Scheme 1.7.** Nickel-catalyzed C–F activation by well-defined (a) NHC and (b) cyclometalated complexes.

The importance of the ligand design in nickel catalysis was showcased by a push-pull strategy for nickel-catalyzed cross-coupling reactions of aryl fluorides with Grignard reagents by Nakamura (Scheme 1.8).^[76] Through careful ligand design, the hydroxyphosphine ligand **23** was able to facilitate C(sp²)-F arylations. DFT calculations and mechanistic experiments indicated that the reaction proceeded through a nickel-

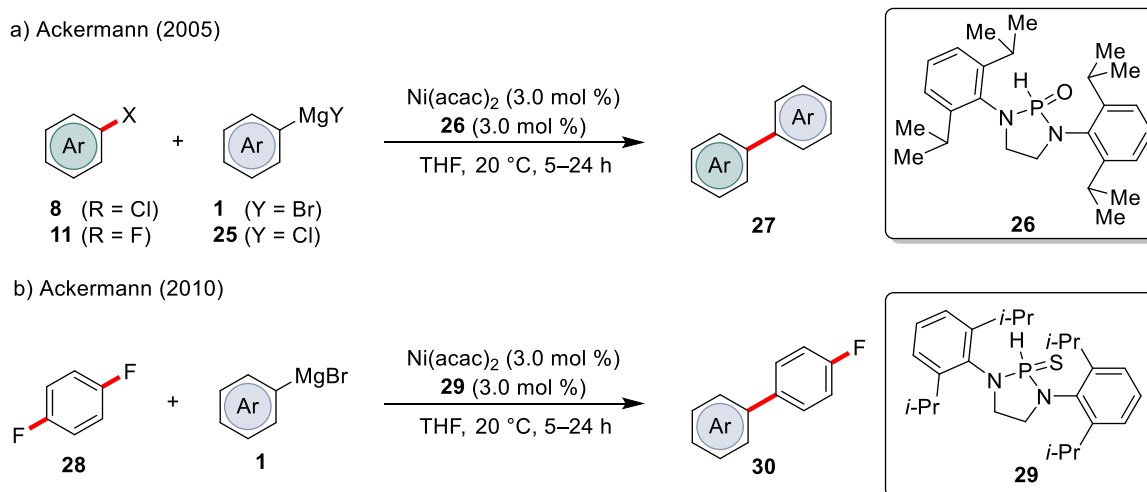
1. Introduction

magnesium bimetallic manifold, that reduces nickel(II) to nickel(0) upon deprotonation of the P–OH ligand.



Scheme 1.8. Hydroxyphosphine ligand **23** for nickel-catalyzed C–F activation.

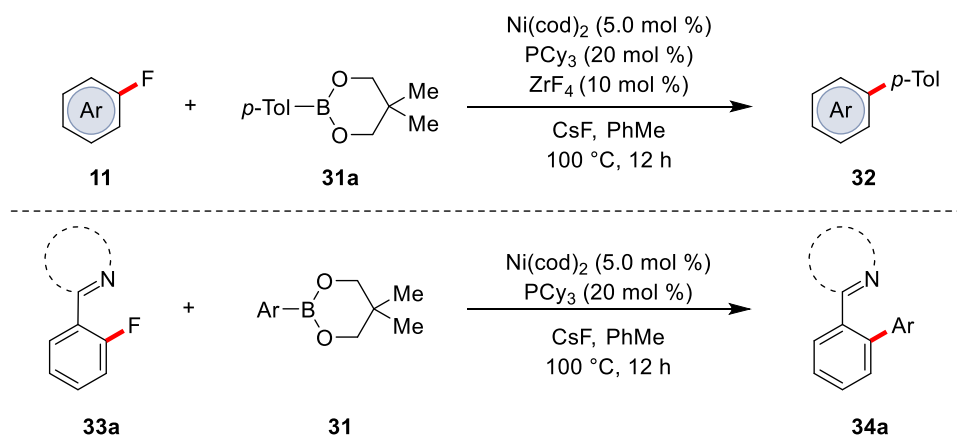
Studies by Ackermann were based on air-stable secondary phosphine oxides (SPO) for the activation of C(aryl)–F bonds. In 2005, Ackermann reported the first use of air-stable SPOs for the activation of C–F bonds. The sterically congested diaminophosphine oxide pre-ligand **26** showed excellent activity at ambient temperature, furnishing numerous biaryl scaffolds (Scheme 1.9a).^[77] Furthermore, Ackermann introduced in 2010 the sterically congested pre-ligand **29** which showed excellent reactivity with a variety of (hetero)arenes at ambient temperature and exclusively yielded monosubstituted products **30**, highlighting the synthetic utility of SPOs in nickel catalysis (Scheme 1.9b).^[78]



Scheme 1.9. Nickel/SPO catalysis for C–F activation.

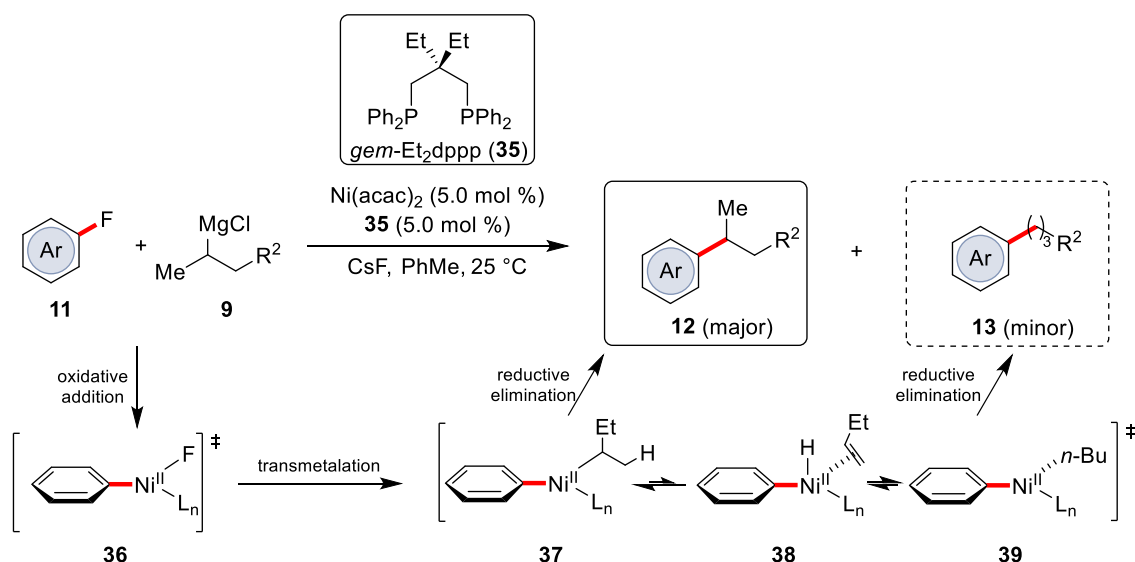
Following these initial reports, it was demonstrated that numerous organometallic reagents in terms of arylation,^[79] alkylation^[80] and alkynylation^[81] among others^[82] were suitable for C–F coupling reactions. Furthermore, the introduction of directing groups resulted in the development of new methods towards unreactive C(sp²)–X bond activations. An approach based on this logic by Chatani described two methods for

nickel-catalyzed Suzuki–Miyaura cross-coupling reaction using zirconium tetrafluoride as co-catalyst or a *N*-containing directing groups (Scheme 1.10).^[83] A variety of functional groups and substituents were tolerated and a change in the turnover-limiting step, from oxidative addition to transmetalation, upon the introduction of directing groups, was observed. It is assumed that zirconium tetrafluoride acts as a LEWIS-acid to facilitate the elimination of the fluorine-atom in an oxidative addition and/or transmetalation process.

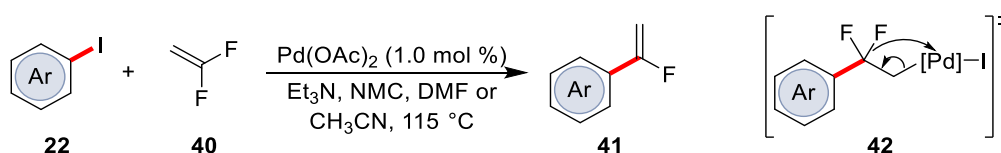


Scheme 1.10. C–F activation enabled by a LEWIS-acid or directing group.

Even though many methods were developed generating C(sp²)–C(sp³) bonds with secondary or tertiary alkyl (pseudo)halides,^[17a, 84] only selected examples showed homologous transformations with secondary and tertiary alkyl nucleophiles and are mostly restricted to reactive aryl halides.^[85] Generally, these protocols rely on the use of highly electron-rich and sterically congested ligands around the metal center to promote fast reductive elimination, thus enhancing selectivity. In terms of nickel-catalyzed C–F activation, the use of branched nucleophiles is especially challenging with respect to selectivity, due to the preferred β -hydride elimination.^[86] In this context, Cornella reported in 2018 on a strategy based on a unique nickel catalyst, which circumvents some of the aforementioned obstacles (Scheme 1.11).^[87] The synthetic efficacy was attributed to the beneficial effect of the *gem*-dialkyl substitution on the ligand **35**, after observing a correlation between the P–Ni–P angle and the chemoselectivities for secondary alkyl nucleophiles.

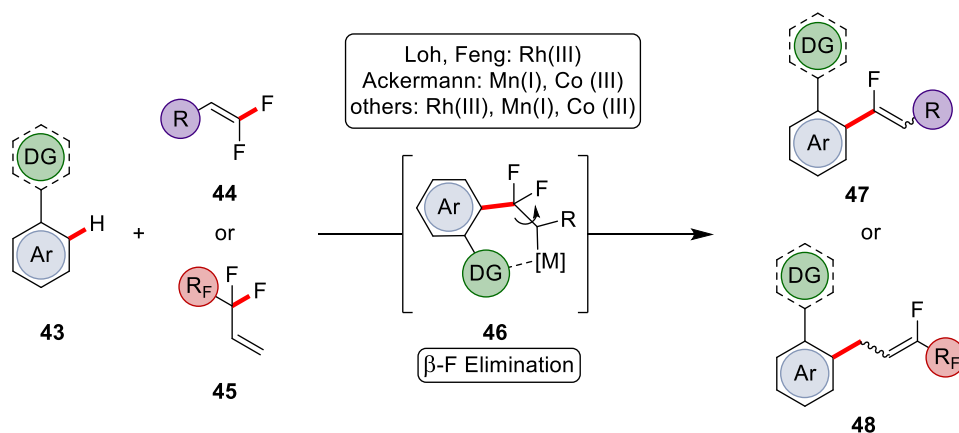


An approach that gained recent attention is the metal-mediated and -catalyzed elimination of α - or β -fluorine atoms, due to milder conditions that are required compared to the oxidative addition into C–F bonds that represents an organometallic C–F activation.^[88] Transformations through these elimination processes typically proceeded by carbon–carbon or carbon–heteroatom bond formations and were increasingly developed as C–F bond activation methods.^[89] The first example of such an elimination approach was reported in 1991 by Heitz, who showed the transition metal-catalyzed activation of a C–F bond by β -fluorine elimination to afford α -fluorostyrenes **41** (Scheme 1.12).^[90]



Taking inspiration from this work, Loh and Feng developed a Rh(III)-catalyzed C–H and C–F activation, based on β -fluorine elimination, to generate fluorovinylated heterocycles.^[91] At the same time, Ackermann^[92] among others^[93] showed that 3d metal catalyst are also well suitable for such kind of transformation. High selectivities of vinylic **44** as well as allylic **45** 1,1-difluoroalkenes and the modification of 7-azaindols,^[92b] important building blocks in pharmaceuticals,^[94] are key developments within these C–H/C–F functionalization manifold (Scheme 1.13). Although different transition metals were used, the mechanism is mainly similar involving (a) chelation-directed C–H

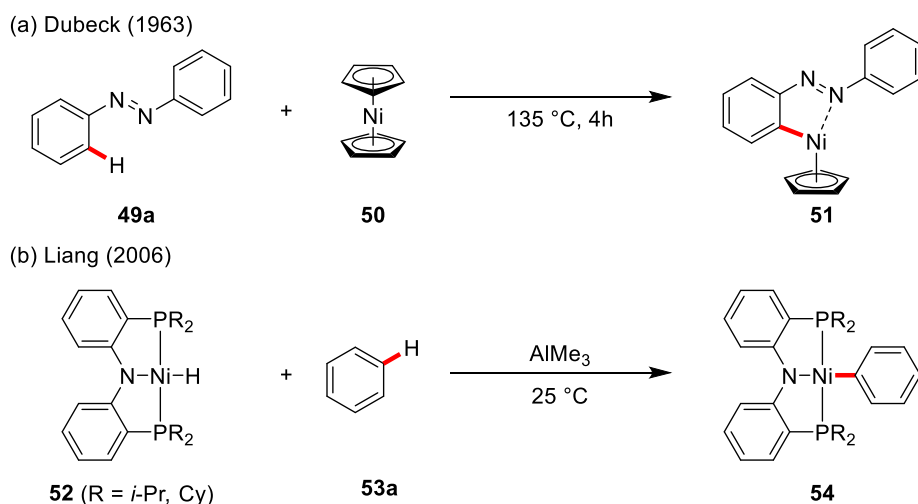
cleavage of (hetero)arenes, (b) migratory insertion of fluoroalkenes and (c) β -fluorine elimination (**46**).



Scheme 1.13. C–H/C–F functionalization by transition metal catalyst.

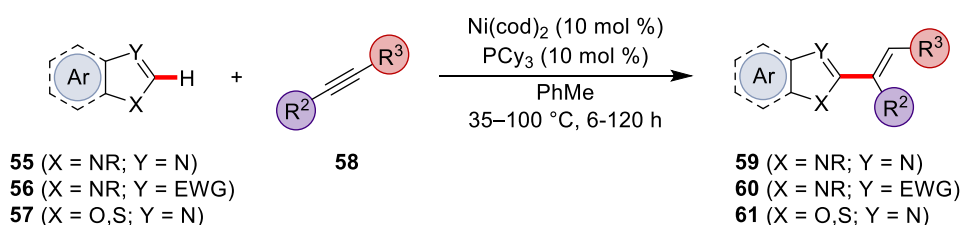
1.4. Nickel-Catalyzed C–H Activation for Alkene Hydroarylations

Catalytic C–H activation using transition metals has received significant interest, because it provides a new strategy to construct carbon–carbon and carbon–heteroatom bonds without pre-functionalization.^[95] Recently, inexpensive catalysts based on 3d transition metals, such as manganese, iron, cobalt and nickel, were increasingly used for catalytic transformations, due to their lower cost and reduced toxicity compared to commonly used 4d-based metal catalysts.^[63, 96] In this context, important contributions to nickel-catalyzed C–H activation were made by Dubeck and Kleiman in 1963, who prepared the cyclonickelated complex **51** *via* C–H nickelation of azobenzene **49a** by nickelocene (Scheme 1.14a).^[97] Thereafter, there was little process on C–H nickelation of non-activated C–H bonds for more than 50 years, yet Liang reported in 2006, that pincer nickel complex **52** could react with benzene to furnish complex **54** *via* oxidative addition of the C–H bond, without the need for a directing group (Scheme 1.14b).^[98]



Scheme 1.14. Nickel-catalyzed C–H activation by (a) directing group assistance and (b) undirected nickelation.

In the same year, Nakao and Hiyama reported the hydroarylation of alkynes **58** as a side reaction in the attempted arylocyanation (Scheme 1.15).^[99] With PCy₃ as the ligand the C–H hydroarylations of several (hetero)arenes **55–57** were accomplished. Taking inspiration from these findings, many nickel-catalyzed C–H activations of activated heteroarenes and unactivated C–H bonds, using monodentate but mostly bidentate chelation-assisted directing groups, were developed.^[100]

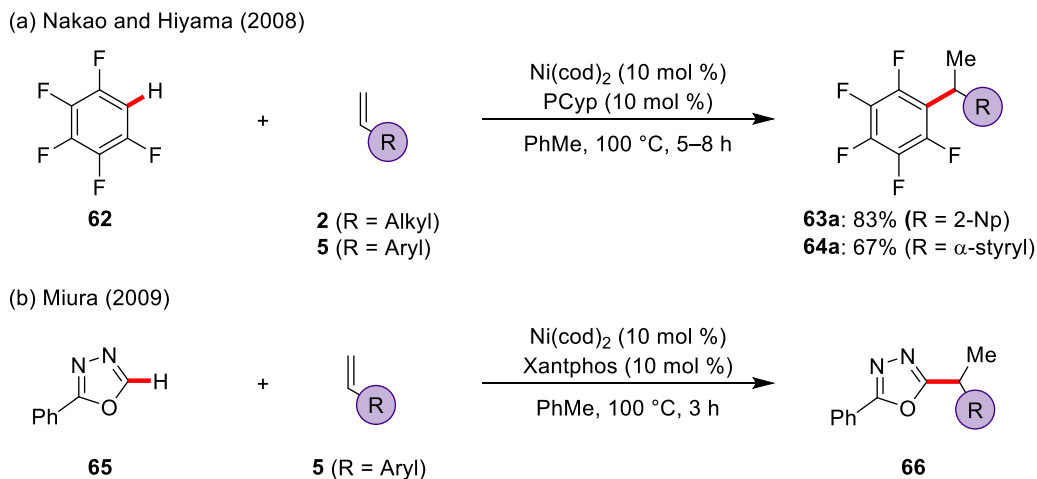


Scheme 1.15. Nickel-catalyzed hydroheteroarylation of alkynes with azoles.

The use of alkynes,^[22b, 96c] alkenes^[101] and allenes^[102] has gained considerable interest in nickel-catalyzed C–H activation due to its excellent atom-economy. Especially, because of their low cost, availability and sustainability, alkenes are particularly attractive for the formation of new C(sp²)–C(sp³) bonds.^[103] Despite the fact that the regioselectivity may be difficult to control, the generation of a stereogenic C(sp³) carbon offers opportunities for the development of asymmetric transformations.

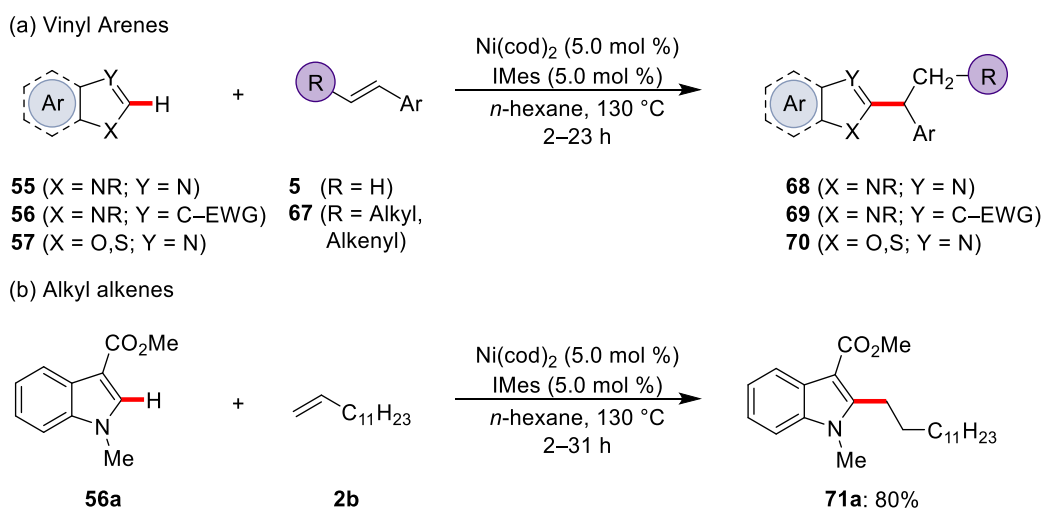
To provide regioselectivity control, Nakao and Hiyama reported in 2008 the unprecedented hydroarylation of conjugated 2-vinyl(arene) with pentafluorobenzene **62** to yield selectively the 1,1-diarylethane products **63a** and **64a** (Scheme 1.16a).^[100e] While the scope was rather limited, Miura reported in 2009 an extension towards the

hydroarylation of easily accessible styrene derivatives **5** with oxadiazole substrates **65** (Scheme 1.16b).^[100c] To achieve high levels of alkene hydroarylation Xantphos was identified as crucial bidentate ligand to form the branched product exclusively.



Scheme 1.16. Early examples of nickel-catalyzed hydroarylations of alkenes with (hetero)arenes.

Since both reports are based on conjugated, thus activated, alkenes, Hiyama reported in 2010 the hydroheteroarylation of unactivated alkenes **5** and **67** at the C2 position of *N*-protected heteroarenes using IMes and Ni(cod)₂ (Scheme 1.17a).^[104] Even though high levels of branched selectivity with conjugated activated alkenes were achieved, unactivated alkene **2b** resulted in the formation of the linear product (Scheme 1.17b). This catalyst would later proved broadly applicable in the hydroarylation of alkenes with various (hetero)arenes.^[22b, 96c]

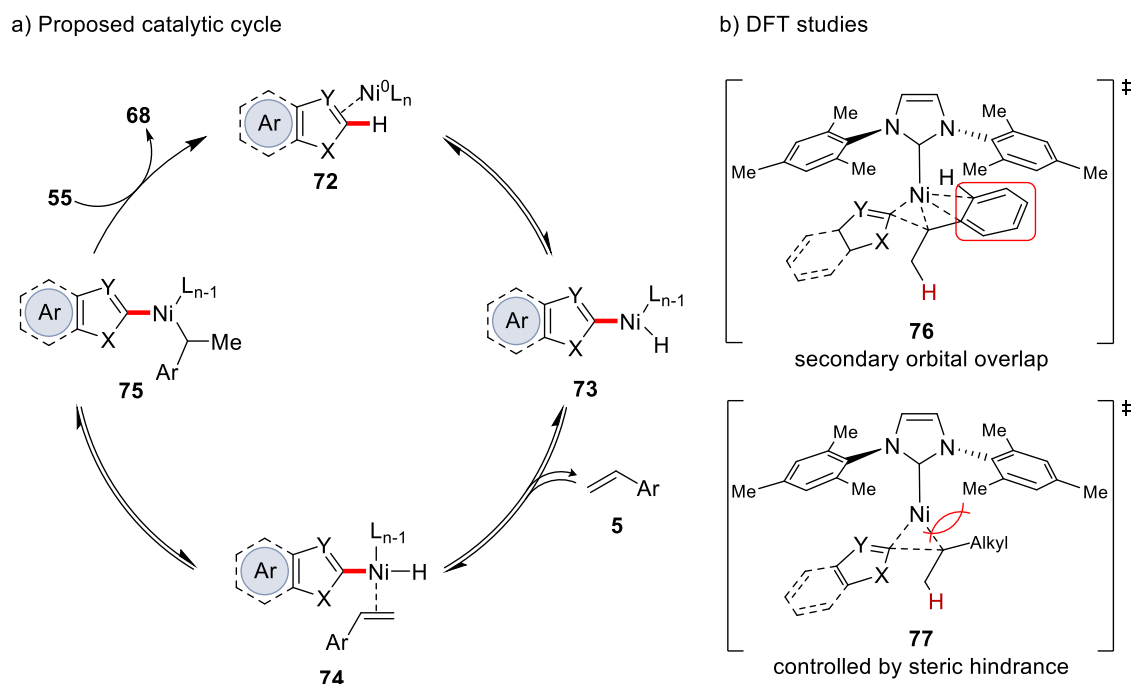


Scheme 1.17. Substrate-guided selectivity in nickel-catalyzed hydroarylations.

Interested in the mechanism and the change in regioselectivity, the authors performed deuterium-labeling experiments, suggesting a reversible oxidative addition step to

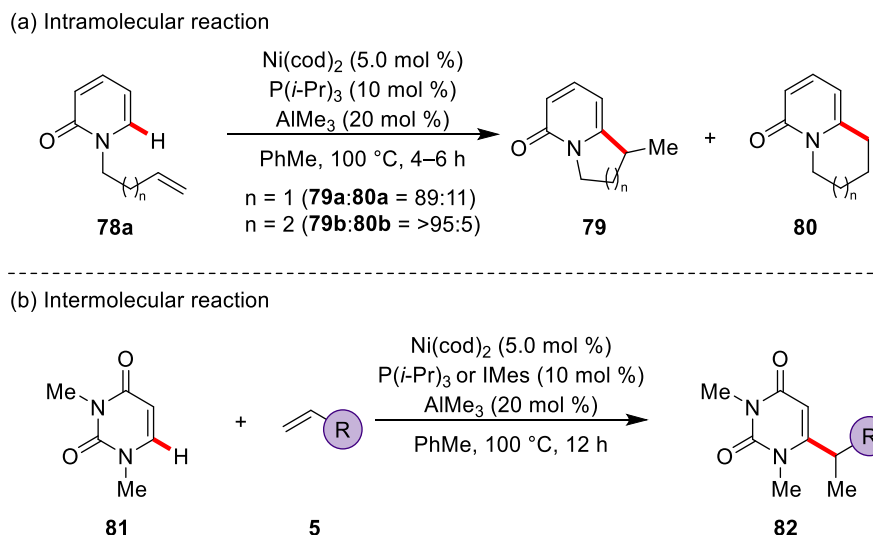
1. Introduction

generate nickel complex **73**.^[100c, 100e, 104] The followed coordination of the alkene **5** and hydronickeleation generates intermediate **75** in a reversible manner, as was based on the observed H/D scrambling. Thereafter, an irreversible and rate-determining reductive elimination delivers product **68** and regenerates intermediate **72** (Scheme 1.18a). To explain the regioselectivity, Nakao and Hiyama as well as Miura proposed the formation of the Markovnikov product to be favored due to the formation of π -benzyl or π -allyl nickel intermediates. Based on DFT studies, Shi supported the mechanism and explained the control in regioselectivity by a secondary orbital overlap between the alkene and the nickel center (Scheme 1.18b).^[105] While the aryl group can overlap with the nickel-center and therefore accelerate the rate-limiting reductive elimination **76**, the alkyl substituted olefins showed no interaction that facilitates the reductive elimination **77**, leading to the sterically less hindered product.



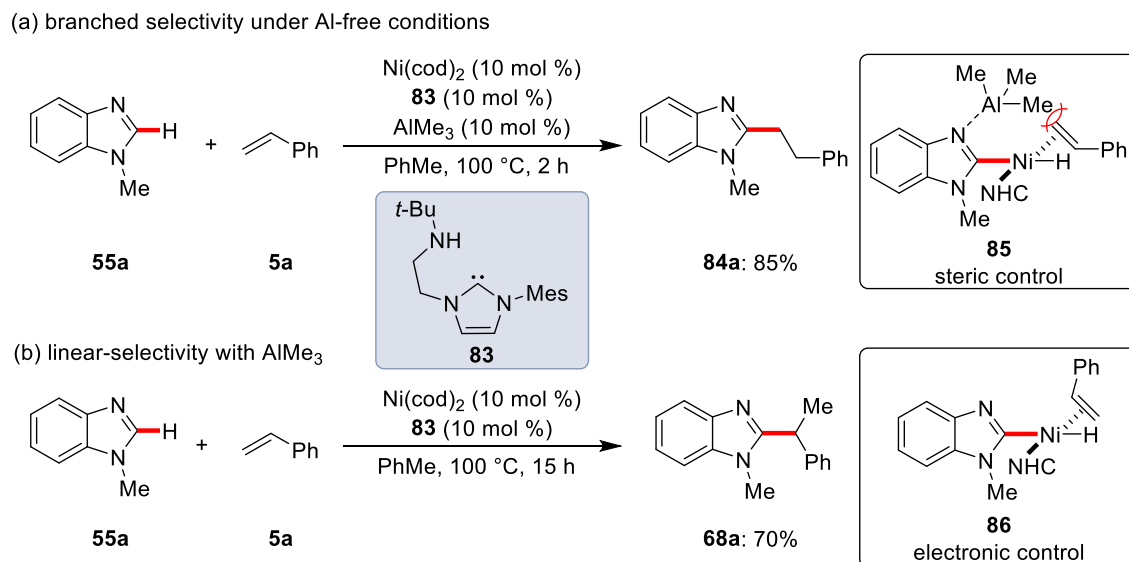
Scheme 1.18. a) Proposed catalytic cycle of the nickel-catalyzed hydroarylation of vinylarenes **5** with azoles **55** and b) key transition states.

Major progress in terms of linear/branch selectivity control and the applicability to unactivated (hetero)arenes and alkenes, was achieved by LEWIS-acidic organoaluminium additives. In this context, the direct functionalization of 2-pyridones **78a** by an intramolecular or intermolecular hydroarylation of alkenes was facilitated efficiently by the addition of organoaluminium additives (Scheme 1.19).^[100b] Inspired by this, numerous hydroarylations of non-conjugated alkenes **2** with various heteroarenes **55-57** were disclosed, reflecting the key role of LEWIS-acids in nickel-catalyzed hydroarylations.^[106]



Scheme 1.19. Nickel-catalyzed hydroarylations of pyridones **78a** and **81** with LEWIS-acid AlMe_3 .

While in most studies just one regioisomer was observed, Ong was able to develop a switch in regioselectivity in the hydroarylation of vinylarene **5a** with benzimidazole **55a** by using Ni(cod)_2 , an amino linked NHC **83** and AlMe_3 as LEWIS-acid (Scheme 1.20).^[107] Interested in the role of the LEWIS-acid, detailed mechanistic studies were performed, revealing that AlMe_3 not only controlled the regioselectivity of the transformation, but also significantly increased the rate of product formation.^[107a]



Scheme 1.20. Regioselectivity control in nickel-catalyzed hydroarylations of styrene **5a** with benzimidazole **55a**.

Mechanistic findings involved the detection of a nickel-hydride species and the isolation of an aluminum-benzimidazole adduct and suggested that in the absence of the organoaluminium additive, the linear selectivity is preferred by less steric hindrance (**85**)

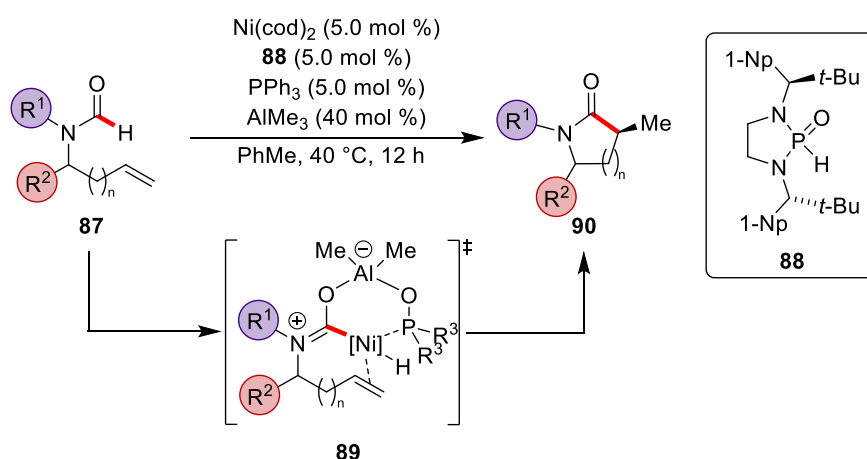
during the insertion of the styrene into the Ni–H bond, whereas hydride insertion at the β -carbon of styrene is electronically favored (**86**).

1.5. Enantioselective Nickel-Catalyzed C–H Activation

“Chirality of organic molecules plays an enormous role [...], yet the synthesis of such entities in one enantiomeric form is one of the most difficult challenges.”

(B. M. Trost)^[108]

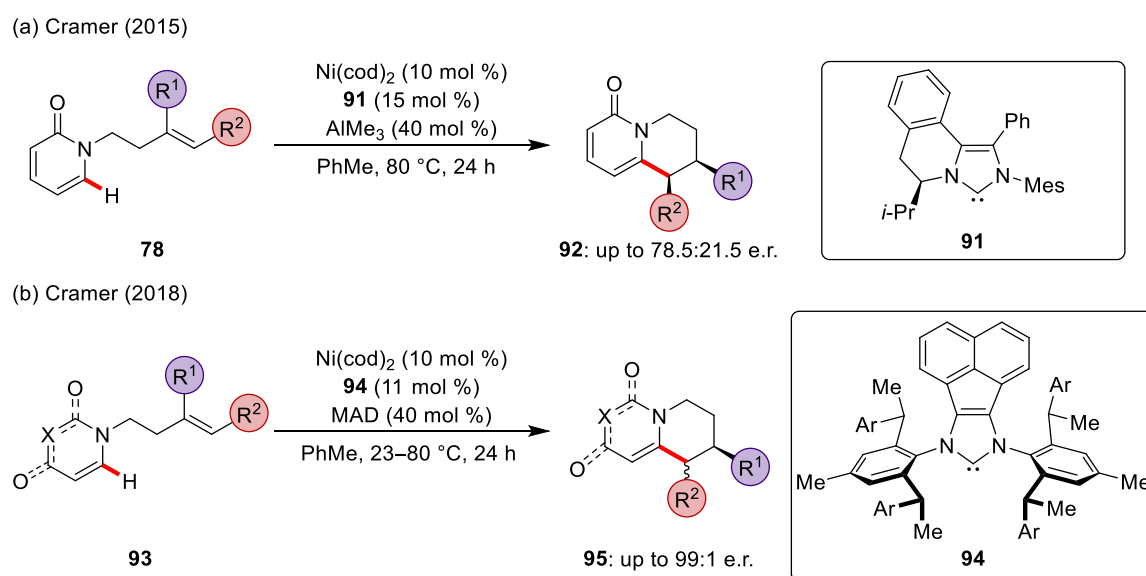
While nickel-catalyzed C–H activations, are nowadays rather well established, asymmetric transformations remain scarce. Thus far, almost all examples involved the asymmetric functionalization of alkenes in an intramolecular fashion.^[109] In this context, a breakthrough was published in 2013 by Cramer,^[109g] based on an enantioselective version of the nickel-catalyzed intramolecular hydrocarbamylation of homoallylic formamides,^[100b] which arguably is the first enantioselective transformation by inner-sphere C–H activation with a 3d transition metal catalyst (Scheme 1.21). Taking advantage of the low bond dissociation energy of the formyl C–H bond^[28, 37a, 110] and the reactive P(III) isomer of the chiral heteroatom-substituted secondary phosphine oxide (HASPO) **88**,^[51] the asymmetric cyclization of substrate **87**, by a nickel/aluminium^[111] heterobimetallic^[22f] activation mode provided pyrrolidinones **90** in high yield and excellent levels of enantiomeric excess (*ee*).



Scheme 1.21. Enantioselective intramolecular nickel-catalyzed hydrocarbamylation of alkenes **87**.

Inspired by the initial results from Nakao and Hiyama,^[100b] Cramer developed a ligand-controlled regiodivergent annulation of pyridone derivatives **78**. With Ni(cod)₂ as the pre-catalyst the *exo*-cyclized product **92** was obtained, whereas the addition of NHC ligand **91**

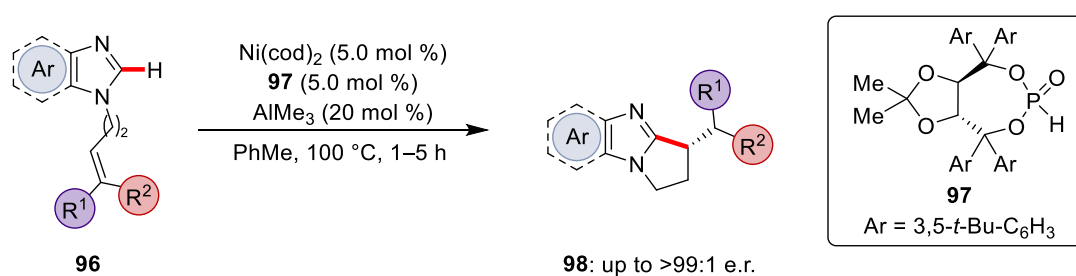
resulted in the selective formation of the *endo* product **92** (Scheme 1.22a).^[109f] The chiral NHC **91**, derived from the design of Hong,^[112] furnished the enantioselective cyclization with up to 78.5:21.5 e.r. Considering the huge potential of chiral NHC ligands, further studies by Cramer, showed the high activity of the novel chiral NHC **94** on the asymmetric cyclization of pyridones with tethered olefins **93** (Scheme 1.22b).^[109e] Inspired by a ligand design by Gawley,^[113] NHC **94** facilitated the formation of the *endo*-cyclized annulated pyridones **95** and uracils from diversely substituted alkenes **93** in excellent yields and enantioselectivities at mild reaction temperatures in the presence of MAD as the LEWIS-acid. This approach was later extended to pyridines by Shi,^[109a] yielding the corresponding tetrahydro(iso)quinolines in excellent diastereo- and regio-selectivities.



Scheme 1.22. Enantioselective nickel-catalyzed hydroarylation with pyridines **78** and **93**.

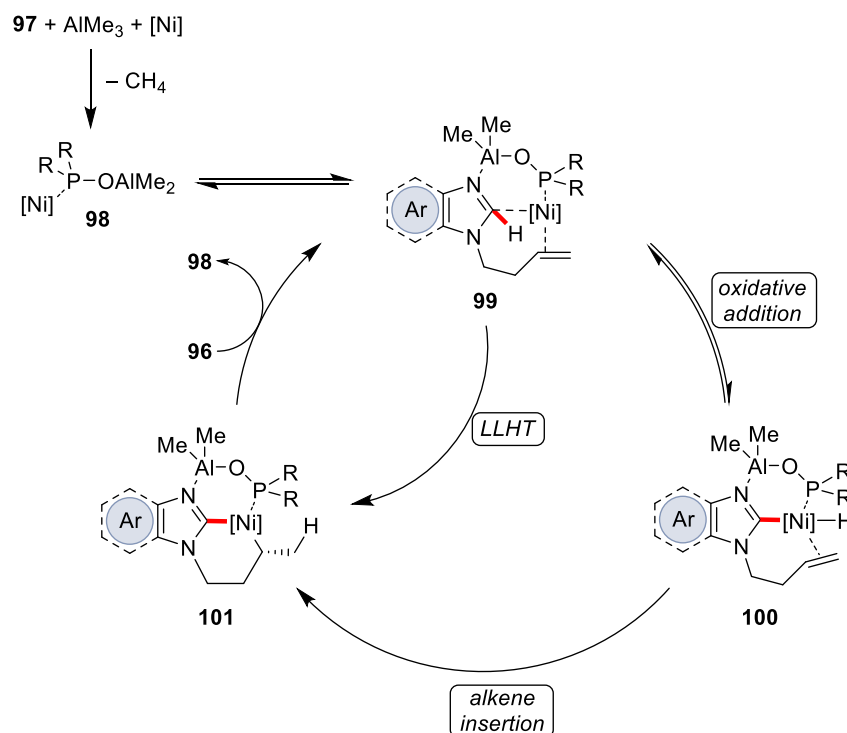
While previous studies on nickel-catalyzed asymmetric C–H activations were limited to pyridones, an extension towards azoles proved viable. Interestingly, since the early studies by Bergman and Ellman^[114] undirected cyclizations with tethered alkenes were long dominated by rhodium(I) catalysts,^[115] with a notable exception by Cavell for the nickel-catalyzed *exo*-selective cyclization of activated (benz)imidazolium salts.^[116] In this context, Ye reported in 2018 on the unprecedented nickel-catalyzed asymmetric *exo*-selective hydroarylation of alkenes with tethered imidazole derivatives **96** (Scheme 1.23).^[109d] Notably, a nickel-aluminum bimetallic catalysis was assumed to occur, which is promoted by the TADDOL based HASPO pre-ligand **97**.^[55] A variety of polycyclic

imidazoles and diversely substituted alkenes proved compatible with the nickel catalysis yielding excellent levels of enantiomeric excess.



Scheme 1.23. Asymmetric nickel-catalyzed *exo*-selective hydroarylation of alkenes **96**.

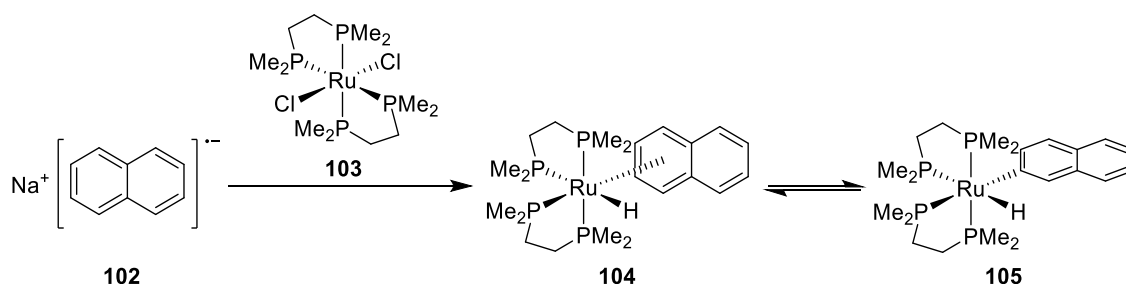
Based on mechanistic experiments a plausible catalytic cycle was proposed (Scheme 1.24). The catalysis is initiated with the formation of the nickel/aluminium bimetallic complex **98** bearing a chiral phosphine oxide ligand. Coordination of the aluminium to the nitrogen *via* dative bond and pre-coordination of the nickel to the olefin yields intermediate **99**. In a hetero-bimetallic mode of activation the C–H bond can be activated through either **100** resulting from an oxidative addition mechanism or **101** resulting from ligand-to-ligand hydrogen transfer (LLHT). The subsequent reductive elimination releases the *exo* product **98**, while the bimetallic active catalyst **99** is regenerated.



Scheme 1.24. Proposed mechanism of the asymmetric nickel-catalyzed *exo*-selective hydroarylation.

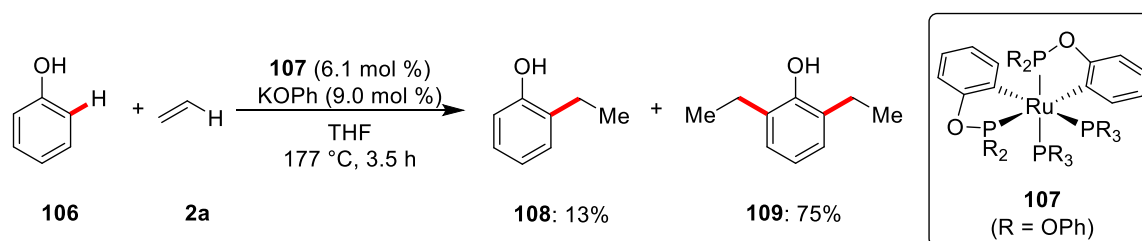
1.6. Ruthenium-Catalyzed C–H Activation

The regioselective direct conversion of C–H bonds into new C–C bonds by precious transition metals, such as palladium-,^[117] rhodium-,^[115a] platinum-^[118] and iridium^[119] complexes, have witnessed an enormous development during the last decades. Recently, the use of less expensive^[120] ruthenium catalysts has tremendously contributed to the discovery of efficient catalytic systems, due to their selective transformation into cyclometalated species, their compatibility with several kinds of oxidants, and the stability of some of them to both air and water.^[38a, 121] The first observation employing ruthenium complexes was reported in 1965 by Chatt and Davidson.^[122] Based on the stoichiometric C–H activation of sodium naphthalene to an in-situ generated ruthenium(0)-phosphine complex an equilibrium between the π -complex **104** and the C–H activated complex **105** was observed (Scheme 1.25).



Scheme 1.25. Early studies on stoichiometric C–H activation with ruthenium complex **103**.

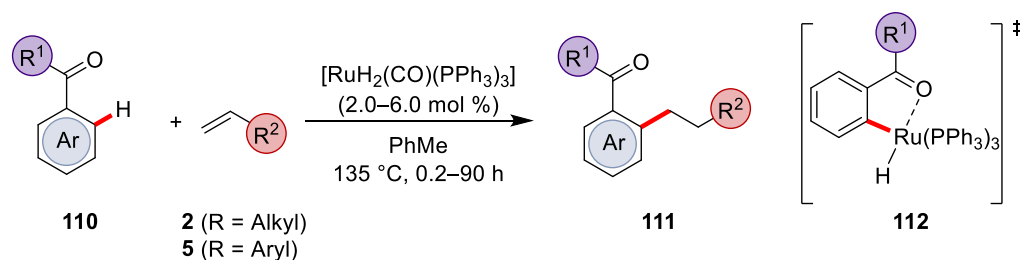
In 1986, Lewis and Smith reported on the ruthenium-catalyzed C–H alkylation of phenol with ethene utilizing phosphites as a transient directing group (Scheme 1.26).^[36, 123] Although the reaction required harsh reaction conditions and was limited to phenol and ethene, this report represented the first example of C–H activation under ruthenium catalysis.



Scheme 1.26. First ruthenium-catalyzed C–H activation.

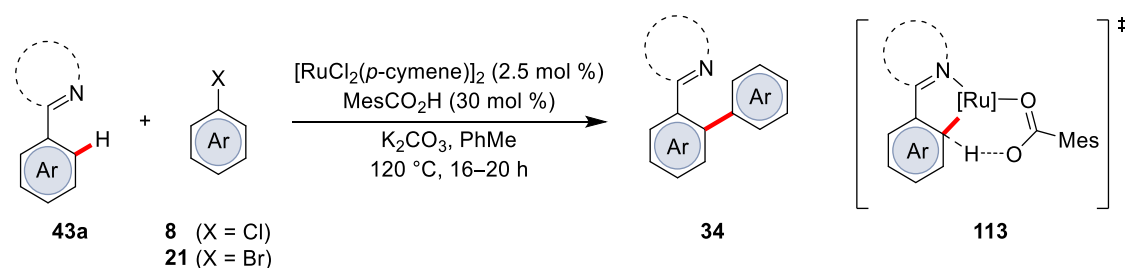
A few years after this pioneering report, Kakiuchi and Murai showed that $[\text{RuH}_2(\text{CO})(\text{PPh}_3)_3]$ was able to catalyze the insertion of a variety of alkenes **2** or **5** into the *ortho* C–H bonds of aromatic ketone derivatives including heteroarenes (Scheme

1.27).^[124] DFT studies by Morokuma^[125] suggested a five-membered ruthenacycle **112** by an initial coordination of the directing group and subsequent oxidative addition of the C–H bond. This important work marked the beginning of a long series of related studies on ruthenium-catalyzed direct C–H activation, such as arylations,^[126] alkylations^[127] and alkenylations^[35b, 43d, 128] among others.^[34, 129]



Scheme 1.27. Pioneering studies on ruthenium-catalyzed direct C–H activation.

Inspired by base-assisted metalation studies by Shaw^[130] and Davies,^[131] Ackermann demonstrated in 2008 a significant breakthrough in ruthenium catalysis using carboxylates as the additives for the arylation of various arenes.^[132] The carboxylate-assisted C–H arylation was not limited to arenes with triazoles, but other directing groups, such as oxazolines, pyridines, and pyrazoles as well as a broad variety of aryl bromides and less reactive aryl chlorides were also applicable (Scheme 1.28). The mechanistic pathway of the C–H activation by carboxylate-assistance was suggested to proceed *via* a six-membered transition state **113**,^[40, 133] with rate acceleration by carboxylates compared to phosphines or phosphates.^[132]

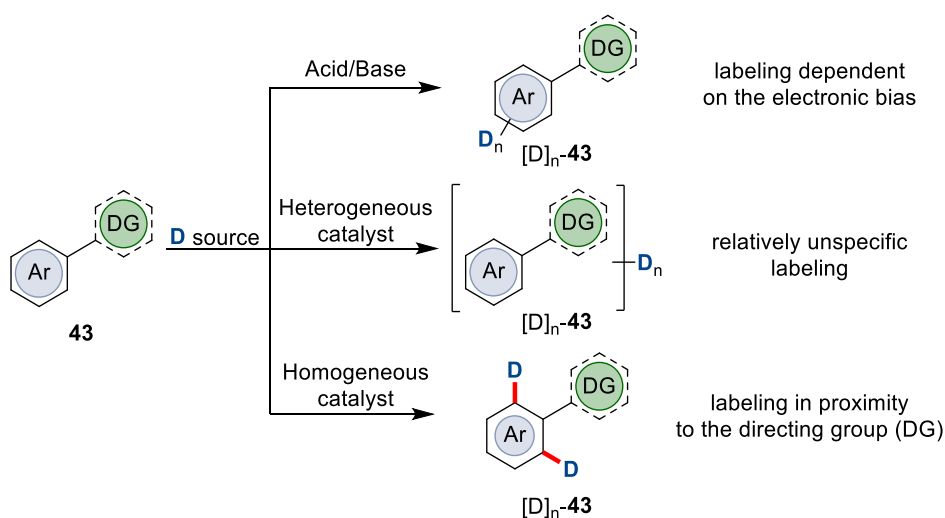


Scheme 1.28. Carboxylate-assisted ruthenium-catalyzed C–H arylation.

Thereafter, carboxylate additives for the development of novel chelation-assisted C–H transformations were broadly applied with major contributions by Ackermann and Dixneuf.^[38a, 121g]

1.7. Ruthenium-Catalyzed Hydrogen Isotope Exchange

The applications for catalytic C–H activations have been largely increased during the last decade with many approaches towards hydrogen isotope exchange (HIE).^[134] In this context, rapid developments in high-performance mass spectrometry to determine isotope ratios,^[135] tools for mechanistic understanding^[136] and the alteration in absorption, distribution, metabolism, and excretion (ADME) properties^[137] of existing drugs showed the importance for selective formations of C–D and C–T bonds.^[138] Compared to conventional multistep syntheses, direct HIE by either acid/base-mediated labeling, heterogeneous or homogeneous catalysis seems more attractive in terms of time and resources (Scheme 1.29).^[139] While acid/base-mediated labeling methods largely depend on the inherent electronics within the target molecules, heterogeneous metal-catalyzed HIE results in relatively unspecific incorporation of numerous isotopes into the target molecule. In contrast, homogeneous metal-catalyzed HIE utilizing a directing group can incorporate numerous isotopes only at specific positions in a molecule.^[140]

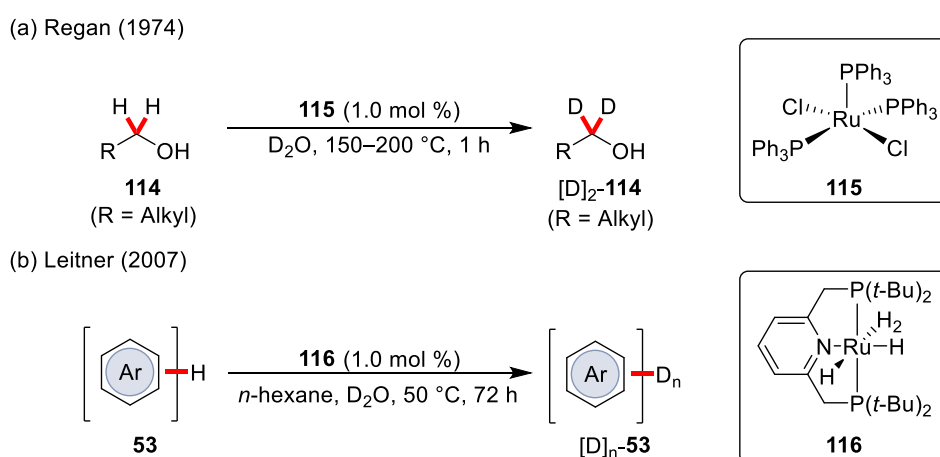


Scheme 1.29. Selectivity control with distinct HIE methods.

In the late 1960s and early 1970s fundamental studies by the research groups of Garnett^[141] and Shilov^[142] resulted in efficient methods for efficient H/D exchange in both aromatic^[134b] and aliphatic^[134a] substrates. While most of these methods required precious metals, such as iridium,^[143] rhodium,^[144] and palladium,^[145] recent developments illustrate the applications of more economic ruthenium^[146] and earth abundant 3d metals.^[147]

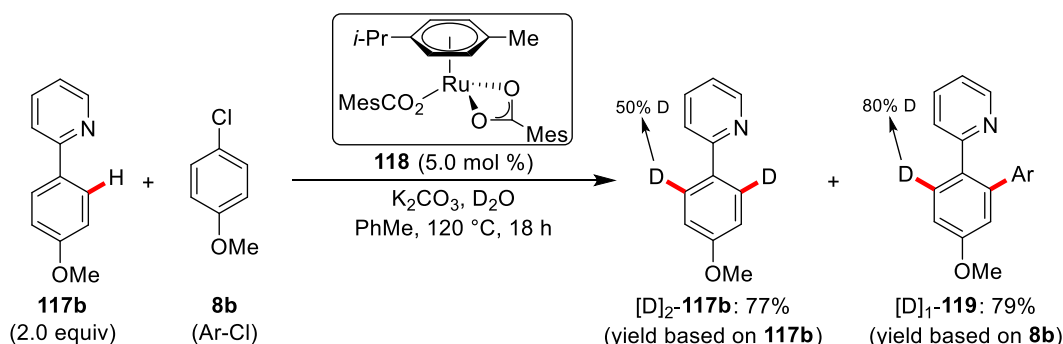
One of the milestones in ruthenium-catalyzed HIE was reported in 1974 by Regan.^[148] Tris(triphenylphosphine)ruthenium(II) dichloride (**115**) was employed as a catalyst in the

deuteration of primary alcohols **114** at high reaction temperatures of 150–200 °C (Scheme 1.30a). In addition to studies on the activation of C–H bonds in α -positions to heteroatoms, the activation of C(sp²)–H bonds gained momentum for HIE methods. An early report based on C(sp²)–H HIE was reported by Leitner on the deuterium-labeling of benzene derivatives and heteroaromatic compounds using the ruthenium complex **116** under milder reaction conditions (Scheme 1.30b).^[149] A combined experimental and computational study showed that strong steric effects furnished the site-selectivity and that the deuteration mechanism was based on a σ -bond metathesis between the aromatic C–H bonds and a hydride ligand of the ruthenium(II) complex **116**.



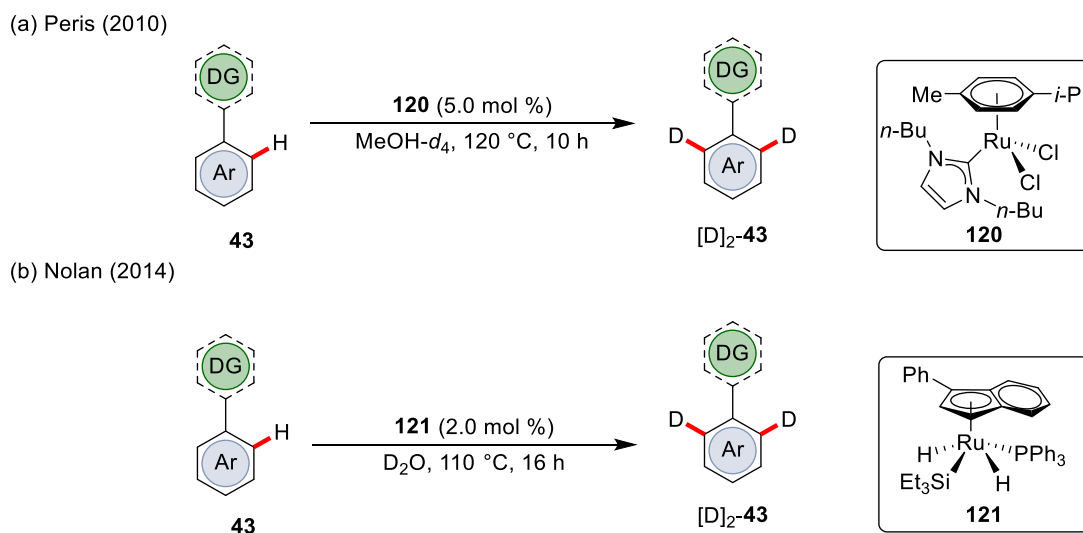
Scheme 1.30. Early examples of ruthenium-catalyzed HIE on (a) activated C(sp³) and (b) unactivated C(sp²).

In 2010, Ackermann reported on the direct arylation with well-defined ruthenium(II) carboxylate catalyst **118**. During mechanistic studies, an incorporation of deuterium into the *ortho* C–H bond of arene **117b** was observed, reflecting the potential for direct HIE (Scheme 1.31).^[126h]



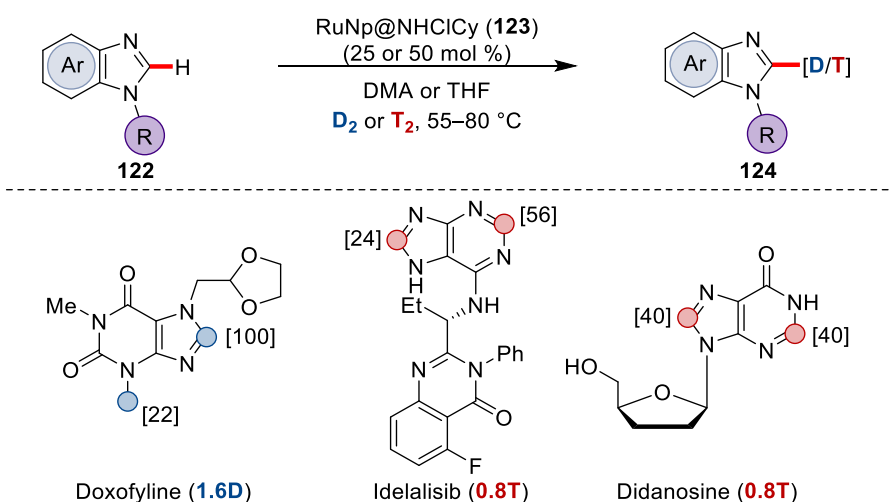
Scheme 1.31. Ruthenium(II) carboxylate catalyzed HIE on arene **117b**.

In the same year, Peris reported on the direct HIE of various arenes bearing *N*-heterocycles using ruthenium-NHC complex **120**, resulting in the *ortho*-selective deuteration in the presence of MeOH-*d*₄ (Scheme 1.32a).^[150] Similarly, Nolan reported on the use of a dihydrosilyl ruthenium catalyst **121** in deuterated water as the isotope source, promoting H/D exchange in a wide range of substituted aromatic and heteroaromatic scaffolds with *N*- or *O*-containing directing groups (Scheme 1.32b).^[151]



Scheme 1.32. Selective ruthenium-catalyzed HIE of arenes containing *N*- or *O*-containing directing groups.

While many deuteration under ruthenium catalysis employed D₂O as simple and easy to handle deuterium source, tritiation in general are dominated by ³H₂ as the isotope source.^[138b, 152] Although many protocols were effective to simple heterocyclic structures, ruthenium-catalyzed late-stage modifications of drugs through deuterium-^[146a, 146b, 146f, 153] and tritium-labeling are rare and mostly achieved by ruthenium nanoparticles.^[154] In this context, a recent publication from Feuillastre and Pieters showed the deuterium and tritium-labeling of nucleobase pharmaceuticals and oligonucleotides by stabilized ruthenium nanoparticles **123** (Scheme 1.33).^[154a] It was highlighted that the isotopic ³H-labeling of didanosine with ³H₂ at low pressure of 13.5 psi led to the selective tritiation at the purine motif with special activities of 23 Ci/mmol.



Scheme 1.33. Rutheniumnanoparticle-catalyzed H/D and H/T exchange of nucleobase pharmaceuticals **122**.

1.8. Remote C–H Activation by Ruthenium Catalysis

The control of site-selectivity in C–H functionalization is one of the biggest challenges facing organic chemist and his most widely achieved by the chelation-assistance of a LEWIS-basic directing group, which facilitates the C–H activation at the *ortho*-position to the directing group.^[155] However, in order to achieve *meta*-selective C–H transformations, various concepts were developed resulting in mainly six different approaches for *meta*-selective C–H functionalizations.^[156]

First, bulky substituents on the arene can inherently prevent the C–H activation at the adjacent positions, resulting in the functionalization at the less-steric hindered *meta*-position (Figure 1.5a).^[157] Unfortunately, this strategy is often limited to iridium-catalyzed borylations. Second, the cleavage of the directing group, such as carboxylic acid, during the course of the reaction, can result in *meta*-selective C–H transformations (Figure 1.5b).^[158] So far, this method is mostly viable in case of arenes with substituents at the *ortho*-position with respect to the directing group. Third, the installation of a template between the arene and the directing group (DG)^[159] brings the catalyst in close proximity to the desired C–H bond at the *meta*-position (Figure 1.5c).^[160] The drawback of this methodology is the requirement of additional synthetic operations for the installation and subsequent removal of the template. In addition, the exact nature of the template is hard to predict. The fourth remote strategy was disclosed by Kuninobu and Kanai. The authors developed a reversible hydrogen bonding urea based linker that allowed selective C–H borylations at the *meta*-position (Figure 1.5d).^[161] Unfortunately,

this transformation is so far largely limited to iridium-catalyzed borylations and is not broadly applicable. The fifth method was pioneered by Catellani^[162] and broadly applied by Yu^[163] and uses norbornene as a transient mediator and a *ortho*-directing group under palladium catalysis, resulting in an efficient way for *meta* C–H functionalization (Figure 1.5e).^[164] Lastly, the formation of cyclometalated ruthenium complexes by chelation-assisted *ortho* C–H metalation strongly increases the electron density on the arene,^[165] thus acting as an *ortho/para*-directing group with respect to the ruthenium and enabling overall functionalizations at a *remote* C–H bond (Figure 1.5f).^[22g, 166]

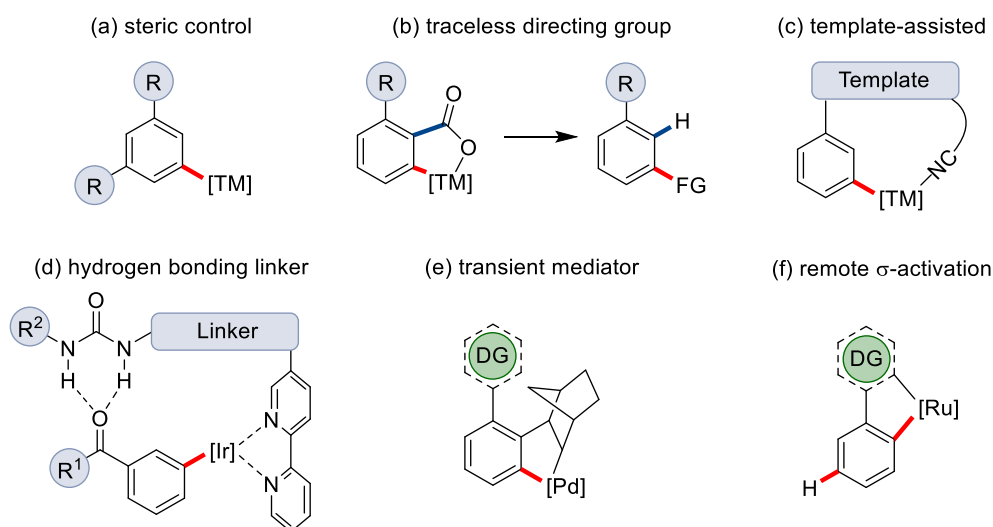
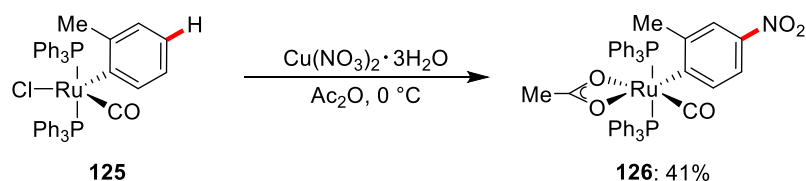
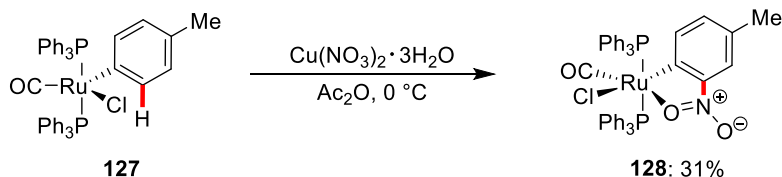


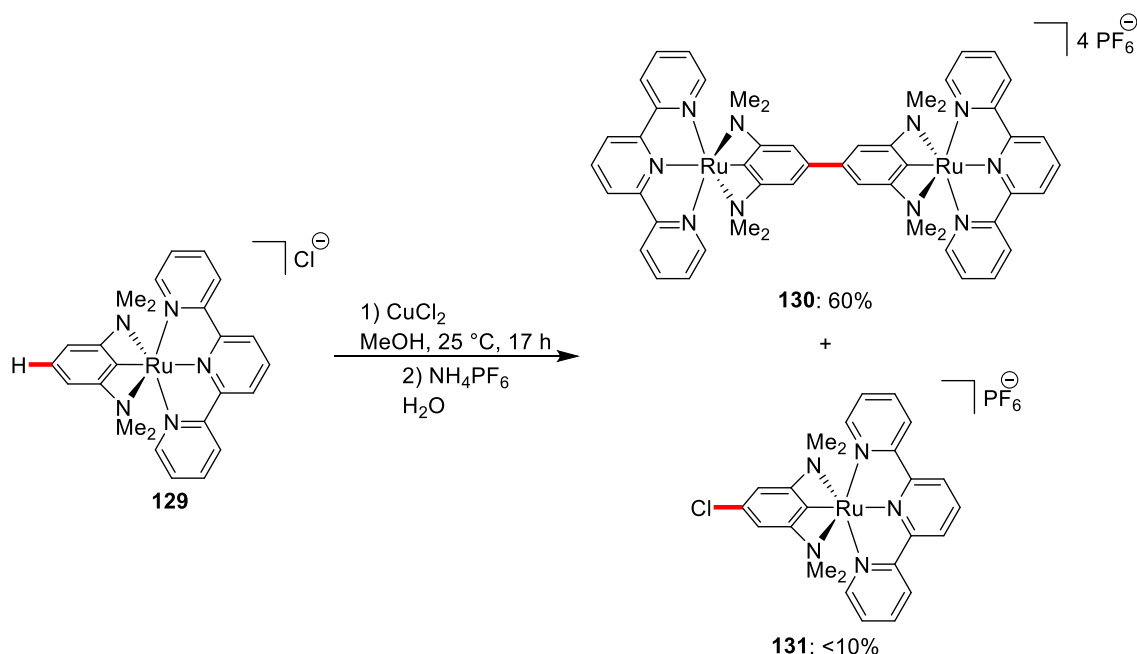
Figure 1.5. Strategies for *meta*-selective C–H activation.

1.8.1. Stoichiometric Remote C–H functionalization of Ruthenium Complexes

In 1994, Roper and Wright demonstrated in a pioneering study the stoichiometric remote C–H nitration of the arene ruthenium complex **125**.^[167] The C–H nitration occurred selectively at the position *para* to the ruthenium metal center (Scheme 1.34a). In contrast, the reaction of ruthenium complex **127** led to the formation of the stable five-membered ruthenacycle **128**, probably due to the *ortho/para*-directing effect of the metal center (Scheme 1.34b).

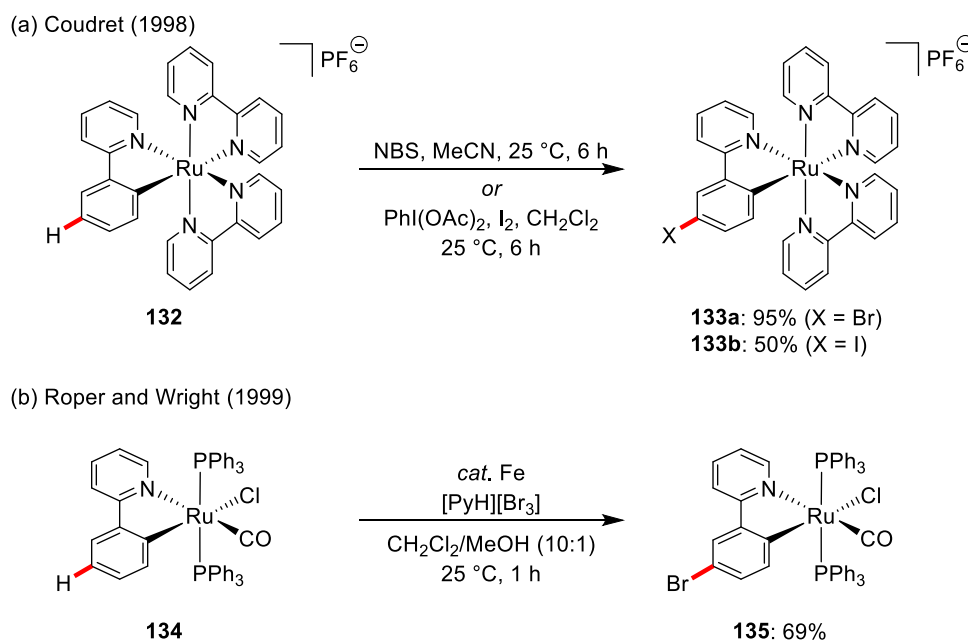
(a) C–H nitration at the *para*-position(b) C–H nitration at the *ortho*-position**Scheme 1.34.** Stoichiometric C–H nitration.

In the same year, the first stoichiometric example of chelation-assisted oxidative remote C–H functionalization was reported by van Koten.^[168] The treatment of the cationic ruthenium complex **129** with CuCl_2 furnished the homocoupled binuclear complex **130** and small amounts of the *para* to the ruthenium chlorinated complex **131** (Scheme 1.35).

**Scheme 1.35.** Oxidative homocoupling of ruthenium complex **129**.

Inspired by these results, Coudret discovered in 1998 the site-selective C–H bromination and iodination of ruthenium complex **132** at the *para*-position to the metal-carbon σ -bond under mild reaction conditions, providing the corresponding complexes **133a** and **133b** in good to high yields (Scheme 1.36a).^[169] One year later, Roper and Wright studied on the remote C–H halogenations of ruthenacycle **134**, affording the mono-brominated product

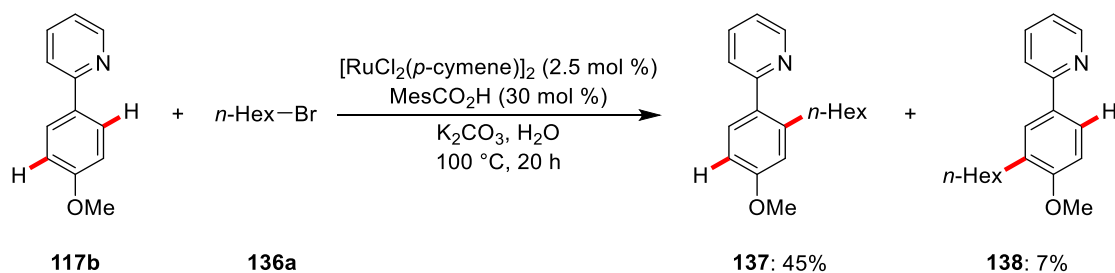
135 solely at the *para*-position with respect to the ruthenium center (Scheme 1.36b).^[170] These transformations were proposed to proceed through an electrophilic aromatic substitution ($S_{\text{E}}\text{Ar}$) process initiated by the *ortho/para*-directing character of the Ru–C σ -bond.



Scheme 1.36. Remote C–H halogenations of cyclometalated ruthenium complexes **132** and **134**.

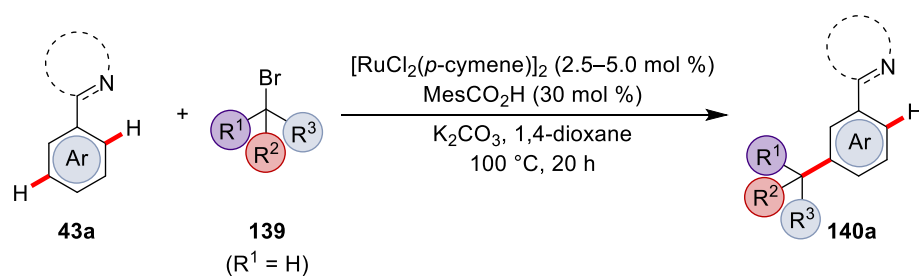
1.8.2. *meta* C–H Alkylation under Ruthenium Catalysis

In 2011, Ackermann reported on the carboxylate-assisted direct C–H alkylations of ketimine derivatives with unactivated primary alkyl bromides.^[127c] However, the alkylation reaction of arylpyridine **117b** provided 41% of the corresponding *ortho*-product **137** along with small amounts (up to 7%) of the *meta* C–H alkylated product **138** (Scheme 1.37). It is noteworthy that it is the first time that *meta*-selectivity under ruthenium catalysis was observed.



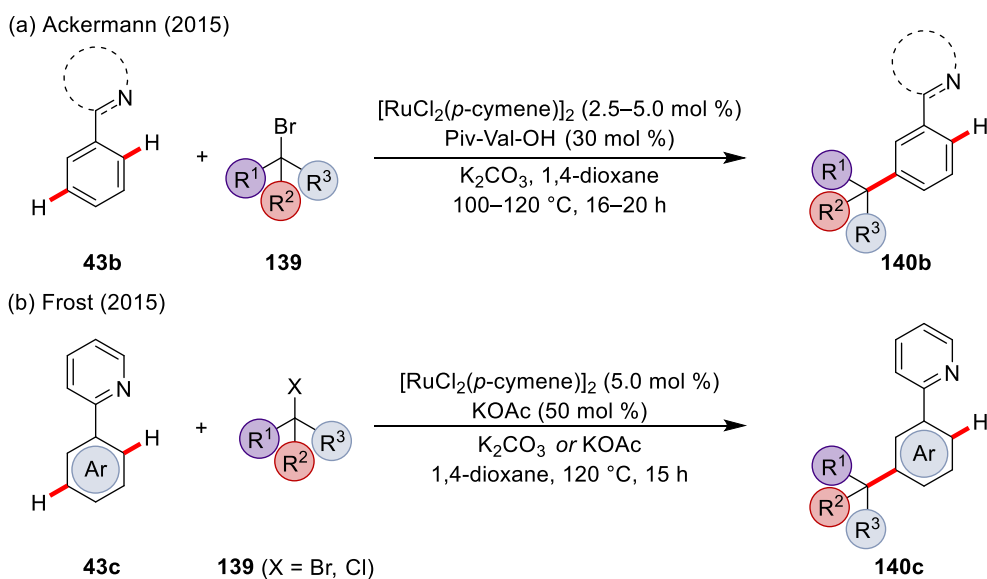
Scheme 1.37. Ruthenium-catalyzed C–H alkylation with *n*-hexyl bromide (**136a**).

Inspired by the observation of the first *meta*-selective ruthenium catalyzed alkylation, Ackermann disclosed thereafter pyridyl- and azole-directed *meta*-selective C–H alkylations with secondary alkyl halides **139** with catalytic amounts of sterically demanding benzoic acid (MesCO₂H) (Scheme 1.38).^[166f] Detailed mechanistic studies on isotope labeling conclusively revealed an initial reversible cycloruthenation which was supportive of a subsequent electrophilic-type alkylation. In addition, by adding stoichiometric amounts of TEMPO no reaction was observed and the reaction of an enantiomerically enriched alkyl halide provided a racemic mixture of the corresponding product.



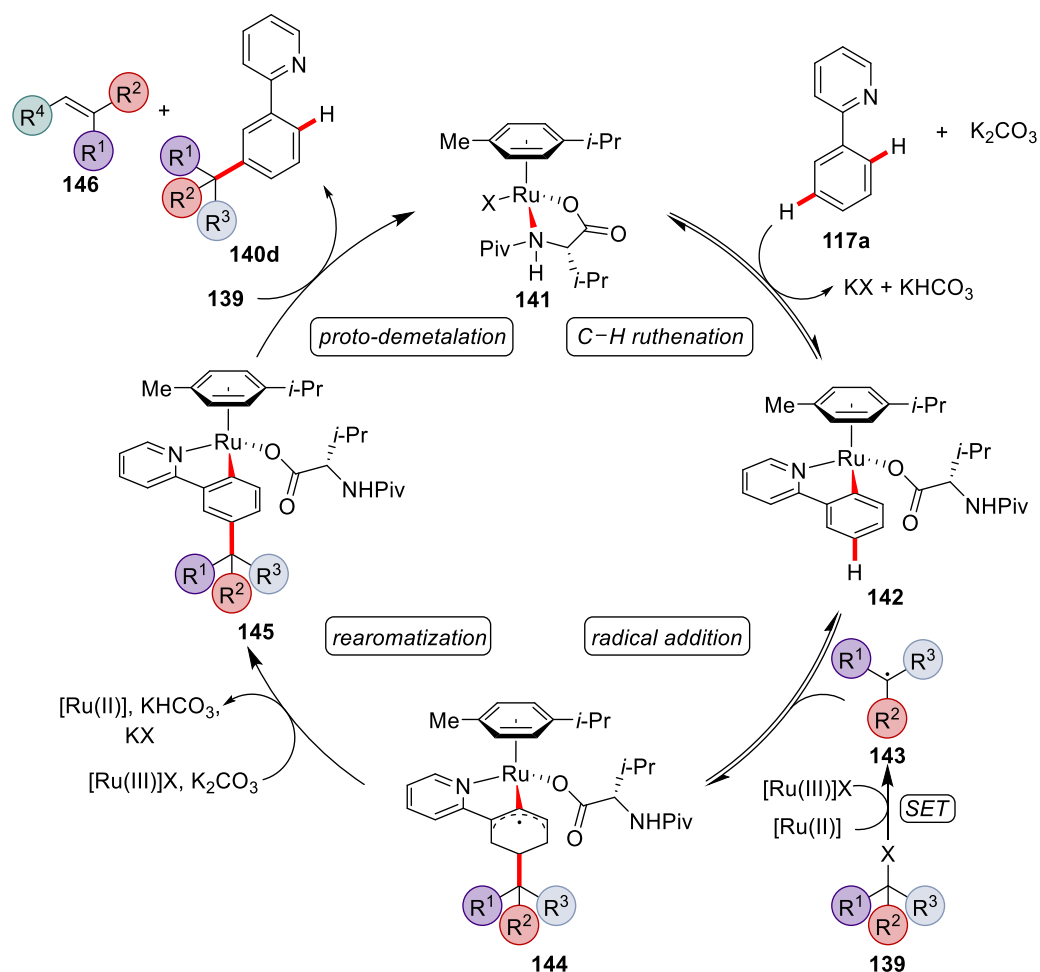
Scheme 1.38. Remote *meta* C–H alkylations with secondary alkyl halides **139**.

In 2015, the groups of Ackermann^[166e] and Frost^[171] independently reported on methods for the *meta*-selective C–H alkylations with tertiary alkyl halides **139** (Scheme 1.39). Notably, Ackermann's protocol used monoprotected amino acids (MPAA) as the carboxylate ligand for the first time in ruthenium-catalyzed C–H activation and a removable auxiliary strategy to access *meta*-substituted anilines (Scheme 1.39a). Both methods showed efficient couplings with secondary and sterically congested tertiary alkyl halides. In this context, Frost's protocol provided the desired products **140c** with less reactive tertiary alkyl chlorides (Scheme 1.39b). Detailed experimental mechanistic studies provided strong evidence for a radical pathway rather than a S_EAr and supported a ruthenium-catalyzed homolytic C–Hal cleavage, reflected by an unusual second-order dependence on the ruthenium concentration.^[166e]



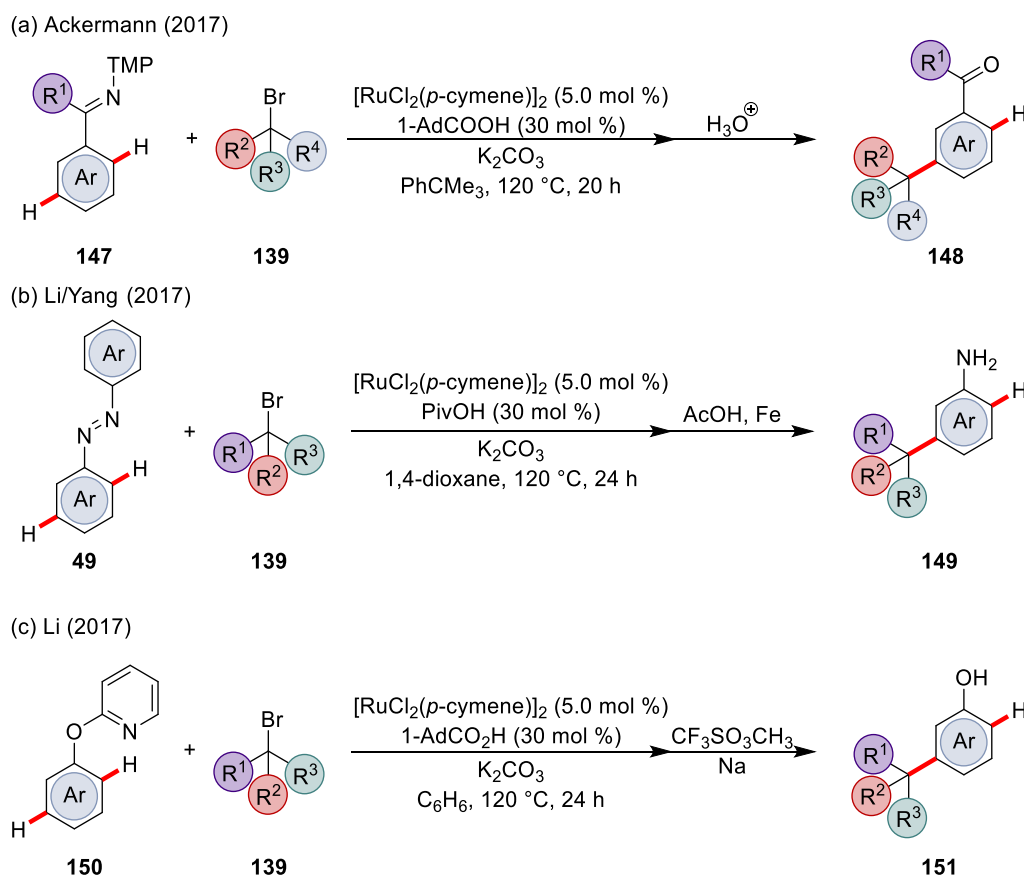
Scheme 1.39. *meta* C–H alkylations with tertiary alkyl halides **139**.

Based on detailed mechanistic studies, such as radical clock experiments, racemization studies and kinetic analysis, Ackermann proposed a detailed catalytic cycle (Scheme 1.40).^[166e] Starting from ruthenium(II) complex **141**, reversible *ortho* C–H metalation generates cyclometalated intermediate **142**. Subsequent radical addition of **143**, which is formed *via* single-electron transfer (SET) from ruthenium(II) to the alkyl halide, occurs at the *para*-position with respect to the ruthenium forming **144**. Afterwards, redox rearomatization and hydrogen-atom abstraction lead to the formation of ruthenacycle **145**. Finally, proto-demetalation delivers the *meta*-alkylated compound **140d** and regenerates the active ruthenium catalyst **141**. Although Frost presented a catalytic cycle in less detail,^[171] both groups suggested a dual role of the ruthenium catalyst, which are cyclometalation and donation of an electron to the alkyl halide *via* SET and therefore facilitating homolytic C–X bond cleavage.^[166e, 171]



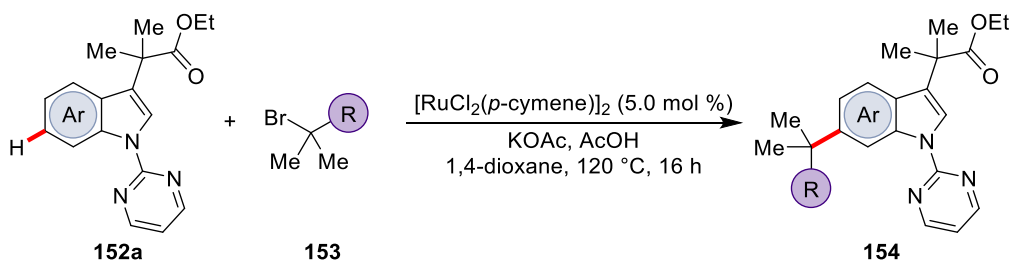
Scheme 1.40. Proposed catalytic cycle for remote C–H alkylations *via ortho*-ruthenation.

Inspired by the removable auxiliary strategy, Ackermann thereafter disclosed a method for the efficient C–H alkylations of easily accessible ketimines **147** with exceptional positional selectivity (Scheme 1.41a). An operationally simple one-pot protocol delivered synthetically useful *meta*-functionalized benzyl amines or *meta/ortho*-substituted arenes and late-stage modified *meta*-substituted arenes, such as ketones, amines, indoles, acids and phenols.^[172] Inspired by these findings, transformable/removable directing groups for *meta* C–H alkylation were expanded to azobenzenes^[173] **49** and phenoxy pyridines^[174] **150** by the groups of Li and Yang, as well as Li, thus providing an access to substituted anilines **149** and phenols **151** after removal of the directing groups (Scheme 1.41b-c).



Scheme 1.41. Remote C–H alkylations of a) ketimines **147**, b) azobenzenes **49** and c) phenoxy pyridines **150**.

In 2017, Frost reported on the remote C–H alkylations of indole derivatives utilizing *N*-pyrimidyl indols with an ester at the C3-position to enable remote C6 alkylation on the benzenoid ring (Scheme 1.42).^[166c] This method benefited from computational chemistry, by means of calculated Fukui indices on organic and inorganic structures, which supported that cyclometalation at the C2-position of the indole increase electron density at the C6-position.

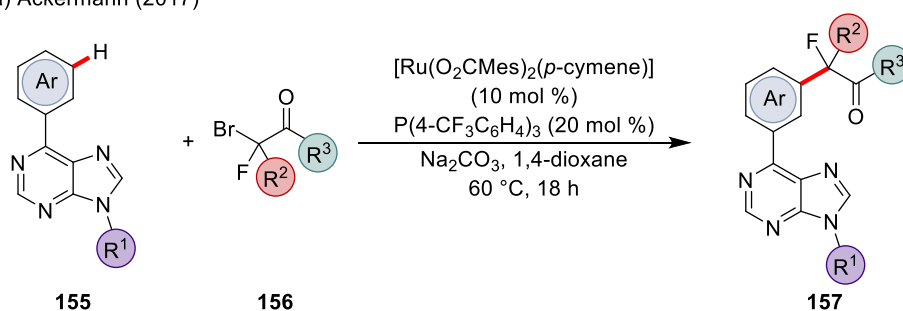


Scheme 1.42. Remote C–H alkylations of indole derivatives **152**.

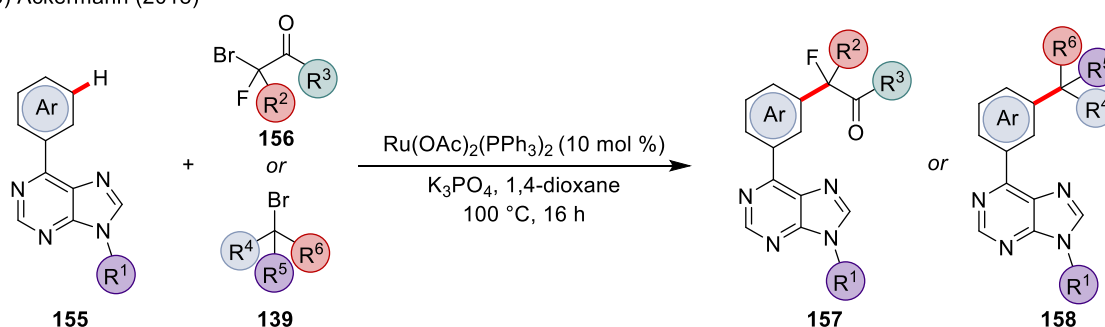
1. Introduction

In the same year, Ackermann reported on the *meta* C–H functionalizations on purines **155** with α -mono/difluorobromoester **156** by assistance of an electron-deficient tertiary phosphine ligand in combination with a congested carboxylate ligand (Scheme 1.43a).^[175] Inspired by this, Ackermann further disclosed the first remote C–H alkylation on purines with an arene-ligand-free ruthenium catalyst.^[176] The C–H alkylation proceeded with various alkyl halides **139** and enabled expedient C–H fluoromethylations (Scheme 1.43b). These approaches highlight the importance of phosphine ligands for challenging *meta* C–H functionalizations, especially late-stage functionalizations of highly sensitive nucleosides.

(a) Ackermann (2017)

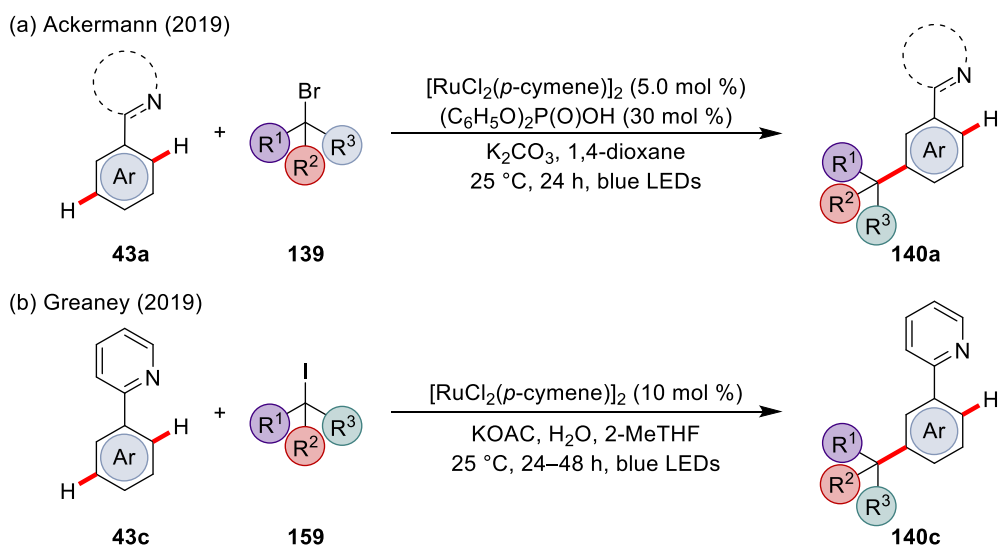


(b) Ackermann (2018)



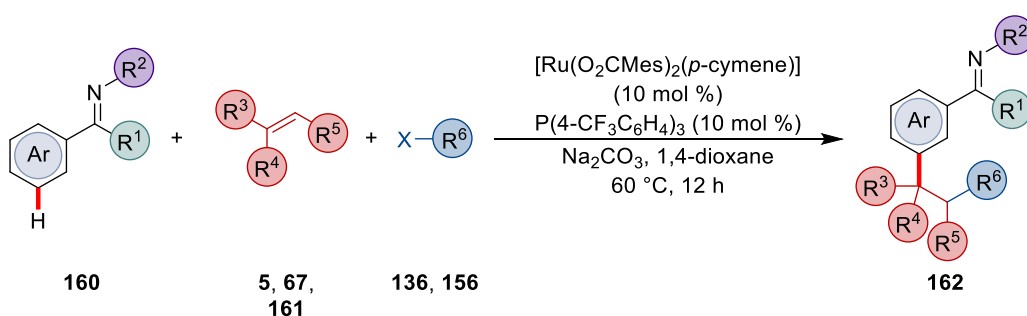
Scheme 1.43. Remote C–H alkylations of purines **155**.

Very recently, a breakthrough in *meta* C–H alkylations by integrating photoredox chemistry was reported by the groups of Ackermann^[177] and Greaney^[178] (Scheme 1.44). Photochemical generation of the alkyl radical species resulted in a significant decrease in the reaction temperature, allowing *meta*-alkylations to proceed at ambient temperature. Although considerably milder reaction conditions were employed and no additional photocatalyst was required, the use of energy-intensive blue LEDs proved to be necessary. Notably, Greaney's system used small amounts of water as an additive, leading to an overall improved catalytic performance (Scheme 1.44b).^[178]



Scheme 1.44. Photochemical remote C–H alkylations of arenes **43**.

Inspired by Ackermann's report on the *meta* C–H functionalizations on purines **155** with α -mono/difluorobromoester,^[175] Liang disclosed in 2019 a three-component ruthenium-catalyzed *meta* C–H functionalization of arenes **160** (Scheme 1.45).^[179] The mild reaction conditions allowed the introduction of styrenes (**5**), internal alkenes (**67**) and acrylates (**161**) together with (fluoro)alkyl halides **136** or **156**, in a one-pot fashion, generating diversely decorated carbon frameworks **162**. Detailed mechanistic and computational studies suggested a radical mechanism through initial SET from the (fluoro)alkyl radical, followed by the radical addition to the alkene. Subsequent, the newly formed radical undergoes C_{Ar}–H bond addition at the *para*-position to the carbon–ruthenium bond.



Scheme 1.45. Three-component ruthenium-catalyzed *meta* C–H functionalization of arenes **160**.

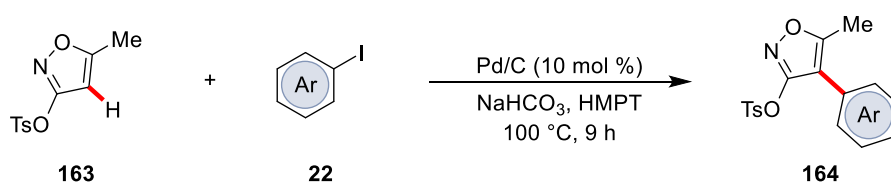
Taking inspiration from these transformations numerous ruthenium-catalyzed remote C–H functionalizations were developed within the last decade, such as benzylations,^[180] carboxylations,^[181] brominations,^[166d, 182] and nitrations.^[183]

1.9. Heterogeneous C–H Functionalization

During the last decades, undisputed advances in transition metal-catalyzed C–H functionalizations had thus far largely been depending on homogeneous catalysts,^[184] however the catalysts featured major disadvantages, especially in terms of catalyst recyclability and trace metal impurities in the isolated products.^[19a, 185] Due to accessibility, recyclability and separability, a number of heterogeneous catalysts were developed in the recent decade with notable progresses for C–H activations, such as arylations,^[186] or carbon–heteroatom^[187] bond formations.

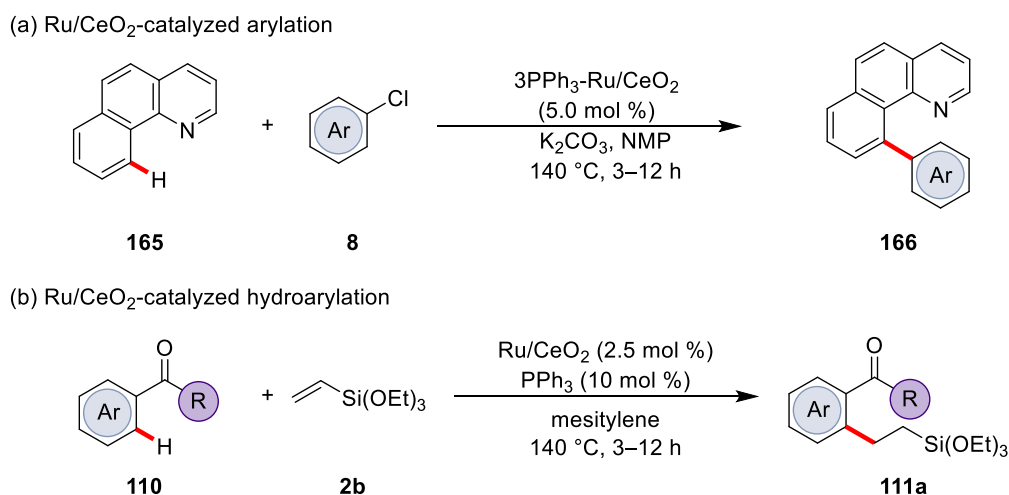
Even though the nature of a catalytic reaction regarding the homo- or heterogeneity is often complicated to determine, common control experiments including a hot filtration test, catalyst poisoning, a three-phase test and recycling studies, are typically required to characterize the heterogeneous nature of the catalytic system.^[19a, 188]

One of the early examples of heterogeneous palladium-catalyzed C–H arylation was reported by Nakamura in 1982,^[189] using palladium on charcoal (Scheme 1.46). Unfortunately, no studies regarding the recyclability and heterogeneity of the reaction were performed.



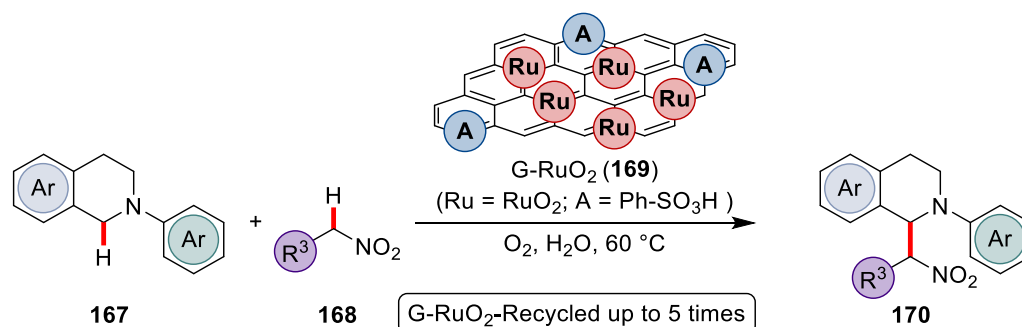
Scheme 1.46. Early example of heterogeneous palladium-catalyzed C–H arylation.

Inspired by this early example, heterogeneous palladium catalysis showed broad applicability to C–H arylation methods,^[186f, 190] however reduced efficiency of the recycled catalyst was often observed. Although palladium is by far the most used metal in heterogeneous C–H functionalizations,^[191] several reports based on other transition metals showed significant potential.^[186a, 187a, 187c, 192] In 2010, Wada demonstrated ruthenium-supported on cerium(IV) oxide as a catalyst for the arylations of benzo[*h*]quinolone **165** (Scheme 1.47a).^[193] Due to the harsh reaction conditions, leaching of the catalyst was detected. In addition, a hot filtration test suggested that the immobilized ruthenium was catalytically active. It is noteworthy that a recycling of the catalyst was possible, albeit the catalyst had to be activated prior to a new run. Based on these results, the same group developed a modified catalytic system for the hydroarylation of vinylsilanes **2b** without any recycling studies (Scheme 1.47b).^[194]



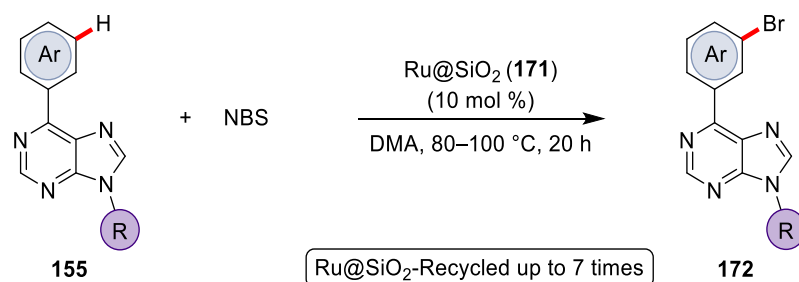
Scheme 1.47. Heterogeneous ruthenium catalysis for (a) arylation of **165** and (b) hydroarylation of vinylsilanes **2b**.

In 2012, Wu reported on the cross-dehydrogenative coupling between tetrahydroisoquinoline derivatives **167** and nitroalkanes **168** using a nanocomposite G-RuO₂ catalyst **169** in water and under an oxygen atmosphere (Scheme 1.48).^[195] Notably, the novel catalyst **169** outperformed established RuCl₃·*n*H₂O or RuO₂·*n*H₂O catalysts even after the fifth run.



Scheme 1.48. Heterogeneous ruthenium catalysis for cross-dehydrogenative couplings.

In 2017, Ackermann reported on the first remote C–H functionalization of aryl-substituted purines **155**, by using a heterogeneous silica-supported ruthenium catalyst **171**.^[196] The ruthenium catalysis regime provided *meta*-halogenated purine derivatives **172**, with excellent recycling and separation properties (Scheme 1.49). In this study, a high dependence of the catalytic activity related to the supporting materials was observed.

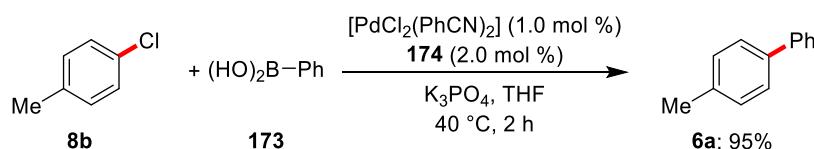


Scheme 1.49. Heterogeneous ruthenium-catalyzed *meta*-selective bromination of purines **155**.

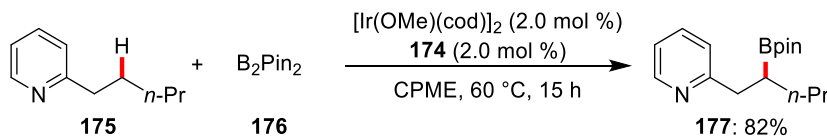
While many catalysts are based on activated carbon or oxide supports,^[197] more research gained recently into metal organic frameworks (MOFs),^[198] nanoparticles^[199] and polymers.^[200] In this context, hybrid systems based on a defined support with a linker that acts as a ligand for the transition metal showed increased importance.^[201] Due to well-known preparation methods and various modification methods hybrid polymers are especially attractive.^[202]

In 2013, Sawamura illustrated a new type of polystyrene(PS)–phosphane covalently bound hybrid towards palladium-catalyzed cross-coupling reactions of unactivated chloroarenes (Scheme 1.50a).^[203] Besides palladium-catalyzed cross-coupling, the hybrid polymer-phosphine **174** was employed to iridium- or rhodium-catalyzed borylations of C(sp³)–H bonds, reflecting the utility of the heterogeneous strategy (Scheme 1.50b-c). Notably, control experiments to support the heterogeneous nature were not performed.

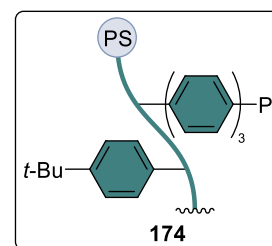
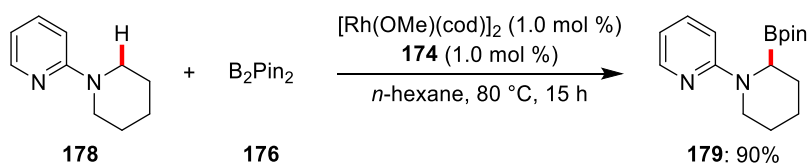
(a) Palladium-catalyzed arylation



(b) Iridium-catalyzed borylation

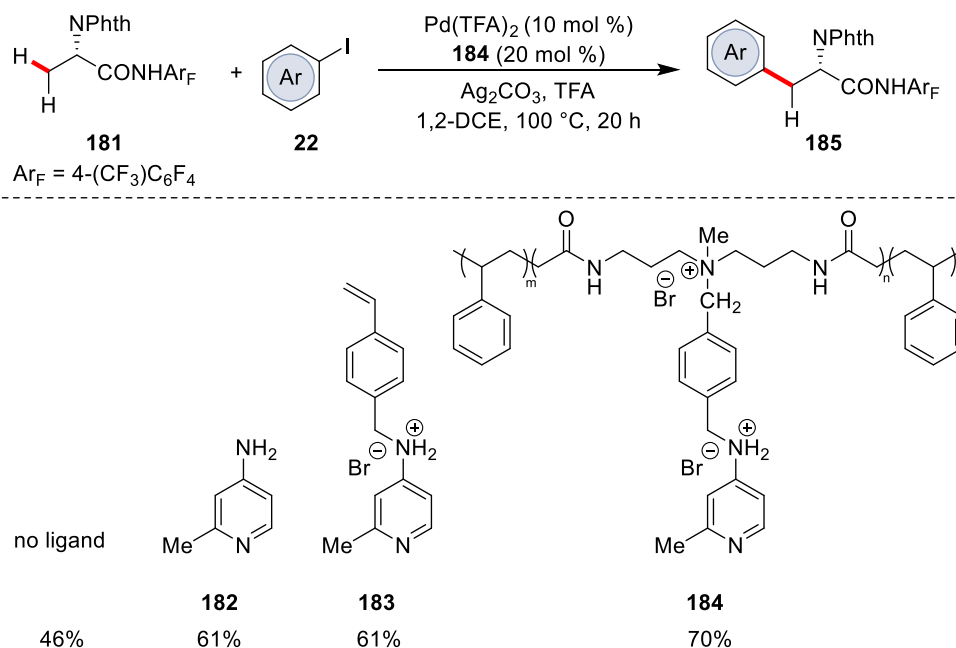


(c) Rhodium-catalyzed borylation



Scheme 1.50. Polymer-supported phosphines **174** in transition metal-catalyzed reactions.

Thereafter, Jones and Yu demonstrated the first example of a polymer-supported catalyst for selective C(sp³)–H monoarylations (Scheme 1.51).^[204] The functionalizable and tunable polymer **184** provided high catalytic efficacy and excellent levels of positional selectivity in palladium-catalyzed monoarylations. In addition, the polymer **184** was reusable without additional palladium catalyst affording an identical catalytic reactivity in the second run.

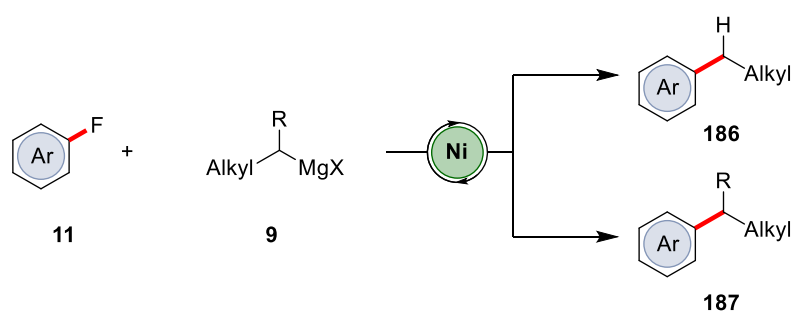


Scheme 1.51. Polymer-supported catalyst for selective palladium-catalyzed C(sp³)–H monoarylations.

2. Objectives

Methods for the selective functionalization of otherwise inert C–H or C–F bonds have been recognized as a transformative method in synthetic chemistry, with applications ranging from the synthesis of bioactive compounds to material sciences.^[22k, 24a, 89, 205] In particular well-defined ligands, such as secondary phosphine oxides, and ruthenium catalysts were recognized as powerful instruments for cross-coupling chemistry and directed C–H transformations.^[60a, 121, 126e, 206] In addition, the development of earth-abundant manganese and nickel catalysts for C–H activations provide an inexpensive and less toxic alternative to their heavier counterparts.^[22b] However, full selectivity control in metal-catalyzed C–H activations are challenging.^[30, 38b, 109c, 207] In this context, the development of novel transition metal catalysts for chemo-, regio- and stereo-selective C–H functionalizations is of great interest.

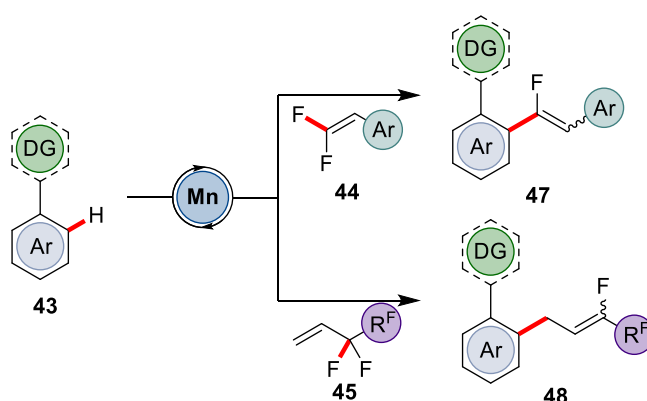
Catalytic C–F bond activation remains a challenge, due to the high BDE of the carbon–fluorine bond, which is typically overcome by using noble metal catalysts or harsh reaction conditions.^[65f, 208] Although many novel methods were developed using well-defined metal complexes,^[79b, 79c, 82b, 209] C(sp²)-C(sp³) couplings remain challenging and hard to control due to the undesirable linear/branched isomerization.^[86-87, 209a, 210] With this in mind, the development of a user-friendly and broadly applicable method for nickel-catalyzed C–F alkylations based on a well-defined nickel catalyst is of great interest (Scheme 2.1).



Scheme 2.1. Broadly applicable nickel-catalyzed C–F activation.

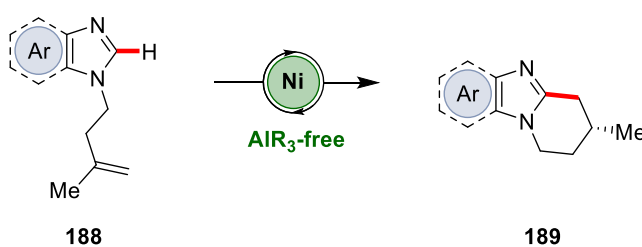
While the activation of C–F bonds is of great interest, the development for novel synthetic methods to install fluorine in organic molecules is also needed.^[94, 211] In this context, various methodologies for transition metal-mediated β -fluorine eliminations were developed, thereby enabling the cleavage of C–F bonds under relatively mild reaction conditions.^[88a-c, 205d] Keeping the tremendous progress by manganese(I) catalysis into

account, ^[22b, 212] the development of a novel manganese(I)-catalyzed C–H/C–F functionalization was intended (Scheme 2.2).^[92b]



Scheme 2.2. Manganese(I)-catalyzed allylative and alkenylative C–H/C–F functionalization.

The enantioselective functionalization of C–H bonds remains largely restricted to noble transition metal catalysts such as palladium, rhodium and iridium.^[207b, 213] Recently, significant progress has been achieved by employing earth-abundant, non-precious 3d metals.^[109c, 207a] Although hydroarylations by nickel-catalyzed C–H activation bear huge potential,^[27] asymmetric intramolecular hydroarylations of unactivated alkenes remain scarce. Since all reported methods require the use of pyrophoric organoaluminium additives, which limits the tolerance of functional groups,^[109a, 109d, 109e] the development and understanding of an organoaluminium-free enantioselective intramolecular cyclization is highly desirable (Scheme 2.3).^[214]

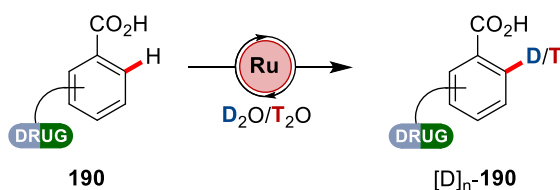


Scheme 2.3. Nickel-catalyzed enantioselective intramolecular C–H cyclization.

Within the last decade, hydrogen isotope exchange (HIE) became a well-established method to accomplish late-stage isotope labeling of challenging scaffolds.^[138a, 138c, 140] In this context, heterogeneous and homogeneous ruthenium catalysts showed a broad applicability.^[134b, 215] In contrast to methods that enabled the labeling of uncomplex molecules, *ortho*-selective HIE with numerous functional groups present remain scarce.^[140] Keeping this limitation in mind, the development of late-stage deuterations

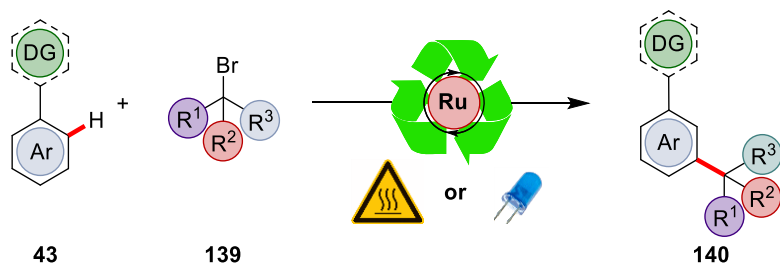
2. Objectives

and tritiations of active pharmaceutical ingredients (API) is highly desirable (Scheme 2.4).^[216]



Scheme 2.4. Selective isotope labeling by ruthenium-catalyzed HIE.

Homogeneous catalysts are by far outnumbering heterogeneous catalysts in the field of C–H functionalizations, even though the recycling of the catalysts is difficult to achieve.^[184] In terms of sustainability heterogeneous catalysts have a clear advantage over homogeneous catalysts.^[19a, 185] In this context, hybrid systems based on easy accessible polymer supports are highly suitable to develop catalysts with a defined coordination sphere around the metal.^[200b, 201a] Taking into account the unique ability of ruthenium to facilitate remote C–H functionalizations,^[22g, 166h] a novel reusable ruthenium-hybrid catalyst for *meta* C–H functionalization of biological relevant motifs is of great interest (Scheme 2.5).



Scheme 2.5. Recyclable ruthenium catalyst for remote C–H functionalizations.

3. Results and Discussion

3.1. SPO-Nickel Catalysts for C–F Alkylations

Transition metal-catalyzed $C(sp^2)$ – $C(sp^3)$ cross-coupling has become a vibrant area of research due to its potential to serve as a strategic C–C bond forming process.^[101, 217] While classical cross-coupling reactions focused on traditional electrophiles, phenol derivatives,^[65e, 218] nitriles^[219] and aryl fluorides^[65c, 65f, 88b, 220] gained more momentum for potential late-stage modifications. In recent years, the importance of fluorinated organic molecules to a variety of applications in modern society is well appreciated and emphasizes the potential for the functionalization of C–F bonds.^[88, 221] Considering the inert nature of the C–F bond during multi-step processes, the wide availability and the relative low costs,^[211a, 222] late stage modifications by metal-catalyzed $C(sp^2)$ – $C(sp^3)$ cross-couplings are a powerful alternative to generate bioactive compounds, pharmaceutical drugs and polymer materials (Figure 3.1.1).^[223]

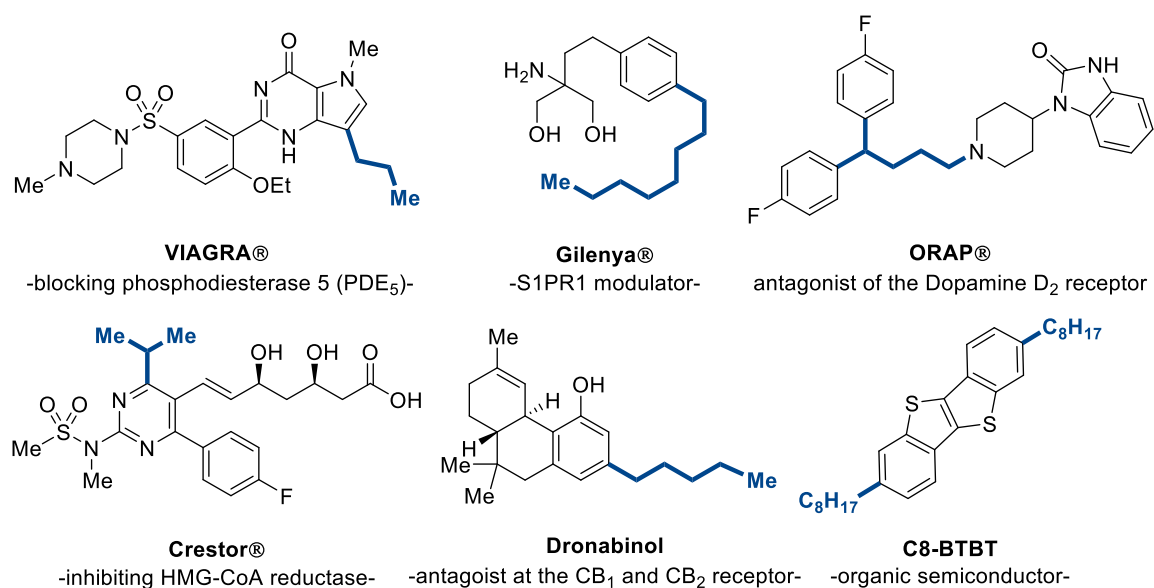


Figure 3.1.1. Selected examples of alkylated pharmaceuticals and semiconductor.

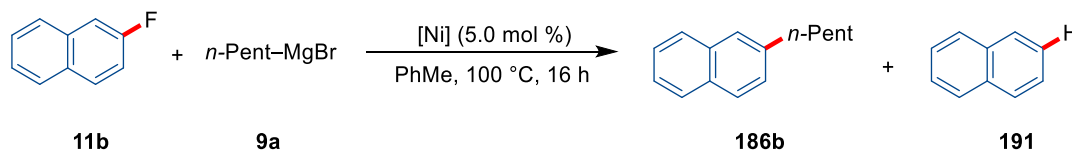
Unfortunately, only a few reports on selective $C(sp^2)$ – $C(sp^3)$ bond formations are known, and mostly restricted to alkyl electrophiles with the aid of sterically-congested ligands.^[17a, 84a, 224] Considerable less attention has been paid on related reactions with branched nucleophiles,^[85, 225] due to competing β -hydride eliminations.^[73, 87, 226] Even though, the pioneering studies of Kumada were accompanied by an undesired isomerization with the finding that a more electron-rich ligand favored β -hydride eliminations,^[73] a general

method towards branched and linear alkylating reagents by efficient nickel catalysis remains elusive.^[87]

3.1.1. Optimization Studies for Primary Alkylmagnesium Reagents

The optimization studies for the nickel(II)-catalyzed C–F activation were commenced by probing various nickel salts for the envisioned C–F alkylation of 2-fluoronaphthalene (**11b**) (Table 3.1.1). Among the tested nickel salts, Ni(acac)₂ turned out to be optimal with 38% isolated yield, albeit a significant amount of defluorinated compound **191** was formed (entry 1). Other nickel salts resulted in the formation of the undesired defluorinated byproduct **191** (entries 2–4). Interestingly, commonly used Ni(cod)₂ facilitated the transformation (entry 5) too, suggesting a nickel(0/II) catalytic manifold.^[65b, 227] It is furthermore worth mentioning that no reaction took place in the absence of a nickel source (entry 6).

Table 3.1.1. Optimization of the nickel source for C–F alkylation with linear alkyl magnesium reagents.^[a]



Entry	[Ni]	Yield / %	186b/191
1	Ni(acac) ₂	38	47/53
2	NiCl ₂ (DME)	18	0/100
3	NiBr ₂ (diglyme)	20	0/100
4	Cp ₂ Ni	12	0/100
5	Ni(cod) ₂	26	62/38
6	-	n.r.	-

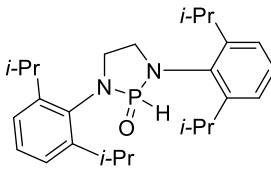
[a] Reaction conditions: **11b** (0.25 mmol), **9a** (0.50 mmol), [Ni] (5.0 mol %), ligand (5.0 mol %), PhMe (0.50 mL), 100 °C, 16 h, under Ar; yield of **186b** and **191** was determined after isolation. The ratio of **186b/191** was determined by ¹H-NMR.

With the best nickel source being identified, further optimization with respect to the (pre)-ligand were performed. As phosphine ligands are broadly implemented in nickel-catalyzed cross-couplings,^[15, 63, 228] various mono- and bidentate-phosphines were screened (Table 3.1.2). Remarkably, SPOs outperformed commonly used ligands, such as dppe and dppf (entries 1–7).^[229] This suggests that highly electron-donating ligands are

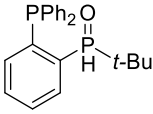
crucial within the catalytic cycle or that the SPO stabilizes essential transition states within catalysis.^[48, 230] In this context, the substitution pattern on the SPO was crucial for the reaction outcome, indicating bulky substituents to be less favored within nickel-catalyzed C–F activations. Considering the previously observed reactivity of Ni(cod)₂ the envisioned transformation was also tested with Ni(cod)₂ in combination with SPO pre-ligand **193** (entry 8). Notably, the desired product was generated in good yield, albeit moderate selectivity. Importantly, the novel bidentate SPO **194** improved the efficiency in terms of yield and selectivity (entry 9), highlighting the importance of this motif in nickel-catalyzed C–F alkylations. Although the transformation could be facilitated by dppe, high temperatures were required (entries 10–11). It is assumed that the SPO-phosphine nickel(II) pre-catalyst and the Grignard reagent formed a nickel/magnesium bimetallic catalytic species that carried out push–pull cooperative activation of the aryl fluoride.^[76c, 209b, 231]

Table 3.1.2. Optimization of phosphine ligands for C–F alkylation with linear alkyl magnesium reagent **9a**.^[a]

Reaction scheme: 11b + *n*-Pent-MgBr (9a) $\xrightarrow[\text{PhMe, 100 } ^\circ\text{C, 16 h}]{[\text{Ni}] (5.0 \text{ mol } \%), \text{ ligand } (5.0 \text{ mol } \%)}$ 186b + 191

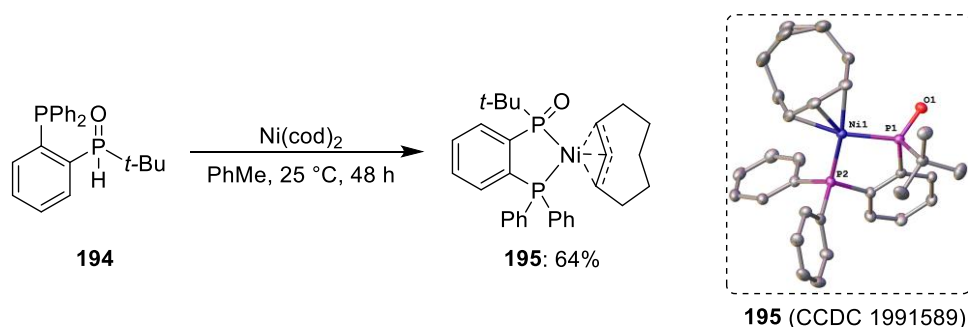
Entry	[Ni]	Ligand	Yield / %	186b/191
1	Ni(acac) ₂	dppe	<10	-
2	Ni(acac) ₂	dppf	<10	-
3	Ni(acac) ₂	(<i>n</i> -Bu) ₂ P(O)H	50	70/30
4	Ni(acac) ₂	(Ad) ₂ P(O)H	25	60/40
5	Ni(acac) ₂		37	57/43
6	Ni(acac) ₂	(Cy) ₂ P(O)H	54	59/41
7	Ni(acac) ₂	(Ph) ₂ P(O)H (193)	52	77/23
8	Ni(cod) ₂	193	87	72/28

3. Results and Discussion

Entry	[Ni]	Ligand	Yield / %	186b/191
9	Ni(cod) ₂	 194	90	78/22
10	Ni(cod) ₂	dppe	95	94/6
11 ^[b]	Ni(cod) ₂	dppe	-	-

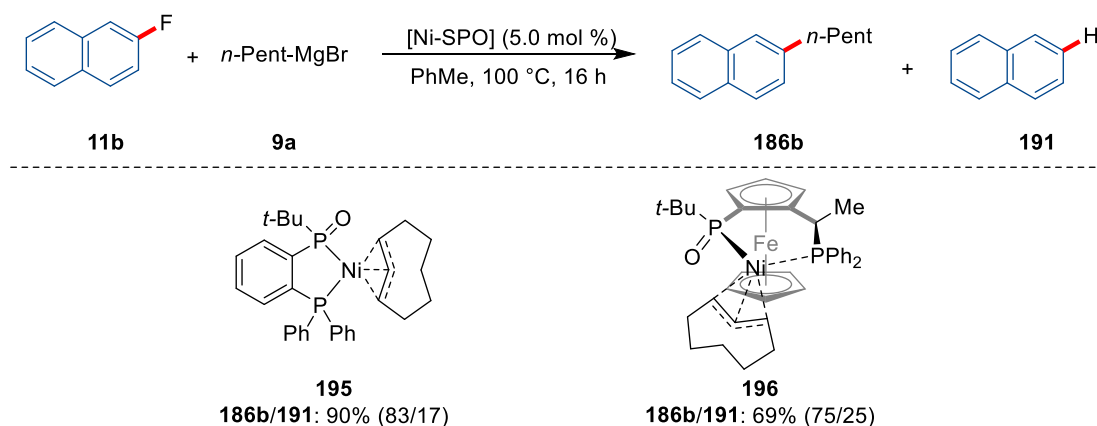
[a] Reaction conditions: **11b** (0.25 mmol), **9a** (0.50 mmol), [Ni] (5.0 mol %), ligand (5.0 mol %), PhMe (0.50 mL), 100 °C, 16 h, under Ar; yield of **186b** and **191** was determined after isolation. The ratio of **186b/191** was determined by ¹H-NMR. [b] THF (0.50 mL) as solvent at 25 °C.

Inspired by the excellent activity of SPO **194**, the preparation of a novel SPO-nickel complex for the nickel-catalyzed C–F alkylation reaction was attempted by Dr. Debasish Ghorai. Thus, treatment of Ni(cod)₂ with pre-ligand **194** resulted in the formation of the novel complex **195**, which was isolated and crystallographically characterized by Dr. Antonis Messinis (Scheme 3.1.1).



Scheme 3.1.1. Synthesis of complex **195**, performed by Dr. Debasish Ghorai. **195** was crystallized by Dr. Antonis Messinis. The crystal structure was measured and resolved by Dr. Christopher Golz.

To our delight complex **195** was found to be even more reactive and selective compared to the previously probed nickel catalyst generated in-situ from pre-ligand **194** (Scheme 3.1.2). Furthermore, the novel SPO-nickel catalyst **195** outperformed the previously reported nickel(II)-JoSPOphos complex **196** in terms of reactivity and selectivity (entry 2),^[214a] highlighting the importance of the ligand backbone.



Scheme 3.1.2. Well-defined SPO-nickel complexes for C–F alkylations.

With the best catalyst in hand, the reaction was optimized regarding different solvents and other reaction parameters (Table 3.1.3). Considering the harsh reaction conditions, it was shown, that the SPO-nickel catalyst **195** was able to facilitate the C–F alkylation at 25 °C. Notably, the mild reaction conditions resulted in better selectivity towards the alkylated product **186b** (entry 1). The use of other aromatic solvents did not result in an improvement (entries 2–4). Using more polar solvents, such as 1,4-dioxane, *n*-Bu₂O or Et₂O, a better selectivity was observed (entries 5–7), probably due to the stabilization of the Grignard reagent by the Schlenk-equilibrium.^[232] Notably, biomass-derived^[18a, 18d, 233] 2-MeTHF was also applied in the envisioned transformation without any deterioration (entry 8). Finally, THF was identified as the optimal solvent, yielding the desired C–F alkylated product **186b** in excellent yield and outstanding selectivity (entries 9–10). With THF, the troublesome evaporation of the solvent of the Grignard could be avoided and the reaction was more easily scalable (entry 11).

Table 3.1.3. Optimization of solvent and temperature for C–F alkylations by SPO-nickel catalysis.^[a]

Entry	Solvent	<i>T</i> / °C	Yield / %	186b/191
1	PhMe	60	83	89/11
2	PhMe	25	79	96/4
3	<i>o</i> -xylene	25	70	93/7
4	<i>p</i> -xylene	25	68	91/9
5	1,4-dioxane	25	73	93/7

3. Results and Discussion

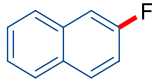
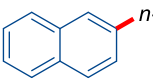
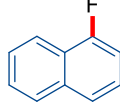
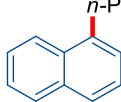
Entry	Solvent	<i>T</i> / °C	Yield / %	186b/191
6	<i>n</i> -Bu ₂ O	25	78	96/4
7	Et ₂ O	25	81	96/4
8	2-MeTHF	25	79	94/6
9	THF	25	79	97/3
10 ^[b]	THF	25	84	98/2
11 ^[b,c]	THF	25	84	98/2

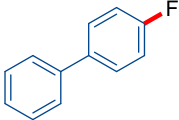
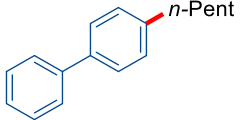
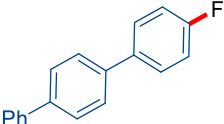
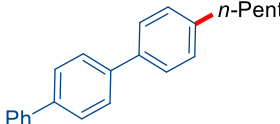
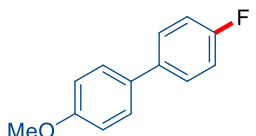
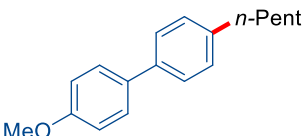
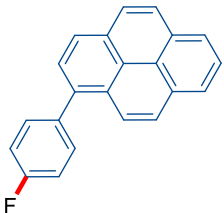
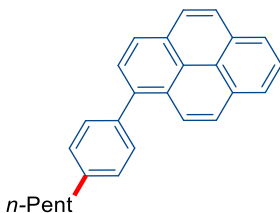
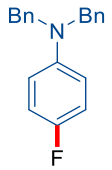
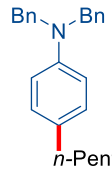
[a] Reaction conditions: **11b** (0.25 mmol), **9a** (0.50 mmol), **195** (5.0 mol %), solvent (0.50 mL), *T*, 16 h, under Ar; yield of **186b** and **191** was determined after isolation. The ratio of **186b/191** was determined by ¹H-NMR. [b] 0.25 M. [c] 0.50 mmol scale.

3.1.2. Scope of the C–F Alkylation using Primary Alkylmagnesium Reagents

The versatility of the SPO-nickel-catalyzed C–F alkylation was tested for differently substituted aryl fluorides **11**. Probing various substitution patterns on the arenes, no limitation was observed and most substituents were well tolerated (Table 3.1.4). Different naphthalenes proved applicable within this transformation (entries 1–2). Furthermore, the method could be applied for the C–F alkylation of different substituted fluorobenzenes **11** yielding the desired products **186d** and **186f** in good yields (entries 3–4). To our delight, the C–O bond was tolerated under the reaction conditions without interference (entry 5), indicating a notable innate chemoselectivity. Finally, pyrene fluorophores and an electron-rich *N*-protected aniline derivative proved to be compatible within the SPO-nickel catalysis regime (entries 6–7).

Table 3.1.4. Scope of aryl fluorides **11** in the SPO-nickel-catalyzed alkylation.^[a]

Entry	Fluoroarene	186	Yield / %
1			82
2			79

Entry	Fluoroarene	186	Yield / %
3	 11d	 186d	73
4	 11f	 186f	72
5	 11g	 186g	60
6	 11h	 186h	72
7	 11i	 186i	71

[a] Reaction conditions: **11** (0.50 mmol), **9a** (1.0 mmol), **195** (5.0 mol %), solvent (2.0 mL), 25 °C, 16 h, isolated yield.

Furthermore, different alkylmagnesium bromides were examined under the reaction regime (Table 3.1.5). Initially, octylmagnesium bromide (**9b**) reacted with excellent regioselectivity without isomerized byproduct being formed (entry 1). No limitations were observed by different chain lengths, indicating the usability towards methylation and ethylation reactions (entry 2-3). Considering, the so called magic methyl effect the introduction of a methyl group highlights the utility of the SPO-nickel catalyst.^[234] Furthermore, a ramification of the alkylmagnesium bromide (**9e**) was well tolerated without isomerization during the course of the reaction.

3. Results and Discussion

Table 3.1.5. Scope of linear alkylmagnesium bromides **9** in the SPO-nickel-catalyzed alkylation.^[a]

Reaction scheme: $\text{Ar-F (11)} + \text{R-MgBr (9)} \xrightarrow[\text{THF, 25 }^\circ\text{C, 16 h}]{\text{195 (5.0 mol \%)}} \text{Ar-R (186)}$

Entry	Alkylmagnesium bromide	186	Yield / %
1	<i>n</i> -OctMgBr (9b)		76
2	MeMgBr (9c)		78
3	EtMgBr (9d)		74
4	2-Et-HexMgBr (9e)		76

[a] Reaction conditions: **11** (0.50 mmol), **9** (1.0 mmol), **195** (5.0 mol %), solvent (2.0 mL), 25 °C, 16 h, isolated yield.

Under the optimized reaction conditions different heterocycles, including indoles and pyridines were probed (Table 3.1.6). Initially, *N*-substituted indoles were tested furnishing the corresponding product **186n-p** in excellent yield and good selectivity, albeit with the formation of a byproduct (entries 1–3).^[100a, 235] Subsequently, various substituents in the C5-position of pyridine were tested, with overall good yields for electron donating and withdrawing substituents (entries 6–7). Moreover, it was demonstrated that pyridine as a substituent is tolerated without interference (entry 8). Notable, no Ziegler alkylation at the reactive α -position of the pyridine was observed.^[236]

3.1. SPO-Nickel Catalysts for C–F Alkylations

Table 3.1.6. Scope of heteroaryl fluorides **11** in the SPO-nickel-catalyzed alkylation.^[a]

Entry	Heteroarene	186	Yield / %
1 ^[b]	 11n	 186na	74
2 ^[b]	 11n	 186nb	72
3	 11p	 186p	72
4	 11q	 186q	76
5	 11r	 186r	74
6	 11s	 186s	73

[a] Reaction conditions: **11** (0.50 mmol), **9** (1.0 mmol), **195** (5.0 mol %), solvent (2.0 mL), 25 °C, 16 h, isolated yield. [b] Mixture of **186** and byproduct.

3.1.3. Optimization Studies for Secondly Alkylmagnesium Reagents

Based on the outstanding selectivity within the linear alkylation, the considerably more challenging alkylation with secondary alkylmagnesium halides **9f-k** was faced. The studies were initiated with **11b** as the model substrate and *sec*-butylmagnesium chloride (**9f**) as the alkylation reagent. It was initially tested whether the formation of the product **187b** is mainly controlled by the ligand (Table 3.1.7). In this context, bidentate phosphine ligands, such as dppe and dppf, failed to give any result (entries 1–2). On the contrary, the monodentate SPO pre-ligand **193** outperformed previously studied phosphine ligands (entry 3). However, a significant amount of isomerized product **186t** was formed. Interestingly, the performance of the novel designed ligand **194** improved the yield, showing the importance of the bidentate nature of the ligand (entry 4). Finally, the novel SPO-nickel(II) complex **195** improved the reactivity and selectivity (entry 5).

Table 3.1.7. Optimization of different phosphine ligands in the SPO-nickel-catalyzed alkylation.^[a]

Entry	[Ni]	Ligand	Yield / %	187b/186t
1	Ni(acac) ₂	dppe	-	-
2	Ni(acac) ₂	dppf	-	-
3	Ni(cod) ₂	193	39	75/25
4	Ni(cod) ₂	 194	47	75/25
5		 195	63	82/18

[a] Reaction conditions: **11b** (0.25 mmol), **9f** (0.50 mmol), [Ni] (5.0 mol %), ligand (5.0 mol %), PhMe (1.0 mL), 100 °C, 16 h, under Ar; yield of isolated products. The ratio of **187b/186t** was determined by ¹H-NMR.

Given the inherent possibility to induce enantioselectivity within the presented C–F alkylation with branched alkylmagnesium halides **9** initial optimization studies were

performed by employing chiral phosphine ligands (Table 3.1.8). Although enantioselective Kumada-Corriu cross-couplings are known,^[237] the use of unactivated fluoroarenes **11** remains elusive.^[238] With different chiral bidentate phosphine ligands no enantiomeric ratio (e.r.) was detected for the branched product (entries 1–2). Inspired by the previous results chiral SPO pre-ligands were tested (entries 3–4).^[239] Unfortunately, the chiral SPO **199** and the SPO **200**^[232b] did not result in a chiral induction. Finally, the chiral JoSPOphos complex **196** was tested at different temperatures (entry 5–6), however, no asymmetric induction was detected (Figure 3.1.2).

Table 3.1.8. Optimization of chiral phosphine ligands in the SPO-nickel-catalyzed alkylation.^[a]

Entry	[Ni]	Ligand	Yield / %	187q/186u	e.r. ^[b]
1	Ni(acac) ₂		40	80/20	-
2	Ni(acac) ₂		41	50/50	-
3	Ni(acac) ₂		22	50/50	-
4	Ni(acac) ₂		43	50/50	-
5			53	98/2	-
6 ^[c]			37	98/2	-

[a] Reaction conditions: **11q** (0.25 mmol), **9f** (0.50 mmol), [Ni] (5.0 mol %), ligand (5.0 mol %), PhMe (1.0 mL), 100 °C, 16 h, under Ar; yield of isolated products. The ratio of **187q/186u** was determined by ¹H-NMR. [b] Determined by chiral HPLC analysis. [c] At 60 °C.

3. Results and Discussion

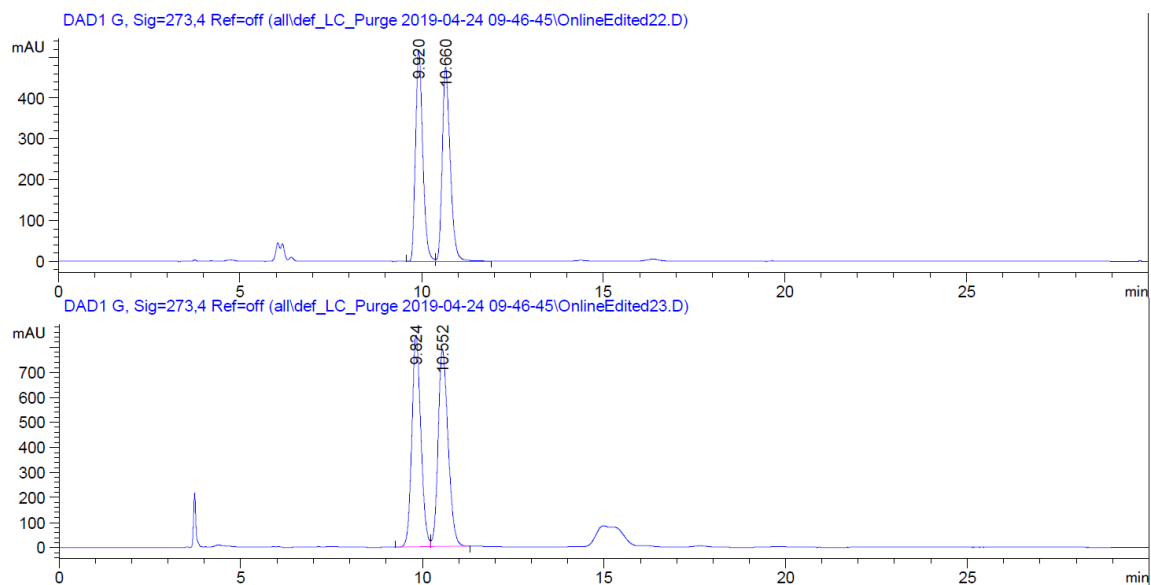
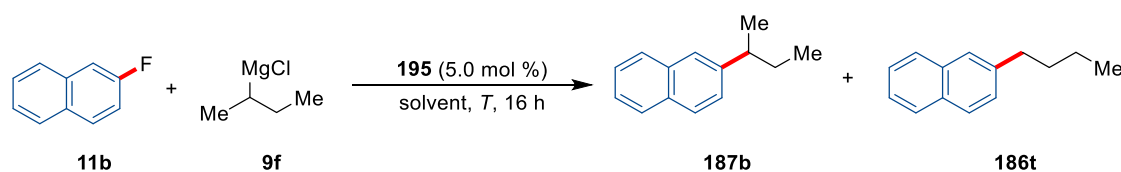


Figure 3.1.2. HPLC chromatogram of *rac*-**187q** (up) and **187q** yielded by JoSPOphos complex **196** (down).

The optimization studies for the SPO-nickel-catalyzed C–F alkylation with branched alkylating reagents **9f** were continued by probing the effect of the reaction temperature and solvent (Table 3.1.9). Notably, SPO-nickel catalyst **195** facilitated the cross-coupling at much milder temperatures and proved to be viable at 25 °C (entries 1–5). However, a diminished yield is accompanied at lower temperature, a clear dependence of the selectivity was detected. Unfortunately, the C–F alkylation was not feasible at 0 °C (entry 6). Moreover, solvent screening resulted in good yields and high selectivities, even when biomass-derived 2-MeTHF was applied (entries 7–10). Control experiments highlighted the unique reactivity of the developed SPO-nickel catalyst **195** compared to other in-situ generated nickel/phosphine catalysts (entries 11–12). By increasing the reaction temperature to 60 °C an improved yield was observed (entry 13).

Table 3.1.9. Optimization of solvent and temperature for branched Grignard reagents.^[a]



Entry	Solvent	<i>T</i> / °C	Yield / %	187b / 186t
1	PhMe	100	64	82/18
2	PhMe	80	72	89/11
3	PhMe	60	78	90/10
4	PhMe	40	55	93/7

Entry	Solvent	<i>T</i> / °C	Yield / %	187b/186t
5	PhMe	25	57	94/6
6	PhMe	0	n.r.	-
7	<i>n</i> -Bu ₂ O	25	56	93/7
8	1,4-dioxane	25	51	92/8
9	2-MeTHF	25	56	93/7
10	THF	25	60	92/8
11 ^[b]	THF	25	n.r.	-
12 ^[c]	THF	25	n.r.	-
13	THF	60	66	96/4

[a] Reaction conditions: **11b** (0.25 mmol), **9f** (0.50 mmol), **195** (5.0 mol %), solvent (1.0 mL), *T*, 16 h, under Ar; yield of isolated products. The ratio of **187b/186t** was determined by ¹H-NMR. [b] Ni(cod)₂ (5.0 mol %) and dppe (5.0 mol %) instead of **195**. [c] Ni(acac)₂ (5.0 mol %) and dppe (5.0 mol %) instead of **195**.

Furthermore, other reaction parameters were tuned for the accomplishment of the envisioned C–F alkylation (Table 3.1.10). Initiated by some control experiments, **187b** was not observed when Ni(acac)₂ and Ni(cod)₂ were used, showing that these nickel salts needed higher activation energies to furnish the examined transformation (entries 1-2). Moreover, different concentrations were evaluated showing no significant role, although a higher selectivity was observed at lower concentrations (entries 3-4). Notably, 5 min of pre-stirring before the addition of **9f** improved the yield dramatically without affecting the selectivity (entry 5). With CsF as the additive, a beneficial effect was not observed, emphasizing a different mechanism compared to related studies (entry 6).^[87, 240] Finally, the reaction was performed at larger scale and a shortened reaction time, reflecting the high reactivity of catalyst **195** towards unactivated C–F bonds (entries 7-8).

Table 3.1.10. Optimization of other reaction parameters for branched Grignard reagents.^[a]

Entry	Solvent	<i>T</i> / °C	Yield / %	187b/186t
1 ^[b]	THF	60	-	-
2 ^[c]	THF	60	-	-
3 ^[d]	THF	60	57	95/5

Entry	Solvent	T / °C	Yield / %	187b/186t
4 ^[e]	THF	60	60	92/8
5 ^[f]	THF	60	84	96/4
6 ^[f,g]	THF	60	71	94/6
7 ^[f,h]	THF	60	84	96/4
8 ^[f,i]	THF	60	77	95/5

[a] Reaction conditions: **11b** (0.25 mmol), **9f** (0.50 mmol), **195** (5.0 mol %), THF (1.0 mL), 60 °C, 16 h, under Ar; yield of isolated products. The ratio of **187b/186t** was determined by ¹H-NMR. [b] Ni(cod)₂ (5.0 mol %) and dppe (5.0 mol %) instead of **195**. [c] Ni(acac)₂ (5.0 mol %) and dppe (5.0 mol %) instead of **195**. [d] 0.125 M. [e] 0.50 M. [f] 5 min pre-stirring then addition of **9f**. [g] CsF (0.50 mmol). [h] 0.50 mmol scale. [i] 30 min.

3.1.4. Scope of the C–F Alkylation using Secondary Alkylmagnesium Reagents

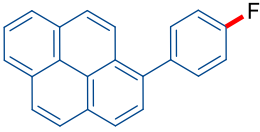
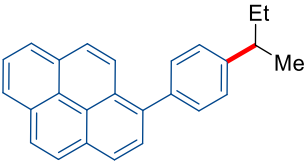
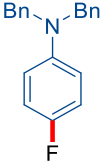
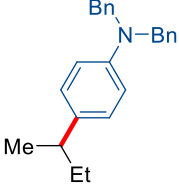
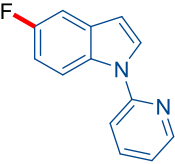
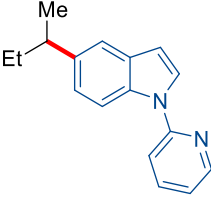
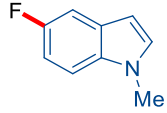
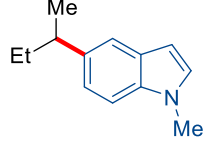
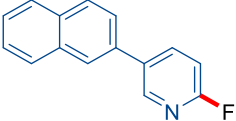
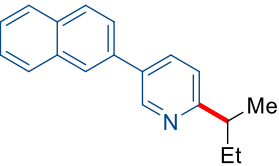
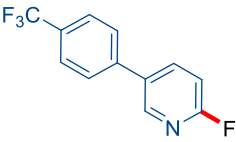
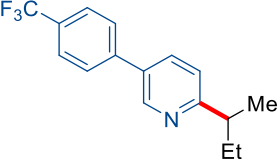
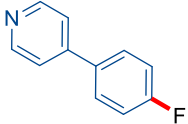
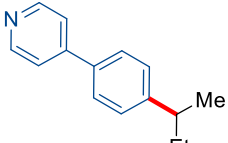
With the optimized reaction conditions in hand, the C–F alkylation of various arenes and heteroarenes with *sec*-butylmagnesium chloride **9f** was investigated (Table 3.1.11). Indeed, different naphthalenes **11b–c** were suitable substrates for this transformation (entries 1–2). Furthermore, a variety of different electron-rich arenes **11d–f** were amenable to the present reaction with overall high selectivities (entries 3–5). Notably, the C–O bond remains intact during the course of the reaction (entry 6) and pyrene fluorophores proved to be compatible within the SPO-nickel catalysis (entry 7). Also, the electron-rich *N*-protected aniline derivative **11i** was converted successfully with an acyclic coupling reagent yielding the *para*-alkylated product **187i** (entry 8).

Next, different biologically relevant heterocyclic motifs, such as indoles or pyridines were probed. *N*-Protected indoles **11o–p** were well tolerated without byproduct formation, probably due to the less-reactive Grignard reagent (entries 9–10).^[68a] Moreover, electron-rich as well as electron-poor pyridines **11q–r** were amenable to the transformation (entries 11–12). Remarkably, fluoroarene **11s** yielded selectively **187s**, highlighting the resistance towards deactivation of the catalyst by coordination or substitutions in the α -position to the heteroatom (entry 13).^[106c, 241]

Table 3.1.11. Scope of the branched-selective alkylation by SPO-nickel catalysis.^[a,b]

Entry	Fluoroarene	187	Yield / %
1			84 (96:4)
2			80 (96:4)
3			75 (78:22)
4			76 (73:27)
5			73 (88:12)
6			68 (76:24)

3. Results and Discussion

Entry	Fluoroarene	187	Yield / %
7	 11h	 187h	89 (93:7)
8	 11i	 187i	76 (65:35)
9	 11o	 187o	69 (88:12)
10	 11p	 187p	70 (87:13)
11	 11q	 187q	75 (98:2)
12	 11r	 187r	74 (79:21)
13	 11s	 187s	89 (85:15)

[a] Reaction conditions: **11** (0.50 mmol), **9f** (1.0 mmol), **195** (5.0 mol %), solvent (2.0 mL), 60 °C, 16 h, under Ar; yield of isolated products. The ratio of **187/186** was determined by ¹H-NMR. Branched/linear selectivities in parentheses.

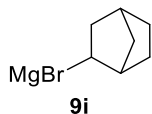
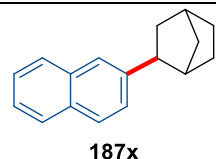
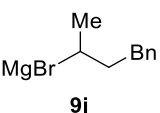
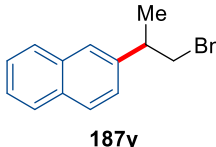
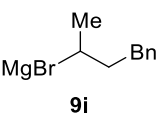
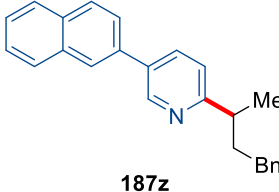
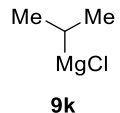
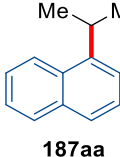
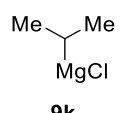
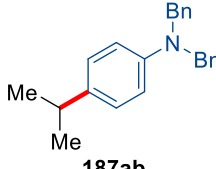
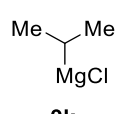
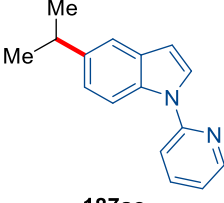
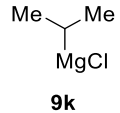
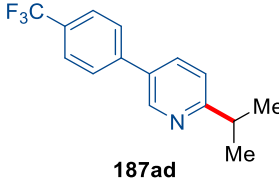
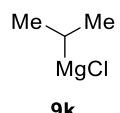
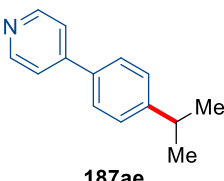
Thereafter, a variety of secondary alkylmagnesium halides **9g-k** were tested in the C–F alkylation (Table 3.1.12). Diverse cyclic alkylmagnesium bromides **9g-h** underwent the nickel-catalyzed cross-coupling with various naphthalenes **11b-c** and electron rich *N*-protected aniline **11i** resulting in excellent yields (entries 1–4). Notable, sterically more constrained norbornene derived Grignard **9i** performed excellently under the reaction regime (entry 5). Furthermore, the sterically more demanding alkylmagnesium bromide **9j** yielded the product with excellent selectivity for the secondary position showing that the tether has no significant influence (entries 6–7). Finally, *iso*-propylmagnesium chloride (**9k**) as alkylating source together with various arenes and heteroarenes **11** were tested (entries 8–12). Remarkable, the desired products **187** were obtained in good yields and excellent selectivities.

Table 3.1.12. Scope of branched Grignard reagents **9** within the SPO-nickel catalysis.^[a,b]

Reaction scheme showing the C–F alkylation of a heteroarene (**11**) with a branched alkylmagnesium halide (**9**) using catalyst **195** (5.0 mol %) in THF at 60 °C for 16 h to yield the alkylated product (**187**).

Entry	Alkylmagnesium halide	187	Yield / %
1			70
2			78
3			79
4			78

3. Results and Discussion

Entry	Alkylmagnesium halide	187	Yield / %
5	 9i	 187x	71
6	 9j	 187y	77 (90:10)
7	 9j	 187z	73 (94:6)
8	 9k	 187aa	81 (96:4)
9	 9k	 187ab	73 (81:19)
10	 9k	 187ac	70 (85:15)
11	 9k	 187ad	73 (99:1)
12	 9k	 187ae	74 (87:13)

[a] Reaction conditions: **11** (0.50 mmol), **9** (1.0 mmol), **195** (5.0 mol %), THF (0.25 M), 60 °C, 16 h, under Ar; yield of isolated products. The ratio of **187/186** was determined by ¹H-NMR. [b] 5 min pre-stirring, then addition of **9**.

3.2. Manganese-Catalyzed Allylative and Alkenylative C–H/C–F Functionalization

In recent years, the unique properties of C–F bonds were well examined and reflected by many fluorine containing pharmaceuticals, agrochemicals and materials (Figure 3.2.1).^[194, 211a, 211d, 242] In this context, conventional C–F bond formations generally require harsh conditions and consequently have limited substrate scopes,^[243] whereas reactions performed in the presence of catalysts can often reduce the activation barrier.^[244]

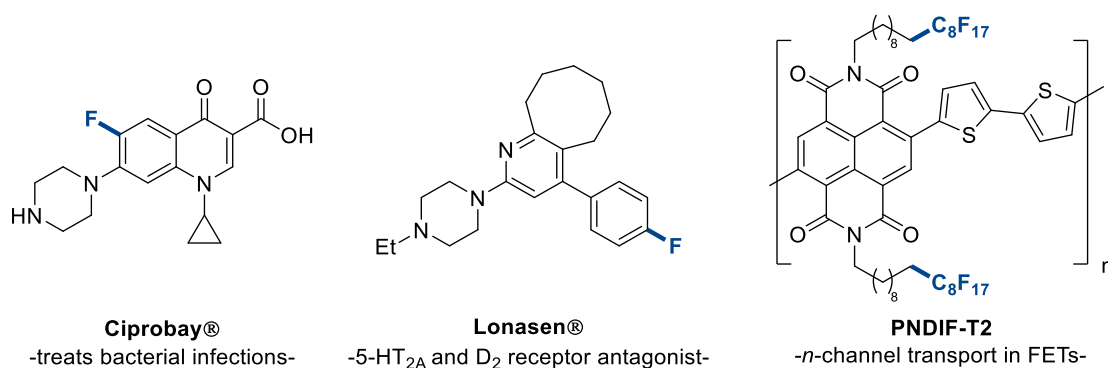


Figure 3.2.1. Selected examples of relevant fluorine containing molecules.

The enormous BDE^[28] ~126 kcal/mol and the accompanied thermodynamically inertness,^[245] make fluorination reactions especially challenging. Nevertheless, photocatalysis^[246] and late transition metals, such as palladium^[247] or silver^[248] proved capable to facilitate these transformations, due to the significantly polarized metal–fluorine σ -bond and sufficient orbital overlap.^[249] However, a sustainable and step-economical access to highly functionalized fluorine-containing molecules by earth-abundant catalysis remained elusive.^[250]

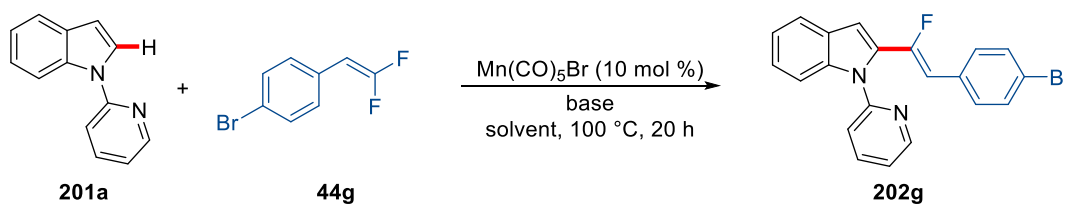
3.2.1. Optimization Studies for the Alkenylative C–H/C–F Functionalization

The optimization studies for the desired C–H/C–F alkenylation were commenced by screening various solvents and bases (Table 3.2.1). First, various solvents were tested showing that ethereal solvents facilitate the envisioned transformation (entries 1–5). Among these, 1,4-dioxane turned out to be the optimal solvent for this reaction (entry 6). Subsequently, the role of a base was studied by comparing different alkali metal carbonates (entries 6–9). The reactivity increased from sodium to potassium carbonate, but significantly dropped, when the heavier analogue like rubidium carbonate was utilized, probably due to the solubility of the formed fluoride salts.^[251] Furthermore, to

3. Results and Discussion

increase the selectivity, different reaction temperatures were probed, revealing an enormous impact on the yield accompanied by the same *Z/E* ratio (entries 10–11). Moreover, an increased amount of substrate **44g** was beneficial, probably due to its low vapor pressure (entries 12–13).^[252] Notably, a higher concentration improved the yield without affecting the selectivity (entry 14). Further optimizations by Uttam Dhawa showed the importance of sodium acetate as additional additive yielding the C–H/C–F alkenylated product **202g** in high yield.

Table 3.2.1. Optimizations for the manganese(I)-catalyzed alkenylative C–H/C–F functionalization.^[a]



Entry	Base	Solvent	Yield / %
1	K ₂ CO ₃	DCE	26
2	K ₂ CO ₃	TFE	11
3	K ₂ CO ₃	PhMe	8
4	K ₂ CO ₃	<i>n</i> -Bu ₂ O	21
5	K ₂ CO ₃	THF	33
6	K ₂ CO ₃	1,4-dioxane	53
7	Na ₂ CO ₃	1,4-dioxane	46
8	Rb ₂ CO ₃	1,4-dioxane	28
9	-	1,4-dioxane	n.r.
10 ^[b]	K ₂ CO ₃	1,4-dioxane	n.r.
11 ^[c]	K ₂ CO ₃	1,4-dioxane	28
12 ^[d]	K ₂ CO ₃	1,4-dioxane	44
13 ^[e]	K ₂ CO ₃	1,4-dioxane	59
14 ^[f]	K ₂ CO ₃	1,4-dioxane	66
15 ^[e,f,g]	K ₂ CO ₃	1,4-dioxane	85

[a] Reaction conditions: **201a** (0.50 mmol), **44g** (1.0 mmol), [MnBr(CO)₅] (10 mol %), base (0.50 mmol), solvent (1.0 mL), 100 °C, 20 h, under Ar; yield of isolated products; all *Z/E* = 92:8, determined by ¹H-NMR. [b] At 80 °C. [c] At 120 °C. [d] **44g** (0.60 mmol). [e] **44g** (1.5 mmol). [f] 1,4-Dioxane (0.50 mL). [g] NaOAc (20 mol %) performed by Uttam Dhawa.

3.2.2. Scope of the Allylative and Alkenylative C–H/C–F Functionalizations

In addition to the optimization of the alkenylative C–H/C–F functionalization, Dr. Daniel Zell optimized the allylative C–H/C–F functionalization on ketimines and together with Uttam Dhawa the allylative C–H/C–F functionalization on indoles. Subsequently, an extensive study on the scope for the allylative and alkenylative manganese(I)-catalyzed C–H/C–F functionalization, including heterocycles and dipeptides was carried out.^[92b]

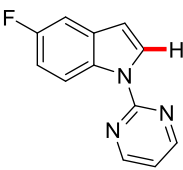
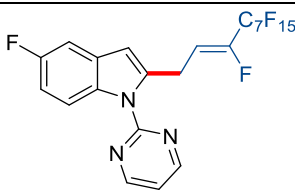
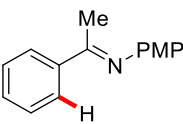
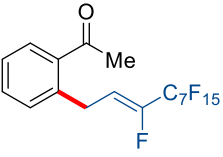
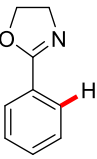
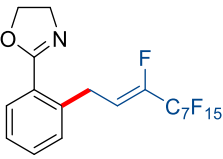
With the optimized catalytic reaction conditions in hand, the substrate scope with respect to different removable directing groups^[35] was explored (Table 3.2.2). Besides indole **201a**, which underwent the desired transformation facily (entry 1), the frequently used pyrimidyl-indole **201b** was also suitable yielding the desired product **203b** in almost quantitative yield (entry 2). Although, β -F elimination is assumed to occur, fluoro substituents were unaffected during the course of the reaction (entry 3). Furthermore, transformable^[172, 253] ketimine **201d** performed well under the optimized reaction conditions, render ketones easily assessable, while oxazoline **203e** was not suitable within this transformation (entries 4–5).

Table 3.2.2. Scope of the manganese(I)-catalyzed allylative C–H/C–F functionalization.^[a]

$\text{201 (X = C, N)} + \text{45a} \xrightarrow[\text{1,4-dioxan, T, 20 h}]{\text{Mn(CO)}_5\text{Br (10 mol \%), NaOAc, K}_2\text{CO}_3} \text{203 (X = C, N)}$

Entry	201	203	Yield / %	Z/E
1 ^[a]	 201a	 203a	97	88:12
2 ^[a]	 201b	 203b	96	87:13

3. Results and Discussion

Entry	201	203	Yield / %	Z/E
3 ^[b]	 201c	 203c	89	85:15
4 ^[b]	 201d	 203d	72	97:3
5 ^[b]	 201e	 203e	n.r.	-

[a] Reaction conditions: **201** (0.50 mmol), **45a** (0.60 mmol), [MnBr(CO)₅] (7.5 mol %), K₂CO₃ (0.50 mmol), 1,4-dioxane (0.50 mL), 80°C, 20 h, isolated yield; Z/E ratios determined by ¹H-NMR spectroscopy.

[b] Reaction conditions: **201** (0.50 mmol), **45a** (1.50 mmol), [MnBr(CO)₅] (10 mol %), NaOAc (40 mol %), K₂CO₃ (0.75 mmol), 1,4-dioxane (0.50 mL), 105 °C, 20 h, isolated yield; Z/E ratios determined by ¹H-NMR spectroscopy.

Inspired by the broad applicability of the manganese(I)-catalyzed allylative C–H/C–F functionalization, various 1,1-difluorostyrenes^[89, 254] **44** were tested under the optimized catalytic reaction conditions for the C–H/C–F alkenylation (Table 3.2.3). A variety of electron-donating substituents in the *ortho*-, *meta*- or *para*-position were tolerated resulting in very good yields and excellent diastereoselectivities (entries 1–4). Furthermore, it was demonstrated that bromo substituents did not react under the reaction regime, although the BDE is significantly lower compared to the cleaved C–F bond (entries 5–7).^[65, 88] Remarkably, an ester group on the styrene was well tolerated and afforded the corresponding product **202h** with excellent selectivity of Z/E = 94:6 (entry 8). Notably, the C–H/C–F alkenylation was not only restricted to 1,1-difluorostyrenes, also 1,1-difluorovinylalkane **44i** underwent the envisioned transformation (entry 9). In this context, citronellal derived compound **44j** was also compatible within this transformation, showing no isomerization or hydroarylation byproduct (entry 10).^[255] The versatile C–H/C–F functionalization however encountered also limitations. 1,1-Difluorostyrenes bearing sterically demanding backbones, such as naphthalene or

3.2. Manganese-Catalyzed Allylative and Alkenylative C–H/C–F Functionalization

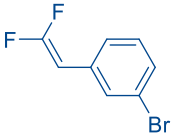
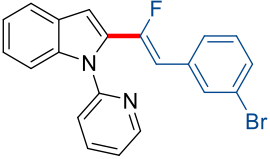
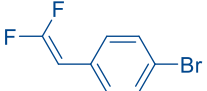
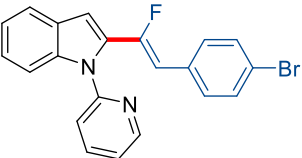
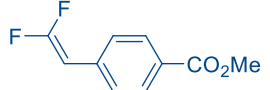
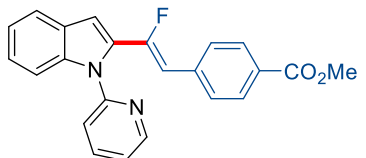
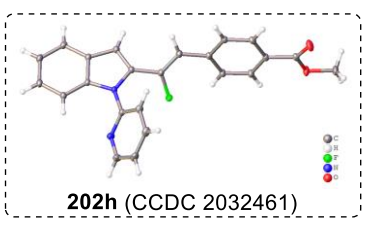
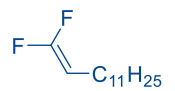
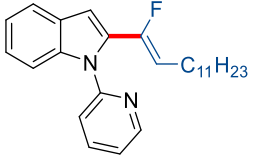
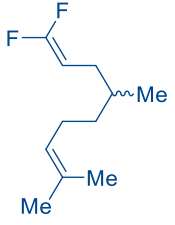
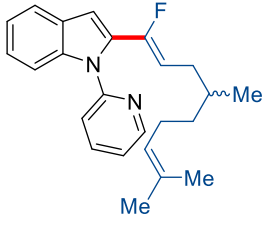
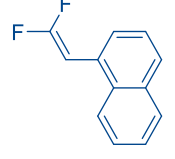
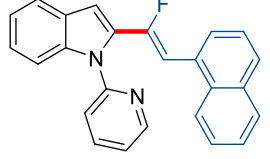
anthracene, could only be converted in low yield and selectivity (entry 11) or did not react at all (entry 12).

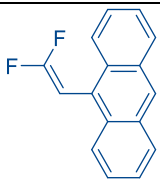
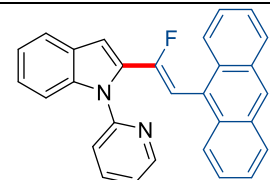
Table 3.2.3. Scope of the manganese(I)-catalyzed alkenylative C–H/C–F functionalization.^[a]

Reaction scheme: 201a + 44 $\xrightarrow[\text{K}_2\text{CO}_3, \text{1,4-dioxan, 100 }^\circ\text{C, 20 h}]{\text{Mn(CO)}_5\text{Br (10 mol \%), NaOAc (20 mol \%)}}$ 202

Entry	44	202	Yield	Z/E
1			87	80:20
2			80	89:11
3			87	87:13
4			81	94:6
5			90	96:4

3. Results and Discussion

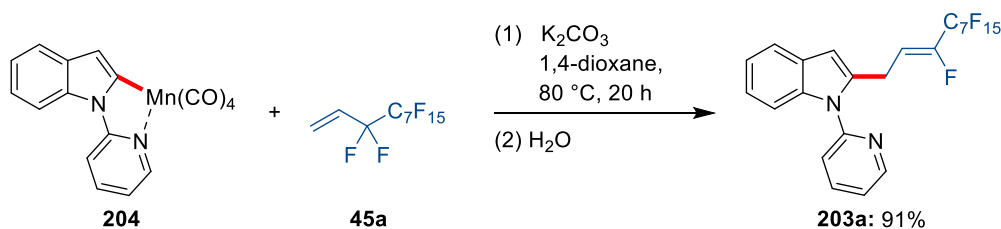
Entry	44	202	Yield	Z/E
6	 <p>44f</p>	 <p>202f</p>	86	96:4
7	 <p>44g</p>	 <p>202g</p>	85	92:8
8	 <p>44h</p>	 <p>202h</p>	92	94:6
		 <p>202h (CCDC 2032461)</p>		
9	 <p>44i</p>	 <p>202i</p>	61	82:18
10	 <p>44j</p>	 <p>202j</p>	58	78:22
11	 <p>44k</p>	 <p>202k</p>	46	65:35

Entry	44	202	Yield	Z/E
12			n.r.	-
	441	2021		

[a] Reaction conditions: **201a** (0.50 mmol), **44** (1.50 mmol), $[\text{MnBr}(\text{CO})_5]$ (10 mol %), NaOAc (20 mol %), K_2CO_3 (0.50 mmol), 1,4-dioxane (0.50 mL), 100 °C, 20 h, isolated yield; Z/E ratios determined by ^1H -NMR spectroscopy. The crystal structure **202h** was measured and resolved by Dr. Christopher Golz.

3.2.3. Experiment with Cyclometalated Complex **204**

Interested in the mechanism of the C–H/C–F functionalization, the formation of product **203a** was studied using the well-defined manganacycle **204** (Scheme 3.2.1).^[43c, 256] The reaction proved viable in an almost quantitative fashion with the same diastereoselectivity compared to the catalytic transformation. Based on this result the formation of manganacycle **204** by a manganese(I)-catalyzed C–H activation pathway is likely operative.



Scheme 3.2.1. Stoichiometric C–H/C–F functionalization of manganacycle **204**.

3.3. Asymmetric Nickel-Catalyzed Hydroarylations by C–H Activation

The progress of modern synthetic organic chemistry is largely related to the discovery of new asymmetric reactions, particularly those catalyzed by chiral catalysts.^[257] This statement is clearly supported by the award of the 2001 Nobel Prize in Chemistry to W. S. Knowles, R. Noyori, and K. B. Sharpless for their work on asymmetric hydrogenation and oxidation reactions, respectively.^[258] In this context, the development of direct asymmetric C–H functionalization reactions are of key importance in modern metallorganic chemistry and heavily rely on rather toxic and expensive 4d and 5d transition metals, such as palladium, rhodium, and iridium.^[207b, 213, 259] On the contrary, recent achievements in the emerged area of catalytic C–H activation by cost effective and sustainable 3d metal catalysts, such as nickel and cobalt among others,^[109b, 109c, 260] significantly expanded synthetic methodologies. In this context, redox neutral hydroarylations of C–C multiple bonds by nickel catalysis have become a powerful tool for challenging transformations.^[27, 96c] Unfortunately, this approach is in many cases restricted to activated heteroarenes or electronically-activated C–C multiple bonds. Notably, recent achievements overcame this issue by applying nickel/aluminium heterobimetallic catalysis.^[111] Even though, the perfect atom economy and the applicability to novel bioactive natural compounds made this methodology especially attractive (Figure 3.3.1),^[261] asymmetric intramolecular C–H hydroarylations are rare and require pyrophoric LEWIS-acidic organoaluminium additives, such as AlMe₃ or MAD.^[109]

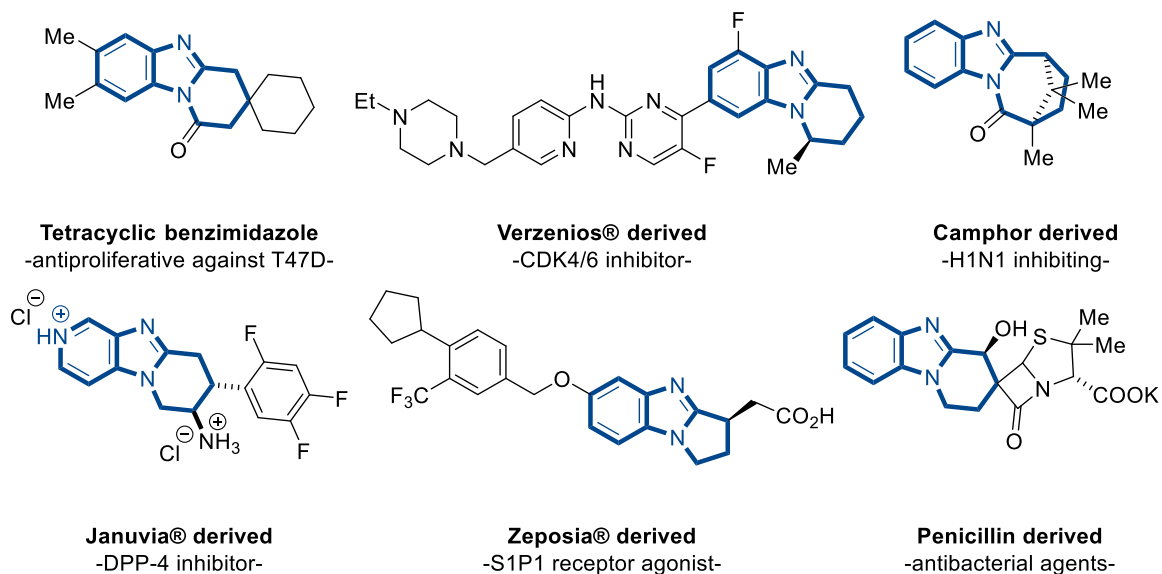
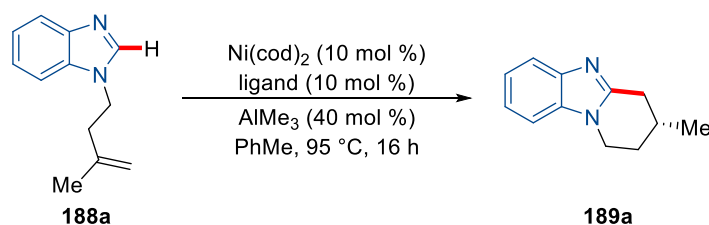


Figure 3.3.1. Selected examples of bioactive polycyclic imidazole motifs.

3.3.1. Optimization Studies for Enantioselective Intramolecular Nickel-Catalyzed Hydroarylations by C–H Activation

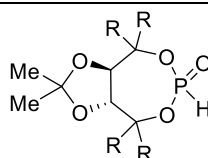
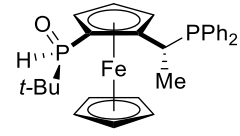
Inspired by early studies based on rhodium(I)-catalyzed intramolecular hydroarylations and the importance of benzimidazole scaffolds in bioactive compounds,^[262] an asymmetric cyclization of *N*-homoallylimidazoles **188a** by nickel catalysis was envisioned. Based on detailed optimization studies by Dr. Joachim Loup, various chiral pre-catalyst and chiral ligands were probed (Table 3.3.1).^[214a] In this context, commercially available chiral nickel(II) (pre)-catalyst **205** and **206** failed to give any conversion (entries 1–2). Further studies were shifted to SPO pre-ligands which were already used in asymmetric organocatalysis^[55d, 263] and asymmetric hydrogenations.^[57b, 239d, 264] Remarkably, with the TADDOL-based SPO **207** a chiral induction was obtained,^[55a, 109d] highlighting the great potential of chiral SPOs within the envisioned asymmetric hydroarylation (entry 3). Thereafter, the chiral JoSPOphos^[264a, 264b, 265] ligand **208** was tested and afforded the desired product **189a** in excellent yield and enantioselectivity (entry 4). Control experiments confirmed the important role of the pre-ligand and the nickel salt (entries 5–6).

Table 3.3.1. Optimization of the catalyst and ligand for the enantioselective nickel-catalyzed cyclization.^[a]



Entry	Ligand	Yield / %	e.r. ^[b]
1 ^[c]	<p>205</p>	n.r.	-
2 ^[c]	<p>206</p>	n.r.	-

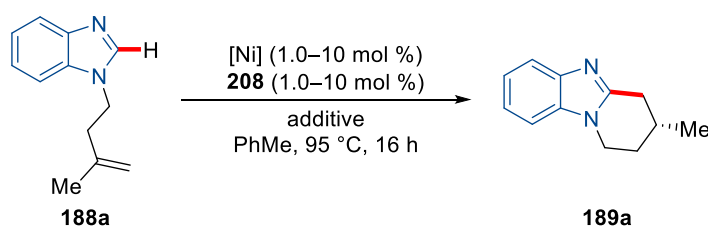
3. Results and Discussion

Entry	Ligand	Yield / %	e.r. ^[b]
3	 207 : R = <i>o</i> -tolyl	69	64:36
4	 208	92	99:1
5 ^[c]	208	n.r.	-
6 ^[d]	-	n.r.	-

[a] Reaction conditions: **188a** (0.50 mmol), Ni(cod)₂ (10 mol %), ligand (10 mol %), AlMe₃ (40 mol %), PhMe (2.0 mL), 16 h, isolated yield. [b] Determined by chiral HPLC analysis. [c] Without Ni(cod)₂. [d] Without **208**.

Considering the air- and moisture instability of Ni(cod)₂, Ni(acac)₂ was tested next as a more robust^[227e, 266] pre-catalyst within the developed asymmetric regime (Table 3.3.2). To our delight, Ni(acac)₂ in combination with JoSPOphos **229** facilitated the asymmetric intramolecular hydroarylation well with an increased yield compared to Ni(cod)₂ (entries 1–3). This finding indicated, that during the course of the reaction the LEWIS-acid likely acted as a reducing agent to generate nickel(0) as active species.^[65b, 227] Further studies, with respect to the catalyst loading showed the excellent reactivity of the catalyst, since even catalyst loadings down to 1 mol % did not affect the conversion and the enantioselectivity (entries 4–5). Finally, different LEWIS-acids were tested indicating that sterically undemanding organoaluminum additives were preferred within the catalytic regime (entries 6–8).

At the same time, Dr. Joachim Loup showed that LEWIS-acids were not required in terms of yield and enantioselectivity, provided that Ni(cod)₂ was used as pre-catalyst (entry 9).^[214a] Considering the unique opportunity for improved functional group tolerance, the focus was shifted to the AlMe₃-free regime.

Table 3.3.2. Optimization of nickel and additive for the enantioselective nickel-catalyzed cyclization.^[a]

Entry	[Ni]	Additive	Yield / %	e.r. ^[b]
1 ^[c]	Ni(acac) ₂	AlMe ₃	92	99:1
2	Ni(cod) ₂	AlMe ₃	82	99:1
3	Ni(acac) ₂	AlMe ₃	93	99:1
4 ^[d]	Ni(acac) ₂	AlMe ₃	93	99:1
5 ^[e]	Ni(acac) ₂	AlMe ₃	90	99:1
6	Ni(acac) ₂	-	n.r.	-
7	Ni(acac) ₂	AlEt ₃	80	99:1
8	Ni(acac) ₂	ZnEt ₂	n.r.	-
9 ^[f]	Ni(cod) ₂	-	96	96:4

[a] Reaction conditions: **188a** (0.50 mmol), [Ni] (1.0–10 mol %), ligand (1.0–10 mol %), additive (40 mol %), PhMe (1.0 mL), 16 h, isolated yield. [b] Determined by chiral HPLC analysis. [c] [Ni] (10 mol %). [d] [Ni] (2.5 mol %). [e] [Ni] (1.0 mol %). [f] Ni(cod)₂ (5.0 mol %), **208** (2.5 mol %), performed by Dr. Joachim Loup.

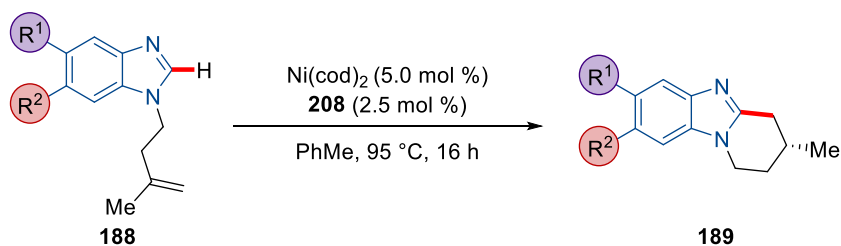
3.3.2. Scope of the Enantioselective Nickel-Catalyzed *endo*-Hydroarylation

With the optimized reaction conditions in hand, the robustness of the enantioselective nickel-catalyzed *endo*-hydroarylation of alkenes *via* C–H activation under aluminum-free conditions was explored. The remarkably simple catalytic system proved able to cyclize various functionalized heteroarenes **188** in outstanding yields and levels of enantioselectivity (Table 3.3.3). Electron-rich as well as electron-deficient poly-substituted benzannulated azoles **188a–c** underwent the desired hydroarylation without a drop in enantioselectivity (entries 1–3). In this context, chloro substituents stayed intact during the course of the reaction, while side reactions, such as cross-coupling^[267] or dehalogenation,^[268] were not detected. Furthermore, substituents in the 5- and 6-position of the benzannulated azole **188d–e** were not affecting the catalytic regime, which was reflected by excellent yields and perfect enantioselectivities (entries 4–5). Notably, sterically demanding fluorescent pyrene derivative **188f** proved to be compatible within

3. Results and Discussion

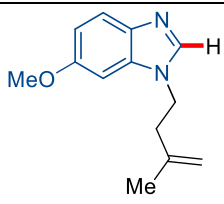
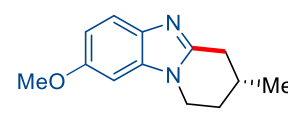
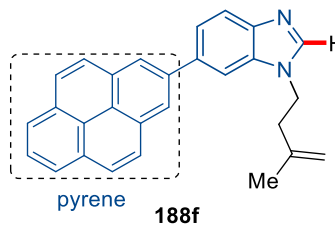
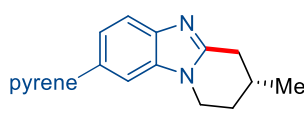
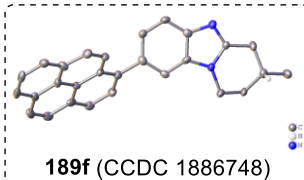
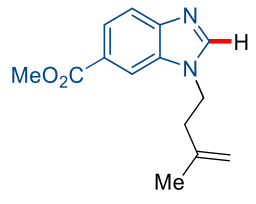
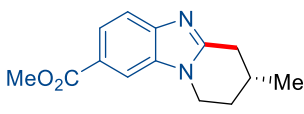
the enantioselective intramolecular nickel-catalyzed hydroarylation (entry 6). X-ray diffraction analysis of product **188f** unambiguously assigned the *R*-configuration of the cyclized product. Finally, ester containing substrate **188g** was converted under the LEWIS-acid free reaction conditions (entry 7).

Table 3.3.3. Scope of benzannulated azoles **188** in the nickel-catalyzed intramolecular hydroarylation.^[a]



Entry	188	189	Yield / %	e.r. ^[b]
1			96	99:1
2			92	96:4
3 ^[c]			84	98:2
4			87	99:1

3.3. Asymmetric Nickel-Catalyzed Hydroarylations by C–H Activation

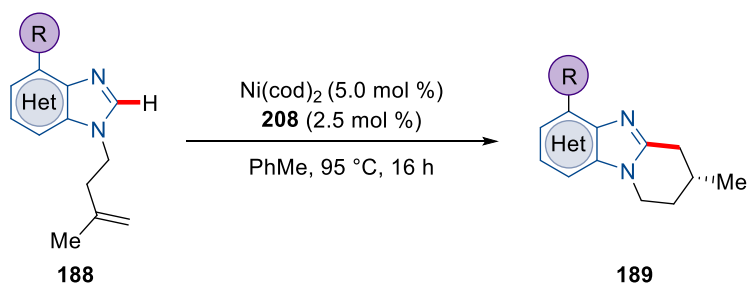
Entry	188	189	Yield / %	e.r. ^[b]
5	 188e	 189e	90	96:4
6	 188f	 189f  189f (CCDC 1886748)	78	99:1
7	 188g	 189g	74	99:1

[a] Reaction conditions: **188** (0.50 mmol), Ni(cod)₂ (5.0 mol %), **208** (2.5 mol %), PhMe (1.0 mL), 16 h, isolated yield. [b] Determined by chiral HPLC analysis. [c] Ni(cod)₂ (10 mol %), **208** (5.0 mol %). The crystal structure **189f** was measured and resolved by Dr. Christopher Golz.

Inspired by the robustness towards diversely decorated benzannulated azoles **188a-g** in the enantioselective nickel-catalyzed *endo*-hydroarylation, a variety of pharmaceutically relevant heterocycles were next probed (Table 3.3.4).^[269] Challenging aza-benzimidazoles^[270] **188h-i** were efficiently converted with excellent yield and high levels of enantioselectivity (entries 1–2). Notably, the coordination of the JoSPOphos pre-ligand to the catalyst was not affected by the bidentate nature of the substrate.^[271] Furthermore, highly functionalized purines, such as biologically relevant morpholine^[272] and fluorescent pyrene derivatives were efficiently converted to the cyclized products (entries 3–5). Finally, pharmaceutical relevant theophylline^[273] derivative **188m** proved to be compatible with the developed enantioselective nickel-catalyzed *endo*-hydroarylation (entry 6).

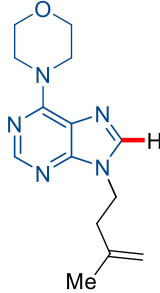
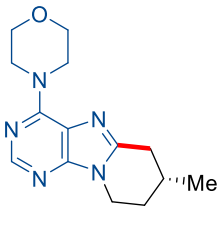
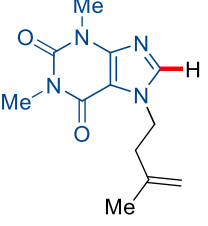
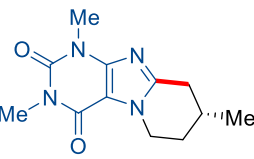
3. Results and Discussion

Table 3.3.4. Scope of pharmaceutically relevant heterocycle **188** in the nickel-catalyzed intramolecular hydroarylation.^[a]



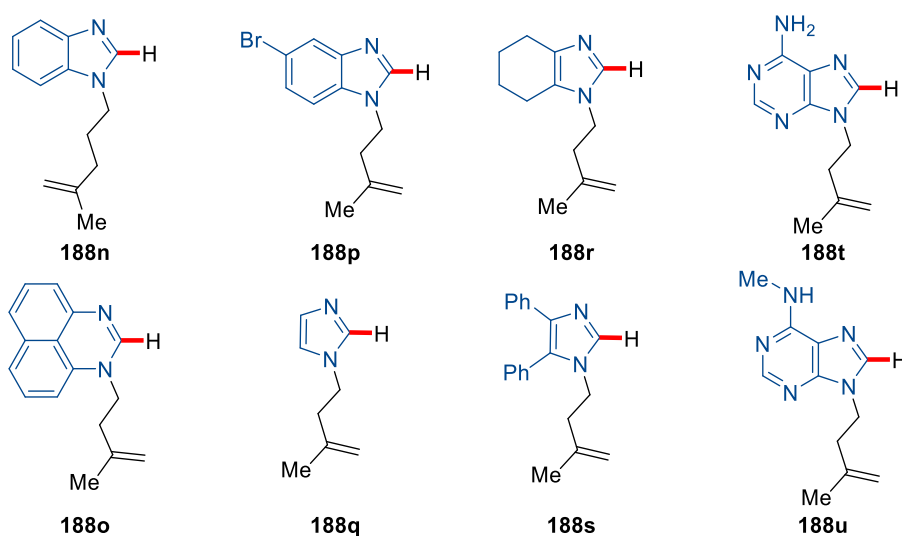
Entry	188	189	Yield / %	e.r. ^[b]
1	<p>188h</p>	<p>189h</p>	82	92:8
2	<p>188i</p>	<p>189i</p>	89	97:3
3	<p>188j</p>	<p>189j</p>	84	95:5
4	<p>188k</p>	<p>189k</p>	82	95:5

3.3. Asymmetric Nickel-Catalyzed Hydroarylations by C–H Activation

Entry	188	189	Yield / %	e.r. ^[b]
5 ^[c]	 188i	 189i	75	95:5
6 ^[c]	 188m	 189m	81	95:5

[a] Reaction conditions: **188** (0.50 mmol), Ni(cod)₂ (5.0 mol %), **208** (2.5 mol %), PhMe (1.0 mL), 16 h, isolated yield. [b] Determined by chiral HPLC analysis. [c] Ni(cod)₂ (10 mol %), **208** (5.0 mol %),

The versatile enantioselective nickel-catalyzed *endo*-hydroarylation however encountered also limitations (Scheme 3.3.1). An elongated carbon tether **188n** and a pyrimidine derived structure **188o** were not feasible within the catalysis, probably because of the kinetically challenging seven-membered ring formation and the higher pK_a.^[31a, 274] Furthermore, bromo-substitutedazole **188p** did not react in a selective fashion probably due to the activation of the relative weak C–Br bond.^[96e, 275] No conversion of the heteroarenes **188q-s** was detected, probably due to a coordinative deactivation pathway with basic amine.^[276]



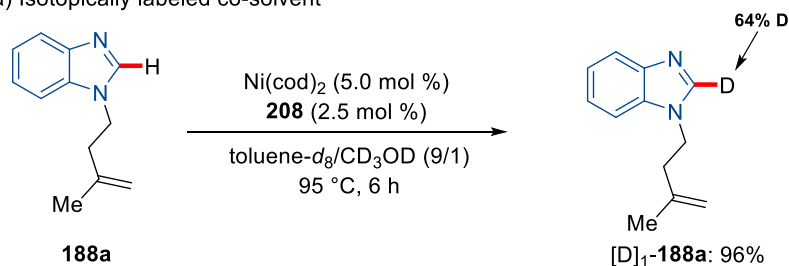
Scheme 3.3.1. Limitations of the nickel-catalyzed intramolecular hydroarylation.

3.3.3. Mechanistic Studies

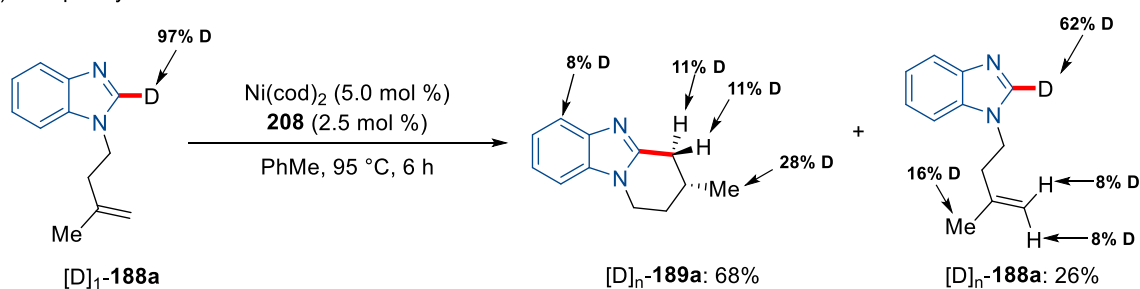
3.3.3.1. H/D-Exchange Experiments

Given the unique features of the asymmetric aluminium-free nickel-catalyzed C–H alkylation, an understanding of its mode of action was desired. To study the mechanism of the C–H activation elementary step, an H/D-exchange experiment with CD₃OD as the co-solvent was conducted (Scheme 3.3.2a). Importantly, a significant H/D-exchange in the C2-position of the reisolated starting material **188a** was detected. Further, a reaction performed with deuterated substrate [D]₁-**188a** revealed H/D scrambling at the methyl group and positions of the former olefin (Scheme 3.3.2b). A possible explanation could be the formation of a nickel-hydride and/or a π -allyl-nickel intermediate that initiates isomerization.^[277] Nevertheless, both observations support a facile and reversible C–H activation step^[278] and are strikingly different from the previous report on nickel-catalyzed *exo*-cyclization.^[109d]

a) Isotopically labeled co-solvent

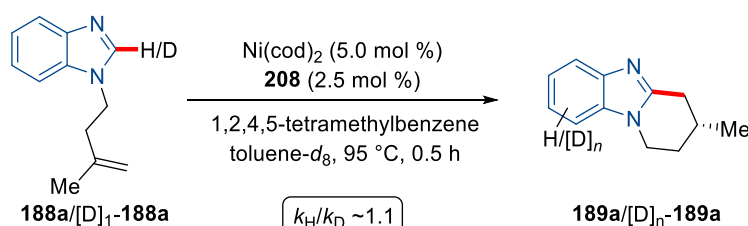


b) Isotopically labeled **188a**



Scheme 3.3.2. H/D-exchange studies.

3.3.3.2. KIE Studies



Scheme 3.3.3. KIE studies.

The kinetic isotope effect (KIE) of the asymmetric aluminium-free nickel-catalyzed C–H hydroarylation was measured by the comparison of independent reaction rates for substrate **188a** and the isotopically labeled analogue [D]₁-**188a**, showing a minor value of $k_{\text{H}}/k_{\text{D}} \sim 1.1$ (Figure 3.3.2). The observed KIE is in good agreement with the results obtained from the H/D-exchange experiments, suggesting the C–H scission step not to be turnover limiting.^[279]

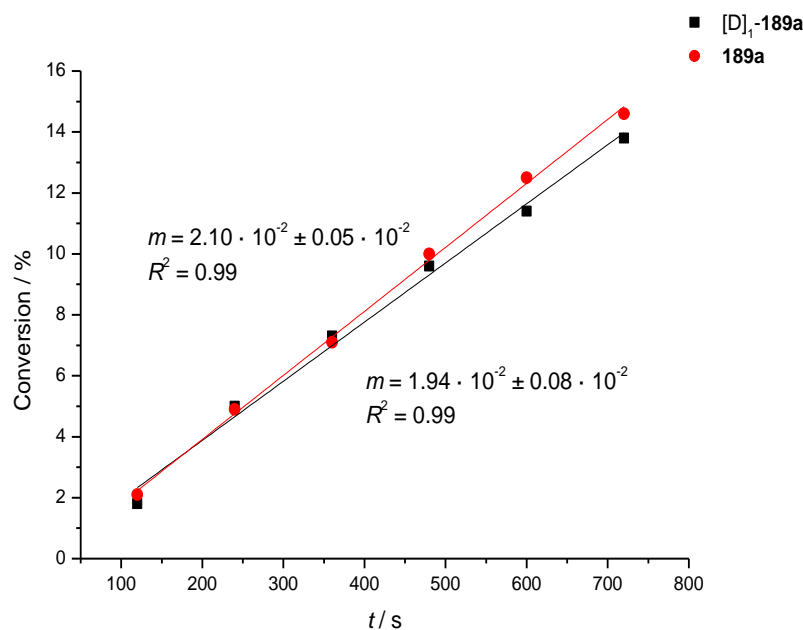
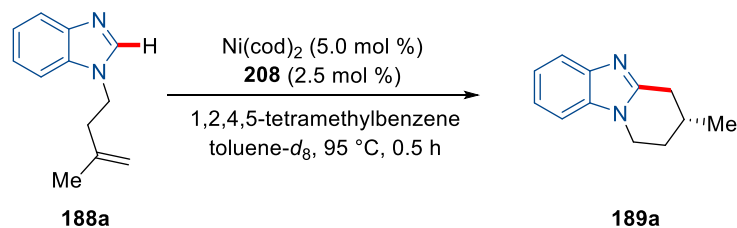


Figure 3.3.2. KIE study of the asymmetric aluminium-free nickel-catalyzed C–H hydroarylation.

3.3.3.3. Kinetic reaction orders

3.3.3.3.1. Reaction order of *N*-homoallylimidazoles **188a**



Scheme 3.3.4. Kinetic order in *N*-homoallylimidazoles **188a**.

The kinetic order of the reaction with respect to the concentration of *N*-homoallylimidazoles **188a** equals $n = 1.06 \pm 0.04$, which likely corresponds to a reaction

order of one (Figure 3.3.3). This result can be interpreted as a clear hint for the participation of substrate **188a** in the turnover-limiting step of the reaction.

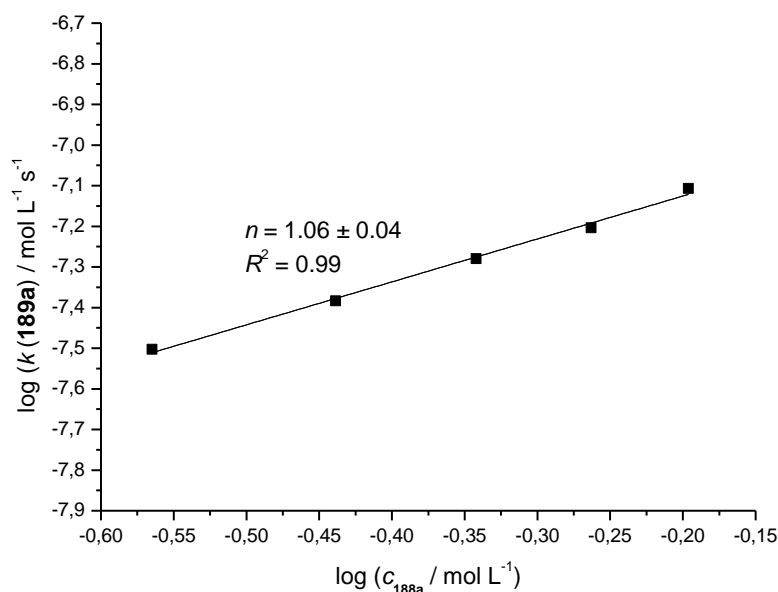
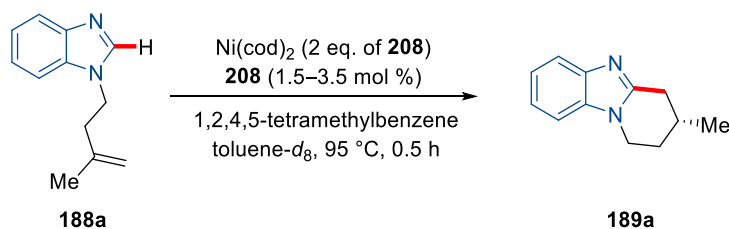


Figure 3.3.3. Kinetic order in [**188a**] in the asymmetric aluminium-free nickel-catalyzed C–H hydroarylation conditions.

3.3.3.3.2. Reaction order of JoSPOphos (**208**)



Scheme 3.3.5. Kinetic order in JoSPOphos (**208**).

The reaction order with respect to the concentration of JoSPOphos (**208**) is roughly one, with $n = 0.96 \pm 0.09$ (Figure 3.3.4), showing that the ligand coordinates during the turnover-limiting step of the catalytic cycle to the metal.

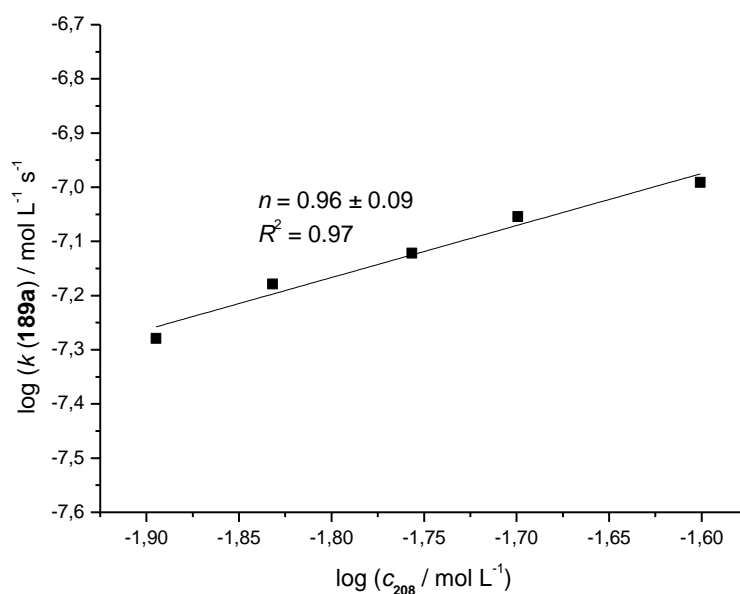
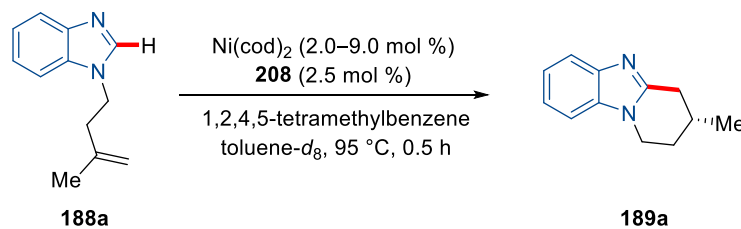


Figure 3.3.4. Kinetic order in [208] in the asymmetric aluminium-free nickel-catalyzed C–H hydroarylation conditions.

3.3.3.3.3. Reaction order of Ni(cod)₂



Scheme 3.3.6. Kinetic order in Ni(cod)₂.

Interestingly, an initial first-order rate dependence in the nickel precursor of $n = 1.06 \pm 0.03$ was observed, followed by an inhibition at higher nickel concentrations (Figure 3.3.5). A possible interpretation to this rather unusual finding could be the existence of a critical nickel concentration, beyond which an autocatalytic deactivation of the catalyst occurs due to aggregation of nickel, as it was proposed for palladium catalysis.^[280] Another explanation to the detrimental effect of higher concentrations of Ni(cod)₂ could be the competitive coordination of free cod to the nickel center, resulting in off-cycle intermediates decelerating the catalysis, as previously reported by Zimmerman and Montgomery.^[281]

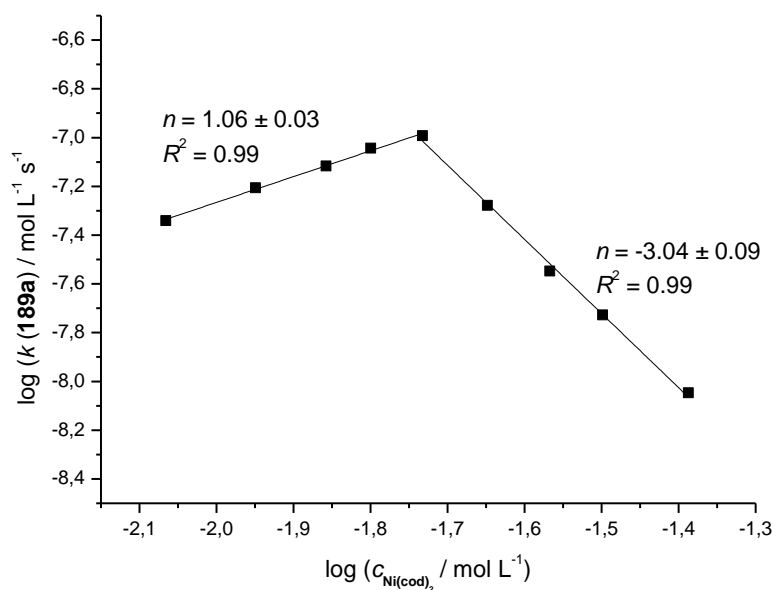
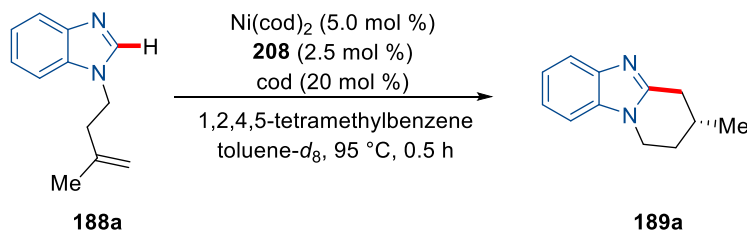


Figure 3.3.5. Kinetic order in $[\text{Ni}(\text{cod})_2]$ in the asymmetric aluminium-free nickel-catalyzed C–H hydroarylation conditions.

3.3.3.4. Effect of the concentration of 1,5-cyclooctadiene on the reaction rate



Scheme 3.3.7. Reaction rate dependence on the concentration of 1,5-cyclooctadiene.

Studies towards high concentrations of 1,5-cyclooctadiene (cod) showed that, in the presence of additional cod, the transformation was found to proceed with a lower rate (Figure 3.3.6). This finding provided support for the hypothesis that an inhibition of the active nickel catalyst is caused by free cod originating from the consumption or degradation of $\text{Ni}(\text{cod})_2$.

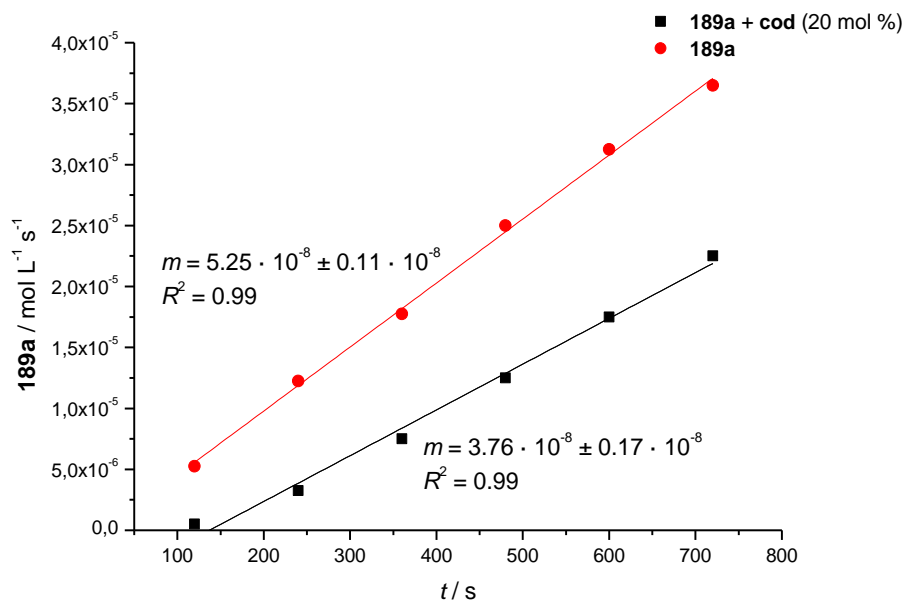


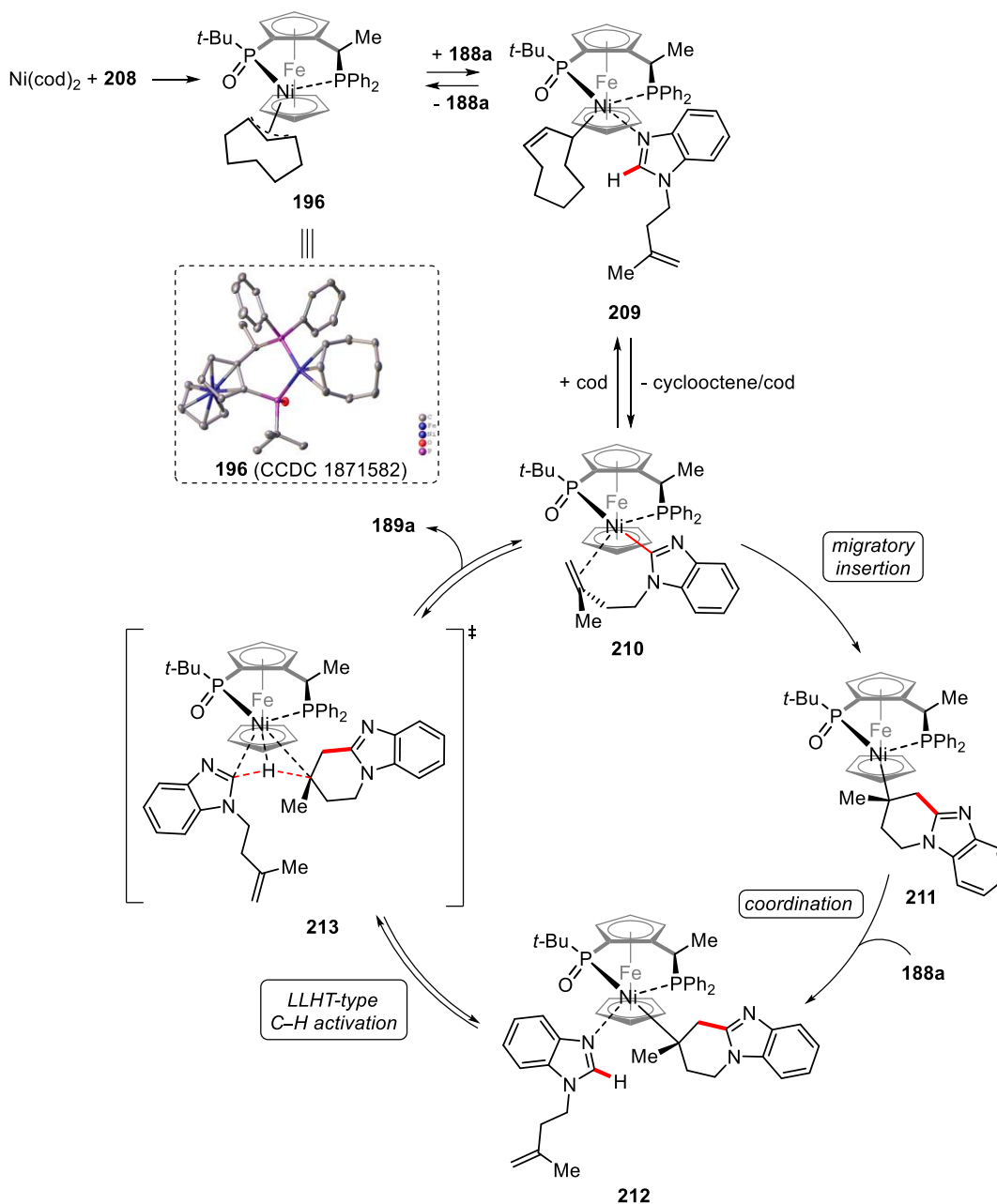
Figure 3.3.6. Effect of the concentration of 1,5-cyclooctadiene in the asymmetric aluminium-free nickel-catalyzed C–H hydroarylation.

3.3.4. Proposed Catalytic Cycle

Based on our detailed mechanistic studies and previous literature reports,^[105, 235b, 282] the catalytic reaction is proposed to be initiated by the formation of the organometallic nickel(II) complex **196** (Scheme 3.3.8). Complex **196** was synthesized by Dr. Debasish Ghorai and found to be active in both stoichiometric and catalytic reactions. A plausible pathway for the generation of nickel(II) complex **196** could be the oxidative addition of nickel(0) into the P(O)–H bond, as it has been previously reported in the literature,^[283] followed by hydride migration to the bond 1,5-cyclooctadiene and chain walking.^[281b] Complex **196** is then coordinated by substrate **188a** to form intermediate **209**. Due to the close proximity an initial C–H activation can occur after loss of a cyclooctene molecule, yielding the proposed active catalyst **210**. Intermediate **210** then undergoes the stereo-determining and C–C bond forming migratory insertion to deliver the cyclized intermediate **211**. Derived from the kinetic reaction order analysis a kinetically relevant coordination of a second substrate **188a** occurs, yielding intermediate **212**. Finally, the facile C–H cleavage was proposed to occur *via* a LLHT manifold **213**,^[277d, 282a, 284] yielding the desired product **189a** and the reformed active catalyst **210**. Taking into account that the formation of the active catalyst is an off-cycle reaction the observed H/D scrambling can be explained since during the oxidative addition of the nickel(0) into the P(O)–H bond a nickel- π -allyl or a nickel-hydride species is possibly

3. Results and Discussion

involved. Furthermore, the isolated complex **196** is a plausible off-cycle intermediate, or a resting state, whose reversible formation is favored by higher concentrations of cod. This can explain the negative order in $\text{Ni}(\text{cod})_2$ above a certain concentration and rationalizing the detrimental effect of adding an excess of free 1,5-cyclooctadiene to the catalytic reaction. Indeed, such cod-incorporating π -allyl complexes are documented to be stable off-cycle intermediates whose formation diminishes the catalytic efficiency.^[281]



Scheme 3.3.8. Proposed catalytic cycle. Complex **196** was prepared and crystallized by Dr. Debasish Ghorai. The crystal structure was measured and resolved by Dr. Christopher Golz.

In this context, detailed DFT studies by Chen and Ackermann revealed in addition to the LLHT and reductive elimination pathway, an unexpected potentially favorable nickel(0)/nickel(II) catalytic cycle comprising P–H oxidative addition, migratory insertion and C(sp²)–H activation *via* σ -CAM (σ -complex-assisted metathesis) and C–C reductive elimination.^[285] Similar to the experimental results the DFT calculations emphasized that complex **196** is probably an off-cycle intermediate, which can be converted to the catalytical active nickel(0) complex by sequential β -hydride elimination and reductive elimination.

3.4. Hydrogen Isotope Exchange by Ruthenium-Catalyzed C–H Activation

Hydrogen isotope exchange (HIE) of otherwise inert C–H bonds promoted by transition metal catalysis has emerged as a valuable tool, since multi-step processes and expensive labeled precursors can be avoided.^[138-139, 139c, 286] Notably, this approach has recently initiated numerous applications towards the detection and quantification of drugs and drug metabolites in a complex matrix by absorption, distribution, metabolism and excretion (ADME) studies.^[152, 287] Consequently, highly selective transition metal-catalyzed HIE of C–H bonds in complex pharmaceuticals is still one of the key challenges for medicinal chemist, because the catalyst needs to be compatible with a variety of functional groups that are commonly present in marketed pharmaceuticals.^[138b, 288] In addition to iridium catalysts,^[143e, 289] recent developments for late-stage labeling of drug candidates were reported by using efficient 3d and 4d transition metals, enabling regioselective direct HIE (Figure 3.4.1).^[139]

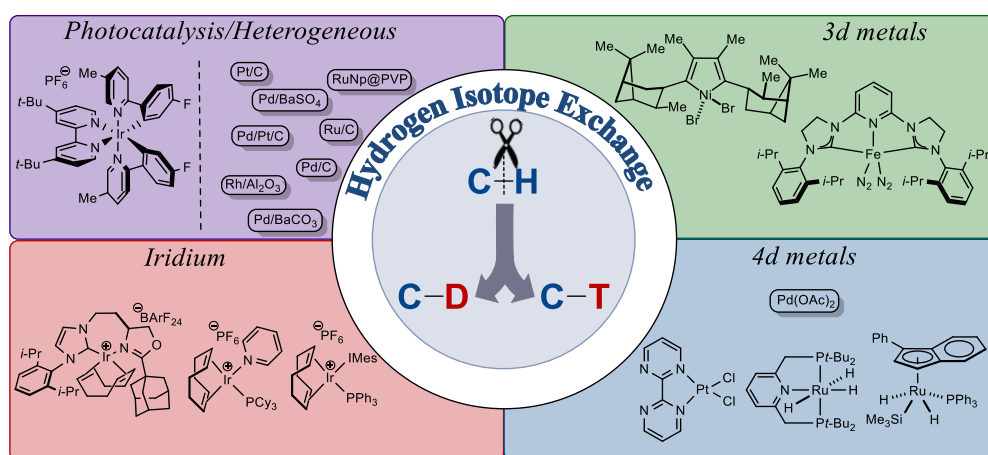


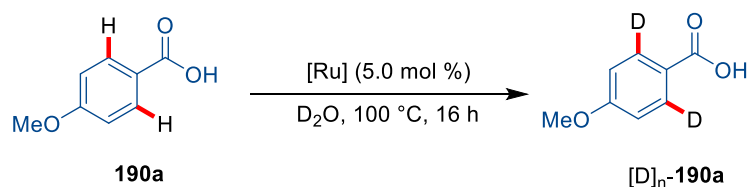
Figure 3.4.1. Transition metal catalysts for HIE of pharmaceuticals.

In order to improve the site-selectivity, the introduction of a directing group in complex organic molecules seems reasonable in HIE reactions to trap the metallacycle with D₂O or T₂O.^[126h, 132, 290] In particular carboxylic acids are especially attractive directing groups due to their commercial availability in large structural diversities,^[291] transformability^[291d, 292] and removability.^[158, 293]

3.4.1. Optimization Studies for Ruthenium(II)-Catalyzed Hydrogen Isotope Exchange

The optimization studies for the envisioned HIE of *p*-anisic acid **190a** were commenced by probing the effect of various ruthenium sources with D₂O (Table 3.4.1). Whereas, simple [RuCl₂(*p*-cymene)]₂ catalyst provided low D-incorporation (entry 1), the use of well-defined ruthenium(II) biscarboxylate complexes afforded high catalytic efficacy in the HIE reaction with excellent D-incorporation (entries 2–4). Therefore, the results were indicative of the essential role of carboxylate ligand in the C–H transformation. Further studies were carried out with [Ru(O₂CAd)₂(*p*-cymene)] as the optimal ruthenium catalyst (entry 5).

Table 3.4.1. Optimization studies for HIE of *p*-anisic acid (**190a**).^[a]



Entry	[Ru]	Yield / %	<i>ortho</i> D / %
1	[RuCl ₂ (<i>p</i> -cymene)] ₂	72	19
2	[Ru(O ₂ Piv) ₂ (<i>p</i> -cymene)]	68	90
3	[Ru(O ₂ Mes) ₂ (<i>p</i> -cymene)]	72	90
4	[Ru(OAc) ₂ (<i>p</i> -cymene)]	73	92
5	[Ru(O ₂ CAd) ₂ (<i>p</i> -cymene)]	76	90

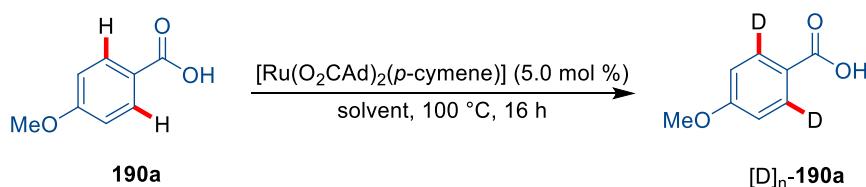
[a] Reaction conditions: **190a** (0.50 mmol), [Ru] (5.0 mol %), D₂O (1.0 mL), 100 °C, 16 h. Yield of isolated products. Degree of D-incorporation was determined by ¹H-NMR.

Next, different deuterium sources (Table 3.4.2) were probed. While solvents, such as MeOD, MeOH-*d*₄ and *i*-PrOH-*d*₈, did not improve the catalytic efficacy, more acidic acetic acid-*d*₄, essential within palladium-catalyzed HIE,^[145b] resulted in a significant reduced yield (entries 1–4). Furthermore, non-acidic deuterium source provided no D-incorporation in the product [D]₂-**190a** (entry 5). Considering solubility problems,^[294] solvent mixtures of deuterium oxide with different aprotic solvents were probed next (entries 6–7). Indeed, a 1:1 mixture of toluene and D₂O increased both the D-incorporation and the isolated yield (entry 8). Notably, biomass-derived GVL^[18a] seemed also suitable for this HIE with excellent levels of isotope-labeling (entry 9). The lower yield can probably be explained by the thermal degradation of GVL accompanied with

3. Results and Discussion

undesired side reactions.^[295] Due to the user-friendly and cost-effective properties,^[296] deuterium oxide was selected as an isotopic labeling source for further studies in the HIE reaction.

Table 3.4.2. Optimization of various deuterium sources for ruthenium(II)-catalyzed HIE of *p*-anisic acid (**190a**).^[a]



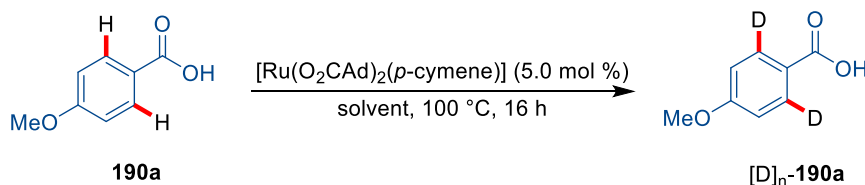
Entry	Solvent	Yield / %	<i>ortho</i> D / %
1	MeOH- <i>d</i> ₄	75	90
2	MeOD	73	92
3	<i>i</i> -PrOH- <i>d</i> ₈	68	80
4	acetic acid- <i>d</i> ₄	56	60
5	chloroform- <i>d</i>	98	0
6 ^[b]	D ₂ O/acetone	62	98
7 ^[b]	D ₂ O/ <i>n</i> -BuOH	73	72
8 ^[b]	D ₂ O/toluene	86	93
9 ^[b]	D ₂ O/GVL	57	91

[a] Reaction conditions: **190a** (0.50 mmol), [Ru(O₂CAAd)₂(*p*-cymene)] (5.0 mol %), solvent (1.0 mL), 100 °C, 16 h, yield of isolated products. Degree of D-incorporation was determined by ¹H-NMR. [b] D₂O/solvent (1/1).

Further optimization studies revealed that the reaction temperature had a significant impact on the deuteration (Table 3.4.3; entries 1–2). In addition, the robustness of the reaction was probed by a successful reaction under air (entry 3). Since 1,4-dioxane is a well-established solvent in many ruthenium-catalyzed C–H activations, it was employed as solvent with 10 equivalents of deuterium oxide, resulting in excellent levels of D-incorporation of **190a** in *ortho*-position (entry 4). A shorter reaction time and a lower amount of ruthenium catalyst did not result in any improved D-incorporation (entries 5–6). Importantly, control experiments showed the essential nature of the catalyst for the HIE (entry 7).

3.4. Hydrogen Isotope Exchange by Ruthenium-Catalyzed C–H Activation

Table 3.4.3. Optimization of ruthenium(II)-catalyzed HIE of *p*-anisic acid (**190a**).^[a]

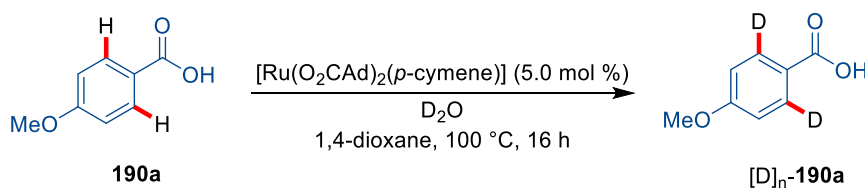


Entry	Solvent	Yield / %	<i>ortho</i> D / %
1 ^[b]	D ₂ O	79	60
2 ^[c]	D ₂ O	72	92
3 ^[d]	D ₂ O	72	94
4 ^[e]	1,4-dioxane	93	95
5 ^[e,f]	1,4-dioxane	91	82
6 ^[e,g]	1,4-dioxane	93	58
7 ^[e,h]	1,4-dioxane	96	-

[a] Reaction conditions: **190a** (0.50 mmol), Ru(O₂CAd)₂(*p*-cymene) (5.0 mol %), solvent (1.0 mL), 100 °C, 16 h, yield of isolated products. Degree of D-incorporation was determined by ¹H-NMR. [b] 45 °C. [c] 110 °C. [d] Under air. [e] D₂O (10 equiv). [f] 6 h. [g] [Ru] 2.5 mol %. [h] Without [Ru].

While deuterium oxide is user-friendly, T₂O is a radiation hazard and larger amounts of T₂O should be avoided.^[297] For further applications, the effectiveness of the envisioned HIE was studied by varying the amount of deuterium oxide (Table 3.4.4). While a decrease in the D-incorporation was observed in the reaction with low amount of deuterium oxide (entry 1–2), amounts of 6.0 to 10 equivalents were overall optimal (entries 3–5). Notably, an excess of deuterium oxide led to a significant drop in yield, (entry 6).

Table 3.4.4. Effect of different quantities of D₂O on the HIE.^[a]



Entry	D ₂ O (X equiv)	Yield / %	<i>ortho</i> D / %
1	2	95	66
2	4	94	71
3	6	94	80

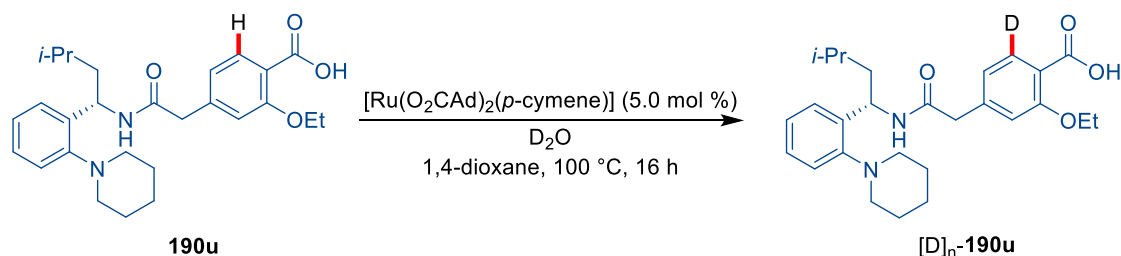
3. Results and Discussion

Entry	D ₂ O (X equiv)	Yield / %	<i>ortho</i> D / %
4	8	95	88
5	10	93	95
6	100	76	95

[a] Reaction conditions: **190a** (0.50 mmol), [Ru(O₂CAd)₂(*p*-cymene)] (5.0 mol %), D₂O (2–100 equiv), 1,4-dioxane (1.0 mL), 100 °C, 16 h, yield of isolated products. Degree of D-incorporation was determined by ¹H-NMR.

With the optimized reaction conditions for the ruthenium(II)-catalyzed HIE reaction in hand, the robustness of the catalytic system towards APIs was studied (Table 3.4.5). Under the optimal reaction conditions 54% D-incorporation of repaglinide^[298] was observed in excellent levels of regioselectivity (entry 1). To improve the efficiency, it was found that a higher concentration was beneficial (entries 2-3). Moreover, an increased catalyst loading slightly ameliorated the degree of deuteration (entry 4). It is noteworthy than an increased amount of catalyst was helpful in case of APIs containing several functional groups, which otherwise could deactivate the ruthenium catalyst. Finally, a significant improvement in the direct deuteration was not observed, when a larger amount of deuterium oxide was employed (entry 5).

Table 3.4.5. Optimization studies for HIE of repaglinide **190u**.^[a]



Entry	Deviation from standard condition	Yield / %	<i>ortho</i> D / %
1	none	81	54
2	2.0 mL instead of 1.0 mL	78	56
3	0.50 mL instead of 1.0 mL	80	72
4	10 mol % [Ru] instead of 5.0 mol %	80	86
5	20 equiv of D ₂ O instead of 10 equiv	79	87

[a] Reaction conditions: **190u** (0.10 mmol), [Ru(O₂CAd)₂(*p*-cymene)] (5.0 mol %), D₂O (1.0 mmol), 1,4-dioxane (1.0 mL), 100 °C, 16 h, yield of isolated products. Degree of D-incorporation was determined by ¹H-NMR.

3.4.2. Scope of the Ruthenium(II)-Catalyzed Hydrogen Isotope Exchange

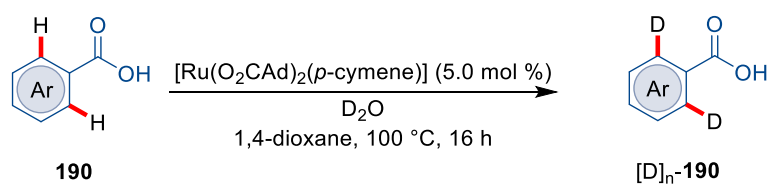
The performance of the ruthenium(II)-catalyzed hydrogen isotope exchange of benzoic acids derivatives **190** was explored under the optimal reaction conditions (Table 3.4.6). The desired isotopic labeled motifs from diversely-substituted benzoic acids **190a-p** were obtained with excellent yields and high levels of D-incorporation (entries 1–16). Indeed, electron-donating and electron-withdrawing substituents at the *ortho*-, *meta*- or *para*-positions were amenable to the HIE reaction, providing in almost all cases D-incorporations higher than 90%.

Although chloroarenes are well known electrophiles in cross-coupling reactions,^[121g] the chloro-substituted benzoic acids **190b**, **190g** and **190k** were fully tolerated. Furthermore, the HIE was fully compatible with valuable functional groups, such as nitro and cyano groups, highlighting the outstanding chemoselectivity of the ruthenium(II)-carboxylate catalysis. It was highlighted that the robustness of the HIE was well reflected by hydroxyl- **190o** or amino-substituents **190p**, while they could act as a potential ligand and therefore led to deactivation of the catalyst.^[299]

Besides the excellent functional group tolerance, the HIE of biologically relevant heterocyclic motifs was investigated. Different (hetero)arenes were tested under the reaction conditions (entries 17–20), yielding the desired products [D]_n-**190q-t** in high chemoselective and good to high levels of D-incorporations. Heterocyclic motifs, including indole **190q** and oxazepine **190t** were well tolerated resulting in the efficient incorporation of two deuterium atoms at the *ortho*-position to the carboxylic acid directing group. The chemoselective nature of the ruthenium(II)-catalyzed HIE regime was also mirrored by the absence of side reactions when bromo-substituted arene **190s** was employed.^[300] It is noteworthy that only poor D-incorporation in the C2-position of **190r** was observed, probably due to repulsive steric interactions.

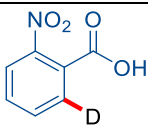
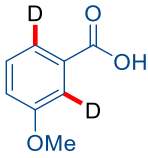
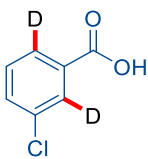
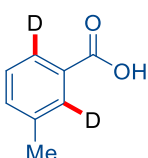
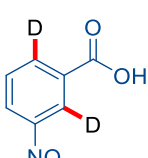
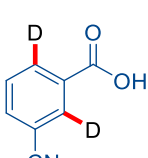
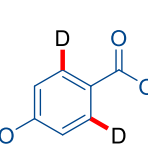
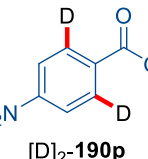
3. Results and Discussion

Table 3.4.6. Substrate scope for the ruthenium(II) biscalboxylate-catalyzed *ortho*-deuterium labeling.^[a]

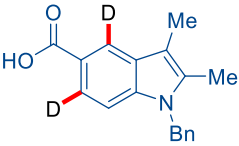
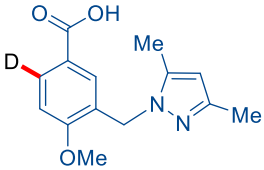
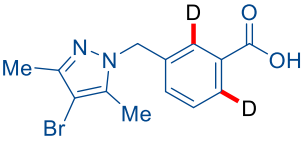
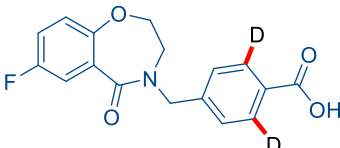


Entry	Product	Yield / %	<i>ortho</i> D / %
1	 [D]₂-190a	93	95
2	 [D]₂-190b	90	60
3	 [D]₂-190c	94	94
4	 [D]₂-190d	79	84
5	 [D]₂-190e	97	93
6	 [D]₁-190f	95	98
7	 [D]₁-190g	94	99
8	 [D]₁-190h	97	97

3.4. Hydrogen Isotope Exchange by Ruthenium-Catalyzed C–H Activation

Entry	Product	Yield / %	<i>ortho</i> D / %
9	 [D] ₁ - 190i	84	90
10	 [D] ₂ - 190j	92	C2: 96 C6: 96
11	 [D] ₂ - 190k	89	C2: 99 C6: 99
12	 [D] ₂ - 190l	95	C2: 98 C6: 98
13	 [D] ₂ - 190m	86	C2: 98 C6: 98
14	 [D] ₂ - 190n	95	C2: 90 C6: 81
15	 [D] ₂ - 190o	87	93
16	 [D] ₂ - 190p	86	87

3. Results and Discussion

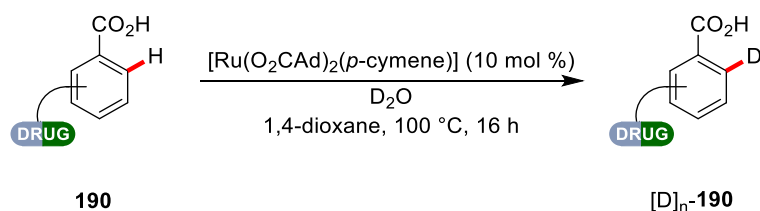
Entry	Product	Yield / %	<i>ortho</i> D / %
17	 [D] ₂ -190q	86	C4: 92 C6: 89
18	 [D] ₁ -190r	82	C6: 89 C2: 17
19	 [D] ₂ -190s	74	C2: 97 C6: 94
20	 [D] ₂ -190t	82	94

[a] Reaction conditions: **190** (0.50 mmol), [Ru(O₂CAd)₂(*p*-cymene)] (5.0 mol %), D₂O (5.0 mmol), 1,4-dioxane (1.0 mL), 100 °C, 16 h, yield of isolated products. Degree of D-incorporation was determined by ¹H-NMR.

Given the excellent performance of the ruthenium(II)-catalyzed HIE, the initial envisioned late-stage labeling of challenging pharmaceuticals was targeted. The HIE protocol was applicable to various APIs, affording the isotopically labeled analogs with moderate to excellent D-incorporation (Table 3.4.7). Important APIs, such as repaglinide -used for promoting insulin release from β-islet cells of the pancreas-, telmisartan -used as an angiotensin II receptor blocker to cardiovascular diseases-^[301] sulfasalazine -a medication to treat rheumatoid arthritis, ulcerative colitis and Crohn's disease-^[302] and bumetanide -a loop diuretic to treat swelling and high blood pressure-^[303] were fully compatible with the HIE reaction and showed excellent position-selective isotope labeling. Notably, the presence of other potential heteroatom-containing directing groups, such as benzimidazole and azo^[304] groups led to unexpected D-incorporation at the *ortho*-position to those groups.^[33a, 34] Moreover, the catalytic HIE was highlighted by tolerating structural motifs, like amide, free sulfonamide, secondary amine and α-amino-pyridines as well as azo-motifs.

3.4. Hydrogen Isotope Exchange by Ruthenium-Catalyzed C–H Activation

Table 3.4.7. Late-stage C–H deuteration of drugs by ruthenium(II) biscalboxylate-catalyzed HIE.^[a]



Entry	API	Product	Yield / %
1	Repaglinide	<p style="text-align: center;">[86] [D] [D]₁-190u</p>	80
2	Telmisartan	<p style="text-align: center;">[50] D [50] [50] D [50] [D]₂-190v</p>	76
3	Sulfasalazine	<p style="text-align: center;">[40] D [40] [40] D [50] [D]₂-190w</p>	72
4	Bumetanid	<p style="text-align: center;">[97] D [97] [95] D [97] [D]₂-190x</p>	73

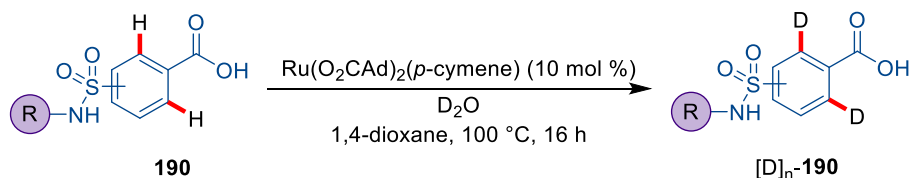
[a] Reaction conditions: **190** (0.10 mmol), [Ru(O₂CAd)₂(*p*-cymene)] (10 mol %), D₂O (1.0 mmol), 1,4-dioxane (0.50 mL), 100 °C, 16 h, yield of isolated products. [X] Degree of D-incorporation was determined by ¹H-NMR.

In addition to complex pharmaceuticals various biologically active sulfonamides were probed (Table 3.4.8).^[305] To our delight, sulfonamides **190y-ab** were all isotopically labeled in an excellent fashion without any solubility issues^[306] or inhibition by functional groups, such as free amino or hydroxyl groups (entries 1–4). In addition, cyclic structures

3. Results and Discussion

like furan **190z** and lactam **190aa** were tolerated under the ruthenium(II)-catalyzed C–H activation regime. Notably, an enforced coordination of the ruthenium catalyst with the carboxylic acid and sulfonamide cannot be ruled out, since both are known directing groups in C–H activation methodologies.^[43d, 305c, 307]

Table 3.4.8. Late-stage C–H deuteration of sulfonamides by ruthenium(II) biscarboxylate-catalyzed HIE.^[a]



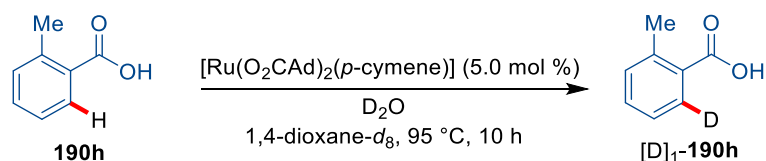
Entry	Product	Yield / %
1	 [97] [D] ₁ - 190y	92
2	 [75] [98] [D] ₁ - 190z	79
3	 [95] [D] ₁ - 190aa	88
4	 [93] [25] [93] [D] ₃ - 190ab	73

[a] Reaction conditions: **190** (0.10 mmol), $\text{Ru}(\text{O}_2\text{CAr})_2(p\text{-cymene})$ (10 mol %), D_2O (1.0 mmol), 1,4-dioxane (0.50 mL), 16 h, 100 °C, yield of isolated products. [X] Degree of D-incorporation was determined by ¹H-NMR.

3.4.3. Mechanistic Studies

3.4.3.1. *In-operando* NMR studies

To gain insights into the HIE the kinetic profile of **190h** was followed by *in-operando* ^1H -NMR spectroscopy (Scheme 3.4.1). The synthetic utility of the ruthenium(II) biscalboxylate-catalyzed HIE was highlighted by the fast rate of the HIE, yielding >78% D-incorporation after 5 h (Figure 3.4.2).



Scheme 3.4.1. *In-operando* NMR studies for the ruthenium(II) biscalboxylate-catalyzed HIE.

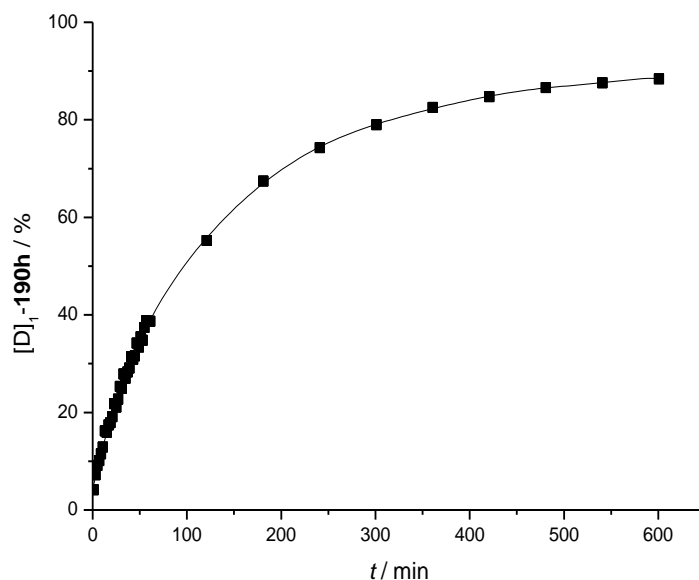
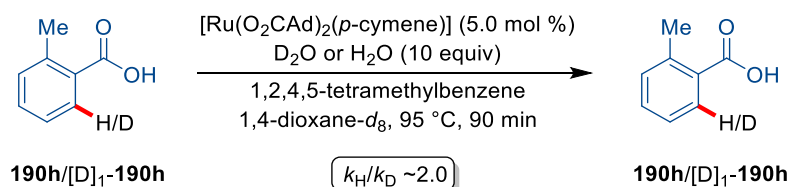


Figure 3.4.2. Reaction profile of the ruthenium(II) biscalboxylate-catalyzed HIE.

3.4.3.2. KIE Studies

To gain a deeper mechanistic understanding of the C–H activation elementary step, independent KIE experiments of *o*-toluic acid (**190h**) and **[D]₁-190h** were performed (Scheme 3.4.2). In this reaction, a KIE of $k_{\text{H}}/k_{\text{D}} \sim 2.0$ was obtained, supporting a rate-determining C–H activation.



Scheme 3.4.2. Independent KIE studies for the ruthenium(II) biscalboxylate-catalyzed HIE.

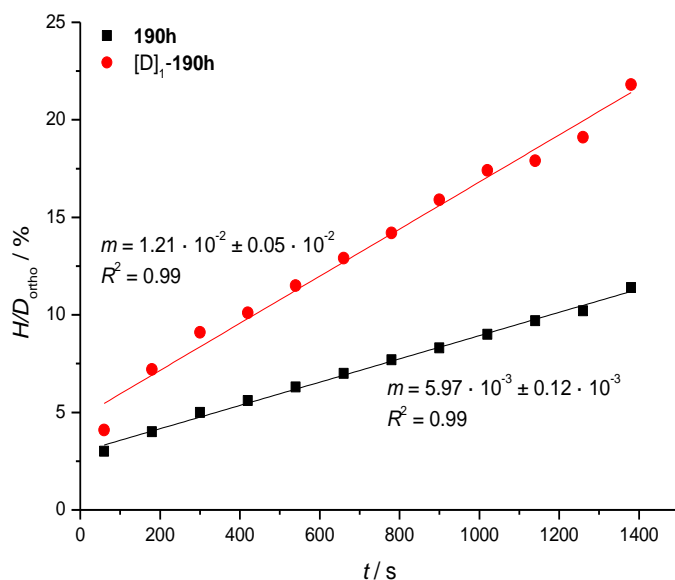
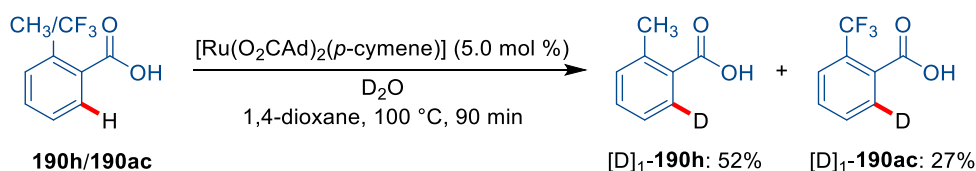


Figure 3.4.3. Independent KIE studies for the ruthenium(II) biscalboxylate-catalyzed HIE.

3.4.3.3. Intermolecular Competition Experiment

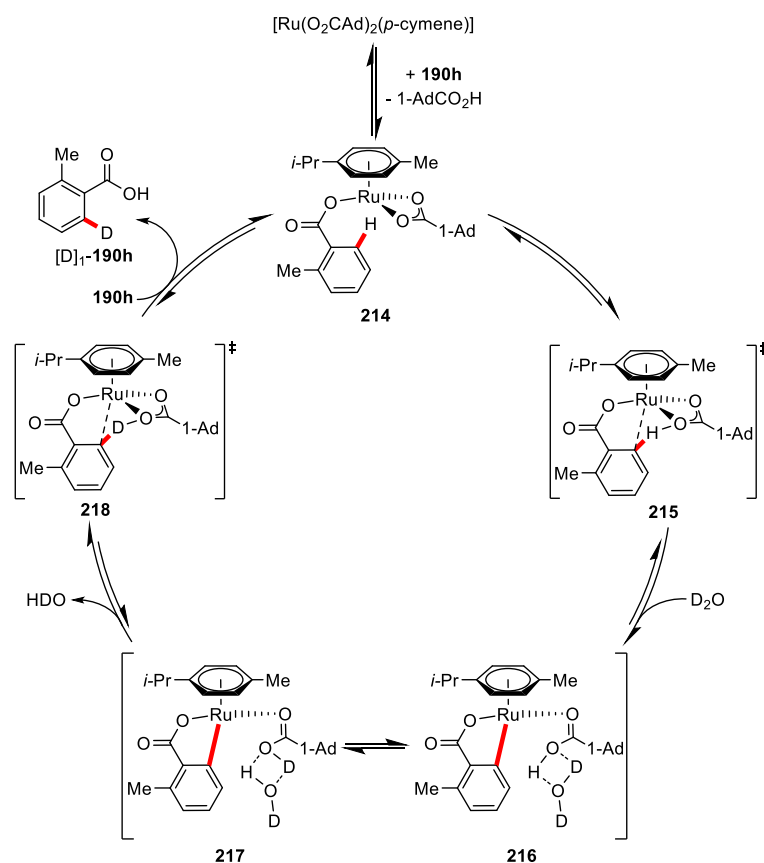
To evaluate the C–H activation mechanism, an intermolecular competition experiment between the electron-rich *o*-toluic acid (**190h**) and electron-poor trifluoromethyl substituted analog **190ac** was conducted (Scheme 3.4.3). Notably the experiment showed a strong preference for the electron-rich substrate **190h** which was indicative of the C–H activation occurring through a BIES-type mechanism.^[43b, 43c, 308]



Scheme 3.4.3. Intermolecular competition experiment by ruthenium(II) biscalboxylate-catalyzed HIE.

3.4.4. Proposed Catalytic Cycle

On the basis of our mechanistic findings and previous reports on directed ruthenium(II)-catalyzed direct C–H activations,^[126h, 132, 290] a plausible catalytic cycle for the present HIE was proposed (Scheme 3.4.4). Initiated by a ligand exchange with **190h**, the ruthenium(II)-carboxylate complex **214** is formed. **214** then undergoes the rate-determining C–H scission step by a BIES type mechanism to form the *ortho*-metalated ruthenacycle **216**. H/D exchange of the hydro-carboxylate ligand with a deuterium oxide leads to a deuterium-carboxylate ligand **217**. Finally, proto-demetalation of the cyclometalated complex **218** facilitated by **190h** generates the desired product [D]₁-**190h** and regenerates the active catalyst **214**.

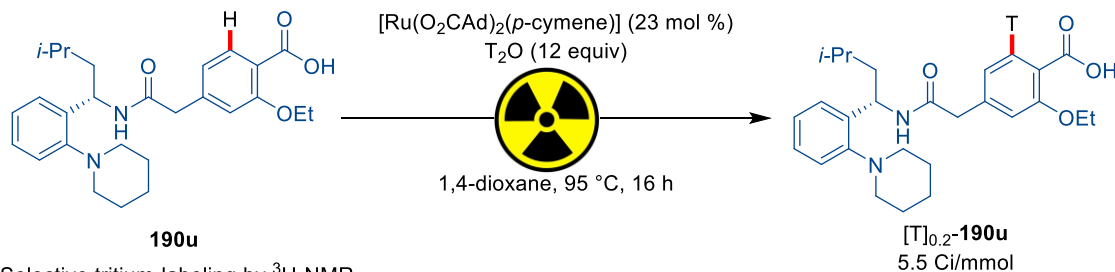


Scheme 3.4.4. Proposed catalytic cycle for ruthenium-catalyzed HIE.

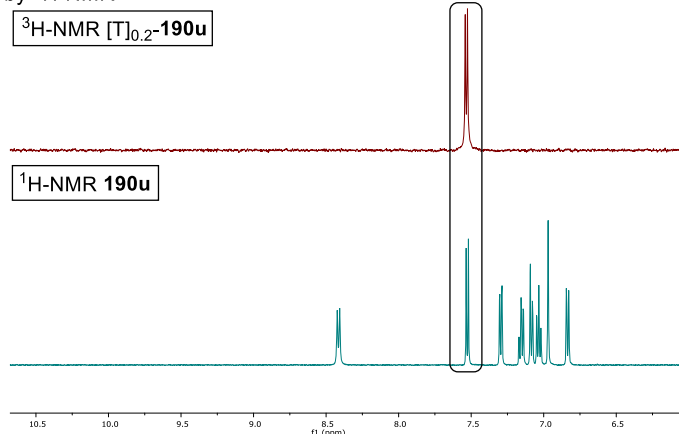
3.4.5. Tritiation of Pharmaceuticals

Based on the high performance of the H/D exchange the *ortho*-selective tritium-labeling of pharmaceuticals with T₂O, generating metabolically stable sites that are compatible to different functional groups was tackled. Considering the previous results, tritium oxide can be suitable to facilitate the HIE, since the reaction with low amounts of deuterium oxide worked well. Therefore, the late-stage tritiation of pharmaceuticals was studied in collaboration with Remo Weck and Dr. Volker Derdau from Sanofi-Aventis Deutschland GmbH. In this context, the HIE with freshly prepared deuterium oxide^[309] resulted in a reduced D-incorporation of the API repaglinide, which was a promising result towards the use of tritium oxide.^[216] Considering that tritium oxide is always a mixture of HDO/HTO,^[310] the developed catalysis seemed suitable due to its reactivity and stability to facilitate first HDO and second HTO activation in an efficient manner. Under slightly modified reaction conditions, tritium was introduced in moderate specific activity highlighting this highly selective C–H activation methodology for late-stage drug modifications (Scheme 3.4.5).

a) Tritiation of repaglinide



b) Selective tritium-labeling by ³H-NMR



Scheme 3.4.5. Ruthenium-catalyzed tritiation performed by Remo Weck and Dr. Volker Derdau of a) repaglinide **190u** in b) a selective fashion.

3.5. Recyclable Ruthenium Catalysts for remote C–H Alkylations

The catalytic functionalization of aromatic C–H bonds by the aid of transition metals has undergone tremendous development during the last decade.^[22] While numerous advances deal with the *ortho*-selective functionalizations of arenes by a directing group approach,^[33a, 36] a deeper understanding of the geometric relationship between the C–H bond and the transition metal furnished advances in *meta*- and *para*-selective transformations,^[22g, 166h] overwriting enthalpic and entropic effects that favor conformationally rigid five-, six-, and occasionally seven-membered cyclometalated intermediates.^[163a] In this context, template- or transient mediator-assisted palladium catalysis^[160] and catalytic σ -activation by *ortho* C–H metalation enabled by ruthenium catalysis^[166] are so far the most promising methods to achieve remote C–H functionalizations. Inspired by the presence of numerous motifs in pharmaceutical drugs and bioactive compounds and the importance of heterogeneous catalysis in chemical industry,^[311] the development of novel recyclable catalysts for remote C–H functionalizations is highly desirable (Figure 3.5.1).^[312]

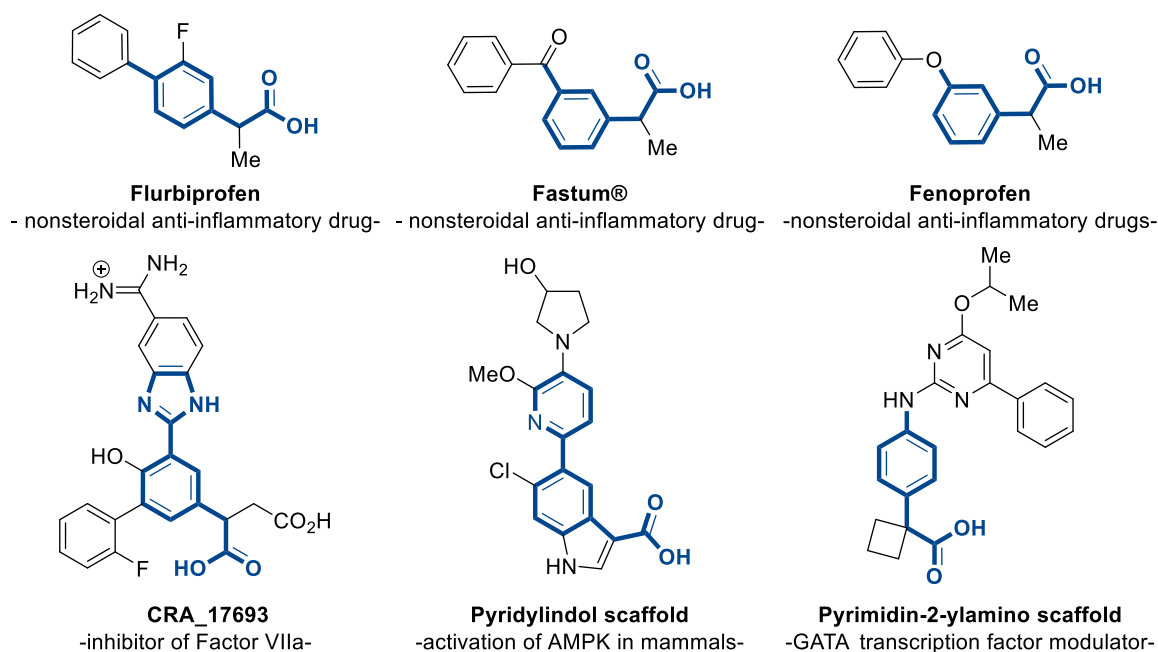
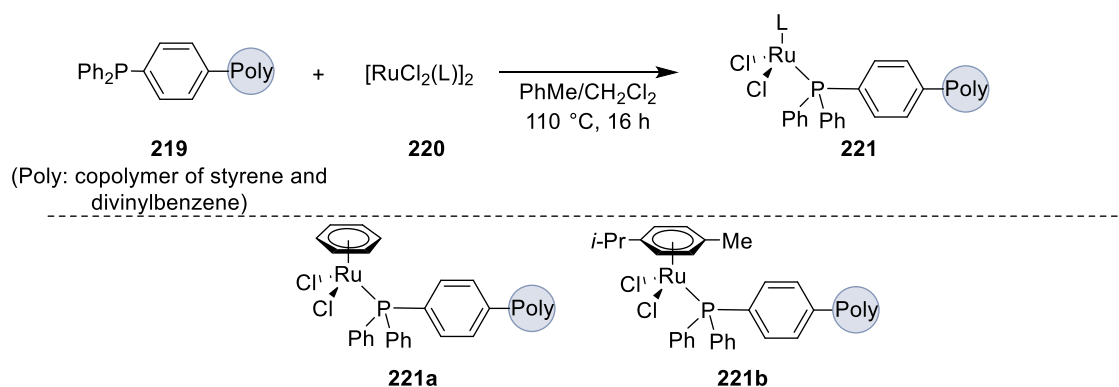


Figure 3.5.1. Selected examples of relevant remote substituted heterocycles.

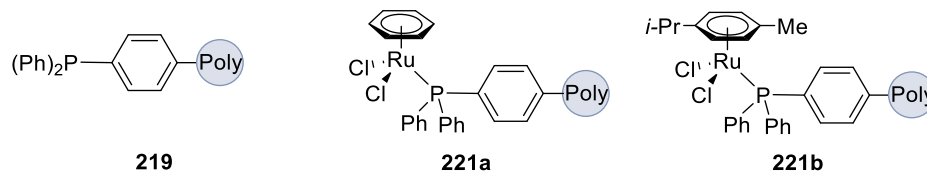
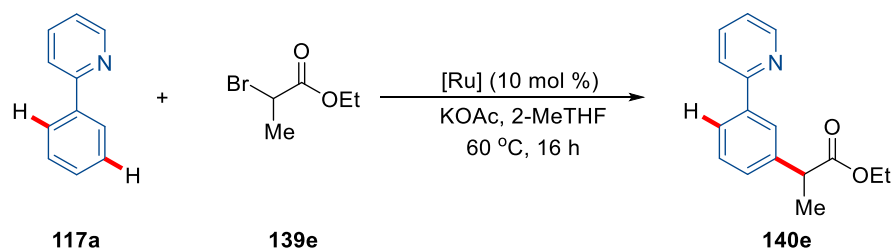
3.5.1. Optimization Studies of *meta* C–H Alkylations by Recyclable Ruthenium Catalyst

Given the broad applicability of remote ruthenium catalysis in combination with phosphine ligands,^[166a, 166b, 175-176] the development of a recyclable catalyst for *meta*-selective functionalizations was attempted. In this context, the preparation of the novel hybrid ruthenium complex **221a** and the previously reported analogue **221b** by polymer-supported phosphine was successful.^[202b, 313] Both hybrid complexes were accessible by an user-friendly protocol (Scheme 3.5.1).



Scheme 3.5.1. Preparation of hybrid ruthenium catalysts **221**.

With the hybrid ruthenium complexes **221a** and **221b** in hand, their reactivity was probed for various *meta*-selective C–H activations. Based on optimization studies by Isaac Choi both hybrid ruthenium catalysts were feasible for *meta* C–H alkylations in biomass-derived 2-MeTHF (Table 3.5.2).^[314] Notably, the good yield and outstanding chemoselectivity of the first run was also achieved when using the recycled catalyst for the second run (entries 1–2). Furthermore, control experiments showed the essential role of the base due to the formation of KBr (entry 3).^[166b, 166e, 166f, 314] Control experiments revealed the necessity of the hybrid ruthenium catalyst and the non-essential nature of the polymer bond phosphine (entries 4–5). When probing other recyclable ruthenium sources,^[196, 315] the important role of the support was reflected, as only the hybrid ruthenium catalysts **221** envisioned the desired functionalization (entries 6–7). Probably the defined metal ligand sphere is key to success for this functionalization, which is achieved far better by the polymer bond phosphine compared to other solid supports.^[201a, 316] In this context, the amounts of ruthenium in the hybrid ruthenium catalysts were determined by detailed inductive coupled plasma-optical emission spectrometry (ICP-OES) analysis.^[314]

Table 3.5.2. *meta* C–H functionalization by heterogeneous ruthenium catalyst.^[a]

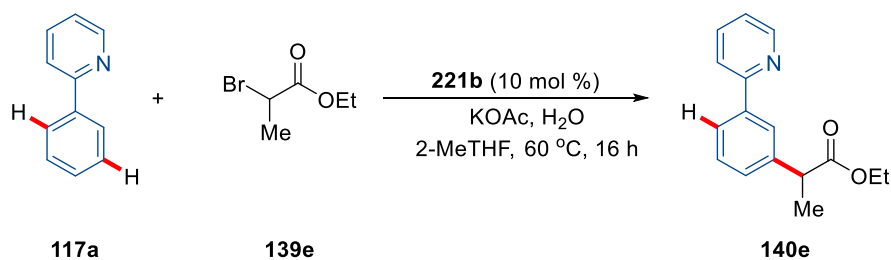
Entry	[Ru]	Yield / %	
		1 st run	2 nd run
1	221a	66	64
2	221b	69	68
3 ^[b]	221a	n.r.	n.d.
4	-	n.r.	n.d.
5	219	n.r.	n.d.
6	Ru@SiO ₂ (191)	n.r.	n.d.
7	Ru@NDCs-800	n.r.	n.d.

[a] Reaction conditions: **117a** (0.25 mmol), **139e** (0.75 mmol), [Ru] (10 mol %), KOAc (0.50 mmol), 2-MeTHF (2.0 mL), 24 h, 60 °C, yield of isolated products. [b] Without KOAc. “n.d.” not determined.

Considering the huge potential of heterogeneous catalysis for industrial processes combined with numerous recent applications in flow^[317] chemistry a flow reaction setup was envisioned. Unfortunately, during the course of the *meta* C–H functionalization by hybrid ruthenium catalyst the formation of insoluble particles prevented the use of flow systems to a certain point. In this context, the addition of various amounts of water to facilitate the solubility was probed (Table 3.5.3). To our delight, no particles due to the added water were observable here. Nevertheless, by adding water the reaction and recycling studies revealed a poorer performance. The results showed clearly that high concentrations of water resulted in a poor conversion combined with no recyclability (entries 1–2). When lowering the amount of added water, a higher reactivity was observed. Nonetheless, the recycling studies revealed that water deactivated the hybrid ruthenium catalyst by cleavage of the coordinated phosphine.^[318]

3. Results and Discussion

Table 3.5.3. Influence of water for the *meta* C–H functionalization by hybrid ruthenium catalyst.^[a]

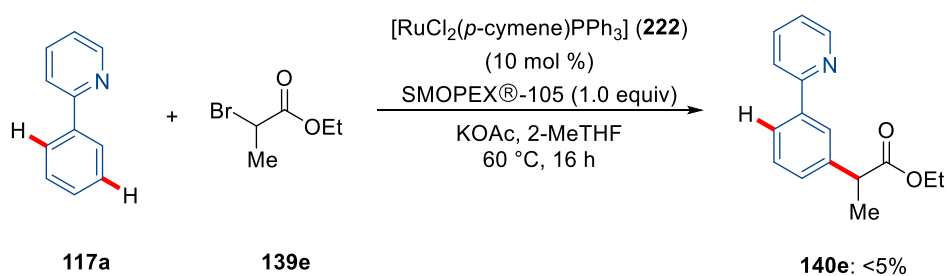
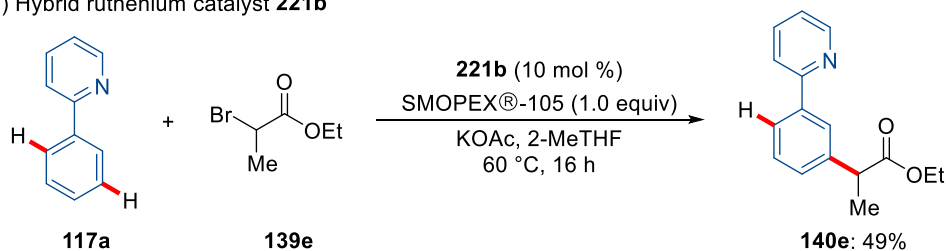


Entry	H ₂ O [mL]	Yield / %	
		1 st run	2 nd run
1	2.0	n.r.	n.d.
2	1.0	13	n.r.
3	0.25	40	34
4	0.10	69	45

[a] Reaction conditions: **117a** (0.25 mmol), **139e** (0.75 mmol), **221b** (10 mol %), KOAc (0.50 mmol), H₂O (0.10–2.0 mL) 2-MeTHF (2.0 mL), 24 h, 60 °C, yield of isolated products. “n.d.” not determined.

3.5.2. Test of Heterogeneity for *meta* C–H Alkylations by Recyclable Ruthenium Catalyst

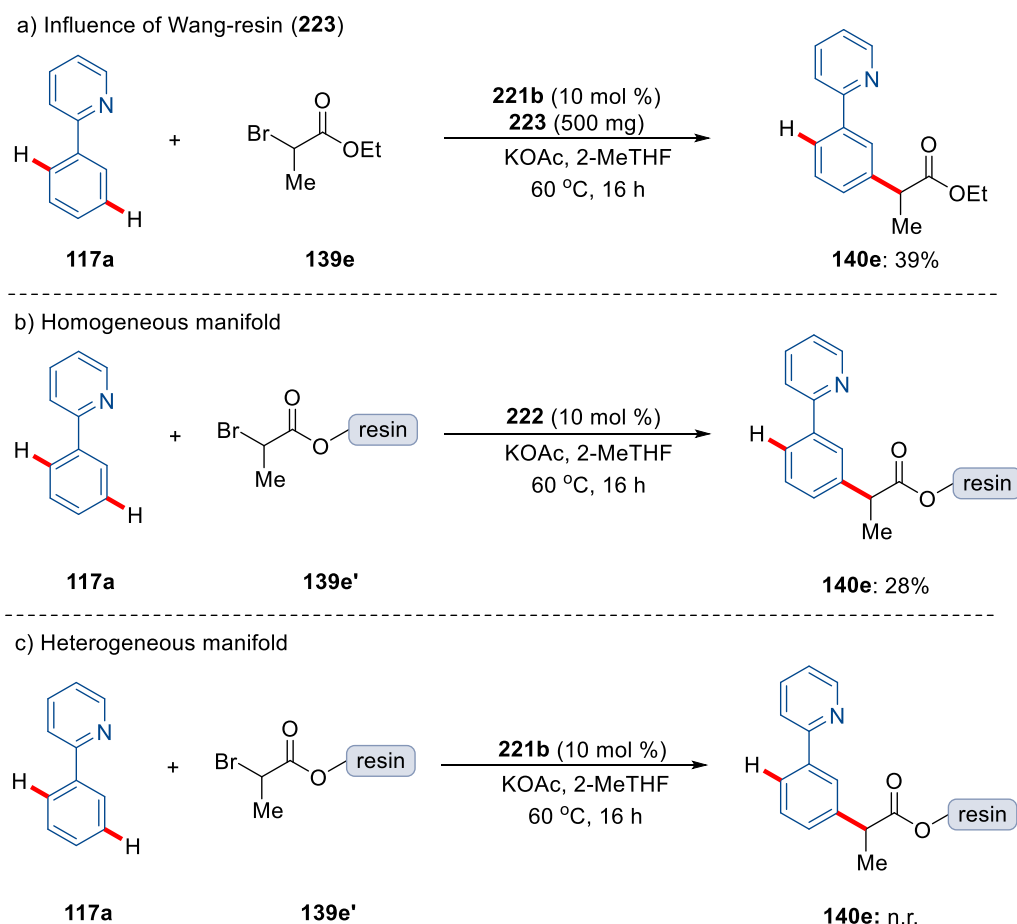
Interested in the heterogeneous and reusable nature of the hybrid ruthenium catalyst, detailed experimental studies to proof the heterogeneity and studied the morphology of the hybrid ruthenium catalysis by spectroscopic and microscopic methods were performed. In this context, the catalyst could be reused up to five times without a significant lack in efficiency. Notably, less than 8 ppm of ruthenium were detected by detailed ICP-OES studies of the reaction mixtures, reflecting a negligible leaching of the transition metal. Based on this excellent reusability and recyclability of the hybrid ruthenium catalyst, the heterogeneous nature was demonstrated. In this context, a poisoning test with SMOPEX®-105 was performed,^[319] which clearly showed the inhibition of the homogeneous ruthenium catalysis (Scheme 3.5.1a). In stark contrast, the hybrid catalysis occurred in the presence of the metal scavenger SMOPEX®-105, emphasizing that trace amounts of leached ruthenium do not facilitate the catalysis (Scheme 3.5.1b).

a) Homogeneous ruthenium catalyst **222**b) Hybrid ruthenium catalyst **221b**

Scheme 3.5.1. Poison test with SMOPEX®-105.

Furthermore, a three-phase test was performed to illustrate the heterogeneous mode of action (Scheme 3.5.2).^[188b, 188c] Therefore, the influence of Wang-resin (**223**) was probed within the catalysis, resulting in a slightly decreased yield, probably due to diffusion control (Scheme 3.5.2a).^[320] Next, the role of the homogeneous ruthenium catalyst $[\text{RuCl}_2(p\text{-cymene})\text{PPh}_3]$ (**222**) was studied by adding the modified Wang-resin **139e'**.^[314] The result showed clearly that the homogeneous catalyst facilitated the reaction (Scheme 3.5.2b). Finally, a three-phase test was performed with the hybrid catalyst **221b** and the modified Wang-resin **139e'** (Scheme 3.5.2c). Notably, no reaction was observed, rendering homogeneous catalysis unlikely to be operative.

3. Results and Discussion



Scheme 3.5.2. Three-phase test.

In addition to the recyclable and reusable nature of the hybrid ruthenium catalyst, the chemical and physical properties were determined (Figure 3.5.2).^[321] Together with Dr. Kai Xue and Dr. Loren Andreas detailed solid-state NMR spectroscopic (ssNMR) studies of **219**, **221b**, and reused **221b** were conducted (Figure 3.5.2a). Interestingly, the ¹³C and ³¹P-NMR spectra showed similar chemical shifts, providing strong evidence that the coordination of the ruthenium by phosphorus remained stable during the course of the catalysis. Furthermore, X-ray photoelectron spectroscopy (XPS) studies by Dr. Yanhui Wang and Dr. Johan G. Alauzun confirmed the presence of a ruthenium(II) species (Figure 3.5.2b). In addition, the excellent stability of coordination between phosphorus and ruthenium was supported by TEM-EDX mapping studies (Figure 3.5.2c). Further characterization studies have been reported elsewhere and are not included in this thesis.^[314]

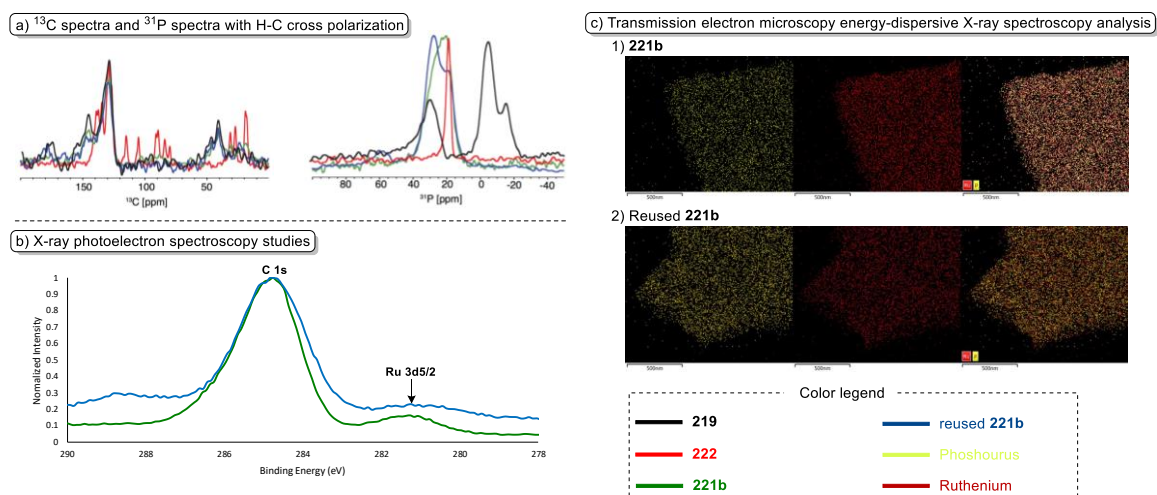


Figure 3.5.2. Characterization of **221b** before and after the catalysis by a) ssNMR spectroscopic by Dr. Kai Xue and Dr. Loren Andreas and b) XPS, c) TEM-EDX by Dr. Yanhui Wang and Dr. Johan G. Alauzun.

3.5.3. Scope of *meta* C–H Alkylations by Recyclable Ruthenium Catalyst

Interested in the versatility of the envisioned recyclable ruthenium-catalyzed *meta* C–H alkylation, the effect of various α -bromoester **139e-s** in combination with 2-phenylpyridine **117a** was probed under the optimized reaction conditions (Table 3.5.4). Among a series of different esters, the tether had no significant influence on the reactivity and selectivity (entries 1–3). Furthermore, a benzyl substituent at the ester is well tolerated without any byproduct formation (entry 4). Nonetheless, a slight drop in yield was observed for α -bromoester **139i** bearing a tetrahydrofuran motif (entry 5). On the same line, the hydroquinone derived alkylating reagent **139j** performed well during the course of the reaction, showing no deactivation of the catalysis due to the hydroxyl group or the reducing nature (entry 6).

Interested in the substitution pattern at the α -position of the ester, various substrates were probed. Among these, sterically more demanding **139k** did not influence the *meta* C–H alkylation (entry 7). Notable, an additional bromo substituent was well tolerated generating the desired product with good yield and excellent selectivity (entry 8). Importantly, the reaction was not limited to α -bromoester, since the amide derived alkylating reagent **139m** showed good reactivity as well (entry 9). Based on the broad applicability towards α -bromoester, esters derived from bioactive scaffolds were tested, such as menthol, cholesterol and borneol. To our delight, the *meta*-selective C–H alkylation proceeded smoothly without byproduct formation or evidence for racemization

3. Results and Discussion

(entries 10–12). Considering the complexity of the natural product derived alkylating reagents the obtained yields are acceptable.

With respect to the limitations of the substrate scope, *tert*-butylbromid (**139q**) was not converted under otherwise identical reaction conditions, probably due to repulsive steric effects (entry 13). In this regard, when using the α -unsubstituted reagent **139r** or the difluoro analog **139s**, only trace amounts of the corresponding products were detected, which is probably a result of the unfavored radical stabilization in the α -position (entries 14–15).^[322]

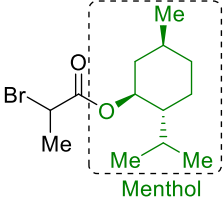
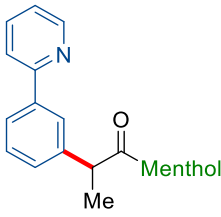
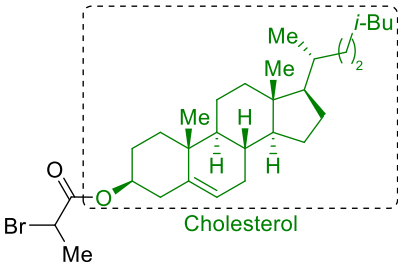
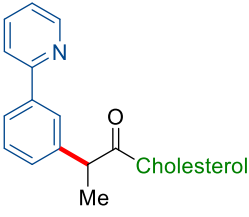
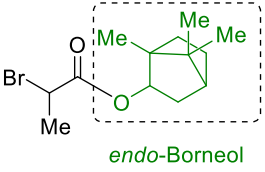
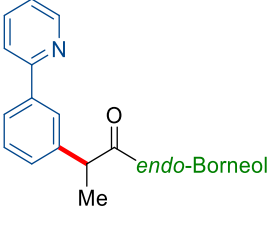
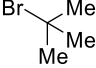
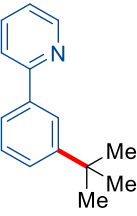
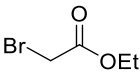
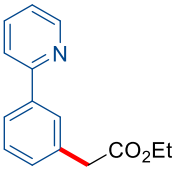
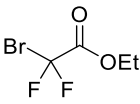
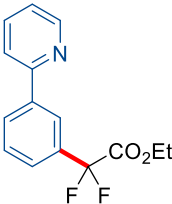
Table 3.5.4. Scope of various α -bromoester for recyclable *meta* C–H functionalization.^[a]

Entry	Alkyl bromid	140	Yield / %
1	 139e	 140e	69
2	 139f	 140f	71
3	 139g	 140g	64

3.5. Recyclable Ruthenium Catalysts for remote C–H Alkylations

Entry	Alkyl bromid	140	Yield / %
4	 139h	 140h	74
5	 139i	 140i	62
6	 139j	 140j	68
7	 139k	 140k	64
8	 139l	 140l	58
9	 139m	 140m	70

3. Results and Discussion

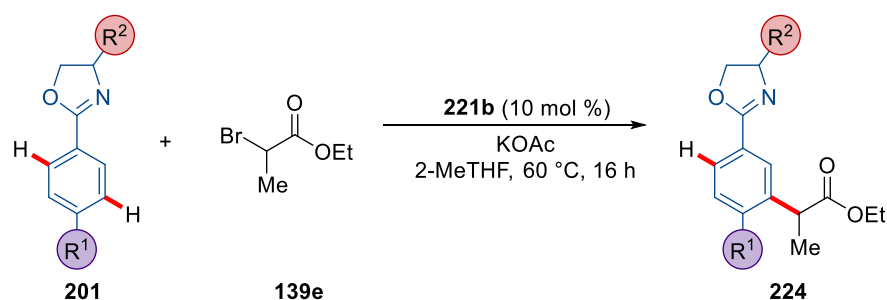
Entry	Alkyl bromid	140	Yield / %
10	 <p>139n</p>	 <p>140n</p>	64
11	 <p>139o</p>	 <p>140o</p>	63
12	 <p>139p</p>	 <p>140p</p>	59
13	 <p>139q</p>	 <p>140q</p>	n.r.
14	 <p>139r</p>	 <p>140r</p>	n.r.
15	 <p>139s</p>	 <p>140s</p>	n.r.

[a] Reaction conditions: **117a** (0.25 mmol), **139** (0.75 mmol), **221b** (10 mol %), KOAc (0.50 mmol), 2-MeTHF (2.0 mL), 24 h, 60 °C, yield of isolated products.

Besides the significant advances towards numerous α -bromoester, the focus was next directed to other valuable directing groups. In this context, oxazolines are key structural motifs in bioactive natural products and readily accessible synthetic intermediates which can easily be modified into a wealth of diverse functional groups.^[323] Especially in terms of remote C–H alkylations 2-aryloxazolines are interesting since *ortho*-functionalizations through directed *ortho*-metalation (DoM),^[324] as well as *ortho*-selective C–H activations are well documented.^[61a, 325]

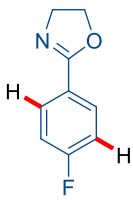
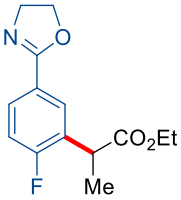
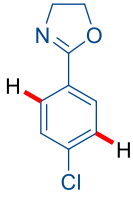
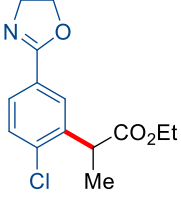
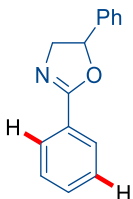
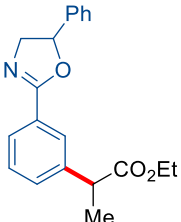
With the optimized hybrid ruthenium system in hand, the versatility and robustness of the recyclable remote C–H alkylation was investigated by using various 2-phenyloxazolines (Table 3.5.5). A wealth of electron-rich as well as electron-deficient substituents were fully tolerated in the transformation, affording products **224e–g** in good to excellent yield (entries 1–3). Remarkably, the chloro-substituent was successfully transformed into the desired product with complete position-selectivity (entry 4). Sterically demanding substituents in the backbone of the oxazoline were fully tolerated and did not affect the catalysis (entry 5).

Table 3.5.5. Scope of various 2-aryloxazolines **201** for recyclable *meta* C–H functionalizations.^[a]



Entry	Oxazoline	224	Yield / %
1	<p style="text-align: center;">201e</p>	<p style="text-align: center;">224e</p>	55
2	<p style="text-align: center;">201f</p>	<p style="text-align: center;">224f</p>	86

3. Results and Discussion

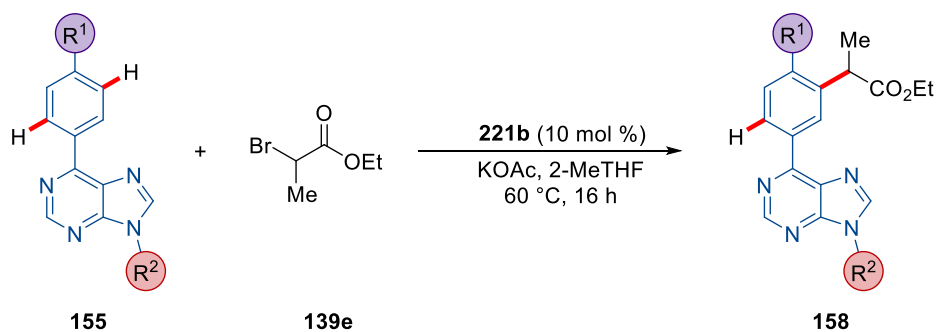
Entry	Oxazoline	224	Yield / %
3	 <p>201g</p>	 <p>224g</p>	65
4	 <p>201h</p>	 <p>224h</p>	66
5	 <p>201i</p>	 <p>224i</p>	69

[a] Reaction conditions: **201** (0.25 mmol), **139e** (0.75 mmol), **221b** (10 mol %), KOAc (0.50 mmol), 2-MeTHF (2.0 mL), 24 h, 60 °C, yield of isolated products.

Inspired by the robustness of the recyclable ruthenium-catalyzed *meta* C–H functionalization, the functionalization of otherwise unreactive C–H bonds in bio-relevant purines were probed,^[326] since modified purine bases were found to exhibit biological activity.^[327] When using the well-defined hybrid ruthenium catalyst **221b**, differently decorated purine-derived substrates **155** were efficiently converted (Table 3.5.6). In this context, *N*-substituted purines **155a–g** performed excellent within the catalysis with no dependence on the *N*-substitution pattern (entries 1–7). Notably, a clear preference for electron-donating substituents was observed, which was supportive of a radical intermediate.^[322b, 322d, 328] Furthermore, the position-selectivity of the hybrid ruthenium catalysis was highlighted by the elusive formation of the desired product **158g**, without byproduct formation due to C–Cl activation.^[121g, 126e, 329] Finally, the *meta* C–H alkylation was found to be scalable and provided product **158f** in a gram-scale reaction without loss of catalytic efficacy.

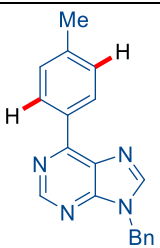
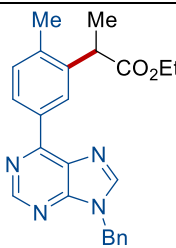
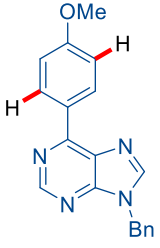
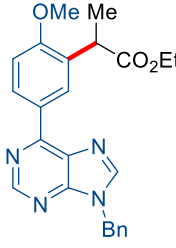
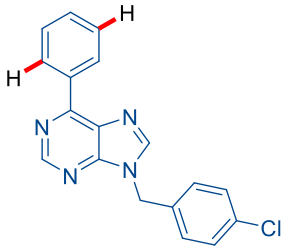
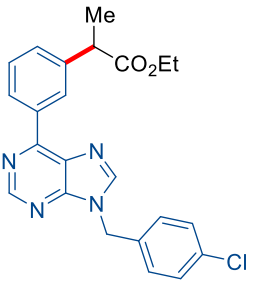
3.5. Recyclable Ruthenium Catalysts for remote C–H Alkylations

Table 3.5.6. Scope of various purines **155** for recyclable *meta* C–H functionalizations.^[a]



Entry	Purine	158	Yield / %
1	<p>155a</p>	<p>158a</p>	92
2	<p>155b</p>	<p>158b</p>	93
3	<p>155c</p>	<p>158c</p>	94
4	<p>155d</p>	<p>158d</p>	81

3. Results and Discussion

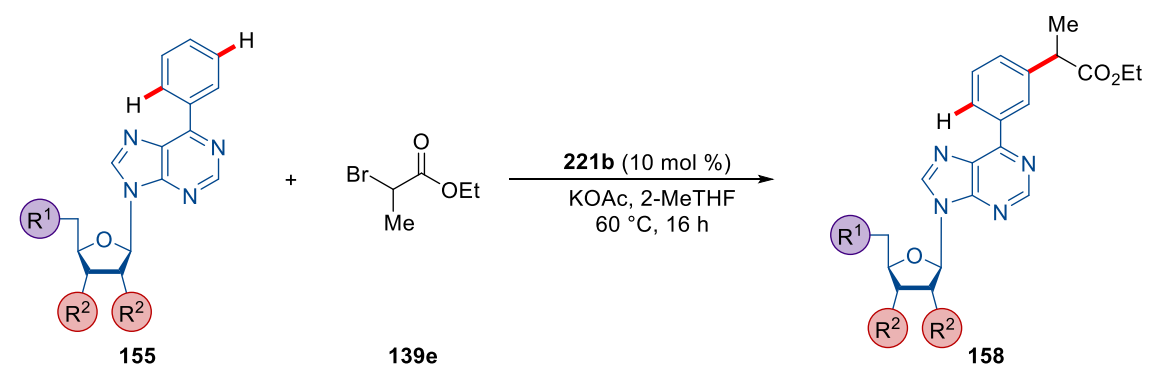
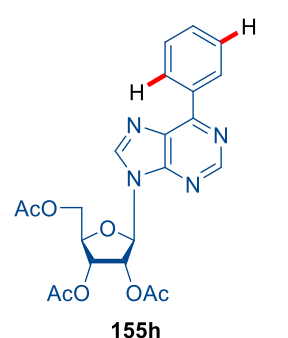
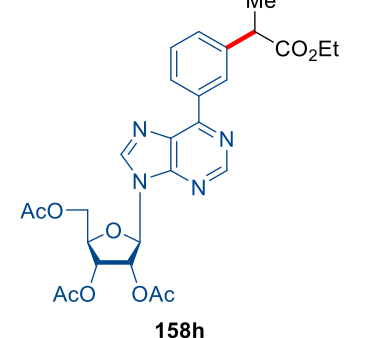
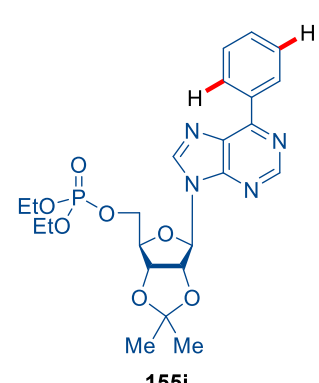
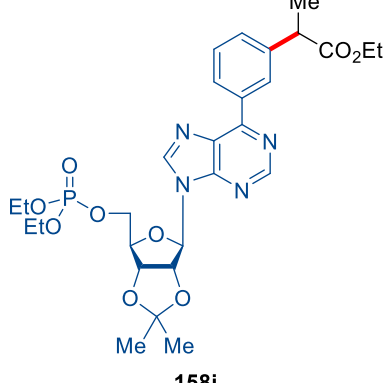
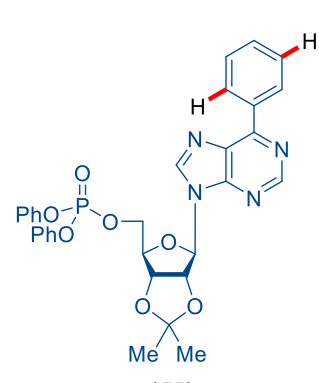
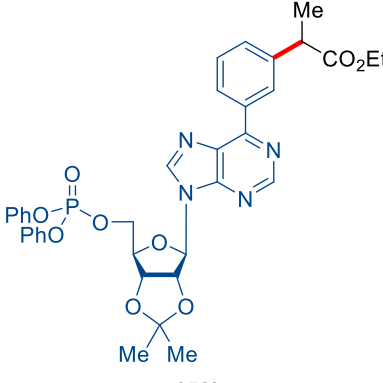
Entry	Purine	158	Yield / %
5	 <p>155e</p>	 <p>158e</p>	83
6	 <p>155f</p>	 <p>158f</p>	88 92 (1.15 g)
7	 <p>155g</p>	 <p>158g</p>	79

[a] Reaction conditions: **155** (0.25 mmol), **139e** (0.75 mmol), **221b** (10 mol %), KOAc (0.50 mmol), 2-MeTHF (2.0 mL), 24 h, 60 °C, yield of isolated products. The yield in parenthesis was obtained in the gram-scale reaction.

Inspired by the broad applicability of the developed hybrid ruthenium *meta* C–H alkylation regime, the late-stage diversification of sensitive nucleosides was subsequently attempted (Table 3.5.7).^[330] Remarkably, the robustness of the catalysis enabled the manipulation of the highly reactive nucleosides unaffected by the *O*-protecting groups (entry 1). Furthermore, it is notable that the catalysis proceeded in an efficient fashion, even when a sensitive phosphorylation was present in the substrates **158i–j** (entries 2–3).

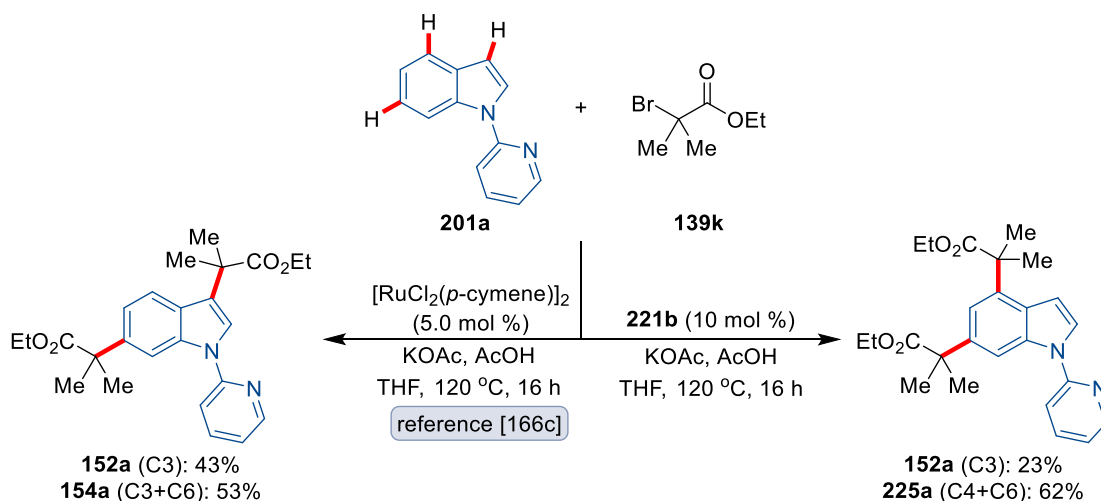
3.5. Recyclable Ruthenium Catalysts for remote C–H Alkylations

Table 3.5.7. Scope of various nucleosides **155** for recyclable *meta* C–H functionalizations.^[a]

Entry	Nucleoside	Product	Yield / %
			
1	 <p>155h</p>	 <p>158h</p>	86
2	 <p>155i</p>	 <p>158i</p>	80
3	 <p>155j</p>	 <p>158j</p>	78

[a] Reaction conditions: **155** (0.25 mmol), **139e** (0.75 mmol), **221b** (10 mol %), KOAc (0.50 mmol), 2-MeTHF (2.0 mL), 24 h, 60 °C, yield of isolated products.

Although a broad range of heteroarenes and alkyl reagents were transformed within the *meta*-selective hybrid ruthenium catalysis, the reactivity remains similar with respect to homogeneous analogs. In this context, a different selectivity with the versatile catalyst **221b** was envisioned. Considering the importance of derivatized biologically relevant indoles and the challenge in achieving position selective C–H functionalizations in those structures,^[331] the recyclable hybrid ruthenium regime was probed for a novel selectivity. As a model system, the remote C3/C6 alkylation of indole **201a** was chosen.^[166c] To our delight, the versatile hybrid ruthenium catalyst **221b** forced the catalysis to a novel selectivity compared to homogeneous ruthenium catalysis (Scheme 3.5.3). Notable, while the homogeneous system yielded the C3/C6-isomer as minor product, the hybrid ruthenium catalyst **221b** yielded the unpresented dialkylated indole **225a** as major product.

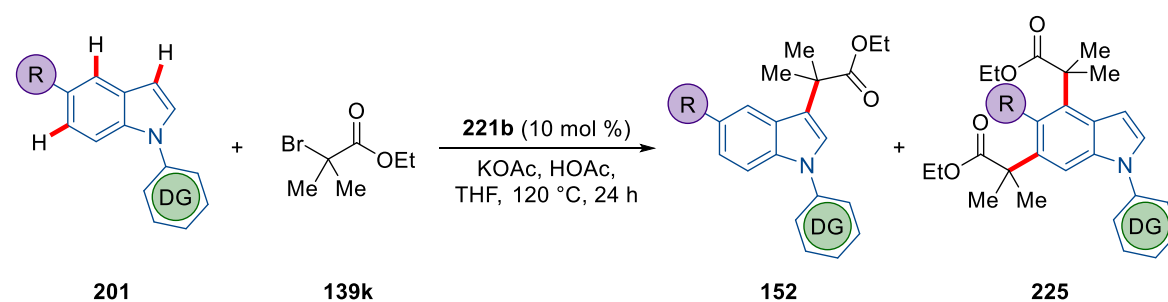


Scheme 3.5.3. Novel selectivity of hybrid ruthenium catalysis **221b**.

Interested in the novel selectivity, the applicability was extended towards various *N*-substituted indoles **201** (Table 3.5.8). Remarkably, both pyridyl- as well as pyrimidyl-directing groups formed the desired C4/C6 dialkylated indoles as the main product (entries 1–4). Nevertheless, the formation of the C3 alkylated indole, as a result of the cyclometalation at the C2-position and the accompanying increase of electron-density was always detected.^[166c] Unfortunately, when the substitution pattern at the indole or the directing group was more complex, a mixture of products was observed (entries 5–10).

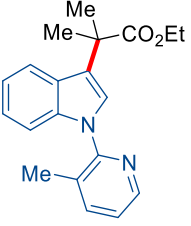
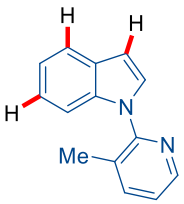
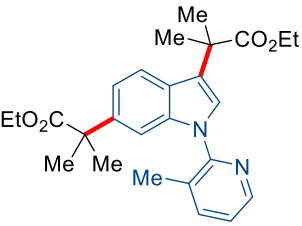
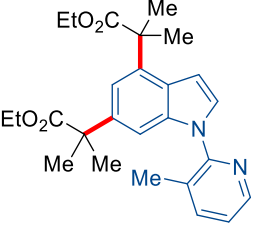
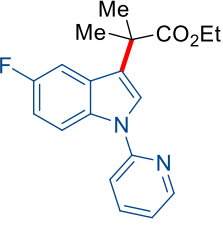
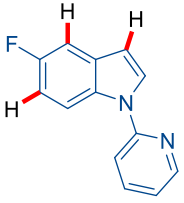
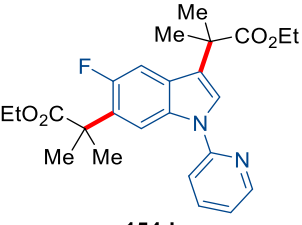
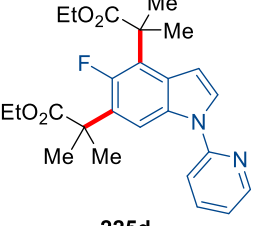
3.5. Recyclable Ruthenium Catalysts for remote C–H Alkylations

Table 3.5.8. Scope of indole **201** for recyclable C4/C6 C–H functionalizations.^[a]



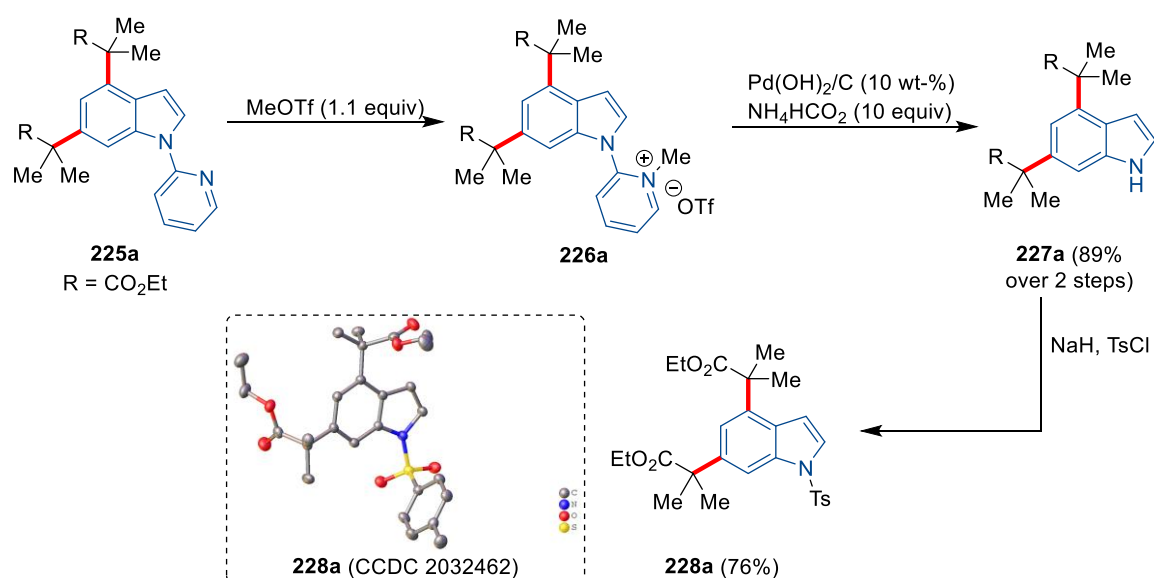
Entry	Indole	Product	Yield / %
1			23
2			62
3			22
4			57

3. Results and Discussion

Entry	Indole	Product	Yield / %
5		 152c	25
6	 201j	 154c	23
7		 225c	26
8		 152d	26
9	 201k	 154d	25
10		 225d	27

[a] Reaction conditions: **201** (0.25 mmol), **139k** (0.75 mmol), **221b** (10 mol %), KOAc (0.50 mmol), AcOH (0.50 mmol), THF (1.0 mL), 24 h, 120 °C, yield of isolated products.

Although the C4/C6 dialkylated indoles **225c** and **225d** were the major formed isomers, the C3/C6 dialkylated indoles **154c** and **154d** and C3 alkylated indoles **152c** and **152d** were also formed, reflecting a high dependence on the electronic nature of the substrate.^[166c] The value of the hybrid ruthenium-catalyzed C–H alkylation was further demonstrated by diversification of the thus obtained product (Scheme 3.5.4). Since the cleavage of the pyridyl group is well documented, the synthetically useful indole **227a** was easily assessable.^[43b, 332] Subsequent functionalization of the NH-free-indole **227a** provided *N*-tosylindole **228a**, which was unambiguously characterized by X-ray diffraction crystallography.

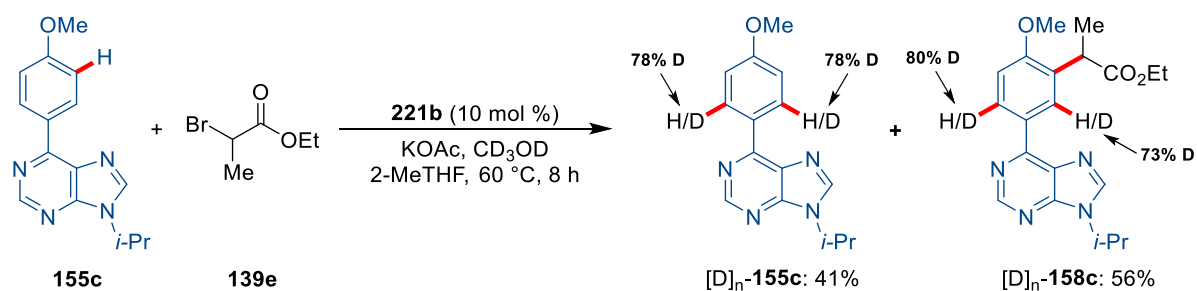


Scheme 3.5.4. Removal of the directing group and diversification of **227a**. The crystal structure **228a** was measured and resolved by Dr. Christopher Golz.

3.5.4. Mechanistic Studies of *meta* C–H Alkylations by Recyclable Ruthenium Catalyst

3.5.4.1. H/D Exchange Experiments

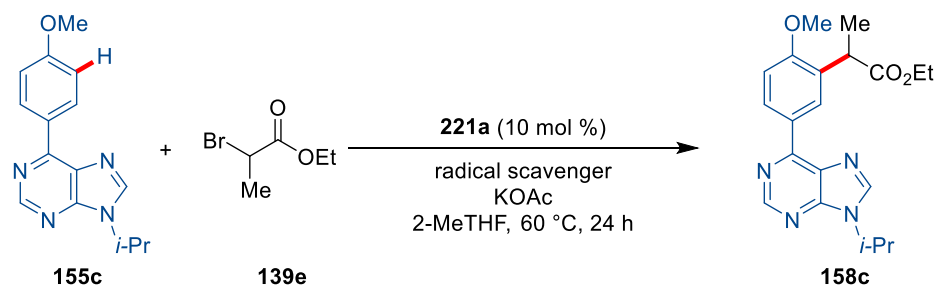
To unravel the mode of action of the hybrid ruthenium catalyst various mechanistic studies were performed. To study the mechanism of the C–H activation elementary step, an H/D-exchange experiment with CD₃OD as the co-solvent was conducted (Scheme 3.5.5). Importantly, a significant H/D-exchange in the *ortho*-position was observed, suggesting a facile and reversible C–H activation.



3.5.4.2. Effect of radical scavenger

Based on experimental evidence detailed experiments with common radical scavengers were conducted. Remarkably, a significant inhibition of the of *meta* C–H alkylation catalyzed by the hybrid ruthenium catalyst **221a** was observed, when typical radical scavengers TEMPO, galvinoxyl free radical, and 1,1-diphenylethylen were added (Table 3.5.9). These results emphasized a SET-type regime to be operative, indicating a radical intermediate. Furthermore, the detection of the TEMPO adduct **229** supported the radical formation at the α -position of the alkylating reagent.

Table 3.5.9. Effect of radical scavengers on remote ruthenium hybrid C–H functionalizations.^[a]

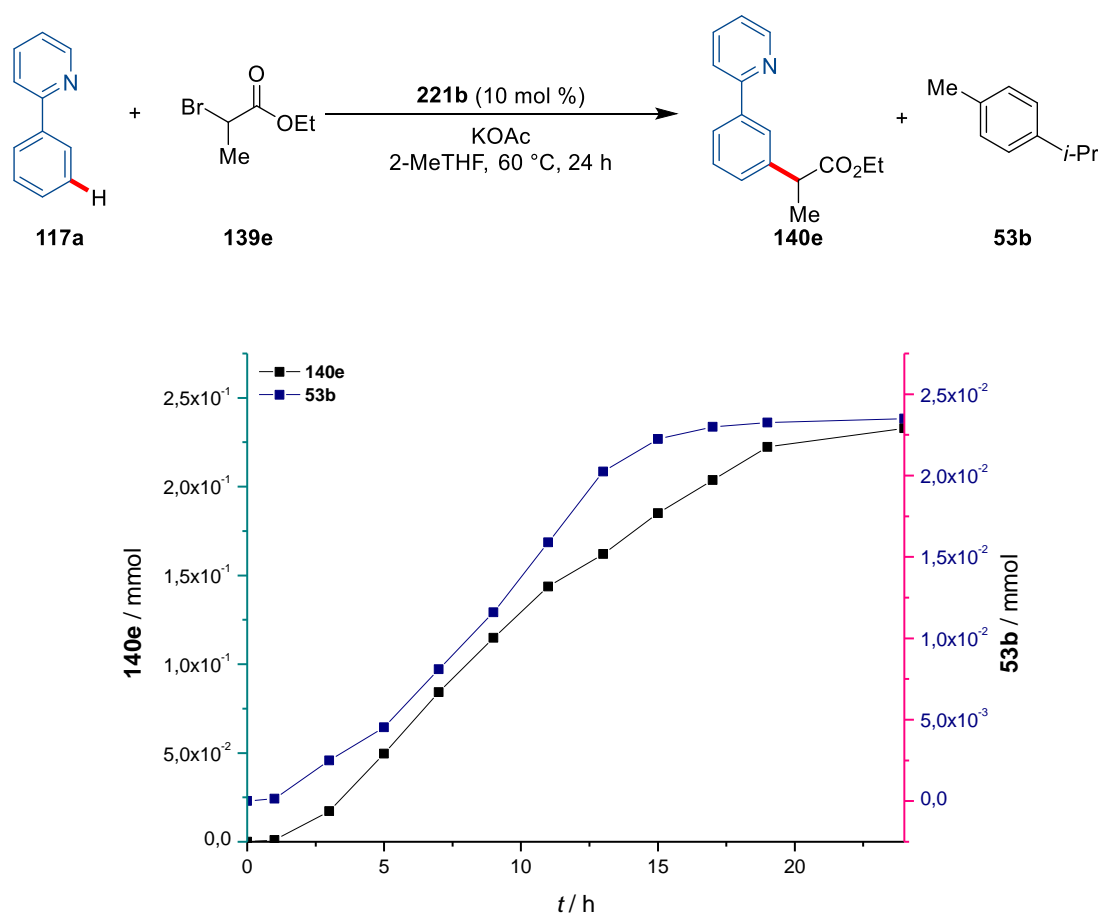


Entry	Radical scavenger	158c / %
1	-	94
2	TEMPO	n.r.
3	Galvinoxyl free radical	n.r.
4	1,1-Diphenylethylene	54

[a] Reaction conditions: **155c** (0.25 mmol), **139e** (0.75 mmol), **221a** (10 mol %), KOAc (0.50 mmol), radical scavenger (0.25 mmol), 2-MeTHF (2.0 mL), 24 h, 60 °C, yield of isolated products.

3.5.4.3. Detection of free *p*-cymene

Considering the importance of the phosphine-ruthenium coordination and the resulting arene dissociation during the course of the reaction, the amount of free *p*-cymene (**53b**) was quantified (Scheme 3.5.6). It is notable that Ackermann reported previously on an arene-free ruthenium pre-catalyst.^[176] The results determined by GC analysis with *n*-dodecane as the internal standard showed, that the dissociation of *p*-cymene is proportional to the formed product **140e**.

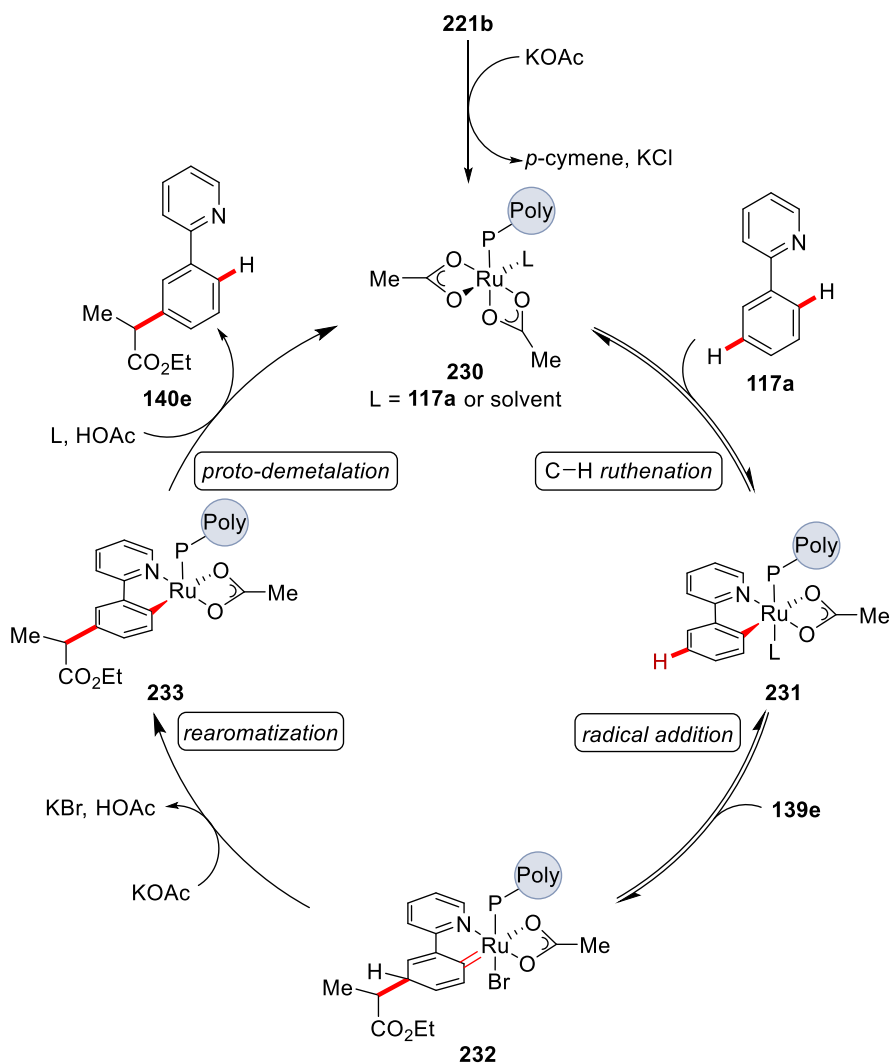
Scheme 3.5.6. Detection of free *p*-cymene (**53b**) by GC analysis.

3.5.5. Proposed Catalytic Cycle

On the basis of our detailed experimental and computational^[314] mechanistic studies a plausible catalytic cycle for the heterogeneous *meta* C–H alkylation was proposed (Scheme 3.5.7). Notably, based on the analogous mechanistic aspects to those in homogeneous catalysis,^[166, 175-176] similar elementary steps were suggested, reflecting that

3. Results and Discussion

hybrid catalysts have a predictable reactivity. The catalysis is initiated by carboxylate-assisted C–H ruthenation, yielding complex **231**.^[38a] Subsequently, ruthenium(III) intermediate is generated *via* a SET from the ruthenium(II) complex **231** to the alkyl halide **139e**. The alkyl radical attacks at the position *para* to ruthenium, giving intermediate **232**. Thereafter, rearomatization generates intermediate **233**, which yields the desired *meta*-alkylated product **140e** and regenerates the catalytically active ruthenium(II) complex **230** *via* proto-demetalation.



Scheme 3.5.7. Proposed catalytic cycle for *meta*-selective hybrid ruthenium catalysis.

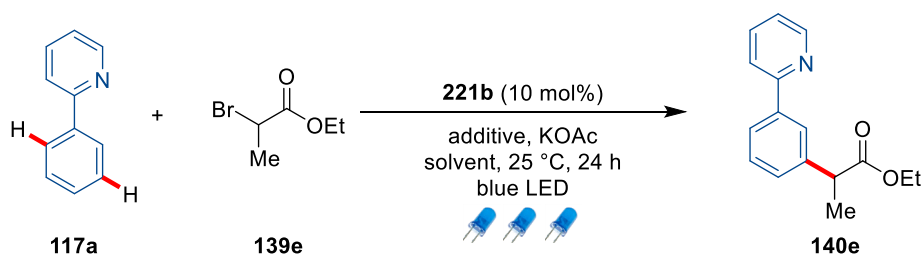
3.5.6. Optimization Studies of Photo-induced *meta* C–H Alkylation by Recyclable Ruthenium Catalyst

Despite indisputable progress, the σ -activation approach is often limited to elevated reaction temperatures, which affect the selectivity and the functional group tolerance.^[22g, 166] In this context, photo-induced C–H functionalization has emerged as a powerful tool for molecular synthesis both in terms of classical *ortho*-functionalizations and homogeneous remote C–H functionalizations.^[177-178, 333] Inspired by the robustness of the developed hybrid ruthenium catalysis, the recyclable photo-induced remote C–H alkylation was tackled.

Initial studies with reaction conditions similar to previously described homogeneous *meta* C–H functionalizations were performed (Table 3.5.10).^[166f, 172, 179] Unfortunately, carboxylic acid or carboxylate additives did not result in good conversion or no recyclability (entries 1–3). Probably, the formation of the well reported ruthenium-biscarboxylate complex $[\text{Ru}(\text{O}_2\text{Mes})_2(p\text{-cymene})]$ furnished the cleavage of the hybrid linker.^[126h] Furthermore, diphenylphosphoric acid established by Ackermann for photo-induced remote C–H alkylation did not facilitate the transformation (entry 4).^[177] In this context, a related methodology developed by Greany showed the beneficial effect of additional water.^[178] The *meta*-alkylated product **140e** was isolated in moderate yield due to the addition of 5 equivalents of H₂O and blue light irradiation at room temperature (entry 5). Notably, the recycled hybrid ruthenium catalyst showed a similar reactivity in the photocatalysis. It is noteworthy that the exact role of water is still under investigation, but it is assumed to facilitate the cycloruthenation.^[178] Control experiments confirmed the essential role of the ruthenium catalyst, the base and the visible light (entries 6–8). In addition, no improvement was observed when various amounts of water or of the catalyst were used (entries 9–10). Remarkably, the catalysis was accessible with water as the solvent, however preventing the recyclability similar to the previous results (entry 11). Furthermore, other solvents proved less efficient for the envisioned recyclable photo-induced C–H functionalization (entries 12–16).

3. Results and Discussion

Table 3.5.10. Optimization for photo-induced *meta* C–H alkylation by recyclable ruthenium catalyst.^[a]



Entry	Additive	Solvent	Yield / %	
			1 st Run	2 nd Run
1	-	2-MeTHF	n.r.	n.d.
2 ^[b]	MesCO ₂ H (30 mol %)	2-MeTHF	43	n.r.
3	MesCO ₂ Na (30 mol %)	2-MeTHF	n.r.	n.d.
4	(C ₆ H ₅ O) ₂ P(O)OH (30 mol %)	2-MeTHF	n.r.	n.d.
5	H ₂ O (5.0 equiv)	2-MeTHF	57	51
6 ^[c]	H ₂ O (5.0 equiv)	2-MeTHF	n.r.	n.d.
7 ^[d]	H ₂ O (5.0 equiv)	2-MeTHF	n.r.	n.d.
8 ^[e]	H ₂ O (5.0 equiv)	2-MeTHF	n.r.	n.d.
9	H ₂ O (10 equiv)	2-MeTHF	52	n.d.
10 ^[f]	H ₂ O (10 equiv)	2-MeTHF	53	n.d.
11	-	H ₂ O	52	n.r.
12	H ₂ O (5.0 equiv)	1,4-dioxane	43	n.d.
13	H ₂ O (5.0 equiv)	PhMe	22	n.d.
14	H ₂ O (5.0 equiv)	<i>m</i> -xylene	n.r.	n.d.
15	H ₂ O (5.0 equiv)	DCE	37	n.d.
16	H ₂ O (5.0 equiv)	THF	13	n.d.

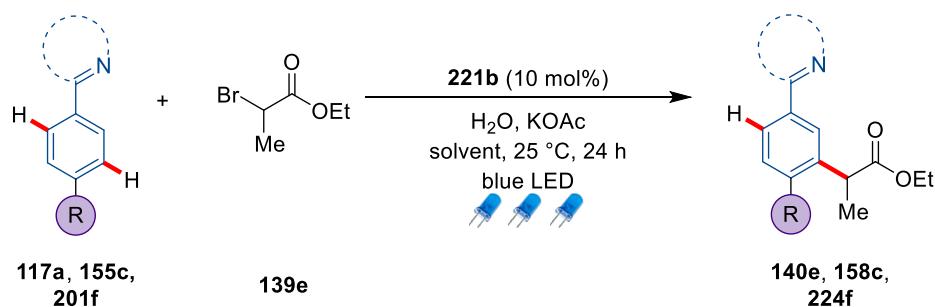
[a] Reaction conditions: **117a** (0.25 mmol), **139e** (0.75 mmol), **221b** (10 mol %), additive (0.30–5.0 equiv), KOAc (0.50 mmol), solvent (2.0 mL), 24 h, 25 °C, blue LED, yield of isolated products. [b] Na₂CO₃ (0.50 mmol) instead of KOAc. [c] The vessel was covered with Al-foil. [d] Without **221b**. [e] Without KOAc. [f] **221b** (20 mol %). “n.d.” not determined.

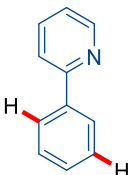
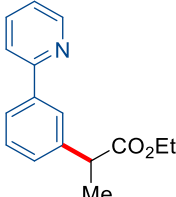
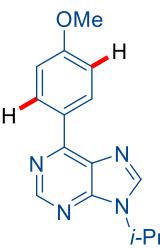
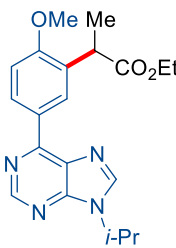
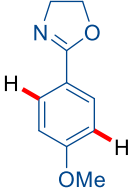
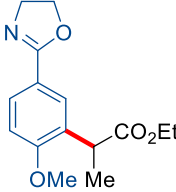
3.5.7. Scope of Photo-induced *meta* C–H Alkylation by Recyclable Ruthenium Catalyst

With the optimized reaction conditions established, the versatility of the photo-induced *meta* C–H alkylation of various heteroarenes was investigated (Table 3.5.11). A variety of biologically important structural motifs were transformed in an acceptable manner within

the novel hybrid ruthenium catalysis (entries 1–3). Remarkably, electron-rich purine **155c** and oxazoline **201f** showed good reactivity with synthetically meaningful α -bromo esters. Although the recycled catalyzed still facilitated the catalysis in a moderate fashion, a decreased activity was observed. Since an oxidation of the phosphine-linker could occur during the photocatalysis, an accompanied cleavage of the hybrid-linker could not be completely ruled out.^[334] Nevertheless, the robust hybrid ruthenium catalysis proved valid for remote C–H alkylations, promoting future methodological developments.

Table 3.5.11. Scope of photo-induced *meta* C–H alkylation by recyclable ruthenium catalyst.^[a]



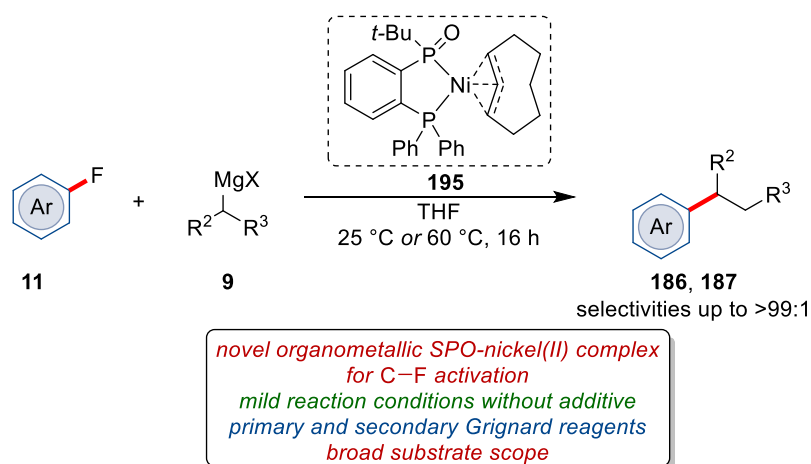
Entry	Substrate	Product	Yield / %	
			1 st Run	2 nd Run
1	 117a	 140e	57	51
2	 155c	 158c	65	54
3	 201f	 224f	62	48

[a] Reaction conditions: **117a/155c/201f** (0.25 mmol), **139e** (0.75 mmol), **221b** (10 mol %), KOAc (0.50 mmol), H₂O (5.0 equiv), solvent (2.0 mL), 24 h, 25 °C, blue LED, yield of isolated products.

4. Summary and Outlook

The development of novel environment-friendly, step- and atom-economical methodologies is one of the main goals in organic chemistry. In this context, the direct functionalization of C–H bonds has emerged as an environmentally-benign alternative that avoids lengthy syntheses and stoichiometric amounts of waste, and has therefore attracted broad interest with applications also to chemical industries. In consideration of the omnipresence of C–H bonds in organic molecules, a selective activation remains challenging and the development of novel methodologies is in high demand. In this thesis, several methods have been devised that revealed the remarkable efficiency, diversity and sustainability of non-expensive ruthenium(II) and earth-abundant manganese(I) and nickel(II) catalysis.

In the first project, the synthesis of the bidentate SPO/nickel catalyst **195** for the activation of otherwise inert C–F bonds was envisioned.^[335] The reduced rate of the β -hydride elimination enabled the utilization of primary and secondary alkylating reagents and resulted in a robust C(sp²)–C(sp³) cross-coupling with high levels of selectivity (Scheme 4.1).^[87] Under the mild reaction conditions, a wealth of electron-rich and electron-deficient arenes **11** proved suitable for this transformation, yielding the alkylated arenes in a position-selective fashion.

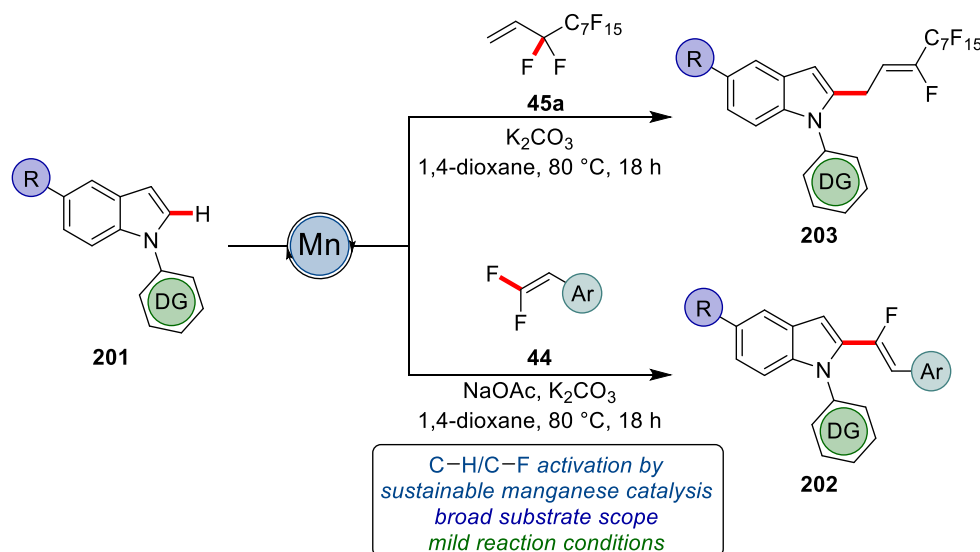


Scheme 4.1. C–F activation for C(sp²)–C(sp³) cross-coupling by a SPO-nickel complex.

These findings highlight the enhanced efficiency of the new tailor-made SPO pre-ligand based-catalyst. One of the main challenges for further research is the development of a catalyst broadly applicable towards various highly stable electrophiles under similar reaction conditions. To this end, a detailed understanding of the mechanism supported by

experimental and computational studies is required.^[231a] Furthermore, based on the excellent branched selectivity, the development of asymmetric nickel-catalyzed C–F activations is a further goal, especially since chiral analogs of established bidentate SPOs were previously reported.^[230]

Due to the importance of fluorine in biologically active compounds and agrochemicals, novel methods to form C–F bonds are in high demand. The second project addressed this challenging C–F bond formation *via* β -fluoroelimination. By earth-abundant manganese catalysis, uncommon C–H/C–F functionalizations were developed utilizing *gem*-difluoro hydrocarbons or *gem*-(per)fluorinated alkenes (Scheme 4.2).^[92b] The C–H/C–F functionalizations set the stage for a variety of step-economical (per)fluoro allylations and alkenylations exclusively resulting in the forming of the (*Z*)-isomer. Furthermore, the manganese regime was characterized by comparatively mild reaction conditions and broad substrate scope, including bromides, ketones and ketimines as well as biologically meaningful indoles and terpenes.

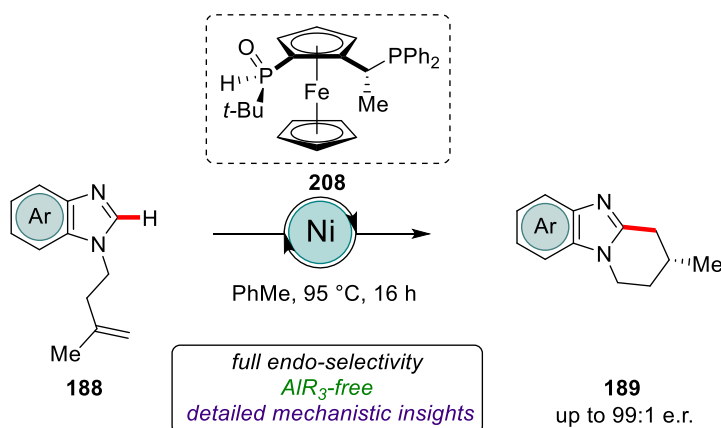


Scheme 4.2. C–H/C–F functionalization by manganese(I) catalysis.

The developed catalysis demonstrates the huge potential of C–H/C–F functionalizations accompanied by C–F bond formation, for catalysis since only a singular example was reported before.^[91] Inspired by this methodology numerous C–H/C–F functionalizations at room temperature,^[92a] with different selectivity^[93b, 336] or broader scope of applications^[93a, 93c] were reported.

4. Summary and Outlook

C–H activation methodologies based on 3d metal catalysts attracted considerable attention during the last decade with a broad applicability in organic synthesis.^[22b] Particular, chiral molecules are of enormous importance for pharmaceutical industry,^[337] thus justifying the development of novel asymmetric C–H functionalizations. Therefore, the development of a nickel-catalyzed asymmetric *endo*-selective cyclization of azoles with alkenes was intended. In sharp contrast to established nickel-catalyzed intramolecular hydroarylations with unactivated alkenes, the developed methodology does not rely on the use of pyrophoric organoaluminium reagents (Scheme 4.3). Various substituted benzimidazoles, including electron-rich and electron-poor derivatives, performed well in this transformation. Moreover, the reaction was not limited to benzimidazoles **188** and a broad variety of bioactive heterocyclic motifs, including highly functionalized purines and theophylline derivatives, were efficiently converted to the cyclized products **189**. Detailed mechanistic studies provided support for the formation of an organometallic nickel(II) species and a kinetically-relevant coordination of a second benzimidazole.

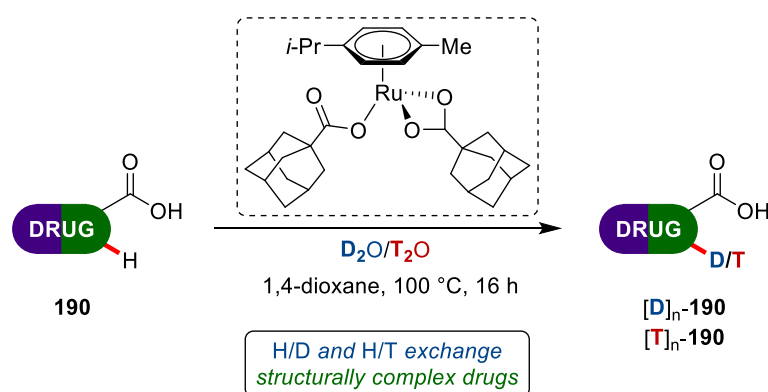


Scheme 4.3. Enantioselective aluminum-free alkene hydroarylations *via* C–H activation by a chiral nickel/JoSPOphos manifold.

The developed nickel(II)-JoSPOphos catalysis bears great potential, since SPO pre-ligands are well-established in cross-coupling chemistry.^[230a, 230b] An application of these methods with respect to asymmetric induction would be an inspiration for future developments. Furthermore, the inherent electronic bias of azoles enabled selective C2 functionalizations. By changing the electronic properties or the reaction regime an extension towards other position-selective functionalizations could be realized.^[338] Finally, since most nickel-catalyzed enantioselective C–H functionalizations are

intramolecular transformations, the need for more challenging intermolecular reactions is high.^[109c, 207a]

Inspired by the broad accessibility of metal-catalyzed C–H activations new methodologies on stable-isotope-labeled compounds were developed.^[135, 137] The undesired multi-step procedures combined with the requirement of easy to handle isotope reagents, characterize HIE as a sustainable methodology. Although methods for the late-stage labeling of APIs were established during the last years, ruthenium catalysts gained momentum, since they need to be compatibility with various functional groups. The well-defined ruthenium(II)-catalyst enabled selective HIE on various challenging carboxylic acids, reflected by the compatibility with numerous functional groups (Scheme 4.4). In addition, various sulfonamides and marked pharmaceutical drugs were successfully labeled *via* late-stage diversification. Remarkably, the robust ruthenium(II) catalysis was further utilized for the step-economical and site-selective synthesis of a tritium labeled drug.



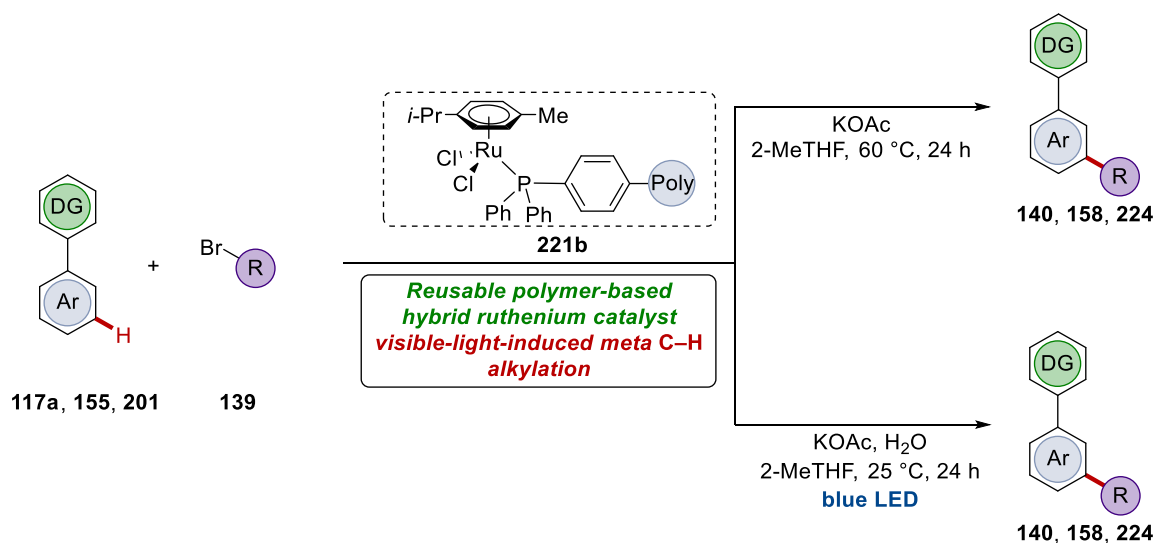
Scheme 4.4. Ruthenium(II)-catalyzed HIE of pharmaceutical drugs by C–H deuteration and C–H tritiation

These finding highlight the applicability of C–H activation for HIE and might inspire future catalyst design, since D_2/T_2 are the preferred isotope sources in industry and in many cases not activated by most ruthenium(II) catalysts used in C–H activations.^[339] Therefore, the design of ruthenium(II) catalysts that activate C–H bonds as well as D_2/T_2 molecules is in high demand for HIE processes. Furthermore, these results might inspire future developments, since many well-established C–H activation methodologies possess the inherent ability to facilitate HIE.^[340]

The last part of this thesis focused on the development of a recyclable catalyst for remote C–H functionalizations to improve their sustainability. Inspired by the main goal to prevent trace metal impurities in target molecules, hybrid ruthenium catalysts

4. Summary and Outlook

immobilized with a defined organic linker on a polymer support bear great potential. Remarkably, with a simple immobilization method, outstanding physical and chemical stabilities were observed by microscopic and spectroscopic analysis of the hybrid ruthenium catalysts **221b**.^[314] Notably, the hybrid ruthenium catalyst featured a high efficacy for *meta* C–H alkylations in a reusable manner with broad applicability towards complex biologically scaffolds (Scheme 4.5). Encouraged by homogeneous remote C–H functionalizations recyclable photo-induced *meta* C–H alkylations extended the applicability of the hybrid ruthenium catalysis.



Scheme 4.5. Recyclable ruthenium catalyst for *meta* C–H functionalization.

The simple immobilization method combined with an easily accessible polymer-based support proved versatile in both preparation and modification and showed an excellent stability.^[341] The broad applicability of the developed catalysis might promote future developments in the field of recyclable hybrid catalysts for C–H functionalizations.^[342]

5. Experimental Part

5.1. General Remarks

Reactions involving air- or moisture-sensitive compounds were conducted under an atmosphere of nitrogen using pre-dried glassware and standard Schlenk- or glovebox-techniques. If not otherwise noted, yields refer to isolated compounds, estimated to be >95% pure by GC and NMR.

Vacuum

The following average pressure was measured on the used rotary vane pump RD4 from Vacuubrand®: $0.8 \cdot 10^{-1}$ mbar (uncorrected value).

Melting points

Melting points were measured on a Stuart® Melting Point Apparatus SMP3 from Barloworld Scientific. All values are uncorrected.

Liquid Chromatography

Analytical thin layer chromatography (TLC) was performed on TLC Silica gel 60 F254 from Merck with detection at 254 nm or 360 nm or developed by treatment with a KMnO_4 solution followed by careful warming. Preparative chromatographic separations were carried out on Merck Geduran® SI 60 (40–63 μm , 70–230 mesh ASTM) silica gel.

Chiral High Performance Liquid Chromatography

Chiral HPLC chromatograms were recorded on an Agilent® 1290 Infinity using CHIRALPAK® IA-3, IB-3, IC-3, ID-3, IE-3 and IF-3 columns (3.0 μm particle size; \varnothing : 4.6 mm and 250 mm length) at ambient temperature.

Gas Chromatography

Gas chromatographic analysis (GC) was performed on an Agilent 7890A or 7890B GC System equipped with an Agilent HP-5 column (30 m, 0.320 mm diameter, 0.25 μm film thickness) and a flame-ionization detector (FID) using hydrogen as the carrier gas. Gas chromatography coupled with mass spectrometry (GC-MS) was performed on the same instrument equipped with an Agilent 5875C Triple-Axis-Detector or an Agilent 5977B

MSD. Mass spectra were obtained with electron-ionization (EI) at 70 eV in positive ion mode.

Mass Spectrometry

Electron-ionization (EI) mass spectra were recorded on a time-of flight mass spectrometer AccuTOF™ from Jeol at 70 eV. Electrospray-ionization (ESI) mass spectra were recorded on a quadrupole time-of-flight maXis or on a time-of-flight mass spectrometer microTOF, both from Bruker Daltonic. The ratios of mass to charge (m/z) are reported and the intensity relative to the base peak ($I = 100$) is given in parenthesis.

Recycling Preparative HPLC

Recycling Preparative HPLC (GPC) was performed on a Japan Analytical Industries (JAI) LC-92XX II NEXT system equipped with a JAIGEL 2.5HR or JAIGEL 2HH column. Chloroform was used as the solvent.

Infrared Spectroscopy

Infrared (IR) spectra of were measured on a Bruker Alpha-P FT-IR spectrometer with a diamond ATR probe in the range of 4000–400 cm^{-1} . In-situ IR measurements were performed with a Mettler-Toledo ReactIR 15 spectrometer equipped with a diamond ATR probe and an MCT detector. Spectra were acquired using Mettler-Toledo iC IR software version 7.0.297 in the range of 650–2200 cm^{-1} with a 4 cm^{-1} resolution. A Pearson's Correction was used as baseline correction in all measurements.

Nuclear Magnetic Resonance Spectroscopy

Nuclear magnetic resonance (NMR) spectra were recorded on Varian MercuryPlus™ 300, Bruker Avance™ III 300, Avance III HD 300, Avance III 400, Avance III HD 400, Avance Neo 400, Avance III HD 500 and Bruker Avance Neo 600 spectrometer. Unless stated otherwise, all measurements were performed at 298 K. Chemical shifts (δ) are reported relative to tetramethylsilane and are referenced using the residual proton or carbon solvent signal.

Table 5.1. Chemical shifts of common deuterated solvents.

Solvent	¹ H-NMR	¹³ C-NMR
CDCl ₃ ^[343]	7.26 ppm	77.16 ppm
DMSO- <i>d</i> ₆ ^[344]	2.50 ppm	39.52 ppm
Acetone- <i>d</i> ₆ ^[344]	2.05 ppm	206.7, 29.92 ppm
Methanol- <i>d</i> ₄ ^[344]	4.78, 3.31 ppm	49.15 ppm
THF- <i>d</i> ₈ ^[344]	3.58, 1.73 ppm	67.57, 25.37 ppm
1,4-Dioxane- <i>d</i> ₈ ^[344]	3.53 ppm	66.66 ppm
Toluene- <i>d</i> ₈ ^[344]	7.09, 7.00, 6.98, 2.09 ppm	137.9, 129.2, 128.3, 125.5, 20.40 ppm

The observed multiplicities are reported as follows: s (singlet), d (doublet), t (triplet), q (quartet), quin (quintet), sext (sextet), sep (septet), m (multiplet) or combinations thereof. A subscript of br indicates a broad signal. The coupling constants *J* are given in Hertz (Hz). All spectra were analyzed using Mestrelab Research MestReNova version 10.0.2 software.

Fluorescence Spectroscopy

Fluorescence spectra were recorded on a Jasco FP-8500 spectrometer as $2.6 \cdot 10^{-7}$ M (**189k**) solutions in MeCN and excitation wavelengths were selected according to the strongest signal.

Optical Rotation

Optical rotation measurements were performed on a Jasco P-2000 polarimeter at 589 nm in chloroform.

Data Analysis and Plots

Analysis of data was performed using OriginLab OriginPro® 8.5G software, which was also employed for linear and non-linear fitting. Histograms were created with Microsoft Excel 2019.

Solvents

All solvents used for work-up and purification were distilled prior to use. Solvents used in reactions involving air- or moisture-sensitive compounds were dried and stored under an inert atmosphere of nitrogen or argon according to the following standard procedures:

Solvents purified by solvent purification system (SPS-800) from M. Braun: Toluene, tetrahydrofuran, diethylether, dichloromethane and *N,N*-dimethylformamide.

Solvents dried and distilled over sodium using benzophenone as indicator: *t*-Amyl alcohol, *o*-, *m*-, *p*-xylene, 1,4-dioxane, 1,2-dimethoxyethane, *n*-butyl ether and methanol.

Solvents dried and distilled over CaH₂: 1,2-Dichloroethane, *N,N*-dimethylacetamide and *N*-methyl-2-pyrrolidone.

Solvents dried over 4 Å molecular sieves and degassed using multiple cycles of freeze-pump-thaw: 2-Methyltetrahydrofuran, *n*-hexane, toluene-*d*₈, and THF-*d*₈.

Water was degassed before its use applying repeated freeze-pump-thaw cycles.

Reagents

Reagents obtained from commercial sources with a purity >95% were used without further purification unless stated otherwise. Pre-ligands **208** (commercial name: SL-J681-1), **205** (SK-J003-1n), and **206** (SK-J004-1n) were obtained from Solvias AG. SMOPEX®-105 was obtained from Johnson Matthey plc and activated before usage.

The following compounds were synthesized according to previously reported procedures:

[Ru(O₂Piv)₂(*p*-cymene)],^[345] [Ru(O₂CAd₂(*p*-cymene)],^[127d] Ru@NDCs-800,^[315]
11e-h,^[346] **11n**,^[347] **44**,^[93b, 348] **117a**,^[349] **139**,^[350] **11o**,^[351] **11p**,^[352] **11r**,^[353] **11s**,^[354]
194,^[355] **196**,^[214a] **201a**,^[356] **201b**,^[356] **201c**,^[356] **201d**,^[357] **201e-l**,^[358] **155**.^[359]

The following compounds were kindly synthesized and/or provided by the persons listed below:

Karsten Rauch: $[\text{RuCl}_2(p\text{-cymene})]_2$ and $[\text{Ru}(\text{OAc})_2p\text{-cymene}]$

Dr. Debasish Ghorai: **188g**

Lorena Capdevila: **9i** and **9j**

Prof. Dr. Hintermann and coworkers (TU München): **200**

Dr. Weiping Liu: **204**

Dr. Joachim Loup: **188a**

Dr. Volker Derdau: **190q-ab**

Dr. Korkit Korvorapun: **158i** and **171**

Nikolaos Kaplaneris: **139g**, **139i**, **139l** and **139m**

5.2. General Procedures

5.2.1. General Procedure A: SPO-Nickel Catalysis with Linear Grignard Reagents

Aryl fluoride **11** (0.50 mmol, 1.00 equiv), **195** (25.0 μmol , 5.00 mol %) and Grignard reagent **9** (1.00 mmol, 2.00 equiv) were placed into an oven-dried 25 mL Schlenk tube equipped with a septum under Ar atmosphere and were stirred for 2 min. Then, the solvent was removed in vacuo and aryl fluoride **11** (0.50 mmol, 1.00 equiv) if liquid and THF (2.00 mL) were added and the mixture was stirred at 25 °C for 16 h. After completion of the reaction, H₂O (5.0 mL) was added and the resulting mixture was extracted with EtOAc (3 x 10 mL). Drying over Na₂SO₄, evaporation of the solvent and purification by column chromatography on silica gel yielded the products **186**.

5.2.2. General Procedure B: SPO-Nickel Catalysis with Branched Grignard

Reagents

Aryl fluoride **11** (0.50 mmol, 1.00 equiv) and **195** (25.0 μmol , 5.00 mol %) in THF (0.50–2.00 mL) were placed into an oven-dried 25 mL Schlenk tube equipped with a septum under Ar atmosphere and vigorously stirred for 5 min. The Grignard reagent **9** (0.50–1.50 mL, 1.00 mmol in THF) was added with a single push of the syringe and the mixture was stirred at 60 °C for 16 h. After completion of the reaction, H₂O (5.0 mL) was added at ambient temperature and the mixture was extracted with EtOAc (3 x 10 mL). Drying over Na₂SO₄, evaporation of the solvent and purification by column chromatography on silica gel yielded the products **187**.

5.2.3. General Procedure C: Manganese(I)-Catalyzed Allylative C–H/C–F

Functionalization

Heteroarene **201** (0.50 mmol, 1.00 equiv), 1*H*,1*H*,2*H*-perfluoroalkene (**45a**) (0.60 mmol, 1.20 equiv), [MnBr(CO)₅] (37.5 μmol , 7.50 mol %) and K₂CO₃ (0.50 mmol, 1.00 equiv) were placed into an oven-dried 25 mL Schlenk tube equipped with a septum under N₂ atmosphere. 1,4-Dioxane (0.50 mL) was added and the mixture was stirred at 80 °C for 20 h. After completion of the reaction, the solvent was removed in vacuo and the

remaining residue was purified by column chromatography on silica gel to afford the desired products **203**.

5.2.4. General Procedure D: Manganese(I)-Catalyzed Allylative or Alkenylative C–H/C–F Functionalization

Heteroarene **201** (0.50 mmol, 1.00 equiv), 1*H*,1*H*,2*H*-per- or 1,1-difluoroalkene **45** or **44** (1.50 mmol, 3.00 equiv), [MnBr(CO)₅] (50.0 μmol, 10.0 mol %), K₂CO₃ (0.50-0.75 mmol, 1.00-1.50 equiv) and NaOAc (0.10-0.20 mmol, 20.0-40.0 mol %) were placed into an oven-dried 25 mL Schlenk tube equipped with a septum under N₂ atmosphere. 1,4-Dioxane (0.50 mL) was added and the mixture was stirred at 100 °C for 20 h. After completion of the reaction, EtOAc (5.0 mL) was added at ambient temperature and the mixture was filtered through a pad of Celite®. Drying over Na₂SO₄, evaporation of the solvent and purification by column chromatography on silica gel yielded the products **202** or **203**.

5.2.5. General Procedure E: Nickel-Catalyzed Enantioselective Intramolecular Hydroarylation

Alkene-tethered azoles **188** (0.50 mmol, 1.00 equiv), Ni(cod)₂ (25.0 μmol, 5.00 mol %), **208** (12.5 μmol, 2.50 mol %) were placed into an oven-dried 25 mL Schlenk tube equipped with a septum under Ar atmosphere. PhMe (1.00 mL) was added and the mixture was stirred at 95 °C for 16 h. After completion of the reaction, EtOAc (5.0 mL) was added at ambient temperature and the mixture was filtered through a short plug of silica gel and rinsed with EtOAc (4 x 10 mL). Drying over Na₂SO₄, evaporation of the solvent and purification by column chromatography on silica gel yielded the products **189**.

5.2.6. General Procedure F: Nickel-Catalyzed Racemic Intramolecular Hydroarylation

The general procedure **GP-E** was followed using Ni(cod)₂ (50.0 μmol, 10.0 mol %), AlMe₃ (0.20 mmol, 0.40 equiv, 2M in PhMe) and *rac*-Ph(*t*-Bu)P(O)H (50 μmol, 10 mol %) instead of **208**.

5.2.7. General Procedure G: HIE of Benzoic Acids and Bioactive Compounds

Benzoic acid **190a-t** (0.50 mmol, 1.00 equiv) or **190u-ab** (0.10 mmol, 1.00 equiv), [Ru(O₂CAd)₂(*p*-cymene)] (10.0–25.0 μmol, 5.00–10.0 mol %) and D₂O (1.00–5.00 mmol, 10.0 equiv) were placed into an oven-dried 25 mL Schlenk tube equipped with a septum under Ar atmosphere. 1,4-Dioxane (0.50 mL or 1.00 mL) was added and the mixture was stirred at 100 °C for 16 h. After completion of the reaction, 1,4-dioxane (10 mL) was added at ambient temperature and the mixture was filtered through a pad of Celite, rinsed with 1,4-dioxane (4 x 10 mL; 5% AcOH). Drying over Na₂SO₄, evaporation of the solvent and purification by column chromatography on silica gel yielded the products [D]_n-**190**.

5.2.8. General Procedure H: Recyclable Ruthenium Catalyst for *meta* C–H Activation

Arenes **117a/201/155** (0.25 mmol, 1.00 equiv), alkyl halides **139** (0.75 mmol, 3.00 equiv), hybrid ruthenium (**221a**, 26.0 mg, 10.0 mol %; **221b**, 30.0 mg, 10.0 mol %) and KOAc (0.50 mmol, 2.00 equiv) were placed into an oven-dried 25 mL Schlenk tube equipped with a septum under Ar atmosphere. 2-MeTHF (2.00 mL) was added and the mixture was stirred at 60 °C for 24 h. After completion of the reaction, hybrid ruthenium was carefully filtered at ambient temperature through a branched filter (Por. 3) and washed with 2-MeTHF (30 mL). The filtrate was concentrated and purification by column chromatography on silica gel yielded the products **140/158/224**.

5.2.9. General Procedure I: Recyclable Ruthenium Catalyst for C4/C6 Dialkylation C–H Activation

Arenes **201** (0.25 mmol, 1.00 equiv), **139k** (0.75 mmol, 3.00 equiv), **221b** (30.0 mg, 10.0 mol %) and NaOAc (0.50 mmol, 2.00 equiv) were placed into an oven-dried 25 mL pressure tube under Ar atmosphere. THF (1.0 mL) and AcOH (30.0 mg, 0.50 mmol, 2.00 equiv) were added and the mixture was stirred at 120 °C for 24 h. After completion of the reaction, **221b** was carefully filtered at ambient temperature through a branched filter (Por. 3) and washed with THF (30 mL). The filtrate was concentrated and purification by column chromatography on silica gel yielded the products **152**, **154** and **225**.

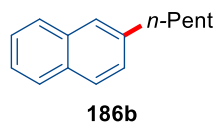
5.2.10. General Procedure J: Recyclable Ruthenium Catalyst for *meta* C–H Activation under Photo-induced Conditions

Arenes **117a/201/155** (0.25 mmol, 1.00 equiv), **139e** (0.75 mmol, 3.00 equiv), **221b** (30.0 mg, 10.0 mol %), KOAc (0.50 mmol, 2.00 equiv) and H₂O (1.25 mmol, 5.00 equiv) were placed in a 10 mL-vial equipped with a septum and wrapped with parafilm, under Ar atmosphere. 2-MeTHF (2.00 mL) was added and the mixture was stirred for 24 h under visible light irradiation (2 x Kessil A360N, $T = 30\text{--}35$ °C). After completion of the reaction, **221b** was carefully filtered at ambient temperature through a branched filter (Por. 3) and washed with 2-MeTHF (30 mL). The filtrate was concentrated and purification by column chromatography on silica gel yielded the products **140/158/224**.

5.3. SPO-Nickel Catalyst for C–F Alkylations

5.3.1. Characterization Data

2-Pentyl-naphthalene (186b)

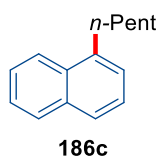


The general procedure **GP-A** was followed using 2-fluoronaphthalene (**11b**) (73.0 mg, 0.50 mmol), pentylmagnesium bromide (**9a**) (0.50 mL, 1.00 mmol) and **195** (13.3 mg, 25.0 μ mol). Purification by column chromatography (*n*-hexane) yielded **186b** (81.3 mg, 82%) as a colourless oil.

¹H-NMR (400 MHz, CDCl₃): δ = 7.89 – 7.72 (m, 3H), 7.65 (dd, J = 1.9, 1.0 Hz, 1H), 7.52 – 7.41 (m, 2H), 7.37 (dd, J = 8.4, 1.8 Hz, 1H), 2.89 – 2.58 (m, 2H), 1.75 (ddd, J = 7.5, 6.1, 2.0 Hz, 2H), 1.49 – 1.32 (m, 4H), 1.02 – 0.88 (m, 3H). **¹³C-NMR** (100 MHz, CDCl₃): δ = 140.6 (C_q), 133.8 (C_q), 132.1 (C_q), 127.9 (CH), 127.7 (CH), 127.6 (CH), 127.5 (CH), 126.4 (CH), 125.9 (CH), 125.1 (CH), 36.24 (CH₂), 31.69 (CH₂), 31.21 (CH₂), 22.73 (CH₂), 14.20 (CH₃). **IR** (ATR): 2955, 2927, 2856, 1508, 1465, 854, 815, 784, 744, 475 cm⁻¹. **MS** (EI) m/z (relative intensity): 198 (29) [M]⁺, 141 (100), 115 (34). **HR-MS** (EI): m/z calcd. for C₁₅H₁₈⁺ [M]⁺ 198.1403, found 198.1402.

The analytical data are in accordance with those previously reported in the literature.^[218b]

1-Pentyl-naphthalene (186c)



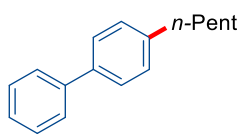
The general procedure **GP-A** was followed using 1-fluoronaphthalene (**11c**) (73.0 mg, 0.50 mmol), pentylmagnesium bromide (**9a**) (0.50 mL, 1.00 mmol) and **195** (13.3 mg, 25.0 μ mol). Purification by column chromatography (*n*-hexane) yielded **186c** (78.3 mg, 79%) as a colourless oil.

¹H-NMR (400 MHz, CDCl₃): δ = 8.10 – 8.03 (m, 1H), 7.88 (dd, J = 8.2, 1.5 Hz, 1H), 7.73 (dt, J = 8.2, 1.1 Hz, 1H), 7.58 – 7.46 (m, 2H), 7.42 (dd, J = 8.1, 7.0 Hz, 1H), 7.38 – 7.32 (m, 1H), 3.67 – 2.91 (m, 2H), 1.95 – 1.65 (m, 2H), 1.58 – 1.21 (m, 4H), 0.95 (t, J = 7.1 Hz, 3H). **¹³C-NMR** (100 MHz, CDCl₃): δ = 139.2 (C_q), 134.0 (C_q), 132. (C_q), 128.9

(CH), 126.5 (CH), 126.0 (CH), 125.7 (CH), 125.7 (CH), 125.5 (CH), 124.0 (CH), 33.24 (CH₂), 32.19 (CH₂), 30.72 (CH₂), 22.76 (CH₂), 14.24 (CH₃). **IR** (ATR): 3046, 2955, 2930, 2859, 1597, 1510, 1465, 1396, 776, 731 cm⁻¹. **MS** (EI) *m/z* (relative intensity): 198 (26) [M]⁺, 141 (100), 115 (24). **HR-MS** (EI): *m/z* calcd. for C₁₅H₁₈⁺ [M]⁺ 198.1403, found 198.1401.

The analytical data are in accordance with those previously reported in the literature.^[360]

4-Pentyl-1,1'-biphenyl (186d)



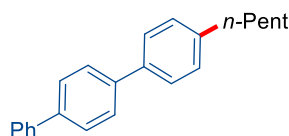
186d

The general procedure **GP-A** was followed using 4-fluoro-1,1'-biphenyl (**11d**) (86.1 mg, 0.50 mmol), pentylmagnesium bromide (**9a**) (0.50 mL, 1.00 mmol) and **195** (13.3 mg, 25.0 μmol). Purification by column chromatography (*n*-hexane) yielded **186d** (81.8 mg, 73%) as a colourless oil.

¹H-NMR (400 MHz, CDCl₃): δ = 7.66 – 7.56 (m, 2H), 7.52 (dd, *J* = 7.8, 2.1 Hz, 2H), 7.43 (dd, *J* = 7.6, 7.6 Hz, 2H), 7.33 (dt, *J* = 7.4, 2.1 Hz, 1H), 7.27 (dd, *J* = 7.8, 2.2 Hz, 2H), 2.66 (t, *J* = 7.0 Hz, 2H), 1.67 (p, *J* = 7.0 Hz, 2H), 1.43 – 1.32 (m, 4H), 0.92 (t, *J* = 6.7 Hz, 3H). **¹³C-NMR** (100 MHz, CDCl₃): δ = 142.3 (C_q), 141.3 (C_q), 138.7 (C_q), 129.0 (CH), 128.8 (CH), 127.1 (CH), 127.1 (CH), 127.1 (CH), 35.73 (CH₂), 31.72 (CH₂), 31.34 (CH₂), 22.72 (CH₂), 14.20 (CH₃). **IR** (ATR): 2955, 2927, 2855, 1486, 1008, 839, 759, 732, 696, 508 cm⁻¹. **MS** (EI) *m/z* (relative intensity): 224 (23) [M]⁺, 167 (100), 152 (14). **HR-MS** (EI): *m/z* calcd. for C₁₇H₂₀⁺ [M]⁺ 224.1560, found 224.1562.

The analytical data are in accordance with those previously reported in the literature.^[209a]

4-Pentyl-1,1':4',1''-terphenyl (186f)



186f

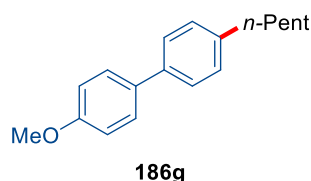
The general procedure **GP-A** was followed using 4-fluoro-1,1':4',1''-terphenyl (**11f**) (124 mg, 0.50 mmol), pentylmagnesium bromide (**9a**) (0.50 mL, 1.00 mmol) and **195**

(13.3 mg, 25.0 μmol). Purification by column chromatography (*n*-hexane) yielded **186f** (108 mg, 72%) as a colourless solid.

M.p.: 174–176 °C. **$^1\text{H-NMR}$** (400 MHz, CDCl_3): δ = 7.71 – 7.63 (m, 6H), 7.62 – 7.54 (m, 2H), 7.47 (dd, J = 7.4, 6.6 Hz, 2H), 7.41 – 7.34 (m, 1H), 7.29 (d, J = 8.0 Hz, 2H), 2.80 – 2.54 (m, 2H), 1.77 – 1.61 (m, 2H), 1.38 (dd, J = 7.0, 5.7 Hz, 4H), 0.93 (dd, J = 6.5, 3.1 Hz, 3H). **$^{13}\text{C-NMR}$** (100 MHz, CDCl_3): δ = 142.4 (C_q), 140.9 (C_q), 140.2 (C_q), 139.9 (C_q), 138.1 (C_q), 129.0 (CH), 128.9 (CH), 127.6 (CH), 127.5 (CH), 127.4 (CH), 127.2 (CH), 127.0 (CH), 35.76 (CH_2), 31.73 (CH_2), 31.34 (CH_2), 22.73 (CH_2), 14.21 (CH_3). **IR** (ATR): 3045, 2954, 2923, 2871, 1484, 1215, 809, 753, 689, 668 cm^{-1} . **MS** (EI) m/z (relative intensity): 300 (33) $[\text{M}]^+$, 243 (100), 165 (9). **HR-MS** (EI): m/z calcd. for $\text{C}_{23}\text{H}_{24}^+ [\text{M}]^+$ 300.1873, found 300.1874.

The analytical data are in accordance with those previously reported in the literature.^[209a]

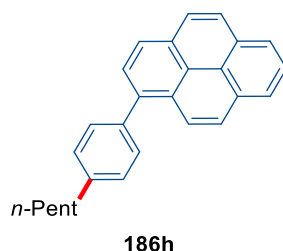
4-Methoxy-4'-pentyl-1,1'-biphenyl (**186g**)



The general procedure **GP-A** was followed using 4-fluoro-4'-methoxy-1,1'-biphenyl (**11g**) (101 mg, 0.50 mmol), pentylmagnesium bromide (**9a**) (0.50 mL, 1.00 mmol) and **195** (13.3 mg, 25.0 μmol). Purification by column chromatography (*n*-hexane) yielded **186g** (76.3 mg, 60%) as a colourless solid.

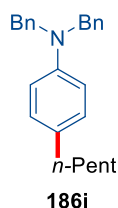
M.p.: 72–74 °C. **$^1\text{H-NMR}$** (400 MHz, CDCl_3): δ = 7.54 (ddd, J = 18.4, 8.5, 1.8 Hz, 4H), 7.32 – 7.20 (m, 2H), 7.08 – 6.95 (m, 2H), 3.89 (s, 3H), 2.68 (dd, J = 8.7, 6.8 Hz, 2H), 1.89 – 1.52 (m, 2H), 1.40 (tt, J = 6.7, 2.5 Hz, 4H), 1.13 – 0.75 (m, 3H). **$^{13}\text{C-NMR}$** (100 MHz, CDCl_3): δ = 159.0 (C_q), 141.6 (C_q), 138.3 (C_q), 133.9 (C_q), 128.9 (CH), 128.1 (CH), 126.7 (CH), 114.3 (CH), 55.45 (CH_3), 35.69 (CH_2), 31.72 (CH_2), 31.36 (CH_2), 22.72 (CH_2), 14.20 (CH_3). **IR** (ATR): 2929, 1610, 1498, 1245, 1216, 1176, 1042, 826, 749, 668 cm^{-1} . **MS** (EI) m/z (relative intensity): 254 (26) $[\text{M}]^+$, 197 (100), 182 (10), 154 (15). **HR-MS** (EI): m/z calcd. for $\text{C}_{18}\text{H}_{22}\text{O}^+ [\text{M}]^+$ 254.1665, found 254.1664.

The analytical data are in accordance with those previously reported in the literature.^[209a]

1-(4-Pentylphenyl)pyrene (186h)

The general procedure **GP-A** was followed using 1-(4-fluorophenyl)pyrene (**11h**) (148 mg, 0.50 mmol), pentylmagnesium bromide (**9a**) (0.50 mL, 1.00 mmol) and **195** (13.3 mg, 25.0 μmol). Purification by column chromatography (*n*-hexane) yielded **186h** (126 mg, 72%) as a brown oil.

$^1\text{H-NMR}$ (400 MHz, CDCl_3): δ = 8.30 – 8.15 (m, 4H), 8.11 (s, 2H), 8.08 – 7.97 (m, 3H), 7.60 d, J = 8.0 Hz, 2H), 7.41 (d, J = 8.0 Hz, 2H), 2.78 (dd, J = 8.8, 6.8 Hz, 2H), 1.88 – 1.72 (m, 2H), 1.47 (dt, J = 7.3, 3.8 Hz, 4H), 1.01 (dd, J = 7.1, 6.0 Hz, 3H). **$^{13}\text{C-NMR}$** (100 MHz, CDCl_3): δ = 142.1 (C_q), 138.6 (C_q), 138.0 (C_q), 131.6 (C_q), 131.1 (C_q), 130.6 (CH), 130.6 (C_q), 128.7 (C_q), 128.5 (CH), 127.8 (CH), 127.6 (CH), 127.4 (CH), 127.4 (CH), 126.1 (CH), 125.6 (CH), 125.1 (CH), 125.1 (C_q), 125.1 (C_q), 124.9 (CH), 124.8 (CH), 35.91 (CH_2), 31.82 (CH_2), 31.41 (CH_2), 22.78 (CH_2), 14.26 (CH_3). **IR** (ATR): 3040, 2954, 2926, 2855, 1499, 1458, 843, 757, 721, 682 cm^{-1} . **MS** (EI) m/z (relative intensity): 348 (100) $[\text{M}]^+$, 291 (95), 276 (27), 138 (6). **HR-MS** (EI): m/z calcd. for $\text{C}_{27}\text{H}_{24}^+ [\text{M}]^+$ 348.1873, found 348.1872.

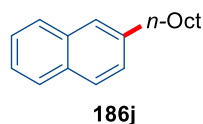
***N,N*-Dibenzyl-4-pentylaniline (186i)**

The general procedure **GP-A** was followed using *N,N*-dibenzyl-4-fluoroaniline (**11i**) (146 mg, 0.50 mmol), pentylmagnesium bromide (**9a**) (0.50 mL, 1.00 mmol) and **195** (13.3 mg, 25.0 μmol). Purification by column chromatography (*n*-hexane/EtOAc: 20/1) yielded **186i** (121 mg, 71%) as a yellow oil.

$^1\text{H-NMR}$ (400 MHz, CDCl_3): δ = 7.39 – 7.33 (m, 4H), 7.32 – 7.27 (m, 6H), 7.04 (dd, J = 8.7, 5.0 Hz, 2H), 6.73 (dd, J = 8.7, 5.0 Hz, 2H), 4.67 (s, 4H), 2.52 (t, J = 7.0 Hz, 2H), 1.61 (q, J = 7.0 Hz, 2H), 1.42 – 1.29 (m, 4H), 0.95 (t, J = 6.8 Hz, 3H). **$^{13}\text{C-NMR}$** (100

MHz, CDCl₃): δ = 147.4 (C_q), 139.1 (C_q), 131.3 (C_q), 129.2 (CH), 128.7 (CH), 126.9 (CH), 126.9 (CH), 112.7 (CH), 54.51 (CH₂), 35.01 (CH₂), 31.8 (CH₂), 31.6 (CH₂), 22.73 (CH₂), 14.21 (CH₃). **IR** (ATR): 2925, 1615, 1519, 1452, 1359, 1229, 957, 803, 729, 696 cm⁻¹. **MS** (ESI) m/z (relative intensity): 366 (3) [M+Na]⁺, 344 [M+H]⁺, 254 (3) [M-Bn]. **HR-MS** (ESI): m/z calcd. for C₂₅H₃₀N⁺ [M+H]⁺ 344.2373, found 344.2375.

2-Octylnaphthalene (186j)

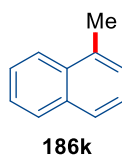


The general procedure **GP-A** was followed using 2-fluoronaphthalene (**11b**) (73.0 mg, 0.50 mmol), octylmagnesium bromide (**9b**) (0.50 mL, 1.00 mmol) and **195** (13.3 mg, 25.0 μ mol). Purification by column chromatography (*n*-hexane) yielded **186j** (91.3 mg, 76%) as a colourless oil.

¹H-NMR (400 MHz, CDCl₃): δ = 8.11 (dd, J = 8.6, 0.9 Hz, 1H), 7.95 – 7.86 (m, 1H), 7.76 (dt, J = 8.1, 1.1 Hz, 1H), 7.59 – 7.48 (m, 2H), 7.45 (dd, J = 8.1, 7.0 Hz, 1H), 7.38 (dd, J = 7.1, 1.3 Hz, 1H), 3.22 – 3.03 (m, 2H), 1.90 – 1.71 (m, 2H), 1.65 – 1.25 (m, 10H), 1.05 – 0.84 (m, 3H). **¹³C-NMR** (100 MHz, CDCl₃): δ = 139.2 (C_q), 134.0 (C_q), 132.1 (C_q), 128.9 (CH), 126.5 (CH), 126.0 (CH), 125.7 (CH), 125.7 (CH), 125.5 (CH), 124.1 (CH), 33.29 (CH₂), 32.08 (CH₂), 31.04 (CH₂), 30.03 (CH₂), 29.69 (CH₂), 29.48 (CH₂), 22.85 (CH₂), 14.27 (CH₃). **IR** (ATR): 2923, 2853, 1597, 1510, 1465, 1396, 789, 775, 725, 424 cm⁻¹. **MS** (EI) m/z (relative intensity): 240 (23) [M]⁺, 141 (100), 115 (22). **HR-MS** (EI): m/z calcd. for C₁₈H₂₄⁺ [M]⁺ 240.1873, found 240.1872.

The analytical data are in accordance with those previously reported in the literature.^[218b]

1-Methylnaphthalene (186k)

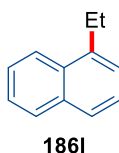


The general procedure **GP-A** was followed using 1-fluoronaphthalene (**11c**) (73.0 mg, 0.50 mmol), MeMgBr bromide (**9c**) (0.33 mL, 1.00 mmol) and **195** (13.3 mg, 25.0 μ mol). Purification by column chromatography (*n*-hexane) yielded **186k** (55.5 mg, 78%) as a colourless oil.

¹H-NMR (400 MHz, CDCl₃): δ = 8.11 – 7.99 (m, 1H), 7.94 – 7.87 (m, 1H), 7.67 (ddd, J = 8.0, 1.4, 0.7 Hz, 1H), 7.62 – 7.49 (m, 2H), 7.43 (dd, J = 8.1, 7.0 Hz, 1H), 7.37 (dp, J = 7.0, 1.1 Hz, 1H), 2.75 (s, 3H). **¹³C-NMR** (100 MHz, CDCl₃): δ = 134.4 (C_q), 133.7 (C_q), 132.8 (C_q), 128.7 (CH), 126.7 (CH), 126.5 (CH), 125.8 (CH), 125.7 (CH), 125.7 (CH), 124.2 (CH), 19.50 (CH₃). **IR** (ATR): 3038, 2928, 1597, 1509, 1398, 1020, 790, 771, 533, 408 cm⁻¹. **MS** (EI) m/z (relative intensity): 142 (83) [M]⁺, 142 (100), 115 (36), 89 (4). **HR-MS** (EI): m/z calcd. for C₁₁H₁₀⁺ [M]⁺ 142.0777, found 142.0776.

The analytical data are in accordance with those previously reported in the literature.^[361]

1-Ethynaphthalene (186l)

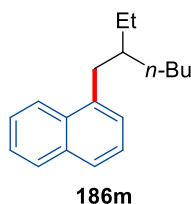


The general procedure **GP-A** was followed using 1-fluoronaphthalene (**11c**) (73.0 mg, 0.50 mmol), EtMgBr (**9d**) (1.00 mL, 1.00 mmol) and **195** (13.3 mg, 25.0 μ mol). Purification by column chromatography (*n*-hexane) yielded **186l** (57.8 mg, 74%) as a colourless oil.

¹H-NMR (400 MHz, CDCl₃): δ = 8.17 – 8.10 (m, 1H), 7.96 – 7.90 (m, 1H), 7.81 – 7.74 (m, 1H), 7.62 – 7.52 (m, 2H), 7.48 (dd, J = 8.1, 7.0 Hz, 1H), 7.41 (dd, J = 7.0, 1.4 Hz, 1H), 3.18 (q, J = 7.5 Hz, 2H), 1.46 (t, J = 7.5 Hz, 3H). **¹³C-NMR** (100 MHz, CDCl₃): δ = 140.4 (C_q), 134.0 (C_q), 131.9 (C_q), 128.9 (CH), 126.5 (CH), 125.8 (2xCH), 125.5 (CH), 125.0 (CH), 123.9 (CH), 26.03 (CH₂), 15.18 (CH₃). **IR** (ATR): 3047, 2966, 2875, 1596, 1510, 1454, 1395, 797, 776, 425 cm⁻¹. **MS** (EI) m/z (relative intensity): 156 (38) [M]⁺, 141 (100), 128 (7), 115 (22). **HR-MS** (EI): m/z calcd. for C₁₂H₁₂⁺ [M]⁺ 156.0934, found 156.0934.

The analytical data are in accordance with those previously reported in the literature.^[361]

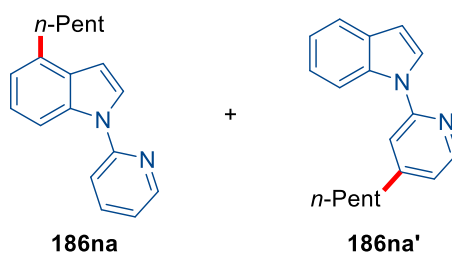
1-(2-Ethylhexyl)naphthalene (186m)



The general procedure **GP-A** was followed using 1-fluoronaphthalene (**11c**) (73.0 mg, 0.50 mmol), 2-Et-HexMgBr (**9e**) (1.00 mL, 1.00 mmol) and **195** (13.3 mg, 25.0 μmol). Purification by column chromatography (*n*-hexane) yielded **186m** (91.3 mg, 76%) as a red oil.

¹H-NMR (400 MHz, CDCl_3): δ = 8.16 – 8.03 (m, 1H), 7.89 (dd, J = 8.0, 1.6 Hz, 1H), 7.75 (d, J = 8.1 Hz, 1H), 7.58 – 7.47 (m, 2H), 7.42 (dd, J = 8.2, 6.9 Hz, 1H), 7.32 (dd, J = 7.1, 1.2 Hz, 1H), 3.19 – 2.89 (m, 2H), 1.83 (dh, J = 12.8, 6.3 Hz, 1H), 1.53 – 1.20 (m, 8H), 0.94 (dt, J = 12.1, 7.2 Hz, 6H). **¹³C-NMR** (100 MHz, CDCl_3): δ = 138.1 (C_q), 134.1 (C_q), 132.4 (C_q), 128.9 (CH), 127.4 (CH), 126.6 (CH), 125.6 (CH), 125.4 (CH), 125.4 (CH), 124.3 (CH), 40.19 (CH), 37.88 (CH_2), 32.91 (CH_2), 28.93 (CH_2), 25.95 (CH_2), 23.31 (CH_2), 14.30 (CH_3), 10.88 (CH_3). **IR** (ATR): 2957, 2925, 2857, 1510, 1459, 1395, 1378, 774, 731, 425 cm^{-1} . **MS** (EI) m/z (relative intensity): 240 (22) [M]⁺, 141 (100), 115 (21). **HR-MS** (EI): m/z calcd. for $\text{C}_{18}\text{H}_{24}^+$ [M]⁺ 240.1873, found 240.1872.

4-Pentyl-1-(pyridin-2-yl)-1*H*-indole (**186na**) and 1-(4-pentylpyridin-2-yl)-1*H*-indole (**186na'**)

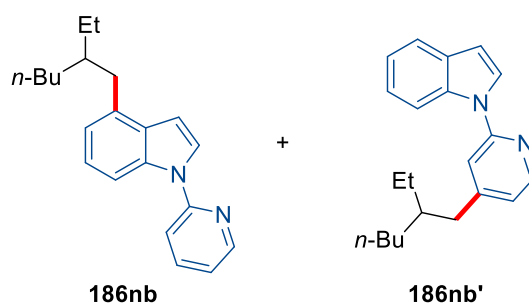


The general procedure **GP-A** was followed using 4-fluoro-1-(pyridin-2-yl)-1*H*-indole (**11n**) (106 mg, 0.50 mmol), pentylmagnesium bromide (**9a**) (0.50 mL, 1.00 mmol) and **195** (13.3 mg, 25.0 μmol). Purification by column chromatography (*n*-hexane/EtOAc: 20/1) yielded a mixture of **186na** and **186na'** (97.8 mg, 74%, **186na/186na'**: 85:15) as a brown oil.

¹H-NMR (400 MHz, CDCl_3): δ = 8.93 (d, J = 7.3 Hz, 0.15H, **186na'**), 8.69 – 8.47 (m, 0.85H, **186na**), 8.03 (d, J = 8.3 Hz, 0.86H, **186na**), 7.89 – 7.80 (m, 0.87H, **186na**), 7.75 (dd, J = 3.5, 1.7 Hz, 0.85H, **186na**; 0.45H, **186na'**), 7.60 (s, 0.18H, **186na'**), 7.54 (dt, J = 8.3, 1.3 Hz, 0.87H, **186na**), 7.32 – 7.21 (m, 0.85H, **186na**; 0.45H, **186na'**), 7.22 – 7.14 (m, 0.84H, **186na**), 7.05 (d, J = 7.2 Hz, 0.87H, **186na**), 6.93 (d, J = 7.3 Hz, 0.15H, **186na'**), 6.79 (dd, J = 3.7, 1.7 Hz, 0.85H, **186na**), 3.39 (t, J = 7.8 Hz, 0.3H, **186na'**), 2.94 (t, J = 7.8 Hz, 1.7H, **186na**), 1.86 – 1.65 (m, 2H), 1.57 – 1.28 (m, 4H), 1.04 – 0.85 (m,

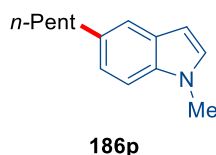
3H). $^{13}\text{C-NMR}$ (100 MHz, CDCl_3): δ = 152.7 (C_q), 149.2 (CH), 138.5 (CH), 135.7 (C_q), 135.1 (C_q), 129.8 (C_q), 125.6 (CH), 123.3 (CH), 120.8 (CH), 120.2 (CH), 114.9 (CH), 110.5 (CH), 104.0 (CH), 33.45 (CH_2), 32.01 (CH_2), 30.60 (CH_2), 22.77 (CH_2), 14.23 (CH_3). **IR** (ATR): 2954, 2928, 2857, 1731, 1687, 1586, 1532, 1472, 1437, 757 cm^{-1} . **MS** (EI) m/z (relative intensity): 264 (28) $[\text{M}]^+$, 207 (100), 180 (10), 130 (5). **HR-MS** (EI): m/z calcd. for $\text{C}_{18}\text{H}_{20}\text{N}_2^+$ $[\text{M}]^+$ 264.1621, found 264.1620.

4-(2-Ethylhexyl)-1-(pyridin-2-yl)-1H-indole (186nb) and 1-[4-(2-ethylhexyl)pyridin-2-yl]-1H-indole (186nb')



The general procedure **GP-A** was followed using 4-fluoro-1-(pyridin-2-yl)-1H-indole (**11n**) (106 mg, 0.50 mmol), 2-Et-HexMgBr (**9e**) (1.00 mL, 1.00 mmol) and **195** (13.3 mg, 25.0 μmol). Purification by column chromatography (*n*-hexane/EtOAc: 20/1) yielded a mixture of **186nb** and **186nb'** (110 mg, 72%, **186nb/186nb'**: 90:10) as a red oil.

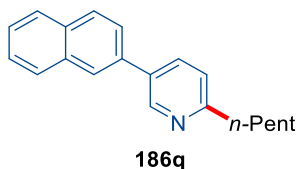
$^1\text{H-NMR}$ (400 MHz, CDCl_3): δ = 8.91 (d, J = 7.3 Hz, 0.1H, **186nb'**), 8.57 (dd, J = 4.9, 2.0 Hz, 0.9H, **186nb**), 8.02 (d, J = 8.4 Hz, 1H), 7.81 (dd, J = 7.9, 1.9 Hz, 1H), 7.72 (d, J = 3.6 Hz, 1H), 7.51 (d, J = 8.2 Hz, 1H), 7.25 – 7.10 (m, 2H), 7.00 (d, J = 7.3 Hz, 1H), 6.75 (d, J = 3.7 Hz, 1H), 3.31 (d, J = 7.1 Hz, 0.2H, **186nb'**), 2.92 – 2.62 (m, 1.8H, **186nb**), 1.77 (q, J = 6.3 Hz, 1H), 1.33 (ddd, J = 10.4, 6.3, 2.9 Hz, 8H), 0.90 (dt, J = 10.4, 7.3 Hz, 6H). $^{13}\text{C-NMR}$ (100 MHz, CDCl_3): δ = 152.7 (C_q), 149.1 (CH), 138.4 (C_q), 135.2 (C_q), 134.8 (C_q), 130.3 (CH), 125.5 (CH), 123.1 (CH), 121.9 (CH), 120.1 (CH), 114.9 (CH), 110.5 (CH), 104.2 (CH), 40.66 (CH), 37.95 (CH_2), 32.92 (CH_2), 29.08 (CH_2), 25.97 (CH_2), 23.27 (CH_2), 14.32 (CH_3), 11.02 (CH_3). **IR** (ATR): 2957, 2926, 1732, 1689, 1586, 1532, 1471, 1343, 777, 756 cm^{-1} . **MS** (EI) m/z (relative intensity): 306 (14) $[\text{M}]^+$, 207 (100), 180 (7). **HR-MS** (EI): m/z calcd. for $\text{C}_{21}\text{H}_{26}\text{N}_2^+$ $[\text{M}]^+$ 306.2091, found 306.2087.

1-Methyl-5-pentyl-1H-indole (186p)

The general procedure **GP-A** was followed using 5-fluoro-1-methyl-1H-indole (**11p**) (74.6 mg, 0.50 mmol), pentylmagnesium bromide (**9a**) (0.50 mL, 1.00 mmol) and **195** (13.3 mg, 25.0 μ mol). Purification by column chromatography (*n*-hexane/EtOAc: 50/1) yielded **186p** (72.5 mg, 72%) as a yellow oil.

¹H-NMR (400 MHz, CDCl₃): δ = 7.52 (dd, *J* = 8.0, 0.7 Hz, 1H), 7.12 (dt, *J* = 1.5, 0.8 Hz, 1H), 6.98 (d, *J* = 3.1 Hz, 1H), 6.97 – 6.94 (m, 1H), 6.43 (dd, *J* = 3.1, 0.9 Hz, 1H), 3.77 (s, 3H), 2.88 – 2.58 (m, 2H), 1.78 – 1.61 (m, 2H), 1.41 – 1.32 (m, 4H), 0.94 – 0.85 (m, 3H). **¹³C-NMR** (100 MHz, CDCl₃): δ = 137.2 (C_q), 136.8 (C_q), 128.4 (CH), 126.6 (C_q), 120.6 (CH), 120.6 (CH), 108.6 (CH), 100.8 (CH), 36.64 (CH₂), 32.89 (CH₃), 32.10 (CH₂), 31.80 (CH₂), 22.78 (CH₂), 14.23 (CH₃). **IR** (ATR): 2955, 2926, 2854, 1714, 1619, 1513, 1468, 1340, 805, 713 cm⁻¹. **MS** (EI) *m/z* (relative intensity): 201 (26) [M]⁺, 144 (100), 115 (6). **HR-MS** (EI): *m/z* calcd. for C₁₄H₁₉N⁺ [M]⁺ 201.1512, found 201.1510.

The analytical data are in accordance with those previously reported in the literature.^[209a]

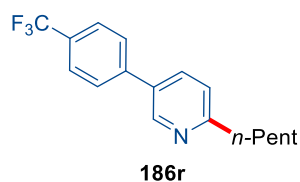
5-(Naphthalen-2-yl)-2-pentylpyridine (186q)

The general procedure **GP-A** was followed using 2-fluoro-5-(naphthalen-2-yl)pyridine (**11q**) (112 mg, 0.50 mmol), pentylmagnesium bromide (**9a**) (0.50 mL, 1.00 mmol) and **195** (13.3 mg, 25.0 μ mol). Purification by column chromatography (*n*-hexane) yielded **186q** (105 mg, 76%) as a light-yellow oil.

¹H-NMR (400 MHz, CDCl₃): δ = 8.68 (d, *J* = 2.4 Hz, 1H), 7.91 (dd, *J* = 9.7, 8.0 Hz, 2H), 7.84 (d, *J* = 8.8 Hz, 1H), 7.76 (dd, *J* = 7.9, 2.3 Hz, 1H), 7.59 – 7.39 (m, 4H), 7.31 (d, *J* = 7.9 Hz, 1H), 3.09 – 2.80 (m, 2H), 1.85 (p, *J* = 7.3 Hz, 2H), 1.43 (dq, *J* = 6.3, 3.5, 2.6 Hz, 4H), 1.06 – 0.86 (m, 3H). **¹³C-NMR** (100 MHz, CDCl₃): δ = 161.3 (C_q), 149.5 (CH), 138.2 (CH), 136.4 (C_q), 133.9 (C_q), 133.8 (C_q), 131.7 (C_q), 128.6 (CH), 128.5 (CH), 127.5 (CH), 126.6 (CH), 126.2 (CH), 125.5 (CH), 125.5 (CH), 122.4 (CH), 38.11 (CH₂), 31.83

(CH₂), 29.79 (CH₂), 22.71 (CH₂), 14.19 (CH₃). **IR** (ATR): 2925, 2856, 1597, 1485, 1376, 1030, 962, 800, 776, 435 cm⁻¹. **MS** (EI) *m/z* (relative intensity): 275 (2) [M]⁺, 246 (9), 232 (22) 219 (100), 189 (7). **HR-MS** (EI): *m/z* calcd. for C₂₀H₂₁N⁺ [M]⁺ 275.1669, found 275.1671.

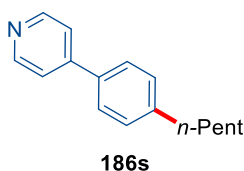
2-Pentyl-5-[4-(trifluoromethyl)phenyl]pyridine (**186r**)



The general procedure **GP-A** was followed using 2-fluoro-5-(4-(trifluoromethyl)phenyl)pyridine (**11r**) (121 mg, 0.50 mmol), pentylmagnesium bromide (**9a**) (0.50 mL, 1.00 mmol) and **195** (13.3 mg, 25.0 μmol). Purification by column chromatography (*n*-hexane/EtOAc: 50/1) yielded **186r** (109 mg, 74%) as a colourless solid.

M.p.: 45–47 °C. **¹H-NMR** (400 MHz, CDCl₃): δ = 8.76 (d, *J* = 2.4 Hz, 1H), 7.80 (dd, *J* = 8.1, 2.4 Hz, 1H), 7.72 (d, *J* = 8.3 Hz, 2H), 7.67 (d, *J* = 8.3 Hz, 2H), 7.25 (d, *J* = 7.8 Hz, 1H), 2.95 – 2.73 (m, 2H), 1.77 (dq, *J* = 11.0, 7.4 Hz, 2H), 1.38 (dp, *J* = 7.4, 3.7, 3.3 Hz, 4H), 1.03 – 0.79 (m, 3H). **¹³C-NMR** (100 MHz, CDCl₃): δ = 162.7 (C_q), 147.8 (CH), 141.7 (C_q), 134.9 (CH), 132.6 (C_q), 130.0 (q, *J* = 32.6 Hz, C_q), 127.4 (CH), 126.1 (q, *J* = 3.8 Hz, CH), 124.3 (q, *J* = 272 Hz, C_q), 122.9 (CH), 38.26 (CH₂), 31.76 (CH₂), 29.73 (CH₂), 22.70 (CH₂), 14.18 (CH₃). **¹⁹F-NMR** (377 MHz, CDCl₃): δ = -62.53. **IR** (ATR): 2930, 1618, 1598, 1483, 1418, 1324, 1167, 1125, 1072, 825 cm⁻¹. **MS** (EI) *m/z* (relative intensity): 293 (2) [M]⁺, 264 (11), 250 (21), 237 (100), 167 (5). **HR-MS** (EI): *m/z* calcd. for C₁₇H₁₈F₃N⁺ [M]⁺ 293.1386, found 293.1391.

4-(4-Pentylphenyl)pyridine (**186s**)



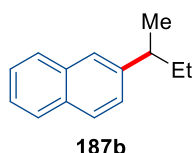
The general procedure **GP-A** was followed using 4-(4-fluorophenyl)pyridine (**11s**) (86.6 mg, 0.50 mmol), pentylmagnesium bromide (**9a**) (0.50 mL, 1.00 mmol) and **195**

(13.3 mg, 25.0 μmol). Purification by column chromatography (*n*-hexane/EtOAc: 20/1) yielded **186s** (82.2 mg, 73%) as a colourless oil.

$^1\text{H-NMR}$ (400 MHz, CDCl_3): δ = 8.64 (d, J = 5.4 Hz, 2H), 7.65 – 7.52 (m, 2H), 7.52 – 7.47 (m, 2H), 7.34 – 7.27 (m, 2H), 2.74 – 2.57 (m, 2H), 1.66 (dt, J = 9.6, 6.8 Hz, 2H), 1.44 – 1.26 (m, 4H), 1.03 – 0.79 (m, 3H). **$^{13}\text{C-NMR}$** (100 MHz, CDCl_3): δ = 150.3 (CH), 148.4 (C_q), 144.4 (C_q), 135.5 (C_q), 129.3 (CH), 127.0 (CH), 121.5 (CH), 35.77 (CH_2), 31.63 (CH_2), 31.19 (CH_2), 22.67 (CH_2), 14.15 (CH_3). **IR** (ATR): 2955, 2927, 2856, 1597, 1488, 1465, 1403, 992, 802, 517 cm^{-1} . **MS** (EI) m/z (relative intensity): 225 (25) $[\text{M}]^+$, 168 (100), 139 (5), 115 (6). **HR-MS** (EI): m/z calcd. for $\text{C}_{16}\text{H}_{19}\text{N}^+$ $[\text{M}]^+$ 225.1512, found 225.1512.

The analytical data are in accordance with those previously reported in the literature.^[362]

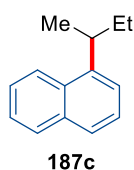
2-(*sec*-Butyl)naphthalene (**187b**)



The general procedure **GP-B** was followed using 2-fluoronaphthalene (**11b**) (73.0 mg, 0.50 mmol), *sec*-BuMgCl (**9f**) (0.50 mL, 1.00 mmol) and **195** (13.3 mg, 25.0 μmol). Purification by column chromatography (*n*-hexane) yielded **187b** (77.3 mg, 84%, b/l: 96:4) as a colorless oil.

$^1\text{H-NMR}$ (400 MHz, CDCl_3): δ = 7.81 (ddd, J = 8.0, 3.0, 1.7 Hz, 3H), 7.63 (dd, J = 1.7, 0.8 Hz, 1H), 7.51 – 7.40 (m, 2H), 7.37 (dd, J = 8.0, 1.8 Hz, 1H), 2.79 (h, J = 7.0 Hz, 1H), 1.87 – 1.62 (m, 2H), 1.35 (d, J = 7.0 Hz, 3H), 0.97 (t, J = 7.3 Hz, 0.13H, 1), 0.88 (t, J = 7.4 Hz, 2.87H, b). **$^{13}\text{C-NMR}$** (100 MHz, CDCl_3): δ = 145.3 (C_q), 133.8 (C_q), 132.3 (C_q), 128.0 (CH), 127.7 (CH), 127.7 (CH), 126.4 (CH), 125.9 (CH), 125.3 (CH), 125.1 (CH), 41.97 (CH), 31.19 (CH_2), 22.02 (CH_3), 12.44 (CH_3). **IR** (ATR): 2959, 2926, 1507, 1454, 1377, 890, 854, 815, 743, 476 cm^{-1} . **MS** (EI) m/z (relative intensity): 184 (23) $[\text{M}]^+$, 155 (100), 141 (11), 128 (10), 115 (9). **HR-MS** (EI): m/z calcd. for $\text{C}_{14}\text{H}_{16}^+$ $[\text{M}]^+$ 184.1247, found 184.1248.

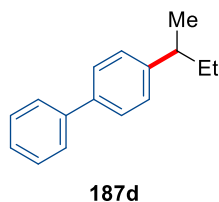
The analytical data are in accordance with those previously reported in the literature.^[363]

1-(*sec*-Butyl)naphthalene (187c)

The general procedure **GP-B** was followed using 1-fluoronaphthalene (**11c**) (73.0 mg, 0.50 mmol), *sec*-BuMgCl (**9f**) (0.50 mL, 1.00 mmol) and **195** (13.3 mg, 25.0 μ mol). Purification by column chromatography (*n*-hexane) yielded **187c** (73.7 mg, 80%, b/l: 96:4) as a colourless oil.

¹H-NMR (400 MHz, CDCl₃): δ = 8.27 – 8.05 (m, 1H), 7.86 (dd, J = 7.8, 1.7 Hz, 1H), 7.70 (dd, J = 8.0, 1.2 Hz, 1H), 7.54 – 7.42 (m, 3H), 7.39 (dd, J = 7.3, 1.3 Hz, 1H), 3.52 (h, J = 6.8 Hz, 1H), 1.93 – 1.78 (m, 1H), 1.72 (dp, J = 13.6, 7.3 Hz, 1H), 1.38 (d, J = 6.9 Hz, 3H), 0.98 (t, J = 7.4 Hz, 0.12H, 1), 0.93 (t, J = 7.4 Hz, 2.88H, b). **¹³C-NMR** (100 MHz, CDCl₃): δ = 143.9 (C_q), 134.1 (C_q), 131.9 (C_q), 129.1 (CH), 126.3 (CH), 125.7 (CH), 125.7 (CH), 125.3 (CH), 123.4 (CH), 122.6 (CH), 35.44 (CH), 30.71 (CH₂), 21.36 (CH₃), 12.42 (CH₃). **IR** (ATR): 2922, 2851, 2163, 2063, 2041, 1712, 1463, 1377, 776, 416 cm⁻¹. **MS** (EI) m/z (relative intensity): 184 (23) [M]⁺, 155 (100), 141 (9), 128 (9), 115 (7). **HR-MS** (EI): m/z calcd. for C₁₄H₁₆⁺ [M]⁺ 184.1247, found 184.1247.

The analytical data are in accordance with those previously reported in the literature.^[363]

4-(*sec*-Butyl)-1,1'-biphenyl (187d)

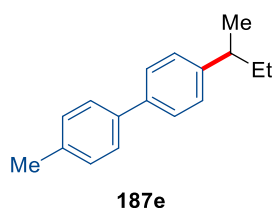
The general procedure **GP-B** was followed using 4-fluoro-1,1'-biphenyl (**11d**) (86.1 mg, 0.50 mmol), *sec*-BuMgCl (**9f**) (0.50 mL, 1.00 mmol) and **195** (13.3 mg, 25.0 μ mol). Purification by column chromatography (*n*-hexane) yielded **187d** (78.8 mg, 75%, b/l: 78:22) as a colorless oil.

¹H-NMR (400 MHz, CDCl₃): δ = 7.64 – 7.59 (m, 2H), 7.58 – 7.52 (m, 2H), 7.45 (ddd, J = 7.8, 1.6, 1.8 Hz 2H), 7.34 (dt J = 7.3, 1.2 Hz, 1H), 7.28 (ddd, J = 8.1, 6.5, 7.3, 7.3 Hz, 2H), 2.67 (h, J = 6.8 Hz, 0.78H, b; 0.42H, 1), 1.74 – 1.60 (m, 1.55H, b; 0.45H, 1), 1.42 (q, J = 7.3 Hz, 0.45H, 1), 1.30 (d, J = 6.9 Hz, 2.33H, b), 0.98 (t, J = 7.3 Hz, 0.68H, 1), 0.89 (t,

$J = 7.4$ Hz, 2.32H, b). $^{13}\text{C-NMR}$ (100 MHz, CDCl_3): $\delta = 147.0$ (C_q), 141.3 (C_q), 138.8 (C_q), 128.8 (CH), 127.6 (CH), 127.1 (CH), 127.1 (CH), 127.1 (CH), 41.50 (CH), 31.32 (CH_2), 21.97 (CH_3), 12.44 (CH_3). **IR** (ATR): 2959, 2927, 2872, 1486, 1455, 1008, 836, 762, 732, 697 cm^{-1} . **MS** (EI) m/z (relative intensity): 210 (19) $[\text{M}]^+$, 181 (100), 165 (38), 152 (12). **HR-MS** (EI): m/z calcd. for $\text{C}_{16}\text{H}_{18}^+$ $[\text{M}]^+$ 210.1403, found 210.1406.

The analytical data are in accordance with those previously reported in the literature.^[364]

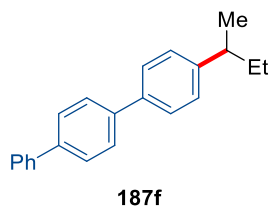
4-(*sec*-Butyl)-4'-methyl-1,1'-biphenyl (**187e**)



The general procedure **GP-B** was followed using 4-fluoro-4'-methyl-1,1'-biphenyl (**11e**) (93.1 mg, 0.50 mmol), *sec*-BuMgCl (**9f**) (0.50 mL, 1.00 mmol) and **195** (13.3 mg, 25.0 μmol). Purification by column chromatography (*n*-hexane) yielded **187e** (85.2 mg, 76%, b/l: 73:27) as a colourless oil.

$^1\text{H-NMR}$ (400 MHz, CDCl_3): $\delta = 7.52$ (ddd, $J = 8.1, 8.1, 2.0$ Hz, 1H), 7.26 (ddd, $J = 8.2, 8.2, 2.3$ Hz, 1H), 2.66 (h, $J = 6.7$ Hz, 0.72H, b; 0.53H, l), 2.41 (s, 3H), 1.71 – 1.60 (m, 1.46H, b; 0.54H, l), 1.42 (q, $J = 7.3$ Hz, 0.54H, l), 1.30 (d, $J = 6.9$ Hz, 2.19H, b), 0.97 (t, $J = 7.3$ Hz, 0.82H, l), 0.89 (t, $J = 7.4$ Hz, 2.18H, b). $^{13}\text{C-NMR}$ (100 MHz, CDCl_3): $\delta = 146.7$ (C_q), 138.8 (C_q), 138.5 (C_q), 136.8 (C_q), 129.6 (CH), 127.6 (CH), 127.0 (CH), 126.9 (CH), 41.48 (CH), 31.33 (CH_2), 21.97 (CH_3), 21.23 (CH_3), 12.45 (CH_3). **IR** (ATR): 3023, 2959, 2925, 2871, 1498, 1455, 1006, 809, 571, 518 cm^{-1} . **MS** (EI) m/z (relative intensity): 224 (47) $[\text{M}]^+$, 195 (100), 181 (56), 165 (39), 152 (7). **HR-MS** (EI): m/z calcd. for $\text{C}_{17}\text{H}_{20}^+$ $[\text{M}]^+$ 224.1560, found 224.1559.

4-(*sec*-Butyl)-1,1':4',1''-terphenyl (**187f**)

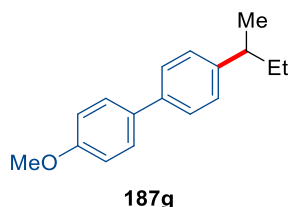


The general procedure **GP-B** was followed using 4-fluoro-1,1':4',1''-terphenyl (**11f**) (124 mg, 0.50 mmol), *sec*-BuMgCl (**9f**) (0.50 mL, 1.00 mmol) and **195** (13.3 mg,

25.0 μmol). Purification by column chromatography (*n*-hexane) yielded **187f** (105 mg, 73%, b/l: 88:12) as a colourless solid.

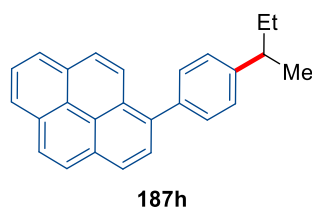
M.p.: 157–159 °C. **$^1\text{H-NMR}$** (400 MHz, CDCl_3): δ = 7.72 – 7.62 (m, 6H), 7.62 – 7.53 (m, 2H), 7.52 – 7.43 (m, 2H), 7.41 – 7.33 (m, 1H), 7.32 – 7.27 (m, 2H), 2.67 (h, J = 7.0 Hz, 1H), 1.66 (pd, J = 7.3, 1.9 Hz, 2H), 1.30 (d, J = 7.0 Hz, 3H), 0.97 (t, J = 7.4 Hz, 0.35H l), 0.89 (t, J = 7.4 Hz, 2.65H, b). **$^{13}\text{C-NMR}$** (100 MHz, CDCl_3): δ = 147.1 (C_q), 140.9 (C_q), 140.3 (C_q), 139.9 (C_q), 138.3 (C_q), 128.9 (CH), 127.7 (CH), 127.6 (CH), 127.5 (CH), 127.4 (CH), 127.2 (CH), 127.0 (CH), 41.52 (CH), 31.33 (CH_2), 21.97 (CH_3), 12.45 (CH_3). **IR** (ATR): 3018, 3006, 2976, 1484, 1215, 827, 744, 698, 668, 586 cm^{-1} . **MS** (EI) m/z (relative intensity): 286 (40) $[\text{M}]^+$, 257 (100), 241 (20), 215 (8), 179 (10). **HR-MS** (EI): m/z calcd. for $\text{C}_{22}\text{H}_{22}^+$ $[\text{M}]^+$ 286.1716, found 286.1717.

4-(*sec*-Butyl)-4'-methoxy-1,1'-biphenyl (**187g**)



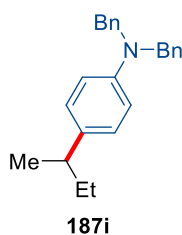
The general procedure **GP-B** was followed using 4-fluoro-4'-methoxy-1,1'-biphenyl (**11g**) (101 mg, 0.50 mmol), *sec*-BuMgCl (**9f**) (0.50 mL, 1.00 mmol) and **195** (13.3 mg, 25.0 μmol). Purification by column chromatography (*n*-hexane) yielded **187g** (81.7 mg, 68%, b/l: 76:24) as a colourless solid.

M.p.: 68–70 °C. **$^1\text{H-NMR}$** (400 MHz, CDCl_3): δ = 7.55 (dd, J = 7.7, 2.4 Hz, 1H), 7.53 (dd, J = 7.1, 2.4 Hz, 1H), 7.52 (dd, J = 7.8, 1.9 Hz, 1H), 7.49 (dd, J = 7.88, 1.9 Hz, 1H), 7.27 – 7.23 (m, 2H), 6.99 (dd, J = 8.9, 2.2 Hz, 2H), 3.86 (s, 3H), 2.65 (h, J = 6.7 Hz, 0.76H b; 0.45H, l), 1.77 – 1.58 (m, 2H), 1.41 (q, J = 7.3 Hz, 0.48H, l), 1.29 (d, J = 7.0 Hz, 2.29H, b), 0.97 (t, J = 7.3 Hz, 0.72H, l), 0.88 (t, J = 7.4 Hz, 2.28H, b). **$^{13}\text{C-NMR}$** (100 MHz, CDCl_3): δ = 159.0 (C_q), 146.3 (C_q), 138.5 (C_q), 133.9 (C_q), 128.1 (CH), 127.6 (CH), 126.7 (CH), 114.3 (CH), 55.45 (CH_3), 41.45 (CH), 31.32 (CH_2), 21.97 (CH_3), 12.44 (CH_3). **IR** (ATR): 2959, 2928, 1606, 1497, 1456, 1250, 1182, 1040, 822, 753 cm^{-1} . **MS** (EI) m/z (relative intensity): 240 (58) $[\text{M}]^+$, 211 (100), 197 (54), 165 (12), 152 (7). **HR-MS** (EI): m/z calcd. for $\text{C}_{17}\text{H}_{20}\text{O}^+$ $[\text{M}]^+$ 240.1509, found 240.1509.

1-[4-(*sec*-Butyl)phenyl]pyrene (187h)

The general procedure **GP-B** was followed using 1-(4-fluorophenyl)pyrene (**11h**) (148 mg, 0.50 mmol), *sec*-BuMgCl (**9f**) (0.50 mL, 1.00 mmol) and **195** (13.3 mg, 25.0 μ mol). Purification by column chromatography (*n*-hexane) yielded **187h** (149 mg, 89%, b/l: 93:7) as an orange oil.

¹H-NMR (400 MHz, CDCl₃): δ = 8.34 – 8.15 (m, 4H), 8.10 (s, 2H), 8.02 (dd, J = 8.4, 7.6 Hz, 3H), 7.66 – 7.54 (m, 2H), 7.48 – 7.34 (m, 2H), 2.77 (h, J = 7.0 Hz, 1H), 1.87 – 1.64 (m, J = 7.0 Hz, 2H), 1.58 – 1.44 (m, 0.2H, 1), 1.39 (d, J = 6.9 Hz, 2.8H, b), 1.03 (t, J = 7.3 Hz, 0.2H, 1), 0.98 (t, J = 7.4 Hz, 2.8H, b). **¹³C-NMR** (100 MHz, CDCl₃): δ = 146.9 (C_q), 138.7 (C_q), 138.0 (C_q), 131.6 (C_q), 131.2 (C_q), 130.6 (CH), 130.6 (C_q), 128.7 (C_q), 128.6 (CH), 128.6 (C_q), 127.8 (CH), 127.6 (CH), 127.4 (CH), 127.2 (CH), 126.1 (CH), 125.6 (CH), 125.1 (CH), 125.1 (C_q), 124.9 (CH), 124.8 (CH), 41.64 (CH), 31.45 (CH₂), 22.01 (CH₃), 12.55 (CH₃). **IR** (ATR): 2958, 2925, 2871, 1499, 1456, 1006, 836, 757, 721, 682 cm⁻¹. **MS** (EI) m/z (relative intensity): 334 (100) [M]⁺, 305 (83), 289 (54), 276 (29), 144 (21). **HR-MS** (EI): m/z calcd. for C₂₆H₂₂⁺ [M]⁺ 334.1716, found 334.1714.

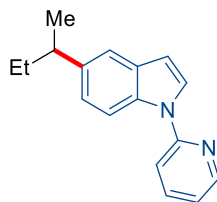
***N,N*-Dibenzyl-4-(*sec*-butyl)aniline (187i)**

The general procedure **GP-B** was followed using *N,N*-dibenzyl-4-fluoroaniline (**11i**) (146 mg, 0.50 mmol), *sec*-BuMgCl (**9f**) (0.50 mL, 1.00 mmol) and **195** (13.3 mg, 25.0 μ mol). Purification by column chromatography (*n*-hexane/EtOAc: 20/1) yielded **187i** (125 mg, 76%, b/l: 65:35) as a yellow oil.

¹H-NMR (400 MHz, CDCl₃): δ = 7.41 – 7.34 (m, 4H), 7.34 – 7.28 (m, 6H), 7.05 (dd, J = 8.7, 2.0 Hz, 2H), 6.72 (dd, J = 8.7, 2.0 Hz, 2H), 4.68 (s, 4H), 2.55 (dt, J = 7.4, 6.8 Hz, 0.63H b; 0.68H, 1), 1.68 – 1.54 (m, 1.30H b; 0.70H, 1), 1.41 (sext, J = 7.3 Hz, 0.70H, 1), 1.25 (d, J = 6.8 Hz, 1.95H, b), 0.98 (t, J = 7.3 Hz, 1.05H, 1), 0.89 (t, J = 7.3 Hz, 1.95H, b).

$^{13}\text{C-NMR}$ (100 MHz, CDCl_3): $\delta = 147.6$ (C_q), 139.1 (C_q), 136.1 (C_q), 128.7 (CH), 128.7 (CH), 127.8 (CH), 126.9 (CH), 112.6 (CH), 54.49 (CH_2), 40.64 (CH), 31.50 (CH_2), 21.93 (CH_3), 12.50 (CH_3). **IR** (ATR): 2958, 2924, 1614, 1519, 1494, 1452, 1360, 1230, 732, 694 cm^{-1} . **MS** (ESI) m/z (relative intensity): 330 (12) $[\text{M}+\text{H}]^+$, 274 (16), 229 (11). **HR-MS** (ESI): m/z calcd. for $\text{C}_{24}\text{H}_{28}\text{N}^+$ $[\text{M}+\text{H}]^+$ 330.2216, found 330.2217.

5-(*sec*-Butyl)-1-(pyridin-2-yl)-1*H*-indole (187o)



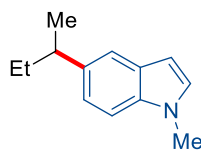
187o

The general procedure **GP-B** was followed using 5-fluoro-1-(pyridin-2-yl)-1*H*-indole (**11o**) (106 mg, 0.50 mmol), *sec*-BuMgCl (**9f**) (0.50 mL, 1.00 mmol) and **195** (13.3 mg, 25.0 μmol). Purification by column chromatography (*n*-hexane/EtOAc: 20:1) yielded **187o** (86.4 mg, 69%, b/l: 88:12) as a yellow oil.

$^1\text{H-NMR}$ (400 MHz, CDCl_3): $\delta = 8.67 - 8.43$ (m, 1H), 8.12 (d, $J = 8.5$ Hz, 1H), 7.87 – 7.73 (m, 1H), 7.71 (d, $J = 3.4$ Hz, 1H), 7.59 – 7.38 (m, 2H), 7.14 (ddd, $J = 8.3, 3.8, 1.1$ Hz, 2H), 6.66 (dd, $J = 3.6, 0.7$ Hz, 1H), 2.80 – 2.58 (m, 1H), 1.67 (dd, $J = 7.4, 1.6$ Hz, 2H), 1.31 (d, $J = 6.9$ Hz, 3H), 0.94 (t, $J = 7.3$ Hz, 0.37H, l), 0.85 (t, $J = 7.4$ Hz, 2.63H, b).

$^{13}\text{C-NMR}$ (100 MHz, CDCl_3): $\delta = 152.8$ (C_q), 149.1 (CH), 140.9 (C_q), 138.4 (CH), 133.8 (C_q), 130.7 (C_q), 126.0 (CH), 122.9 (CH), 119.9 (CH), 119.1 (CH), 114.4 (CH), 112.9 (CH), 105.6 (CH), 41.82 (CH), 31.72 (CH_2), 22.61 (CH_3), 12.54 (CH_3). **IR** (ATR): 2959, 2925, 1691, 1592, 1476, 1435, 1340, 1215, 774, 722 cm^{-1} . **MS** (EI) m/z (relative intensity): 250 (21) $[\text{M}]^+$, 221 (100), 206 (45), 115 (4). **HR-MS** (EI): m/z calcd. for $\text{C}_{17}\text{H}_{18}\text{N}_2^+$ $[\text{M}]^+$ 250.1465, found 250.1465.

5-(*sec*-Butyl)-1-methyl-1*H*-indole (187p)



187p

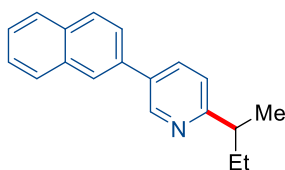
The general procedure **GP-B** was followed using 5-fluoro-1-methyl-1*H*-indole (**11p**) (74.6 mg, 0.50 mmol), *sec*-BuMgCl (**9f**) (0.50 mL, 1.00 mmol) and **195** (13.3 mg,

25.0 μmol). Purification by column chromatography *n*-hexane/EtOAc: 50:1) yielded **187p** (65.6 mg, 70%, b/l: 87:13) as a yellow oil.

$^1\text{H-NMR}$ (400 MHz, CDCl_3): δ = 7.53 (dd, J = 8.1, 6.3 Hz, 1H), 7.15 – 7.09 (m, 1H), 7.04 – 6.89 (m, 2H), 6.44 (dt, J = 3.1, 0.7 Hz, 1H), 3.78 (d, J = 3.6 Hz, 3H), 2.73 (dq, J = 14.1, 7.4 Hz, 1H), 1.68 (pt, J = 6.7, 4.6 Hz, 2H), 1.32 (d, J = 6.9 Hz, 3H), 0.95 (t, J = 7.4 Hz, 0.41H, l), 0.86 (t, J = 7.4 Hz, 2.6H, b). **$^{13}\text{C-NMR}$** (100 MHz, CDCl_3): δ = 141.7 (C_q), 128.4 (C_q), 126.8 (CH), 120.6 (C_q), 119.2 (CH), 108.7 (CH), 107.3 (CH), 100.7 (CH), 42.34 (CH_3), 32.90 (CH), 31.78 (CH_2), 22.66 (CH_3), 12.61 (CH_3). **IR** (ATR): 2958, 2926, 2872, 1513, 1469, 1340, 1321, 810, 713 cm^{-1} . **MS** (EI) m/z (relative intensity): 187 (47) $[\text{M}]^+$, 158 (100), 144 (47), 77 (13). **HR-MS** (EI): m/z calcd. for $\text{C}_{13}\text{H}_{17}\text{N}^+$ $[\text{M}]^+$ 187.1356, found 187.1355.

The analytical data are in accordance with those previously reported in the literature.^[87]

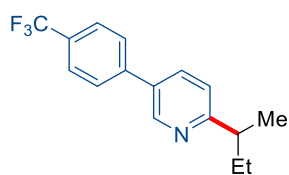
2-(*sec*-Butyl)-5-(naphthalen-2-yl)pyridine (**187q**)



187q

The general procedure **GP-B** was followed using 2-fluoro-5-(naphthalen-2-yl)pyridine (**11q**) (112 mg, 0.50 mmol), *sec*-BuMgCl (**9f**) (0.50 mL, 1.00 mmol) and **195** (13.3 mg, 25.0 μmol). Purification by column chromatography (*n*-hexane/EtOAc: 50:1) yielded **187q** (98.0 mg, 75%, b/l: 98:2) as an orange oil.

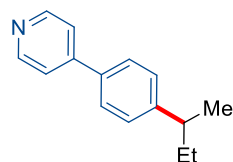
$^1\text{H-NMR}$ (400 MHz, CDCl_3): δ = 8.71 (d, J = 2.2 Hz, 1H), 7.97 – 7.88 (m, 2H), 7.83 (d, J = 8.3 Hz, 2H), 7.60 – 7.39 (m, 4H), 7.34 (d, J = 7.9 Hz, 1H), 3.00 (d, J = 11.8 Hz, 1H), 1.96 – 1.81 (m, 1H), 1.74 (dp, J = 14.2, 7.2 Hz, 1H), 1.41 (d, J = 6.9 Hz, 3H), 1.00 (t, J = 7.40 Hz, 0.07H, l), 0.95 (t, J = 7.4 Hz, 2.93H, b). **$^{13}\text{C-NMR}$** (100 MHz, CDCl_3): δ = 165.0 (C_q), 148.9 (CH), 138.9 (CH), 136.2 (C_q), 134.2 (C_q), 134.0 (C_q), 131.6 (C_q), 128.6 (CH), 127.6 (CH), 127.1 (CH), 126.7 (CH), 126.2 (CH), 125.6 (CH), 125.4 (CH), 121.5 (CH), 43.13 (CH), 30.21 (CH_2), 20.49 (CH_3), 12.34 (CH_3). **IR** (ATR): 2960, 2927, 1596, 1484, 1459, 1379, 1019, 846, 800, 775 cm^{-1} . **MS** (EI) m/z (relative intensity): 261 (1) $[\text{M}]^+$, 260 (6), 246 (50), 233 (100), 219 (16), 176 (10). **HR-MS** (EI): m/z calcd. for $\text{C}_{19}\text{H}_{19}\text{N}^+$ $[\text{M}]^+$ 261.1517, found 261.1522.

2-(*sec*-Butyl)-5-[4-(trifluoromethyl)phenyl]pyridine (187r)**187r**

The general procedure **GP-B** was followed using 2-fluoro-5-[4-(trifluoromethyl)phenyl]pyridine (**11r**) (121 mg, 0.50 mmol), *sec*-BuMgCl (**9f**) (0.50 mL, 1.00 mmol) and **195** (13.3 mg, 25.0 μ mol). Purification by column chromatography (*n*-hexane/EtOAc: 50/1) yielded **187r** (103 mg, 74%, b/l: 79:21) as a colourless solid.

M.p.: 70–72 °C. **$^1\text{H-NMR}$** (400 MHz, CDCl_3): δ = 8.78 (dd, J = 9.0, 2.4 Hz, 1H), 7.81 (dd, J = 9.0, 2.4 Hz, 1H), 7.70 (dd, J = 8.3, 8.3 Hz, 4H), 7.25 (s, 1H), 2.99 – 2.77 (m, 0.81H b; 0.42H, l), 1.89 – 1.59 (m, 2H), 1.42 (h, J = 7.4 Hz, 0.43H, l), 1.33 (d, J = 6.9 Hz, 2.43H, b), 0.96 (t, J = 7.3 Hz, 0.65H, l), 0.88 (t, J = 7.4 Hz, 2.43H, b). **$^{13}\text{C-NMR}$** (100 MHz, CDCl_3): δ = 166.6 (C_q), 147.6 (CH), 141.7 (C_q), 135.0 (CH), 132.8 (C_q), 130.0 (C_q , $^2J_{\text{C-F}}$ = 32.6 Hz, C_q), 127.4 (CH), 126.12 (q, $^3J_{\text{C-F}}$ = 3.8 Hz, CH), 125.7 (q, $^1J_{\text{C-F}}$ = 276 Hz, C_q), 121.8 (CH), 43.52 (CH), 30.12 (CH_2), 20.50 (CH_3), 12.28 (CH_3). **$^{19}\text{F-NMR}$** (377 MHz, CDCl_3): δ = –62.54. **IR** (ATR): 2969, 1616, 1487, 1320, 1163, 1127, 1071, 1017, 864, 830 cm^{-1} . **MS** (EI) m/z (relative intensity): 278 (2) $[\text{M-H}]^-$, 264 (57), 251 (100) 237 (15), 202 (13). **HR-MS** (EI): m/z calcd. for $\text{C}_{16}\text{H}_{15}\text{F}_3\text{N}^-$ $[\text{M-H}]^-$ 278.1151, found 278.1151.

The analytical data are in accordance with those previously reported in the literature.^[87]

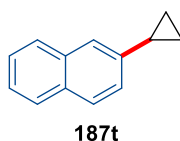
4-[4-(*sec*-Butyl)phenyl]pyridine (187s)**187s**

The general procedure **GP-B** was followed using 4-(4-fluorophenyl)pyridine (**11s**) (86.6 mg, 0.50 mmol), *sec*-BuMgCl (**9f**) (0.50 mL, 1.00 mmol) and **195** (13.3 mg, 25.0 μ mol). Purification by column chromatography (*n*-hexane/EtOAc: 20/1) yielded **187s** (72.8 mg, 69%, b/l: 94:6) as a yellow oil.

$^1\text{H-NMR}$ (400 MHz, CDCl_3): δ = 8.65 (br, 2H), 7.60 (dd, J = 8.2, 3.7 Hz, 2H), 7.51 (d, J = 5.0 Hz, 2H), 7.36 (dd, J = 8.2, 3.7 Hz, 2H), 2.98 (hept, J = 7.0 Hz, 0.93H, b), 2.64 (dd,

$J = 7.4, 7.3$ Hz, 0.26H, l), 1.69 (sext, $J = 7.4$ Hz, 0.27H, b), 1.30 (d, $J = 7.0$ Hz, 5.61H, b), 0.97 (t, $J = 7.4$ Hz, 0.39H, l). $^{13}\text{C-NMR}$ (126 MHz, CDCl_3): $\delta = 150.6$ (C_q), 149.6 (CH), 149.1 (C_q), 135.4 (C_q), 127.5 (CH), 127.2 (CH), 127.0 (CH), 122.0 (CH), 34.09 (CH), 24.04 (CH_3). **IR** (ATR): 2959, 2926, 1595, 1489, 1455, 1403, 992, 810, 575, 526 cm^{-1} . **MS** (EI) m/z (relative intensity): 211 (12) $[\text{M}]^+$, 182 (100), 167 (38), 115 (2). **HR-MS** (EI): m/z calcd. for $\text{C}_{15}\text{H}_{17}\text{N}^+$ $[\text{M}]^+$ 211.1356, found 211.1356.

2-Cyclopropylnaphthalene (187t)

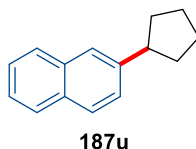


The general procedure **GP-B** was followed using 2-fluoronaphthalene (**11b**) (73.0 mg, 0.50 mmol), cyclopropylmagnesium bromide (**9g**) (1.00 mL, 1.00 mmol) and **195** (13.3 mg, 25.0 μmol). Purification by column chromatography (*n*-hexane) yielded **187t** (58.9 mg, 70%) as a colourless oil.

$^1\text{H-NMR}$ (400 MHz, CDCl_3): $\delta = 7.84 - 7.72$ (m, 3H), 7.54 – 7.52 (m, 1H), 7.49 – 7.37 (m, 2H), 7.20 (dd, $J = 8.5, 1.9$ Hz, 1H), 2.07 (tt, $J = 8.4, 5.1$ Hz, 1H), 1.10 – 0.96 (m, 2H), 0.87 – 0.76 (m, 2H). $^{13}\text{C-NMR}$ (100 MHz, CDCl_3): $\delta = 141.6$ (C_q), 133.7 (C_q), 132.0 (C_q), 128.0 (CH), 127.7 (CH), 127.4 (CH), 126.1 (CH), 125.0 (CH), 124.8 (CH), 123.9 (CH), 15.80 (CH), 9.30 (CH_2). **IR** (ATR): 3054, 3000, 1599, 1510, 1015, 920, 906, 816, 742, 480 cm^{-1} . **MS** (EI) m/z (relative intensity): 168 (61) $[\text{M}]^+$, 167 (100), 153 (53), 141 (14), 115 (16). **HR-MS** (EI): m/z calcd. for $\text{C}_{13}\text{H}_{12}^+$ $[\text{M}]^+$ 168.0934, found 168.0933.

The analytical data are in accordance with those previously reported in the literature.^[365]

2-Cyclopentylnaphthalene (187u)

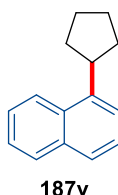


The general procedure **GP-B** was followed using 2-fluoronaphthalene (**11b**) (73.0 mg, 0.50 mmol), cyclopentylmagnesium bromide (**9h**) (0.50 mL, 1.00 mmol) and **195** (13.3 mg, 25.0 μmol). Purification by column chromatography (*n*-hexane) yielded **187u** (76.6 mg, 78%, b/l) as a colourless oil.

¹H-NMR (400 MHz, CDCl₃): δ = 7.87 – 7.71 (m, 3H), 7.67 (dt, J = 1.8, 0.7 Hz, 1H), 7.53 – 7.34 (m, 3H), 3.29 – 3.07 (m, 1H), 2.24 – 2.07 (m, 2H), 1.98 – 1.81 (m, 2H), 1.81 – 1.65 (m, 4H). **¹³C-NMR** (100 MHz, CDCl₃): δ = 144.1 (C_q), 133.7 (C_q), 132.2 (C_q), 127.9 (CH), 127.7 (CH), 127.6 (CH), 126.4 (CH), 126.0 (CH), 125.1 (CH), 125.0 (CH), 46.20 (CH), 34.69 (CH₂), 25.79 (CH₂). **IR** (ATR): 3053, 2952, 2866, 1601, 1508, 888, 852, 815, 745, 476 cm⁻¹. **MS** (EI) m/z (relative intensity): 196 (90) [M]⁺, 181 (22), 167 (100), 152 (53), 141 (39), 128 (35), 115 (16). **HR-MS** (EI): m/z calcd. for C₁₅H₁₆⁺ [M]⁺ 196.1247, found 196.1245.

The analytical data are in accordance with those previously reported in the literature.^[218b]

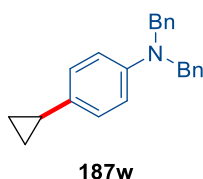
1-Cyclopentyl-naphthalene (187v)



The general procedure **GP-B** was followed using 1-fluoronaphthalene (**11c**) (73.0 mg, 0.50 mmol), cyclopentylmagnesium bromide (**9h**) (0.50 mL, 1.00 mmol) and **195** (13.3 mg, 25.0 μ mol). Purification by column chromatography (*n*-hexane) yielded **187v** (77.5 mg, 79%, b/l) as a colourless oil.

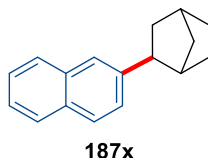
¹H-NMR (400 MHz, CDCl₃): δ = 8.23 – 8.13 (m, 1H), 7.91 – 7.81 (m, 1H), 7.76 – 7.64 (m, 1H), 7.55 – 7.47 (m, 2H), 7.44 (d, J = 5.7 Hz, 2H), 3.80 (p, J = 8.1 Hz, 1H), 2.30 – 2.13 (m, 2H), 1.97 – 1.69 (m, 6H). **¹³C-NMR** (100 MHz, CDCl₃): δ = 142.3 (C_q), 134.0 (C_q), 132.4 (C_q), 128.9 (CH), 126.4 (CH), 125.7 (CH), 125.6 (CH), 125.4 (CH), 124.1 (CH), 122.1 (CH), 41.34 (CH), 33.75 (CH₂), 25.51 (CH₂). **IR** (ATR): 3047, 2952, 2867, 1597, 1510, 1452, 1397, 795, 776, 432 cm⁻¹. **MS** (EI) m/z (relative intensity): 196 (92) [M]⁺, 181 (34), 167 (100), 153 (75), 141 (41), 128 (33), 115 (16). **HR-MS** (EI): m/z calcd. for C₁₅H₁₆⁺ [M]⁺ 196.1247, found 196.1248.

The analytical data are in accordance with those previously reported in the literature.^[209a]

***N,N*-Dibenzyl-4-cyclopropylaniline (187w)**

The general procedure **GP-B** was followed using *N,N*-dibenzyl-4-fluoroaniline (**11i**) (146 mg, 0.50 mmol), cyclopropylmagnesium bromide (**9g**) (1.00 mL, 1.00 mmol) and **195** (13.3 mg, 25.0 μmol). Purification by column chromatography (*n*-hexane/EtOAc: 20/1) yielded **187w** (122 mg, 78%) as a yellow oil.

$^1\text{H-NMR}$ (400 MHz, CDCl_3): δ = 7.39 – 7.33 (m, 4H), 7.32 – 7.27 (m, 6H), 6.96 (dd, J = 8.7, 1.9 Hz, 2H), 6.71 (dd, J = 8.7 Hz, 2H), 4.66 (s, 4H), 1.84 (dt, J = 8.5, 5.1 Hz, 1H), 0.87 (dt, J = 8.5, 6.0 Hz, 2H), 0.60 (dt, J = 8.5, 6.0 Hz, 2H). **$^{13}\text{C-NMR}$** (100 MHz, CDCl_3): δ = 147.4 (C_q), 139.0 (C_q), 131.9 (C_q), 128.7 (2CH), 126.9 (CH), 126.9 (CH), 112.8 (CH), 54.53 (CH_2), 14.55 (CH), 8.30 (CH_2). **IR** (ATR): 3027, 1616, 1519, 1493, 1452, 1360, 1231, 956, 810, 732 cm^{-1} . **MS** (ESI) m/z (relative intensity): 336 (3) $[\text{M}+\text{Na}]^+$, 314 (100) $[\text{M}+\text{H}]^+$, 223 (9). **HR-MS** (ESI): m/z calcd. for $\text{C}_{23}\text{H}_{24}\text{N}^+$ $[\text{M}+\text{H}]^+$ 314.1903, found 314.1906.

2-(Bicyclo[2.2.1]heptan-2-yl)naphthalene (187x)

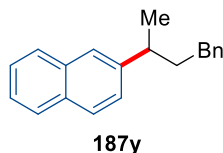
The general procedure **GP-B** was followed using 2-fluoronaphthalene (**11b**) (73.0 mg, 0.50 mmol), (bicyclo[2.2.1]heptan-2-yl)magnesium bromide (**9i**) (1.50 mL, 1.00 mmol) and **195** (13.3 mg, 25.0 μmol). Purification by column chromatography (*n*-hexane) yielded **187x** (78.9 mg, 71%) as a colourless oil.

$^1\text{H-NMR}$ (400 MHz, CDCl_3): δ = 7.86 – 7.72 (m, 3H), 7.64 (d, J = 1.7 Hz, 1H), 7.50 – 7.32 (m, 3H), 2.92 (dd, J = 8.8, 5.8 Hz, 1H), 2.58 – 2.46 (m, 1H), 2.41 (d, J = 4.2 Hz, 1H), 1.90 – 1.75 (m, 2H), 1.73 – 1.54 (m, 3H), 1.44 (ddd, J = 10.5, 7.0, 2.6 Hz, 1H), 1.38 – 1.11 (m, 2H). **$^{13}\text{C-NMR}$** (100 MHz, CDCl_3): δ = 145.1 (C_q), 133.6 (C_q), 131.9 (C_q), 127.9 (CH), 127.8 (CH), 127.6 (CH), 127.2 (CH), 125.9 (CH), 125.1 (CH), 124.3 (CH), 47.57 (CH), 42.92 (CH), 39.04 (CH_2), 37.10 (CH), 36.24 (CH_2), 30.74 (CH_2), 29.15 (CH_2). **IR** (ATR): 2950, 2868, 1600, 1507, 1454, 946, 854, 814, 744, 476 cm^{-1} . **MS** (EI)

m/z (relative intensity): 222 (26) $[M]^+$, 178 (12), 154 (23), 142 (100), 128 (10). **HR-MS** (EI): m/z calcd. for $C_{17}H_{18}^+$ $[M]^+$ 222.1403, found 222.1402.

The analytical data are in accordance with those previously reported in the literature.^[366]

2-(4-Phenylbutan-2-yl)naphthalene (187y)

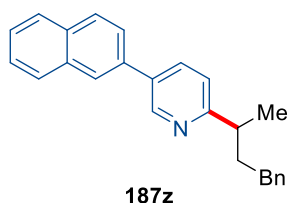


The general procedure **GP-B** was followed using 2-fluoronaphthalene (**11b**) (73.0 mg, 0.50 mmol), (4-phenylbutan-2-yl)magnesium bromide (**9j**) (1.50 mL, 1.00 mmol) and **195** (13.3 mg, 25.0 μ mol). Purification by column chromatography (*n*-hexane) yielded **187y** (100 mg, 77%, b/l: 90:10) as a colourless oil.

¹H-NMR (400 MHz, $CDCl_3$): δ = 7.85 (dt, J = 8.5, 3.2 Hz, 3H), 7.67 (d, J = 1.9 Hz, 1H), 7.56 – 7.37 (m, 3H), 7.30 (ddd, J = 9.6, 4.9, 1.5 Hz, 2H), 7.27 – 7.15 (m, 3H), 3.02 – 2.89 (m, 0.9H, b), 2.85 (t, J = 7.2 Hz, 0.2H, l), 2.70 (t, J = 7.3 Hz, 0.2H, l), 2.67 – 2.49 (m, 1.8H, b), 2.19 – 1.94 (m, 1.8H, b), 1.88 – 1.70 (m, 0.4H, l), 1.46 – 1.34 (m, 2.7H, b). **¹³C-NMR** (100 MHz, $CDCl_3$): δ = 144.8 (C_q), 142.6 (C_q), 133.8 (C_q), 132.4 (C_q), 128.5 (CH), 128.4 (CH), 128.2 (CH), 127.7 (CH), 127.7 (CH), 126.0 (CH), 125.9 (CH), 125.8 (CH), 125.5 (CH), 125.3 (CH), 39.97 (CH_2), 39.78 (CH), 34.11 (CH_2), 22.67 (CH_3). **IR** (ATR): 2957, 2924, 2854, 1601, 1496, 855, 818, 745, 699, 477 cm^{-1} . **MS** (EI) m/z (relative intensity): 260 (13) $[M]^+$, 156 (100), 141 (46), 128 (14), 115 (10). **HR-MS** (EI): m/z calcd. for $C_{20}H_{20}^+$ $[M]^+$ 260.1560, found 260.1560.

The analytical data are in accordance with those previously reported in the literature.^[367]

5-(Naphthalen-2-yl)-2-(4-phenylbutan-2-yl)pyridine (187z)

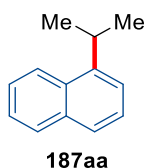


The general procedure **GP-B** was followed using 2-fluoro-5-(naphthalen-2-yl)pyridine (**11q**) (112 mg, 0.50 mmol), (4-phenylbutan-2-yl)magnesium bromide (**9j**) (1.50 mL,

1.00 mmol) and **195** (13.3 mg, 25.0 μmol). Purification by column chromatography (*n*-hexane/EtOAc 50:1) yielded **187z** (123 mg, 73%, b/l: 94:6) as a yellow oil.

$^1\text{H-NMR}$ (400 MHz, CDCl_3): δ = 8.74 (d, J = 2.3 Hz, 1H), 7.92 (dt, J = 18.3, 8.8 Hz, 3H), 7.79 (dd, J = 8.0, 2.2 Hz, 1H), 7.65 – 7.42 (m, 4H), 7.36 – 7.14 (m, 6H), 3.09 (h, J = 7.0 Hz, 0.94H, b), 2.97 (t, J = 7.7 Hz, 0.06H, l), 2.68 (dd, J = 14.1, 11.9, 6.1 Hz, 2H), 2.36 – 2.14 (m, 1H), 2.04 (ddt, J = 13.2, 9.9, 6.4 Hz, 1H), 1.46 (d, J = 6.9 Hz, 3H). **$^{13}\text{C-NMR}$** (100 MHz, CDCl_3): δ = 165.1 (C_q), 150.0 (CH), 142.5 (C_q), 138.0 (CH), 136.6 (C_q), 134.0 (C_q), 133.9 (C_q), 131.7 (C_q), 128.6 (CH), 128.6 (CH), 128.4 (2CH), 127.5 (CH), 126.6 (CH), 126.2 (CH), 125.8 (CH), 125.6 (CH), 125.6 (CH), 121.3 (CH), 41.52 (CH), 38.91 (CH_2), 34.14 (CH_2), 21.09 (CH_3). **IR** (ATR): 2921, 2852, 1597, 1485, 1454, 1029, 801, 777, 746, 699 cm^{-1} . **MS** (EI) m/z (relative intensity): 337 (1) $[\text{M}]^+$, 233 (100), 204 (6), 176 (3). **HR-MS** (EI): m/z calcd. for $\text{C}_{25}\text{H}_{23}\text{N}^+$ $[\text{M}]^+$ 337.1825, found 337.1824.

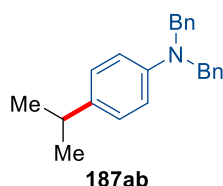
1-Isopropyl-naphthalene (**187aa**)



The general procedure **GP-B** was followed using 1-fluoronaphthalene (**11c**) (73.0 mg, 0.50 mmol), *i*-PrMgBr (**9k**) (0.50 mL, 1.00 mmol) and **195** (13.3 mg, 25.0 μmol). Purification by column chromatography (*n*-hexane) yielded **187aa** (68.9 mg, 81%, b/l: 93:7) as a colourless oil.

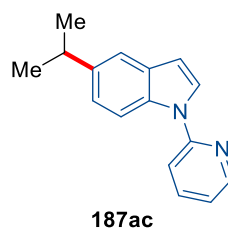
$^1\text{H-NMR}$ (400 MHz, CDCl_3): δ = 8.17 (dd, J = 8.4, 1.6 Hz, 0.93H, b), 8.09 (dd, J = 8.5, 1.3 Hz, 0.07H, l), 7.98 (dd, J = 8.4, 4.1 Hz, 0.14H, l), 7.89 (dd, J = 7.8, 1.3 Hz, 1H), 7.73 (dd, J = 7.4, 1.9 Hz, 1H), 7.62 (dd, J = 8.1, 7.1 Hz, 0.08H, l), 7.59 – 7.43 (m, 4H), 7.38 – 7.30 (m, 0.16H, l), 3.80 (hept, J = 6.9 Hz, 0.92H, b), 3.09 (dd, J = 8.7, 6.7 Hz, 0.14H, l), 1.83 (h, J = 7.4 Hz, 0.13H l), 1.45 (dd, J = 6.9, 0.7 Hz, 5.52H, b), 1.07 (t, J = 7.3 Hz, 0.21H, l). **$^{13}\text{C-NMR}$** (100 MHz, CDCl_3): δ = 144.8 (C_q), 134.0 (C_q), 131.5 (C_q), 129.0 (CH), 126.4 (CH), 125.8 (CH), 125.8 (CH), 125.4 (CH), 123.4 (CH), 121.8 (CH), 28.67 (CH), 23.70 (CH_3). **IR** (ATR): 3047, 2962, 1597, 1510, 1463, 1395, 1006, 796, 776, 435 cm^{-1} . **MS** (EI) m/z (relative intensity): 170 (30) $[\text{M}]^+$, 155 (100), 128 (12), 115 (7). **HR-MS** (EI): m/z calcd. for $[\text{C}_{13}\text{H}_{14}]^+$ $[\text{M}]^+$ 170.1090, found 170.1090.

The analytical data are in accordance with those previously reported in the literature.^[361]

***N,N*-Dibenzyl-4-isopropylaniline (187ab)**

The general procedure **GP-B** was followed using *N,N*-dibenzyl-4-fluoroaniline (**11i**) (146 mg, 0.50 mmol), *i*-PrMgBr (**9k**) (0.50 mL, 1.00 mmol) and **195** (13.3 mg, 25.0 μ mol). Purification by column chromatography (*n*-hexane/EtOAc: 20/1) yielded **187ab** (115 mg, 73%, b/l: 81:19) as a yellow oil.

¹H-NMR (400 MHz, CDCl₃): δ = 7.42 – 7.36 (m, 4H), 7.36 – 7.28 (m, 6H), 7.12 (dd, J = 8.4, 1.8, 1.35H, b), 7.08 – 7.03 (dd, J = 8.4, 1.8, 0.65H, l), 6.77 (dd, J = 8.4, 1.8, 2H), 4.69 (s, 4H), 2.88 (hept, J = 6.9 Hz, 0.68H, b), 2.55 (dd, J = 7.5, 6.4 Hz, 0.64H, l), 1.66 (q, J = 7.4 Hz, 0.65H l), 1.28 (d, J = 6.9 Hz, 4.15H, b), 1.00 (t, J = 7.3 Hz, 0.97H, l). **¹³C-NMR** (100 MHz, CDCl₃): δ = 147.5 (C_q), 139.1 (C_q), 137.2 (C_q), 128.7 (2xCH), 126.9 (CH), 126.9 (CH), 112.6 (CH), 54.50 (CH₂), 33.09 (CH), 24.32 (CH₃). **IR** (ATR): 2957, 1614, 1519, 1452, 1360, 1231, 957, 813, 732, 697 cm⁻¹. **MS** (ESI) m/z (relative intensity): 338 (5) [M+Na]⁺, 316 (100) [M+H]⁺, 225 (3). **HR-MS** (ESI): m/z calcd. for C₂₃H₂₆N⁺ [M+H]⁺ 316.2060, found 316.2064.

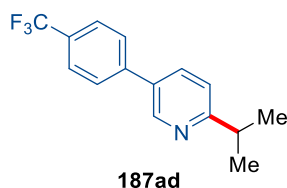
5-Isopropyl-1-(pyridin-2-yl)-1*H*-indole (187ac)

The general procedure **GP-B** was followed using 5-fluoro-1-methyl-1*H*-indole (**11o**) (74.6 mg, 0.50 mmol), *i*-PrMgBr (**9k**) (0.50 mL, 1.00 mmol) and **195** (13.3 mg, 25.0 μ mol). Purification by column chromatography (*n*-hexane/EtOAc: 50:1) yielded **187ac** (82.6 mg, 70%, b/l: 85:15) as a red oil.

¹H-NMR (400 MHz, CDCl₃): δ = 8.56 (dd, J = 4.8, 2.0, 1H), 8.13 (ddd, J = 8.5, 2.2, 1.5 Hz, 1H), 7.81 (ddd, J = 8.3, 7.3, 1.9 Hz, 1H), 7.72 (dd, J = 7.0, 3.5 Hz, 1H), 7.55 – 7.42 (m, 2H), 7.23 – 7.09 (m, 2H), 6.67 (ddd, J = 5.4, 3.6, 0.9 Hz, 1H), 3.05 (p, J = 6.9 Hz, 0.74H, b), 2.67 (t, J = 7.3 Hz, 0.54H, l), 1.74 (h, J = 7.6 Hz, 0.55H, l), 1.34 (d, J = 7.0 Hz, 4.44H, b), 0.98 (t, J = 7.3 Hz, 0.79H, l). **¹³C-NMR** (100 MHz, CDCl₃): δ = 152.7 (C_q),

149.1 (C_q), 142.1 (C_q), 138.4 (C_q), 133.7 (CH), 130.8 (CH), 126.1 (CH), 122.4 (CH), 119.9 (CH), 118.2 (CH), 114.4 (CH), 112.9 (CH), 105.6 (CH), 34.22 (CH), 24.68 (CH₃). **IR** (ATR): 2957, 2924, 1591, 1475, 1435, 1341, 1292, 1261, 775, 720 cm⁻¹. **MS** (EI) *m/z* (relative intensity): 259 (21) [M+Na]⁺, 237 (100) [M+H]⁺, 195 (8). **HR-MS** (ESI): *m/z* calcd. for C₁₆H₁₇N₂⁺ [M+H]⁺ 237.1386, found 237.1388.

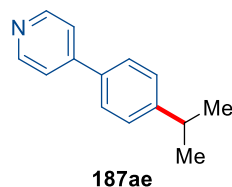
2-Isopropyl-5-[4-(trifluoromethyl)phenyl]pyridine (187ad)



The general procedure **GP-B** was followed using 2-fluoro-5-[4-(trifluoromethyl)phenyl]pyridine (**11r**) (121 mg, 0.50 mmol), *i*-PrMgBr (**9k**) (0.50 mL, 1.00 mmol) and **195** (13.3 mg, 25.0 μmol). Purification by column chromatography (*n*-hexane/EtOAc: 50/1) yielded **187ad** (96.8 mg, 73%, b/l: >99:1) as an orange oil.

¹H-NMR (400 MHz, CDCl₃): δ = 8.80 (t, *J* = 3.0 Hz, 1H), 7.86 (dt, *J* = 8.2, 3.0 Hz, 1H), 7.80 – 7.60 (m, 4H), 7.32 (dd, *J* = 8.1, 3.4 Hz, 1H), 3.18 (dq, *J* = 7.0, 3.5 Hz, 1H), 1.38 (dd, *J* = 7.0, 3.5 Hz, 6H). **¹³C-NMR** (100 MHz, CDCl₃): δ = 167.3 (C_q), 147.4 (CH), 141.6 (C_q), 135.4 (CH), 132.9 (C_q), 130.09 (q, ²*J*_{C-F} = 33.2 Hz, C_q), 127.4 (CH), 126.2 (q, ³*J*_{C-F} = 3.6 Hz, CH), 124.28 (q, ¹*J*_{C-F} = 272.1 Hz, C_q), 121.0 (CH), 36.14 (CH), 22.68 (CH₃). **¹⁹F-NMR** (282 MHz, CDCl₃): δ = -62.54. **IR** (ATR): 2967, 1486, 1324, 1165, 1111, 1071, 1017, 854, 828, 603 cm⁻¹. **MS** (EI) *m/z* (relative intensity): 265 (19) [M]⁺, 250 (100), 237 (57), 202 (12). **HR-MS** (EI): *m/z* calcd. for C₁₅H₁₄F₃N⁺ [M]⁺ 265.1073, found 265.1074.

4-(4-Isopropylphenyl)pyridine (187ae)



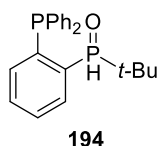
The general procedure **GP-B** was followed using 4-(4-fluorophenyl)pyridine (**11s**) (86.6 mg, 0.50 mmol), *i*-PrMgBr (**9k**) (0.50 mL, 1.00 mmol) and **195** (13.3 mg, 25.0 μmol). Purification by column chromatography (*n*-hexane/EtOAc: 50/1) yielded **187ae** (74.0 mg, 74%, b/l: 85:15) as a colourless oil.

¹H-NMR (400 MHz, CDCl₃): δ = 8.64 (d, J = 4.6 Hz, 2H), 7.59 (dd, J = 6.4, 4.5 Hz, 2H), 7.50 (dd, J = 6.3, 1.5 Hz, 2H), 7.30 (dd, J = 6.3, 1.5 Hz, 2H), 2.67 (h, J = 7.2 Hz, 1H), 1.64 (p, J = 7.4 Hz, 2H), 1.28 (d, J = 6.9 Hz, 2.55H, b), 0.95 (t, J = 7.3 Hz, 0.45H, l), 0.86 (t, J = 7.4 Hz, 2.55H, b). **¹³C-NMR** (100 MHz, CDCl₃): δ = 150.3 (CH), 149.1 (C_q), 148.4 (C_q), 135.7 (C_q), 128.0 (CH), 127.0 (CH), 121.6 (CH), 41.60 (CH), 31.22 (CH₂), 21.89 (CH₃), 12.37 (CH₃). **IR** (ATR): 2964, 2926, 1593, 1540, 1488, 1402, 1061, 1029, 809, 515 cm⁻¹. **MS** (EI) m/z (relative intensity): 197 (26) [M]⁺, 182 (100), 167 (42), 152 (6). **HR-MS** (EI): m/z calcd. for C₁₄H₁₅N⁺ [M]⁺ 197.1199, found 197.1198.

The analytical data are in accordance with those previously reported in the literature.^[368]

5.3.2. Synthesis of 194 and 195

tert-Butyl (2-(diphenylphosphaneyl)phenyl)phosphine oxide (194)



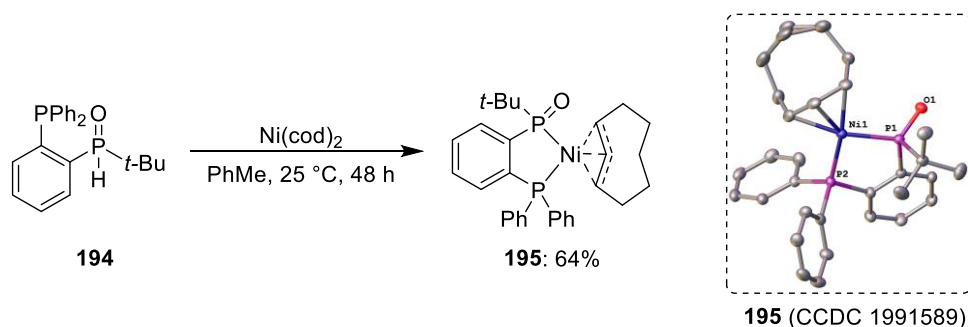
(2-Bromophenyl)diphenylphosphine (1.98 g 5.8 mmol) in THF (10 mL) was added dropwise, at -78°C , to a solution of *n*-butyllithium (3.8 mL, 5.8 mmol, 1.6 M in hexane) and the mixture was stirred at -78°C for 2 hours. The reaction solution is then transferred, at 0°C , to a reaction vessel, in which a solution of *tert*-butyldichlorophosphine (1.05 g, 5.8 mmol) in 5 mL of THF was placed and stirred for 1.5 h. Then H₂O (50 mL) was added and the mixture was warmed to ambient temperature overnight. NaCl (20 mL) was added and the mixture was extracted with CH₂Cl₂ (3 x 40 mL), dried over Na₂SO₄ and concentrated in vacuo. Purification of the remaining crude product by column chromatography on silica gel (EtOAc) yielded **194** (1.15 g, 54%) as a colourless viscous oil.

¹H-NMR (400 MHz, CDCl₃): δ = 8.00 (d, J = 8.5 Hz, 1H), 7.48 (dt, J = 30.2, 7.4 Hz, 3H), 7.34 (dt, J = 10.3, 3.0 Hz, 6H), 7.27 – 7.19 (m, 2H), 7.18 – 7.07 (m, 1H), 1.25 (d, J = 15.7 Hz, 9H). **¹³C-NMR** (101 MHz, CDCl₃): δ = 140.7 (dd, $^1J_{\text{C-P}}$ = 20.9, 7.5 Hz, C_q), 135.9 (d, $^1J_{\text{C-P}}$ = 9.8 Hz, C_q), 135.6 (d, $^1J_{\text{C-P}}$ = 11.2 Hz, C_q), 135.1 (d, $^3J_{\text{C-P}}$ = 7.6 Hz, CH), 133.9 (d, $^2J_{\text{C-P}}$ = 19.5 Hz, CH), 133.5 (d, $^2J_{\text{C-P}}$ = 19.5 Hz, CH), 133.1 (t, $^3J_{\text{C-P}}$ = 7.4 Hz, CH), 132.0 (CH), 129.1 (d, $^3J_{\text{C-P}}$ = 2.1 Hz, CH), 128.8 (t, $^2J_{\text{C-P}}$ = 13.8 Hz), 66.26 (d, $^1J_{\text{C-P}}$

5. Experimental Part

= 7.8 Hz), 24.51 (d, $^2J_{C-P}$ = 4.0 Hz). $^{31}\text{P-NMR}$ (162 MHz, CDCl_3): δ = 36.37 (dd, J = 474, 70.4 Hz), -15.67 (d, J = 70.4 Hz). $^{31}\text{P}\{\text{H}\}\text{-NMR}$ (162 MHz, CDCl_3): δ = 36.37 (d, J = 70.4 Hz), -15.59 (d, J = 70.4 Hz). **IR** (ATR): 2959, 2340, 1475, 1434, 1167, 911, 726, 695, 613, 524 cm^{-1} . **MS** (ESI) m/z (relative intensity): 756 (100) $[2\text{M}+\text{Na}]^+$, 569 (14), 389 (68) $[\text{M}+\text{Na}]^+$, 367 (78) $[\text{M}+\text{H}]^+$. **HR-MS** (ESI): m/z calcd. for $\text{C}_{22}\text{H}_{25}\text{OP}_2^+$ $[\text{M}+\text{H}]^+$ 367.1375, found 367.1382.

Synthesis of **195**



Under an Ar atmosphere a mixture of $\text{Ni}(\text{cod})_2$ (138 mg, 0.50 mmol) and **194** (183 mg, 0.50 mmol) in toluene (5.0 mL) was stirred at ambient temperature for 48 h. The solvent was removed *in vacuo* and the resulting residue was washed with dry *n*-hexane (3 x 10 mL) under an Ar atmosphere. The remaining solid was dried in vacuum to provide **195** (176 mg, 64%) as a brown solid. **195** was transferred to a glovebox, where it stays stable for months.

M.p.: 195–199 (decomposition). $^1\text{H-NMR}$ (400 MHz, toluene- d_8): δ = 8.41 (d, J = 6.6 Hz, 1H), 7.59 (ddd, J = 10.2, 6.5, 2.9 Hz, 2H), 7.28 (t, J = 7.4 Hz, 2H), 7.13 (d, J = 4.0 Hz, 5H), 6.96 – 6.81 (m, 4H), 5.18 (d, J = 9.5 Hz, 1H), 4.64 (t, J = 8.5 Hz, 1H), 4.26 (dq, J = 8.7, 4.2 Hz, 1H), 2.97 (dd, J = 14.7, 6.8 Hz, 1H), 1.89 (dtt, J = 27.0, 11.0, 5.5 Hz, 2H), 1.63 – 1.39 (m, 2H), 1.34 – 1.07 (m, 5H), 1.01 (d, J = 13.7 Hz, 9H). $^{13}\text{C-NMR}$ (101 MHz, toluene- d_8): δ = 135.9 (d, J = 42.2 Hz, C_q), 135.9 (d, J = 42.2 Hz, C_q), 134.2 (d, J = 12.4 Hz, CH), 132.2 (d, J = 11.7 Hz, CH), 132.0 (d, J = 11.4 Hz, CH), 131.5 (d, J = 42.2 Hz, C_q), 131.3 (d, J = 42.2 Hz, C_q), 130.8 (d, J = 2.3 Hz, CH), 130.6 (t, J = 3.2 Hz, CH), 129.8 (d, J = 6.0 Hz, CH), 129.5 (d, J = 2.2 Hz, CH), , 129.0 (CH), 128.9 (CH), 128.5 (CH), 109.8 (d, J = 2.7 Hz, CH), 76.90 (d, J = 18.0 Hz, CH), 74.88 (d, J = 20.3 Hz, CH), 38.56 (d, J = 28.1 Hz, C_q), 30.85 (d, J = 49.0 Hz, 2 CH_2), 29.35 (d, J = 5.0 Hz, CH_2), 28.78 (t, J = 3.6 Hz, CH_2), 26.94 (d, J = 5.5 Hz, CH_3), 23.68 (CH_2). $^{31}\text{P-NMR}$ (162 MHz, toluene- d_8): δ = 125.9 (d, J = 17.6 Hz), 59.09 (d, J = 17.4 Hz). **IR** (ATR): 2933, 1435,

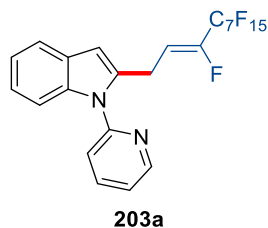
1109, 1088, 1044, 998, 744, 694, 547, 486 cm^{-1} . **MS** (LIFDI) m/z (relative intensity): 532 (100) $[\text{M}]^+$. **HR-MS** (ESI): m/z calcd. for $\text{C}_{30}\text{H}_{36}\text{NiOP}_2^+$ $[\text{M}+\text{H}]^+$ 533.1668, found 533.1646.

Crystals suitable for X-Ray crystallography were grown from a saturated solution of complex **195** in toluene at $-25\text{ }^\circ\text{C}$.

5.4. Manganese(I)-Catalyzed Allylative and Alkenylative C–H/C–F Functionalization

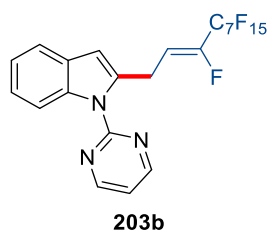
5.4.1. Characterization Data

(*Z*)-2-(1*H*,1*H*,2*H*-Perfluorodec-2-en-1-yl)-1-(pyridin-2-yl)-1*H*-indole (**203a**)



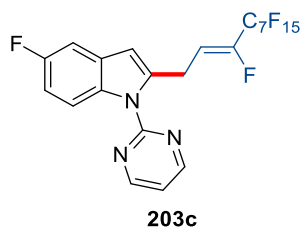
The general procedure **GP-C** was followed using 1-(pyridin-2-yl)-1*H*-indole (**201a**) (97.1 mg, 0.50 mmol), 1*H*,1*H*,2*H*-perfluorodec-1-ene (**45a**) (268 mg, 0.60 mmol) and [MnBr(CO)₅] (10.3 mg, 37.5 μmol). Purification by column chromatography (*n*-hexane/EtOAc: 10/1) yielded **203a** (301 mg, 97%, *Z/E*: 88:12) as a yellow oil.

¹H-NMR (400 MHz, CDCl₃): δ = 8.66 (dd, *J* = 4.9, 1.8 Hz, 1H), 7.90 (dd, *J* = 7.8, 2.0 Hz, 1H), 7.68 – 7.56 (m, 1H), 7.50 (d, *J* = 7.9 Hz, 1H), 7.45 – 7.37 (m, 1H), 7.33 (ddd, *J* = 7.5, 4.8, 1.1 Hz, 1H), 7.25 – 7.16 (m, 2H), 6.53 (s, 1H), 6.18 (dt, *J* = 22.4, 8.2 Hz, 0.12H, *E*), 5.84 (dt, *J* = 32.7, 7.5 Hz, 0.88H, *Z*), 3.93 (dd, *J* = 7.6, 2.4 Hz, 1.76H, *Z*), 3.87 (dd, *J* = 7.8, 1.2 Hz, 0.24H, *E*). **¹³C-NMR** (101 MHz, CDCl₃): δ = 151.0 (C_q), 149.9 (C_q), 146.3 (dt, ¹*J*_{C–F} = 261 Hz, ²*J*_{C–F} = 29.1 Hz, C_q), 138.6 (CH), 137.3 (C_q), 136.3 (C_q), 128.5 (C_q), 122.6 (CH), 122.3 (CH), 121.2 (CH), 120.7 (CH), 120.6 (CH), 117.3 (dt, ¹*J*_{C–F} = 289 Hz, ²*J*_{C–F} = 32.9 Hz, C_q), 113.5 (dt, ²*J*_{C–F} = 8.8 Hz, ³*J*_{C–F} = 4.5 Hz, CH), 112.9 (m, C_q), 111.4 (m, C_q), 111.0 (m, C_q), 110.7 (m, C_q), 110.3 (CH), 108.7 (m, C_q), 107.0 (m, C_q), 103.9 (CH), 22.84 (d, ³*J*_{C–F} = 4.3 Hz, CH₂). **¹⁹F-NMR** (377 MHz, CDCl₃): δ = –80.9 (m), –114.9 (m), –117.50 (m), –122.1 (m), –122.8 (m), –123.0 (m), –126.2 (m), –130.8 (m). **IR** (ATR): 1588, 1471, 1457, 1439, 1237, 1201, 1145, 909, 732, 663 cm^{–1}. **MS** (ESI) *m/z* (relative intensity): 643 (83) [M+Na]⁺, 621 (100) [M+H]⁺, 346 (9). **HR-MS** (ESI): *m/z* calcd. for C₂₃H₁₃F₁₆N₂⁺ [M+H]⁺ 621.0818, found 621.0811.

(Z)-2-(1*H*,1*H*,2*H*-Perfluorodec-2-en-1-yl)-1-(pyrimidin-2-yl)-1*H*-indole (203b)

The general procedure **GP-C** was followed using 1-(pyrimidin-2-yl)-1*H*-indole (**201b**) (97.6 mg, 0.50 mmol), 1*H*,1*H*,2*H*-perfluorodec-1-ene (**45a**) (268 mg, 0.60 mmol) and [MnBr(CO)₅] (10.3 mg, 37.5 μmol). Purification by column chromatography (*n*-hexane/EtOAc: 10/1) yielded **203b** (298 mg, 96%, *Z/E*: 87:13) as an orange solid.

M.p.: 54–56 °C. **¹H-NMR** (400 MHz, CDCl₃): δ = 8.66 (d, *J* = 4.8 Hz, 2H), 8.31 (d, *J* = 8.1 Hz, 1H), 7.46 (d, *J* = 7.6 Hz, 1H), 7.15 (dt, *J* = 25.1, 7.4 Hz, 2H), 7.02 (dd, *J* = 4.8, 3.3 Hz, 1H), 6.42 (s, 1H), 6.16 (dt, *J* = 22.7, 7.9 Hz, 0.13H, *E*), 5.81 (dt, *J* = 33.2, 7.4 Hz, 0.87H, *Z*), 4.08 (d, *J* = 7.6 Hz, 2H). **¹³C-NMR** (101 MHz, CDCl₃): δ = 158.2 (CH), 146.1 (dt, ¹*J*_{C-F} = 260 Hz, ²*J*_{C-F} = 28.9 Hz, C_q), 137.2 (C_q), 136.7 (C_q), 129.1 (C_q), 123.5 (CH), 122.4 (CH), 120.2 (CH), 117.3 (dt, ¹*J*_{C-F} = 288 Hz, ²*J*_{C-F} = 32.8 Hz, C_q), 117.2 (CH), 114.7 (CH), 114.5 (dt, ²*J*_{C-F} = 8.5 Hz, ³*J*_{C-F} = 4.4 Hz, CH), 113.4 (m, C_q), 113.0 (m, C_q), 111.0 (m, C_q), 110.6 (m, C_q), 110.4 (m, C_q), 108.4 (m, C_q), 108.0 (m, C_q), 107.6 (CH), 25.10 (d, ³*J*_{C-F} = 4.0 Hz, CH₂). **¹⁹F-NMR** (377 MHz, CDCl₃): δ = –80.85 (m), –114.9 (m), –117.4 (m), –122.0 (m), –122.8 (m), –122.9 (m), –126.2 (m), –130.9 (m). **IR** (ATR): 1564, 1455, 1429, 1198, 1144, 1108, 804, 744, 664, 530 cm^{–1}. **MS** (ESI) *m/z* (relative intensity): 644 (49) [M+Na]⁺, 622 (100) [M+H]⁺, 346 (11). **HR-MS** (ESI): *m/z* calcd. for C₂₂H₁₂F₁₆N₃⁺ [M+H]⁺ 622.0770, found 622.0751.

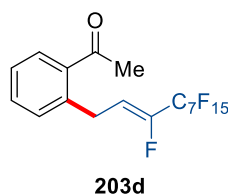
(Z)-2-(1*H*,1*H*,2*H*-Perfluorodec-2-en-1-yl)-5-fluoro-1-(pyrimidin-2-yl)-1*H*-indole (203c)

The general procedure **GP-C** was followed using 5-fluoro-1-(pyrimidin-2-yl)-1*H*-indole (**201c**) (107 mg, 0.50 mmol), 1*H*,1*H*,2*H*-perfluorodec-1-ene (**45a**) (268 mg, 0.60 mmol)

and $[\text{MnBr}(\text{CO})_5]$ (10.3 mg, 37.5 μmol). Purification by column chromatography (*n*-hexane/EtOAc: 10/1) yielded **203c** (285 mg, 89%, *Z/E*: 85:15) as a red solid.

M.p.: 61–63 °C. **$^1\text{H-NMR}$** (400 MHz, CDCl_3): δ = 8.85 – 8.54 (m, 2H), 8.39 (dd, J = 9.0, 4.4 Hz, 1H), 7.22 – 7.16 (m, 1H), 7.14 (dd, J = 4.7, 1.4 Hz, 1H), 7.06 – 6.91 (m, 1H), 6.46 (d, J = 3.5 Hz, 1H), 6.25 (dt, J = 22.2, 8.0 Hz, 0.15H, *E*), 5.90 (dt, J = 33.0, 7.3 Hz, 0.85H, *Z*), 4.17 (d, J = 5.1 Hz, 2H). **$^{13}\text{C-NMR}$** (101 MHz, CDCl_3): δ = 159.2 (d, $^1J_{\text{C-F}}$ = 238 Hz, C_q), 158.2 (CH), 158.0 (C_q), 146.2 (dt, $^1J_{\text{C-F}}$ = 261 Hz, $^2J_{\text{C-F}}$ = 28.9 Hz, C_q), 138.4 (C_q), 133.5 (C_q), 129.8 (d, $^3J_{\text{C-F}}$ = 10.1 Hz, C_q), 117.3 (CH), 116.7 (dt, $^1J_{\text{C-F}}$ = 288 Hz, $^2J_{\text{C-F}}$ = 32.9 Hz, C_q), 115.95 (d, $^2J_{\text{C-F}}$ = 9.0 Hz, CH), 114.16 (dt, $^2J_{\text{C-F}}$ = 8.4 Hz, $^3J_{\text{C-F}}$ = 4.5 Hz, CH), 113.6 (m, C_q), 113.0 (m, C_q), 111.2 (d, $^2J_{\text{C-F}}$ = 24.9 Hz, CH), 110.8 (m, C_q), 110.4 (m, C_q), 108.4 (m, C_q), 107.9 (m, C_q), 107.4 (d, $^3J_{\text{C-F}}$ = 4.0 Hz, CH), 105.4 (d, $^2J_{\text{C-F}}$ = 23.6 Hz, CH), 25.28 (d, $^3J_{\text{C-F}}$ = 4.0 Hz, CH_2). **$^{19}\text{F-NMR}$** (377 MHz, CDCl_3): δ = –80.90 (m), –114.9 (m), –117.5 (m), –121.0 (m), –122.8 (m), –122.9 (m), –123.6 (m), –126.2 (m), –131.1 (m). **IR** (ATR): 1578, 1473, 1450, 1431, 1201, 1148, 1111, 803, 709, 665 cm^{-1} . **MS** (ESI) m/z (relative intensity): 662 (6) $[\text{M}+\text{Na}]^+$, 640 (100) $[\text{M}+\text{H}]^+$, 355 (26). **HR-MS** (ESI): m/z calcd. for $\text{C}_{22}\text{H}_{11}\text{F}_{17}\text{N}_3^+$ $[\text{M}+\text{H}]^+$ 640.0676, found 640.0677.

(*Z*)-1-[2-(1*H*,1*H*,2*H*-Perfluorodec-2-en-1-yl)phenyl]ethan-1-one (**203d**)

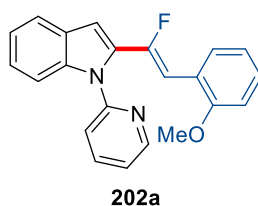


The general procedure **GP-D** was followed using *N*-(4-methoxyphenyl)-1-phenylethan-1-imine (**201d**) (113 mg, 0.50 mmol), 1*H*,1*H*,2*H*-perfluorodec-1-ene (**45a**) (669 mg, 1.50 mmol), $[\text{MnBr}(\text{CO})_5]$ (13.7 mg, 50.0 μmol), NaOAc (16.4 mg, 0.20 mmol) and K_2CO_3 (104 mg, 0.75 mmol). Hydrolysis with HCl (5 mL, 1M) and purification by column chromatography (*n*-hexane/EtOAc: 20/1) yielded **203d** (197 mg, 72%, *Z/E*: 97:3) as a yellow oil.

$^1\text{H-NMR}$ (300 MHz, CDCl_3): δ = 7.79 (dd, J = 7.7, 1.4 Hz, 1H), 7.47 (dd, J = 7.5, 1.3 Hz, 1H), 7.37 (dd, J = 7.6, 1.4 Hz, 1H), 7.29 (dd, J = 7.6, 1.3 Hz, 1H), 6.16 (dt, J = 23.7, 8.5 Hz, 0.3H, *E*), 5.93 (dt, J = 33.7, 7.7 Hz, 0.97H, *Z*), 3.83 (dd, J = 7.7, 2.3 Hz, 2H), 2.62 (s, 3H). **$^{13}\text{C-NMR}$** (151 MHz, CDCl_3): δ = 201.2 (C_q), 145.9 (dt, $^1J_{\text{C-F}}$ = 259 Hz, $^2J_{\text{C-F}}$ = 29.4 Hz, C_q), 138.1 (C_q), 136.9 (C_q), 132.6 (CH), 131.7 (CH), 130.3 (CH), 127.3 (CH), 117.30

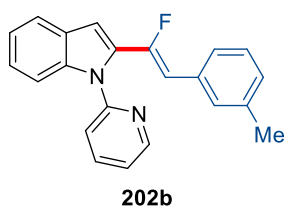
(dt, $^1J_{C-F} = 289$, $^2J_{C-F} = 33.3$ Hz C_q), 115.5 (CH), 112.9 (m), 112.2 (m), 111.3 (m), 110.7 (m), 110.3 (m), 108.90 (m), 29.30 (CH₃), 28.88 (CH₂). **^{19}F -NMR** (282 MHz, CDCl₃): $\delta = -80.87$ (m), -117.5 (m), -122.0 (m), -122.1 (m), -122.8 (m), -123.0 (m), -126.2 (m), -132.4 (m). **IR** (ATR): 1687, 1358, 1236, 1198, 1144, 1106, 759, 708, 664, 600 cm⁻¹. **MS** (ESI) m/z (relative intensity): 1115 (3) [2M+Na]⁺, 569 (100) [M+Na]⁺, 507 (10), 309 (8). **HR-MS** (ESI): m/z calcd. for C₁₈H₁₁F₁₆O⁺ [M+H]⁺ 547.0549, found 547.0545.

(Z)-2-[1-Fluoro-2-(2-methoxyphenyl)vinyl]-1-(pyridin-2-yl)-1H-indole (202a)



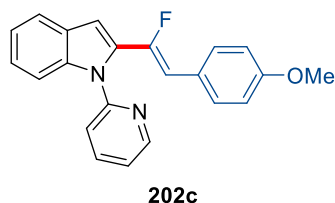
The general procedure **GP-D** was followed using 1-(pyridin-2-yl)-1H-indole (**201a**) (97.1 mg, 0.50 mmol), 1-(2,2-difluorovinyl)-2-methoxybenzene (**44a**) (255 mg, 1.50 mmol), [MnBr(CO)₅] (13.7 mg, 50.0 μ mol), NaOAc (8.20 mg, 0.10 mmol) and K₂CO₃ (69.1 mg, 0.50 mmol). Purification by column chromatography (*n*-hexane/EtOAc: 10/1) yielded **202a** (149 mg, 87%, *Z/E*: 80:20) as a yellow oil.

1H -NMR (300 MHz, CDCl₃): $\delta = 8.70$ (ddd, $J = 4.9, 2.0, 0.8$ Hz, 0.8H, *Z*), 8.53 (ddd, $J = 4.9, 2.0, 0.8$ Hz, 0.2H, *E*), 7.91 – 7.82 (m, 1H), 7.74 – 7.69 (m, 1H), 7.58 (dd, $J = 8.4, 0.9$ Hz, 1H), 7.46 (dt, $J = 8.0, 0.9$ Hz, 1H), 7.38 – 7.29 (m, 2H), 7.26 (dt, $J = 7.3, 1.5$ Hz, 2H), 7.09 (d, $J = 0.9$ Hz, 1H), 7.03 – 6.94 (m, 1H), 6.88 (dd, $J = 8.3, 1.1$ Hz, 1H), 6.67 (d, $J = 21.6$ Hz, 0.2H, *E*), 6.54 (d, $J = 39.9$ Hz, 0.8H, *Z*), 3.80 (s, 2.4H, *Z*), 3.69 (s, 0.6H, *E*). **^{13}C -NMR** (125 MHz, CDCl₃): $\delta = 156.3$ (C_q), 151.8 (C_q), 150.7 (d, $^1J_{C-F} = 255$ Hz, C_q), 149.7 (C_q), 149.3 (CH), 138.7 (C_q), 138.3 (CH), 132.7 (d, $^2J_{C-F} = 31.3$ Hz, C_q), 129.7 (d, $^3J_{C-F} = 13.6$ Hz, CH), 128.7 (CH), 127.7 (C_q), 124.1 (CH), 122.2 (CH), 121.5 (CH), 121.2 (CH), 120.9 (CH), 120.7 (CH), 111.3 (CH), 110.5 (CH), 107.2 (d, $^4J_{C-F} = 4.3$ Hz, CH), 103.6 (d, $^3J_{C-F} = 7.4$ Hz, CH), 55.6 (CH₃). **^{19}F -NMR** (282 MHz, CDCl₃): $\delta = -94.2$ (dd, $J = 19.1, 2.5$ Hz, 0.20F; *E*), -108.2 (d, $J = 40.0$ Hz, 0.80F, *Z*). **IR** (ATR): 3073, 2836, 1586, 1466, 1436, 1245, 1028, 906, 779, 725 cm⁻¹. **MS** (EI) m/z (relative intensity): 344 (100) [M]⁺, 313 (80), 237 (29). **HR-MS** (EI): m/z calcd. for C₂₂H₁₇FN₂O⁺ [M]⁺ 344.1325, found 344.1312.

(Z)-2-[1-Fluoro-2-(*m*-tolyl)vinyl]-1-(pyridin-2-yl)-1*H*-indole (202b)

The general procedure **GP-D** was followed using 1-(pyridin-2-yl)-1*H*-indole (**201a**) (97.1 mg, 0.50 mmol), 1-(2,2-difluorovinyl)-3-methylbenzene (**44b**) (231 mg, 1.50 mmol), [MnBr(CO)₅] (13.7 mg, 50.0 μmol), NaOAc (8.20 mg, 0.10 mmol) and K₂CO₃ (69.1 mg, 0.50 mmol). Purification by column chromatography (*n*-hexane/EtOAc: 10/1) yielded **202b** (131 mg, 80%, *Z/E*: 89:11) as a yellow oil.

¹H-NMR (300 MHz, CDCl₃): δ = 8.69 (dd, *J* = 4.9, 1.8 Hz, 0.89H, *Z*), 8.60 – 8.49 (m, 0.11H, *E*), 7.87 (dd, *J* = 7.8, 1.9 Hz, 1H), 7.69 (d, *J* = 7.8 Hz, 1H), 7.57 (d, *J* = 8.1 Hz, 1H), 7.45 (d, *J* = 8.0 Hz, 1H), 7.38 – 7.18 (m, 6H), 7.08 (d, *J* = 7.5 Hz, 1H), 7.04 – 7.01 (m, 1H), 6.46 (d, *J* = 19.1 Hz, 0.11H, *E*), 6.02 (d, *J* = 37.6 Hz, 0.89H, *Z*), 2.35 (s, 2.67H, *Z*), 2.21 (s, 0.33H, *E*). ¹³C-NMR (100 MHz, CDCl₃): δ = 151.0 (d, ¹*J*_{C-F} = 257 Hz, C_q), 151.9 (C_q), 149.6 (CH), 138.7 (C_q), 138.5 (CH), 138.2 (C_q), 133.4 (C_q), 132.4 (d, ²*J*_{C-F} = 30.1 Hz, C_q), 129.6 (d, ³*J*_{C-F} = 7.6 Hz, CH), 128.6 (CH), 128.5 (CH), 127.9 (C_q), 126.2 (d, ⁴*J*_{C-F} = 7.7 Hz, CH), 124.4 (CH), 122.4 (CH), 121.7 (CH), 121.3 (CH), 120.7 (CH), 111.4 (CH), 110.3 (d, ³*J*_{C-F} = 9.5 Hz, CH), 107.5 (d, ⁴*J*_{C-F} = 4.5 Hz, CH), 21.6 (CH₃). ¹⁹F-NMR (376 MHz, CDCl₃): δ = -92.4 (dd, *J* = 19.0, 2.9 Hz, 0.11F, *E*), -105.9 (d, *J* = 38.0 Hz, 0.89F, *Z*). IR (ATR): 3051, 1586, 1468, 1348, 1146, 1436, 906, 777, 730, 669 cm⁻¹. MS (EI) *m/z* (relative intensity): 328 (100) [M]⁺, 307 (75), 237 (30). HR-MS (EI): *m/z* calcd. for C₂₂H₁₇FN₂⁺ [M]⁺ 328.1376, found 328.1377.

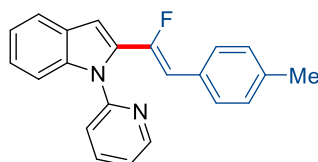
(Z)-2-[1-Fluoro-2-(4-methoxyphenyl)vinyl]-1-(pyridin-2-yl)-1*H*-indole (202c)

The general procedure **GP-D** was followed using 1-(pyridin-2-yl)-1*H*-indole (**201a**) (97.1 mg, 0.50 mmol), 1-(2,2-difluorovinyl)-4-methoxybenzene (**44c**) (255 mg, 1.50 mmol), [MnBr(CO)₅] (13.7 mg, 50.0 μmol), NaOAc (8.20 mg, 0.10 mmol) and K₂CO₃ (69.1 mg,

0.50 mmol). Purification by column chromatography (*n*-hexane/EtOAc: 10/1) yielded **202c** (149 mg, 87%, *Z/E*: 87:13) as a yellow oil.

¹H-NMR (300 MHz, CDCl₃): δ = 8.72 – 8.61 (m, 0.87H, *Z*), 8.54 (ddd, *J* = 4.9, 2.0, 0.8 Hz, 0.13H, *E*), 7.84 (dd, *J* = 7.8, 1.9 Hz, 1H), 7.68 – 7.63 (m, 1H), 7.57 – 7.50 (m, 1H), 7.46 – 7.38 (m, 3H), 7.35 – 7.29 (m, 1H), 7.26 – 7.17 (m, 3H), 6.97 (d, *J* = 1.0 Hz, 1H), 6.86 – 6.79 (m, 1H), 6.42 (d, *J* = 19.1 Hz, 0.13H, *E*), 5.97 (d, *J* = 38.2 Hz, 0.87H, *Z*), 3.80 (s, 2.61H, *Z*), 3.72 (s, 0.39H, *E*). **¹³C-NMR** (125 MHz, CDCl₃): δ = 159.0 (C_q), 151.9 (C_q); 149.8 (d, ¹*J*_{C–F} = 254 Hz, C_q), 149.5 (CH), 138.6 (C_q), 138.5 (CH), 132.6 (d, ²*J*_{C–F} = 30.5 Hz, C_q), 130.3 (d, ³*J*_{C–F} = 7.6 Hz, CH), 128.0 (C_q), 126.2 (d, ⁴*J*_{C–F} = 3.6 Hz, C_q), 124.2 (CH), 122.4 (CH), 121.7 (CH), 121.3 (CH), 120.8 (CH), 114.1 (CH), 111.4 (CH), 109.8 (d, ³*J*_{C–F} = 9.9 Hz, CH), 107.1 (d, ⁴*J*_{C–F} = 4.0 Hz, CH), 55.4 (CH₃). **¹⁹F-NMR** (471 MHz, CDCl₃): δ = –94.0 (dd, *J* = 19.1, 3.1 Hz, 0.17F, *E*), –108.9 (d, *J* = 38.2 Hz, 0.83F, *Z*). **IR** (ATR): 3053, 2836, 1606, 1467, 1449, 1436, 1248, 1178, 856, 737 cm^{–1}. **MS** (EI) *m/z* (relative intensity): 344 (100) [M]⁺, 324 (45), 309 (44), 380 (32). **HR-MS** (EI): *m/z* calcd. for C₂₂H₁₇FN₂O⁺ [M]⁺ 344.1325, found 344.1322.

(*Z*)-2-[1-Fluoro-2-(*p*-tolyl)vinyl]-1-(pyridin-2-yl)-1*H*-indole (202d)



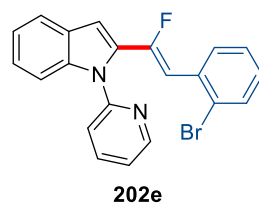
202d

The general procedure **GP-D** was followed using 1-(pyridin-2-yl)-1*H*-indole (**201a**) (97.1 mg, 0.50 mmol), 1-(2,2-difluorovinyl)-4-methylbenzene (**44d**) (231 mg, 1.50 mmol), [MnBr(CO)₅] (13.7 mg, 50.0 μmol), NaOAc (8.20 mg, 0.10 mmol) and K₂CO₃ (69.1 mg, 0.50 mmol). Purification by column chromatography (*n*-hexane/EtOAc: 10/1) yielded **202d** (133 mg, 81%, *Z/E*: 94:6) as a yellow oil.

¹H-NMR (300 MHz, CDCl₃): δ = 8.68 (dd, *J* = 5.0, 1.8 Hz, 0.94H, *Z*), 8.56 (dd, *J* = 4.9, 1.8 Hz, 0.06H, *E*), 7.86 (dd, *J* = 7.8, 1.9 Hz, 1H), 7.71 – 7.65 (m, 1H), 7.56 (dt, *J* = 8.3, 1.0 Hz, 1H), 7.47 – 7.43 (m, 1H), 7.40 (d, *J* = 8.0 Hz, 2H), 7.34 (ddd, *J* = 7.5, 4.9, 1.0 Hz, 1H), 7.29 – 7.21 (m, 2H), 7.15 (d, *J* = 7.9 Hz, 2H), 7.02 (t, *J* = 0.9 Hz, 1H), 6.47 (d, *J* = 19.1 Hz, 0.06H, *E*), 6.02 (d, *J* = 38.3 Hz, 0.94H, *Z*), 2.36 (s, 2.82H, *Z*), 2.28 (s, 0.18H, *E*). **¹³C-NMR** (100 MHz, CDCl₃): δ = 151.8 (C_q), 150.6 (d, ¹*J*_{C–F} = 263 Hz, C_q), 149.5 (CH), 138.7 (C_q), 138.5 (CH), 137.6 (d, ⁴*J*_{C–F} = 2.5 Hz, C_q), 132.5 (d, ²*J*_{C–F} = 30.1 Hz, C_q),

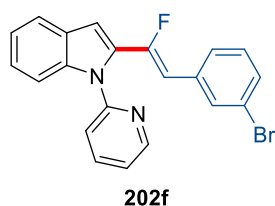
130.7 (d, $^4J_{C-F} = 3.8$ Hz, C_q), 129.4 (CH), 128.9 (d, $^3J_{C-F} = 7.7$ Hz, CH), 128.0 (C_q), 124.3 (CH), 122.4 (CH), 121.7 (CH), 121.3 (CH), 120.8 (CH), 111.4 (CH), 110.1 (d, $^3J_{C-F} = 9.6$ Hz, CH), 107.3 (d, $^4J_{C-F} = 4.5$ Hz, CH), 21.4 (CH₃). **$^{19}\text{F-NMR}$** (376 MHz, CDCl₃): $\delta = -92.7$ (dd, $J = 19.3, 3.2$ Hz, 0.06F, *E*), -106.9 (d, $J = 38.3$ Hz, 0.94F, *Z*). **IR** (ATR): 3051, 1585, 1467, 1449, 1436, 1380, 1348, 1212, 1147, 737 cm⁻¹. **MS** (EI) m/z (relative intensity): 328 (100) [M]⁺, 307 (85), 237 (22). **HR-MS** (EI): m/z calcd. for C₂₂H₁₇FN₂⁺ [M]⁺ 328.1376, found 328.1389.

(Z)-2-[2-(2-Bromophenyl)-1-fluorovinyl]-1-(pyridin-2-yl)-1H-indole (202e)



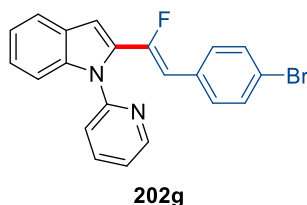
The general procedure **GP-D** was followed using 1-(pyridin-2-yl)-1*H*-indole (**201a**) (97.1 mg, 0.50 mmol), 1-bromo-2-(2,2-difluorovinyl)benzene (**44e**) (329 mg, 1.50 mmol), [MnBr(CO)₅] (13.7 mg, 50.0 μmol), NaOAc (8.20 mg, 0.10 mmol) and K₂CO₃ (69.1 mg, 0.50 mmol). Purification by column chromatography (*n*-hexane/EtOAc: 10/1) yielded **202e** (176 mg, 90%, *Z/E*: 96:4) as a yellow oil.

$^1\text{H-NMR}$ (300 MHz, CDCl₃): $\delta = 8.70$ (dd, $J = 4.9, 1.9$ Hz, 0.96H, *Z*), 8.58 (dd, $J = 4.9, 1.8$ Hz, 0.04H, *E*), 7.88 (ddd, $J = 7.9, 5.8, 1.8$ Hz, 2H), 7.76 – 7.67 (m, 1H), 7.61 – 7.41 (m, 3H), 7.38 – 7.22 (m, 4H), 7.14 (s, 1H), 7.08 (dd, $J = 7.7, 1.6$ Hz, 1H), 6.58 (d, $J = 17.7$ Hz, 0.04H, *E*), 6.36 (d, $J = 37.7$ Hz, 0.96H, *Z*). **$^{13}\text{C-NMR}$** (100 MHz, CDCl₃): $\delta = 151.8$ (d, $^1J_{C-F} = 258$ Hz, C_q), 151.6 (C_q), 149.7 (CH), 139.1 (C_q), 138.6 (CH), 133.0 (d, $^4J_{C-F} = 4.1$ Hz, C_q), 132.8 (CH), 131.8 (d, $^2J_{C-F} = 33.0$ Hz, C_q), 130.4 (d, $^3J_{C-F} = 13.3$ Hz, CH), 128.7 (CH), 127.7 (C_q), 127.4 (CH), 124.5 (CH), 123.7 (C_q), 122.6 (CH), 121.7 (CH), 121.4 (CH), 121.1 (CH), 111.3 (CH), 108.1 (d, $^3J_{C-F} = 9.7$ Hz, CH), 108.0 (CH). **$^{19}\text{F-NMR}$** (376 MHz, CDCl₃): $\delta = -93.3$ (dd, $J = 17.5, 2.1$ Hz, 0.04F, *E*), -107.2 (d, $J = 37.8$ Hz, 0.96F, *Z*). **IR** (ATR): 3060, 1653, 1586, 1467, 1436, 1382, 1349, 1147, 1021, 741 cm⁻¹. **MS** (EI) m/z (relative intensity): 392 (23) [M]⁺, 313 (100), 293 (36), 237 (20). **HR-MS** (EI): m/z calcd. for C₂₁H₁₄⁷⁹BrFN₂⁺ [M]⁺ 392.0324, found 392.0322.

(Z)-2-[2-(3-Bromophenyl)-1-fluorovinyl]-1-(pyridin-2-yl)-1H-indole (202f)

The general procedure **GP-D** was followed using 1-(pyridin-2-yl)-1*H*-indole (**201a**) (97.1 mg, 0.50 mmol), 1-bromo-3-(2,2-difluorovinyl)benzene (**44f**) (329 mg, 1.50 mmol), [MnBr(CO)₅] (13.7 mg, 50.0 μmol), NaOAc (8.20 mg, 0.10 mmol) and K₂CO₃ (69.1 mg, 0.50 mmol). Purification by column chromatography (*n*-hexane/EtOAc: 10/1) yielded **202f** (169 mg, 86%, *Z/E*: 96:4) as a yellow oil.

¹H-NMR (300 MHz, CDCl₃): δ = 8.66 (d, *J* = 4.8 Hz, 0.96H, *Z*), 8.51 (d, *J* = 4.6 Hz, 0.04H, *E*), 7.86 (t, *J* = 7.7 Hz, 1H), 7.70 – 7.60 (m, 2H), 7.51 (d, *J* = 8.1 Hz, 1H), 7.43 (d, *J* = 8.0 Hz, 1H), 7.40 – 7.31 (m, 3H), 7.28 – 7.15 (m, 3H), 7.02 (s, 1H), 6.35 (d, *J* = 18.1 Hz, 0.04H, *E*), 5.95 (d, *J* = 37.1 Hz, 0.96H, *Z*). ¹³C-NMR (126 MHz, CDCl₃): δ = 151.9 (d, ¹*J*_{C-F} = 258 Hz, C_q), 151.6 (C_q), 149.6 (CH), 138.8 (C_q), 138.5 (CH), 135.4 (d, ⁴*J*_{C-F} = 3.7 Hz, C_q), 131.8 (d, ²*J*_{C-F} = 30.1 Hz, C_q), 131.5 (d, ³*J*_{C-F} = 8.7 Hz, CH), 130.4 (CH), 130.0 (CH), 127.7 (C_q), 127.4 (d, ⁴*J*_{C-F} = 7.6 Hz, CH), 124.6 (CH), 122.7 (C_q), 122.6 (CH), 121.8 (CH), 121.4 (CH), 120.7 (CH), 111.3 (CH), 108.5 (d, ³*J*_{C-F} = 9.0 Hz, CH), 108.0 (d, ⁴*J*_{C-F} = 4.6 Hz, CH). ¹⁹F-NMR (282 MHz, CDCl₃): δ = –90.9 (dd, *J* = 18.0, 2.6 Hz, 0.04F, *E*), –104.1 (d, *J* = 37.2 Hz, 0.96F, *Z*). IR (ATR): 3055, 1659, 1586, 1467, 1436, 1380, 1146, 1074, 730, 683 cm⁻¹. MS (EI) *m/z* (relative intensity): 392 (100) [M]⁺, 373 (55), 292 (42), 237 (78). HR-MS (EI): *m/z* calcd. for C₂₁H₁₄⁷⁹BrFN₂⁺ [M]⁺ 392.0324, found 392.0332.

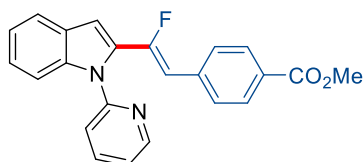
(Z)-2-(2-(4-Bromophenyl)-1-fluorovinyl)-1-(pyridin-2-yl)-1H-indole (202g):

The general procedure **GP-D** was followed using 1-(pyridin-2-yl)-1*H*-indole (**201a**) (97.1 mg, 0.50 mmol), 1-bromo-4-(2,2-difluorovinyl)benzene (**44g**) (329 mg, 1.50 mmol), [MnBr(CO)₅] (13.7 mg, 50.0 μmol), NaOAc (8.20 mg, 0.10 mmol) and K₂CO₃ (69.1 mg,

0.50 mmol). Purification by column chromatography (*n*-hexane/EtOAc: 10/1) yielded **202g** (167 mg, 85%, *Z/E* = 92/8) as a yellow oil.

¹H-NMR (300 MHz, CDCl₃): δ = 8.67 (ddd, *J* = 4.9, 2.0, 0.8 Hz, 0.92H, *Z*), 8.54 (ddd, *J* = 4.9, 1.9, 0.9 Hz, 0.08H, *E*), 7.88 (dd, *J* = 8.0, 2.0 Hz, 1H), 7.68 (ddd, *J* = 7.5, 1.5, 0.8 Hz, 1H), 7.57 – 7.48 (m, 1H), 7.48 – 7.41 (m, 3H), 7.38 – 7.32 (m, 3H), 7.29 (dd, *J* = 7.1, 1.4 Hz, 1H), 7.24 – 7.18 (m, 1H), 7.03 (s, 0.92H, *Z*), 6.94 (s, 0.08H, *E*), 6.38 (d, *J* = 18.2 Hz, 0.08H, *E*), 5.96 (d, *J* = 37.4 Hz, 0.92H, *Z*). **¹³C-NMR** (100 MHz, CDCl₃): δ = 151.9 (C_q), 151.7 (d, ¹*J*_{C-F} = 258 Hz, C_q), 149.7 (CH), 138.8 (C_q), 138.6 (C_q), 131.8 (CH), 131.6 (CH), 132.4 (d, ⁴*J*_{C-F} = 3.7 Hz, C_q), 130.4 (d, *J* = 8.0 Hz, (CH), 127.9 (C_q), 124.6 (CH), 122.6 (CH), 121.8 (CH), 121.5 (CH), 121.4 (d, ⁴*J*_{C-F} = 3.7 Hz, C_q), 120.8 (CH), 111.3 (CH), 108.9 (d, ³*J*_{C-F} = 9.5 Hz, CH), 107.9 (d, ⁴*J*_{C-F} = 4.6 Hz, CH). **¹⁹F-NMR** (376 MHz, CDCl₃): δ = -91.08 (dd, *J* = 18.3, 2.9 Hz, 0.08F, *E*), -105.04 (d, *J* = 37.6 Hz, 0.92F, *Z*). **IR** (ATR): 3053, 2959, 1585, 1468, 1449, 1436, 1381, 1331, 1073, 1009 cm⁻¹. **MS** (ESI) *m/z* (relative intensity): 415 (100) [M+Na]⁺, 393 (51) [M+H]⁺. **HR-MS** (ESI): *m/z* calcd. for C₂₁H₁₅⁷⁹BrFN₂⁺ [M+H]⁺ 393.0397, found 393.0401.

Methyl (*Z*)-4-{2-fluoro-2-[1-(pyridin-2-yl)-1*H*-indol-2-yl]vinyl}benzoate (**202h**)



202h

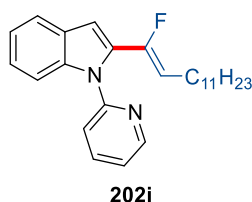
The general procedure **GP-D** was followed using 1-(pyridin-2-yl)-1*H*-indole (**201a**) (97.1 mg, 0.50 mmol), methyl 4-(2,2-difluorovinyl)benzoate (**44h**) (297 mg, 1.50 mmol), [MnBr(CO)₅] (13.7 mg, 50.0 μmol), NaOAc (8.20 mg, 0.10 mmol) and K₂CO₃ (69.1 mg, 0.50 mmol). Purification by column chromatography (*n*-hexane/EtOAc: 10/1) yielded **202h** (171 mg, 92%, *Z/E*: 94:6) as a yellow solid.

M.p.: 150–153 °C. **¹H-NMR** (400 MHz, CDCl₃): δ = 8.67 (d, *J* = 4.8 Hz, 0.94H, *Z*), 8.52 (d, *J* = 4.8 Hz, 0.6H, *E*), 7.99 (d, *J* = 7.7 Hz, 2H), 7.94 – 7.82 (m, 1H), 7.69 (d, *J* = 7.9 Hz, 1H), 7.52 (dd, *J* = 8.3, 3.7 Hz, 3H), 7.45 (d, *J* = 8.0 Hz, 1H), 7.35 (dd, *J* = 7.5, 4.9 Hz, 1H), 7.28 (t, *J* = 7.8 Hz, 1H), 7.22 (t, *J* = 7.5 Hz, 1H), 7.07 (s, 1H), 6.47 (d, *J* = 18.0 Hz, 0.06H, *E*), 6.06 (d, *J* = 37.4 Hz, 0.94H, *Z*), 3.91 (s, 2.79H, *Z*), 3.87 (s, 0.18H, *E*). **¹³C-NMR** (100 MHz, CDCl₃): δ = 166.8 (C_q), 152.6 (d, ¹*J*_{C-F} = 260 Hz, C_q), 151.6 (C_q), 149.7 (CH), 138.9 (C_q), 138.6 (CH), 138.0 (C_q), 138.0 (C_q), 131.8 (d, ²*J*_{C-F} = 29.8 Hz, C_q),

129.9 (CH), 128.7 (d, $^3J_{\text{C-F}} = 8.6$ Hz, CH), 127.8 (C_q), 124.7 (CH), 122.6 (CH), 121.9 (CH), 121.5 (CH), 120.7 (CH), 111.3 (CH), 109.0 (d, $^3J_{\text{C-F}} = 9.0$ Hz, CH), 108.2 (d, $^4J_{\text{C-F}} = 4.5$ Hz, CH), 52.17 (CH₃). **¹⁹F-NMR** (377 MHz, CDCl₃): $\delta = -88.99$ (dd, $J = 18.1, 3.0$ Hz, 0.06F, *E*), -102.88 (d, $J = 37.5$ Hz, 0.94F, *Z*). **IR** (ATR): 1714, 1606, 1468, 1435, 1275, 1183, 1108, 907, 727, 697 cm⁻¹. **MS** (ESI) m/z (relative intensity): 767 (23) [2M+Na]⁺, 395 (89) [M+Na]⁺, 373 (100) [M+H]⁺, 353 (17). **HR-MS** (ESI): m/z calcd. for C₂₃H₁₈FN₂O₂⁺ [M+H]⁺ 373.1347, found 373.1350.

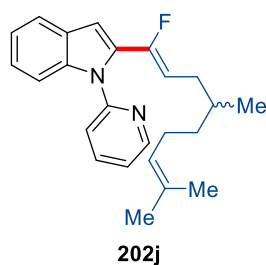
Crystals suitable for X-ray crystallography were grown by slow evaporation from a solution of **202h** in *i*-PrOH.

(Z)-2-(1-Fluorotridec-1-en-1-yl)-1-(pyridin-2-yl)-1H-indole (202i)



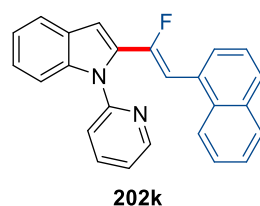
The general procedure **GP-D** was followed using 1-(pyridin-2-yl)-1H-indole (**201a**) (97.1 mg, 0.50 mmol), 1,1-difluorotridec-1-ene (**44i**) (328 mg, 1.50 mmol), [MnBr(CO)₅] (13.7 mg, 50.0 μ mol), NaOAc (8.20 mg, 0.10 mmol) and K₂CO₃ (69.1 mg, 0.50 mmol). Purification by column chromatography (*n*-hexane/EtOAc: 10/1) yielded **202i** (120 mg, 61%, *Z/E*: 82:18) as a yellow oil.

¹H-NMR (400 MHz, CDCl₃): $\delta = 8.66$ (dd, $J = 4.9, 1.8$ Hz, 1H), 7.85 (dd, $J = 7.8, 1.8$ Hz, 1H), 7.63 (dd, $J = 7.2, 1.5$ Hz, 1H), 7.51 (d, $J = 8.1$ Hz, 1H), 7.39 (d, $J = 8.0$ Hz, 1H), 7.32 (ddd, $J = 7.5, 4.9, 1.1$ Hz, 1H), 7.25 – 7.14 (m, 2H), 6.85 (s, 1H), 5.50 (dt, $J = 19.4, 8.1$ Hz, 0.18H, *E*), 5.07 (dt, $J = 36.1, 7.7$ Hz, 0.82H, *Z*), 2.18 (qd, $J = 7.3, 1.8$ Hz, 2H), 1.42 – 1.15 (m, 18H), 0.89 (t, $J = 6.8$ Hz, 3H). **¹³C-NMR** (125 MHz, CDCl₃): $\delta = 151.8$ (C_q), 150.4 (d, $^1J_{\text{C-F}} = 243$ Hz, C_q), 149.3 (CH), 138.2 (C_q), 138.2 (CH), 132.2 (d, $^2J_{\text{C-F}} = 32.4$ Hz, C_q), 127.9 (C_q), 123.8 (CH), 122.2 (CH), 121.4 (CH), 121.1 (CH), 120.8 (CH), 111.5 (d, $^2J_{\text{C-F}} = 16.7$ Hz, CH), 111.3 (CH), 106.5 (CH), 32.1 (CH₂), 29.9 (CH₂), 29.6 (CH₂), 29.5 (CH₂), 29.3 (CH₂), 24.4 (CH₂), 22.9 (CH₂), 14.3 (CH₃). **¹⁹F-NMR** (282 MHz, CDCl₃): $\delta = -98.5$ (d, $J = 19.2$ Hz, 0.18F, *E*), -111.8 (d, $J = 36.1$ Hz, 0.82F, *Z*). **IR** (ATR): 2922, 2852, 1587, 1468, 1450, 1436, 1381, 1347, 798, 737 cm⁻¹. **MS** (EI) m/z (relative intensity): 392 (25) [M]⁺, 237 (100), 231 (36). **HR-MS** (EI): m/z calcd. for C₂₆H₃₃FN₂⁺ [M]⁺ 392.2628, found 392.2636.

(Z)-2-(1-Fluoro-4,8-dimethylnona-1,7-dien-1-yl)-1-(pyridin-2-yl)-1H-indole (202j)

The general procedure **GP-D** was followed using 1-(pyridin-2-yl)-1H-indole (**201a**) (97.1 mg, 0.50 mmol), 1,1-difluoro-4,8-dimethylnona-1,7-diene (**44j**) (283 mg, 1.50 mmol), [MnBr(CO)₅] (13.7 mg, 50.0 μmol), NaOAc (8.20 mg, 0.10 mmol) and K₂CO₃ (69.1 mg, 0.50 mmol). Purification by column chromatography (*n*-hexane/EtOAc: 10/1) yielded **202j** (104 mg, 58%, *Z/E*: 78:22) as a yellow oil.

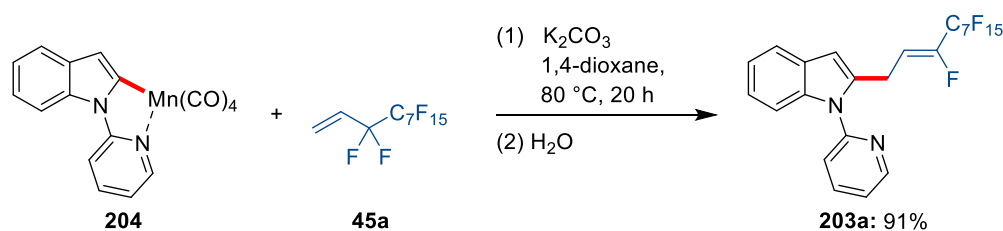
¹H-NMR (400 MHz, CDCl₃): δ = 8.65 (ddd, *J* = 4.9, 2.0, 0.9 Hz, 1H), 7.85 (ddd, *J* = 8.0, 7.4, 1.9 Hz, 1H), 7.63 (dt, *J* = 7.6, 0.9 Hz, 1H), 7.50 (dd, *J* = 8.2, 0.9 Hz, 1H), 7.39 (dt, *J* = 8.0, 0.9 Hz, 1H), 7.34 – 7.29 (m, 1H), 7.22 (dt, *J* = 8.0, 1.2 Hz, 1H), 7.20 – 7.15 (m, 1H), 6.85 (d, *J* = 1.1 Hz, 1H), 5.52 (dt, *J* = 19.7, 7.9 Hz, 0.22H, *E*), 5.15 – 4.99 (m, 1.78H, *Z*), 2.22 – 1.89 (m, 4H), 1.69 (dd, *J* = 6.9, 1.4 Hz, 3H), 1.60 (d, *J* = 1.2 Hz, 3H), 1.55 – 1.47 (m, 1H), 1.33 (ddt, *J* = 13.0, 9.6, 6.0 Hz, 1H), 1.21 – 1.12 (m, 1H), 0.88 (dd, *J* = 6.7, 1.4 Hz, 3H). ¹³C-NMR (125 MHz, CDCl₃): δ = 150.9 (d, ¹*J*_{C-F} = 244 Hz, C_q), 149.4 (CH), 138.3 (C_q), 138.2 (CH), 137.3 (C_q), 132.3 (d, ²*J*_{C-F} = 32.7, C_q), 131.3 (C_q), 127.9 (C_q), 124.8 (CH), 123.9 (CH), 122.3 (CH), 121.4 (CH), 121.1 (CH), 120.8 (CH), 111.3 (CH), 109.9 (d, ³*J*_{C-F} = 16.7 Hz, CH), 106.5 (d, ⁴*J*_{C-F} = 3.3 Hz, CH), 36.7 (CH₂), 33.0 (CH), 31.4 (CH₂), 26.0 (CH₃), 25.8 (CH₂), 19.7 (CH₃), 17.9 (CH₃). ¹⁹F-NMR (282 MHz, CDCl₃): δ = -96.8 (d, *J* = 19.6 Hz, 0.22F, *E*), -111.2 (d, *J* = 36.1 Hz, 0.78F, *Z*). IR (ATR): 2956, 2924, 1697, 1588, 1469, 1451, 1437, 1379, 780, 742 cm⁻¹. MS (EI) *m/z* (relative intensity): 362 (28) [M]⁺, 327 (35), 231 (100). HR-MS (EI): *m/z* calcd. for C₂₄H₂₇FN₂⁺ [M]⁺ 362.2158, found 362.2157.

(Z)-2-[1-Fluoro-2-(naphthalen-1-yl)vinyl]-1-(pyridin-2-yl)-1H-indole (202k)

The general procedure **GP-D** was followed using 1-(pyridin-2-yl)-1*H*-indole (**201a**) (97.1 mg, 0.50 mmol), 1-(2,2-difluorovinyl)naphthalene (**44k**) (285 mg, 1.50 mmol), [MnBr(CO)₅] (13.7 mg, 50.0 μmol), NaOAc (8.20 mg, 0.10 mmol) and K₂CO₃ (69.1 mg, 0.50 mmol). Purification by column chromatography (*n*-hexane/EtOAc: 10/1) yielded **202k** (83.8 mg, 46%, *Z/E*: 65:35) as a yellow oil.

¹H-NMR (400 MHz, CDCl₃): δ = 8.75 (dd, *J* = 5.0, 2.0 Hz, 0.65H, *Z*), 8.28 (dd, *J* = 5.0, 2.0 Hz, 0.35H, *E*), 7.96 – 7.66 (m, 5H), 7.64 – 7.33 (m, 6H), 7.28 (s, 1H), 7.24 – 7.16 (m, 2H), 7.02 – 6.88 (m, 1H), 6.76 (ddd, *J* = 7.5, 4.9, 1.0 Hz, 0.35H), 6.66 (d, *J* = 36.0 Hz, 0.65H). ¹³C-NMR (100 MHz, CDCl₃): δ = 152.0 (C_q), 151.6 (d, ¹J_{C-F} = 256 Hz, C_q), 149.8 (CH), 149.0 (CH), 139.0 (CH), 138.7 (CH), 133.8 (C_q), 133.4 (C_q), 132.4 (d, ²J = 32.0 Hz, C_q), 131.4 (C_q), 129.3 (d, ²J_{C-F} = 2.9 Hz, C_q), 128.8 (CH), 127.9 (C_q), 126.2 (CH), 125.8 (CH), 125.7 (CH), 124.5 (CH), 123.9 (CH), 122.6 (CH), 121.8 (CH), 121.5 (CH), 121.2 (CH), 111.4 (CH), 107.8 (d, ⁴J_{C-F} = 4.1 Hz, CH), 106.5 (d, ³J_{C-F} = 10.6 Hz, CH). ¹⁹F-NMR (377 MHz, CDCl₃): δ = -94.35 (d, *J* = 18.2 Hz, 0.35, *E*), -107.38 (d, *J* = 36.1 Hz, 0.65, *Z*). IR (ATR): 3055, 1663, 1587, 1468, 1449, 1437, 1348, 1231, 777, 741 cm⁻¹. MS (ESI) *m/z* (relative intensity): 387 (49) [M+Na]⁺, 365 (100) [M+H]⁺, 345 (28). HR-MS (ESI): *m/z* calcd. for C₂₅H₁₇FN₂⁺ [M+H]⁺ 365.1449, found 365.1453.

5.4.2. Experiments with Cyclometalated Complex **204**

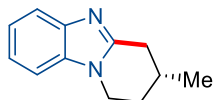


Scheme 5.1. Experiment with cyclometalated complex **204**.

Complex **204** (72.0 mg, 0.20 mmol, 1.00 equiv), 1*H*,1*H*,2*H*-perfluorodecene (**45a**) (107 mg, 0.24 mmol, 1.20 equiv), K₂CO₃ (27.6 mg, 0.20 mmol, 1.00 equiv) were placed into an oven-dried 25 mL Schlenk tube equipped with a septum under N₂ atmosphere. 1,4-Dioxane (0.20 mL) was added and the mixture was stirred at 80 °C for 20 h. After completion of the reaction, H₂O (10 mL) was added at ambient temperature and the resulting mixture was extracted with Et₂O (3 x 15 mL). Drying over Na₂SO₄, evaporation of the solvent and purification by column chromatography yielded **203a** (113 mg, 91%, *Z/E*: 88:12) as a yellow oil.

5.5. Asymmetric Nickel-Catalyzed Hydroarylations by C–H Activation

5.5.1. Characterization Data

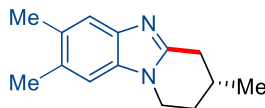
(R)-3-Methyl-1,2,3,4-tetrahydrobenzo[4,5]imidazo[1,2-*a*]pyridine (189a)

189a

The general procedure **GP-E** was followed using 1-(3-methylbut-3-en-1-yl)-1*H*-benzo[*d*]imidazole (**188a**) (93.6 mg, 0.50 mmol), Ni(cod)₂ (6.90 mg, 25.0 μmol) and **208** (6.30 mg, 12.5 μmol). Purification by column chromatography (*n*-hexane/EtOAc: 1/1) yielded **189a** (89.5 mg, 96%) as a colourless solid.

M.p.: 134–136 °C. **¹H-NMR** (400 MHz, CDCl₃): δ = 7.82 – 7.64 (m, 1H), 7.39 – 7.21 (m, 3H), 4.25 (ddd, *J* = 12.0, 5.8, 2.9 Hz, 1H), 3.99 (ddd, *J* = 12.0, 11.1, 5.1 Hz, 1H), 3.25 (ddd, *J* = 17.1, 4.7, 1.8 Hz, 1H), 2.68 (dd, *J* = 17.1, 10.4 Hz, 1H), 2.34 – 2.08 (m, 2H), 1.83 (dd, *J* = 11.1, 5.8 Hz, 1H), 1.24 (d, *J* = 6.6 Hz, 3H). **¹³C-NMR** (101 MHz, CDCl₃): δ = 151.9 (C_q), 143.2 (C_q), 134.6 (C_q), 122.1 (CH), 121.7 (CH), 119.0 (CH), 108.8 (CH), 41.65 (CH₂), 33.56 (CH₂), 30.57 (CH₂), 27.71 (CH), 21.18 (CH₃). **IR** (ATR): 2956, 2925, 1514, 1457, 1416, 1319, 1285, 1230, 738, 437 cm⁻¹. **MS** (ESI) *m/z* (relative intensity): 187 (100) [M+H]⁺, 117 (3). **HR-MS** (ESI): *m/z* calcd. for C₁₂H₁₅N₂⁺ [M+H]⁺ 187.1230, found 187.1234. **[α]_D²⁰**: +62.5 (c = 1.00, CHCl₃). **HPLC separation** (Chiralpak® IC-3, *n*-hexane/*i*PrOH: 80/20, 1.0 mL/min, detection at 273 nm): *t_r* (major) = 17.3 min, *t_r* (minor) = 19.0 min, 99:1 e.r.

The analytical data are in accordance with those previously reported in the literature for the racemic compound.^[369]

(R)-3,7,8-Trimethyl-1,2,3,4-tetrahydrobenzo[4,5]imidazo[1,2-*a*]pyridine (189b)

189b

The general procedure **GP-E** was followed using 5,6-dimethyl-1-(3-methylbut-3-en-1-yl)-1*H*-benzo[*d*]imidazole (**188b**) (107 mg, 0.50 mmol), Ni(cod)₂ (6.90 mg, 25.0 μmol)

and **208** (6.30 mg, 12.5 μmol). Purification by column chromatography (*n*-hexane/EtOAc: 2/1) yielded **189b** (98.0 mg, 92%) as a colourless solid.

M.p.: 177–179 °C. **$^1\text{H-NMR}$** (400 MHz, CDCl_3): δ = 7.44 (s, 1H), 7.05 (s, 1H), 4.15 (ddd, J = 12.0, 5.9, 3.0 Hz, 1H), 3.90 (ddd, J = 12.3, 11.1, 4.9 Hz, 1H), 3.17 (ddd, J = 17.0, 4.7, 1.8 Hz, 1H), 2.60 (dd, J = 17.0, 10.4 Hz, 1H), 2.37 (s, 3H), 2.35 (s, 3H), 2.22–2.02 (m, 2H), 1.76 (dd, J = 11.2, 5.8 Hz, 1H), 1.17 (d, J = 6.6 Hz, 3H). **$^{13}\text{C-NMR}$** (100 MHz, CDCl_3): δ = 151.0 (C_q), 141.5 (C_q), 133.1 (C_q), 130.9 (C_q), 130.7 (C_q), 119.1 (CH), 109.2 (CH), 41.7 (CH_2), 33.5 (CH_2), 30.7 (CH_2), 27.8 (CH), 21.2 (CH_3), 20.6 (CH_3), 20.4 (CH_3). **IR** (ATR): 2953, 2867, 1516, 1488, 1462, 1421, 1322, 907, 847, 728 cm^{-1} . **MS** (EI) m/z (relative intensity): 214 (100) $[\text{M}]^+$, 199 (36), 172 (39), 157 (14). **HR-MS** (EI): m/z calcd. for $\text{C}_{14}\text{H}_{18}\text{N}_2^+$ $[\text{M}]^+$ 214.1470, found 214.1469. **$[\alpha]_D^{20}$** : +48 (c = 1.00, CHCl_3). **HPLC separation** (Chiralpak® ID-3, *n*-hexane/THF: 70/30, 0.75 mL/min, detection at 250 nm): t_r (minor) = 33.9 min, t_r (major) = 35.2 min, 4:96 e.r.

(*R*)-7,8-Dichloro-3-methyl-1,2,3,4-tetrahydrobenzo[4,5]imidazo[1,2-*a*]pyridine (189c)



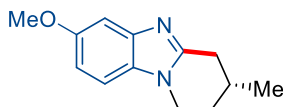
189c

The general procedure **GP-E** was followed using 5,6-dichloro-1-(3-methylbut-3-en-1-yl)-1*H*-benzo[*d*]imidazole (**188c**) (128 mg, 0.50 mmol), $\text{Ni}(\text{cod})_2$ (13.8 mg, 50.0 μmol) and **208** (12.6 mg, 25.0 μmol). Purification by column chromatography (*n*-hexane/EtOAc: 2/1) yielded **189c** (107 mg, 84%) as a colourless solid.

M.p.: 157–159 °C. **$^1\text{H-NMR}$** (300 MHz, CDCl_3): δ = 7.74 (s, 1H), 7.37 (s, 1H), 4.16 (ddd, J = 12.0, 5.8, 2.9 Hz, 1H), 3.92 (dd, J = 11.1, 4.7 Hz, 1H), 3.19 (ddd, J = 17.4, 4.7, 1.8 Hz, 1H), 2.62 (dd, J = 17.4, 10.5 Hz, 1H), 2.30–2.01 (m, 2H), 1.79 (dd, J = 11.2, 5.8 Hz, 1H), 1.19 (d, J = 6.5 Hz, 3H). **$^{13}\text{C-NMR}$** (125 MHz, CDCl_3): δ = 154.0 (C_q), 142.2 (C_q), 133.8 (C_q), 126.2 (C_q), 125.8 (C_q), 120.1 (CH), 110.4 (CH), 42.1 (CH_2), 33.5 (CH_2), 30.4 (CH_2), 27.6 (CH), 21.2 (CH_3). **IR** (ATR): 2957, 2928, 1510, 1483, 1456, 1403, 1383, 1094, 855, 575 cm^{-1} . **MS** (EI) m/z (relative intensity): 254 (100) $[\text{M}]^+$, 219 (28), 212 (70), 185 (14). **HR-MS** (EI): m/z calcd. for $\text{C}_{12}\text{H}_{12}^{35}\text{Cl}_2\text{N}_2^+$ $[\text{M}]^+$ 254.0378, found 254.0375. **$[\alpha]_D^{20}$** : +60 (c = 1.00, CHCl_3). **HPLC separation** (Chiralpak® ID-3, *n*-

hexane/THF: 70/30, 1.0 mL/min, detection at 280 nm): t_r (major) = 11.2 min, t_r (minor) = 12.0 min, 98:2 e.r.

(R)-7-Methoxy-3-methyl-1,2,3,4-tetrahydrobenzo[4,5]imidazo[1,2-*a*]pyridine (189d)

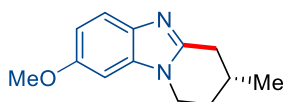


189d

The general procedure **GP-E** was followed using 5-methoxy-1-(3-methylbut-3-en-1-yl)-1*H*-benzo[*d*]imidazole (**188d**) (108 mg, 0.50 mmol), Ni(cod)₂ (6.90 mg, 25.0 μmol) and **208** (6.30 mg, 12.5 μmol). Purification by column chromatography (*n*-hexane/EtOAc: 2/1) yielded **189d** (94.0 mg, 87%) as a colourless solid.

M.p.: 127–129 °C. **¹H-NMR** (300 MHz, CDCl₃): δ = 7.56 (dd, *J* = 8.7, 0.5 Hz, 1H), 6.87 (dd, *J* = 8.7, 2.4 Hz, 1H), 6.76 (dd, *J* = 2.4, 0.5 Hz, 1H), 4.16 (ddd, *J* = 12.0, 5.9, 2.9 Hz, 1H), 3.97–3.82 (m, 4H), 3.18 (ddd, *J* = 17.0, 4.7, 1.8 Hz, 1H), 2.61 (dd, *J* = 17.0, 10.4 Hz, 1H), 2.30–1.96 (m, 2H), 1.78 (dd, *J* = 11.1, 5.7 Hz, 1H), 1.19 (d, *J* = 6.5 Hz, 3H). **¹³C-NMR** (125 MHz, CDCl₃): δ = 156.1 (C_q), 151.0 (C_q), 137.1 (C_q), 135.0 (C_q), 119.3 (CH), 111.0 (CH), 93.2 (CH), 56.1 (CH₃), 41.8 (CH₂), 33.6 (CH₂), 30.7 (CH₂), 27.9 (CH), 21.3 (CH₃). **IR** (ATR): 2926, 1624, 1523, 1455, 1418, 1247, 1213, 1155, 815, 728 cm⁻¹. **MS** (EI) *m/z* (relative intensity): 216 (83) [M]⁺, 201 (100), 159 (49), 131 (15). **HR-MS** (EI): *m/z* calcd. for C₁₃H₁₆N₂O⁺ [M]⁺ 216.1263, found 216.1264. [α]_D²⁰: +56 (c = 1.00, CHCl₃). **HPLC separation** (Chiralpak® ID-3, *n*-hexane/THF: 75/25, 0.75 mL/min, detection at 280 nm): t_r (minor) = 49.3 min, t_r (major) = 52.1 min, 1:99 e.r.

(R)-8-Methoxy-3-methyl-1,2,3,4-tetrahydrobenzo[4,5]imidazo[1,2-*a*]pyridine (189e)

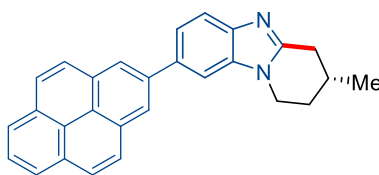


189e

The general procedure **GP-E** was followed using 6-methoxy-1-(3-methylbut-3-en-1-yl)-1*H*-benzo[*d*]imidazole (**188e**) (108 mg, 0.50 mmol), Ni(cod)₂ (6.90 mg, 25.0 μmol) and **208** (6.30 mg, 12.5 μmol). Purification by column chromatography (*n*-hexane/EtOAc: 2/1) yielded **189e** (97.0 mg, 90%) as a colourless solid.

M.p.: 142–144 °C. **¹H-NMR** (300 MHz, CDCl₃): δ = 7.31 (s, 1H), 7.24 (d, J = 8.6 Hz, 1H), 6.94 (dd, J = 8.7, 2.2 Hz, 1H), 4.26 (ddd, J = 12.2, 5.8, 2.9 Hz, 1H), 4.01 (dd, J = 11.5, 5.1 Hz, 1H), 3.91 (s, 3H), 3.30 (dd, J = 17.3, 4.8 Hz, 1H), 2.70 (dd, J = 17.3, 10.3 Hz, 1H), 2.22 (d, J = 14.1 Hz, 2H), 1.84 (dd, J = 11.1, 5.8 Hz, 1H), 1.24 (d, J = 6.5 Hz, 3H). **¹³C-NMR** (125 MHz, CDCl₃): δ = 156.8 (C_q), 151.7 (C_q), 141.8 (C_q), 128.6 (C_q), 112.3 (CH), 109.6 (CH), 101.0 (CH), 56.1 (CH₃), 41.9 (CH₂), 32.9 (CH₂), 30.4 (CH₂), 27.4 (CH), 21.1 (CH₃). **IR** (ATR): 2924, 1489, 1513, 1441, 1419, 1268, 1152, 1116, 1029, 801 cm⁻¹. **MS** (EI) m/z (relative intensity): 216 (100) [M]⁺, 201 (100), 159 (24), 131 (13). **HR-MS** (EI): m/z calcd. for C₁₃H₁₆N₂O⁺ [M]⁺ 216.1263, found 216.1260. **[α]_D²⁰**: +64 (c = 1.00, CHCl₃). **HPLC separation** (Chiralpak® IC-3, *n*-hexane/EtOH + EDA (0.1%): 91/9, 1.0 mL/min, detection at 250 nm): t_r (major) = 25.0 min, t_r (minor) = 26.5 min, 96:4 e.r.

(R)-3-Methyl-8-(pyren-1-yl)-1,2,3,4-tetrahydrobenzo[4,5]imidazo[1,2-*a*]pyridine (189f)



189f

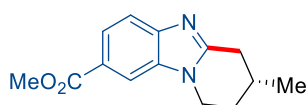
The general procedure **GP-E** was followed using 1-(3-methylbut-3-en-1-yl)-6-(pyren-1-yl)-1H-benzo[*d*]imidazole (**188f**) (193 mg, 0.50 mmol), Ni(cod)₂ (13.8 mg, 50.0 μ mol) and **208** (12.6 mg, 25.0 μ mol). Purification by column chromatography (*n*-hexane/EtOAc: 2/1) yielded **189f** (151 mg, 78%) as a yellow solid.

M.p.: 249–251 °C. **¹H-NMR** (600 MHz, CDCl₃): δ = 8.25 – 8.17 (m, 3H), 8.16 (dd, J = 7.4, 0.9 Hz, 1H), 8.13 – 8.07 (m, 2H), 8.04 (d, J = 7.8 Hz, 1H), 8.01 (dd, J = 8.4, 6.8 Hz, 2H), 7.89 – 7.82 (m, 1H), 7.54 – 7.49 (m, 2H), 4.26 (ddd, J = 12.1, 5.8, 3.0 Hz, 1H), 4.01 (dd, J = 12.1, 4.9 Hz, 1H), 3.29 (ddd, J = 17.1, 4.9, 1.8 Hz, 1H), 2.72 (dd, J = 17.1, 10.5 Hz, 1H), 2.30 – 2.14 (m, 2H), 1.91 – 1.72 (m, 1H), 1.23 (d, J = 6.5 Hz, 3H). **¹³C-NMR** (125 MHz, CDCl₃): δ = 152.7 (C_q), 142.5 (C_q), 138.6 (C_q), 135.1 (C_q), 134.9 (C_q), 131.7 (C_q), 131.1 (C_q), 130.5 (C_q), 128.9 (C_q), 128.2 (CH), 127.6 (CH), 127.5 (CH), 127.4 (CH), 126.1 (CH), 125.7 (CH), 125.3 (CH), 125.2 (CH), 125.1 (C_q), 125.1 (C_q), 124.9 (CH), 124.7 (CH), 118.7 (CH), 110.9 (CH), 41.87 (CH₂), 33.73 (CH₂), 30.65 (CH₂), 27.82 (CH), 21.27 (CH₃). **IR** (ATR): 2953, 2926, 1517, 1453, 1419, 1068, 847, 831, 755,

721 cm^{-1} . **MS** (EI) m/z (relative intensity): 386 (100) $[\text{M}]^+$, 331 (61), 276 (23), 165 (18). **HR-MS** (EI): m/z calcd. for $\text{C}_{28}\text{H}_{22}\text{N}_2^+$ $[\text{M}]^+$ 386.1783, found 386.1779. $[\alpha]_{\text{D}}^{20}$: +14.3 ($c = 0.42$, CHCl_3). **HPLC separation** (Chiralpak® IC-3, n -hexane/ i PrOH: 80/20, 1.0 mL/min, detection at 250 nm): t_r (major) = 22.8 min, t_r (minor) = 26.5 min, 99:1 e.r.

Crystals suitable for X-ray crystallography were grown by slow evaporation from a solution of **189f** in CHCl_3 .

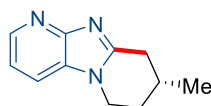
(R)-Methyl-3-methyl-1,2,3,4-tetrahydrobenzo[4,5]imidazo[1,2-*a*]pyridine-8-carboxylate (189g)



189g

The general procedure **GP-E** was followed using methyl 1-(3-methylbut-3-en-1-yl)-1*H*-benzo[*d*]imidazole-6-carboxylate (**188g**) (122 mg, 0.50 mmol), $\text{Ni}(\text{cod})_2$ (6.90 mg, 25.0 μmol) and **208** (6.30 mg, 12.5 μmol). Purification by column chromatography (n -hexane/ EtOAc : 1/1) yielded **189g** (90.0 mg, 74%) as a colourless solid.

M.p.: 134–136 °C. **$^1\text{H-NMR}$** (400 MHz, CDCl_3): $\delta = 8.39$ (dd, $J = 3.2, 1.6$ Hz, 1H), 7.97 (dd, $J = 8.6, 1.6$ Hz, 1H), 7.31 (dd, $J = 8.6, 3.2$ Hz, 1H), 4.27 (ddd, $J = 12.0, 6.1, 3.0$ Hz, 1H), 4.06 – 3.94 (m, 1H), 3.94 (s, 3H), 3.34 – 3.05 (m, 1H), 2.67 (ddd, $J = 17.2, 10.4, 3.5$ Hz, 1H), 2.19 (dd, $J = 6.4, 3.5$ Hz, 2H), 1.96 – 1.72 (m, 1H), 1.21 (d, $J = 6.5$ Hz, 3H). **$^{13}\text{C-NMR}$** (101 MHz, CDCl_3): $\delta = 168.0$ (C_q), 153.8 (C_q), 142.9 (C_q), 137.9 (C_q), 124.4 (C_q), 123.6 (CH), 121.4 (CH), 108.6 (CH), 52.17 (CH_3), 42.02 (CH_2), 33.68 (CH_2), 30.52 (CH_2), 27.68 (CH), 21.23 (CH_3). **IR** (ATR): 2953, 2930, 1719, 1440, 1411, 1301, 1205, 1088, 773, 756 cm^{-1} . **MS** (ESI) m/z (relative intensity): 267 (8) $[\text{M}+\text{Na}]^+$, 245 (100) $[\text{M}+\text{H}]^+$. **HR-MS** (ESI): m/z calcd. for $\text{C}_{14}\text{H}_{17}\text{N}_2\text{O}_2^+$ $[\text{M}+\text{H}]^+$ 245.1285, found 245.1286. $[\alpha]_{\text{D}}^{20}$: +40.0 ($c = 1.00$, CHCl_3). **HPLC separation** (Chiralpak® IA-3, n -hexane/THF: 60/40, 1.0 mL/min, detection at 250 nm): t_r (major) = 12.3 min, t_r (minor) = 13.2 min, 99:1 e.r.

(R)-8-Methyl-6,7,8,9-tetrahydroimidazo[1,2-*a*:4,5-*b'*]dipyridine (189h)**189h**

The general procedure **GP-E** was followed using 1-(3-methylbut-3-en-1-yl)-1*H*-imidazo[4,5-*b*]pyridine (**188h**) (94.0 mg, 0.50 mmol), Ni(cod)₂ (6.90 mg, 25.0 μmol) and **208** (6.30 mg, 12.5 μmol). Purification by column chromatography (acetone) yielded **189h** (77.0 mg, 82%) as a grey solid.

M.p.: 171–173 °C. **¹H-NMR** (400 MHz, CDCl₃): δ = 8.49 (d, *J* = 4.7 Hz, 1H), 7.60 (d, *J* = 7.8 Hz, 1H), 7.13 (dd, *J* = 7.7, 4.6 Hz, 1H), 4.30–4.16 (m, 1H), 4.00 (dd, *J* = 11.4, 4.5 Hz, 1H), 3.39–3.20 (m, 1H), 2.69 (dd, *J* = 17.4, 10.2 Hz, 1H), 2.26–2.11 (m, 2H), 1.91–1.70 (m, 1H), 1.20 (d, *J* = 6.2 Hz, 3H). **¹³C-NMR** (75 MHz, CDCl₃): δ = 155.8 (C_q), 154.7 (C_q), 144.6 (CH), 126.8 (C_q), 117.1 (CH), 116.9 (CH), 42.0 (CH₂), 33.6 (CH₂), 30.3 (CH₂), 27.5 (CH), 21.2 (CH₃). **IR** (ATR): 3382, 2957, 1614, 1482, 1409, 1279, 787, 755, 620, 548 cm⁻¹. **MS** (EI) *m/z* (relative intensity): 187 (100) [M]⁺, 172 (17), 145 (89), 133 (15). **HR-MS** (EI): *m/z* calcd. for C₁₁H₁₃N₃⁺ [M]⁺ 187.1109, found 187.1108. **[α]_D²⁰**: +40 (c = 1.00, CHCl₃). **HPLC separation** (Chiralpak® IC-3, *n*-hexane/EtOH + EDA (0.1%): 90/10, 0.8 mL/min, detection at 273 nm): *t_r* (major) = 163 min, *t_r* (minor) = 172 min, 92:8 e.r.

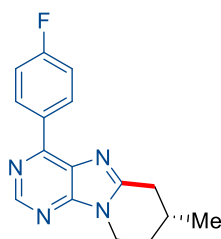
(R)-7-Methyl-6,7,8,9-tetrahydroimidazo[1,2-*a*:5,4-*b'*]dipyridine (189i)**189i**

The general procedure **GP-E** was followed using 3-(3-methylbut-3-en-1-yl)-3*H*-imidazo[4,5-*b*]pyridine (**188i**) (94.0 mg, 0.50 mmol), Ni(cod)₂ (6.90 mg, 25.0 μmol) and **208** (6.30 mg, 12.5 μmol). Purification by column chromatography (*n*-hexane/EtOAc: 1/10) yielded **189i** (83.1 mg, 89%) as a colourless solid.

M.p.: 116–118 °C. **¹H-NMR** (400 MHz, CDCl₃): δ = 8.26 (dd, *J* = 4.8, 1.4 Hz, 1H), 7.89 (dd, *J* = 7.9, 1.5 Hz, 1H), 7.15 (dd, *J* = 8.0, 4.8 Hz, 1H), 4.42 (ddd, *J* = 12.8, 5.8, 2.9 Hz, 1H), 3.99 (ddd, *J* = 12.8, 11.0, 4.8 Hz, 1H), 3.19 (ddd, *J* = 17.4, 4.8, 1.8 Hz, 1H), 2.63 (dd, *J* = 17.4, 10.5 Hz, 1H), 2.26–2.04 (m, 2H), 1.74 (dd, *J* = 11.2, 5.7 Hz, 1H), 1.17 (d, *J*

= 6.5 Hz, 3H). $^{13}\text{C-NMR}$ (75 MHz, CDCl_3): δ = 153.5 (C_q), 147.7 (C_q), 142.9 (CH), 135.1 (C_q), 126.2 (CH), 118.3 (CH), 40.8 (CH_2), 33.7 (CH_2), 30.3 (CH_2), 27.5 (CH), 21.2 (CH_3). **IR** (ATR): 3415, 2953, 2939, 1508, 1439, 1390, 1341, 1280, 804, 778 cm^{-1} . **MS** (EI) m/z (relative intensity): 187 (100) $[\text{M}]^+$, 172 (18), 145 (88), 133 (14). **HR-MS** (EI): m/z calcd. for $\text{C}_{11}\text{H}_{13}\text{N}_3^+$ $[\text{M}]^+$ 187.1109, found 187.1104. $[\alpha]_{\text{D}}^{20}$: +68 ($c = 1.00$, CHCl_3). **HPLC separation** (Chiralpak® IC-3, n -hexane/ i PrOH: 80/20, 1.0 mL/min, detection at 273 nm): t_r (minor) = 20.6 min, t_r (major) = 22.1 min, 3:97 e.r.

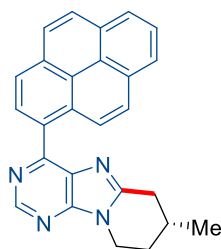
(R)-4-(4-Fluorophenyl)-7-methyl-6,7,8,9-tetrahydropyrido[1,2-*e*]purine (189j)



189j

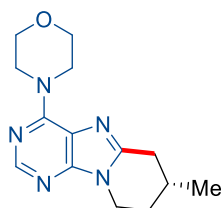
The general procedure **GP-E** was followed using 6-(4-fluorophenyl)-9-(3-methylbut-3-en-1-yl)-9*H*-purine (**188j**) (141 mg, 0.50 mmol), $\text{Ni}(\text{cod})_2$ (6.90 mg, 25.0 μmol) and **208** (6.30 mg, 12.5 μmol). Purification by column chromatography (n -hexane/EtOAc: 2/1) yielded **189j** (118 mg, 84%) as a colourless solid.

M.p.: 164–166 °C. $^1\text{H-NMR}$ (500 MHz, CDCl_3): δ = 8.90 (s, 1H), 8.79 (ddd, $J = 8.7, 5.5, 3.0$ Hz, 2H), 7.25–7.19 (m, 2H), 4.45 (ddd, $J = 12.8, 8.7, 3.0$ Hz, 1H), 4.04 (ddd, $J = 12.8, 11.0, 4.9$ Hz, 1H), 3.29 (ddd, $J = 17.6, 4.8, 1.8$ Hz, 1H), 2.70 (dd, $J = 17.6, 10.4$ Hz, 1H), 2.31–2.15 (m, 2H), 1.88–1.70 (m, 1H), 1.22 (d, $J = 6.6$ Hz, 3H). $^{13}\text{C-NMR}$ (125 MHz, CDCl_3): δ = 164.5 (d, $^1J_{\text{C-F}} = 250$ Hz, C_q), 154.4 (C_q), 153.2 (C_q), 151.7 (C_q), 151.3 (CH), 132.2 (d, $^4J_{\text{C-F}} = 3.0$ Hz, C_q), 131.9 (d, $^3J_{\text{C-F}} = 8.8$ Hz, CH), 130.8 (C_q), 115.8 (d, $^2J_{\text{C-F}} = 22.7$ Hz, CH), 41.1 (CH_2), 33.9 (CH_2), 30.0 (CH_2), 27.6 (CH), 21.2 (CH_3). $^{19}\text{F-NMR}$ (471 MHz, CDCl_3): δ = -109.78 (dq, $J = 12.8, 5.5$ Hz). **IR** (ATR): 2956, 2928, 1582, 1510, 1444, 1341, 1322, 1160, 849, 806 cm^{-1} . **MS** (EI) m/z (relative intensity): 282 (100) $[\text{M}]^+$, 267 (18), 239 (20), 213 (17). **HR-MS** (EI): m/z calcd. for $\text{C}_{16}\text{H}_{15}\text{FN}_4^+$ $[\text{M}]^+$ 282.1281, found 282.1277. $[\alpha]_{\text{D}}^{20}$: +12 ($c = 1.00$, CHCl_3). **HPLC separation** (Chiralpak® IA-3, n -hexane/ i PrOH: 70/30, 0.75 mL/min, detection at 250 nm): t_r (major) = 8.8 min, t_r (minor) = 9.7 min, 95:5 e.r.

(R)-7-Methyl-4-(pyren-1-yl)-6,7,8,9-tetrahydropyrido[1,2-*e*]purine (189k)**189k**

The general procedure **GP-E** was followed using 9-(3-methylbut-3-en-1-yl)-6-(pyren-1-yl)-9*H*-purine (**188k**) (194 mg, 0.50 mmol), Ni(cod)₂ (6.90 mg, 25.0 μmol) and **208** (6.30 mg, 12.5 μmol). Purification by column chromatography (*n*-hexane/EtOAc: 2/1) yielded **189k** (159 mg, 82%) as a yellow solid.

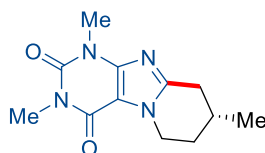
M.p.: 238–240 °C. **¹H-NMR** (300 MHz, CDCl₃): δ = 9.15 (s, 1H), 8.55 (d, *J* = 8.2, 1H), 8.52 (d, *J* = 6.7, 1H), 8.32 (d, *J* = 8.0 Hz, 1H), 8.25 – 8.17 (m, 2H), 8.16–7.98 (m, 4H), 4.54 (ddd, *J* = 12.8, 5.7, 2.9 Hz, 1H), 4.12 (ddd, *J* = 12.8, 11.0, 4.9 Hz, 1H), 3.26 (ddd, *J* = 17.8, 4.7, 1.7 Hz, 1H), 2.67 (dd, *J* = 17.8, 10.5 Hz, 1H), 2.34–2.11 (m, 2H), 1.94–1.76 (m, 1H), 1.20 (d, *J* = 6.5 Hz, 3H). **¹³C-NMR** (75 MHz, CDCl₃): δ = 156.3 (C_q), 154.8 (C_q), 153.0 (C_q), 151.4 (CH), 133.0 (C_q), 132.5 (C_q), 132.5 (C_q), 131.4 (C_q), 131.0 (C_q), 130.3 (C_q), 129.5 (C_q), 129.0 (CH), 128.5 (CH), 128.2 (CH), 127.5 (CH), 126.1 (CH), 125.6 (CH), 125.5 (CH), 125.4 (CH), 124.9 (CH), 124.8 (C_q), 41.3 (CH₂), 34.0 (CH₂), 30.1 (CH₂), 27.6 (CH), 21.2 (CH₃). **IR** (ATR): 2957, 1580, 1440, 1389, 1333, 1317, 848, 749, 723, 687 cm⁻¹. **MS** (ESI) *m/z* (relative intensity): 777 (85) [2M+H]⁺, 389 (100) [M+H]⁺. **HR-MS** (ESI): *m/z* calcd. for C₂₆H₂₁N₄⁺ [M+H]⁺ 389.1761, found 389.1765. **[α]_D²⁰**: +20 (c = 1.00, CHCl₃). **HPLC separation** (Chiralpak® IA-3, *n*-hexane/EtOH + EDA (0.1%): 80/20, 1.0 mL/min, detection at 250 nm): *t_r* (major) = 18.0 min, *t_r* (minor) = 23.5 min, 95:5 e.r.

(R)-4-(7-Methyl-6,7,8,9-tetrahydropyrido[1,2-*e*]purin-4-yl)morpholine (189l)**189l**

The general procedure **GP-E** was followed using 4-[9-(3-methylbut-3-en-1-yl)-9*H*-purin-6-yl]morpholine (**188l**) (137 mg, 0.50 mmol), Ni(cod)₂ (13.8 mg, 50.0 μmol) and **208** (12.6 mg, 25.0 μmol). Purification by column chromatography (*n*-hexane/EtOAc: 2/1) yielded **189l** (102 mg, 75%) as a colourless solid.

M.p.: 147–149 °C. **¹H-NMR** (500 MHz, CDCl₃): δ = 8.31 (s, 1H), 4.33 (ddd, *J* = 12.8, 5.7, 3.0 Hz, 1H), 4.25 (d, *J* = 5.0 Hz, 4H), 3.93 (ddd, *J* = 12.8, 10.9, 4.9 Hz, 1H), 3.86–3.76 (m, 4H), 3.11 (ddd, *J* = 17.1, 4.8, 1.7 Hz, 1H), 2.55 (dd, *J* = 17.1, 10.4 Hz, 1H), 2.22–2.07 (m, 2H), 1.73 (dd, *J* = 11.1, 5.8 Hz, 1H), 1.18 (d, *J* = 6.5 Hz, 3H). **¹³C-NMR** (125 MHz, CDCl₃): δ = 153.1 (C_q), 151.3 (C_q), 151.3 (CH), 147.8 (C_q), 119.5 (C_q), 67.1 (CH₂), 45.6 (CH₂), 40.8 (CH₂), 33.5 (CH₂), 30.1 (CH₂), 27.6 (CH), 21.0 (CH₃). **IR** (ATR): 2921, 2853, 1582, 1441, 1327, 1284, 1253, 1112, 1030, 959 cm⁻¹. **MS** (ESI) *m/z* (relative intensity): 274 (100) [M+H]⁺. **HR-MS** (ESI): *m/z* calcd. for C₁₄H₂₀N₅O [M+H]⁺ 274.1662, found 274.1667. **[α]_D²⁰:** +40 (c = 1.00, CHCl₃). **HPLC separation** (Chiralpak® IF-3, *n*-hexane/EtOH + EDA (0.1%): 80/20, 1.0 mL/min, detection at 273 nm): *t_r* (major) = 22.1 min, *t_r* (minor) = 26.1 min, 95:5 e.r.

(*R*)-1,3,8-Trimethyl-6,7,8,9-tetrahydropyrido[2,1-*f*]purine-2,4(1*H*,3*H*)-dione (189m)



189m

The general procedure **GP-E** was followed using 1,3-dimethyl-7-(3-methylbut-3-en-1-yl)-1*H*-purine-2,6(3*H*,7*H*)-dione (**188m**) (124 mg, 0.50 mmol), Ni(cod)₂ (13.8 mg, 50.0 μmol) and **208** (12.6 mg, 25.0 μmol). Purification by column chromatography (*n*-hexane/EtOAc: 2/1) yielded **189m** (101 mg, 81%) as a colourless solid.

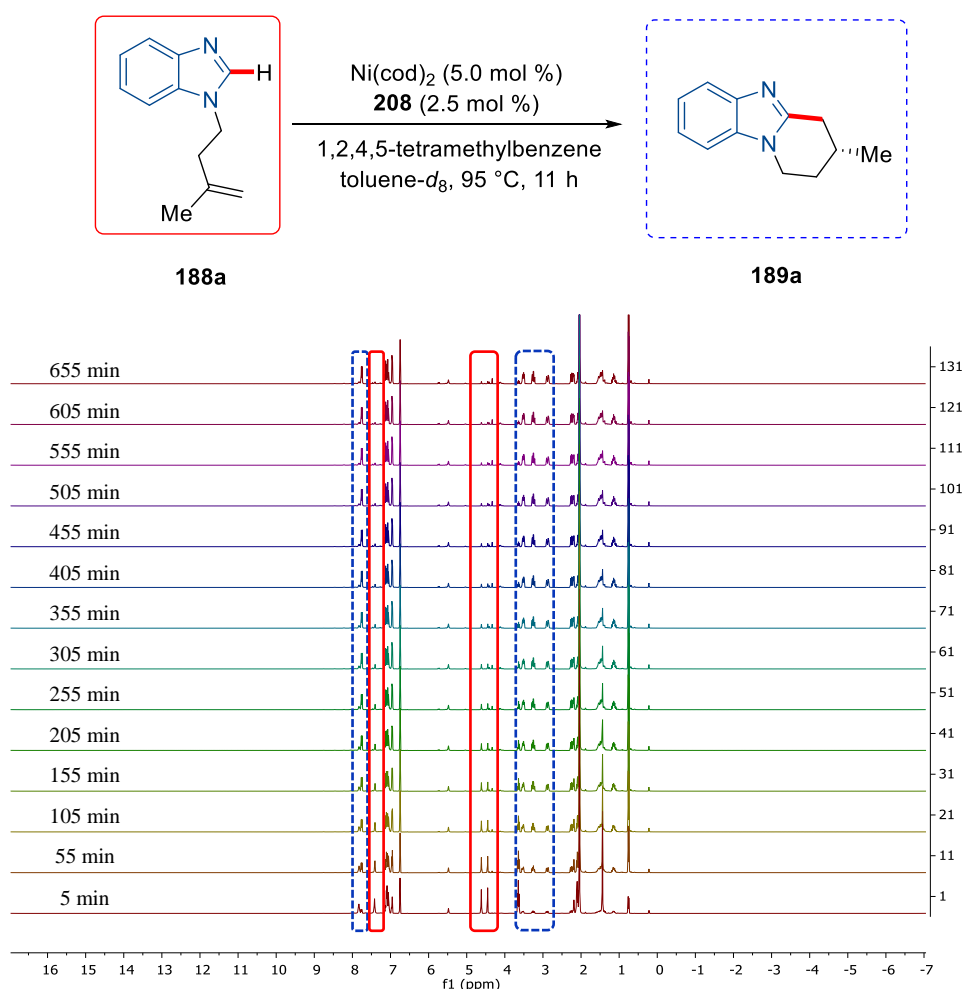
M.p.: 183–185 °C. **¹H-NMR** (500 MHz, CDCl₃): δ = 4.54 (ddd, *J* = 13.6, 5.8, 3.1 Hz, 1H), 4.09 (ddd, *J* = 14.2, 11.1, 4.7 Hz, 1H), 3.53 (s, 3H), 3.36 (s, 3H), 3.03 (ddd, *J* = 17.4, 5.1, 1.7 Hz, 1H), 2.46 (dd, *J* = 17.5, 10.1 Hz, 1H), 2.15 – 2.00 (m, 2H), 1.68 (dd, *J* = 11.1, 5.6 Hz, 1H), 1.14 (d, *J* = 6.5 Hz, 3H). **¹³C-NMR** (125 MHz, CDCl₃): δ = 155.1 (C_q), 151.9 (C_q), 150.5 (C_q), 148.6 (C_q), 106.7 (C_q), 44.1 (CH₂), 32.9 (CH₂), 30.0 (CH₂), 29.8 (CH₃), 27.9 (CH), 26.8 (CH₃), 21.0 (CH₃). **IR** (ATR): 2930, 2925, 2854, 1701, 1656, 1546, 1463, 1427, 1234, 747 cm⁻¹. **MS** (ESI) *m/z* (relative intensity): 271 (100) [M+Na]⁺, 249 (82) [M+H]⁺. **HR-MS** (ESI): *m/z* calcd. for C₁₂H₁₇N₄O₂ [M+H]⁺ 249.1346, found

249.1347. $[\alpha]_D^{20}$: +28 ($c = 1.00$, CHCl_3). **HPLC separation** (Chiralpak® IA-3, *n*-hexane/*i*PrOH: 80/20, 1.2 mL/min, detection at 273 nm): t_r (major) = 18.5 min, t_r (minor) = 21.7 min, 95:5 e.r.

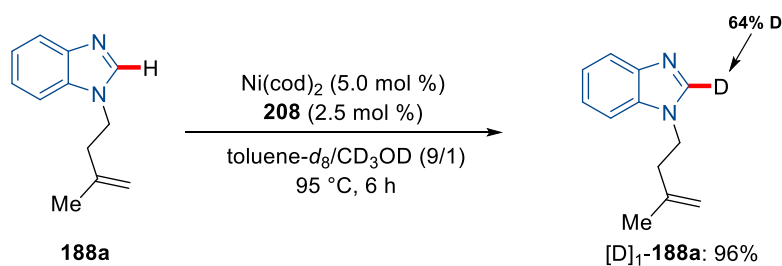
5.5.2. Mechanistic Studies

In-Operando NMR studies

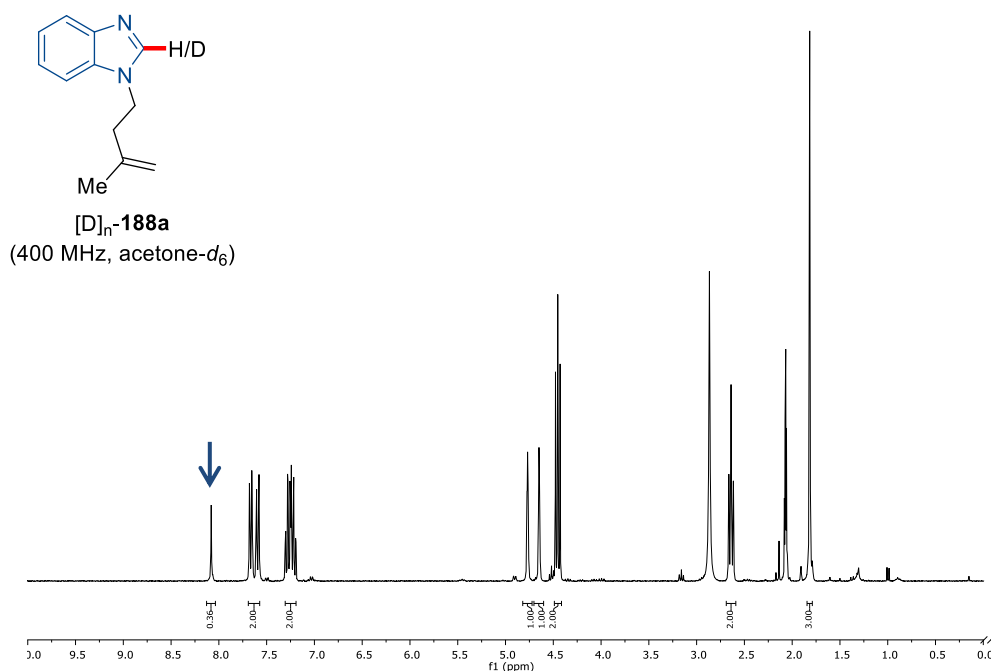
Inside a nitrogen-filled glovebox, an oven-dried Young NMR tube was charged with **188a** (46.6 mg, 0.25 mmol, 1.00 equiv), $\text{Ni}(\text{cod})_2$ (3.45 mg, 12.5 μmol , 5.00 mol %), **208** (3.15 mg, 6.25 μmol , 2.50 mol %) and 1,2,4,5-tetramethylbenzene (13.4 mg, 0.10 mmol). Toluene- d_8 (0.50 mL) was added and the Young NMR tube was closed, removed from the glovebox, and placed in a Bruker Avance III HD 400 spectrometer. After locking and shimming of the sample, periodic measurements (every 50 min, with 8 scans) at 95 °C for 11 h provided the following spectra.

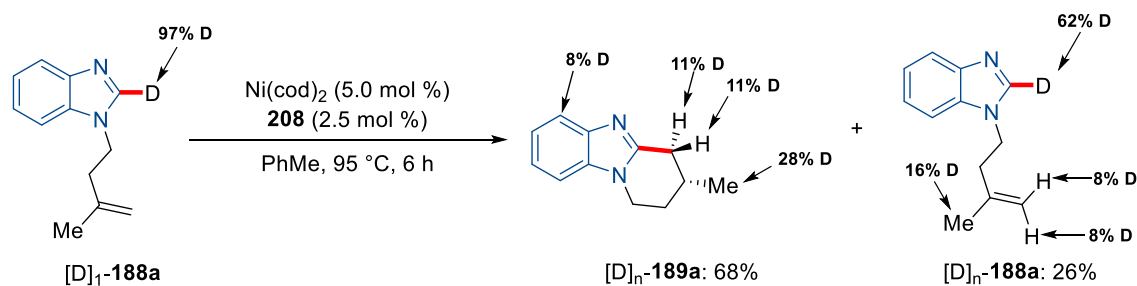


Scheme 5.2. *In-operando* NMR studies with **188a**.

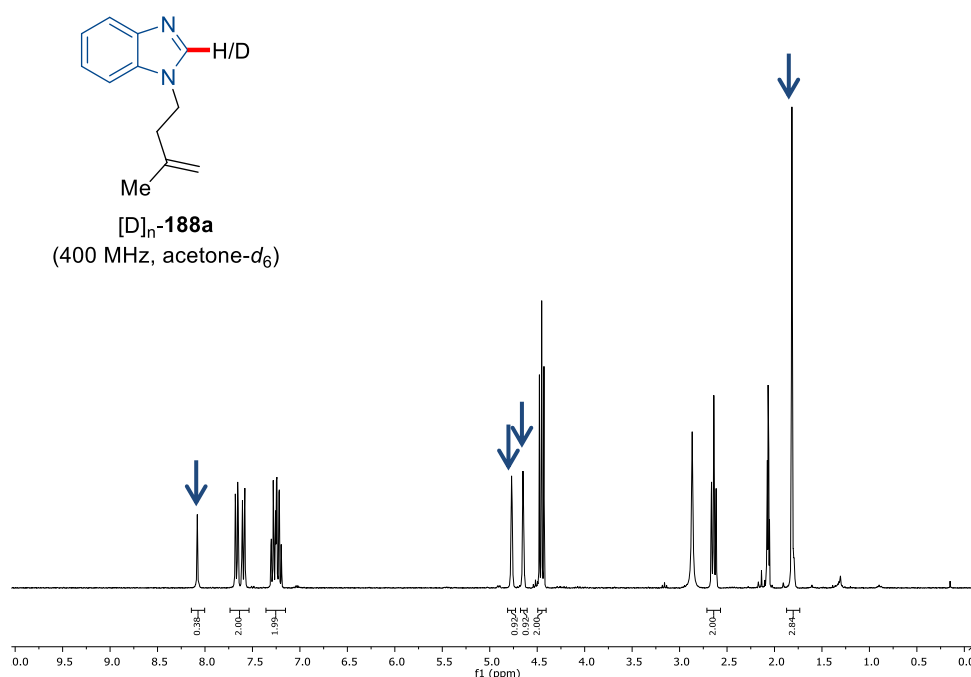
H/D-Exchange with Isotopically-Labeled CD₃ODScheme 5.3. H/D-exchange with CD₃OD and **188a**.

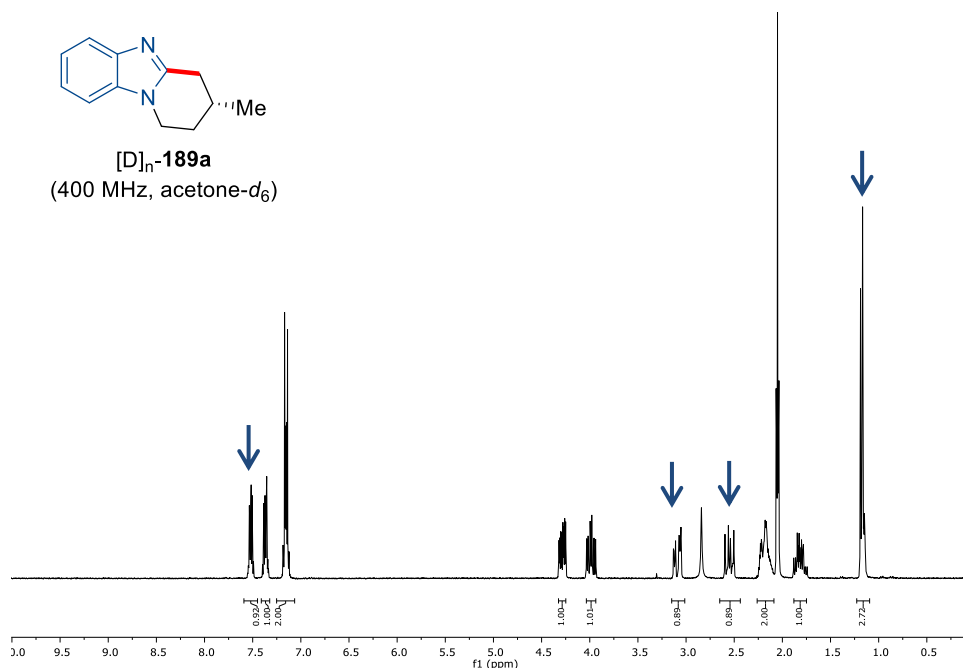
188a (93.6 mg, 0.50 mmol, 1.00 equiv), Ni(cod)₂ (6.90 mg, 25.0 μmol, 5.00 mol %), **208** (6.30 mg, 12.5 μmol, 2.50 mol %) were placed into an oven-dried 25 mL Schlenk tube equipped with a septum under N₂ atmosphere. Toluene (0.90 mL) and CD₃OD (0.10 mL) were added and the mixture was stirred at 95 °C. After 16 h, the reaction was cooling to 25 °C and diluted with EtOAc (10 mL). The mixture was filtered through a short plug of silica gel, rinsed with EtOAc (4 x 10 mL) and concentrated under reduced pressure. Purification by column chromatography (*n*-hexane/EtOAc: 2/1) yielded [D]₁-**188a** (89.9 mg, 96%).

Figure 5.1. H/D-exchange with CD₃OD and **188a**.

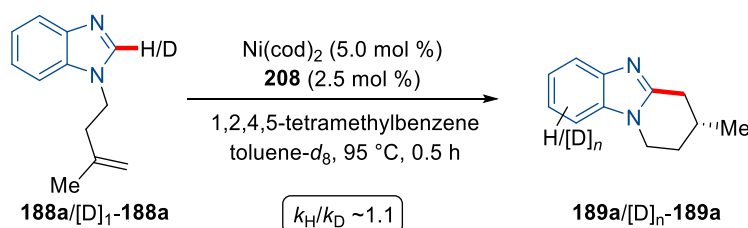
H/D-Exchange with Isotopically-Labeled [D]₁-188aScheme 5.4. H/D-exchange with [D]₁-188a.

[D]₁-188a (93.6 mg, 0.50 mmol, 1.00 equiv), Ni(cod)₂ (6.90 mg, 25.0 μmol, 5.00 mol %), **208** (6.30 mg, 12.5 μmol, 2.50 mol %) were placed into an oven-dried 25 mL Schlenk tube equipped with a septum under N₂ atmosphere. Toluene (1.00 mL) was added and the mixture was stirred at 95 °C. After 6 h, the reaction was cooling to 25 °C and diluted with EtOAc (10 mL). The mixture was filtered through a short plug of silica gel, rinsed with EtOAc (4 x 10 mL) and concentrated under reduced pressure. Purification by column chromatography (*n*-hexane/EtOAc: 2/1) yielded [D]_n-189a (63.7 mg, 68%) and reisolated [D]_n-188a (24.3 mg, 26%).



Figure 5.2. H/D-exchange with [D]₁-**188a**.

Kinetic Isotope Effect (KIE)

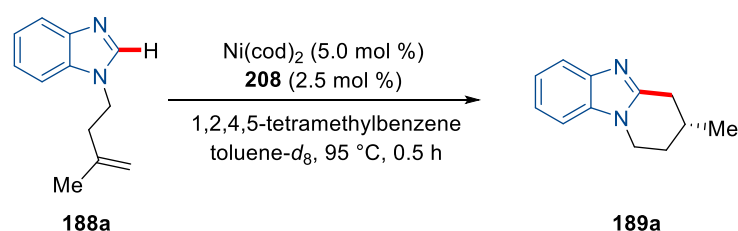
Scheme 5.5. KIE studies with **188a** and [D]₁-**188a**.

Two independent reactions were performed respectively to determine the KIE value by comparison of the initial reaction rates by *in-operando* NMR-analysis with 1,2,4,5-tetramethylbenzene as the internal standard.

Inside a nitrogen-filled glovebox, an oven-dried Young NMR tube was charged with **188a** (46.6 mg, 0.25 mmol, 1.00 equiv) or [D]₁-**188a** (46.8 mg, 0.25 mmol, 1.00 equiv), Ni(cod)₂ (3.45 mg, 12.5 μmol, 5.00 mol %), **208** (3.15 mg, 6.25 μmol, 2.50 mol %) and 1,2,4,5-tetramethylbenzene (13.4 mg, 0.10 mmol). Toluene-*d*₈ (0.5 mL) was added and the Young NMR tube was closed, removed from the glovebox, and placed in a Bruker Avance III HD 400 spectrometer. After locking and shimming of the sample, periodic measurements (every 2 min, with 4 scans) at 95 °C for 12 min provided the following data.

Table 5.2. Conversion *versus* time for **188a** and [D]₁-**188a**.

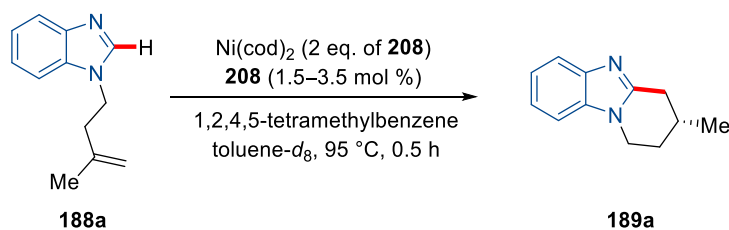
<i>t</i> / s	120	240	360	480	600	720
188a / %	2.10	4.90	7.10	10.0	12.5	14.6
[D] ₁ - 188a / %	1.80	5.00	7.30	9.60	11.4	13.8

Determination of the reaction order of **188a**Scheme 5.6. Reaction order in **188a**.

The reaction order was examined using the initial rate method. Inside a nitrogen-filled glovebox, oven-dried Young NMR tubes were charged with a stock solution (0.50 mL) consisting of Ni(cod)₂ (17.3 mg, 62.5 μmol), **208** (15.8 mg, 31.3 μmol) and 1,2,4,5-tetramethylbenzene (67.1 mg, 0.50 mmol) in toluene-*d*₈ (2.50 mL). Substrate **188a** (0.15, 0.20, 0.25, 0.30, 0.35 mmol) was then added. The Young NMR tubes were closed, removed from the glovebox, and placed in a Bruker Avance III HD 400 spectrometer. After locking and shimming of the samples, periodic measurements (every 2 min, with 4 scans) at 95 °C for 30 min provided the following data.

Table 5.3. Reaction order in [**188a**].

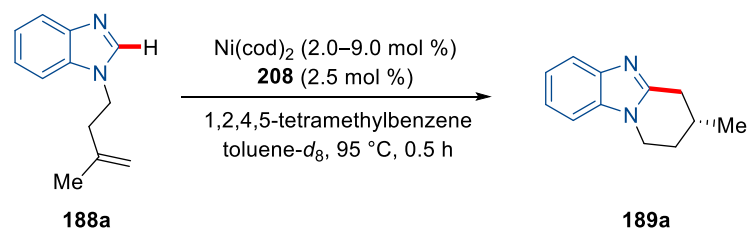
Entry	<i>c</i> / mol L ⁻¹	<i>k</i> / mol L ⁻¹ s ⁻¹	log (<i>c</i> / mol L ⁻¹)	log (<i>k</i> / mol L ⁻¹ s ⁻¹)
1	0.272	3.140·10 ⁻⁸	-0.565	-7.503
2	0.364	4.133·10 ⁻⁸	-0.439	-7.384
3	0.455	5.250·10 ⁻⁸	-0.342	-7.280
4	0.546	6.250·10 ⁻⁸	-0.263	-7.204
5	0.637	7.819·10 ⁻⁸	-0.196	-7.107

Determination of the reaction order of **208**Scheme 5.7. Reaction order in **208**.

The reaction order was examined using the initial rate method. Inside a nitrogen-filled glovebox, oven-dried Young NMR tubes were charged with a stock solution (0.50 mL) consisting of Ni(cod)_2 (17.3 mg, 62.5 μmol , 5.00 mol %), **188a** (233 mg, 1.25 mmol, 1.00 equiv) and 1,2,4,5-tetramethylbenzene (67.1 mg, 0.50 mmol) in toluene- d_8 (2.50 mL). **208** (1.5, 2.0, 2.5, 3.0, 3.5 mol %) was then added. The Young NMR tubes were closed, removed from the glovebox, and placed in a Bruker Avance III HD 400 spectrometer. After locking and shimming of the samples, periodic measurements (every 2 min, with 4 scans) at 95 °C for 30 min provided the following data.

Table 5.4. Reaction order in [**208**].

Entry	$c / \text{mol L}^{-1}$	$k / \text{mol L}^{-1} \text{s}^{-1}$	$\log(c / \text{mol L}^{-1})$	$\log(k / \text{mol L}^{-1} \text{s}^{-1})$
1	$1.274 \cdot 10^{-2}$	$5.260 \cdot 10^{-8}$	-1.895	-7.279
2	$1.473 \cdot 10^{-2}$	$6.625 \cdot 10^{-8}$	-1.832	-7.179
3	$1.752 \cdot 10^{-2}$	$7.551 \cdot 10^{-8}$	-1.757	-7.122
4	$1.999 \cdot 10^{-2}$	$8.824 \cdot 10^{-8}$	-1.699	-7.054
5	$2.508 \cdot 10^{-2}$	$1.021 \cdot 10^{-7}$	-1.601	-6.991

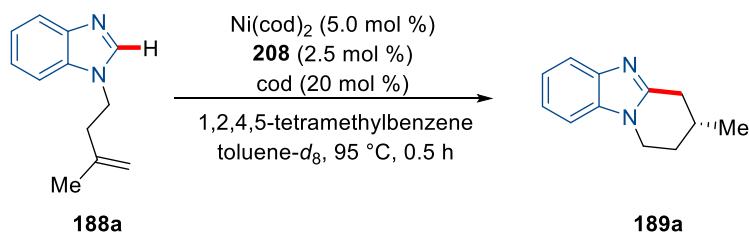
Determination of the reaction order of Ni(cod)₂**Scheme 5.8.** Reaction order in Ni(cod)₂.

The reaction order was examined using the initial rate method. Inside a nitrogen-filled glovebox, oven-dried Young NMR tubes were charged with a stock solution (0.50 mL) consisting of **188a** (419 mg, 2.25 mmol, 1.00 equiv), **208** (28.4 mg, 56.3 μmol, 2.50 mol %) and 1,2,4,5-tetramethylbenzene (121 mg, 0.90 mmol) in toluene-*d*₈ (4.50 mL). Ni(cod)₂ (2.0, 2.5, 3.0, 3.5, 4.0, 5.0, 6.0, 7.0, 9.0 mol %) was then added. The Young NMR tubes were closed, removed from the glovebox, and placed in a Bruker Avance III HD 400 spectrometer. After locking and shimming of the samples, periodic measurements (every 2 min, with 4 scans) at 95 °C for 30 min provided the following data.

Table 5.5. Reaction order in [Ni(cod)₂].

Entry	$c / \text{mol L}^{-1}$	$k / \text{mol L}^{-1} \text{s}^{-1}$	$\log (c / \text{mol L}^{-1})$	$\log (k / \text{mol L}^{-1} \text{s}^{-1})$
1	$8.593 \cdot 10^{-3}$	$4.561 \cdot 10^{-8}$	-2.066	-7.341
2	$1.124 \cdot 10^{-2}$	$6.214 \cdot 10^{-8}$	-1.949	-7.207
3	$1.388 \cdot 10^{-2}$	$7.644 \cdot 10^{-8}$	-1.858	-7.117
4	$1.586 \cdot 10^{-2}$	$9.047 \cdot 10^{-8}$	-1.800	-7.044
5	$1.851 \cdot 10^{-2}$	$1.018 \cdot 10^{-7}$	-1.733	-6.992
6	$2.247 \cdot 10^{-2}$	$5.260 \cdot 10^{-8}$	-1.648	-7.279
7	$2.710 \cdot 10^{-2}$	$2.837 \cdot 10^{-8}$	-1.567	-7.547
8	$3.173 \cdot 10^{-2}$	$1.874 \cdot 10^{-8}$	-1.499	-7.727
9	$4.098 \cdot 10^{-2}$	$8.964 \cdot 10^{-9}$	-1.387	-8.047

Effect of the concentration of 1,5-cyclooctadien on the reaction rate



Scheme 5.9. Effect of additional cod on the reaction rate.

Two independent reactions were performed respectively to determine the initial reaction rates by *in-operando* NMR-analysis with 1,2,4,5-tetramethylbenzene as the internal standard. Inside a nitrogen-filled glovebox, an oven-dried Young NMR tube was charged with **188a** (46.6 mg, 0.25 mmol, 1.00 equiv), $\text{Ni}(\text{cod})_2$ (3.45 mg, 12.5 μmol , 5.00 mol %), **208** (3.15 mg, 6.25 μmol , 2.50 mol %), 1,2,4,5-tetramethylbenzene (13.4 mg, 0.10 mmol) and toluene- d_8 (0.5 mL). 1,5-Cyclooctadiene (5.04 mg, 50 μmol , 20 mol%) was added and the Young NMR tube was closed, removed from the glovebox, and placed in a Bruker Avance III HD 400 spectrometer. After locking and shimming of the sample, periodic measurements (every 2 min, with 4 scans) at 95 °C for 12 min provided the following data.

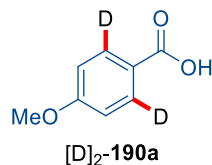
Tabelle 5.6. Effect of additional cod on the reaction rate.

t / s	120	240	360	480	600	720
189a / %	2.10	4.90	7.10	10.0	12.5	14.6
189a + cod / %	0.20	1.30	3.10	4.90	7.00	9.10

5.6. Hydrogen Isotope Exchange by Ruthenium-Catalyzed C–H Activation

5.6.1. Characterization Data

4-Methoxybenzoic-2,6-*d*₂ acid ([D]₂-190a)

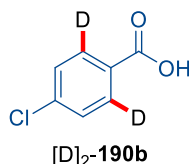


The general procedure **GP-G** was followed using 4-methoxybenzoic acid (**190a**) (76.1 mg, 0.50 mmol), [Ru(O₂CAd)₂(*p*-cymene)] (14.9 mg, 5.00 mol %) and D₂O (90.0 μL, 5.00 mmol). Purification by column chromatography (*n*-hexane/EtOAc/AcOH: 8/1/0.1) yielded [D]₂-**190a** (68.6 mg, 93%) as a colourless solid. Incorporation expected at $\delta = 8.07$ ppm and determined against the integral at $\delta = 3.88$. Degree of Deuteration: 95%.

¹H-NMR (300 MHz, CDCl₃): $\delta = 8.07$ (d, $J = 9.3$ Hz, 0.1H), 6.95 (s, 2H), 3.88 (s, 3H).

¹³C-NMR (125 MHz, CDCl₃): $\delta = 171.6$ (C_q), 164.2 (C_q), 132.1 (t, $J = 25.2$ Hz, CD), 121.6 (C_q), 113.8 (CH), 55.6 (CH₃). **MS** (EI) m/z (relative intensity): 154 (100) [M]⁺, 137 (40), 109 (25). **HR-MS** (EI): m/z calcd. for C₈H₆D₂O₃⁺ [M]⁺ 154.0599, found 154.0602.

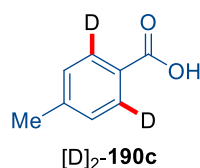
4-Chlorobenzoic-2,6-*d*₂ acid ([D]₂-190b)



The general procedure **GP-G** was followed using 2-chlorobenzoic acid (**190b**) (78.3 mg, 0.50 mmol), [Ru(O₂CAd)₂(*p*-cymene)] (14.9 mg, 5.00 mol %) and D₂O (90.0 μL, 5.00 mmol). Purification by column chromatography (*n*-hexane/EtOAc/AcOH: 8/1/0.1) yielded [D]₂-**190b** (71.1 mg, 90%) as a colourless solid. Incorporation expected at $\delta = 8.04$ ppm and determined against the integral at $\delta = 7.54$ – 7.38 . Degree of Deuteration: 60%

¹H-NMR (400 MHz, CDCl₃): $\delta = 8.04$ (d, $J = 8.4$ Hz, 0.8H), 7.54 – 7.38 (m, 2H). ¹³C-

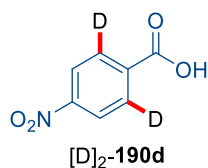
NMR (100 MHz, MeOH-*d*₄): $\delta = 168.9$ (C_q), 140.2 (C_q), 132.3 (t, $J = 25.4$ Hz, CD), 129.7 (C_q), 129.6 (CH). **MS** (EI) m/z (relative intensity): 158 (75) [M]⁺, 141 (100), 113 (59). **HR-MS** (ESI): m/z calcd. for C₇H₂³⁵ClD₂O₂⁻ [M–H]⁻ 157.0031, found 157.0001 and for C₇H₄³⁵ClO₂⁻ [M–H]⁻ 154.9905, found 154.9906.

4-Methylbenzoic-2,6-*d*₂ acid ([D]₂-190c)

The general procedure **GP-G** was followed using 4-methylbenzoic acid (**190**) (68.1 mg, 0.50 mmol), [Ru(O₂CAd)₂(*p*-cymene)] (14.9 mg, 5.00 mol %) and D₂O (90.0 μL, 5.00 mmol). Purification by column chromatography (*n*-hexane/EtOAc/AcOH: 8/1/0.1) yielded [D]₂-**190c** (64.9 mg, 94%) as a colourless solid. Incorporation expected at $\delta = 8.03$ and determined against the integral at $\delta = 2.46$. Degree of Deuteration: 94%.

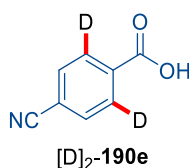
¹H-NMR (400 MHz, CDCl₃): $\delta = 8.03$ (d, $J = 8.2$ Hz, 0.12H), 7.30 (s, 2H), 2.46 (s, 3H).

¹³C-NMR (100 MHz, CDCl₃): $\delta = 172.6$ (C_q), 144.8 (C_q), 130.2 (t, $J = 24.9$ Hz, CD), 129.2 (CH), 128.9 (C_q), 21.9 (CH₃). **MS** (EI) m/z (relative intensity): 138 (88) [M]⁺, 121 (71), 93 (100). **HR-MS** (EI): m/z calcd. for C₈H₆D₂O₂⁺ [M]⁺ 138.0650, found 138.0654.

4-Nitrobenzoic-2,6-*d*₂ acid ([D]₂-190d)

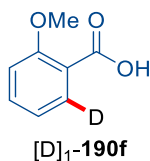
The general procedure **GP-G** was followed using 4-nitrobenzoic acid (**190d**) (83.6 mg, 0.50 mmol), [Ru(O₂CAd)₂(*p*-cymene)] (14.9 mg, 5.00 mol %) and D₂O (90.0 μL, 5.00 mmol). Purification by column chromatography (*n*-hexane/EtOAc/AcOH: 8/1/0.1) yielded [D]₂-**190d** (66.4 mg, 79%) as a colourless solid. Incorporation expected at $\delta = 8.17$ ppm and determined against the integral at $\delta = 8.33$. Degree of Deuteration: 84%.

¹H-NMR (300 MHz, DMSO-*d*₆): $\delta = 8.33$ (d, $J = 8.6$ Hz, 2H), 8.17 (d, $J = 8.9$ Hz, 0.32H). **¹³C-NMR** (100 MHz, DMSO-*d*₆): $\delta = 165.8$ (C_q), 150.0 (C_q), 130.3 (t, $J = 27.9$ Hz, CD), 123.7 (C_q) 123.6 (CH). **MS** (EI) m/z (relative intensity): 168 (100) [M-H]⁻, 124 (49). **HR-MS** (ESI): m/z calcd. for C₇H₂D₂NO₄⁻ [M-H]⁻ 168.0271, found 168.0275 and for C₇H₄NO₄⁻ [M-H]⁻ 166.0146, found 166.0151.

4-Cyanobenzoic-2,6-*d*₂ acid ([D]₂-190e)

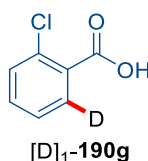
The general procedure **GP-G** was followed using 4-cyanobenzoic acid (**190e**) (73.6 mg, 0.50 mmol), [Ru(O₂CAd)₂(*p*-cymene)] (14.9 mg, 5.00 mol %) and D₂O (90.0 μL, 5.00 mmol). Purification by column chromatography (*n*-hexane/EtOAc/AcOH: 8/1/0.1) yielded [D]₂-**190e** (71.8 mg, 97%) as a colourless solid. Incorporation expected at $\delta = 8.08$ ppm and determined against the integral at $\delta = 7.98$. Degree of Deuteration: 93%.

¹H-NMR (300 MHz, DMSO-*d*₆): $\delta = 8.08$ (d, $J = 8.4$ Hz, 0.13H), 7.98 (s, 2H). **¹³C-NMR** (125 MHz, DMSO-*d*₆): $\delta = 166.1$ (C_q), 134.7 (C_q), 132.6 (CH), 129.6 (t, $J = 25.5$ Hz, CD), 118.2 (C_q), 115.1 (C_q). **MS** (EI) m/z (relative intensity): 148 (100) [M–H][–], 104 (43). **HR-MS** (ESI): m/z calcd. for C₈H₂D₂NO₂[–] [M–H][–] 148.0373, found 148.0374 and for C₇H₂D₂N[–] [M–CO₂H][–] 104.0475, found 104.0469.

2-Methoxybenzoic-6-*d* acid ([D]₁-190f)

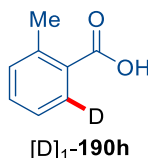
The general procedure **GP-G** was followed using 2-methoxybenzoic acid (**190f**) (76.1 mg, 0.50 mmol), [Ru(O₂CAd)₂(*p*-cymene)] (14.9 mg, 5.00 mol %) and D₂O (90.0 μL, 5.00 mmol). Purification by column chromatography (*n*-hexane/EtOAc/AcOH: 8/1/0.1) yielded [D]₁-**190f** (72.8 mg, 95%) as a colourless solid. Incorporation expected at $\delta = 8.18$ ppm and determined against the integral at $\delta = 4.08$. Degree of Deuteration: 98%.

¹H-NMR (300 MHz, CDCl₃): $\delta = 8.18$ (d, $J = 8.3$ Hz, 0.02H), 7.69 – 7.49 (m, 1H), 7.14 (d, $J = 7.3$ Hz, 1H), 7.06 (d, $J = 8.3$ Hz, 1H), 4.08 (s, 3H). **¹³C-NMR** (125 MHz, CDCl₃): $\delta = 165.8$ (C_q), 158.2 (C_q), 135.2 (CH), 133.3 (t, $J = 25.1$ Hz, CD), 122.1 (CH), 117.6 (C_q), 111.8 (CH), 56.8 (CH₃). **MS** (EI) m/z (relative intensity): 153 (55) [M]⁺, 136 (30), 124 (69), 106 (100). **HR-MS** (EI): m/z calcd. for C₈H₇DO₃⁺ [M]⁺ 153.0536, found 153.0535.

2-Chlorobenzoic-6-*d* acid ([D]₁-190g)

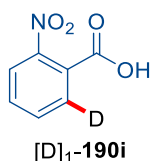
The general procedure **GP-G** was followed using 2-chlorobenzoic acid (**190g**) (78.3 mg, 0.50 mmol), [Ru(O₂CAd)₂(*p*-cymene)] (14.9 mg, 5.00 mol %) and D₂O (90.0 μL, 5.00 mmol). Purification by column chromatography (*n*-hexane/EtOAc/AcOH: 8/1/0.1) yielded [D]₁-**190g** (73.8 mg, 94%) as a colourless solid. Incorporation expected at $\delta = 8.03$ and determined against the integral at $\delta = 7.36$. Degree of Deuteration: 99%.

¹H-NMR (400 MHz, CDCl₃): $\delta = 8.03$ (d, $J = 7.8$ Hz, 0.01H), 7.57 – 7.42 (m, 2H), 7.36 (dd, $J = 6.3, 2.3$ Hz, 1H). **¹³C-NMR** (100 MHz, CDCl₃): $\delta = 170.9$ (C_q), 134.9 (C_q), 133.8 (CH), 132.5 (t, $J = 25.5$ Hz, CD), 131.7 (CH), 128.5 (C_q), 126.7 (CH). **MS** (EI) m/z (relative intensity): 157 (75) [M]⁺, 140 (100), 112 (63). **HR-MS** (EI): m/z calcd. for C₇H₄D³⁷ClO₂⁺ [M]⁺ 159.0015, found 159.0027 and for C₇H₄D³⁵ClO₂⁺ [M]⁺ 157.0041, found 157.0042.

2-Methylbenzoic-6-*d* acid ([D]₁-190h)

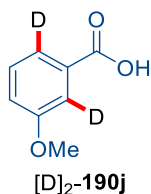
The general procedure **GP-G** was followed using 2-methylbenzoic acid (**190h**) (68.1 mg, 0.50 mmol), [Ru(O₂CAd)₂(*p*-cymene)] (14.9 mg, 5.00 mol %) and D₂O (90.0 μL, 5.00 mmol). Purification by column chromatography (*n*-hexane/EtOAc/AcOH: 8/1/0.1) yielded [D]₁-**190h** (66.5 mg, 97%) as a colourless solid. Incorporation expected at $\delta = 8.10$ ppm and determined against the integral at $\delta = 2.69$. Degree of Deuteration: 97%.

¹H-NMR (300 MHz, CDCl₃): $\delta = 8.10$ (d, $J = 8.1$ Hz, 0.03H), 7.49 (t, $J = 7.5$ Hz, 1H), 7.38 – 7.25 (m, 2H), 2.69 (s, 3H). **¹³C-NMR** (100 MHz, CDCl₃): $\delta = 173.8$ (C_q), 141.5 (C_q), 133.1 (CH), 132.1 (CH), 131.7 (CH), 128.5 (C_q), 125.9 (CD), 22.3 (CH₃). **MS** (EI) m/z (relative intensity): 137 (71) [M]⁺, 119 (100). **HR-MS** (EI): m/z calcd. for C₈H₇DO₂⁺ [M]⁺ 137.0587, found 137.0589.

2-Nitrobenzoic-6-*d* acid ([D]₁-190i)

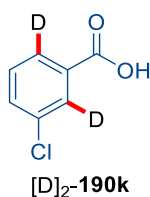
The general procedure **GP-G** was followed using 2-nitrobenzoic acid (**190i**) (83.6 mg, 0.50 mmol), [Ru(O₂CAd)₂(*p*-cymene)] (14.9 mg, 5.00 mol %) and D₂O (90.0 μL, 5.00 mmol). Purification by column chromatography (*n*-hexane/EtOAc/AcOH: 8/1/0.1) yielded [D]₁-**190i** (70.6 mg, 84%) as a colourless solid. Incorporation expected at $\delta = 7.86$ ppm and determined against the integral at $\delta = 7.96$. Degree of Deuteration: 90%.

¹H-NMR (300 MHz, DMSO-*d*₆): $\delta = 7.96$ (dd, $J = 7.0, 2.1$ Hz, 1H), 7.86 (d, $J = 2.3$ Hz, 0.1H), 7.85 – 7.70 (m, 2H). **¹³C-NMR** (125 MHz, DMSO-*d*₆): $\delta = 166.0$ (C_q), 148.4 (C_q), 133.0 (CH), 132.4 (CH), 129.7 (t, $J = 25.4$ Hz, CD), 127.3 (C_q), 123.7 (CH). **MS** (EI) m/z (relative intensity): 167 (33) [M–H][–], 151 (46), 124 (28), 94 (49). **HR-MS** (ESI): m/z calcd. for C₇H₃DNO₄[–] [M–H][–] 167.0209, found 167.0209 and for C₇H₄NO₄[–] [M–H][–] 166.0146, found 166.0144.

3-Methoxybenzoic-2,6-*d*₂ acid ([D]₂-190j)

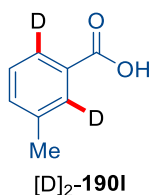
The general procedure **GP-G** was followed using 3-methoxybenzoic acid (**190j**) (76.1 mg, 0.50 mmol), [Ru(O₂CAd)₂(*p*-cymene)] (14.9 mg, 5.00 mol %) and D₂O (90.0 μL, 5.00 mmol). Purification by column chromatography (*n*-hexane/EtOAc/AcOH: 8/1/0.1) yielded [D]₂-**190j** (70.9 mg, 92%) as a colourless solid. Incorporation expected at $\delta = 7.71$ and 7.63 ppm and determined against the integral at $\delta = 3.87$. Degree of Deuteration: 96%.

¹H-NMR (300 MHz, CDCl₃): $\delta = 7.71$ (s, 0.04H), 7.63 (s, 0.04H), 7.39 (d, $J = 8.3$ Hz, 1H), 7.16 (d, $J = 8.3$ Hz, 1H), 3.87 (s, 3H). **¹³C-NMR** (100 MHz, CDCl₃): $\delta = 172.2$ (C_q), 159.7 (C_q), 130.5 (C_q), 129.6 (CH), 122.7 (t, $J = 25.0$ Hz, CD), 120.7 (CH), 114.2 (t, $J = 25.3$ Hz, CD), 55.6 (CH₃). **MS** (EI) m/z (relative intensity): 154 (100) [M]⁺, 137 (40), 106 (25). **HR-MS** (EI): m/z calcd. for C₈H₆D₂O₃⁺ [M]⁺ 154.0599, found 153.0601.

3-Chlorobenzoic-2,6-*d*₂ acid ([D]₂-190k)

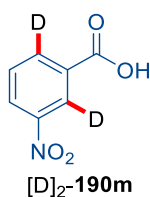
The general procedure **GP-G** was followed using 2-chlorobenzoic acid (**190k**) (78.3 mg, 0.50 mmol), [Ru(O₂CAd)₂(*p*-cymene)] (14.9 mg, 5.00 mol %) and D₂O (90.0 μL, 5.00 mmol). Purification by column chromatography (*n*-hexane/EtOAc/AcOH: 8/1/0.1) yielded [D]₂-**190k** (70.6 mg, 89%) as a colourless solid. Incorporation expected at $\delta = 8.10$ and 8.00 ppm and determined against the integral at $\delta = 7.43$. Degree of Deuteration: 99%.

¹H-NMR (400 MHz, CDCl₃): $\delta = 8.10$ (d, $J = 2.1$ Hz, 0.01H), 8.00 (dd, $J = 7.8, 1.1$ Hz, 0.01H), 7.60 (d, $J = 8.0$ Hz, 1H), 7.43 (d, $J = 8.0$ Hz, 1H). **¹³C-NMR** (100 MHz, CDCl₃): $\delta = 170.7$ (C_q), 134.8 (C_q), 134.1 (CH), 130.9 (C_q), 130.3 (t, $J = 26.3$ Hz, CD), 129.9 (CH), 128.2 (t, $J = 25.1$ Hz, CD). **MS** (EI) m/z (relative intensity): 158 (100), [M]⁺, 141 (90), 113 (62). **HR-MS** (EI): m/z calcd. for C₇H₃D₂³⁷ClO₂⁺ [M]⁺ 160.0078, found 160.0077 and for C₇H₃D₂³⁵ClO₂⁺ [M]⁺ 158.0104, found 158.0104.

3-Methylbenzoic-2,6-*d*₂ acid ([D]₂-190l)

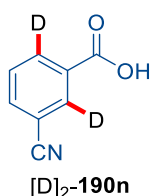
The general procedure **GP-G** was followed using 3-methylbenzoic acid (**190l**) (68.1 mg, 0.50 mmol), [Ru(O₂CAd)₂(*p*-cymene)] (14.9 mg, 5.00 mol %) and D₂O (90.0 μL, 5.00 mmol). Purification by column chromatography (*n*-hexane/EtOAc/AcOH: 8/1/0.1) yielded [D]₂-**190l** (65.6 mg, 95%) as a colourless solid. Incorporation expected at $\delta = 7.95$ ppm and determined against the integral at $\delta = 2.45$. Degree of Deuteration: 98%.

¹H-NMR (400 MHz, CDCl₃): $\delta = 7.95$ (d, $J = 8.6$ Hz, 0.04H), 7.46 (d, $J = 7.6$ Hz, 1H), 7.39 (d, $J = 7.6$ Hz, 1H), 2.45 (s, 3H). **¹³C-NMR** (100 MHz, CDCl₃): $\delta = 172.3$ (C_q), 138.4 (C_q), 134.7 (CH), 130.6 (t, $J = 26.7$ Hz, CD), 129.4 (C_q), 128.4 (CH), 127.3 (t, $J = 25.1$ Hz, CD), 21.4 (CH₃). **MS** (EI) m/z (relative intensity): 138 (87) [M]⁺, 121 (45), 93 (100). **HR-MS** (EI): m/z calcd. for C₈H₆D₂O₂⁺ [M]⁺ 138.0560, found 138.0650.

3-Nitrobenzoic-2,6-*d*₂ acid ([D]₂-190m)

The general procedure **GP-G** was followed using 3-nitrobenzoic acid (**190m**) (83.6 mg, 0.50 mmol), [Ru(O₂CAd)₂(*p*-cymene)] (14.9 mg, 5.00 mol %) and D₂O (90.0 μL, 5.00 mmol). Purification by column chromatography (*n*-hexane/EtOAc/AcOH: 8/1/0.1) yielded [D]₂-**190m** (71.9 mg, 86%) as a colourless solid. Incorporation expected at $\delta = 8.60$ and 8.33 ppm and determined against the integral at $\delta = 7.80$ ppm. Degree of Deuteration: 98%.

¹H-NMR (300 MHz, DMSO-*d*₆): $\delta = 8.60$ (d, $J = 2.5$ Hz, 0.02H), 8.45 (d, $J = 8.2$ Hz, 1H), 8.33 (d, $J = 8.2$ Hz, 0.02H), 7.80 (d, $J = 8.2$ Hz, 1H). **¹³C-NMR** (125 MHz, DMSO-*d*₆): $\delta = 165.5$ (C_q), 147.8 (C_q), 134.7 (t, $J = 25.2$ Hz, CD), 132.4 (C_q), 130.4 (CH), 127.4 (CH), 123.7 (t, $J = 25.7$ Hz, CD). **MS** (EI) m/z (relative intensity): 359 (15) [(2M–2H)+Na]⁺, 168 (100) [M–H]⁺, 124 (49), 124 (28), 94 (49). **HR-MS** (ESI): m/z calcd. for C₇H₂D₂NO₄⁺ [M–H]⁺ 168.0271, found 168.0274 and for C₆H₂D₂NO₂⁺ [M–COO]⁺ 124.0373, found 124.0373.

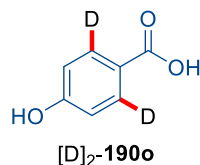
3-Cyanobenzoic-2,6-*d*₂ acid ([D]₂-190n)

The general procedure **GP-G** was followed using 3-cyanobenzoic acid (**190n**) (73.6 mg, 0.50 mmol), [Ru(O₂CAd)₂(*p*-cymene)] (14.9 mg, 5.00 mol %) and D₂O (90.0 μL, 5.00 mmol). Purification by column chromatography (*n*-hexane/EtOAc/AcOH: 8/1/0.1) yielded [D]₂-**190n** (70.8 mg, 95%) as a colourless solid. Incorporation expected at $\delta = 8.29$ and 8.24 ppm and determined against the integral at $\delta = 7.74$ ppm. Degree of Deuteration: 86%.

¹H-NMR (300 MHz, DMSO-*d*₆): $\delta = 8.29$ (d, $J = 1.7$ Hz, 0.1H), 8.24 (dd, $J = 7.9, 1.2$ Hz, 0.19H), 8.11 (d, $J = 7.9$ Hz, 1H), 7.74 (dd, $J = 7.9, 4.2$ Hz, 1H). **¹³C-NMR** (125 MHz, DMSO-*d*₆): $\delta = 165.7$ (C_q), 136.3 (CH), 133.5 (t, $J = 25.1$ Hz, CD), 132.6 (t, $J = 25.5$ Hz, CD), 132.0 (CH), 130.0 (C_q), 118.1 (C_q), 111.8 (C_q). **MS** (EI) m/z (relative intensity): 148

(100) $[M-H]^-$, 104 (35). **HR-MS** (ESI): m/z calcd. for $C_8H_2D_2NO_2^-$ $[M-H]^-$ 148.0373, found 148.0374.

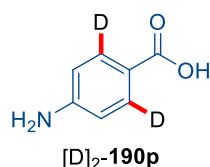
4-Hydroxybenzoic-2,6- d_2 acid ($[D]_2$ -**190o**)



The general procedure **GP-G** was followed using 4-hydroxybenzoic acid (**190o**) (69.1 mg, 0.50 mmol), $[Ru(O_2CAd)_2(p\text{-cymene})]$ (14.9 mg, 5.00 mol %) and D_2O (90.0 μ L, 5.00 mmol). Purification by column chromatography (*n*-hexane/EtOAc/AcOH: 8/1/0.1) yielded $[D]_2$ -**190o** (61.0 mg, 87%) as a colourless solid. Incorporation expected at $\delta = 7.87$ ppm and determined against the integral at $\delta = 6.81$. Degree of Deuteration: 93%.

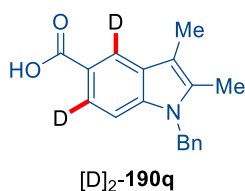
1H -NMR (400 MHz, Methanol- d_4): $\delta = 7.87$ (d, $J = 9.2$ Hz, 0.13H), 6.81 (s, 2H). **^{13}C -NMR** (100 MHz, Methanol- d_4): $\delta = 170.1$ (C_q), 163.3 (C_q), 132.9 (t, $J = 25.2$ Hz, CD), 122.6 (C_q), 115.9 (CH). **MS** (ESI) m/z (relative intensity): 139 (100), $[M-H]^-$, 95 (12). **HR-MS** (ESI): m/z calcd. for $C_7H_3D_2O_3^-$ $[M-H]^-$ 139.0370, found 139.0370.

4-Aminobenzoic-2,6- d_2 acid ($[D]_2$ -**190p**)



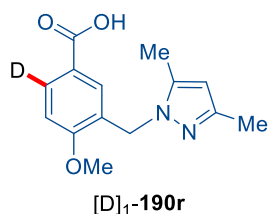
The general procedure **GP-G** was followed using 4-aminobenzoic acid (**190p**) (68.6 mg, 0.50 mmol), $[Ru(O_2CAd)_2(p\text{-cymene})]$ (14.9 mg, 5.00 mol %) and D_2O (90.0 μ L, 5.00 mmol). Purification by column chromatography (*n*-hexane/EtOAc/AcOH: 8/1/0.1) yielded $[D]_2$ -**190p** (59.4 mg, 86%) as a brown solid. Incorporation expected at $\delta = 7.61$ ppm and determined against the integral at $\delta = 6.54$. Degree of Deuteration: 87%.

1H -NMR (400 MHz, DMSO- d_6): $\delta = 7.61$ (d, $J = 9.1$ Hz, 0.26H), 6.54 (s, 2H), 5.83 (s, 2H). **^{13}C -NMR** (125 MHz, DMSO- d_6): $\delta = 167.7$ (C_q), 153.0 (C_q), 131.2 (C_q), 130.8 (t, $J = 23.8$ Hz, CD), 112.4 (CH). **MS** (ESI) m/z (relative intensity): 138 (100) $[M-H]^-$, 94 (15). **HR-MS** (ESI) m/z : calcd. for $C_7H_4D_2NO_2^-$ $[M-H]^-$ 138.0530, found 138.0524 and for $C_7H_5DNO_2$ $[M-H]^-$ 137.0467, found 137.0461.

1-Benzyl-2,3-dimethyl-1*H*-indole-5-carboxylic-4,6-*d*₂ acid ([D]₂-190q**)**

The general procedure **GP-G** was followed using 1-benzyl-2,3-dimethyl-1*H*-indole-5-carboxylic acid (**190q**) (140 mg, 0.50 mmol), [Ru(O₂CAd)₂(*p*-cymene)] (14.9 mg, 5.00 mol %) and D₂O (90.0 μL, 5.00 mmol). Purification by column chromatography (*n*-hexane/EtOAc/AcOH: 8/1/0.1) yielded [D]₂-**190q** (121 mg, 86%) as a yellow solid. Incorporation expected at $\delta = 8.11$ and 7.66 ppm and determined against the integral at $\delta = 7.42$ ppm. Degree of Deuteration: 92%.

¹H-NMR (500 MHz, DMSO-*d*₆): $\delta = 8.11$ (s, 0.05H), 7.66 (d, $J = 8.6$ Hz, 0.11H), 7.42 (s, 1H), 7.33 – 7.25 (m, 2H), 7.25 – 7.18 (m, 1H), 7.03 – 6.92 (m, 2H), 5.43 (s, 2H), 2.28 (d, $J = 0.8$ Hz, 3H), 2.25 (d, $J = 0.8$ Hz, 3H). **¹³C-NMR** (125 MHz, DMSO-*d*₆): $\delta = 168.4$ (C_q), 138.5 (C_q), 138.2 (C_q), 134.4 (C_q), 128.7 (CH), 128.7 (CH), 127.6 (C_q), 127.0 (CH), 126.1 (CH), 126.1 (CH), 121.9 (CD), 121.0 (C_q), 109.0 (CD), 108.8 (CH), 107.5 (C_q), 46.0 (CH₂), 10.0 (CH₃), 8.6 (CH₃). **MS** (EI) m/z (relative intensity): 280 (100) [M–H][–], 255 (14), 179 (59). **HR-MS** (ESI): m/z calcd. for C₁₈H₁₄D₂NO₂[–] [M–H][–] 280.1312, found 280.1314 and for C₁₈H₁₅D₁NO₂[–] [M–H][–] 279.1249, found 279.1250.

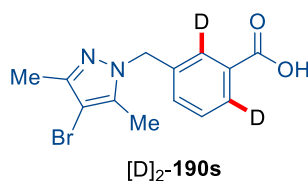
3-[(3,5-Dimethyl-1*H*-pyrazol-1-yl)methyl]-4-methoxybenzoic-6-*d* acid ([D]₁-190r**)**

The general procedure **GP-G** was followed using 3-[(3,5-dimethyl-1*H*-pyrazol-1-yl)methyl]-4-methoxybenzoic acid (**190r**) (130 mg, 0.50 mmol), [Ru(O₂CAd)₂(*p*-cymene)] (14.9 mg, 5.00 mol %) and D₂O (90.0 μL, 5.00 mmol). Purification by column chromatography (*n*-hexane/EtOAc/AcOH: 8/1/0.1) yielded [D]₂-**190r** (107 mg, 82%) as a colourless solid. Incorporation expected at $\delta = 7.87$ and 7.21 ppm and determined against the integral at $\delta = 5.11$ ppm. Degree of Deuteration: 50%.

¹H-NMR (500 MHz, DMSO-*d*₆): $\delta = 7.87$ (dd, $J = 8.6, 2.2$ Hz, 0.11H), 7.21 (q, $J = 1.0$ Hz, 0.89H), 7.11 (s, 1H), 5.93 – 5.79 (m, 0.9H), 5.11 (s, 2H), 3.90 (s, 3H), 2.15 (d, $J = 0.8$

Hz, 3H), 2.09 (s, 3H). $^{13}\text{C-NMR}$ (100 MHz, MeOH- d_4): δ = 169.5 (C_q), 161.6 (C_q), 149.2 (C_q), 141.9 (C_q), 132.4 (CD), 130.0 (C_q), 127.0 (C_q), 124.2 (CD), 111.0 (CH), 106.5 (CH), 56.4 (CH₃), 47.9 (CH₂), 13.2 (CH₃), 10.8 (CH₃). **MS** (EI) m/z (relative intensity): 260 (100) [M-H]⁻, 216 (9). **HR-MS** (ESI) (relative intensity): m/z calcd. for C₁₄H₁₄N₂O₃⁻ [M-H]⁻ 260.1151, found 260.1152 (89) and for C₁₄H₁₅N₂O₃⁻ [M-H]⁻ 259.1088, found 259.1090 (11).

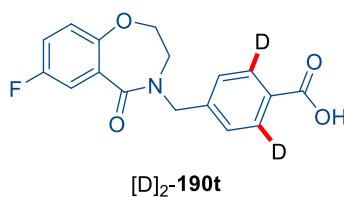
3-[(4-Bromo-3,5-dimethyl-1H-pyrazol-1-yl)methyl]benzoic-2,6- d_2 acid ([D]₂-190s)



The general procedure **GP-G** was followed using 3-[(4-bromo-3,5-dimethyl-1H-pyrazol-1-yl)methyl]benzoic acid (**190s**) (155 mg, 0.50 mmol), [Ru(O₂CAd)₂(*p*-cymene)] (14.9 mg, 5.00 mol %) and D₂O (90.0 μL , 5.00 mmol). Purification by column chromatography (*n*-hexane/EtOAc/AcOH: 8/1/0.1) yielded [D]₂-**190s** (114 mg, 74%) as a brown solid. Incorporation expected at δ = 7.85 and 7.73 ppm and determined against the integral at δ = 5.35 ppm. Degree of Deuteration: 95%.

$^1\text{H-NMR}$ (300 MHz, DMSO- d_6): δ = 7.85 (d, J = 7.6 Hz, 0.06H), 7.73 (s, 0.03H), 7.46 (d, J = 7.6 Hz, 1H), 7.34 (d, J = 7.7 Hz, 1H), 5.35 (s, 2H), 2.18 (s, 3H), 2.12 (s, 3H). $^{13}\text{C-NMR}$ (125 MHz, MeOH- d_4): δ = 169.6 (C_q), 147.6 (C_q), 139.6 (C_q), 138.6 (C_q), 132.8 (C_q), 132.2 (CH), 130.0 (t, J = 14.1 Hz, CD), 129.9 (CH), 128.7 (t, J = 23.1 Hz, CD), 95.4 (C_q), 53.9 (CH₂), 12.1 (CH₃), 10.3 (CH₃). **MS** (EI) m/z (relative intensity): 311 (100) [M-H]⁻, 265 (5), 232 (5), 173 (10). **HR-MS** (ESI): m/z calcd. for C₁₃H₁₀⁸¹BrD₂N₂O₂⁻ [M-H]⁻ 311.0193, found 311.0200 and for C₁₃H₁₀⁷⁹BrD₂N₂O₂⁻ [M-H]⁻ 309.0213, found 302.0217.

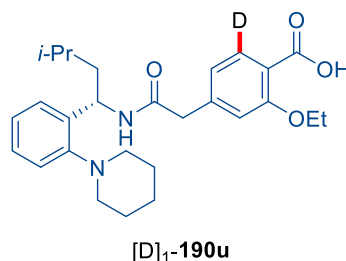
4-[[7-Fluoro-5-oxo-2,3-dihydrobenzo[*f*][1,4]oxazepin-4(5H)-yl]methyl]benzoic-2,6- d_2 acid ([D]₂-190t)



The general procedure **GP-G** was followed using 4-[[7-fluoro-5-oxo-2,3-dihydrobenzo[*f*][1,4]oxazepin-4(5*H*)-yl]methyl]benzoic acid (**190t**) (158 mg, 0.50 mmol), [Ru(O₂CAd)₂(*p*-cymene)] (14.9 mg, 5.00 mol %) and D₂O (90.0 μL, 5.00 mmol). Purification by column chromatography (*n*-hexane/EtOAc/AcOH: 8/1/0.1) yielded [D]₂-**190t** (130 mg, 82%) as a brown solid. Incorporation expected at $\delta = 7.93$ ppm and determined against the integral at $\delta = 4.83$ ppm. Degree of Deuteration: 94%.

¹H-NMR (500 MHz, DMSO-*d*₆): $\delta = 7.93$ (d, *J* = 8.5 Hz, 0.12H), 7.44 (q, *J* = 3.1 Hz, 2.8H), 7.40 – 7.31 (m, 1H), 7.09 (dd, *J* = 8.9, 4.7 Hz, 1H), 4.83 (s, 2H), 4.21 (dd, *J* = 5.6, 4.8 Hz, 2H), 3.54 (t, *J* = 5.2 Hz, 2H). ¹³C-NMR (125 MHz, DMSO-*d*₆): $\delta = 167.1$ (C_q), 166.6 (d, ⁴*J*_{C-F} = 2.1 Hz, C_q), 157.7 (d, ¹*J*_{C-F} = 240 Hz, C_q), 149.8 (d, ⁴*J*_{C-F} = 2.1 Hz, C_q), 142.7 (C_q), 129.8 (C_q), 129.3 (t, *J* = 25.1 Hz, CD), 128.9 (d, ³*J*_{C-F} = 7.5 Hz, C_q), 127.6 (CH), 123.5 (d, ³*J*_{C-F} = 8.1 Hz, CH), 119.7 (d, ²*J*_{C-F} = 23.2 Hz, CH), 116.4 (d, ²*J*_{C-F} = 24.6 Hz, CH), 73.2 (CH₂), 49.9 (CH₂), 45.9 (CH₂). ¹⁹F-NMR (282 MHz, DMSO-*d*₆): $\delta = -119.7$ (s). **MS** (EI) *m/z* (relative intensity): 316 (100) [M–H][–], 272 (6). **HR-MS** (ESI): *m/z* calcd. for C₁₇H₁₁D₂FNO₄[–] [M–H][–] 316.0975, found 316.0975.

(S)-2-Ethoxy-4-(2-{3-methyl-1-[2-(piperidin-1-yl)phenyl]butyl}amino)-2-(oxoethyl)benzoic-6-*d* acid ([D]₁-190u)

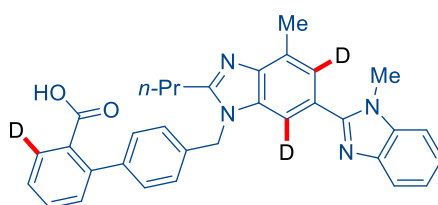


The general procedure **GP-G** was followed using (*S*)-2-ethoxy-4-{2-{3-methyl-1-[2-(piperidin-1-yl)phenyl]butyl}amino}-2-(oxoethyl)benzoic acid (**repaglinide**) (**190u**) (45.3 mg, 0.10 mmol), [Ru(O₂CAd)₂(*p*-cymene)] (5.96 mg, 10.0 mol %) and D₂O (20.0 μL, 1.00 mmol). Purification by column chromatography (*n*-hexane/EtOAc/AcOH: 8/2/0.1) yielded [D]₁-**190u** (36.2 mg, 80%) as a colourless solid. Incorporation expected at $\delta = 7.54$ ppm and determined against the integral at $\delta = 5.37$ ppm. Degree of Deuteration: 86%.

¹H-NMR (300 MHz, DMSO-*d*₆): $\delta = 8.45$ (d, *J* = 8.5 Hz, 1H), 7.54 (d, *J* = 7.8 Hz, 0.14H), 7.30 (dd, *J* = 7.6, 1.6 Hz, 1H), 7.22 – 7.12 (m, 1H), 7.12 – 6.94 (m, 3H), 6.84 (s, 1H), 5.37 (qd, *J* = 9.2, 4.9 Hz, 1H), 4.01 (q, *J* = 7.0 Hz, 2H), 3.47 (s, 4H), 3.05 (s, 2H),

1.83 – 1.40 (m, 9H), 1.31 (t, $J = 7.0$ Hz, 3H), 0.89 (dd, $J = 6.5, 2.4$ Hz, 6H). $^{13}\text{C-NMR}$ (100 MHz, MeOH- d_4): $\delta = 172.1$ (C_q), 169.5 (C_q), 159.6 (C_q), 153.4 (C_q), 143.9 (C_q), 140.7 (C_q), 133.1–132.3 (t, $J = 24.9$ Hz, CD), 128.8 (CH), 127.3 (CH), 125.6 (CH), 122.3 (C_q), 122.2 (CH), 122.2 (CH), 114.9 (CH), 66.0 (CH₂), 48.2 (CH), 47.5 (CH₂), 44.0 (CH₂), 27.8 (CH₂), 26.6 (CH), 25.4 (CH₂), 23.6 (CH₃), 22.6 (CH₃), 14.9 (CH₃). **MS** (EI) m/z (relative intensity): 452 (100) [M–H][–], 408 (6). **HR-MS** (ESI) m/z (relative intensity): calcd. for C₂₇H₃₄DN₂O₄[–] [M–H][–] 452.2665, found 452.2663 and for C₂₇H₃₅N₂O₄[–] [M–H][–] 451.2602, found 451.2595.

4'-{[2'-(Butyl-1-*d*)-1,7'-dimethyl-1*H*,3'*H*-[2,5'-bibenzo[*d*]imidazol]-3'-yl]-4',6'-*d*₂]methyl}-[1,1'-biphenyl]-3-*d*-2-carboxylic acid ([D]₂-190v)



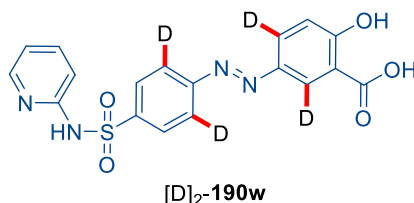
[D]₂-190v

The general procedure **GP-G** was followed using 4'-{[(1,7'-dimethyl-2'-propyl-1*H*,3'*H*-[2,5'-bibenzo[*d*]imidazol]-3'-yl)methyl]-[1,1'-biphenyl]-2-carboxylic acid (**telmisartan**) (**190v**) (51.5 mg, 0.10 mmol), [Ru(O₂CAd)₂(*p*-cymene)] (5.96 mg, 10.0 mol %) and D₂O (20.0 μL , 1.00 mmol). Purification by column chromatography (*n*-hexane/EtOAc/AcOH: 7/3/0.1) yielded [D]₂-**190v** (39.5 mg, 76%) as a colourless solid. Incorporation expected at $\delta = 7.70$ and determined against the integral at $\delta = 5.37$ ppm. Degree of Deuteration: 50%.

$^1\text{H-NMR}$ (300 MHz, DMSO- d_6): $\delta = 7.70$ (dd, $J = 15.1, 7.8$ Hz, 2H), 7.58 (d, $J = 7.6$ Hz, 1H), 7.52 (dd, $J = 7.6, 7.5$ Hz, 1H), 7.48 (s, 0.50H), 7.43 (d, $J = 7.9$ Hz, 1H), 7.36 – 7.20 (m, 5H), 7.18 (d, $J = 8.1$ Hz, 2H), 5.61 (s, 2H), 3.82 (s, 3H), 2.92 (q, $J = 7.1$ Hz, 1H), 2.63 (s, 3H), 1.82 (p, $J = 6.9$ Hz, 2H), 1.01 (t, $J = 7.3$ Hz, 3H). $^{13}\text{C-NMR}$ (100 MHz, DMSO- d_6): $\delta = 169.7$ (C_q), 156.2 (C_q), 154.0 (C_q), 142.7 (C_q), 142.4 (C_q), 140.3 (C_q), 140.2 (C_q), 136.6 (C_q), 135.9 (C_q), 134.7 (C_q), 130.7 (CH), 130.3 (CH), 129.0 (CH), 128.7 (CH), 128.7 (C_q), 128.4 (C_q), 128.2 (CH), 127.2 (d, $J = 11.0$ Hz, CD), 126.4 (CH), 126.4 (CH), 123.1 (CD), 123.4 (C_q), 122.1 (CH), 121.8 (CH), 118.7 (CH), 110.4 (CH), 109.3 (CD), 46.2 (CH₂), 31.8 (CH₃), 28.8 (CH₂), 20.8 (CH₂), 16.4 (CH₃), 13.9 (CH₃). **MS** (EI) m/z (relative intensity): 519 (100) [M]⁺, 378 (9), 307 (5). **HR-MS** (ESI): m/z calcd. for C₃₃H₂₆D₃N₄O₂[–] [M–H][–] 518.2630, found 518.2635.

The analytical data are in accordance with those previously reported in the literature for the unlabeled compound.^[370]

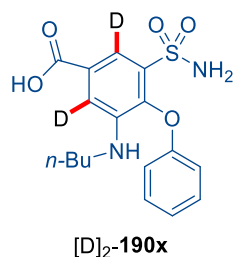
(*E*)-2-Hydroxy-5-({4-[*N*-(pyridin-2-yl-6-*d*)sulfamoyl]phenyl-2-*d*}diazenyl)benzoic-4,6-*d*₂ acid ([D]₂-190w)



The general procedure **GP-G** was followed using (*E*)-2-hydroxy-5-({4-[*N*-(pyridin-2-yl)sulfamoyl]phenyl}diazenyl)benzoic acid (**sulfasalazine**) (**190w**) (39.8 mg, 0.10 mmol), [Ru(O₂CAd)₂(*p*-cymene)] (5.96 mg, 10.0 mol %) and D₂O (20.0 μL, 1.00 mmol). Purification by column chromatography (*n*-hexane/EtOAc/AcOH: 7/3/0.1) yielded [D]₂-**190w** (28.7 mg, 72%) as a yellow solid. Incorporation expected at $\delta = 8.35$ ppm and determined against the integral at $\delta = 6.86$ ppm. Degree of Deuteration: 50%.

¹H-NMR (300 MHz, DMSO-*d*₆): $\delta = 8.35$ (d, $J = 2.1$ Hz, 0.5H), 8.16 – 7.89 (m, 4.8H), 7.77 (ddd, $J = 8.7, 7.0, 1.8$ Hz, 1H), 7.23 (d, $J = 8.9$ Hz, 1H), 7.17 – 7.10 (m, 1H), 6.86 (t, $J = 6.5$ Hz, 1H). **¹³C-NMR** (125 MHz, MeOH-*d*₄): $\delta = 166.7$ (C_q), 155.9 (C_q), 155.8 (d, $J = 6.1$ Hz, C_q), 155.1 (C_q), 146.4 (C_q), 146.3 (d, $J = 6.9$ Hz, C_q), 144.5 (C_q), 142.8 (CD) 142.4 (CH), 129.1 (CH), 129.0 (CH), 128.9 (CD), 123.8 (CH), 123.8 (CH), 119.0 (CH), 118.9 (CD), 116.5 (CD), 116.4 (CH). **MS** (ESI) m/z (relative intensity): 398 (100) [M–H][–], 397 (100), 283 (2). **HR-MS** (ESI): m/z calcd. for C₁₈H₉D₄N₄O₅S[–] [M–H][–] 401.0863, found 401.0848, for C₁₈H₁₁D₂N₄O₅S[–] [M–H][–] 399.0738, found 399.0718, for C₁₈H₁₂DN₄O₅S[–] [M–H][–] 398.0675, found 398.0666 and for C₁₈H₁₃N₄O₅S[–] [M–H][–] 397.0612, found 397.0616.

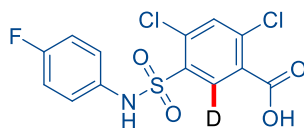
4-Benzyl-3-(*n*-butylamino)-5-sulfamoylbenzoic-2,6-*d*₂ acid ([D]₂-190x)



The general procedure **GP-G** was followed using 4-benzyl-3-(butylamino)-5-sulfamoylbenzoic acid (**bumetanide**) (**190x**) (36.4 mg, 0.10 mmol), [Ru(O₂CAd)₂(*p*-cymene)] (5.96 mg, 10.0 mol %) and D₂O (20.0 μL, 1.00 mmol). Purification by column chromatography (*n*-hexane/EtOAc/AcOH: 8/2/0.1) yielded [D]₂-**190x** (26.7 mg, 73%) as a colourless solid. Incorporation expected at $\delta = 7.69$ and 7.42 ppm and determined against the integral at $\delta = 5.05$ ppm. Degree of Deuteration: 96%.

¹H-NMR (300 MHz, DMSO-*d*₆): $\delta = 7.69$ (s, 0.03H), 7.42 (s, 0.05H), 7.34 – 7.21 (m, 4H), 7.07 – 6.94 (m, 1H), 6.89 – 6.78 (m, 2H), 5.05 (t, $J = 5.8$ Hz, 1H), 3.06 (q, $J = 6.6$ Hz, 2H), 1.48 – 1.27 (m, 2H), 1.19 – 1.02 (m, 2H), 0.77 (t, $J = 7.3$ Hz, 3H). **¹³C-NMR** (125 MHz, MeOH-*d*₄): $\delta = 169.1$ (C_q), 157.8 (C_q), 157.8 (C_q), 143.8 (C_q), 141.4 (C_q), 138.3 (C_q), 130.6 (CH), 130.6 (CH), 129.9 (CD), 124.0 (CH), 117.1 (CD), 116.6 (CH), 116.6 (CH), 43.7 (CH₂), 32.0 (CH₂), 20.9 (CH₂), 14.02 (CH₃). **MS** (ESI) m/z (relative intensity): 365 (100) [M–H][–], 283 (100), 255 (6). **HR-MS** (ESI): m/z calcd. for C₁₇H₁₇D₂N₂O₅S[–] [M–H][–] 365.1146, found 365.1137.

2,4-Dichloro-5-[*N*-(4-fluorophenyl)sulfamoyl]benzoic-6-*d* acid ([D]₁-**190y**)

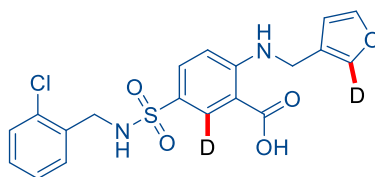


[D]₁-**190y**

The general procedure **GP-G** was followed using 2,4-dichloro-5-[*N*-(4-fluorophenyl)sulfamoyl]benzoic acid (**190y**) (36.4 mg, 0.10 mmol), [Ru(O₂CAd)₂(*p*-cymene)] (5.96 mg, 10.0 mol %) and D₂O (20.0 μL, 1.00 mmol). Purification by column chromatography (*n*-hexane/EtOAc/AcOH: 8/2/0.1) yielded [D]₁-**190y** (33.4 mg, 92%) as a colourless solid. Incorporation expected at $\delta = 8.29$ ppm and determined against the integral at $\delta = 7.94$ ppm. Degree of Deuteration: 97%.

¹H-NMR (300 MHz, DMSO-*d*₆): $\delta = 8.29$ (s, 0.03H), 7.94 (s, 1H), 7.11 (d, $J = 6.7$ Hz, 4H). **¹³C-NMR** (100 MHz, MeOH-*d*₄): $\delta = 161.7$ (d, $^1J_{C-F} = 244$ Hz, C_q), 139.6 (C_q), 136.8 (C_q), 135.8 (C_q), 134.8 (CH), 133.8 (C_q), 133.8 (C_q), 124.9 (t, $J = 24.8$ Hz, CD), 124.8 (d, $^3J_{C-F} = 8.3$ Hz, CH), 116.9 (d, $^2J_{C-F} = 23.2$ Hz, CH). **¹⁹F-NMR** (377 MHz, MeOH-*d*₄): $\delta = -119.1$ (d, $J = 4.5$ Hz). **MS** (ESI) m/z (relative intensity): 363 (100) [M–H][–], 319 (29), 283 (32). **HR-MS** (ESI): m/z calcd. for C₁₃H₆D³⁵Cl₂FNO₄S[–] [M–H][–] 362.9525, found 362.9531 and for C₁₂H₆D³⁵Cl₂FNO₂S[–] [M–H][–] 318.9627, found 318.9628.

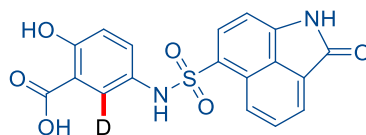
5-[N-(2-Chlorobenzyl)sulfamoyl]-2-[(furan-3-ylmethyl)amino]benzoic-6-*d* acid ([D]₁-190z)

[D]₁-190z

The general procedure **GP-G** was followed using 5-[N-(2-chlorobenzyl)sulfamoyl]-2-[(furan-3-ylmethyl)amino]benzoic acid (**190z**) (42.1 mg, 0.10 mmol), [Ru(O₂CAd)₂(*p*-cymene)] (5.96 mg, 10.0 mol %) and D₂O (20.0 μL, 1.00 mmol). Purification by column chromatography (*n*-hexane/EtOAc/AcOH: 8/2/0.1) yielded [D]₁-**190z** (33.2 mg, 79%) as a colourless solid. Incorporation expected at $\delta = 8.31$ ppm and determined against the integral at $\delta = 6.78$ ppm. Degree of Deuteration: 98%.

¹H-NMR (400 MHz, MeOH-*d*₄): $\delta = 8.31$ (d, $J = 2.4$ Hz, 0.02H), 7.69 (d, $J = 9.0$ Hz, 1H), 7.47 (d, $J = 1.7$ Hz, 0.25H), 7.34 (dd, $J = 5.7, 3.6$ Hz, 0.77H), 7.37 – 7.11 (m, 3H), 6.87 (d, $J = 9.0$ Hz, 1H), 6.34 (dd, $J = 25.0, 3.2$ Hz, 2H), 4.49 (s, 2H), 4.16 (s, 2H). **¹³C-NMR** (100 MHz, MeOH-*d*₄): $\delta = 170.8$ (C_q), 154.4 (CH), 152.9 (C_q), 143.6 (C_q), 136.0 (C_q), 134.3 (C_q), 133.5 (CH), 131.2 (CH), 130.3 (CH), 129.9 (CH), 128.0 (CH), 127.9 (C_q), 126.7 (C_q), 112.6 (CH), 111.3 (CH), 111.2 (t, $J = 27.5$ Hz, CD), 108.3 (CH), 45.3 (CH₂), 40.6 (CH₂). **MS** (ESI) m/z (relative intensity): 421 (100) [M–H][–], 377 (5). **HR-MS** (ESI): m/z calcd. for C₁₉H₁₄D₂³⁵ClN₂O₅S[–] [M–H][–] 421.0599, found 421.0596 and for C₁₉H₁₅D³⁵ClN₂O₅S[–] [M–H][–] 420.0537, found 420.0527.

2-Hydroxy-5-[(2-oxo-1,2-dihydrobenzo[*cd*]indole)-6-sulfonamido]benzoic-6-*d* acid ([D]₁-190aa)

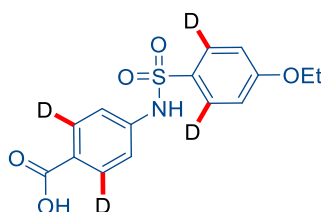
[D]₁-190aa

The general procedure **GP-G** was followed using 2-hydroxy-5-[(2-oxo-1,2-dihydrobenzo[*cd*]indole)-6-sulfonamido]benzoic acid (**190aa**) (38.3 mg, 0.10 mmol), [Ru(O₂CAd)₂(*p*-cymene)] (5.96 mg, 10.0 mol %) and D₂O (20.0 μL, 1.00 mmol). Purification by column chromatography (*n*-hexane/EtOAc/AcOH: 7/3/0.1) yielded [D]₁-

190aa (33.9 mg, 88%) as a brown solid. Incorporation expected at $\delta = 6.60$ ppm and determined against the integral at $\delta = 7.75$ ppm. Degree of Deuteration: 95%.

$^1\text{H-NMR}$ (500 MHz, MeOH- d_4): $\delta = 7.75$ (d, $J = 8.4$ Hz, 1H), 7.24 (d, $J = 7.0$ Hz, 1H), 7.15 (d, $J = 7.5$ Hz, 1H), 6.99 (dd, $J = 8.4, 7.0$ Hz, 1H), 6.60 (s, 0.05H), 6.14 (dd, $J = 15.4, 8.2$ Hz, 2H), 5.82 (d, $J = 8.7$ Hz, 1H). **$^{13}\text{C-NMR}$** (100 MHz, MeOH- d_4): $\delta = 171.4$ (C_q), 161.0 (C_q), 144.1 (C_q), 134.6 (CH), 131.3 (CH), 131.2 (CH), 131.1 (CH), 129.6 (C_q), 128.8 (C_q), 128.2 (C_q), 127.7 (C_q), 126.4 (C_q), 126.1 (CH) 126.1 (CH), 118.1 (C_q), 111.4 (C_q), 105.9 (CH). **MS** (ESI) m/z (relative intensity): 384 (100) $[\text{M-H}]^-$, 355 (9), 232 (28). **HR-MS** (ESI): m/z calcd. for $\text{C}_{18}\text{H}_{10}\text{DN}_2\text{O}_6\text{S}^-$ $[\text{M-H}]^-$ 384.0406, found 384.0416.

4-[(4-Ethoxyphenyl)sulfonamido-2,6- d_2]benzoic-2,6- d_2 acid ($[\text{D}]_3$ -**190ab**)



$[\text{D}]_3$ -**190ab**

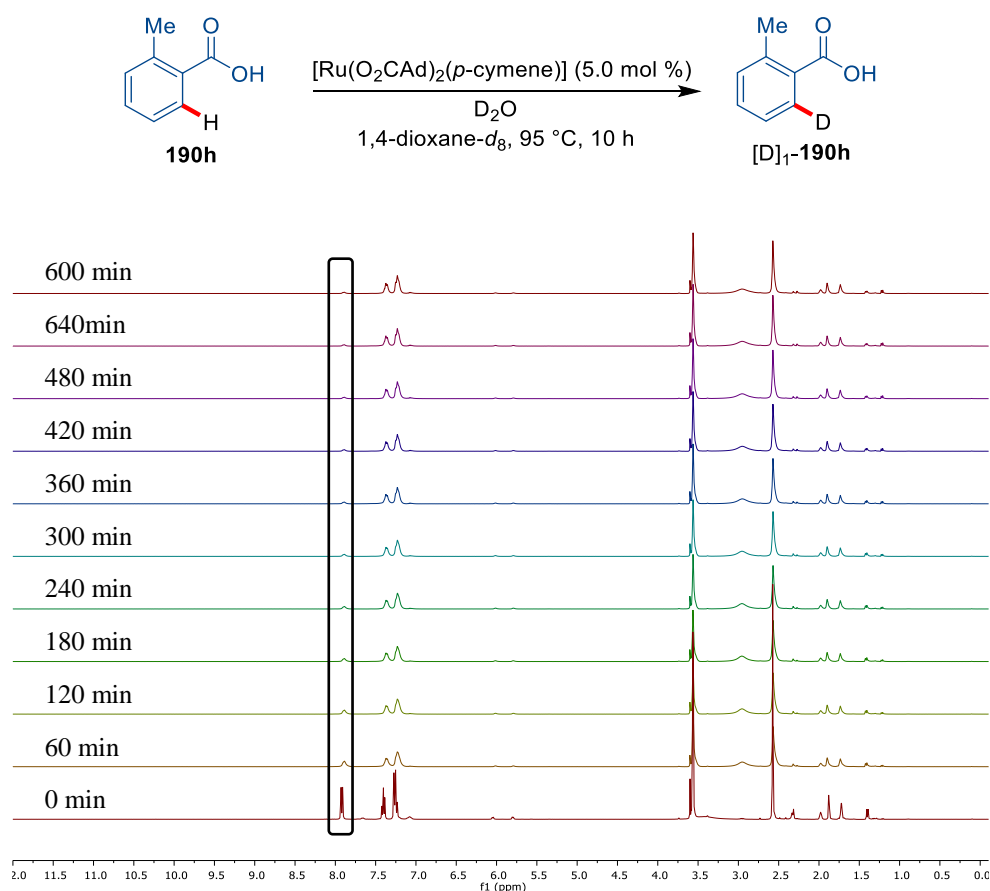
The general procedure **GP-G** was followed using 4-[(4-ethoxyphenyl)sulfonamide]benzoic acid (**190ab**) 32.1 mg, 0.10 mmol), $[\text{Ru}(\text{O}_2\text{CAd})_2(p\text{-cymene})]$ (5.96 mg, 10.0 mol %) and D_2O (20.0 μL , 1.00 mmol.). Purification by column chromatography (n -hexane/EtOAc/AcOH: 8/2/0.1) yielded $[\text{D}]_3$ -**190ab** (23.6 mg, 73%) as a yellow solid. Incorporation expected at $\delta = 7.87$ ppm and determined against the integral at $\delta = 4.06$ ppm. Degree of Deuteration: 93%.

$^1\text{H-NMR}$ (300 MHz, MeOH- d_4): $\delta = 7.87$ (s, 0.14H), 7.77 (dd, $J = 7.1, 6.7$ Hz, 1.5H), 7.21 (s, 2H), 7.10 – 6.73 (m, 2H), 4.06 (q, $J = 7.0$ Hz, 2H), 1.37 (t, $J = 7.0$ Hz, 3H). **$^{13}\text{C-NMR}$** (100 MHz, MeOH- d_4): $\delta = 164.1$ (C_q), 143.8 (C_q), 132.1 (CD), 132.1 (C_q), 130.4 (CH), 119.7 (C_q), 119.6 (CH), 115.7 (CH), 115.6 (C_q), 65.1 (CH_2), 14.9 (CH_3). **MS** (ESI) m/z (relative intensity): 322 (4) $[\text{M-H}]^-$, 283 (100), 255 (4). **HR-MS** (ESI): m/z calcd. for $\text{C}_{15}\text{H}_{11}\text{D}_3\text{NO}_5\text{S}^-$ $[\text{M-H}]^-$ 323.0786, found 323.0795 and for $\text{C}_{15}\text{H}_{12}\text{D}_2\text{NO}_5\text{S}^-$ $[\text{M-H}]^-$ 322.0724, found 322.0739.

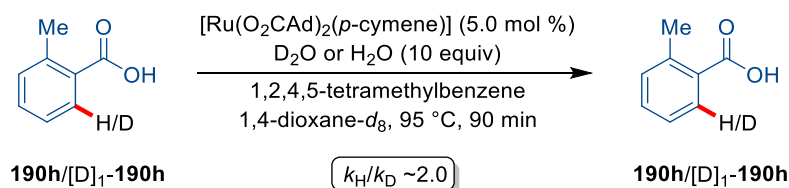
5.6.2. Mechanistic Studies

In-Operando NMR studies

Inside a nitrogen-filled glovebox, an oven-dried Young NMR tube was charged with 2-methylbenzoic acid (**190h**) (13.6 mg, 0.10 mmol, 1.00 equiv), $[\text{Ru}(\text{O}_2\text{CAd})_2(p\text{-cymene})]$ (2.97 mg, 5.00 μmol , 5.00 mol %) and D_2O (20.0 mg, 10.0 mmol, 10.0 equiv). 1,4-Dioxane- d_8 (0.50 mL) was added and the Young NMR tube was closed, removed from the glovebox, and placed in a Bruker Avance III HD 400 NMR spectrometer. After locking and shimming of the sample, periodic measurements (every 2 min, with 5 scans) at 95 °C for 10 h provided the following spectra.

Scheme 5.9. *In-operando* NMR studies of **190h**.

Kinetic Isotope Effect (KIE)

Scheme 5.10. KIE studies of **190h** and $[\text{D}]_1\text{-190h}$.

5. Experimental Part

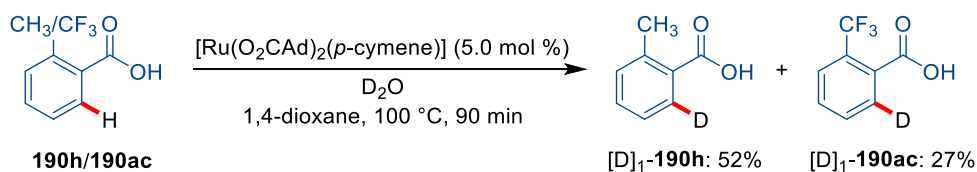
Two independent reactions were performed respectively to determine the KIE value by comparison of the initial reaction rates by *in-operando* NMR-analysis with 1,2,4,5-tetramethylbenzene as the internal standard.

Inside a nitrogen-filled glovebox, two oven-dried Young NMR tubes were charged with **190h** (13.6 mg, 0.10 mmol, 1.00 equiv) or [D]₁-**190h** (13.7 mg, 0.10 mmol, 1.00 equiv), [Ru(O₂CAd)₂(*p*-cymene)] (2.97 mg, 5.0 μmol, 5.0 mol %), H₂O (18.0 mg, 1.00 mmol, 10.0 equiv) or D₂O (20.0 mg, 1.00 mmol, 10.0 equiv), respectively, and 1,2,4,5-tetramethylbenzene (13.4 mg, 0.10 mmol). 1,4-Dioxane-*d*₈ (0.50 mL) was added and the Young NMR tubes were closed, taken out of the glovebox, and placed in a Bruker Avance III HD 400 spectrometer. After locking and shimming of the samples, periodic measurements (every 2 min, with 5 scans) at 95 °C for 23 min provided the following data.

Table 5.7. Conversion *versus* time for the formation of [D]₁-**190h** and **190h**.

<i>t</i> / s	[D] ₁ - 190 / %	190 / %
60	4.10	3.00
180	7.20	4.10
300	9.10	5.00
420	10.1	5.60
540	11.5	6.30
660	12.9	7.00
780	16.2	7.70
900	15.9	8.30
1020	17.4	9.00
1140	17.9	9.70
1260	19.1	10.2
1380	21.8	11.4

Intermolecular Competition Experiment



Scheme 5.11. Intermolecular competition experiment between **190h** and **190ac**.

2-Methylbenzoic acid (**190h**) (13.6 mg, 0.10 mmol, 1.00 equiv), 2-(trifluoromethyl)benzoic acid (**190ac**) (19.0 mg, 0.10 mmol, 1.00 equiv), $[\text{Ru}(\text{O}_2\text{CAd})_2(\textit{p}\text{-cymene})]$ (2.97 mg, 5.00 μmol , 5.00 mol %), and D_2O (20.0 mg, 10.0 mmol, 10.0 equiv) were placed into an oven-dried 25 mL Schlenk tube equipped with a septum under Ar atmosphere. 1,4-Dioxane (0.50 mL) was added and the mixture was stirred at 100 $^\circ\text{C}$ for 1.5 h. After completion of the reaction, the mixture was filtered through a pad of Celite, rinsed with 1,4-dioxane (4 x 10 mL; 5% AcOH) and concentrated in vacuum. The crude mixture was analyzed by means of $^1\text{H-NMR}$ spectroscopy with 1,2,4,5-tetramethylbenzene (13.4 mg, 0.10 mmol) as the internal standard to furnish the following degrees of deuteration: $[\text{D}]_1\text{-190h}$ (52%) and $[\text{D}]_1\text{-190ac}$ (27%).

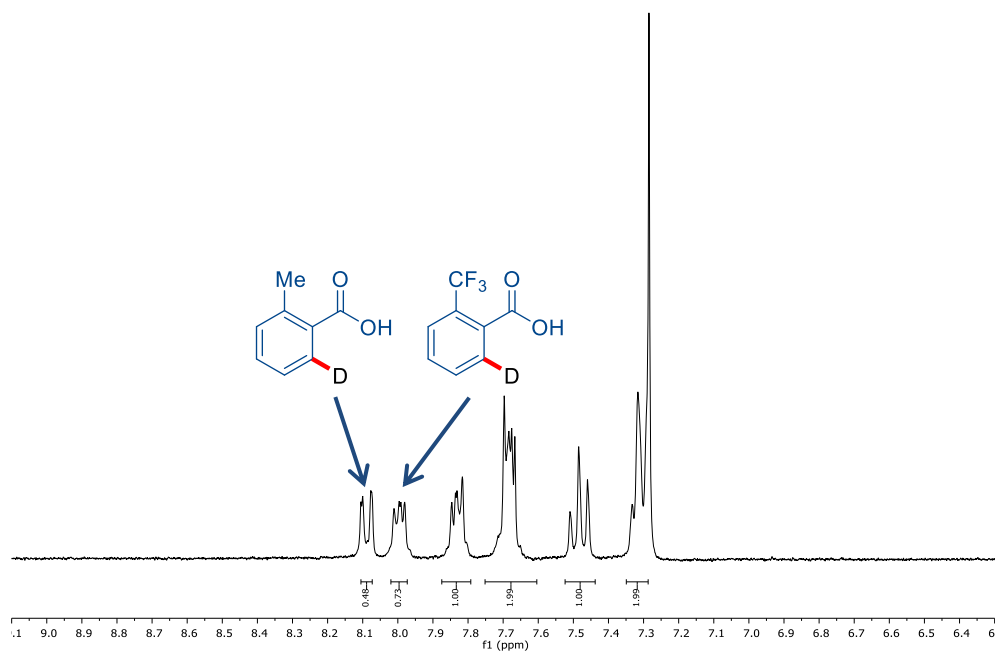


Figure 5.3. Intermolecular competition experiment between **190h** and **190ac**.

5.7. Recyclable Ruthenium Catalyst for remote C–H Activation

5.7.1. Synthesis of Hybrid Ruthenium catalysts 221a and 221b

Hybrid Ruthenium 221a

[RuCl₂(C₆H₆)₂] (0.25 g, 0.50 mmol, 1.00 equiv) and polymer-bound triphenylphosphine (0.50 g, 0.85 mmol, 1.70 equiv, 1.4–2.0 mmol/g, Fluorochem) were placed in a 100 mL flask equipped with a reflux condenser. CH₂Cl₂ (15 mL) and PhMe (15 mL) were added and the mixture was refluxed at 110 °C for 4 h. After completion of the reaction, the suspension was filtered through a branched filter (Por. 3), rinsed with DCE (30 mL) and dried *in vacuo* for 24 h. **221a** was isolated (630 mg, 52%) as an air stable deep red solid. ICP-OES analysis by Dr. Volker Karius yielded a ruthenium concentration of 9.72 wt.%.

$$\frac{n_{\text{Cat}} \cdot M_{\text{Ru}}}{\text{ICP-OES result}} = m_{\text{Cat}}$$

$$\text{for GP-H} = \frac{2.50 \cdot 10^{-5} \text{ mol} \cdot 101.07 \frac{\text{g}}{\text{mol}}}{0.0972} = 2.60 \cdot 10^{-2} \text{ g} = 26.0 \text{ mg}$$

Hybrid Ruthenium 221b ^[313b]

[RuCl₂(*p*-cymene)₂] (0.30 g, 0.50 mmol) and polymer-bound triphenylphosphine (0.50 g, 0.85 mmol, 1.70 equiv, 1.4–2.0 mmol/g, Fluorochem) were placed in a 100 mL flask equipped with a reflux condenser. CH₂Cl₂ (15 mL) and PhMe (15 mL) were added and the mixture was refluxed at 110 °C for 4 h. After completion of the reaction, the suspension was filtered through a branched filter (Por. 3), rinsed with DCE (30 mL) and dried *in vacuo* for 24 h. **221b** was isolated (646mg, 58%) as an air stable deep red solid ICP-OES analysis by Dr. Volker Karius yielded a Ru concentration of 8.40 wt.%.

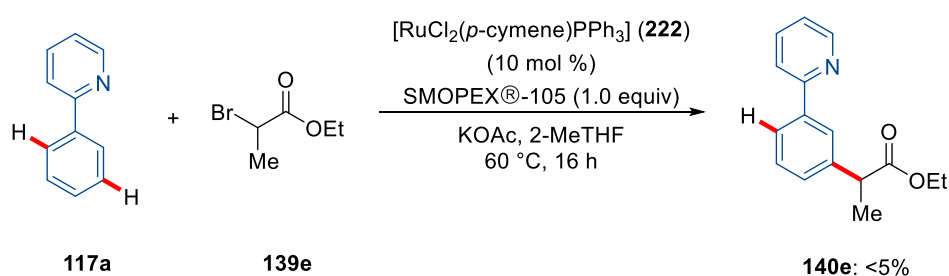
$$\frac{n_{\text{Cat}} \cdot M_{\text{Ru}}}{\text{ICP-OES result}} = m_{\text{Cat}}$$

$$\text{for GP-H} = \frac{2.50 \cdot 10^{-5} \text{ mol} \cdot 101.07 \frac{\text{g}}{\text{mol}}}{0.0840} = 3.00 \cdot 10^{-2} \text{ g} = 30.0 \text{ mg}$$

5.7.2. Test of Heterogeneity for *meta* C–H Alkylations by Recyclable Ruthenium Catalyst

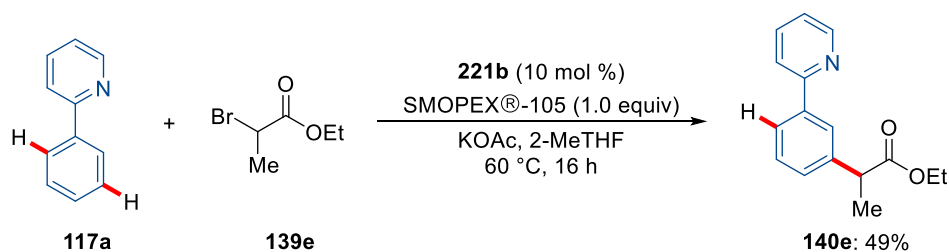
5.7.2.1. Poison test

A suspension of 2-phenylpyridine **117a** (38.8 mg, 0.25 mmol), ethyl 2-bromopropanoate **139e** (136 mg, 0.75 mmol), RuCl₂PPh₃(*p*-cymene) (**222**) (14.2 mg, 10 mol %), SMOPEX®-105 (3.7 mmol/g, 70.0 mg) and KOAc (49.1 mg, 0.50 mmol) in 2-MeTHF (2.0 mL) was stirred at 60 °C for 16 h under N₂. After cooling to ambient temperature, the mixture was concentrated *in vacuo*. Purification by column chromatography on silica gel afforded **140e** (3.17 mg, 4.9%) as a colourless oil.



Scheme 5.12. Poison test with **222** and SMOPEX®-105.

A suspension of 2-phenylpyridine **117a** (38.8 mg, 0.25 mmol), ethyl 2-bromopropanoate **139e** (136 mg, 0.75 mmol), **221b** (30.0 mg, 10 mol %), SMOPEX®-105 (3.7 mmol/g, 70.0 mg) and KOAc (49.1 mg, 0.50 mmol) in 2-MeTHF (2.0 mL) was stirred at 60 °C for 16 h under N₂. After cooling to ambient temperature, the mixture was concentrated *in vacuo*. Purification by column chromatography on silica gel afforded **140e** (31.2 mg, 49%) as a colourless oil.

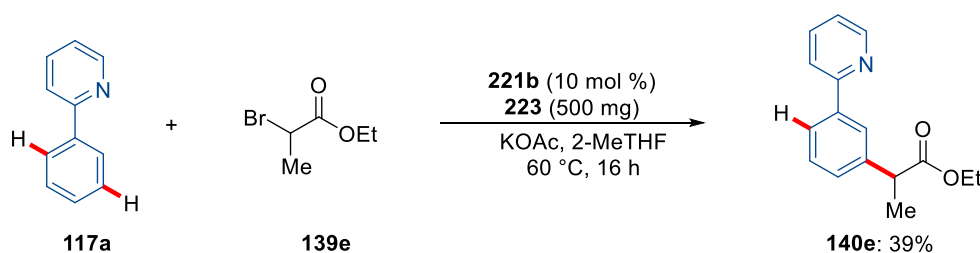


Scheme 5.13. Poison test with **221b** and SMOPEX®-105.

5.7.2.2. Three-phase test

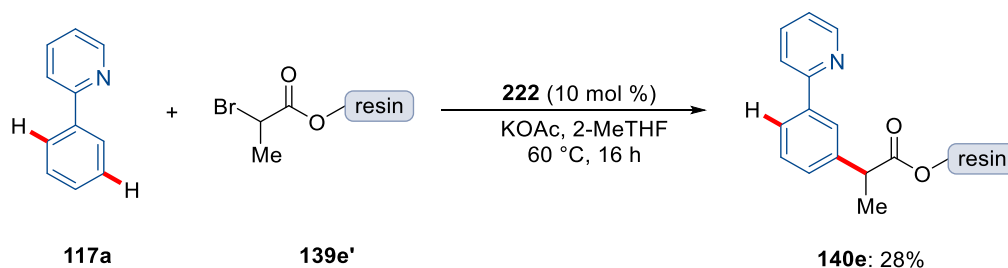
Test 1

A suspension of 2-phenylpyridine **117a** (38.8 mg, 0.25 mmol), ethyl 2-bromopropanoate **139e** (136 mg, 0.75 mmol), **221b** (30.0 mg, 10 mol %), modified Wang resin **223** (500 mg, 0.20 mmol), and KOAc (49.1 mg, 0.50 mmol) in 2-MeTHF (4.0 mL) was stirred at 60 °C for 16 h under N₂. After cooling to ambient temperature, the mixture was concentrated *in vacuo*. Purification by column chromatography on silica gel afforded **140e** (24.9 mg, 39%) as a colourless oil.

Scheme 5.14. Influence of Wang-resin **223**.

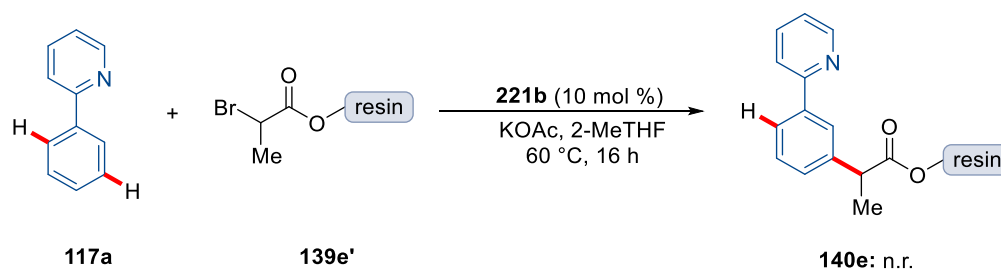
Test 2

A suspension of 2-phenylpyridine **117a** (38.8 mg, 0.25 mmol), modified Wang resin (**139e'**) (500 mg, 0.20 mmol), RuCl₂PPh₃(*p*-cymene) (**222**) (30.0 mg, 10 mol %) and KOAc (49.1 mg, 0.50 mmol) in 2-MeTHF (4.0 mL) was stirred at 60 °C for 16 h under N₂. After cooling to ambient temperature, the reaction mixture was filtered through a branched filter (Por. 3) and washed with 2-MeTHF (30 mL). The filtered resin was cleaved^[314] and ¹H NMR was used for determination of the yield of **140e** (17.8 mg, 28%) with 1,3,5-trimethoxybenzene as an internal standard.

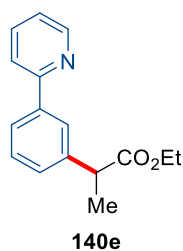
Scheme 5.15. Homogeneous manifold with modified Wang-resin **139e'**.

Test 3

A suspension of 2-phenylpyridine **117a** (38.8 mg, 0.25 mmol), modified Wang resin (139e') (500 mg, 0.20 mmol), **221b** (30.0 mg, 10 mol %) and KOAc (49.1 mg, 0.50 mmol) in 2-MeTHF (4.0 mL) was stirred at 60 °C for 16 h under N₂. After cooling to ambient temperature, the reaction mixture was filtered through a branched filter (Por. 3) and washed with 2-MeTHF (30 mL). The filtered resin was cleaved^[314] and ¹H NMR was used for determination of the yield of **140e** with 1,3,5-trimethoxybenzene as an internal standard.



Scheme 5.16. Heterogeneous manifold with modified Wang-resin **139e'**.

5.7.3. Characterization Data**Ethyl 2-[3-(pyridin-2-yl)phenyl]propanoate (140e)**

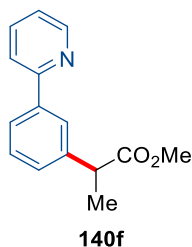
The general procedure **GP-H** was followed using 2-phenylpyridine (**117a**) (38.8 mg, 0.25 mmol), ethyl 2-bromopropanoate (**139e**) (136 mg, 0.75 mmol), **221a** (26.0 mg, 10.0 mol %) and KOAc (49.1 mg, 0.50 mmol). Purification by column chromatography (*n*-hexane/EtOAc: 10/1) yielded **140e** (42.2 mg, 66%) as a colourless oil.

The general procedure **GP-H** was followed using 2-phenylpyridine (**117a**) (38.8 mg, 0.25 mmol), ethyl 2-bromopropanoate (**139e**) (136 mg, 0.75 mmol), **221b** (30.0 mg, 10.0 mol %) and KOAc (49.1 mg, 0.50 mmol). Purification by column chromatography (*n*-hexane/EtOAc: 10/1) yielded **140e** (44.7 mg, 69%) as a colourless oil.

The general procedure **GP-J** was followed using 2-phenylpyridine (**117a**) (38.8 mg, 0.25 mmol), ethyl 2-bromopropanoate (**139e**) (136 mg, 0.75 mmol), **221b** (30.0 mg, 10.0 mol %), KOAc (49.1 mg, 0.50 mmol) and H₂O (22.5 μ L, 1.25 mmol). Purification by column chromatography (*n*-hexane/EtOAc: 10/1) yielded **140e** (36.4 mg, 57%) as a colourless oil. **¹H-NMR** (400 MHz, CDCl₃): δ = 8.62 (dd, *J* = 4.8, 1.4 Hz, 1H), 7.92 (dd, *J* = 1.8, 0.6 Hz, 1H), 7.82 (dd, *J* = 7.5, 1.8 Hz, 1H), 7.65 (d, *J* = 1.4 Hz, 1H), 7.64 (dd, *J* = 2.3, 1.4 Hz, 1H), 7.37 (dd, *J* = 7.5, 0.6 Hz, 1H), 7.32 (dd, *J* = 7.5, 1.8 Hz, 1H), 7.15 – 7.11 (m, 1H), 4.14 – 3.99 (m, 2H), 3.76 (q, *J* = 7.1 Hz, 1H), 1.50 (d, *J* = 7.1 Hz, 3H), 1.14 (t, *J* = 7.1 Hz, 3H). **¹³C-NMR** (100 MHz, CDCl₃): δ = 174.6 (C_q), 157.4 (C_q), 149.8 (CH), 141.4 (C_q), 139.9 (C_q), 136.9 (CH), 129.2 (CH), 128.1 (CH), 126.5 (CH), 125.8 (CH), 122.3 (CH), 120.8 (CH), 60.92 (CH₂), 45.80 (CH), 18.88 (CH₃), 14.28 (CH₃). **IR** (ATR): 2980, 1730, 1585, 1462, 1248, 1195, 1165, 1066, 770, 699 cm⁻¹. **MS** (ESI) *m/z* (relative intensity): 278 (22) [M+Na]⁺, 256 (100) [M+H]⁺, 156 (17). **HR-MS** (ESI): *m/z* calcd. for C₁₆H₁₈NO₂⁺ [M+H]⁺ 256.1332, found: 256.1332.

The analytical data are in accordance with those previously reported in the literature.^[371]

Ethyl 2-[3-(pyridin-2-yl)phenyl]propanoate (**140f**)

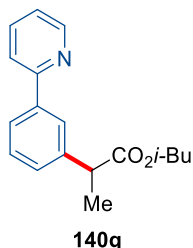


The general procedure **GP-H** was followed using 2-phenylpyridine (**117a**) (38.8 mg, 0.25 mmol), methyl 2-bromopropanoate (**139f**) (125 mg, 0.75 mmol), **221b** (30.0 mg, 10.0 mol %) and KOAc (49.1 mg, 0.50 mmol). Purification by column chromatography (*n*-hexane/EtOAc: 10/1) yielded **140f** (42.8 mg, 71%) as a colourless oil.

¹H-NMR (400 MHz, CDCl₃): δ = 8.69 (dd, *J* = 5.2, 1.4 Hz, 1H), 8.02 – 7.91 (m, 1H), 7.86 (dd, *J* = 7.7, 1.5 Hz, 1H), 7.80 – 7.68 (m, 2H), 7.43 (t, *J* = 7.7 Hz, 1H), 7.36 (dd, *J* = 7.7, 1.5 Hz, 1H), 7.23 (ddd, *J* = 6.6, 4.8, 2.0 Hz, 1H), 3.83 (q, *J* = 7.1 Hz, 1H), 3.66 (s, 3H), 1.56 (d, *J* = 7.2 Hz, 3H). **¹³C-NMR** (100 MHz, CDCl₃): δ = 175.1 (C_q), 157.4 (C_q), 149.8 (CH), 141.2 (C_q), 139.9 (C_q), 136.9 (CH), 129.2 (CH), 128.1 (CH), 126.5 (CH), 125.9 (CH), 122.3 (CH), 120.8 (CH), 52.19 (CH₃), 45.64 (CH), 18.80 (CH₃). **IR** (ATR):

2980, 2951, 1733, 1585, 1566, 1462, 1435, 1202, 1165, 770 cm^{-1} . **MS** (EI) m/z (relative intensity): 241 (28) $[\text{M}]^+$, 182 (100), 167 (55). **HR-MS** (EI): m/z calcd. for $\text{C}_{15}\text{H}_{15}\text{NO}_2^+$ $[\text{M}]^+$ 241.1103, found: 241.1102.

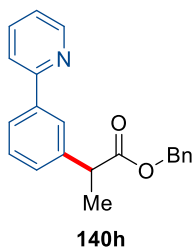
Isobutyl 2-[3-(pyridin-2-yl)phenyl]propanoate (**140g**)



The general procedure **GP-H** was followed using 2-phenylpyridine (**117a**) (38.8 mg, 0.25 mmol), isobutyl 2-bromopropanoate (**139g**) (157 mg, 0.75 mmol), **221b** (30.0 mg, 10.0 mol %) and KOAc (49.1 mg, 0.50 mmol). Purification by column chromatography (*n*-hexane/EtOAc: 10/1) yielded **140g** (45.3 mg, 64%) as a colourless oil.

$^1\text{H-NMR}$ (400 MHz, CDCl_3): δ = 8.69 (dd, J = 4.9, 1.4 Hz, 1H), 7.94 (dd, J = 1.6, 1.4 Hz, 1H), 7.87 (dd, J = 7.6, 1.4 Hz, 1H), 7.81 – 7.67 (m, 2H), 7.43 (dd, J = 7.6, 7.5 Hz, 1H), 7.39 (dd, J = 7.5, 1.6 Hz, 1H), 7.23 (ddd, J = 6.6, 4.9, 2.0 Hz, 1H), 3.88 – 3.83 (m, 3H), 1.88 (q, J = 6.7 Hz, 1H), 1.57 (d, J = 7.1 Hz, 3H), 0.84 (d, J = 6.7 Hz, 6H). **$^{13}\text{C-NMR}$** (100 MHz, CDCl_3): δ = 174.6 (C_q), 157.4 (C_q), 149.8 (CH), 141.4 (C_q), 139.8 (C_q), 136.9 (CH), 129.1 (CH), 128.2 (CH), 126.5 (CH), 125.8 (CH), 122.3 (CH), 120.8 (CH), 70.98 (CH_2), 45.88 (CH), 27.89 (CH), 19.12 (CH_3), 18.71 (CH_3). **IR** (ATR): 2963, 1731, 1585, 1566, 1462, 1436, 1241, 1195, 1164, 769 cm^{-1} . **MS** (EI) m/z (relative intensity): 283 (22) $[\text{M}]^+$, 225 (13), 182 (100), 167 (53). **HR-MS** (EI): m/z calcd. for $\text{C}_{18}\text{H}_{21}\text{NO}_2^+$ $[\text{M}]^+$ 283.1572, found: 283.1574.

Benzyl 2-(3-(pyridin-2-yl)phenyl)propanoate (**140h**)

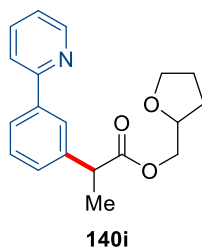


The general procedure **GP-H** was followed using 2-phenylpyridine (**117a**) (38.8 mg, 0.25 mmol), benzyl 2-bromopropanoate (**139h**) (182 mg, 0.75 mmol), **221b** (30.0 mg, 10.0

mol %) and KOAc (49.1 mg, 0.50 mmol). Purification by column chromatography (*n*-hexane/EtOAc: 10/1) yielded **140h** (58.7 mg, 74%) as a colourless oil.

¹H-NMR (400 MHz, CDCl₃): δ = 8.82 – 8.63 (m, 1H), 7.96 (d, *J* = 2.0 Hz, 1H), 7.91 (dd, *J* = 7.7, 1.6 Hz, 1H), 7.76 (dd, *J* = 7.6, 1.8 Hz, 1H), 7.70 (d, *J* = 7.9 Hz, 1H), 7.46 (dd, *J* = 7.7, 7.7 Hz, 1H), 7.43 – 7.37 (m, 1H), 7.37 – 7.22 (m, 6H), 5.53 – 4.70 (m, 2H), 3.91 (q, *J* = 7.1 Hz, 1H), 1.61 (d, *J* = 7.2 Hz, 3H). **¹³C-NMR** (100 MHz, CDCl₃): δ = 174.4 (C_q), 157.3 (C_q), 149.7 (CH), 141.1 (C_q), 139.8 (C_q), 136.9 (CH), 136.1 (C_q), 129.2 (CH), 128.6 (CH), 128.2 (CH), 128.2 (CH), 128.1 (CH), 126.5 (CH), 125.9 (CH), 122.3 (CH), 120.8 (CH), 66.60 (CH₂), 45.76 (CH), 18.73 (CH₃). **IR** (ATR): 2932, 1731, 1584, 1566, 1461, 1378, 1158, 769, 742, 697 cm⁻¹. **MS** (ESI) *m/z* (relative intensity): 340 (6) [M+Na]⁺, 318 (100) [M+H]⁺. **HR-MS** (ESI): *m/z* calcd. for C₂₁H₂₀NO₂⁺ [M+H]⁺ 318.1489, found: 318.1490.

(Tetrahydrofuran-2-yl)methyl 2-[3-(pyridin-2-yl)phenyl]propanoate (**140i**)

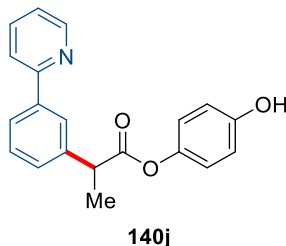


The general procedure **GP-H** was followed using 2-phenylpyridine (**117a**) (38.8 mg, 0.25 mmol), (tetrahydrofuran-2-yl)methyl 2-bromopropanoate (**139i**) (178 mg, 0.75 mmol), **221b** (30.0 mg, 10.0 mol %) and KOAc (49.1 mg, 0.50 mmol). Purification by column chromatography (*n*-hexane/EtOAc: 10/1) yielded **140i** (48.2 mg, 62%) as a colourless oil.

¹H-NMR (400 MHz, CDCl₃): δ = 8.71 (dd, *J* = 5.0, 1.4 Hz, 1H), 7.97 (d, *J* = 1.7 Hz, 1H), 7.90 (d, *J* = 7.3 Hz, 1H), 7.77 (d, *J* = 1.8 Hz, 1H), 7.75 (d, *J* = 1.2 Hz, 1H), 7.45 (dd, *J* = 7.8, 7.6 Hz, 1H), 7.40 (dd, *J* = 7.6, 1.4 Hz, 1H), 7.25 (ddd, *J* = 7.3, 5.0, 2.5 Hz, 1H), 4.23 – 4.02 (m, 3H), 3.89 (q, *J* = 7.1, 1.4 Hz, 1H), 3.82 – 3.70 (m, 2H), 1.96 – 1.76 (m, 3H), 1.59 (dd, *J* = 7.2, 1.4 Hz, 3H), 1.56 – 1.47 (m, 1H). **¹³C-NMR** (100 MHz, CDCl₃): δ = 174.6 (C_q), 157.4 (d, *J* = 1.8 Hz, C_q), 149.8 (CH), 141.2 (C_q), 139.9 (C_q), 136.8 (CH), 129.1 (CH), 128.2 (CH), 126.5 (d, *J* = 1.5 Hz, CH), 125.9 (CH), 122.3 (CH), 120.8 (d, *J* = 2.2 Hz, CH), 76.59 (d, *J* = 7.9 Hz, CH), 68.60 (d, *J* = 8.0 Hz, CH₂), 66.80 (d, *J* = 19.0 Hz, CH₂), 45.69 (d, *J* = 4.7 Hz, CH), 28.04 (d, *J* = 14.1 Hz, CH₂), 25.76 (d, *J* = 8.0 Hz, CH₂), 18.75 (d, *J* = 6.3 Hz, CH₃). **IR** (ATR): 2977, 2873, 1732, 1584, 1461, 1436, 1194, 1165, 1080, 770 cm⁻¹. **MS** (EI) *m/z* (relative intensity): 311 (7) [M]⁺, 268 (25), 241 (31), 183

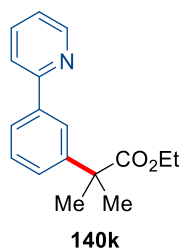
(100), 167 (68). **HR-MS** (ED): m/z calcd. for $C_{19}H_{21}N_2O_3^+$ $[M]^+$ 311.1521, found: 311.1523.

4-Hydroxyphenyl 2-(3-(pyridin-2-yl)phenyl)propanoate (**140j**)



The general procedure **GP-H** was followed using 2-phenylpyridine (**117a**) (38.8 mg, 0.25 mmol), 4-hydroxyphenyl-2-bromopropanoate (**139j**) (184 mg, 0.75 mmol), **221b** (30.0 mg, 10.0 mol %) and KOAc (49.1 mg, 0.50 mmol). Purification by column chromatography (*n*-hexane/EtOAc: 10/1) yielded **140j** (54.3 mg, 68%) as a colourless oil. **¹H-NMR** (400 MHz, CDCl₃): δ = 8.71 (ddd, J = 4.9, 1.8, 1.0 Hz, 1H), 8.02 (d, J = 1.8 Hz, 1H), 7.88 (dd, J = 7.1, 1.9 Hz, 1H), 7.82 (dd, J = 7.7, 1.8 Hz, 1H), 7.77 (dd, J = 7.9, 1.2 Hz, 1H), 7.54 – 7.44 (m, 2H), 7.34 – 7.29 (m, 1H), 6.80 – 6.70 (m, 2H), 6.70 – 6.63 (m, 2H), 4.02 (q, J = 7.1 Hz, 1H), 1.65 (d, J = 7.2 Hz, 3H). **¹³C-NMR** (100 MHz, CDCl₃): δ = 173.7 (C_q), 157.4 (C_q), 154.1 (C_q), 149.5 (CH), 143.9 (C_q), 141.0 (C_q), 139.7 (C_q), 137.5 (CH), 129.4 (CH), 128.3 (CH), 126.8 (CH), 126.3 (CH), 122.6 (CH), 122.2 (CH), 121.4 (CH), 45.80 (CH), 18.65 (CH₃). **IR** (ATR): 2929, 1750, 1594, 1566, 1509, 1463, 1190, 1160, 1146, 773 cm⁻¹. **MS** (ESI) m/z (relative intensity): 342 (11) $[M+Na]^+$, 320 (100) $[M+H]^+$. **HR-MS** (ESI): m/z calcd. for $C_{20}H_{17}NO_3^+$ $[M+H]^+$ 320.1281, found: 320.1283.

Ethyl 2-methyl-2-[3-(pyridin-2-yl)phenyl]propanoate (**140k**)



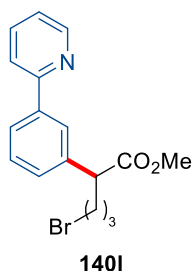
The general procedure **GP-H** was followed using 2-phenylpyridine (**117a**) (38.8 mg, 0.25 mmol), ethyl 2-bromo-2-methylpropanoate (**139k**) (146 mg, 0.75 mmol), **221b** (30.0 mg, 10.0 mol %) and KOAc (49.1 mg, 0.50 mmol). Purification by column

chromatography (*n*-hexane/EtOAc: 10/1) yielded **140k** (42.9 mg, 64%) as a colourless oil.

¹H-NMR (400 MHz, CDCl₃): δ = 8.70 (dd, *J* = 4.8, 1.5 Hz, 1H), 7.99 (dd, *J* = 1.9, 1.5 Hz, 1H), 7.84 (dd, *J* = 7.4, 1.6 Hz, 1H), 7.78 – 7.67 (m, 2H), 7.43 (dd, *J* = 7.5, 7.4 Hz, 2H), 7.23 (ddd, *J* = 7.5, 4.8, 1.5 Hz, 1H), 4.14 (q, *J* = 7.1 Hz, 2H), 1.65 (s, 6H), 1.19 (t, *J* = 7.1 Hz, 3H). **¹³C-NMR** (100 MHz, CDCl₃): δ = 176.9 (C_q), 157.7 (C_q), 149.8 (CH), 145.5 (C_q), 139.7 (C_q), 136.8 (CH), 128.9 (CH), 126.6 (CH), 125.4 (CH), 124.4 (CH), 122.2 (CH), 120.9 (CH), 60.99 (CH₂), 46.77 (C_q), 26.74 (CH₃), 14.22 (CH₃). **IR** (ATR): 2979, 1726, 1585, 1566, 1463, 1253, 1146, 1025, 771, 700 cm⁻¹. **MS** (EI) *m/z* (relative intensity): 269 (20) [M]⁺, 196 (100), 180 (21), 167 (18). **HR-MS** (EI): *m/z* calcd. for C₁₇H₁₉NO₂⁺ [M]⁺ 269.1416, found: 269.1415.

The analytical data are in accordance with those previously reported in the literature.^[171]

Methyl 6-bromo-2-[3-(pyridin-2-yl)phenyl]hexanoate (**140l**)

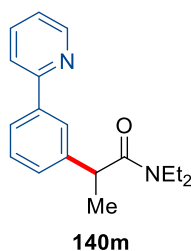


The general procedure **GP-H** was followed using 2-phenylpyridine (**117a**) (38.8 mg, 0.25 mmol), methyl 2,6-dibromohexanoate (**139l**) (216 mg, 0.75 mmol), **221b** (30.0 mg, 10.0 mol %) and KOAc (49.1 mg, 0.50 mmol). Purification by column chromatography (*n*-hexane/EtOAc: 10/1) yielded **140l** (50.3 mg, 58%) as a brown oil.

¹H-NMR (400 MHz, CDCl₃): δ = 8.69 (dd, *J* = 5.0, 1.2 Hz, 1H), 7.93 (dd, *J* = 1.8, 1.7 Hz, 1H), 7.88 (dd, *J* = 7.7, 1.7 Hz, 1H), 7.80 – 7.68 (m, 2H), 7.44 (dd, *J* = 7.8, 7.7 Hz, 1H), 7.37 (dd, *J* = 7.8, 1.2 Hz, 1H), 7.24 (ddd, *J* = 6.6, 5.0, 1.8 Hz, 1H), 3.67 (s, 3H), 3.67 (t, *J* = 7.6 Hz, 1H), 3.39 (t, *J* = 6.6 Hz, 2H), 2.3 – 2.20 (m, 1H), 2.10 – 2.00 (m, 1H), 1.90 – 1.80 (m, 2H). **¹³C-NMR** (100 MHz, CDCl₃): δ = 174.1 (C_q), 157.2 (C_q), 149.8 (CH), 140.1 (C_q), 139.2 (C_q), 136.9 (CH), 129.3 (CH), 128.4 (CH), 126.8 (CH), 126.2 (CH), 122.4 (CH), 120.8 (CH), 52.27 (CH₃), 50.99 (CH), 33.17 (CH₂), 32.13 (CH₂), 30.80 (CH₂). **IR** (ATR): 2951, 1732, 1584, 1566, 1461, 1435, 1261, 1203, 1164, 771 cm⁻¹. **MS** (EI) *m/z* (relative intensity): 347 (14) [M]⁺, 288 (18), 268 (100), 208 (61), 168 (61). **HR-MS** (EI): *m/z* calcd. for C₁₇H₁₈⁷⁹BrNO₂⁺ [M]⁺ 347.0521, found: 347.0520.

The analytical data are in accordance with those previously reported in the literature.^[166b]

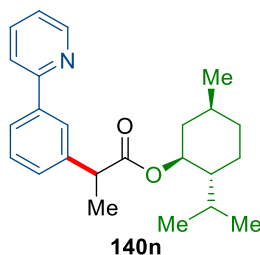
***N,N*-Diethyl-2-[3-(pyridin-2-yl)phenyl]propanamide (140m)**



The general procedure **GP-H** was followed using 2-phenylpyridine (**117a**) (38.8 mg, 0.25 mmol), 2-bromo-*N,N*-diethylpropanamide (**139m**) (156 mg, 0.75 mmol), **221b** (30.0 mg, 10.0 mol %) and KOAc (49.1 mg, 0.50 mmol). Purification by column chromatography (*n*-hexane/EtOAc: 10/1) yielded **140m** (49.4 mg, 70%) as a yellow oil.

¹H-NMR (400 MHz, CDCl₃): δ = 8.69 (d, J = 5.0 Hz, 1H), 7.91 (s, 1H), 7.85 (dd, J = 7.6, 1.2 Hz, 1H), 7.76 – 7.70 (m, 2H), 7.42 (dd, J = 7.6, 7.5 Hz, 1H), 7.35 (dd, J = 7.6, 1.2 Hz, 1H), 7.236 – 7.22 (m, 1H), 3.94 (q, J = 7.0 Hz, 1H), 3.53 (dq, J = 7.6, 7.1 Hz, 1H), 3.36 (dq, J = 7.6, 7.1 Hz, 1H), 3.23 (dq, J = 7.6, 7.1 Hz, 1H), 3.10 (dq, J = 7.6, 7.1 Hz, 1H), 1.49 (d, J = 7.0 Hz, 3H), 1.10 (t, J = 7.1 Hz, 3H), 1.01 (t, J = 7.1 Hz, 3H). **¹³C-NMR** (100 MHz, CDCl₃): δ = 172.8 (C_q), 157.3 (C_q), 149.7 (C_q), 143.2 (CH), 139.8 (C_q), 137.0 (CH), 129.4 (CH), 128.0 (CH), 126.2 (CH), 125.5 (CH), 122.4 (CH), 120.9 (CH), 43.29 (CH₂), 41.85 (CH₂), 40.45 (CH), 21.18 (CH₃), 14.45 (CH₃), 12.99 (CH₃). **IR** (ATR): 2973, 2932, 1636, 1584, 1566, 1461, 1433, 1264, 774, 702 cm⁻¹. **MS** (EI) m/z (relative intensity): 282 (18) [M]⁺, 225 (14), 182 (26), 167 (30), 100 (100). **HR-MS** (EI): m/z calcd. for C₁₈H₂₂N₂O⁺ [M]⁺ 282.1732, found: 282.1730.

(1*R*,2*S*,5*R*)-2-Isopropyl-5-methylcyclohexyl 2-[3-(pyridin-2-yl)phenyl]propanoate (140n)

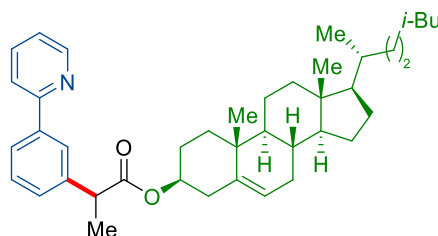


The general procedure **GP-H** was followed using 2-phenylpyridine (**117a**) (38.8 mg, 0.25 mmol), (1*R*,2*S*,5*R*)-2-isopropyl-5-methylcyclohexyl 2-bromopropanoate (**139n**) (218 mg, 0.75 mmol), **221b** (30.0 mg, 10.0 mol %) and KOAc (49.1 mg, 0.50 mmol).

Purification by column chromatography (*n*-hexane/EtOAc: 10/1) yielded **140n** (58.3 mg, 64%) as a colourless oil.

¹H-NMR (400 MHz, CDCl₃): δ = 8.69 (dd, *J* = 4.9, 1.4 Hz, 1H), 7.92 (dd, *J* = 3.9, 1.9 Hz, 1H), 7.87 (dd, *J* = 7.7, 1.5 Hz, 1H), 7.79 – 7.65 (m, 2H), 7.49 – 7.32 (m, 2H), 7.22 (ddd, *J* = 6.5, 4.8, 2.1 Hz, 1H), 4.69 – 4.60 (m, 1H), 3.82 – 3.76 (m, 1H), 2.06 – 1.76 (m, 2H), 1.71 – 1.58 (m, 2H), 1.56 (d, *J* = 2.7 Hz, 1H), 1.54 (d, *J* = 2.7 Hz, 1H), 1.51 – 1.39 (m, 1H), 1.38 – 1.23 (m, 2H), 1.02 – 0.93 (m, 2H), 0.95 – 0.72 (m, 7H), 0.71 (d, *J* = 6.9 Hz, 1H), 0.64 (d, *J* = 7.0 Hz, 1H), 0.49 (d, *J* = 6.9 Hz, 1H). **¹³C-NMR** (100 MHz, CDCl₃): δ = 174.2 (C_q), 157.5 (C_q), 149.8 (CH), 141.5 (C_q), 139.8 (C_q), 136.8 (CH), 129.0 (CH), 128.1 (CH), 126.4 (CH), 125.7 (CH), 122.3 (CH), 120.7 (CH), 74.68 (CH), 47.14 (CH), 46.10 (CH₂), 40.80 (CH), 34.38 (CH₂), 31.50 (CH₂), 26.10 (CH), 23.40 (CH), 22.14 (CH₃), 20.82 (CH₃), 18.73 (CH₃), 16.18 (CH₃). **IR** (ATR): 2953, 2869, 1726, 1585, 1461, 1243, 1198, 1170, 1151, 768 cm⁻¹. **MS** (EI) *m/z* (relative intensity): 365 (18) [M]⁺, 228 (28), 183 (100), 167 (42), 83 (72). **HR-MS** (EI): *m/z* calcd. for C₂₄H₃₁NO₂⁺ [M]⁺ 365.2355, found: 365.2362.

(3*S*,8*S*,9*S*,10*R*,13*R*,14*S*,17*R*)-10,13-Dimethyl-17-[(*R*)-6-methylheptan-2-yl]-2,3,4,7,8,9,10,11,12,13,14,15,16,17-tetradecahydro-1*H*-cyclopenta[*a*]phenanthren-3-yl 2-[3-(pyridin-2-yl)phenyl]propanoate (140o**)**



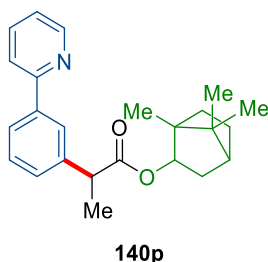
140o

The general procedure **GP-H** was followed using 2-phenylpyridine (**117a**) (38.8 mg, 0.25 mmol), (3*S*,8*S*,9*S*,10*R*,13*R*,14*S*,17*R*)-10,13-dimethyl-17-((*R*)-6-methylheptan-2-yl)-2,3,4,7,8,9,10,11,12,13,14,15,16,17-tetradecahydro-1*H*-cyclopenta[*a*]phenanthren-3-yl 2-bromopropanoate (**139o**) (391 mg, 0.75 mmol), **221b** (30.0 mg, 10.0 mol %) and KOAc (49.1 mg, 0.50 mmol). Purification by column chromatography (*n*-hexane/EtOAc: 10/1) yielded **140o** (93.9 mg, 63%) as a colourless oil.

¹H-NMR (400 MHz, CDCl₃): δ = 8.70 (dd, *J* = 5.0, 1.5 Hz, 1H), 7.94 (dd, *J* = 1.7, 1.7 Hz, 1H), 7.87 (dd, *J* = 7.6, 1.5 Hz, 1H), 7.74 (dd, *J* = 6.6, 1.7 Hz, 2H), 7.43 (dd, *J* = 7.6, 7.6 Hz, 2H), 7.23 (ddd, *J* = 6.6, 5.0, 2.1 Hz, 1H), 5.33 (dd, *J* = 4.3, 1.8 Hz, 1H), 4.75 –

4.51 (m, 1H), 3.78 (q, $J = 7.2$ Hz, 1H), 2.40 – 2.27 (m, 1H), 2.25 – 2.17 (m, 1H), 2.05 – 1.75 (m, 5H), 1.61 – 1.25 (m, 14H), 1.22 – 0.95 (m, 13H), 0.94 – 0.88 (m, 3H), 0.86 (dd, $J = 6.6, 1.8$ Hz, 6H), 0.66 (s, 3H). $^{13}\text{C-NMR}$ (100 MHz, CDCl_3): $\delta = 174.0$ (C_q), 157.4 (C_q), 149.7 (CH), 141.6 (C_q), 139.8 (C_q), 139.7 (C_q), 136.9 (CH), 129.1 (CH), 128.1 (CH), 126.5 (CH), 125.8 (CH), 122.7 (CH), 122.3 (CH), 120.8 (CH), 74.40 (CH), 56.81 (CH), 56.26 (CH), 50.12 (CH), 45.97 (CH), 42.43 (CH_2), 39.85 (CH_2), 39.65 (CH_2), 38.17 (C_q), 37.94 (CH_2), 36.71 (CH_2), 36.31 (CH_2), 35.92 (CH), 32.04 (CH_2), 32.01 (CH), 28.36 (CH_2), 28.15 (CH), 27.84 (C_q), 24.41 (CH_2), 23.96 (CH_2), 22.70 (CH_3), 21.15 (CH_2), 19.45 (CH_3), 18.96 (CH_3), 18.94 (CH_3), 11.98 (CH_3). **IR** (ATR): 2935, 2867, 1731, 1585, 1462, 1437, 1376, 1195, 1165, 769 cm^{-1} . **MS** (ESI) m/z (relative intensity): 618 (100) $[\text{M}+\text{Na}]^+$, 596 (30) $[\text{M}+\text{H}]^+$. **HR-MS** (ESI): m/z calcd. for $\text{C}_{41}\text{H}_{58}\text{NO}_2^+$ $[\text{M}+\text{H}]^+$ 596.4462, found: 596.4465.

Endo-(1,7,7-trimethylbicyclo[2.2.1]heptan-2-yl 2-(3-(pyridin-2-yl)phenyl)propanoate (140p)

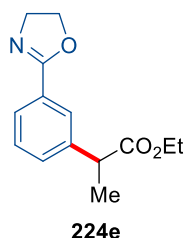


The general procedure **GP-H** was followed using 2-phenylpyridine (**117a**) (38.8 mg, 0.25 mmol), (\pm)-1,7,7-trimethylbicyclo[2.2.1]heptan-2-yl-2-bromopropanoate (**139p**) (217 mg, 0.75 mmol), **221b** (30.0 mg, 10.0 mol %) and KOAc (49.1 mg, 0.50 mmol). Purification by column chromatography (*n*-hexane/EtOAc: 10/1) yielded **140p** (53.6 mg, 59%) as a colourless oil.

$^1\text{H-NMR}$ (400 MHz, CDCl_3): $\delta = 8.72$ (d, $J = 4.8$ Hz, 1H), 7.98 (d, $J = 1.7$ Hz, 1H), 7.90 (dd, $J = 7.5, 1.6$ Hz, 1H), 7.76 (dd, $J = 6.7, 1.6$ Hz, 2H), 7.49 – 7.38 (m, 2H), 7.30 – 7.20 (m, 1H), 5.04 – 4.57 (m, 1H), 3.84 (dd, $J = 7.2, 2.9$ Hz, 1H), 2.40 – 2.25 (m, 1H), 1.84 (ddd, $J = 12.7, 9.3, 3.9$ Hz, 1H), 1.77 – 1.55 (m, 6H), 1.33 – 1.13 (m, 1H), 1.09 – 0.96 (m, 1H), 0.89 (d, $J = 1.8$ Hz, 3H), 0.87 – 0.82 (m, 4H), 0.81 – 0.76 (m, 1H), 0.69 (s, 1H). $^{13}\text{C-NMR}$ (100 MHz, CDCl_3): $\delta = 174.8$ (C_q), 157.4 (C_q), 149.7 (CH), 141.5 (C_q), 139.6 (C_q), 137.0 (CH), 129.1 (CH), 128.2 (CH), 126.5 (CH), 125.8 (CH), 122.3 (CH), 120.8 (CH), 80.30 (CH), 48.96 (C_q), 47.96 (CH), 46.09 (C_q), 44.97 (CH_2), 36.77 (CH), 28.05 (CH_2), 27.15 (CH_2), 19.77 (CH_3), 18.97 (CH_3), 18.52 (CH_3), 13.56 (CH_3). **IR** (ATR): 2953,

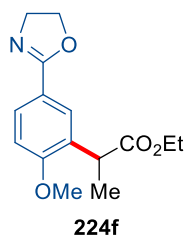
2875, 1729, 1585, 1461, 1426, 1248, 1197, 1160, 767 cm^{-1} . **MS** (ESI) m/z (relative intensity): 386 (8) $[\text{M}+\text{Na}]^+$, 364 (100) $[\text{M}+\text{H}]^+$. **HR-MS** (ESI): m/z calcd. for $\text{C}_{24}\text{H}_{30}\text{NO}_2^+$ $[\text{M}+\text{H}]^+$ 364.2271, found: 364.2273.

Ethyl 2-[3-(4,5-dihydrooxazol-2-yl)phenyl]propanoate (**224e**)



The general procedure **GP-H** was followed using 2-phenyl-4,5-dihydrooxazole (**201e**) (38.8 mg, 0.25 mmol), ethyl 2-bromopropanoate (**139e**) (136 mg, 0.75 mmol), **221b** (30.0 mg, 10.0 mol %) and KOAc (49.1 mg, 0.50 mmol). Purification by column chromatography (*n*-hexane/EtOAc: 10/1) yielded **224e** (34.0 mg, 55%) as a colourless oil. **¹H-NMR** (400 MHz, CDCl_3): δ = 7.89 (dd, J = 1.6, 1.6 Hz, 1H), 7.83 (dd, J = 7.7, 1.6 Hz, 1H), 7.43 (dd, J = 7.7, 1.6 Hz, 1H), 7.36 (dd, J = 7.7, 7.7 Hz, 1H), 4.43 (t, J = 9.5 Hz, 2H), 4.23 – 3.99 (m, 4H), 3.74 (q, J = 7.1 Hz, 1H), 1.51 (d, J = 7.2 Hz, 3H), 1.19 (t, J = 7.1 Hz, 3H). **¹³C-NMR** (100 MHz, CDCl_3): δ = 174.3 (C_q), 164.7 (C_q), 141.1 (C_q), 130.5 (CH), 128.8 (CH), 128.2 (C_q), 127.6 (CH), 127.1 (CH), 67.76 (CH_2), 60.89 (CH_2), 55.07 (CH_2), 45.56 (CH), 18.63 (CH_3), 14.25 (CH_3). **IR** (ATR): 2980, 1732, 1650, 1362, 1194, 1067, 950, 711, 422, 375 cm^{-1} . **MS** (EI) m/z (relative intensity): 247 (21) $[\text{M}]^+$, 174 (100), 131 (33), 103 (26). **HR-MS** (EI): m/z calcd. for $\text{C}_{14}\text{H}_{17}\text{NO}_3^+$ $[\text{M}]^+$ 247.1208, found: 247.1210.

Ethyl 2-[5-(4,5-dihydrooxazol-2-yl)-2-methoxyphenyl]propanoate (**224f**)



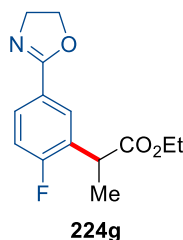
The general procedure **GP-H** was followed using 2-(4-methoxyphenyl)-4,5-dihydrooxazole (**201f**) (44.3 mg, 0.25 mmol), ethyl 2-bromopropanoate (**139e**) (136 mg, 0.75 mmol), **221b** (30.0 mg, 10.0 mol %) and KOAc (49.1 mg, 0.50 mmol). Purification

by column chromatography (*n*-hexane/EtOAc: 10/1) yielded **224f** (59.6 mg, 86%) as a colourless solid.

The general procedure **GP-J** was followed using 2-(4-methoxyphenyl)-4,5-dihydrooxazole (**201f**) (44.3 mg, 0.25 mmol), ethyl 2-bromopropanoate (**139e**) (136 mg, 0.75 mmol), **221b** (30.0 mg, 10.0 mol %) and KOAc (49.1 mg, 0.50 mmol) and H₂O (22.5 μ L, 1.25 mmol). Purification by column chromatography (*n*-hexane/EtOAc: 10/1) yielded **224f** (42.9 mg, 62%) as a colourless solid.

M.p.: 121–123 °C. **¹H-NMR** (400 MHz, CDCl₃): δ = 7.88 – 7.77 (m, 2H), 6.86 (d, *J* = 8.5 Hz, 1H), 4.38 (t, *J* = 9.5, Hz, 2H), 4.11 (q, *J* = 7.2 Hz, 2H), 4.00 (t, *J* = 9.5 Hz, 2H), 3.95 (t, *J* = 7.2 Hz, 1H), 3.83 (s, 3H), 1.47 (d, *J* = 7.2 Hz, 3H), 1.17 (t, *J* = 7.2 Hz, 3H). **¹³C-NMR** (100 MHz, CDCl₃): δ = 174.6 (C_q), 164.5 (C_q), 159.4 (C_q), 129.7 (C_q), 128.7 (CH), 128.4 (CH), 120.3 (C_q), 110.2 (CH), 67.61 (CH₂), 60.63 (CH₂), 55.64 (CH₃), 54.96 (CH₂), 39.78 (CH), 17.00 (CH₃), 14.29 (CH₃). **IR** (ATR): 2978, 1728, 1647, 1500, 1363, 1254, 1179, 1075, 1024, 949 cm⁻¹. **MS** (EI) *m/z* (relative intensity): 277 (55) [M]⁺, 204 (100), 161 (29), 131 (22). **HR-MS** (EI): *m/z* calcd. for C₁₅H₁₉NO₄⁺ [M]⁺ 277.1314, found: 277.1313.

Ethyl 2-[5-(4,5-dihydrooxazol-2-yl)-2-fluorophenyl]propanoate (**224g**)

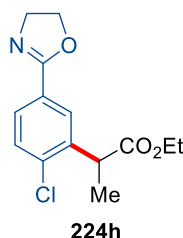


The general procedure **GP-H** was followed using 2-(4-fluorophenyl)-4,5-dihydrooxazole (**201g**) (41.3 mg, 0.25 mmol), ethyl 2-bromopropanoate (**139e**) (136 mg, 0.75 mmol), **221b** (30.0 mg, 10.0 mol %) and KOAc (49.1 mg, 0.50 mmol). Purification by column chromatography (*n*-hexane/EtOAc: 10/1) yielded **224g** (43.1 mg, 65%) as a colourless oil.

¹H-NMR (400 MHz, CDCl₃): δ = 7.91 (dd, *J* = 7.3, 1.0 Hz, 1H), 7.84 (ddd, *J* = 8.3, 5.0, 1.5 Hz, 1H), 7.07 (dd, *J* = 8.3, 1.0 Hz, 1H), 4.49 – 4.32 (m, 2H), 4.14 (q, *J* = 7.1 Hz, 2H), 4.08 – 3.97 (m, 3H), 1.52 (d, *J* = 7.2 Hz, 3H), 1.20 (t, *J* = 7.1, 3H). **¹³C-NMR** (100 MHz, CDCl₃): δ = 173.5 (C_q), 163.9 (C_q), 162.5 (d, ¹*J*_{C-F} = 251.8 Hz, C_q), 129.4 (d, ³*J*_{C-F} = 5.0 Hz, CH), 129.1 (d, ³*J*_{C-F} = 9.2 Hz, CH), 128.4 (d, ²*J*_{C-F} = 15.7 Hz, C_q), 124.3 (d, ⁴*J*_{C-F} = 3.5 Hz, C_q), 115.7 (d, ²*J*_{C-F} = 23.3 Hz, CH), 67.90 (CH₂), 61.17 (CH₂), 55.10 (CH₂), 38.87 (d, ⁴*J*_{C-F} = 2.4 Hz, CH), 17.37 (CH₃), 14.22 (CH₃). **¹⁹F-NMR** (282 MHz, CDCl₃): δ

–113.2. **IR** (ATR): 2981, 1731, 1651, 1499, 1363, 1253, 1181, 1073, 949, 833 cm^{-1} . **MS** (EI) m/z (relative intensity): 265 (22) $[\text{M}]^+$, 192 (100), 149 (43), 101 (17). **HR-MS** (EI): m/z calcd. for $\text{C}_{14}\text{H}_{16}\text{FNO}_3^+$ $[\text{M}]^+$ 265.1114, found: 265.1112.

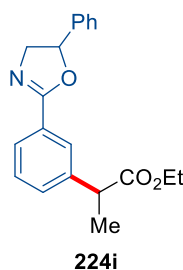
Ethyl 2-[2-chloro-5-(4,5-dihydrooxazol-2-yl)phenyl]propanoate (**224h**)



The general procedure **GP-H** was followed using 2-(4-chlorophenyl)-4,5-dihydrooxazole (**201h**) (45.4 mg, 0.25 mmol), ethyl 2-bromopropanoate (**139e**) (136 mg, 0.75 mmol), **221b** (30.0 mg, 10.0 mol %) and KOAc (49.1 mg, 0.50 mmol). Purification by column chromatography (*n*-hexane/EtOAc: 10/1) yielded **224h** (46.4 mg, 66%) as a colourless oil.

¹H-NMR (400 MHz, CDCl_3): δ = 7.91 (d, J = 1.9 Hz, 1H), 7.77 (ddd, J = 8.3, 1.9, 1.4 Hz, 1H), 7.41 (dd, J = 8.3, 1.4 Hz, 1H), 4.43 (t, J = 9.6 Hz, 2H), 4.20 – 4.10 (m, 3H), 4.05 (t, J = 9.6 Hz, 2H), 1.54 (d, J = 7.2 Hz, 3H), 1.21 (t, J = 7.1 Hz, 3H). **¹³C-NMR** (100 MHz, CDCl_3): δ = 173.6 (C_q), 163.9 (C_q), 138.8 (C_q), 137.1 (C_q), 129.8 (CH), 128.5 (CH), 128.0 (CH), 127.0 (C_q), 67.92 (CH_2), 61.19 (CH_2), 55.14 (CH_2), 42.50 (CH), 17.43 (CH_3), 14.25 (CH_3). **IR** (ATR): 2980, 2936, 1730, 1651, 1475, 1337, 1244, 1191, 1074, 949 cm^{-1} . **MS** (EI) m/z (relative intensity): 281 (9) $[\text{M}]^+$, 246 (88), 208 (100), 165 (45). **HR-MS** (EI): m/z calcd. for $\text{C}_{14}\text{H}_{16}^{35}\text{ClNO}_3^+$ $[\text{M}]^+$ 281.0819, found: 281.0817.

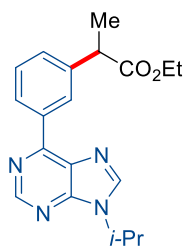
Ethyl 2-[3-(4-phenyl-4,5-dihydrooxazol-2-yl)phenyl]propanoate (**224i**)



The general procedure **GP-H** was followed using 2,5-diphenyl-4,5-dihydrooxazole (**201i**) (55.8 mg, 0.25 mmol), ethyl 2-bromopropanoate (**139e**) (136 mg, 0.75 mmol), **221b** (30.0 mg, 10.0 mol %) and KOAc (49.1 mg, 0.50 mmol). Purification by column chromatography (*n*-hexane/EtOAc: 10/1) yielded **224i** (55.7 mg, 69%) as a colourless oil.

¹H-NMR (400 MHz, CDCl₃): δ = 7.96 (s, 1H), 7.91 (dd, J = 7.6, 1.5 Hz, 1H), 7.47 (d, J = 7.9 Hz, 1H), 7.44 – 7.31 (m, 6H), 5.66 (dd, J = 10.2, 8.0 Hz, 1H), 4.48 (dd, J = 14.9, 10.2 Hz, 1H), 4.20 – 4.05 (m, 2H), 4.00 (dd, J = 14.9, 8.0 Hz, 1H), 3.76 (q, J = 7.2 Hz, 1H), 1.52 (d, J = 7.2 Hz, 3H), 1.20 (t, J = 7.2 Hz, 3H). **¹³C-NMR** (100 MHz, CDCl₃): δ = 174.3 (C_q), 164.0 (C_q), 141.1 (C_q), 130.7 (CH), 129.0 (CH), 129.0 (CH), 128.9 (CH), 128.5 (CH), 128.1 (C_q), 127.8 (C_q), 127.2 (CH), 125.9 (CH), 81.27 (CH₂), 63.32 (CH), 61.00 (CH₂), 45.58 (CH), 18.65 (CH₃), 14.26 (CH₃). **IR** (ATR): 2979, 1731, 1651, 1454, 1357, 1337, 1249, 1193, 1064, 699 cm⁻¹. **MS** (EI) m/z (relative intensity): 323 (4) [M]⁺, 250 (10), 217 (100), 189 (12). **HR-MS** (EI): m/z calcd. for C₂₀H₂₁NO₃⁺ [M]⁺ 323.1521, found: 323.1523.

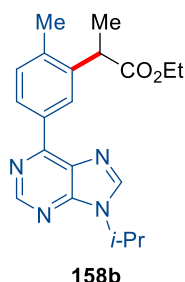
Ethyl 2-[3-(9-isopropyl-9H-purin-6-yl)phenyl]propanoate (**158a**)



158a

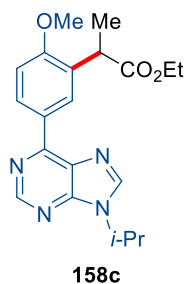
The general procedure **GP-H** was followed using 9-isopropyl-6-phenyl-9H-purine (**155a**) (59.6 mg, 0.25 mmol), ethyl 2-bromopropanoate (**139e**) (136 mg, 0.75 mmol), **221b** (30.0 mg, 10.0 mol %) and KOAc (49.1 mg, 0.50 mmol). Purification by column chromatography (*n*-hexane/EtOAc: 3/1) yielded **158a** (77.8 mg, 92%) as a colourless oil.

¹H-NMR (400 MHz, CDCl₃): δ = 9.00 (s, 1H), 8.72 (dd, J = 7.4, 1.7 Hz, 1H), 8.68 (dd, J = 1.7, 0.8 Hz, 1H), 8.17 (s, 1H), 7.55 – 7.45 (m, 2H), 4.97 (sept, J = 6.8 Hz, 1H), 4.12 (q, J = 7.2 Hz, 2H), 3.86 (q, J = 7.2 Hz, 1H), 1.66 (d, J = 6.8 Hz, 6H), 1.57 (d, J = 7.2 Hz, 3H), 1.19 (t, J = 7.2 Hz, 3H). **¹³C-NMR** (100 MHz, CDCl₃): δ = 174.6 (C_q), 154.6 (C_q), 152.2 (C_q), 152.1 (CH), 142.1 (CH), 141.3 (C_q), 136.2 (C_q), 131.6 (C_q), 129.9 (CH), 129.0 (CH), 129.0 (CH), 60.87 (CH₂), 47.35 (CH), 45.77 (CH), 22.68 (CH₃), 18.82 (CH₃), 14.23 (CH₃). **IR** (ATR): 2979, 1727, 1568, 1446, 1325, 1219, 1176, 1064, 797, 647 cm⁻¹. **MS** (EI) m/z (relative intensity): 338 (60) [M]⁺, 265 (81), 223 (100), 208 (52). **HR-MS** (EI): m/z calcd. for C₁₉H₂₂N₄O₂⁺ [M]⁺ 338.1743, found: 338.1735.

Ethyl 2-[5-(9-isopropyl-9H-purin-6-yl)-2-methylphenyl]propanoate (158b)

The general procedure **GP-H** was followed using 9-isopropyl-6-(*p*-tolyl)-9H-purine (**155b**) (63.1 mg, 0.25 mmol), ethyl 2-bromopropanoate (**139e**) (136 mg, 0.75 mmol), **221b** (30.0 mg, 10.0 mol %) and KOAc (49.1 mg, 0.50 mmol). Purification by column chromatography (*n*-hexane/EtOAc: 3/1) yielded **158b** (81.9 mg, 93%) as a colourless oil.

¹H-NMR (400 MHz, CDCl₃): δ = 8.97 (s, 1H), 8.73 (d, J = 1.8 Hz, 1H), 8.62 (dd, J = 8.0, 1.8 Hz, 1H), 8.16 (s, 1H), 7.34 (d, J = 8.0 Hz, 1H), 4.96 (sept, J = 6.8 Hz, 1H), 4.13 (q, J = 7.1 Hz, 2H), 4.01 (q, J = 7.1 Hz, 1H), 2.43 (s, 3H), 1.64 (d, J = 6.8 Hz, 6H), 1.60 (d, J = 7.1 Hz, 3H), 1.19 (t, J = 7.1 Hz, 3H). **¹³C-NMR** (100 MHz, CDCl₃): δ = 174.7 (C_q), 154.7 (C_q), 152.1 (CH), 141.8 (CH), 139.7 (C_q), 139.2 (C_q), 134.1 (C_q), 131.5 (C_q), 130.9 (CH), 128.6 (CH), 128.3 (CH), 60.87 (CH₂), 47.23 (CH), 41.99 (CH), 22.69 (CH₃), 19.88 (CH₃), 17.87 (CH₃), 14.25 (CH₃). **IR** (ATR): 2979, 1727, 1576, 1445, 1324, 1218, 1187, 1061, 806, 647 cm⁻¹. **MS** (EI) m/z (relative intensity): 352 (84) [M]⁺, 306 (34), 279 (89), 237 (100), 222 (56). **HR-MS** (EI): m/z calcd. for C₂₀H₂₄N₄O₂⁺ [M]⁺ 352.1899, found: 352.1901.

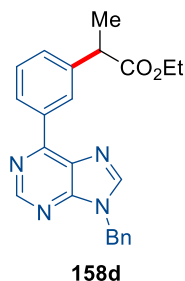
Ethyl 2-[5-(9-isopropyl-9H-purin-6-yl)-2-methoxyphenyl]propanoate (158c)

The general procedure **GP-H** was followed using 9-isopropyl-6-(4-methoxyphenyl)-9H-purine (**155c**) (67.1 mg, 0.25 mmol), ethyl 2-bromopropanoate (**139e**) (136 mg, 0.75 mmol), **221b** (30.0 mg, 10.0 mol %) and KOAc (49.1 mg, 0.50 mmol). Purification by column chromatography (*n*-hexane/EtOAc: 3/1) yielded **158c** (86.5 mg, 94%) as a colourless oil.

The general procedure **GP-J** was followed using 9-isopropyl-6-(4-methoxyphenyl)-9*H*-purine (**155c**) (67.1 mg, 0.25 mmol), ethyl 2-bromopropanoate (**139e**) (136 mg, 0.75 mmol), **221b** (30.0 mg, 10.0 mol %) and KOAc (49.1 mg, 0.50 mmol) and H₂O (22.5 μL, 1.25 mmol). Purification by column chromatography (*n*-hexane/EtOAc: 3/1) yielded **158c** (59.9 mg, 65%) as a colourless oil.

¹H-NMR (400 MHz, CDCl₃): δ = 8.94 (s, 1H), 8.81 (dd, *J* = 8.7, 2.2 Hz, 1H), 8.71 (d, *J* = 2.2 Hz, 1H), 8.14 (s, 1H), 7.01 (d, *J* = 8.7 Hz, 1H), 4.95 (sept, *J* = 6.8 Hz, 1H), 4.14 (q, *J* = 7.1 Hz, 2H), 4.04 (q, *J* = 7.2 Hz, 1H), 3.88 (s, 3H), 1.64 (d, *J* = 6.8 Hz, 6H), 1.56 (d, *J* = 7.2 Hz, 3H), 1.18 (t, *J* = 7.1 Hz, 3H). ¹³C-NMR (100 MHz, CDCl₃): δ = 174.9 (C_q), 159.3 (C_q), 154.5 (C_q), 152.1 (CH), 152.0 (C_q), 141.5 (CH), 131.1 (C_q), 130.7 (CH), 130.1 (C_q), 130.0 (CH), 128.5 (C_q), 110.5 (CH), 60.61 (CH₂), 55.65 (CH), 47.19 (CH₃), 40.39 (CH), 22.69 (CH₃), 17.13 (CH₃), 14.31 (CH₃). IR (ATR): 2978, 1728, 1574, 1505, 1449, 1325, 1254, 1184, 1027, 806 cm⁻¹. MS (EI) *m/z* (relative intensity): 368 (59) [M]⁺, 295 (100), 253 (90), 237 (27). HR-MS (EI): *m/z* calcd. for C₂₀H₂₄N₄O₃⁺ [M]⁺ 368.1848, found: 368.1846.

Ethyl 2-[3-(9-benzyl-9*H*-purin-6-yl)phenyl]propanoate (**158d**)

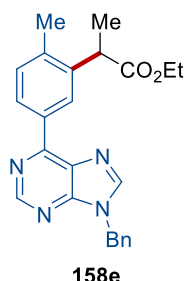


The general procedure **GP-H** was followed using 9-benzyl-6-phenyl-9*H*-purine (**155d**) (71.6 mg, 0.25 mmol), ethyl 2-bromopropanoate (**139e**) (136 mg, 0.75 mmol), **221b** (30.0 mg, 10.0 mol %) and KOAc (49.1 mg, 0.50 mmol). Purification by column chromatography (*n*-hexane/EtOAc: 3/1) yielded **158d** (78.2 mg, 81%) as a colourless oil.

¹H-NMR (400 MHz, CDCl₃): δ = 9.05 (s, 1H), 8.74 (dd, *J* = 7.3, 1.8 Hz, 1H), 8.71 (d, *J* = 1.8 Hz, 1H), 8.09 (s, 1H), 7.58 – 7.46 (m, 2H), 7.39 – 7.28 (m, 5H), 5.47 (s, 2H), 4.22 – 3.99 (m, 2H), 3.87 (q, *J* = 7.2 Hz, 1H), 1.58 (d, *J* = 7.2 Hz, 3H), 1.20 (t, *J* = 7.1 Hz, 3H). ¹³C-NMR (100 MHz, CDCl₃): δ = 174.6 (C_q), 154.8 (C_q), 152.7 (CH), 152.6 (C_q), 144.3 (CH), 141.3 (C_q), 136.1 (C_q), 135.3 (C_q), 131.1 (C_q), 130.1 (CH), 129.3 (CH), 129.1 (CH), 129.0 (CH), 129.0 (CH), 128.7 (CH), 127.9 (CH), 60.91 (CH₂), 47.38 (CH₂), 45.78 (CH), 18.83 (CH₃), 14.25 (CH₃). IR (ATR): 2979, 1726, 1569, 1455, 1323, 1192, 1177,

797, 728, 700 cm^{-1} . **MS** (EI) m/z (relative intensity): 386 (48) $[\text{M}]^+$, 313 (92), 221 (8), 132 (72), 91 (100). **HR-MS** (EI): m/z calcd. for $\text{C}_{23}\text{H}_{22}\text{N}_4\text{O}_2^+$ $[\text{M}]^+$ 386.1743, found: 386.1741.

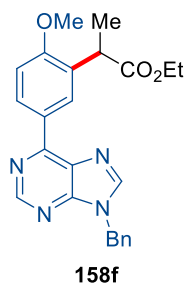
Ethyl 2-[5-(9-benzyl-9H-purin-6-yl)-2-methylphenyl]propanoate (**158e**)



The general procedure **GP-H** was followed using 9-benzyl-6-(*p*-tolyl)-9H-purine (**155e**) (75.1 mg, 0.25 mmol), ethyl 2-bromopropanoate (**139e**) (136 mg, 0.75 mmol), **221b** (30.0 mg, 10.0 mol %) and KOAc (49.1 mg, 0.50 mmol). Purification by column chromatography (*n*-hexane/EtOAc: 3/1) yielded **158e** (83.0 mg, 83%) as a colourless solid.

M.p.: 98–100 °C. **$^1\text{H-NMR}$** (400 MHz, CDCl_3): δ = 9.02 (s, 1H), 8.76 (d, J = 1.8 Hz, 1H), 8.64 (dd, J = 8.0, 1.8 Hz, 1H), 8.06 (s, 1H), 7.39 – 7.27 (m, 6H), 5.46 (s, 2H), 4.14 (q, J = 7.1 Hz, 2H), 4.02 (q, J = 7.2 Hz, 1H), 2.45 (s, 3H), 1.60 (d, J = 7.2 Hz, 3H), 1.19 (t, J = 7.1 Hz, 3H). **$^{13}\text{C-NMR}$** (100 MHz, CDCl_3): δ = 174.7 (C_q), 154.9 (C_q), 152.7 (CH), 152.6 (C_q), 144.0 (CH), 139.8 (C_q), 139.4 (C_q), 135.4 (C_q), 134.0 (C_q), 131.0 (CH), 129.2 (CH), 129.2 (CH), 128.6 (CH), 128.6 (C_q), 128.3 (CH), 127.9 (CH), 60.88 (CH_2), 47.31 (CH_2), 42.01 (CH), 19.91 (CH_3), 17.88 (CH_3), 14.27 (CH_3). **IR** (ATR): 2979, 1726, 1578, 1561, 1448, 1322, 1194, 805, 728, 648 cm^{-1} . **MS** (EI) m/z (relative intensity): 400 (35) $[\text{M}]^+$, 327 (52), 235 (13), 132 (39), 91 (100). **HR-MS** (EI): m/z calcd. for $\text{C}_{24}\text{H}_{24}\text{N}_4\text{O}_2^+$ $[\text{M}]^+$ 400.1899, found: 400.1898.

Ethyl 2-[5-(9-benzyl-9H-purin-6-yl)-2-methoxyphenyl]propanoate (**158f**)

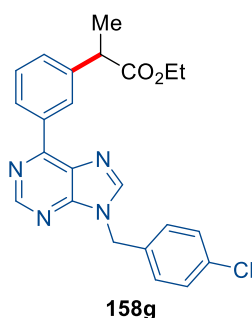


The general procedure **GP-H** was followed using 9-benzyl-6-(4-methoxyphenyl)-9*H*-purine (**155f**) (79.1 mg, 0.25 mmol), ethyl 2-bromopropanoate (**139e**) (136 mg, 0.75 mmol), **221b** (30.0 mg, 10.0 mol %) and KOAc (49.1 mg, 0.50 mmol). Purification by column chromatography (*n*-hexane/EtOAc: 3/1) yielded **158f** (91.6 mg, 88%) as a colourless solid.

The general procedure **GP-H** was followed using 9-benzyl-6-(4-methoxyphenyl)-9*H*-purine (**155f**) (949 mg, 3.00 mmol), ethyl 2-bromopropanoate (**139e**) (1.63 g, 9.00 mmol), **221b** (360 mg, 10.0 mol %) and KOAc (589 mg, 6.00 mmol) in 2-MeTHF (10 mL). Purification by column chromatography (*n*-hexane/EtOAc: 3/1) yielded **158f** (1.15 g, 92%) as a colourless solid.

M.p.: 122–124 °C. **¹H-NMR** (400 MHz, CDCl₃): δ = 8.98 (s, 1H), 8.83 (dd, *J* = 8.6, 2.2 Hz, 1H), 8.74 (d, *J* = 2.2 Hz, 1H), 8.04 (s, 1H), 7.39 – 7.27 (m, 5H), 7.02 (d, *J* = 8.6 Hz, 1H), 5.45 (s, 2H), 4.20 – 4.10 (m, 2H), 4.05 (q, *J* = 7.2 Hz, 1H), 3.89 (s, 3H), 1.57 (d, *J* = 7.2 Hz, 3H), 1.19 (t, *J* = 7.1 Hz, 3H). **¹³C-NMR** (100 MHz, CDCl₃): δ = 174.9 (C_q), 159.4 (C_q), 154.6 (C_q), 152.6 (CH), 152.4 (C_q), 143.8 (CH), 135.5 (C_q), 130.7 (CH), 130.6 (C_q), 130.2 (CH), 130.0 (C_q), 129.2 (CH), 128.6 (CH), 128.4 (C_q), 127.9 (CH), 110.6 (CH), 60.62 (CH₂), 55.66 (CH₃), 47.28 (CH₂), 40.40 (CH), 17.14 (CH₃), 14.33 (CH₃). **IR** (ATR): 2979, 1727, 1578, 1507, 1451, 1324, 1255, 1183, 1027, 728 cm⁻¹. **MS** (EI) *m/z* (relative intensity): 416 (51) [M]⁺, 343 (100), 327 (8), 91 (100). **HR-MS** (EI): *m/z* calcd. for C₂₄H₂₄N₄O₃⁺ [M]⁺ 416.1848, found: 416.1850.

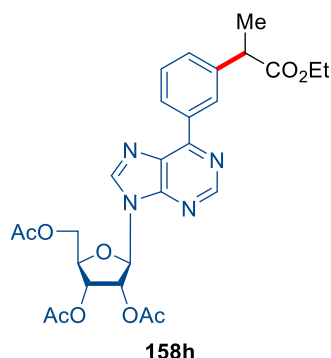
Ethyl 2-{3-[9-(4-chlorobenzyl)-9*H*-purin-6-yl]phenyl}propanoate (**158g**)



The general procedure **GP-H** was followed using 9-(4-chlorobenzyl)-6-phenyl-9*H*-purine (**155g**) (80.2 mg, 0.25 mmol), ethyl 2-bromopropanoate (**139e**) (136 mg, 0.75 mmol), **221b** (30.0 mg, 10.0 mol %) and KOAc (49.1 mg, 0.50 mmol). Purification by column chromatography (*n*-hexane/EtOAc: 3/1) yielded **158g** (83.0 mg, 79%) as a colourless solid.

M.p.: 138–140 °C. **¹H-NMR** (400 MHz, CDCl₃): δ = 9.05 (s, 1H), 8.74 (dd, J = 7.2, 1.7 Hz, 1H), 8.72 (d, J = 1.5 Hz, 1H), 8.10 (s, 1H), 7.59 – 7.46 (m, 2H), 7.35 (d, J = 8.4, 2H), 7.27 (d, J = 8.4, 2H), 5.46 (s, 2H), 4.22 – 4.06 (m, 2H), 3.88 (q, J = 7.2 Hz, 1H), 1.60 (d, J = 7.2 Hz, 3H), 1.21 (t, J = 7.2 Hz, 3H). **¹³C-NMR** (100 MHz, CDCl₃): δ = 174.6 (C_q), 155.0 (C_q), 152.8 (CH), 152.6 (C_q), 144.0 (CH), 141.4 (C_q), 136.0 (C_q), 134.8 (C_q), 133.9 (C_q), 131.1 (C_q), 130.2 (CH), 129.5 (CH), 129.3 (CH), 129.1 (CH), 129.1 (CH), 129.0 (CH), 60.94 (CH₂), 46.75 (CH₂), 45.80 (CH), 18.85 (CH₃), 14.27 (CH₃). **IR** (ATR): 2980, 1726, 1569, 1484, 1323, 1178, 1094, 1017, 761, 641 cm⁻¹. **MS** (EI) m/z (relative intensity): 420 (25) [M]⁺, 347 (62), 125 (100). **HR-MS** (EI): m/z calcd. for C₂₃H₂₁³⁵ClN₄O₂⁺ [M]⁺ 420.1353, found: 420.1351.

(2R,3R,4R,5R)-2-(Acetoxymethyl)-5-{6-[3-(1-ethoxy-1-oxopropan-2-yl)phenyl]-9H-purin-9-yl}tetrahydrofuran-3,4-diyl diacetate (158h**)**

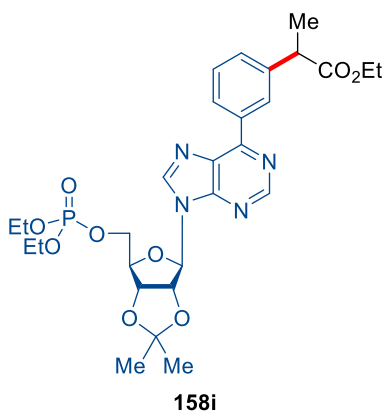


The general procedure **GP-H** was followed using (2R,3R,4R,5R)-2-(acetoxymethyl)-5-(6-phenyl-9H-purin-9-yl)tetrahydrofuran-3,4-diyl diacetate (**155h**) (114 mg, 0.25 mmol), ethyl 2-bromopropanoate (**139e**) (136 mg, 0.75 mmol), **221b** (30.0 mg, 10.0 mol %) and KOAc (49.1 mg, 0.50 mmol). Purification by column chromatography (*n*-hexane/EtOAc: 1/1) yielded **158h** (119 mg, 86%) as a colourless oil.

¹H-NMR (400 MHz, CDCl₃): δ = 9.02 (s, 1H), 8.71 (dd, J = 7.1, 1.8 Hz, 1H), 8.68 (d, J = 1.8 Hz, 1H), 8.27 (s, 1H), 7.57 – 7.44 (m, 2H), 6.30 (d, J = 5.5 Hz, 1H), 6.00 (t, J = 5.5 Hz, 1H), 5.70 (dd, J = 5.5, 4.3 Hz, 1H), 4.50 – 4.43 (m, 2H), 4.43 – 4.76 (m, 1H), 4.22 – 4.04 (m, 2H), 3.86 (q, J = 7.2 Hz, 1H), 2.16 (s, 3H), 2.15 (s, 3H), 2.08 (s, 3H), 1.58 (d, J = 7.2 Hz, 3H), 1.20 (t, J = 7.1 Hz, 3H). **¹³C-NMR** (100 MHz, CDCl₃): δ = 174.5 (C_q), 170.4 (C_q), 169.7 (C_q), 169.5 (C_q), 155.4 (C_q), 152.8 (CH), 152.2 (C_q), 142.6 (CH), 141.4 (C_q), 135.8 (C_q), 131.8 (C_q), 130.3 (CH), 129.1 (CH), 129.1 (CH), 129.0 (CH), 86.46 (CH), 80.53 (CH), 73.20 (CH), 70.80 (CH), 63.21 (CH₂), 60.94 (CH₂), 45.78 (CH), 20.92 (CH₃), 20.69 (CH₃), 20.53 (CH₃), 18.82 (CH₃), 14.26 (CH₃). **IR** (ATR): 2983, 1747,

1569, 1372, 1326, 1216, 1047, 904, 756, 702 cm^{-1} . **MS** (ESI) m/z (relative intensity): 1131 (100) $[2\text{M}+\text{Na}]^+$, 577 (36) $[\text{M}+\text{Na}]^+$. **HR-MS** (ESI): m/z calcd. for $\text{C}_{27}\text{H}_{31}\text{N}_4\text{O}_9^+$ $[\text{M}+\text{H}]^+$ 555.2086, found: 555.2083.

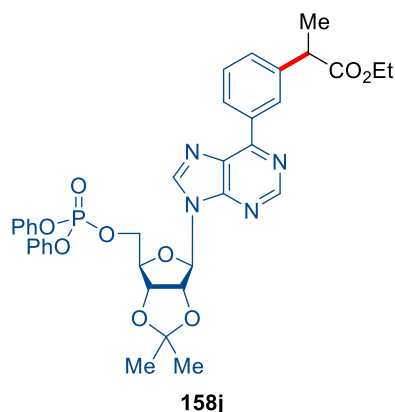
Ethyl 2-{3-[9-((3*aR*,4*R*,6*R*,6*aR*)-6-[(diethoxyphosphoryl)oxy]methyl)-2,2-dimethyl-tetrahydrofuro[3,4-*d*][1,3]dioxol-4-yl)-9*H*-purin-6-yl]phenyl}propanoate (158i**)**



The general procedure **GP-H** was followed using [(3*aR*,4*R*,6*R*,6*aR*)-2,2-dimethyl-6-(6-phenyl-9*H*-purin-9-yl)tetrahydrofuro[3,4-*d*][1,3]dioxol-4-yl)methyl diethyl phosphate (**155i**) (126 mg, 0.25 mmol), ethyl 2-bromopropanoate (**139e**) (136 mg, 0.75 mmol), **221b** (30.0 mg, 10.0 mol %) and KOAc (49.1 mg, 0.50 mmol). Purification by column chromatography (*n*-hexane/EtOAc: 1/1) yielded **158i** (121 mg, 80%) as a yellow oil.

¹H-NMR (400 MHz, CDCl_3): δ = 9.02 (s, 1H), 8.72 (dd, J = 7.1, 1.8 Hz, 1H), 8.69 (d, J = 1.8 Hz, 1H), 8.29 (s, 1H), 7.59 – 7.45 (m, 2H), 6.26 (d, J = 2.5 Hz, 1H), 5.45 (dd, J = 6.3, 2.5 Hz, 1H), 5.13 (dd, J = 6.3, 3.0 Hz, 1H), 4.57 – 4.44 (m, 1H), 4.29 (ddd, J = 10.8, 6.3, 4.4 Hz, 1H), 4.25 – 4.19 (m, 1H), 4.19 – 4.12 (m, 2H), 4.12 – 3.99 (m, 3H), 3.86 (q, J = 7.1 Hz, 1H), 1.78 (s, 1H), 1.65 (s, 3H), 1.58 (d, J = 7.2 Hz, 3H), 1.41 (s, 3H), 1.27 (t, J = 7.1 Hz, 3H), 1.25 (t, J = 7.1 Hz, 3H), 1.20 (t, J = 7.1 Hz, 3H). **¹³C-NMR** (100 MHz, CDCl_3): δ = 174.5 (C_q), 155.1 (C_q), 152.6 (CH), 151.9 (C_q), 143.3 (CH), 143.3 (CH), 141.4 (C_q), 135.9 (C_q), 131.9 (C_q), 130.3 (CH), 129.1 (CH), 129.1 (CH), 114.9 (C_q), 91.21 (d, $^4J_{\text{C-P}}$ = 2.3 Hz, CH), 85.45 (d, $^3J_{\text{C-P}}$ = 7.8 Hz, CH), 84.38 (CH), 81.49 (CH), 66.75 (d, $^2J_{\text{C-P}}$ = 5.5 Hz, CH_2), 64.28 (d, $^2J_{\text{C-P}}$ = 5.9 Hz, CH_2), 60.94 (CH_2), 45.78 (CH), 27.31 (CH_3), 25.49 (CH_3), 18.82 (CH_3), 16.20 (d, $^3J_{\text{C-P}}$ = 6.6 Hz, CH_3), 14.26 (CH_3). **³¹P-NMR** (120 MHz, CDCl_3): δ = -1.04. **IR** (ATR): 2983, 1730, 1569, 1263, 1209, 1159, 1075, 1024, 979, 864 cm^{-1} . **MS** (ESI) m/z (relative intensity): 1231 (100) $[2\text{M}+\text{Na}]^+$, 627 (48) $[\text{M}+\text{Na}]^+$. **HR-MS** (ESI): m/z calcd. for $\text{C}_{28}\text{H}_{38}\text{N}_4\text{O}_9\text{P}^+$ $[\text{M}+\text{H}]^+$ 605.2371, found: 605.2368.

Ethyl 2-{3-[9-((3a*R*,4*R*,6*R*,6a*R*)-6-[(diphenoxyphosphoryl)oxy]methyl)-2,2-dimethyl tetrahydrofuro[3,4-*d*][1,3]dioxol-4-yl)-9*H*-purin-6-yl]phenyl}propanoate (155j**)**

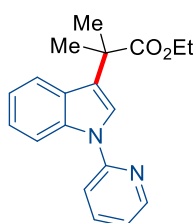


The general procedure **GP-H** was followed using [(3a*R*,4*R*,6*R*,6a*R*)-2,2-dimethyl-6-(6-phenyl-9*H*-purin-9-yl)tetrahydrofuro[3,4-*d*][1,3]dioxol-4-yl]methyl diphenyl phosphate (**155j**) (150 mg, 0.25 mmol), ethyl 2-bromopropanoate (**139e**) (136 mg, 0.75 mmol), **221b** (30.0 mg, 10.0 mol %) and KOAc (49.1 mg, 0.50 mmol). Purification by column chromatography (*n*-hexane/EtOAc: 1/1) yielded **155j** (137 mg, 78%) as a yellow oil.

¹H-NMR (400 MHz, CDCl₃): δ = 8.97 (s, 1H), 8.71 (dd, *J* = 6.9, 1.9 Hz, 1H), 8.69 – 8.66 (m, 1H), 8.19 (s, 1H), 7.60 – 7.45 (m, 2H), 7.31 – 7.16 (m, 4H), 7.18 – 7.05 (m, 6H), 6.21 (d, *J* = 2.4 Hz, 1H), 5.34 (dd, *J* = 6.3, 2.4 Hz, 1H), 5.08 (dd, *J* = 6.3, 2.9 Hz, 1H), 4.60 – 4.40 (m, 3H), 4.21 – 4.07 (m, 2H), 3.87 (q, *J* = 7.2 Hz, 1H), 1.62 (s, 3H), 1.59 (dd, *J* = 7.2, 1.3 Hz, 3H), 1.37 (s, 3H), 1.20 (t, *J* = 7.2 Hz, 3H). **¹³C-NMR** (100 MHz, CDCl₃): δ = 174.5 (C_q), 155.1 (C_q), 152.5 (CH), 151.7 (C_q), 150.3 (d, ²*J*_{C-P} = 7.0 Hz, C_q), 143.3 (CH), 141.3 (C_q), 135.8 (C_q), 131.8 (C_q), 130.2 (C_q), 129.9 (CH), 129.8 (CH), 129.1 (CH), 129.0 (C_q), 129.0 (CH), 125.6 (CH), 120.0 (CH), 120.0 (CH), 119.9 (CH), 119.9 (CH), 114.9 (CH), 91.15 (d, ⁴*J*_{C-P} = 2.8 Hz, CH), 85.21 (d, ³*J*_{C-P} = 8.2 Hz, CH), 84.20 (CH), 81.31 (CH), 68.06 (d, ³*J*_{C-P} = 6.0 Hz, CH₂), 60.90 (CH₂), 45.75 (CH), 27.22 (CH₃), 25.37 (CH₃), 18.80 (CH₃), 14.23 (CH₃). **³¹P-NMR** (120 MHz, CDCl₃): δ = -12.11. **IR** (ATR): 2985, 1730, 1581, 1489, 1211, 1187, 1162, 1025, 953, 768 cm⁻¹. **MS** (ESI) *m/z* (relative intensity): 1423 (100) [2M+Na]⁺, 723 (33) [M+Na]⁺. **HR-MS** (ESI): *m/z* calcd. for C₃₆H₃₈N₄O₉P⁺ [M+H]⁺ 701.2371, found: 701.2366.

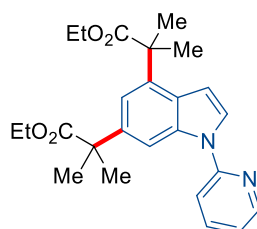
Ethyl 2-methyl-2-[1-(pyridin-2-yl)-1*H*-indol-3-yl]propanoate (152a) and diethyl 2,2'-[1-(pyridin-2-yl)-1*H*-indole-4,6-diyl]bis(2-methylpropanoate) (225a)

The modified procedure **GP-I** was followed using 1-(pyridin-2-yl)-1*H*-indole (**201a**) (48.6 mg, 0.25 mmol), ethyl 2-bromo-2-methylpropanoate (**139k**) (146 mg, 0.75 mmol), **221b** (30.0 mg, 10.0 mol %), KOAc (49.1 mg, 0.50 mmol) and AcOH (30.0 mg, 0.50 mmol) in THF (1.00 mL). Purification by column chromatography (*n*-hexane/EtOAc: 5/1) yielded **152a** (17.7 mg, 23%) and **225a** (65.3 mg, 62%) as a yellow oil.

**152a**

¹H-NMR (400 MHz, CDCl₃): δ = 8.58 – 8.47 (m, 1H), 8.09 (dd, J = 8.2, 1.3 Hz, 1H), 7.77 (ddd, J = 9.2, 5.3, 1.8 Hz, 1H), 7.67 – 7.58 (m, 2H), 7.48 (dd, J = 8.2, 1.3 Hz, 1H), 7.23 (dd, J = 7.3, 1.3 Hz, 1H), 7.19 – 7.06 (m, 2H), 4.10 (q, J = 7.1 Hz, 2H), 1.70 (s, 6H), 1.11 (t, J = 7.1 Hz, 3H) **¹³C-NMR** (100 MHz, CDCl₃): δ = 176.9 (C_q), 152.4 (C_q), 149.1 (CH), 138.5 (CH), 135.9 (C_q), 128.5 (C_q), 123.7 (C_q), 123.2 (CH), 122.6 (CH), 121.0 (CH), 120.7 (CH), 120.1 (CH), 114.8 (CH), 112.9 (CH), 61.00 (CH₂), 42.16 (C_q), 26.19 (2 x CH₃), 14.27 (CH₃). **IR** (ATR): 2978, 1721, 1590, 1470, 1438, 1236, 1138, 1023, 780, 739 cm⁻¹. **MS** (ESI) m/z (relative intensity): 331 (48) [M+Na]⁺, 309 (10) [M+H]⁺. **HR-MS** (ESI): m/z calcd. for C₁₉H₂₁N₂O₂⁺ [M+H]⁺ 309.1598, found: 309.1602.

The analytical data are in accordance with those previously reported in the literature.^[166c]

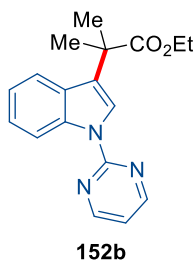
**225a**

¹H-NMR (400 MHz, CDCl₃): δ = 8.57 (ddd, J = 4.9, 1.9, 0.9 Hz, 1H), 8.12 (dd, J = 1.6, 0.8 Hz, 1H), 7.83 (ddd, J = 8.3, 7.4, 2.0 Hz, 1H), 7.62 (d, J = 3.6 Hz, 1H), 7.45 (dd, J =

8.3, 1.0 Hz, 1H), 7.18 (ddd, $J = 7.4, 4.9, 1.0$ Hz, 1H), 7.15 (d, $J = 1.6$ Hz, 1H), 6.65 (dd, $J = 3.6, 0.8$ Hz, 1H), 4.14 (q, $J = 7.1$ Hz, 2H), 4.10 (q, $J = 7.1$ Hz, 2H), 1.68 (s, 6H), 1.66 (s, 6H), 1.18 (t, $J = 7.1$ Hz, 3H), 1.11 (t, $J = 7.1$ Hz, 3H). $^{13}\text{C-NMR}$ (100 MHz, CDCl_3): $\delta = 177.9$ (C_q), 177.3 (C_q), 152.6 (C_q), 149.2 (CH), 139.9 (C_q), 138.5 (CH), 137.1 (C_q), 135.6 (C_q), 126.9 (C_q), 126.0 (CH), 120.4 (CH), 115.9 (CH), 115.3 (CH), 108.6 (CH), 104.4 (CH), 60.91 (CH_2), 60.81 (CH_2), 47.06 (C_q), 46.70 (C_q), 27.07 (CH_3), 26.50 (CH_3), 14.26 (CH_3), 14.24 (CH_3). **IR** (ATR): 2978, 1725, 1590, 1522, 1471, 1439, 1262, 1141, 1026, 777 cm^{-1} . **MS** (ESI) m/z (relative intensity): 445 (74) $[\text{M}+\text{Na}]^+$, 423 (100) $[\text{M}+\text{H}]^+$, 231 (22). **HR-MS** (ESI): m/z calcd. for $\text{C}_{25}\text{H}_{32}\text{N}_2\text{O}_4^+$ $[\text{M}+\text{H}]^+$ 423.2278, found: 423.2279.

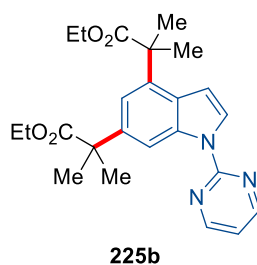
Ethyl 2-methyl-2-[1-(pyrimidin-2-yl)-1H-indol-3-yl]propanoate (**152b**) and diethyl 2,2'-[1-(pyrimidin-2-yl)-1H-indole-4,6-diyl]bis(2-methylpropanoate) (**225b**)

The modified procedure **GP-I** was followed using 1-(pyrimidin-2-yl)-1H-indole (**201b**) (48.8 mg, 0.25 mmol), ethyl 2-bromo-2-methylpropanoate (**139k**) (146 mg, 0.75 mmol), **221b** (30.0 mg, 10.0 mol %), KOAc (49.1 mg, 0.50 mmol) and AcOH (30.0 mg, 0.50 mmol) in THF (1.00 mL). Purification by column chromatography (*n*-hexane/EtOAc: 5/1) yielded **152b** (17.0 mg, 22%) and **225b** (60.4 mg, 57%) as a yellow oil.



$^1\text{H-NMR}$ (400 MHz, CDCl_3): $\delta = 8.82$ (d, $J = 8.3$ Hz, 1H), 8.69 (d, $J = 5.0$ Hz, 2H), 8.17 (s, 1H), 7.60 (d, $J = 7.9$ Hz, 1H), 7.33 (dd, $J = 7.8, 7.8$ Hz, 1H), 7.21 (dd, $J = 7.5, 7.5$ Hz, 1H), 7.02 (d, $J = 4.8$ Hz, 1H), 4.13 (q, $J = 7.1$ Hz, 2H), 1.73 (s, 6H), 1.13 (t, $J = 7.0$ Hz, 3H). $^{13}\text{C-NMR}$ (100 MHz, CDCl_3): $\delta = 176.9$ (C_q), 158.2 (CH), 157.8 (C_q), 136.3 (C_q), 129.5 (C_q), 125.1 (C_q), 123.8 (CH), 122.1 (CH), 122.0 (CH), 120.3 (CH), 116.5 (CH), 116.0 (CH), 61.05 (CH_2), 42.19 (C_q), 26.10 (2 x CH_3), 14.26 (CH_3). **IR** (ATR): 2979, 1722, 1577, 1562, 1427, 1383, 1246, 1138, 801, 746 cm^{-1} . **MS** (ESI) m/z (relative intensity): 332 (100) $[\text{M}+\text{Na}]^+$, 310 (57) $[\text{M}+\text{H}]^+$. **HR-MS** (ESI): m/z calcd. for $\text{C}_{18}\text{H}_{20}\text{N}_3\text{O}_2^+$ $[\text{M}+\text{H}]^+$ 310.1550, found: 310.1549.

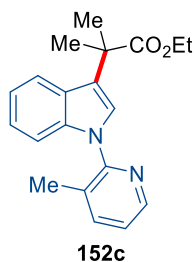
The analytical data are in accordance with those previously reported in the literature.^[166c]



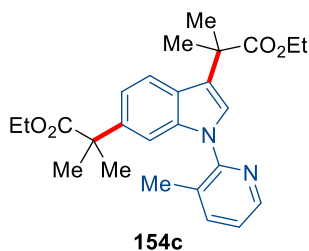
¹H-NMR (400 MHz, CDCl₃): δ = 8.85 (d, J = 1.6 Hz, 1H), 8.67 (d, J = 4.8 Hz, 2H), 8.21 (d, J = 3.8 Hz, 1H), 7.19 (d, J = 1.7 Hz, 1H), 7.02 (d, J = 4.8 Hz, 1H), 6.65 (d, J = 3.8 Hz, 1H), 4.16 (q, J = 7.1 Hz, 2H), 4.10 (q, J = 7.1 Hz, 2H), 1.70 (s, 6H), 1.68 (s, 6H), 1.20 (t, J = 7.1 Hz, 3H), 1.11 (t, J = 7.1 Hz, 3H). **¹³C-NMR** (100 MHz, CDCl₃): δ = 177.9 (C_q), 177.4 (C_q), 158.2 (CH), 157.8 (C_q), 140.5 (C_q), 136.8 (C_q), 135.9 (C_q), 127.8 (C_q), 125.7 (CH), 116.6 (CH), 116.3 (CH), 112.2 (CH), 105.6 (CH), 60.91 (C_q), 60.78 (C_q), 47.20 (CH₂), 46.61 (CH₂), 27.15 (CH₃), 26.57 (CH₃), 14.25 (CH₃), 14.20 (CH₃). **IR** (ATR): 2974, 2927, 1726, 1577, 1526, 1443, 1387, 1251, 1140, 1027 cm⁻¹. **MS** (ESI) m/z (relative intensity): 446 (100) [M+Na]⁺, 424 (63) [M+H]⁺. **HR-MS** (ESI): m/z calcd. for C₂₄H₃₀N₃O₄⁺ [M+H]⁺ 424.2231, found: 424.2234.

Ethyl 2-methyl-2-[1-(3-methylpyridin-2-yl)-1H-indol-3-yl]propanoate (152c), diethyl 2,2'-[1-(3-methylpyridin-2-yl)-1H-indole-3,6-diyl]bis(2-methylpropanoate) (154c) and diethyl 2,2'-[1-(3-methylpyridin-2-yl)-1H-indole-4,6-diyl]bis(2-methylpropanoate) (225c)

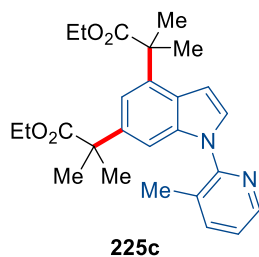
The modified procedure **GP-I** was followed using 1-(3-methylpyridin-2-yl)-1H-indole (**201j**) (52.0 mg, 0.25 mmol), ethyl 2-bromo-2-methylpropanoate (**139k**) (146 mg, 0.75 mmol), **221b** (30.0 mg, 10.0 mol %), KOAc (49.1 mg, 0.50 mmol) and AcOH (30.0 mg, 0.50 mmol) in THF (1.00 mL). Purification by column chromatography (*n*-hexane/EtOAc: 5/1) and HPLC purification (*n*-hexane/*i*-PrOH 80:20, 5.0 mL min⁻¹) yielded **152c** (20.2 mg, 25%) as a colorless oil, **154c** (25.1 mg, 23%) as a colorless oil and **225c** (28.4 mg, 26%) as a colorless oil.



$^1\text{H-NMR}$ (400 MHz, CDCl_3): δ = 8.47 (dd, J = 4.9, 1.8 Hz, 1H), 7.73 (dd, J = 7.8, 1.6, 1.2 Hz, 2H), 7.30 – 7.23 (m, 2H), 7.21 – 7.10 (m, 3H), 4.12 (q, J = 7.1 Hz, 2H), 2.22 (s, 3H), 1.73 (s, 6H), 1.15 (t, J = 7.1 Hz, 3H). **$^{13}\text{C-NMR}$** (101 MHz, CDCl_3): δ = 177.0 (C_q), 151.0 (C_q), 147.1 (CH), 140.6 (CH), 137.0 (C_q), 129.1 (C_q), 126.9 (C_q), 124.0 (CH), 122.9 (CH), 122.4 (CH), 122.1 (C_q), 120.8 (CH), 120.1 (CH), 111.4 (CH), 60.86 (CH_2), 42.20 (C_q), 26.23 (CH_3), 18.09 (CH_3), 14.25 (CH_3). **IR** (ATR): 2978, 1723, 1574, 1461 1363, 1237, 1141, 1022, 799, 743 cm^{-1} . **MS** (ESI) m/z (relative intensity): 345 (34) $[\text{M}+\text{Na}]^+$, 323 (100) $[\text{M}+\text{H}]^+$. **HR-MS** (ESI): m/z calcd. for $\text{C}_{20}\text{H}_{23}\text{N}_2\text{O}_2^+$ $[\text{M}+\text{H}]^+$ 323.1754, found: 323.1759.



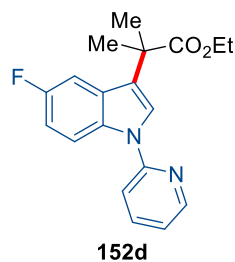
$^1\text{H-NMR}$ (400 MHz, CDCl_3): δ = 8.45 (dd, J = 4.7, 1.8 Hz, 1H), 7.72 (ddd, J = 7.6, 1.9, 0.8 Hz, 1H), 7.64 (dd, J = 8.3, 0.8 Hz, 1H), 7.27 (dd, J = 7.6, 4.8 Hz, 1H), 7.19 (s, 1H), 7.13 – 7.07 (m, 2H), 4.08 (q, J = 7.1 Hz, 4H), 2.18 (s, 3H), 1.68 (s, 6H), 1.55 (s, 6H), 1.13 (t, J = 7.1 Hz, 6H). **$^{13}\text{C-NMR}$** (100 MHz, CDCl_3): δ = 177.2 (C_q), 176.9 (C_q), 151.0 (C_q), 147.2 (CH), 140.7 (CH), 139.4 (C_q), 137.0 (C_q), 129.0 (C_q), 125.6 (C_q), 124.4 (CH), 122.9 (CH), 121.9 (C_q), 120.7 (CH), 118.4 (CH), 108.4 (CH), 60.89 (CH_2), 60.81 (CH_2), 46.64 (C_q), 42.24 (C_q), 27.03 (CH_3), 26.26 (CH_3), 18.18 (CH_3), 14.28 (CH_3), 14.17 (CH_3). **IR** (ATR): 2976, 2930, 1726, 1574, 1456, 1456, 1253, 1144, 1026, 802 cm^{-1} . **MS** (ESI) m/z (relative intensity): 459 (44) $[\text{M}+\text{Na}]^+$, 437 (100) $[\text{M}+\text{H}]^+$. **HR-MS** (ESI): m/z calcd. for $\text{C}_{26}\text{H}_{33}\text{N}_2\text{O}_4^+$ $[\text{M}+\text{H}]^+$ 437.2435, found: 437.2438.



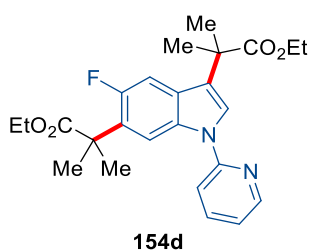
¹H-NMR (400 MHz, CDCl₃): δ = 8.44 (dd, J = 4.9, 1.8 Hz, 1H), 7.72 (dd, J = 7.5, 1.2 Hz, 1H), 7.27 (dd, J = 7.6, 4.8 Hz, 1H), 7.25 (s, 1H), 7.08 (s, 2H), 6.61 (d, J = 3.3 Hz, 1H), 4.08 (q, J = 7.1 Hz, 4H), 2.20 (s, 3H), 1.67 (s, 6H), 1.56 (s, 6H), 1.11 (t, J = 7.1 Hz, 6H). **¹³C-NMR** (100 MHz, CDCl₃): δ = 177.9 (C_q), 177.3 (C_q), 151.1 (C_q), 147.1 (CH), 140.7 (CH), 139.2 (C_q), 137.1 (C_q), 136.6 (C_q), 129.1 (CH), 127.2 (C_q), 125.4 (C_q), 123.0 (CH), 115.1 (CH), 107.2 (CH), 102.9 (CH), 60.83 (CH₂), 60.74 (CH₂), 46.87 (C_q), 46.78 (C_q), 27.01 (CH₃), 26.48 (CH₃), 18.13 (CH₃), 14.24 (CH₃), 14.20 (CH₃). **IR** (ATR): 2978, 2929, 1725, 1573, 1511, 1455, 1253, 1139, 1027, 780 cm⁻¹. **MS** (ESI) m/z (relative intensity): 459 (41) [M+Na]⁺, 437 (100) [M+H]⁺. **HR-MS** (ESI): m/z calcd. for C₂₆H₃₃N₂O₄⁺ [M+H]⁺ 437.2435, found: 437.2439.

Ethyl 2-[5-fluoro-1-(pyridin-2-yl)-1H-indol-3-yl]-2-methylpropanoate (152d), diethyl 2,2'-[5-fluoro-1-(pyridin-2-yl)-1H-indole-3,6-diyl]bis(2-methylpropanoate) (154d) and diethyl 2,2'-[5-fluoro-1-(pyridin-2-yl)-1H-indole-4,6-diyl]bis(2-methylpropanoate) (225d)

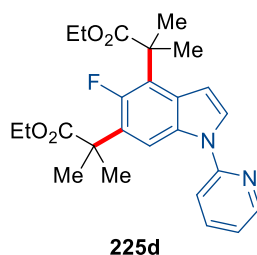
The modified procedure **GP-I** was followed using 5-fluoro-1-(pyridin-2-yl)-1H-indole (**201k**) (53.1 mg, 0.25 mmol), ethyl 2-bromo-2-methylpropanoate (**139k**) (146 mg, 0.75 mmol), **221b** (30.0 mg, 10.0 mol %), KOAc (49.1 mg, 0.50 mmol) and AcOH (30.0 mg, 0.50 mmol) in THF (1.00 mL). Purification by column chromatography (*n*-hexane/EtOAc: 5/1) and HPLC purification (*n*-hexane/*i*-PrOH 80:20, 5.0 mL min⁻¹) yielded **152d** (21.2 mg, 26%) as a colorless oil, **154d** (27.5 mg, 25%) as a colorless solid and **225d** (29.7 mg, 27%) as a colorless oil.



¹H-NMR (400 MHz, CDCl₃): δ = 8.59 – 8.43 (m, 1H), 8.16 (dd, J = 9.1, 4.7 Hz, 1H), 7.94 – 7.75 (m, 1H), 7.63 (s, 1H), 7.52 – 7.41 (m, 1H), 7.33 (dd, J = 9.8, 2.6 Hz, 1H), 7.16 (ddd, J = 7.3, 4.8, 1.0 Hz, 1H), 7.01 (dd, J = 9.0, 2.6 Hz, 1H), 4.15 (q, J = 7.1 Hz, 2H), 1.71 (s, 6H), 1.18 (t, J = 7.1 Hz, 3H). **¹³C-NMR** (100 MHz, CDCl₃): δ = 176.5 (C_q), 158.3 (d, $^1J_{C-F}$ = 237 Hz, C_q), 152.3 (C_q), 149.1 (CH), 138.6 (CH), 132.5 (C_q), 129.0 (d, $^3J_{C-F}$ = 9.6 Hz, C_q), 123.9 (CH), 123.5 (d, $^4J_{C-F}$ = 4.4 Hz, C_q), 120.2 (CH), 114.4 (CH), 114.2 (d, $^3J_{C-F}$ = 9.3 Hz, CH), 111.3 (d, $^2J_{C-F}$ = 25.4 Hz, CH), 106.0 (d, $^3J_{C-F}$ = 24.1 Hz, CH), 61.14 (CH₂), 42.11 (C_q), 26.04 (CH₃), 14.26 (CH₃). **¹⁹F-NMR** (282 MHz, CDCl₃): δ = –122.4. **IR** (ATR): 2979, 1723, 1592, 1470, 1380, 1245, 1135, 1024, 849, 774 cm⁻¹. **MS** (ESI) m/z (relative intensity): 349 (48) [M+Na]⁺, 327 (100) [M+H]⁺. **HR-MS** (ESI): m/z calcd. for C₁₉H₂₀FN₂O₂⁺ [M+H]⁺ 327.1503, found: 327.1508.

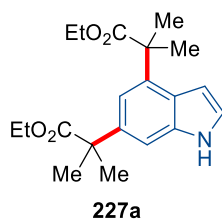


M.p.: 104–106 °C. **¹H-NMR** (400 MHz, CDCl₃): δ = 8.56 (dd, J = 5.1, 1.8 Hz, 1H), 8.24 (d, J = 6.8 Hz, 1H), 7.83 (dd, J = 7.9, 1.9 Hz, 1H), 7.56 (s, 1H), 7.45 (d, J = 8.2 Hz, 1H), 7.30 (d, J = 12.3 Hz, 1H), 7.17 (dd, J = 7.3, 4.9 Hz, 1H), 4.65 – 3.72 (m, 4H), 1.70 (s, 6H), 1.62 (s, 6H), 1.17 (t, J = 7.1 Hz, 6H). **¹³C-NMR** (100 MHz, CDCl₃): δ = 177.3 (C_q), 176.5 (C_q), 156.5 (d, $^1J_{C-F}$ = 239 Hz, C_q), 152.5 (C_q), 149.1 (CH), 138.2 (CH), 132.5 (C_q), 129.0 (d, $^2J_{C-F}$ = 16.9 Hz, C_q), 127.5 (d, $^2J_{C-F}$ = 10.4 Hz, C_q), 123.5 (CH), 123.4 (d, $^3J_{C-F}$ = 4.3 Hz, C_q), 120.2 (CH), 114.5 (CH), 110.9 (d, $^4J_{C-F}$ = 5.4 Hz, CH), 106.4 (d, $^3J_{C-F}$ = 25.8 Hz, CH), 61.13 (CH₂), 60.95 (CH₂), 44.65 (C_q), 42.13 (C_q), 26.19 (2 x CH₃), 26.06 (2 x CH₃), 14.25 (CH₃), 14.19 (CH₃). **¹⁹F-NMR** (282 MHz, CDCl₃): δ = –122.1 (s). **IR** (ATR): 2979, 1726, 1590, 1440, 1382, 1251, 1134, 1025, 849, 776 cm⁻¹. **MS** (ESI) m/z (relative intensity): 463 (69) [M+Na]⁺, 441 (100) [M+H]⁺. **HR-MS** (ESI): m/z calcd. for C₂₅H₃₀FN₂O₄⁺ [M+H]⁺ 441.2184, found: 441.2186.



¹H-NMR (400 MHz, CDCl₃): δ = 8.72 – 8.51 (m, 1H), 8.20 (dd, J = 6.6, 3.2 Hz, 1H), 7.84 (dd, J = 5.4, 1.7 Hz, 1H), 7.62 (d, J = 3.5 Hz, 1H), 7.43 (dd, J = 7.0, 3.2 Hz, 1H), 7.25 – 7.16 (m, 1H), 6.82 (d, J = 3.4 Hz, 1H), 4.14 (q, J = 7.2 Hz, 4H), 1.76 (s, 6H), 1.60 (s, 6H), 1.16 (t, J = 7.3 Hz, 6H). **¹³C-NMR** (100 MHz, CDCl₃): δ = 177.8 (C_q), 177.4 (C_q), 154.7 (d, $^1J_{C-F}$ = 239 Hz, C_q), 152.5 (C_q), 149.1 (CH), 138.7 (CH), 132.1 (C_q), 129.6 (d, $^2J_{C-F}$ = 19.4 Hz, C_q), 127.5 (d, $^3J_{C-F}$ = 6.50 Hz, C_q), 126.6 (CH), 123.1 (d, $^2J_{C-F}$ = 15.1 Hz, C_q), 120.6 (CH), 115.2 (CH), 109.5 (d, $^4J_{C-F}$ = 6.2 Hz, CH), 105.0 (d, $^4J_{C-F}$ = 5.0 Hz, CH), 60.99 (CH₂), 60.84 (CH₂), 46.56 (C_q), 44.80 (C_q), 27.23 (CH₃), 27.19 (CH₃), 26.26 (CH₃), 26.25 (CH₃), 14.26 (CH₃), 14.23 (CH₃). **¹⁹F-NMR** (282 MHz, CDCl₃): δ = –121.2 (s). **IR** (ATR): 2980, 1732, 1590, 1475, 1437, 1421, 1256, 1192, 1138, 778 cm⁻¹. **MS** (ESI) m/z (relative intensity): 463 (68) [M+Na]⁺, 441 (100) [M+H]⁺. **HR-MS** (ESI): m/z calcd. for C₂₅H₃₀FN₂O₄⁺ [M+H]⁺ 441.2184, found: 441.2187.

Diethyl 2,2'-(1H-indole-4,6-diyl)bis(2-methylpropanoate) (**227a**)

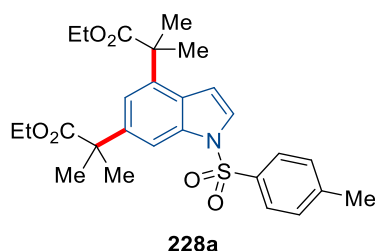


To a solution of **225a** (423 mg, 1.0 mmol, 1.0 equiv) in CH₂Cl₂ (2.0 mL) was added MeOTf (181 mg, 120 μ L, 1.1 mmol, 1.1 equiv) dropwise at 0 °C. After 30 min, the mixture was allowed to warm up to 25 °C and stirred for 16 h. After removal of the solvent, Pd(OH)₂/C (38.6 mg, 10 wt.%) and ammonium formate (630 mg, 10.0 mmol, 10.0 equiv) were added. The mixture was diluted with MeOH (4.0 mL, 0.25 M) and stirred at 60 °C for 16 h. After addition of EtOAc (20 mL) at ambient temperature, the mixture was filtered through a short pad of Celite® and the solvents were removed *in vacuo*. Purification by flash column chromatography on silica gel (*n*-hexane/EtOAc: 5/1) yielded **227a** (307 mg, 89%) as a pale colorless oil.

¹H-NMR (400 MHz, CDCl₃): δ = 8.33 (s, 1H), 7.28 (d, J = 2.3 Hz, 1H), 7.11 – 7.01 (m, 2H), 6.47 (d, J = 2.3 Hz, 1H), 4.14 (q, J = 7.1 Hz, 2H), 4.09 (q, J = 7.1 Hz, 2H), 1.68 (s, 6H), 1.64 (s, 6H), 1.18 (t, J = 7.1 Hz, 3H), 1.10 (t, J = 7.1 Hz, 3H). **¹³C-NMR** (100 MHz, CDCl₃): δ = 178.0 (C_q), 177.4 (C_q), 138.6 (C_q), 136.8 (C_q), 136.2 (C_q), 124.3 (C_q), 124.0 (CH), 114.3 (CH), 107.1 (CH), 101.6 (CH), 60.80 (CH₂), 60.80 (CH₂), 46.77 (C_q), 46.72

(C_q), 26.95 (CH₃), 26.95 (CH₃), 26.32 (CH₃), 26.32 (CH₃), 14.20 (CH₃), 14.16 (CH₃). **IR** (ATR): 3374, 2977, 1707, 1467, 1254, 1137, 1024, 858, 779, 730 cm⁻¹. **MS** (ESI) *m/z* (relative intensity): 368 (100) [M+Na]⁺, 346 (41) [M+H]⁺. **HR-MS** (ESI): *m/z* calcd. for C₂₀H₂₈NO₄⁺ [M+H]⁺ 346.2013, found: 346.2014.

Diethyl 2,2'-(1-tosyl-1*H*-indole-4,6-diyl)bis(2-methylpropanoate) (**228a**)



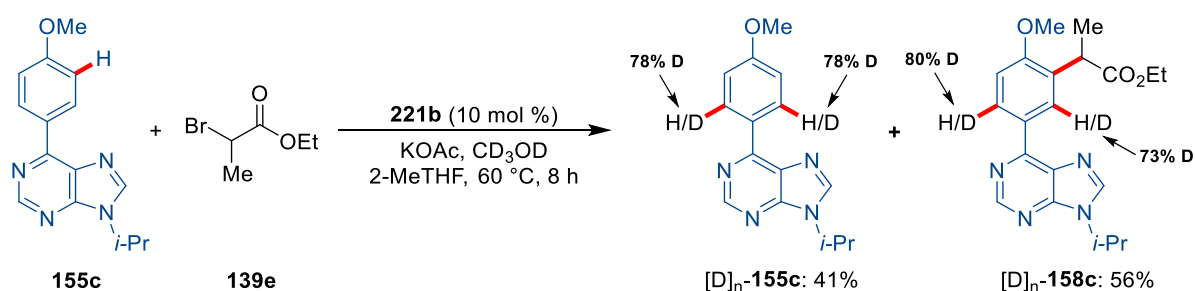
To a solution of **227a** (100 mg, 0.30 mmol, 1.0 equiv) in CH₃CN (15 mL) was added NaH (17.4 mg, 0.44 mmol, 1.5 equiv) at 0 °C. The mixture was stirred for 30 min and TsCl (60.8 mg, 0.32 mmol, 1.1 equiv) was added. Then, the mixture was allowed to reach room temperature and was stirred for additional 4 h. The reaction was quenched with a saturated aqueous solution of NH₄Cl (5.0 mL) and was extracted with ethyl acetate (3 x 20 mL). The combined organic phases were washed with brine, dried over Na₂SO₄ and concentrated *in vacuo*. Purification by flash column chromatography on silica gel (*n*-hexane/EtOAc: 5/1) yielded **228a** (114 mg, 76%) as a colorless solid.

M.p.: 91–93 °C. **¹H-NMR** (400 MHz, CDCl₃): δ = 7.91 (dd, *J* = 1.6, 0.8 Hz, 1H), 7.76 (d, *J* = 8.4 Hz, 2H), 7.51 (d, *J* = 3.8 Hz, 1H), 7.23 (d, *J* = 7.8 Hz, 2H), 7.16 (d, *J* = 1.6 Hz, 1H), 6.60 (dd, *J* = 3.8, 0.8 Hz, 1H), 4.14 (q, *J* = 7.1 Hz, 2H), 4.04 (q, *J* = 7.1 Hz, 2H), 2.35 (s, 3H), 1.64 (s, 6H), 1.58 (s, 6H), 1.18 (t, *J* = 7.1 Hz, 3H), 1.02 (t, *J* = 7.1 Hz, 3H). **¹³C-NMR** (100 MHz, CDCl₃): δ = 177.3 (C_q), 176.8 (C_q), 145.1 (C_q), 141.55 (C_q), 137.6 (C_q), 135.4 (C_q), 135.3 (C_q), 130.0 (CH), 127.3 (C_q), 127.1 (CH), 126.0 (CH), 117.7 (CH), 109.5 (CH), 107.5 (CH), 60.95 (CH₂), 60.95 (CH₂), 47.03 (C_q), 46.59 (C_q), 27.01 (2 x CH₃), 26.41 (2 x CH₃), 21.69 (CH₃), 14.20 (CH₃), 14.09 (CH₃). **IR** (ATR): 2978, 1723, 1366, 1252, 1171, 1140, 1091, 1027, 668, 582 cm⁻¹. **MS** (ESI) *m/z* (relative intensity): 522 (92) [M+Na]⁺, 500 (35) [M+H]⁺. **HR-MS** (ESI): *m/z* calcd. for C₂₇H₃₄NO₆S⁺ [M+H]⁺ 500.2101, found: 500.2098.

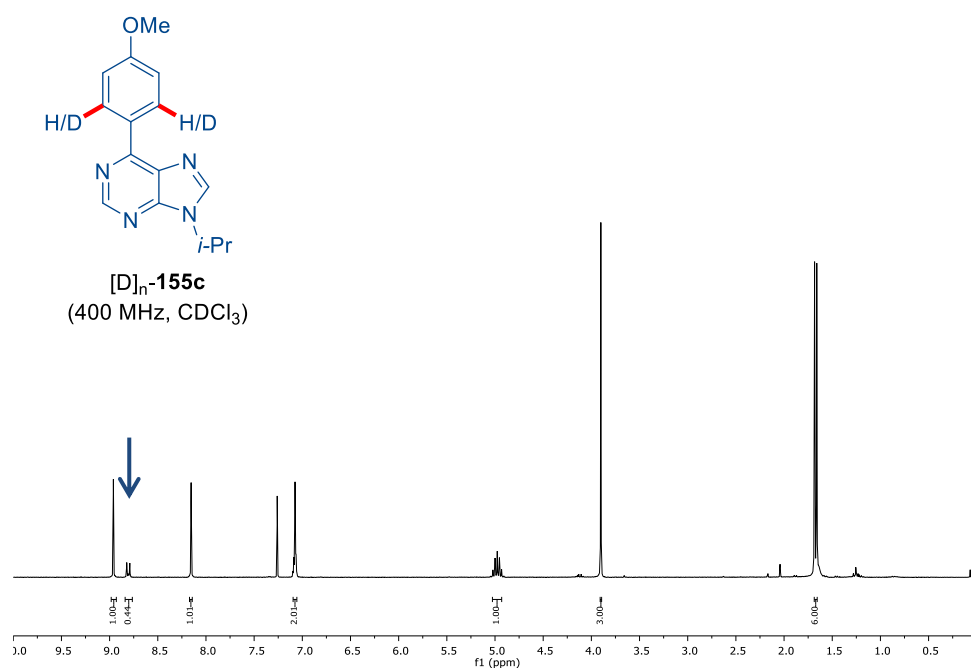
Crystals suitable for X-ray crystallography were grown by slow evaporation from a solution of **228a** in *i*-PrOH.

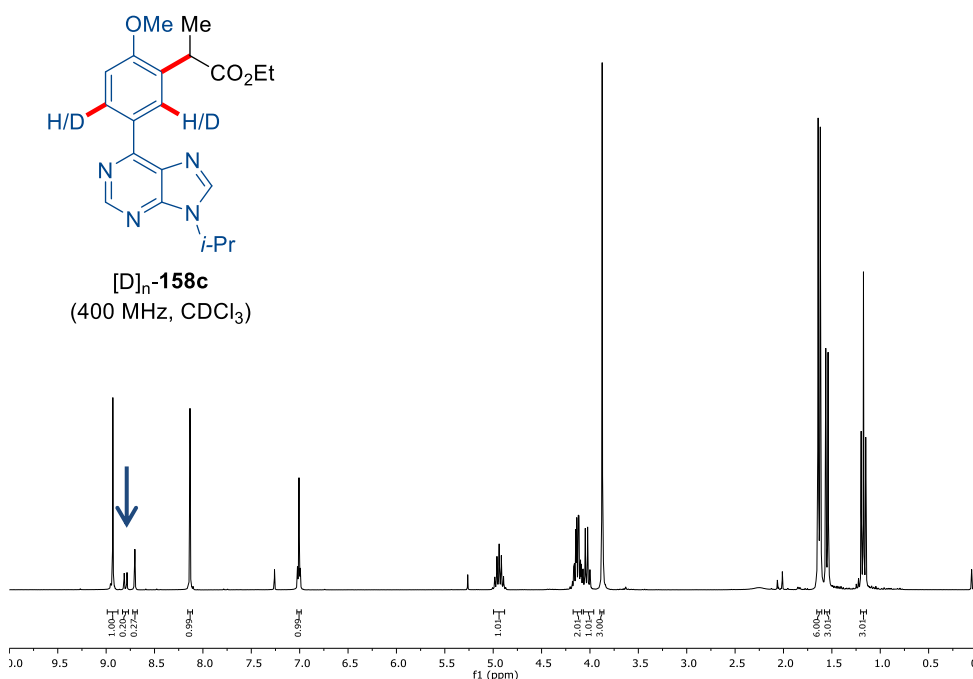
5.7.4. Mechanistic Studies

H/D Exchange

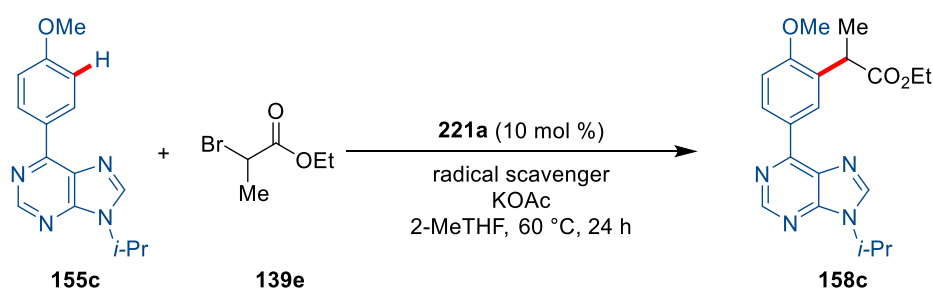
Scheme 5.17. H/D exchange of **155c** with CD_3OD .

The modified procedure **GP-H** was followed using 9-isopropyl-6-(4-methoxyphenyl)-9H-purine (**155c**) (67.1 mg, 0.25 mmol), ethyl 2-bromopropanoate (**139e**) (136 mg, 0.75 mmol), **221b** (30.0 mg, 10.0 mol %), KOAc (49.1 mg, 0.50 mmol) and CD_3OD (80.1 mg, 2.50 mmol) for 8 h. Purification by column chromatography (*n*-hexane/EtOAc: 3/1) yielded $[\text{D}]_n\text{-155c}$ (27.5 mg, 41%) and $[\text{D}]_n\text{-158c}$ (51.5 mg, 56%).



Figure 5.4. H/D exchange of **155c** with CD₃OD.

Effect of Radical Scavengers on the *meta* C–H Alkylation



Scheme 5.18. Effect of radical scavengers.

9-Isopropyl-6-(4-methoxyphenyl)-9*H*-purine (**155c**) (67.1 mg, 0.25 mmol), ethyl 2-bromopropanoate (**139e**) (136 mg, 0.75 mmol), **221a** (26.0 mg, 10 mol %), KOAc (49.1 mg, 0.50 mmol), radical scavenger (TEMPO, 39.1 mg, 0.25 mmol; galvinoxyl free radical, 105.4 mg, 0.25 mmol; 1,1-diphenylethylene, 45.1 mg, 0.25 mmol) were placed into an oven-dried 25 mL Schlenk tube equipped with a septum under Ar atmosphere. 2-MeTHF (2.00 mL) was added and the mixture was stirred at 60 °C for 24 h. **221a** was carefully filtered through a branched filter (Por. 3) and washed with 2-MeTHF (30 mL). The crude filtrate of the reaction with radical scavenger TEMPO was directly analyzed by

5.7. Recyclable Ruthenium Catalyst for remote C–H Activation

HR-MS. All filtrates were concentrated and purification by column chromatography (*n*-hexane/EtOAc: 3/1) provide the following yields of **158c**.

Table 5.8. Effect of radical scavengers TEMPO, galvinoxyl free radical and 1,1-diphenylethylene.

Entry	Radical scavenger (1.0 equiv)	158c / %
1	--	94
2	TEMPO	0
3	Galvinoxyl free radical	0
4	1,1-Diphenylethylene	54

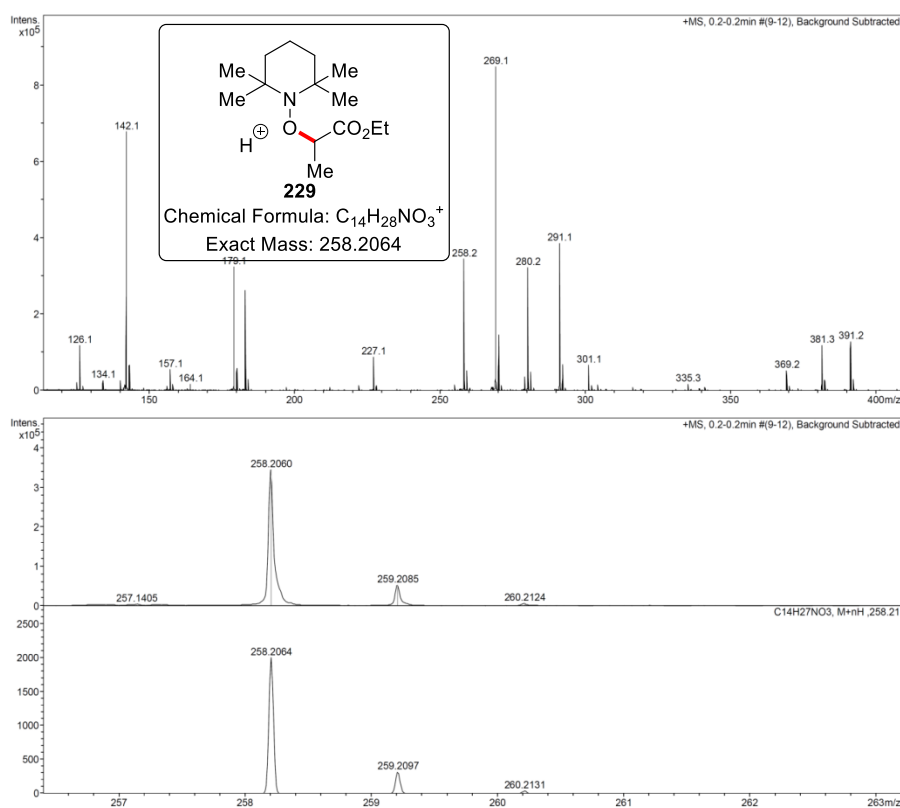
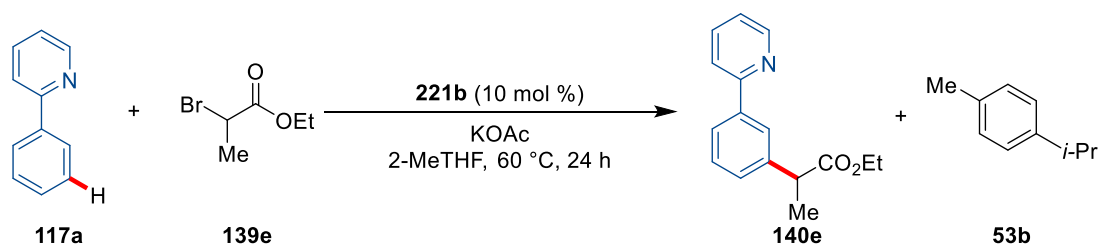


Figure 5.5. Detection of TEMPO adduct **229** by HR-MS.

Detection of free *p*-cymene (**53b**) by gas chromatography (GC) studiesScheme 5.19. Detection of free *p*-cymene.

Independent reactions of 2-phenylpyridine (**117a**) (38.8 mg, 0.25 mmol), ethyl 2-bromopropanoate (**139e**) (136 mg, 0.75 mmol), **221b** (30.0 mg, 10.0 mol %), KOAc (49.1 mg, 0.50 mmol) and *n*-dodecane (30 μ L) were placed into an oven-dried 25 mL Schlenk tube equipped with a septum under Ar atmosphere. 2-MeTHF (2.00 mL) was added and the mixture was stirred at 60 °C for 1, 3, 5, 7, 9, 11, 13, 15, 17, 19 h. After cooling in an ice-bath, an aliquot (0.20 mL) was taken from each reaction by a syringe. The aliquots were diluted with EtOAc, filtered through a short plug of silica gel and analyzed by gas chromatography, provide the following data.

Table 5.9. Conversion *versus* time for **140e** and **53b**.

<i>t</i> / h	140e / mmol	53b / mmol
1	$9.30 \cdot 10^{-4}$	$1.51 \cdot 10^{-4}$
3	$1.72 \cdot 10^{-2}$	$2.49 \cdot 10^{-3}$
5	$4.96 \cdot 10^{-2}$	$4.53 \cdot 10^{-3}$
7	$8.42 \cdot 10^{-2}$	$8.10 \cdot 10^{-3}$
9	$1.15 \cdot 10^{-1}$	$1.16 \cdot 10^{-2}$
11	$1.44 \cdot 10^{-1}$	$1.59 \cdot 10^{-2}$
13	$1.62 \cdot 10^{-1}$	$2.03 \cdot 10^{-2}$
15	$1.85 \cdot 10^{-1}$	$2.23 \cdot 10^{-2}$
17	$2.04 \cdot 10^{-1}$	$2.30 \cdot 10^{-2}$
19	$2.22 \cdot 10^{-1}$	$2.33 \cdot 10^{-2}$
24	$2.33 \cdot 10^{-1}$	$2.35 \cdot 10^{-2}$

5.8. Crystallographic Data

The crystal structures of **195**, **202h**, **189f** and **228a** were measured and resolved by Dr. Christopher Golz.

A suitable crystal was selected and mounted on a 'Bruker APEX-II CCD' diffractometer. The crystal was kept at 100.0 K during data collection. Using Olex2,^[372] the structure was resolved with the XT^[373] structure solution program using Intrinsic Phasing and refined with the SHELXL^[374] refinement package using Least Squares minimisation.

X-Ray Crystallographic Data of **195**

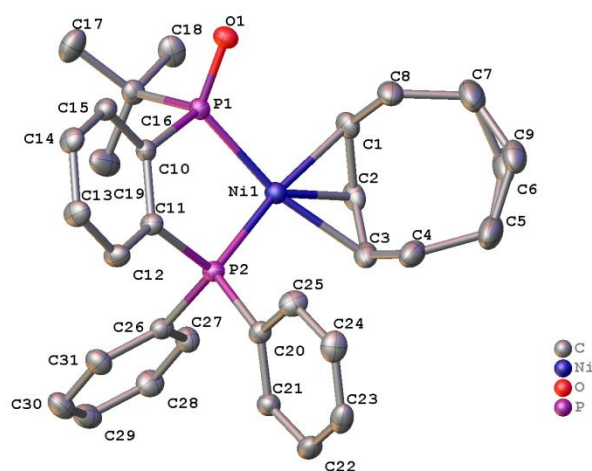


Figure 5.6. Molecular structure of **195** with thermal ellipsoids at 50% probability level. The hydrogen atoms are omitted for clarity.

Table 5.9. Crystal data and structure refinement for **195**.

Compound	195
CCDC number	1991589
Identification code	0730_CG_0m
Empirical formula	C ₃₀ H ₃₆ NiOP ₂
Formula weight	533.24
Temperature/K	100.0
Crystal system	monoclinic
Space group	P2 ₁ /n
a/Å	16.4441(17)
b/Å	10.3116(9)
c/Å	16.7804(17)

$\alpha/^\circ$	90
$\beta/^\circ$	106.122(3)
$\gamma/^\circ$	90
Volume/ \AA^3	2733.5(5)
Z	4
$\rho_{\text{calc}}/\text{g/cm}^3$	1.296
μ/mm^{-1}	0.847
F(000)	1128.0
Crystal size/ mm^3	$0.672 \times 0.195 \times 0.148$
Radiation	MoK α ($\lambda = 0.71073$)
2 Θ range for data collection/ $^\circ$	4.69 to 57.5
Index ranges	$-21 \leq h \leq 22, -13 \leq k \leq 12, -22 \leq l \leq 22$
Reflections collected	46944
Independent reflections	7061 [$R_{\text{int}} = 0.0241, R_{\text{sigma}} = 0.0155$]
Data/restraints/parameters	7061/0/356
Goodness-of-fit on F^2	1.043
Final R indexes [$I > 2\sigma(I)$]	$R_1 = 0.0279, wR_2 = 0.0717$
Final R indexes [all data]	$R_1 = 0.0304, wR_2 = 0.0736$
Largest diff. peak/hole / $e \text{\AA}^{-3}$	0.91/-0.51

Table 5.10. Bond lengths [\AA] for 195.

Atom	Atom	Length/ \AA	Atom	Atom	Length/ \AA
Ni1	P1	2.1881(4)	C10	C11	1.3977(18)
Ni1	P2	2.1300(4)	C10	C15	1.3995(18)
Ni1	C1	2.0360(14)	C11	C12	1.3996(18)
Ni1	C2	1.9624(13)	C12	C13	1.387(2)
Ni1	C3	2.0930(14)	C13	C14	1.391(2)
P1	O1	1.5134(10)	C14	C15	1.3879(19)
P1	C10	1.8485(13)	C16	C17	1.528(2)
P1	C16	1.8717(14)	C16	C18	1.5270(19)
P2	C11	1.8189(13)	C16	C19	1.527(2)
P2	C20	1.8169(13)	C20	C21	1.3907(18)
P2	C26	1.8172(14)	C20	C25	1.3975(19)

Atom	Atom	Length/Å	Atom	Atom	Length/Å
C1	C2	1.416(2)	C21	C22	1.3947(19)
C1	C8	1.516(2)	C22	C23	1.383(2)
C2	C3	1.401(2)	C23	C24	1.385(2)
C3	C4	1.516(2)	C24	C25	1.385(2)
C4	C5	1.546(2)	C26	C27	1.3977(19)
C5	C6	1.529(3)	C26	C31	1.3926(19)
C5	C9	1.500(16)	C27	C28	1.3900(19)
C6	C7	1.509(3)	C28	C29	1.383(2)
C7	C8	1.540(2)	C29	C30	1.389(2)
C7	C9	1.529(17)	C30	C31	1.386(2)

Table 5.11. Bond angles [°] for **195**.

Atom	Atom	Atom	Angle/°	Atom	Atom	Atom	Angle/°
P2	Ni1	P1	91.360(14)	C9	C7	C8	118.7(6)
C1	Ni1	P1	94.97(4)	C1	C8	C7	114.01(14)
C1	Ni1	P2	171.43(4)	C5	C9	C7	119.2(10)
C1	Ni1	C3	73.91(6)	C11	C10	P1	119.62(9)
C2	Ni1	P1	132.56(5)	C11	C10	C15	118.79(12)
C2	Ni1	P2	134.33(5)	C15	C10	P1	121.19(10)
C2	Ni1	C1	41.43(6)	C10	C11	P2	115.33(9)
C2	Ni1	C3	40.25(6)	C10	C11	C12	120.50(12)
C3	Ni1	P1	166.86(4)	C12	C11	P2	123.89(10)
C3	Ni1	P2	99.05(4)	C13	C12	C11	119.68(13)
O1	P1	Ni1	120.75(4)	C12	C13	C14	120.41(13)
O1	P1	C10	107.53(6)	C15	C14	C13	119.76(12)
O1	P1	C16	108.41(6)	C14	C15	C10	120.85(12)
C10	P1	Ni1	103.11(4)	C17	C16	P1	109.50(10)
C10	P1	C16	103.87(6)	C18	C16	P1	107.55(9)
C16	P1	Ni1	111.66(5)	C18	C16	C17	108.79(12)
C11	P2	Ni1	107.39(4)	C18	C16	C19	109.60(12)
C20	P2	Ni1	117.77(5)	C19	C16	P1	110.51(10)
C20	P2	C11	104.03(6)	C19	C16	C17	110.82(13)

5. Experimental Part

Atom	Atom	Atom	Angle/°	Atom	Atom	Atom	Angle/°
C20	P2	C26	104.71(6)	C21	C20	P2	122.81(10)
C26	P2	Ni1	113.97(4)	C21	C20	C25	119.47(13)
C26	P2	C11	108.24(6)	C25	C20	P2	117.51(10)
C2	C1	Ni1	66.50(8)	C20	C21	C22	119.91(13)
C2	C1	C8	124.51(14)	C23	C22	C21	120.25(14)
C8	C1	Ni1	106.14(10)	C22	C23	C24	119.94(13)
C1	C2	Ni1	72.07(8)	C25	C24	C23	120.30(14)
C3	C2	Ni1	74.90(8)	C24	C25	C20	120.13(14)
C3	C2	C1	123.64(13)	C27	C26	P2	117.97(10)
C2	C3	Ni1	64.85(8)	C31	C26	P2	123.07(10)
C2	C3	C4	125.21(13)	C31	C26	C27	118.96(13)
C4	C3	Ni1	106.27(9)	C28	C27	C26	120.24(13)
C3	C4	C5	113.86(15)	C29	C28	C27	120.11(14)
C6	C5	C4	117.46(15)	C28	C29	C30	120.17(14)
C9	C5	C4	120.4(6)	C31	C30	C29	119.77(14)
C7	C6	C5	118.54(18)	C30	C31	C26	120.75(14)
C6	C7	C8	116.81(15)				

X-Ray Crystallographic Data of 202h

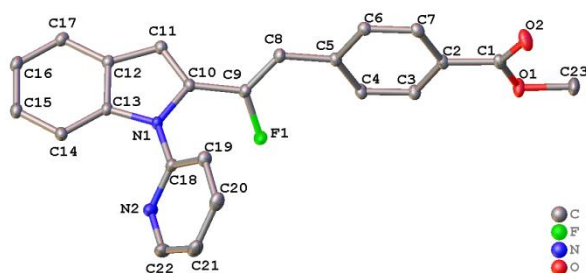


Figure 5.7. Molecular structure of **202h** with thermal ellipsoids at 50% probability level. The hydrogen atoms are omitted for clarity.

Table 5.12. Crystal data and structure refinement for **202h**.

Compound	202h
CCDC number	2032461
Identification code	mo_1023_CG_0m

Empirical formula	C ₂₃ H ₁₇ FN ₂ O ₂
Formula weight	372.38
Temperature/K	100.0
Crystal system	monoclinic
Space group	P2 ₁ /n
a/Å	13.7070(8)
b/Å	8.8511(8)
c/Å	14.7691(14)
α/°	90
β/°	94.024(3)
γ/°	90
Volume/Å ³	1787.4(3)
Z	4
ρ _{calc} /g/cm ³	1.384
μ/mm ⁻¹	0.096
F(000)	776.0
Crystal size/mm ³	0.477 × 0.261 × 0.151
Radiation	MoKα (λ = 0.71073)
2θ range for data collection/°	3.92 to 61.078
Index ranges	-19 ≤ h ≤ 19, -12 ≤ k ≤ 12, -21 ≤ l ≤ 21
Reflections collected	99403
Independent reflections	5466 [R _{int} = 0.0226, R _{sigma} = 0.0092]
Data/restraints/parameters	5466/0/254
Goodness-of-fit on F ²	1.033
Final R indexes [I ≥ 2σ (I)]	R ₁ = 0.0368, wR ₂ = 0.0989
Final R indexes [all data]	R ₁ = 0.0384, wR ₂ = 0.1007
Largest diff. peak/hole / e Å ⁻³	0.43/-0.23

Table 5.13. Bond lengths [Å] for 202h.

Atom	Atom	Length/Å	Atom	Atom	Length/Å
F1	C9	1.3641(9)	C6	C7	1.3878(11)
O1	C1	1.3347(11)	C8	C9	1.3351(11)
O1	C23	1.4400(10)	C9	C10	1.4573(11)

5. Experimental Part

Atom	Atom	Length/Å	Atom	Atom	Length/Å
O2	C1	1.2103(10)	C10	C11	1.3737(11)
N1	C10	1.3968(10)	C11	C12	1.4334(11)
N1	C13	1.3917(9)	C12	C13	1.4114(11)
N1	C18	1.4200(10)	C12	C17	1.4070(11)
N2	C18	1.3338(11)	C13	C14	1.3978(11)
N2	C22	1.3418(12)	C14	C15	1.3849(11)
C1	C2	1.4868(11)	C15	C16	1.4080(12)
C2	C3	1.3979(11)	C16	C17	1.3824(12)
C2	C7	1.3963(11)	C18	C19	1.3898(11)
C3	C4	1.3903(11)	C19	C20	1.3921(12)
C4	C5	1.4057(11)	C20	C21	1.3886(14)
C5	C6	1.4044(11)	C21	C22	1.3851(14)
C5	C8	1.4678(11)			

Table 5.14. Bond angles [°] for 202h.

Atom	Atom	Atom	Angle/°	Atom	Atom	Atom	Angle/°
C1	O1	C23	115.99(7)	N1	C10	C9	121.89(7)
C10	N1	C18	126.69(7)	C11	C10	N1	109.52(7)
C13	N1	C10	108.20(6)	C11	C10	C9	128.22(7)
C13	N1	C18	124.64(7)	C10	C11	C12	107.20(7)
C18	N2	C22	116.67(8)	C13	C12	C11	107.27(7)
O1	C1	C2	112.32(7)	C17	C12	C11	133.52(8)
O2	C1	O1	123.52(8)	C17	C12	C13	119.21(7)
O2	C1	C2	124.16(8)	N1	C13	C12	107.81(7)
C3	C2	C1	121.82(7)	N1	C13	C14	129.60(7)
C7	C2	C1	118.15(7)	C14	C13	C12	122.59(7)
C7	C2	C3	120.03(7)	C15	C14	C13	116.80(8)
C4	C3	C2	120.10(7)	C14	C15	C16	121.70(8)
C3	C4	C5	120.43(7)	C17	C16	C15	121.19(7)
C4	C5	C8	123.66(7)	C16	C17	C12	118.50(8)
C6	C5	C4	118.71(7)	N2	C18	N1	115.22(7)
C6	C5	C8	117.63(7)	N2	C18	C19	124.30(8)

Atom	Atom	Atom	Angle/°	Atom	Atom	Atom	Angle/°
C7	C6	C5	120.95(7)	C19	C18	N1	120.48(7)
C6	C7	C2	119.76(7)	C18	C19	C20	117.86(8)
C9	C8	C5	127.87(7)	C21	C20	C19	118.91(8)
F1	C9	C10	112.68(6)	C22	C21	C20	118.37(8)
C8	C9	F1	119.99(7)	N2	C22	C21	123.87(9)
C8	C9	C10	127.31(7)				

X-Ray Crystallographic Data of 189f

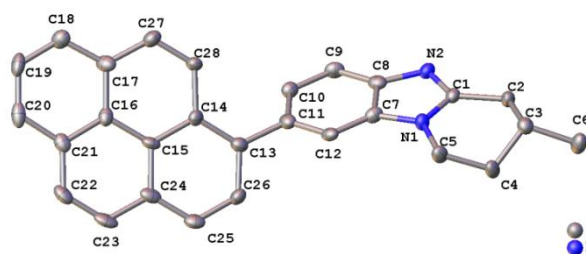


Figure 5.8. Molecular structure of **189f** with thermal ellipsoids at 50% probability level. The hydrogen atoms are omitted for clarity.

Table 5.15. Crystal data and structure refinement for **189f**.

Compound	189f
CCDC number	1886748
Empirical formula	C ₂₈ H ₂₂ N ₂
Formula weight	386.47
Temperature/K	100.01
Crystal system	triclinic
Space group	P1
a/Å	8.3387(3)
b/Å	8.3450(3)
c/Å	28.1990(11)
α/°	97.8300(10)
β/°	96.8240(10)
γ/°	90.1480(10)
Volume/Å ³	1929.85(12)

Z	4
$\rho_{\text{calc}}/\text{g}/\text{cm}^3$	1.330
μ/mm^{-1}	0.596
F(000)	816.0
Crystal size/ mm^3	$0.211 \times 0.169 \times 0.114$
Radiation	CuK α ($\lambda = 1.54178$)
2Θ range for data collection/ $^\circ$	6.374 to 149.142
Index ranges	$-10 \leq h \leq 10, -10 \leq k \leq 10, -34 \leq l \leq 35$
Reflections collected	49175
Independent reflections	14978 [$R_{\text{int}} = 0.0312, R_{\text{sigma}} = 0.0320$]
Data/restraints/parameters	14978/3/1086
Goodness-of-fit on F^2	1.085
Final R indexes [$I > 2\sigma(I)$]	$R_1 = 0.0830, wR_2 = 0.2176$
Final R indexes [all data]	$R_1 = 0.0831, wR_2 = 0.2177$
Largest diff. peak/hole / $e \text{ \AA}^{-3}$	0.48/-0.39
Flack parameter	0.09(11)

Table 5.16. Bond lengths [\AA] for **189f**.

Atom	Atom	Length/ \AA	Atom	Atom	Length/ \AA
N1	C1	1.383(8)	C13	C26	1.411(9)
N1	C5	1.470(8)	C14	C15	1.423(9)
N1	C7	1.384(9)	C14	C28	1.452(9)
N2	C1	1.321(8)	C15	C16	1.431(10)
N2	C8	1.404(9)	C15	C24	1.417(9)
C1	C2	1.496(9)	C16	C17	1.437(10)
C2	C3	1.537(10)	C16	C21	1.414(9)
C3	C4	1.512(9)	C17	C18	1.396(11)
C3	C6	1.533(10)	C17	C27	1.437(10)
C4	C5	1.500(10)	C18	C19	1.380(10)
C7	C8	1.405(9)	C19	C20	1.355(12)
C7	C12	1.376(9)	C20	C21	1.421(11)
C8	C9	1.387(10)	C21	C22	1.404(10)
C9	C10	1.393(10)	C22	C23	1.361(12)

Atom	Atom	Length/Å	Atom	Atom	Length/Å
C10	C11	1.398(9)	C23	C24	1.429(10)
C11	C12	1.382(10)	C24	C25	1.388(11)
C11	C13	1.502(9)	C25	C26	1.392(10)
C13	C14	1.403(10)	C27	C28	1.344(10)

Table 5.17. Bond angles [°] for **189f**.

Atom	Atom	Atom	Angle/°	Atom	Atom	Atom	Angle/°
C1	N1	C5	124.3(5)	C15	C14	C28	117.3(6)
C1	N1	C7	108.3(5)	C14	C15	C16	121.1(6)
C7	N1	C5	127.3(5)	C24	C15	C14	120.3(6)
C1	N2	C8	105.6(5)	C24	C15	C16	118.6(6)
N1	C1	C2	122.3(6)	C15	C16	C17	119.3(6)
N2	C1	N1	111.4(6)	C21	C16	C15	119.8(6)
N2	C1	C2	126.1(6)	C21	C16	C17	120.9(6)
C1	C2	C3	112.0(6)	C24	C15	C16	118.6(6)
C4	C3	C2	111.2(5)	C15	C16	C17	119.3(6)
C4	C3	C6	109.8(6)	C21	C16	C15	119.8(6)
C6	C3	C2	109.5(6)	C21	C16	C17	120.9(6)
C5	C4	C3	112.7(6)	C16	C17	C27	118.4(6)
N1	C5	C4	110.0(6)	C18	C17	C16	117.4(6)
N1	C7	C8	104.6(6)	C18	C17	C27	124.2(7)
C12	C7	N1	131.4(6)	C19	C18	C17	121.7(7)
C12	C7	C8	124.0(6)	C20	C19	C18	120.8(7)
N2	C8	C7	110.0(6)	C19	C20	C21	121.6(7)
C9	C8	N2	131.3(6)	C16	C21	C20	117.5(7)
C9	C8	C7	118.5(6)	C22	C21	C16	120.2(7)
C8	C9	C10	118.4(6)	C22	C21	C20	122.3(7)
C9	C10	C11	121.4(6)	C23	C22	C21	120.7(7)
C10	C11	C13	120.3(6)	C22	C23	C24	120.9(7)
C12	C11	C10	121.1(6)	C15	C24	C23	119.8(7)
C12	C11	C13	118.5(6)	C25	C24	C15	119.0(7)
C7	C12	C11	116.6(6)	C25	C24	C23	121.2(6)

Atom	Atom	Atom	Angle/°	Atom	Atom	Atom	Angle/°
C14	C13	C11	123.9(6)	C24	C25	C26	120.6(6)
C14	C13	C26	118.2(6)	C25	C26	C13	121.7(6)
C26	C13	C11	117.9(6)	C28	C27	C17	121.8(7)
C13	C14	C15	120.1(6)	C27	C28	C14	122.0(6)
C13	C14	C28	122.6(6)				

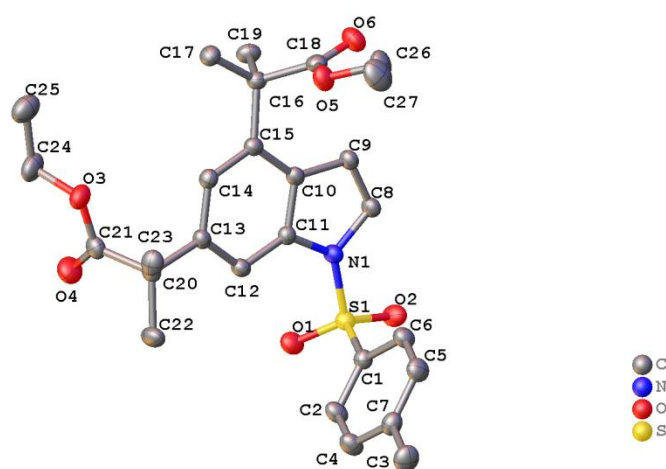
X-Ray Crystallographic Data of **228a**

Figure 5.9. Molecular structure of **228a** with thermal ellipsoids at 50% probability level. The hydrogen atoms are omitted for clarity.

Table 5.18. Crystal data and structure refinement for **228a**.

Compound	228a
CCDC number	2032462
Identification code	mo_1077_CG_0m
Empirical formula	$C_{27}H_{33}NO_6S$
Formula weight	499.60
Temperature/K	100.0
Crystal system	triclinic
Space group	P-1
a/Å	12.6388(14)
b/Å	13.6307(14)
c/Å	15.2519(17)

$\alpha/^\circ$	83.546(3)
$\beta/^\circ$	83.600(3)
$\gamma/^\circ$	87.659(3)
Volume/ \AA^3	2593.5(5)
Z	4
$\rho_{\text{calc}}/\text{g/cm}^3$	1.280
μ/mm^{-1}	0.166
F(000)	1064.0
Crystal size/ mm^3	$0.382 \times 0.278 \times 0.126$
Radiation	MoK α ($\lambda = 0.71073$)
2 Θ range for data collection/ $^\circ$	3.992 to 61.208
Index ranges	$-17 \leq h \leq 18, -19 \leq k \leq 18, -21 \leq l \leq 21$
Reflections collected	164957
Independent reflections	15828 [$R_{\text{int}} = 0.0336, R_{\text{sigma}} = 0.0197$]
Data/restraints/parameters	15828/0/645
Goodness-of-fit on F^2	1.028
Final R indexes [$I \geq 2\sigma(I)$]	$R_1 = 0.0376, wR_2 = 0.0910$
Final R indexes [all data]	$R_1 = 0.0468, wR_2 = 0.1000$
Largest diff. peak/hole / $e \text{\AA}^{-3}$	0.47/-0.54

Table 5.19. Bond lengths [\AA] for 228a.

Atom	Atom	Length/ \AA	Atom	Atom	Length/ \AA
S1	O1	1.4305(8)	S2	O7	1.4311(9)
S1	O2	1.4317(8)	S2	O8	1.4312(9)
S1	N1	1.6557(9)	S2	N2	1.6645(10)
S1	C1	1.7512(11)	S2	C28	1.7494(11)
O3	C21	1.3410(14)	O9	C45	1.3447(16)
O3	C24	1.4590(14)	O9	C51	1.4554(16)
O4	C21	1.2090(14)	O10	C45	1.2023(15)
O5	C18	1.3416(14)	O11	C49	1.3290(14)
O5	C26	1.4619(14)	O11	C53	1.4615(15)
O6	C18	1.2037(14)	O12	C49	1.2040(14)
N1	C8	1.3997(13)	N2	C35	1.4049(13)

5. Experimental Part

Atom	Atom	Length/Å	Atom	Atom	Length/Å
N1	C11	1.4026(13)	N2	C42	1.4041(13)
C1	C2	1.3863(15)	C28	C29	1.3911(15)
C1	C6	1.3934(15)	C28	C33	1.3932(15)
C2	C3	1.3878(16)	C29	C30	1.3889(17)
C3	C4	1.3932(16)	C30	C31	1.3957(17)
C4	C5	1.3970(16)	C31	C32	1.3956(17)
C4	C7	1.5021(16)	C31	C34	1.5047(17)
C5	C6	1.3872(16)	C32	C33	1.3862(16)
C8	C9	1.3499(15)	C35	C36	1.3539(16)
C9	C10	1.4474(14)	C36	C37	1.4490(14)
C10	C11	1.4030(14)	C37	C38	1.4109(15)
C10	C15	1.4105(14)	C37	C42	1.4093(14)
C11	C12	1.3949(14)	C38	C39	1.3880(14)
C12	C13	1.3849(15)	C38	C47	1.5321(14)
C13	C14	1.4165(14)	C39	C40	1.4155(15)
C13	C20	1.5400(14)	C40	C41	1.3837(15)
C14	C15	1.3880(14)	C40	C43	1.5342(15)
C15	C16	1.5324(14)	C41	C42	1.3953(14)
C16	C17	1.5372(15)	C43	C44	1.5340(17)
C16	C18	1.5384(15)	C43	C45	1.5315(17)
C16	C19	1.5393(15)	C43	C46	1.5366(16)
C20	C21	1.5348(15)	C47	C48	1.5385(16)
C20	C22	1.5324(16)	C47	C49	1.5325(15)
C20	C23	1.5396(16)	C47	C50	1.5393(16)
C24	C25	1.4943(19)	C51	C52	1.5073(19)
C26	C27	1.4982(19)	C53	C54	1.496(2)

Table 5.20. Bond angles [°] for 228a.

Atom	Atom	Atom	Angle/°	Atom	Atom	Atom	Angle/°
O1	S1	O2	119.90(5)	O7	S2	N2	106.67(5)
O1	S1	N1	108.03(5)	O7	S2	C28	108.66(5)
O1	S1	C1	108.31(5)	O8	S2	O7	120.69(5)

Atom	Atom	Atom	Angle/°	Atom	Atom	Atom	Angle/°
O2	S1	N1	104.78(5)	O8	S2	N2	104.91(5)
O2	S1	C1	110.59(5)	O8	S2	C28	109.41(5)
N1	S1	C1	104.01(5)	N2	S2	C28	105.40(5)
C21	O3	C24	115.26(9)	C45	O9	C51	116.03(11)
C18	O5	C26	115.04(9)	C49	O11	C53	115.95(10)
C8	N1	S1	124.52(7)	C35	N2	S2	124.17(8)
C8	N1	C11	108.60(8)	C42	N2	S2	126.32(7)
C11	N1	S1	126.73(7)	C42	N2	C35	108.49(9)
C2	C1	S1	118.10(8)	C29	C28	S2	119.81(9)
C2	C1	C6	121.39(10)	C29	C28	C33	121.16(10)
C6	C1	S1	120.50(8)	C33	C28	S2	119.02(9)
C1	C2	C3	118.89(10)	C30	C29	C28	118.98(11)
C2	C3	C4	121.13(10)	C29	C30	C31	121.02(11)
C3	C4	C5	118.80(10)	C30	C31	C34	120.90(11)
C3	C4	C7	120.11(11)	C32	C31	C30	118.77(11)
C5	C4	C7	121.08(11)	C32	C31	C34	120.34(11)
C6	C5	C4	121.00(10)	C33	C32	C31	121.17(11)
C5	C6	C1	118.79(10)	C32	C33	C28	118.91(11)
C9	C8	N1	109.23(9)	C36	C35	N2	109.29(9)
C8	C9	C10	107.91(9)	C35	C36	C37	107.94(9)
C11	C10	C9	107.10(9)	C38	C37	C36	134.05(10)
C11	C10	C15	118.57(9)	C42	C37	C36	107.03(9)
C15	C10	C9	134.34(10)	C42	C37	C38	118.91(9)
N1	C11	C10	107.11(9)	C37	C38	C47	121.19(9)
C12	C11	N1	128.95(9)	C39	C38	C37	117.12(9)
C12	C11	C10	123.91(10)	C39	C38	C47	121.59(10)
C13	C12	C11	117.26(9)	C38	C39	C40	123.20(10)
C12	C13	C14	119.55(9)	C39	C40	C43	118.35(10)
C12	C13	C20	120.70(9)	C41	C40	C39	119.93(10)
C14	C13	C20	119.75(9)	C41	C40	C43	121.70(9)
C15	C14	C13	123.08(10)	C40	C41	C42	117.09(10)
C10	C15	C16	119.99(9)	N2	C42	C37	107.22(9)

5. Experimental Part

Atom	Atom	Atom	Angle/°	Atom	Atom	Atom	Angle/°
C14	C15	C10	117.47(9)	C41	C42	N2	129.11(10)
C14	C15	C16	122.40(9)	C41	C42	C37	123.67(10)
C15	C16	C17	112.87(9)	C40	C43	C46	112.88(9)
C15	C16	C18	109.10(8)	C44	C43	C40	109.53(9)
C15	C16	C19	108.47(9)	C44	C43	C46	109.54(10)
C17	C16	C18	108.82(9)	C45	C43	C40	106.84(9)
C17	C16	C19	108.53(9)	C45	C43	C44	108.80(10)
C18	C16	C19	108.97(9)	C45	C43	C46	109.14(10)
O5	C18	C16	112.19(9)	O9	C45	C43	111.05(10)
O6	C18	O5	123.00(10)	O10	C45	O9	123.76(12)
O6	C18	C16	124.80(10)	O10	C45	C43	125.17(12)
C21	C20	C13	106.58(8)	C38	C47	C48	109.37(9)
C21	C20	C23	111.27(9)	C38	C47	C49	110.68(9)
C22	C20	C13	112.56(9)	C38	C47	C50	112.34(9)
C22	C20	C21	107.61(9)	C48	C47	C50	109.32(9)
C22	C20	C23	108.68(9)	C49	C47	C48	108.53(9)
C23	C20	C13	110.12(9)	C49	C47	C50	106.50(9)
O3	C21	C20	112.60(9)	O11	C49	C47	111.60(9)
O4	C21	O3	123.06(11)	O12	C49	O11	123.67(10)
O4	C21	C20	124.29(11)	O12	C49	C47	124.67(10)
O3	C24	C25	107.89(10)	O9	C51	C52	111.39(11)
O5	C26	C27	107.96(10)	O11	C53	C54	111.82(12)

6. References

- [1] J. Garcia - Martinez, E. Serrano - Torregrosa, *The Chemical Element: Chemistry's Contribution to Our Global Future, First Edition*, Wiley-VCH, Weinheim, **2011**.
- [2] a) P. T. Anastas, M. M. Kirchhoff, *Acc. Chem. Res.* **2002**, *35*, 686–694; b) P. T. Anastas, J. C. Warner, *Green Chemistry: Theory and Practice*, Oxford University Press, Oxford, **1998**.
- [3] D. Rodríguez-Padrón, A. R. Puente-Santiago, A. M. Balu, M. J. Muñoz-Batista, R. Luque, *ChemCatChem* **2019**, *11*, 18–38.
- [4] a) B. M. Trost, *Angew. Chem. Int. Ed.* **1995**, *34*, 259–281; b) B. M. Trost, *Science* **1991**, *254*, 1471–1477.
- [5] C. C. C. Johansson Seechurn, M. O. Kitching, T. J. Colacot, V. Snieckus, *Angew. Chem. Int. Ed.* **2012**, *51*, 5062–5085.
- [6] C. Glaser, *Ber. Dtsch. Chem. Ges.* **1869**, *2*, 422–424.
- [7] F. Ullmann, J. Bielecki, *Ber. Dtsch. Chem. Ges.* **1901**, *34*, 2174–2185.
- [8] a) N. Miyaura, A. Suzuki, *Chem. Rev.* **1995**, *95*, 2457–2483; b) N. Miyaura, K. Yamada, A. Suzuki, *Tetrahedron Lett.* **1979**, *20*, 3437–3440; c) N. Miyaura, A. Suzuki, *Chem. Commun.* **1979**, 866–867.
- [9] a) E.-i. Negishi, A. O. King, N. Okukado, *J. Org. Chem.* **1977**, *42*, 1821–1823; b) A. O. King, N. Okukado, E.-i. Negishi, *Chem. Commun.* **1977**, 683–684.
- [10] a) R. F. Heck, J. P. Nolley, *J. Org. Chem.* **1972**, *37*, 2320–2322; b) M. Tsutomu, M. Kunio, O. Atsumu, *Bull. Chem. Soc. Jpn.* **1971**, *44*, 581–581.
- [11] a) K. Tamao, K. Sumitani, M. Kumada, *J. Am. Chem. Soc.* **1972**, *94*, 4374–4376; b) R. J. P. Corriu, J. P. Masse, *Chem. Commun.* **1972**, 144–144.
- [12] a) T. Hiyama, *J. Organomet. Chem.* **2002**, *653*, 58–61; b) Y. Hatanaka, T. Hiyama, *J. Org. Chem.* **1988**, *53*, 918–920.
- [13] a) J. K. Stille, *Angew. Chem. Int. Ed.* **1986**, *25*, 508–524; b) D. Milstein, J. K. Stille, *J. Am. Chem. Soc.* **1979**, *101*, 4992–4998; c) D. Milstein, J. K. Stille, *J. Am. Chem. Soc.* **1978**, *100*, 3636–3638.
- [14] a) R. Chinchilla, C. Nájera, *Chem. Soc. Rev.* **2011**, *40*, 5084–5121; b) K. Sonogashira, *J. Organomet. Chem.* **2002**, *653*, 46–49; c) K. Sonogashira, Y. Tohda, N. Hagihara, *Tetrahedron Lett.* **1975**, *16*, 4467–4470.

- [15] A. de Meijere, S. Bräse, M. Oestreich, *Metal-Catalyzed Cross-Coupling Reactions and More*, Wiley-VCH, Weinheim, **2014**.
- [16] The Nobel Prize in Chemistry 2010, NobelPrize.org Nobel Media AB, accessed on 08.11.2020, retrieved from <https://www.nobelprize.org/prizes/chemistry/2010/summary/>.
- [17] a) A. Piontek, E. Bisz, M. Szostak, *Angew. Chem. Int. Ed.* **2018**, *57*, 11116–11128; b) T. Iwasaki, N. Kambe, *Top. Curr. Chem.* **2016**, *374*, 66; c) L. N. Cavalcanti, G. A. Molander, *Top. Curr. Chem.* **2016**, *374*, 39; d) E. Nakamura, T. Hatakeyama, S. Ito, K. Ishizuka, L. Ilies, M. Nakamura, *Org. React.* **2014**, 1–210.
- [18] a) P. Gandeepan, N. Kaplaneris, S. Santoro, L. Vaccaro, L. Ackermann, *ACS Sustain. Chem. Eng.* **2019**, *7*, 8023–8040; b) E. Bisz, M. Szostak, *ChemSusChem* **2018**, *11*, 1290–1294; c) S. Santoro, F. Ferlin, L. Luciani, L. Ackermann, L. Vaccaro, *Green Chem.* **2017**, *19*, 1601–1612; d) S. Monticelli, L. Castoldi, I. Murgia, R. Senatore, E. Mazzeo, J. Wackerlig, E. Urban, T. Langer, V. Pace, *Monatsh. Chem.* **2017**, *148*, 37–48.
- [19] a) S. Santoro, S. I. Kozhushkov, L. Ackermann, L. Vaccaro, *Green Chem.* **2016**, *18*, 3471–3493; b) Á. Molnár, *Chem. Rev.* **2011**, *111*, 2251–2320; c) M. Benaglia, *Recoverable and Recyclable Catalysts*, Wiley-VCH, Weinheim, **2009**.
- [20] a) T. Gensch, M. J. James, T. Dalton, F. Glorius, *Angew. Chem. Int. Ed.* **2018**, *57*, 2296–2306; b) J.-C. Hierso, M. Beaupérin, P. Meunier, *Eur. J. Inorg. Chem.* **2007**, *2007*, 3767–3780.
- [21] C.-J. Li, *Green Processes*, Wiley-VCH, Weinheim, **2012**.
- [22] a) T. H. Meyer, L. H. Finger, P. Gandeepan, L. Ackermann, *Trends Chem.* **2019**, *1*, 63–76; b) P. Gandeepan, T. Müller, D. Zell, G. Cera, S. Warratz, L. Ackermann, *Chem. Rev.* **2019**, *119*, 2192–2452; c) C.-S. Wang, P. H. Dixneuf, J.-F. Soulé, *Chem. Rev.* **2018**, *118*, 7532–7585; d) J. C. K. Chu, T. Rovis, *Angew. Chem. Int. Ed.* **2018**, *57*, 62–101; e) Y. Park, Y. Kim, S. Chang, *Chem. Rev.* **2017**, *117*, 9247–9301; f) M. M. Lorion, K. Maindan, A. R. Kapdi, L. Ackermann, *Chem. Soc. Rev.* **2017**, *46*, 7399–7420; g) J. A. Leitch, C. G. Frost, *Chem. Soc. Rev.* **2017**, *46*, 7145–7153; h) J. He, M. Wasa, K. S. L. Chan, Q. Shao, J.-Q. Yu, *Chem. Rev.* **2017**, *117*, 8754–8786; i) Q.-Z. Zheng, N. Jiao, *Chem. Soc. Rev.* **2016**, *45*, 4590–4627; j) O. Daugulis, J. Roane, L. D. Tran, *Acc. Chem. Res.* **2015**, *48*, 1053–1064; k) J. Wencel-Delord, F. Glorius, *Nat. Chem.* **2013**, *5*, 369–375; l) G. Rouquet, N. Chatani, *Angew. Chem. Int. Ed.* **2013**, *52*, 11726–11743; m) L.

-
- Ackermann, R. Vicente, A. R. Kapdi, *Angew. Chem. Int. Ed.* **2009**, *48*, 9792–9826; n) L. Ackermann, *Modern Arylation Methods*, Wiley-VCH, Weinheim, **2009**; o) R. G. Bergman, *Nature* **2007**, *446*, 391–393.
- [23] a) S. D. Friis, M. J. Johansson, L. Ackermann, *Nat. Chem.* **2020**, *12*, 511–519; b) M. Seki, *Org. Process Res. Dev.* **2016**, *20*, 867–877; c) L. Ackermann, *Org. Process Res. Dev.* **2015**, *19*, 260–269.
- [24] a) J. Zhang, L. J. Kang, T. C. Parker, S. B. Blakey, C. K. Luscombe, S. R. Marder, *Molecules* **2018**, *23*, 922; b) J.-R. Pouliot, F. Grenier, J. T. Blaskovits, S. Beaupré, M. Leclerc, *Chem. Rev.* **2016**, *116*, 14225–14274; c) D. J. Schipper, K. Fagnou, *Chem. Mater.* **2011**, *23*, 1594–1600.
- [25] a) C. Liu, J. Yuan, M. Gao, S. Tang, W. Li, R. Shi, A. Lei, *Chem. Rev.* **2015**, *115*, 12138–12204; b) S. A. Girard, T. Knauber, C.-J. Li, in *From C-H to C-C Bonds: Cross-Dehydrogenative-Coupling*, The Royal Society of Chemistry, **2015**, pp. 1–32; c) C. S. Yeung, V. M. Dong, *Chem. Rev.* **2011**, *111*, 1215–1292.
- [26] N. Sauermann, T. H. Meyer, Y. Qiu, L. Ackermann, *ACS Catal.* **2018**, *8*, 7086–7103.
- [27] L. Ackermann, B. T. Gunnoe, L. G. Habgood, *Catalytic Hydroarylation of Carbon-Carbon Multiple Bonds*, Wiley-VCH, Weinheim, **2017**.
- [28] Y. R. Luo, *Handbook of bond dissociation energies in organic compounds*, CRC Press, Boca Raton, Florida, **2003**.
- [29] J. F. Hartwig, M. A. Larsen, *ACS Cent. Sci.* **2016**, *2*, 281–292.
- [30] V. K. Tiwari, M. Kapur, *Org. Biomol. Chem.* **2019**, *17*, 1007–1026.
- [31] a) K. Shen, Y. Fu, J.-N. Li, L. Liu, Q.-X. Guo, *Tetrahedron* **2007**, *63*, 1568–1576; b) I. V. Seregin, V. Gevorgyan, *Chem. Soc. Rev.* **2007**, *36*, 1173–1193.
- [32] J. F. Hartwig, *Acc. Chem. Res.* **2012**, *45*, 864–873.
- [33] a) C. Sambigioglio, D. Schönbauer, R. Blicke, T. Dao-Huy, G. Pototschnig, P. Schaaf, T. Wiesinger, M. F. Zia, J. Wencel-Delord, T. Besset, B. U. W. Maes, M. Schnürch, *Chem. Soc. Rev.* **2018**, *47*, 6603–6743; b) W. Ma, P. Gandeepan, J. Li, L. Ackermann, *Organic Chemistry Frontiers* **2017**, *4*, 1435–1467; c) Z. Chen, B. Wang, J. Zhang, W. Yu, Z. Liu, Y. Zhang, *Org. Chem. Front.* **2015**, *2*, 1107–1295.
- [34] S. De Sarkar, W. Liu, S. I. Kozhushkov, L. Ackermann, *Adv. Synth. Catal.* **2014**, *356*, 1461–1479.

- [35] a) S. Rej, N. Chatani, *Angew. Chem. Int. Ed.* **2019**, *58*, 8304–8329; b) W. Ma, P. Gandeepan, J. Li, L. Ackermann, *Org. Chem. Front.* **2017**, *4*, 1435–1467; c) F. Zhang, D. R. Spring, *Chem. Soc. Rev.* **2014**, *43*, 6906–6919; d) G. Rousseau, B. Breit, *Angew. Chem. Int. Ed.* **2011**, *50*, 2450–2494; e) J. Cornella, M. Righi, I. Larrosa, *Angew. Chem. Int. Ed.* **2011**, *50*, 9429–9432.
- [36] P. Gandeepan, L. Ackermann, *Chem* **2018**, *4*, 199–222.
- [37] a) H. Yi, G. Zhang, H. Wang, Z. Huang, J. Wang, A. K. Singh, A. Lei, *Chem. Rev.* **2017**, *117*, 9016–9085; b) J.-T. Yu, C. Pan, *Chem. Commun.* **2016**, *52*, 2220–2236.
- [38] a) L. Ackermann, *Chem. Rev.* **2011**, *111*, 1315–1345; b) D. Balcells, E. Clot, O. Eisenstein, *Chem. Rev.* **2010**, *110*, 749–823; c) Y. Boutadla, D. L. Davies, S. A. Macgregor, A. I. Poblador-Bahamonde, *Dalton Trans.* **2009**, 5820–5831; d) J. A. Labinger, J. E. Bercaw, *Nature* **2002**, *417*, 507–514.
- [39] B. Biswas, M. Sugimoto, S. Sakaki, *Organometallics* **2000**, *19*, 3895–3908.
- [40] a) L. David, F. Keith, *Chem. Lett.* **2010**, *39*, 1118–1126; b) S. I. Gorelsky, D. Lapointe, K. Fagnou, *J. Am. Chem. Soc.* **2008**, *130*, 10848–10849.
- [41] a) R. A. Alharis, C. L. McMullin, D. L. Davies, K. Singh, S. A. Macgregor, *Faraday Discuss.* **2019**, *220*, 386–403; b) R. A. Alharis, C. L. McMullin, D. L. Davies, K. Singh, S. A. Macgregor, *J. Am. Chem. Soc.* **2019**, *141*, 8896–8906; c) Y. Boutadla, D. L. Davies, S. A. Macgregor, A. I. Poblador-Bahamonde, *Dalton Trans.* **2009**, 5887–5893.
- [42] a) D. García-Cuadrado, A. A. C. Braga, F. Maseras, A. M. Echavarren, *J. Am. Chem. Soc.* **2006**, *128*, 1066–1067; b) L.-C. Campeau, M. Parisien, A. Jean, K. Fagnou, *J. Am. Chem. Soc.* **2006**, *128*, 581–590.
- [43] a) T. Rogge, J. C. A. Oliveira, R. Kuniyil, L. Hu, L. Ackermann, *ACS Catal.* **2020**, *10*, 10551–10558; b) D. Zell, M. Bursch, V. Müller, S. Grimme, L. Ackermann, *Angew. Chem. Int. Ed.* **2017**, *56*, 10378–10382; c) W. Liu, S. C. Richter, Y. Zhang, L. Ackermann, *Angew. Chem. Int. Ed.* **2016**, *55*, 7747–7750; d) W. Ma, R. Mei, G. Tenti, L. Ackermann, *Chem. Eur. J.* **2014**, *20*, 15248–15251.
- [44] P. C. J. Kamer, P. W. N. M. van Leeuwen, *Phosphorus(III) Ligands in Homogeneous Catalysis: Design and Synthesis*, Wiley, Chichester, **2012**.
- [45] a) E. Peris, *Chem. Rev.* **2018**, *118*, 9988–10031; b) M. D. Wodrich, X. Hu, *Nat. Rev. Chem.* **2017**, *2*, 0099; c) F. Glaser, O. S. Wenger, *Coord. Chem. Rev.* **2020**,

-
- 405, 213129; d) M. A. W. Lawrence, K.-A. Green, P. N. Nelson, S. C. Lorraine, *Polyhedron* **2018**, *143*, 11–27.
- [46] M. R. Netherton, G. C. Fu, *Org. Lett.* **2001**, *3*, 4295–4298.
- [47] P. W. N. M. van Leeuwen, C. F. Roobeek, R. L. Wife, J. H. G. Frijns, *Chem. Commun.* **1986**, 31–33.
- [48] T. M. Shaikh, C.-M. Weng, F.-E. Hong, *Coord. Chem. Rev.* **2012**, *256*, 771–803.
- [49] L. Ackermann, *Chiral Secondary Phosphine Oxides as Preligands*, Wiley-VCH, Weinheim, **2008**.
- [50] a) H. Clavier, G. Buono, *Chem. Rec.* **2017**, *17*, 399–414; b) V. Cadierno, *Appl. Sci.* **2015**, *5*, 380–401.
- [51] a) A. Christiansen, C. Li, M. Garland, D. Selent, R. Ludwig, R. Franke, A. Börner, *ChemCatChem* **2010**, *2*, 1278–1285; b) D. Moraleda, D. Gatineau, D. Martin, L. Giordano, G. Buono, *Chem. Commun.* **2008**, 3031–3033; c) L. Ackermann, *Synthesis* **2006**, *10*, 1557–1571; d) T. L. Emmick, R. L. Letsinger, *J. Am. Chem. Soc.* **1968**, *90*, 3459–3465.
- [52] a) C. A. Busacca, J. C. Lorenz, N. Grinberg, N. Haddad, M. Hrapchak, B. Latli, H. Lee, P. Sabila, A. Saha, M. Sarvestani, S. Shen, R. Varsolona, X. Wei, C. H. Senanayake, *Org. Lett.* **2005**, *7*, 4277–4280; b) W. B. Farnham, R. A. Lewis, R. K. Murray, K. Mislow, *J. Am. Chem. Soc.* **1970**, *92*, 5808–5809; c) L. D. Quin, R. E. Montgomery, *J. Org. Chem.* **1963**, *28*, 3315–3320.
- [53] a) L. Ackermann, R. Born, *Angew. Chem. Int. Ed.* **2005**, *44*, 2444–2447; b) G. Y. Li, *J. Organomet. Chem.* **2002**, *653*, 63–68; c) G. Y. Li, *Angew. Chem. Int. Ed.* **2001**, *40*, 1513–1516.
- [54] L.-Y. Jung, S.-H. Tsai, F.-E. Hong, *Organometallics* **2010**, *29*, 282–282.
- [55] a) Q.-S. Liu, D.-Y. Wang, Z.-J. Yang, Y.-X. Luan, J.-F. Yang, J.-F. Li, Y.-G. Pu, M. Ye, *J. Am. Chem. Soc.* **2017**, *139*, 18150–18153; b) M. R. Nahm, J. R. Potnick, P. S. White, J. S. Johnson, *J. Am. Chem. Soc.* **2006**, *128*, 2751–2756; c) M. R. Nahm, X. Linghu, J. R. Potnick, C. M. Yates, P. S. White, J. S. Johnson, *Angew. Chem. Int. Ed.* **2005**, *44*, 2377–2379; d) X. Linghu, J. R. Potnick, J. S. Johnson, *J. Am. Chem. Soc.* **2004**, *126*, 3070–3071; e) D. Enders, L. Tedeschi, J. W. Bats, *Angew. Chem. Int. Ed.* **2000**, *39*, 4605–4607.
- [56] a) T. Nemoto, Y. Hamada, *Tetrahedron* **2011**, *67*, 667–687; b) T. Nemoto, *Chem. Pharm. Bull.* **2008**, *56*, 1213–1228.

- [57] a) D. Berthold, B. Breit, *Org. Lett.* **2018**, *20*, 598–601; b) H. Landert, F. Spindler, A. Wyss, H.-U. Blaser, B. Pugin, Y. Ribourduille, B. Gschwend, B. Ramalingam, A. Pfaltz, *Angew. Chem. Int. Ed.* **2010**, *49*, 6873–6876.
- [58] a) S.-G. Li, M. Yuan, F. Topic, Z. S. Han, C. H. Senanayake, Y. S. Tsantrizos, *J. Org. Chem.* **2019**, *84*, 7291–7302; b) Z. S. Han, H. Wu, Y. Xu, Y. Zhang, B. Qu, Z. Li, D. R. Caldwell, K. R. Fandrick, L. Zhang, F. Roschangar, J. J. Song, C. H. Senanayake, *Org. Lett.* **2017**, *19*, 1796–1799; c) L. Copey, L. Jean-Gérard, B. Andrioletti, E. Framery, *Tetrahedron Lett.* **2016**, *57*, 543–545; d) F. A. Kortmann, M.-C. Chang, E. Otten, E. P. A. Couzijn, M. Lutz, A. J. Minnaard, *Chem. Sci.* **2014**, *5*, 1322–1327; e) D. Gatineau, L. Giordano, G. Buono, *J. Am. Chem. Soc.* **2011**, *133*, 10728–10731.
- [59] a) T. Achard, *CHIMIA International Journal for Chemistry* **2016**, *70*, 8–19; b) B. Walther, *Coord. Chem. Rev.* **1984**, *60*, 67–105; c) D. M. Roundhill, R. F. Sperline, W. B. Beaulied, *Coord. Chem. Rev.* **1978**, *26*, 263–279.
- [60] a) A. Gallen, A. Riera, X. Verdaguer, A. Grabulosa, *Catalysis Science & Technology* **2019**, *9*, 5504–5561; b) P. Sutra, A. Igau, *Coord. Chem. Rev.* **2016**, *308*, 97–116.
- [61] a) D. Zell, S. Warratz, D. Gelman, S. J. Garden, L. Ackermann, *Chem. Eur. J.* **2016**, *22*, 1248–1252; b) L. V. Graux, M. Giorgi, G. Buono, H. Clavier, *Dalton Trans.* **2016**, *45*, 6491–6502.
- [62] T. Chu, G. I. Nikonov, *Chem. Rev.* **2018**, *118*, 3608–3680.
- [63] S. Z. Tasker, E. A. Standley, T. F. Jamison, *Nature* **2014**, *509*, 299–309.
- [64] V. P. Ananikov, *ACS Catal.* **2015**, *5*, 1964–1971.
- [65] a) S. Ogoshi, *Nickel Catalysis in Organic Synthesis: Methods and Reactions*, Wiley-VCH, Weinheim, **2020**; b) E. Richmond, J. Moran, *Synthesis* **2018**, *50*, 499–513; c) J.-D. Hamel, J.-F. Paquin, *Chem. Commun.* **2018**, *54*, 10224–10239; d) M. Tobisu, N. Chatani, *Top. Curr. Chem.* **2016**, *374*, 41; e) M. Tobisu, N. Chatani, *Acc. Chem. Res.* **2015**, *48*, 1717–1726; f) T. Ahrens, J. Kohlmann, M. Ahrens, T. Braun, *Chem. Rev.* **2015**, *115*, 931–972; g) M. F. Kuehnel, D. Lentz, T. Braun, *Angew. Chem. Int. Ed.* **2013**, *52*, 3328–3348; h) J. Burdeniuc, B. Jedicka, R. H. Crabtree, *Chem. Ber.* **1997**, *130*, 145–154.
- [66] P. Barbier, *C. R. Hebd. Séances Acad. Sci.* **1899**, *238*, 110–111.
- [67] V. Grignard, *C. R. Acad. Sci.* **1900**, *130*, 1322–1324.

-
- [68] a) R. Li-Yuan Bao, R. Zhao, L. Shi, *Chem. Commun.* **2015**, *51*, 6884–6900; b) P. Knochel, A. Krasovskiy, I. Sapountzis, in *Handbook of Functionalized Organometallics: Applications in Synthesis* (Ed.: P. Knochel), Wiley-VCH, Weinheim, **2005**, pp. 109–172.
- [69] A. Job, R. Reich, *C. R. Acad. Sci. Paris* **1924**, *179*, 330–332.
- [70] M. S. Kharasch, E. K. Fields, *J. Am. Chem. Soc.* **1941**, *63*, 2316–2320.
- [71] M. S. Kharasch, C. F. Fuchs, *J. Am. Chem. Soc.* **1943**, *65*, 504–507.
- [72] M. Kumada, *Pure Appl. Chem.* **1980**, *52*, 669–679.
- [73] Y. Kiso, K. Tamao, M. Kumada, *J. Organomet. Chem.* **1973**, *50*, C12–C14.
- [74] V. P. W. Böhm, C. W. K. Gstöttmayr, T. Weskamp, W. A. Herrmann, *Angew. Chem. Int. Ed.* **2001**, *40*, 3387–3389.
- [75] T. Braun, R. N. Perutz, M. I. Sladek, *Chem. Commun.* **2001**, 2254–2255.
- [76] a) S. Asako, L. Ilies, P. Verma, S. Ichikawa, E. Nakamura, *Chem. Lett.* **2014**, *43*, 726–728; b) Y. Nakamura, N. Yoshikai, L. Ilies, E. Nakamura, *Org. Lett.* **2012**, *14*, 3316–3319; c) N. Yoshikai, H. Matsuda, E. Nakamura, *J. Am. Chem. Soc.* **2009**, *131*, 9590–9599.
- [77] L. Ackermann, R. Born, J. H. Spatz, D. Meyer, *Angew. Chem. Int. Ed.* **2005**, *44*, 7216–7219.
- [78] L. Ackermann, C. Wechsler, A. R. Kapdi, A. Althammer, *Synlett* **2010**, 294–298.
- [79] a) H. Shi, W. Dai, B. Wang, S. Cao, *Organometallics* **2018**, *37*, 459–463; b) J. Zhou, J. H. J. Berthel, M. W. Kuntze-Fechner, A. Friedrich, T. B. Marder, U. Radius, *J. Org. Chem.* **2016**, *81*, 5789–5794; c) F. Zhu, Z.-X. Wang, *J. Org. Chem.* **2014**, *79*, 4285–4292; d) A. D. Sun, J. A. Love, *Org. Lett.* **2011**, *13*, 2750–2753; e) L.-G. Xie, Z.-X. Wang, *Chem. Eur. J.* **2010**, *16*, 10332–10336; f) A. Steffen, M. I. Sladek, T. Braun, B. Neumann, H.-G. Stammler, *Organometallics* **2005**, *24*, 4057–4064.
- [80] a) J.-R. Wang, K. Manabe, *Org. Lett.* **2009**, *11*, 741–744; b) B.-T. Guan, S.-K. Xiang, T. Wu, Z.-P. Sun, B.-Q. Wang, K.-Q. Zhao, Z.-J. Shi, *Chem. Commun.* **2008**, 1437–1439.
- [81] G. Jin, X. Zhang, S. Cao, *Org. Lett.* **2013**, *15*, 3114–3117.
- [82] a) T. Niwa, H. Ochiai, Y. Watanabe, T. Hosoya, *J. Am. Chem. Soc.* **2015**, *137*, 14313–14318; b) X.-W. Liu, J. Echavarren, C. Zarate, R. Martin, *J. Am. Chem. Soc.* **2015**, *137*, 12470–12473.

- [83] M. Tobisu, T. Xu, T. Shimasaki, N. Chatani, *J. Am. Chem. Soc.* **2011**, *133*, 19505–19511.
- [84] a) Z. T. Ariki, Y. Maekawa, M. Nambo, C. M. Crudden, *J. Am. Chem. Soc.* **2018**, *140*, 78–81; b) Z. Zuo, D. T. Ahneman, L. Chu, J. A. Terrett, A. G. Doyle, D. W. C. MacMillan, *Science* **2014**, *345*, 437–440; c) S. L. Zultanski, G. C. Fu, *J. Am. Chem. Soc.* **2013**, *135*, 624–627; d) S. E. Denmark, A. J. Cresswell, *J. Org. Chem.* **2013**, *78*, 12593–12628.
- [85] a) D. N. Primer, G. A. Molander, *J. Am. Chem. Soc.* **2017**, *139*, 9847–9850; b) C. Lohre, T. Dröge, C. Wang, F. Glorius, *Chem. Eur. J.* **2011**, *17*, 6052–6055; c) A. Joshi-Pangu, C.-Y. Wang, M. R. Biscoe, *J. Am. Chem. Soc.* **2011**, *133*, 8478–8481.
- [86] D. Heijnen, J.-B. Gualtierotti, V. Hornillos, B. L. Feringa, *Chem. Eur. J.* **2016**, *22*, 3991–3995.
- [87] M. J. O'Neill, T. Riesebeck, J. Cornella, *Angew. Chem. Int. Ed.* **2018**, *57*, 9103–9107.
- [88] a) T. A. Unzner, T. Magauer, *Tetrahedron Lett.* **2015**, *56*, 877–883; b) Q. Shen, Y.-G. Huang, C. Liu, J.-C. Xiao, Q.-Y. Chen, Y. Guo, *J. Fluorine Chem.* **2015**, *179*, 14–22; c) T. Stahl, H. F. T. Klare, M. Oestreich, *ACS Catal.* **2013**, *3*, 1578–1587; d) H. Amii, K. Uneyama, *Chem. Rev.* **2009**, *109*, 2119–2183.
- [89] T. Fujita, K. Fuchibe, J. Ichikawa, *Angew. Chem. Int. Ed.* **2019**, *58*, 390–402.
- [90] W. Heitz, A. Knebelkamp, *Macromol. Rapid Commun.* **1991**, *12*, 69–75.
- [91] P. Tian, C. Feng, T.-P. Loh, *Nat. Commun.* **2015**, *6*, 7472.
- [92] a) D. Zell, V. Müller, U. Dhawa, M. Bursch, R. R. Presa, S. Grimme, L. Ackermann, *Chem. Eur. J.* **2017**, *23*, 12145–12148; b) D. Zell, U. Dhawa, V. Müller, M. Bursch, S. Grimme, L. Ackermann, *ACS Catal.* **2017**, *7*, 4209–4213.
- [93] a) N. Murakami, M. Yoshida, T. Yoshino, S. Matsunaga, *Chem. Pharm. Bull.* **2018**, *66*, 51–54; b) S.-H. Cai, L. Ye, D.-X. Wang, Y.-Q. Wang, L.-J. Lai, C. Zhu, C. Feng, T.-P. Loh, *Chem. Commun.* **2017**, *53*, 8731–8734; c) L. Kong, X. Zhou, X. Li, *Org. Lett.* **2016**, *18*, 6320–6323.
- [94] J. Wang, M. Sánchez-Roselló, J. L. Aceña, C. del Pozo, A. E. Sorochinsky, S. Fustero, V. A. Soloshonok, H. Liu, *Chem. Rev.* **2014**, *114*, 2432–2506.
- [95] a) F. Roudesly, J. Oble, G. Poli, *J. Mol. Catal. A Chem.* **2017**, *426*, 275–296; b) R. H. Crabtree, A. Lei, *Chem. Rev.* **2017**, *117*, 8481–8482.

-
- [96] a) X.-h. Cai, B. Xie, *ARKIVOC* **2015**, 2015, 184–211; b) T. K. Hyster, *Catal. Lett.* **2015**, 145, 458–467; c) Y. Nakao, *Chem. Rec.* **2011**, 11, 242–251; d) L. C. M. Castro, N. Chatani, *Chem. Lett.* **2015**, 44, 410–421; e) J. Yamaguchi, K. Muto, K. Itami, *Eur. J. Org. Chem.* **2013**, 2013, 19–30; f) M. S. Khan, A. Haque, M. K. Al-Suti, P. R. Raithby, *J. Organomet. Chem.* **2015**, 793, 144–133.
- [97] J. P. Kleiman, M. Dubeck, *J. Am. Chem. Soc.* **1963**, 85, 1544–1545.
- [98] L.-C. Liang, P.-S. Chien, Y.-L. Huang, *J. Am. Chem. Soc.* **2006**, 128, 15562–15563.
- [99] Y. Nakao, K. S. Kanyiva, S. Oda, T. Hiyama, *J. Am. Chem. Soc.* **2006**, 128, 8146–8147.
- [100] a) Y. Nakao, Y. Yamada, N. Kashihara, T. Hiyama, *J. Am. Chem. Soc.* **2010**, 132, 13666–13668; b) Y. Nakao, H. Idei, K. S. Kanyiva, T. Hiyama, *J. Am. Chem. Soc.* **2009**, 131, 15996–15997; c) T. Mukai, K. Hirano, T. Satoh, M. Miura, *J. Org. Chem.* **2009**, 74, 6410–6413; d) K. S. Kanyiva, F. Löbermann, Y. Nakao, T. Hiyama, *Tetrahedron Lett.* **2009**, 50, 3463–3466; e) Y. Nakao, N. Kashihara, K. S. Kanyiva, T. Hiyama, *J. Am. Chem. Soc.* **2008**, 130, 16170–16171; f) Kyalo Stephen Kanyiva, Y. Nakao, T. Hiyama, *Heterocycles* **2007**, 72, 677–680; g) K. S. Kanyiva, Y. Nakao, T. Hiyama, *Angew. Chem. Int. Ed.* **2007**, 46, 8872–8874.
- [101] Z. Dong, Z. Ren, S. J. Thompson, Y. Xu, G. Dong, *Chem. Rev.* **2017**, 117, 9333–9403.
- [102] S. Nakanowatari, T. Müller, J. C. A. Oliveira, L. Ackermann, *Angew. Chem. Int. Ed.* **2017**, 56, 15891–15895.
- [103] Y. Nakao, in *Catalytic Hydroarylation of Carbon-Carbon Multiple Bonds* (Ed.: T. B. G. L. Ackermann, L. G. Habgood), Wiley-VCH, Weinheim, **2017**, pp. 175–192.
- [104] Y. Nakao, N. Kashihara, K. S. Kanyiva, T. Hiyama, *Angew. Chem. Int. Ed.* **2010**, 49, 4451–4454.
- [105] Y.-Y. Jiang, Z. Li, J. Shi, *Organometallics* **2012**, 31, 4356–4366.
- [106] a) P. A. Donets, N. Cramer, *Angew. Chem. Int. Ed.* **2015**, 54, 633–637; b) R. Tamura, Y. Yamada, Y. Nakao, T. Hiyama, *Angew. Chem. Int. Ed.* **2012**, 51, 5679–5682; c) Y. Nakao, K. S. Kanyiva, T. Hiyama, *J. Am. Chem. Soc.* **2008**, 130, 2448–2449.

- [107] a) W.-C. Chen, Y.-C. Lai, W.-C. Shih, M.-S. Yu, G. P. A. Yap, T.-G. Ong, *Chem. Eur. J.* **2014**, *20*, 8099–8105; b) W.-C. Shih, W.-C. Chen, Y.-C. Lai, M.-S. Yu, J.-J. Ho, G. P. A. Yap, T.-G. Ong, *Org. Lett.* **2012**, *14*, 2046–2049.
- [108] B. M. Trost, *Proc. Natl. Acad. Sci. U.S.A.* **2004**, *101*, 5348–5355.
- [109] a) W.-B. Zhang, X.-T. Yang, J.-B. Ma, Z.-M. Su, S.-L. Shi, *J. Am. Chem. Soc.* **2019**, *141*, 5628–5634; b) Ł. Woźniak, N. Cramer, *Trends Chem.* **2019**, *1*, 471–484; c) J. Loup, U. Dhawa, F. Pesciaioli, J. Wencel-Delord, L. Ackermann, *Angew. Chem. Int. Ed.* **2019**, *58*, 12803–12818; d) Y.-X. Wang, S.-L. Qi, Y.-X. Luan, X.-W. Han, S. Wang, H. Chen, M. Ye, *J. Am. Chem. Soc.* **2018**, *140*, 5360–5364; e) J. Diesel, A. M. Finogenova, N. Cramer, *J. Am. Chem. Soc.* **2018**, *140*, 4489–4493; f) P. A. Donets, N. Cramer, *Angew. Chem. Int. Ed.* **2015**, *54*, 633–637; g) P. A. Donets, N. Cramer, *J. Am. Chem. Soc.* **2013**, *135*, 11772–11775; h) K. Ogata, Y. Atsuumi, D. Shimada, S.-i. Fukuzawa, *Angew. Chem. Int. Ed.* **2011**, *50*, 5896–5899.
- [110] a) S. K. Murphy, V. M. Dong, *Chem. Commun.* **2014**, *50*, 13645–13649; b) J. C. Leung, M. J. Krische, *Chem. Sci.* **2012**, *3*, 2202–2209; c) M. C. Willis, *Chem. Rev.* **2010**, *110*, 725–748.
- [111] Y.-X. Wang, M. Ye, *Sci. China Chem.* **2018**, *61*, 1004–1013.
- [112] D. Hirsch-Weil, K. A. Abboud, S. Hong, *Chem. Commun.* **2010**, *46*, 7525–7527.
- [113] a) A. Albright, D. Eddings, R. Black, C. J. Welch, N. N. Gerasimchuk, R. E. Gawley, *J. Org. Chem.* **2011**, *76*, 7341–7351; b) A. Albright, R. E. Gawley, *J. Am. Chem. Soc.* **2011**, *133*, 19680–19683.
- [114] J. C. Lewis, R. G. Bergman, J. A. Ellman, *Acc. Chem. Res.* **2008**, *41*, 1013–1025.
- [115] a) D. A. Colby, R. G. Bergman, J. A. Ellman, *Chem. Rev.* **2010**, *110*, 624–655; b) A. S. Tsai, R. M. Wilson, H. Harada, R. G. Bergman, J. A. Ellman, *Chem. Commun.* **2009**, 3910–3912.
- [116] A. T. Normand, S. K. Yen, H. V. Huynh, T. S. A. Hor, K. J. Cavell, *Organometallics* **2008**, *27*, 3153–3160.
- [117] T. W. Lyons, M. S. Sanford, *Chem. Rev.* **2010**, *110*, 1147–1169.
- [118] J. A. Labinger, *Chem. Rev.* **2017**, *117*, 8483–8496.
- [119] S. Pan, T. Shibata, *ACS Catal.* **2013**, *3*, 704–712.
- [120] Ruthenium (320\$ oz.tr.), Accessed on 19.02.2021, retrieved from <http://www.platinum.matthey.com/prices/price-tables>.

-
- [121] a) K. S. Singh, *Catalysts* **2019**, *9*, 173; b) G. Duarah, P. P. Kaishap, T. Begum, S. Gogoi, *Adv. Synth. Catal.* **2019**, *361*, 654–672; c) C. Shan, L. Zhu, L.-B. Qu, R. Bai, Y. Lan, *Chem. Soc. Rev.* **2018**, *47*, 7552–7576; d) L. Ackermann, *Acc. Chem. Res.* **2014**, *47*, 281–295; e) B. Li, P. H. Dixneuf, *Chem. Soc. Rev.* **2013**, *42*, 5744–5767; f) S. I. Kozhushkov, L. Ackermann, *Chem. Sci.* **2013**, *4*, 886–896; g) P. B. Arockiam, C. Bruneau, P. H. Dixneuf, *Chem. Rev.* **2012**, *112*, 5879–5918.
- [122] J. Chatt, J. M. Davidson, *J. Chem. Soc.* **1965**, 843–855.
- [123] L. N. Lewis, J. F. Smith, *J. Am. Chem. Soc.* **1986**, *108*, 2728–2735.
- [124] S. Murai, F. Kakiuchi, S. Sekine, Y. Tanaka, A. Kamatani, M. Sonoda, N. Chatani, *Nature* **1993**, *366*, 529–531.
- [125] a) T. Matsubara, N. Koga, D. G. Musaev, K. Morokuma, *Organometallics* **2000**, *19*, 2318–2329; b) T. Matsubara, N. Koga, D. G. Musaev, K. Morokuma, *J. Am. Chem. Soc.* **1998**, *120*, 12692–12693.
- [126] a) K. Korvorapun, J. Struwe, R. Kuniyil, A. Zangarelli, A. Casnati, M. Waeterschoot, L. Ackermann, *Angew. Chem. Int. Ed.* **2020**, *59*, 18103–18109; b) S. R. Yetra, T. Rogge, S. Warratz, J. Struwe, W. Peng, P. Vana, L. Ackermann, *Angew. Chem. Int. Ed.* **2019**, *58*, 7490–7494; c) T. Rogge, L. Ackermann, *Angew. Chem. Int. Ed.* **2019**, *58*, 15640–15645; d) M. Simonetti, D. M. Cannas, X. Just-Baringo, I. J. Vitorica-Yrezabal, I. Larrosa, *Nat. Chem.* **2018**, *10*, 724–731; e) P. Nareddy, F. Jordan, M. Szostak, *ACS Catal.* **2017**, *7*, 5721–5745; f) G.-F. Zha, H.-L. Qin, E. A. B. Kantchev, *RSC Adv.* **2016**, *6*, 30875–30885; g) M. Simonetti, G. J. P. Perry, X. C. Cambeiro, F. Juliá-Hernández, J. N. Arokianathar, I. Larrosa, *J. Am. Chem. Soc.* **2016**, *138*, 3596–3606; h) L. Ackermann, R. Vicente, H. K. Potukuchi, V. Pirovano, *Org. Lett.* **2010**, *12*, 5032–5035; i) L. Ackermann, A. Althammer, R. Born, *Synlett* **2007**, 2833–2836.
- [127] a) K. Korvorapun, M. Moselage, J. Struwe, T. Rogge, A. M. Messinis, L. Ackermann, *Angew. Chem. Int. Ed.* **2020**, *59*, 18795–18803; b) J. Loup, D. Zell, J. C. A. Oliveira, H. Keil, D. Stalke, L. Ackermann, *Angew. Chem. Int. Ed.* **2017**, *56*, 14197–14201; c) L. Ackermann, N. Hofmann, R. Vicente, *Org. Lett.* **2011**, *13*, 1875–1877; d) L. Ackermann, P. Novák, R. Vicente, N. Hofmann, *Angew. Chem. Int. Ed.* **2009**, *48*, 6045–6048.
- [128] a) R. Manikandan, M. Jeganmohan, *Chem. Commun.* **2017**, *53*, 8931–8947; b) N. Y. P. Kumar, A. Bechtoldt, K. Raghuvanshi, L. Ackermann, *Angew. Chem. Int. Ed.* **2016**, *55*, 6929–6932; c) A. Bechtoldt, C. Tirler, K. Raghuvanshi, S. Warratz,

- C. Kornhaaß, L. Ackermann, *Angew. Chem. Int. Ed.* **2016**, *55*, 264–267; d) H. Weissman, X. Song, D. Milstein, *J. Am. Chem. Soc.* **2001**, *123*, 337–338.
- [129] a) S. De Sarkar, N. Y. P. Kumar, L. Ackermann, *Chem. Eur. J.* **2017**, *23*, 84–87; b) R. Mei, C. Zhu, L. Ackermann, *Chem. Commun.* **2016**, *52*, 13171–13174; c) M. Zhang, Y. Zhang, X. Jie, H. Zhao, G. Li, W. Su, *Org. Chem. Front.* **2014**, *1*, 843–895.
- [130] a) J. C. Gaunt, B. L. Shaw, *J. Organomet. Chem.* **1975**, *102*, 511–516; b) J. M. Duff, B. E. Mann, B. L. Shaw, B. Turtle, *Dalton Trans.* **1974**, 139–145; c) J. M. Duff, B. L. Shaw, *Dalton Trans.* **1972**, 2219–2225.
- [131] D. L. Davies, O. Al-Duaij, J. Fawcett, M. Giardiello, S. T. Hilton, D. R. Russell, *Dalton Trans.* **2003**, 4132–4138.
- [132] L. Ackermann, R. Vicente, A. Althammer, *Org. Lett.* **2008**, *10*, 2299–2302.
- [133] a) M. Lafrance, K. Fagnou, *J. Am. Chem. Soc.* **2006**, *128*, 16496–16497; b) V. I. Sokolov, L. L. Troitskaya, O. A. Reutov, *J. Organomet. Chem.* **1979**, *182*, 537–546.
- [134] a) M. Valero, V. Derdau, *J. Labelled Compd. Radiopharm.* **2020**, *63*, 266–280; b) D. Hesk, *J. Labelled Compd. Radiopharm.* **2019**, *63*, 247–265; c) Y. A. Zolotarev, A. K. Dadayan, Y. A. Borisov, V. S. Kozik, *Chem. Rev.* **2010**, *110*, 5425–5446.
- [135] a) D. M. Freund, A. D. Hegeman, *Curr. Opin. Biotechnol.* **2017**, *43*, 41–48; b) M. Larance, A. I. Lamond, *Nat. Rev. Mol.* **2015**, *16*, 269–280.
- [136] M. Gómez-Gallego, M. A. Sierra, *Chem. Rev.* **2011**, *111*, 4857–4963.
- [137] a) P. Asadi-Atoi, P. Barraud, C. Tisne, S. Kellner, *Biol. Chem.* **2019**, *400*, 847–865; b) S. L. Harbeson, R. D. Tung, *Med. Chem. News* **2014**, *2*, 8–22; c) T. G. Gant, *J. Med. Chem.* **2014**, *57*, 3595–3611.
- [138] a) J. Atzrodt, V. Derdau, W. J. Kerr, M. Reid, *Angew. Chem. Int. Ed.* **2018**, *57*, 1758–1784; b) D. Hesk, C. F. Lavey, P. McNamara, *J. Labelled Compd. Radiopharm.* **2010**, *53*, 722–730; c) J. Atzrodt, V. Derdau, T. Fey, J. Zimmermann, *Angew. Chem. Int. Ed.* **2007**, *46*, 7744–7765.
- [139] a) H. Yang, D. Hesk, *J. Labelled Compd. Radiopharm.* **2020**, *63*, 296–307; b) W. J. Kerr, G. J. Knox, L. C. Paterson, *J. Labelled Compd. Radiopharm.* **2020**, *63*, 281–295; c) D. Hesk, *J. Labelled Compd. Radiopharm.* **2020**, *63*, 247–265.
- [140] J. Atzrodt, V. Derdau, W. J. Kerr, M. Reid, *Angew. Chem. Int. Ed.* **2018**, *57*, 3022–3047.

-
- [141] a) J. L. Garnett, M. A. Long, A. B. McLaren, K. B. Peterson, *Chem. Commun.* **1973**, 749–750; b) J. L. Garnett, R. J. Hodges, *J. Am. Chem. Soc.* **1967**, *89*, 4546–4547; c) J. L. Garnett, R. J. Hodges, *Chem. Commun.* **1967**, 1001–1003.
- [142] a) R. H. Crabtree, *Chem. Rev.* **1985**, *85*, 245–269; b) N. F. Gol'dshleger, V. V. EsNkova, A. E. Shilov, A. A. Shteinman, *Zh. Fiz. Khim.* **1972**, *46*, 785–786; c) N. F. Gol'dshleger, M. B. Tyabin, A. E. Shilov, A. A. Shteinman, *Zh. Fiz. Khim.* **1969**, *43*, 1222–1223.
- [143] a) M. Valero, D. Bouzouita, A. Palazzolo, J. Atzrodt, C. Dugave, S. Tricard, S. Feuillastre, G. Pieters, B. Chaudret, V. Derdau, *Angew. Chem. Int. Ed.* **2020**, *59*, 3517–3522; b) M. Valero, R. Weck, S. Güssregen, J. Atzrodt, V. Derdau, *Angew. Chem. Int. Ed.* **2018**, *57*, 8159–8163; c) Y. Y. Loh, K. Nagao, A. J. Hoover, D. Hesk, N. R. Rivera, S. L. Colletti, I. W. Davies, D. W. C. MacMillan, *Science* **2017**, *358*, 1182–1187; d) W. J. Kerr, D. M. Lindsay, M. Reid, J. Atzrodt, V. Derdau, P. Rojahn, R. Weck, *Chem. Commun.* **2016**, *52*, 6669–6672; e) W. J. Kerr, M. Reid, T. Tuttle, *ACS Catal.* **2015**, *5*, 402–410; f) M. Parmentier, T. Hartung, A. Pfaltz, D. Muri, *Chem. Eur. J.* **2014**, *20*, 11496–11504; g) J. A. Brown, A. R. Cochrane, S. Irvine, W. J. Kerr, B. Mondal, J. A. Parkinson, L. C. Paterson, M. Reid, T. Tuttle, S. Andersson, G. N. Nilsson, *Adv. Synth. Catal.* **2014**, *356*, 3551–3562; h) M. J. Hickey, L. P. Kingston, W. J. S. Lockley, P. Allen, A. Mather, D. J. Wilkinson, *J. Labelled Compd. Radiopharm.* **2007**, *50*, 286–289.
- [144] a) A. L. Garreau, H. Zhou, M. C. Young, *Org. Lett.* **2019**, *21*, 7044–7048; b) A. Di Giuseppe, R. Castarlenas, J. J. Pérez-Torrente, F. J. Lahoz, L. A. Oro, *Chem. Eur. J.* **2014**, *20*, 8391–8403; c) J. L. Rhinehart, K. A. Manbeck, S. K. Buzak, G. M. Lippa, W. W. Brennessel, K. I. Goldberg, W. D. Jones, *Organometallics* **2012**, *31*, 1943–1952; d) A. Di Giuseppe, R. Castarlenas, J. J. Pérez-Torrente, F. J. Lahoz, V. Polo, L. A. Oro, *Angew. Chem. Int. Ed.* **2011**, *50*, 3938–3942; e) J. Campos, A. C. Esqueda, J. López-Serrano, L. Sánchez, F. P. Cossio, A. de Cozar, E. Álvarez, C. Maya, E. Carmona, *J. Am. Chem. Soc.* **2010**, *132*, 16765–16767; f) S. Chen, G. Song, X. Li, *Tetrahedron Lett.* **2008**, *49*, 6929–6932.
- [145] a) V. P. Shevchenko, I. A. Razzhivina, M. G. Chernysheva, G. A. Badun, I. Y. Nagaev, K. V. Shevchenko, N. F. Myasoedov, *Radiochemistry* **2015**, *57*, 312–320; b) S. Ma, G. Villa, P. S. Thuy-Boun, A. Homs, J.-Q. Yu, *Angew. Chem. Int. Ed.* **2014**, *53*, 734–737; c) V. P. Shevchenko, I. Y. Nagaev, K. V. Shevchenko, N.

- F. Myasoedov, *Radiochemistry* **2013**, *55*, 545–551; d) P. Hermange, A. T. Lindhardt, R. H. Taaning, K. Bjerglund, D. Lupp, T. Skrydstrup, *J. Am. Chem. Soc.* **2011**, *133*, 6061–6071.
- [146] a) L. V. A. Hale, N. K. Szymczak, *J. Am. Chem. Soc.* **2016**, *138*, 13489–13492; b) B. Chatterjee, V. Krishnakumar, C. Gunanathan, *Org. Lett.* **2016**, *18*, 5892–5895; c) W. Bai, K.-H. Lee, S. K. S. Tse, K. W. Chan, Z. Lin, G. Jia, *Organometallics* **2015**, *34*, 3686–3698; d) S. H. Lee, S. I. Gorelsky, G. I. Nikonov, *Organometallics* **2013**, *32*, 6599–6604; e) Y. Sawama, Y. Yabe, H. Iwata, Y. Fujiwara, Y. Monguchi, H. Sajiki, *Chem. Eur. J.* **2012**, *18*, 16436–16442; f) L. Neubert, D. Michalik, S. Bähn, S. Imm, H. Neumann, J. Atzrodt, V. Derdau, W. Holla, M. Beller, *J. Am. Chem. Soc.* **2012**, *134*, 12239–12244; g) B. G. Hashiguchi, K. J. H. Young, M. Yousufuddin, W. A. Goddard, R. A. Periana, *J. Am. Chem. Soc.* **2010**, *132*, 12542–12545; h) Y. Fujiwara, H. Iwata, Y. Sawama, Y. Monguchi, H. Sajiki, *Chem. Commun.* **2010**, *46*, 4977–4979; i) T. Maegawa, Y. Fujiwara, Y. Inagaki, Y. Monguchi, H. Sajiki, *Adv. Synth. Catal.* **2008**, *350*, 2215–2218.
- [147] a) C. Zarate, H. Yang, M. J. Bezdek, D. Hesk, P. J. Chirik, *J. Am. Chem. Soc.* **2019**, *141*, 5034–5044; b) C. Kingston, M. A. Wallace, A. J. Allentoff, J. N. deGruyter, J. S. Chen, S. X. Gong, S. Bonacorsi, P. S. Baran, *J. Am. Chem. Soc.* **2019**, *141*, 774–779; c) H. Yang, C. Zarate, W. N. Palmer, N. Rivera, D. Hesk, P. J. Chirik, *ACS Catal.* **2018**, *8*, 10210–10218; d) W. N. Palmer, P. J. Chirik, *ACS Catal.* **2017**, *7*, 5674–5678; e) R. Pony Yu, D. Hesk, N. Rivera, I. Pelczer, P. J. Chirik, *Nature* **2016**, *529*, 195–199.
- [148] S. L. Regen, *J. Org. Chem.* **1974**, *39*, 260–261.
- [149] M. H. G. Pechtl, M. Hölscher, Y. Ben-David, N. Theyssen, R. Loschen, D. Milstein, W. Leitner, *Angew. Chem. Int. Ed.* **2007**, *46*, 2269–2272.
- [150] A. Prades, M. Poyatos, E. Peris, *Adv. Synth. Catal.* **2010**, *352*, 1155–1162.
- [151] L. Piola, J. A. Fernández-Salas, S. Manzini, S. P. Nolan, *Org. Biomol. Chem.* **2014**, *12*, 8683–8688.
- [152] P. H. Allen, M. J. Hickey, L. P. Kingston, D. J. Wilkinson, *J. Labelled Compd. Radiopharm.* **2010**, *53*, 731–738.
- [153] D. Hesk, K. Voronin, P. McNamara, P. Royster, D. Koharski, S. Hendershot, S. Saluja, V. Truong, T. M. Chan, *J. Labelled Compd. Radiopharm.* **2007**, *50*, 131–137.

-
- [154] a) A. Palazzolo, S. Feuillastre, V. Pfeifer, S. Garcia-Argote, D. Bouzouita, S. Tricard, C. Chollet, E. Marcon, D.-A. Buisson, S. Cholet, F. Fenaille, G. Lippens, B. Chaudret, G. Pieters, *Angew. Chem. Int. Ed.* **2019**, *58*, 4891–4895; b) G. Pieters, C. Taglang, E. Bonnefille, T. Gutmann, C. Puente, J.-C. Berthet, C. Dugave, B. Chaudret, B. Rousseau, *Angew. Chem. Int. Ed.* **2014**, *53*, 230–234.
- [155] M. H. Emmert, C. J. Legacy, in *Arene Chemistry: Reaction Mechanisms and Methods for Aromatic Compounds* (Ed.: J. Mortier), John Wiley & Sons, Hoboken, NJ, **2015**, pp. 647–674.
- [156] J. Li, S. De Sarkar, L. Ackermann, in *C–H Bond Activation and Catalytic Functionalization I. Topics in Organometallic Chemistry* (Eds.: P. Dixneuf, H. Doucet), Springer, Cham, **2016**, pp. 217–258.
- [157] a) D. W. Robbins, J. F. Hartwig, *Angew. Chem. Int. Ed.* **2013**, *52*, 933–937; b) J.-Y. Cho, M. K. Tse, D. Holmes, R. E. Maleczka, M. R. Smith, *Science* **2002**, *295*, 305–308.
- [158] Y. Wei, P. Hu, M. Zhang, W. Su, *Chem. Rev.* **2017**, *117*, 8864–8907.
- [159] a) S. Das, C. D. Incarvito, R. H. Crabtree, G. W. Brudvig, *Science* **2006**, *312*, 1941–1943; b) R. Breslow, X. Zhang, Y. Huang, *J. Am. Chem. Soc.* **1997**, *119*, 4535–4536.
- [160] a) H. Shi, Y. Lu, J. Weng, K. L. Bay, X. Chen, K. Tanaka, P. Verma, K. N. Houk, J.-Q. Yu, *Nat. Chem.* **2020**, *12*, 399–404; b) S. Porey, X. Zhang, S. Bhowmick, V. Kumar Singh, S. Guin, R. S. Paton, D. Maiti, *J. Am. Chem. Soc.* **2020**, *142*, 3762–3774; c) Z. Fan, K. L. Bay, X. Chen, Z. Zhuang, H. S. Park, K.-S. Yeung, K. N. Houk, J.-Q. Yu, *Angew. Chem. Int. Ed.* **2020**, *59*, 4770–4777; d) K.-Y. Yoon, G. Dong, *Angew. Chem. Int. Ed.* **2018**, *57*, 8592–8596; e) H. Shi, A. N. Herron, Y. Shao, Q. Shao, J.-Q. Yu, *Nature* **2018**, *558*, 581–585; f) R. Li, G. Dong, *Angew. Chem. Int. Ed.* **2018**, *57*, 1697–1701; g) R. Jayarajan, J. Das, S. Bag, R. Chowdhury, D. Maiti, *Angew. Chem. Int. Ed.* **2018**, *57*, 7659–7663; h) Z. Zhang, K. Tanaka, J.-Q. Yu, *Nature* **2017**, *543*, 538–542; i) G. Cheng, P. Wang, J.-Q. Yu, *Angew. Chem. Int. Ed.* **2017**, *56*, 8183–8186; j) M. Bera, S. Agasti, R. Chowdhury, R. Mondal, D. Pal, D. Maiti, *Angew. Chem. Int. Ed.* **2017**, *56*, 5272–5276; k) Z. Dong, J. Wang, G. Dong, *J. Am. Chem. Soc.* **2015**, *137*, 5887–5890; l) L. Chu, M. Shang, K. Tanaka, Q. Chen, N. Pissarnitski, E. Streckfuss, J.-Q. Yu, *ACS Cent. Sci.* **2015**, *1*, 394–399; m) D. Leow, G. Li, T.-S. Mei, J.-Q. Yu, *Nature* **2012**, *486*, 518–522.

- [161] Y. Kuninobu, H. Ida, M. Nishi, M. Kanai, *Nat. Chem.* **2015**, *7*, 712–717.
- [162] a) M. Catellani, E. Motti, N. Della Ca', *Acc. Chem. Res.* **2008**, *41*, 1512–1522; b) M. Catellani, F. Frignani, A. Rangoni, *Angew. Chem. Int. Ed.* **1997**, *36*, 119–122.
- [163] a) G. Meng, N. Y. S. Lam, E. L. Lucas, T. G. Saint-Denis, P. Verma, N. Chekshin, J.-Q. Yu, *J. Am. Chem. Soc.* **2020**, *142*, 10571–10591; b) X.-C. Wang, W. Gong, L.-Z. Fang, R.-Y. Zhu, S. Li, K. M. Engle, J.-Q. Yu, *Nature* **2015**, *519*, 334–338.
- [164] a) J. Wang, G. Dong, *Chem. Rev.* **2019**, *119*, 7478–7528; b) P. Wang, M. E. Farmer, X. Huo, P. Jain, P.-X. Shen, M. Ishoey, J. E. Bradner, S. R. Wisniewski, M. D. Eastgate, J.-Q. Yu, *J. Am. Chem. Soc.* **2016**, *138*, 9269–9276; c) N. Della Ca', M. Fontana, E. Motti, M. Catellani, *Acc. Chem. Res.* **2016**, *49*, 1389–1400.
- [165] M. Gagliardo, D. J. M. Snelders, P. A. Chase, R. J. M. Klein Gebbink, G. P. M. van Klink, G. van Koten, *Angew. Chem. Int. Ed.* **2007**, *46*, 8558–8573.
- [166] a) K. Korvorapun, R. Kuniyil, L. Ackermann, *ACS Catal.* **2020**, *10*, 435–440; b) K. Korvorapun, N. Kaplaneris, T. Rogge, S. Warratz, A. C. Stückl, L. Ackermann, *ACS Catal.* **2018**, *8*, 886–892; c) J. A. Leitch, C. L. McMullin, M. F. Mahon, Y. Bhonoah, C. G. Frost, *ACS Catal.* **2017**, *7*, 2616–2623; d) C. J. Teskey, A. Y. W. Lui, M. F. Greaney, *Angew. Chem. Int. Ed.* **2015**, *54*, 11677–11680; e) J. Li, S. Warratz, D. Zell, S. De Sarkar, E. E. Ishikawa, L. Ackermann, *J. Am. Chem. Soc.* **2015**, *137*, 13894–13901; f) N. Hofmann, L. Ackermann, *J. Am. Chem. Soc.* **2013**, *135*, 5877–5884; g) O. Saidi, J. Marafie, A. E. W. Ledger, P. M. Liu, M. F. Mahon, G. Kociok-Köhn, M. K. Whittlesey, C. G. Frost, *J. Am. Chem. Soc.* **2011**, *133*, 19298–19301; h) M. Ghosh, S. De Sarkar, *Asian J. Org. Chem.* **2018**, *7*, 1236–1255.
- [167] G. R. Clark, C. E. L. Headford, W. R. Roper, L. J. Wright, V. P. D. Yap, *Inorg. Chim. Acta* **1994**, *220*, 261–272.
- [168] J.-P. Sutter, D. M. Grove, M. Beley, J.-P. Collin, N. Veldman, A. L. Spek, J.-P. Sauvage, G. van Koten, *Angew. Chem. Int. Ed.* **1994**, *33*, 1282–1285.
- [169] C. Coudret, S. Fraysse, *Chem. Commun.* **1998**, 663–664.
- [170] A. M. Clark, C. E. F. Rickard, W. R. Roper, L. J. Wright, *Organometallics* **1999**, *18*, 2813–2820.
- [171] A. J. Paterson, S. St John-Campbell, M. F. Mahon, N. J. Press, C. G. Frost, *Chem. Commun.* **2015**, *51*, 12807–12810.
- [172] J. Li, K. Korvorapun, S. De Sarkar, T. Rogge, D. J. Burns, S. Warratz, L. Ackermann, *Nat. Commun.* **2017**, *8*, 15430.

-
- [173] G. Li, X. Lv, K. Guo, Y. Wang, S. Yang, L. Yu, Y. Yu, J. Wang, *Org. Chem. Front.* **2017**, *4*, 1145–1148.
- [174] G. Li, P. Gao, X. Lv, C. Qu, Q. Yan, Y. Wang, S. Yang, J. Wang, *Org. Lett.* **2017**, *19*, 2682–2685.
- [175] Z. Ruan, S.-K. Zhang, C. Zhu, P. N. Ruth, D. Stalke, L. Ackermann, *Angew. Chem. Int. Ed.* **2017**, *56*, 2045–2049.
- [176] F. Fumagalli, S. Warratz, S.-K. Zhang, T. Rogge, C. Zhu, A. C. Stückl, L. Ackermann, *Chem. Eur. J.* **2018**, *24*, 3984–3988.
- [177] P. Gandeepan, J. Koeller, K. Korvorapun, J. Mohr, L. Ackermann, *Angew. Chem. Int. Ed.* **2019**, *58*, 9820–9825.
- [178] A. Sagadevan, M. F. Greaney, *Angew. Chem. Int. Ed.* **2019**, *58*, 9826–9830.
- [179] X.-G. Wang, Y. Li, H.-C. Liu, B.-S. Zhang, X.-Y. Gou, Q. Wang, J.-W. Ma, Y.-M. Liang, *J. Am. Chem. Soc.* **2019**, *141*, 13914–13922.
- [180] a) G. Li, D. Li, J. Zhang, D.-Q. Shi, Y. Zhao, *ACS Catal.* **2017**, *7*, 4138–4143; b) B. Li, S.-L. Fang, D.-Y. Huang, B.-F. Shi, *Org. Lett.* **2017**, *19*, 3950–3953.
- [181] H. L. Barlow, C. J. Teskey, M. F. Greaney, *Org. Lett.* **2017**, *19*, 6662–6665.
- [182] Q. Yu, L. a. Hu, Y. Wang, S. Zheng, J. Huang, *Angew. Chem. Int. Ed.* **2015**, *54*, 15284–15288.
- [183] a) Z. Fan, H. Lu, A. Zhang, *J. Org. Chem.* **2018**, *83*, 3245–3251; b) Z. Fan, J. Li, H. Lu, D.-Y. Wang, C. Wang, M. Uchiyama, A. Zhang, *Org. Lett.* **2017**, *19*, 3199–3202; c) Z. Fan, J. Ni, A. Zhang, *J. Am. Chem. Soc.* **2016**, *138*, 8470–8475.
- [184] S. Hübner, J. G. de Vries, V. Farina, *Adv. Synth. Catal.* **2016**, *358*, 3–25.
- [185] I. Fechete, Y. Wang, J. C. Védrine, *Catal. Today* **2012**, *189*, 2–27.
- [186] a) F. Ferlin, A. Marini, N. Ascani, L. Ackermann, D. Lanari, L. Vaccaro, *ChemCatChem* **2020**, *12*, 449–454; b) I. Choi, V. Müller, G. Lole, R. Köhler, V. Karius, W. Viöl, C. Jooss, L. Ackermann, *Chem. Eur. J.* **2020**, *26*, 3509–3514; c) S. Wang, D. Hu, W. Hua, J. Gu, Q. Zhang, X. Jia, K. Xi, *RSC Adv.* **2015**, *5*, 53935–53939; d) W. Zhang, Y. Tian, N. Zhao, Y. Wang, J. Li, Z. Wang, *Tetrahedron* **2014**, *70*, 6120–6126; e) N. T. S. Phan, C. K. Nguyen, T. T. Nguyen, T. Truong, *Catal. Sci. Technol.* **2014**, *4*, 369–377; f) J. Malmgren, A. Nagendiran, C.-W. Tai, J.-E. Bäckvall, B. Olofsson, *Chem. Eur. J.* **2014**, *20*, 13531–13535; g) H. T. N. Le, T. T. Nguyen, P. H. L. Vu, T. Truong, N. T. S. Phan, *J. Mol. Catal. A Chem.* **2014**, *391*, 74–82; h) E. Y. Lee, J. Park, *ChemCatChem* **2011**, *3*, 1127–1129.

- [187] a) T. Truong, K. D. Nguyen, S. H. Doan, N. T. S. Phan, *Appl Catal A Gen* **2016**, *510*, 27–33; b) S. Vásquez-Céspedes, A. Ferry, L. Candish, F. Glorius, *Angew. Chem. Int. Ed.* **2015**, *54*, 5772–5776; c) P. Pal, H. Singh, A. B. Panda, S. C. Ghosh, *Asian J. Org. Chem.* **2015**, *4*, 879–883; d) H. Fei, S. M. Cohen, *J. Am. Chem. Soc.* **2015**, *137*, 2191–2194; e) P. Pal, A. K. Giri, H. Singh, S. C. Ghosh, A. B. Panda, *Chem. Asian J.* **2014**, *9*, 2392–2396; f) K. Manna, T. Zhang, W. Lin, *J. Am. Chem. Soc.* **2014**, *136*, 6566–6569; g) L. L. Chng, J. Zhang, J. Yang, M. Amoura, J. Y. Ying, *Adv. Synth. Catal.* **2011**, *353*, 2988–2998; h) S. Kawamorita, H. Ohmiya, K. Hara, A. Fukuoka, M. Sawamura, *J. Am. Chem. Soc.* **2009**, *131*, 5058–5059.
- [188] a) A. F. Schmidt, A. A. Kurokhtina, *Kinet. Catal.* **2012**, *53*, 714–730; b) R. H. Crabtree, *Chem. Rev.* **2012**, *112*, 1536–1554; c) J. A. Widegren, R. G. Finke, *J. Mol. Catal. A Chem.* **2003**, *198*, 317–341.
- [189] N. Nakamura, Y. Tajima, K. Saka, *Heterocycles* **1982**, *17*, 235–245.
- [190] a) M. Cao, D. Wu, W. Su, R. Cao, *J. Catal.* **2015**, *321*, 62–69; b) D.-T. D. Tang, K. D. Collins, J. B. Ernst, F. Glorius, *Angew. Chem. Int. Ed.* **2014**, *53*, 1809–1813; c) D.-T. D. Tang, K. D. Collins, F. Glorius, *J. Am. Chem. Soc.* **2013**, *135*, 7450–7453; d) V. A. Zinovyeva, M. A. Vorotyntsev, I. Bezverkhyy, D. Chaumont, J.-C. Hierso, *Adv. Funct. Mater.* **2011**, *21*, 1064–1075; e) L. Wang, W.-b. Yi, C. Cai, *Chem. Commun.* **2011**, *47*, 806–808; f) Y. Huang, Z. Lin, R. Cao, *Chem. Eur. J.* **2011**, *17*, 12706–12712; g) S. Hernández, I. Moreno, R. SanMartin, G. Gómez, M. T. Herrero, E. Domínguez, *J. Org. Chem.* **2010**, *75*, 434–441.
- [191] a) A. J. Reay, L. K. Neumann, I. J. S. Fairlamb, *Synlett* **2016**, 1211–1216; b) R. Cano, A. F. Schmidt, G. P. McGlacken, *Chem. Sci.* **2015**, *6*, 5338–5346; c) L. Djakovitch, F.-X. Felpin, *ChemCatChem* **2014**, *6*, 2175–2187.
- [192] a) Y. Budnikova, O. Bochkova, M. Khrizanforov, I. Nizameev, K. Kholin, T. Gryaznova, A. Laskin, Y. Dudkina, S. Strelakova, S. Fedorenko, A. Kononov, A. Mustafina, *ChemCatChem* **2019**, *11*, 5615–5624; b) S. Vásquez-Céspedes, K. M. Chepiga, N. Möller, A. H. Schäfer, F. Glorius, *ACS Catal.* **2016**, *6*, 5954–5961; c) L. He, K. Natta, J. Rabeah, C. Taeschler, H. Neumann, A. Brückner, M. Beller, *Angew. Chem. Int. Ed.* **2015**, *54*, 4320–4324; d) N. T. S. Phan, P. H. L. Vu, T. T. Nguyen, *J. Catal.* **2013**, *306*, 38–46.
- [193] H. Miura, K. Wada, S. Hosokawa, M. Inoue, *Chem. Eur. J.* **2010**, *16*, 4186–4189.

-
- [194] H. Miura, K. Wada, S. Hosokawa, M. Inoue, *ChemCatChem* **2010**, *2*, 1223–1225.
- [195] Q.-Y. Meng, Q. Liu, J.-J. Zhong, H.-H. Zhang, Z.-J. Li, B. Chen, C.-H. Tung, L.-Z. Wu, *Org. Lett.* **2012**, *14*, 5992–5995.
- [196] S. Warratz, D. J. Burns, C. Zhu, K. Korvorapun, T. Rogge, J. Scholz, C. Jooss, D. Gelman, L. Ackermann, *Angew. Chem. Int. Ed.* **2017**, *56*, 1557–1560.
- [197] a) N. J. O'Connor, A. S. M. Jonayat, M. J. Janik, T. P. Senftle, *Nat. Catal.* **2018**, *1*, 531–539; b) N. Yang, S. F. Bent, *J. Catal.* **2017**, *351*, 49–58; c) E. Lam, J. H. T. Luong, *ACS Catal.* **2014**, *4*, 3393–3410; d) M. Misono, in *Stud. Surf. Sci. Catal.* (Ed.: M. Misono), Elsevier, **2013**, pp. 25–65; e) U. Díaz, D. Brunel, A. Corma, *Chem. Soc. Rev.* **2013**, *42*, 4083–4097; f) F. Rodríguez-reinoso, *Carbon* **1998**, *36*, 159–175.
- [198] a) M. Safaei, M. M. Foroughi, N. Ebrahimpoor, S. Jahani, A. Omid, M. Khatami, *Trends Anal. Chem.* **2019**, *118*, 401–425; b) M. Liu, J. Wu, H. Hou, *Chem. Eur. J.* **2019**, *25*, 2935–2948.
- [199] a) L. Liu, A. Corma, *Chem. Rev.* **2018**, *118*, 4981–5079; b) D. Pla, M. Gómez, *ACS Catal.* **2016**, *6*, 3537–3552.
- [200] a) S. Itsuno, in *Encyclopedia of Polymeric Nanomaterials* (Eds.: S. Kobayashi, K. Müllen), Springer Berlin Heidelberg, Berlin, Heidelberg, **2014**, pp. 1–9; b) N. Kann, *Molecules* **2010**, *15*, 6306; c) J. Lu, P. H. Toy, *Chem. Rev.* **2009**, *109*, 815–838; d) M. R. Buchmeiser, *Chem. Rev.* **2009**, *109*, 303–321; e) N. Madhavan, C. W. Jones, M. Weck, *Acc. Chem. Res.* **2008**, *41*, 1153–1165.
- [201] a) R. Ye, J. Zhao, B. B. Wickemeyer, F. D. Toste, G. A. Somorjai, *Nat. Catal.* **2018**, *1*, 318–325; b) O. Deutschmann, H. Knözinger, K. Kochloefl, T. Turek, in *Ullmann's Encyclopedia of Industrial Chemistry*, Wiley - VCH, Weinheim, **2009**, pp. 457–482.
- [202] a) M. Benaglia, A. Puglisi, F. Cozzi, *Chem. Rev.* **2003**, *103*, 3401–3430; b) N. E. Leadbeater, M. Marco, *Chem. Rev.* **2002**, *102*, 3217–3274.
- [203] T. Iwai, T. Harada, K. Hara, M. Sawamura, *Angew. Chem. Int. Ed.* **2013**, *52*, 12322–12326.
- [204] L.-C. Lee, J. He, J.-Q. Yu, C. W. Jones, *ACS Catal.* **2016**, *6*, 5245–5250.
- [205] a) Y. Segawa, T. Maekawa, K. Itami, *Angew. Chem. Int. Ed.* **2015**, *54*, 66–81; b) J. Yamaguchi, A. D. Yamaguchi, K. Itami, *Angew. Chem. Int. Ed.* **2012**, *51*,

- 8960–9009; c) S. K. Sinha, G. Zanoni, D. Maiti, *Asian J. Org. Chem.* **2018**, *7*, 1178–1192; d) H. Amii, K. Uneyama, *Chem. Rev.* **2009**, *109*, 2119–2183.
- [206] a) C. Bruneau, P. H. Dixneuf, in *C-H Bond Activation and Catalytic Functionalization I. Topics in Organometallic Chemistry* (Ed.: H. D. P. Dixneuf), Springer, Cham, **2015**, pp. 137–188; b) T. M. Shaikh, C.-M. Weng, F.-E. Hong, *Coord. Chem. Rev.* **2012**, *256*, 771–803.
- [207] a) Ł. Woźniak, N. Cramer, *Trends Chem.* **2019**, *1*, 471–484; b) C. G. Newton, S.-G. Wang, C. C. Oliveira, N. Cramer, *Chem. Rev.* **2017**, *117*, 8908–8976.
- [208] T. Braun, R. P. Hughes, *Organometallic Fluorine Chemistry*, Springer, Cham, **2015**.
- [209] a) Y. A. Ho, M. Leiendecker, X. Liu, C. Wang, N. Alandini, M. Rueping, *Org. Lett.* **2018**, *20*, 5644–5647; b) Z. Jin, Y.-J. Li, Y.-Q. Ma, L.-L. Qiu, J.-X. Fang, *Chem. Eur. J.* **2012**, *18*, 446–450.
- [210] a) B. Atwater, N. Chandrasoma, D. Mitchell, M. J. Rodriguez, M. Pompeo, R. D. J. Froese, M. G. Organ, *Angew. Chem. Int. Ed.* **2015**, *54*, 9502–9506; b) D. Yu, C.-S. Wang, C. Yao, Q. Shen, L. Lu, *Org. Lett.* **2014**, *16*, 5544–5547; c) S.-H. Xiao, Y. Xiong, X.-X. Zhang, S. Cao, *Tetrahedron* **2014**, *70*, 4405–4411; d) A. D. Sun, K. Leung, A. D. Restivo, N. A. LaBerge, H. Takasaki, J. A. Love, *Chem. Eur. J.* **2014**, *20*, 3162–3168; e) X. Yang, H. Sun, S. Zhang, X. Li, *J. Organomet. Chem.* **2013**, *723*, 36–42.
- [211] a) H. Mei, J. Han, S. Fustero, M. Medio-Simon, D. M. Sedgwick, C. Santi, R. Ruzziconi, V. A. Soloshonok, *Chem. Eur. J.* **2019**, *25*, 11797–11819; b) Q. Cheng, T. Ritter, *Trends Chem.* **2019**, *1*, 461–470; c) M. G. Campbell, T. Ritter, *Chem. Rev.* **2015**, *115*, 612–633; d) R. Berger, G. Resnati, P. Metrangolo, E. Weber, J. Hulliger, *Chem. Soc. Rev.* **2011**, *40*, 3496–3508.
- [212] W. Liu, L. Ackermann, *ACS Catal.* **2016**, *6*, 3743–3752.
- [213] T. G. Saint-Denis, R.-Y. Zhu, G. Chen, Q.-F. Wu, J.-Q. Yu, *Science* **2018**, *359*, 747–759.
- [214] a) J. Loup, V. Müller, D. Ghorai, L. Ackermann, *Angew. Chem. Int. Ed.* **2019**, *58*, 1749–1753; b) J. Diesel, D. Grosheva, S. Kodama, N. Cramer, *Angew. Chem. Int. Ed.* **2019**, *58*, 11044–11048.
- [215] a) M. Valero, V. Derdau, *J. Labelled Compd. Radiopharm.* **2019**, *63*, 266–280; b) W. J. S. Lockley, D. Hesk, *J. Labelled Compd. Radiopharm.* **2010**, *53*, 704–715.

-
- [216] V. Müller, R. Weck, V. Derdau, L. Ackermann, *ChemCatChem* **2020**, *12*, 100–104.
- [217] a) A. W. Dombrowski, N. J. Gesmundo, A. L. Aguirre, K. A. Sarris, J. M. Young, A. R. Bogdan, M. C. Martin, S. Gedeon, Y. Wang, *ACS Med. Chem. Lett.* **2020**, *11*, 597–604; b) M. M. Heravi, V. Zadsirjan, P. Hajiabbasi, H. Hamidi, *Monatsh. Chem.* **2019**, *150*, 535–591; c) J. B. Diccianni, T. Diao, *Trends Chem.* **2019**, *1*, 830–844; d) L.-C. Campeau, N. Hazari, *Organometallics* **2019**, *38*, 3–35; e) P. M. Edwards, L. L. Schafer, *Chem. Commun.* **2018**, *54*, 12543–12560; f) K. Zhao, L. Shen, Z.-L. Shen, T.-P. Loh, *Chem. Soc. Rev.* **2017**, *46*, 586–602; g) D. Haas, J. M. Hammann, R. Greiner, P. Knochel, *ACS Catal.* **2016**, *6*, 1540–1552; h) C. Cordovilla, C. Bartolomé, J. M. Martínez-Ilarduya, P. Espinet, *ACS Catal.* **2015**, *5*, 3040–3053; i) S. P. Nolan, O. Navarro, in *Reference Module in Chemistry, Molecular Sciences and Chemical Engineering*, Elsevier, **2013**, pp. 1–37.
- [218] a) A. Piontek, W. Ochędzan-Siodłak, E. Bisz, M. Szostak, *Adv. Synth. Catal.* **2019**, *361*, 2329–2336; b) X. Liu, C.-C. Hsiao, I. Kalvet, M. Leiendecker, L. Guo, F. Schoenebeck, M. Rueping, *Angew. Chem. Int. Ed.* **2016**, *55*, 6093–6098; c) L. Guo, C.-C. Hsiao, H. Yue, X. Liu, M. Rueping, *ACS Catal.* **2016**, *6*, 4438–4442; d) M. Tobisu, T. Takahira, N. Chatani, *Org. Lett.* **2015**, *17*, 4352–4355; e) B.-J. Li, D.-G. Yu, C.-L. Sun, Z.-J. Shi, *Chem. Eur. J.* **2011**, *17*, 1728–1759.
- [219] a) K. M. Korch, D. A. Watson, *Chem. Rev.* **2019**, *119*, 8192–8228; b) N. Liu, Z.-X. Wang, *Adv. Synth. Catal.* **2012**, *354*, 1641–1645; c) D.-G. Yu, M. Yu, B.-T. Guan, B.-J. Li, Y. Zheng, Z.-H. Wu, Z.-J. Shi, *Org. Lett.* **2009**, *11*, 3374–3377; d) J. A. Miller, J. W. Dankwardt, *Tetrahedron Lett.* **2003**, *44*, 1907–1910; e) J. J. Garcia, N. M. Brunkan, W. D. Jones, *J. Am. Chem. Soc.* **2002**, *124*, 9547–9555; f) J. A. Miller, *Tetrahedron Lett.* **2001**, *42*, 6991–6993.
- [220] a) N. A. LaBerge, J. A. Love, *Activation and Formation of Aromatic C–F Bonds*, Springer, Cham, **2015**; b) E. Clot, O. Eisenstein, N. Jasim, S. A. Macgregor, J. E. McGrady, R. N. Perutz, *Acc. Chem. Res.* **2011**, *44*, 333–348.
- [221] J. A. Olsen, D. W. Banner, P. Seiler, B. Wagner, T. Tschopp, U. Obst-Sander, M. Kansy, K. Müller, F. Diederich, *ChemBioChem* **2004**, *5*, 666–675.
- [222] a) L. Keyes, J. A. Love, in *C–H and C–X Bond Functionalization: Transition Metal Mediation* (Ed.: X. Ribas), The Royal Society of Chemistry, **2013**, pp. 159–192; b)

- [223] a) C. Citti, P. Linciano, F. Russo, L. Luongo, M. Iannotta, S. Maione, A. Laganà, A. L. Capriotti, F. Forni, M. A. Vandelli, G. Gigli, G. Cannazza, *Sci Rep.* **2019**, *9*, 20335; b) Y. Yuan, G. Giri, A. L. Ayzner, A. P. Zoombelt, S. C. B. Mannsfeld, J. Chen, D. Nordlund, M. F. Toney, J. Huang, Z. Bao, *Nat. Commun.* **2014**, *5*, 3005; c) M. Sanford, *Drugs* **2014**, *74*, 1411–1433; d) M. Mothi, S. Sampson, *Cochrane Database Syst. Rev.* **2013**, 1465–1858; e) A. Luvai, W. Mbagaya, A. S. Hall, J. H. Barth, *Clinical Medicine Insights: Cardiology* **2012**, *6*, 17–33; f) N. A. McGrath, M. Brichacek, J. T. Njardarson, *J. Chem. Educ.* **2010**, *87*, 1348–1349; g) D. J. Nichols, G. J. Muirhead, J. A. Harness, *Br. J. Clin. Pharmacol.* **2002**, *53*, 5S–12S.
- [224] a) Y. Shen, Y. Gu, R. Martin, *J. Am. Chem. Soc.* **2018**, *140*, 12200–12209; b) I. Kalvet, T. Sperger, T. Scattolin, G. Magnin, F. Schoenebeck, *Angew. Chem. Int. Ed.* **2017**, *56*, 7078–7082; c) J. Wang, T. Qin, T.-G. Chen, L. Wimmer, J. T. Edwards, J. Cornella, B. Vokits, S. A. Shaw, P. S. Baran, *Angew. Chem. Int. Ed.* **2016**, *55*, 9676–9679.
- [225] a) Y. Yang, K. Niedermann, C. Han, S. L. Buchwald, *Org. Lett.* **2014**, *16*, 4638–4641; b) A. Joshi-Pangu, M. Ganesh, M. R. Biscoe, *Org. Lett.* **2011**, *13*, 1218–1221.
- [226] a) J. A. van Rijn, M. A. Siegler, A. L. Spek, E. Bouwman, E. Drent, *Organometallics* **2009**, *28*, 7006–7014; b) K. L. Arthur, Q. L. Wang, D. M. Bregel, N. A. Smythe, B. A. O’Neil, K. I. Goldberg, K. G. Moloy, *Organometallics* **2005**, *24*, 4624–4628; c) J. J. Low, W. A. Goddard, *J. Am. Chem. Soc.* **1984**, *106*, 6928–6937.
- [227] a) Y. Li, Y. Luo, L. Peng, Y. Li, B. Zhao, W. Wang, H. Pang, Y. Deng, R. Bai, Y. Lan, G. Yin, *Nat. Commun.* **2020**, *11*, 417; b) D. D. Dawson, V. F. Oswald, A. S. Borovik, E. R. Jarvo, *Chem. Eur. J.* **2020**, *26*, 3044–3048; c) G. J. Harkness, M. L. Clarke, *Catal. Sci. Technol.* **2018**, *8*, 328–334; d) E. A. Standley, S. J. Smith, P. Müller, T. F. Jamison, *Organometallics* **2014**, *33*, 2012–2018; e) E. A. Standley, T. F. Jamison, *J. Am. Chem. Soc.* **2013**, *135*, 1585–1592.
- [228] a) A. L. Clevenger, R. M. Stolley, J. Aderibigbe, J. Louie, *Chem. Rev.* **2020**, *120*, 6124–6196; b) T. Inatomi, Y. Koga, K. Matsubara, *Molecules* **2018**, *23*, 140; c) K. K. Chow, W. Levason, C. A. McAuliffe, in *Transition Metal Complexes of Phosphorus, Arsenic and Antimony Ligands* (Ed.: C. A. McAuliffe), Macmillan Education UK, London, **1973**, pp. 33–204.

-
- [229] a) P. W. N. M. van Leeuwen, in *Organophosphorus Chemistry: From Molecules to Applications* (Ed.: V. Iaroshenko), Wiley-VCH, Weinheim, **2019**, pp. 1–58; b) C. Nataro, S. M. Fosbenner, *J. Chem. Educ.* **2009**, *86*, 1412; c) M.-N. Birkholz, Z. Freixa, P. W. N. M. van Leeuwen, *Chem. Soc. Rev.* **2009**, *38*, 1099–1118; d) P. Dierkes, P. W. N. M. van Leeuwen, *Dalton Trans.* **1999**, 1519–1530.
- [230] a) P. W. N. M. van Leeuwen, I. Cano, Z. Freixa, *ChemCatChem* **2020**, *12*, 3982–3994; b) A. Gallen, A. Riera, X. Verdaguer, A. Grabulosa, *Catal. Sci. Technol.* **2019**, *9*, 5504–5561; c) D. Hérault, D. H. Nguyen, D. Nuel, G. Buono, *Chem. Soc. Rev.* **2015**, *44*, 2508–2528; d) L. Ackermann, *Synthesis* **2006**, *2006*, 1557–1571.
- [231] a) C. Wu, S. P. McCollom, Z. Zheng, J. Zhang, S.-C. Sha, M. Li, P. J. Walsh, N. C. Tomson, *ACS Catal.* **2020**, *10*, 7934–7944; b) L. Ackermann, A. Althammer, *Chem. unserer Zeit* **2009**, *43*, 74–83; c) N. Yoshikai, H. Mashima, E. Nakamura, *J. Am. Chem. Soc.* **2005**, *127*, 17978–17979.
- [232] a) R. M. Peltzer, J. Gauss, O. Eisenstein, M. Cascella, *J. Am. Chem. Soc.* **2020**, *142*, 2984–2994; b) S. Koller, J. Gatzka, K. M. Wong, P. J. Altmann, A. Pöthig, L. Hintermann, *J. Org. Chem.* **2018**, *83*, 15009–15028; c) M. Westerhausen, A. Koch, H. Görls, S. Krieck, *Chem. Eur. J.* **2017**, *23*, 1456–1483; d) R. M. Peltzer, O. Eisenstein, A. Nova, M. Cascella, *J. Phys. Chem. B* **2017**, *121*, 4226–4237; e) D. Seyferth, *Organometallics* **2009**, *28*, 1598–1605; f) W. Schlenk, W. Schlenk jun., *Ber. dtsch. Chem. Ges. A/B* **1929**, *62*, 920–924.
- [233] C. S. Slater, M. J. Savelski, D. Hitchcock, E. J. Cavanagh, *J. Environ. Sci. Health A* **2016**, *51*, 487–494.
- [234] a) Y. Chen, *Adv. Synth. Catal.* **2020**, *362*, 998–1014; b) K. W. Kuntz, J. E. Campbell, H. Keilhack, R. M. Pollock, S. K. Knutson, M. Porter-Scott, V. M. Richon, C. J. Sneeringer, T. J. Wigle, C. J. Allain, C. R. Majer, M. P. Moyer, R. A. Copeland, R. Chesworth, *J. Med. Chem.* **2016**, *59*, 1556–1564; c) H. Schönherr, T. Cernak, *Angew. Chem. Int. Ed.* **2013**, *52*, 12256–12267; d) E. J. Barreiro, A. E. Kümmerle, C. A. M. Fraga, *Chem. Rev.* **2011**, *111*, 5215–5246.
- [235] a) M. Balkenhohl, P. Knochel, *SynOpen* **2018**, *02*, 78–95; b) V. Singh, Y. Nakao, S. Sakaki, M. M. Deshmukh, *J. Org. Chem.* **2017**, *82*, 289–301; c) W.-C. Lee, C.-H. Chen, C.-Y. Liu, M.-S. Yu, Y.-H. Lin, T.-G. Ong, *Chem. Commun.* **2015**, *51*, 17104–17107.
- [236] a) F.-F. Zhuo, W.-W. Xie, Y.-X. Yang, L. Zhang, P. Wang, R. Yuan, C.-S. Da, *J. Org. Chem.* **2013**, *78*, 3243–3249; b) H. G. Richey, J. Farkas, *Tetrahedron Lett.*

- 1985**, 26, 275–278; c) K. Ziegler, H. Zeiser, *Ber. dtsch. Chem. Ges. A/B* **1930**, 63, 1847–1851.
- [237] a) M. S. Eno, A. Lu, J. P. Morken, *J. Am. Chem. Soc.* **2016**, 138, 7824–7827; b) M. Jin, L. Adak, M. Nakamura, *J. Am. Chem. Soc.* **2015**, 137, 7128–7134; c) S. Lou, G. C. Fu, *J. Am. Chem. Soc.* **2010**, 132, 1264–1266; d) J. Mao, F. Liu, M. Wang, L. Wu, B. Zheng, S. Liu, J. Zhong, Q. Bian, P. J. Walsh, *J. Am. Chem. Soc.* **2014**, 136, 17662–17668; e) H. Horibe, Y. Fukuda, K. Kondo, H. Okuno, Y. Murakami, T. Aoyama, *Tetrahedron* **2004**, 60, 10701–10709.
- [238] Y. Kiso, K. Tamao, N. Miyake, K. Yamamoto, M. Kumada, *Tetrahedron Lett.* **1974**, 15, 3–6.
- [239] a) X.-B. Wang, M. Goto, L.-B. Han, *Chem. Eur. J.* **2014**, 20, 3631–3635; b) D. Gatineau, D. Moraleda, J.-V. Naubron, T. Bürgi, L. Giordano, G. Buono, *Tetrahedron: Asym.* **2009**, 20, 1912–1917; c) J. Bigeault, L. Giordano, G. Buono, *Angew. Chem. Int. Ed.* **2005**, 44, 4753–4757; d) X.-b. Jiang, A. J. Minnaard, B. Hessen, B. L. Feringa, A. L. L. Duchateau, J. G. O. Andrien, J. A. F. Boogers, J. G. de Vries, *Org. Lett.* **2003**, 5, 1503–1506; e) W.-M. Dai, K. K. Y. Yeung, W. H. Leung, R. K. Haynes, *Tetrahedron: Asym.* **2003**, 14, 2821–2826.
- [240] R. J. Somerville, L. V. A. Hale, E. Gómez-Bengoa, J. Burés, R. Martin, *J. Am. Chem. Soc.* **2018**, 140, 8771–8780.
- [241] a) L. S. Jongbloed, N. Vogt, A. Sandleben, B. de Bruin, A. Klein, J. I. van der Vlugt, *Eur. J. Inorg. Chem.* **2018**, 2018, 2408–2418; b) Muriel Durandetti, J. Maddaluno, in *Encyclopedia of Reagents for Organic Synthesis*, **2014**, pp. 1–3; c) J. Holzbock, W. Sawodny, L. Walz, *Z. Kristallogr. – Cryst. Mater.* **1997**, 212, 115–120; d) G. Liptay, T. Wadsten, A. Borbély-Kuszmán, *J. Therm. Anal.* **1990**, 36, 93–97; e) G. Liptay, T. Wadsten, A. Borbély-Kuszmán, *J. Therm. Anal.* **1986**, 31, 845–852; f) C. Ai-Hua, W. Ai-Jian, W. Ling, S. Yu-Tong, *Crystallogr. Rep.* **2018**, 63, 942–946; g) J. Zhang, S. Liu, A. Li, H. Ye, Z. Li, *New J. Chem.* **2016**, 40, 7027–7033; h) G. J. Long, P. J. Clarke, *Inorg. Chem.* **1978**, 17, 1394–1401; i) M. R. Rosenthal, R. S. Drago, *Inorg. Chem.* **1965**, 4, 840–844.
- [242] a) Y. Zhou, J. Wang, Z. Gu, S. Wang, W. Zhu, J. L. Aceña, V. A. Soloshonok, K. Izawa, H. Liu, *Chem. Rev.* **2016**, 116, 422–518; b) B. Kang, R. Kim, S. B. Lee, S.-K. Kwon, Y.-H. Kim, K. Cho, *J. Am. Chem. Soc.* **2016**, 138, 3679–3686; c) T. Fujiwara, D. O’Hagan, *J. Fluorine Chem.* **2014**, 167, 16–29; d) F. Liu, D. W. Grainger, in *Biomaterials Science (Third Edition)* (Eds.: B. D. Ratner, A. S.

-
- Hoffman, F. J. Schoen, J. E. Lemons), Academic Press, **2013**, pp. 92–103; e) E. D. Deeks, G. M. Keating, *CNS Drugs* **2010**, *24*, 65–84.
- [243] a) J. A. Wilkinson, *Chem. Rev.* **1992**, *92*, 505–519; b) M. R. C. Gerstenberger, A. Haas, *Angew. Chem. Int. Ed.* **1981**, *20*, 647–667.
- [244] a) X. Li, X. Shi, X. Li, D. Shi, *Beilstein J. Org. Chem.* **2019**, *15*, 2213–2270; b) D. E. Yerien, S. Bonesi, A. Postigo, *Org. Biomol. Chem.* **2016**, *14*, 8398–8427; c) T. Liang, C. N. Neumann, T. Ritter, *Angew. Chem. Int. Ed.* **2013**, *52*, 8214–8264.
- [245] a) Q. Cheng, T. Ritter, *Trends Chem.* **2019**, *1*, 461–470; b) J. A. Dean, in *Lange's Handbook of Chemistry (15th Ed)* (Ed.: J. A. Dean), McGraw-Hill, Inc., New-York, **1999**, pp. 4.1–4.81.
- [246] a) H. Egami, S. Masuda, Y. Kawato, Y. Hamashima, *Org. Lett.* **2018**, *20*, 1367–1370; b) J. G. West, T. A. Bedell, E. J. Sorensen, *Angew. Chem. Int. Ed.* **2016**, *55*, 8923–8927; c) M. B. Nodwell, A. Bagai, S. D. Halperin, R. E. Martin, H. Knust, R. Britton, *Chem. Commun.* **2015**, *51*, 11783–11786; d) J.-B. Xia, C. Zhu, C. Chen, *Chem. Commun.* **2014**, *50*, 11701–11704; e) S. D. Halperin, H. Fan, S. Chang, R. E. Martin, R. Britton, *Angew. Chem. Int. Ed.* **2014**, *53*, 4690–4693; f) J.-B. Xia, C. Zhu, C. Chen, *J. Am. Chem. Soc.* **2013**, *135*, 17494–17500.
- [247] a) K. Yamamoto, J. Li, J. A. O. Garber, J. D. Rolfes, G. B. Boursalian, J. C. Borghs, C. Genicot, J. Jacq, M. van Gastel, F. Neese, T. Ritter, *Nature* **2018**, *554*, 511–514; b) H. Park, P. Verma, K. Hong, J.-Q. Yu, *Nat. Chem.* **2018**, *10*, 755–762; c) R.-Y. Zhu, K. Tanaka, G.-C. Li, J. He, H.-Y. Fu, S.-H. Li, J.-Q. Yu, *J. Am. Chem. Soc.* **2015**, *137*, 7067–7070; d) S.-J. Lou, D.-Q. Xu, Z.-Y. Xu, *Angew. Chem. Int. Ed.* **2014**, *53*, 10330–10335; e) M.-G. Braun, A. G. Doyle, *J. Am. Chem. Soc.* **2013**, *135*, 12990–12993; f) K. B. McMurtrey, J. M. Racowski, M. S. Sanford, *Org. Lett.* **2012**, *14*, 4094–4097; g) K. S. L. Chan, M. Wasa, X. Wang, J.-Q. Yu, *Angew. Chem. Int. Ed.* **2011**, *50*, 9081–9084; h) X. Wang, T.-S. Mei, J.-Q. Yu, *J. Am. Chem. Soc.* **2009**, *131*, 7520–7521; i) K. L. Hull, W. Q. Anani, M. S. Sanford, *J. Am. Chem. Soc.* **2006**, *128*, 7134–7135.
- [248] a) P. Xu, S. Guo, L. Wang, P. Tang, *Angew. Chem. Int. Ed.* **2014**, *53*, 5955–5958; b) P. S. Fier, J. F. Hartwig, *Science* **2013**, *342*, 956–960; c) H. Schroeder, E. Kober, H. Ulrich, R. Rätz, H. Agahigian, C. Grundmann, *J. Org. Chem.* **1962**, *27*, 2580–2584.

- [249] a) T. Furuya, A. S. Kamlet, T. Ritter, *Nature* **2011**, *473*, 470–477; b) T. Furuya, J. E. M. N. Klein, T. Ritter, *Synthesis* **2010**, *2010*, 1804–1821; c) D. O'Hagan, *Chem. Soc. Rev.* **2008**, *37*, 308–319.
- [250] a) T. Truong, K. Klimovica, O. Daugulis, *J. Am. Chem. Soc.* **2013**, *135*, 9342–9345; b) W. Liu, J. T. Groves, *Angew. Chem. Int. Ed.* **2013**, *52*, 6024–6027; c) W. Liu, X. Huang, M.-J. Cheng, R. J. Nielsen, W. A. Goddard, J. T. Groves, *Science* **2012**, *337*, 1322–1325; d) S. Bloom, C. R. Pitts, D. C. Miller, N. Haselton, M. G. Holl, E. Urheim, T. Lectka, *Angew. Chem. Int. Ed.* **2012**, *51*, 10580–10583.
- [251] H. Stephen, T. S. Pergamon, *Solubilities of Inorganic and Organic Compounds: Binary Systems*, Pergamon Press Ltd., Oxford, **1963**.
- [252] a) A. E. Robel, K. Marshall, M. Dickinson, D. Lunderberg, C. Butt, G. Peaslee, H. M. Stapleton, J. A. Field, *Environ. Sci. Technol.* **2017**, *51*, 9022–9032; b) Y. Y. Stoilov, *Langmuir* **1998**, *14*, 5685–5690; c) C. E. Redemann, S. W. Chaikin, R. B. Fearing, G. J. Rotariu, J. Savit, D. v. Hoesen, *J. Am. Chem. Soc.* **1948**, *70*, 3604–3606.
- [253] a) J. R. Hummel, J. A. Boerth, J. A. Ellman, *Chem. Rev.* **2017**, *117*, 9163–9227; b) R. W. Layer, *Chem. Rev.* **1963**, *63*, 489–510; c) E. H. Cordes, W. P. Jencks, *J. Am. Chem. Soc.* **1963**, *85*, 2843–2848.
- [254] a) C. Liu, C. Zhu, Y. Cai, Z. Yang, H. Zeng, F. Chen, H. Jiang, *Chem. Eur. J.* **2020**, *26*, 1953–1957; b) S. Koley, R. A. Altman, *Isr. J. Chem.* **2020**, *60*, 313–339; c) L. Yang, W.-W. Ji, E. Lin, J.-L. Li, W.-X. Fan, Q. Li, H. Wang, *Org. Lett.* **2018**, *20*, 1924–1927; d) P. Gao, C. Yuan, Y. Zhao, Z. Shi, *Chem* **2018**, *4*, 2201–2211; e) X. Lu, Y. Wang, B. Zhang, J.-J. Pi, X.-X. Wang, T.-J. Gong, B. Xiao, Y. Fu, *J. Am. Chem. Soc.* **2017**, *139*, 12632–12637; f) S. B. Lang, R. J. Wiles, C. B. Kelly, G. A. Molander, *Angew. Chem. Int. Ed.* **2017**, *56*, 15073–15077; g) R. T. Thornbury, F. D. Toste, *Angew. Chem. Int. Ed.* **2016**, *55*, 11629–11632; h) X. Zhang, W. Dai, W. Wu, S. Cao, *Org. Lett.* **2015**, *17*, 2708–2711; i) W. Dai, J. Xiao, G. Jin, J. Wu, S. Cao, *J. Org. Chem.* **2014**, *79*, 10537–10546; j) G. Chelucci, *Chem. Rev.* **2012**, *112*, 1344–1462.
- [255] a) B. R. Reiner, A. A. Kassie, C. R. Wade, *Dalton Trans.* **2019**, *48*, 9588–9595; b) D. Lichosyt, Y. Zhang, K. Hurej, P. Dydio, *Nat. Catal.* **2019**, *2*, 114–122; c) L. E. Hanna, M. O. Konev, E. R. Jarvo, *Eur. J. Org. Chem.* **2019**, *2019*, 184–187; d) S. M. Jing, V. Balasanthiran, V. Pagar, J. C. Gallucci, T. V. RajanBabu, *J. Am. Chem. Soc.* **2017**, *139*, 18034–18043; e) S. W. M. Crossley, R. M. Martinez, S.

-
- Guevara-Zuluaga, R. A. Shenvi, *Org. Lett.* **2016**, *18*, 2620–2623; f) H. T. Dao, C. Li, Q. Michaudel, B. D. Maxwell, P. S. Baran, *J. Am. Chem. Soc.* **2015**, *137*, 8046–8049; g) Jean - Pierre Bégué, D. Bonnet - Delpon, in *Bioorganic and Medicinal Chemistry of Fluorine* (Ed.: D. B. D. Jean - Pierre Bégué), **2008**, pp. 1–22.
- [256] a) Z. Ruan, N. Sauermann, E. Manoni, L. Ackermann, *Angew. Chem. Int. Ed.* **2017**, *56*, 3172–3176; b) W. Liu, D. Zell, M. John, L. Ackermann, *Angew. Chem. Int. Ed.* **2015**, *54*, 4092–4096.
- [257] a) H. Pellissier, *Adv. Synth. Catal.* **2019**, *361*, 1733–1755; b) M. Ghosh, V. S. Shinde, M. Rueping, *Beilstein J. Org. Chem.* **2019**, *15*, 2710–2746; c) Y. Yamashita, T. Yasukawa, W.-J. Yoo, T. Kitanosono, S. Kobayashi, *Chem. Soc. Rev.* **2018**, *47*, 4388–4480; d) X.-P. Zeng, Z.-Y. Cao, Y.-H. Wang, F. Zhou, J. Zhou, *Chem. Rev.* **2016**, *116*, 7330–7396; e) V. Šunjić, V. P. Peroković, *Organic Chemistry from Retrosynthesis to Asymmetric Synthesis*, Springer International Publishing, Switzerland, **2016**; f) A. H. Cherney, N. T. Kadunce, S. E. Reisman, *Chem. Rev.* **2015**, *115*, 9587–9652; g) C. Bolm, J. A. Gladysz, *Chem. Rev.* **2003**, *103*, 2761–2762; h) G. R. Stephenson, *Advanced Asymmetric Synthesis*, Springer, Netherlands, **1996**.
- [258] The Nobel Prize in Chemistry 2001, NobelPrize.org. Nobel Media AB, accessed on 12.09.2020, retrieved from <https://www.nobelprize.org/prizes/chemistry/2001/summary/>.
- [259] a) K. Liao, T. C. Pickel, V. Boyarskikh, J. Bacsá, D. G. Musaev, H. M. L. Davies, *Nature* **2017**, *551*, 609–613; b) B. Ye, N. Cramer, *Acc. Chem. Res.* **2015**, *48*, 1308–1318; c) C. Zheng, S.-L. You, *RSC Adv.* **2014**, *4*, 6173–6214; d) R. Giri, B.-F. Shi, K. M. Engle, N. Mangel, J.-Q. Yu, *Chem. Soc. Rev.* **2009**, *38*, 3242–3272; e) H. M. L. Davies, J. R. Manning, *Nature* **2008**, *451*, 417–424; f) N. Cramer, J. Mas-Roselló, A. G. Herraiz, B. Audic, A. Laverny, *Angew. Chem. Int. Ed.* **2020**, *59*, 2–29.
- [260] F. Colobert, J. Wencel-Delord, *C–H Activation for Asymmetric Synthesis*, Wiley-VCH, Weinheim, **2019**.
- [261] a) V. V. Chernyshov, O. I. Yarovaya, D. S. Fadeev, Y. V. Gatilov, Y. L. Esaulkova, A. S. Muryleva, K. O. Sinegubova, V. V. Zarubaev, N. F. Salakhutdinov, *Mol. Divers.* **2020**, *24*, 61–67; b) Y. Wang, J. Wang, L. Wang,

- Benzimidazole derivatives, preparation methods and uses thereof*, WO 2018/113771 A1, **2018**; c) A. Kumar, S. Banerjee, P. Roy, S. M. Sondhi, A. Sharma, *Mol. Divers.* **2018**, *22*, 113–127; d) R. M. Jones, D. J. Buzard, A. M. Kawasaki, S. H. Kim, L. Thoresen, J. Lehmann, X. Zhu, (Arena Pharmaceuticals, Inc.), *Preparation of substituted tricyclic acid derivatives as SIPI receptor agonists useful in the treatment of autoimmune and inflammatory disorders*, WO 2010/027431 A1, **2010**; e) S. D. Edmondson, A. Mastracchio, J. M. Cox, G. J. Eiermann, H. He, K. A. Lyons, R. A. Patel, S. B. Patel, A. Petrov, G. Scapin, J. K. Wu, S. Xu, B. Zhu, N. A. Thornberry, R. S. Roy, A. E. Weber, *Bioorg. Med. Chem. Lett.* **2009**, *19*, 4097–4101; f) Y. L. Chen, K. Hedberg, K. Guarino, J. A. Retsema, M. Anderson, M. Manousos, J. Barrett, *J. Antibiot.* **1991**, *44*, 870–884.
- [262] a) D. Song, S. Ma, *ChemMedChem* **2016**, *11*, 646–659; b) P. Singla, V. Luxami, K. Paul, *RSC Adv.* **2014**, *4*, 12422–12440; c) M. Gaba, S. Singh, C. Mohan, *Eur. J. Med. Chem.* **2014**, *76*, 494–505; d) Y. Bansal, O. Silakari, *Biorg. Med. Chem.* **2012**, *20*, 6208–6236.
- [263] a) T. N. Nguyen, P.-A. Chen, K. Setthakarn, J. A. May, *Molecules* **2018**, *23*, 2317; b) K. Gratzer, M. Waser, *Synthesis* **2012**, *44*, 3661–3670.
- [264] a) M. R. Friedfeld, H. Zhong, R. T. Ruck, M. Shevlin, P. J. Chirik, *Science* **2018**, *360*, 888–893; b) M. Christensen, A. Nolting, M. Shevlin, M. Weisel, P. E. Maligres, J. Lee, R. K. Orr, C. W. Plummer, M. T. Tudge, L.-C. Campeau, R. T. Ruck, *J. Org. Chem.* **2016**, *81*, 824–830; c) X.-b. Jiang, M. van den Berg, A. J. Minnaard, B. L. Feringa, J. G. de Vries, *Tetrahedron: Asym.* **2004**, *15*, 2223–2229.
- [265] a) X.-H. Yang, V. M. Dong, *J. Am. Chem. Soc.* **2017**, *139*, 1774–1777; b) K. Xu, W. Raimondi, T. Bury, B. Breit, *Chem. Commun.* **2015**, *51*, 10861–10863; c) K. Xu, N. Thieme, B. Breit, *Angew. Chem. Int. Ed.* **2014**, *53*, 7268–7271.
- [266] L. Nattmann, R. Saeb, N. Nöthling, J. Cornella, *Nat. Catal.* **2020**, *3*, 6–13.
- [267] a) S. Kim, M. J. Goldfogel, M. M. Gilbert, D. J. Weix, *J. Am. Chem. Soc.* **2020**, *142*, 9902–9907; b) J.-L. Tao, Z.-X. Wang, *Asian J. Org. Chem.* **2016**, *5*, 521–527; c) L.-Y. Liao, X.-R. Kong, X.-F. Duan, *J. Org. Chem.* **2014**, *79*, 777–782.
- [268] a) A. J. Nett, S. Cañellas, Y. Higuchi, M. T. Robo, J. M. Kochkodan, M. T. Haynes, J. W. Kampf, J. Montgomery, *ACS Catal.* **2018**, *8*, 6606–6611; b) X. Jurvilliers, R. Schneider, Y. Fort, J. Ghanbaja, *Appl. Organomet. Chem.* **2001**, *15*, 744–748.

-
- [269] a) M. Gaba, C. Mohan, *Med. Chem. Res.* **2016**, *25*, 173–210; b) T. Wang, M. A. Block, S. Cowen, A. M. Davies, E. Devereaux, L. Gingipalli, J. Johannes, N. A. Larsen, Q. Su, J. A. Tucker, D. Whitston, J. Wu, H.-J. Zhang, M. Zinda, C. Chuaqui, *Bioorg. Med. Chem. Lett.* **2012**, *22*, 2063–2069.
- [270] a) A. Srivastava, S. Ramachandran, S. P. Hameed, V. Ahuja, V. P. Hosagrahara, *Chem. Res. Toxicol.* **2014**, *27*, 1586–1597; b) T. Chappie, M. Heyward, N. Patel, P. Verhoest, (Pfizer Inc.), *Azabenzimidazole compounds as inhibitors of pde4 isozymes for the treatment of cns and other disorders*, WO2014/128585A1, **2014**;
c) T. Wang, M. A. Block, S. Cowen, A. M. Davies, E. Devereaux, L. Gingipalli, J. Johannes, N. A. Larsen, Q. Su, J. A. Tucker, D. Whitston, J. Wu, H.-J. Zhang, M. Zinda, C. Chuaqui, *Bioorg. Med. Chem. Lett.* **2012**, *22*, 2063–2069; d) R. A. Stavenger, H. Cui, S. E. Dowdell, R. G. Franz, D. E. Gaitanopoulos, K. B. Goodman, M. A. Hilfiker, R. L. Ivy, J. D. Leber, J. P. Marino, H.-J. Oh, A. Q. Viet, W. Xu, G. Ye, D. Zhang, Y. Zhao, L. J. Jolivette, M. S. Head, S. F. Semus, P. A. Elkins, R. B. Kirkpatrick, E. Dul, S. S. Khandekar, T. Yi, D. K. Jung, L. L. Wright, G. K. Smith, D. J. Behm, C. P. Doe, R. Bentley, Z. X. Chen, E. Hu, D. Lee, *J. Med. Chem.* **2007**, *50*, 2–5.
- [271] a) Y.-Y. Zhou, C. Uyeda, *Science* **2019**, *363*, 857–862; b) C.-L. Hsieh, T.-J. Liu, Y. Song, G.-H. Lee, B.-Y. Jin, T.-S. Lin, S.-M. Peng, *Dalton Trans.* **2019**, *48*, 9912–9915; c) C.-C. Chiu, G.-H. Lee, T.-S. Lin, S.-M. Peng, *Dalton Trans.* **2019**, *48*, 8464–8477; d) A. K. Maity, M. Zeller, C. Uyeda, *Organometallics* **2018**, *37*, 2437–2441; e) S. Pal, Y.-Y. Zhou, C. Uyeda, *J. Am. Chem. Soc.* **2017**, *139*, 11686–11689.
- [272] a) A. Tzara, D. Xanthopoulos, A. P. Kourounakis, *ChemMedChem* **2020**, *15*, 392–403; b) V. A. Pal'chikov, *Russ. J. Org. Chem.* **2013**, *49*, 787–814.
- [273] a) Y. J. Ma, D. Q. Jiang, J. X. Meng, M. X. Li, H. H. Zhao, Y. Wang, L. Q. Wang, *J. Clin. Pharm.* **2016**, *41*, 594–601; b) P. J. Barnes, *Pharmaceuticals* **2010**, *3*, 725–747; c) K. Ito, S. Lim, G. Caramori, B. Cosio, K. F. Chung, I. M. Adcock, P. J. Barnes, *Proc. Natl. Acad. Sci. U.S.A.* **2002**, *99*, 8921–8926.
- [274] a) Li Ran, Xu XueTao, Y. Mengchun, *Chin. J. Org. Chem.* **2020**, *40*, DOI: 10.6023/cjoc202005056; b) A. S. Kleinke, D. Webb, T. F. Jamison, *Tetrahedron* **2012**, *68*, 6999–7018; c) S. K. Chattopadhyay, S. Karmakar, T. Biswas, K. C. Majumdar, H. Rahaman, B. Roy, *Tetrahedron* **2007**, *63*, 3919–3952; d) G. A. Molander, *Acc. Chem. Res.* **1998**, *31*, 603–609.

- [275] a) S. Bajo, G. Laidlaw, A. R. Kennedy, S. Sproules, D. J. Nelson, *Organometallics* **2017**, *36*, 1662–1672; b) D. A. Everson, B. A. Jones, D. J. Weix, *J. Am. Chem. Soc.* **2012**, *134*, 6146–6159.
- [276] a) K. Gonzalez Nieves, D. M. Pinero Cruz, *Acta Crystallogr. E* **2020**, *76*, 314–317; b) N. Türkel, *Bioinorg. Chem. Appl.* **2015**, *2015*, 374782; c) R. H. Crabtree, *Chem. Rev.* **2015**, *115*, 127–150; d) M. D. Argyle, C. H. Bartholomew, *Catalysts* **2015**, *5*, 145–269; e) C. L. Weeks, P. Turner, R. R. Fenton, P. A. Lay, *Dalton Trans.* **2002**, 931–940; f) A. Baiker, D. Monti, Y. S. Fan, *J. Catal.* **1984**, *88*, 81–88.
- [277] a) Y. He, Y. Cai, S. Zhu, *J. Am. Chem. Soc.* **2017**, *139*, 1061–1064; b) M. Gaydou, T. Moragas, F. Juliá-Hernández, R. Martin, *J. Am. Chem. Soc.* **2017**, *139*, 12161–12164; c) I. Buslov, J. Becouse, S. Mazza, M. Montandon-Clerc, X. Hu, *Angew. Chem. Int. Ed.* **2015**, *54*, 14523–14526; d) J. S. Bair, Y. Schramm, A. G. Sergeev, E. Clot, O. Eisenstein, J. F. Hartwig, *J. Am. Chem. Soc.* **2014**, *136*, 13098–13101; e) W.-C. Lee, C.-H. Wang, Y.-H. Lin, W.-C. Shih, T.-G. Ong, *Org. Lett.* **2013**, *15*, 5358–5361.
- [278] D. Gallego, E. A. Baquero, *Open Chemistry* **2018**, *16*, 1001–1058.
- [279] E. M. Simmons, J. F. Hartwig, *Angew. Chem. Int. Ed.* **2012**, *51*, 3066–3072.
- [280] a) A. A. Ádám, M. Szabados, K. Musza, P. Bélteky, Z. Kónya, Á. Kukovecz, P. Sipos, I. Pálinkó, *React. Kinet. Mech. Catal.* **2019**, *126*, 841–855; b) A. F. Schmidt, V. V. Smirnov, A. Al-Halaiga, *Kinet. Catal.* **2007**, *48*, 390–397.
- [281] a) A. J. Nett, J. Montgomery, P. M. Zimmerman, *ACS Catal.* **2017**, *7*, 7352–7362; b) A. J. Nett, W. Zhao, P. M. Zimmerman, J. Montgomery, *J. Am. Chem. Soc.* **2015**, *137*, 7636–7639.
- [282] a) S. Tang, O. Eisenstein, Y. Nakao, S. Sakaki, *Organometallics* **2017**, *36*, 2761–2771; b) Y. Gao, K. N. Houk, C.-Y. Ho, X. Hong, *Org. Biomol. Chem.* **2017**, *15*, 7131–7139; c) X. Hong, J. Wang, Y.-F. Yang, L. He, C.-Y. Ho, K. N. Houk, *ACS Catal.* **2015**, *5*, 5545–5555.
- [283] a) L.-B. Han, Y. Ono, H. Yazawa, *Org. Lett.* **2005**, *7*, 2909–2911; b) L.-B. Han, C. Zhang, H. Yazawa, S. Shimada, *J. Am. Chem. Soc.* **2004**, *126*, 5080–5081.
- [284] a) O. Eisenstein, J. Milani, R. N. Perutz, *Chem. Rev.* **2017**, *117*, 8710–8753; b) L.-J. Xiao, X.-N. Fu, M.-J. Zhou, J.-H. Xie, L.-X. Wang, X.-F. Xu, Q.-L. Zhou, *J. Am. Chem. Soc.* **2016**, *138*, 2957–2960; c) J. Guihaumé, S. Halbert, O. Eisenstein, R. N. Perutz, *Organometallics* **2012**, *31*, 1300–1314.

-
- [285] J.-B. Liu, X. Wang, A. Messinis, X.-J. Liu, R. Kuniyil, D. Chen, L. Ackermann, *Chem. Sci.* **2020**, 718–729.
- [286] V. Derdau, *Chem. unserer Zeit* **2019**, 53, 224–231.
- [287] a) D. Gao, X. Chen, X. Yang, Q. Wu, F. Jin, H. Wen, Y. Jiang, H. Liu, *J. Am. Soc. Mass Spectrom. Chem.* **2015**, 26, 686–694; b) C. S. Elmore, R. A. Bragg, *Bioorg. Med. Chem. Lett.* **2015**, 25, 167–171; c) O. Chahrour, D. Cobice, J. Malone, *J. Pharm. Biomed. Anal.* **2015**, 113, 2–20; d) J. J. Vrbanac, A. Hilgers, T. Dubnicka, F. B. Shilliday, D. Humphries, R. N. Hayes, *Rapid Commun. Mass Spectrom.* **2012**, 26, 2569–2576; e) N. Penner, L. Xu, C. Prakash, *Chem. Res. Toxicol.* **2012**, 25, 513–531; f) I. Jacobo, S. Lekha, A. V. Dietrich, *Curr. Drug Metab.* **2012**, 13, 1213–1225; g) R. C. A. Schellekens, F. Stellaard, H. J. Woerdenbag, H. W. Frijlink, J. G. W. Kosterink, *Br. J. Clin. Pharmacol.* **2011**, 72, 879–897; h) A. E. Mutlib, *Chem. Res. Toxicol.* **2008**, 21, 1672–1689.
- [288] a) M. Moir, J. J. Danon, T. A. Reekie, M. Kassiou, *Expert Opin. Drug Discov.* **2019**, 14, 1137–1149; b) K. Chen, X. Lei, *Curr. Opin. Green Sustain. Chem.* **2018**, 11, 9–14; c) D. Basu, S. Kumar, S. S. V, R. Bandichhor, *J. Chem. Sci.* **2018**, 130, 71; d) C. Schmidt, *Nat. Biotechnol.* **2017**, 35, 493–494; e) T. Gensch, M. N. Hopkinson, F. Glorius, J. Wencel-Delord, *Chem. Soc. Rev.* **2016**, 45, 2900–2936.
- [289] a) M. Valero, D. Becker, K. Jess, R. Weck, J. Atzrodt, T. Bannenberg, V. Derdau, M. Tamm, *Chem. Eur. J.* **2019**, 25, 6517–6522; b) W. J. Kerr, R. J. Mudd, M. Reid, J. Atzrodt, V. Derdau, *ACS Catal.* **2018**, 8, 10895–10900; c) W. J. Kerr, M. Reid, T. Tuttle, *Angew. Chem. Int. Ed.* **2017**, 56, 7808–7812; d) E. R. M. Habraken, P. Haspeslagh, M. Vliegen, T. Noël, *J. Flow Chem.* **2015**, 5, 2–5; e) J. J. Verendel, O. Pàmies, M. Diéguez, P. G. Andersson, *Chem. Rev.* **2014**, 114, 2130–2169; f) W. J. Kerr, R. J. Mudd, L. C. Paterson, J. A. Brown, *Chem. Eur. J.* **2014**, 20, 14604–14607; g) D. Hesk, P. R. Das, B. Evans, *J. Labelled Compd. Radiopharm.* **1995**, 36, 497–502.
- [290] a) A. Bechtoldt, M. E. Baumert, L. Vaccaro, L. Ackermann, *Green Chem.* **2018**, 20, 398–402; b) S. Warratz, C. Kornhaaß, A. Cajaraville, B. Niepötter, D. Stalke, L. Ackermann, *Angew. Chem. Int. Ed.* **2015**, 54, 5513–5517; c) L. Ackermann, J. Pospesch, *Org. Lett.* **2011**, 13, 4153–4155.
- [291] a) S.-S. Yan, Q. Fu, L.-L. Liao, G.-Q. Sun, J.-H. Ye, L. Gong, Y.-Z. Bo-Xue, D.-G. Yu, *Coord. Chem. Rev.* **2018**, 374, 439–463; b) in *Bioactive Carboxylic Compound Classes*, **2016**, pp. 221–236; c) C. Lamberth, J. Dinges, *Bioactive*

- Carboxylic Compound Classes: Pharmaceuticals and Agrochemicals*, Wiley-VCH, Weinheim, **2016**; d) L. J. Gooßen, N. Rodríguez, K. Gooßen, *Angew. Chem. Int. Ed.* **2008**, *47*, 3100–3120; e) L. S. Hegedus, L. Wade, in *Compendium of Organic Synthetic Methods* (Ed.: L. W. Louis S. Hegedus), John Wiley & Sons, Hoboken, NJ, **1977**, pp. 8–32.
- [292] a) Z. Wang, X. Wang, Y. Nishihara, *Chem. Asian J.* **2020**, *15*, 1234–1247; b) P. A. Dub, T. Ikariya, *ACS Catal.* **2012**, *2*, 1718–1741; c) L. J. Gooßen, K. Gooßen, N. Rodríguez, M. Blanchot, C. Linder, B. Zimmermann, *Pure Appl. Chem.* **2008**, *80*, 1725–1733.
- [293] a) R. Kluger, G. W. Howe, S. O. C. Mundle, in *Adv. Phys. Org. Chem.* (Eds.: I. H. Williams, N. H. Williams), Academic Press, **2013**, pp. 85–128; b) S. Rajadurai, *Catalysis Reviews* **1994**, *36*, 385–403.
- [294] a) S. E. David, P. Timmins, B. R. Conway, *Drug Dev. Ind. Pharm.* **2012**, *38*, 93–103; b) C. M. Romero, F. Suárez, *J. Solution Chem.* **2009**, *38*, 315–320; c) J. N. Starr, C. J. King, *Ind. Eng. Chem.* **1992**, *31*, 2572–2579.
- [295] C. Y. Y. Wong, A. W.-T. Choi, M. Y. Lui, B. Fridrich, A. K. Horváth, L. T. Mika, I. T. Horváth, *J. Struct. Chem.* **2017**, *28*, 423–429.
- [296] a) J. Dong, X. Wang, Z. Wang, H. Song, Y. Liu, Q. Wang, *Chem. Sci.* **2020**, *11*, 1026–1031; b) R. Zhou, J. Li, H. W. Cheo, R. Chua, G. Zhan, Z. Hou, J. Wu, *Chem. Sci.* **2019**, *10*, 7340–7344.
- [297] a) B. I. Synzynys, O. A. Momot, O. A. Mirzeabasov, A. V. Zemnova, E. R. Lyapunova, M. G. Yu, A. A. Oudalova, *KnE Engineering* **2018**, *3*, 249–260; b) I. Fairlie, *Med Confl Surviv* **2008**, *24*, 306–319; c) J. J. Katz, in *Kirk - Othmer Encyclopedia of Chemical Technology*, **2000**, pp. 1–13; d) Review of Risk from Tritium 2007, Advisory Group on Ionising Radiation, accessed on 12.11.2020, retrieved from http://www.rachel.org/lib/tritium_risks.070601.pdf.
- [298] a) C. R. Culy, B. Jarvis, *Drugs* **2001**, *61*, 1625–1660; b) R. Moses, *Expert Opin. Pharmacother.* **2000**, *1*, 1455–1467; c) M. Massi-Benedetti, P. Damsbo, *Expert Opin. Investig. Drugs* **2000**, *9*, 885–898.
- [299] a) X. Fang, B. Li, J. Zheng, X. Wang, H. Zhu, Y. Yuan, *Dalton Trans.* **2019**, *48*, 2290–2294; b) S. Parveen, M. Hanif, S. Movassaghi, M. P. Sullivan, M. Kubanik, M. A. Shaheen, T. Söhnel, S. M. F. Jamieson, C. G. Hartinger, *Eur. J. Inorg. Chem.* **2017**, *2017*, 1721–1727; c) J. Hubrich, L. Ackermann, *Eur. J. Org. Chem.*

-
- 2016, *2016*, 3700–3704; d) T. G. Scrase, M. J. O'Neill, A. J. Peel, P. W. Senior, P. D. Matthews, H. Shi, S. R. Boss, P. D. Barker, *Inorg. Chem.* **2015**, *54*, 3118–3124; e) L. Schäffler, U. R. Werz, G. Maas, *Inorg. Chim. Acta* **2005**, *358*, 3152–3158.
- [300] a) G.-W. Wang, M. Wheatley, M. Simonetti, D. M. Cannas, I. Larrosa, *Chem* **2020**, *6*, 1459–1468; b) A. Sagadevan, A. Charitou, F. Wang, M. Ivanova, M. Vuagnat, M. F. Greaney, *Chem. Sci.* **2020**, *11*, 4439–4443; c) L. Huang, D. J. Weix, *Org. Lett.* **2016**, *18*, 5432–5435; d) A. Biafora, T. Krause, D. Hackenberger, F. Belitz, L. J. Gooßen, *Angew. Chem. Int. Ed.* **2016**, *55*, 14752–14755.
- [301] a) J. E. Frampton, *Drugs* **2011**, *71*, 651–677; b) M. Destro, F. Cagnoni, G. P. Dognini, V. Galimberti, C. Taietti, C. Cavalleri, E. Galli, *Expert Opin. Pharmacother.* **2011**, *12*, 2719–2735; c) S. Deppe, R. H. Böger, J. Weiss, R. A. Benndorf, *Expert Opin. Drug Metab. Toxicol.* **2010**, *6*, 863–871; d) A. J. Battershill, L. J. Scott, *Drugs* **2006**, *66*, 51–83.
- [302] a) G. L. Plosker, K. F. Croom, *Drugs* **2005**, *65*, 1825–1849; b) C. P. Rains, S. Noble, D. Faulds, *Drugs* **1995**, *50*, 137–156; c) T. S. Gagarella, R. E. Walsh, *Dig. Dis. Sci.* **1992**, *37*, 801–812; d) K. M. Das, *Gastroenterol. Clin. North Am.* **1989**, *18*, 1–20.
- [303] a) S. C. Kharod, S. K. Kang, S. D. Kadam, *Front. Neurosci.* **2019**, *13*, 310; b) D. M. van Andel, J. J. Sprengers, B. Oranje, F. E. Scheepers, F. E. Jansen, H. Bruining, *Mol. Autism* **2020**, *11*, 30–34; c) A. Ward, R. C. Heel, *Drugs* **1984**, *28*, 426–464.
- [304] J. Hubrich, T. Himmler, L. Rodefeld, L. Ackermann, *ACS Catal.* **2015**, *5*, 4089–4093.
- [305] a) C. T. Supuran, *Molecules* **2017**, *22*, 1642; b) Y. Kwon, J. Song, H. Lee, E.-Y. Kim, K. Lee, S. K. Lee, S. Kim, *J. Med. Chem.* **2015**, *58*, 7749–7762; c) H.-X. Dai, A. F. Stepan, M. S. Plummer, Y.-H. Zhang, J.-Q. Yu, *J. Am. Chem. Soc.* **2011**, *133*, 7222–7228.
- [306] a) D. P. Elder, R. Holm, H. L. d. Diego, *Int. J. Pharm.* **2013**, *453*, 88–100; b) K. T. Savjani, A. K. Gajjar, J. K. Savjani, *ISRN Pharmaceutics* **2012**, *2012*, 195727; c) C. A. Lipinski, F. Lombardo, B. W. Dominy, P. J. Feeney, *Adv. Drug Deliv. Rev.* **2001**, *46*, 3–26.

- [307] a) K.-X. Tang, C.-M. Wang, T.-H. Gao, L. Chen, L. Fan, L.-P. Sun, *Adv. Synth. Catal.* **2019**, *361*, 26–38; b) Y. Dong, X. Zhang, J. Chen, W. Zou, S. Lin, H. Xu, *Chem. Sci.* **2019**, *10*, 8744–8751.
- [308] a) L. Wang, B. P. Carrow, *ACS Catal.* **2019**, *9*, 6821–6836; b) K. Naksomboon, J. Poater, F. M. Bickelhaupt, M. Á. Fernández-Ibáñez, *J. Am. Chem. Soc.* **2019**, *141*, 6719–6725.
- [309] M. Saljoughian, *Synthesis* **2002**, *2002*, 1781–1801.
- [310] a) J. V. Kondakova, C. D. Khoroshilova, A. B. Sazonov, *Radiochim. Acta* **2020**, *108*, 375–382; b) S. Heinze, T. Stolz, D. Ducret, J.-C. Colson, *Fusion Sci. Technol.* **2005**, *48*, 673–679; c) T. Stolz, D. Ducret, S. Heinze, G. Baldacchino, J. C. Colson, B. Dedieu, T. Pelletier, *Fusion Eng. Des.* **2003**, *69*, 57–60; d) E. Collinson, F. S. Dainton, J. Kroh, *Proc. Math. Phys. Eng. Sci.* **1962**, *265*, 422–429; e) A. H. Price, *Nature* **1958**, *181*, 262–262.
- [311] a) S. Waclawek, V. V. T. Padil, M. Černík, *Ecol. Chem. Eng. S* **2018**, *25*, 9–34; b) M. Schmal, *Heterogeneous Catalysis and its Industrial Applications*, Springer International Publishing, Switzerland, **2016**; c) Uwe Dingerdissen, Andreas Martin, Daniel Herein, Hans Jürgen Wernicke, in *Handbook of Heterogeneous Catalysis* (Ed.: H. K. G. Ertl, F. Schüth and J. Weitkamp), Wiley-VCH, Weinheim, **2008**, pp. 37–56.
- [312] a) S. Bhattacharya, Kumar;, K. Cameron, O'Keefe;, M. Dowling, Scott;, D. Ebner, Christopher;, D. Edmons, James, (Pfizer Inc.), *Indole compounds that activate AMPK*, WO 2014/140704 A1, **2014**; b) C. W. Alexander, D. De, I. K. Khanna, S. Pillarisetti, (Dr. Reddy's Laboratories Ltd.), *Heterocyclic compounds as gata modulators*, WO 2010/028179 A1, **2010**; c) W. D. Shrader, A. Kolesnikov, J. Burgess-Henry, R. Rai, J. Hendrix, H. Hu, S. Torkelson, T. Ton, W. B. Young, B. A. Katz, C. Yu, J. Tang, R. Cabuslay, E. Sanford, J. W. Janc, P. A. Sprengeler, *Bioorg. Med. Chem. Lett.* **2006**, *16*, 1596–1600; d) T. G. Kantor, *Pharmacotherapy* **1986**, *6*, 93–102; e) R. N. Brogden, R. C. Heel, T. M. Speight, G. S. Avery, *Drugs* **1979**, *18*, 417–438; f) R. N. Brogden, R. M. Finder, T. M. Speight, G. S. Avery, *Drugs* **1977**, *13*, 241–265.
- [313] a) Z. Moussa, Z. M. A. Judeh, S. A. Ahmed, *RSC Adv.* **2019**, *9*, 35217–35272; b) N. E. Leadbeater, K. A. Scott, L. J. Scott, *J. Org. Chem.* **2000**, *65*, 3231–3232.
- [314] I. Choi, V. Müller, Y. Wang, K. Xue, R. Kuniyil, V. Karius, L. B. Andreas, J. G. Alauzun, L. Ackermann, *Chem. Eur. J.* **2020**, *26*, 15290–15297.

-
- [315] X. Cui, A.-E. Surkus, K. Junge, C. Topf, J. Radnik, C. Kreyenschulte, M. Beller, *Nat. Commun.* **2016**, *7*, 11326.
- [316] a) P. T. Smith, E. M. Nichols, Z. Cao, C. J. Chang, *Acc. Chem. Res.* **2020**, *53*, 575–587; b) M. P. Conley, C. Copéret, C. Thieuleux, *ACS Catal.* **2014**, *4*, 1458–1469; c) U. Díaz, M. Boronat, A. Corma, *Proc. Math. Phys. Eng. Sci.* **2012**, *468*, 1927–1954.
- [317] a) T. Yu, Z. Ding, W. Nie, J. Jiao, H. Zhang, Q. Zhang, C. Xue, X. Duan, Y. M. A. Yamada, P. Li, *Chem. Eur. J.* **2020**, *26*, 5729–5747; b) M. Trojanowicz, *Molecules* **2020**, *25*, 1434; c) H. Ishitani, Y. Saito, B. Laroche, X. Rao, S. Kobayashi, in *Flow Chemistry: Integrated Approaches for Practical Applications* (Eds.: V. L. Santiago, E. Garcia-Verdugo), The Royal Society of Chemistry, **2020**, pp. 1–49; d) R. L. Hartman, *Curr. Opin. Chem. Eng.* **2020**, *29*, 42–50; e) S. Govaerts, A. Nyuchev, T. Noel, *J. Flow Chem.* **2020**, *10*, 13–71; f) S. Santoro, F. Ferlin, L. Ackermann, L. Vaccaro, *Chem. Soc. Rev.* **2019**, *48*, 2767–2782; g) R. Ciriminna, M. Pagliaro, R. Luque, *Preprints* **2019**, DOI: doi.org/10.1016/j.gee.2020.1009.1013; h) F. M. Akwi, P. Watts, *Chem. Commun.* **2018**, *54*, 13894–13928; i) A. Tanimu, S. Jaenicke, K. Alhooshani, *Chem. Eng. J.* **2017**, *327*, 792–821; j) M. B. Plutschack, B. Pieber, K. Gilmore, P. H. Seeberger, *Chem. Rev.* **2017**, *117*, 11796–11893; k) T. Noël, S. L. Buchwald, *Chem. Soc. Rev.* **2011**, *40*, 5010–5029.
- [318] a) I. Turel, J. Kljun, F. Perdih, E. Morozova, V. Bakulev, N. Kasyanenko, J. A. W. Byl, N. Osheroff, *Inorg. Chem.* **2010**, *49*, 10750–10752; b) M. F. Mahon, M. K. Whittlesey, P. T. Wood, *Organometallics* **1999**, *18*, 4068–4074.
- [319] S. Phillips, P. Kauppinen, *Platin. Met. Rev.* **2010**, *54*, 69–70.
- [320] a) A. R. Riscoe, C. J. Wrasman, A. A. Herzing, A. S. Hoffman, A. Menon, A. Boubnov, M. Vargas, S. R. Bare, M. Cargnello, *Nat. Catal.* **2019**, *2*, 852–863; b) V. I. Dybkov, *J. Mater. Sci.* **1986**, *21*, 3085–3090; c) T. K. Sherwood, *Pure Appl. Chem.* **1965**, *10*, 595–609; d) J. F. Zimmerman, *J. Phys. Chem.* **1949**, *53*, 562–569.
- [321] M. Che, J. C. Vedrine, *Characterization of Solid Materials and Heterogeneous Catalysts: From Structure to Surface Reactivity*, Wiley-VCH, Weinheim, **2012**.
- [322] a) B. Tang, J. Zhao, J.-F. Xu, X. Zhang, *Chem. Sci.* **2020**, *11*, 1192–1204; b) D. Leifert, A. Studer, *Angew. Chem. Int. Ed.* **2020**, *59*, 74–108; c) M. L. Poutsma, J.

- Org. Chem.* **2011**, *76*, 270–276; d) J. Hioe, H. Zipse, *Org. Biomol. Chem.* **2010**, *8*, 3609–3617.
- [323] a) T. G. Gant, A. I. Meyers, *Tetrahedron* **1994**, *50*, 2297–2360; b) A. I. Meyers, E. D. Mihelich, *Angew. Chem. Int. Ed.* **1976**, *15*, 270–281; c) J. A. Frump, *Chem. Rev.* **1971**, *71*, 483–505.
- [324] a) C. A. Quesnelle, V. Snieckus, *Synthesis* **2018**, *50*, 4413–4428; b) K. R. Campos, *Chem. Soc. Rev.* **2007**, *36*, 1069–1084; c) J. Epszajn, A. Jozwiak, A. K. Szczesniak, *Curr. Org. Chem.* **2006**, *10*, 1817–1848; d) M. Schlosser, *Angew. Chem. Int. Ed.* **2005**, *44*, 376–393; e) C. G. Hartung, V. Snieckus, in *Modern Arene Chemistry* (Ed.: D. Astruc), Wiley - VCH, Weinheim, **2002**, pp. 330–367; f) V. Snieckus, *Chem. Rev.* **1990**, *90*, 879–933.
- [325] a) M. Tobisu, K. Yasui, Y. Aihara, N. Chatani, *Angew. Chem. Int. Ed.* **2017**, *56*, 1877–1880; b) R. Mei, J. Loup, L. Ackermann, *ACS Catal.* **2016**, *6*, 793–797; c) R. Mei, L. Ackermann, *Adv. Synth. Catal.* **2016**, *358*, 2443–2448.
- [326] a) M. Mondal, T. Begum, P. Bharali, *Catal. Sci. Technol.* **2018**, *8*, 6029–6056; b) V. Gayakhe, Y. S. Sanghvi, I. J. S. Fairlamb, A. R. Kapdi, *Chem. Commun.* **2015**, *51*, 11944–11960; c) M. K. Lakshman, A. C. Deb, R. R. Chamala, P. Pradhan, R. Pratap, *Angew. Chem. Int. Ed.* **2011**, *50*, 11400–11404.
- [327] a) W. Xu, K. M. Chan, E. T. Kool, *Nat. Chem.* **2017**, *9*, 1043–1055; b) A. M. Pedley, S. J. Benkovic, *Trends Biochem. Sci.* **2017**, *42*, 141–154; c) M. Hocek, *Nucleic Acids Symp. Ser.* **2005**, *49*, 29–30.
- [328] H. G. Viehe, Z. Janousek, R. Merenyi, L. Stella, *Acc. Chem. Res.* **1985**, *18*, 148–154.
- [329] M. Arpad, P. Attila, *Curr. Org. Chem.* **2016**, *20*, 381–458.
- [330] a) G. Ni, Y. Du, F. Tang, J. Liu, H. Zhao, Q. Chen, *RSC Adv.* **2019**, *9*, 14302–14320; b) K. L. Seley-Radtke, M. K. Yates, *Antivir. Res.* **2018**, *154*, 66–86; c) A. R. Kapdi, D. Maiti, Y. S. Sanghvi, *Palladium-Catalyzed Modification of Nucleosides, Nucleotides and Oligonucleotides*, Elsevier, Oxford, **2018**; d) Z. Jahnz-Wechmann, G. R. Framski, P. A. Januszczuk, J. Boryski, *Front. Chem.* **2016**, *4*, DOI: 10.3389/fchem.2016.00019; e) K. H. Shaughnessy, *Molecules* **2015**, *20*, 9419; f) Y. Liang, S. F. Wnuk, *Molecules* **2015**, *20*, 4874; g) L. P. Jordheim, D. Durantel, F. Zoulim, C. Dumontet, *Nat. Rev. Drug Discov.* **2013**, *12*,

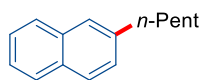
-
- 447–464; h) J. Štambaský, M. Hocek, P. Kočovský, *Chem. Rev.* **2009**, *109*, 6729–6764.
- [331] a) R. A. Jagtap, B. Punji, *Asian J. Org. Chem.* **2020**, *9*, 326–342; b) J. A. Leitch, Y. Bhonoah, C. G. Frost, *ACS Catal.* **2017**, *7*, 5618–5627; c) A. H. Sandtorv, *Adv. Synth. Catal.* **2015**, *357*, 2403–2435.
- [332] a) W. Liu, J. Bang, Y. Zhang, L. Ackermann, *Angew. Chem. Int. Ed.* **2015**, *54*, 14137–14140; b) V. Smout, A. Peschiulli, S. Verbeeck, E. A. Mitchell, W. Herrebout, P. Bultinck, C. M. L. Vande Velde, D. Berthelot, L. Meerpoel, B. U. W. Maes, *J. Org. Chem.* **2013**, *78*, 9803–9814.
- [333] a) L. Guillemard, J. Wencel-Delord, *Beilstein J. Org. Chem.* **2020**, *16*, 1754–1804; b) K. Korvorapun, J. Struwe, R. Kuniyil, A. Zangarelli, A. Casnati, M. Waeterschoot, L. Ackermann, *Angew. Chem. Int. Ed.*, *59*, 18103–18109.
- [334] a) M. März, M. Kohout, T. Nevesely, J. Chudoba, D. Prukała, S. Niziński, M. Sikorski, G. Burdziński, R. Cibulka, *Org. Biomol. Chem.* **2018**, *16*, 6809–6817; b) C.-S. Wang, P. H. Dixneuf, J.-F. Soulé, *ChemCatChem* **2017**, *9*, 3117–3120; c) Y. Unoh, T. Satoh, K. Hirano, M. Miura, *ACS Catal.* **2015**, *5*, 6634–6639; d) S. Yasui, S. Tojo, T. Majima, *J. Org. Chem.* **2005**, *70*, 1276–1280; e) N. Somasundaram, C. Srinivasan, *J. Org. Chem.* **1996**, *61*, 2895–2896; f) G. I. Nikishin, V. G. Glukhovtsev, M. A. Peikova, A. V. Ignatenko, *Bulletin of the Academy of Sciences of the USSR, Division of chemical science* **1971**, *20*, 2202–2204.
- [335] V. Müller, D. Ghorai, L. Capdevila, A. M. Messinis, X. Ribas, L. Ackermann, *Org. Lett.* **2020**, *22*, 7034–7040.
- [336] U. Dhawa, D. Zell, R. Yin, S. Okumura, M. Murakami, L. Ackermann, *J. Catal.* **2018**, *364*, 14–18.
- [337] a) M. Abram, M. Jakubiec, K. Kamiński, *ChemMedChem* **2019**, *14*, 1744–1761; b) H. Alkadi, R. Jbeily, *Infect. Disord. Drug Targets* **2018**, *18*, 88–95.
- [338] a) G.-L. Gao, C. Yang, W. Xia, *Chem. Commun.* **2017**, *53*, 1041–1044; b) J. Gui, Q. Zhou, C.-M. Pan, Y. Yabe, A. C. Burns, M. R. Collins, M. A. Ornelas, Y. Ishihara, P. S. Baran, *J. Am. Chem. Soc.* **2014**, *136*, 4853–4856.
- [339] Pierre H. Dixneuf, Christian Bruneau, *Ruthenium in Catalysis*, Springer, Cham, Switzerland **2014**.
- [340] J. Zhang, S. Zhang, T. Gogula, H. Zou, *ACS Catal.* **2020**, *10*, 7486–7494.

- [341] O. Piermatti, R. Abu - Reziq, L. Vaccaro, in *Catalyst Immobilization* (Eds.: M. Benaglia, A. Puglisi), Wiley-VCH, Weinheim, **2020**, pp. 1–22.
- [342] D. Meng, J. Bi, Y. Dong, B. Hao, K. Qin, T. Li, D. Zhu, *Chem. Commun.* **2020**, 56, 2889–2892.
- [343] H. E. Gottlieb, V. Kotlyar, A. Nudelman, *J. Org. Chem.* **1997**, 62, 7512–7515.
- [344] M. J. O'Neil, P. E. Heckelman, C. B. Koch, K. J. Roman, *The Merck Index, an Encyclopedia of Chemicals, Drugs, and Biologicals – Fourteenth Edition*, Merck & Co., Inc., Whitehouse Station, NJ, **2006**.
- [345] P. B. Arockiam, C. Fischmeister, C. Bruneau, P. H. Dixneuf, *Angew. Chem. Int. Ed.* **2010**, 49, 6629–6632.
- [346] J.-H. Li, W.-J. Liu, *Org. Lett.* **2004**, 6, 2809–2811.
- [347] R. N. Gaykar, A. Guin, S. Bhattacharjee, A. T. Biju, *Org. Lett.* **2019**, 21, 9613–9617.
- [348] a) V. Müller, Cobalt- und Ruthenium-katalysierte C–H Alkylierung und Alkenylierung, Master-Thesis, Georg-August-Universität Göttingen **2016**; b) R. Loska, K. Szachowicz, D. Szydlik, *Org. Lett.* **2013**, 15, 5706–5709; c) H. Sakaguchi, Y. Uetake, M. Ohashi, T. Niwa, S. Ogoshi, T. Hosoya, *J. Am. Chem. Soc.* **2017**, 139, 12855–12862; d) J. Hu, X. Han, Y. Yuan, Z. Shi, *Angew. Chem. Int. Ed.* **2017**, 56, 13342–13346.
- [349] X. Rao, C. Liu, J. Qiu, Z. Jin, *Org. Biomol. Chem.* **2012**, 10, 7875–7883.
- [350] a) S. Vishwakarma, A. Kumari, K. Mitra, S. Singh, R. Singh, J. Singh, S. K. Sen Gupta, B. Ray, *J. Appl. Polym. Sci.* **2019**, 136, 47964–47964; b) P. M. Morrison, P. J. Foley, S. L. Warriner, M. E. Webb, *Chem. Commun.* **2015**, 51, 13470–13473; c) A. A. S. Gietter, P. G. Gildner, A. P. Cinderella, D. A. Watson, *Org. Lett.* **2014**, 16, 3166–3169.
- [351] L. Liang, S. Fu, D. Lin, X.-Q. Zhang, Y. Deng, H. Jiang, W. Zeng, *J. Org. Chem.* **2014**, 79, 9472–9480.
- [352] X.-H. Xu, G.-K. Liu, A. Azuma, E. Tokunaga, N. Shibata, *Org. Lett.* **2011**, 13, 4854–4857.
- [353] A. M. Thompson, P. D. O'Connor, A. Blaser, V. Yardley, L. Maes, S. Gupta, D. Launay, D. Martin, S. G. Franzblau, B. Wan, Y. Wang, Z. Ma, W. A. Denny, *J. Med. Chem.* **2016**, 59, 2530–2550.

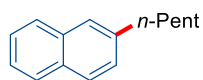
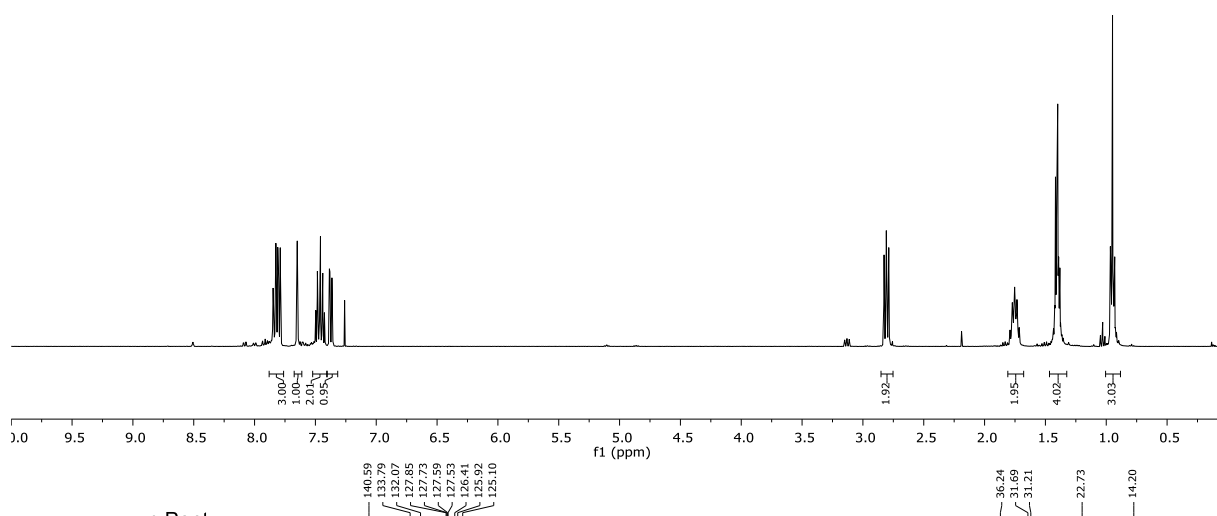
-
- [354] A. Czompa, B. L. Pásztor, J. A. Sahar, Z. Mucsi, D. Bogdán, K. Ludányi, Z. Varga, I. M. Mándity, *RSC Adv.* **2019**, *9*, 37818–37824.
- [355] L. C. Wilkins, Y. Kim, E. D. Litle, F. P. Gabbai, *Angew. Chem. Int. Ed.* **2019**, *58*, 18266–18270.
- [356] D. Tu, X. Cheng, Y. Gao, P. Yang, Y. Ding, C. Jiang, *Org. Biomol. Chem.* **2016**, *14*, 7443–7446.
- [357] Q. Sun, N. Yoshikai, *Org. Lett.* **2019**, *21*, 5238–5242.
- [358] M. Ishihara, H. Togo, *Tetrahedron* **2007**, *63*, 1474–1480.
- [359] a) Q. Gou, W. Li, Q. Zhao, J. Xie, P. Luo, G. Cao, S. Chen, J. Qin, *Eur. J. Org. Chem.* **2018**, *2018*, 4089–4094; b) M. A. Ali, X. Yao, H. Sun, H. Lu, *Org. Lett.* **2015**, *17*, 1513–1516; c) M. Martín-Ortíz, M. Gómez-Gallego, C. Ramírez de Arellano, M. A. Sierra, *Chem. Eur. J.* **2012**, *18*, 12603–12608; d) I. Čerňa, R. Pohl, B. Klepetářová, M. Hocek, *J. Org. Chem.* **2008**, *73*, 9048–9054; e) M. Havelková, D. Dvořák, M. Hocek, *Synthesis* **2001**, *2001*, 1704–1710; f) V. B. Oza, R. C. Corcoran, *J. Org. Chem.* **1995**, *60*, 3680–3684.
- [360] M. Tobisu, T. Takahira, T. Morioka, N. Chatani, *J. Am. Chem. Soc.* **2016**, *138*, 6711–6714.
- [361] G. Dilauro, A. Francesca Quivelli, P. Vitale, V. Capriati, F. M. Perna, *Angew. Chem. Int. Ed.* **2019**, *58*, 1799–1802.
- [362] H. Yu, T. Szilvási, P. Rai, R. J. Twieg, M. Mavrikakis, N. L. Abbott, *Adv. Funct. Mater.* **2018**, *28*, 1703581.
- [363] D. Heijnen, F. Tosi, C. Vila, M. C. A. Stuart, P. H. Elsinga, W. Szymanski, B. L. Feringa, *Angew. Chem. Int. Ed.* **2017**, *56*, 3354–3359.
- [364] W. Liu, J. Li, P. Querard, C.-J. Li, *J. Am. Chem. Soc.* **2019**, *141*, 6755–6764.
- [365] Y.-Y. Zhou, C. Uyeda, *Angew. Chem. Int. Ed.* **2016**, *55*, 3171–3175.
- [366] M. Catellani, L. Ferioli, *Synthesis* **1996**, *1996*, 769–772.
- [367] B. Zhou, H. Sato, L. Ilies, E. Nakamura, *ACS Catal.* **2018**, *8*, 8–11.
- [368] E. L. Gall, C. Gosmini, J.-Y. Nédélec, J. Périchon, *Tetrahedron* **2001**, *57*, 1923–1927.
- [369] K. L. Tan, A. Vasudevan, R. G. Bergman, J. A. Ellman, A. J. Souers, *Org. Lett.* **2003**, *5*, 2131–2134.
- [370] A. A. A.-E. A. H. H. Bakheit, B. Mustafa, A. Haque, T. A. Wani, in *Profiles of Drug Substances, Excipients and Related Methodology* (Ed.: H. G. Brittain), Elsevier Science Publishing Co Inc, San Diego, USA, **2015**, pp. 371–429.

- [371] A. J. Paterson, C. J. Heron, C. L. McMullin, M. F. Mahon, N. J. Press, C. G. Frost, *Org. Biomol. Chem.* **2017**, *15*, 5993–6000.
- [372] O. V. Dolomanov, L. J. Bourhis, R. J. Gildea, J. A. K. Howard, H. Puschmann, *J. Appl. Crystallogr.* **2009**, *42*, 339–341.
- [373] G. Sheldrick, *Acta Crystallogr. E* **2015**, *A71*, 3–8.
- [374] G. Sheldrick, *Acta Crystallogr. E* **2015**, *C71*, 3–8.

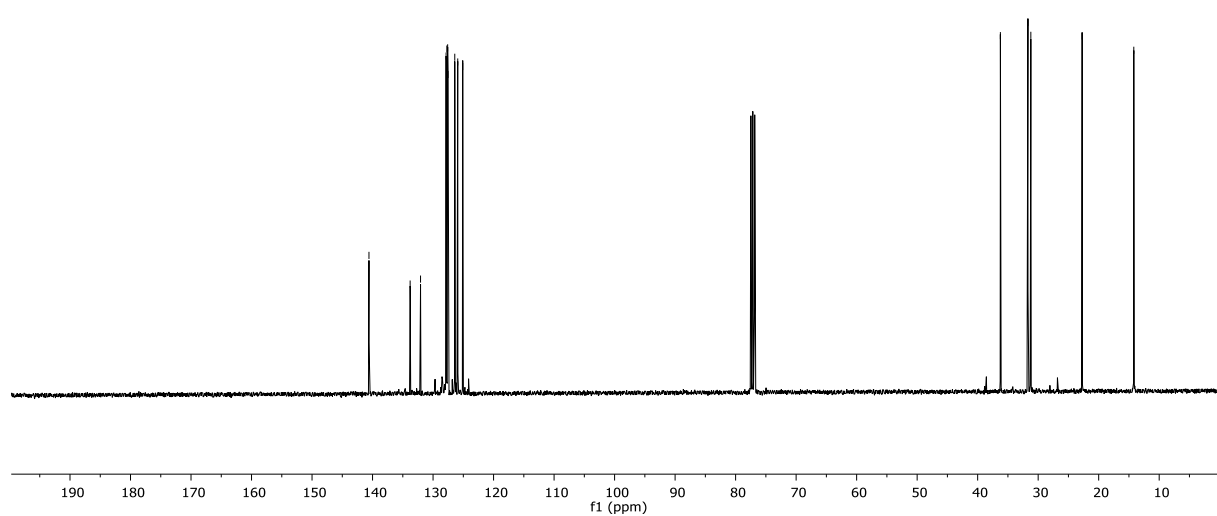
7. Appendix: NMR-Spectra and HPLC Chromatograms



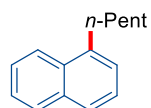
186b
(400 MHz, CDCl₃)



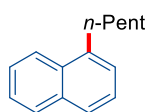
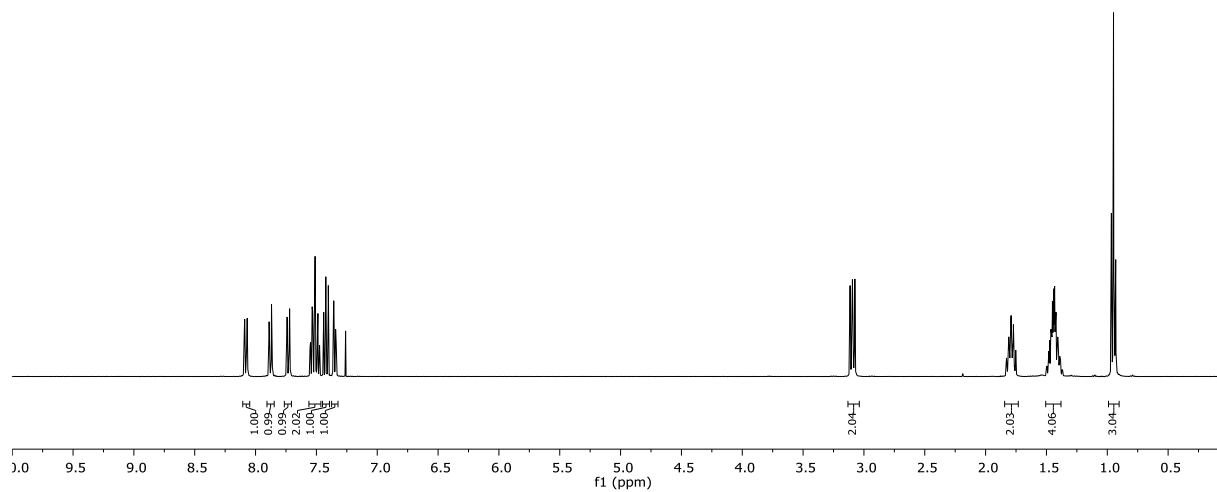
186b
(100 MHz, CDCl₃)



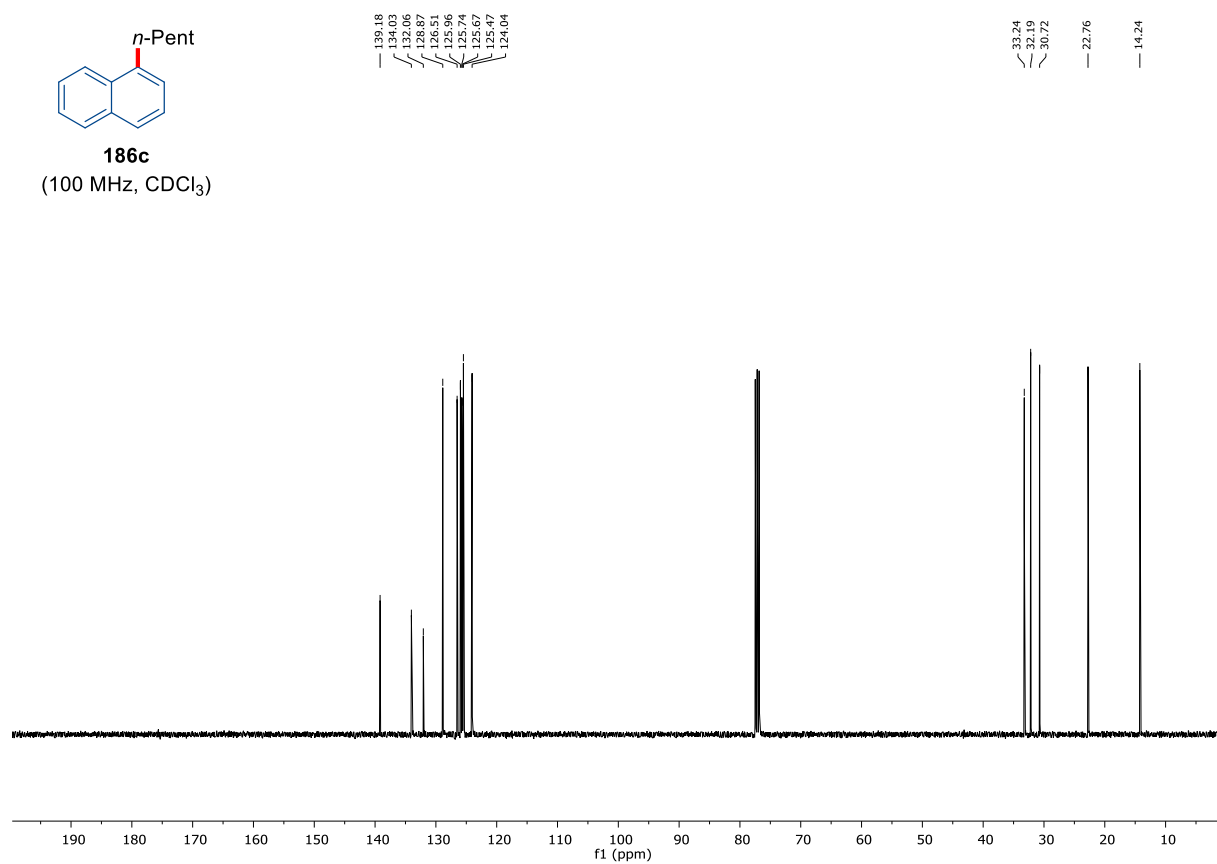
7. Appendix: NMR-Spectra and HPLC Chromatograms

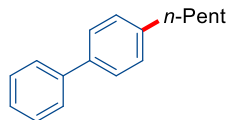


186c
(400 MHz, CDCl₃)

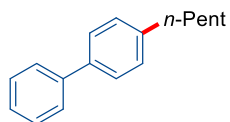
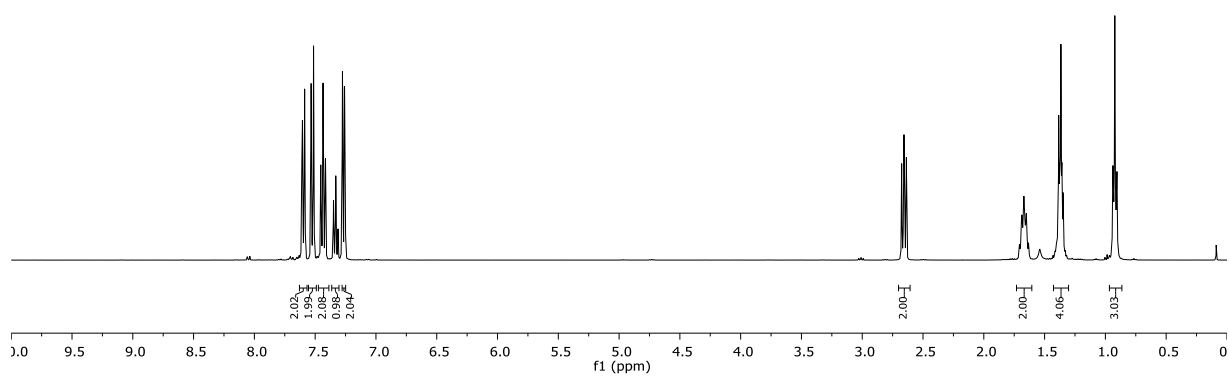


186c
(100 MHz, CDCl₃)

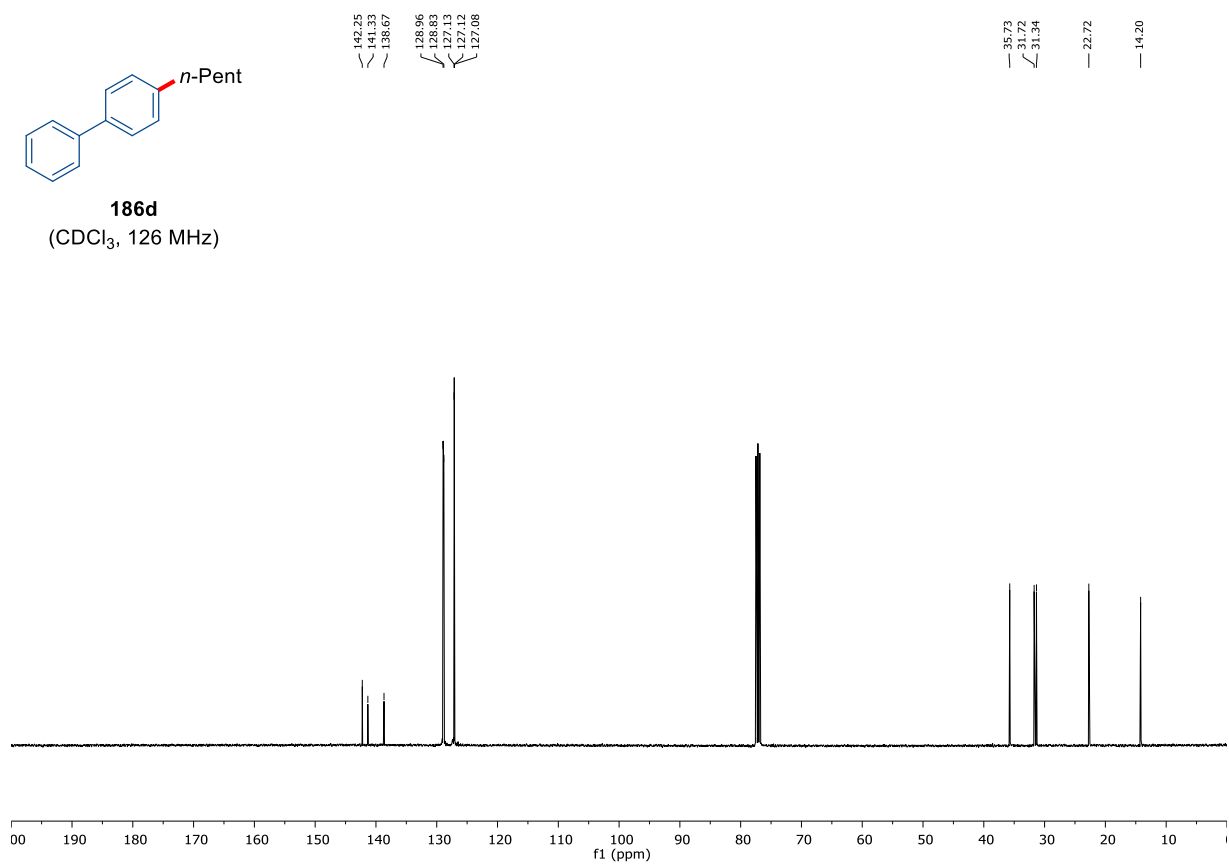




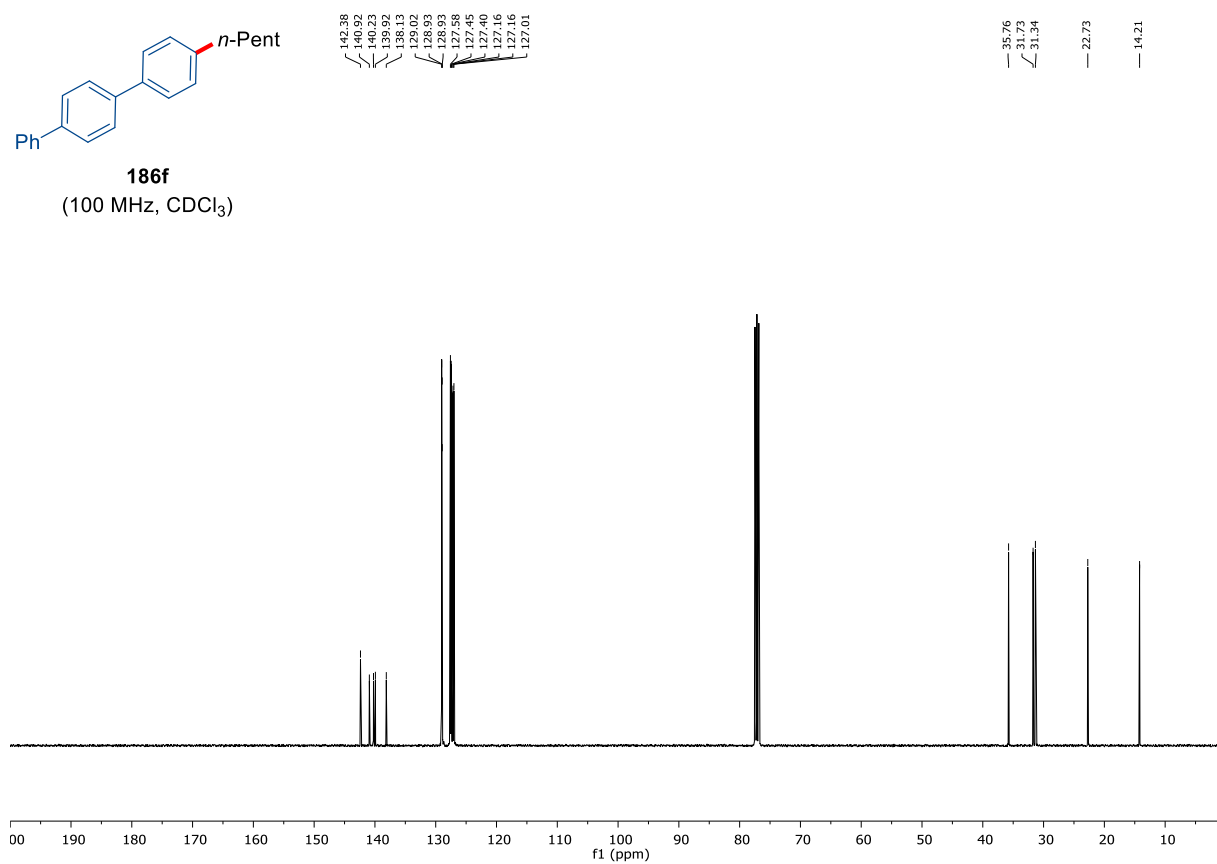
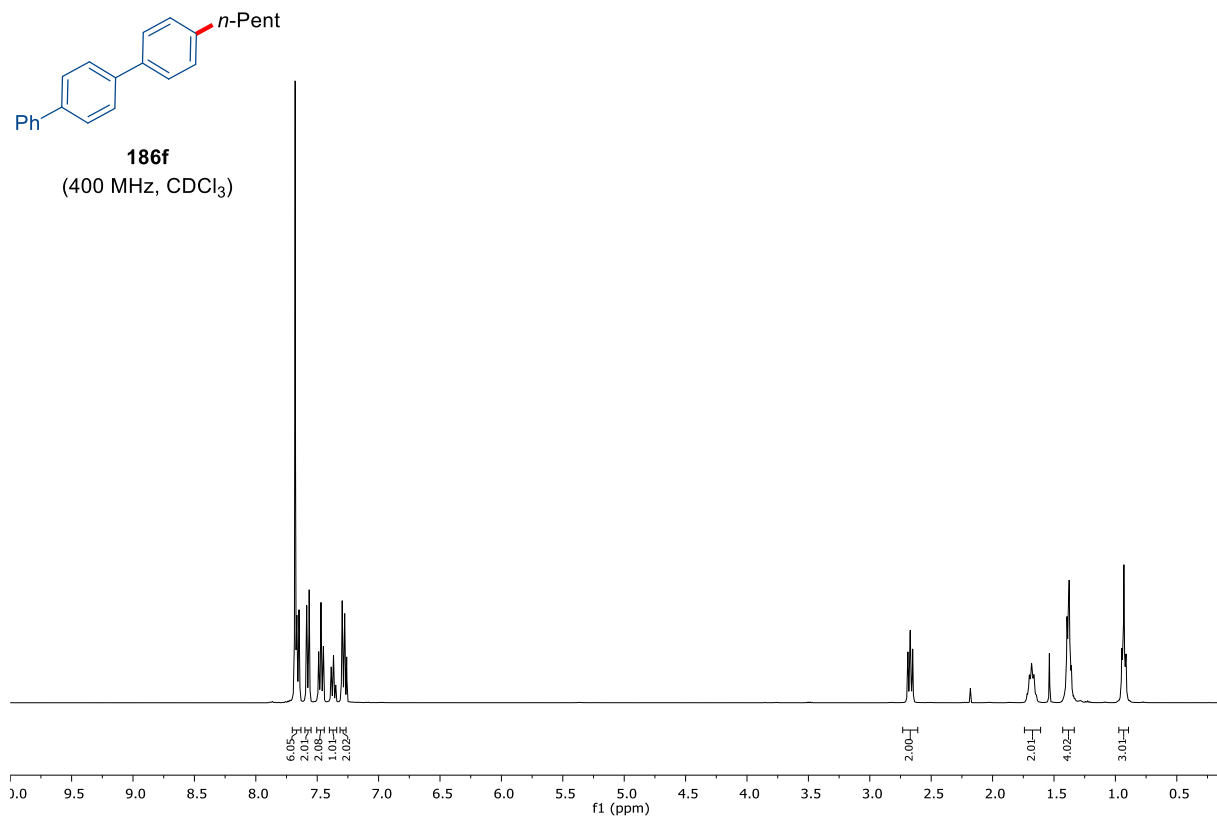
186d
(CDCl₃, 400 MHz)

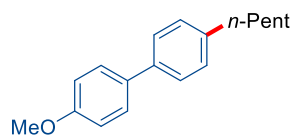


186d
(CDCl₃, 126 MHz)

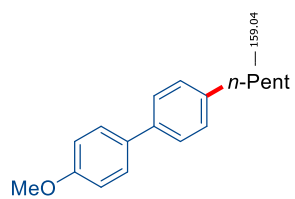
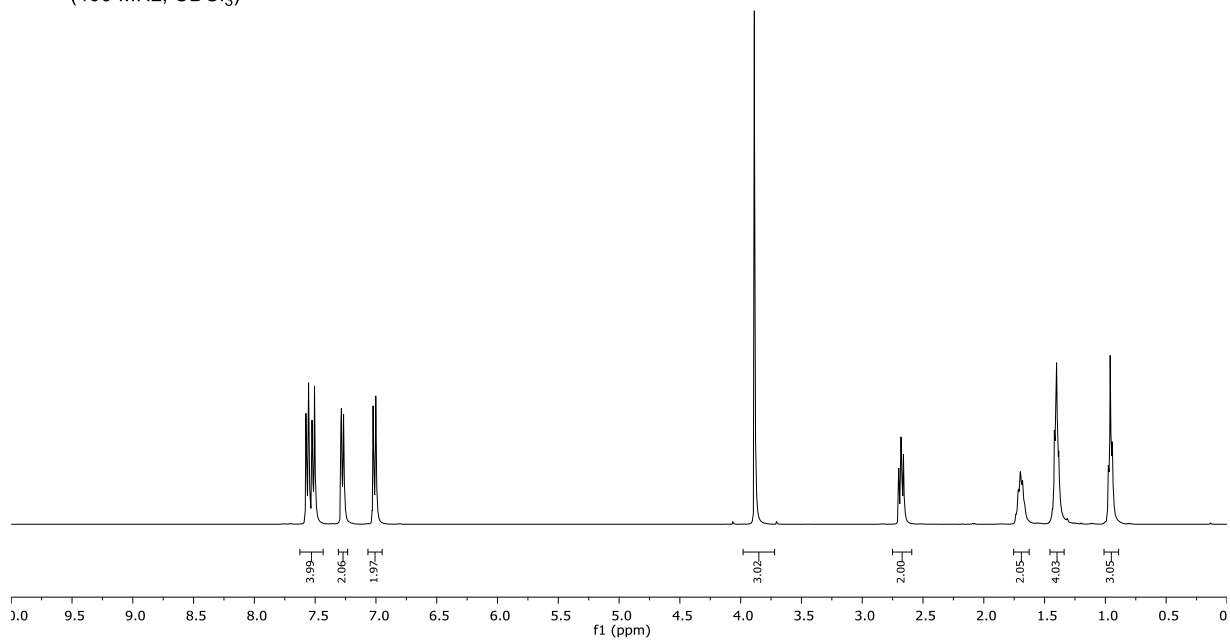


7. Appendix: NMR-Spectra and HPLC Chromatograms

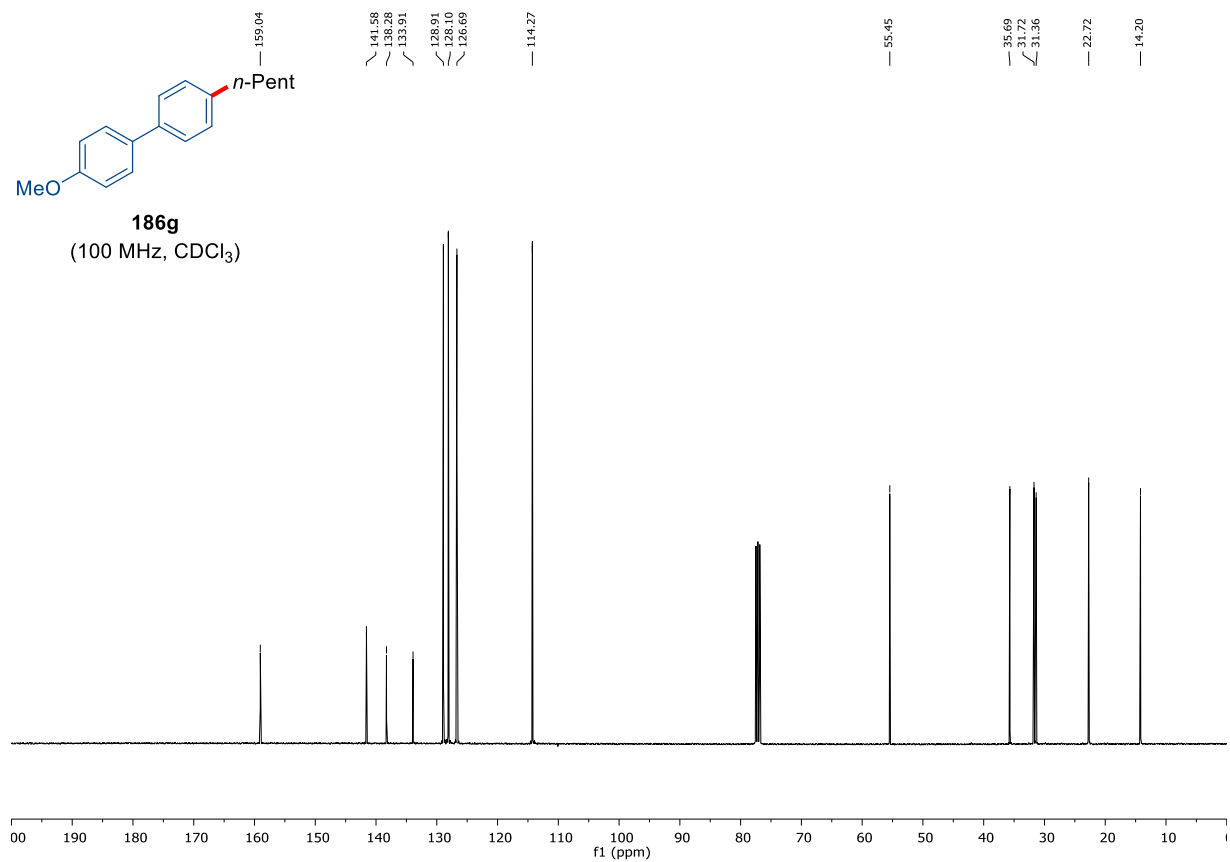




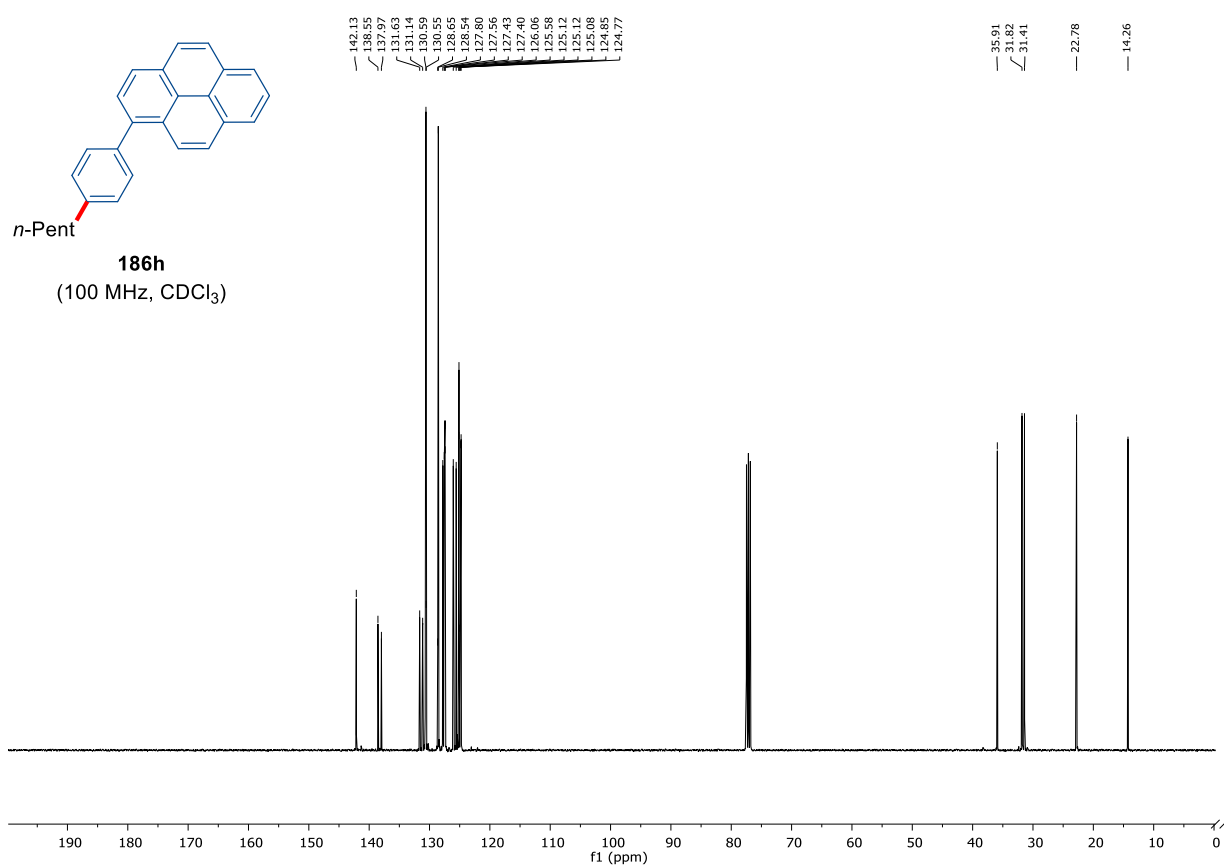
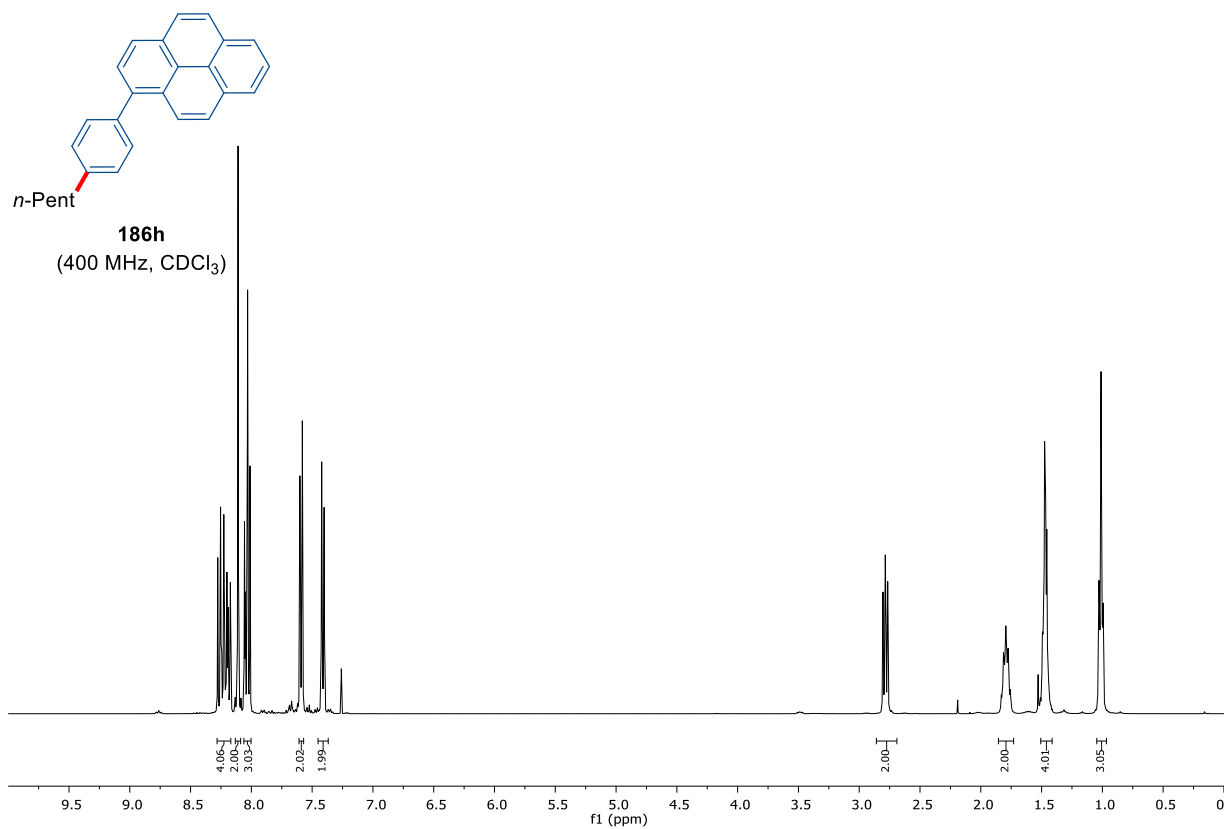
186g
(400 MHz, CDCl₃)

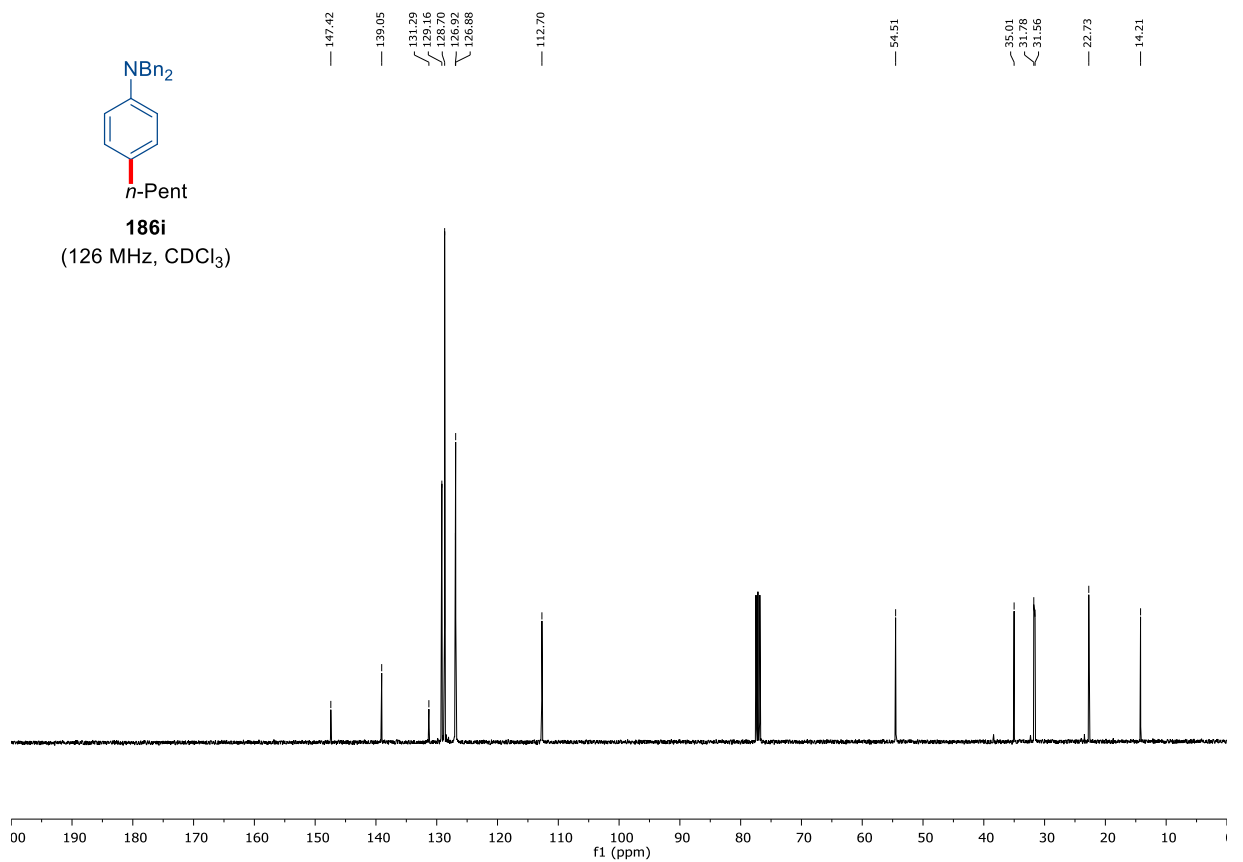
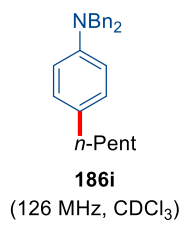
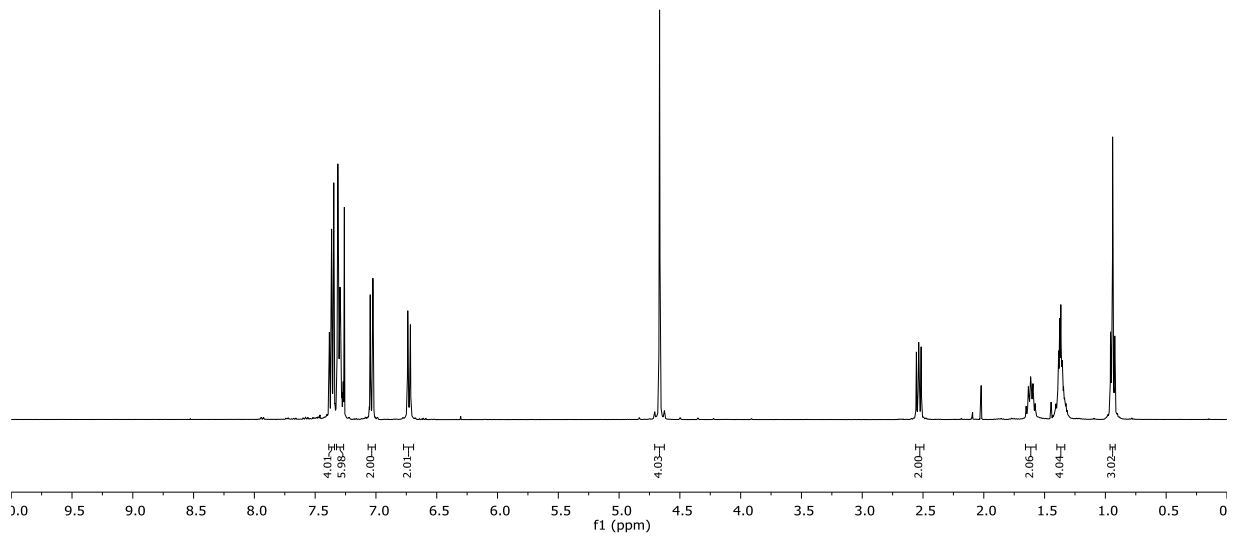
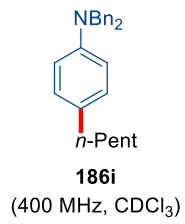


186g
(100 MHz, CDCl₃)

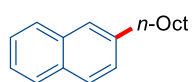


7. Appendix: NMR-Spectra and HPLC Chromatograms

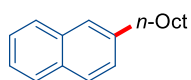
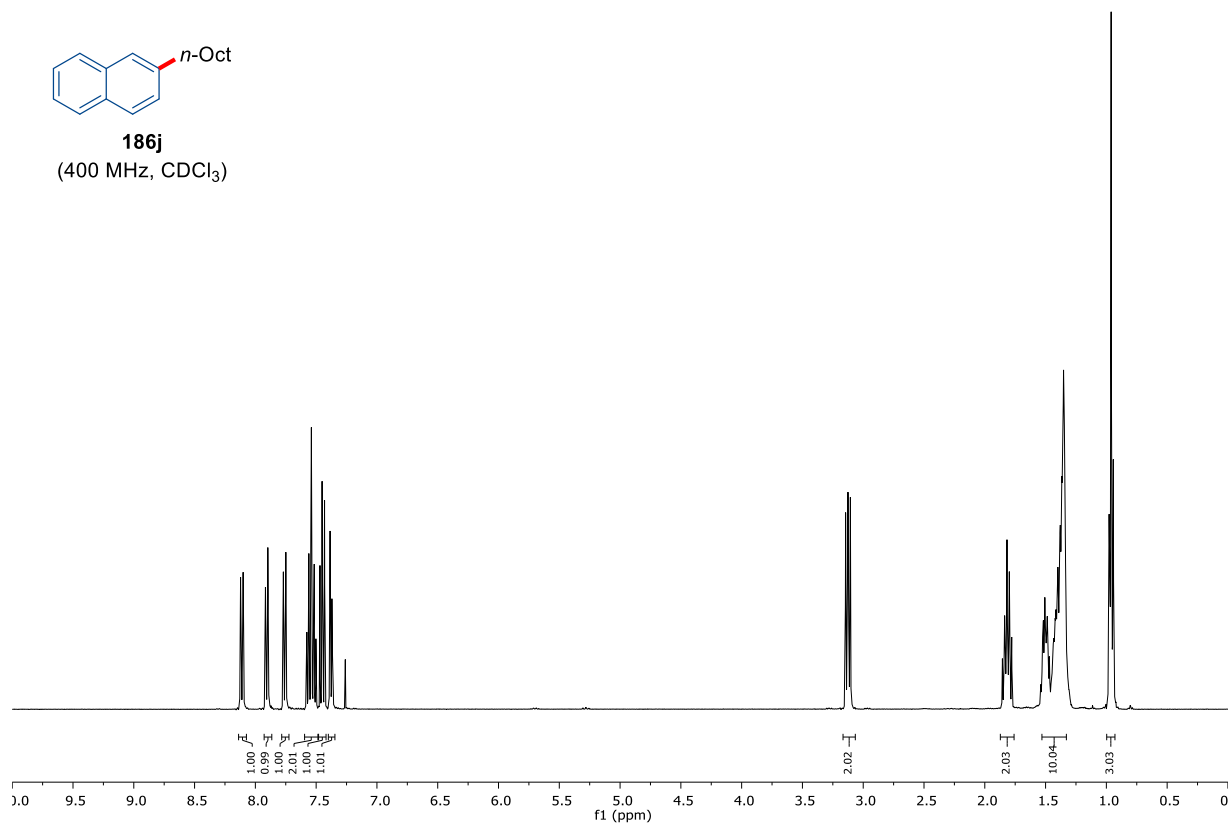




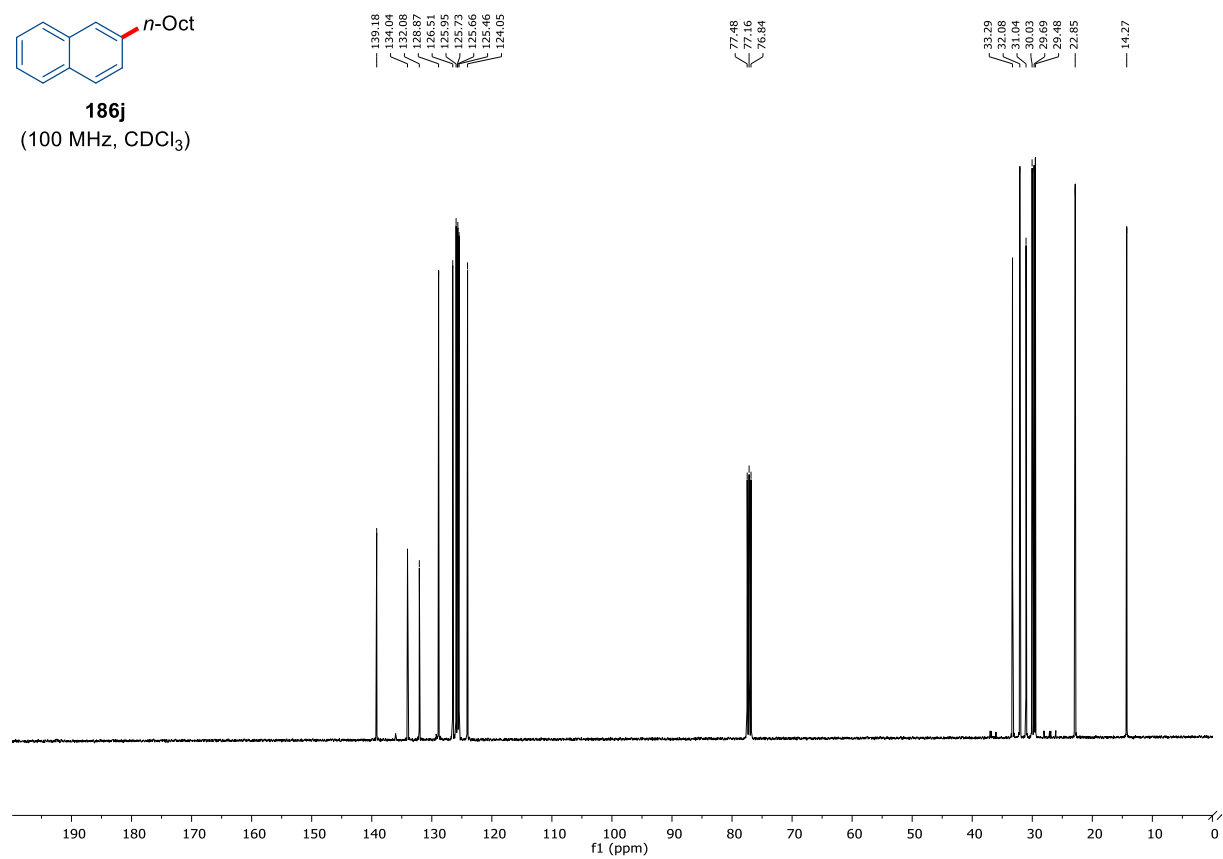
7. Appendix: NMR-Spectra and HPLC Chromatograms

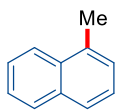


186j
(400 MHz, CDCl₃)

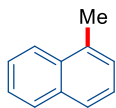
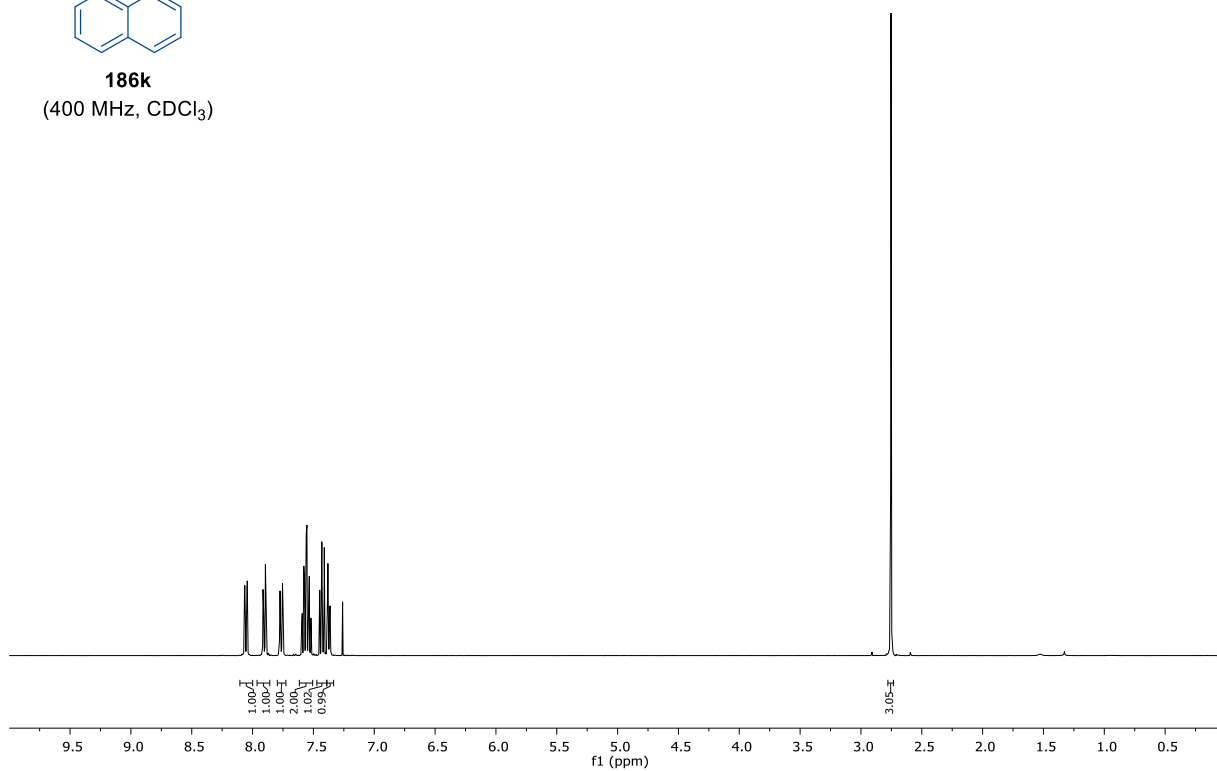


186j
(100 MHz, CDCl₃)

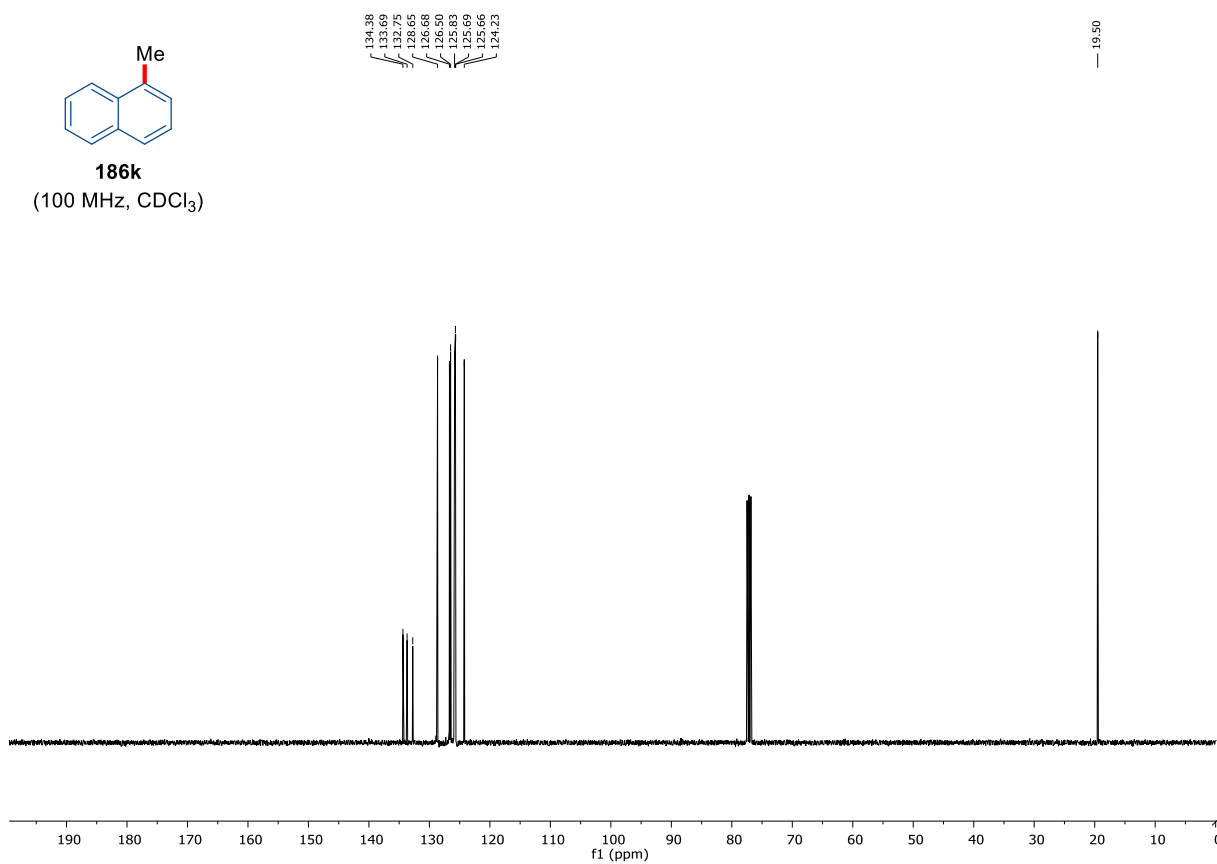




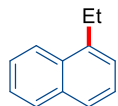
186k
(400 MHz, CDCl₃)



186k
(100 MHz, CDCl₃)

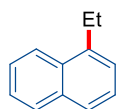
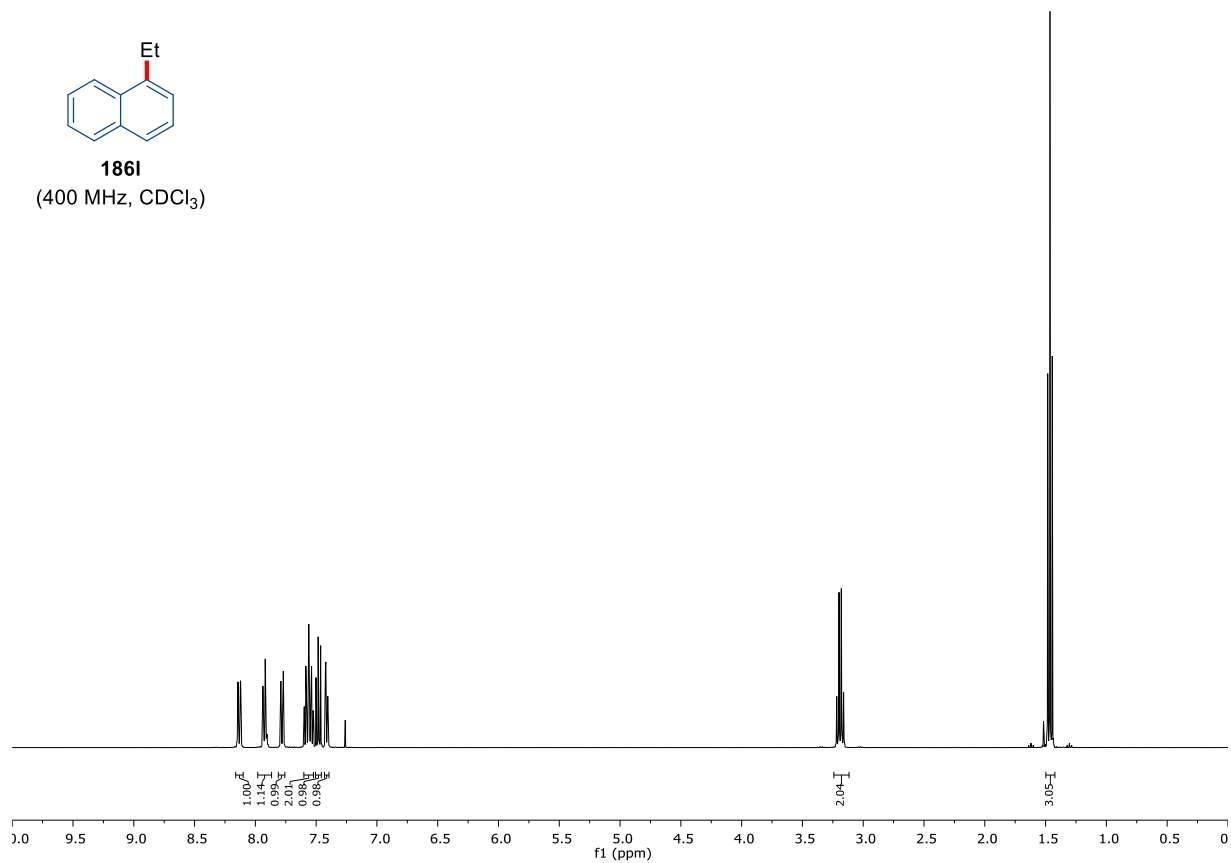


7. Appendix: NMR-Spectra and HPLC Chromatograms



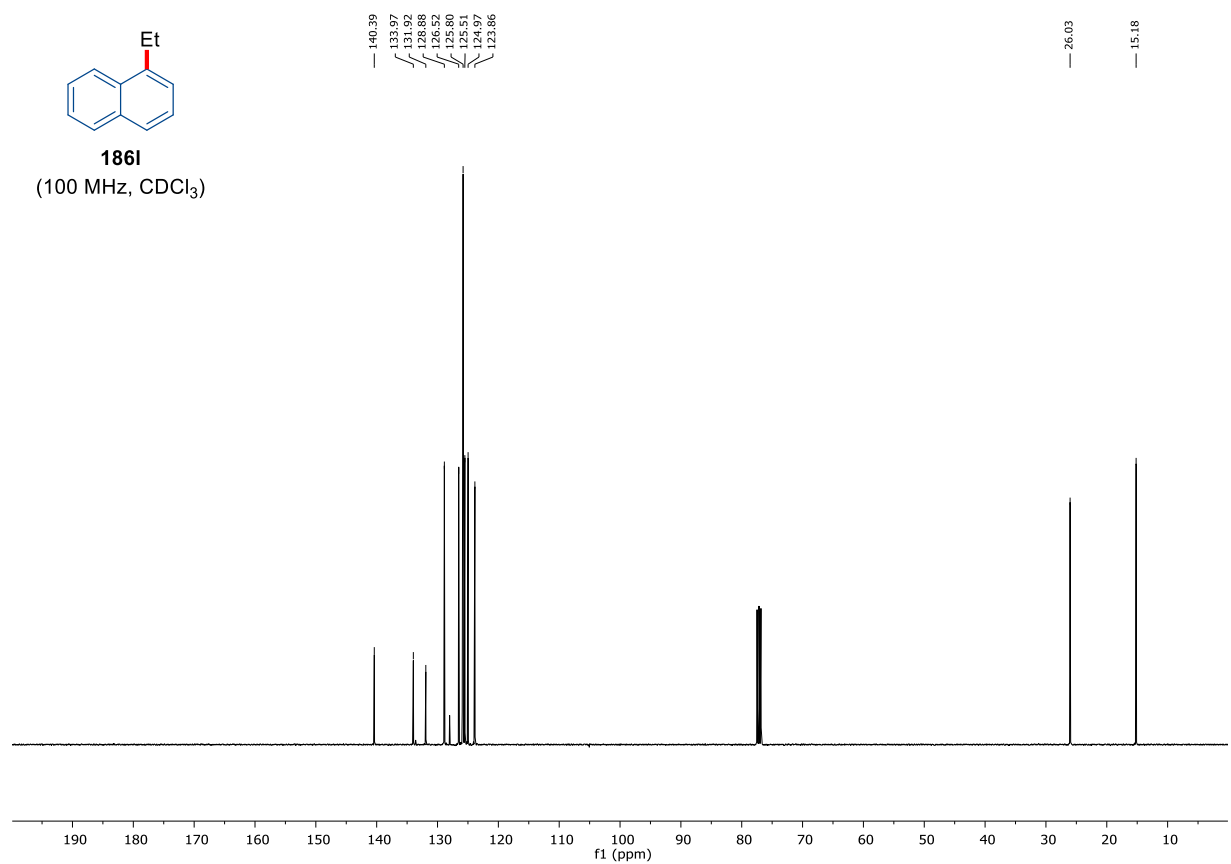
186I

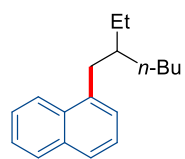
(400 MHz, CDCl₃)



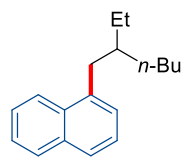
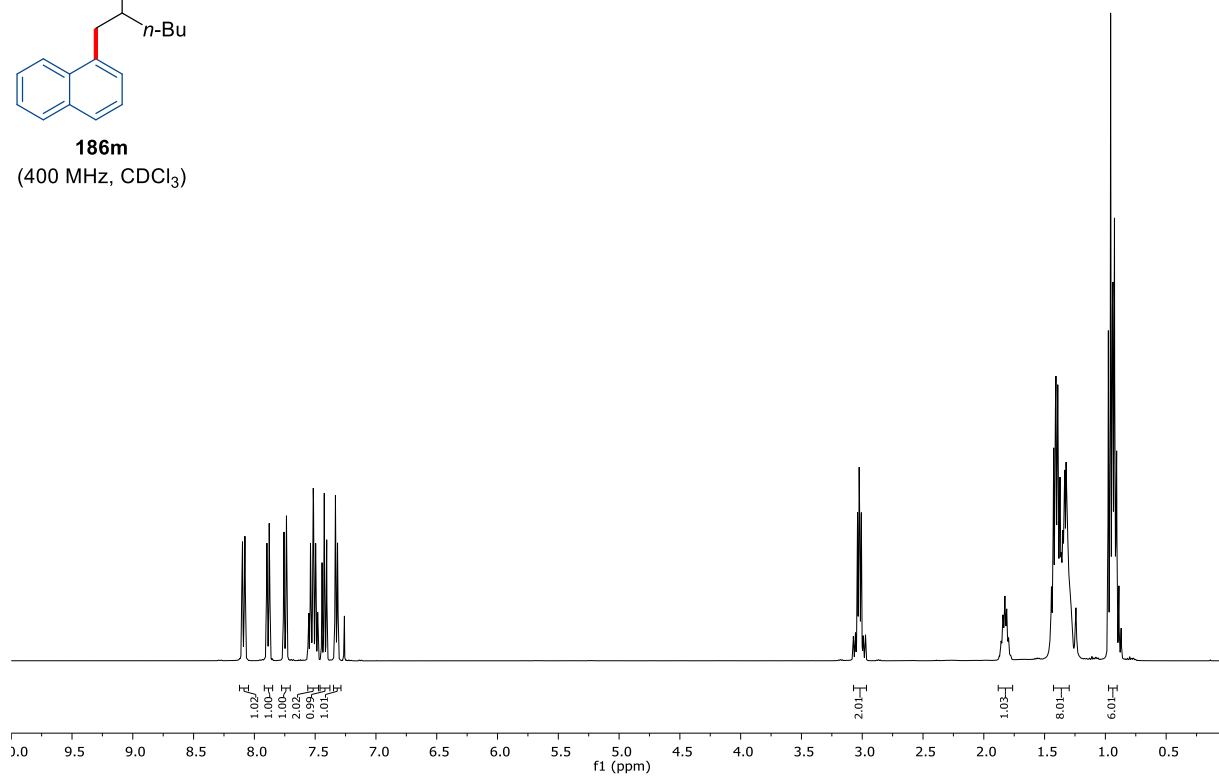
186I

(100 MHz, CDCl₃)

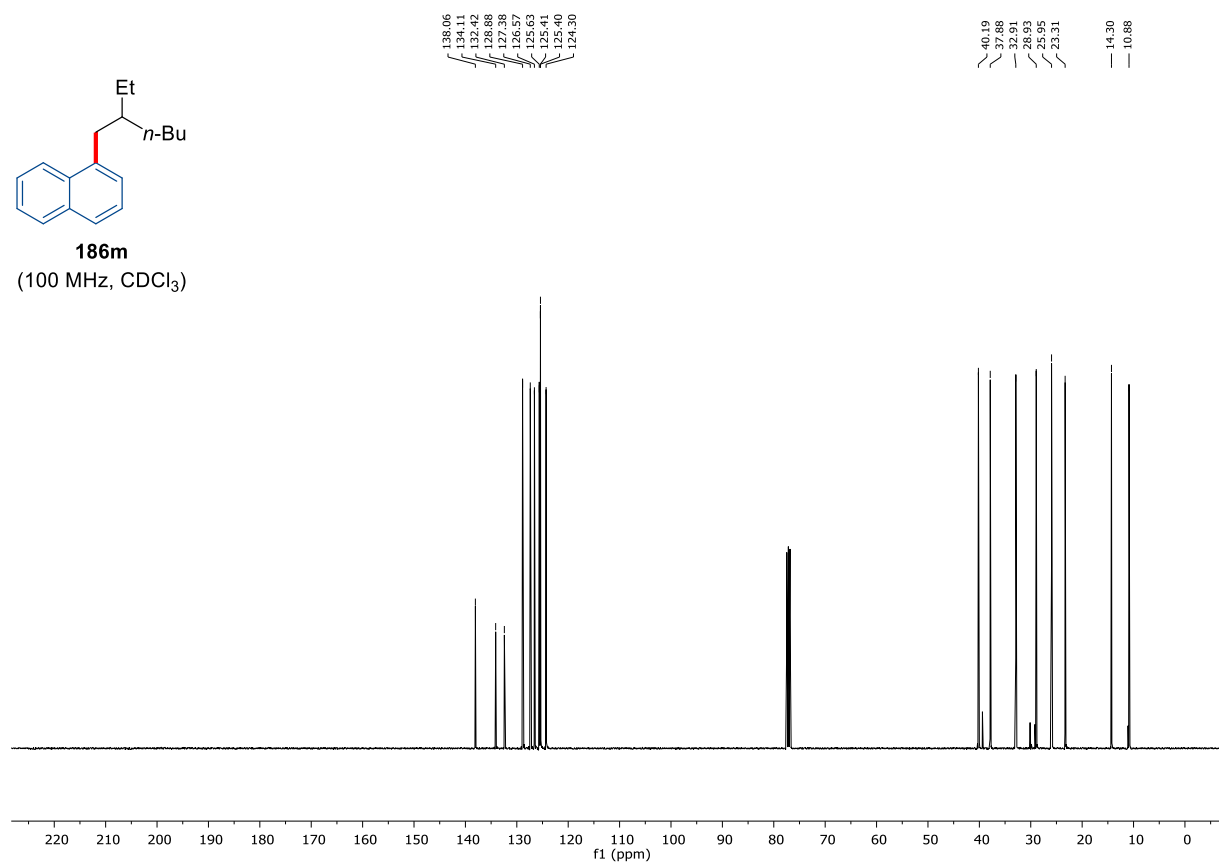




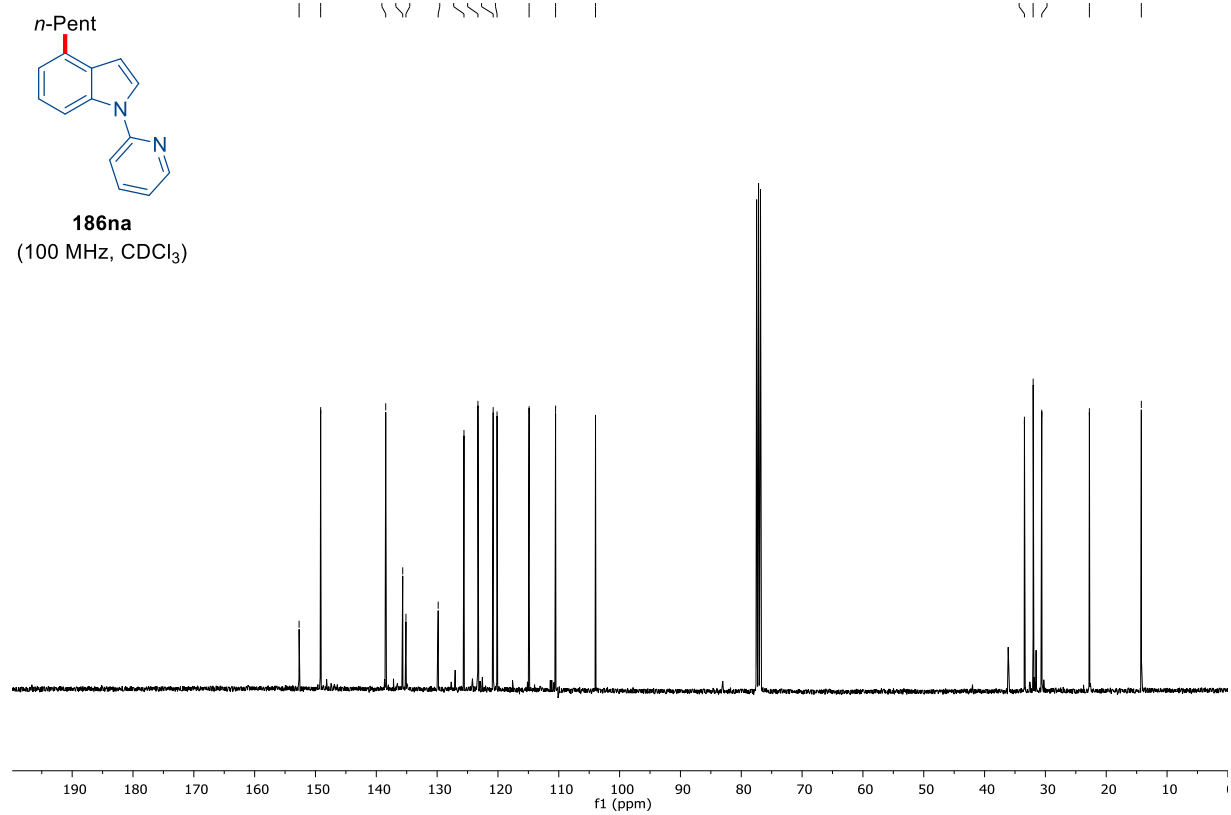
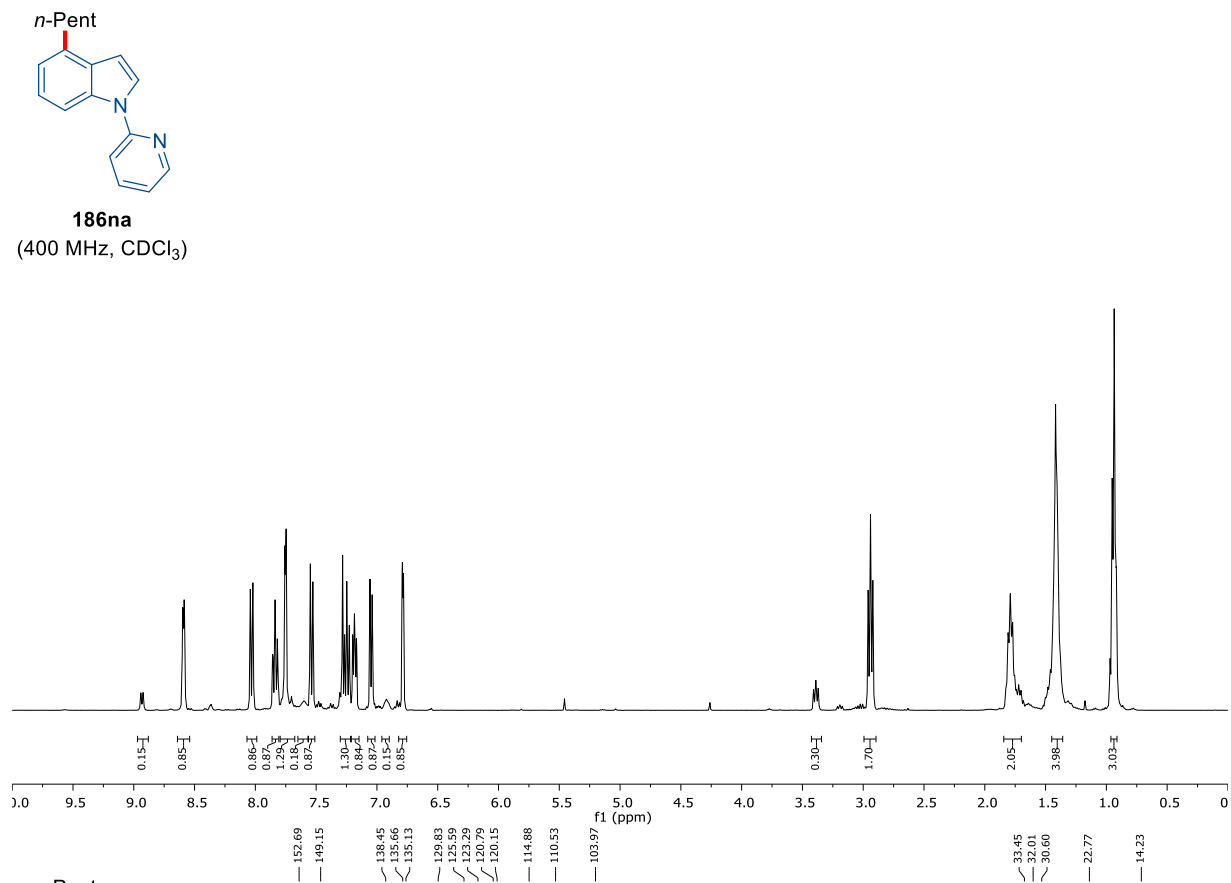
186m
(400 MHz, CDCl₃)

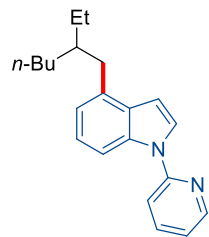
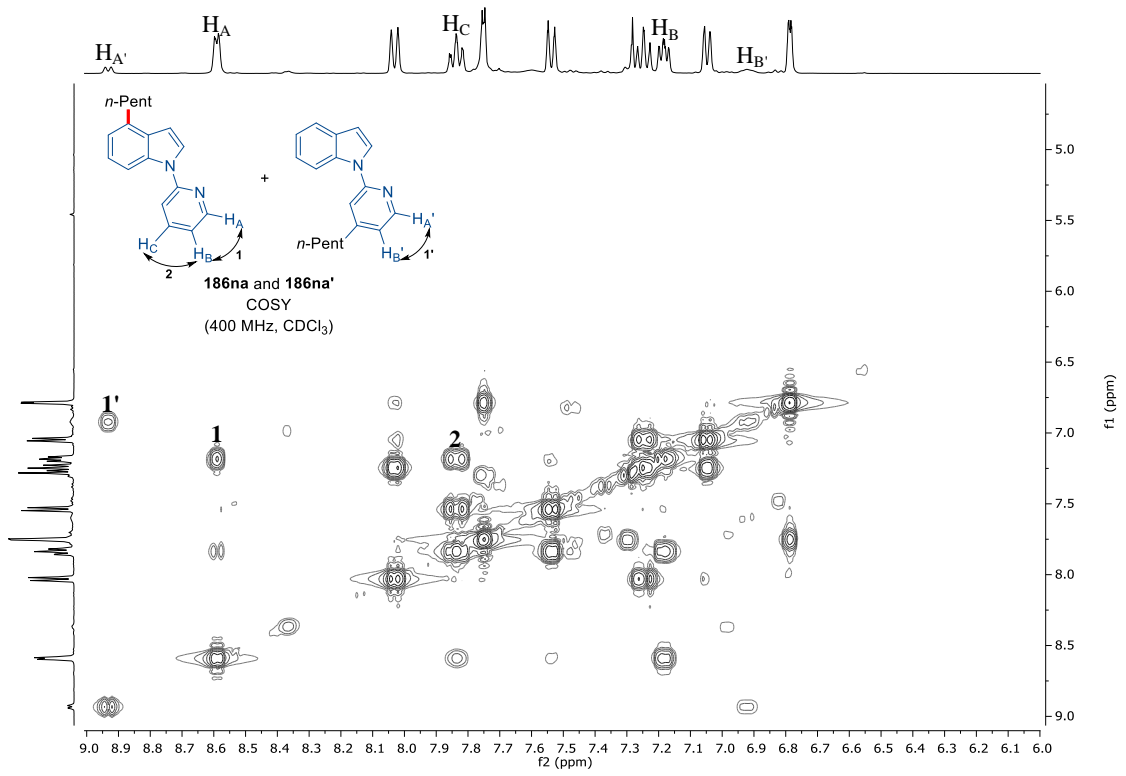


186m
(100 MHz, CDCl₃)

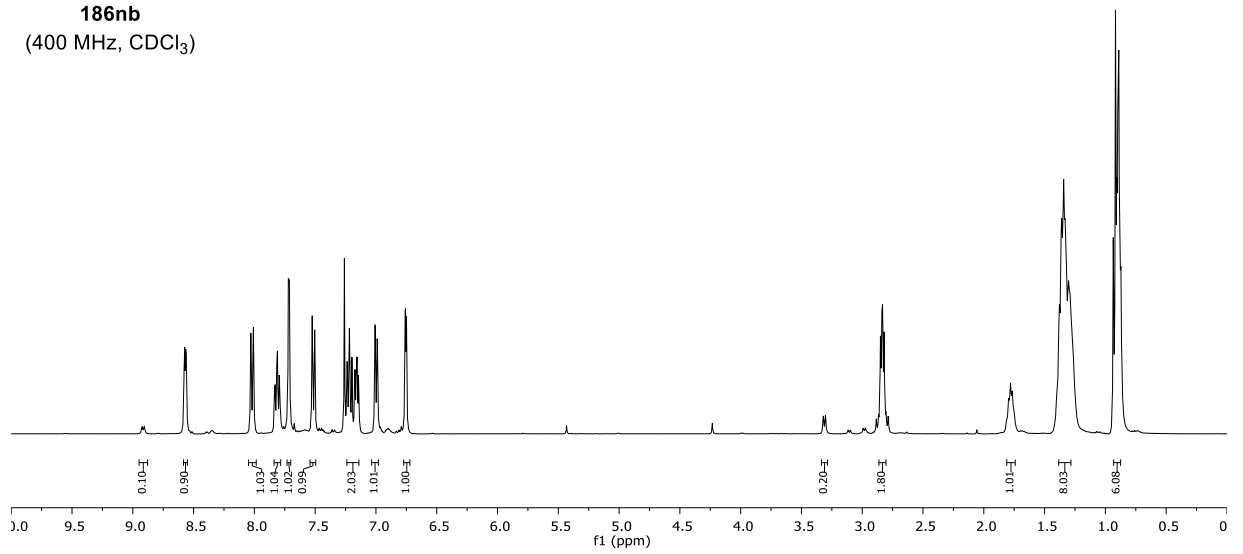


7. Appendix: NMR-Spectra and HPLC Chromatograms

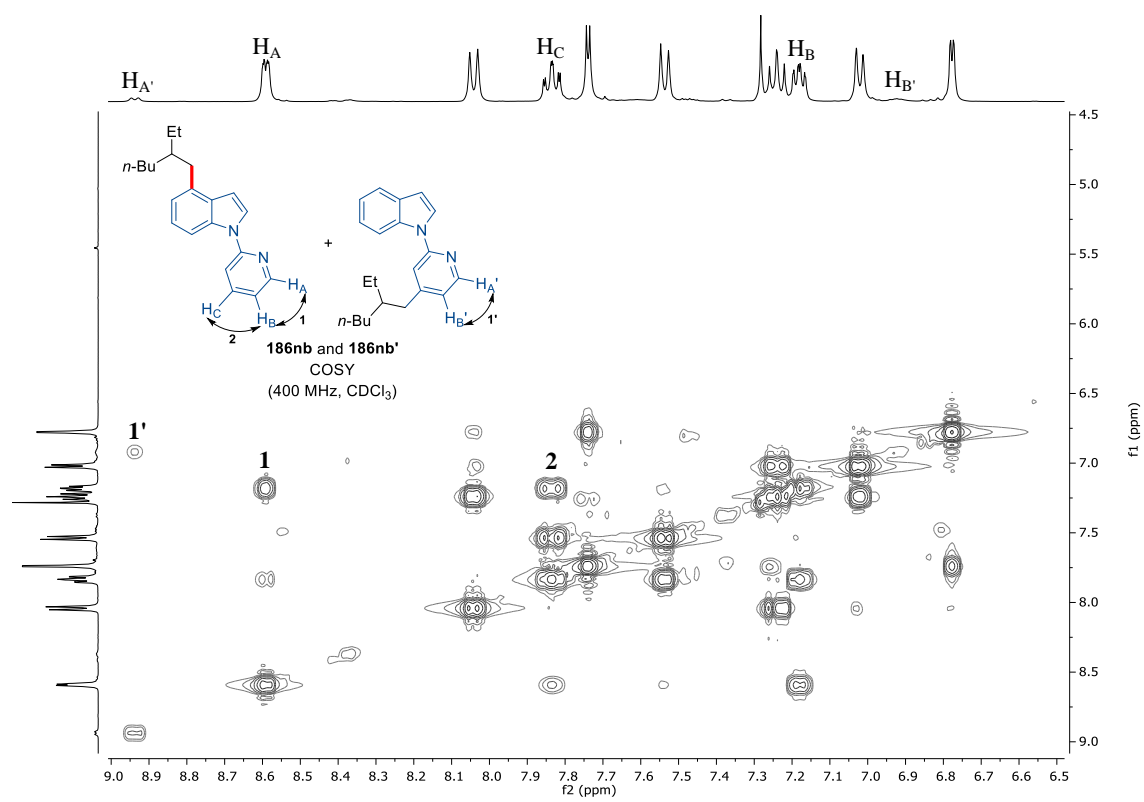
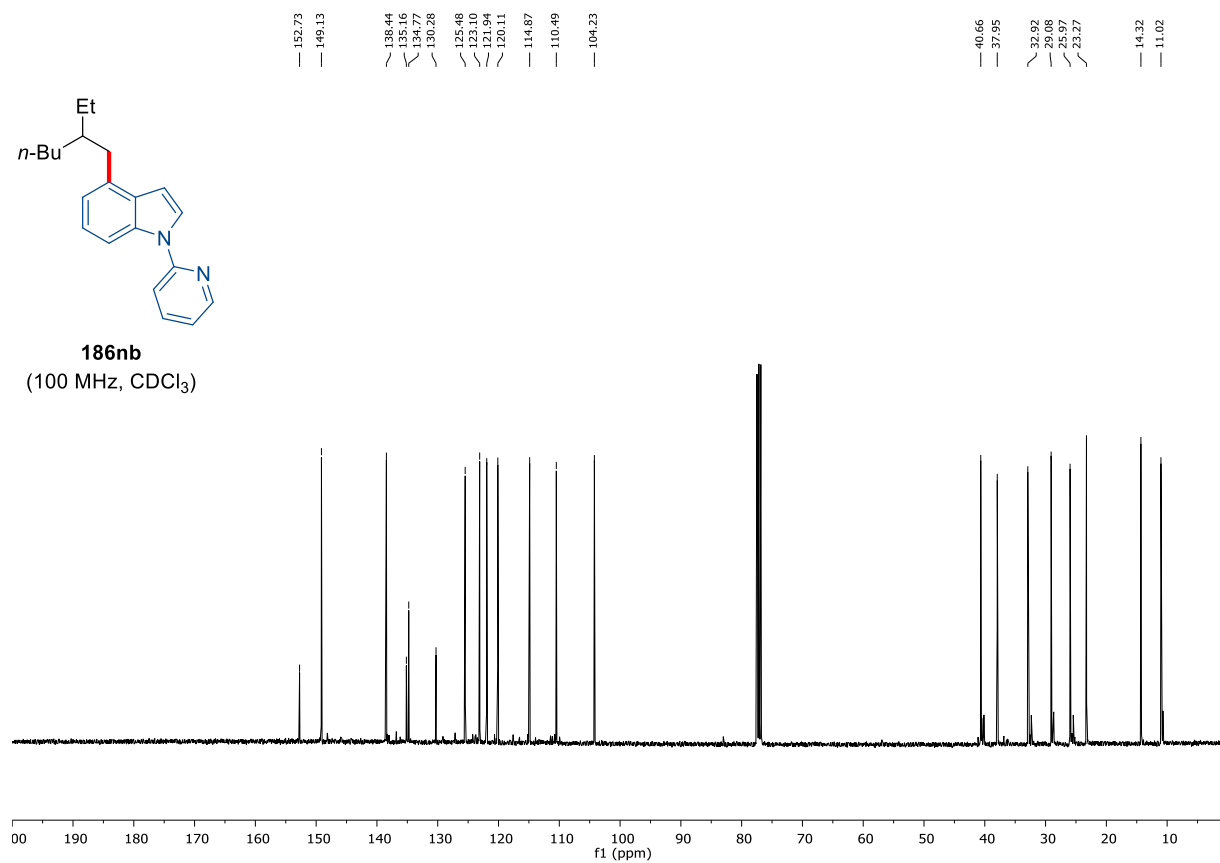


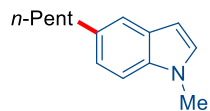


186nb
 (400 MHz, $CDCl_3$)

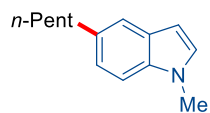
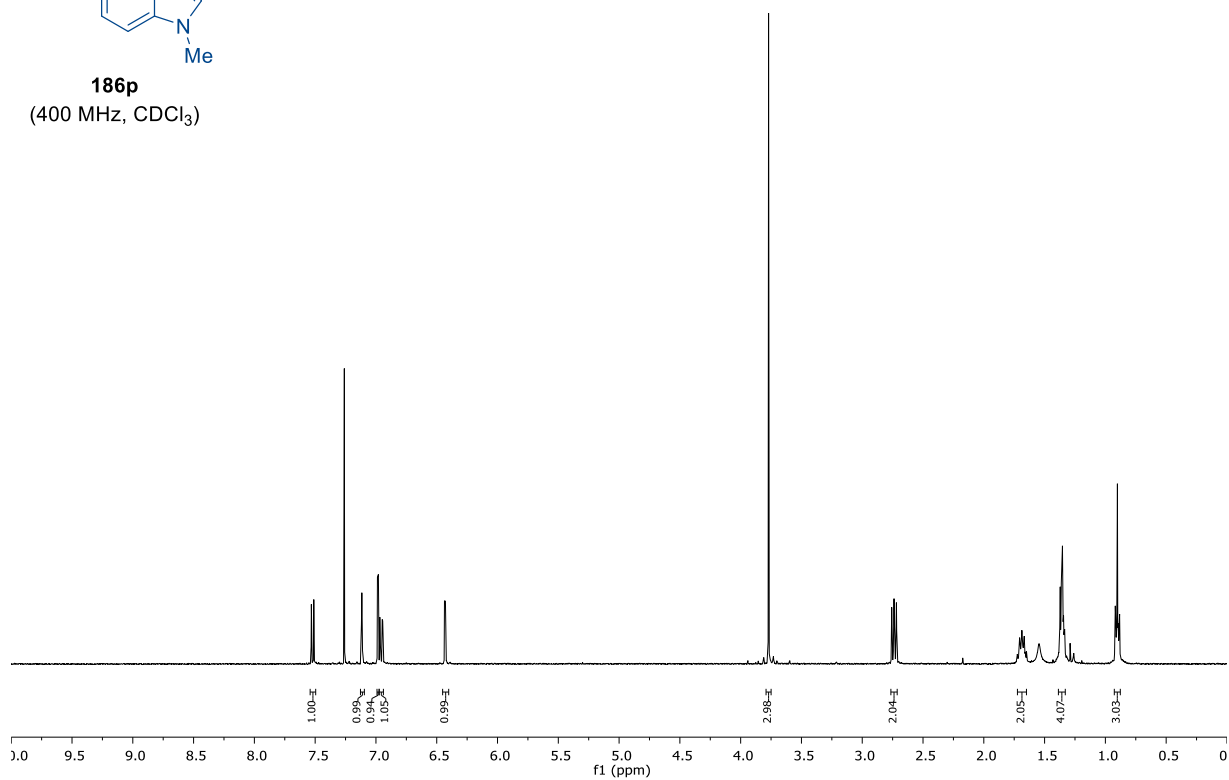


7. Appendix: NMR-Spectra and HPLC Chromatograms

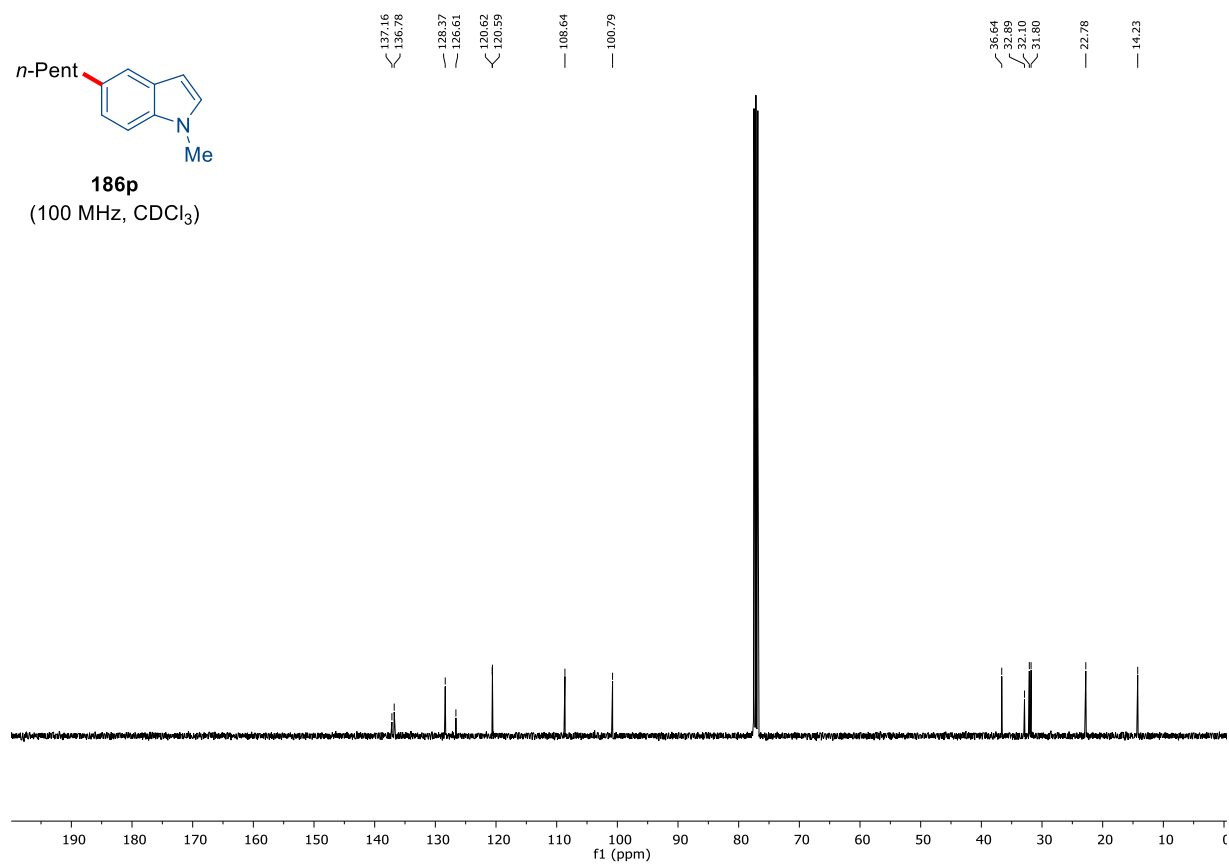




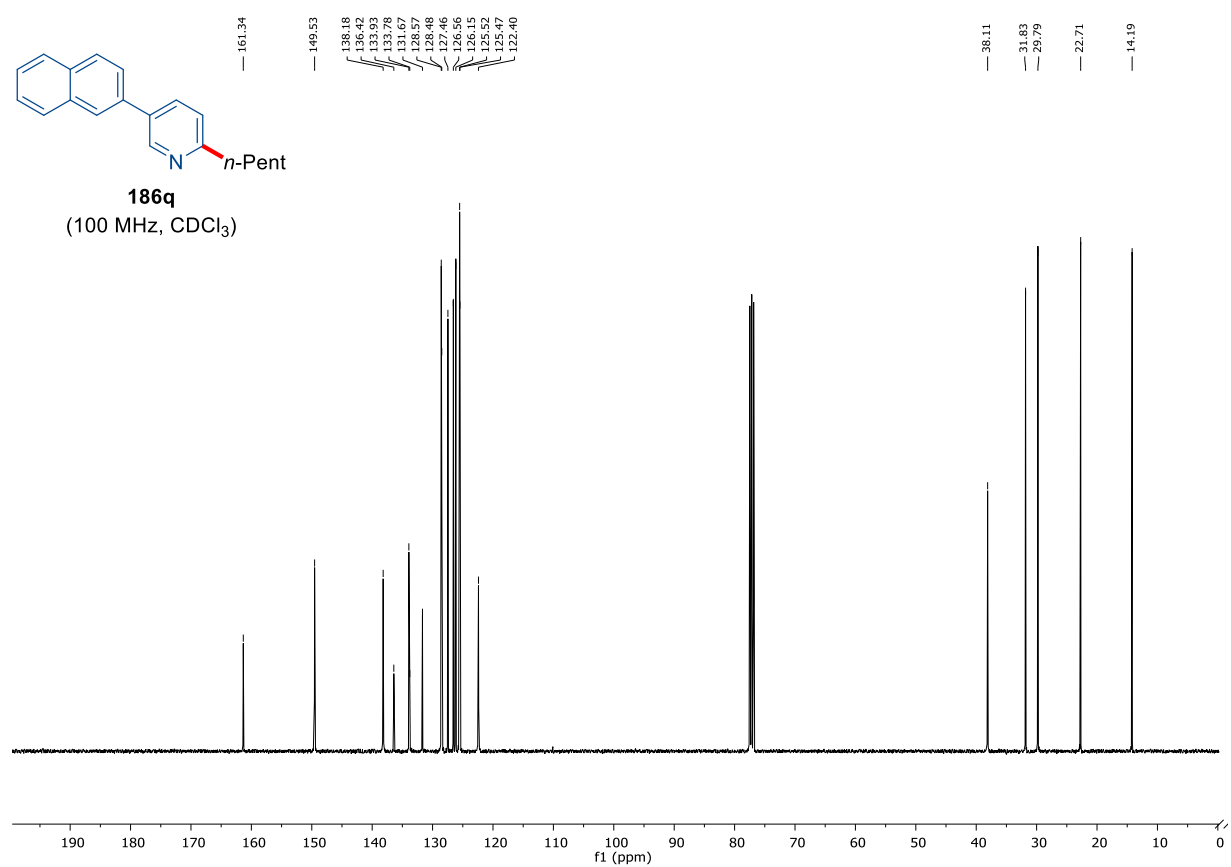
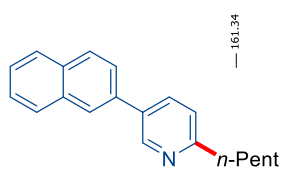
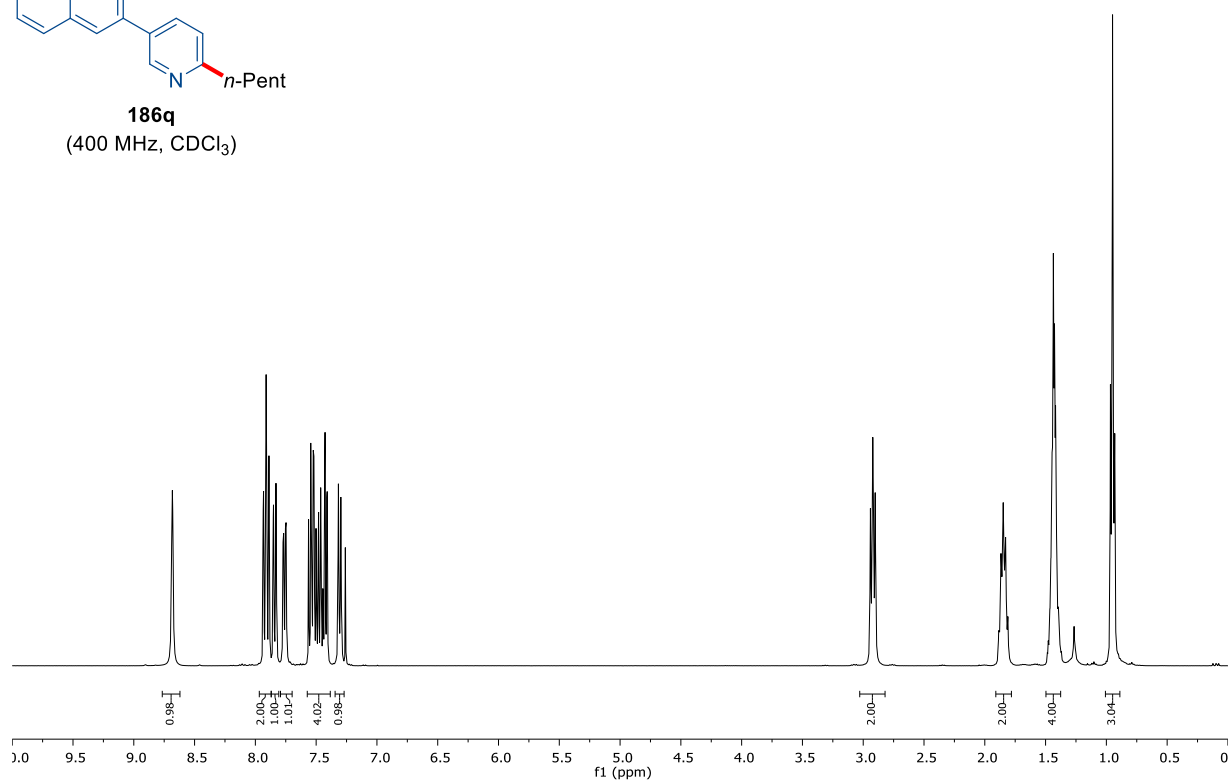
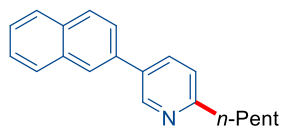
186p
(400 MHz, CDCl₃)

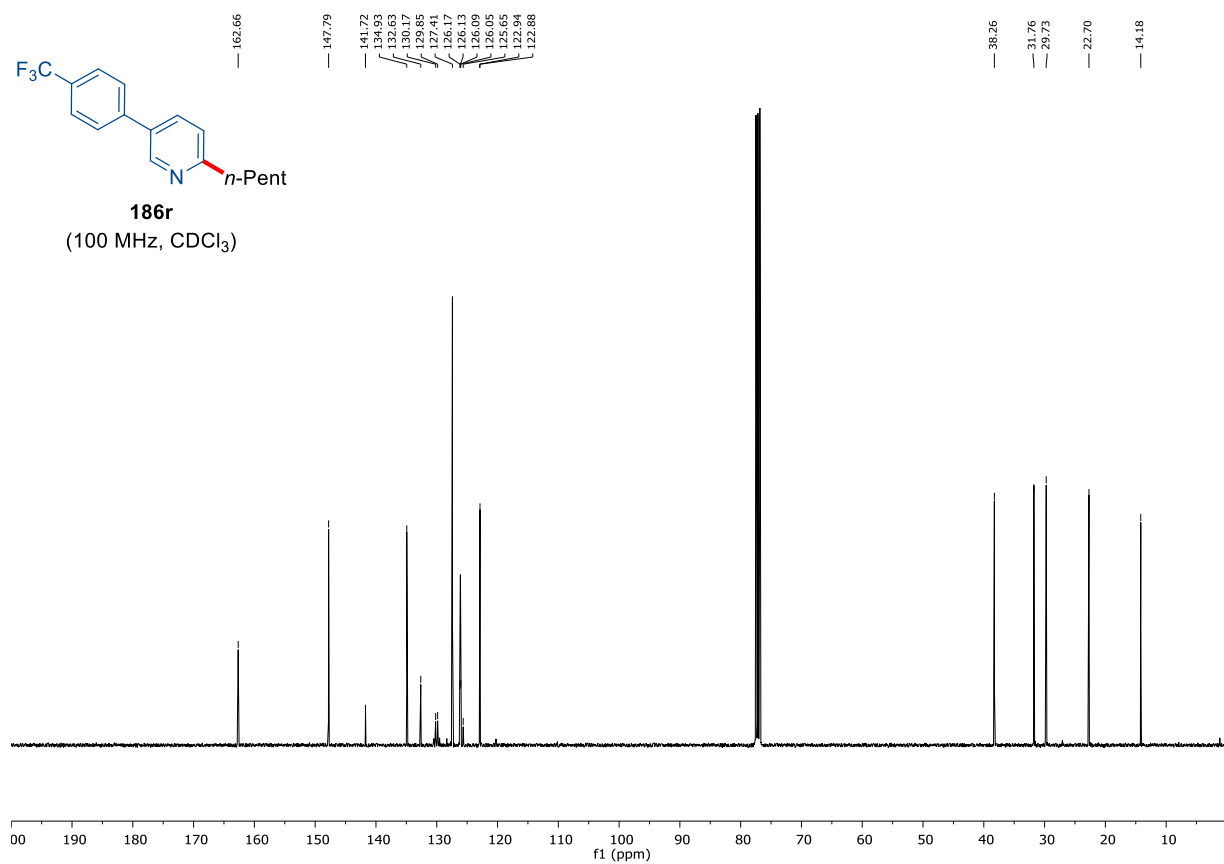
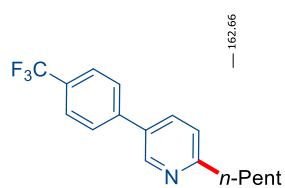
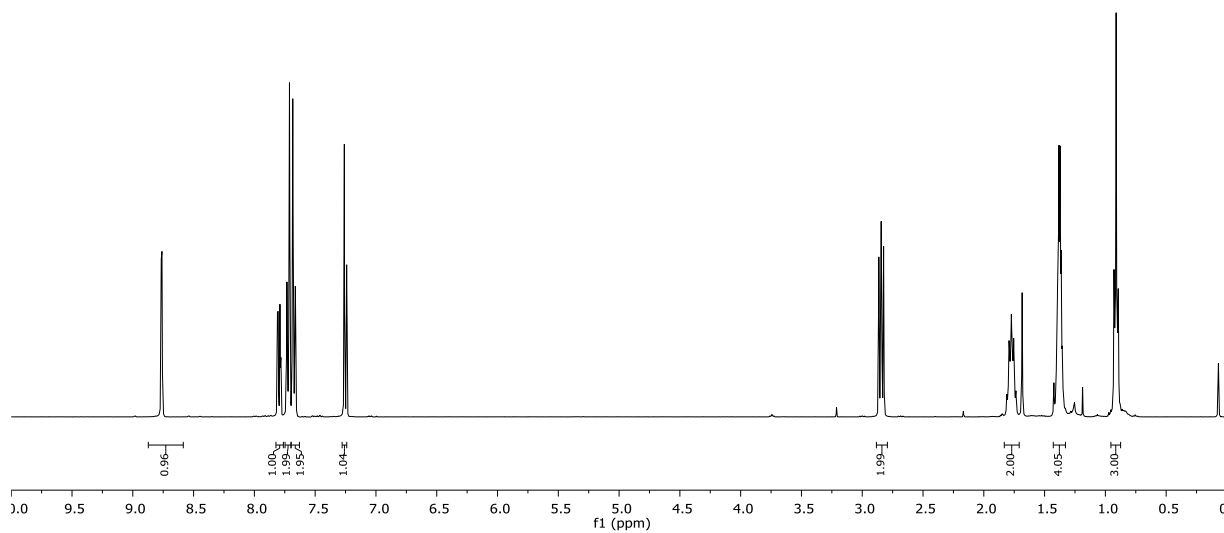
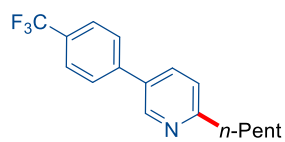


186p
(100 MHz, CDCl₃)

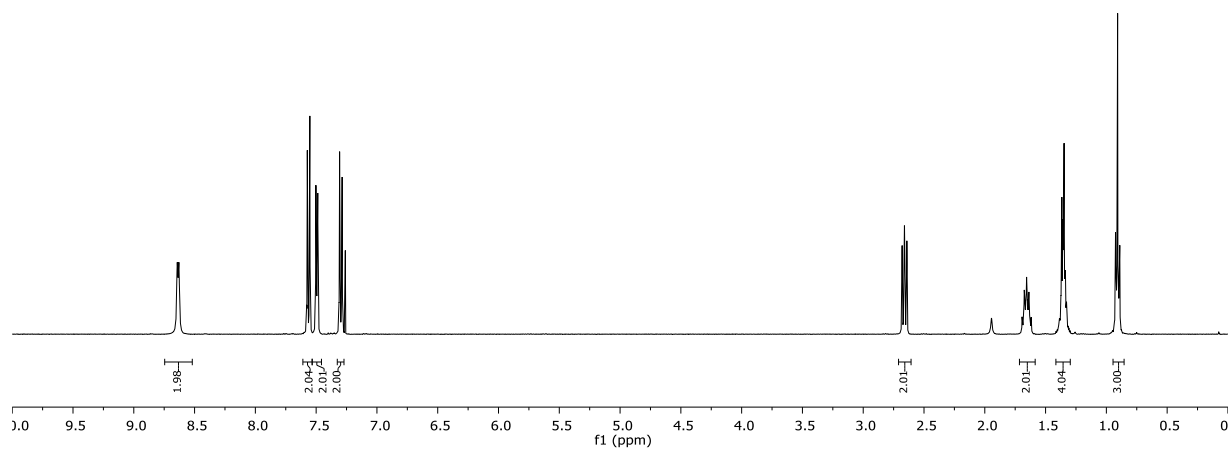
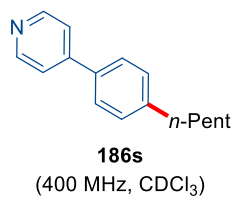
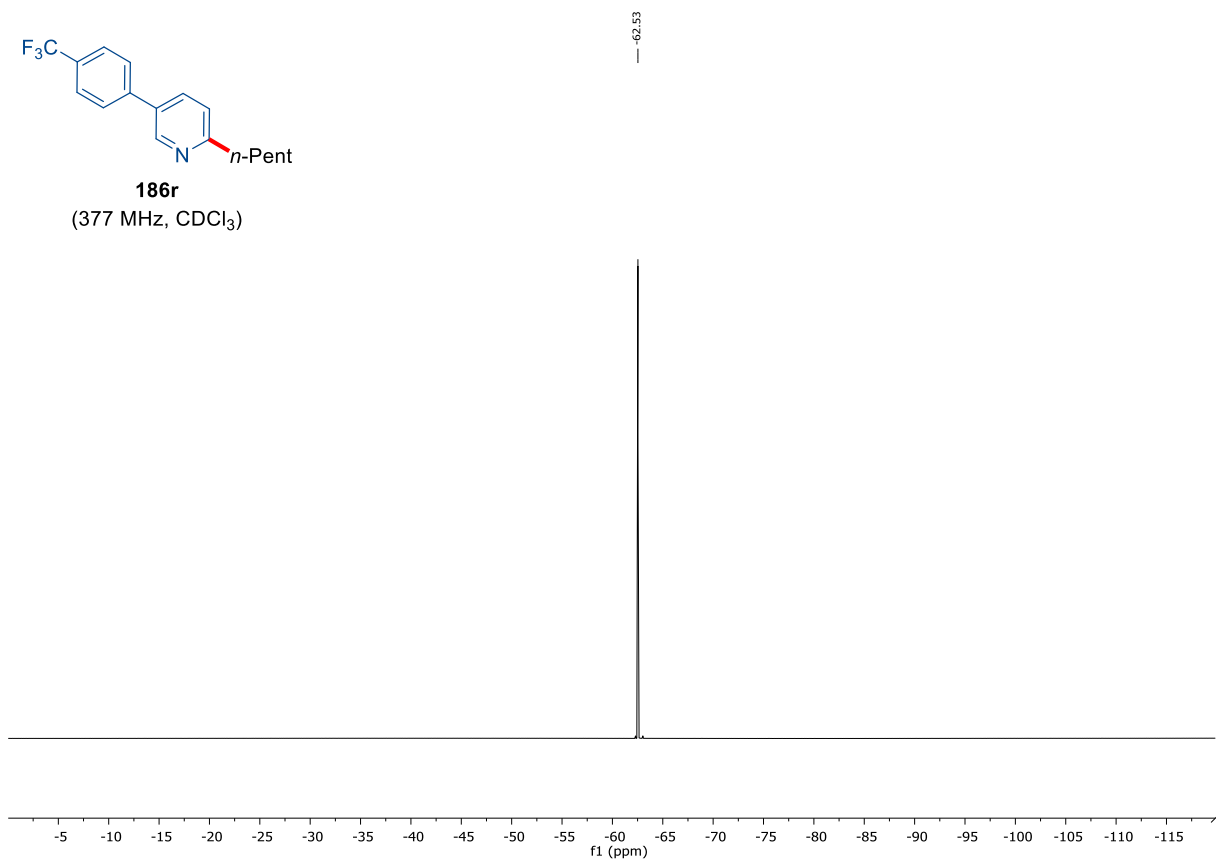
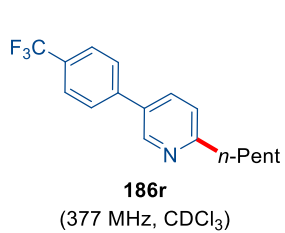


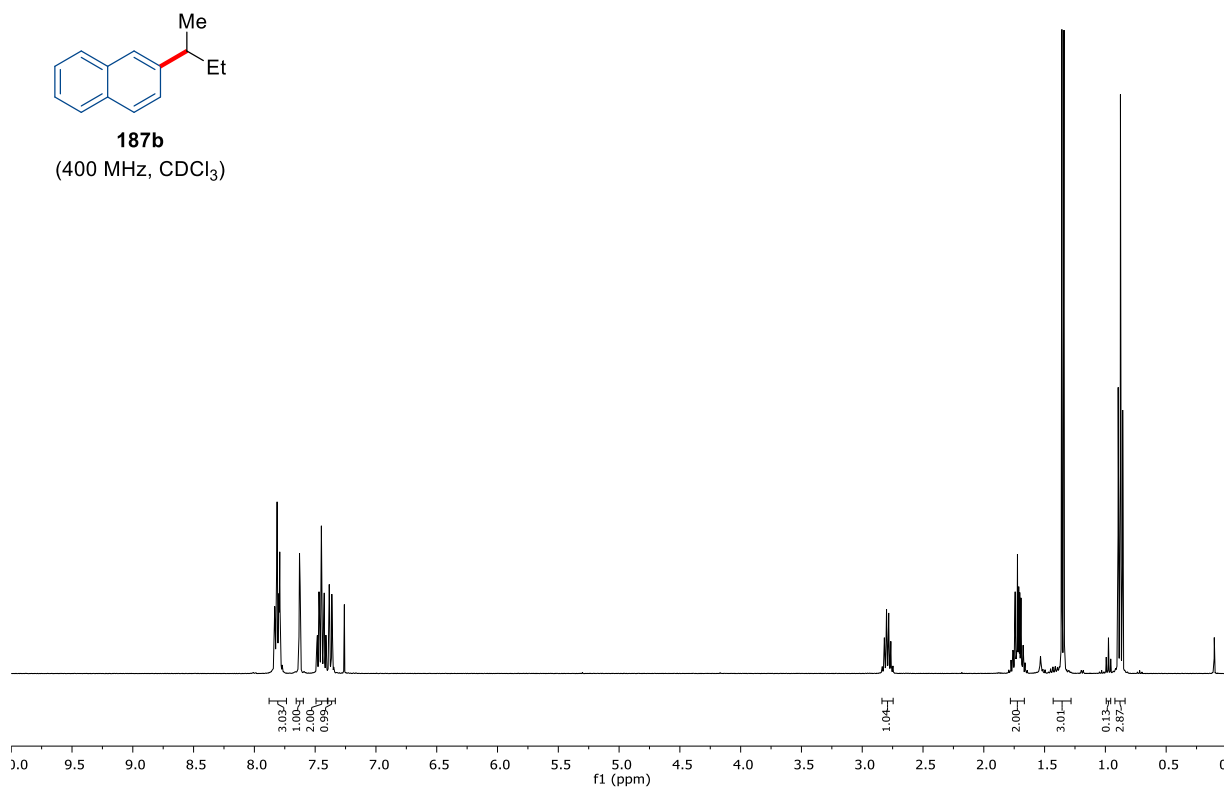
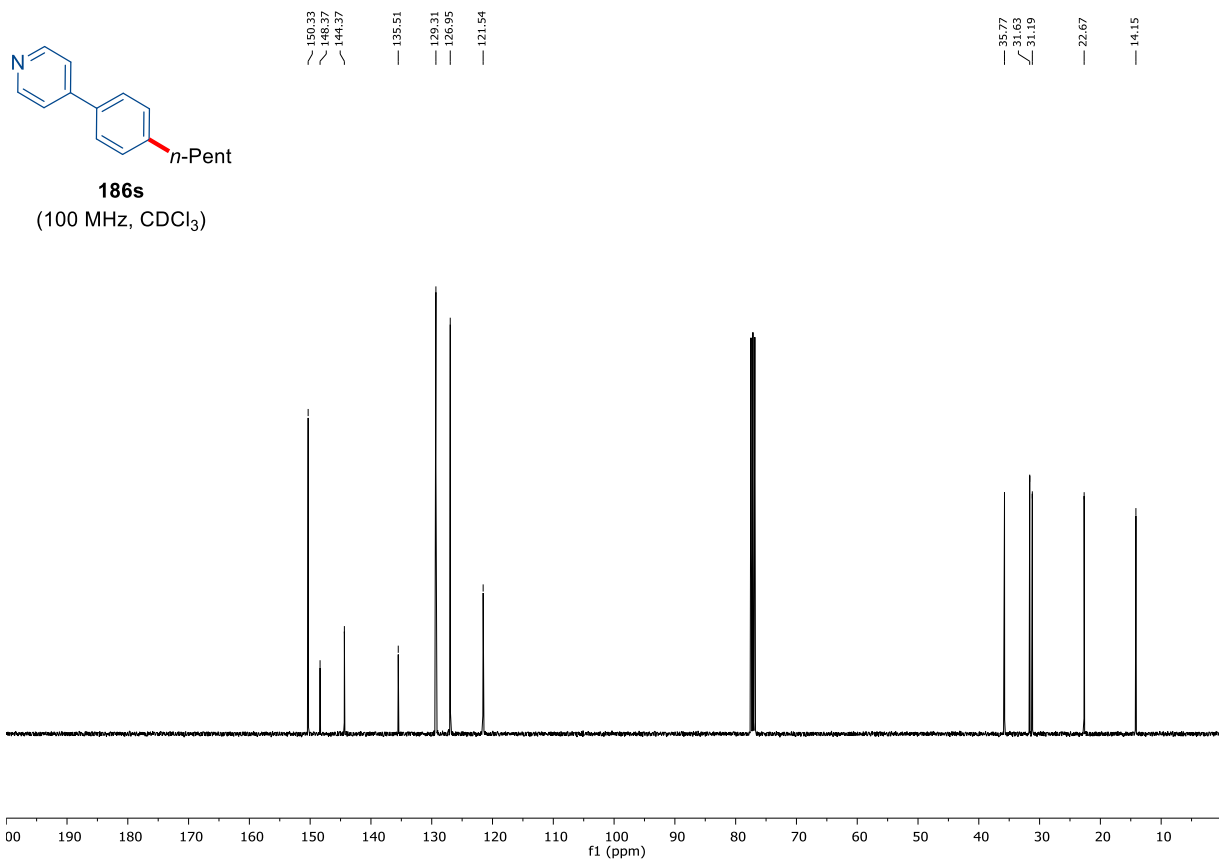
7. Appendix: NMR-Spectra and HPLC Chromatograms



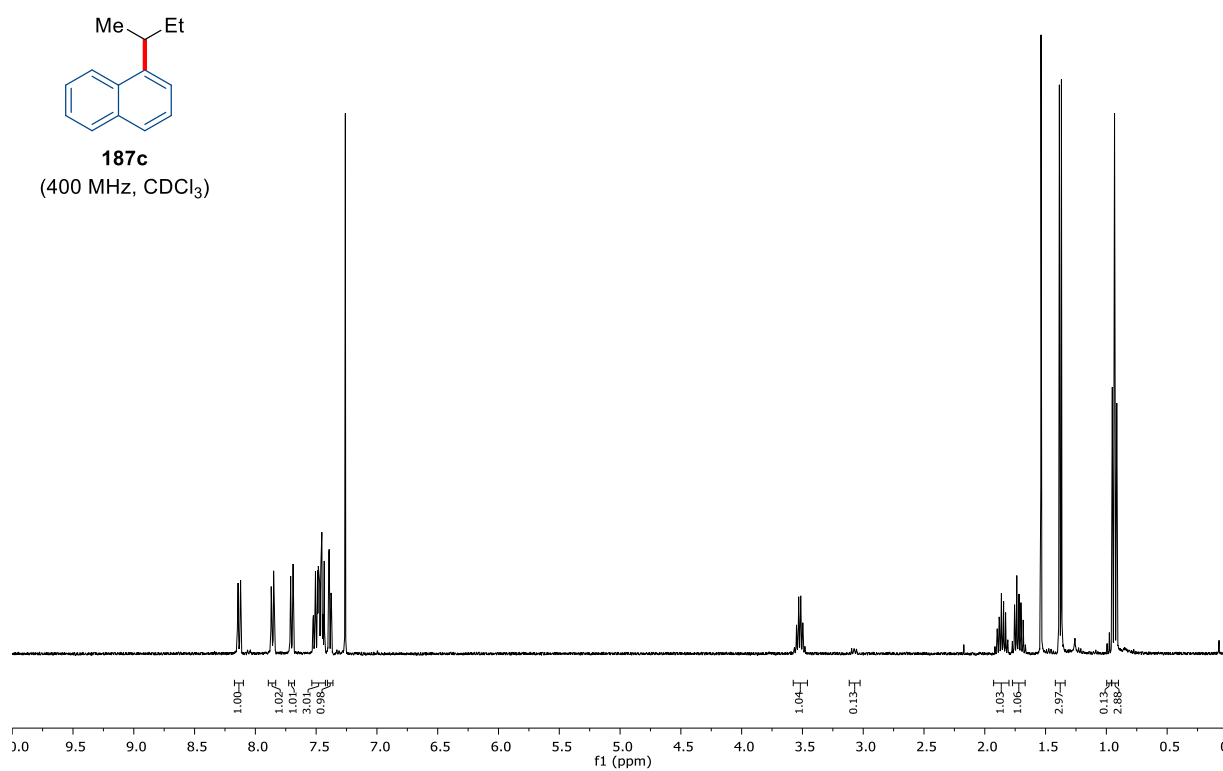
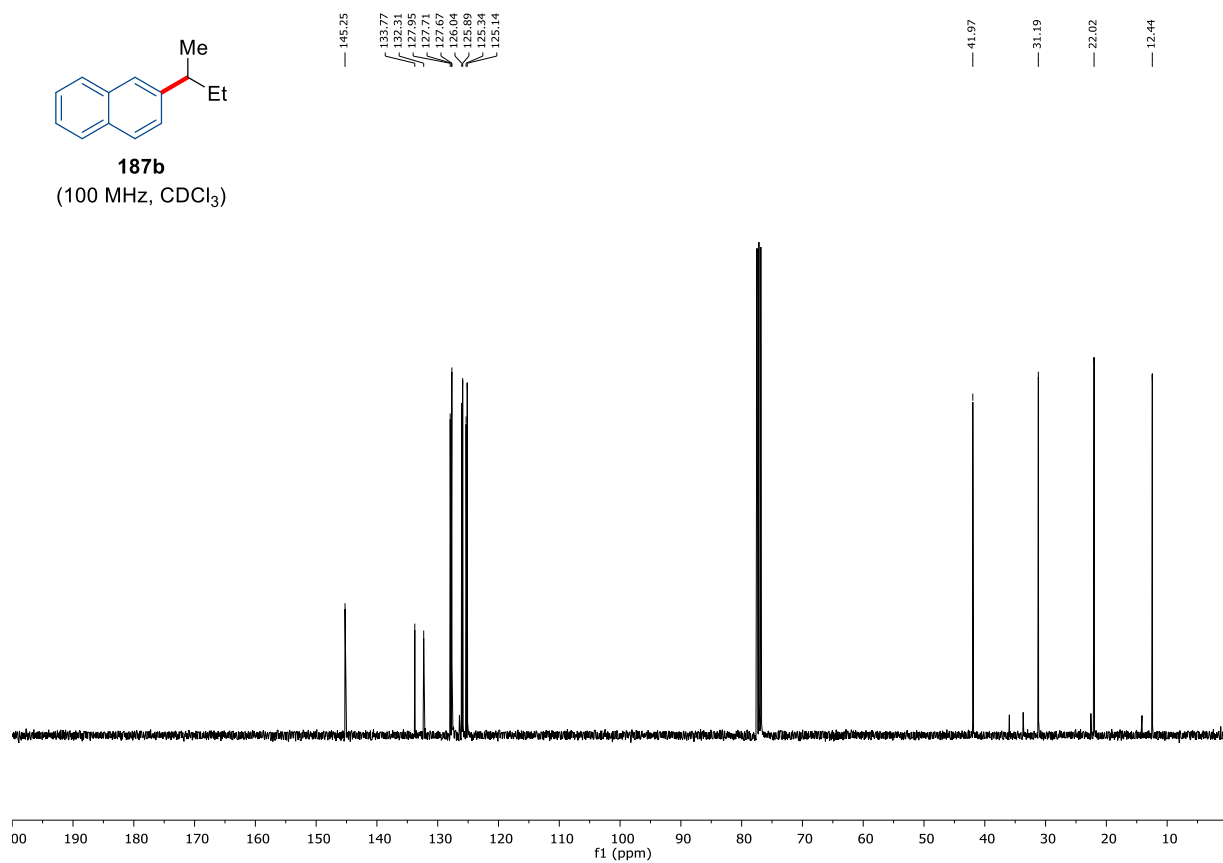


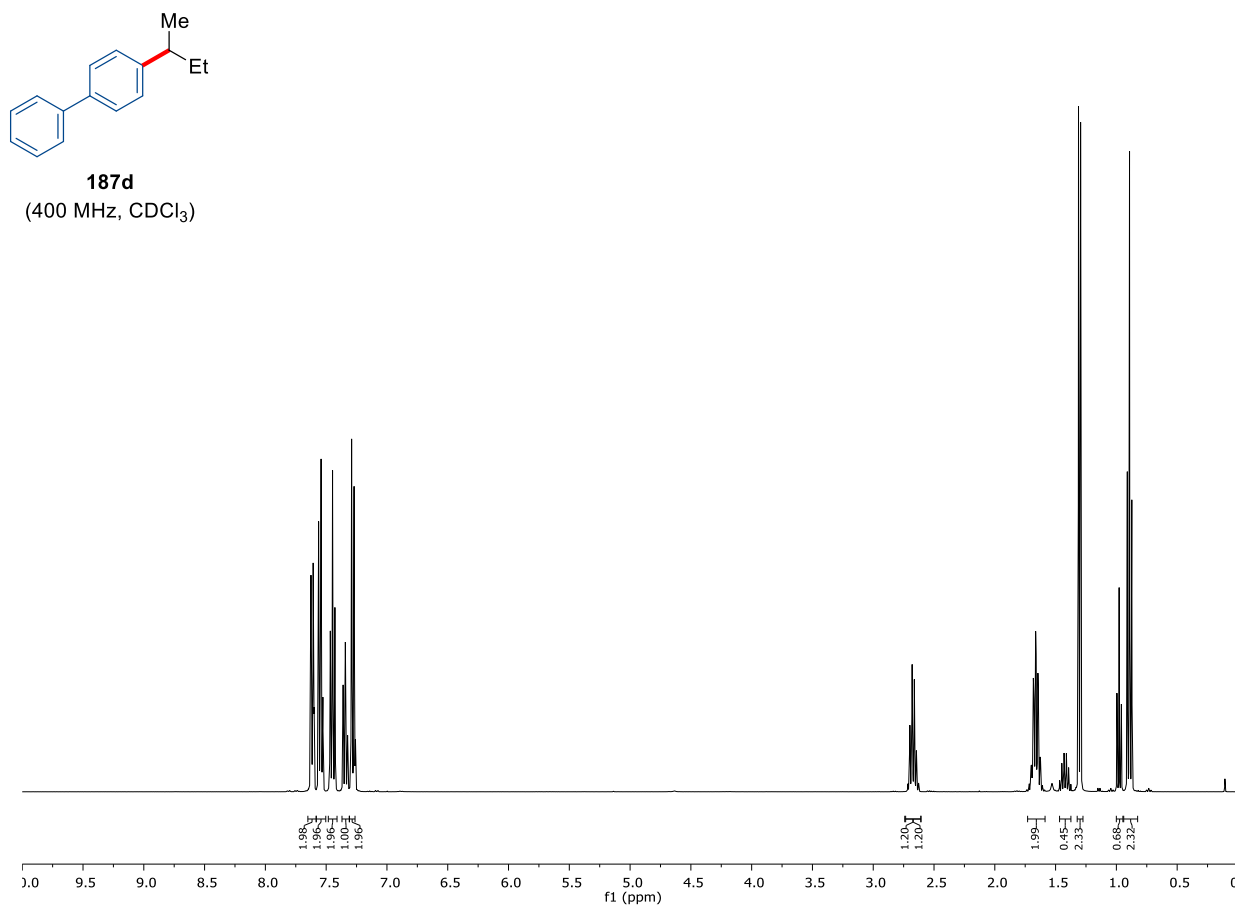
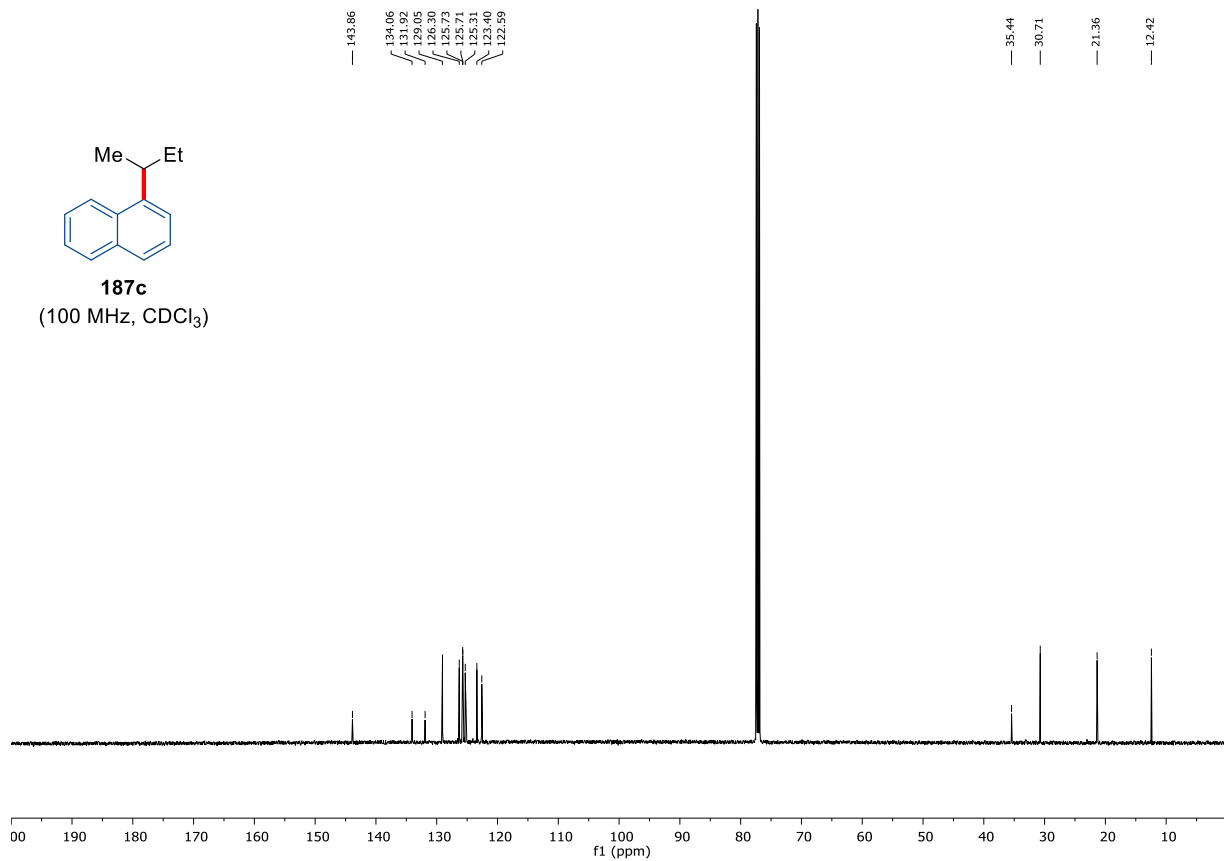
7. Appendix: NMR-Spectra and HPLC Chromatograms



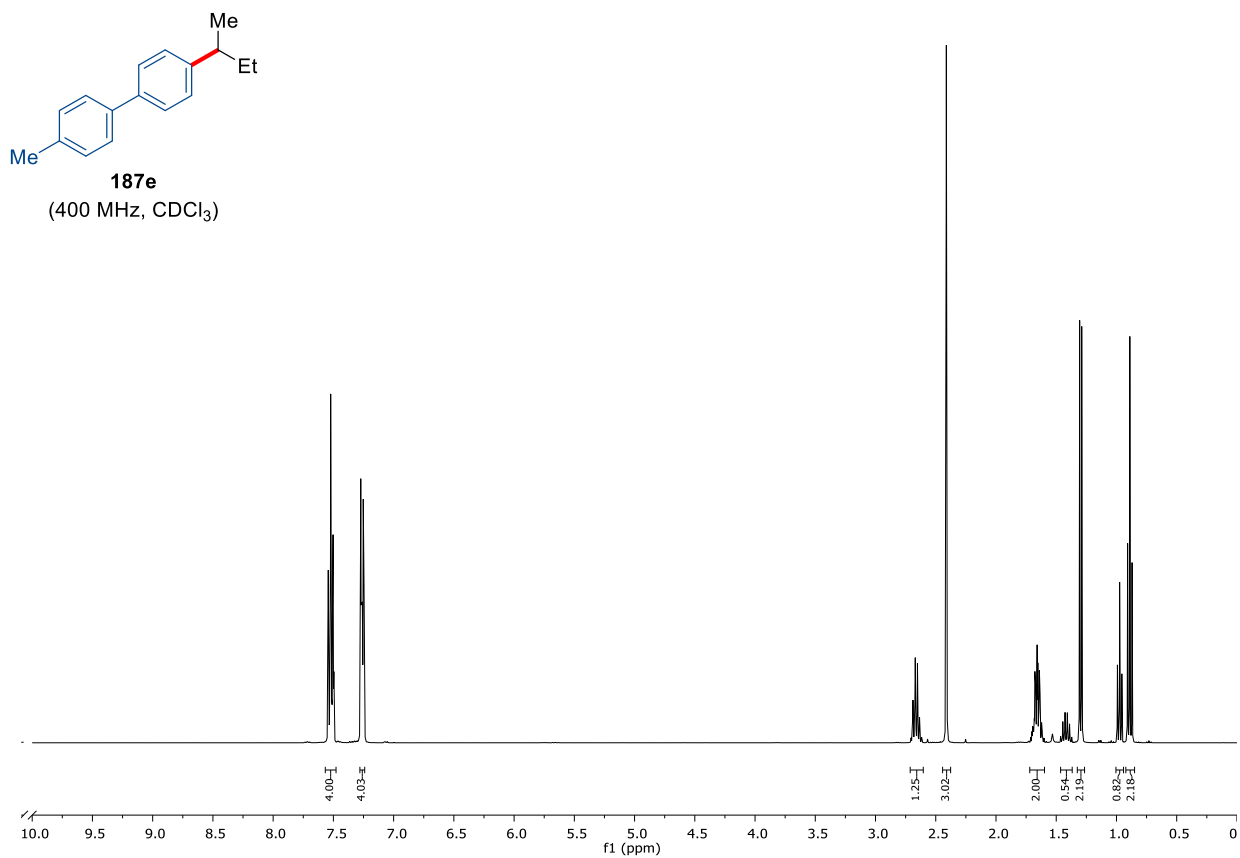
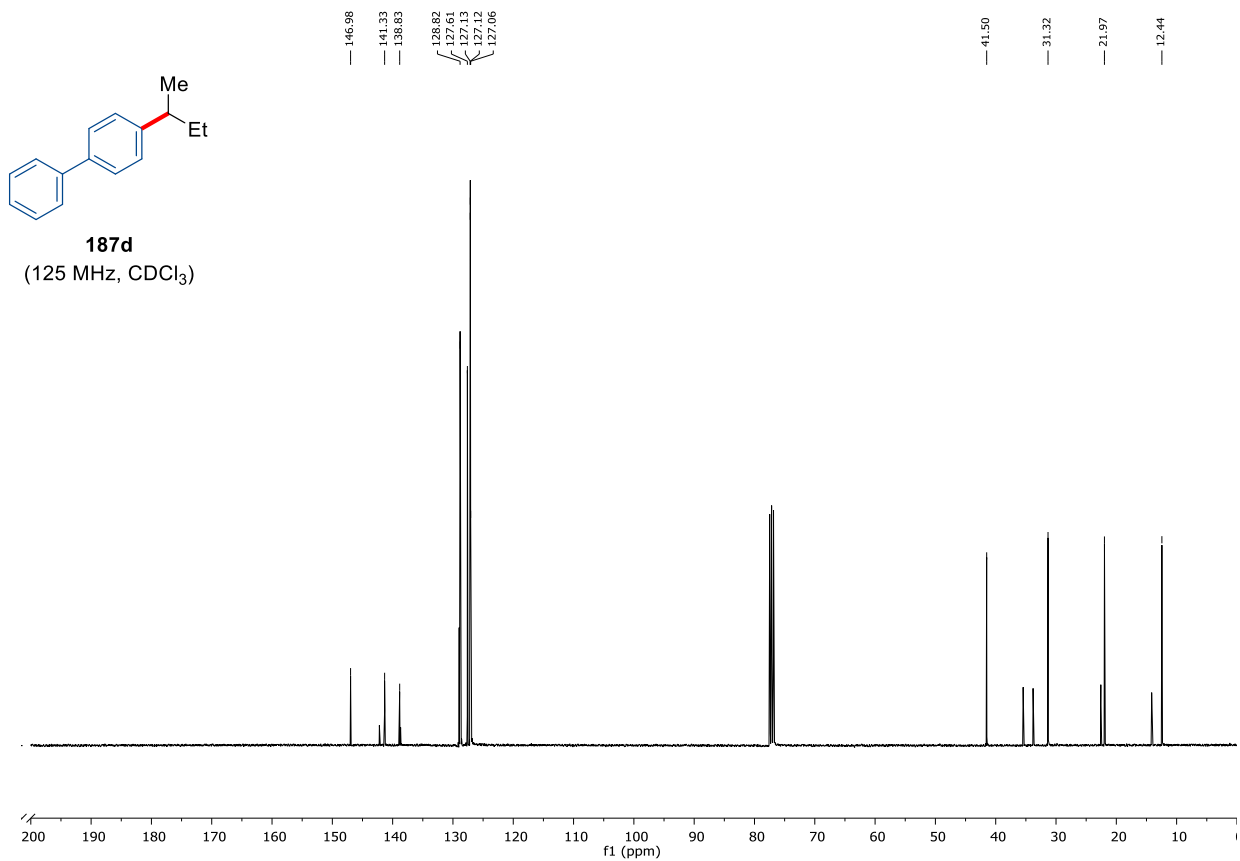


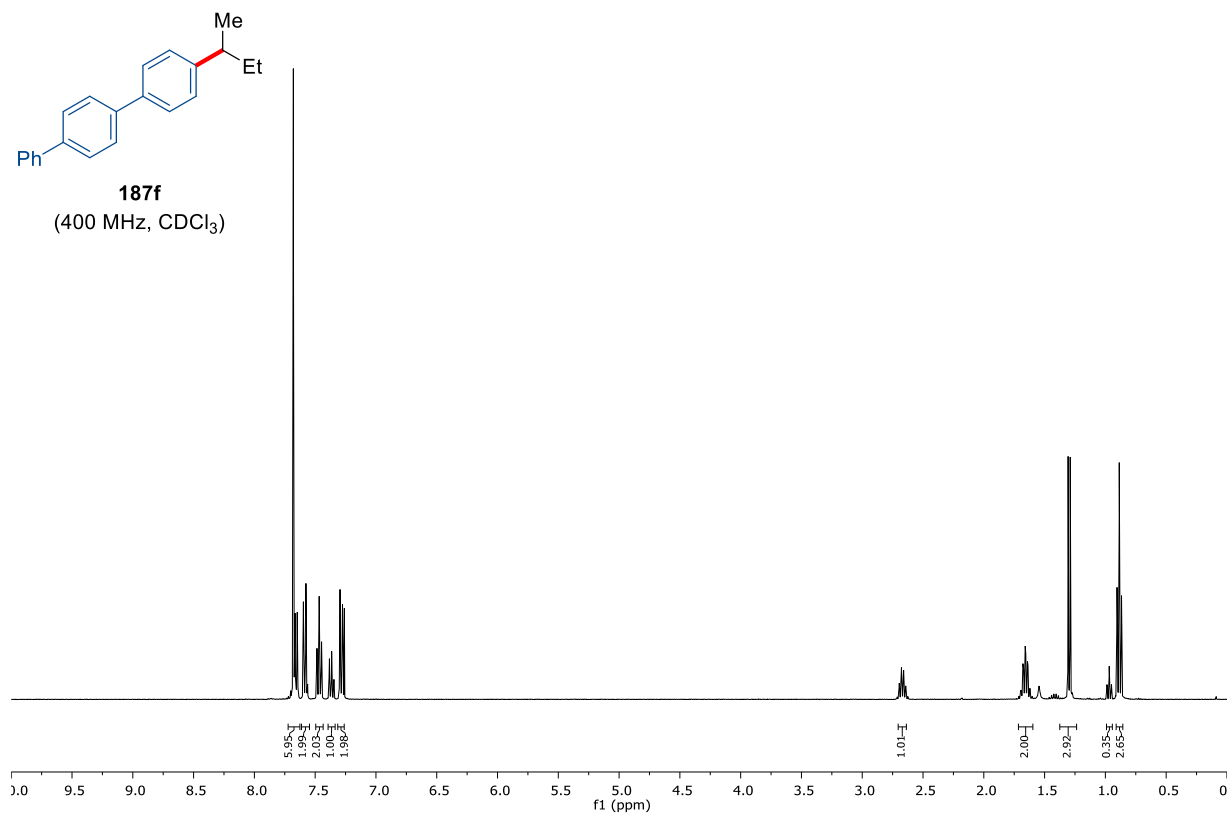
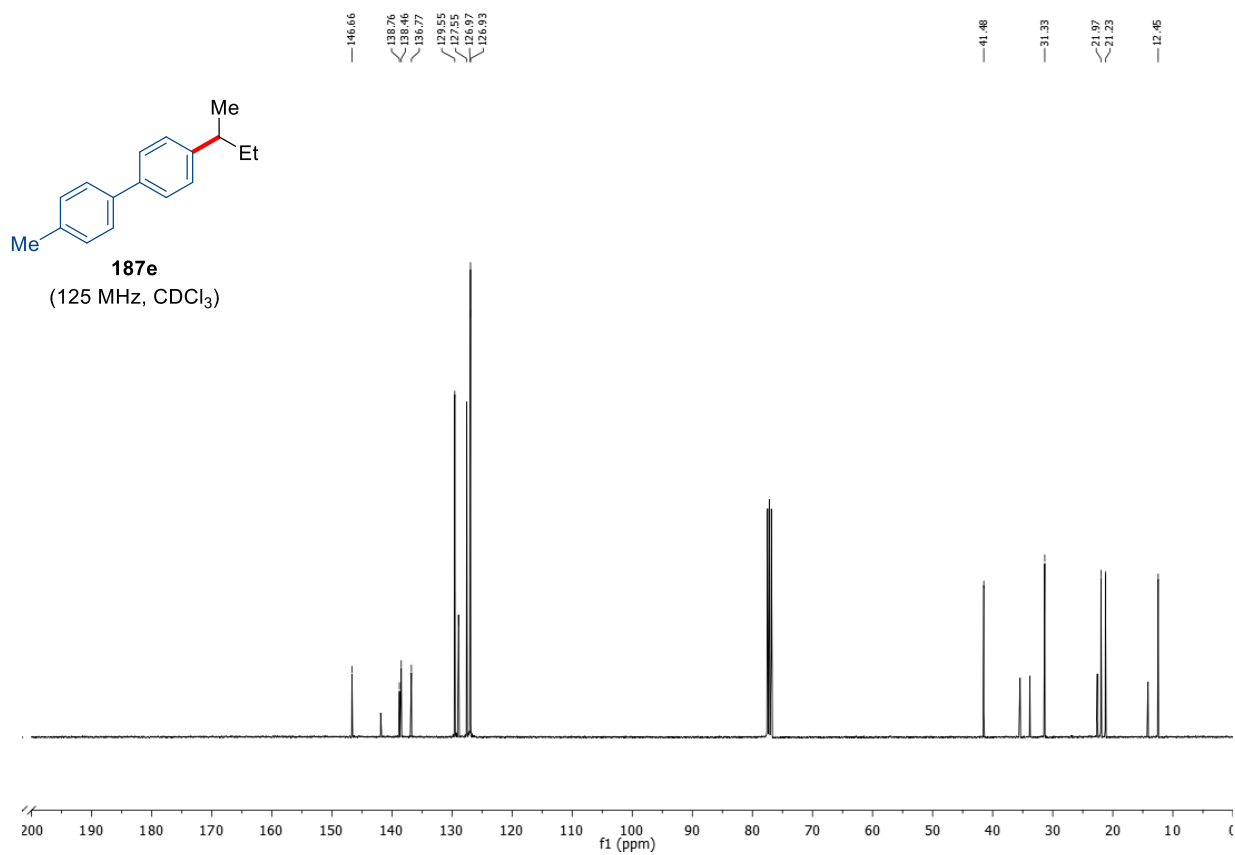
7. Appendix: NMR-Spectra and HPLC Chromatograms



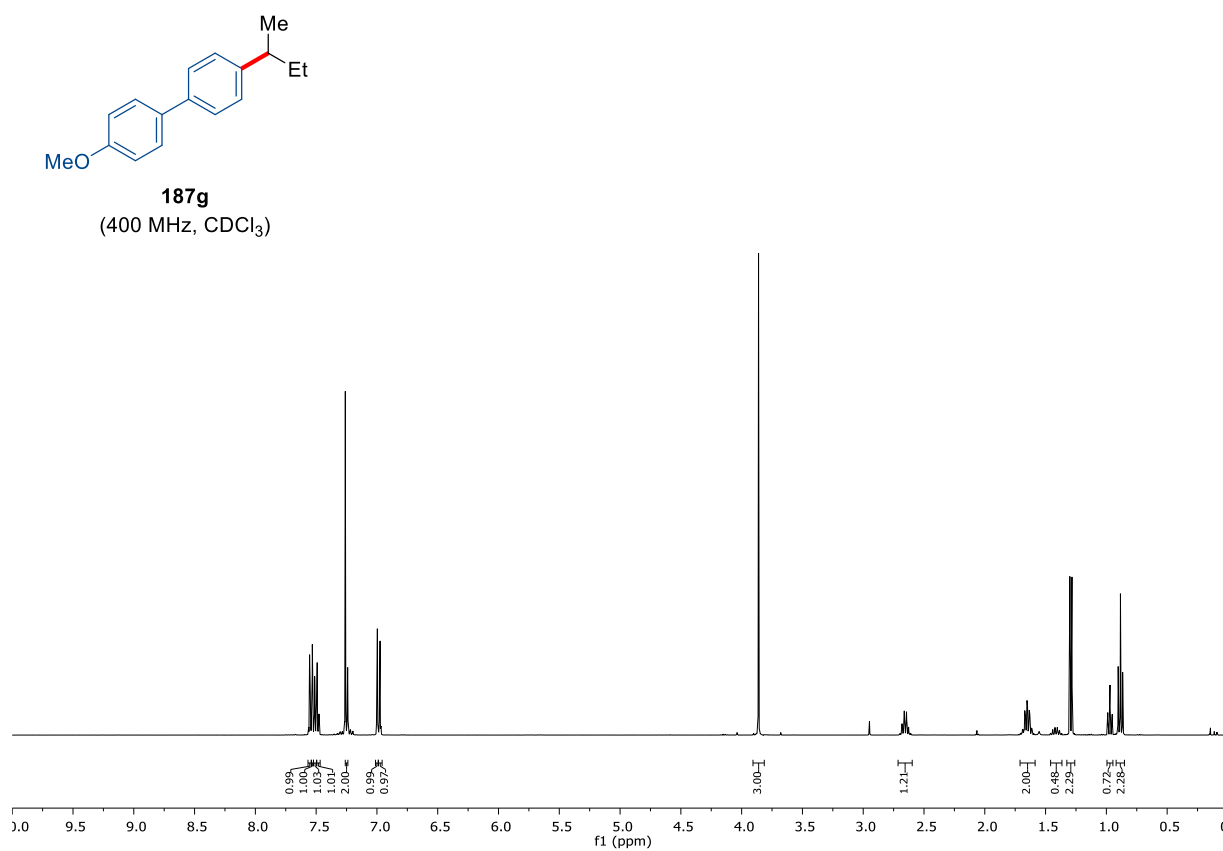
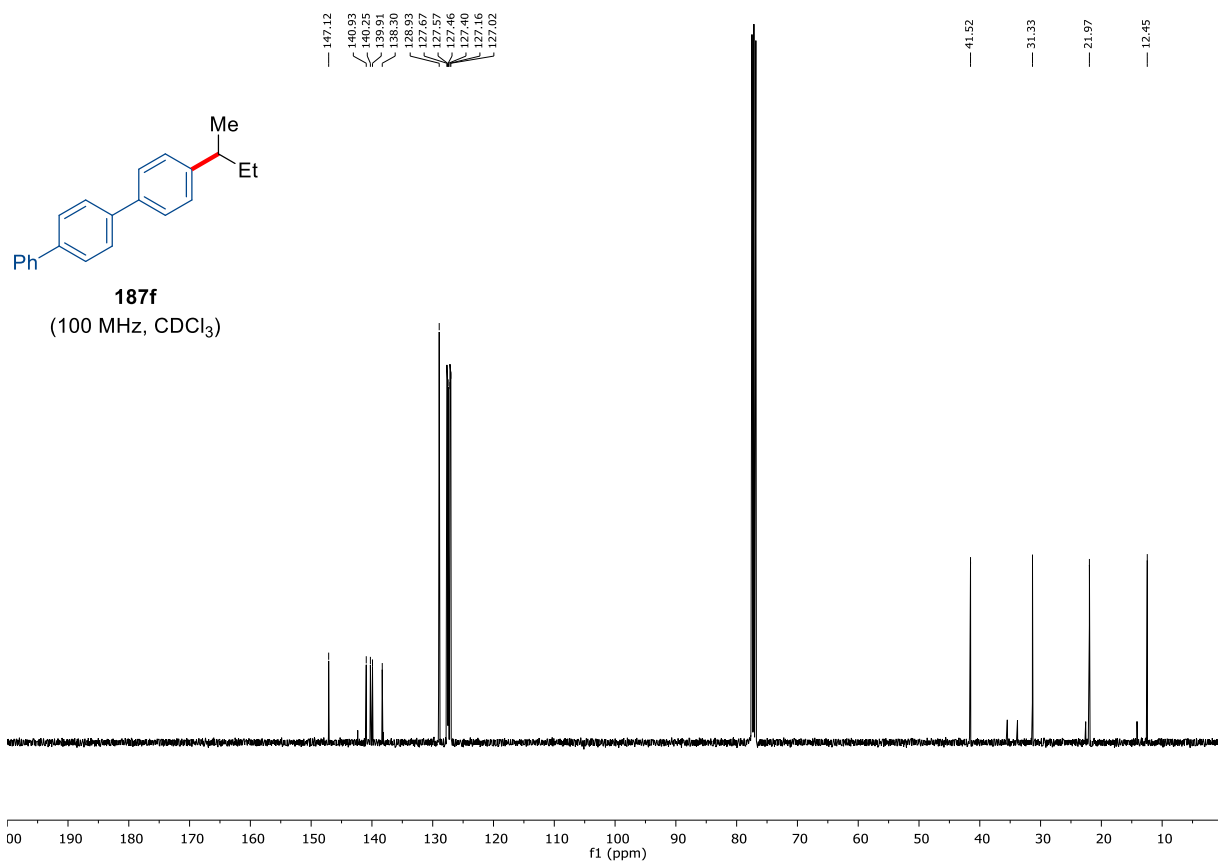


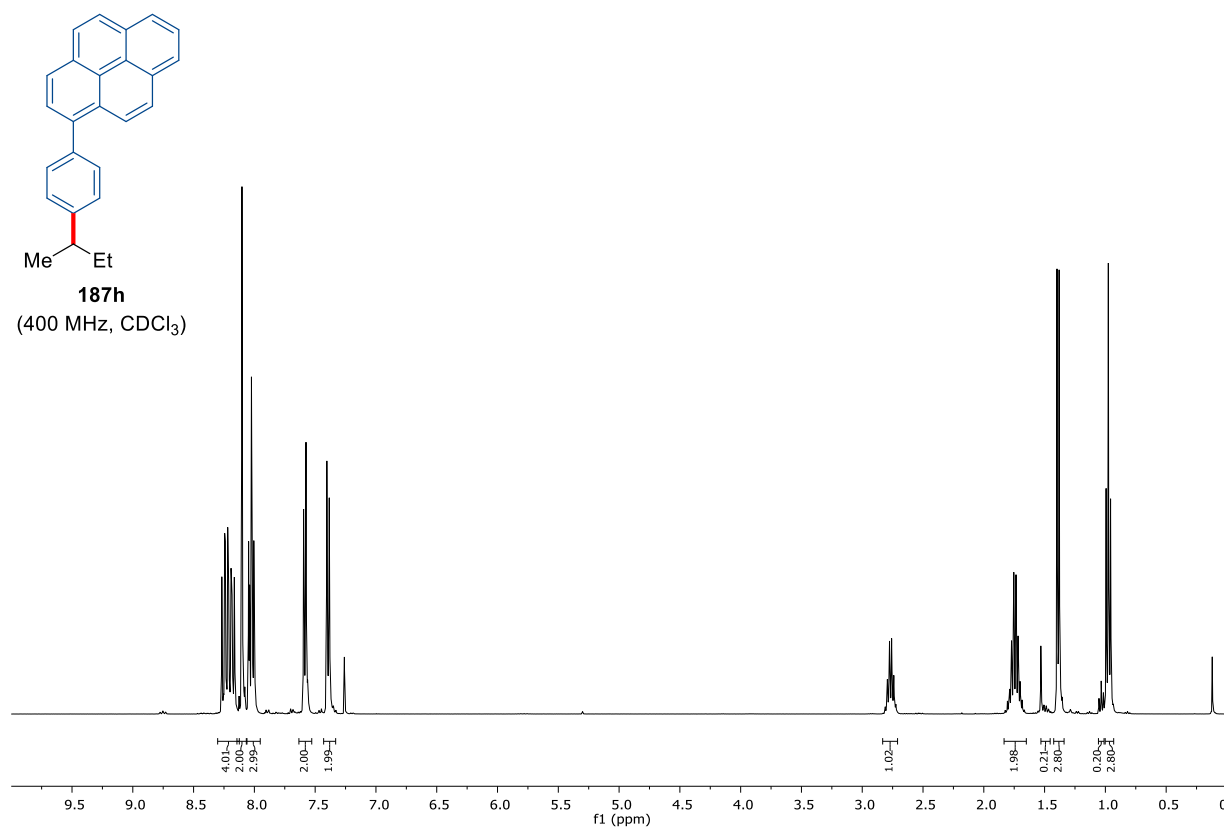
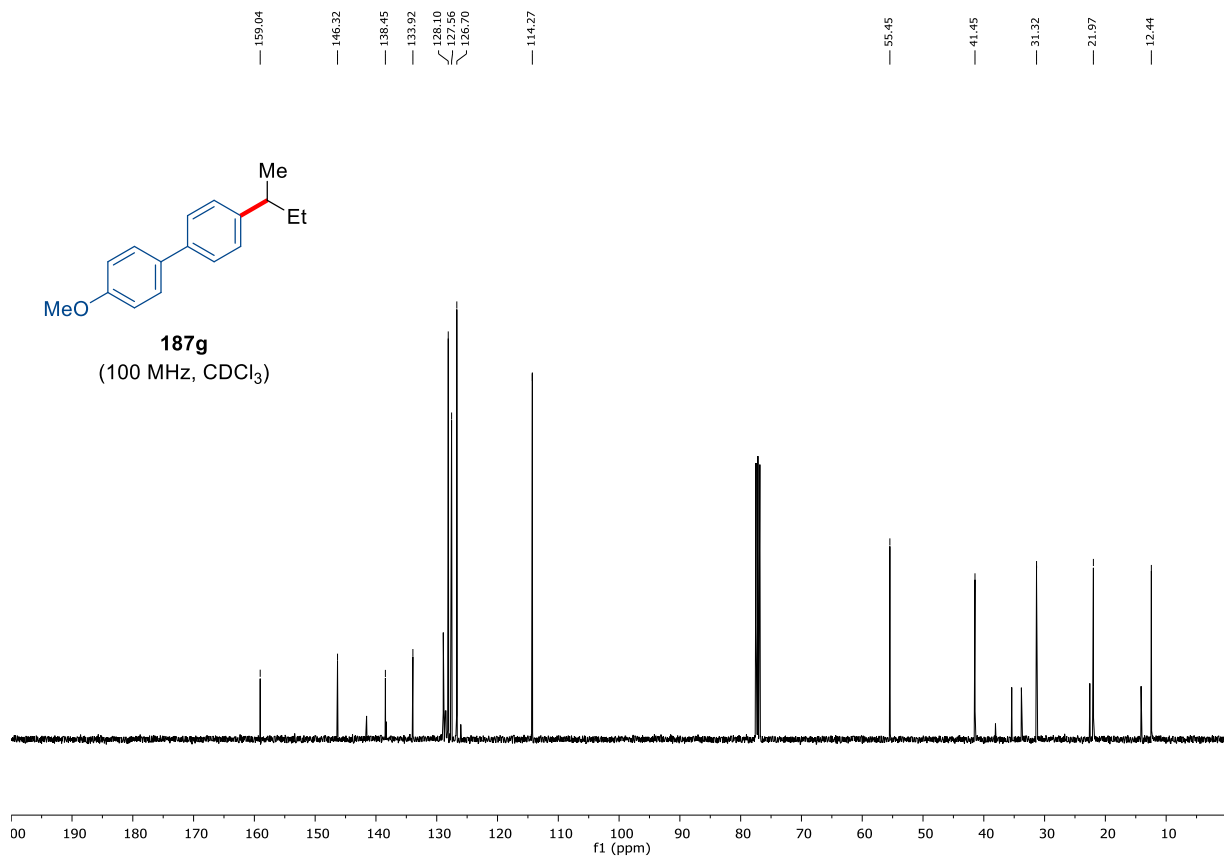
7. Appendix: NMR-Spectra and HPLC Chromatograms



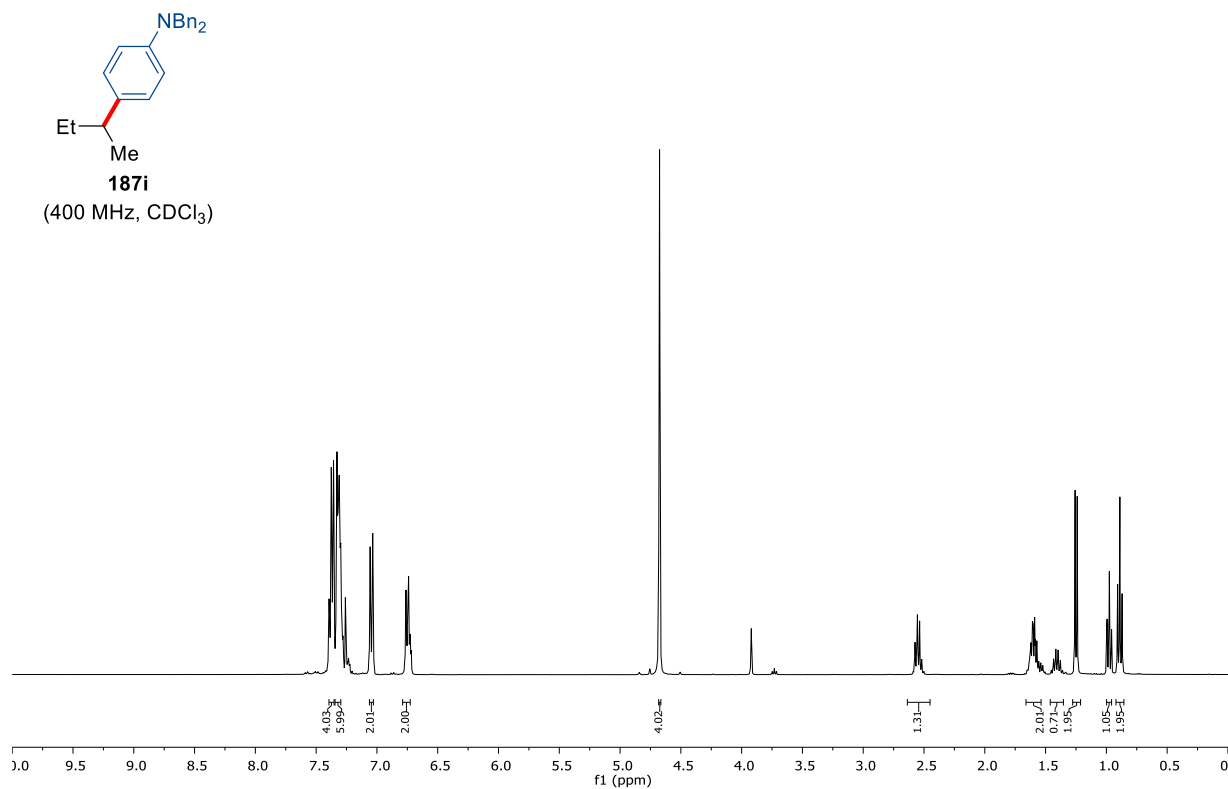
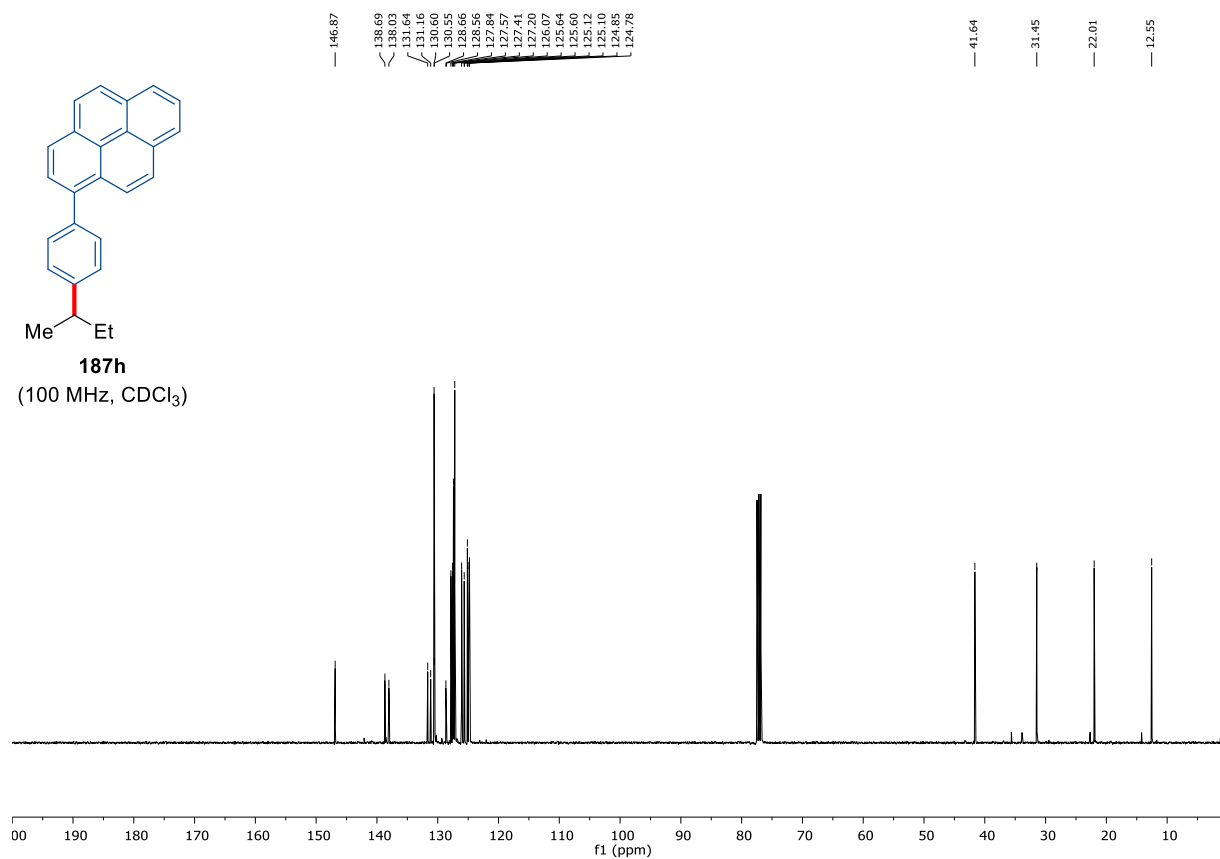


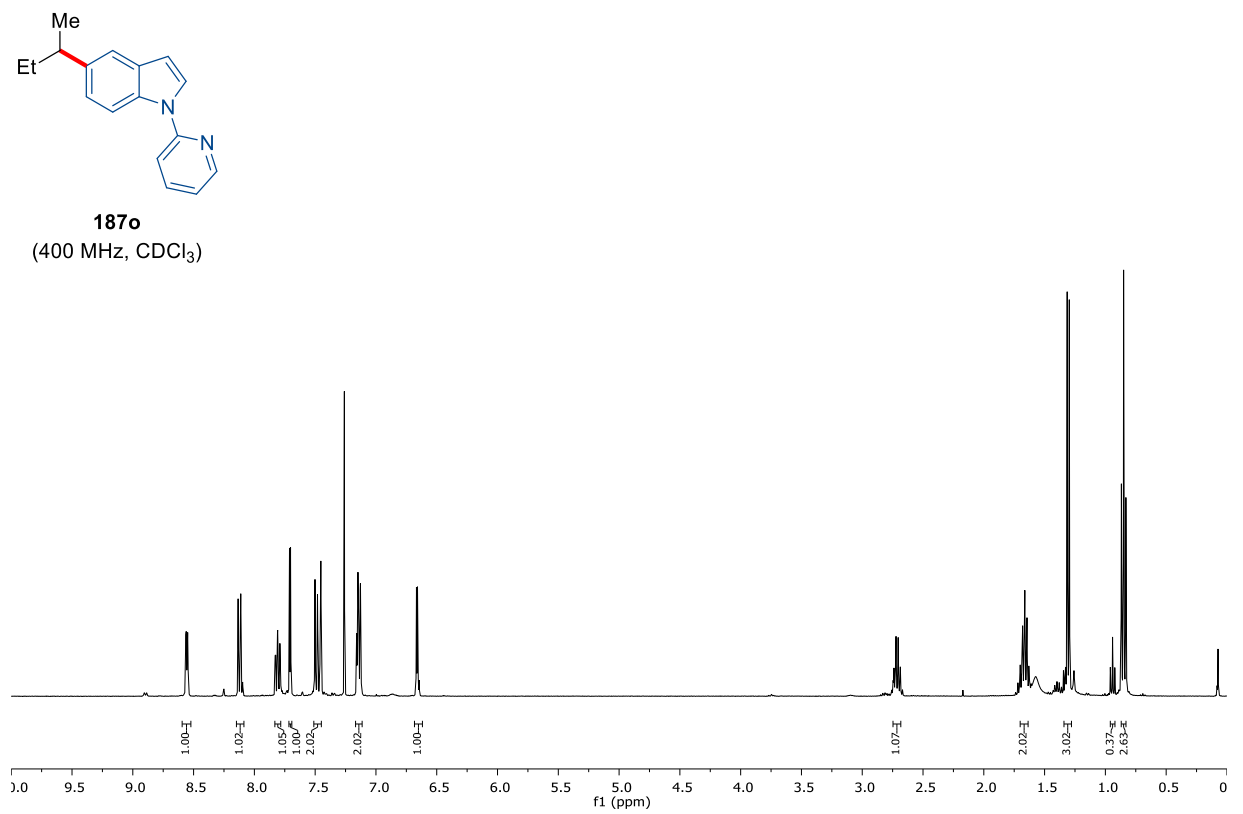
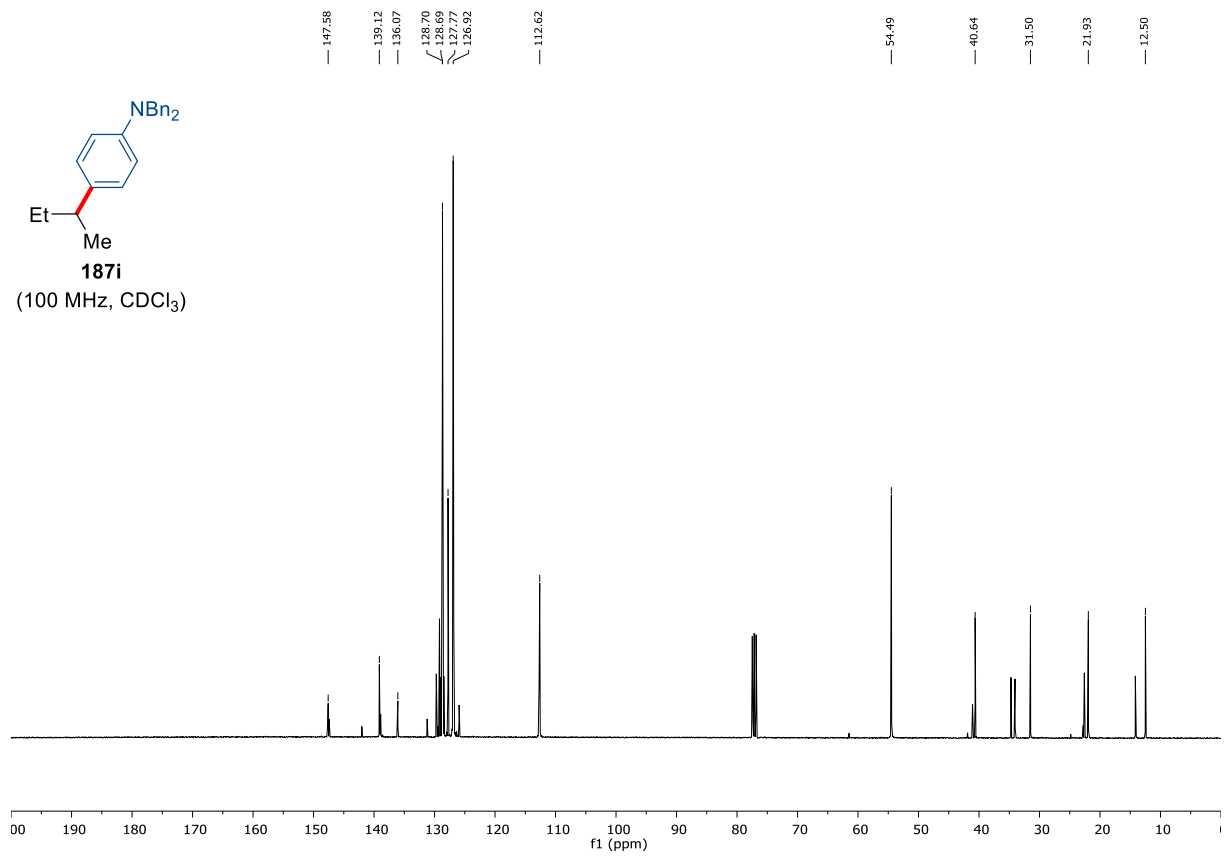
7. Appendix: NMR-Spectra and HPLC Chromatograms



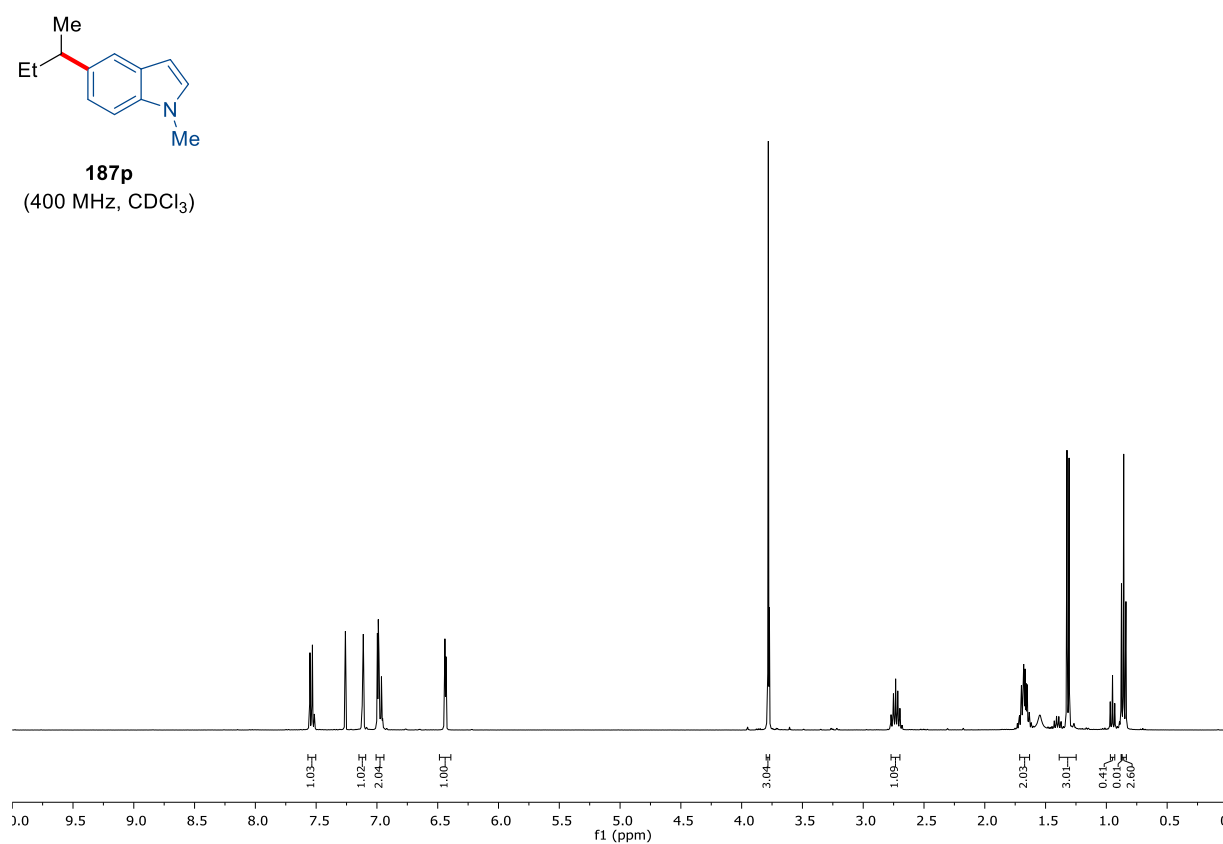
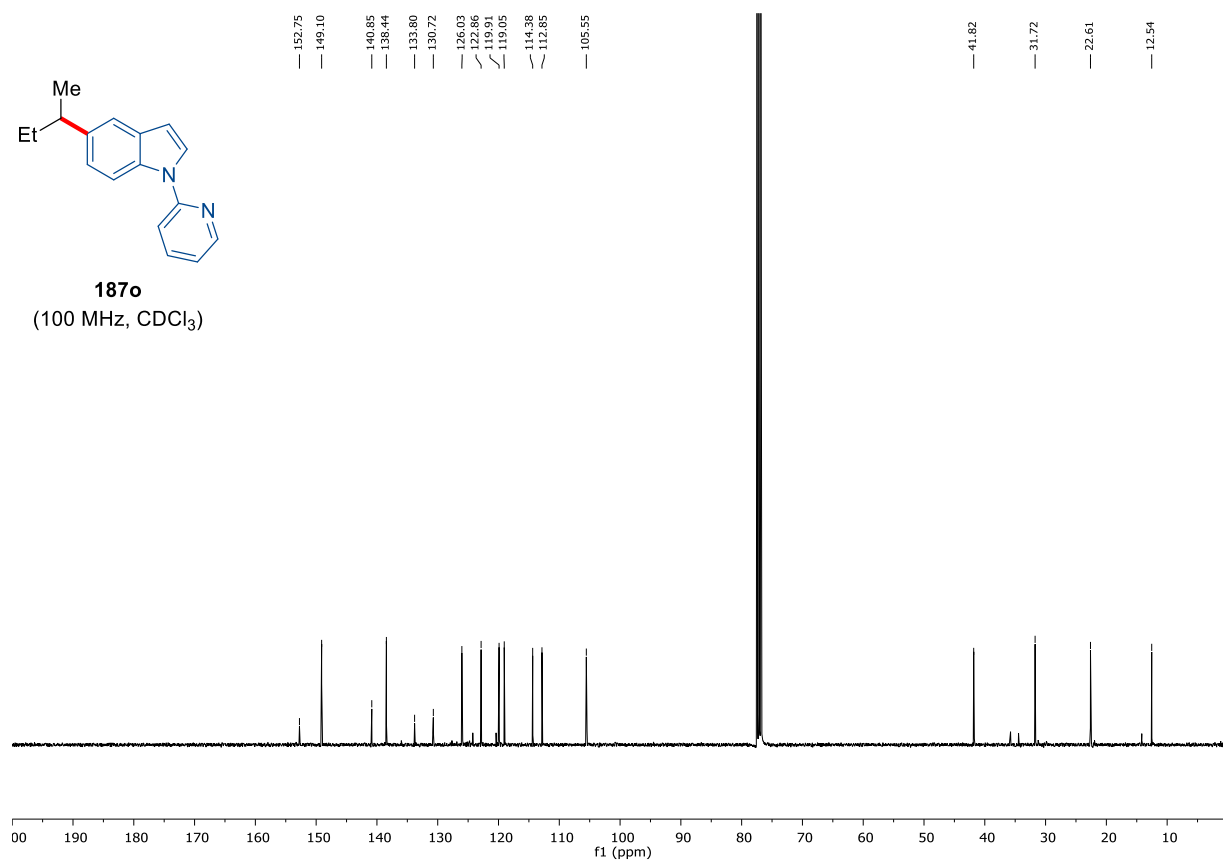


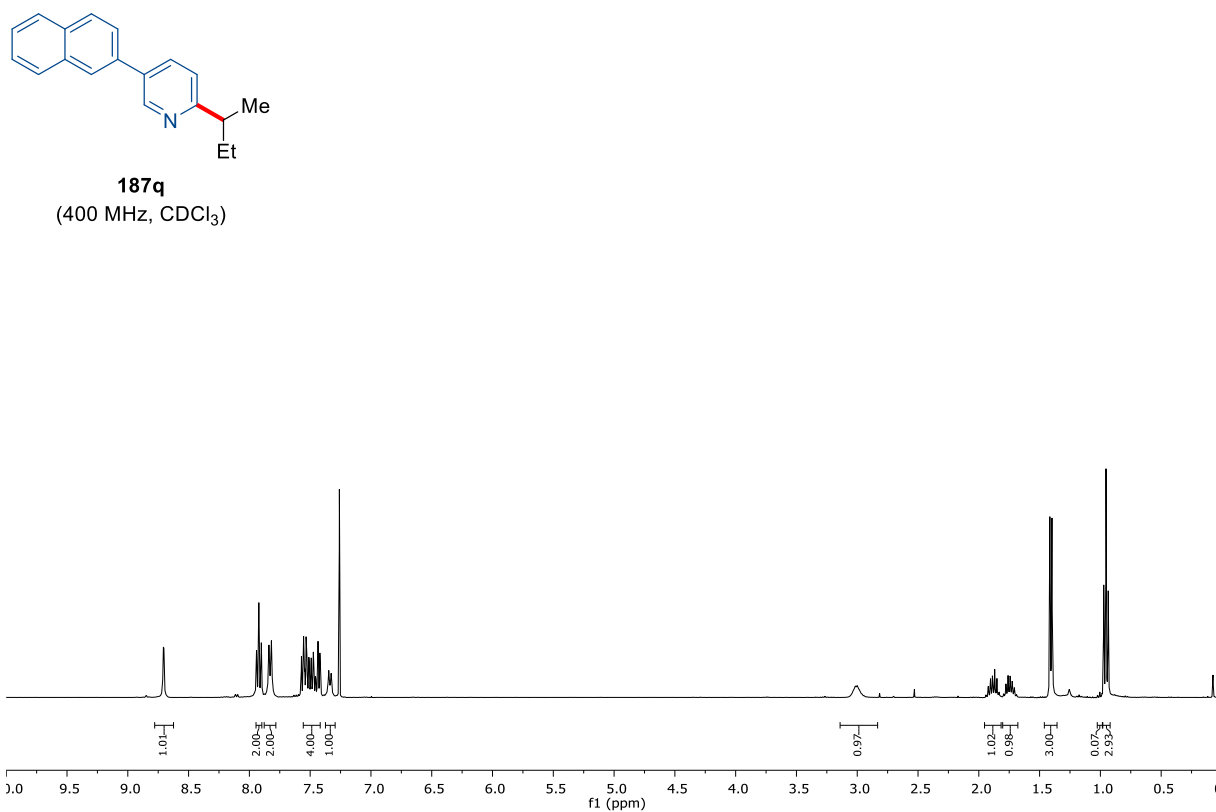
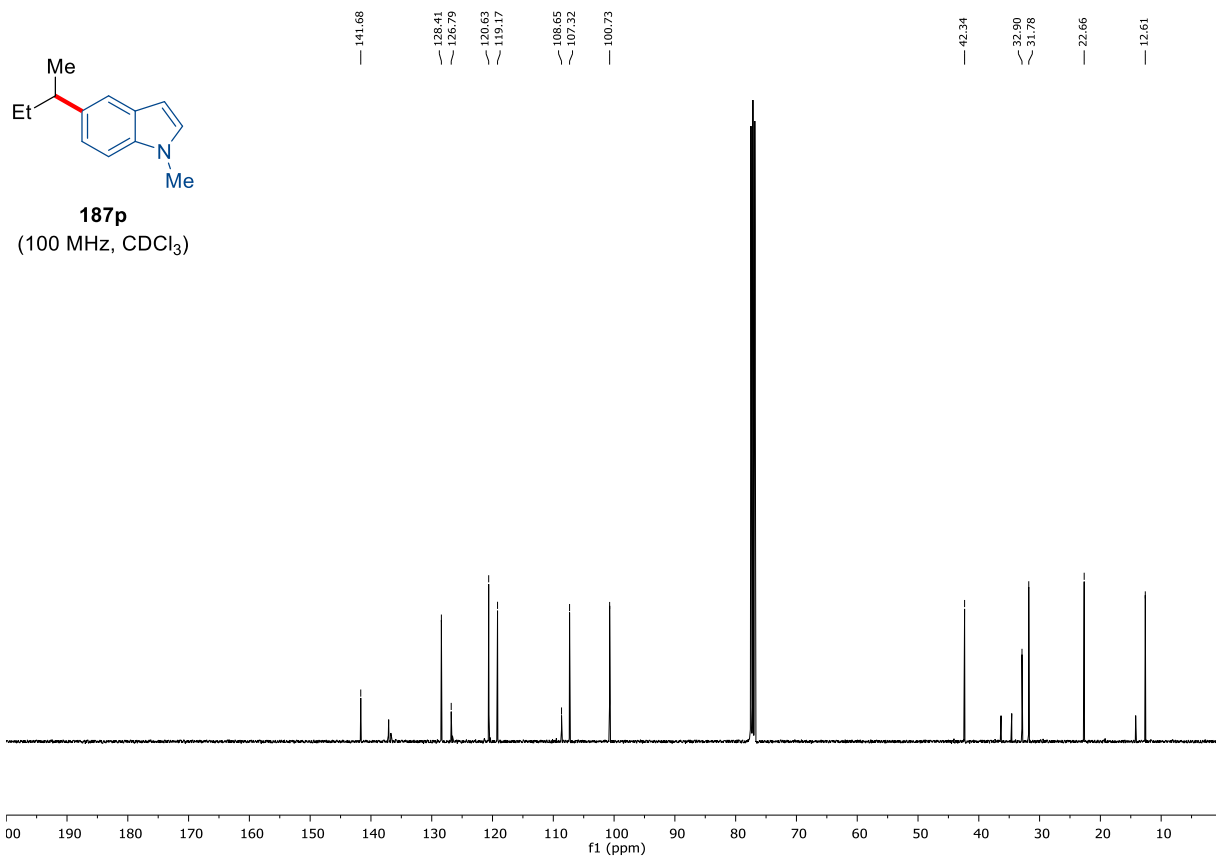
7. Appendix: NMR-Spectra and HPLC Chromatograms



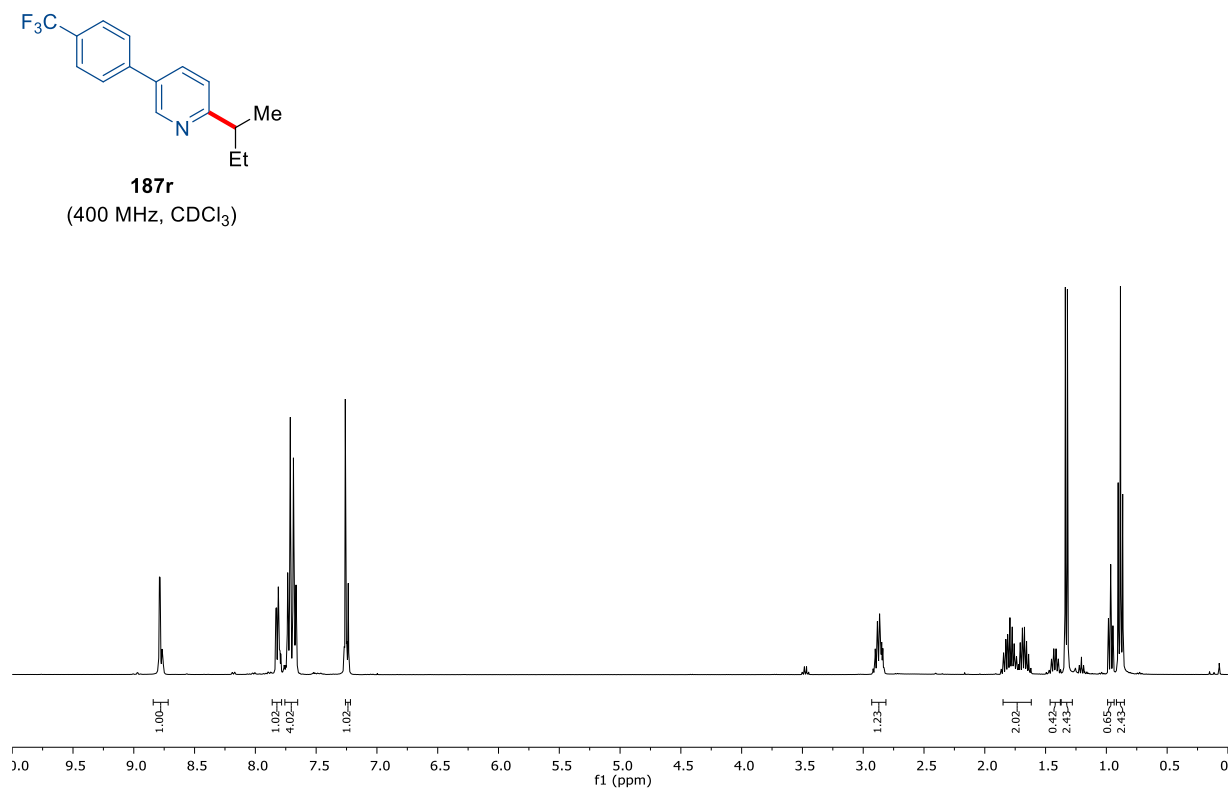
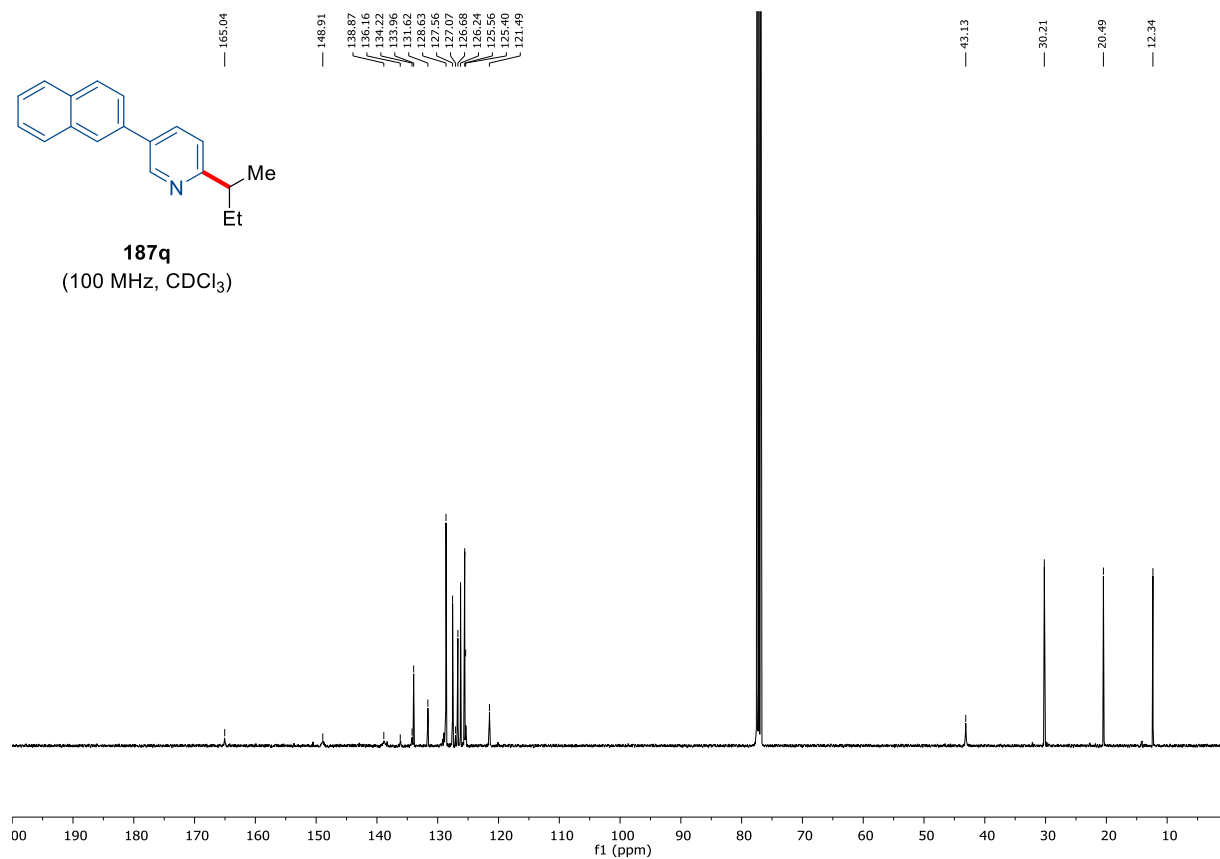


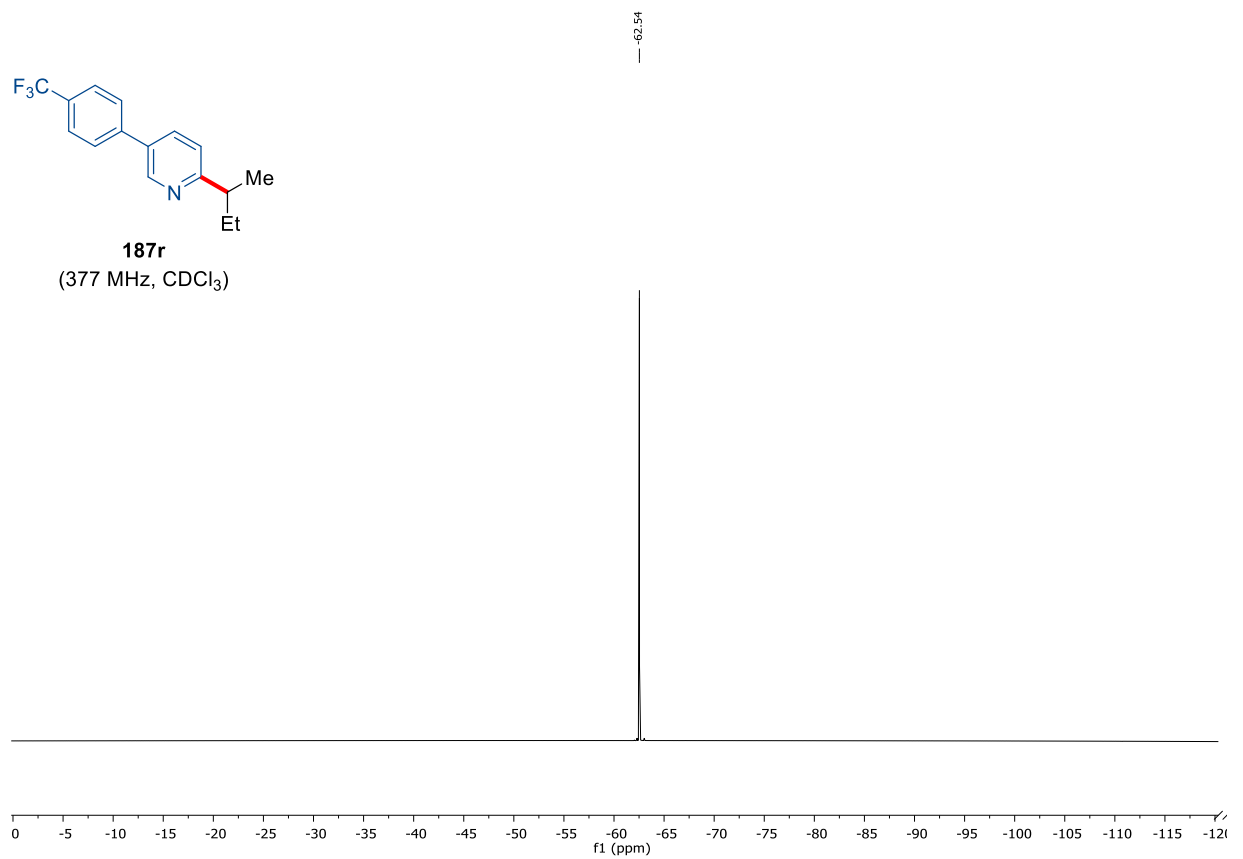
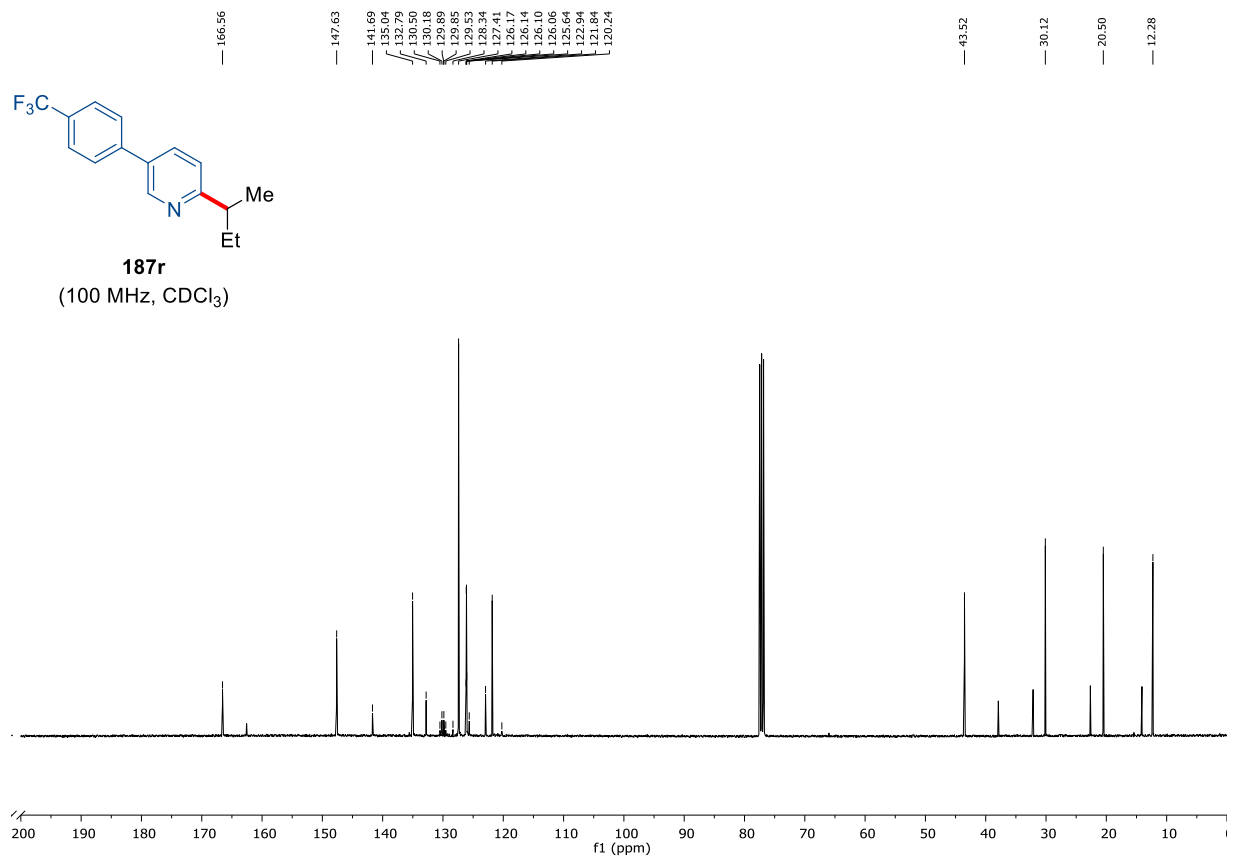
7. Appendix: NMR-Spectra and HPLC Chromatograms



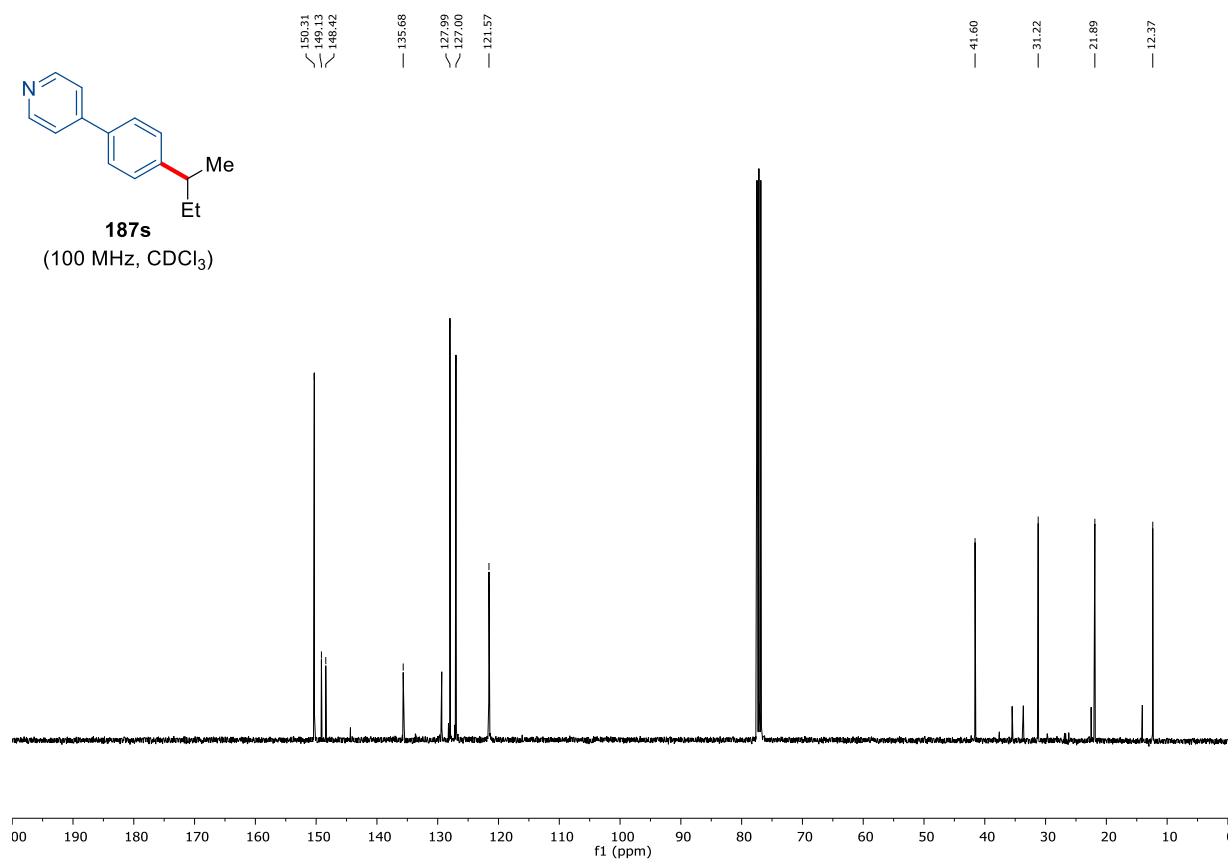
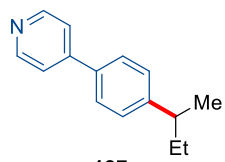
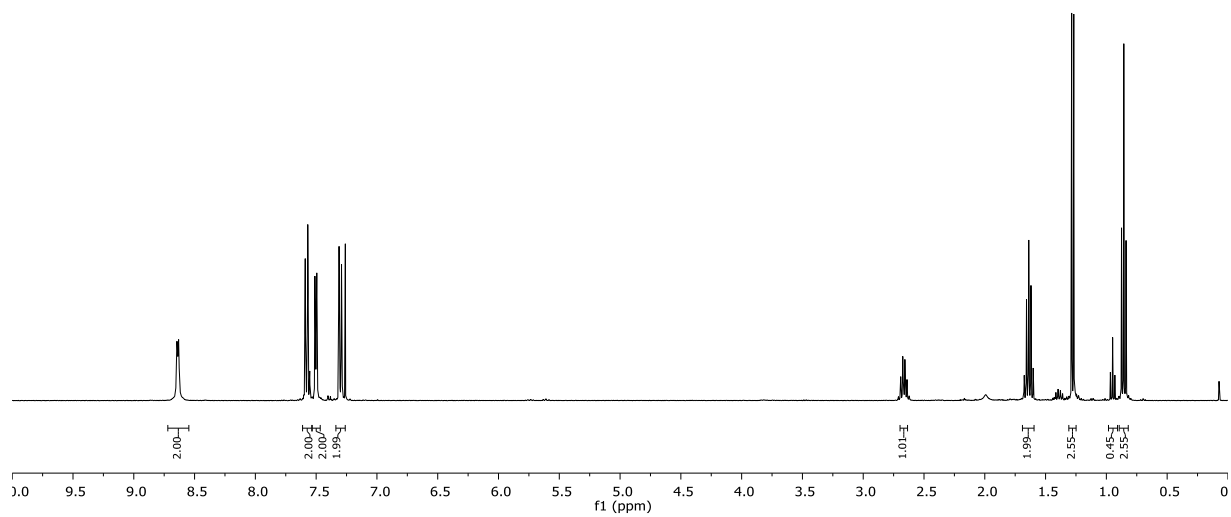
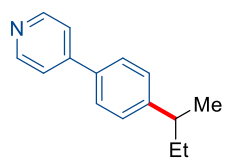


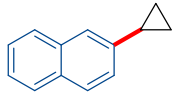
7. Appendix: NMR-Spectra and HPLC Chromatograms



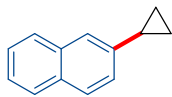
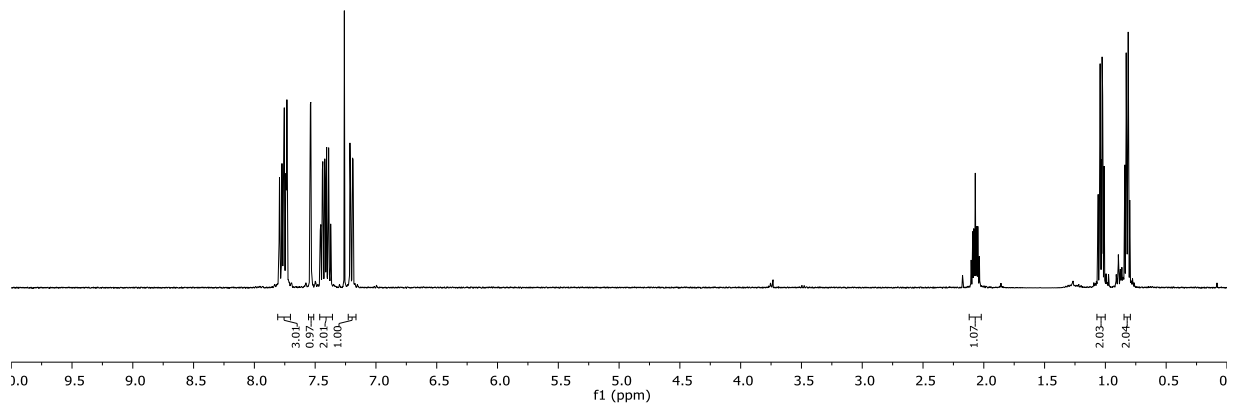


7. Appendix: NMR-Spectra and HPLC Chromatograms

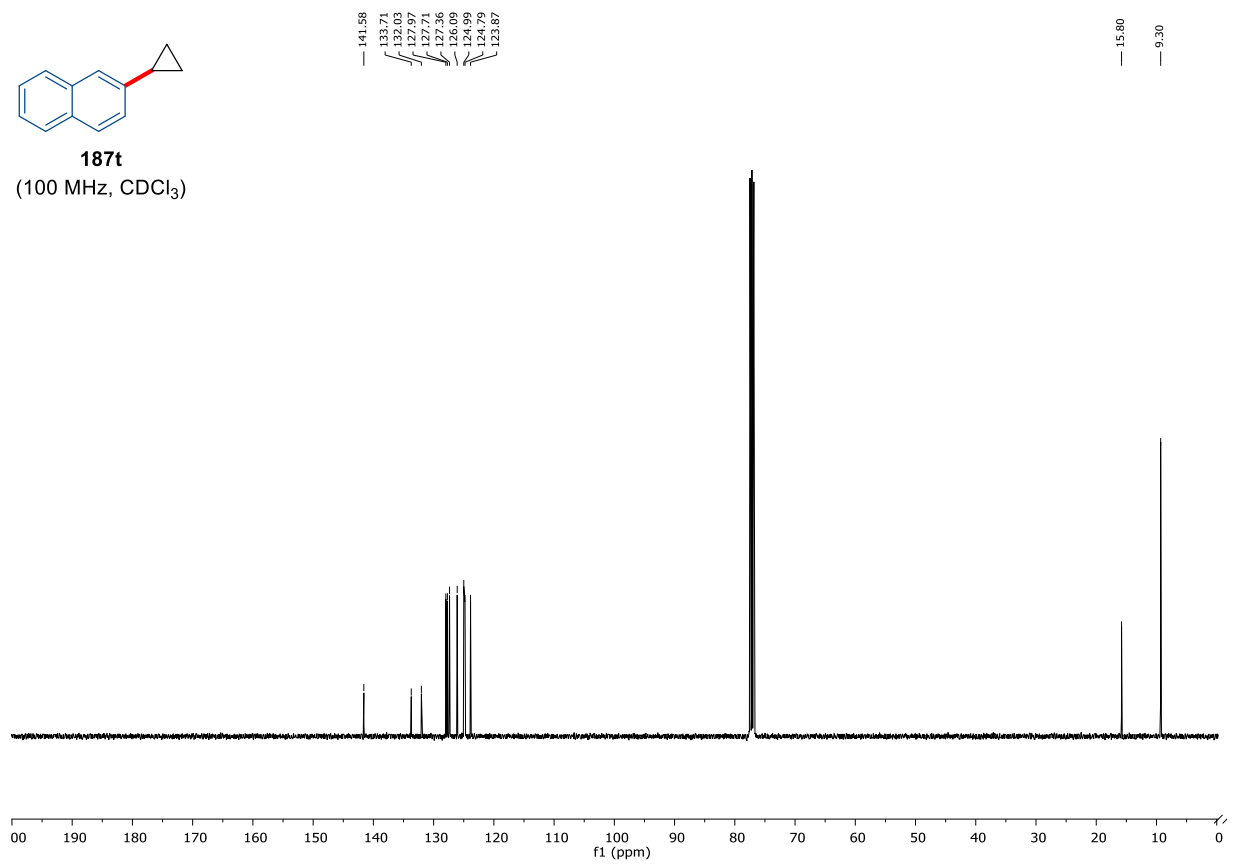




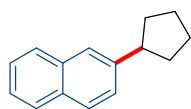
187t
(400 MHz, CDCl₃)



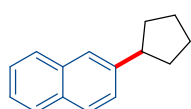
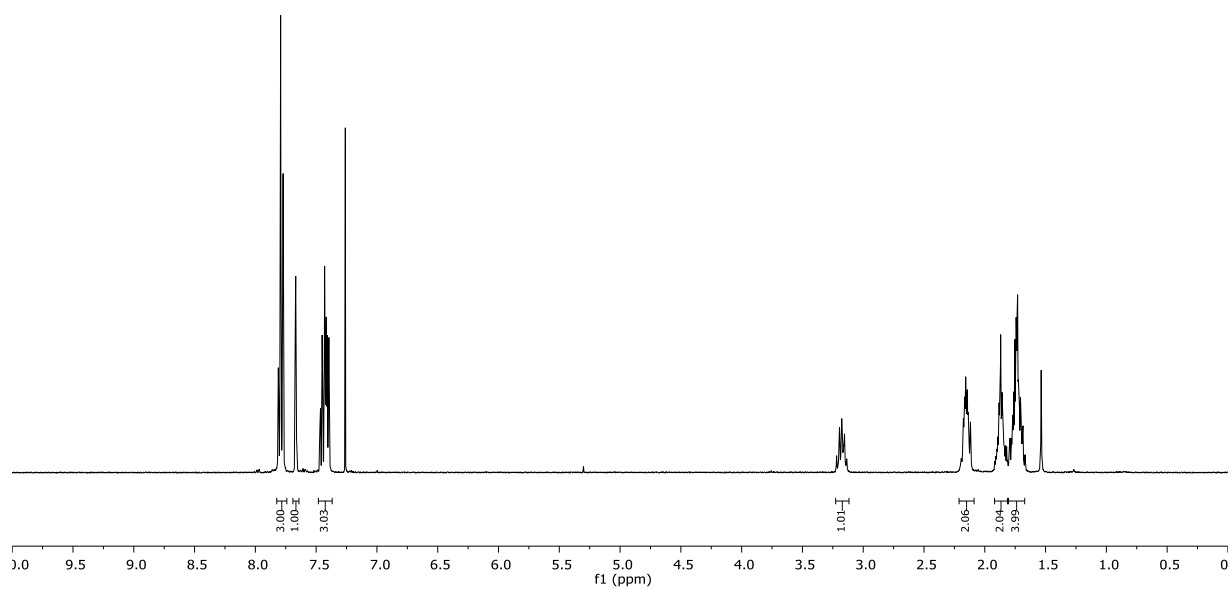
187t
(100 MHz, CDCl₃)



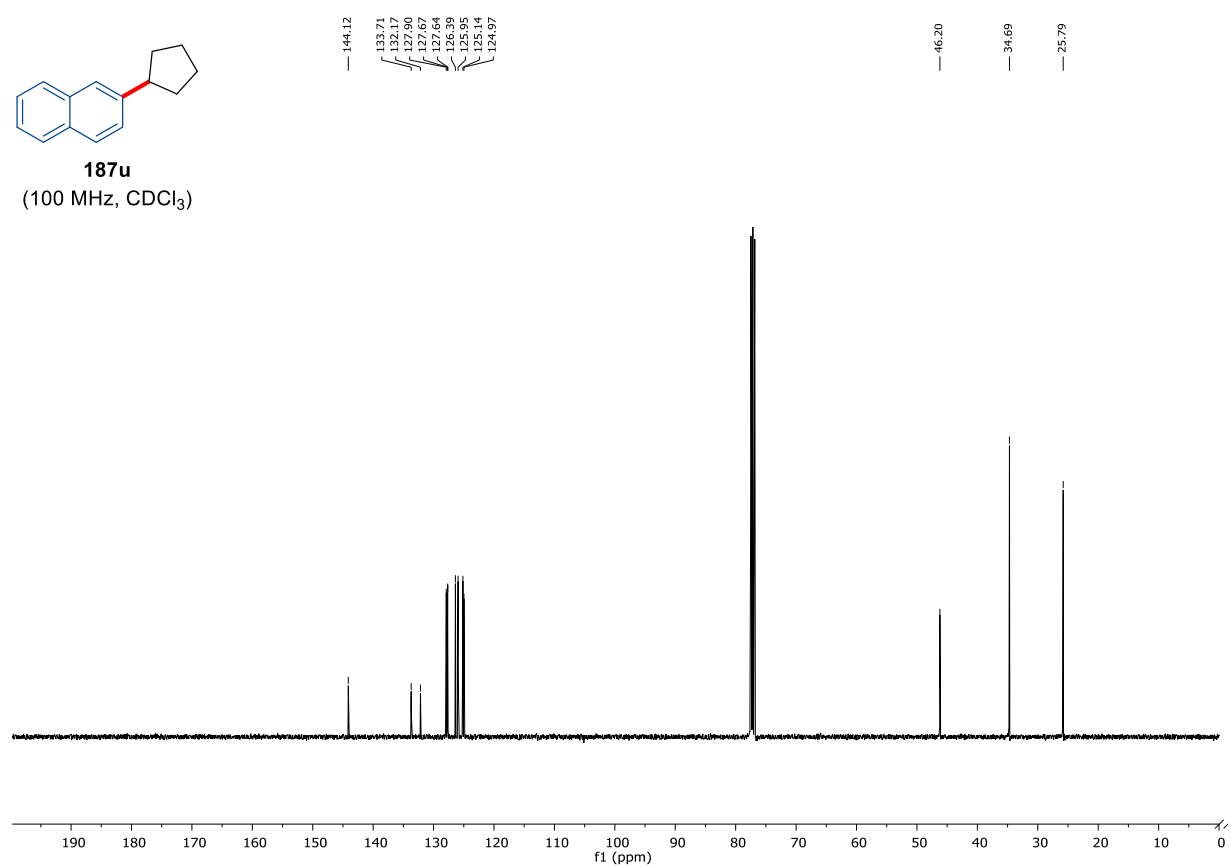
7. Appendix: NMR-Spectra and HPLC Chromatograms

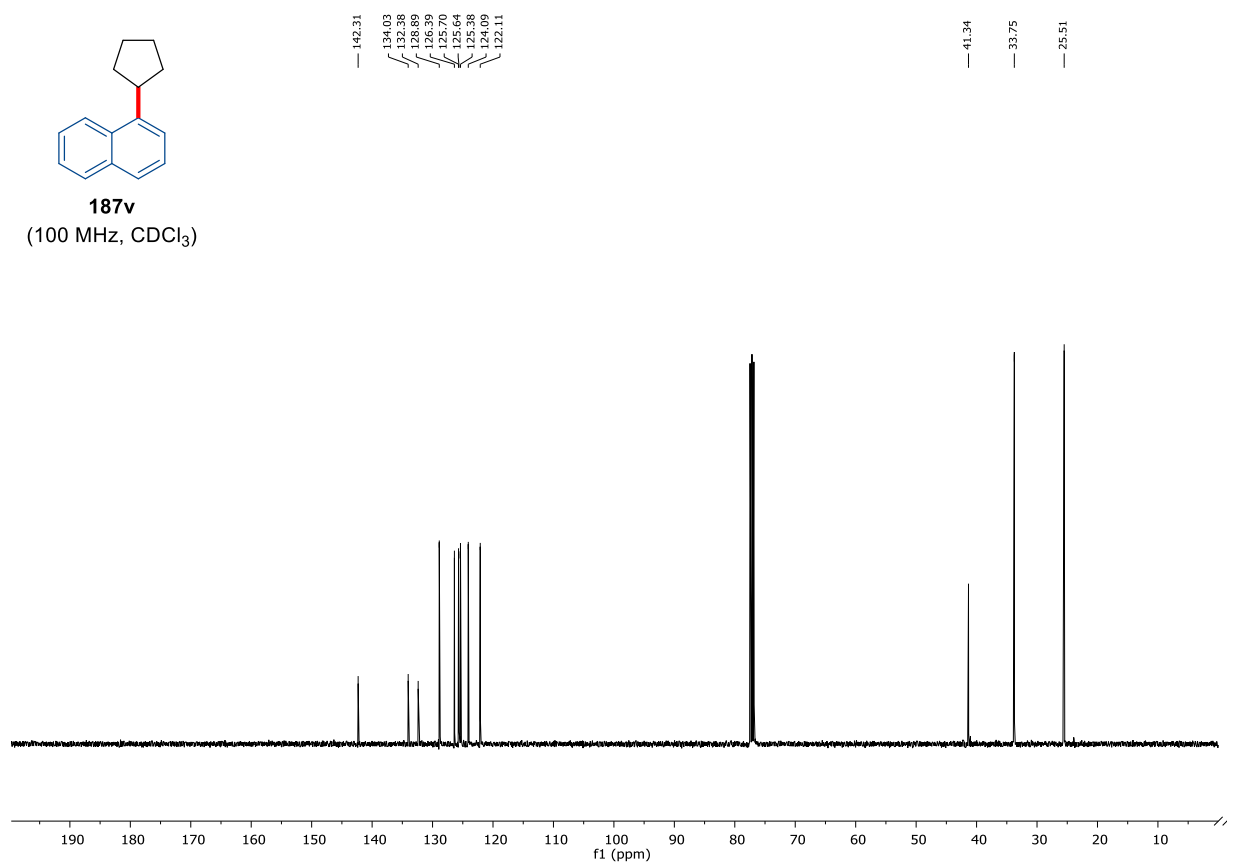
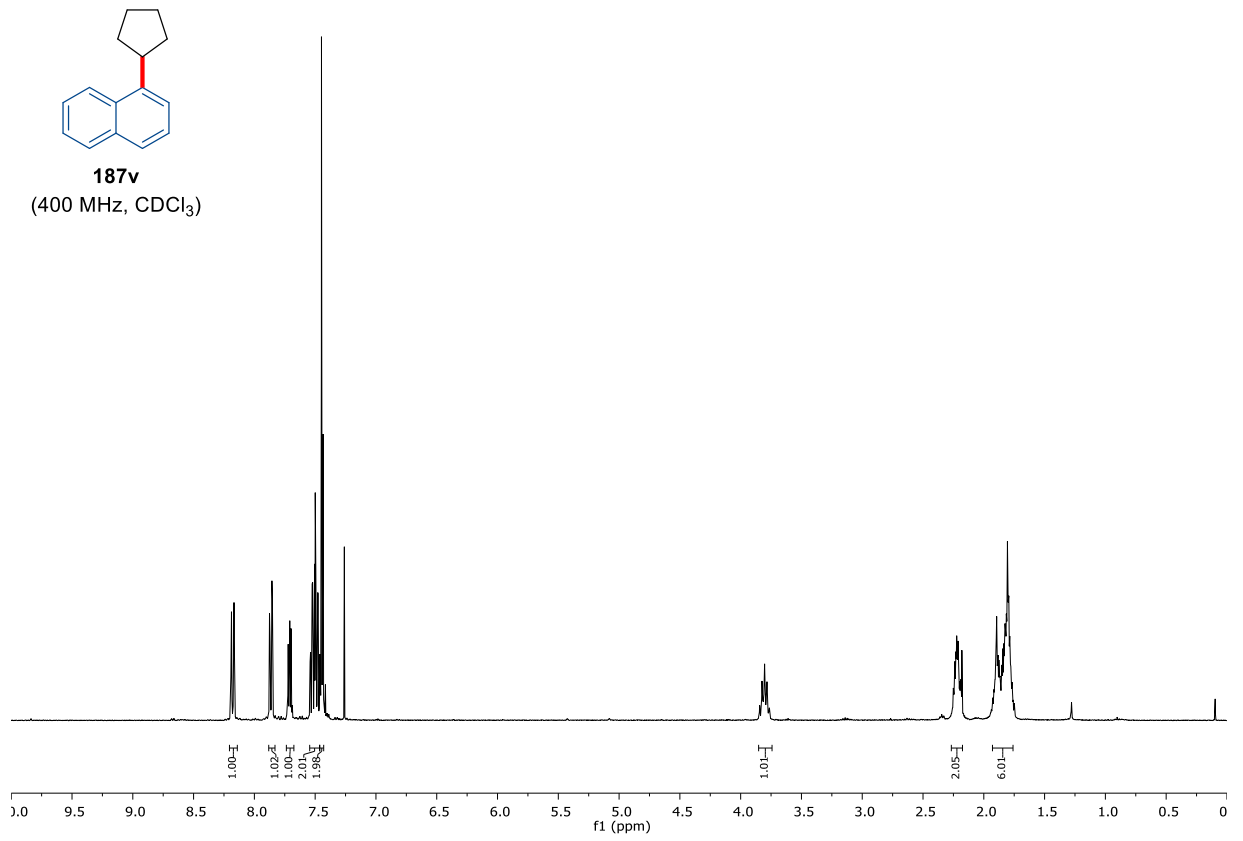


187u
(400 MHz, CDCl₃)

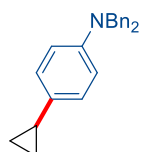


187u
(100 MHz, CDCl₃)

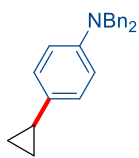
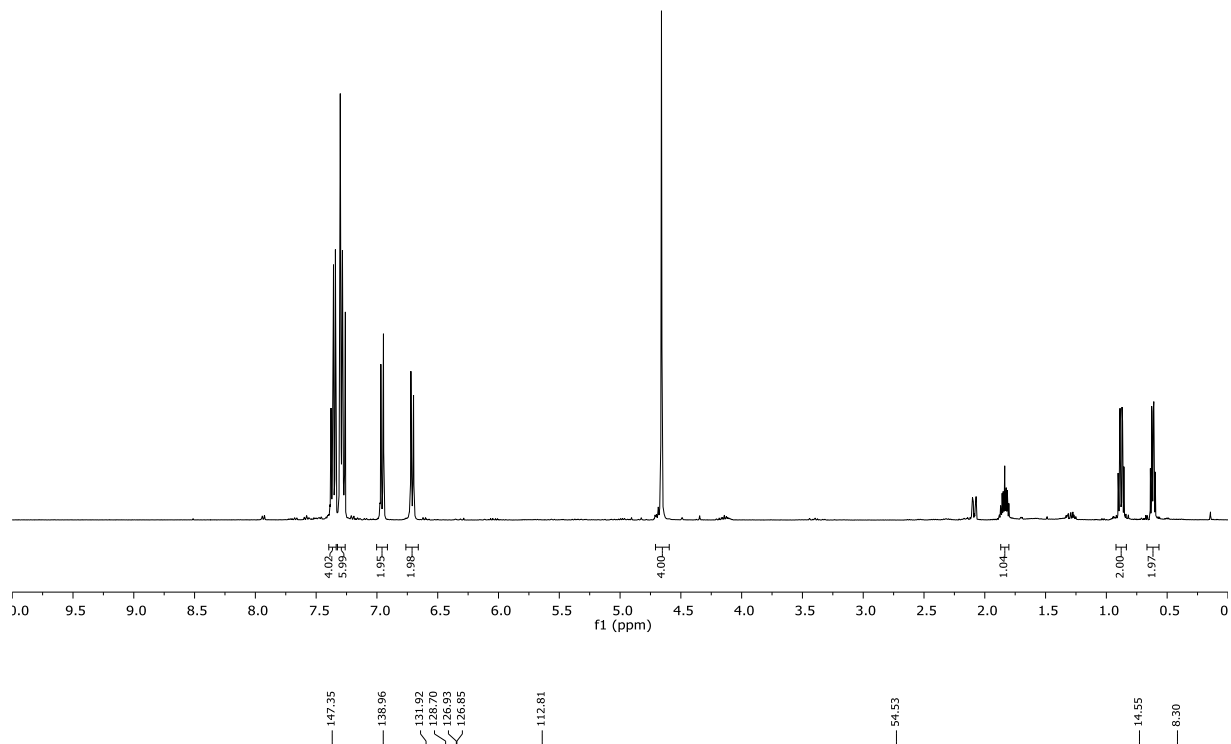




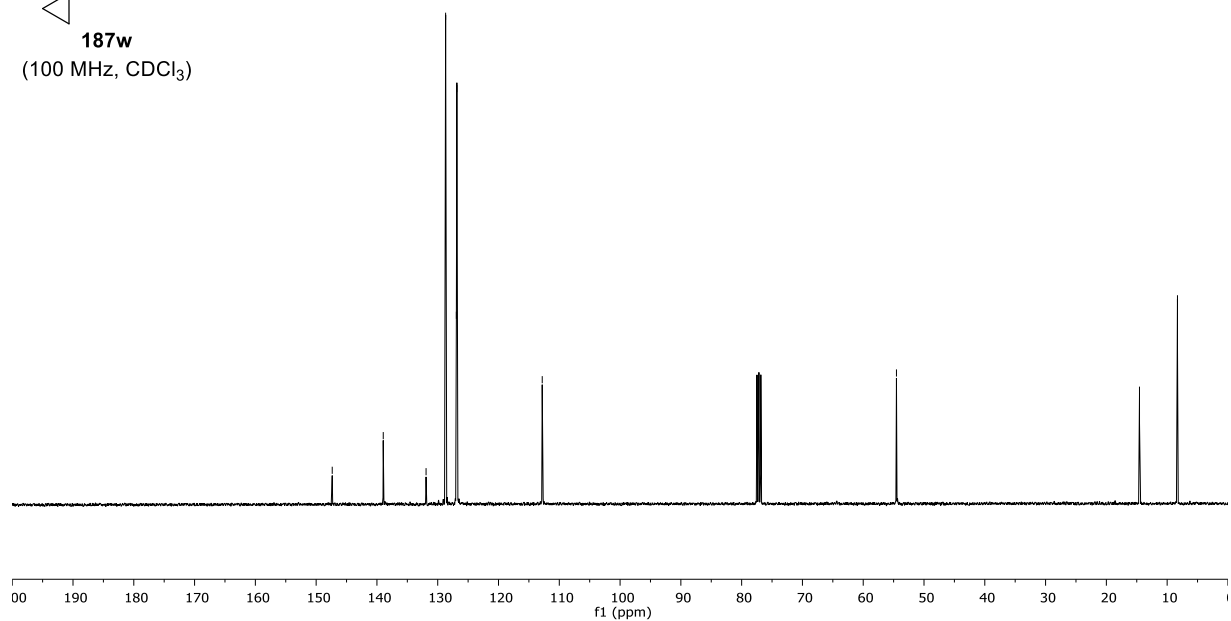
7. Appendix: NMR-Spectra and HPLC Chromatograms

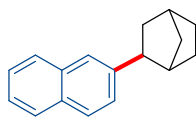


187w
(400 MHz, CDCl₃)

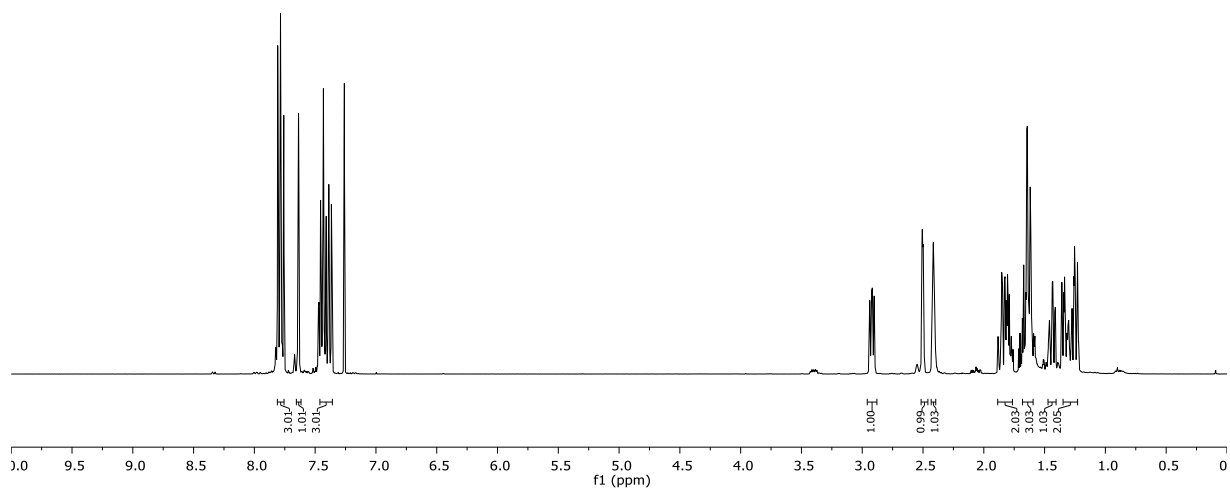


187w
(100 MHz, CDCl₃)



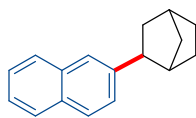


187x
(400 MHz, CDCl₃)

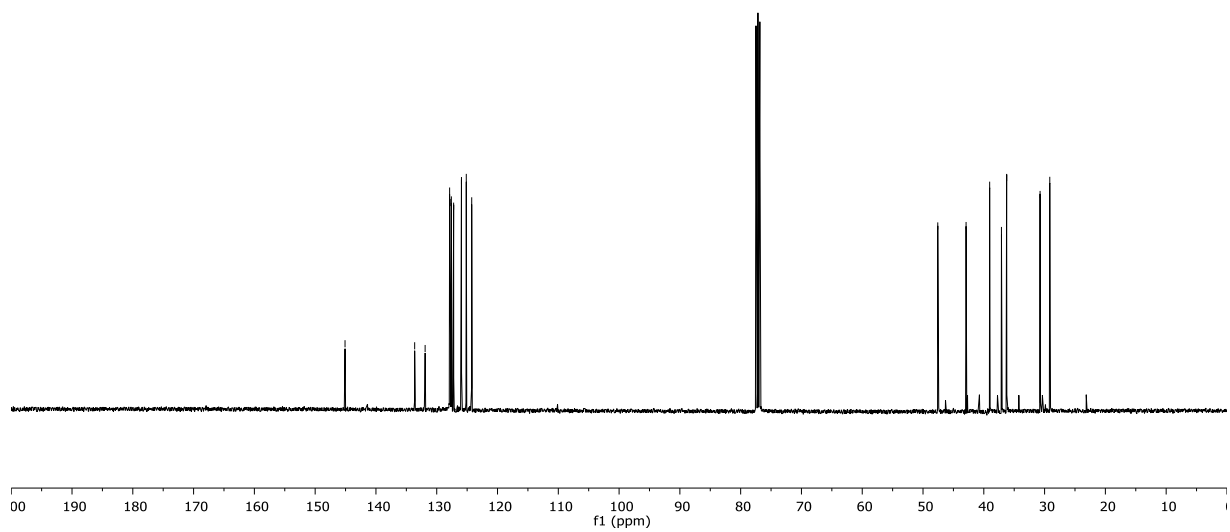


145.08
133.63
131.91
127.88
127.79
127.59
127.02
126.66
125.14
124.25

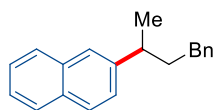
47.57
46.82
46.00
37.10
36.24
30.74
29.15



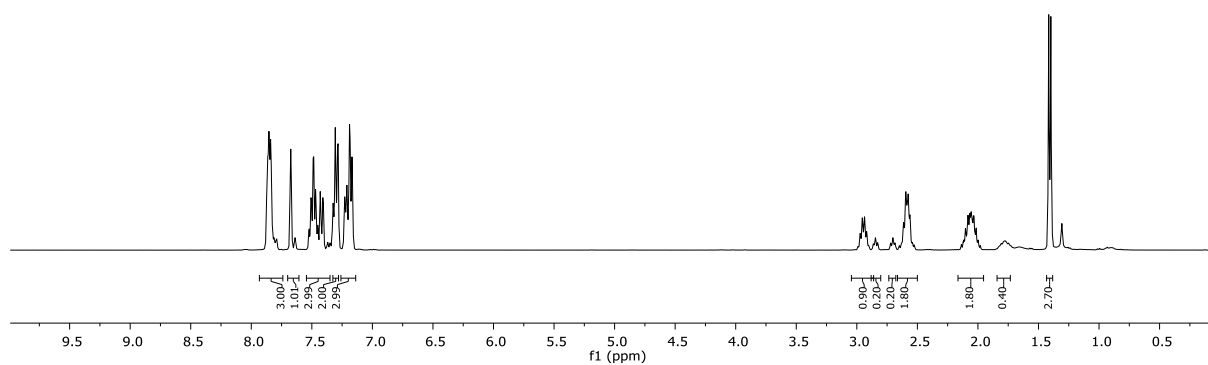
187x
(100 MHz, CDCl₃)



7. Appendix: NMR-Spectra and HPLC Chromatograms

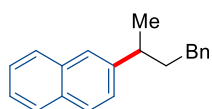


187y
(400 MHz, CDCl₃)

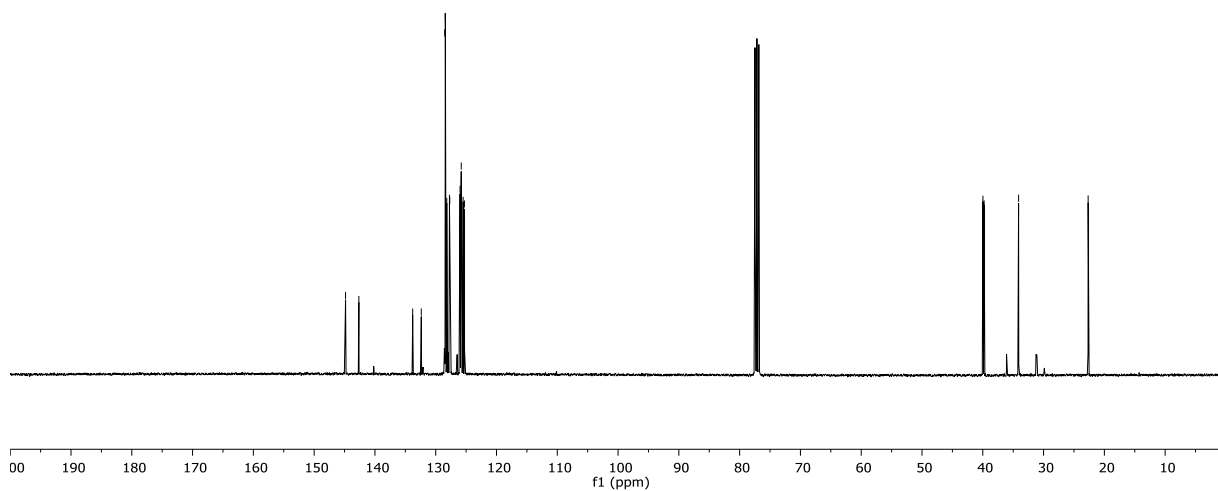


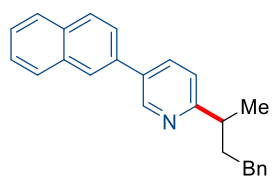
144.63
144.61
133.79
132.37
128.52
128.42
128.18
127.74
127.69
125.88
125.80
125.49
125.28

38.97
38.78
34.11
22.67

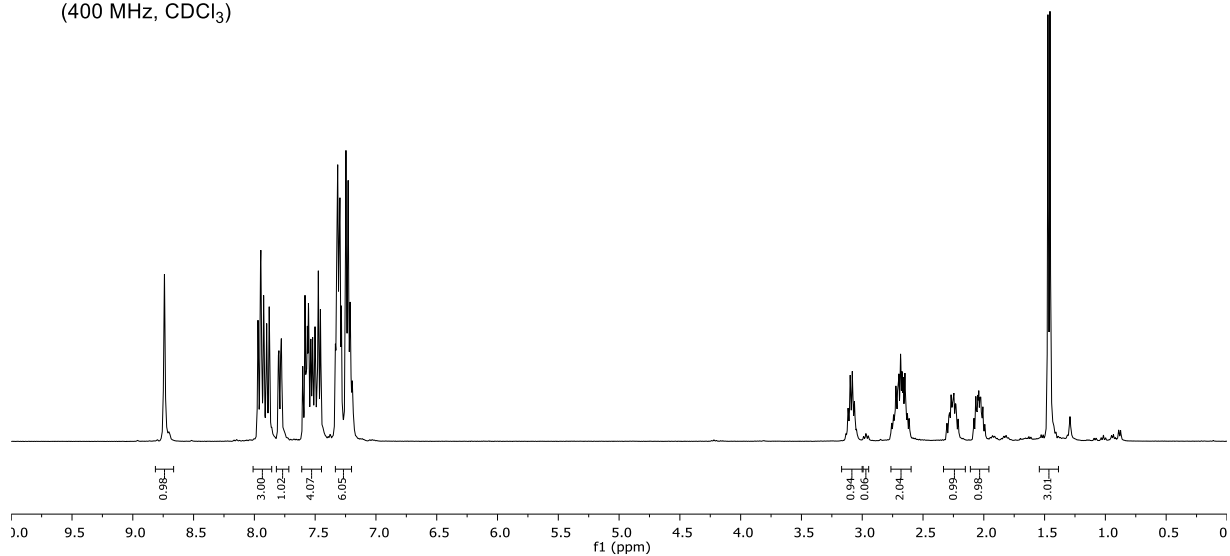


187y
(100 MHz, CDCl₃)

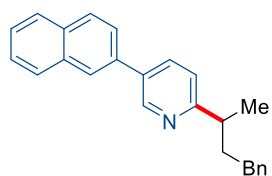




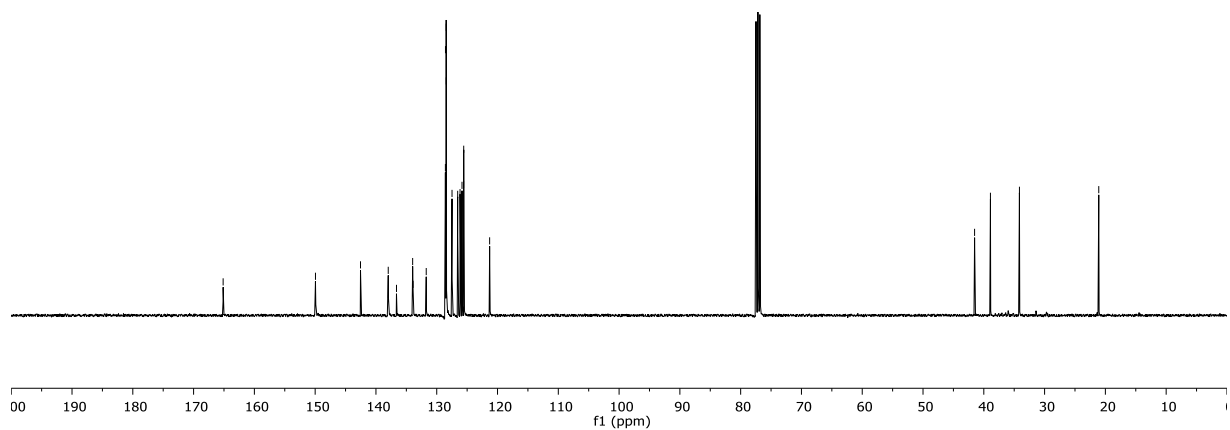
187z
(400 MHz, CDCl₃)



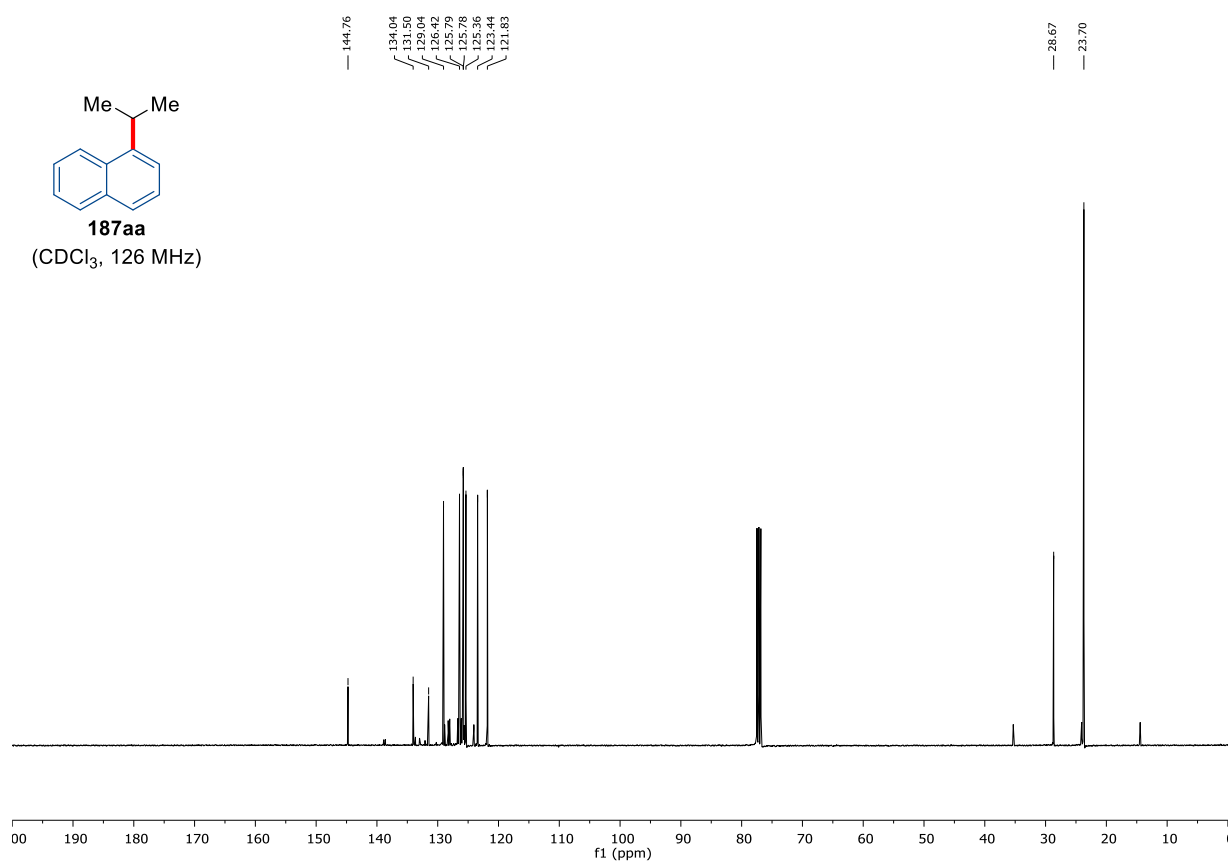
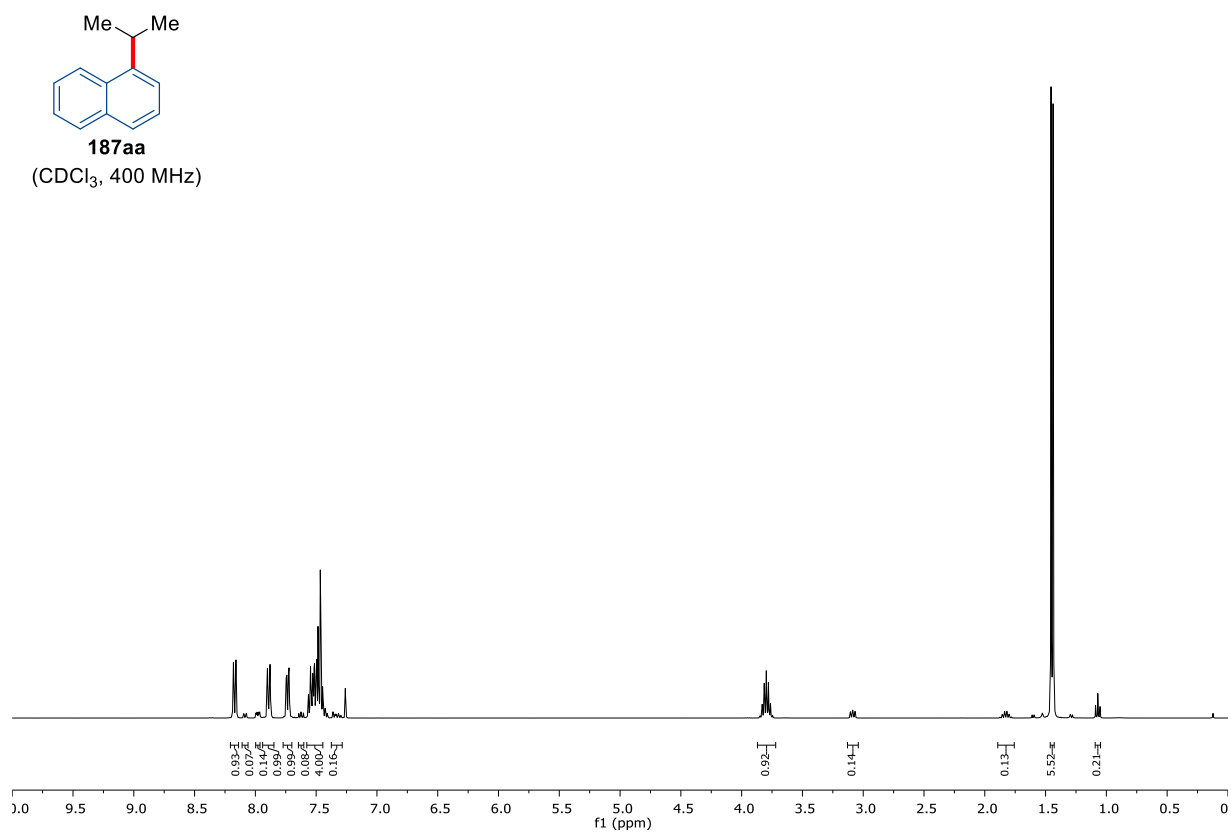
165.14
149.95
147.86
137.98
136.62
133.96
133.89
131.73
128.58
128.56
128.44
127.49
126.55
126.16
125.84
125.58
125.56
121.30
41.52
38.91
34.14
21.09

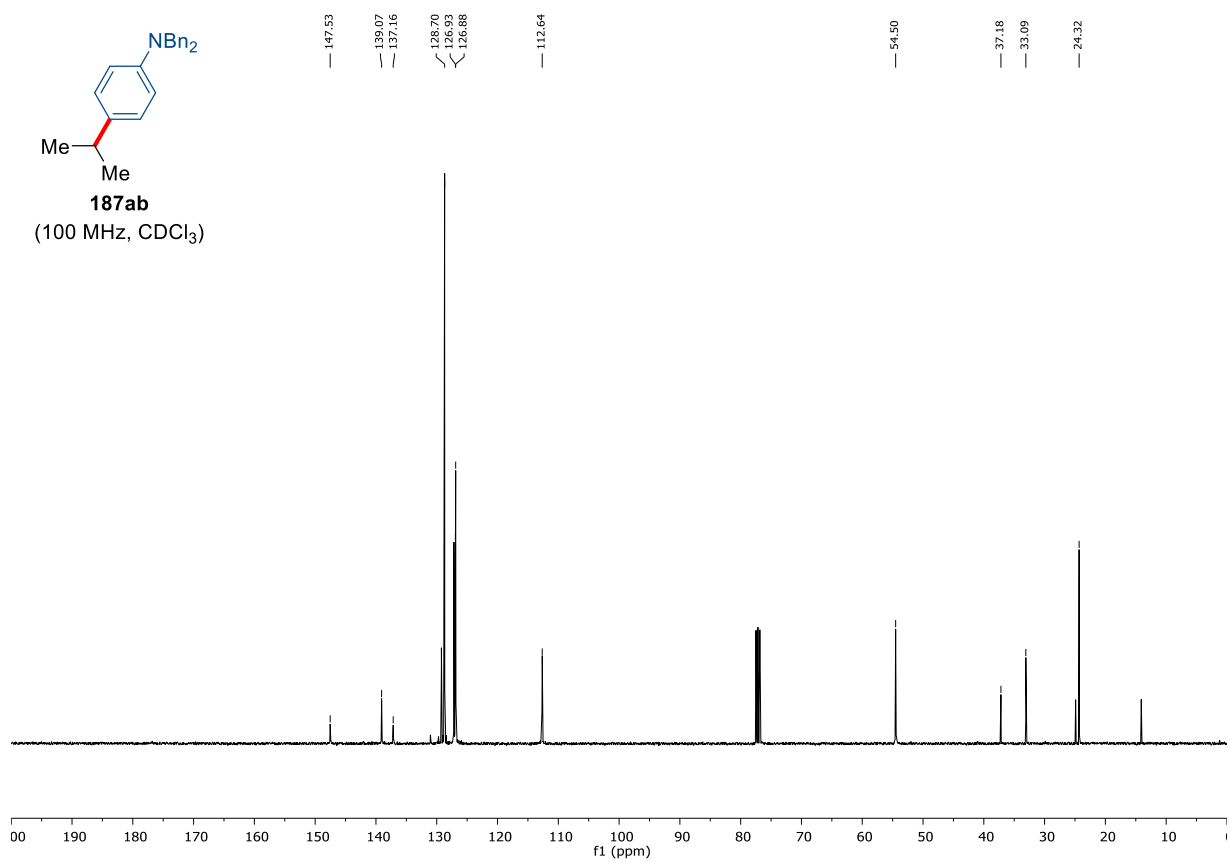
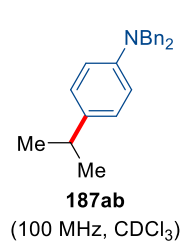
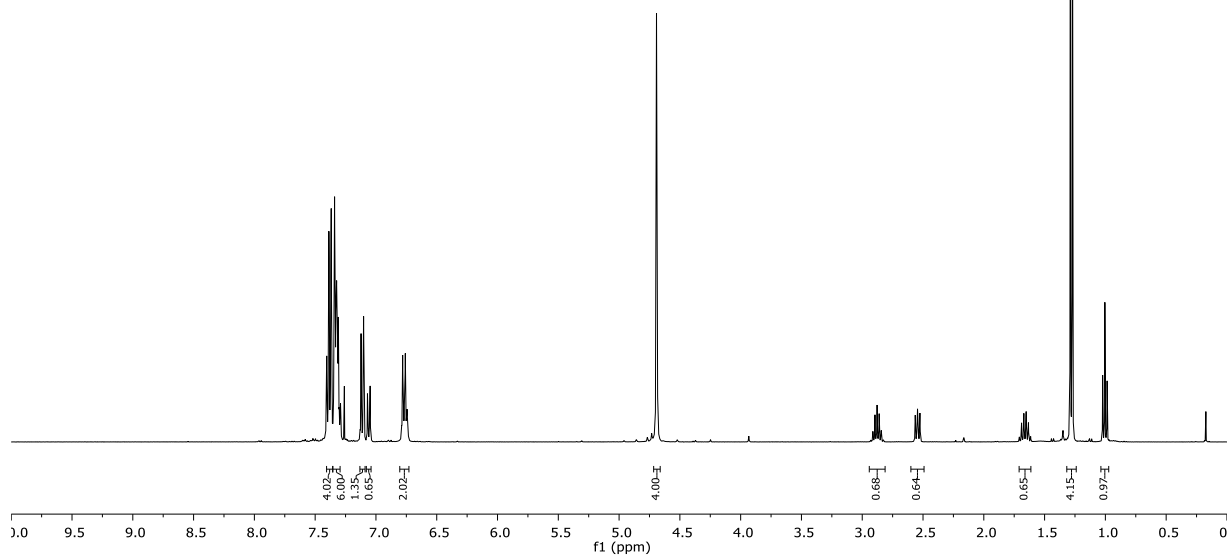
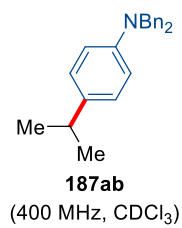


187z
(100 MHz, CDCl₃)

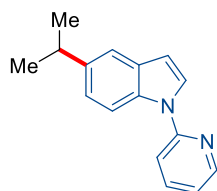


7. Appendix: NMR-Spectra and HPLC Chromatograms

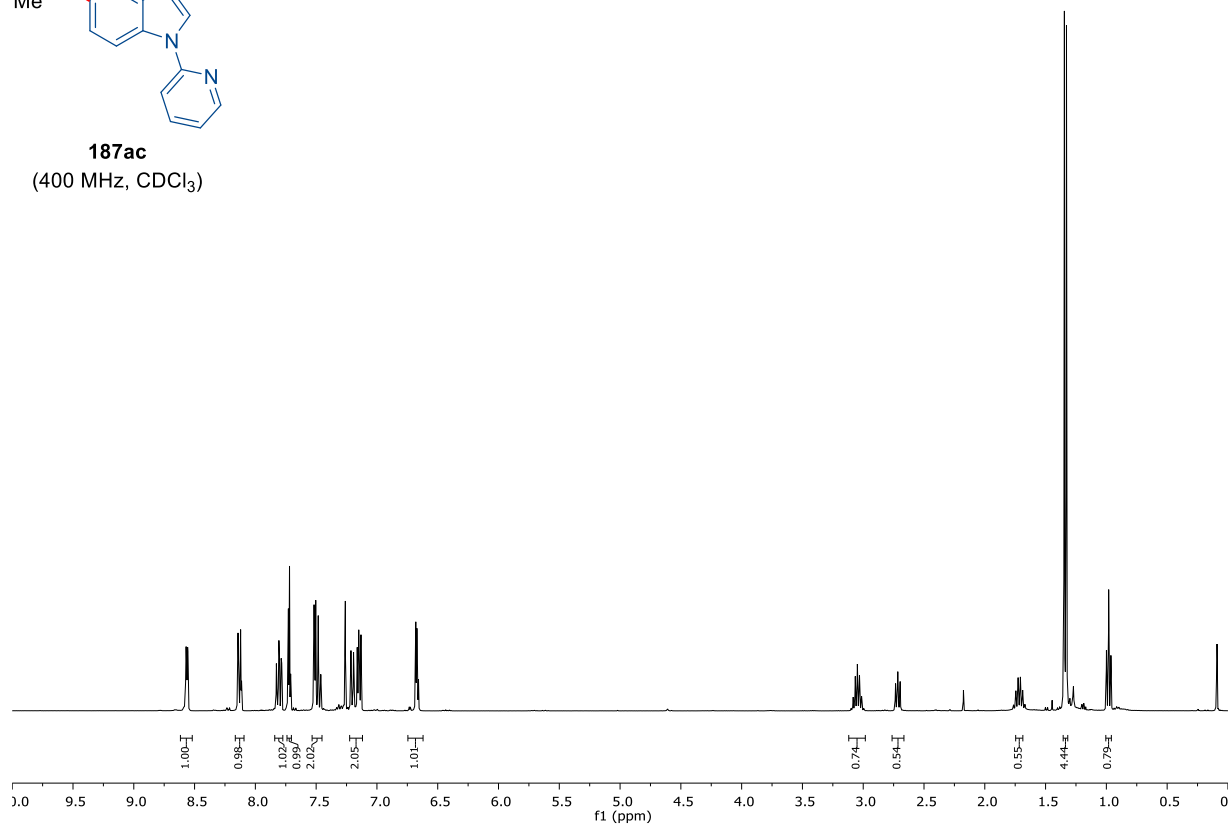




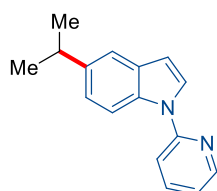
7. Appendix: NMR-Spectra and HPLC Chromatograms



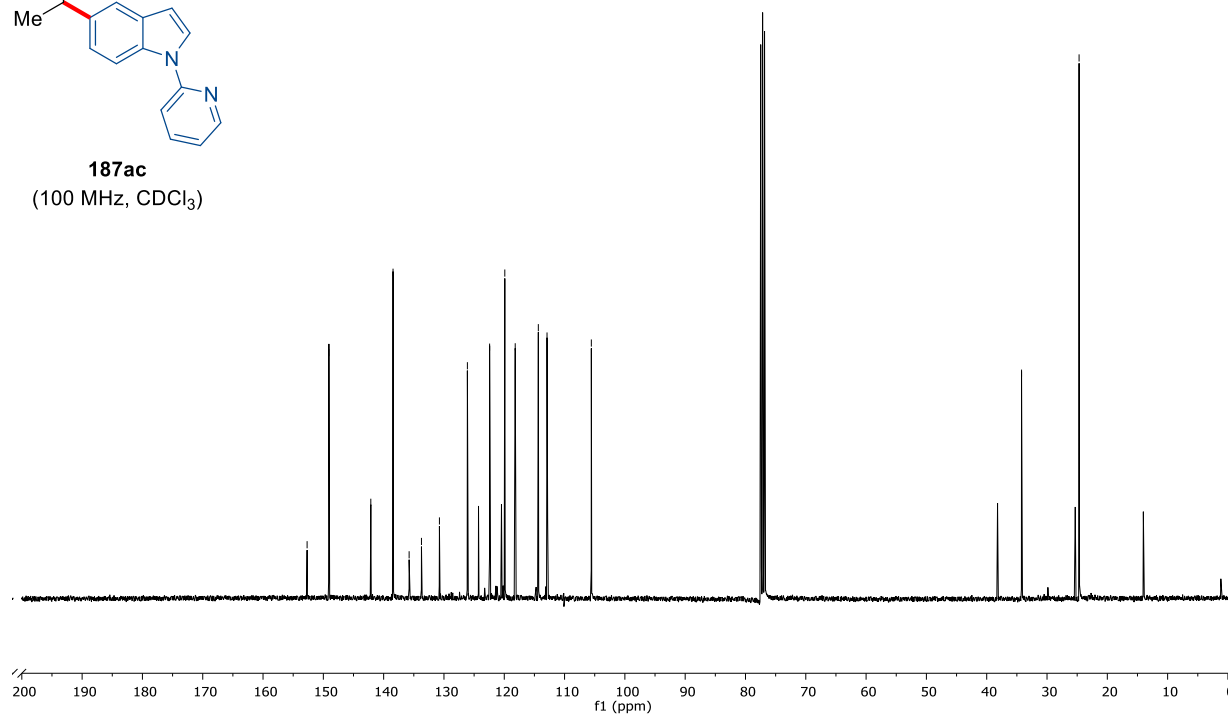
187ac
(400 MHz, CDCl₃)

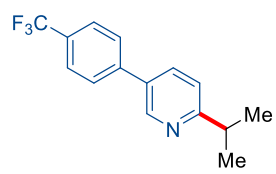


152.69
149.09
142.13
138.44
135.78
133.73
130.75
126.11
122.43
119.91
118.18
114.35
112.91
34.22
24.68

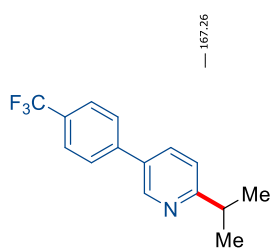
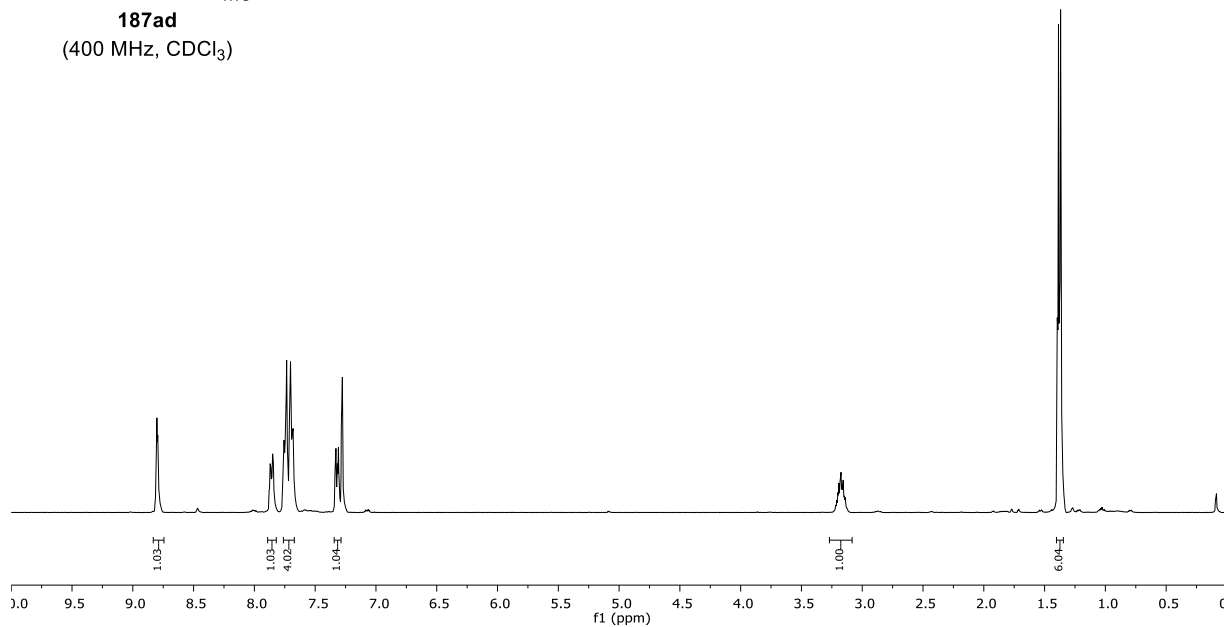


187ac
(100 MHz, CDCl₃)

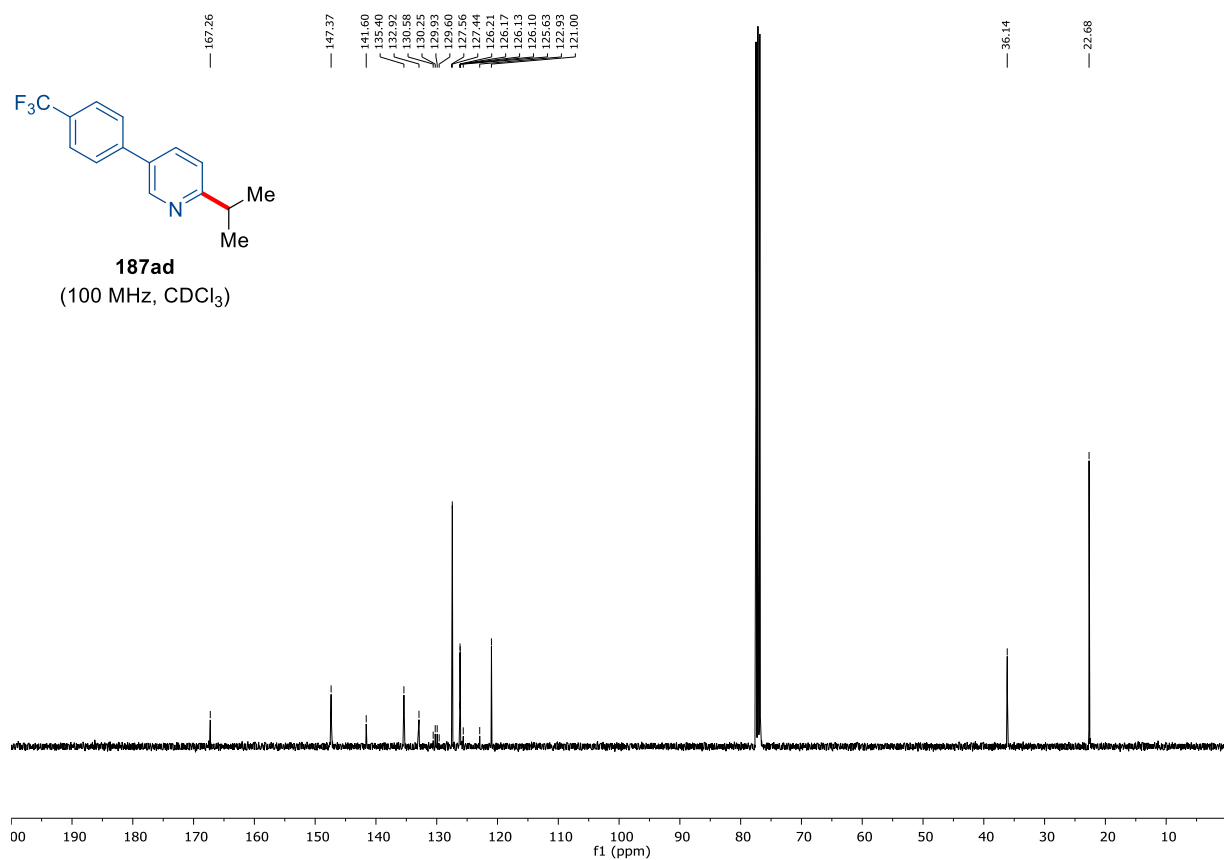




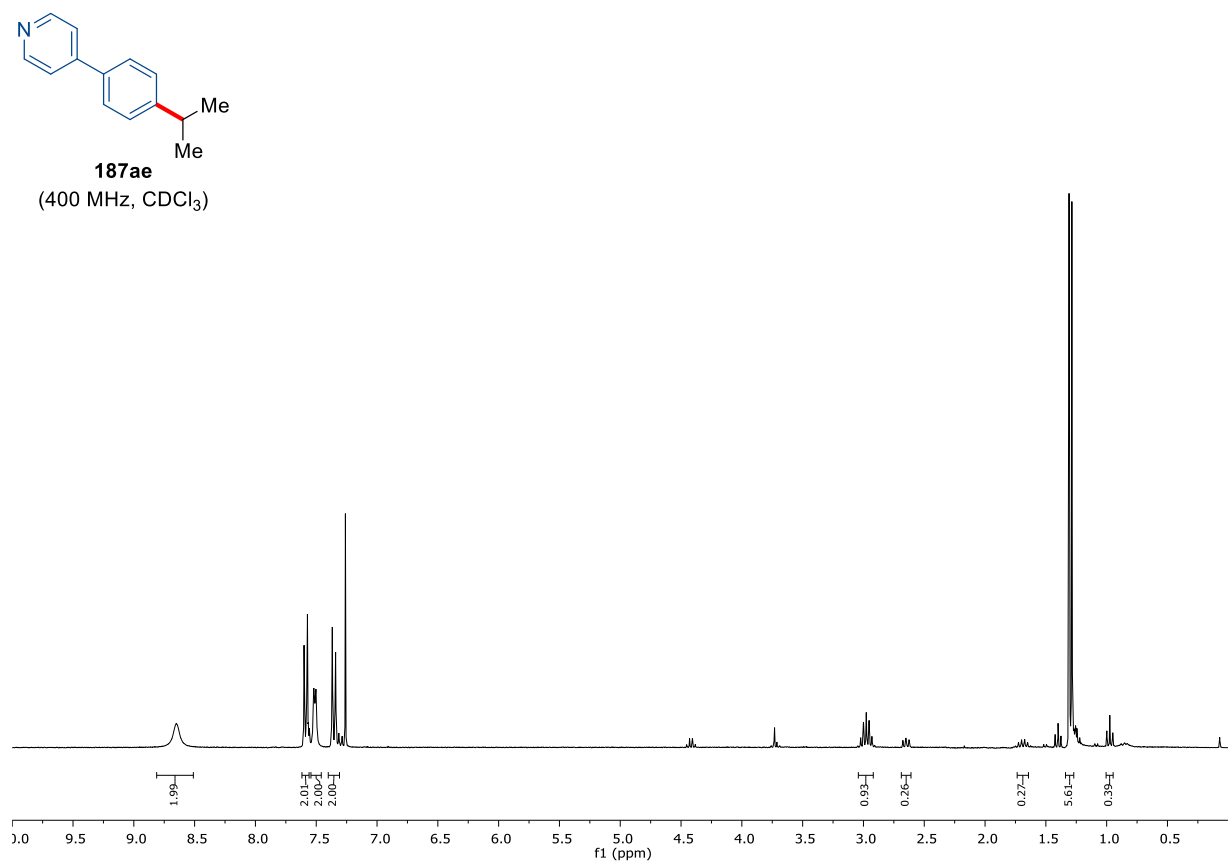
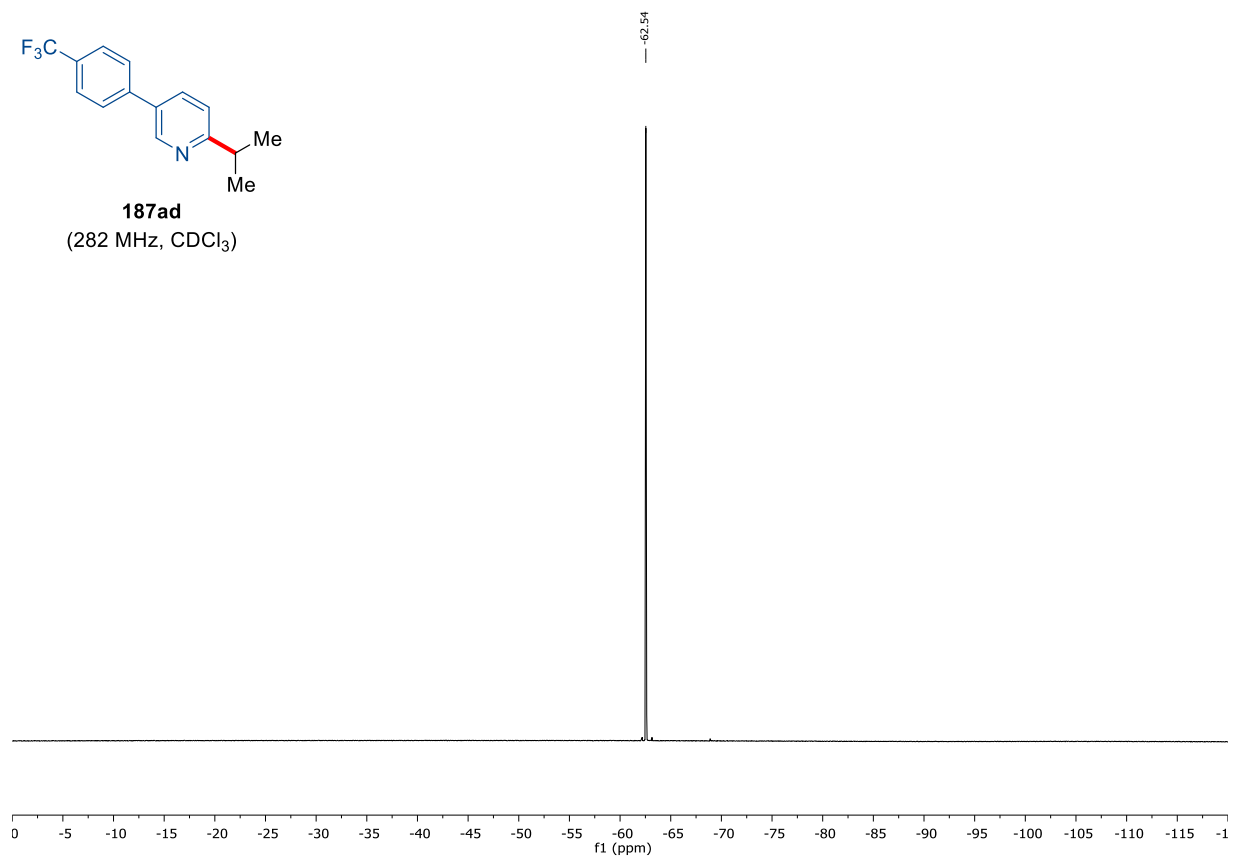
187ad
(400 MHz, CDCl₃)

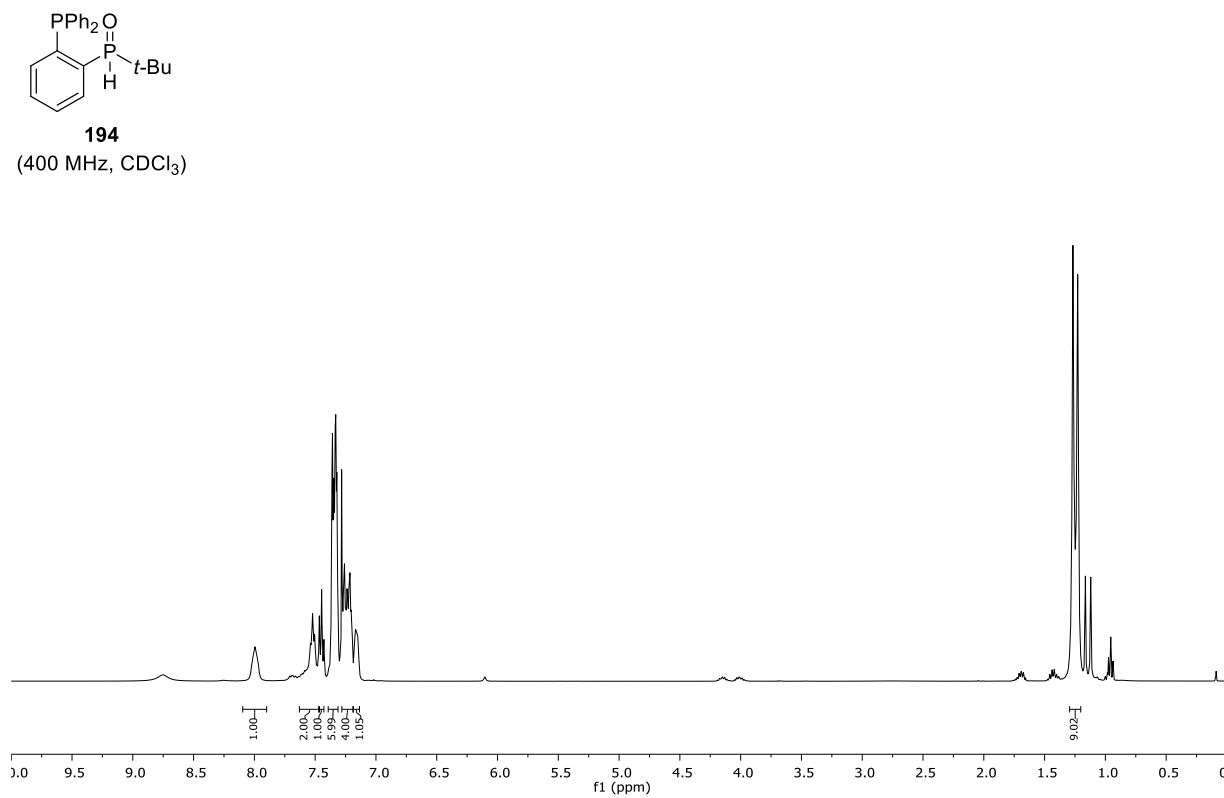
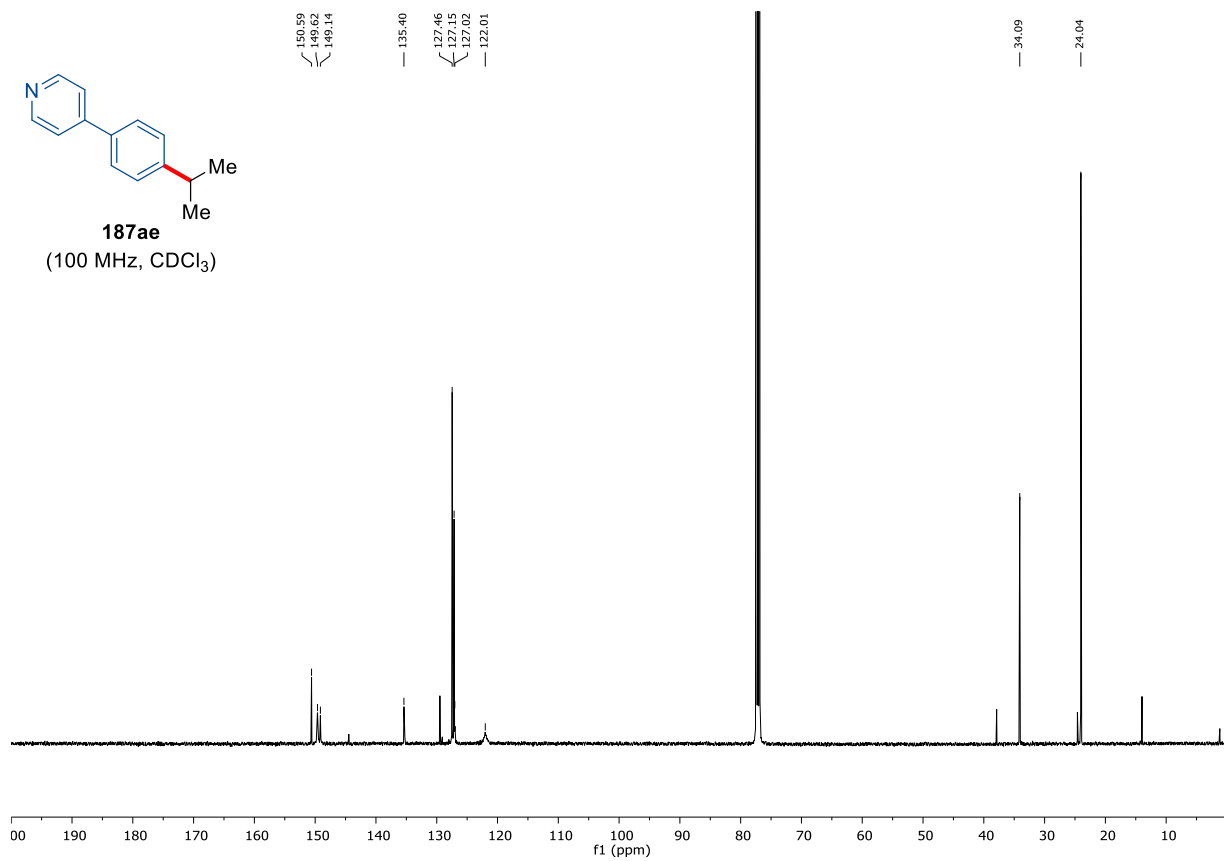


187ad
(100 MHz, CDCl₃)

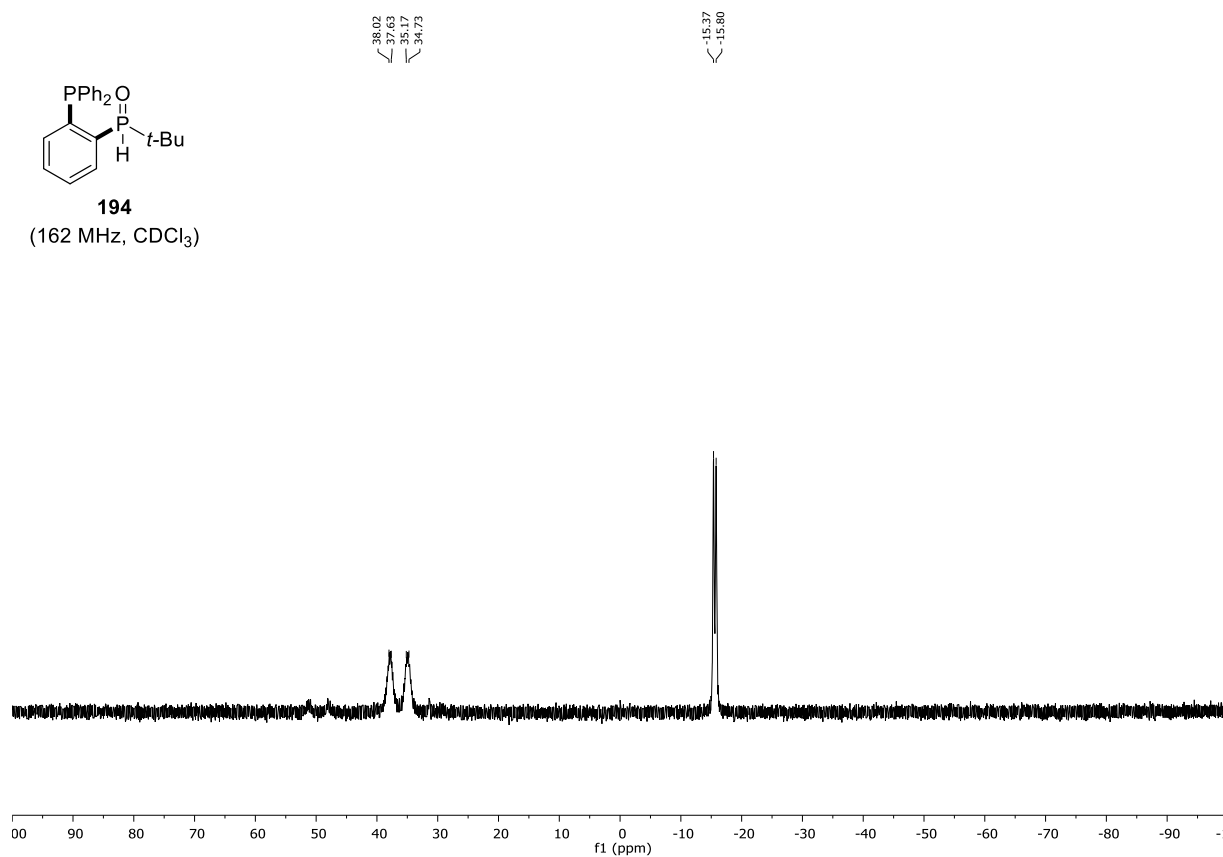
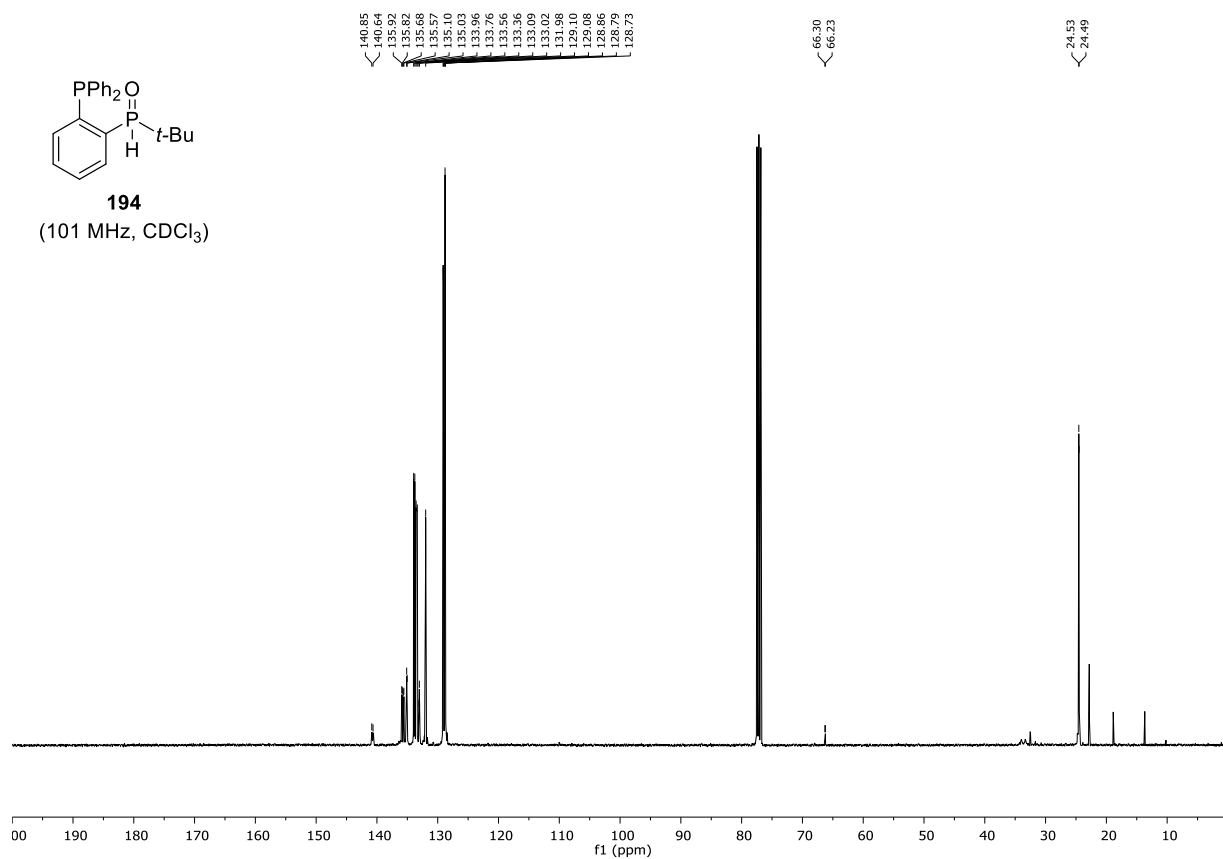


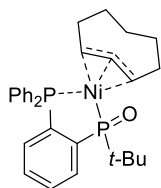
7. Appendix: NMR-Spectra and HPLC Chromatograms





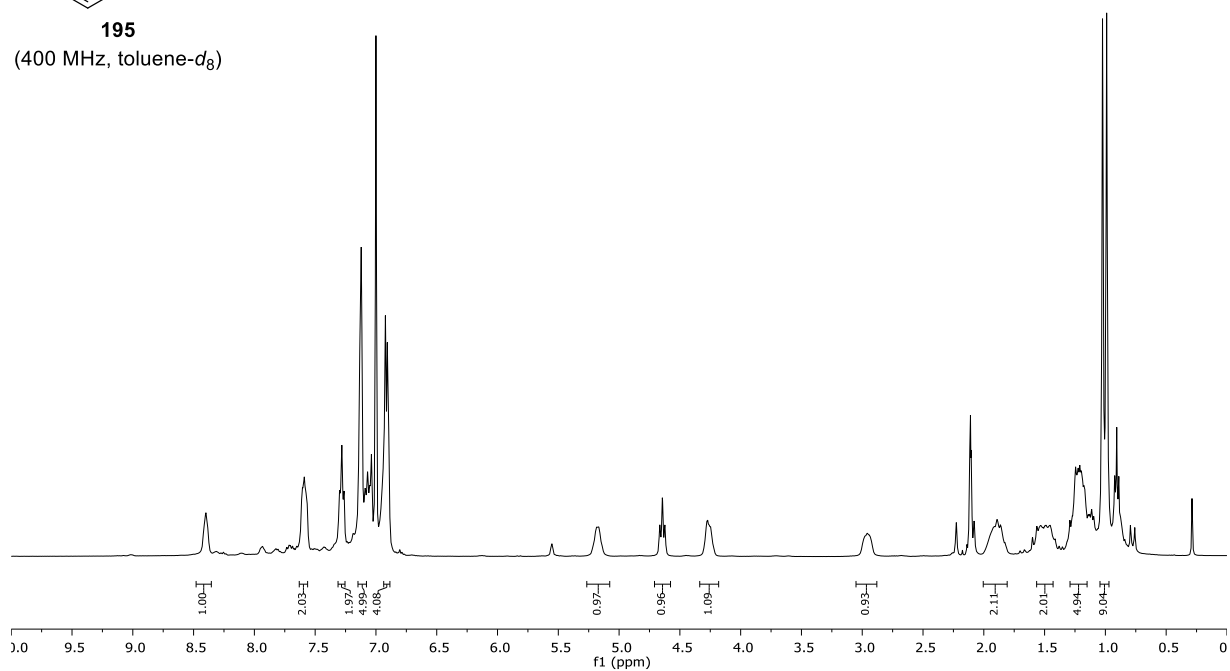
7. Appendix: NMR-Spectra and HPLC Chromatograms



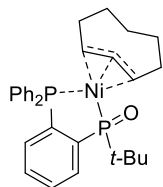


195

(400 MHz, toluene- d_6)

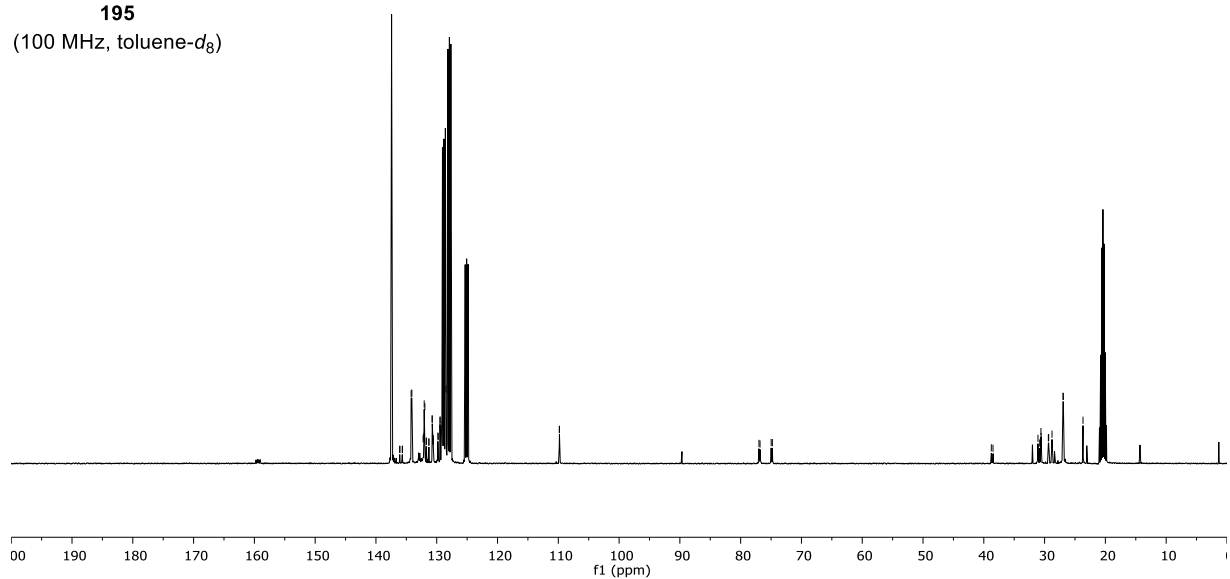


136.09, 136.07, 135.66, 135.64, 134.22, 134.09, 132.24, 132.12, 132.06, 131.95, 131.71, 131.71, 131.29, 131.29, 130.76, 130.73, 130.63, 130.59, 130.59, 129.86, 129.86, 129.75, 129.46, 129.44, 129.00, 129.00, 128.47, 109.84, 109.81, 76.99, 76.81, 74.78, 74.78, 38.76, 38.49, 37.09, 30.60, 30.60, 30.57, 29.38, 29.33, 28.81, 28.78, 28.74, 26.92, 23.68

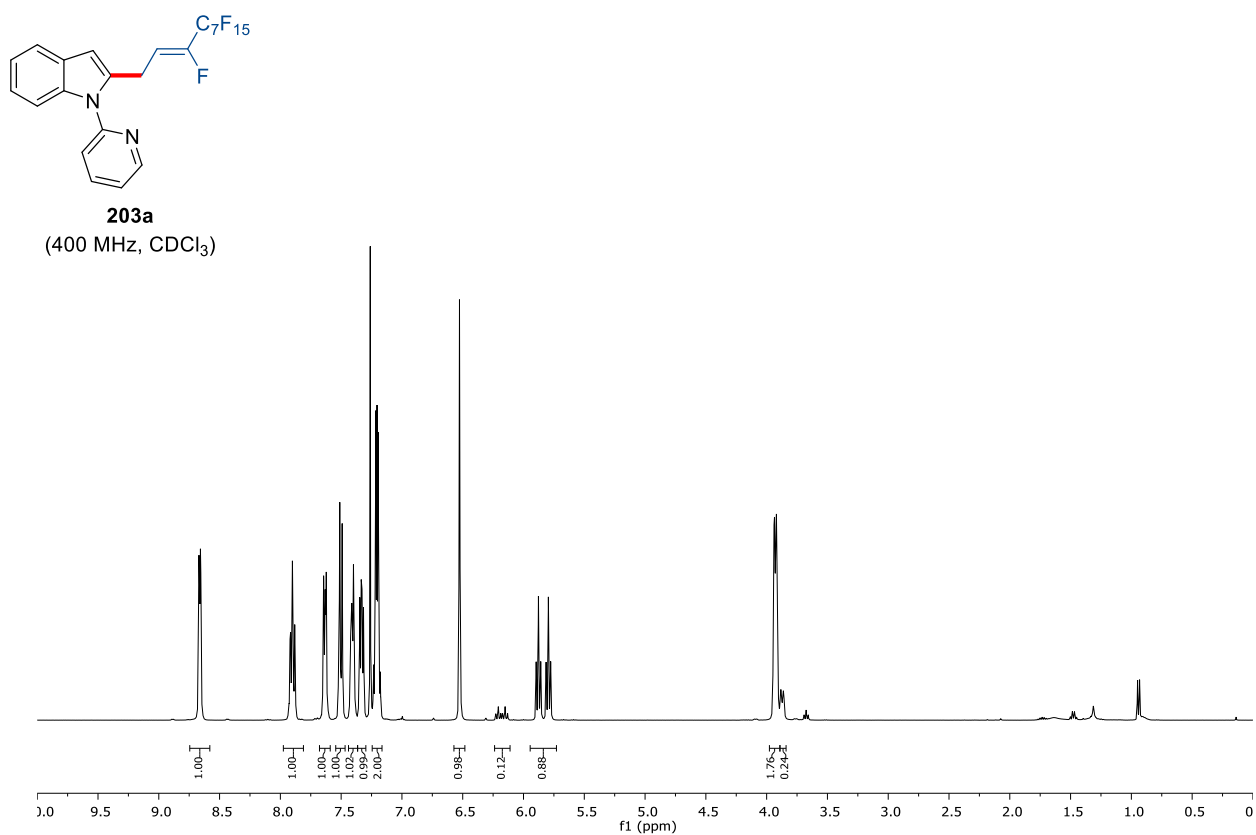
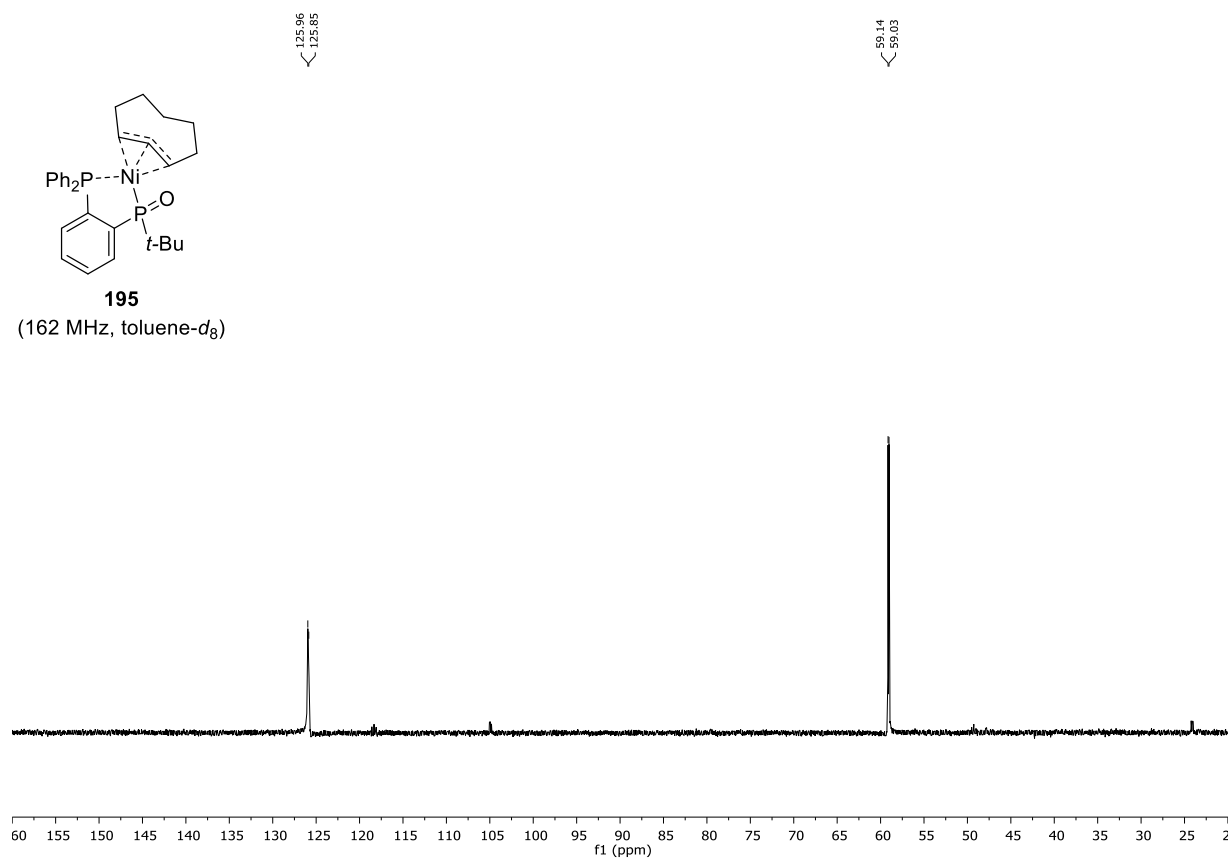


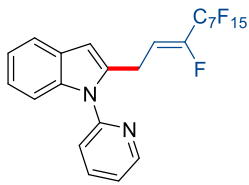
195

(100 MHz, toluene- d_6)

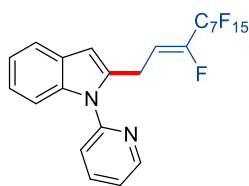
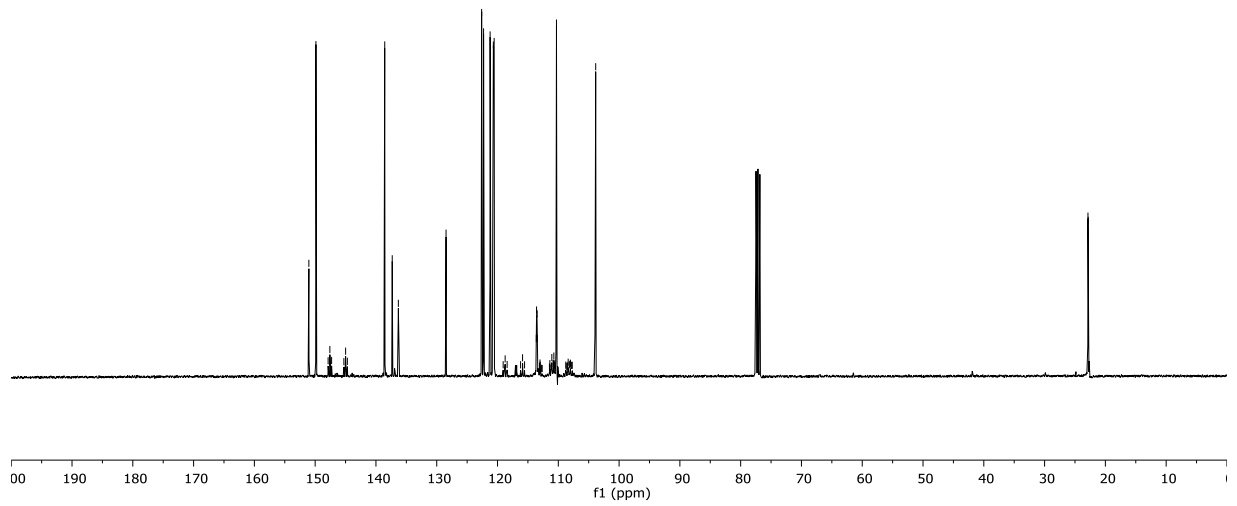


7. Appendix: NMR-Spectra and HPLC Chromatograms

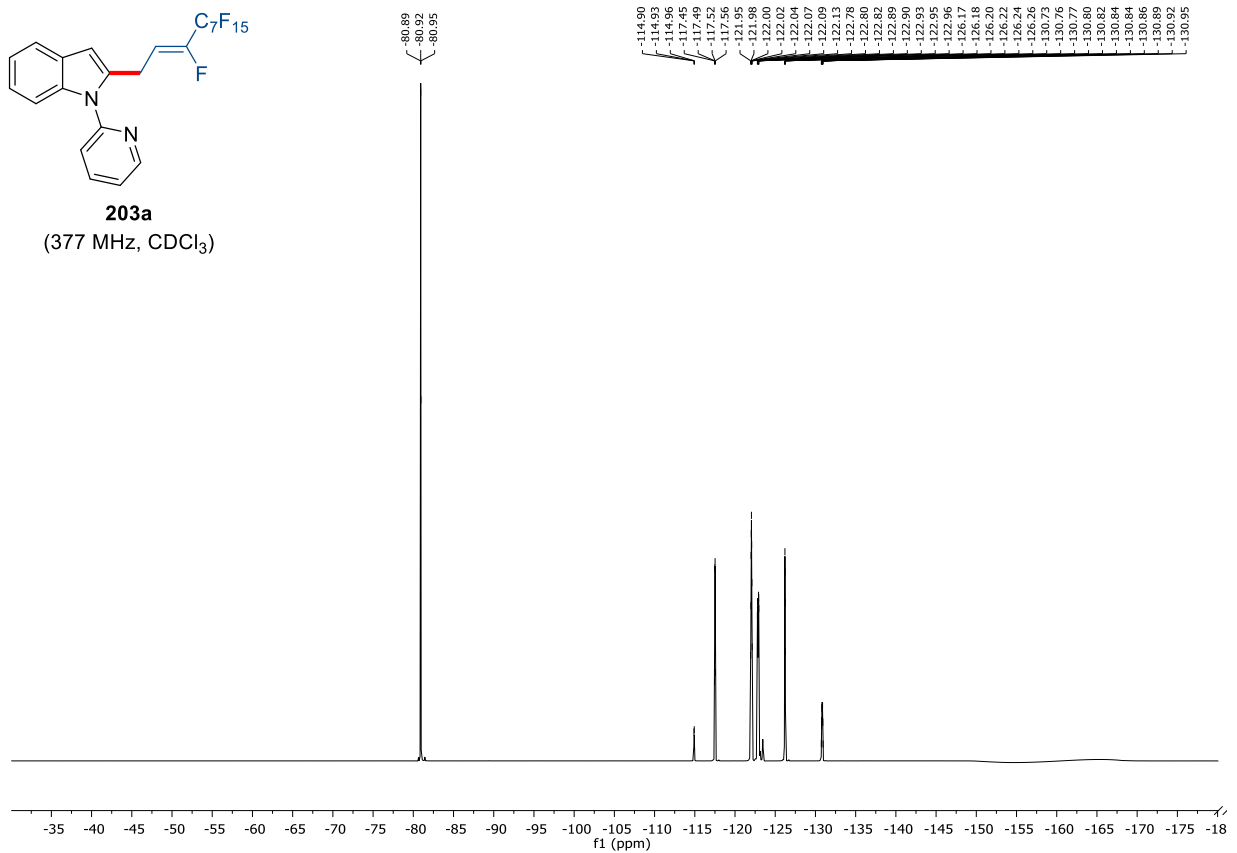




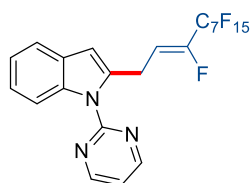
203a
(100 MHz, CDCl₃)



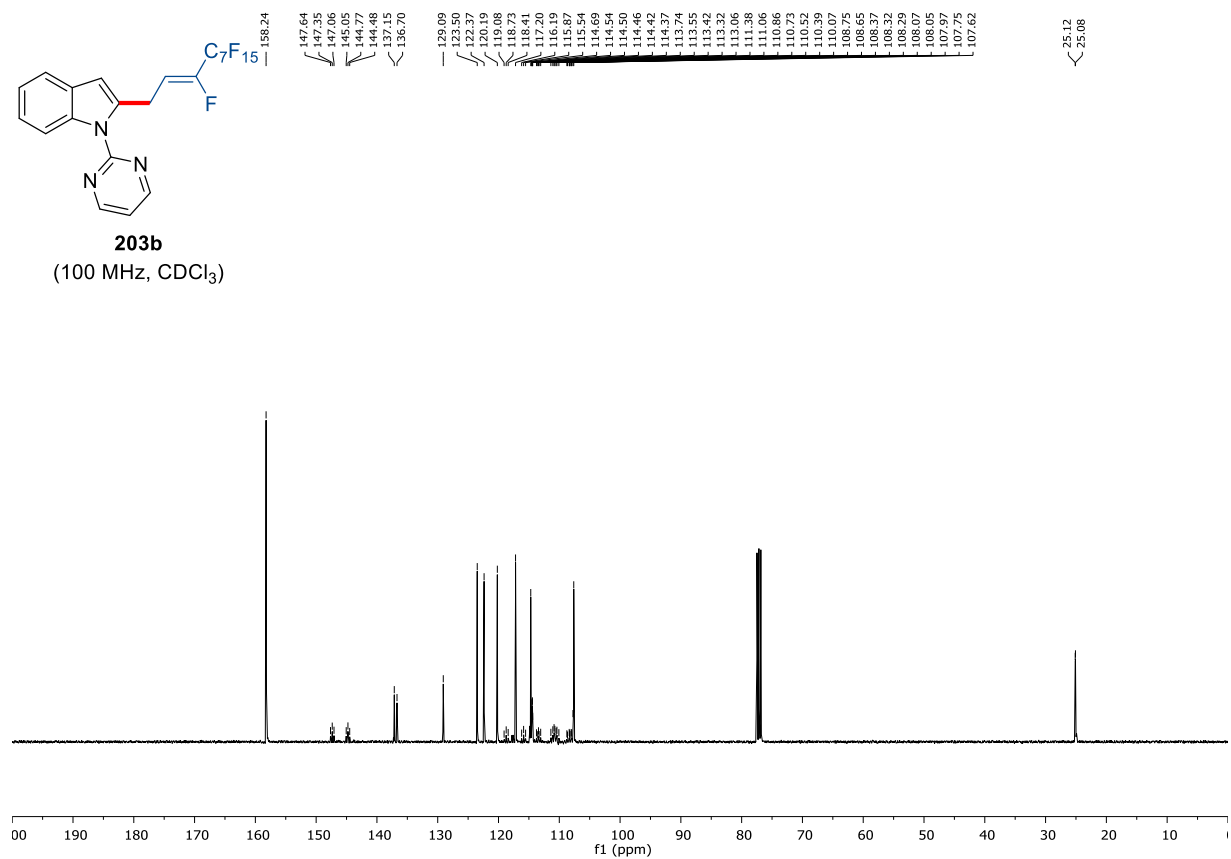
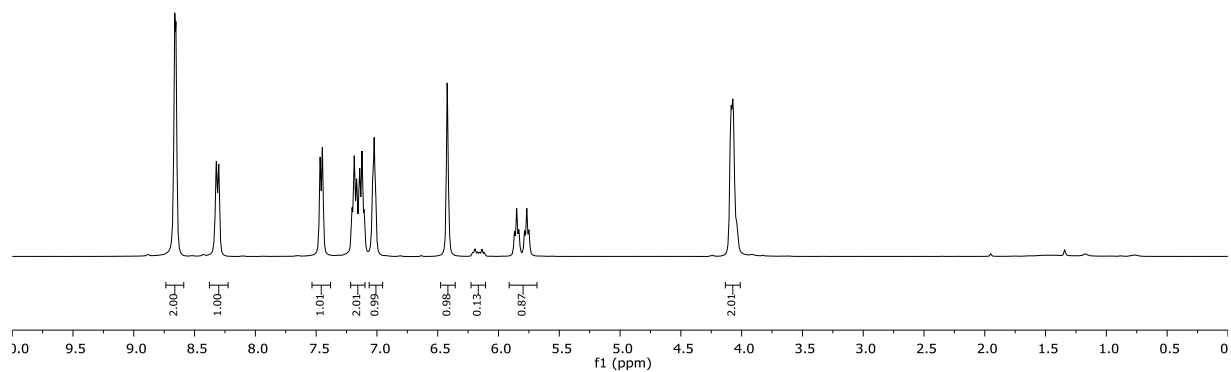
203a
(377 MHz, CDCl₃)

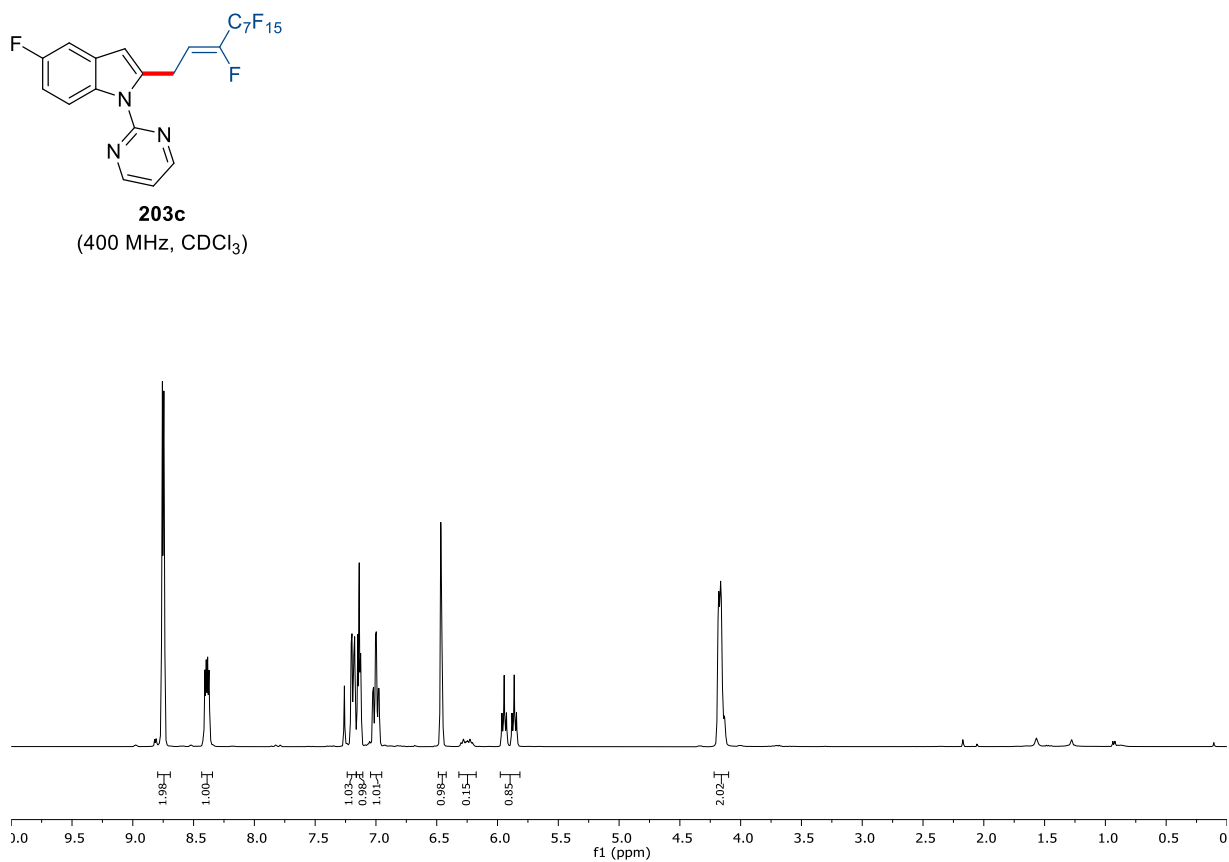
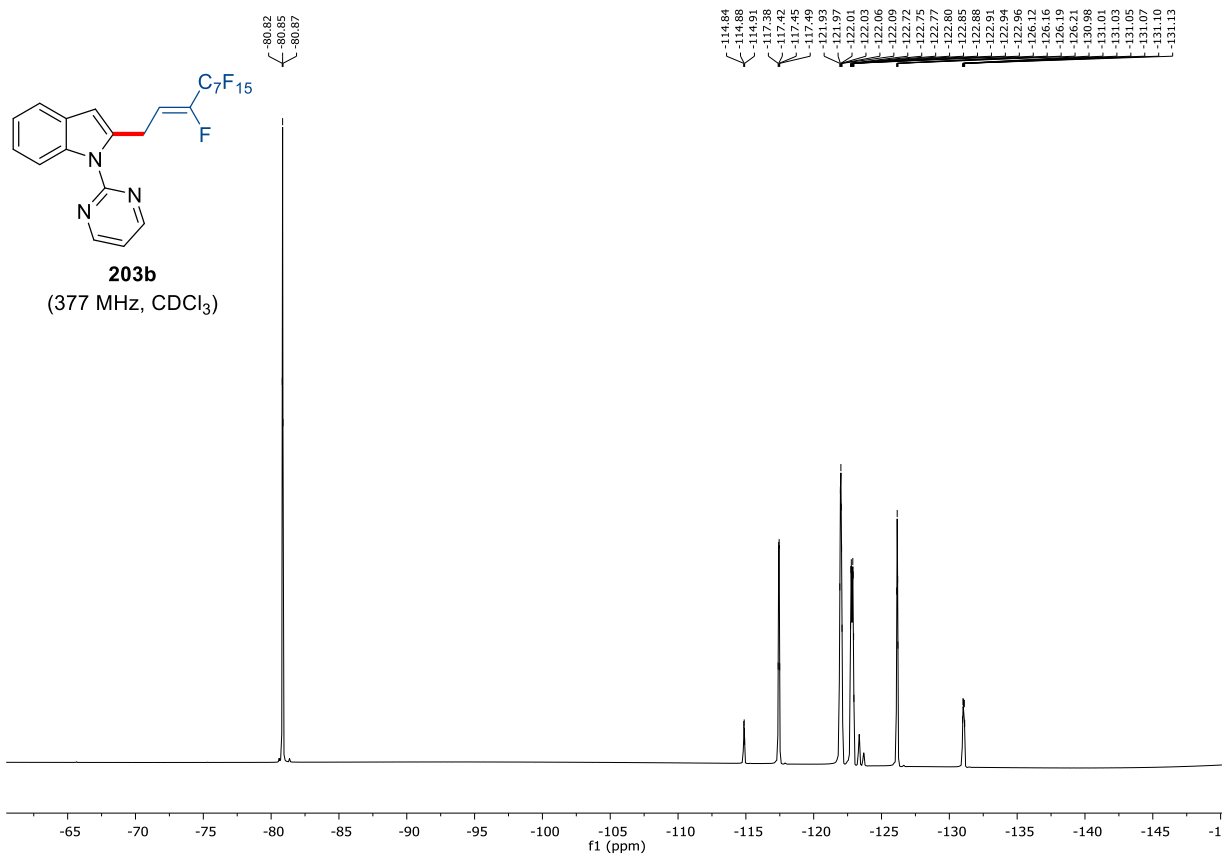


7. Appendix: NMR-Spectra and HPLC Chromatograms

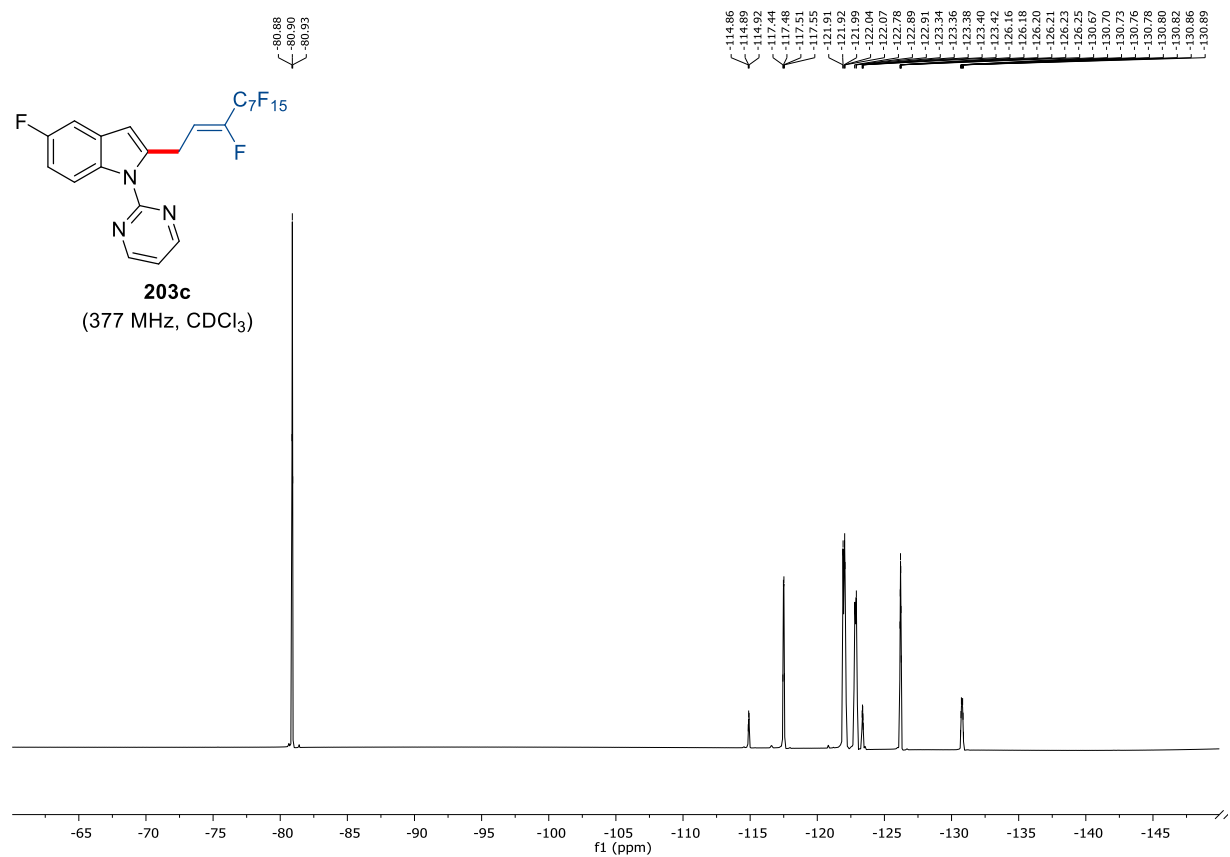
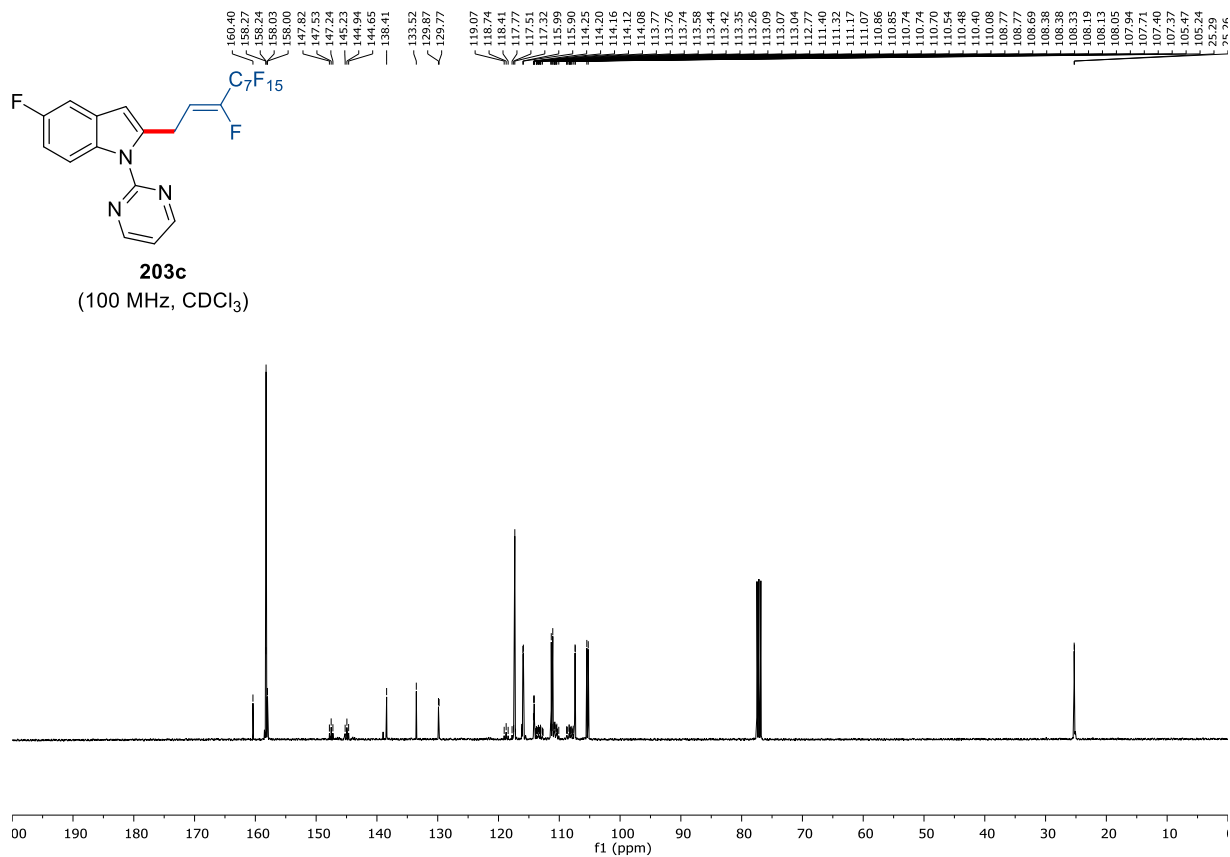


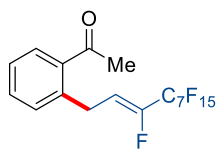
203b
(400 MHz, CDCl₃)



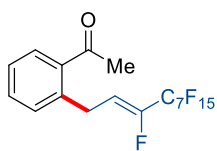
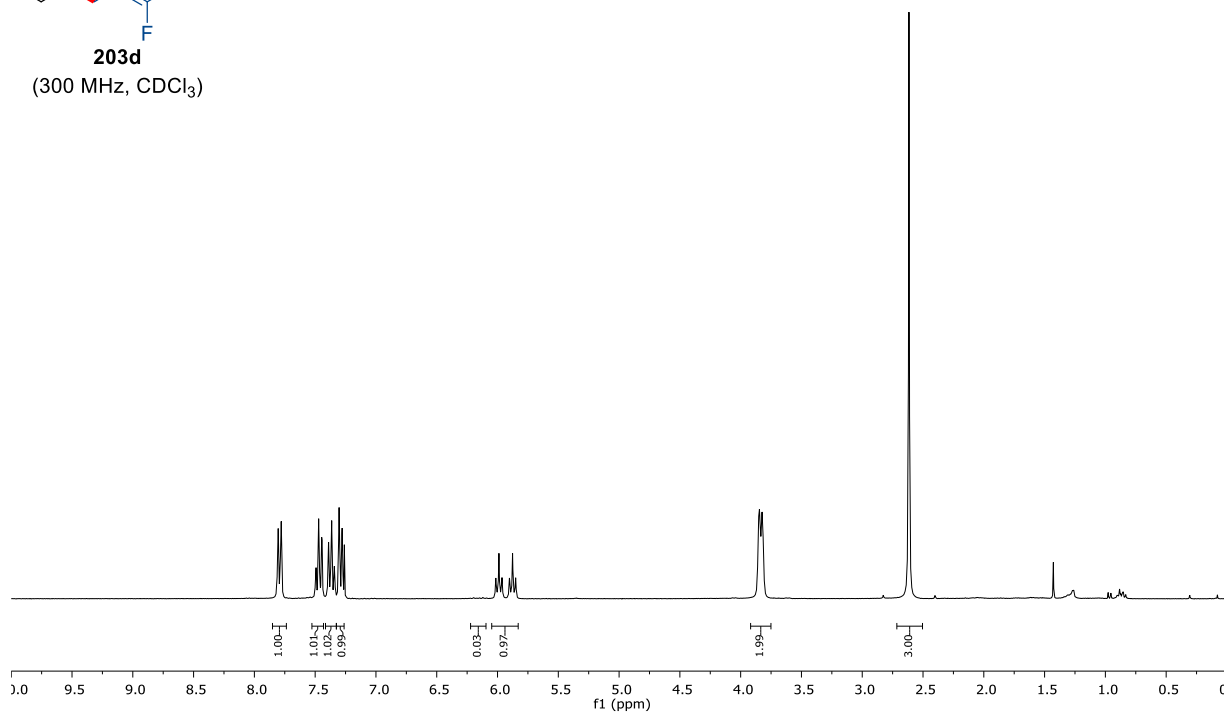


7. Appendix: NMR-Spectra and HPLC Chromatograms

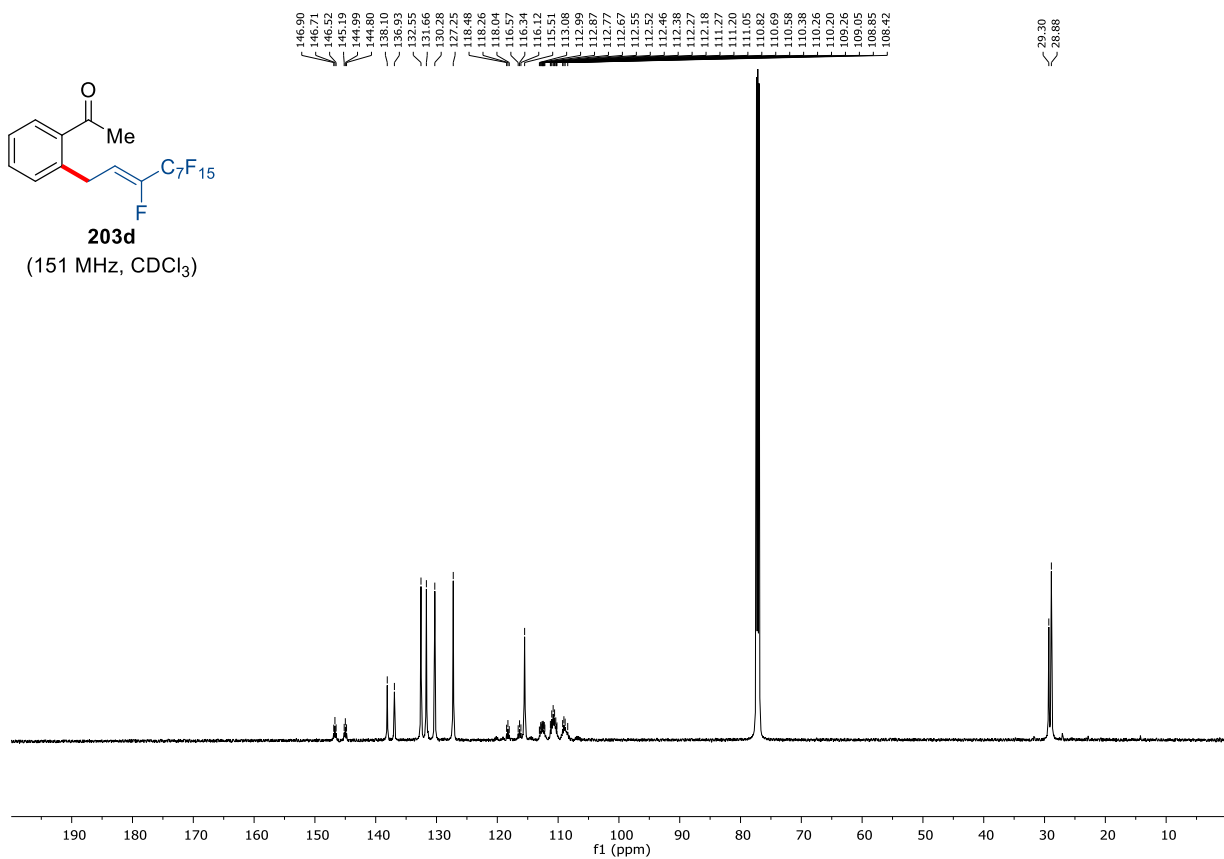




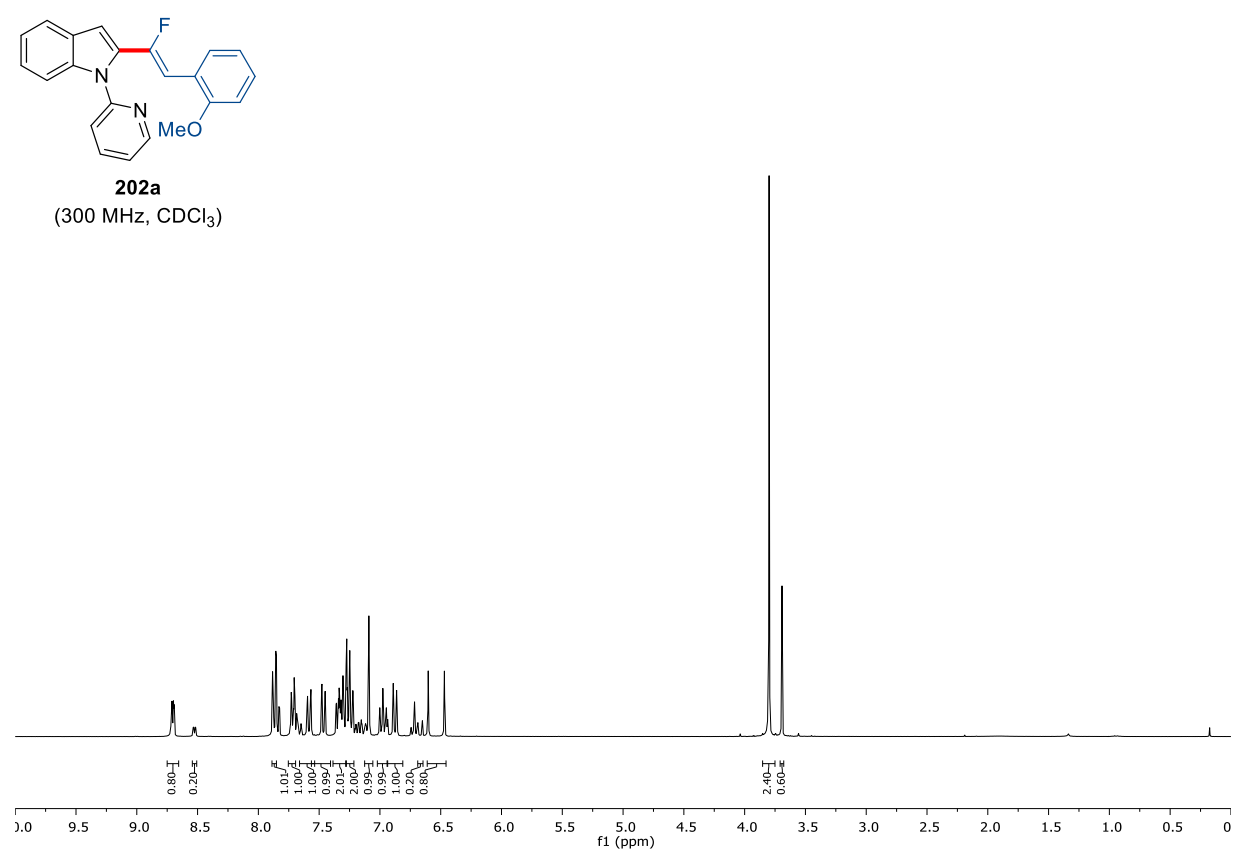
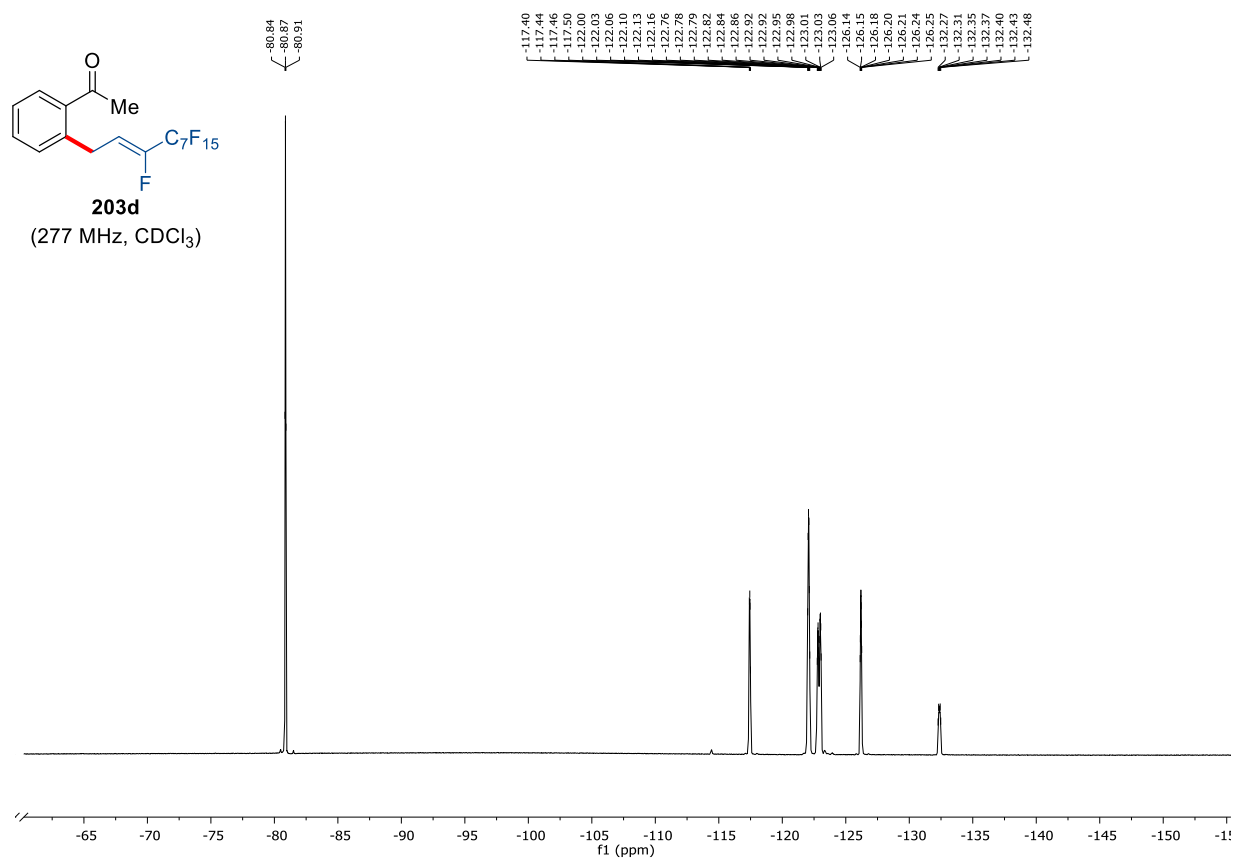
(300 MHz, CDCl₃)

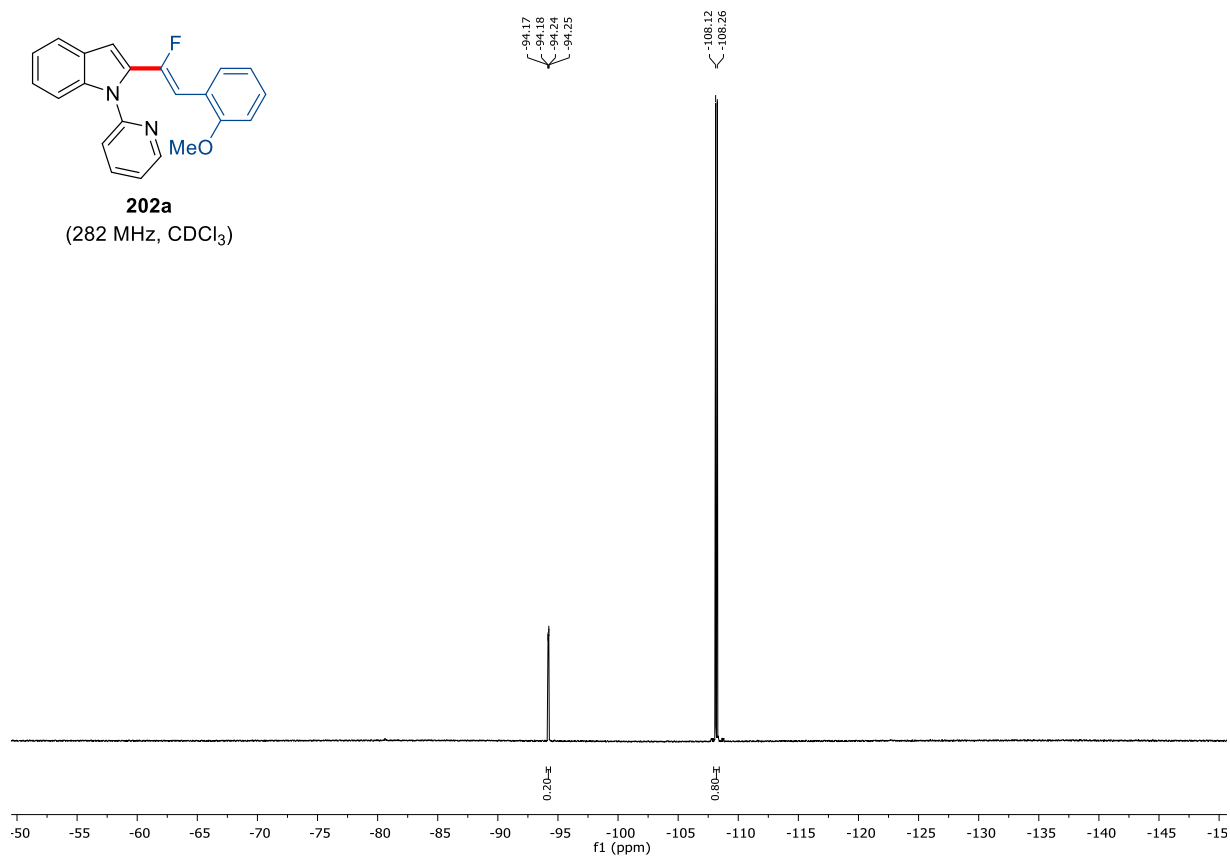
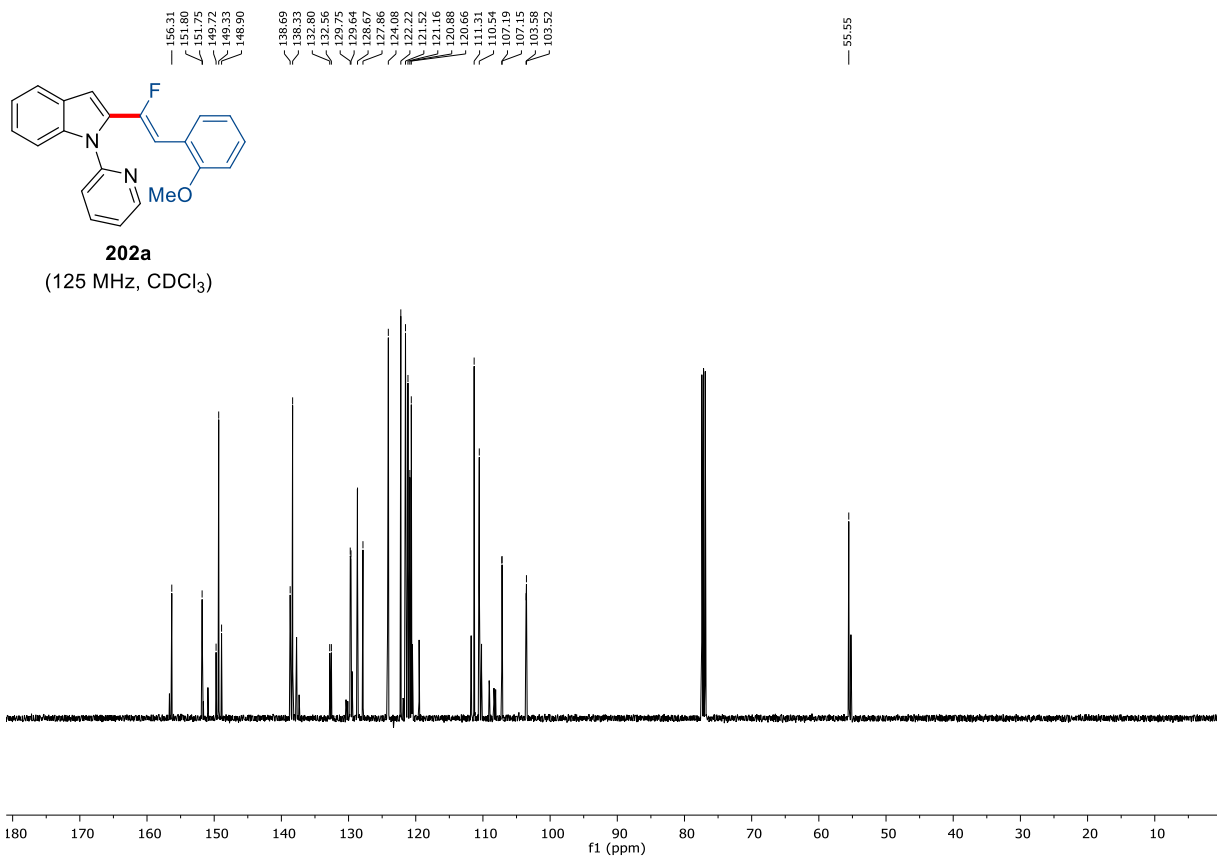


(151 MHz, CDCl₃)

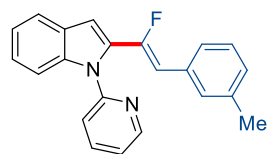


7. Appendix: NMR-Spectra and HPLC Chromatograms

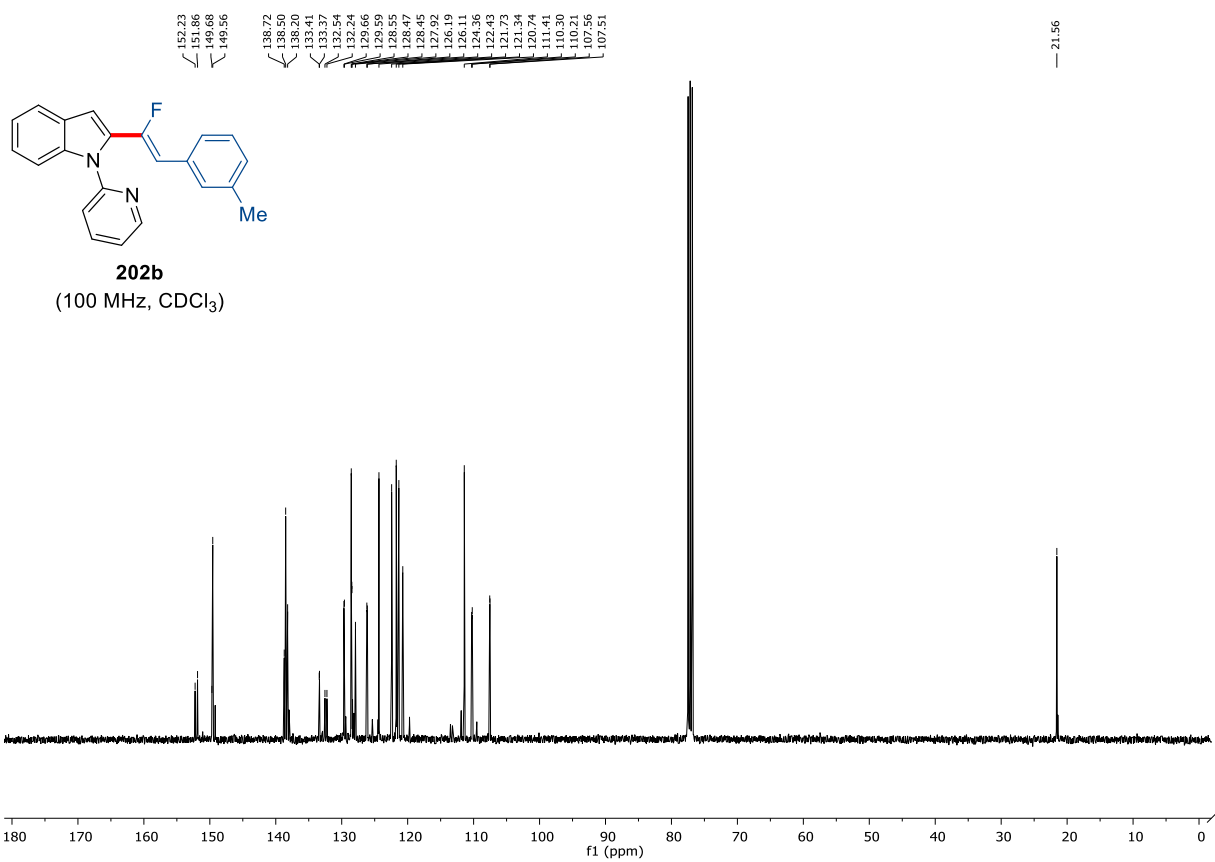
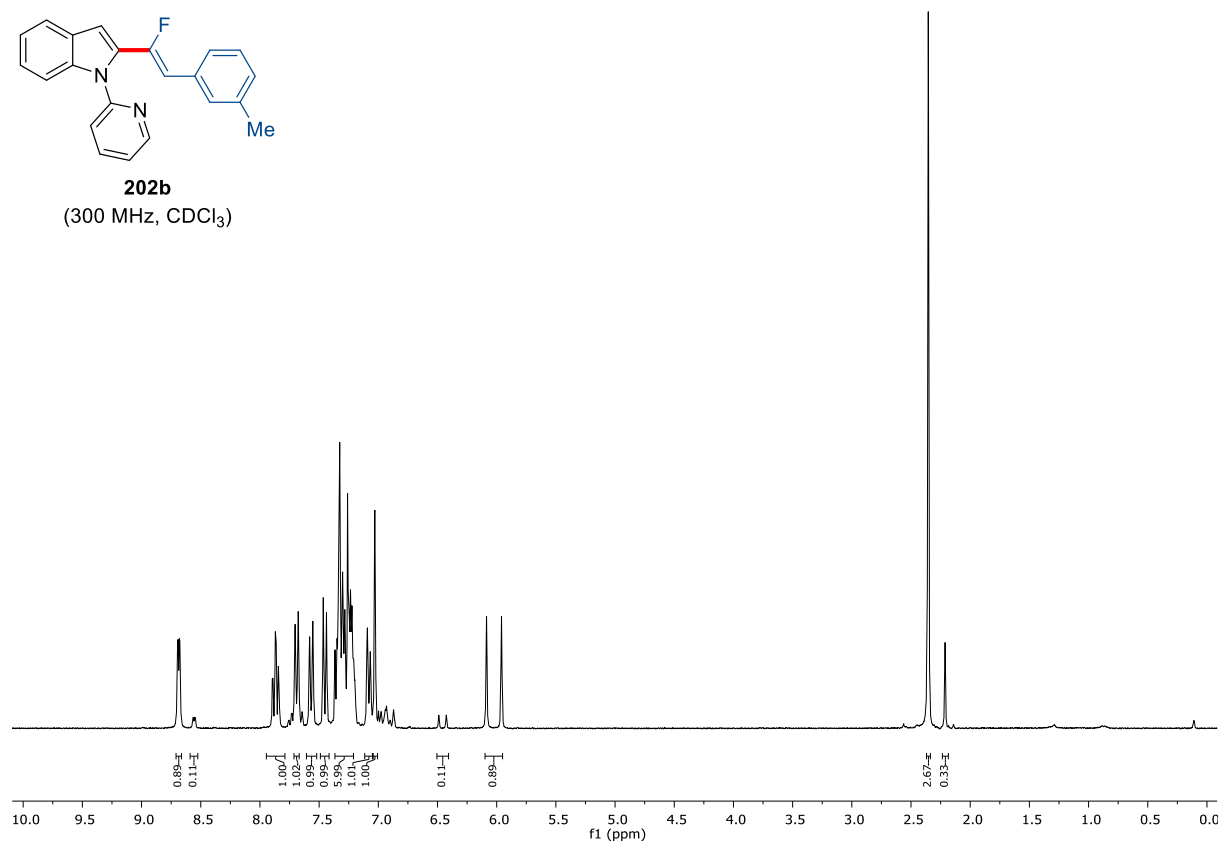


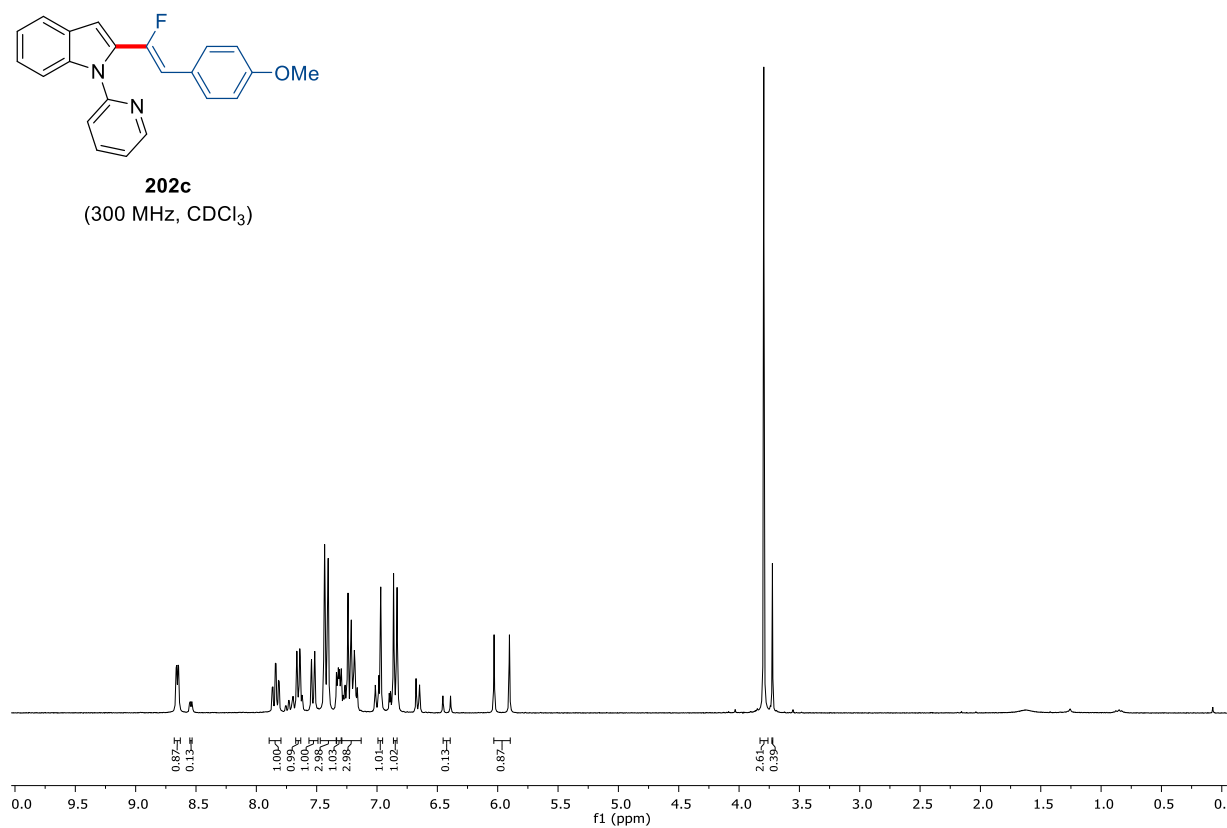
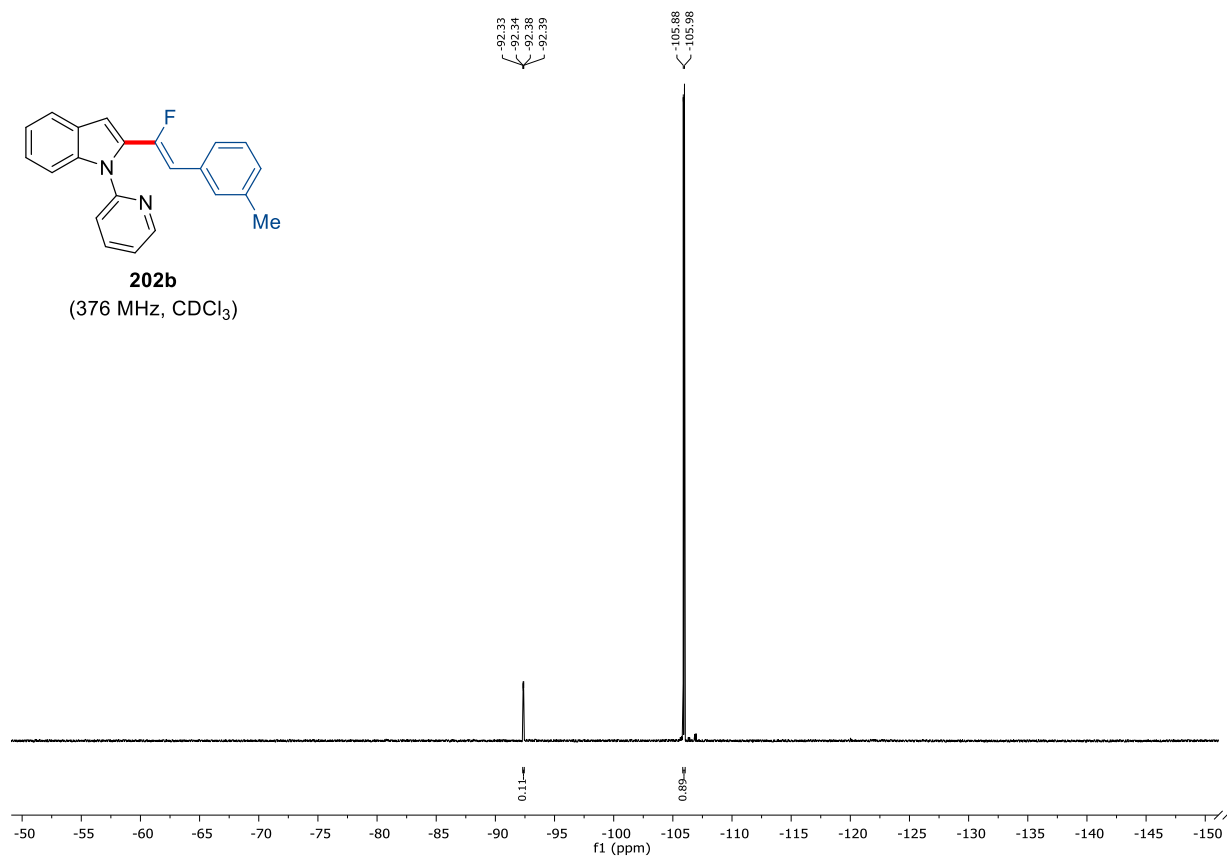


7. Appendix: NMR-Spectra and HPLC Chromatograms

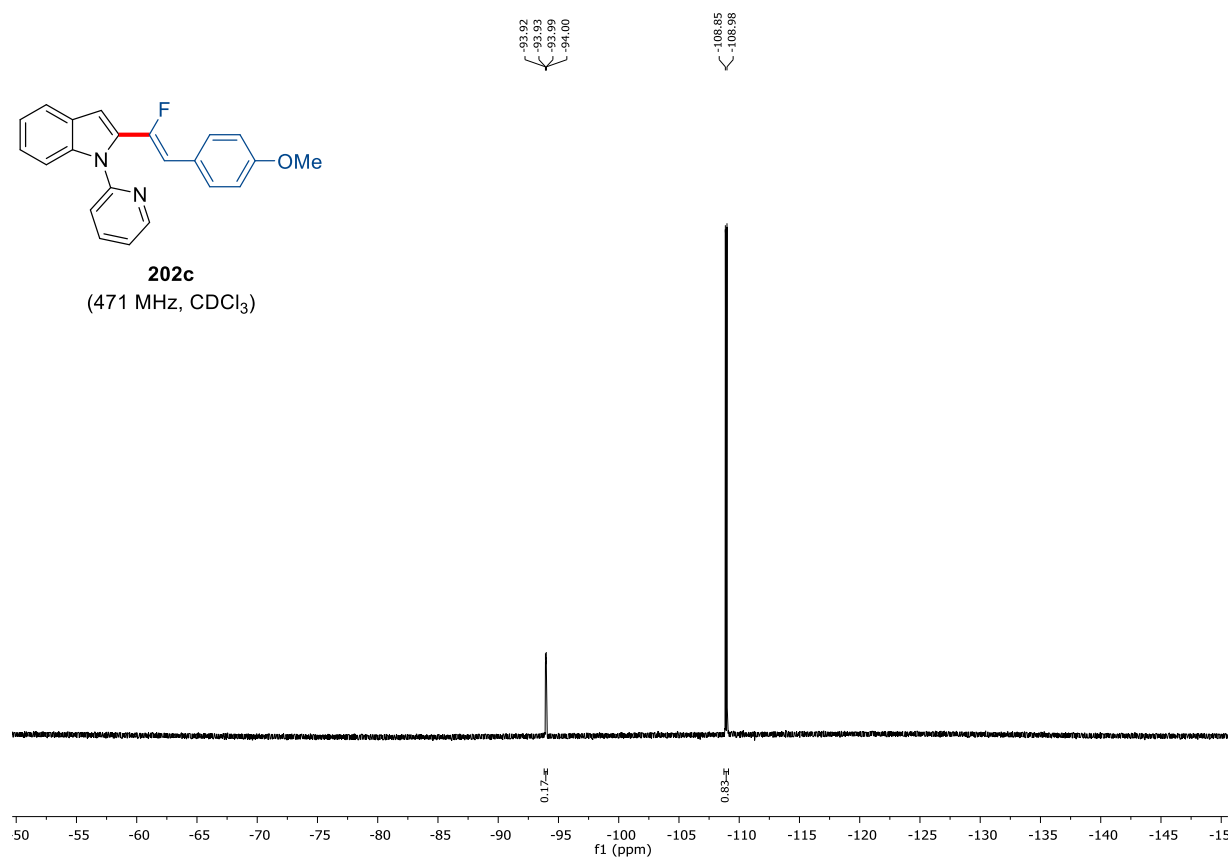
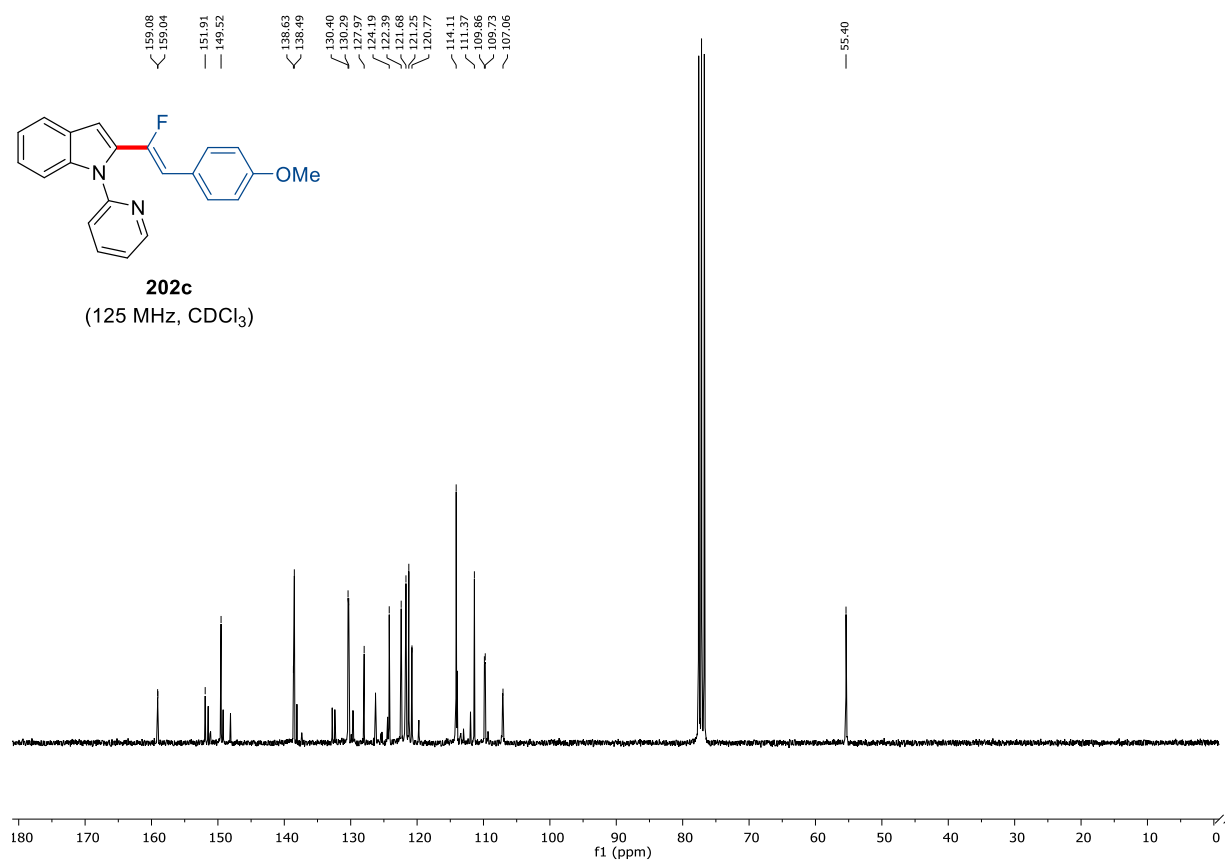


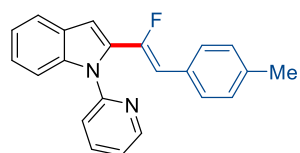
202b
(300 MHz, CDCl₃)



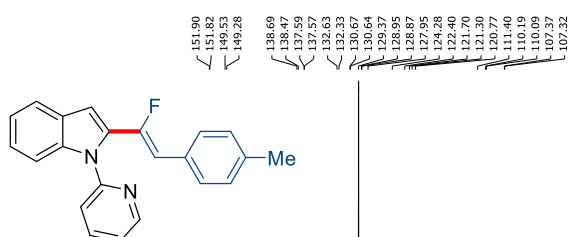
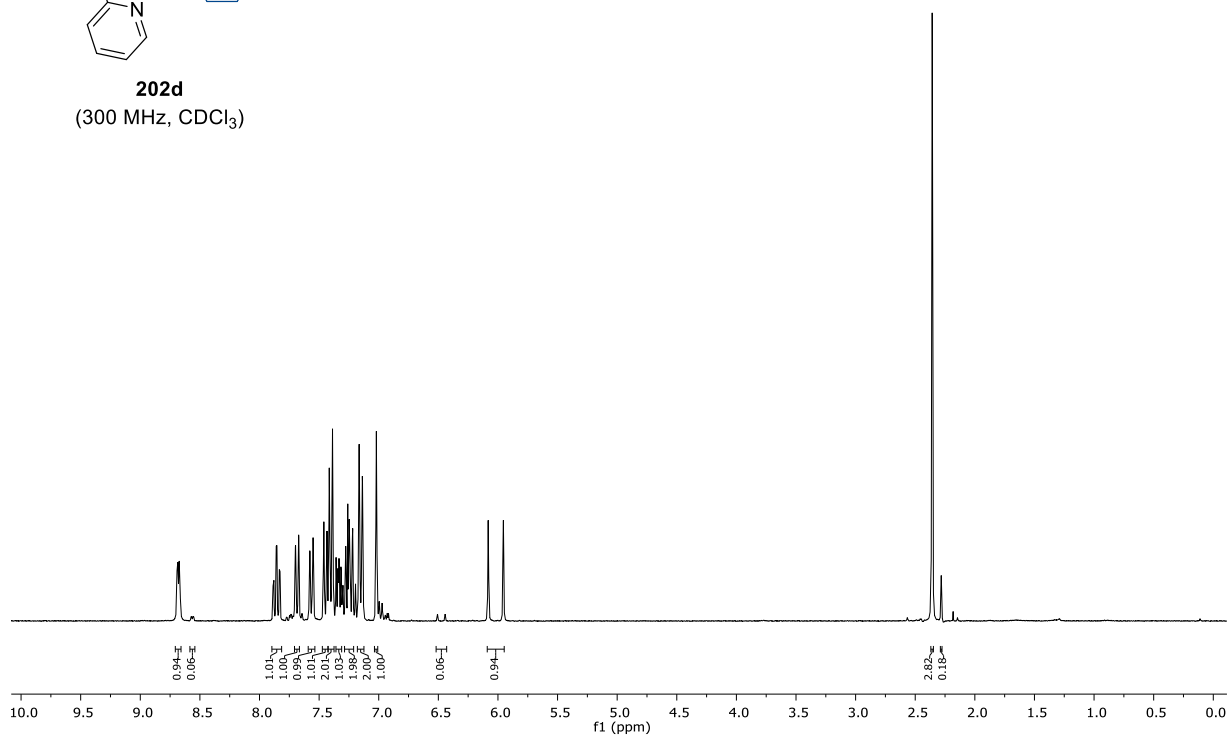


7. Appendix: NMR-Spectra and HPLC Chromatograms

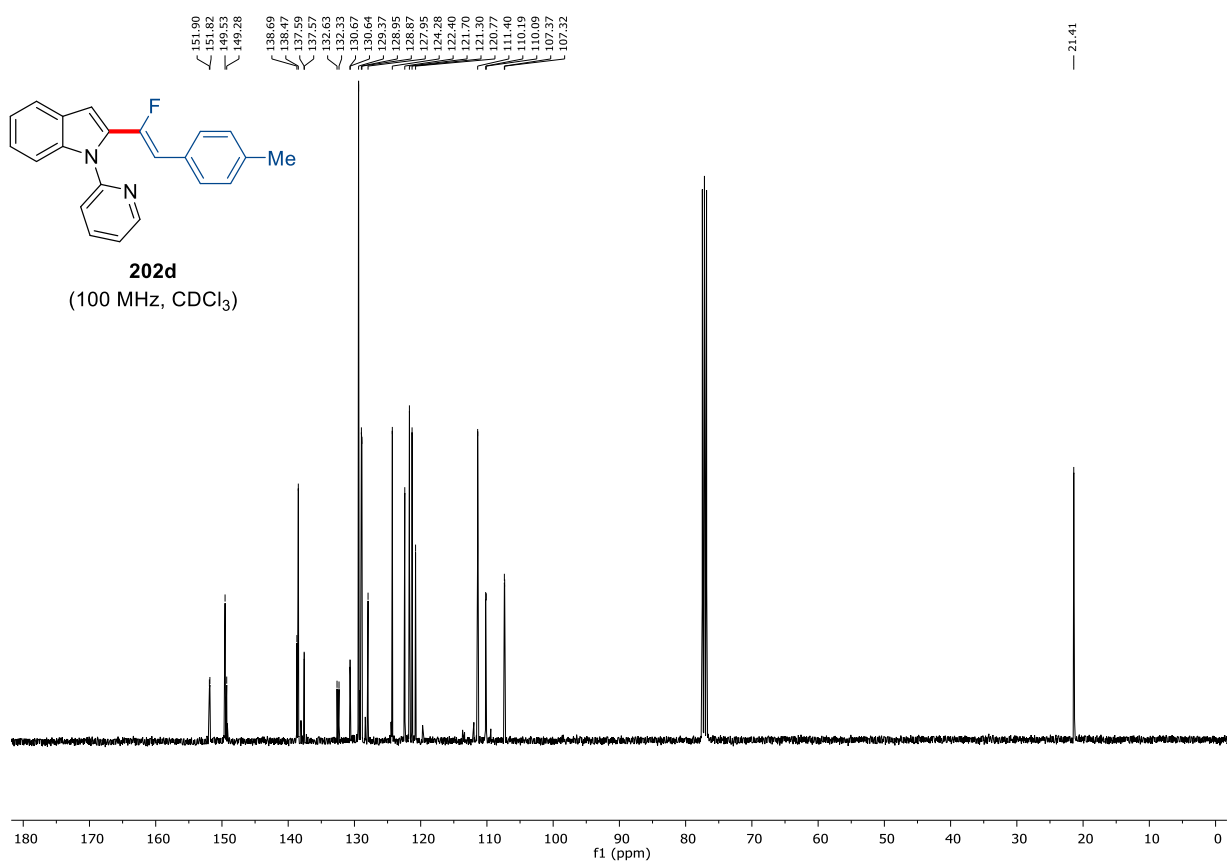




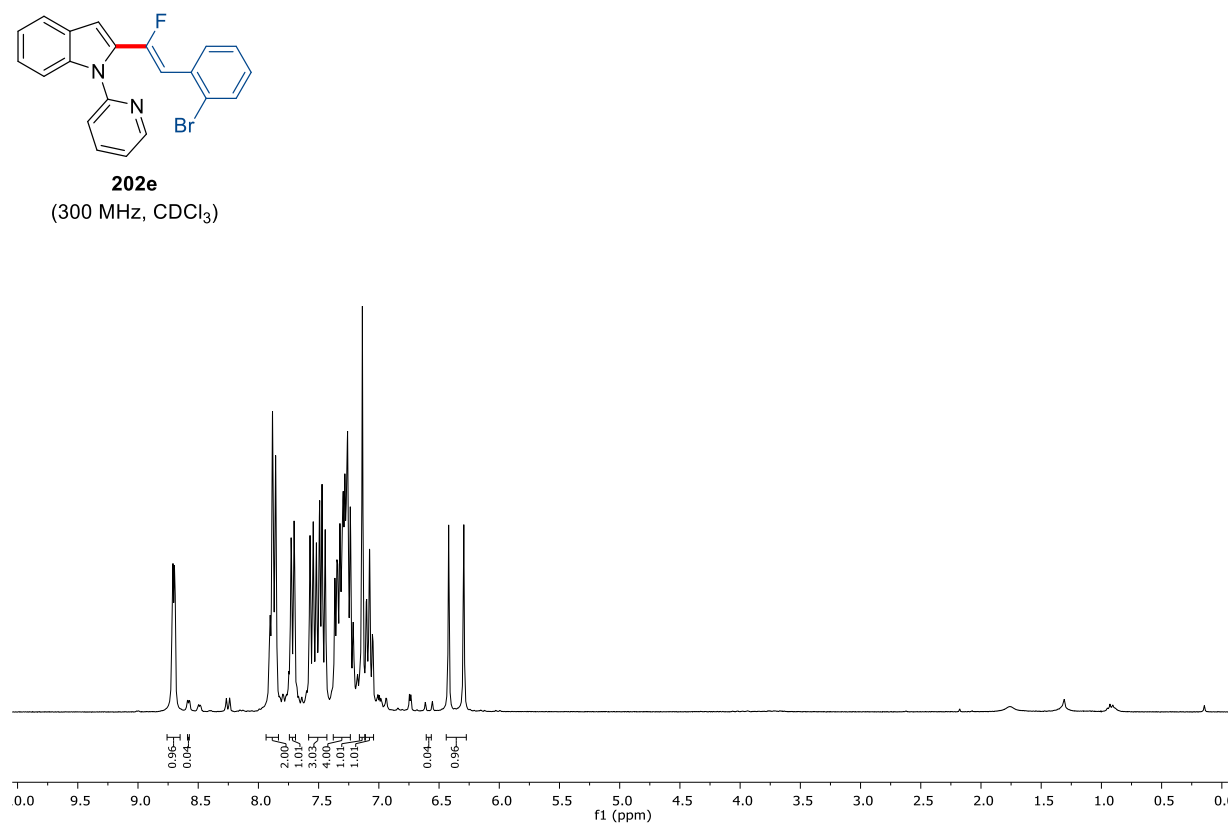
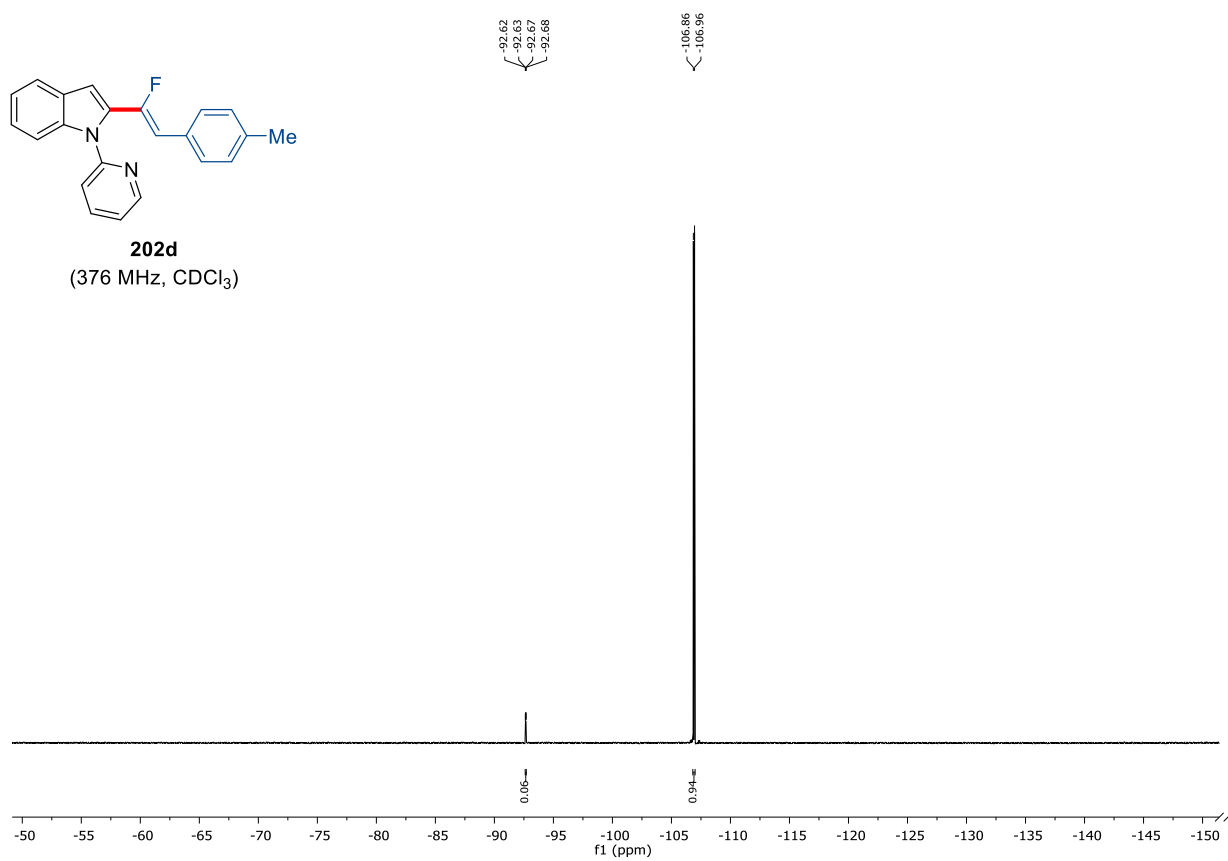
202d
(300 MHz, CDCl₃)

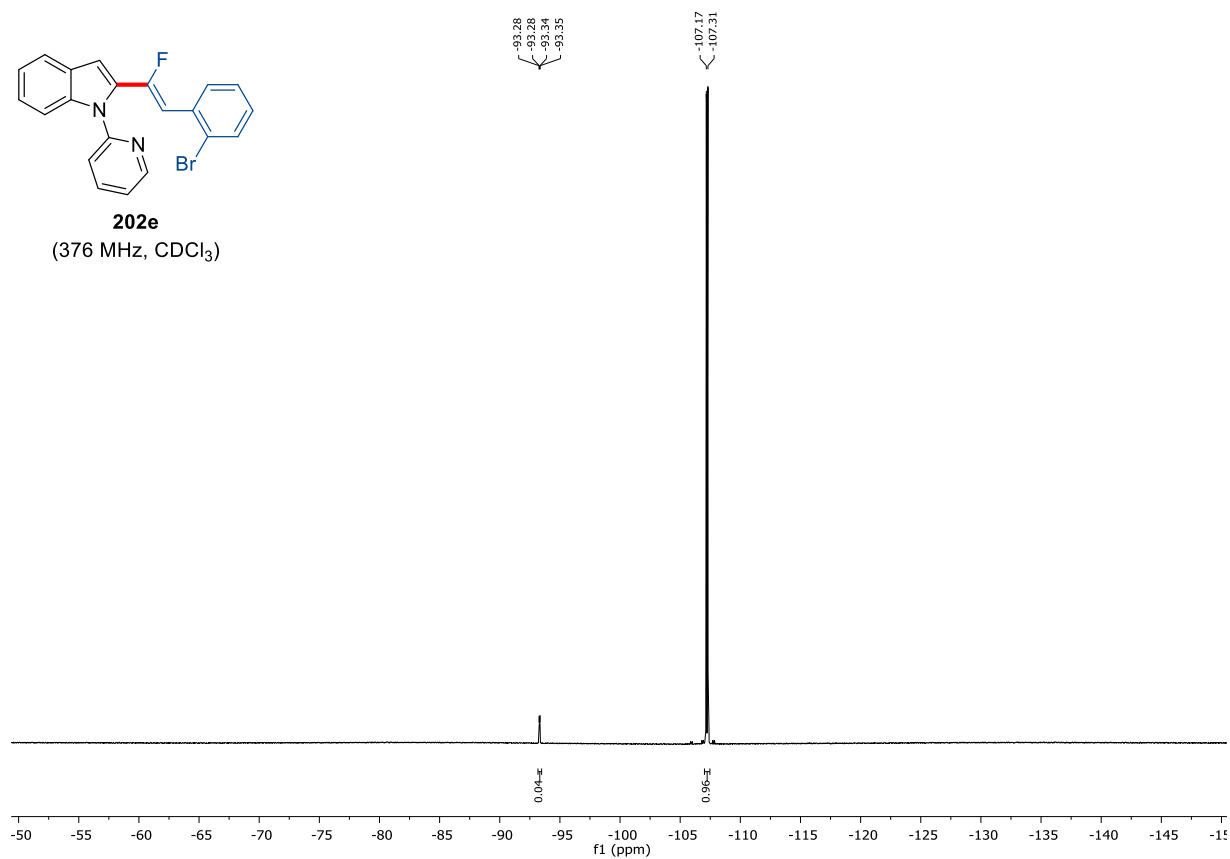
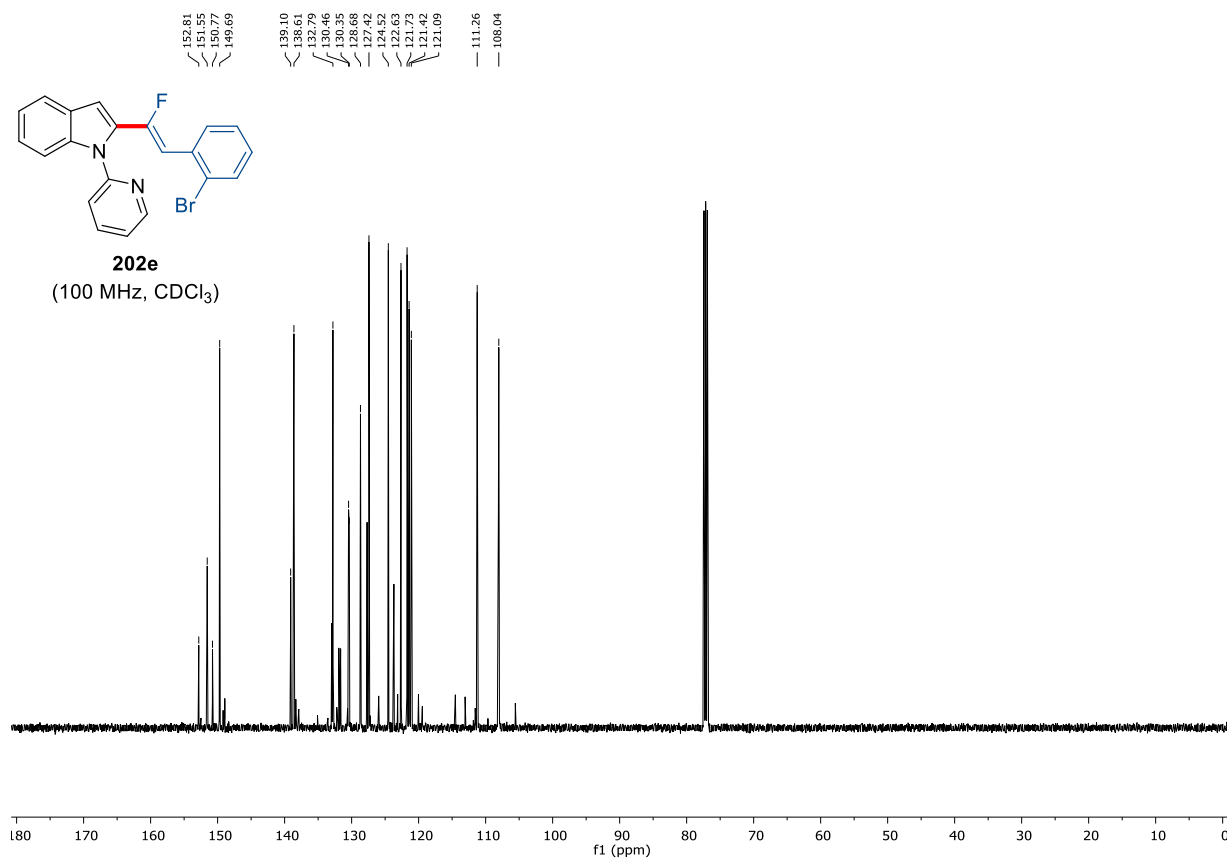


202d
(100 MHz, CDCl₃)

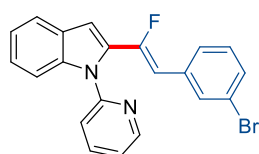


7. Appendix: NMR-Spectra and HPLC Chromatograms

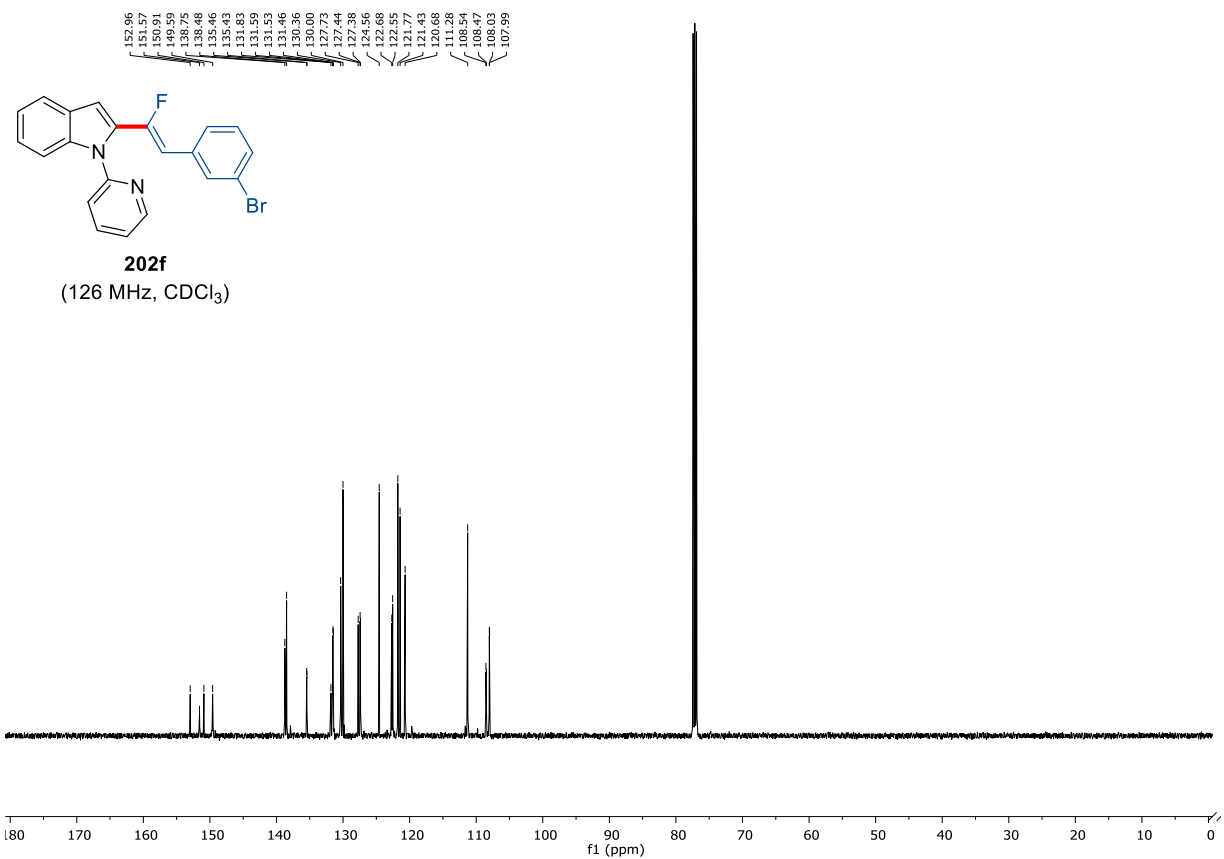
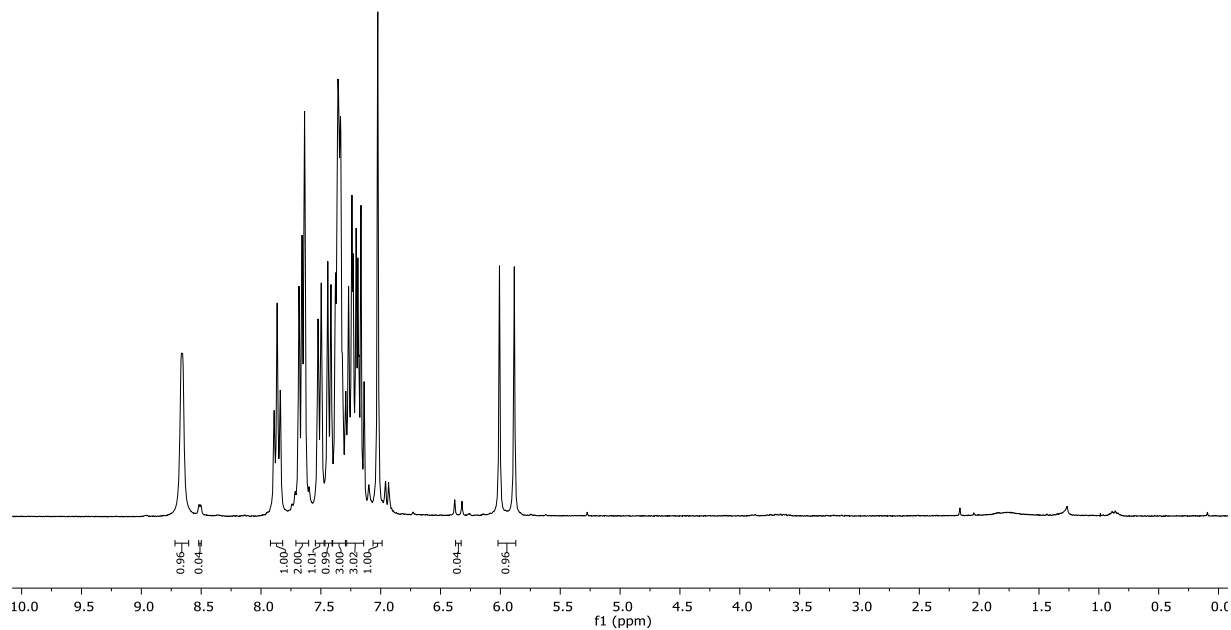


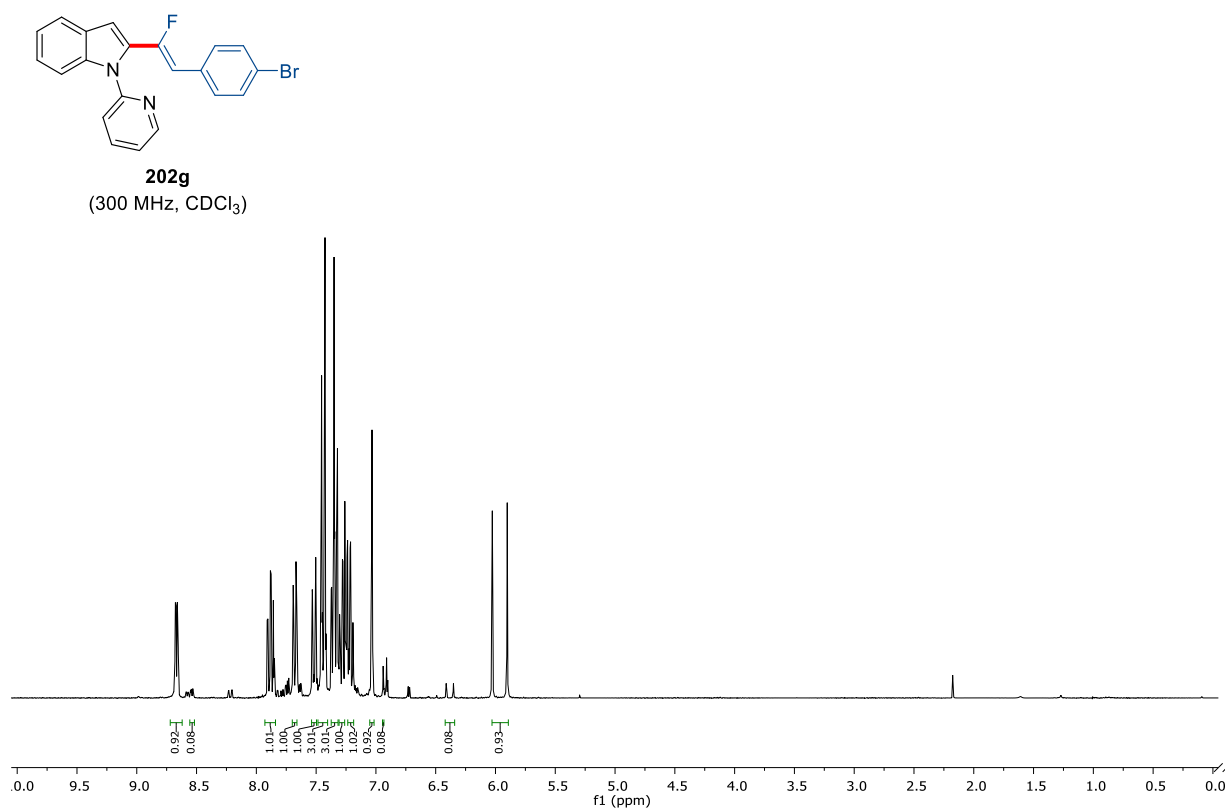
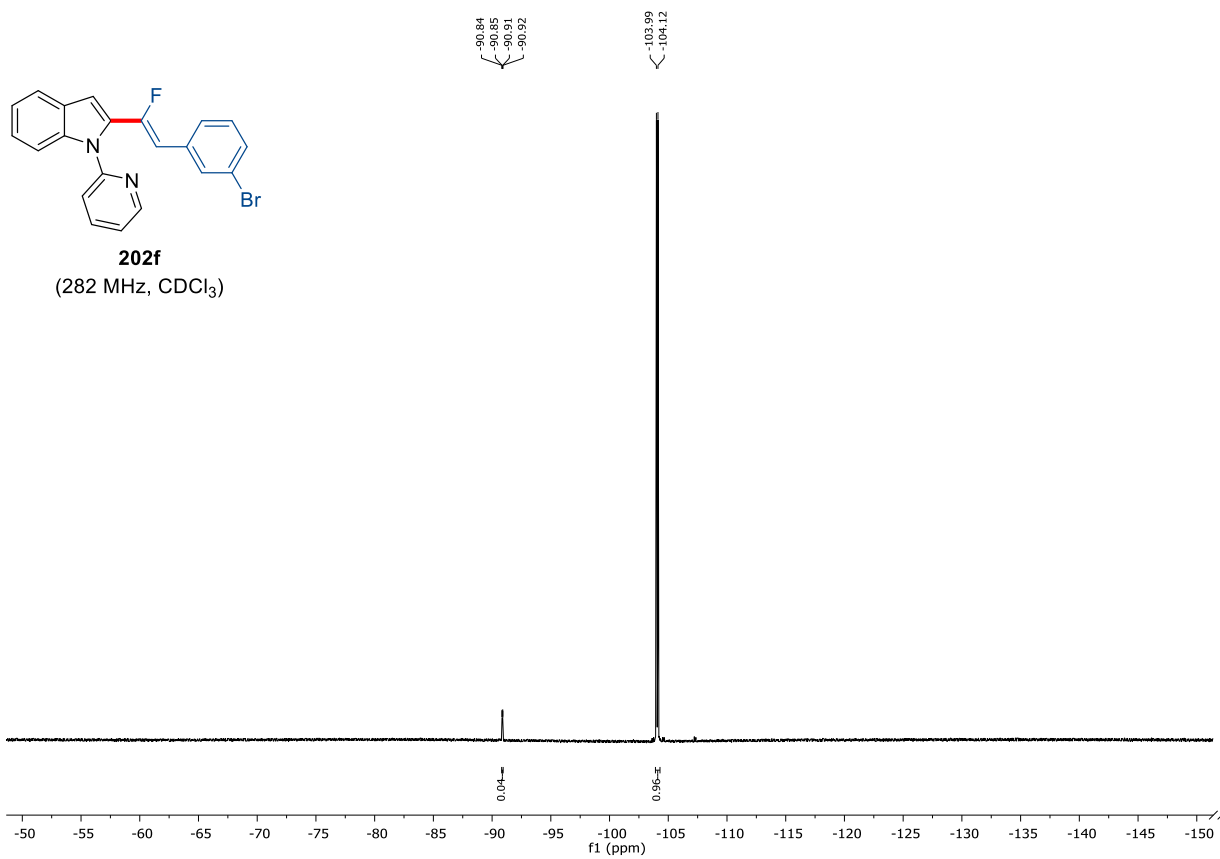


7. Appendix: NMR-Spectra and HPLC Chromatograms

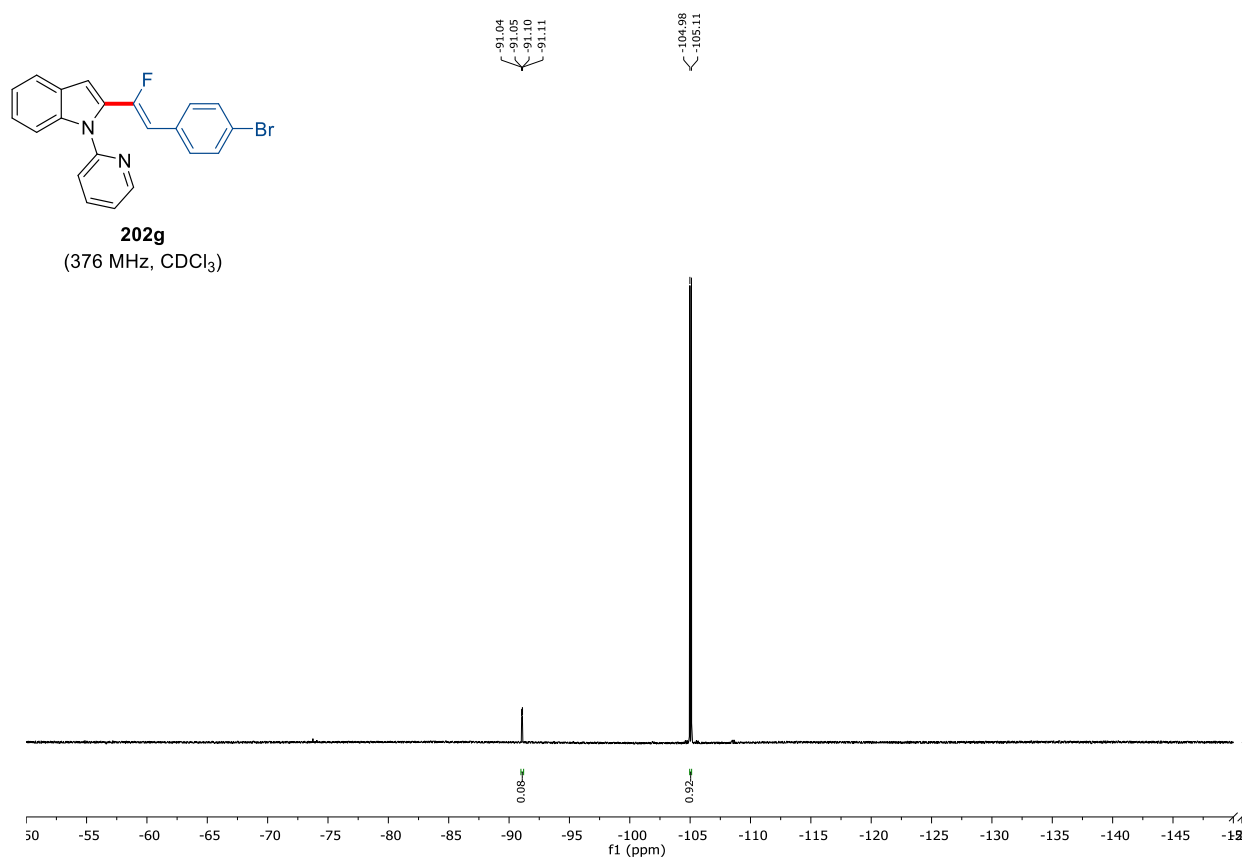
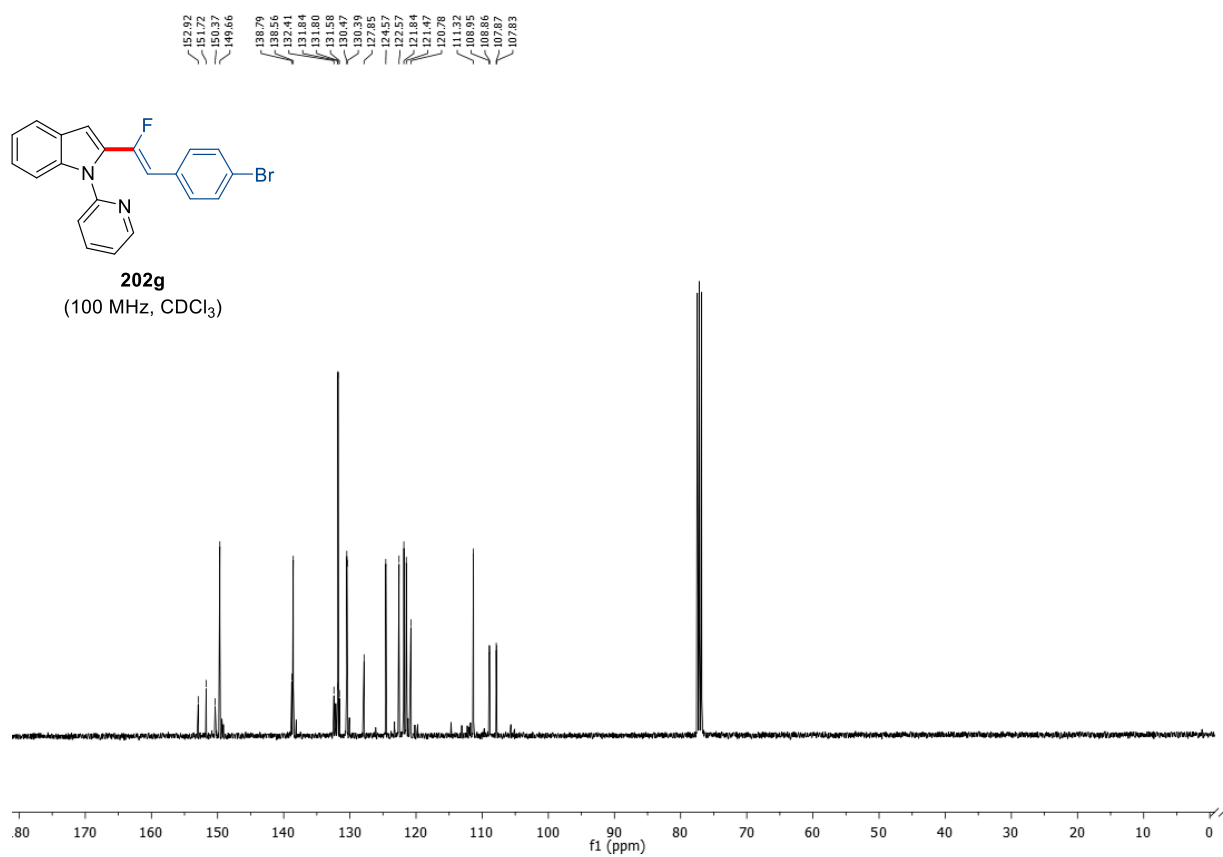


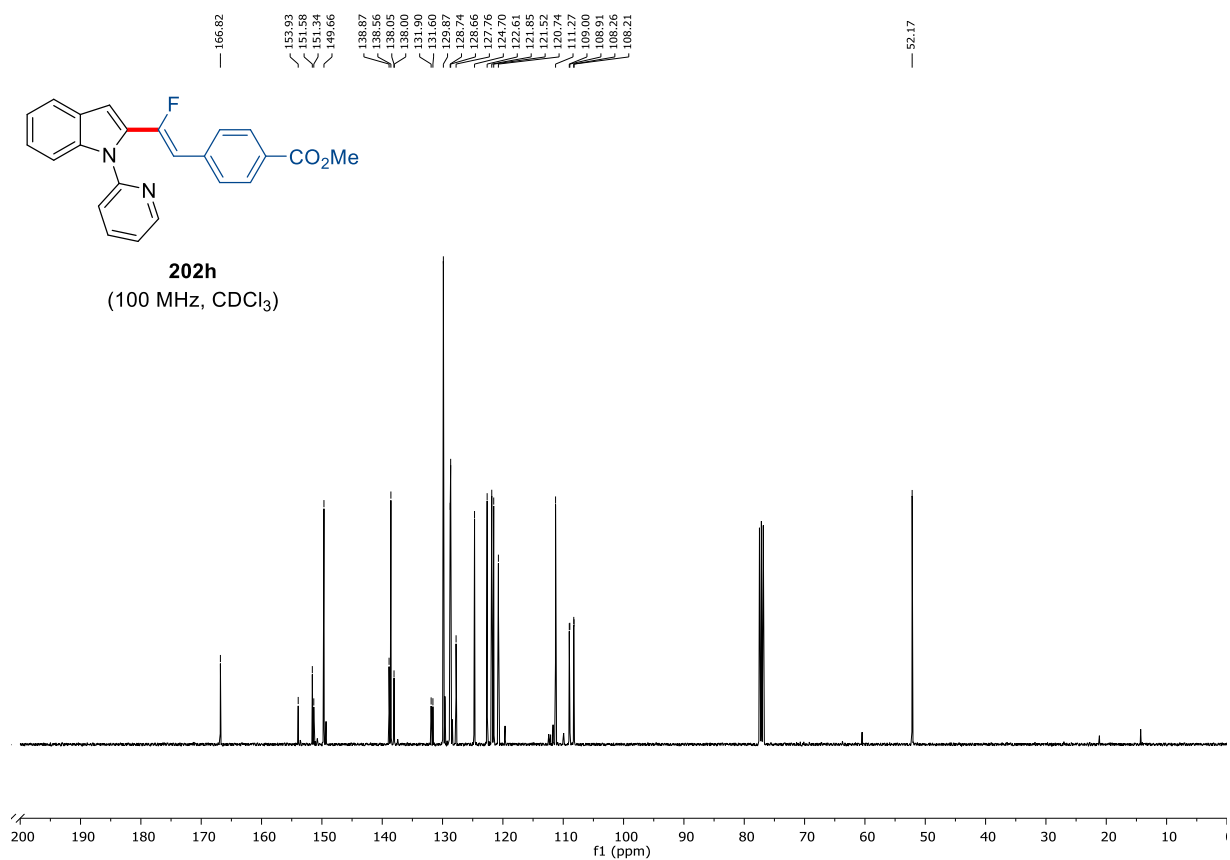
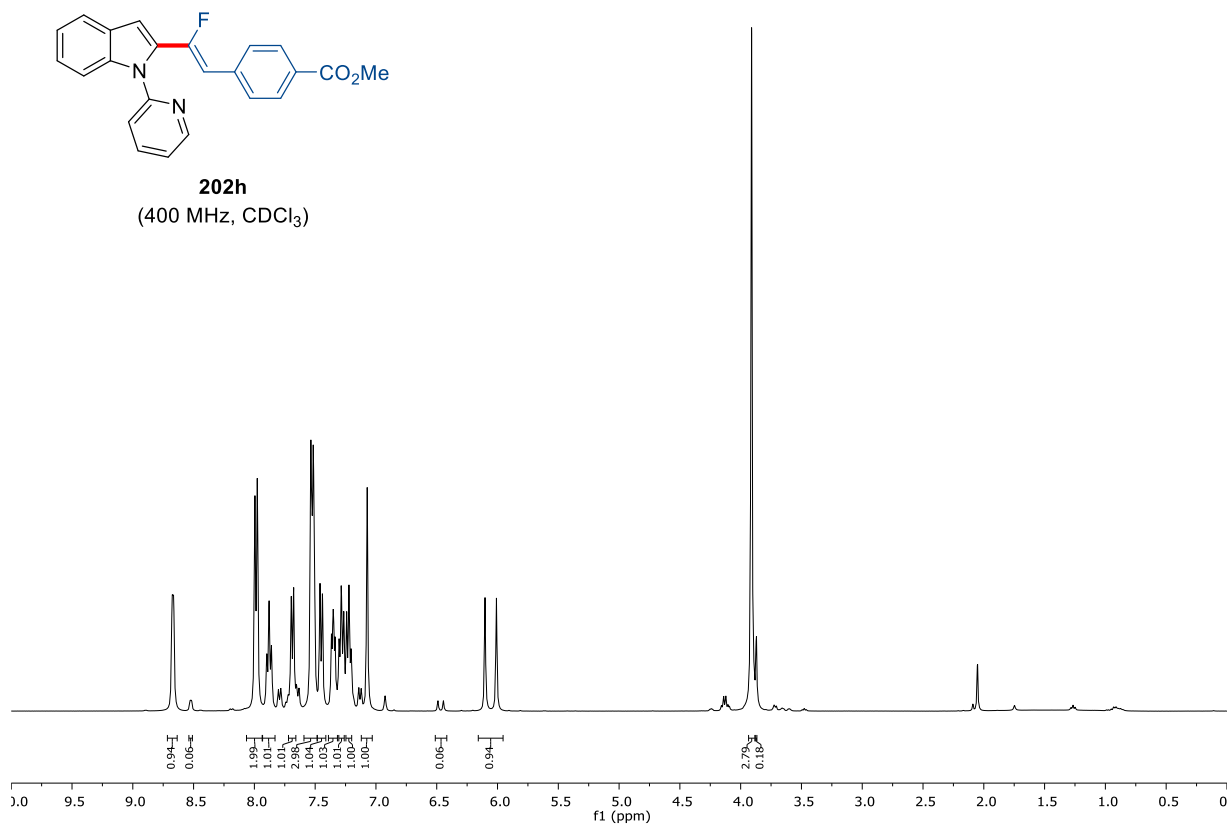
202f
(300 MHz, CDCl₃)



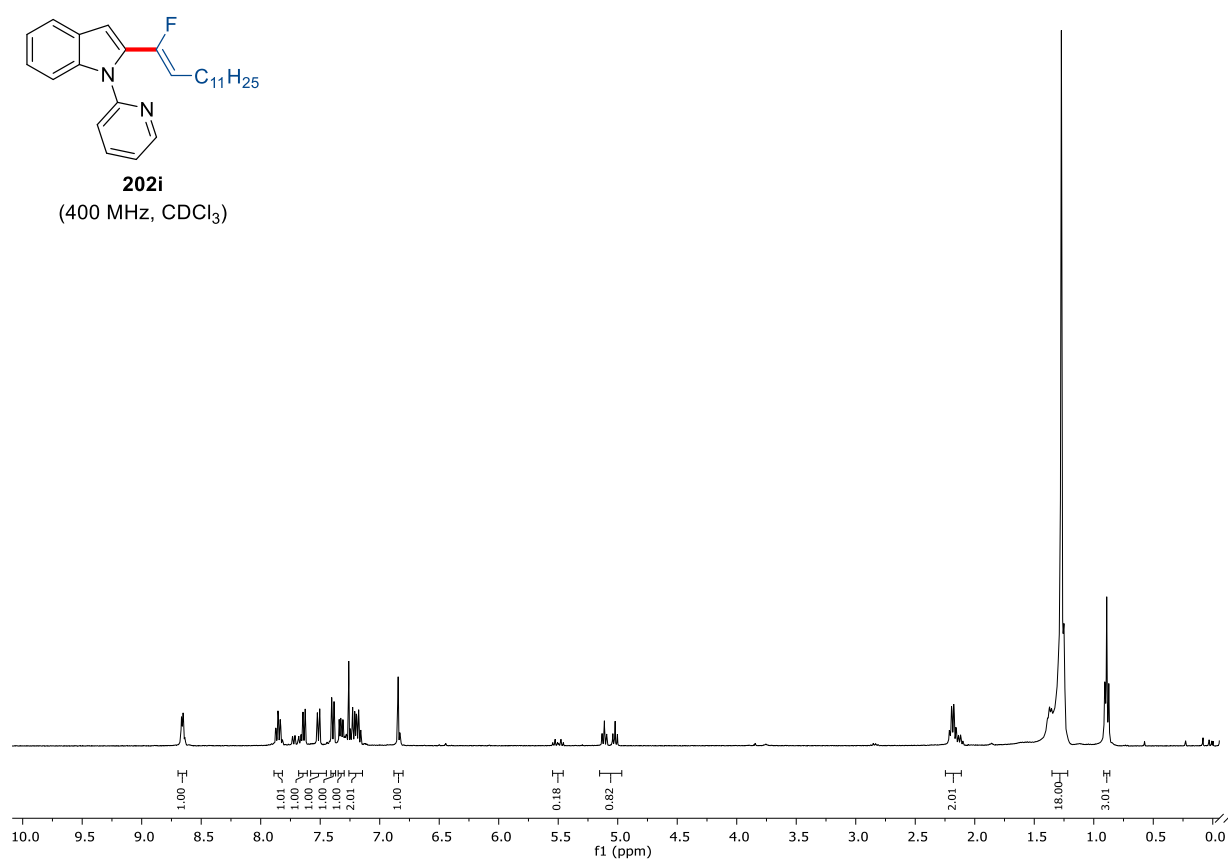
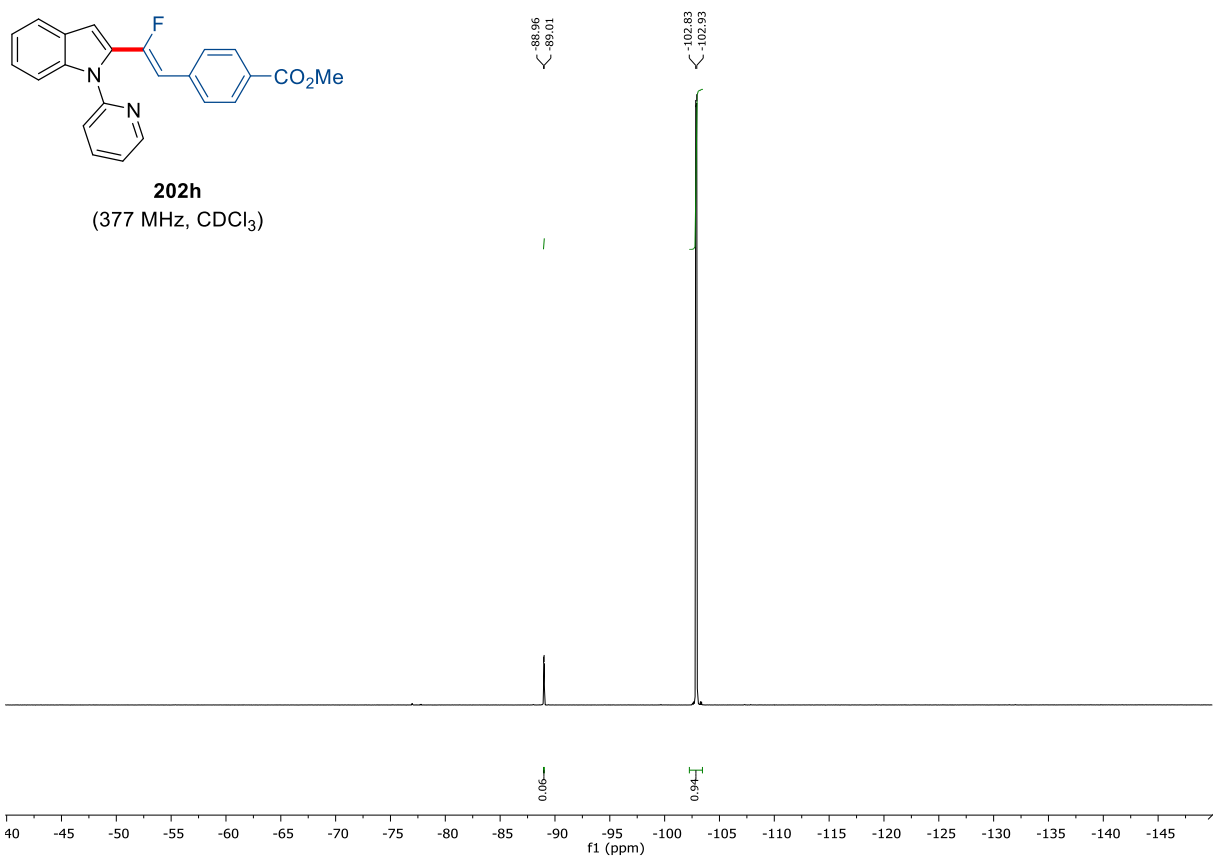


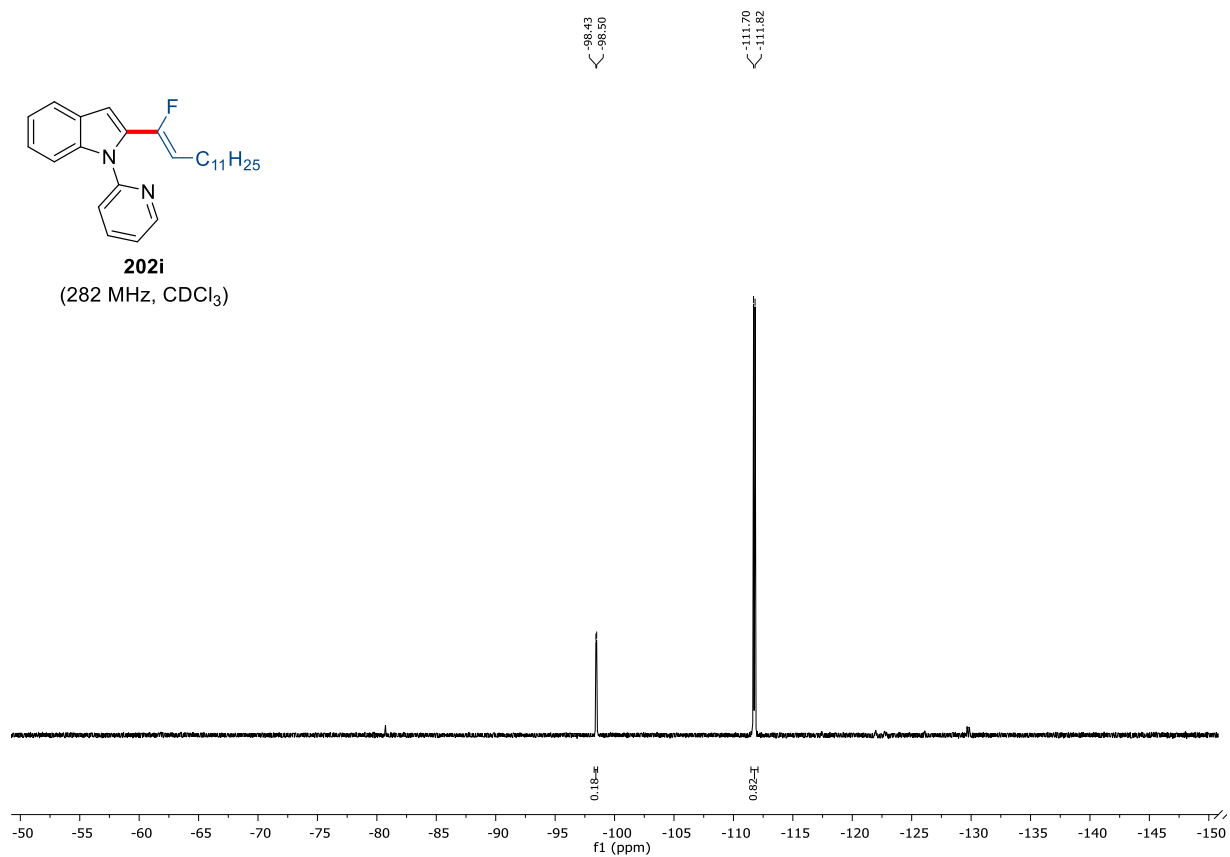
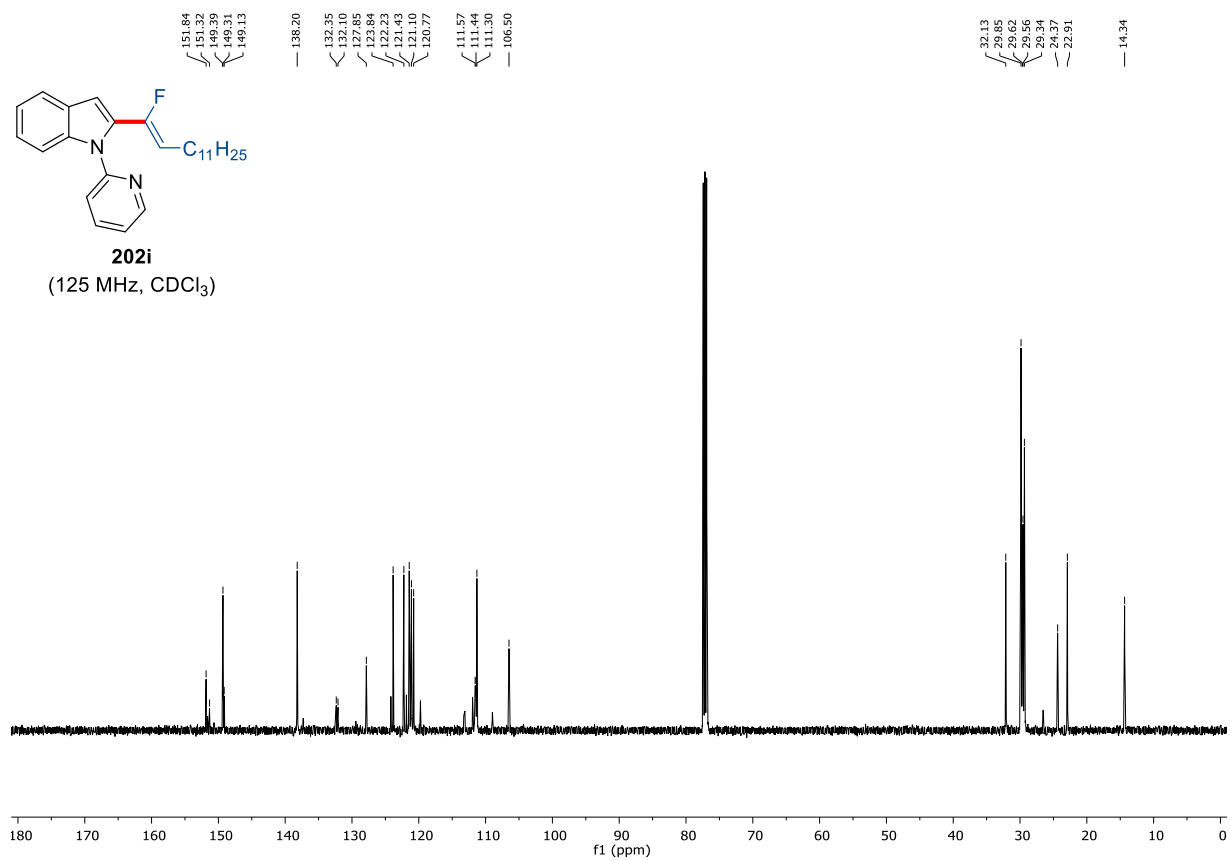
7. Appendix: NMR-Spectra and HPLC Chromatograms



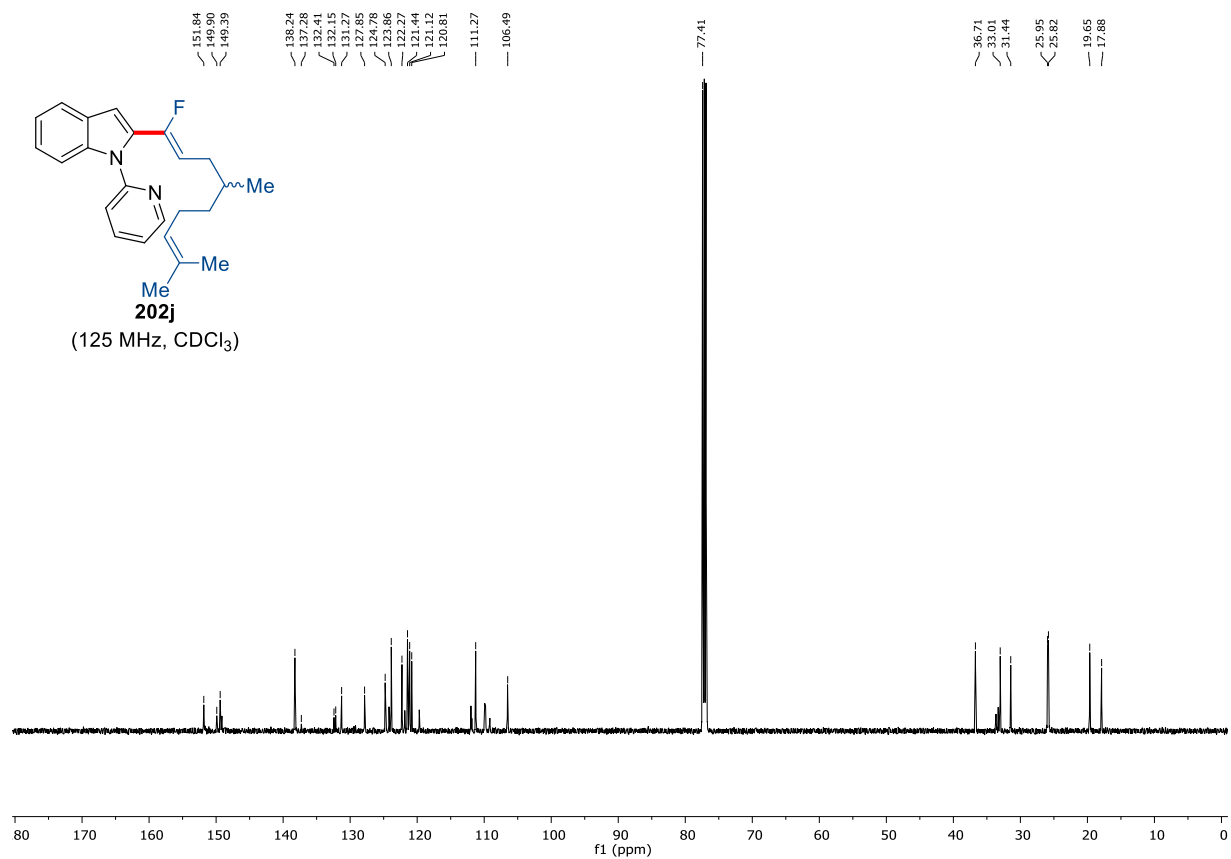
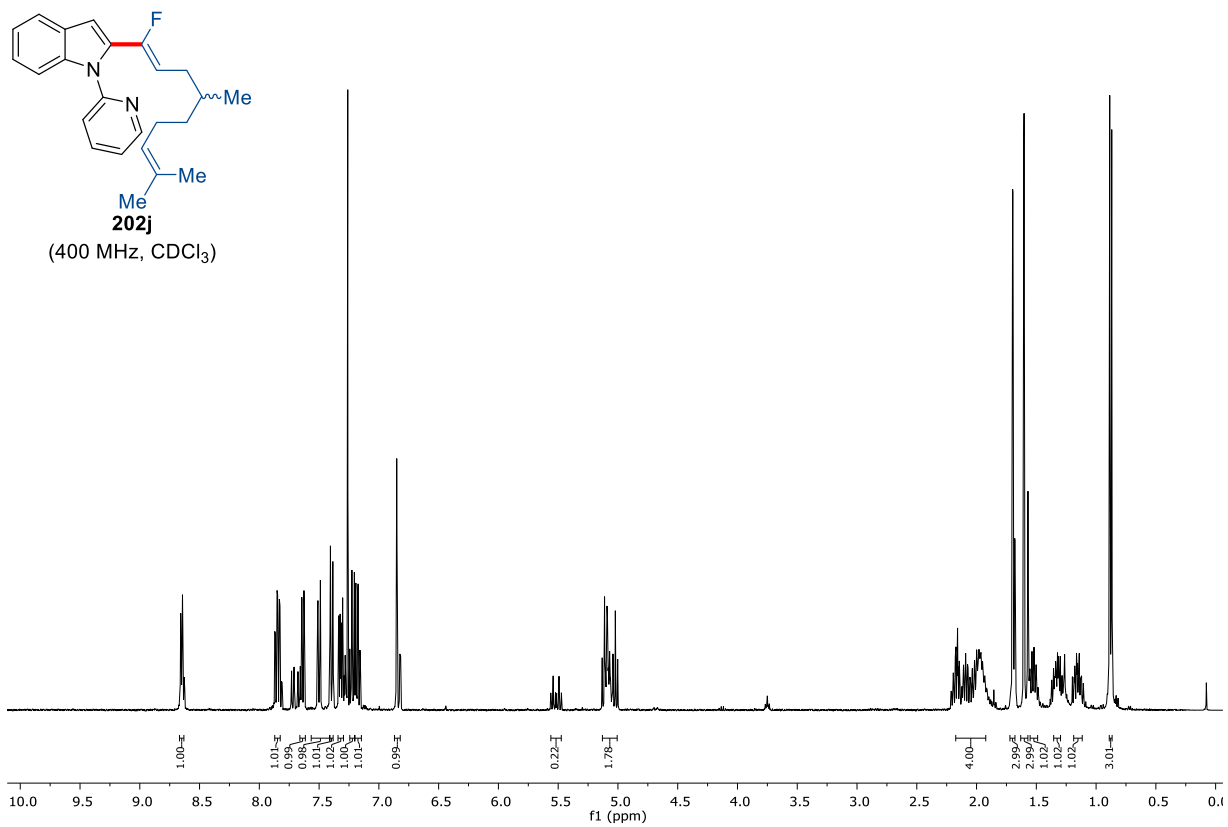


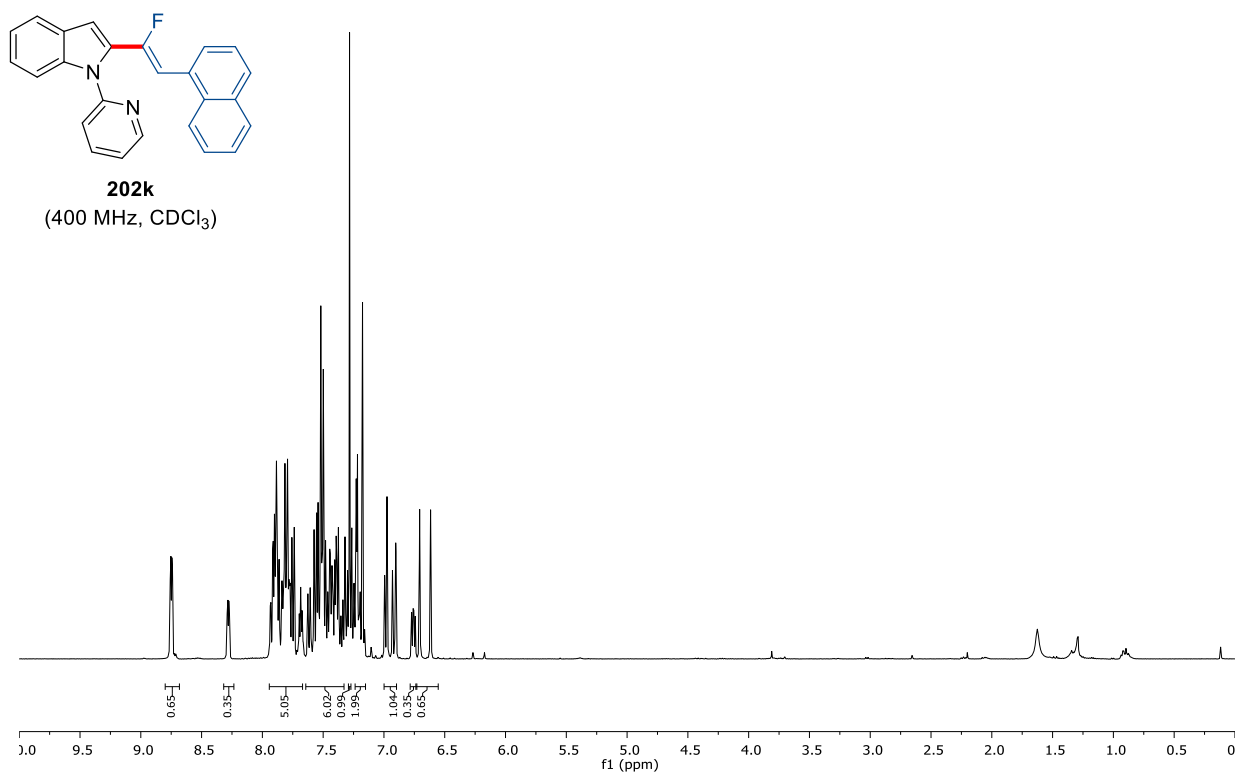
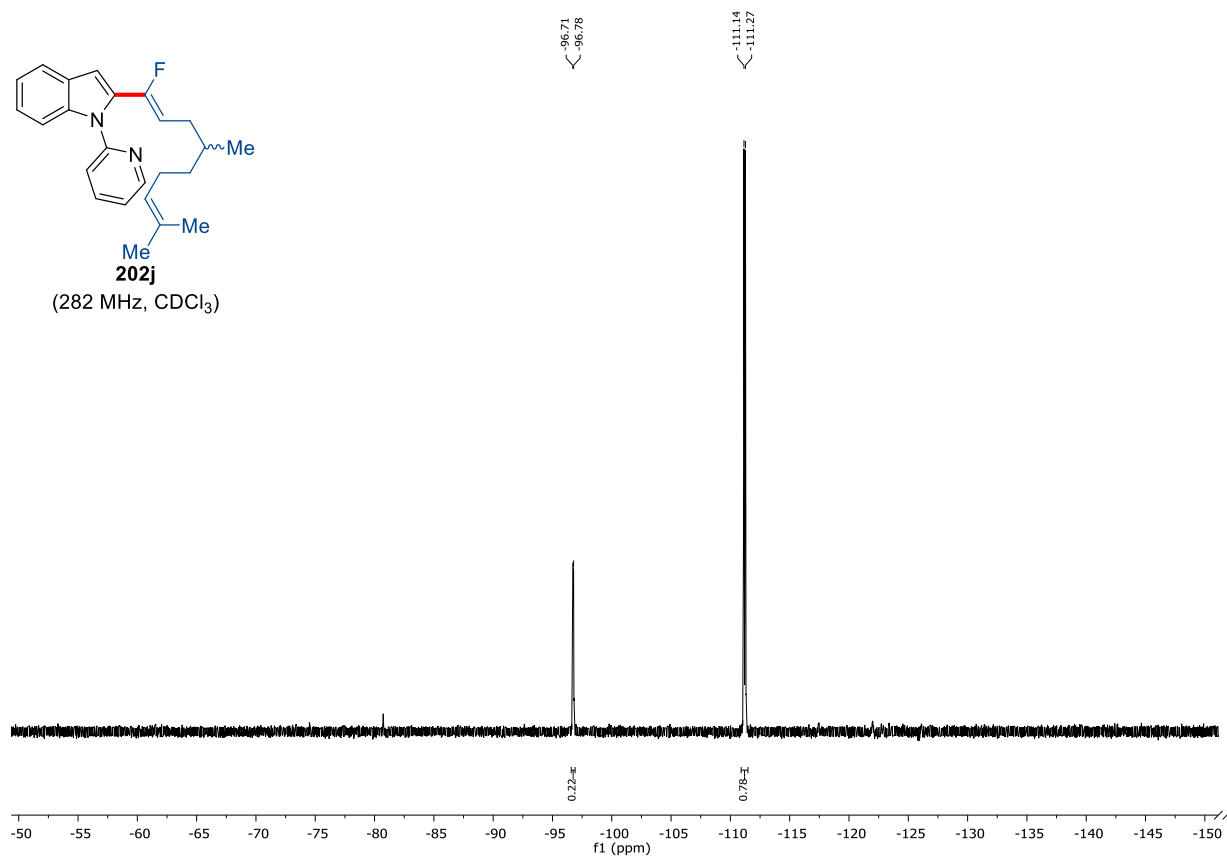
7. Appendix: NMR-Spectra and HPLC Chromatograms



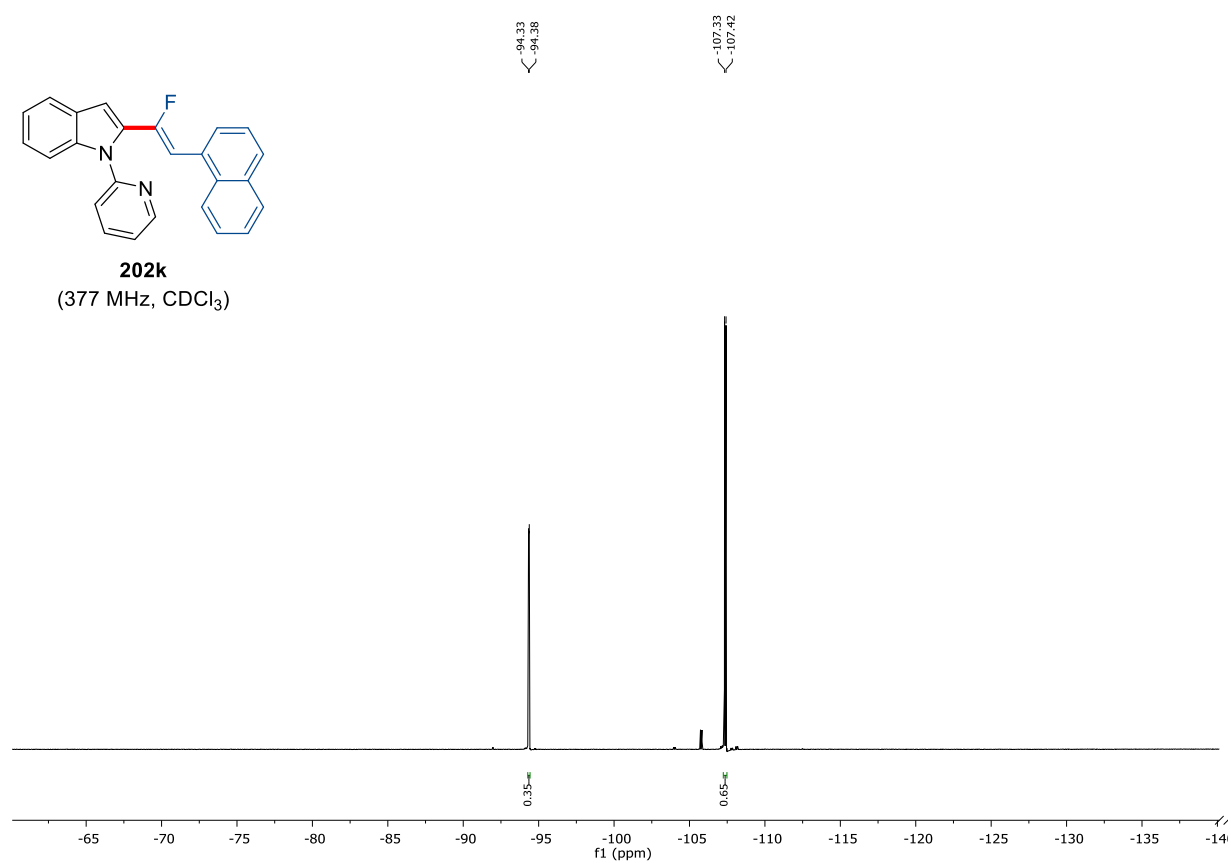
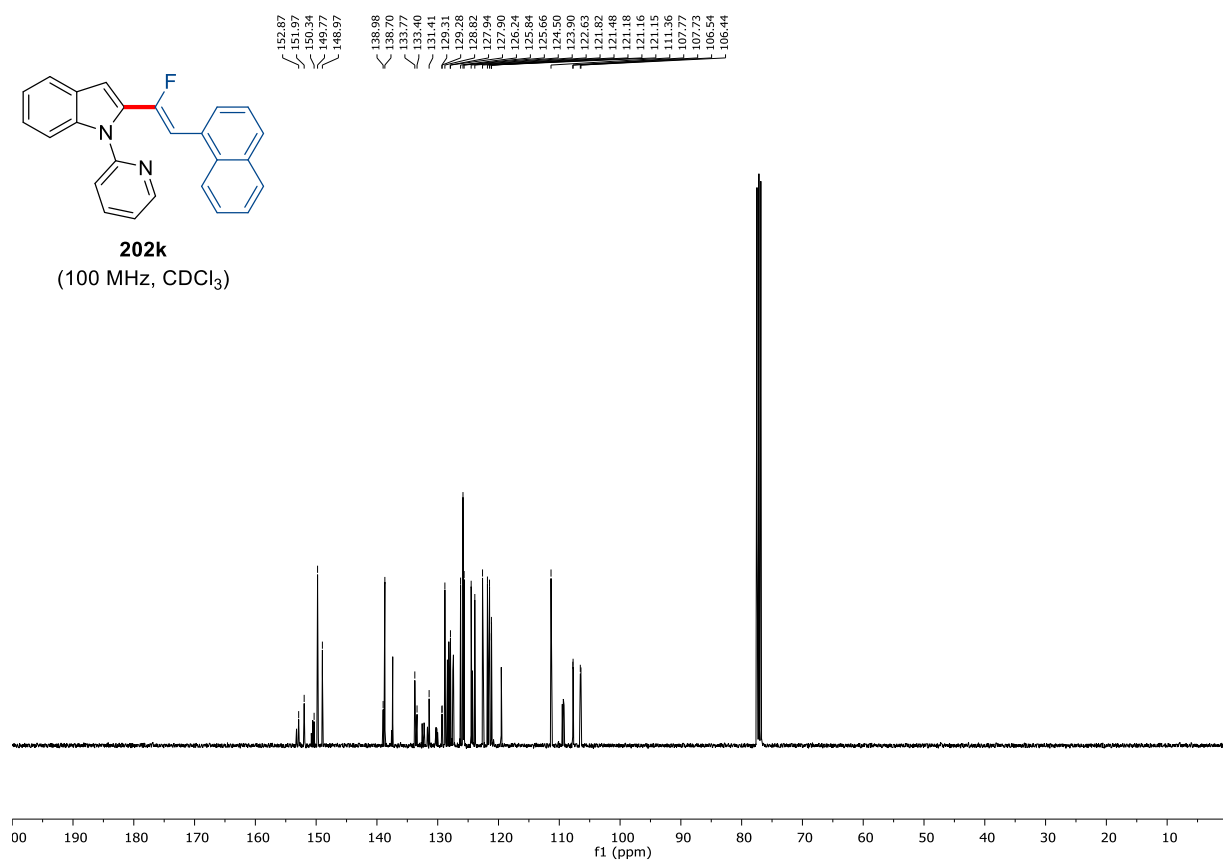


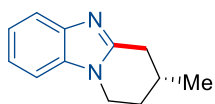
7. Appendix: NMR-Spectra and HPLC Chromatograms



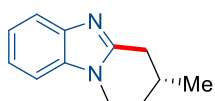
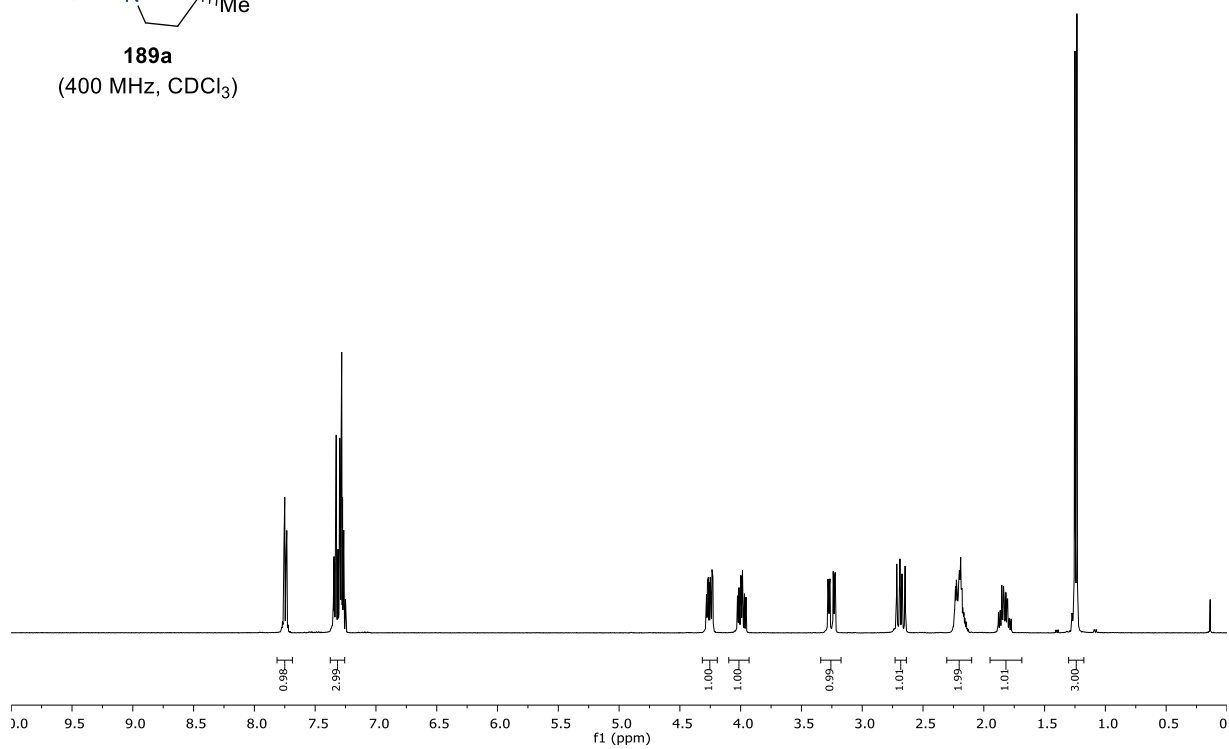


7. Appendix: NMR-Spectra and HPLC Chromatograms

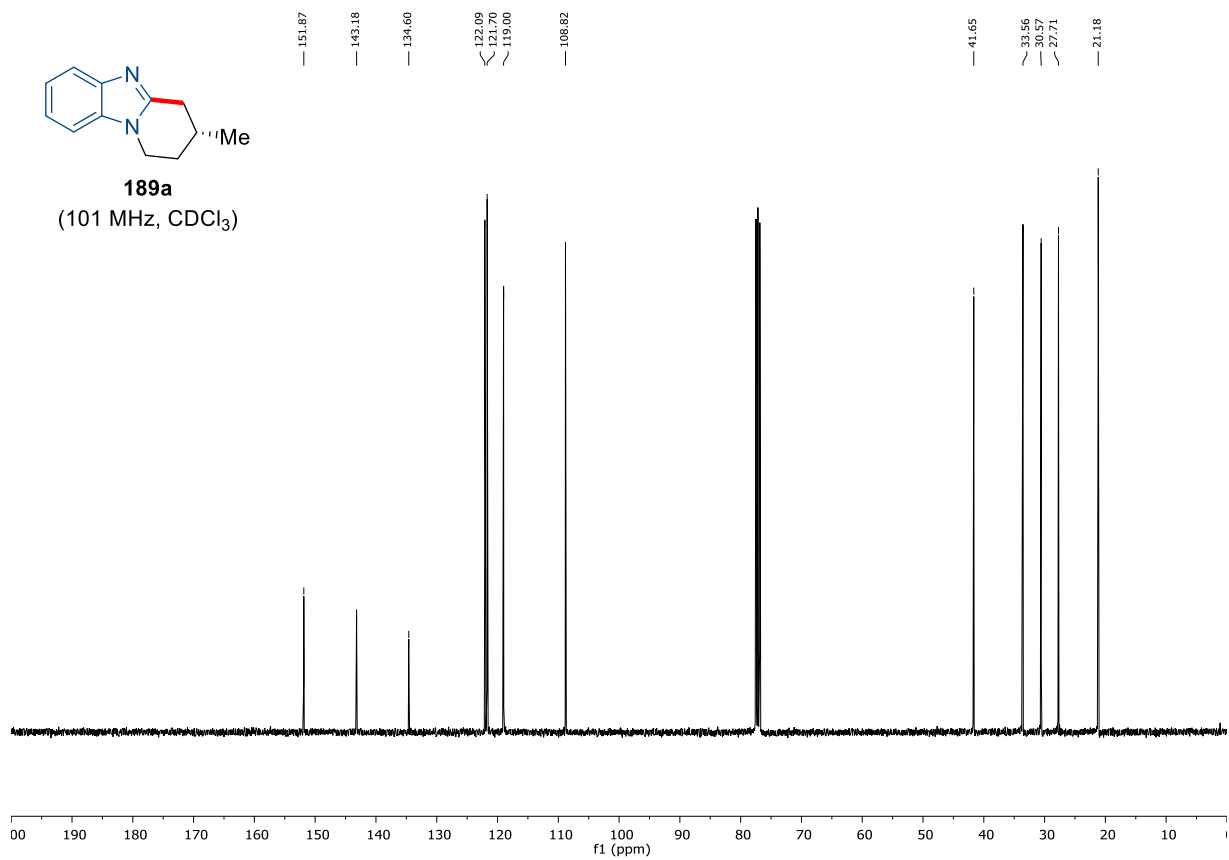




189a
(400 MHz, CDCl₃)

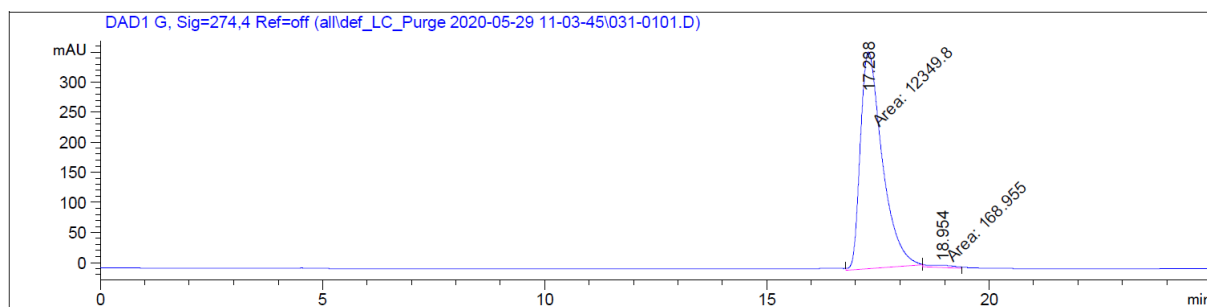


189a
(101 MHz, CDCl₃)

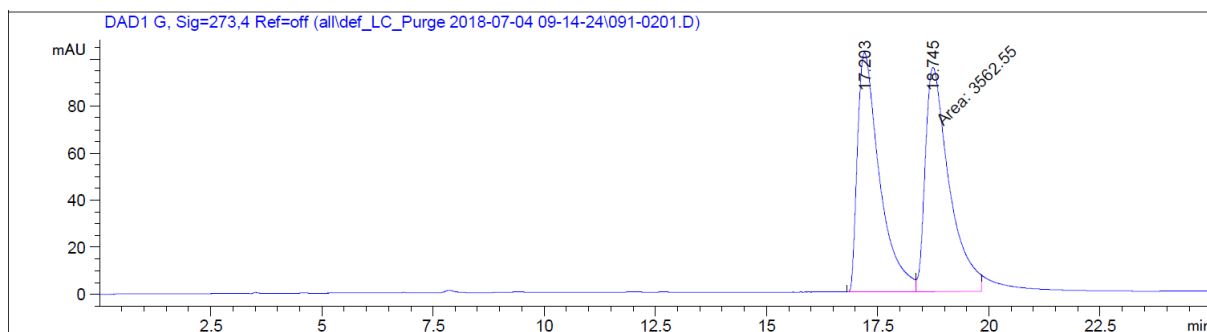


7. Appendix: NMR-Spectra and HPLC Chromatograms

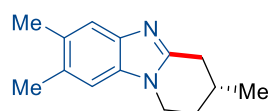
Chiral HPLC of **189a**



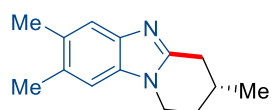
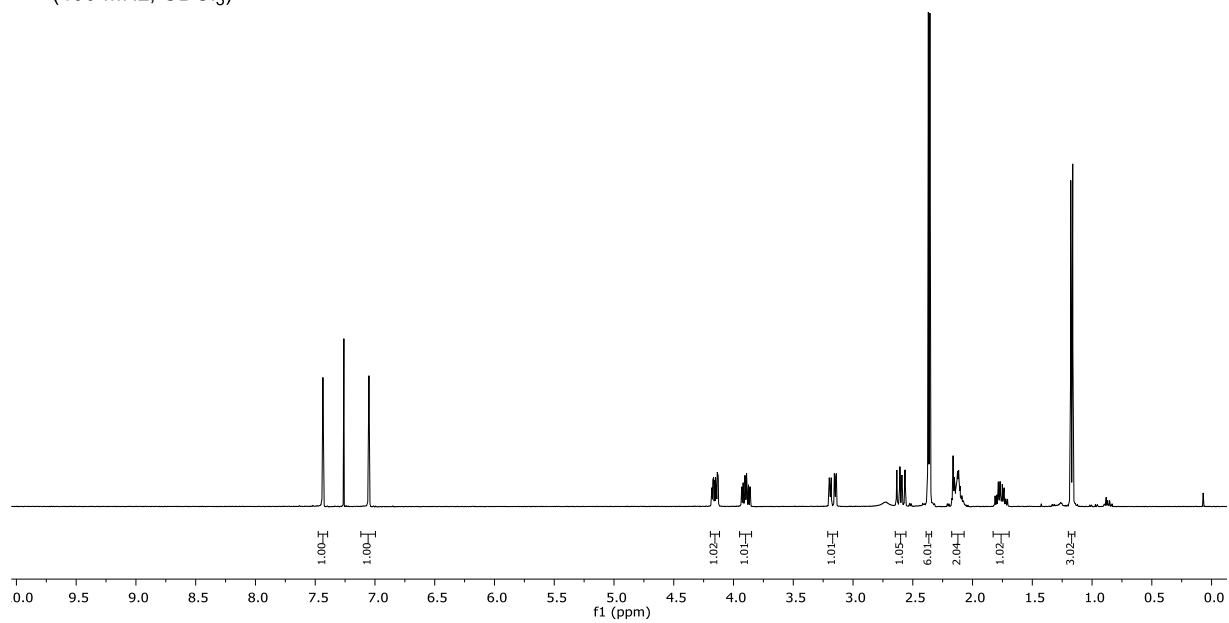
Peak #	RetTime [min]	Type	Width [min]	Area [mAU*s]	Height [mAU]	Area %
1	17.288	MM	0.5712	1.23498e4	360.37155	98.6504
2	18.954	MM	0.6959	168.95505	4.04670	1.3496



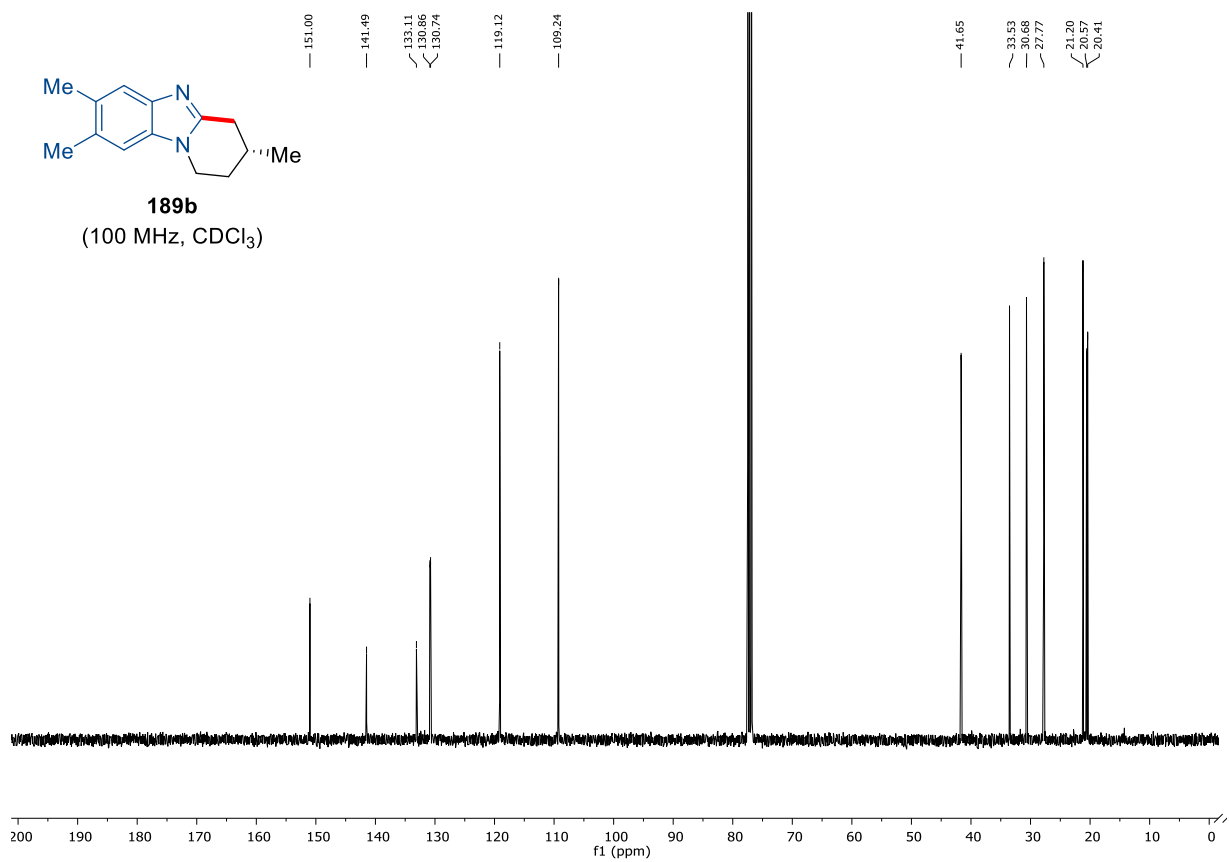
Peak #	RetTime [min]	Type	Width [min]	Area [mAU*s]	Height [mAU]	Area %
1	17.203	BV	0.5119	3516.55786	101.82705	49.6752
2	18.745	MF	0.6232	3562.54932	95.27898	50.3248

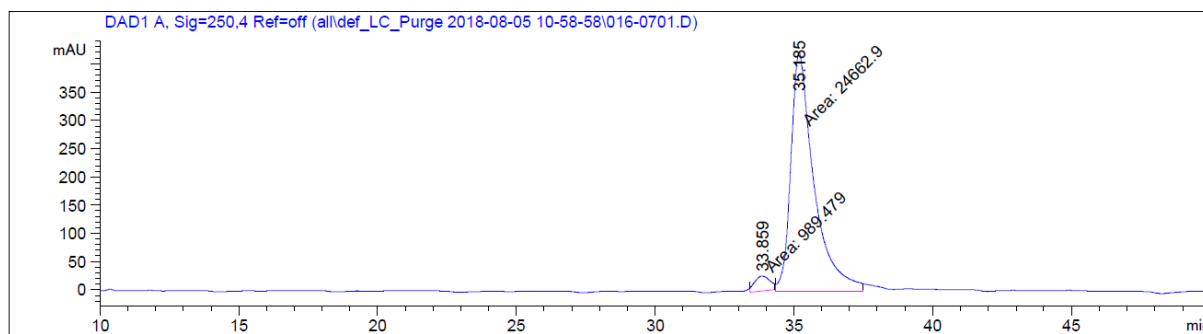


189b
(400 MHz, CDCl₃)

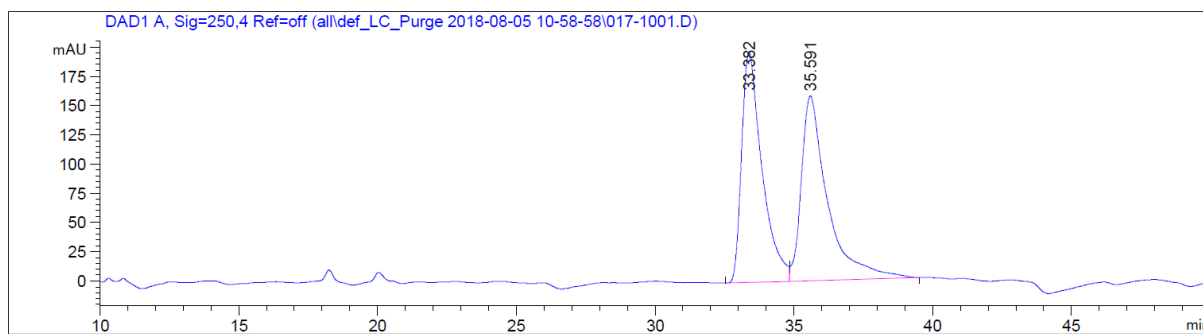


189b
(100 MHz, CDCl₃)

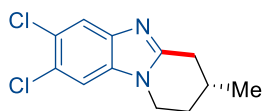


Chiral HPLC of **189b**

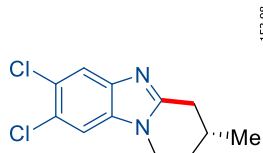
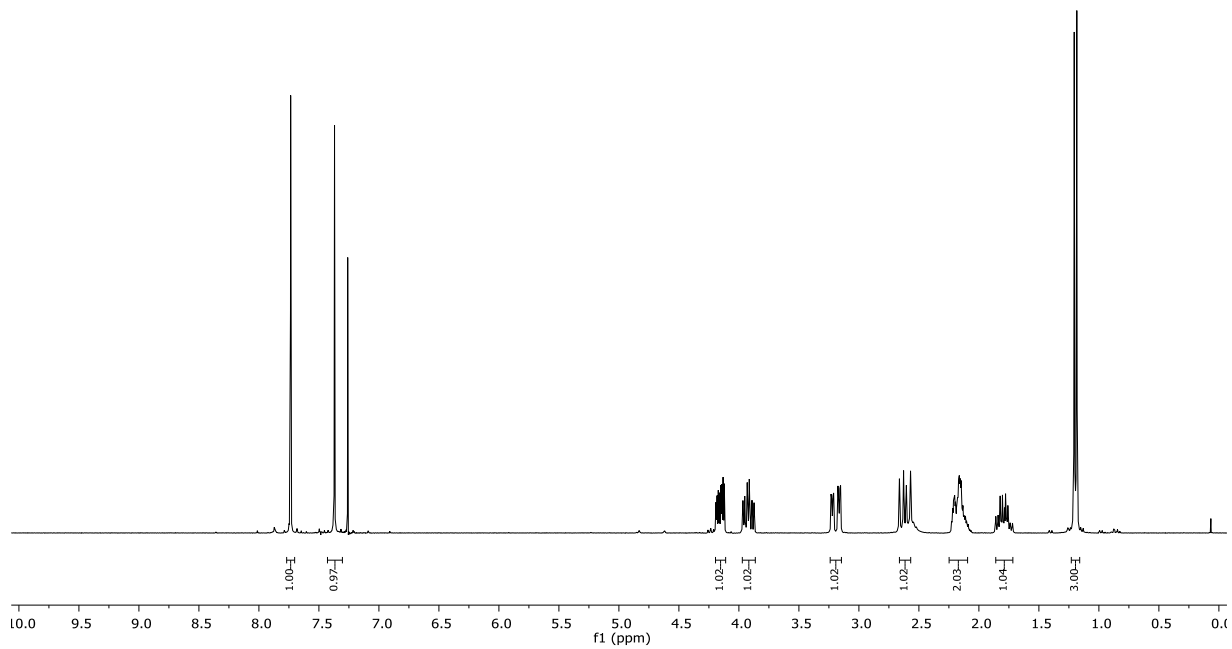
Peak #	RetTime [min]	Type	Width [min]	Area [mAU*s]	Height [mAU]	Area %
1	33.859	MM	0.6314	989.47949	26.11733	3.8573
2	35.185	MM	0.9713	2.46629e4	423.19061	96.1427



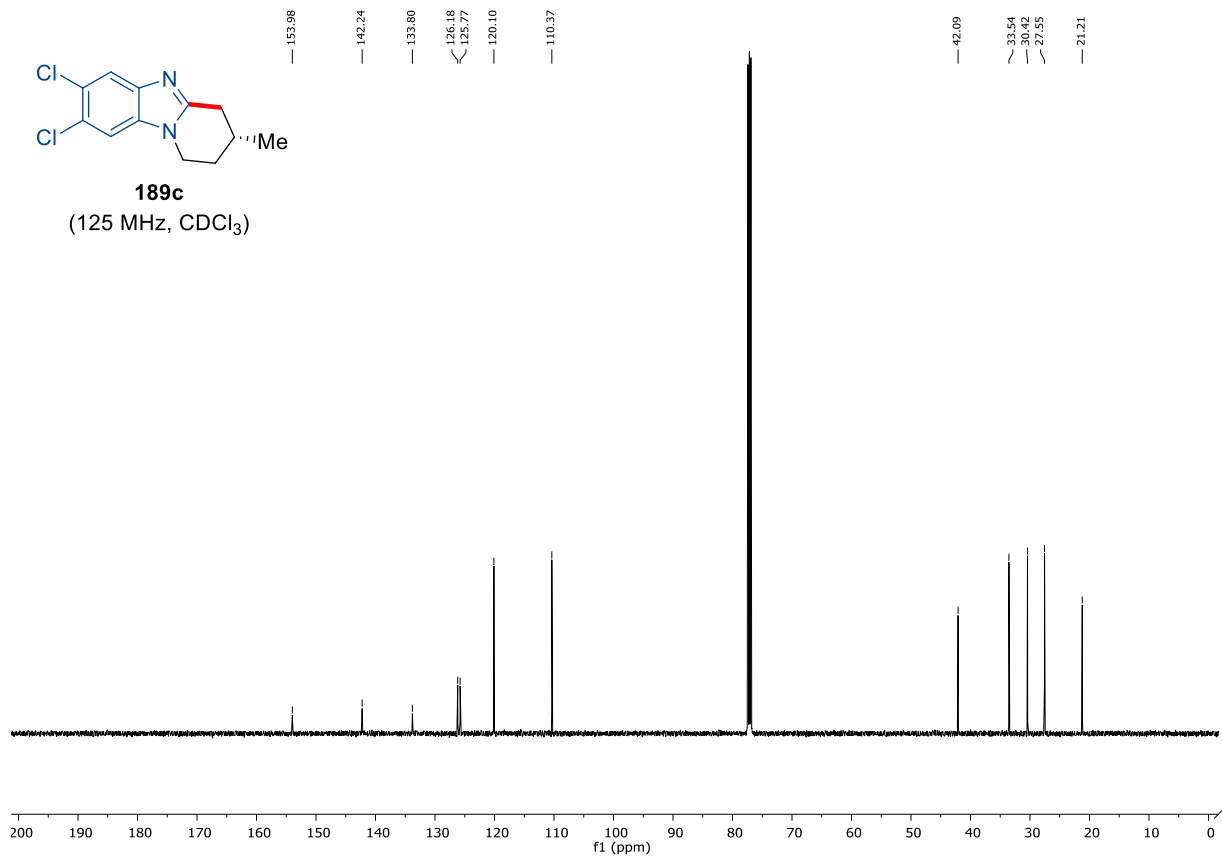
Peak #	RetTime [min]	Type	Width [min]	Area [mAU*s]	Height [mAU]	Area %
1	33.382	BV	0.7449	1.00634e4	196.68741	49.1858
2	35.591	VB	0.9349	1.03965e4	157.95943	50.8142



189c
(300 MHz, CDCl₃)

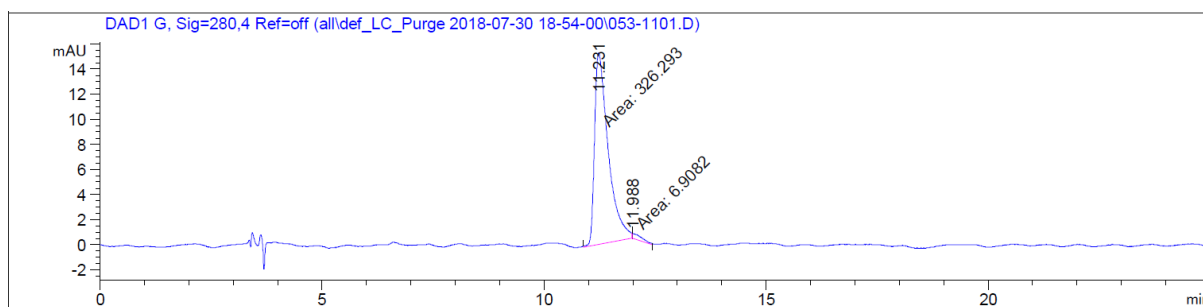


189c
(125 MHz, CDCl₃)

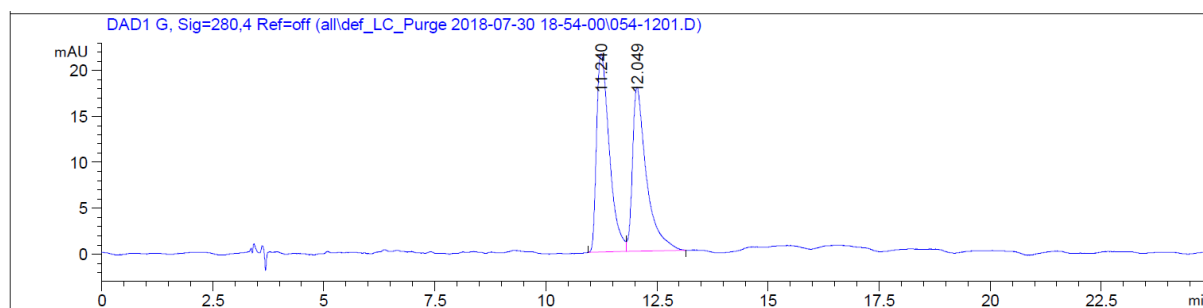


7. Appendix: NMR-Spectra and HPLC Chromatograms

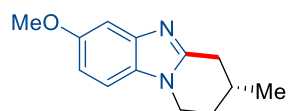
Chiral HPLC of **189c**



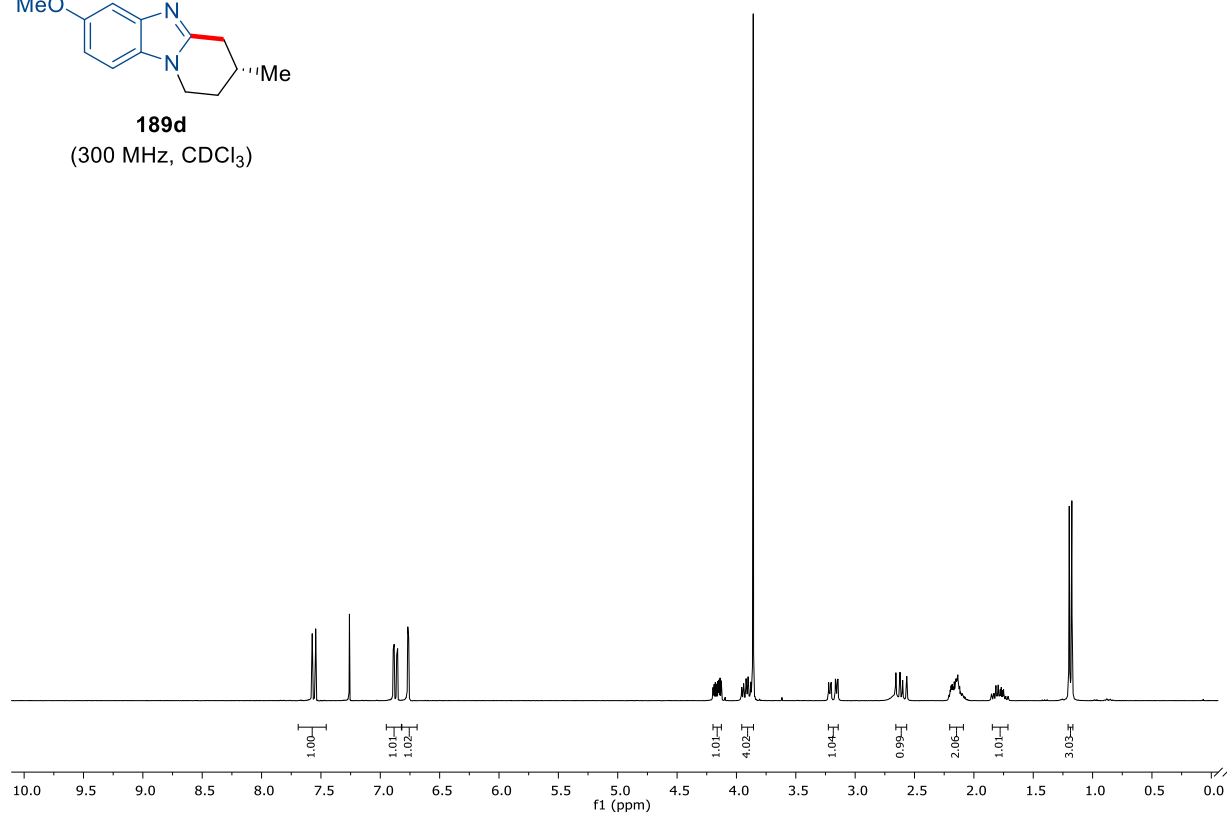
Peak #	RetTime [min]	Type	Width [min]	Area [mAU*s]	Height [mAU]	Area %
1	11.231	MM	0.3554	326.29340	15.30031	97.9267
2	11.988	MM	0.2834	6.90820	4.06213e-1	2.0733



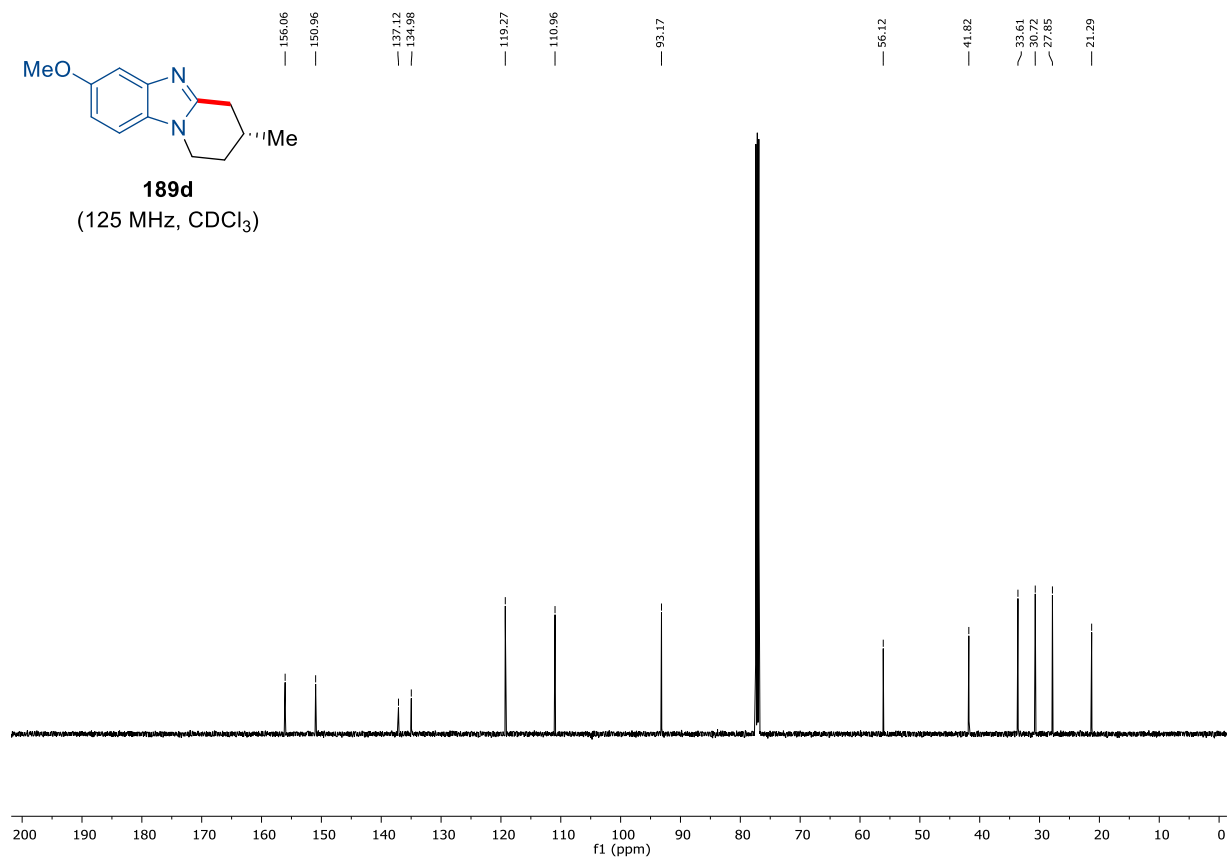
Peak #	RetTime [min]	Type	Width [min]	Area [mAU*s]	Height [mAU]	Area %
1	11.240	BV	0.3042	431.77551	21.59795	52.4443
2	12.049	VB	0.3107	391.52829	17.86267	47.5557

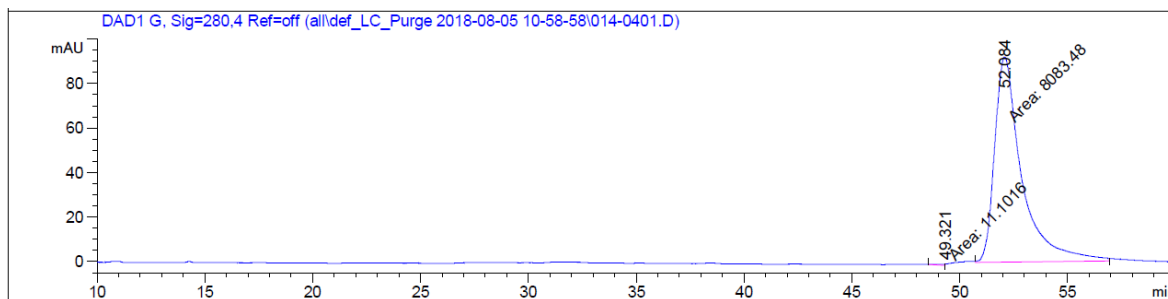


189d
(300 MHz, CDCl₃)

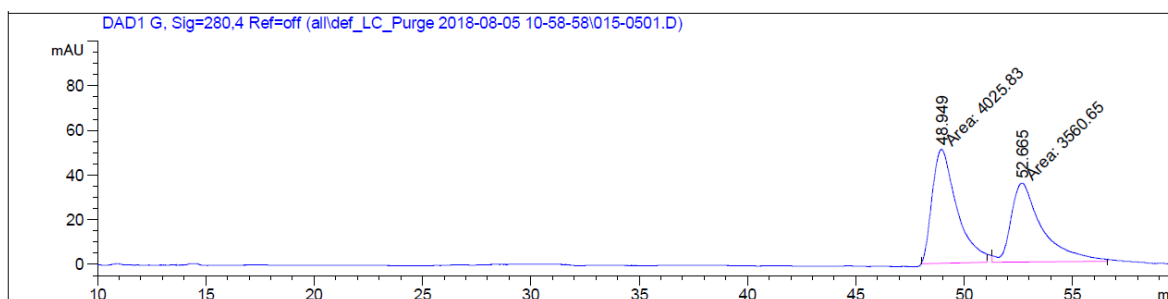


189d
(125 MHz, CDCl₃)

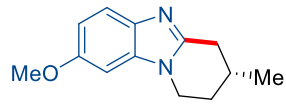


Chiral HPLC of **189d**

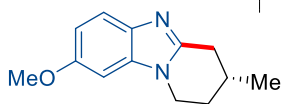
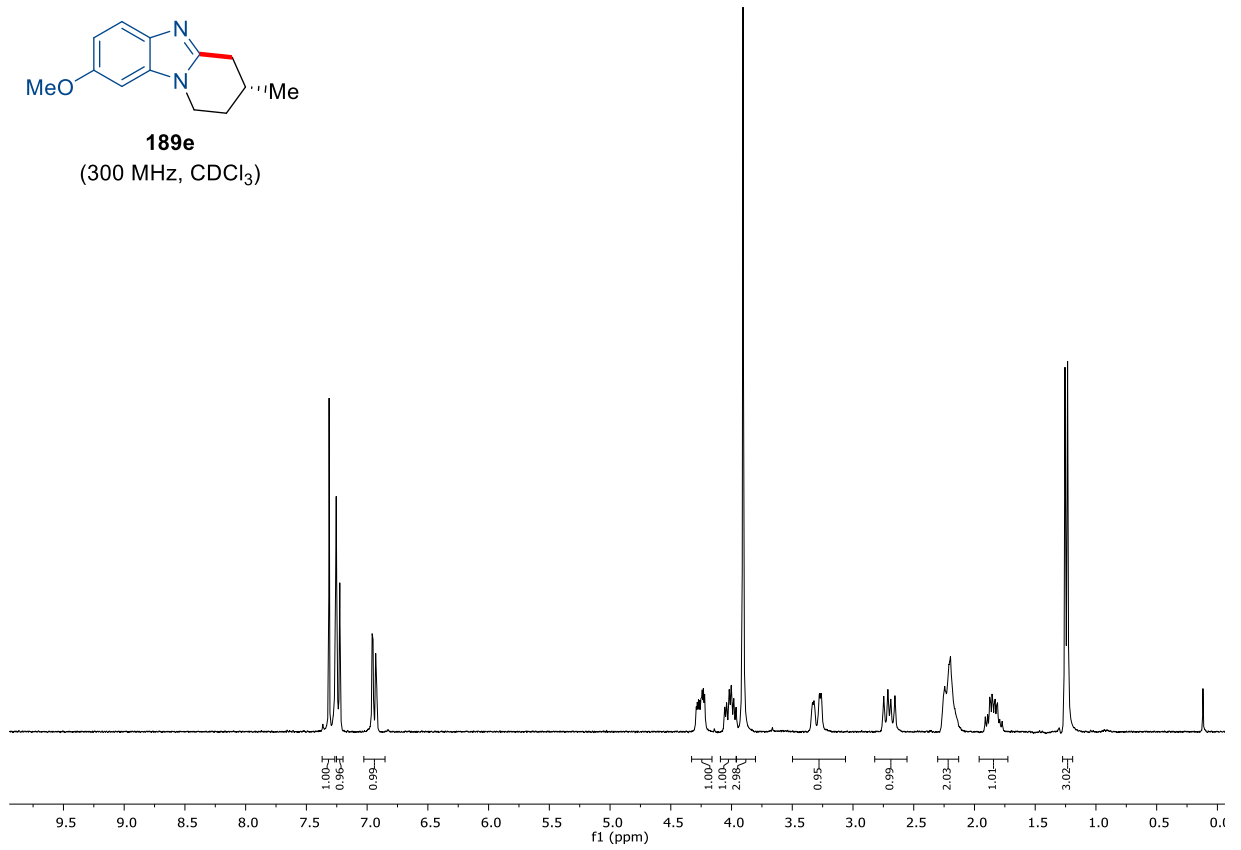
Peak #	RetTime [min]	Type	Width [min]	Area [mAU*s]	Height [mAU]	Area %
1	49.321	MM	0.3402	11.10163	5.43940e-1	0.1371
2	52.084	MM	1.4592	8083.47949	92.32921	99.8629



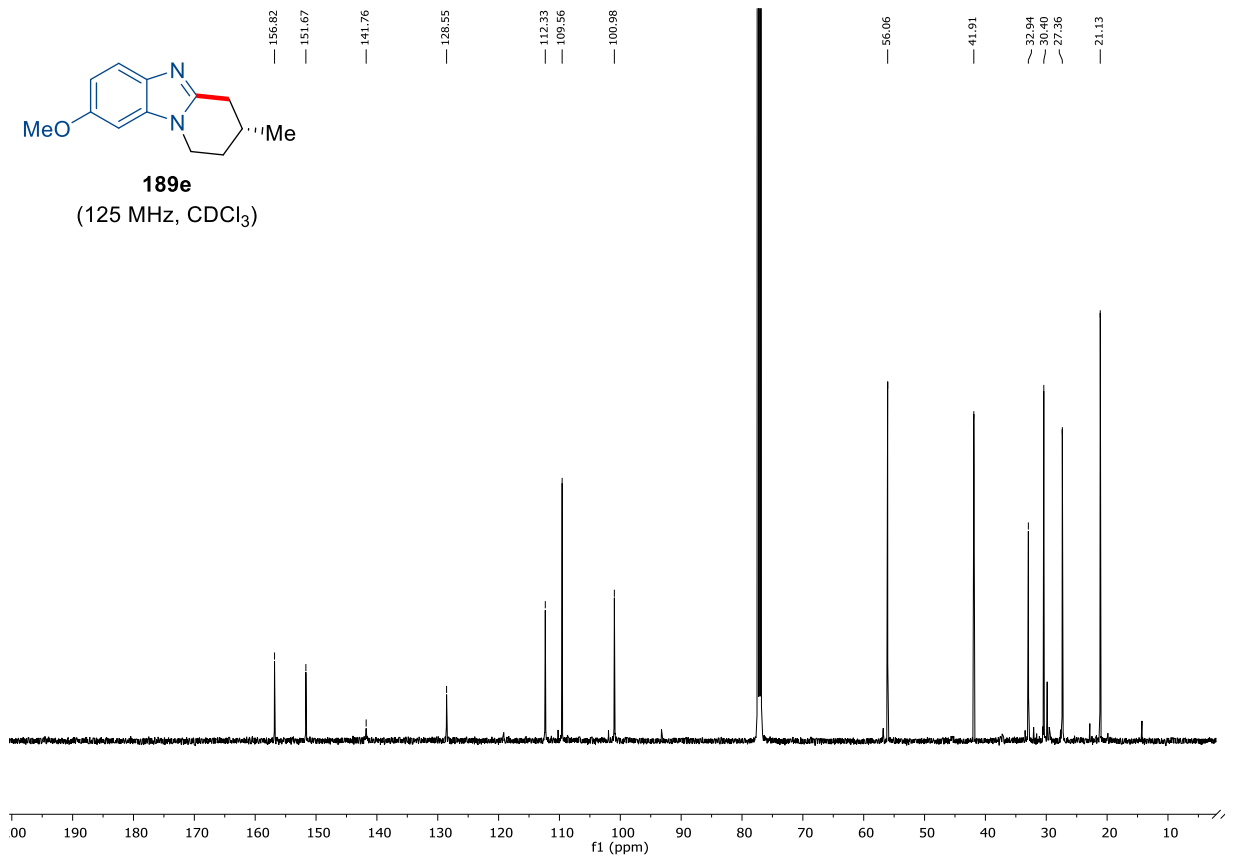
Peak #	RetTime [min]	Type	Width [min]	Area [mAU*s]	Height [mAU]	Area %
1	48.949	MM	1.3151	4025.82739	51.02060	53.0658
2	52.665	MM	1.6762	3560.64868	35.40374	46.9342



189e
(300 MHz, CDCl₃)

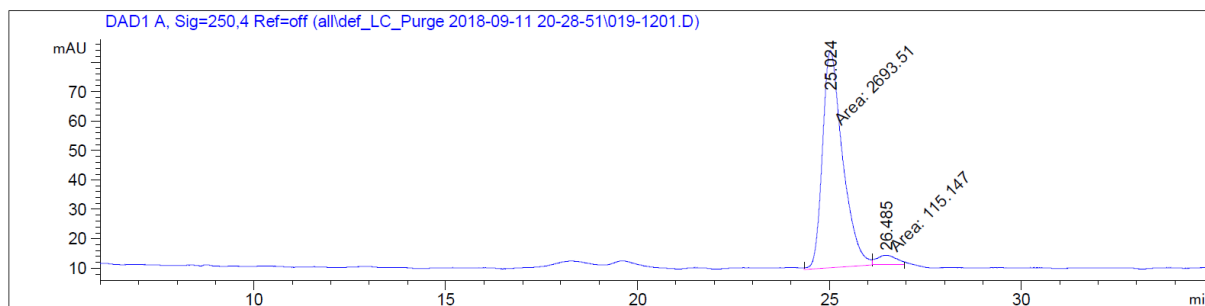


189e
(125 MHz, CDCl₃)

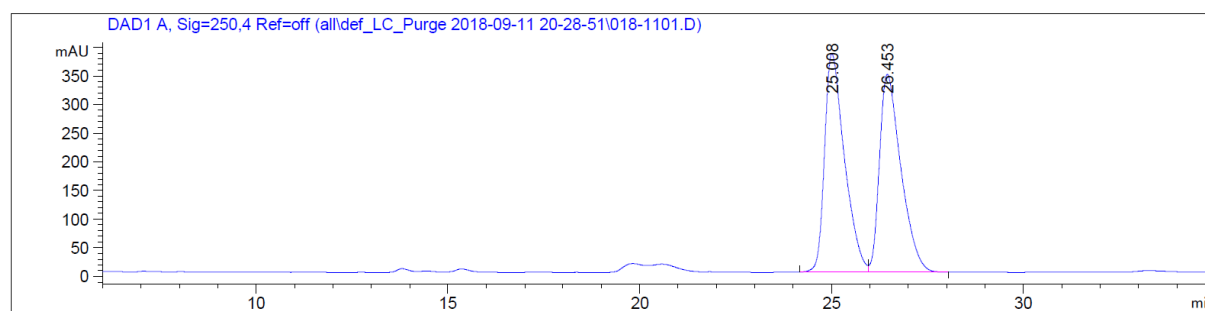


7. Appendix: NMR-Spectra and HPLC Chromatograms

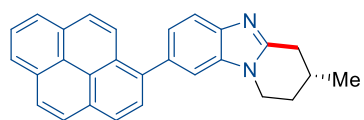
Chiral HPLC of **189e**



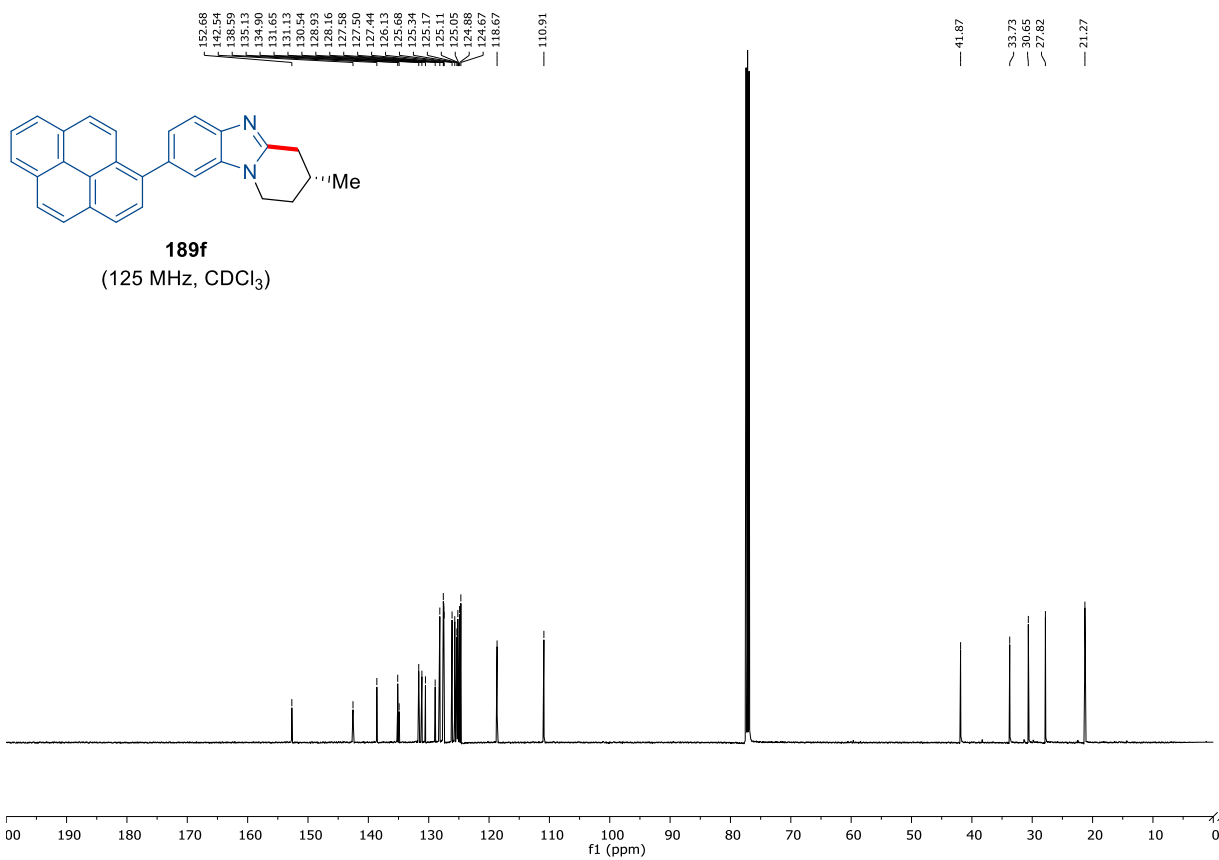
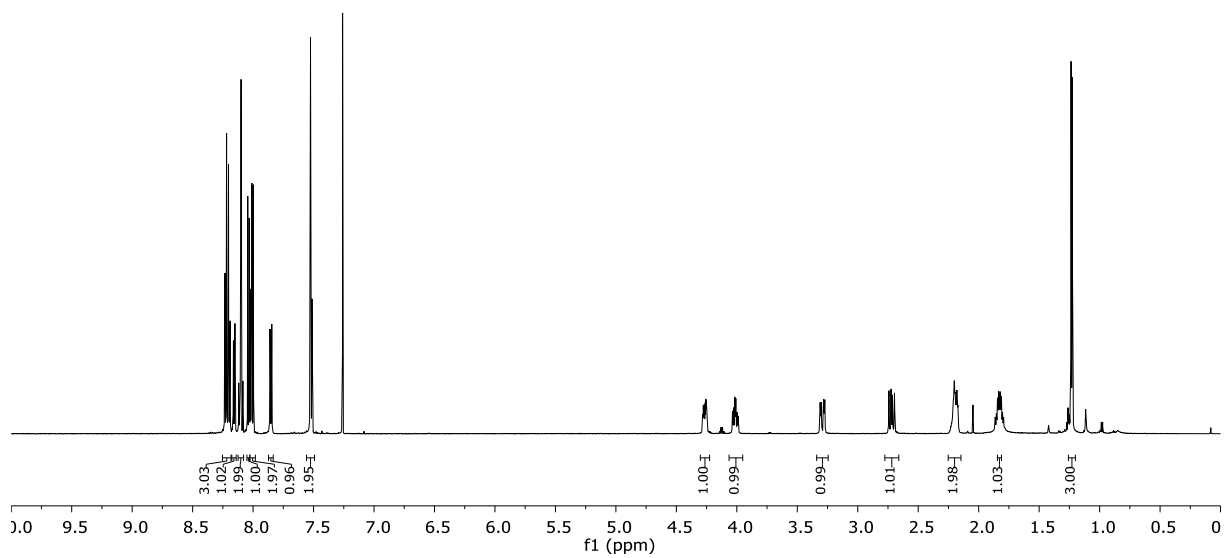
Peak #	RetTime [min]	Type	Width [min]	Area [mAU*s]	Height [mAU]	Area %
1	25.024	MM	0.6086	2693.50537	73.76445	95.9003
2	26.485	MM	0.6029	115.14696	3.18296	4.0997

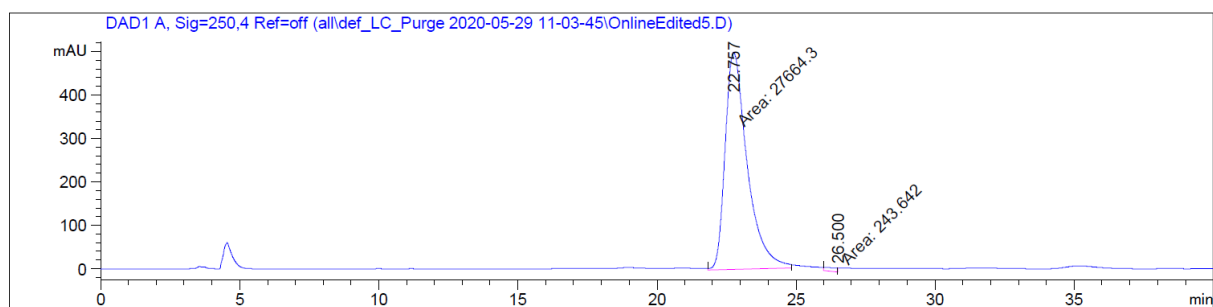


Peak #	RetTime [min]	Type	Width [min]	Area [mAU*s]	Height [mAU]	Area %
1	25.008	BV	0.5307	1.37499e4	381.29388	50.5553
2	26.453	VB	0.5710	1.34479e4	345.54178	49.4447

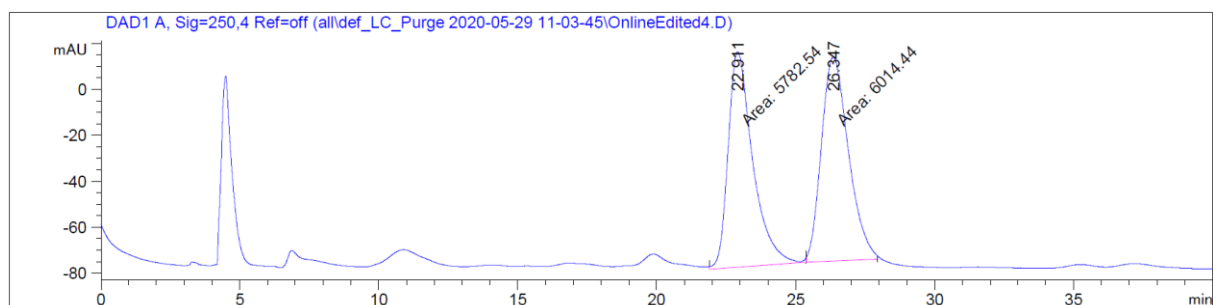


189f
(600 MHz, CDCl₃)

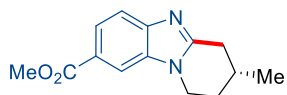


Chiral HPLC of **189f**

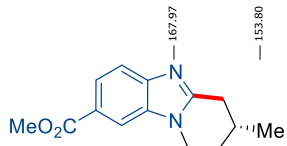
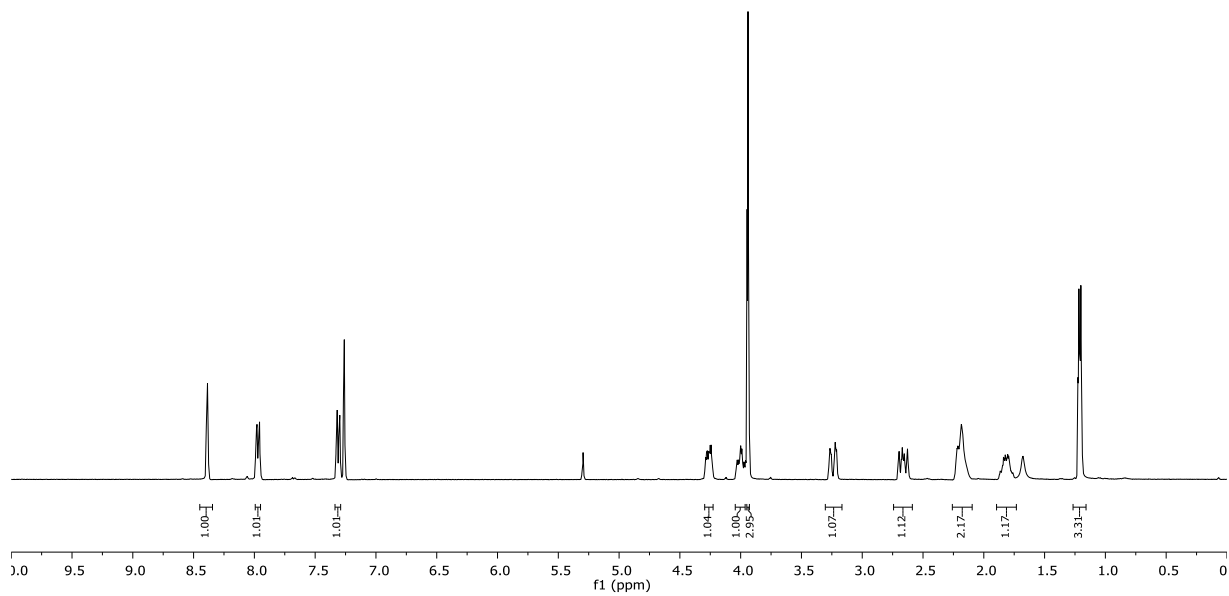
Peak #	RetTime [min]	Type	Width [min]	Area [mAU*s]	Height [mAU]	Area %
1	22.757	MM	0.9220	2.76643e4	500.07278	99.1270
2	26.500	MM	0.4372	243.64198	9.28818	0.8730



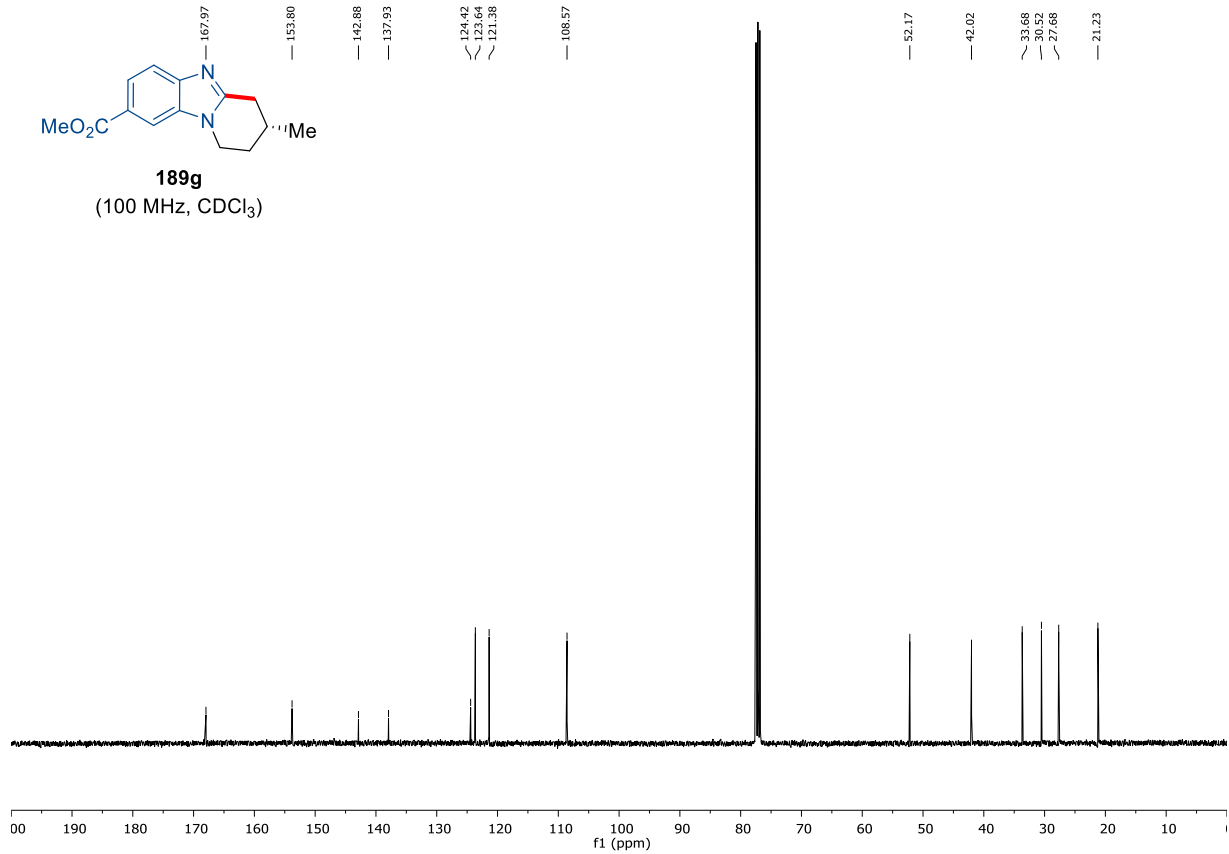
Peak #	RetTime [min]	Type	Width [min]	Area [mAU*s]	Height [mAU]	Area %
1	22.911	MM	1.0257	5782.54199	93.96201	49.0171
2	26.347	MM	1.1287	6014.43652	88.80775	50.9829



189g
(400 MHz, CDCl₃)

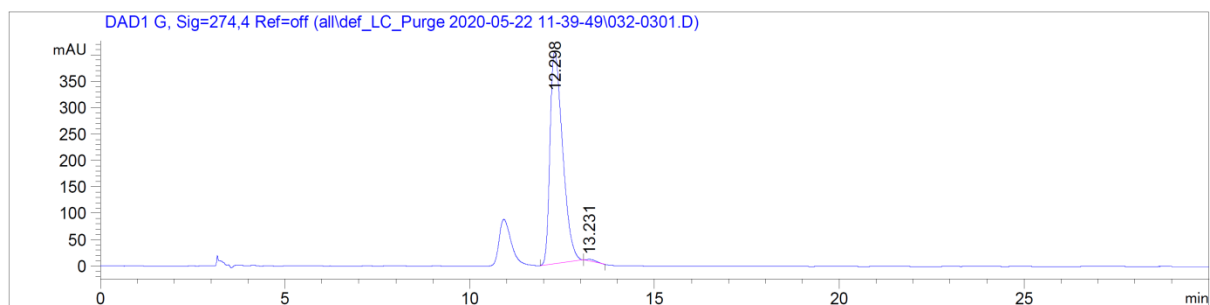


189g
(100 MHz, CDCl₃)

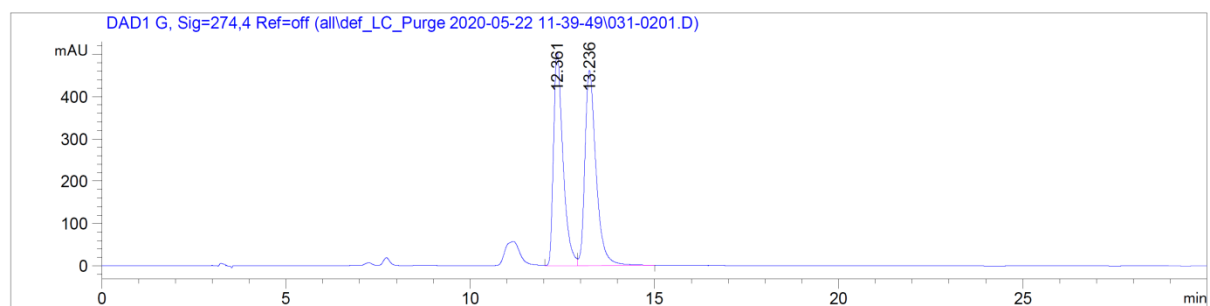


7. Appendix: NMR-Spectra and HPLC Chromatograms

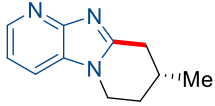
Chiral HPLC of **189g**



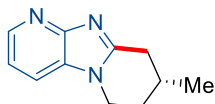
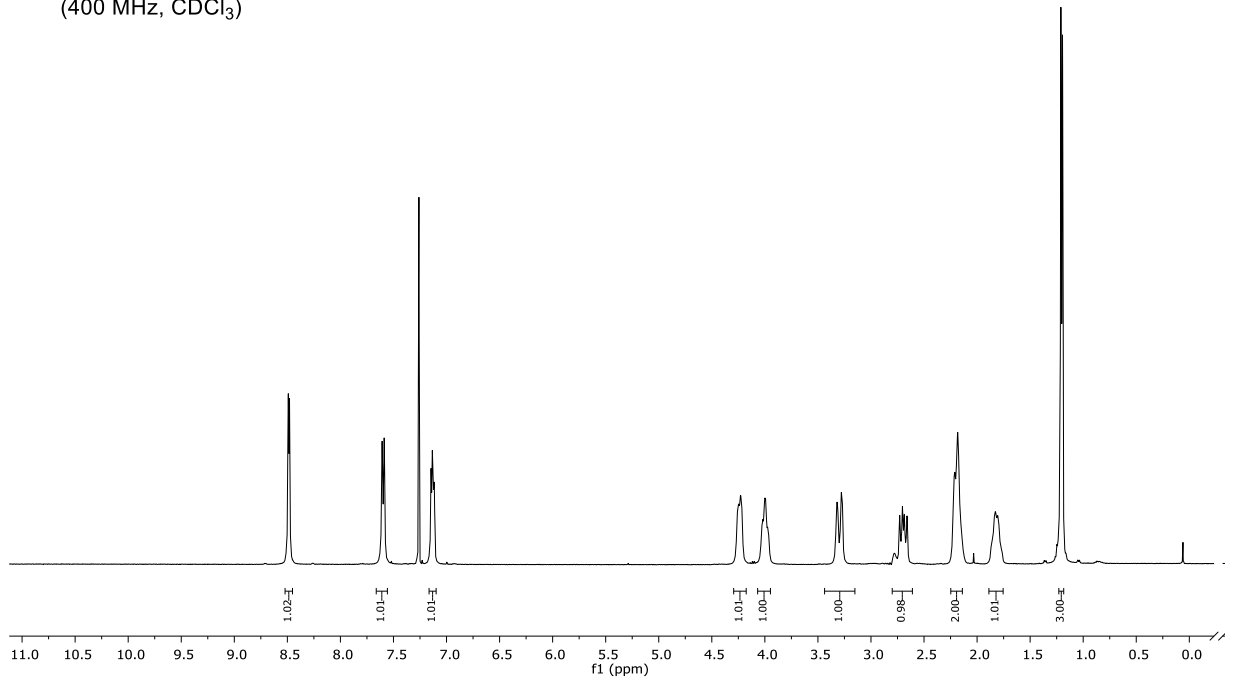
Peak #	RetTime [min]	Type	Width [min]	Area [mAU*s]	Height [mAU]	Area %
1	12.298	BB	0.3727	9539.14453	402.27072	99.3085
2	13.231	BB	0.2895	66.41808	3.31827	0.6915



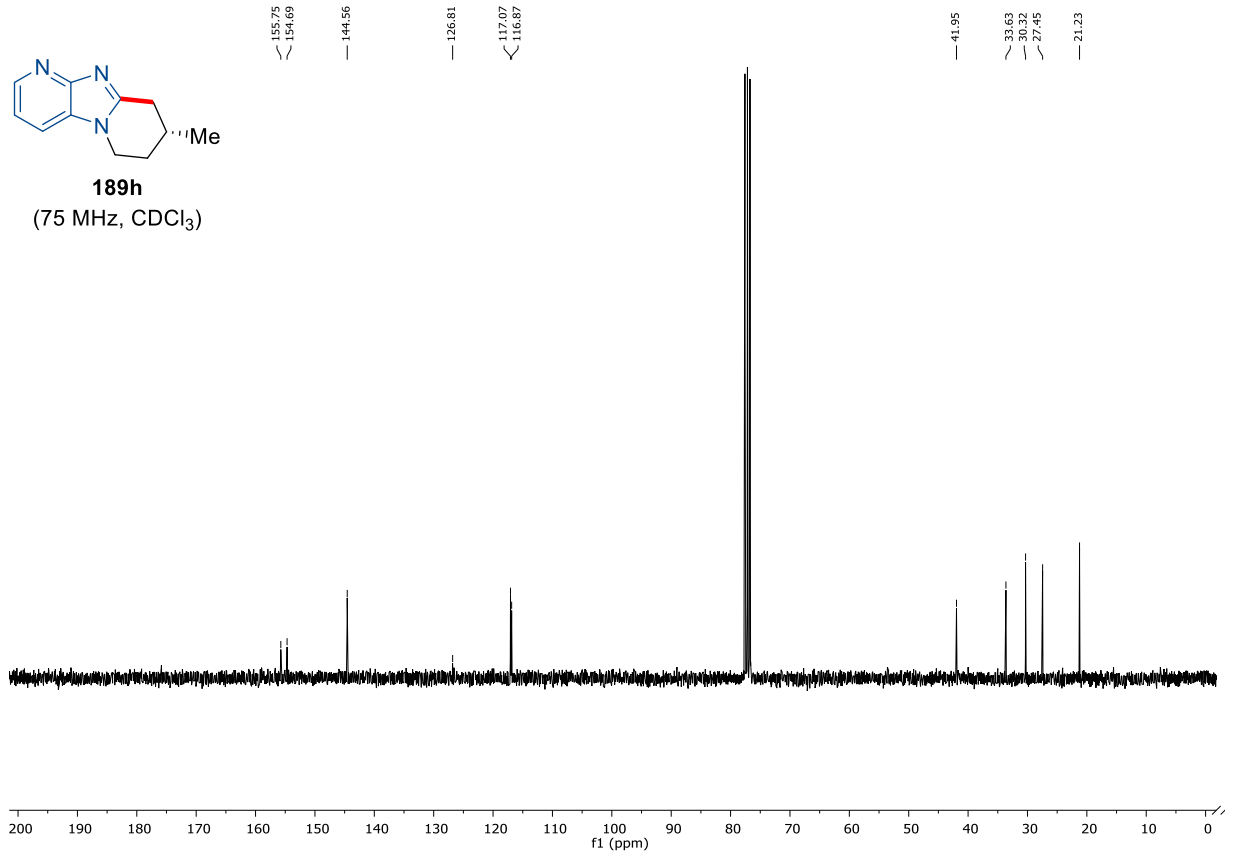
Peak #	RetTime [min]	Type	Width [min]	Area [mAU*s]	Height [mAU]	Area %
1	12.361	VV	0.2681	8986.92676	503.84906	48.1402
2	13.236	VB	0.3179	9681.32324	461.16260	51.8598

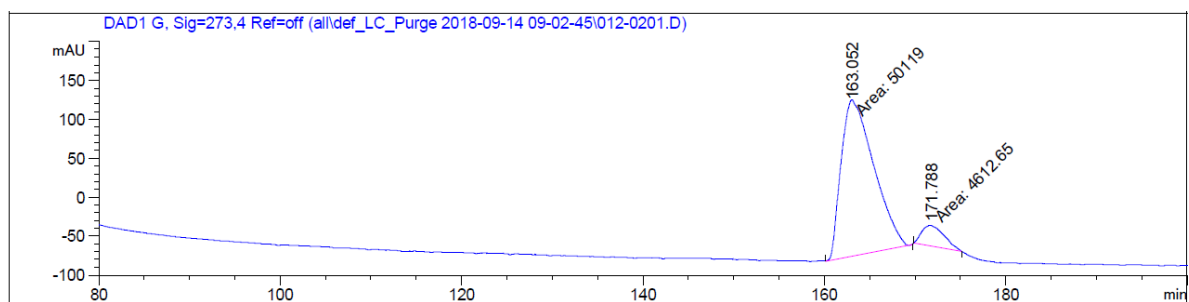


189h
(400 MHz, CDCl₃)

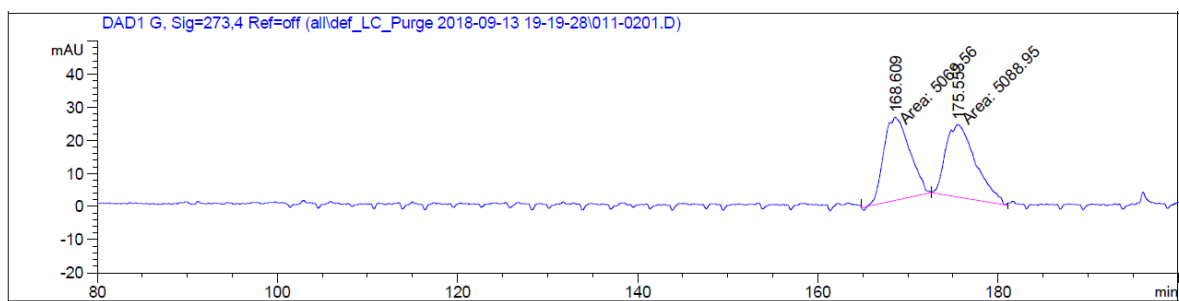


189h
(75 MHz, CDCl₃)

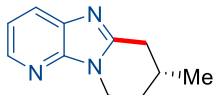


Chiral HPLC of **189h**

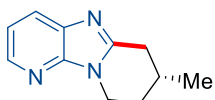
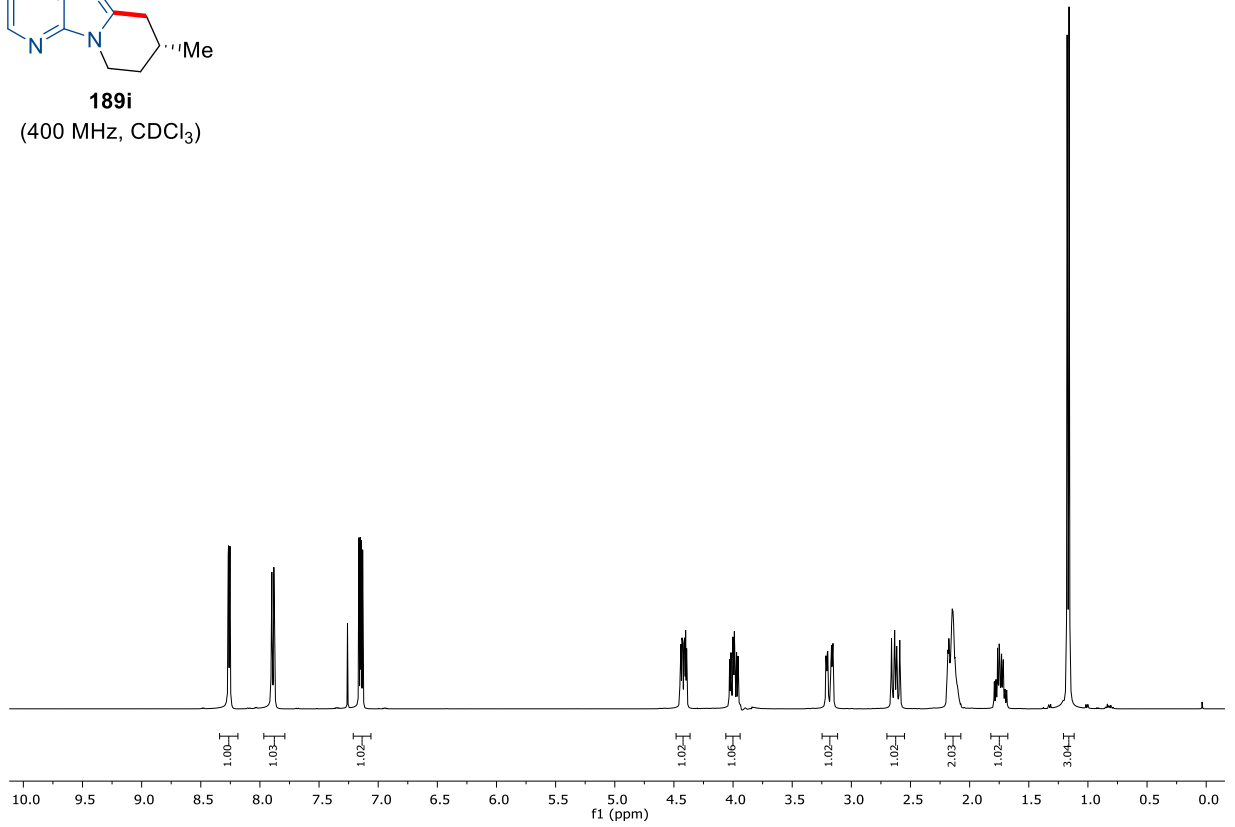
Peak #	RetTime [min]	Type	Width [min]	Area [mAU*s]	Height [mAU]	Area %
1	163.052	MM	4.1569	5.01190e4	200.94647	91.5722
2	171.788	MM	2.9064	4612.65430	26.45112	8.4278



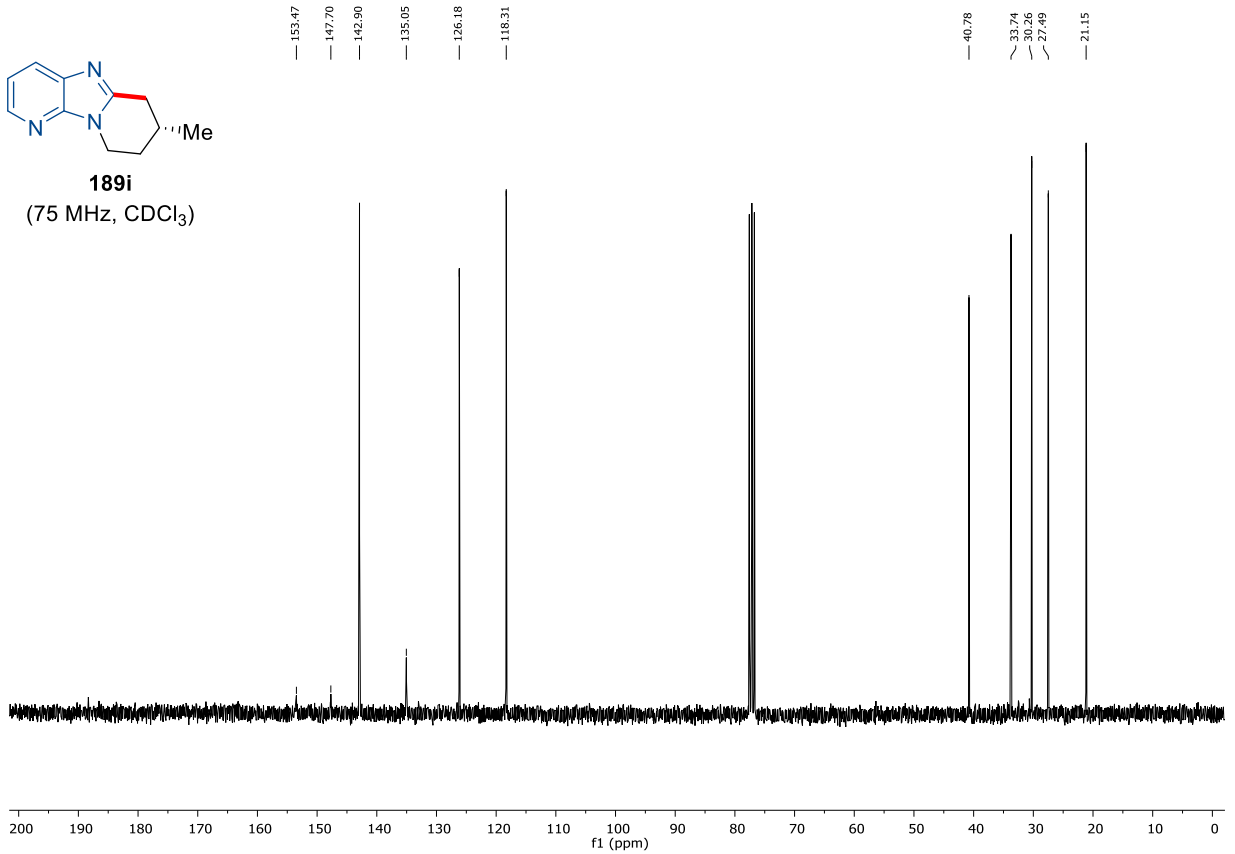
Peak #	RetTime [min]	Type	Width [min]	Area [mAU*s]	Height [mAU]	Area %
1	168.609	MM	3.3619	5069.55615	25.13269	49.9045
2	175.553	MM	3.8593	5088.95459	21.97717	50.0955



189i
(400 MHz, CDCl₃)

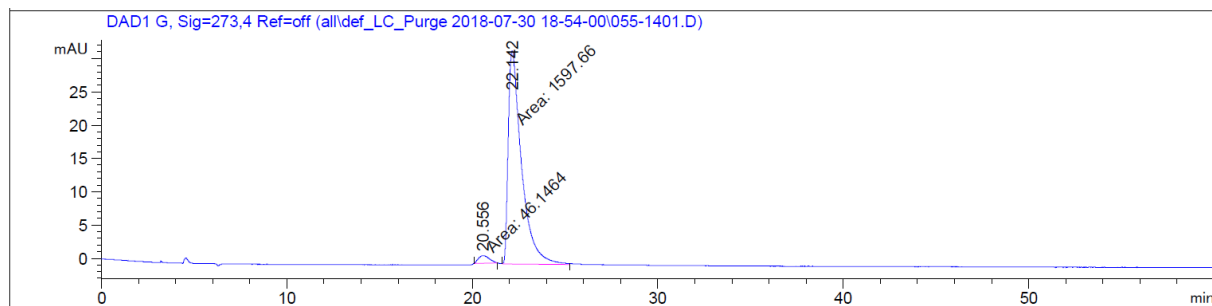


189i
(75 MHz, CDCl₃)

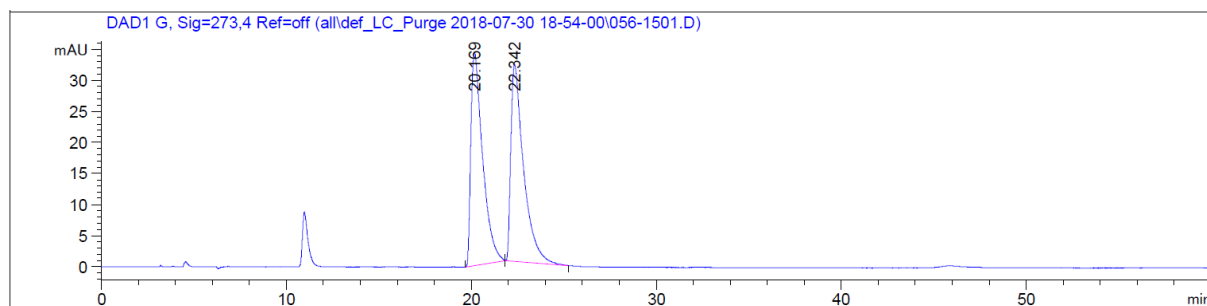


7. Appendix: NMR-Spectra and HPLC Chromatograms

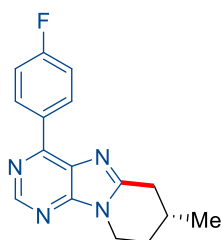
Chiral HPLC of **189i**



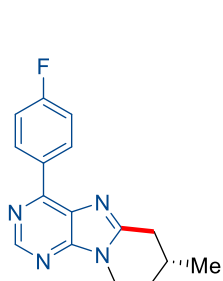
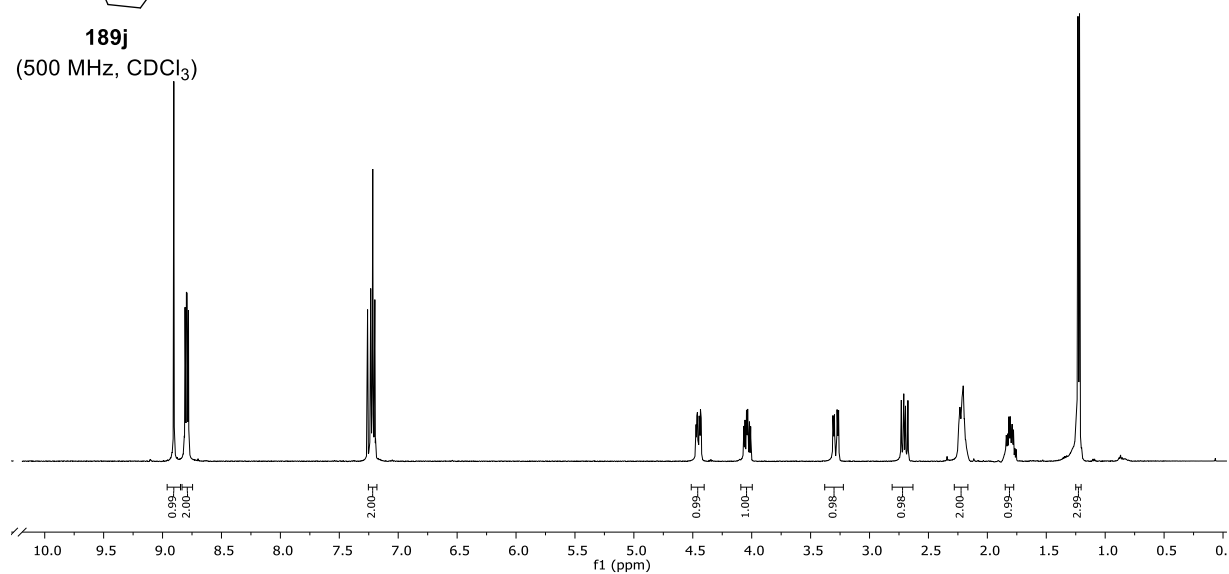
Peak #	RetTime [min]	Type	Width [min]	Area [mAU*s]	Height [mAU]	Area %
1	20.556	MM	0.6844	46.14644	1.12370	2.8073
2	22.142	MF	0.8302	1597.65625	32.07220	97.1927



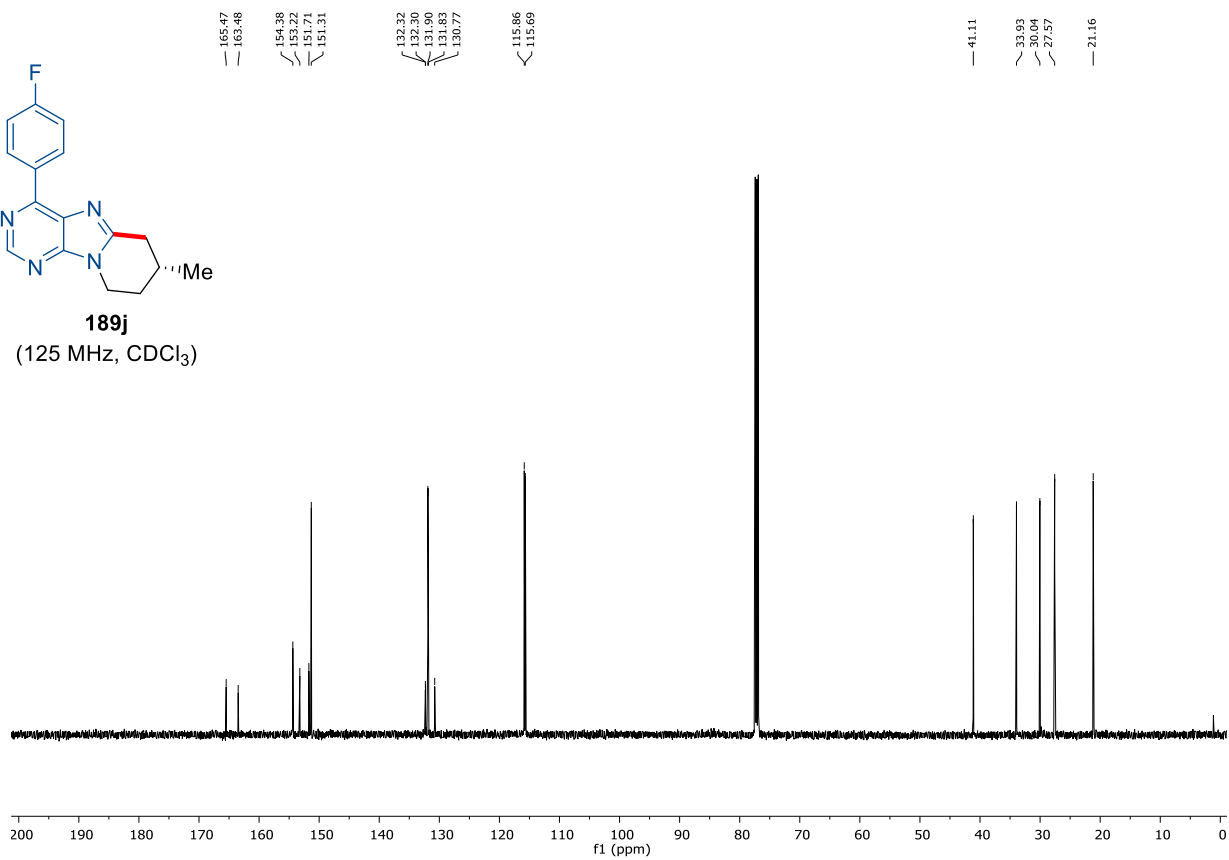
Peak #	RetTime [min]	Type	Width [min]	Area [mAU*s]	Height [mAU]	Area %
1	20.169	BB	0.6179	1511.71252	34.38778	49.9431
2	22.342	BB	0.6681	1515.15942	31.61507	50.0569



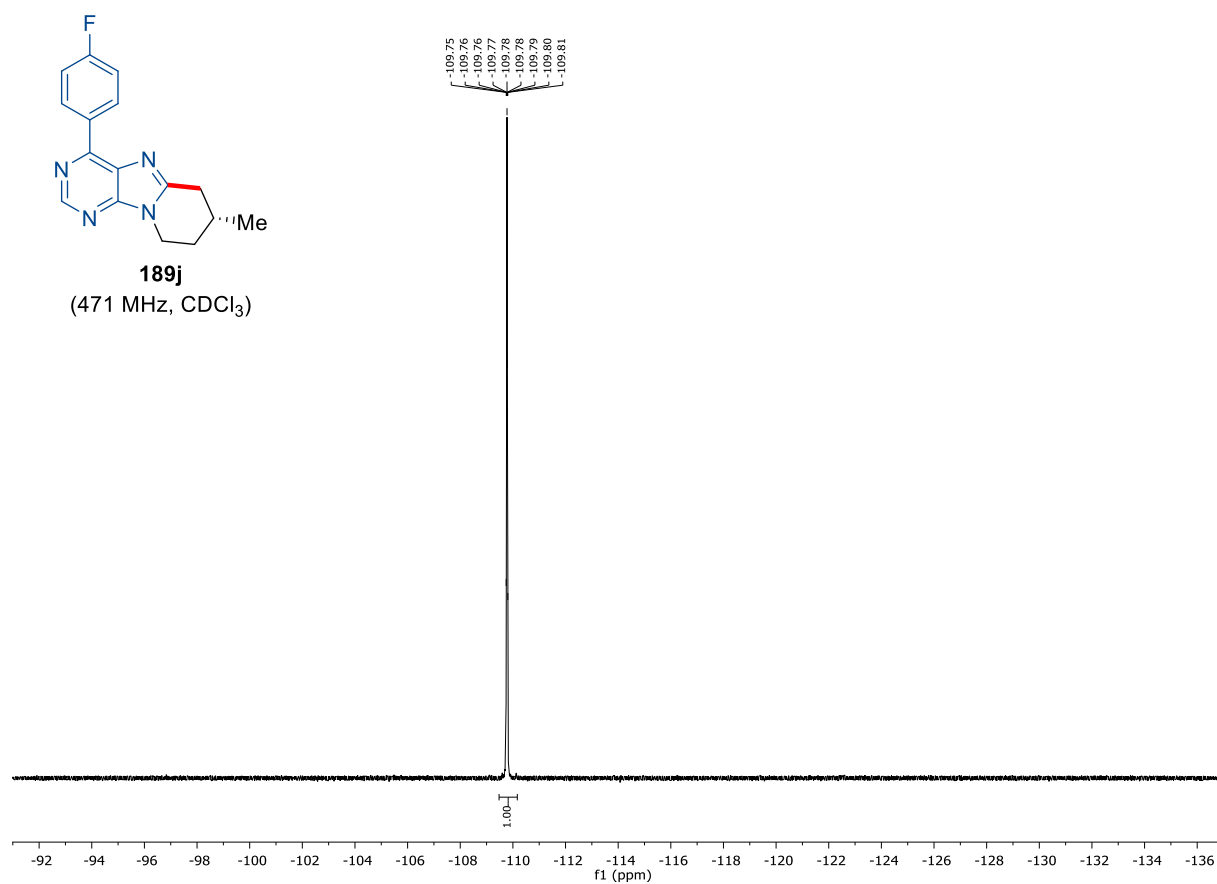
189j
(500 MHz, CDCl₃)



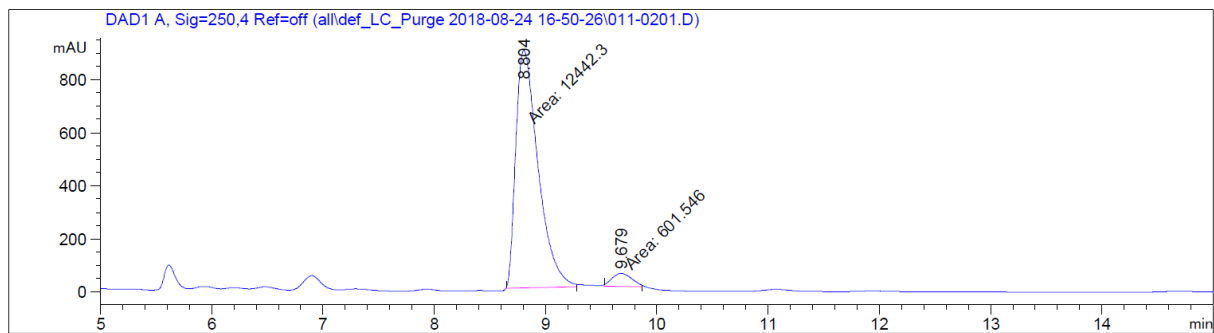
189j
(125 MHz, CDCl₃)



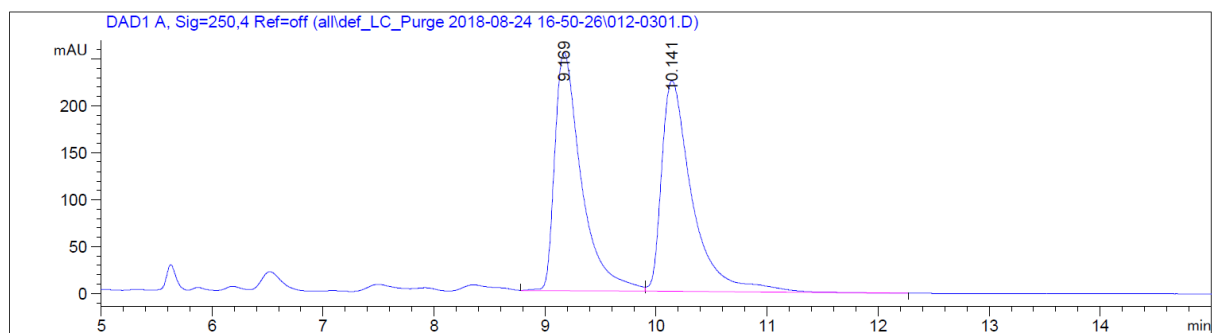
7. Appendix: NMR-Spectra and HPLC Chromatograms



Chiral HPLC of **189j**

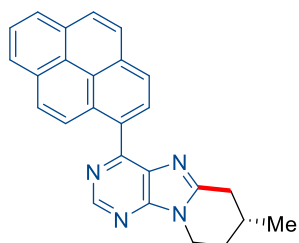


Peak #	RetTime [min]	Type	Width [min]	Area [mAU*s]	Height [mAU]	Area %
1	8.804	MM	0.2319	1.24423e4	894.41425	95.3883
2	9.679	MM	0.2055	601.54602	48.79048	4.6117

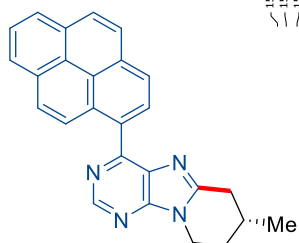
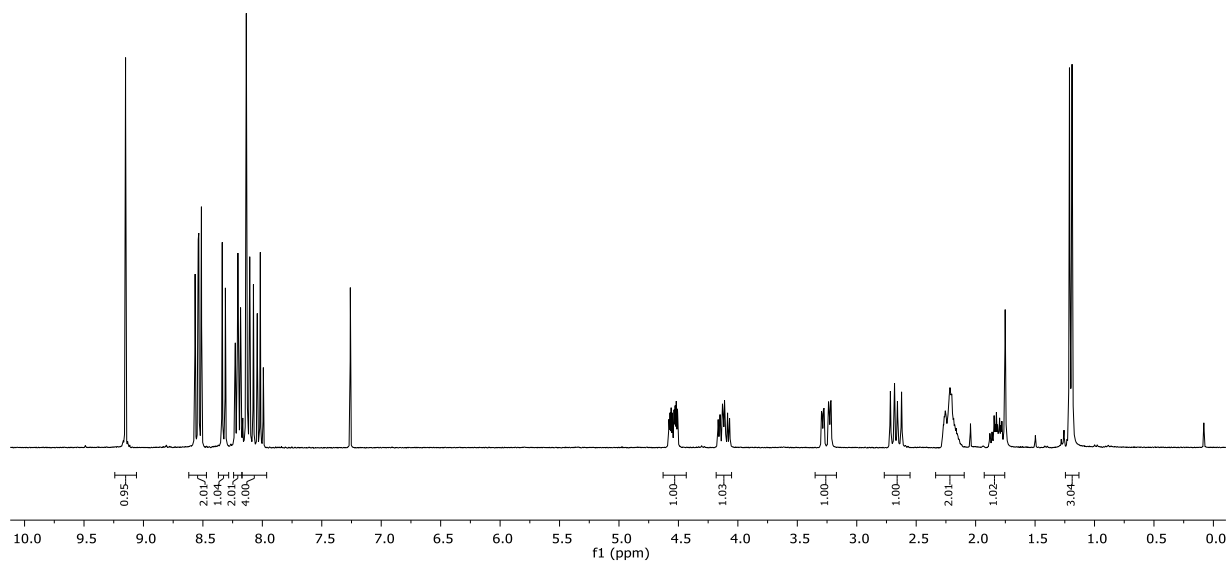


Peak #	RetTime [min]	Type	Width [min]	Area [mAU*s]	Height [mAU]	Area %
1	9.169	BV	0.2487	4229.35449	253.41176	49.4846
2	10.141	VB	0.2846	4317.45947	224.30168	50.5154

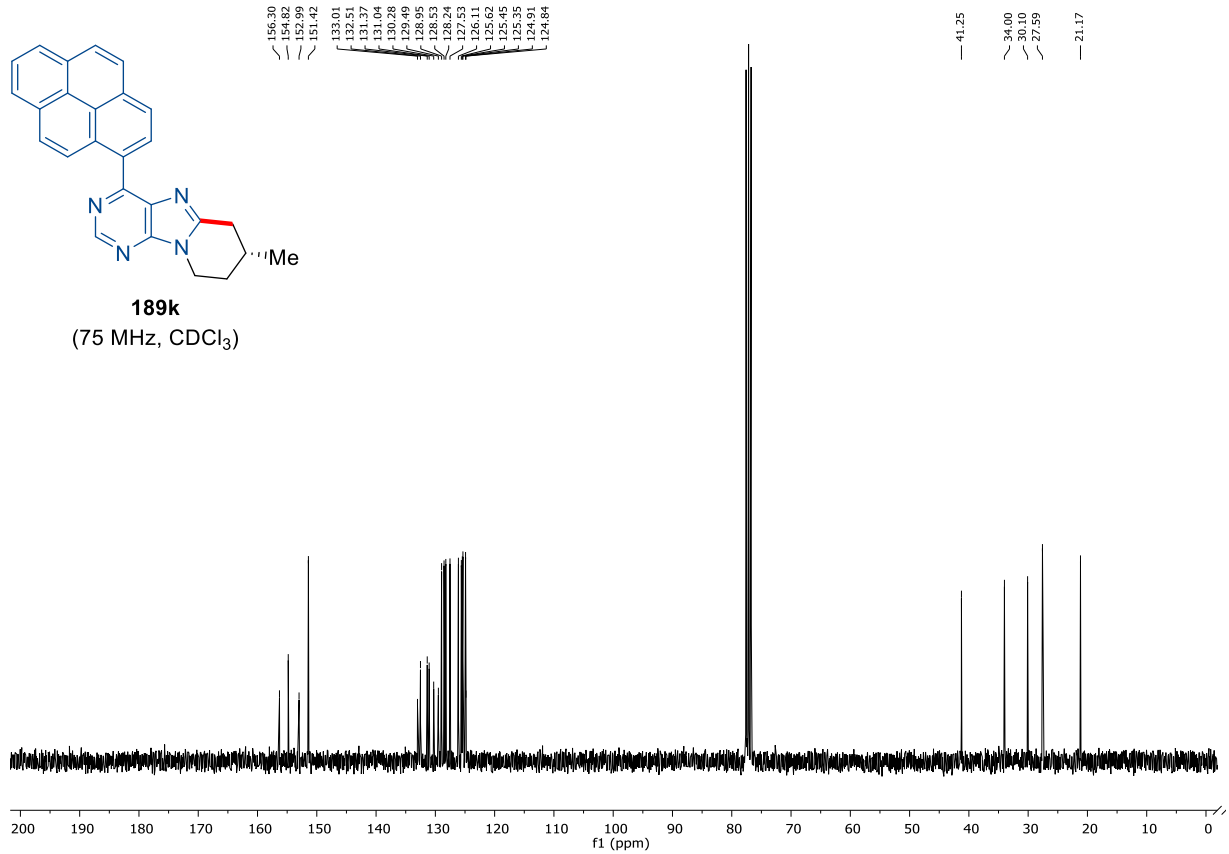
7. Appendix: NMR-Spectra and HPLC Chromatograms



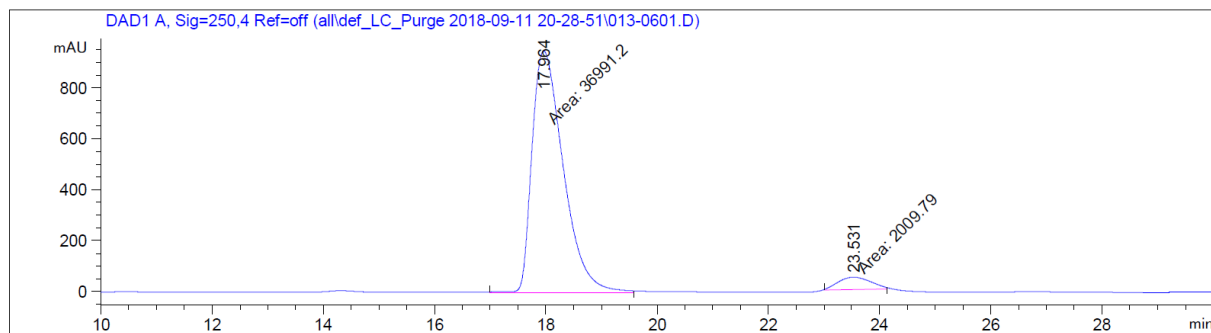
189k
(300 MHz, CDCl₃)



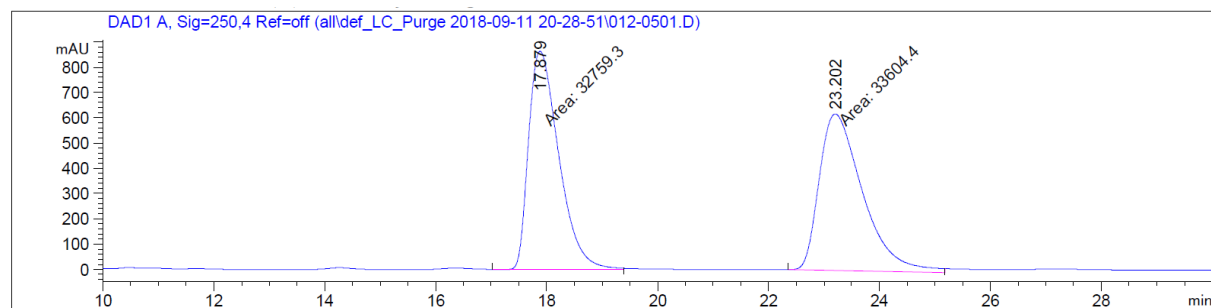
189k
(75 MHz, CDCl₃)



Chiral HPLC of **189k**

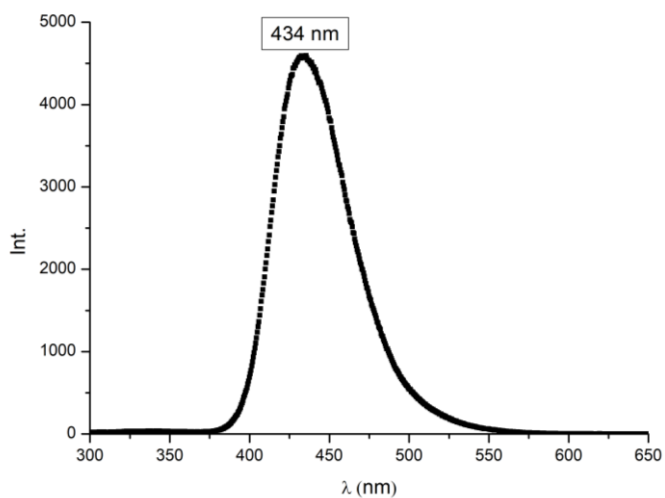


Peak #	RetTime [min]	Type	Width [min]	Area [mAU*s]	Height [mAU]	Area %
1	17.964	MM	0.6503	3.69912e4	948.01892	94.8468
2	23.531	MM	0.6867	2009.79150	48.77616	5.1532

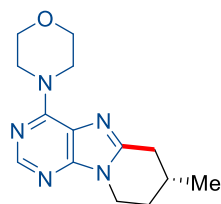


Peak #	RetTime [min]	Type	Width [min]	Area [mAU*s]	Height [mAU]	Area %
1	17.879	MM	0.6318	3.27593e4	864.11041	49.3633
2	23.202	MM	0.9047	3.36044e4	619.08929	50.6367

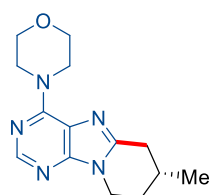
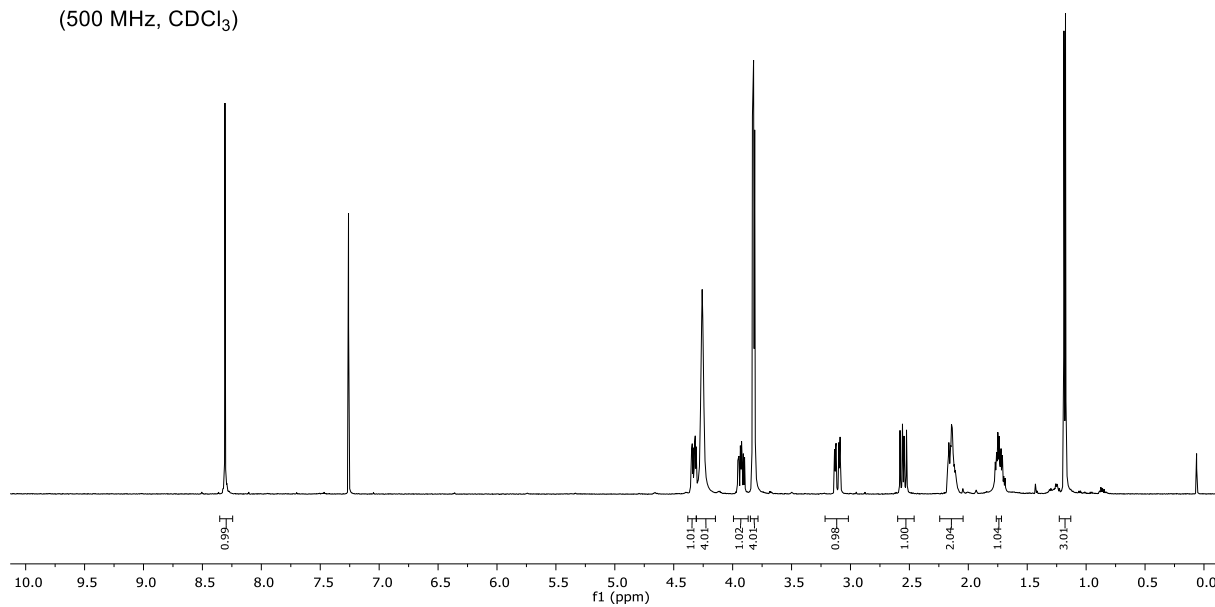
Emission fluorescence spectra of **189k** (excitation at 250 nm)



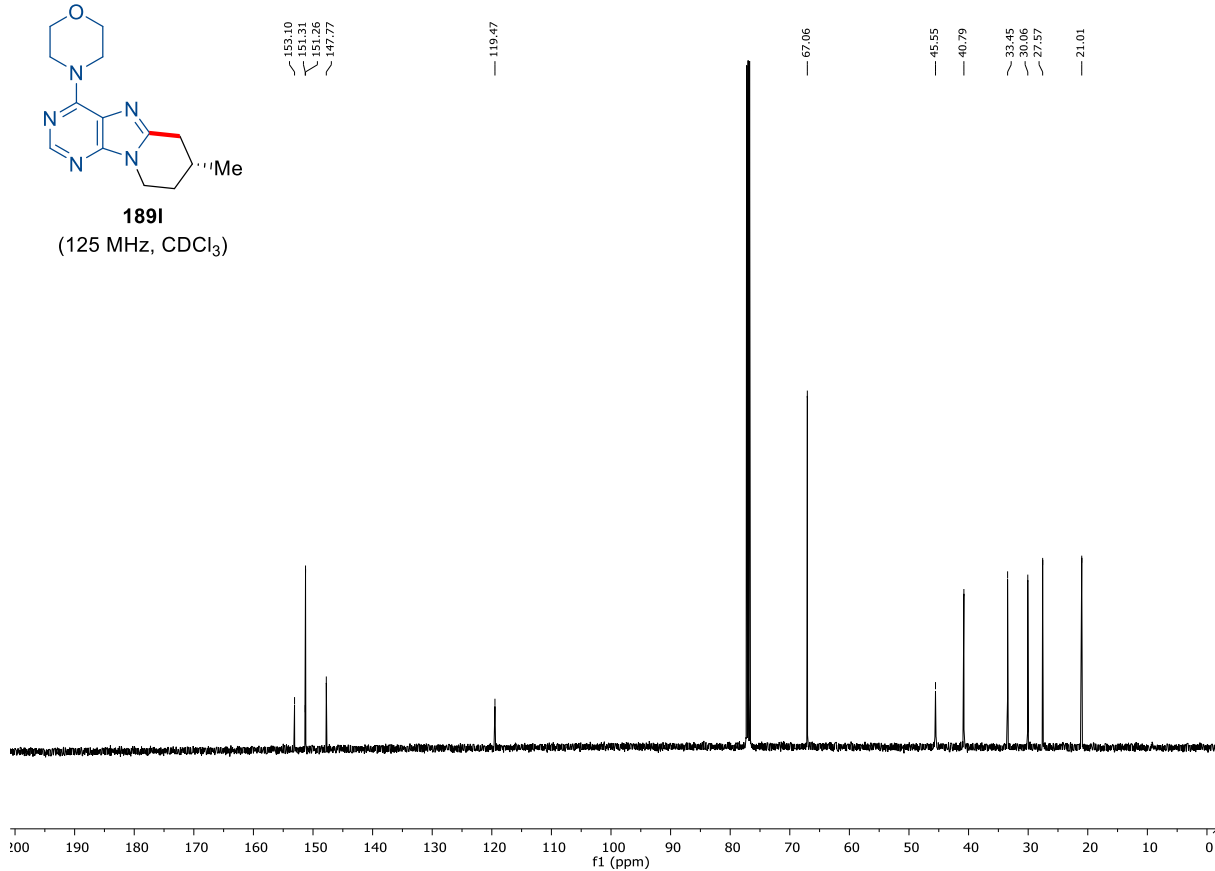
7. Appendix: NMR-Spectra and HPLC Chromatograms



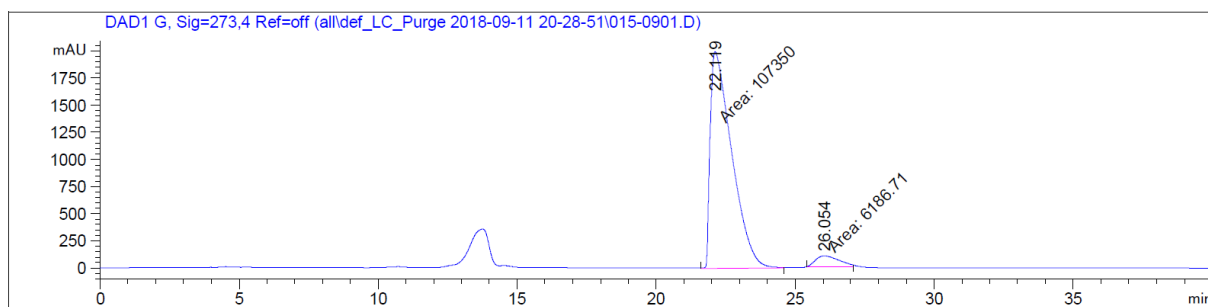
189
(500 MHz, CDCl₃)



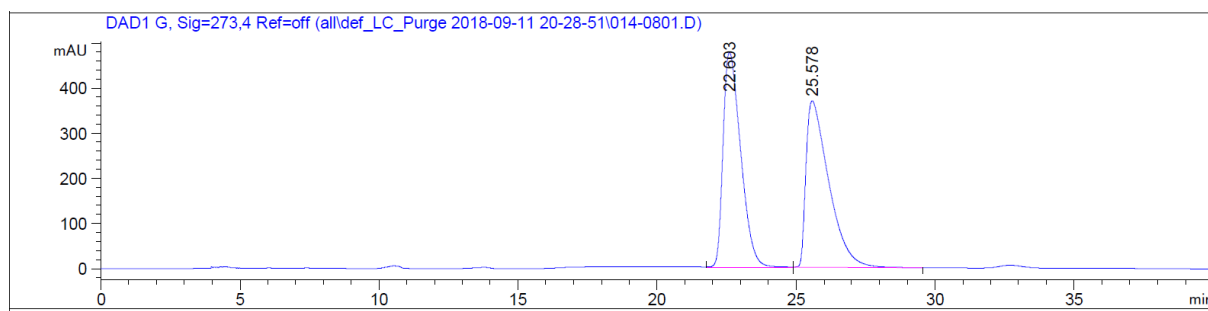
189
(125 MHz, CDCl₃)



Chiral HPLC of 189I

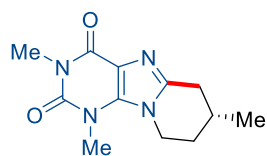


Peak #	RetTime [min]	Type	Width [min]	Area [mAU*s]	Height [mAU]	Area %
1	22.119	MM	0.8956	1.07350e5	1997.71045	94.5509
2	26.054	MM	1.0004	6186.70508	103.07303	5.4491

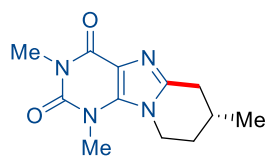
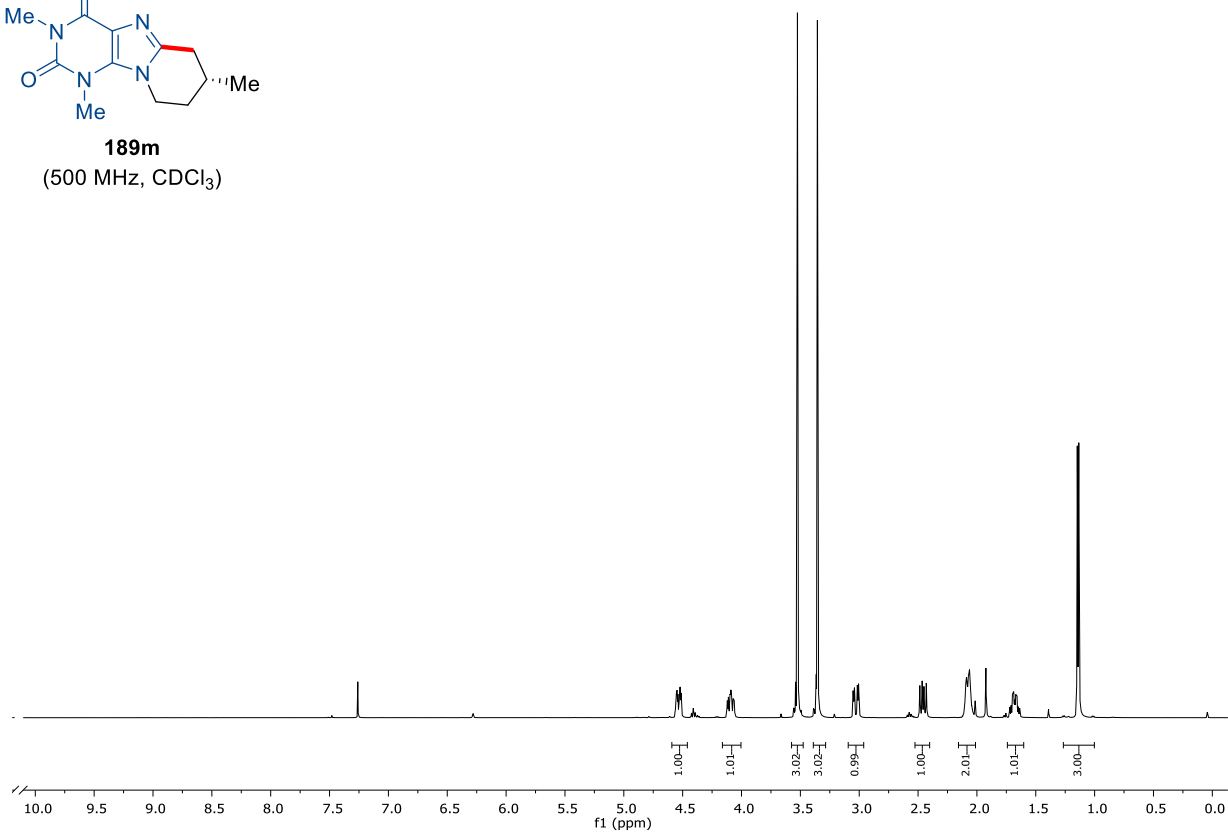


Peak #	RetTime [min]	Type	Width [min]	Area [mAU*s]	Height [mAU]	Area %
1	22.603	BB	0.6704	2.08296e4	476.08545	49.8449
2	25.578	BB	0.8262	2.09592e4	368.67932	50.1551

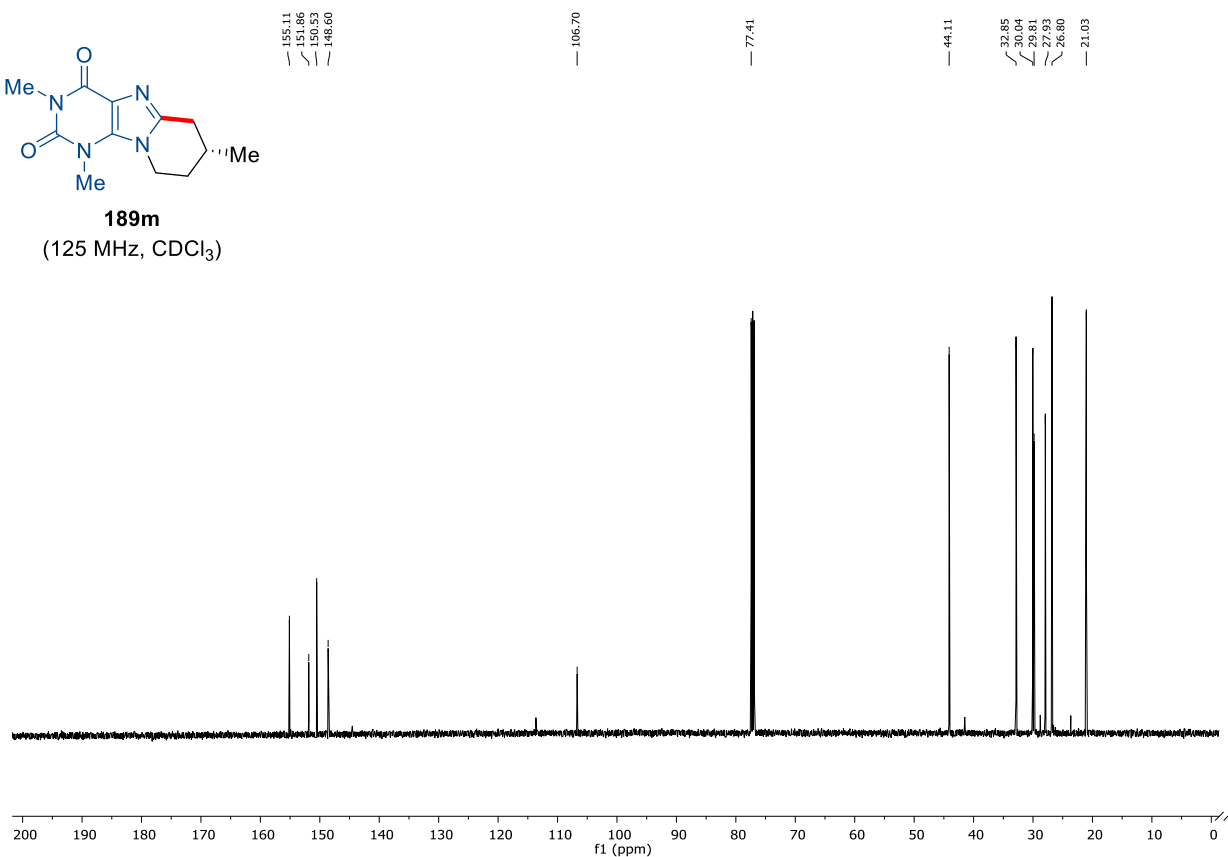
7. Appendix: NMR-Spectra and HPLC Chromatograms



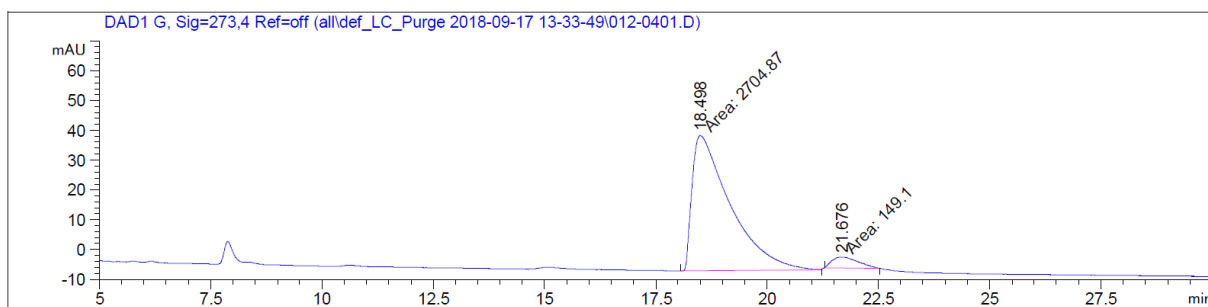
189m
(500 MHz, CDCl₃)



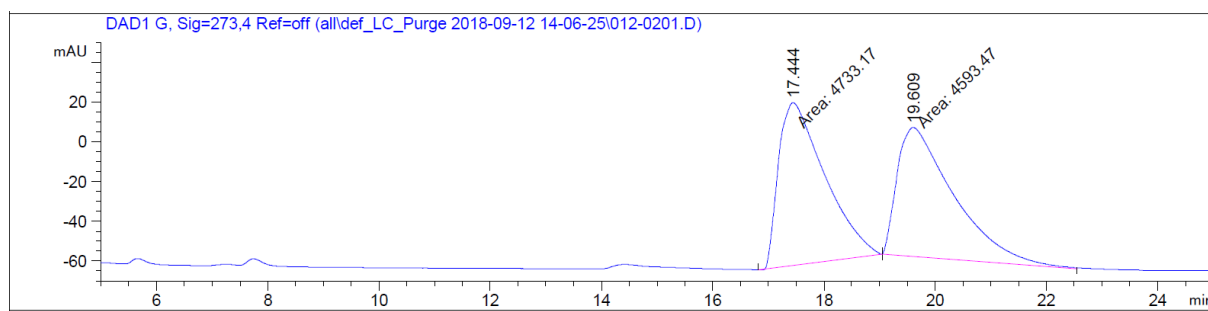
189m
(125 MHz, CDCl₃)



Chiral HPLC of 189m

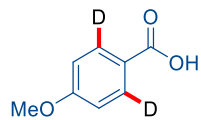


Peak #	RetTime [min]	Type	Width [min]	Area [mAU*s]	Height [mAU]	Area %
1	18.498	MM	0.9939	2704.86719	45.35829	94.7757
2	21.676	MM	0.6785	149.09972	3.66234	5.2243

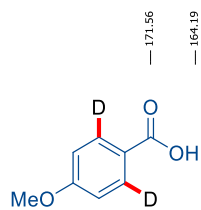
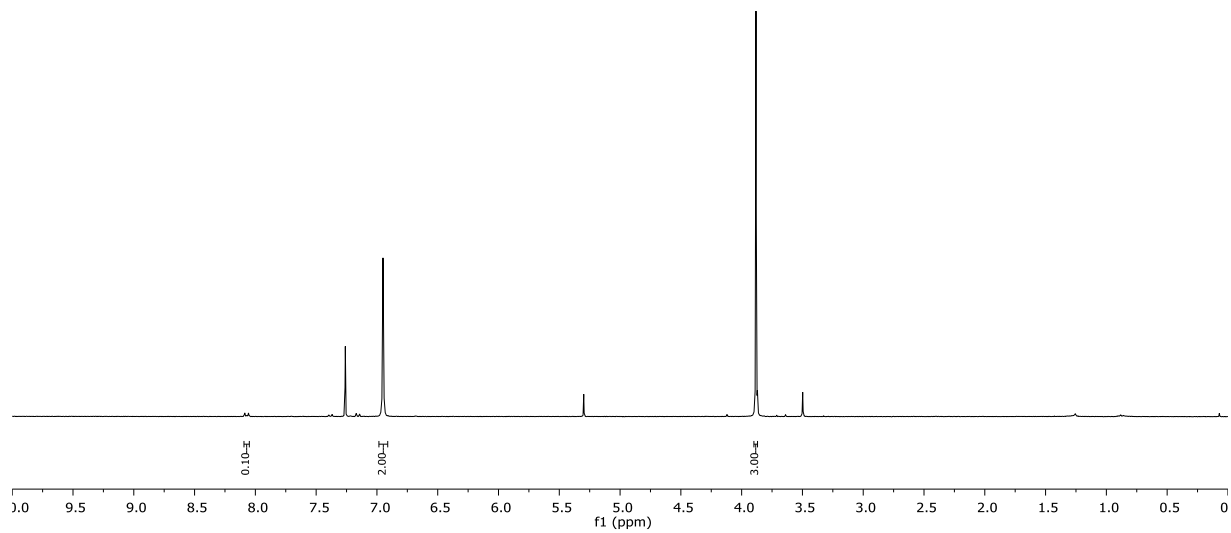


Peak #	RetTime [min]	Type	Width [min]	Area [mAU*s]	Height [mAU]	Area %
1	17.444	MM	0.9613	4733.17090	82.05954	50.7490
2	19.609	MM	1.1764	4593.46631	65.07555	49.2510

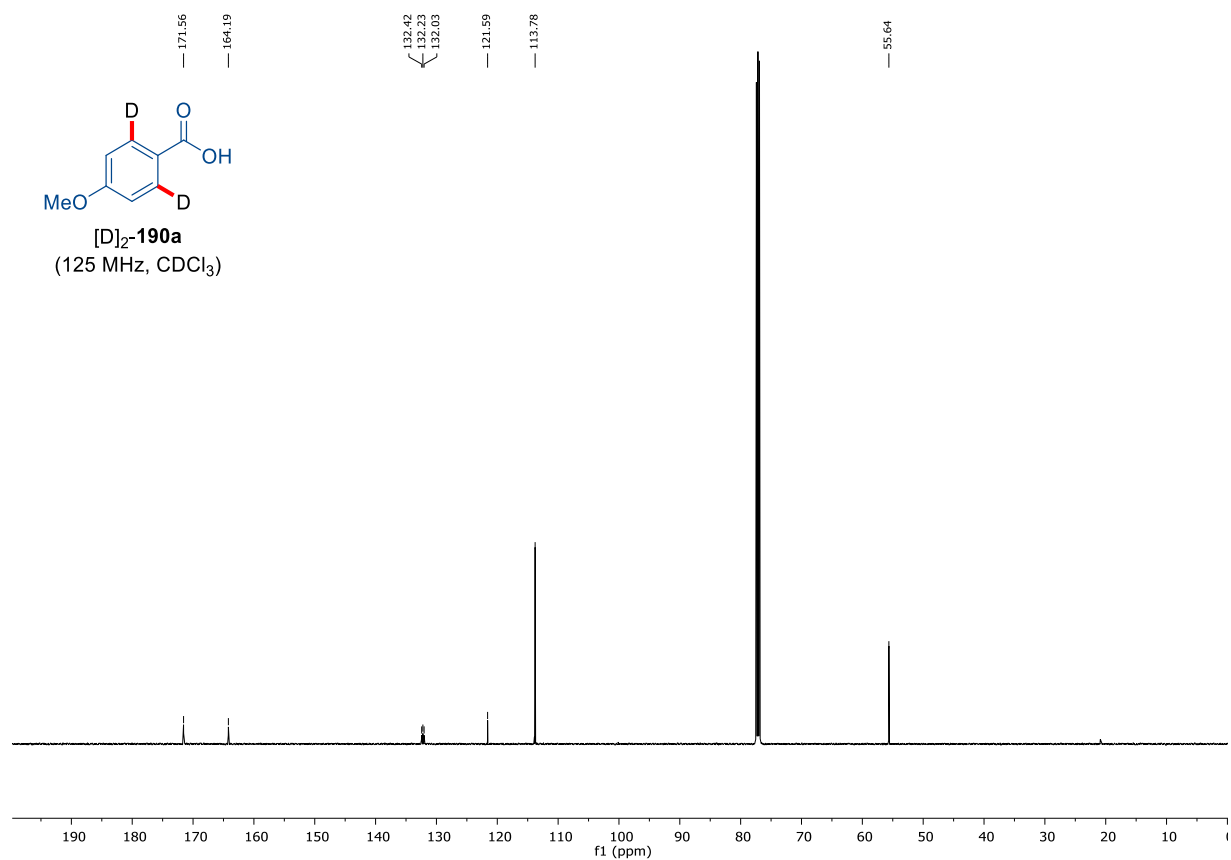
7. Appendix: NMR-Spectra and HPLC Chromatograms

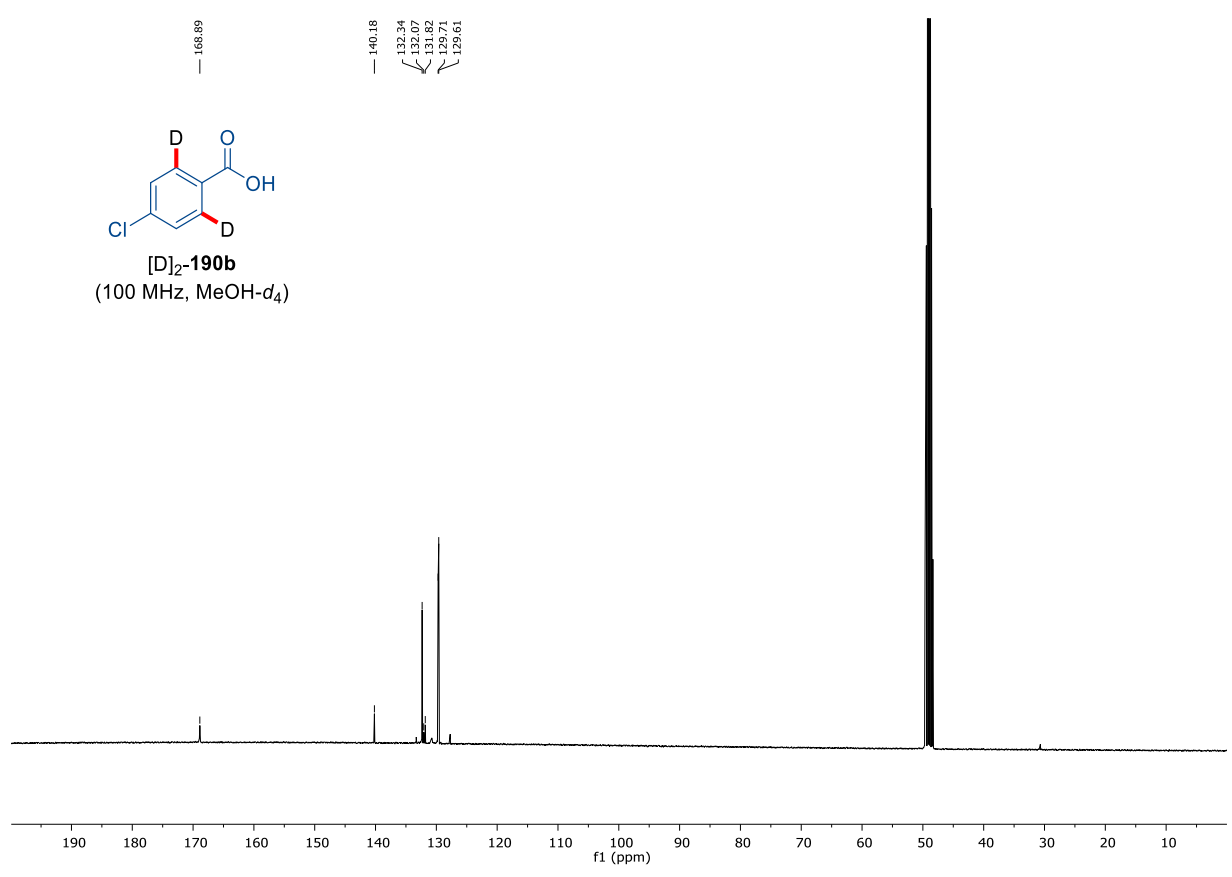
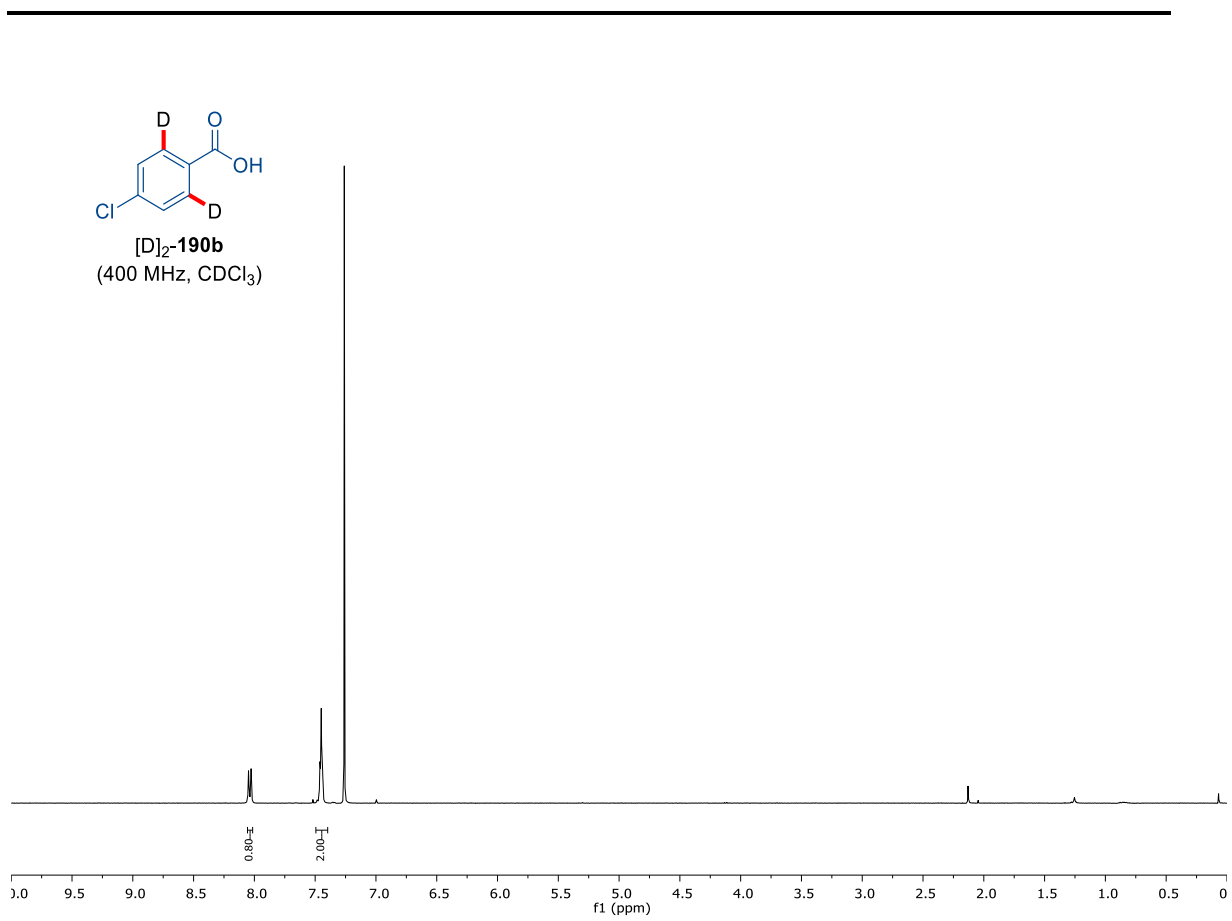


[D]₂-190a
(300 MHz, CDCl₃)

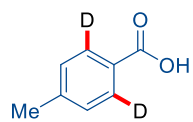


[D]₂-190a
(125 MHz, CDCl₃)

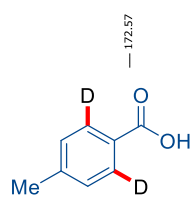
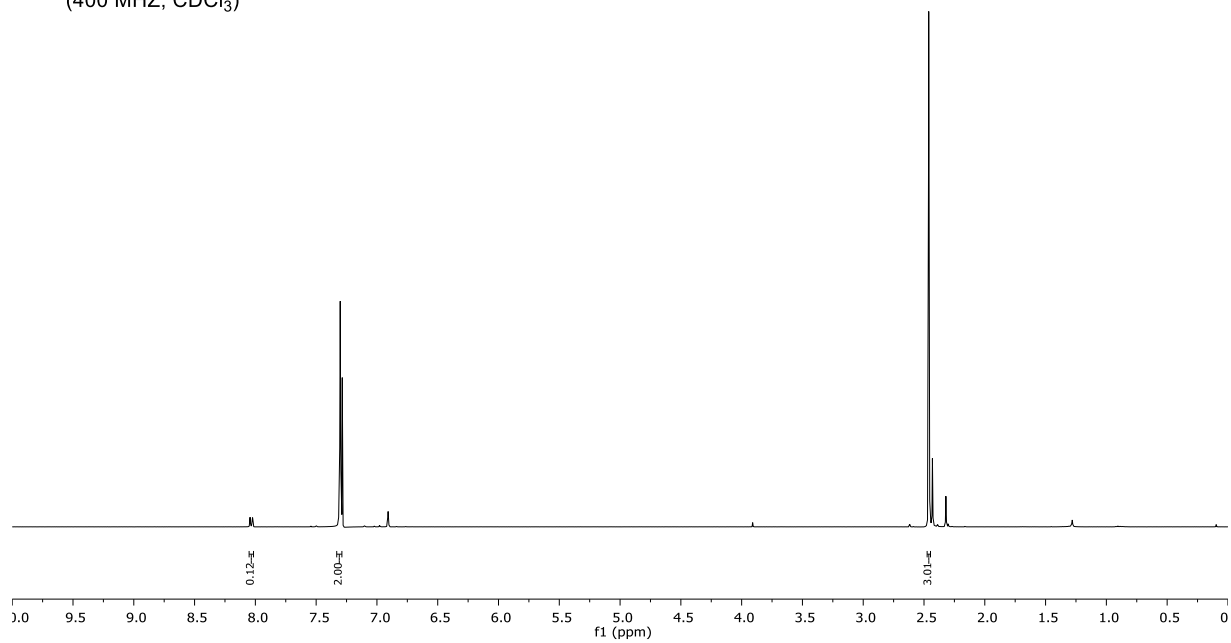




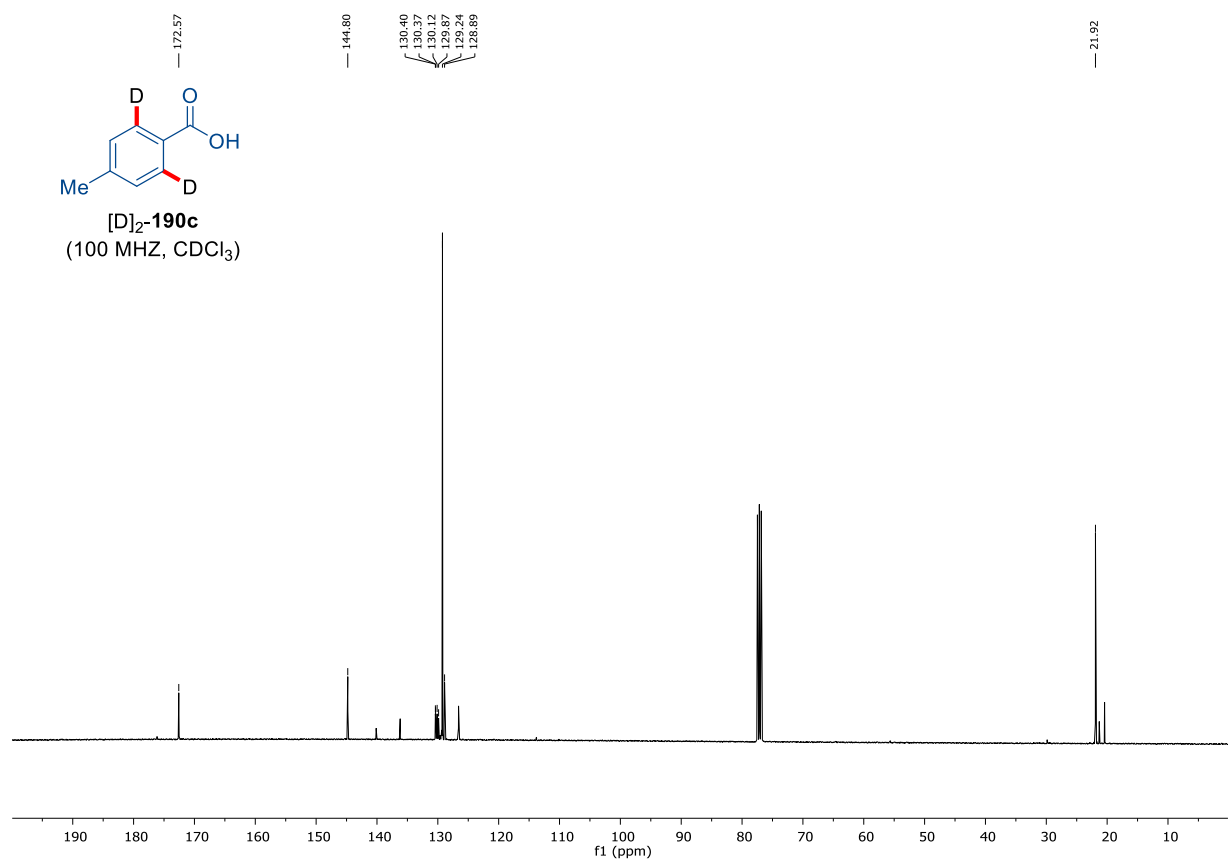
7. Appendix: NMR-Spectra and HPLC Chromatograms

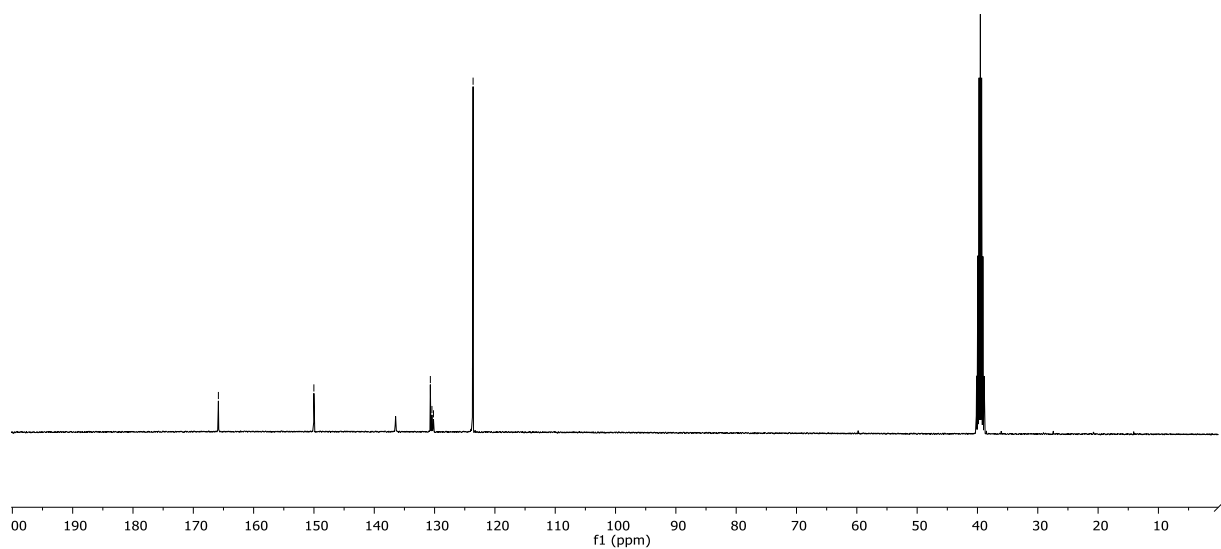
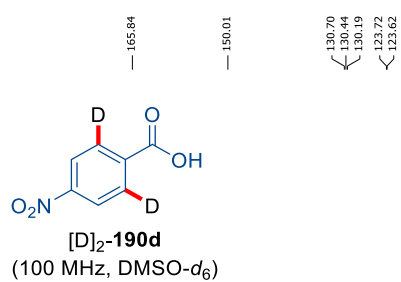
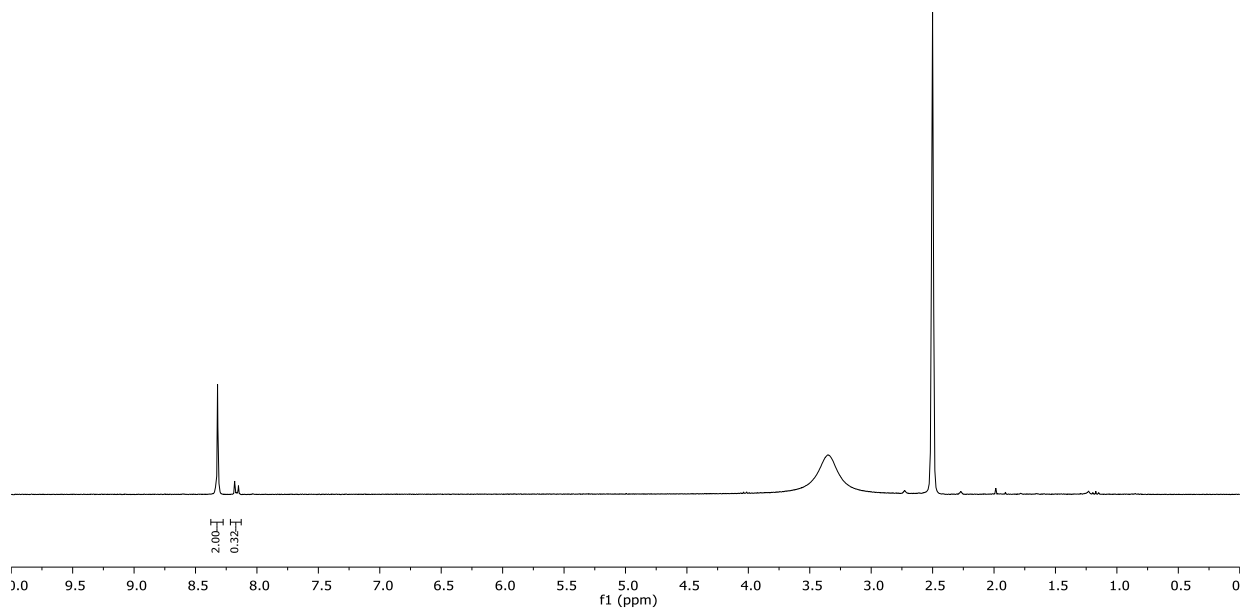
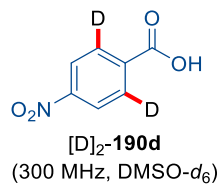


[D]₂-190c
(400 MHz, CDCl₃)

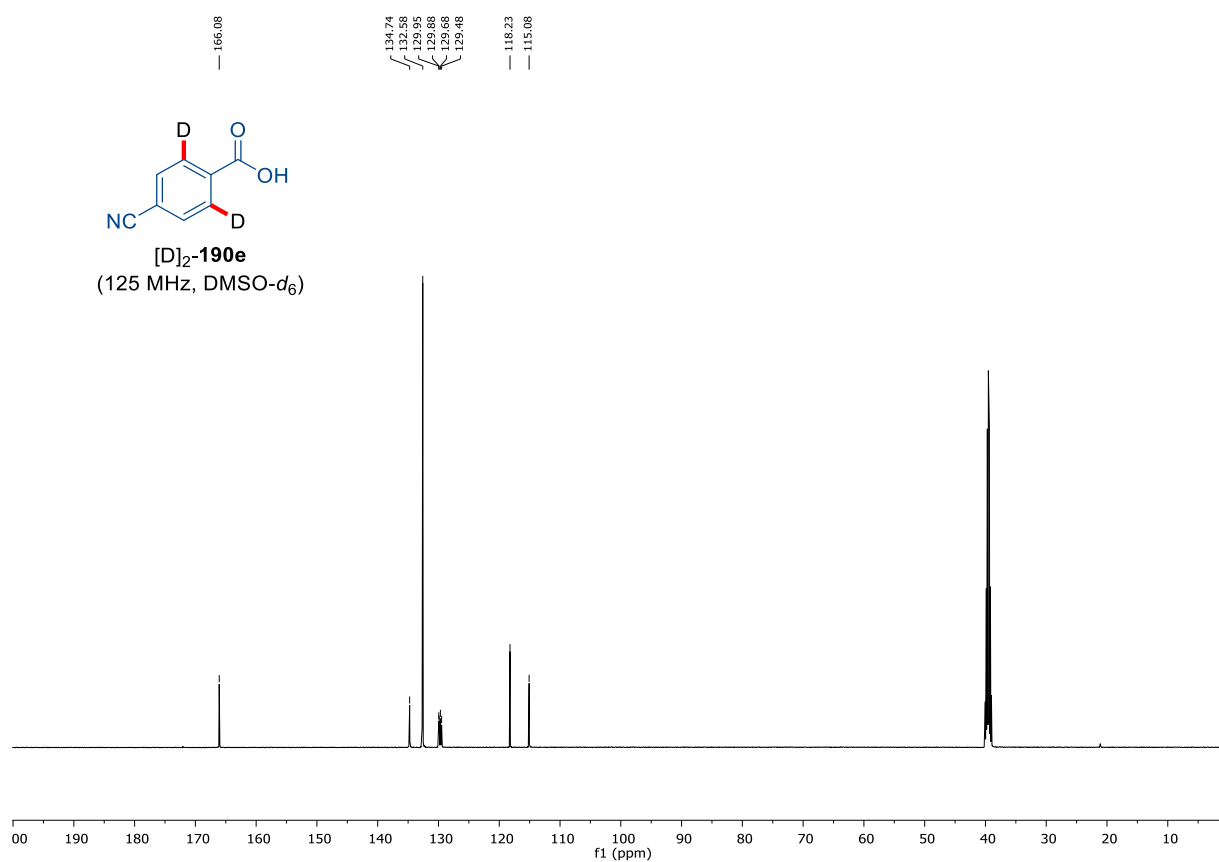
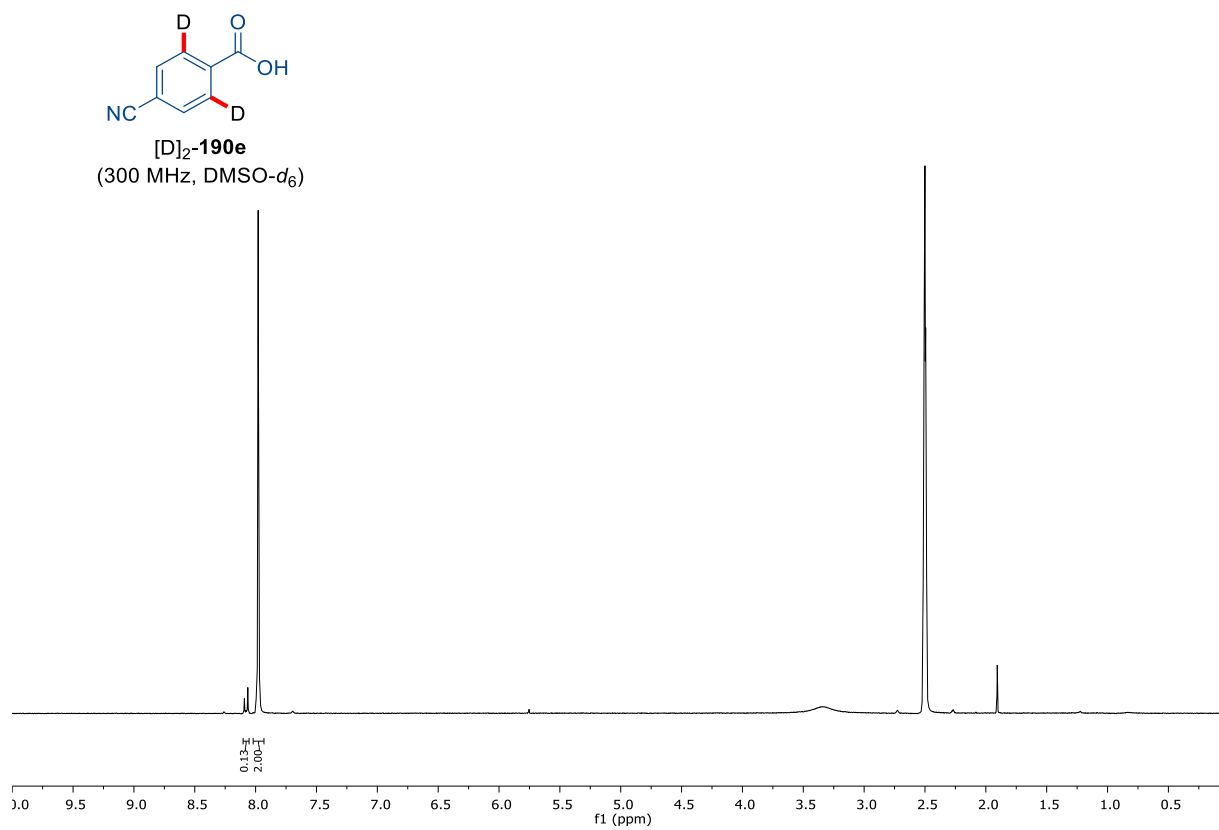


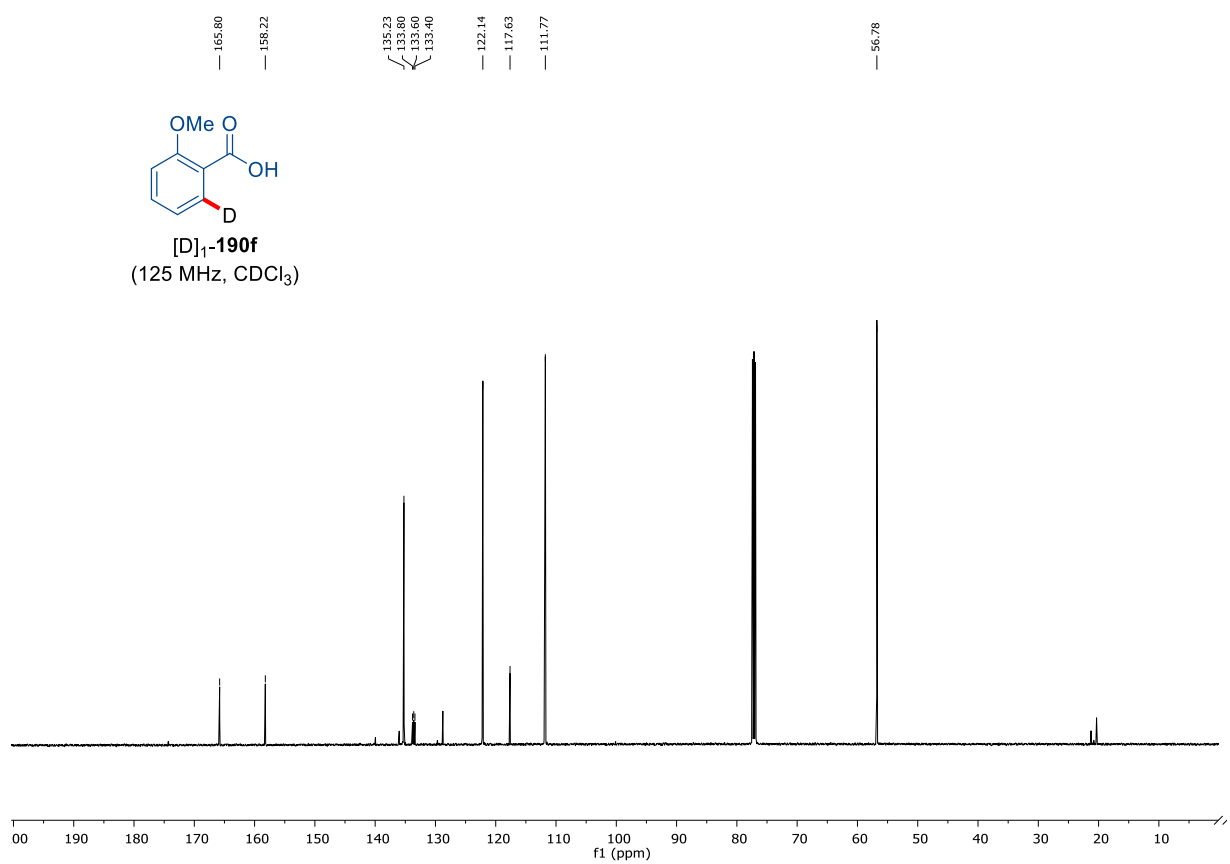
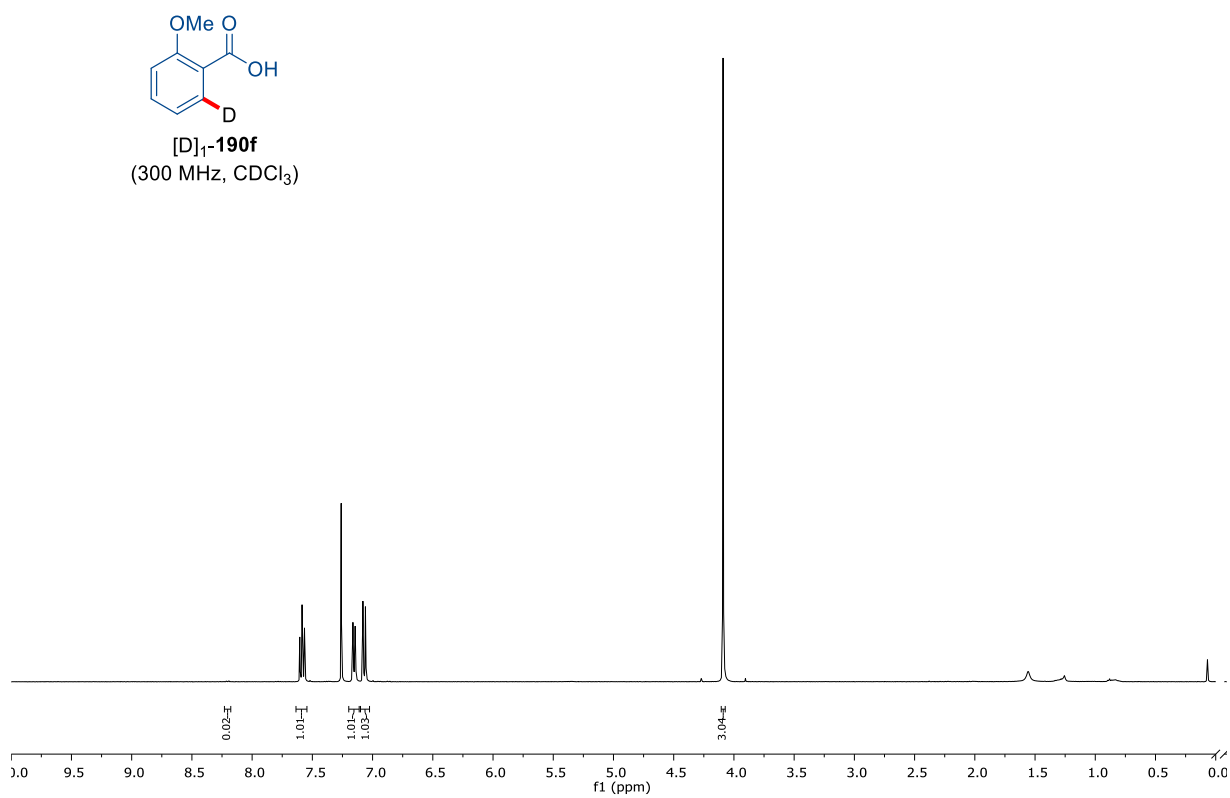
[D]₂-190c
(100 MHz, CDCl₃)



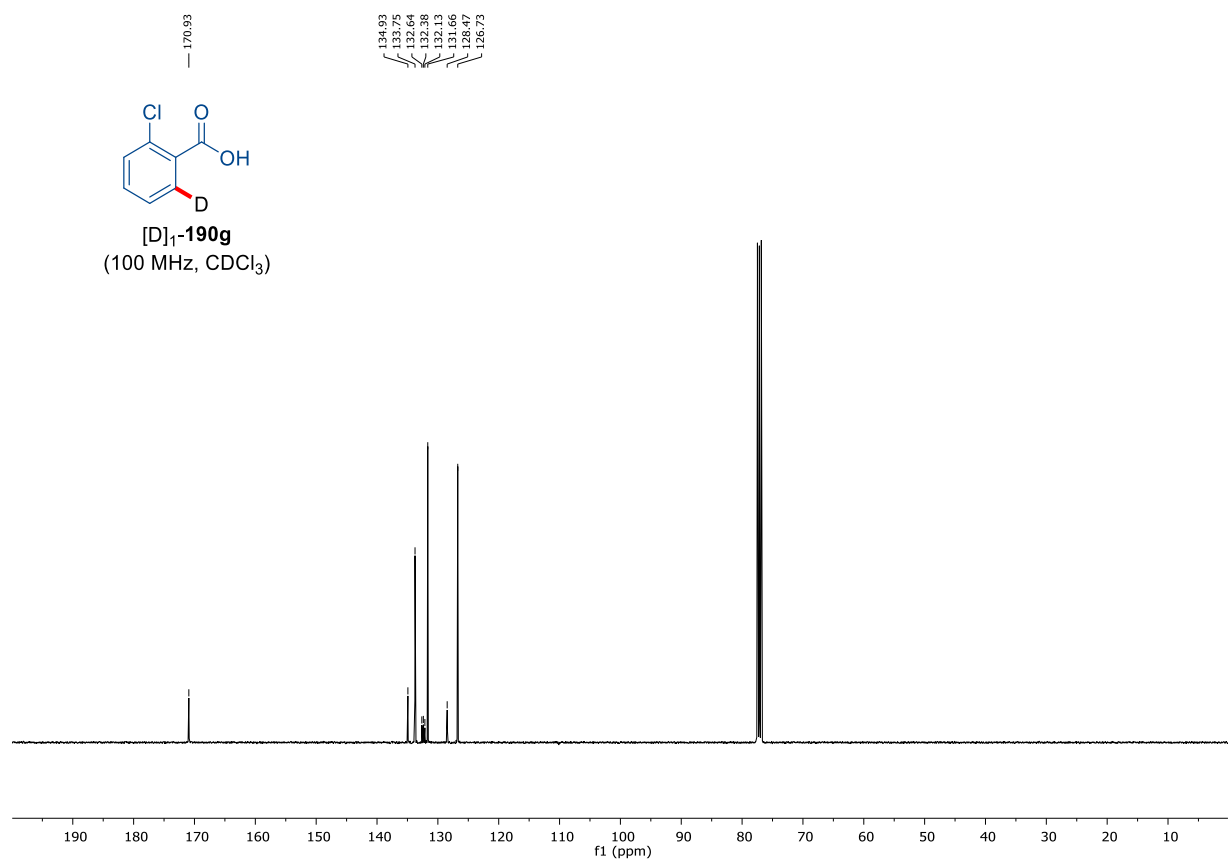
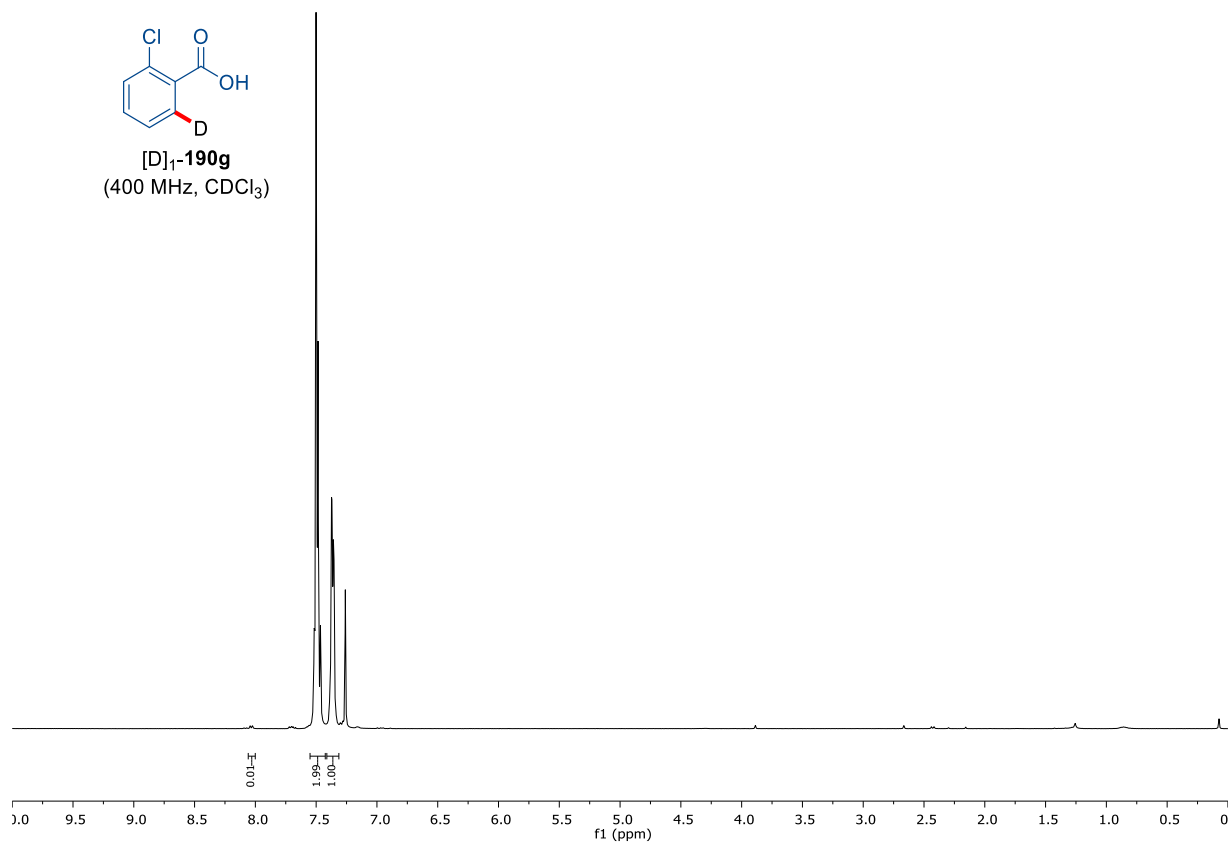


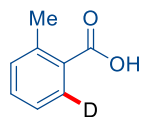
7. Appendix: NMR-Spectra and HPLC Chromatograms



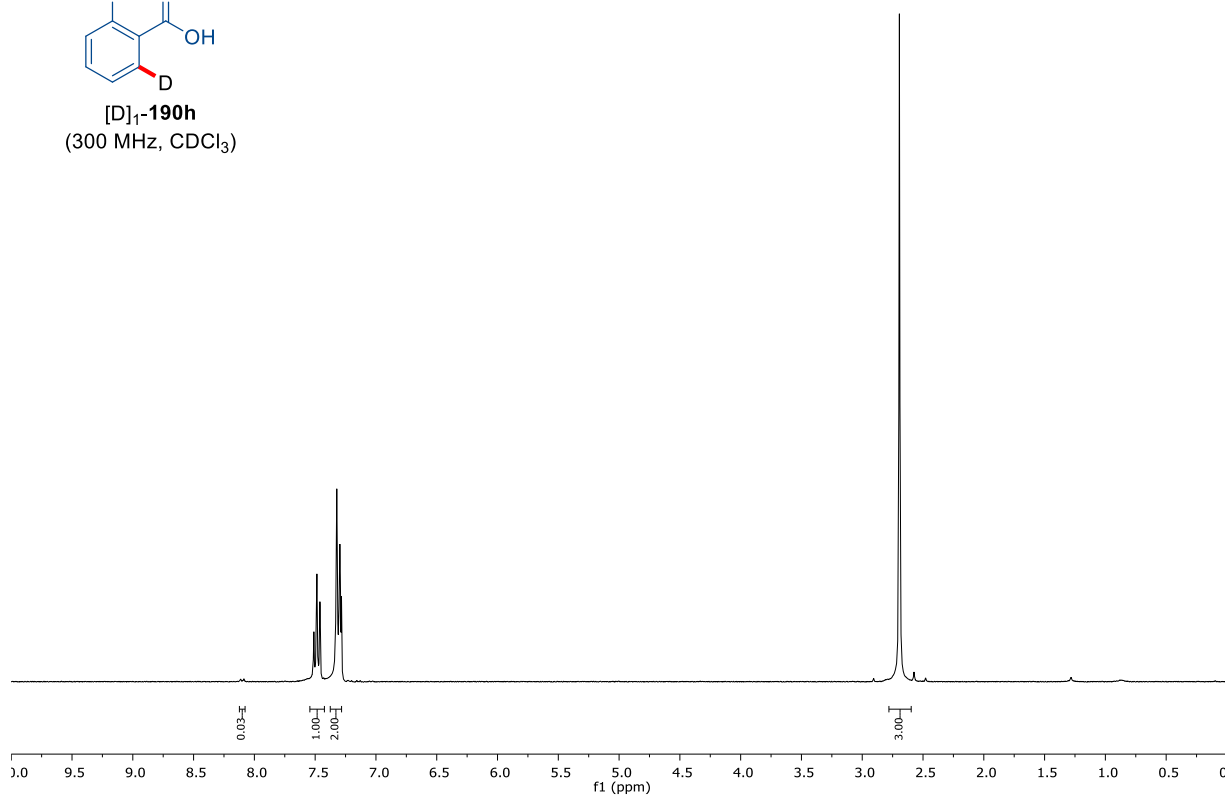


7. Appendix: NMR-Spectra and HPLC Chromatograms





[D]₁-**190h**
(300 MHz, CDCl₃)



173.76

141.50

133.09

132.06

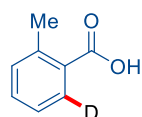
131.74

128.49

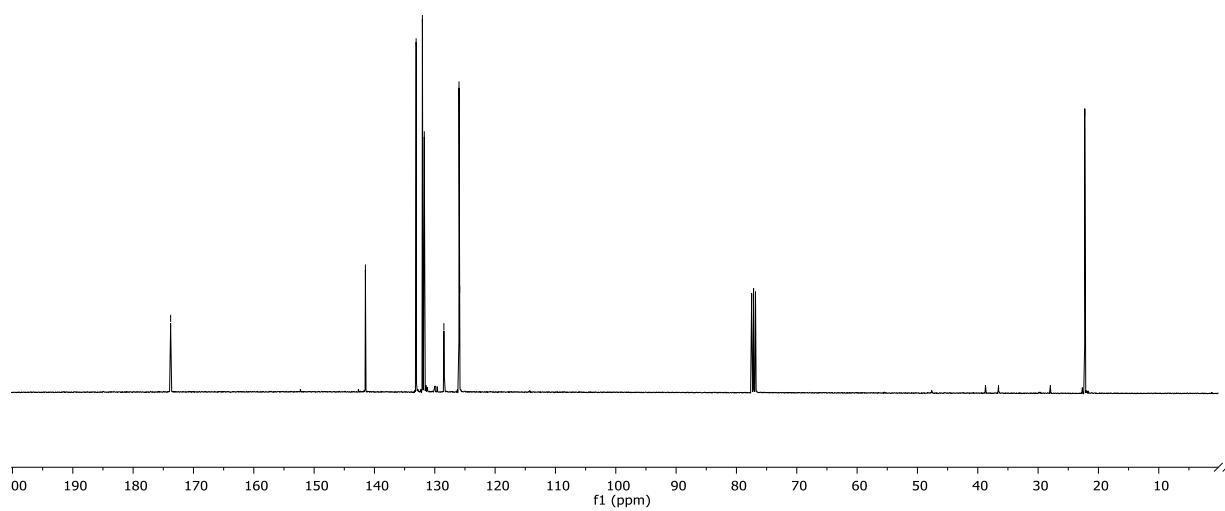
125.99

125.87

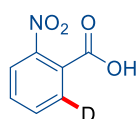
22.27



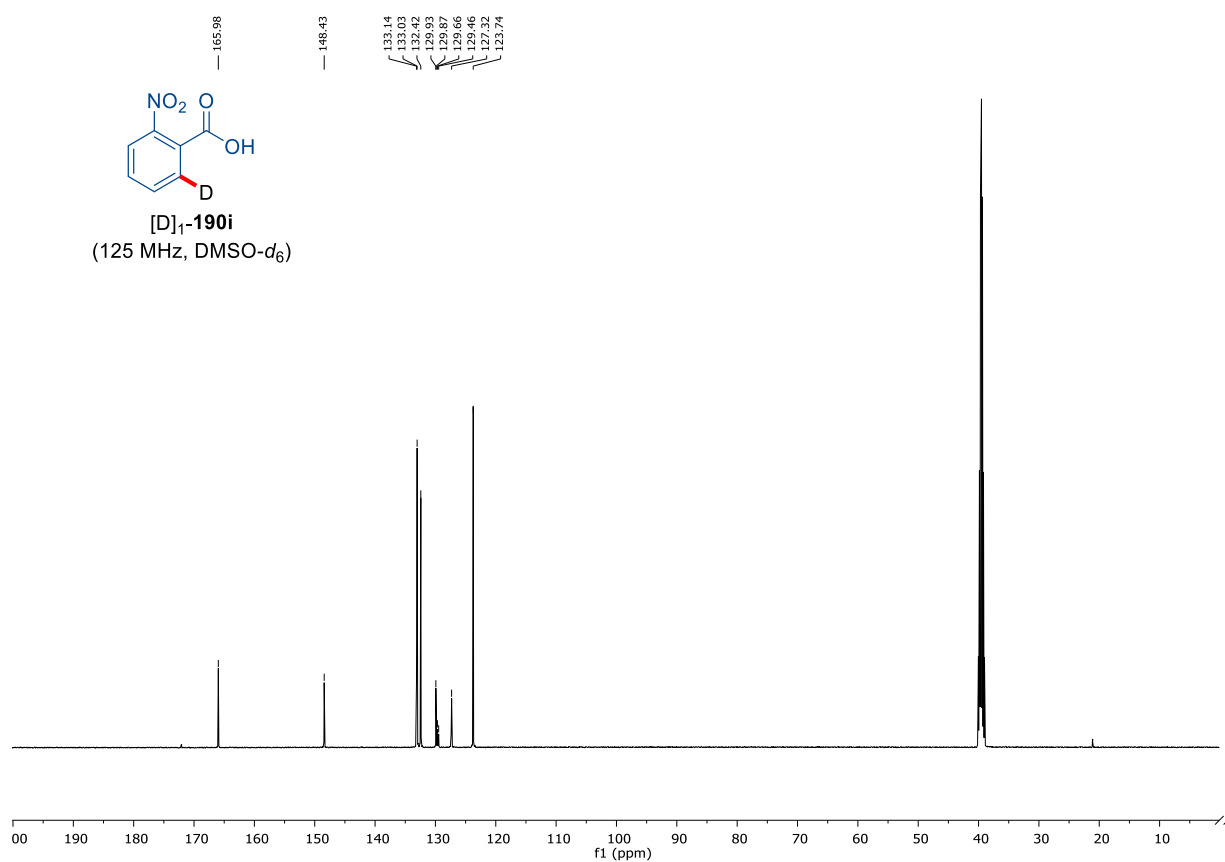
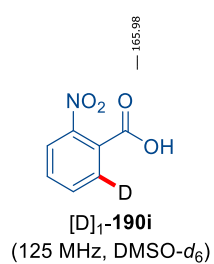
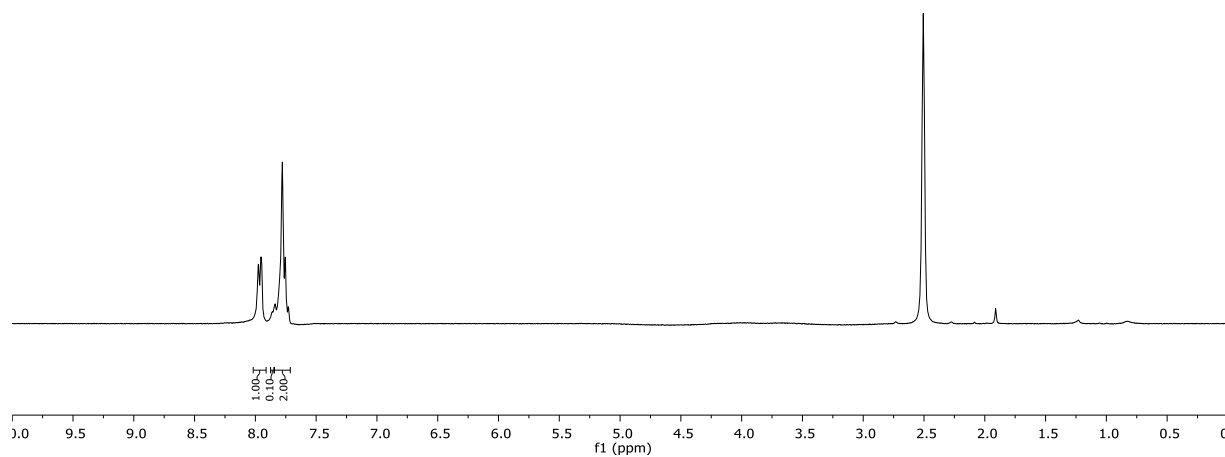
[D]₁-**190h**
(100 MHz, CDCl₃)

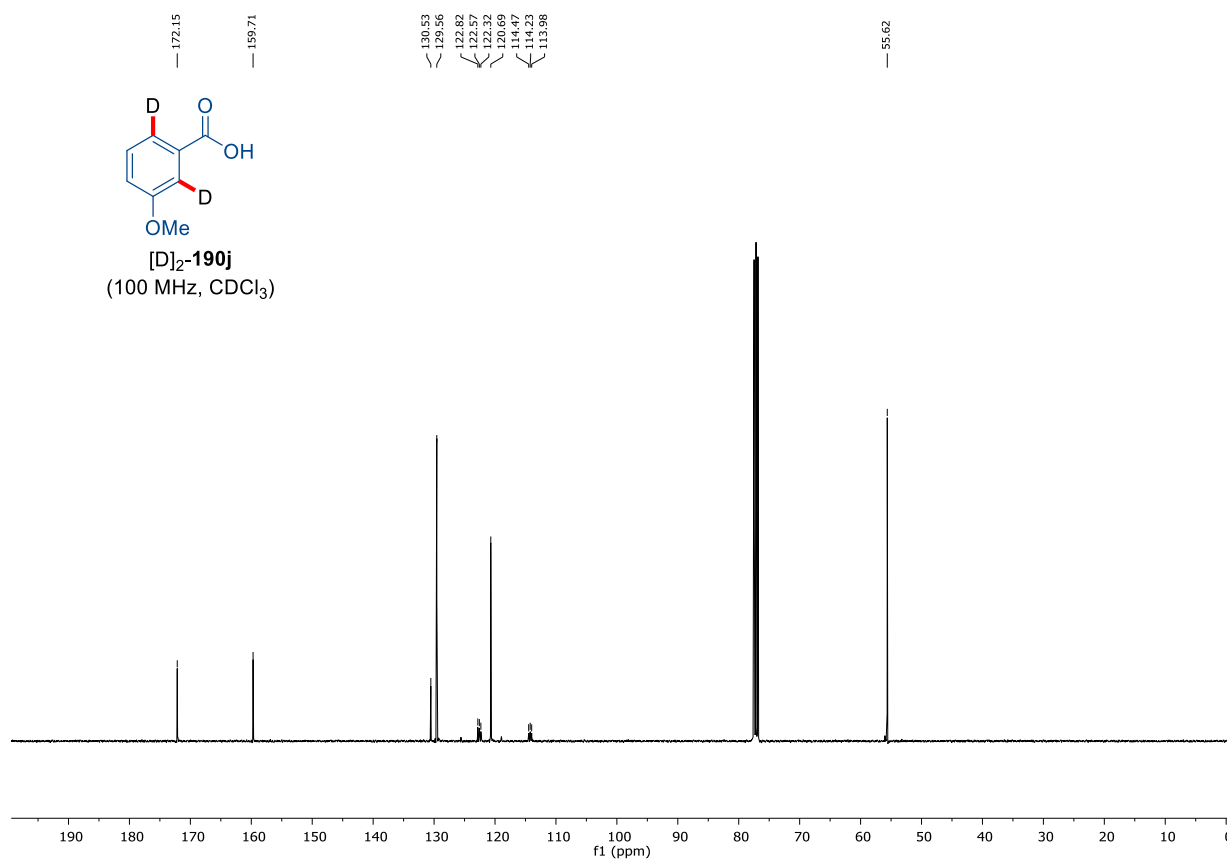
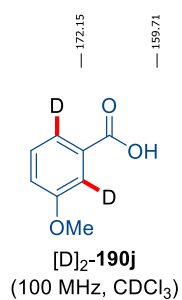
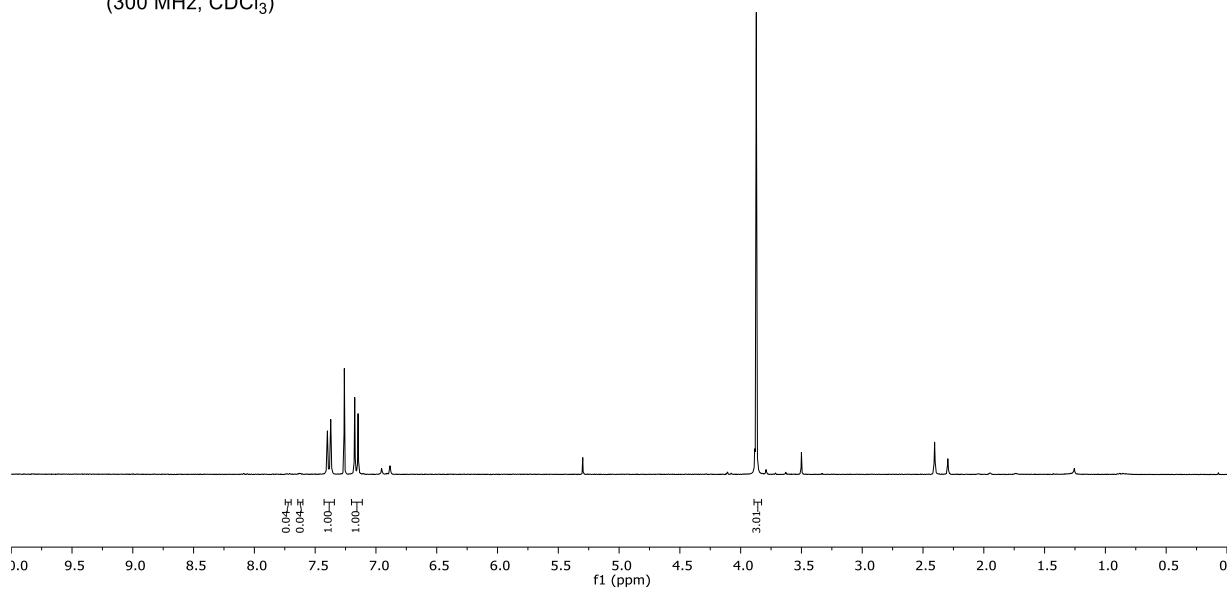
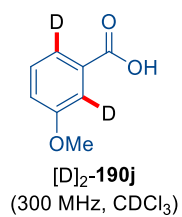


7. Appendix: NMR-Spectra and HPLC Chromatograms

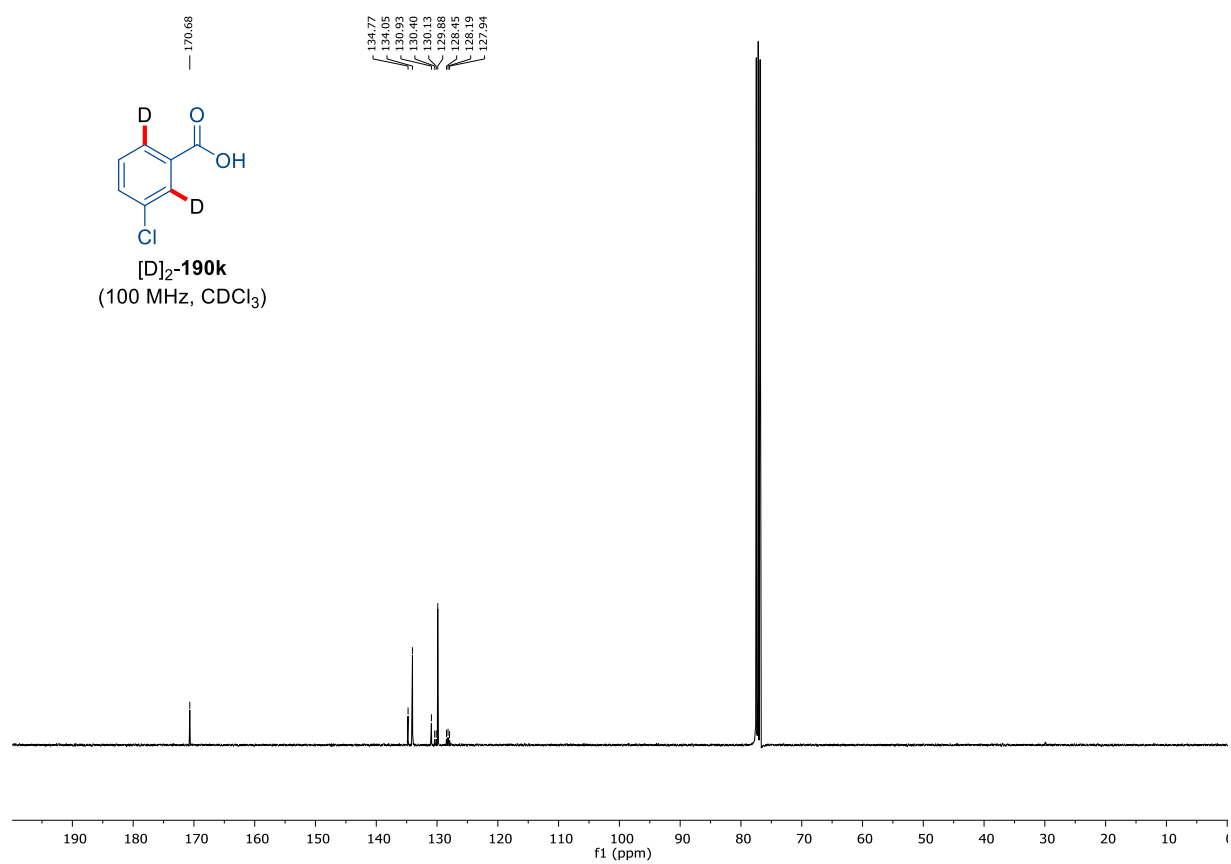
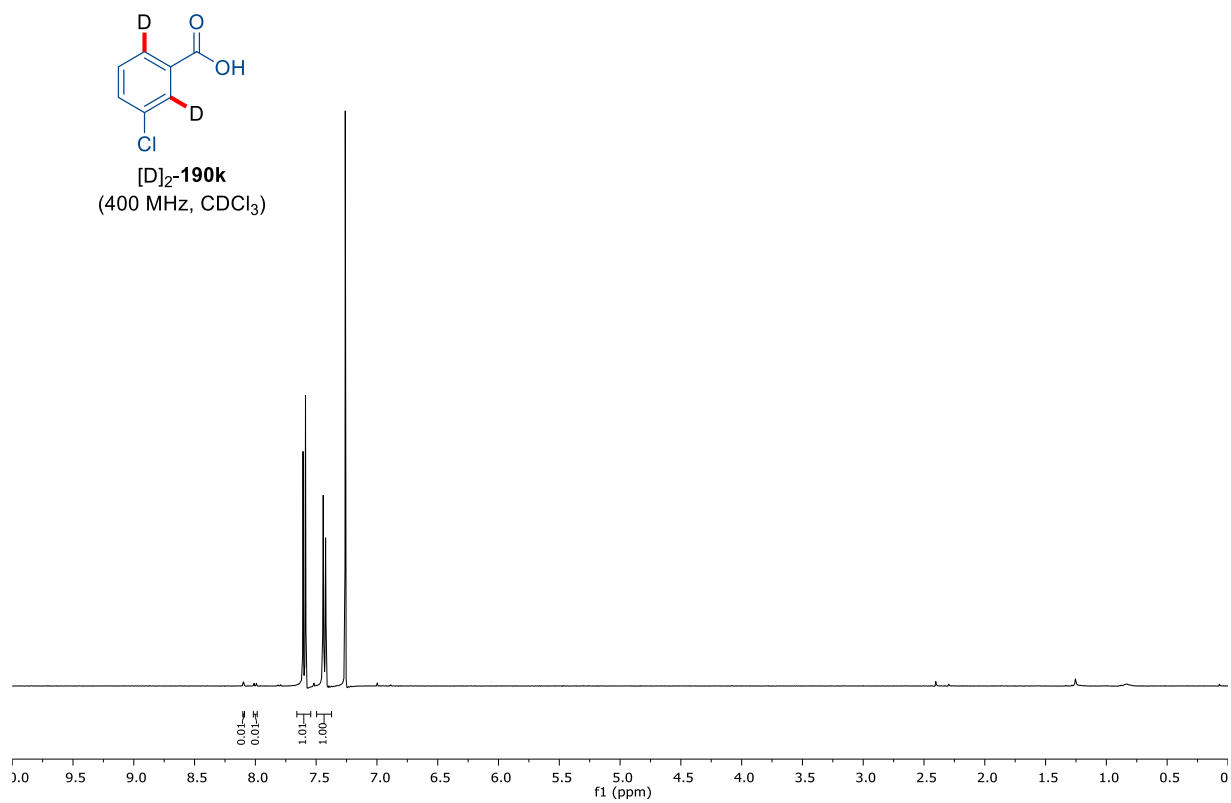


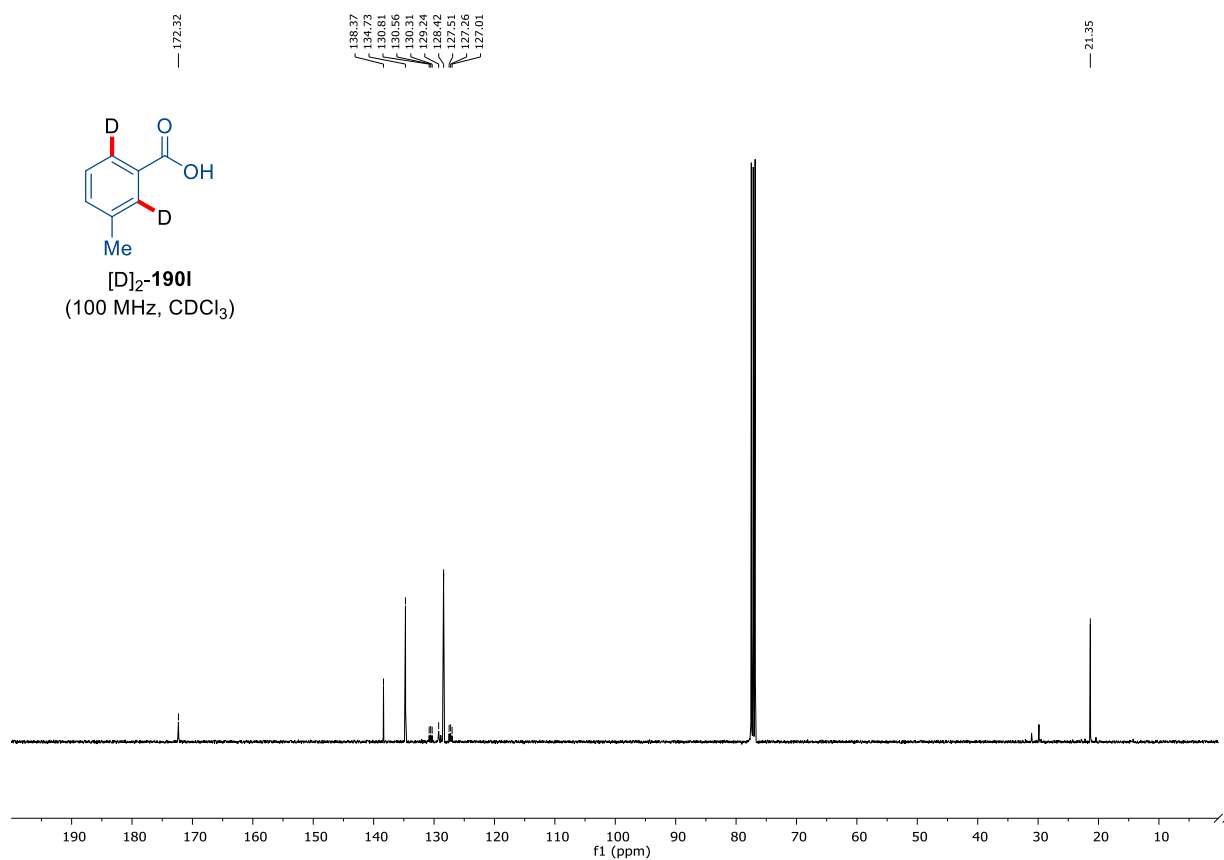
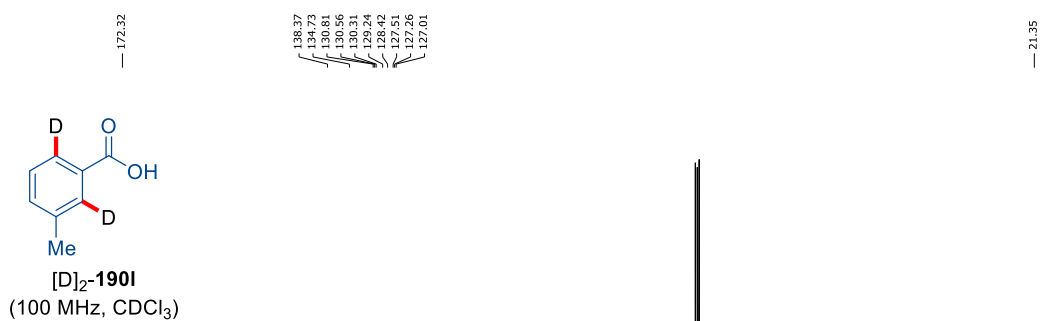
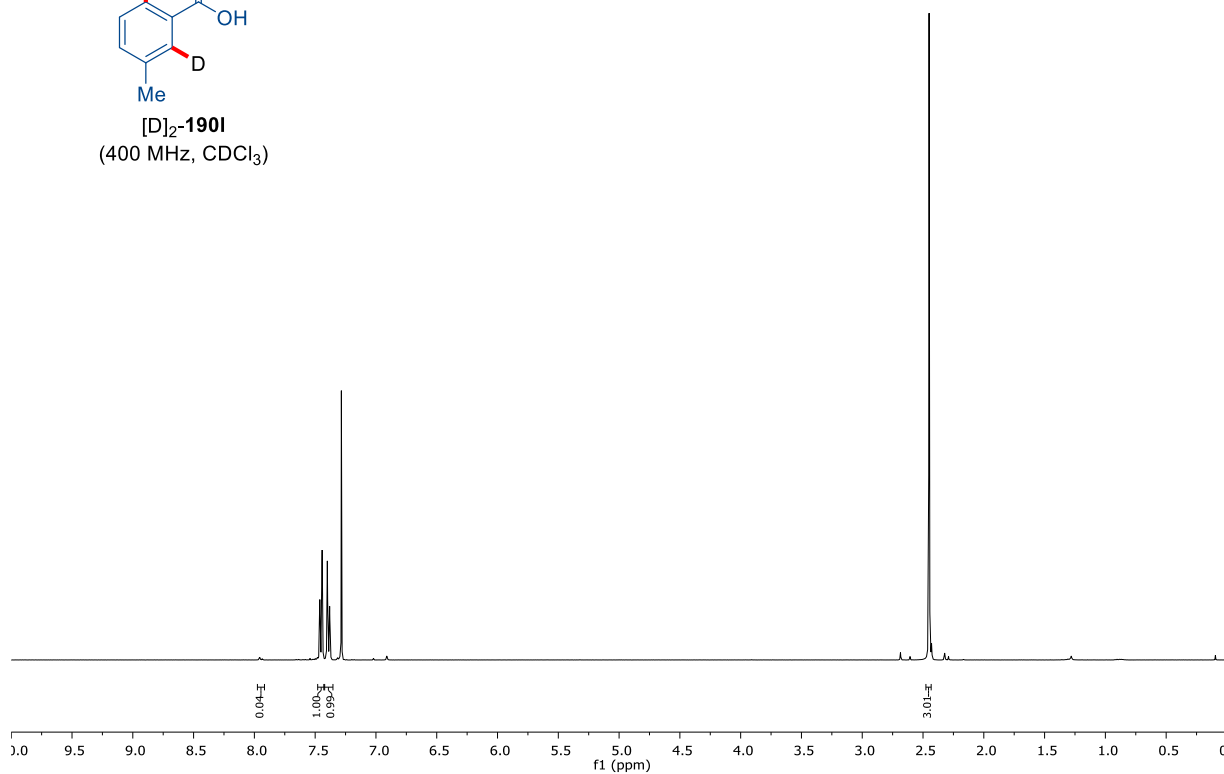
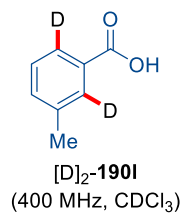
[D]₁-**190i**
(300 MHz, DMSO-*d*₆)



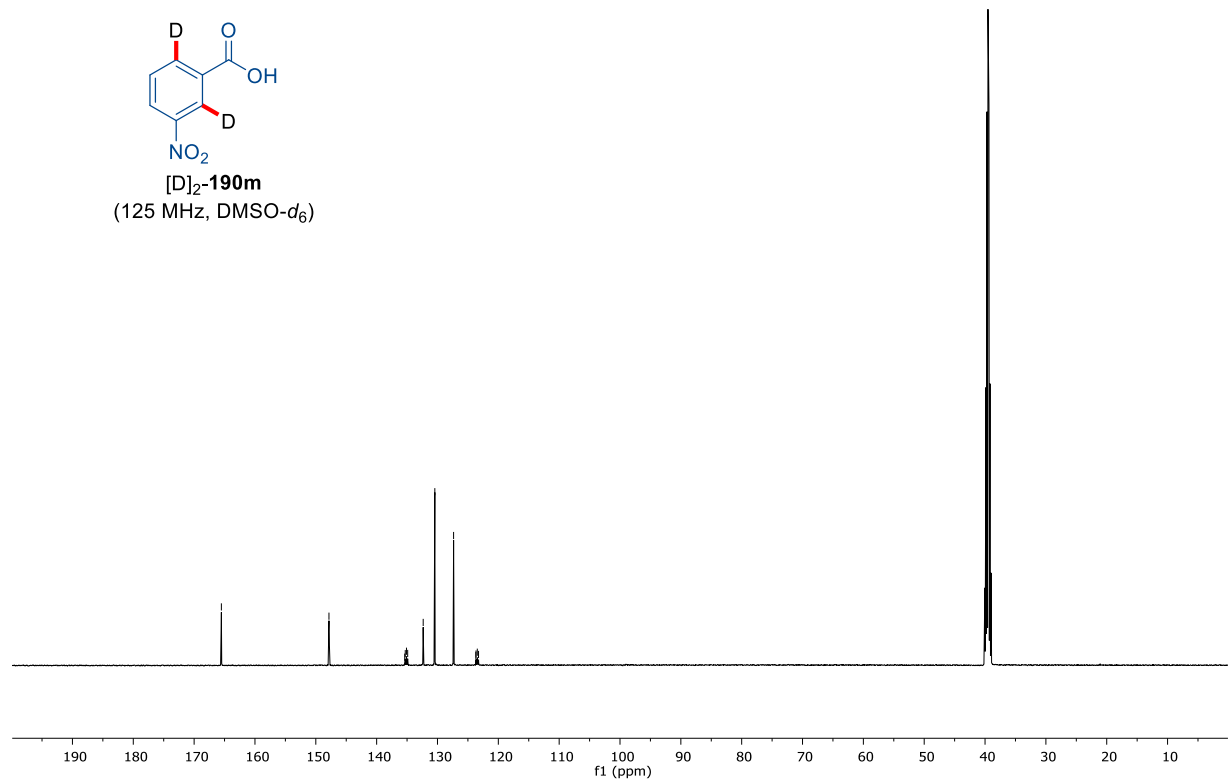
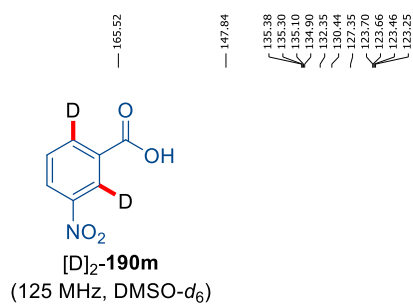
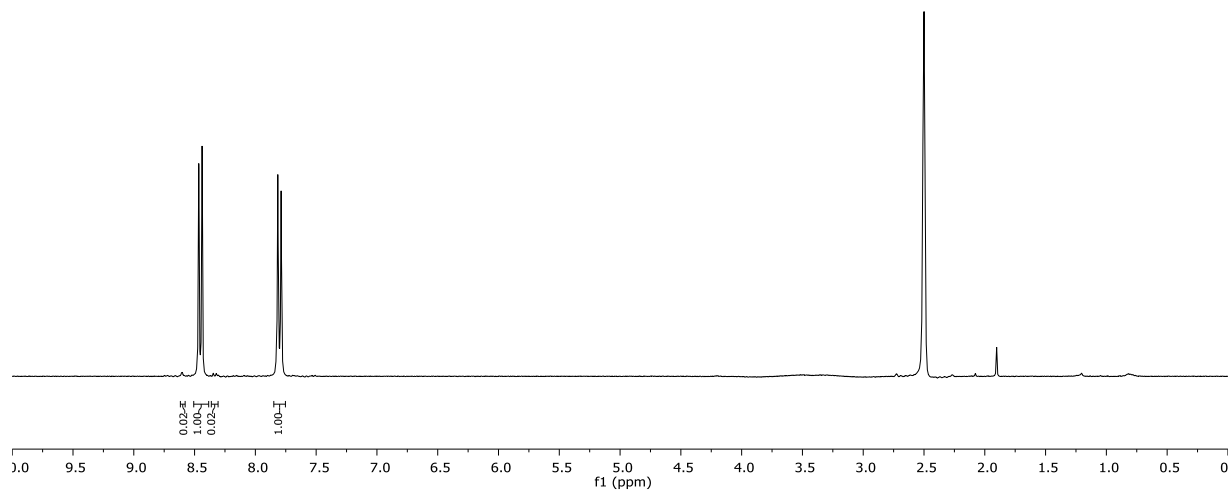
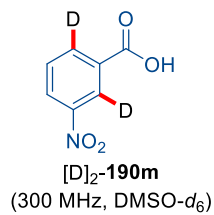


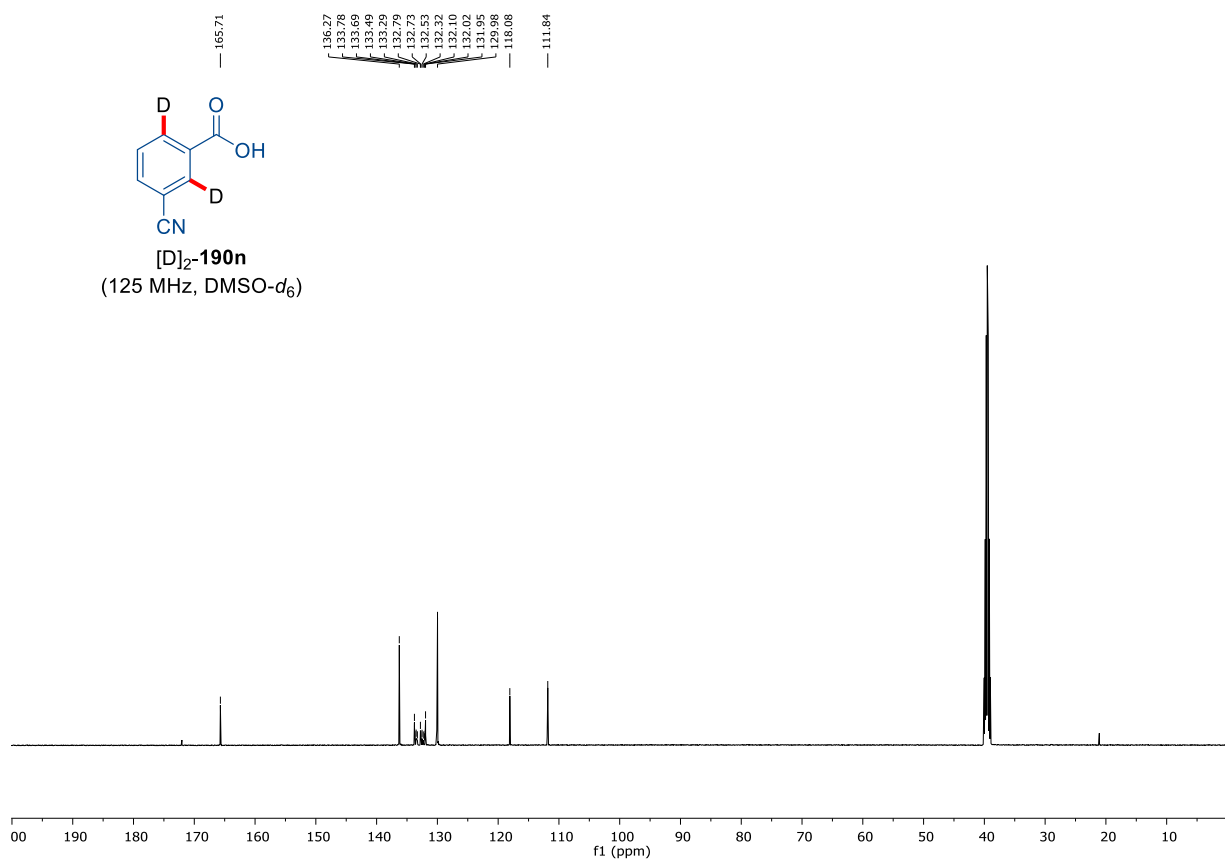
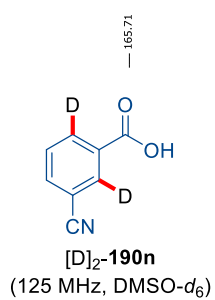
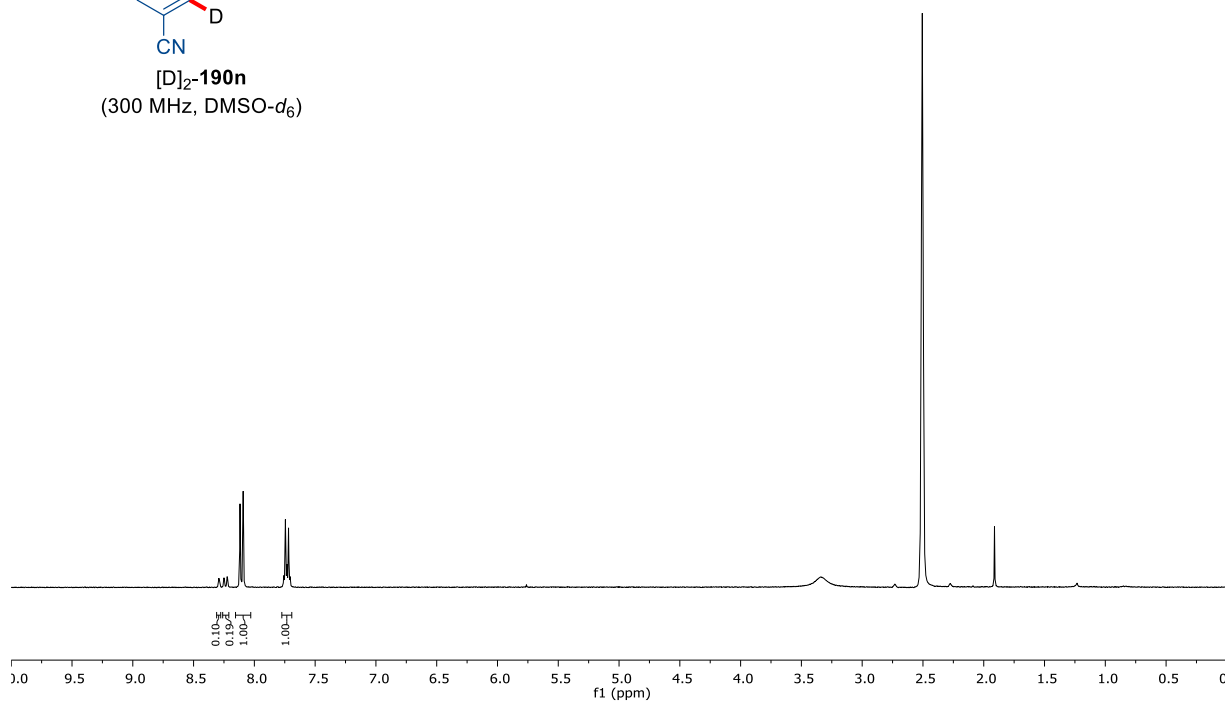
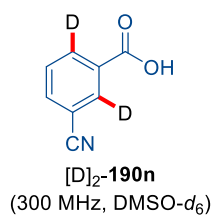
7. Appendix: NMR-Spectra and HPLC Chromatograms



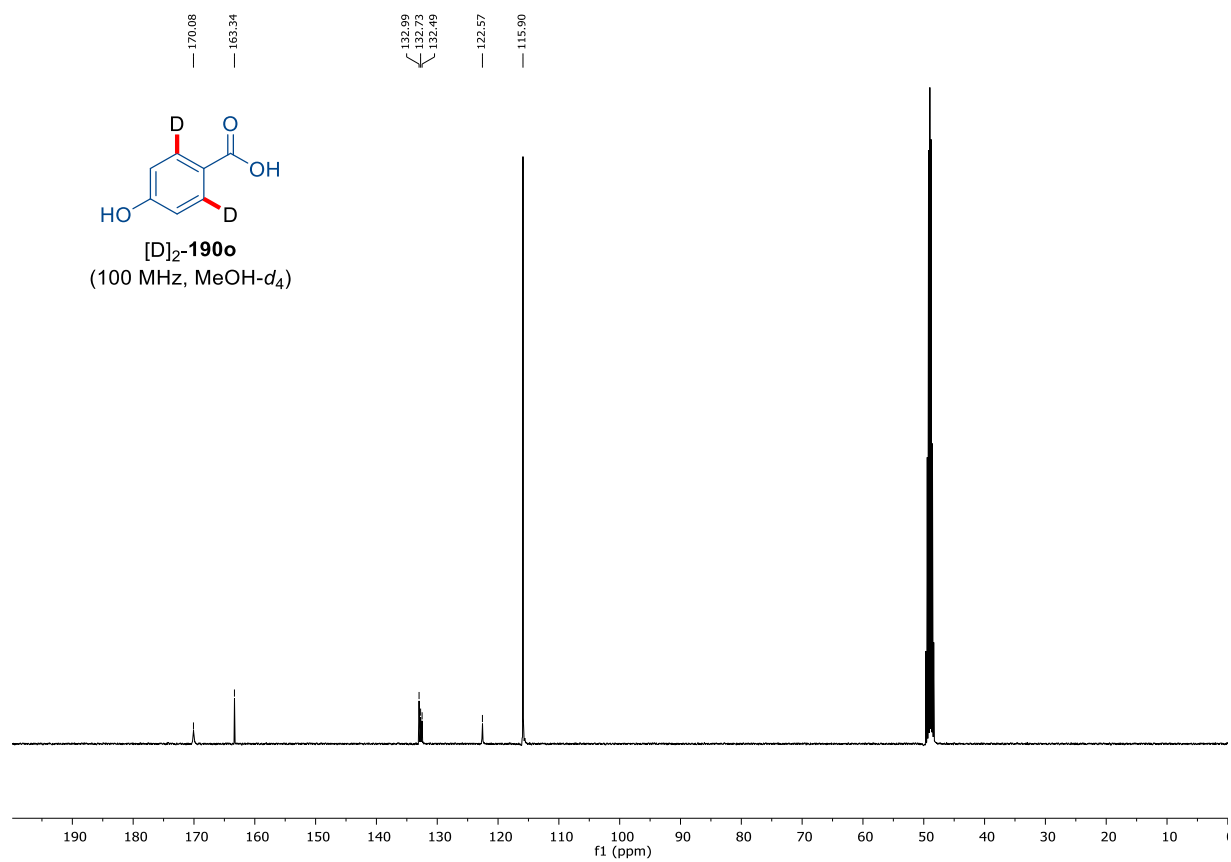
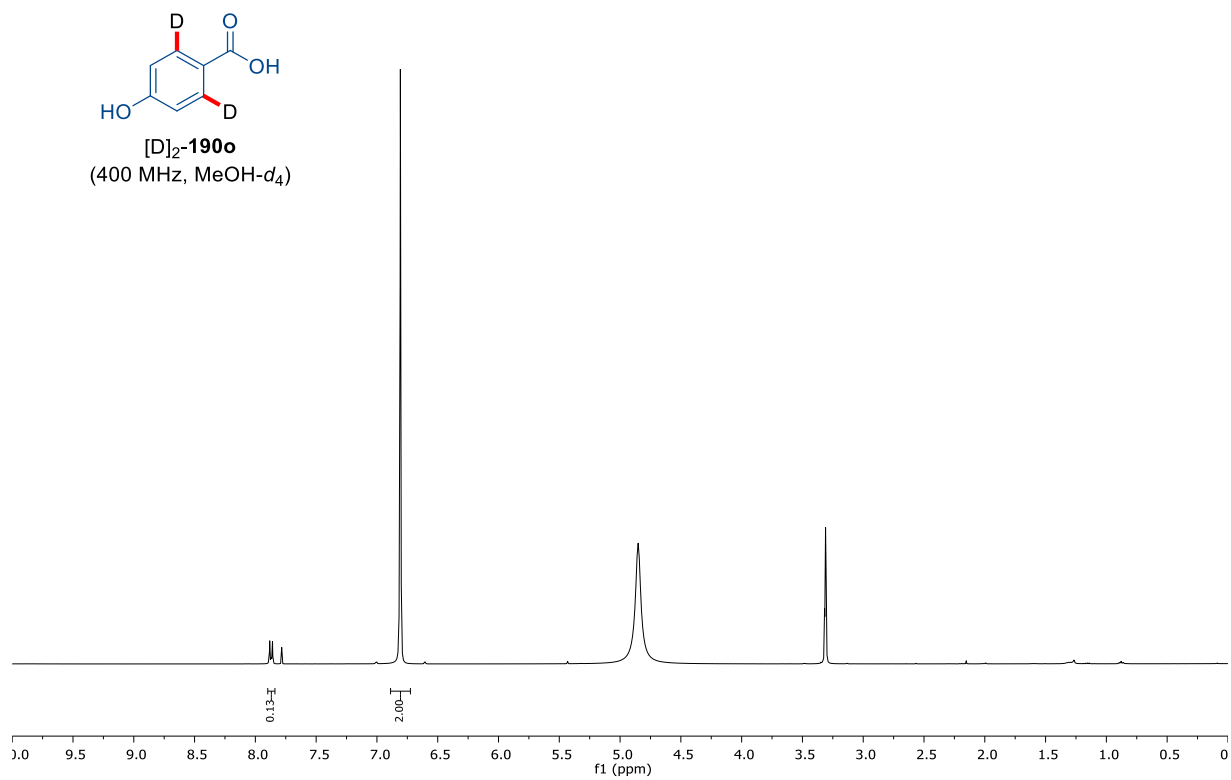


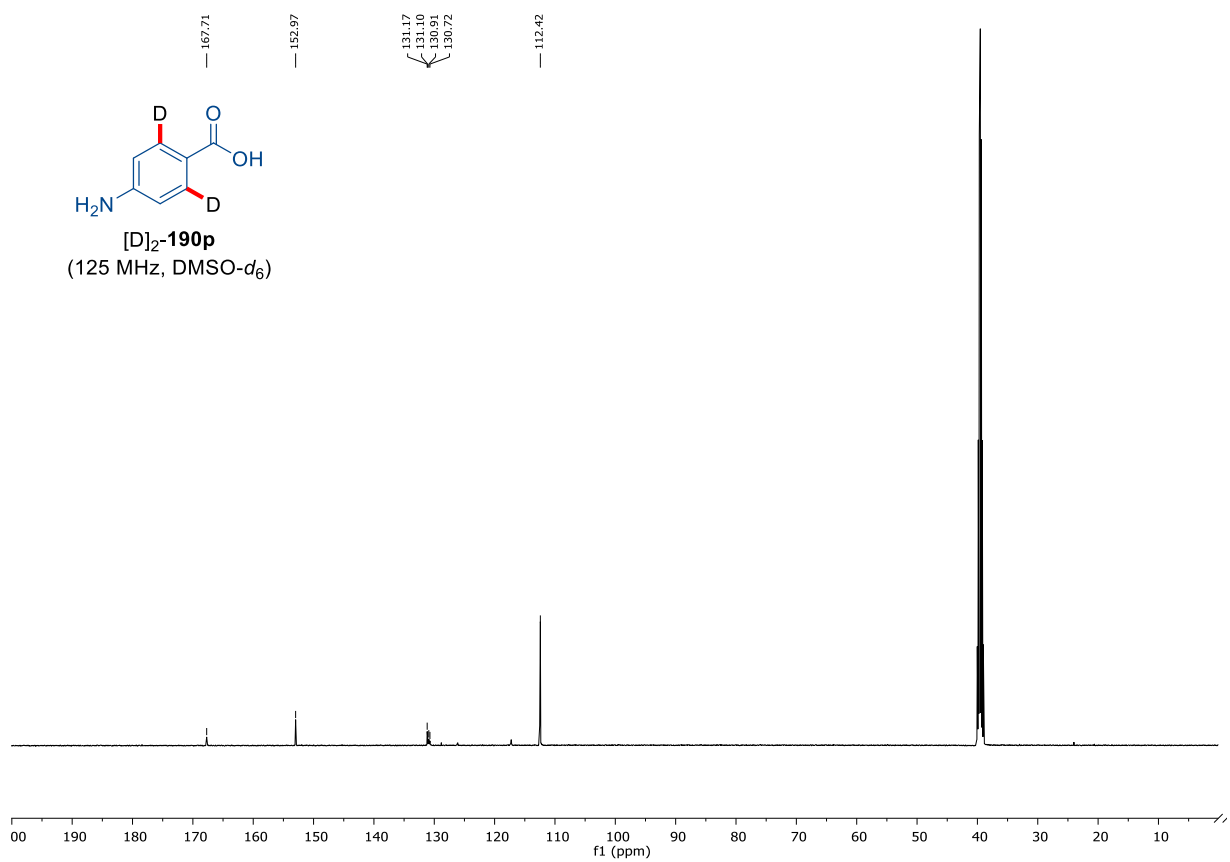
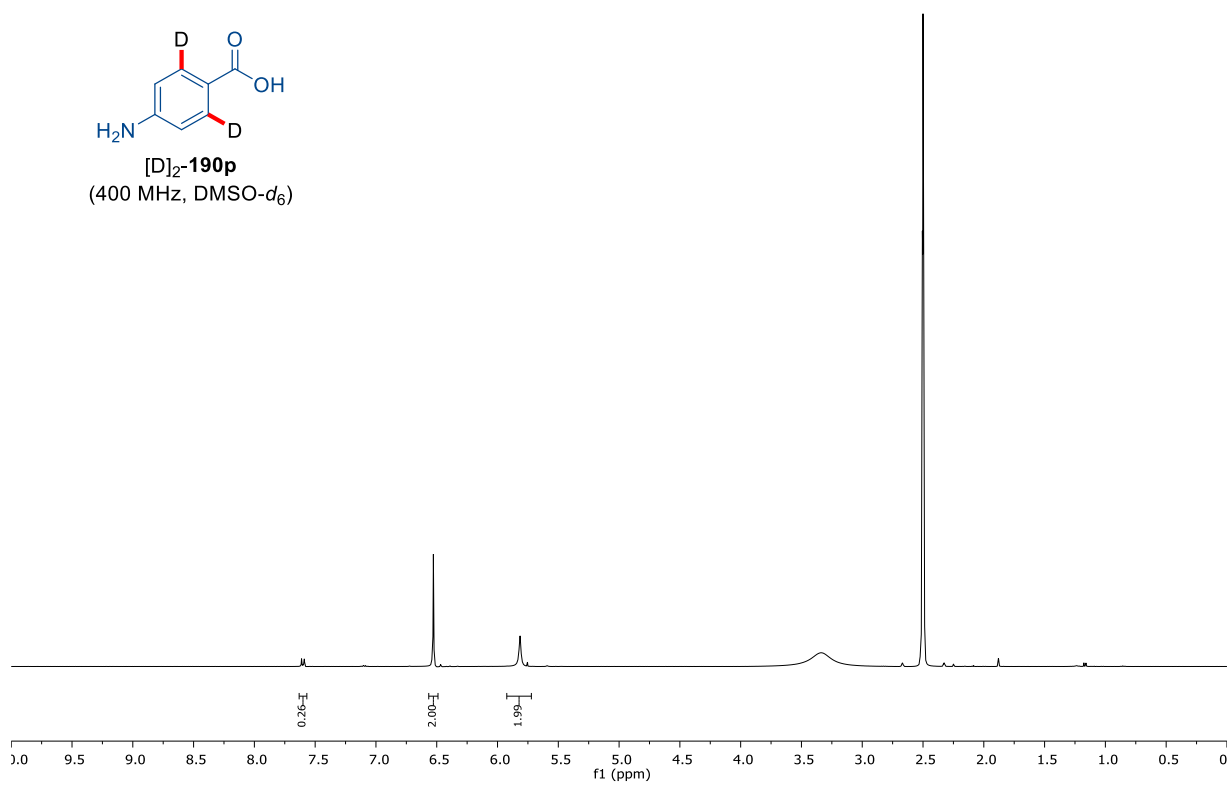
7. Appendix: NMR-Spectra and HPLC Chromatograms



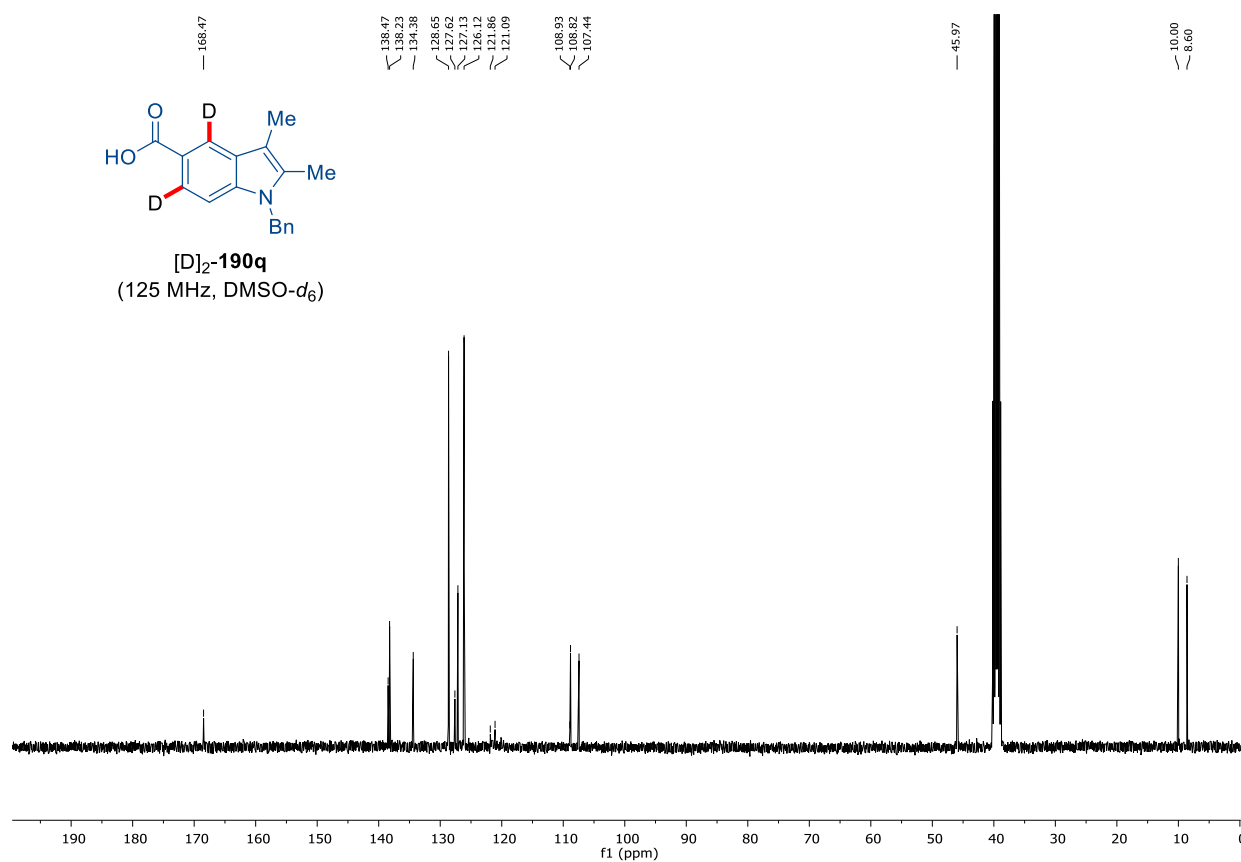
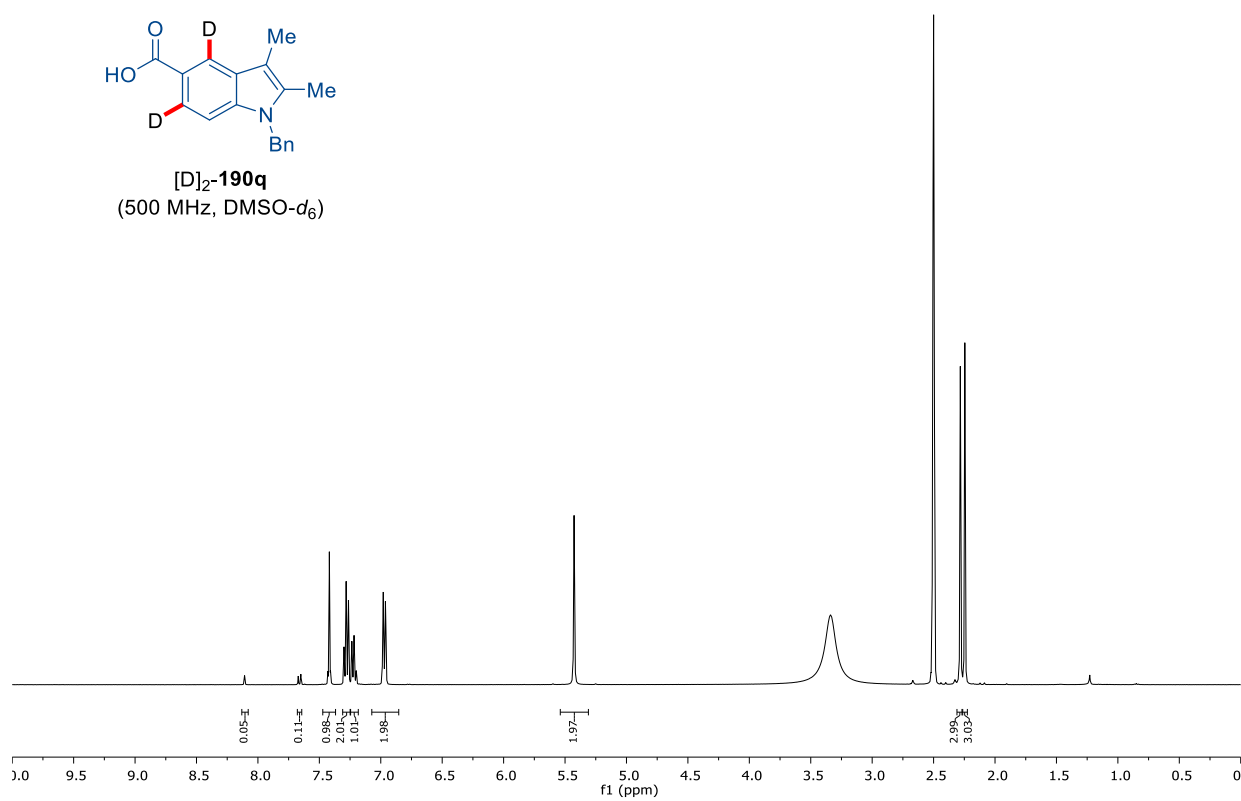


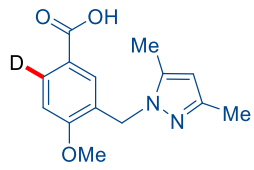
7. Appendix: NMR-Spectra and HPLC Chromatograms



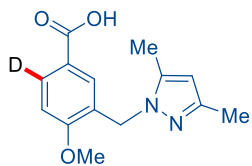
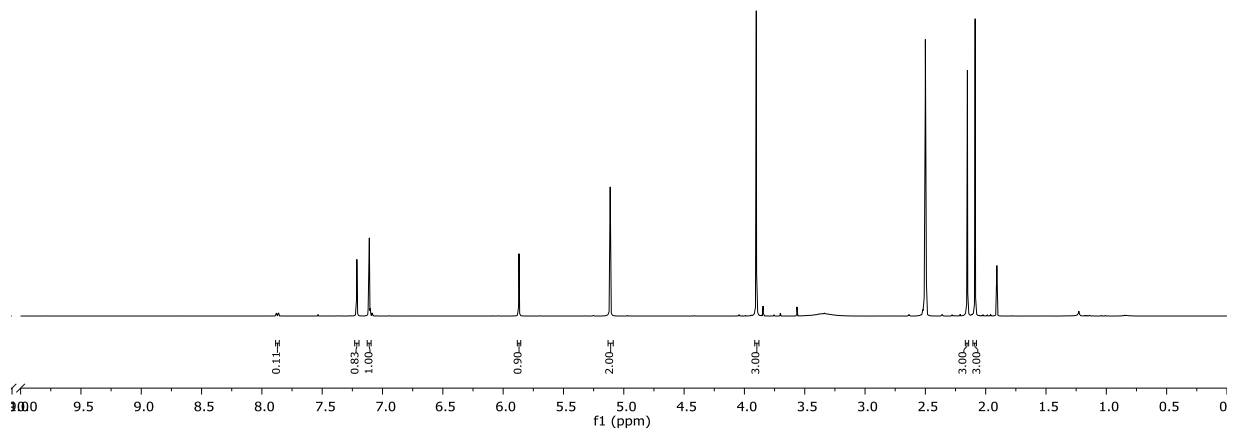


7. Appendix: NMR-Spectra and HPLC Chromatograms

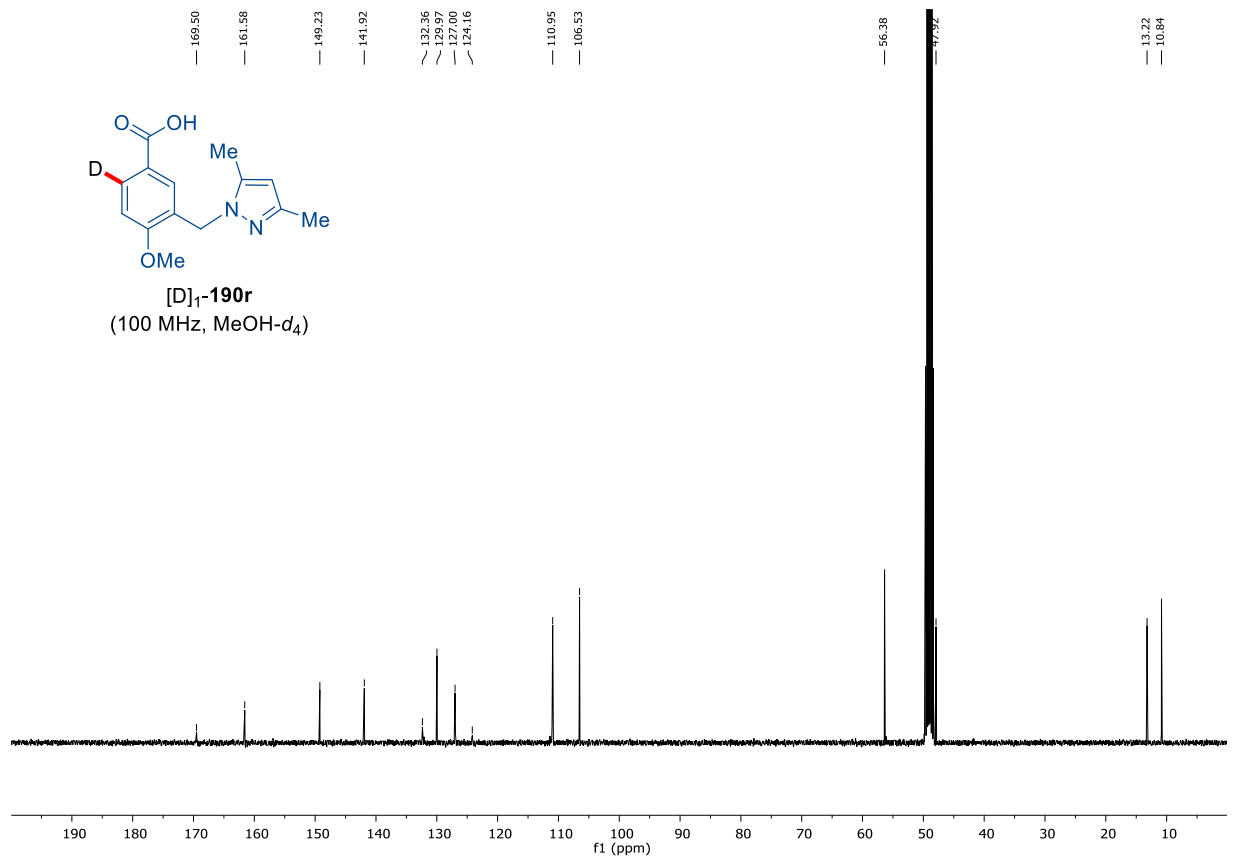




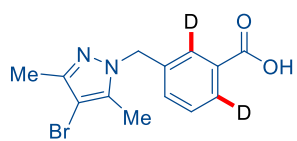
[D]₁-190r
(500 MHz, DMSO-d₆)



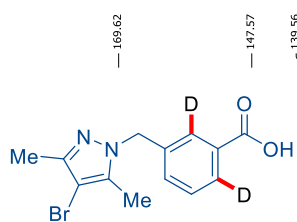
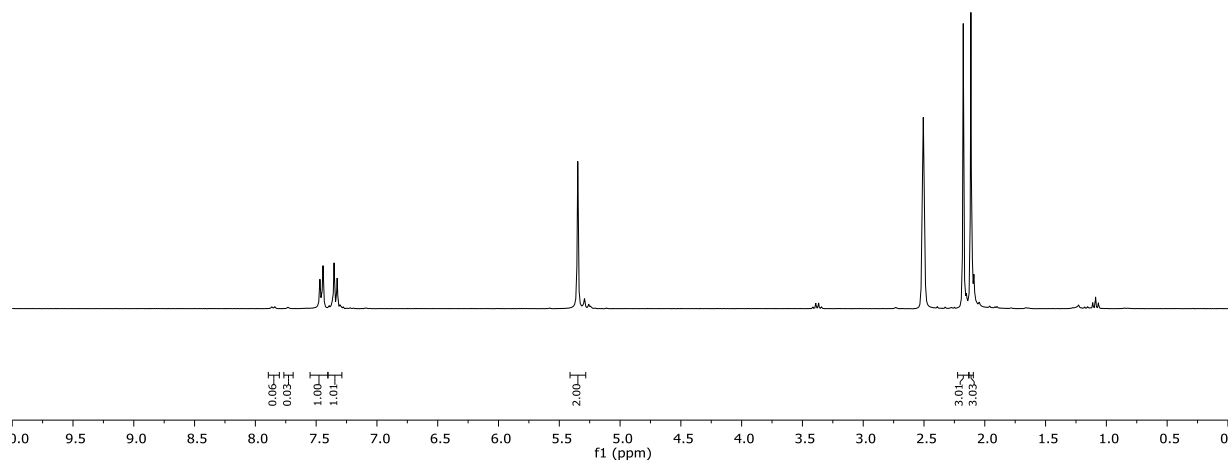
[D]₁-190r
(100 MHz, MeOH-d₄)



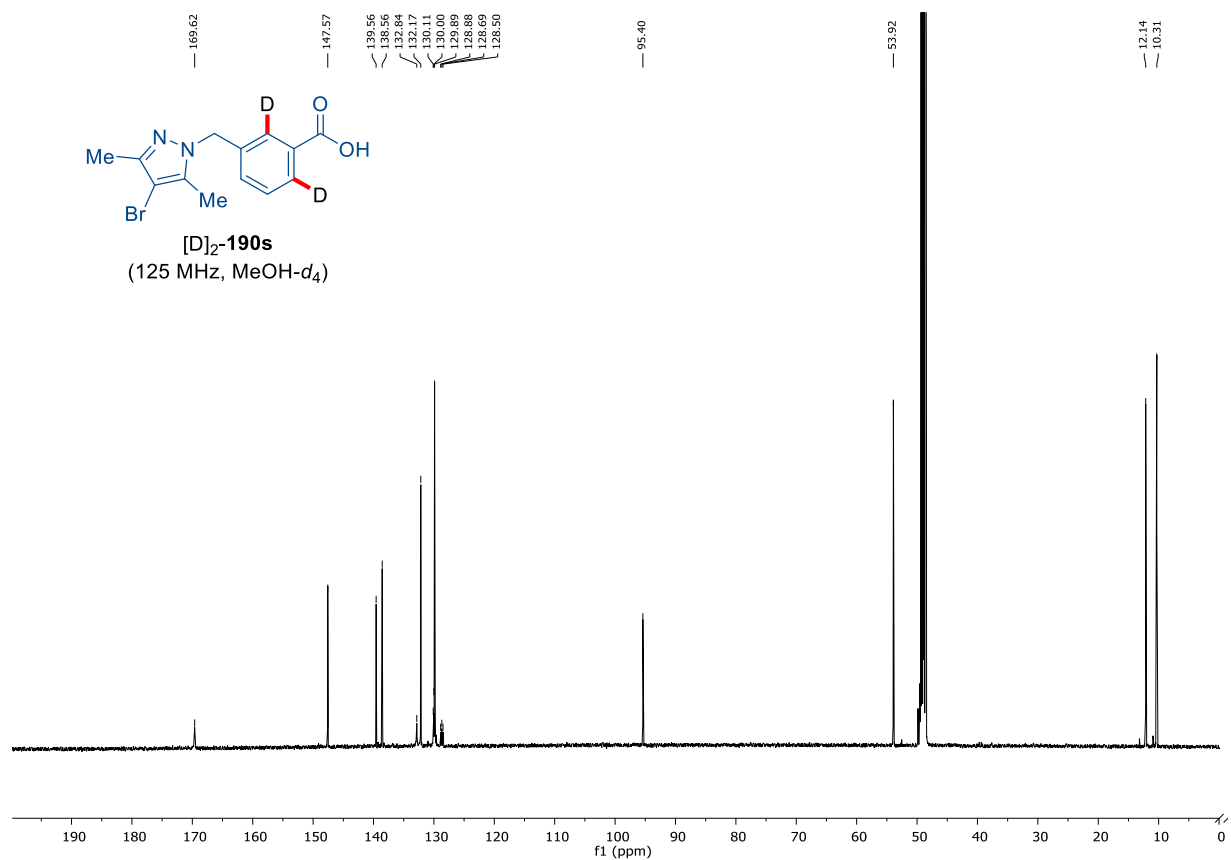
7. Appendix: NMR-Spectra and HPLC Chromatograms

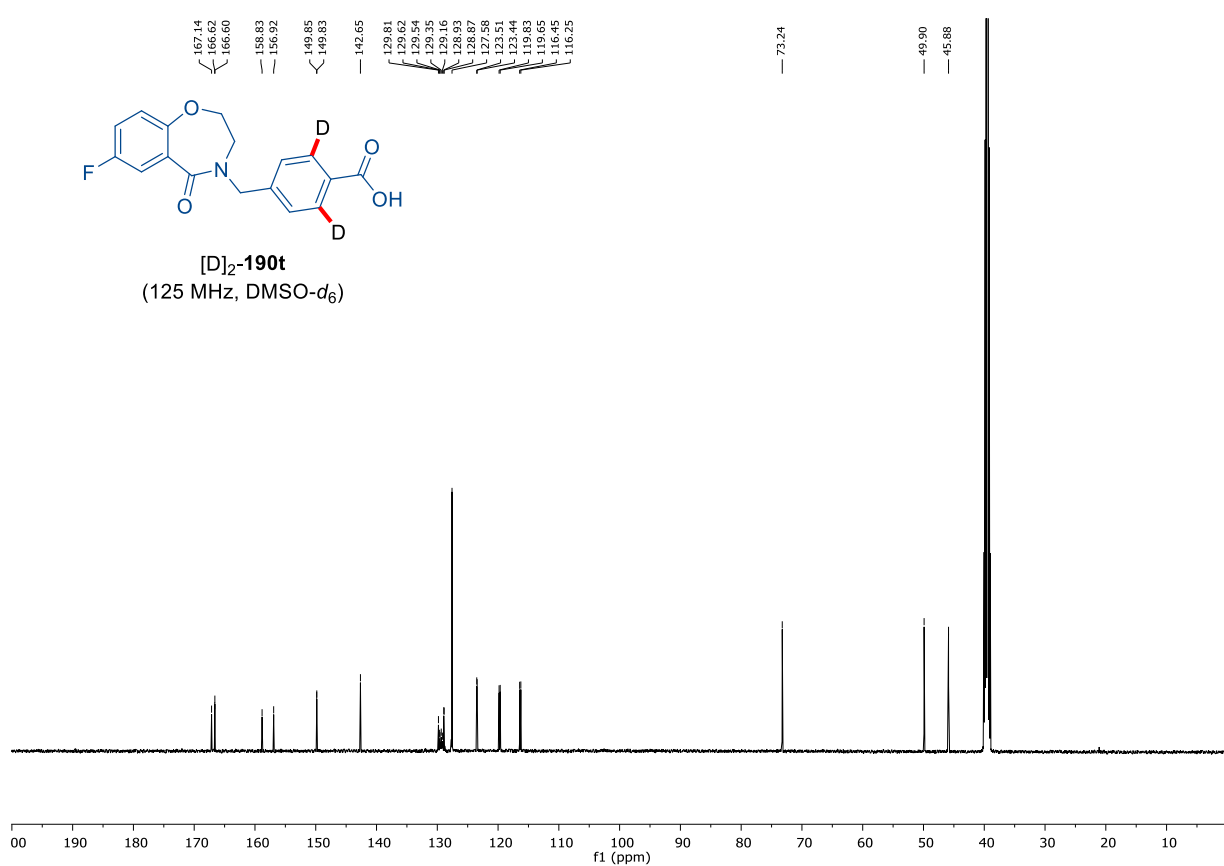
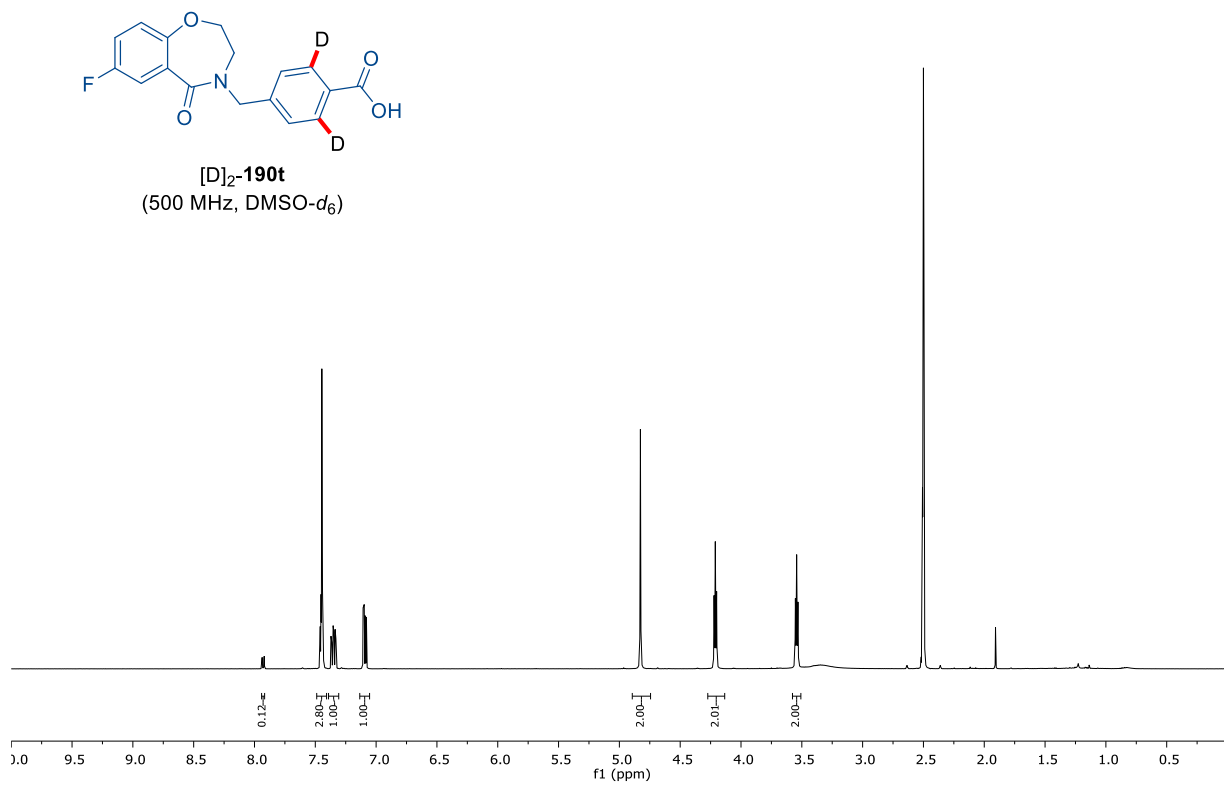


[D]₂-190s
(300 MHz, DMSO-*d*₆)

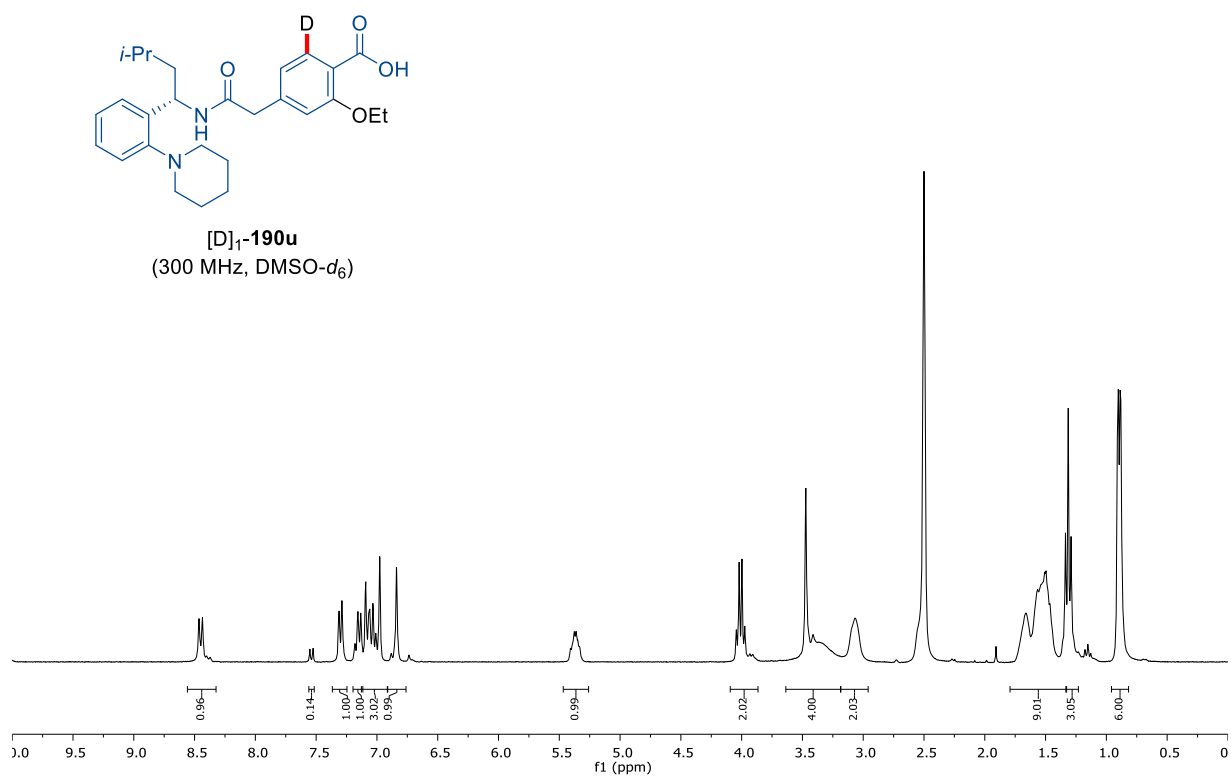
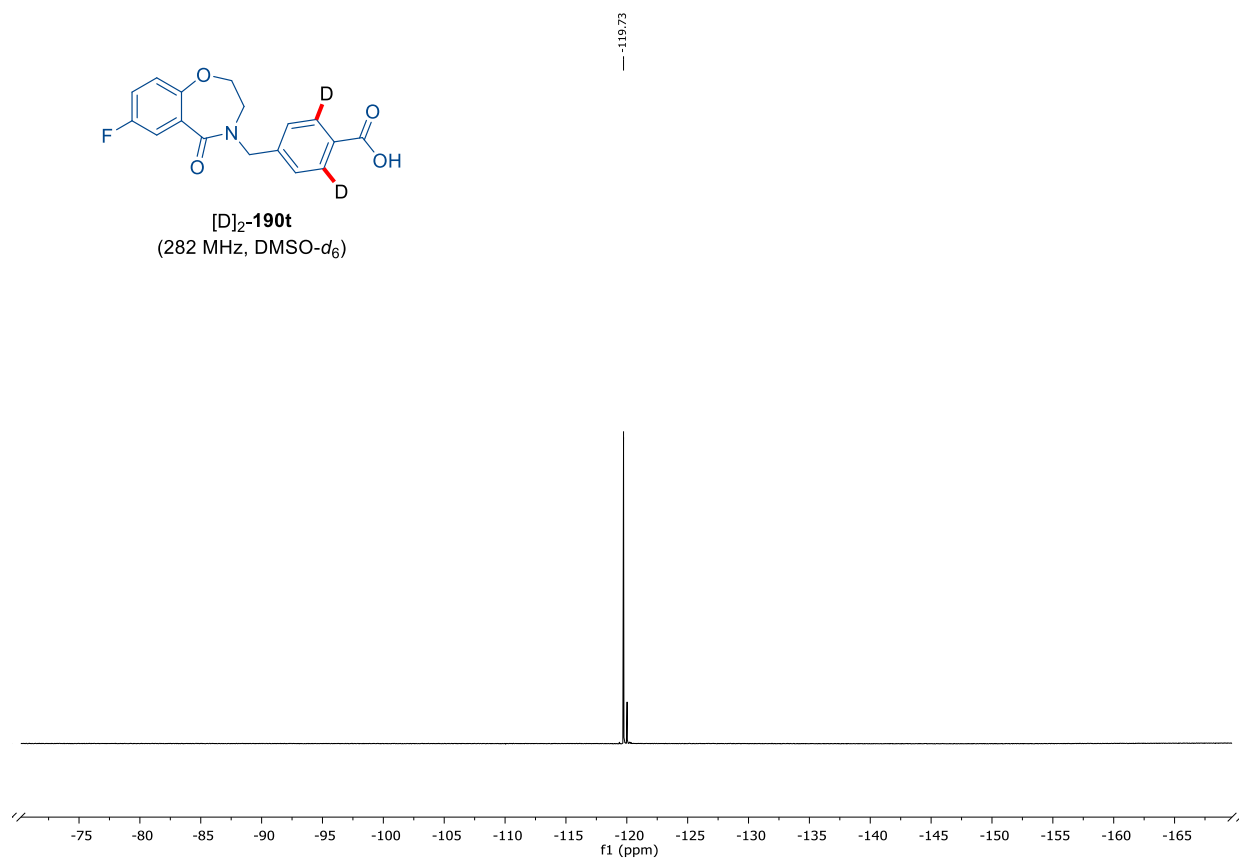


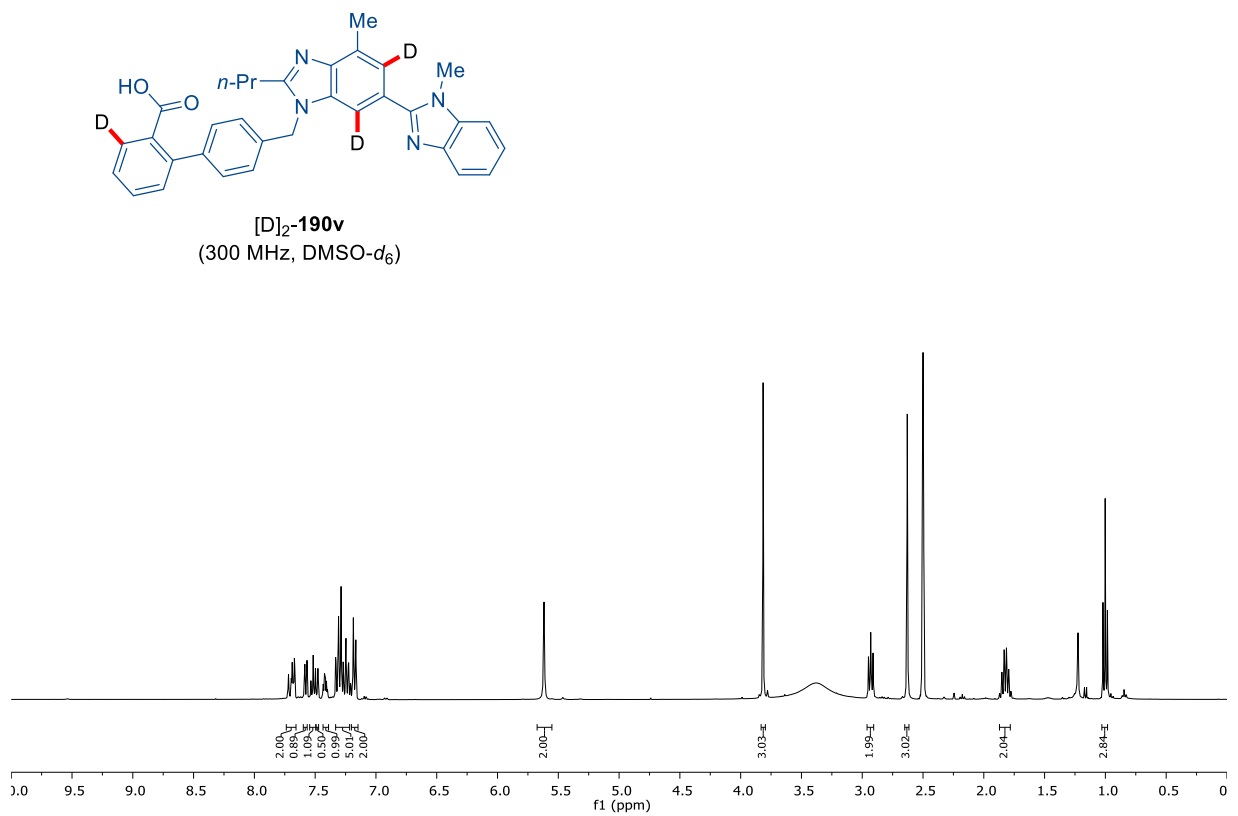
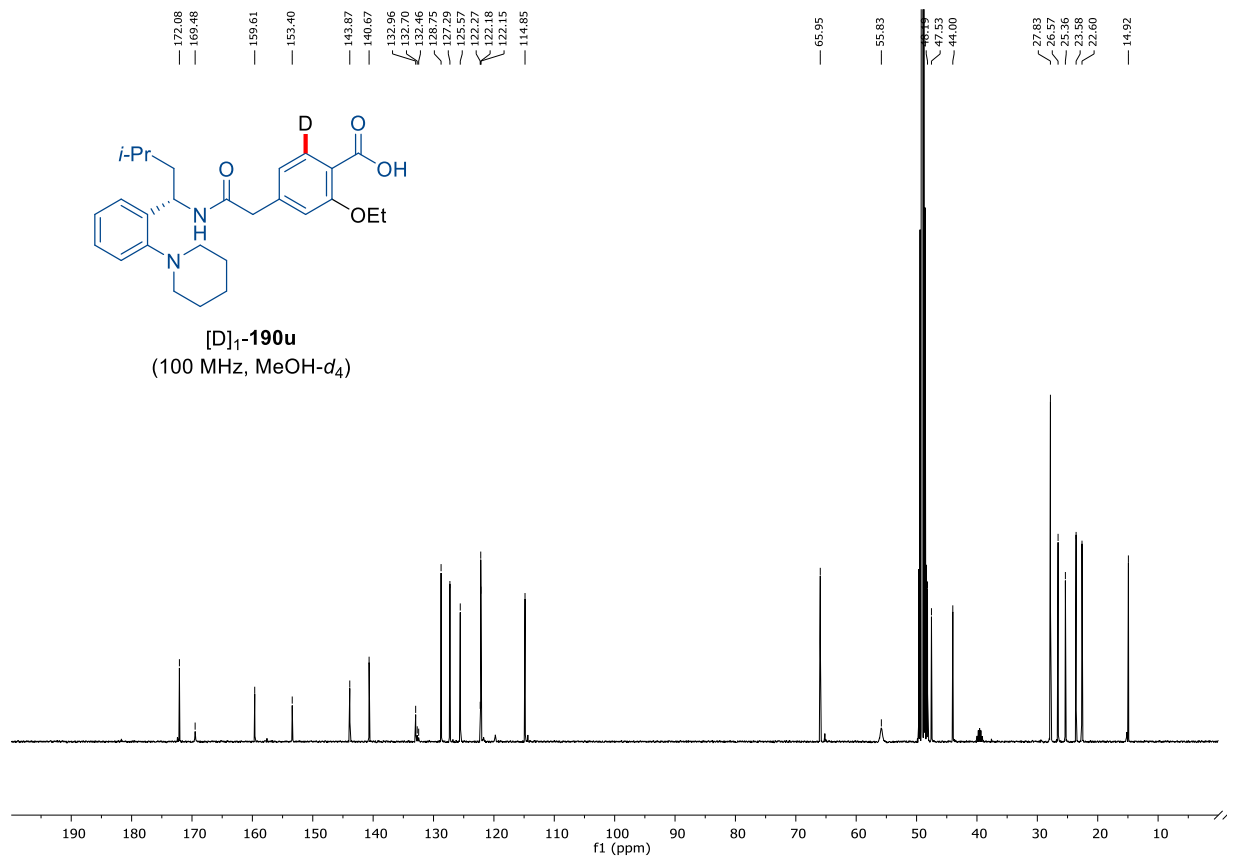
[D]₂-190s
(125 MHz, MeOH-*d*₄)



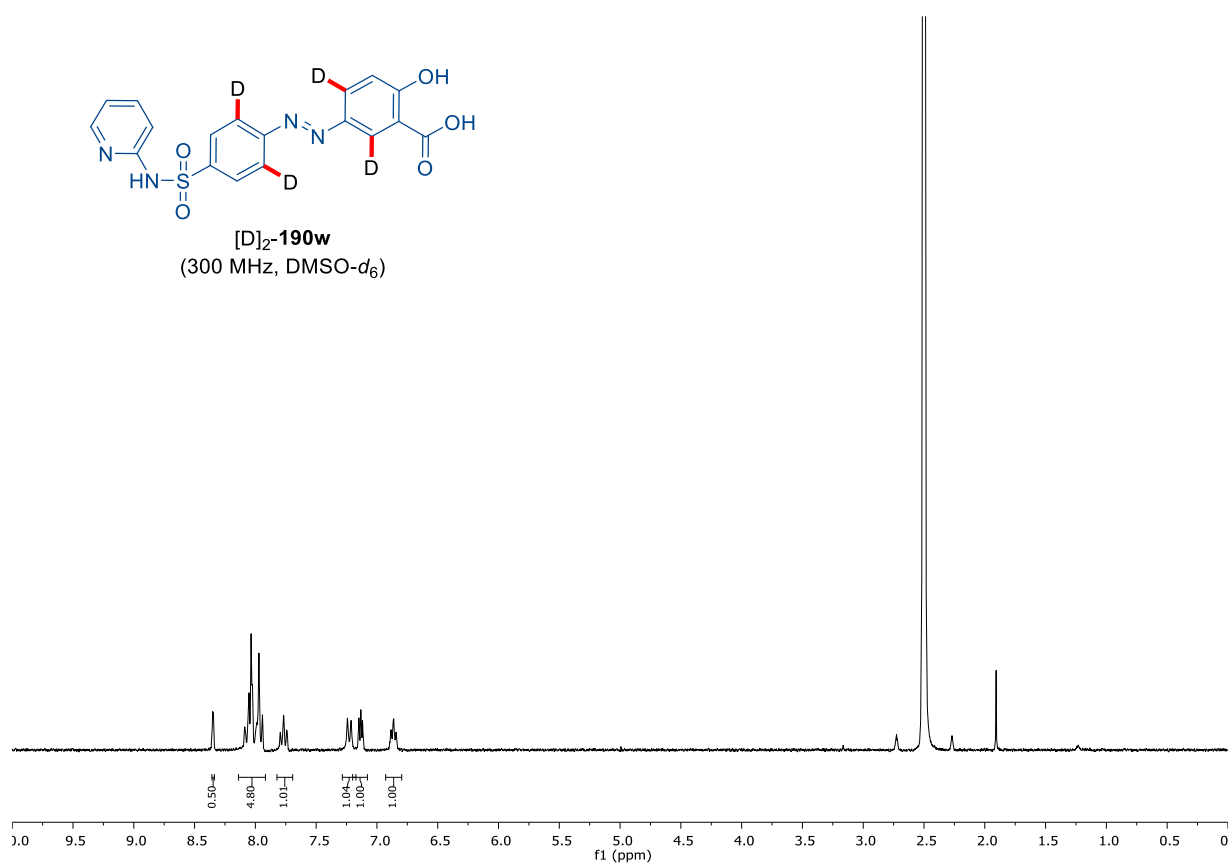
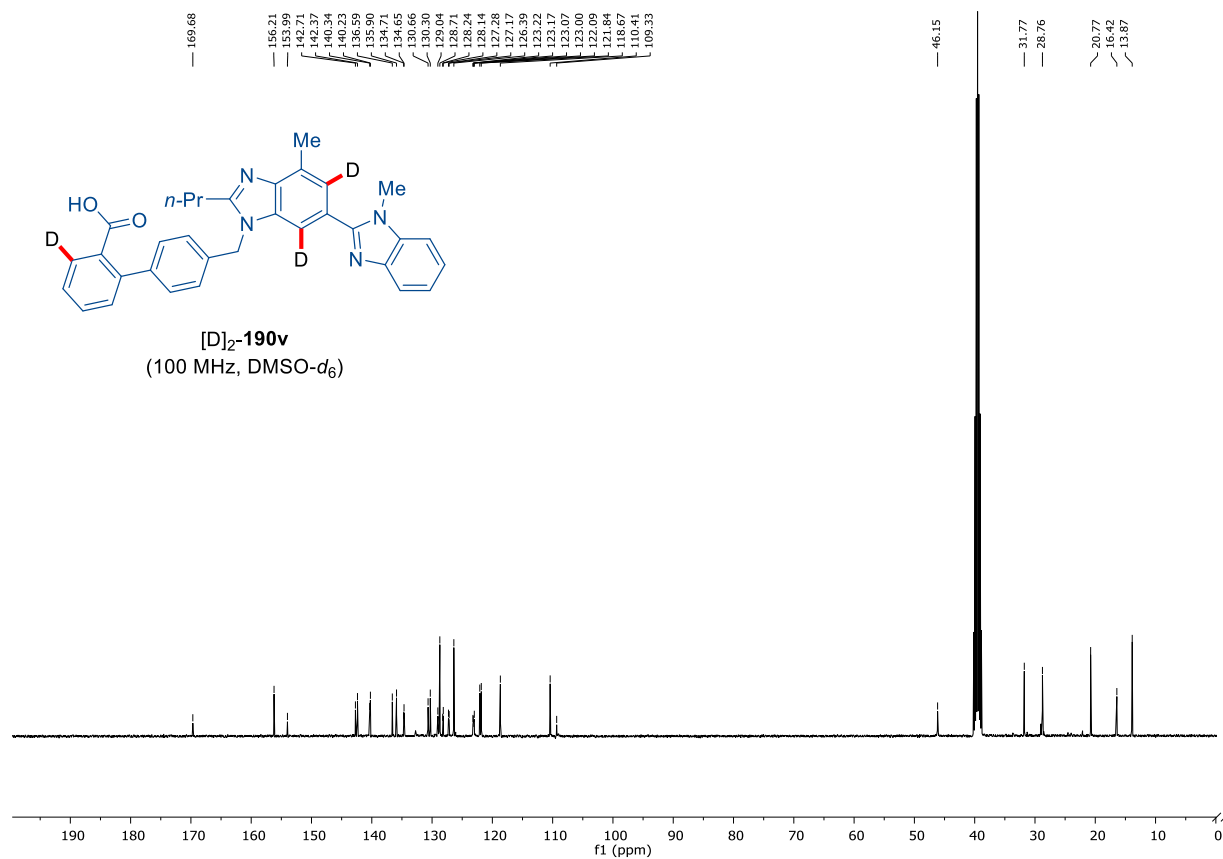


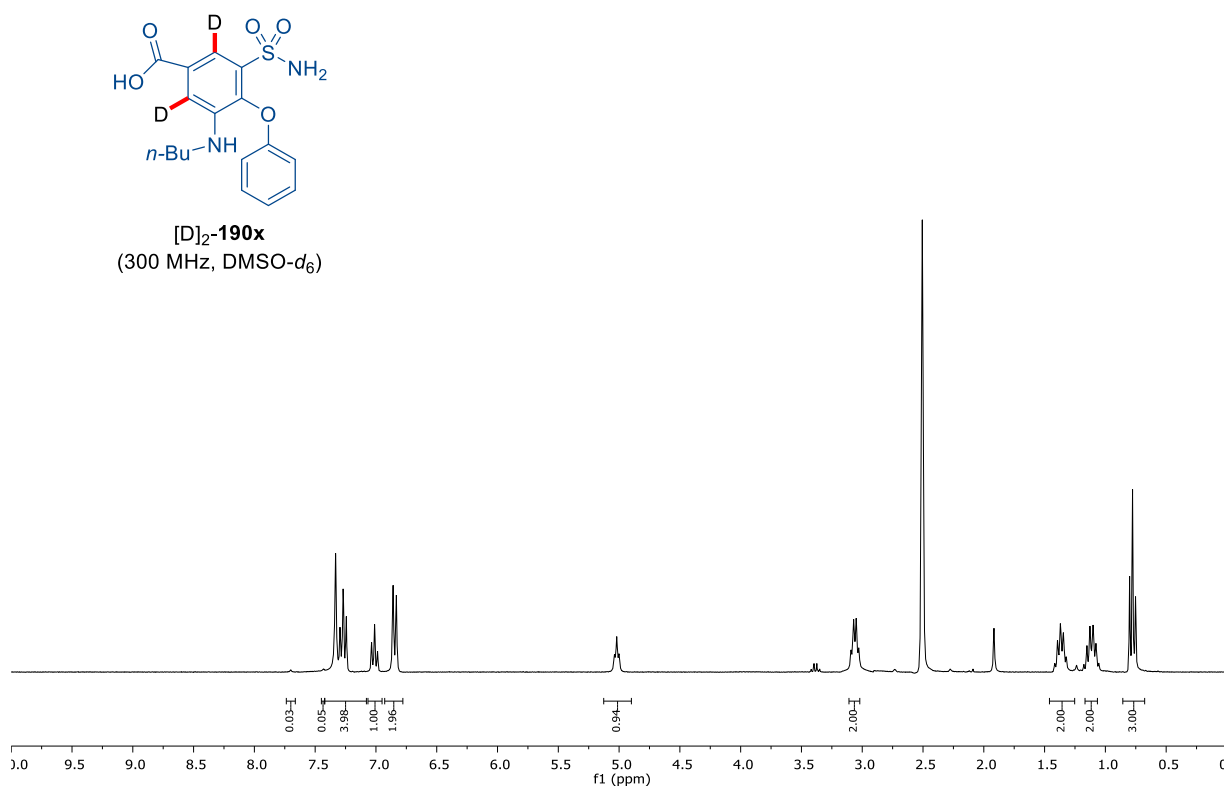
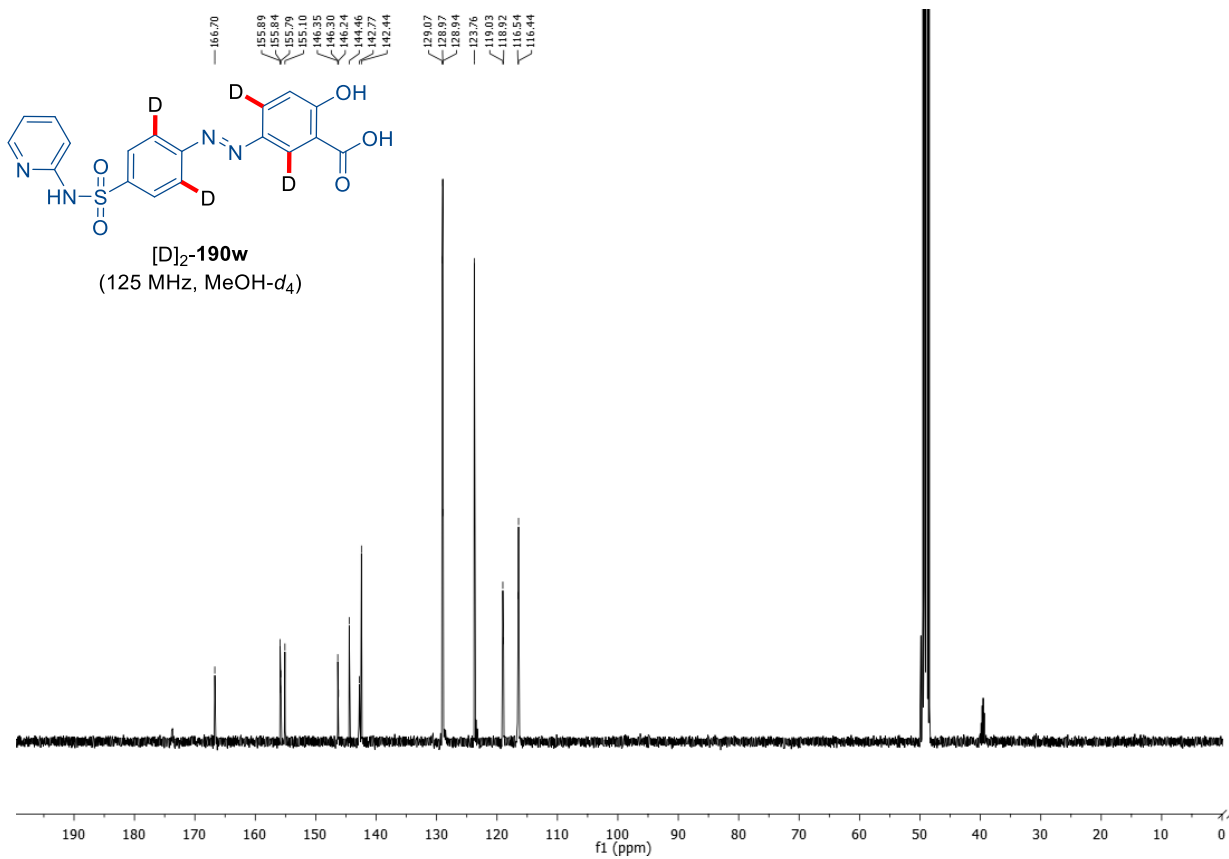
7. Appendix: NMR-Spectra and HPLC Chromatograms



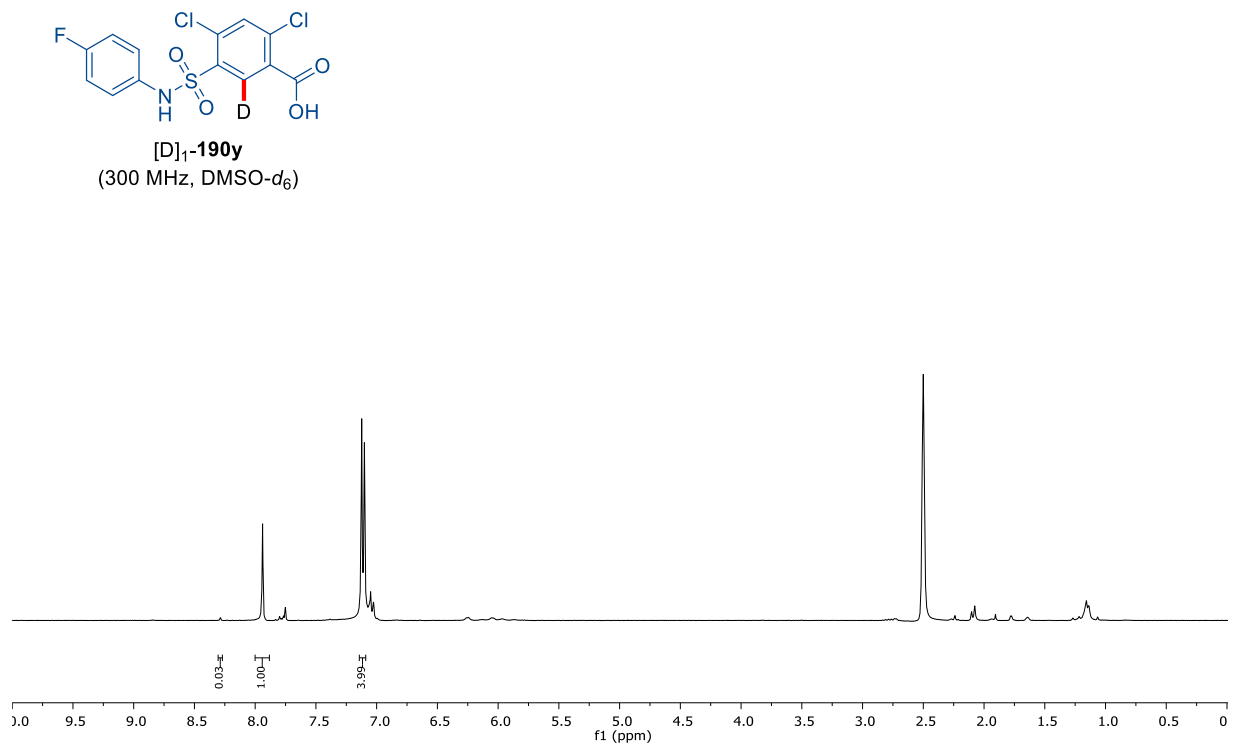
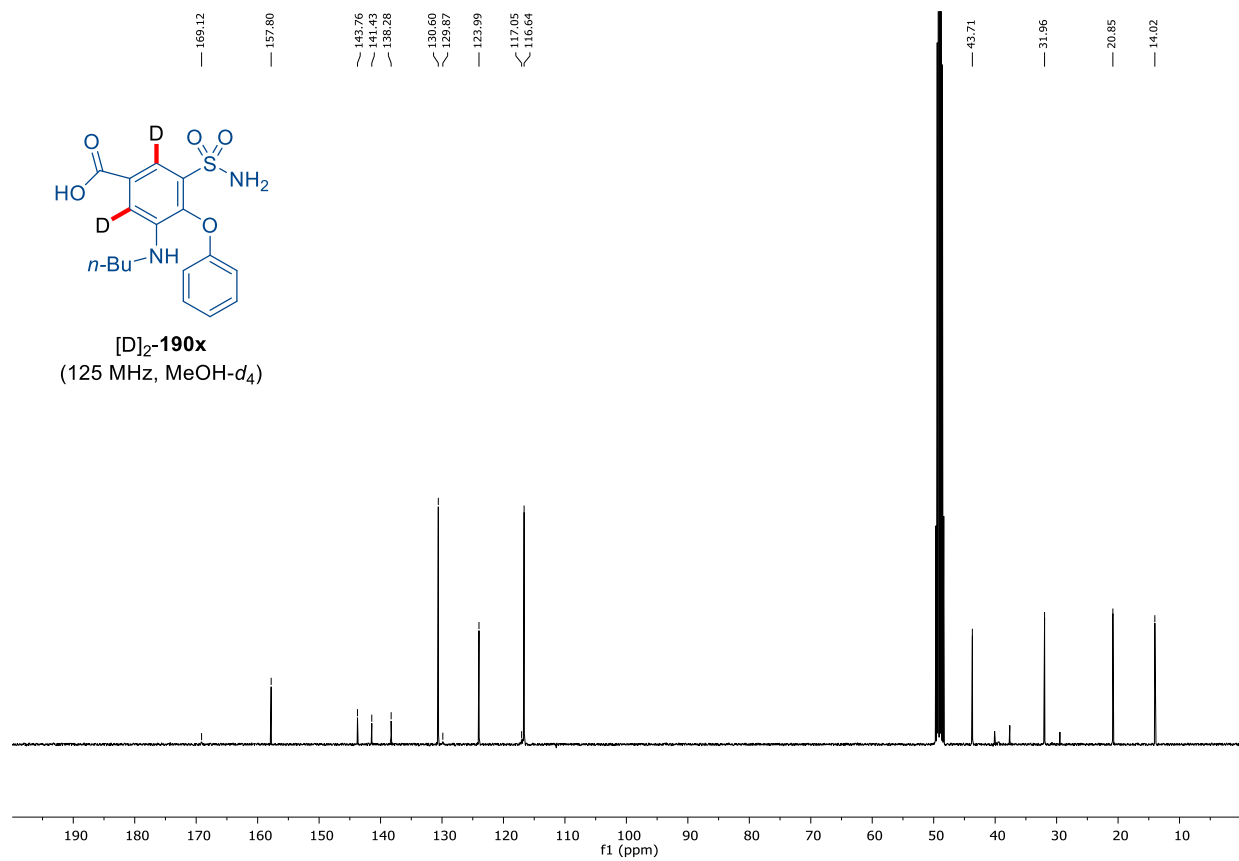


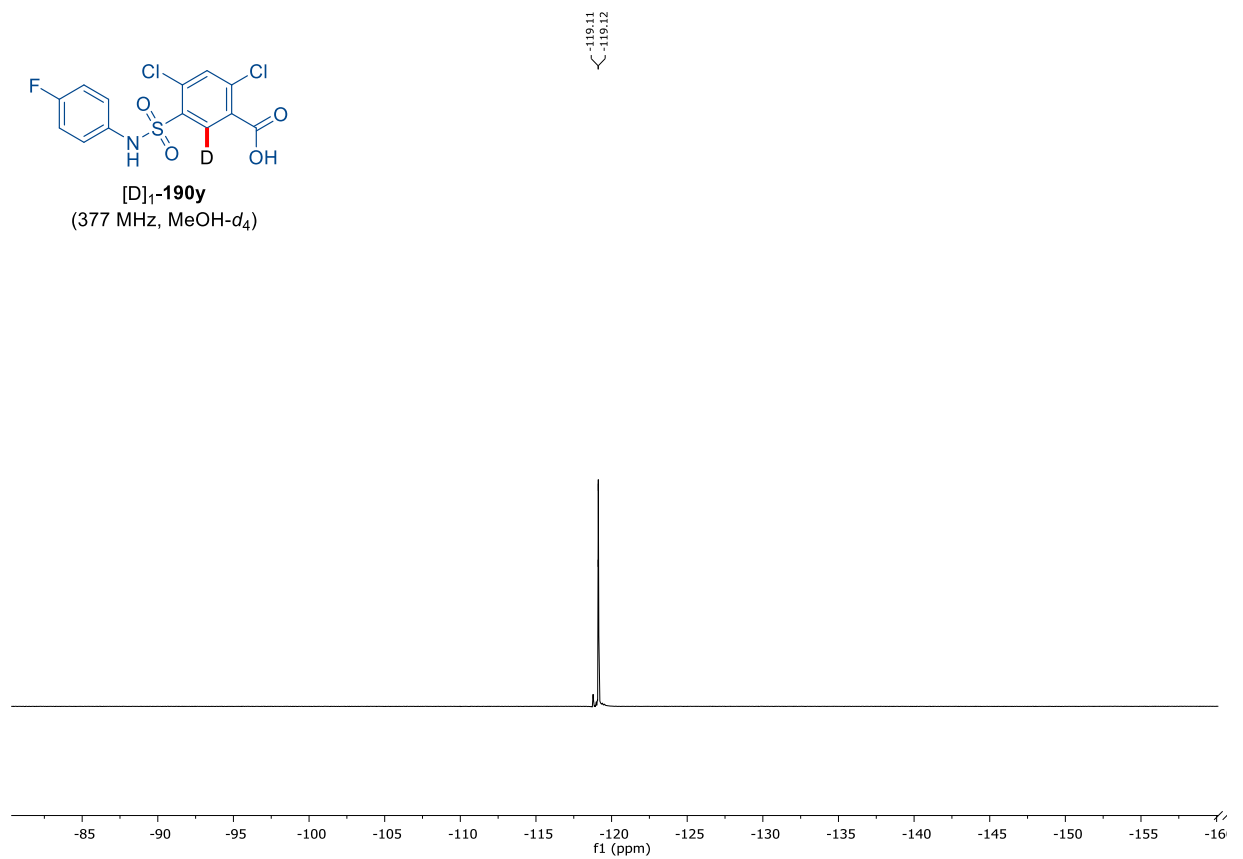
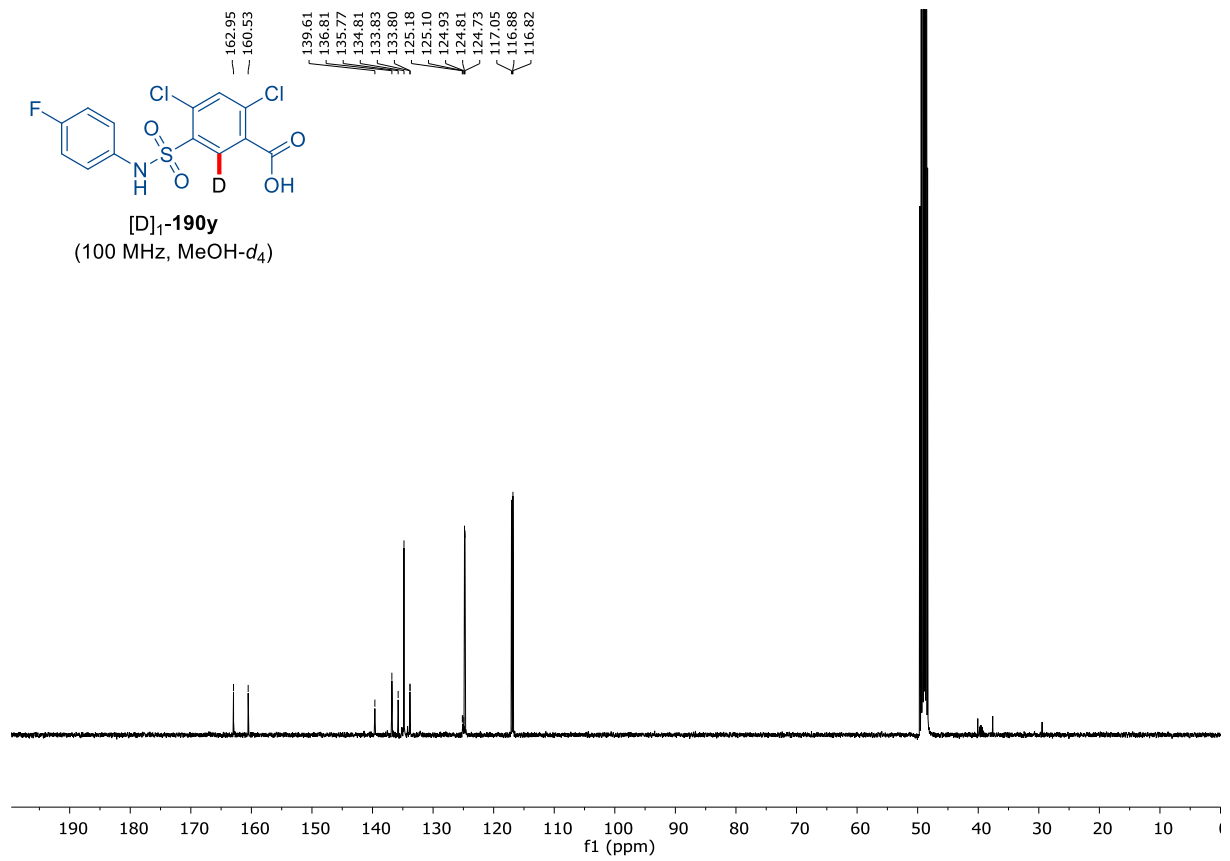
7. Appendix: NMR-Spectra and HPLC Chromatograms



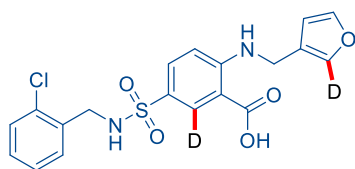


7. Appendix: NMR-Spectra and HPLC Chromatograms

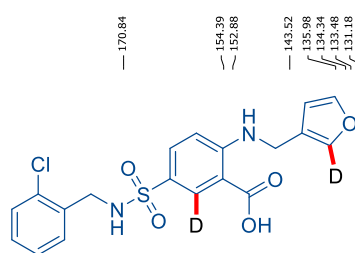
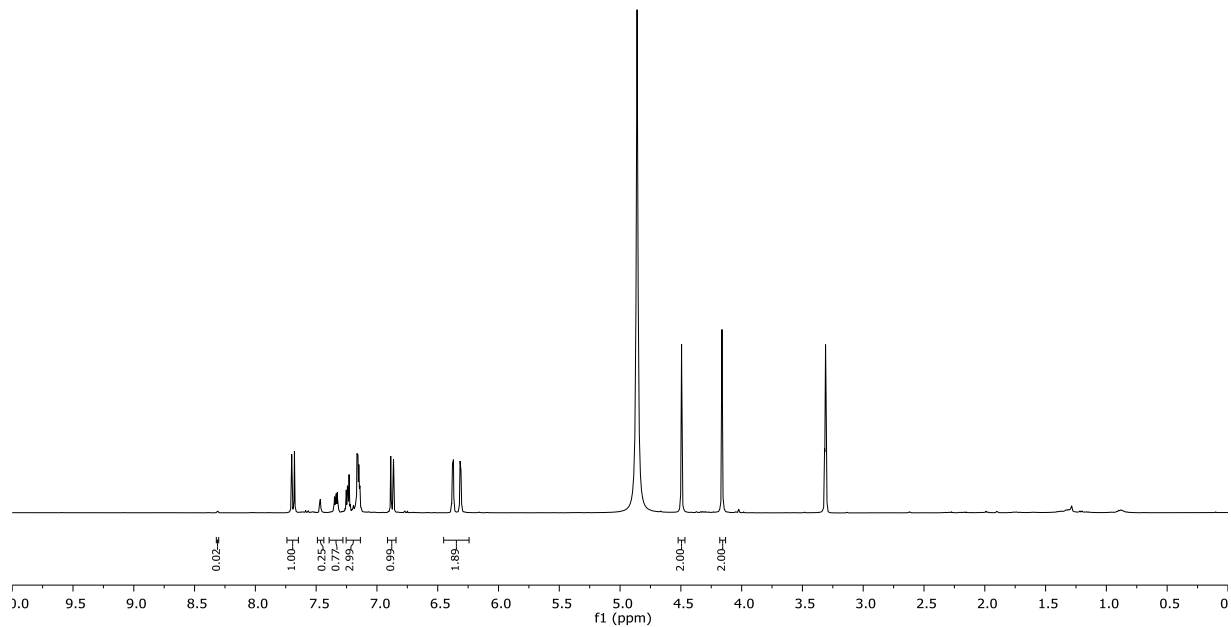




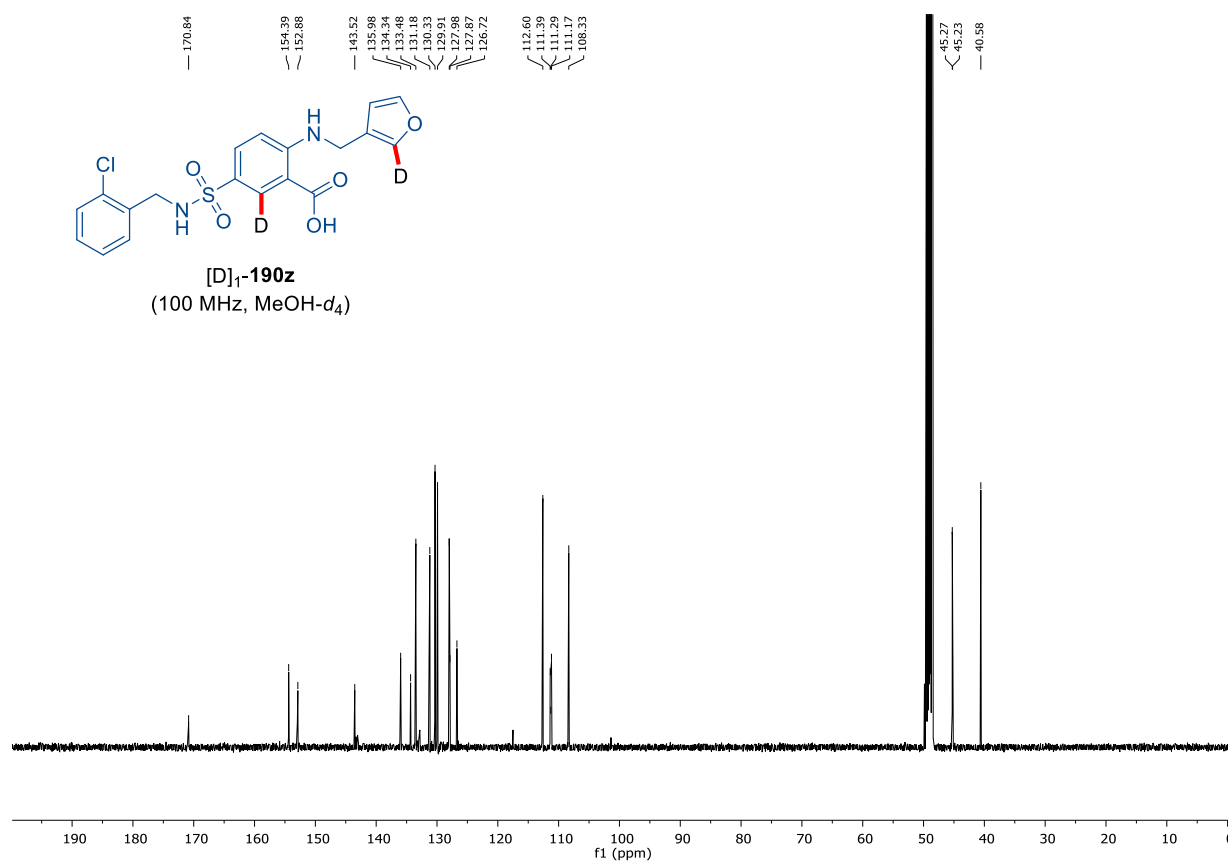
7. Appendix: NMR-Spectra and HPLC Chromatograms

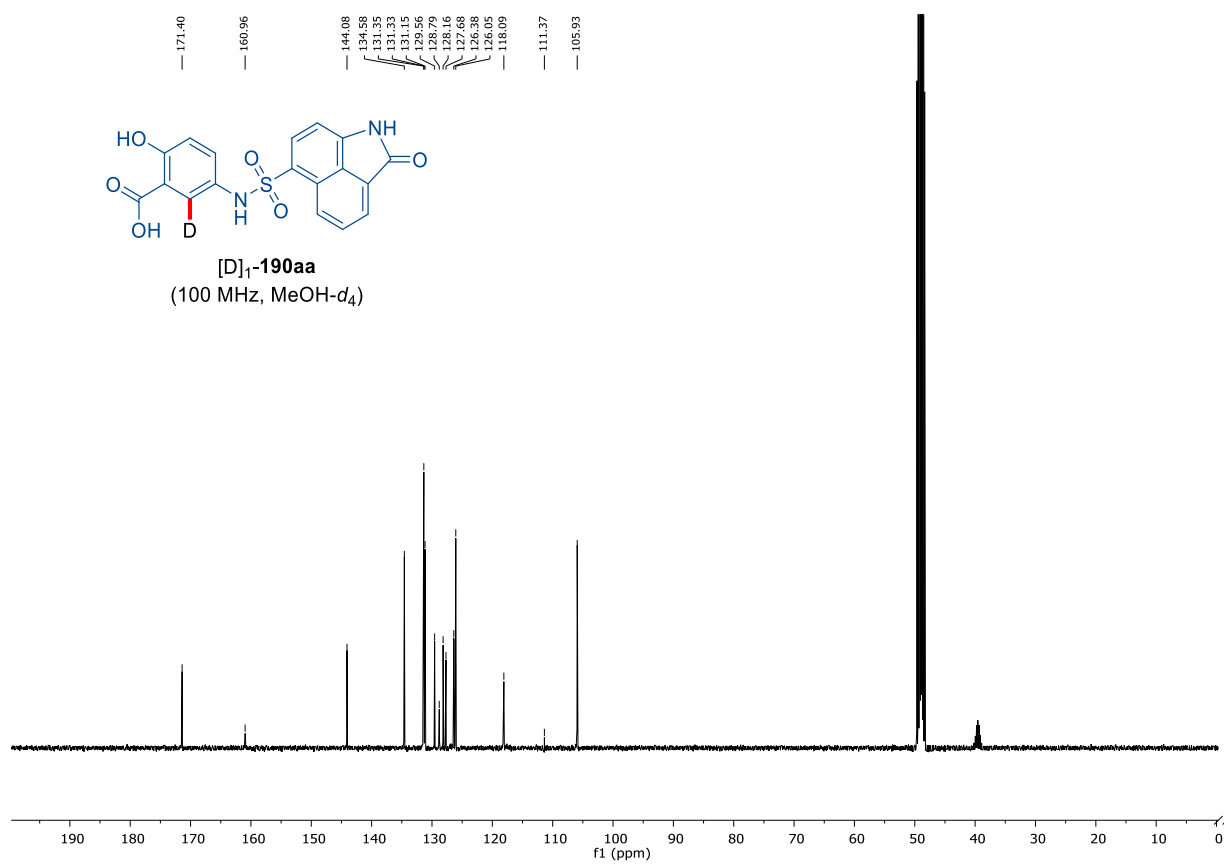
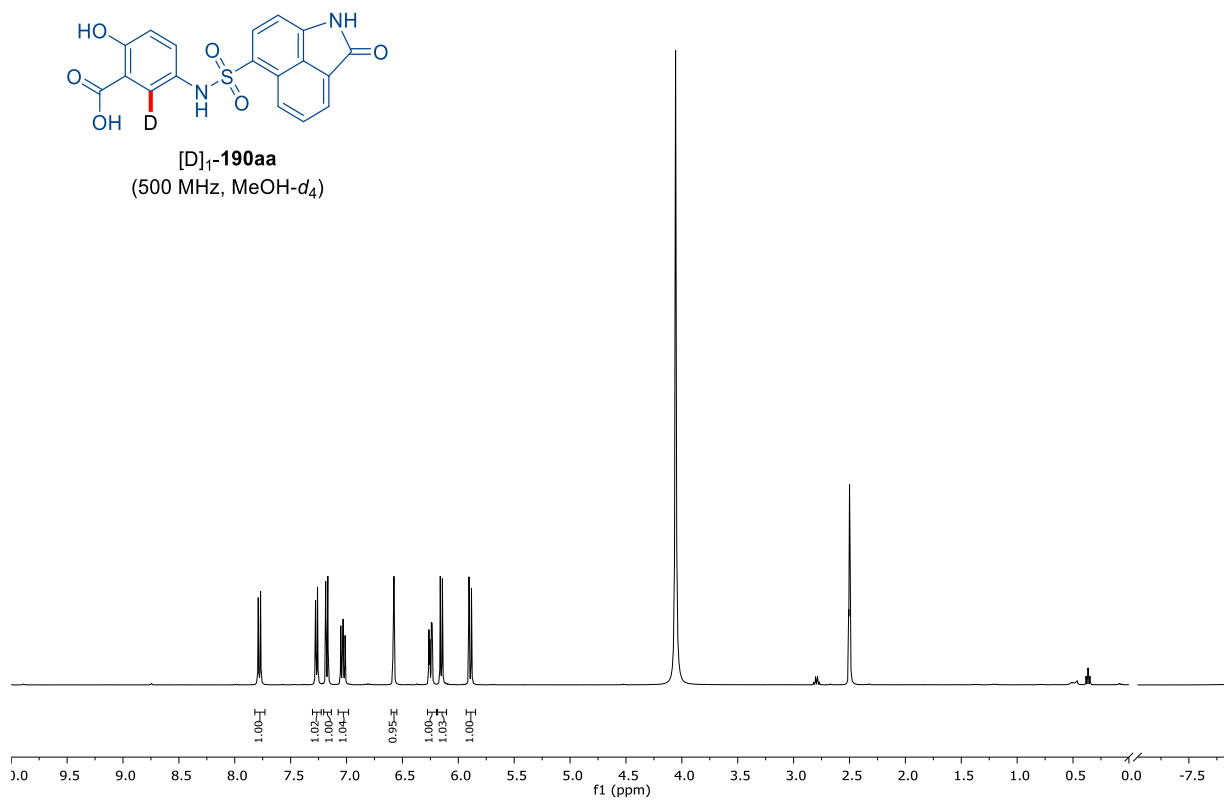


[D]₁-190z
(400 MHz, MeOH-d₄)

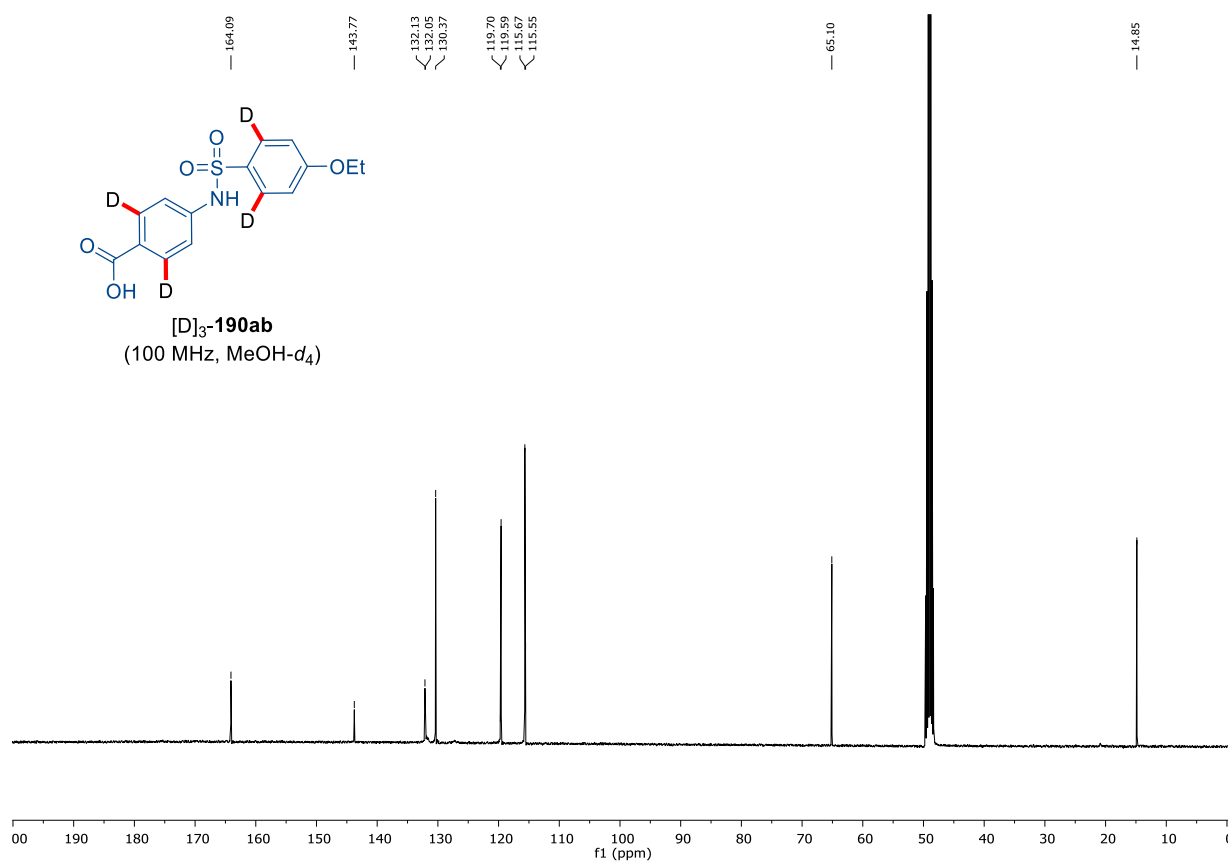
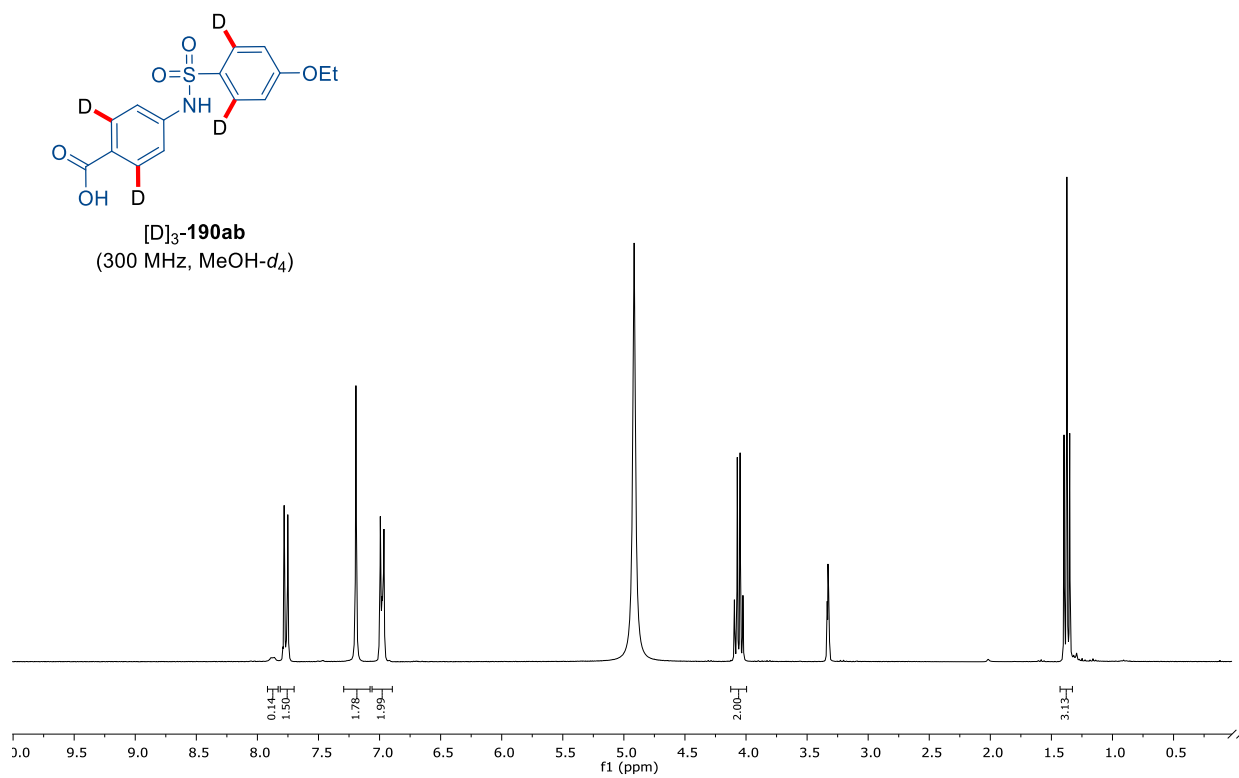


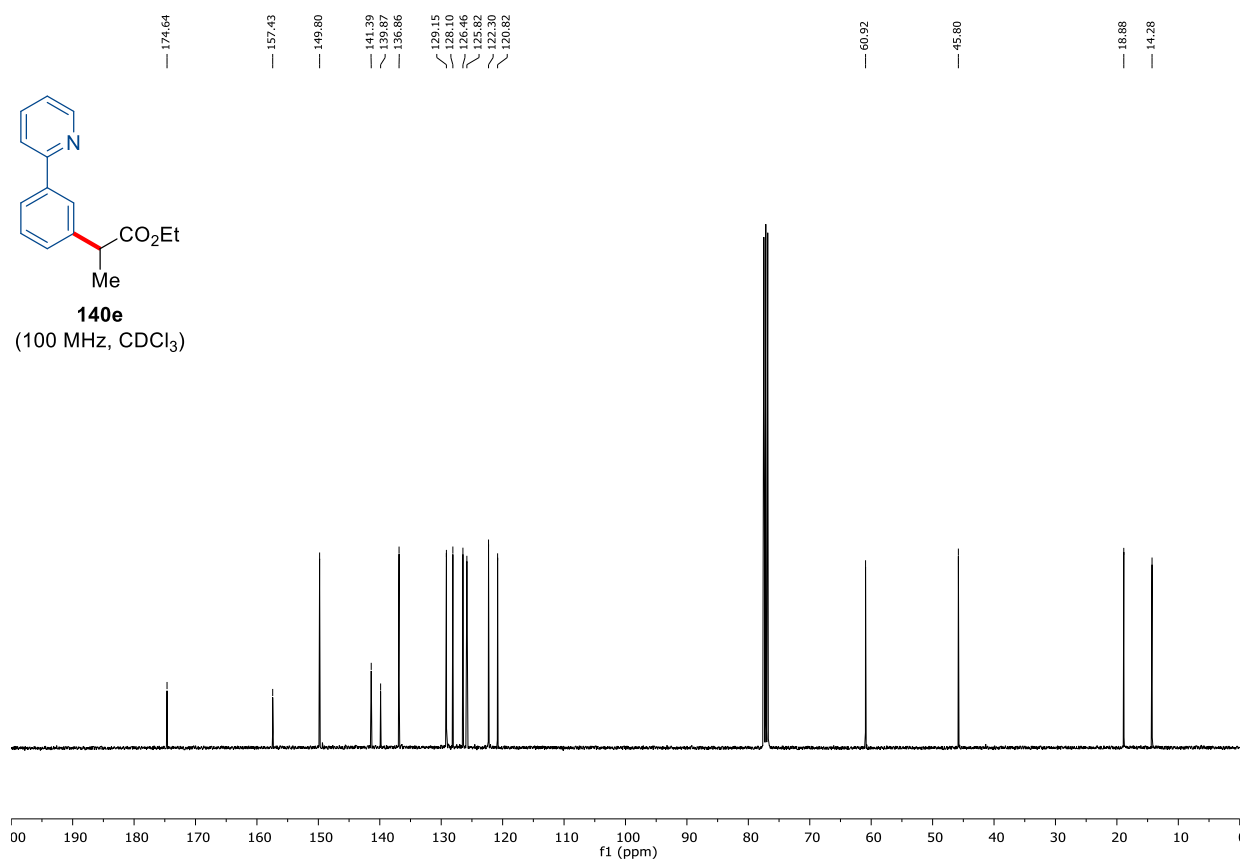
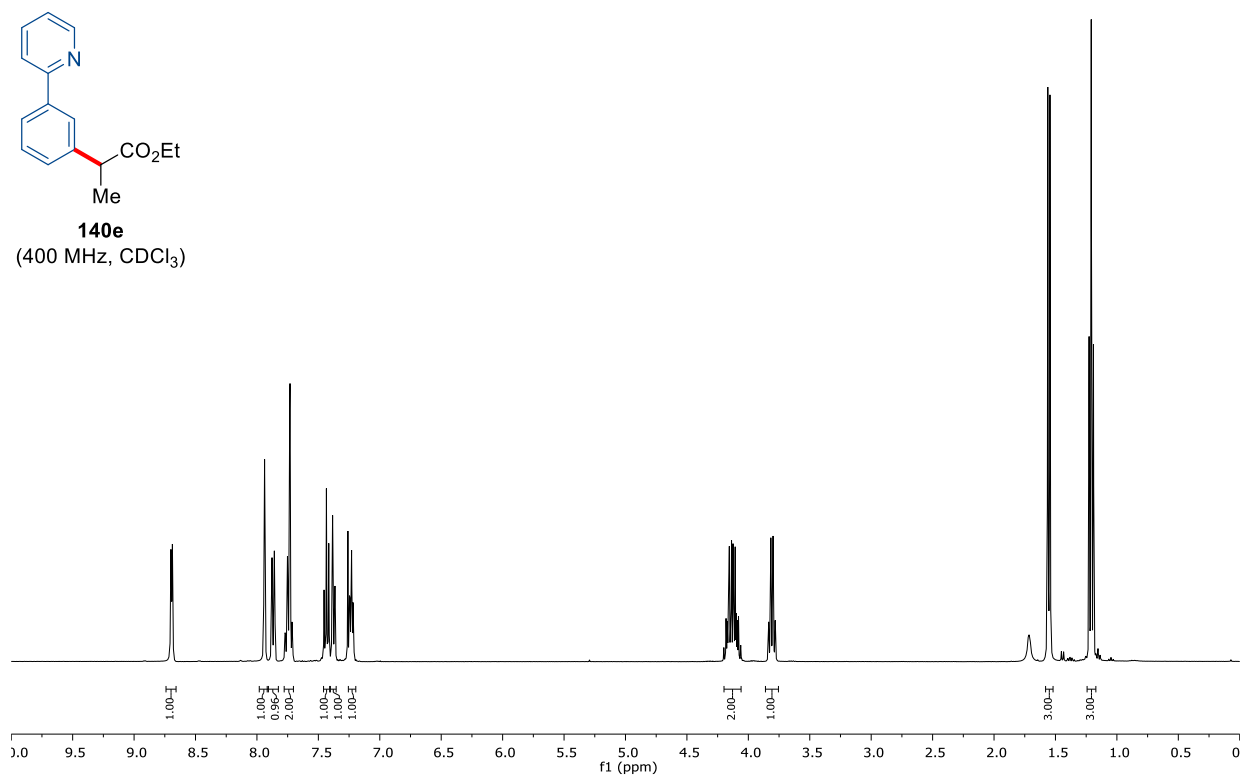
[D]₁-190z
(100 MHz, MeOH-d₄)



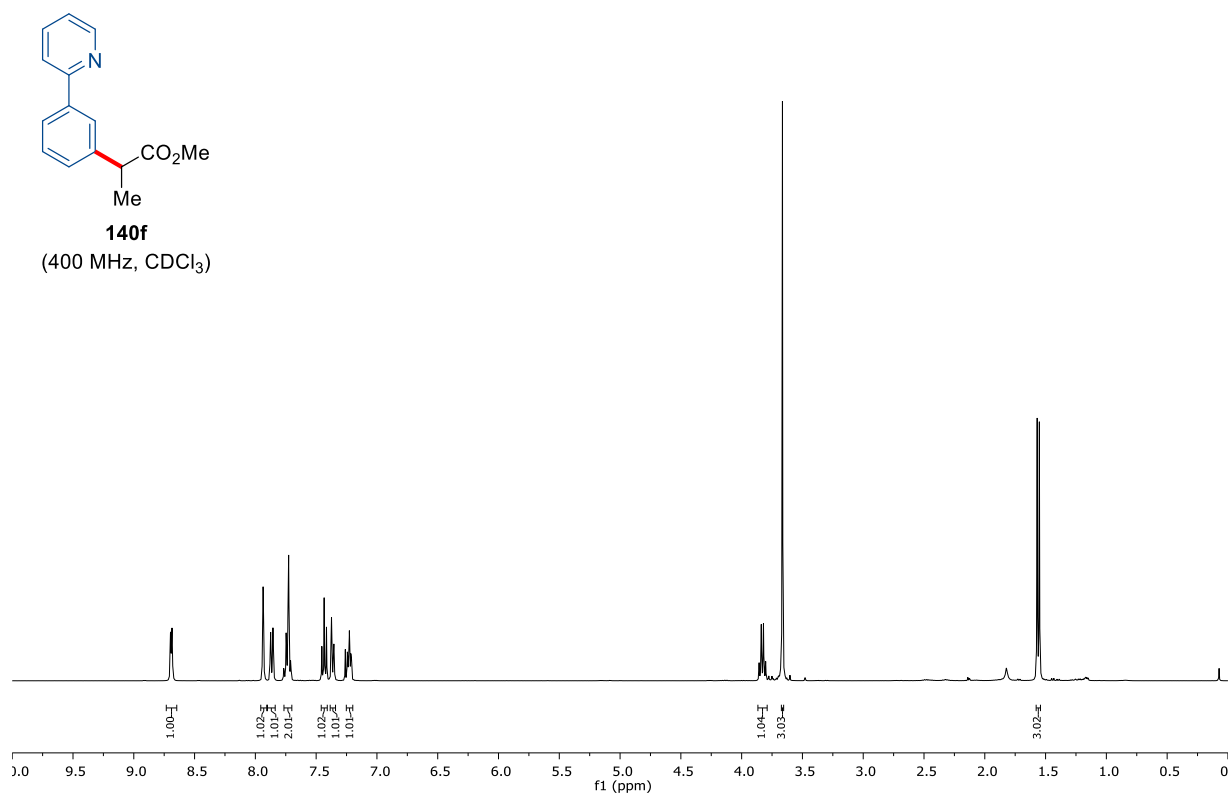
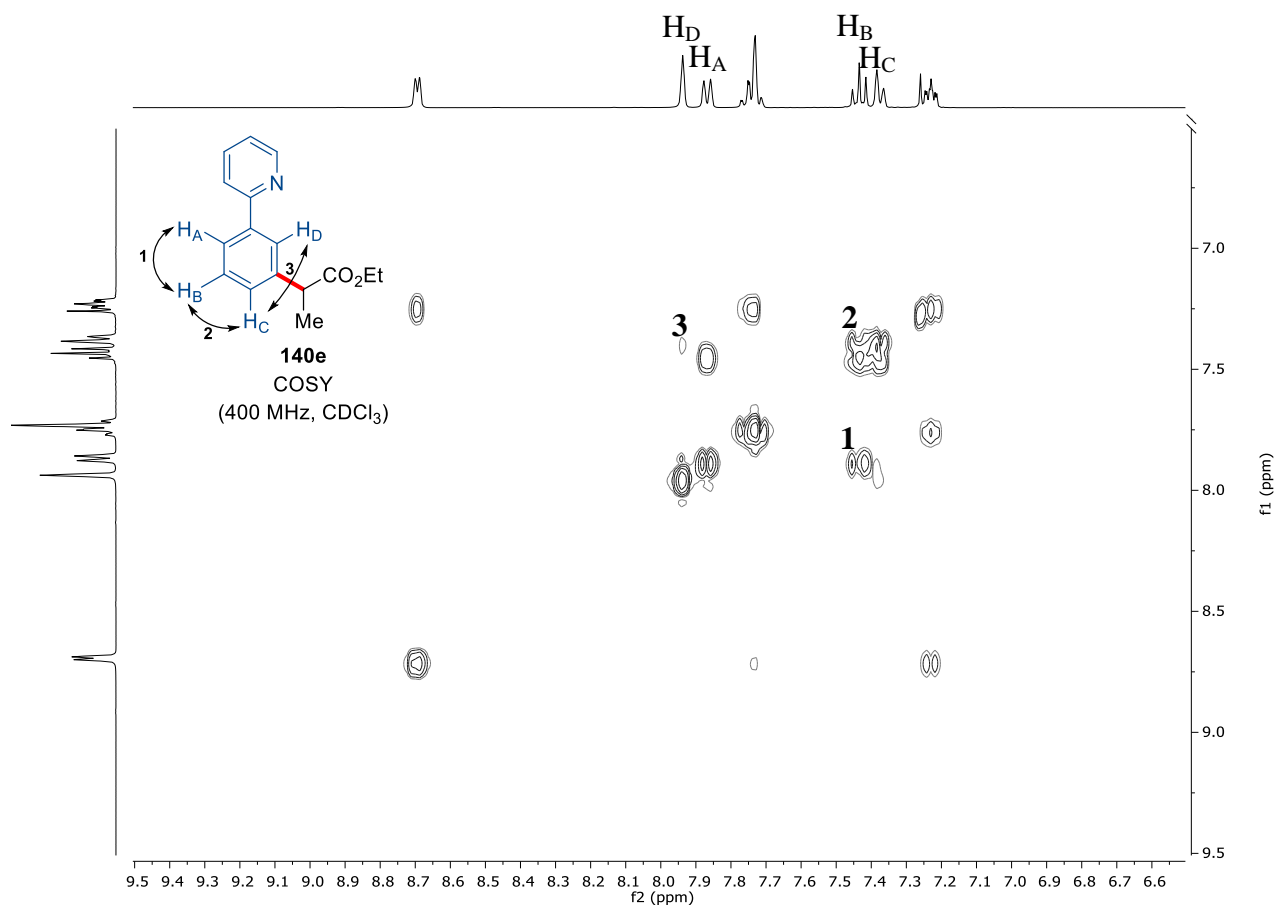


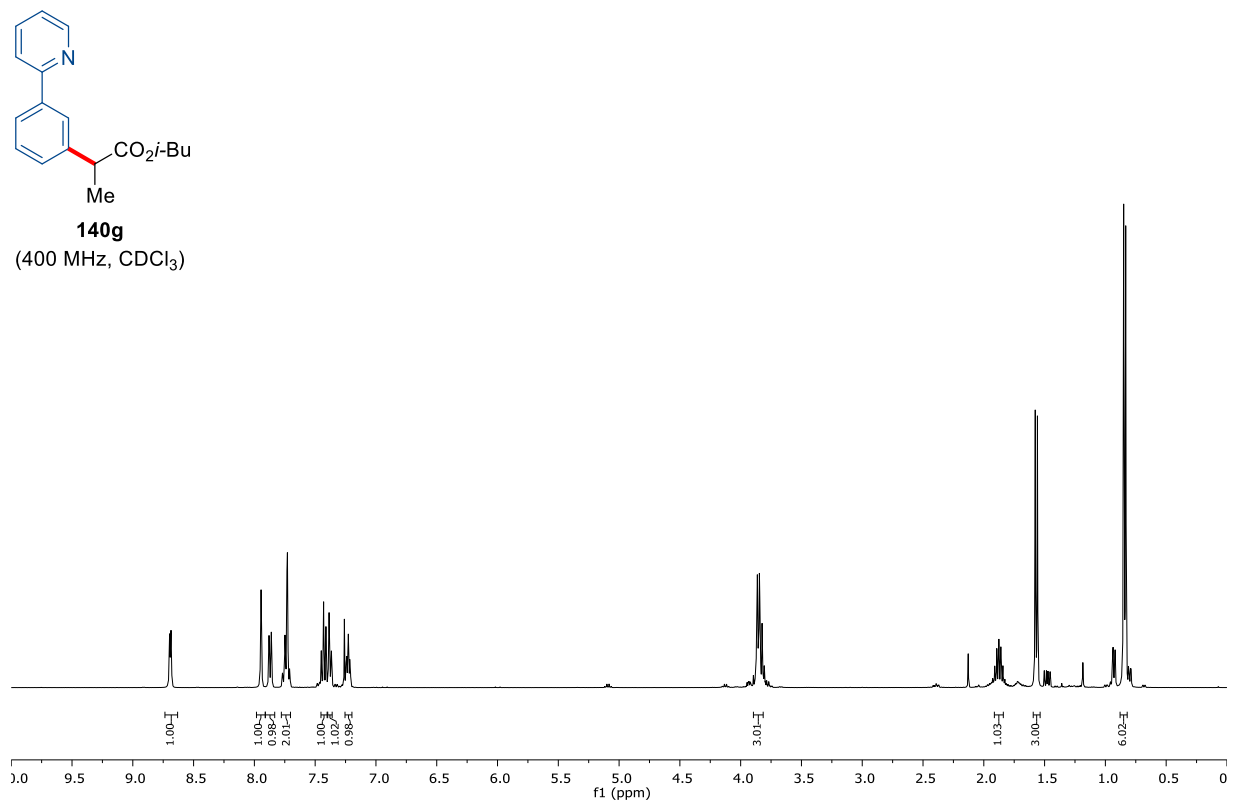
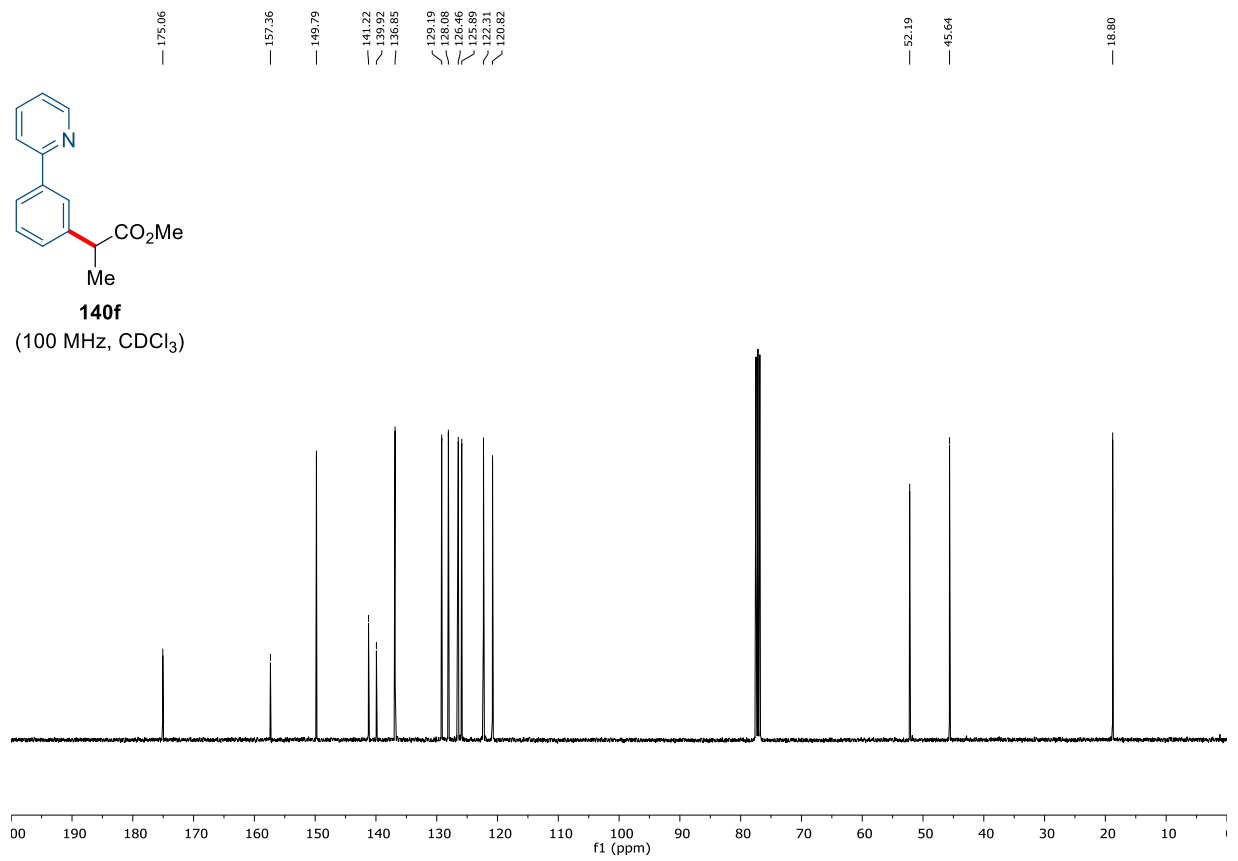
7. Appendix: NMR-Spectra and HPLC Chromatograms



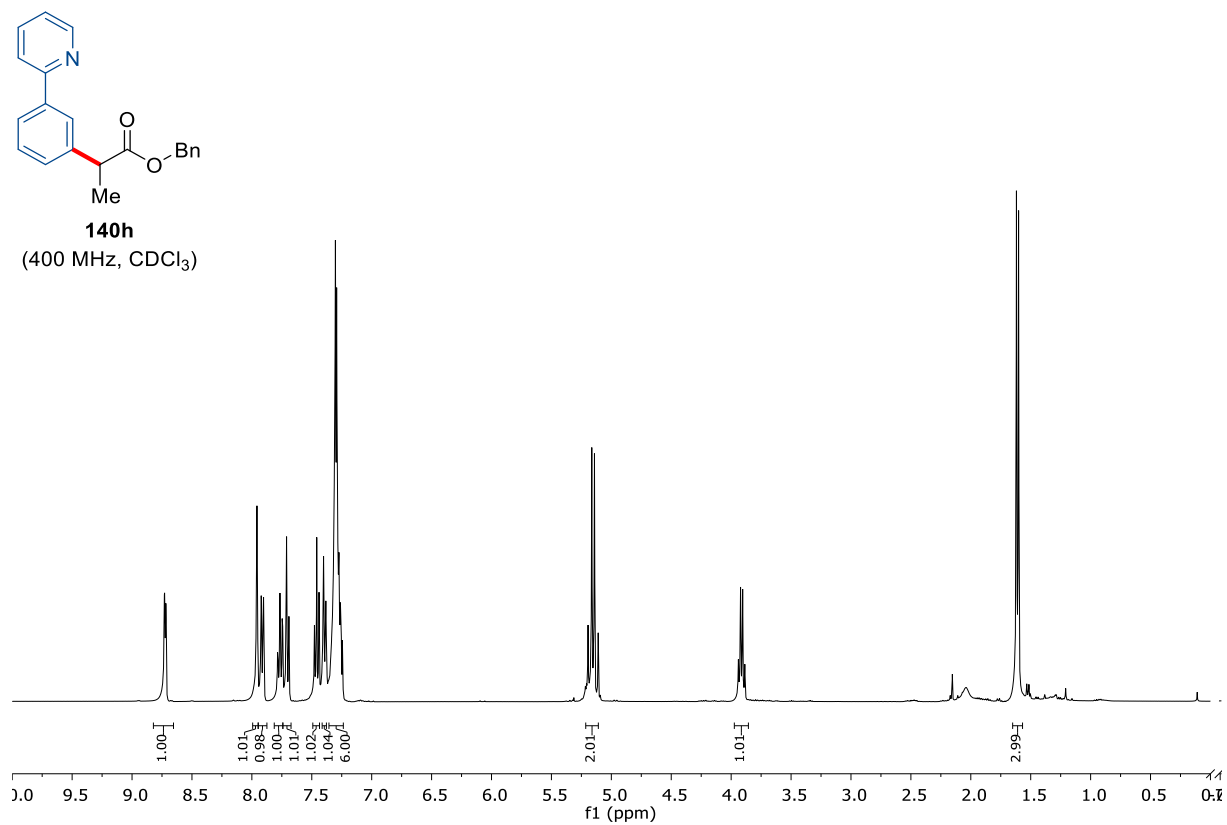
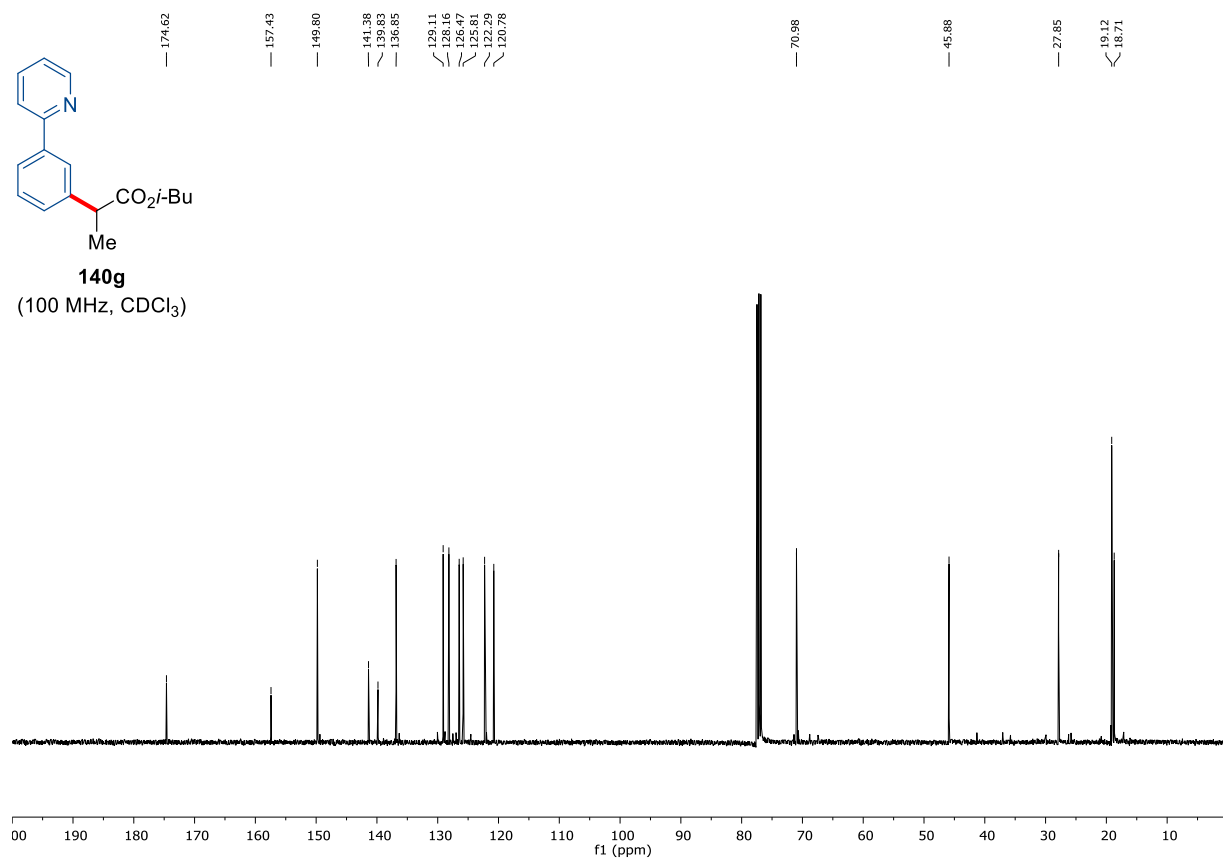


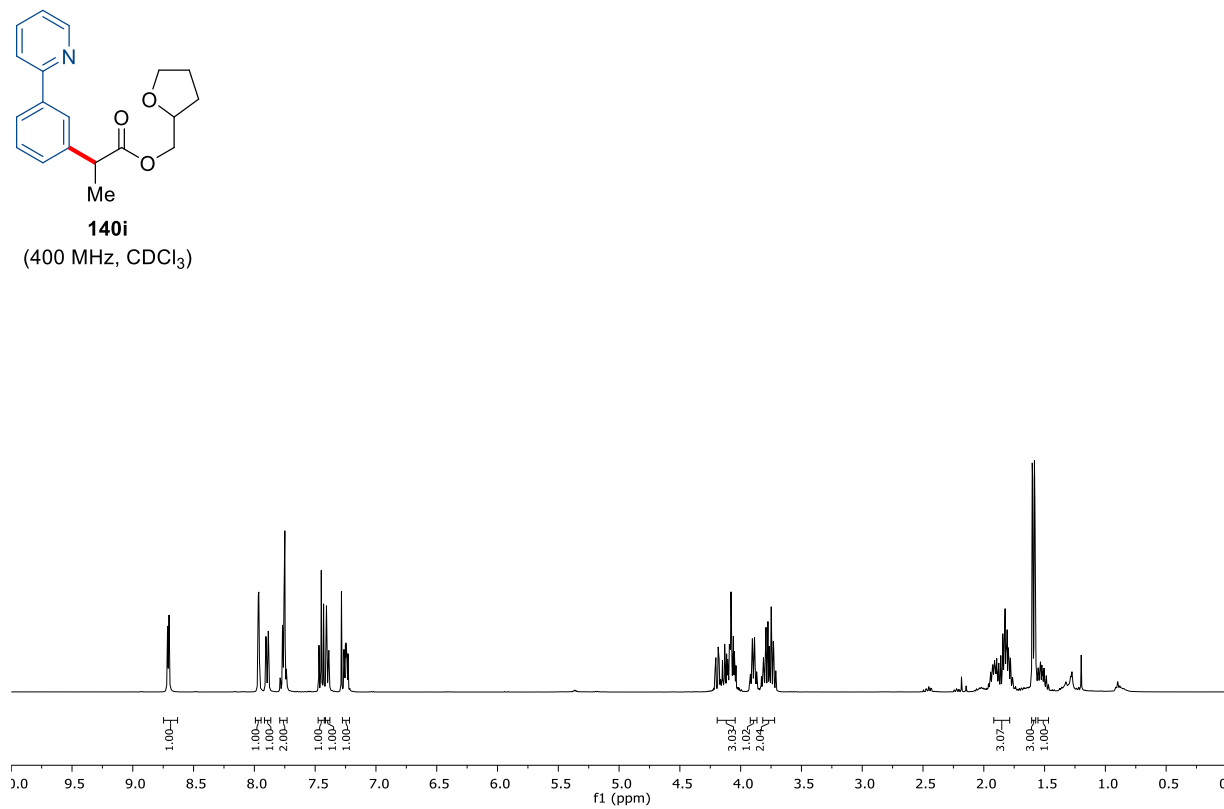
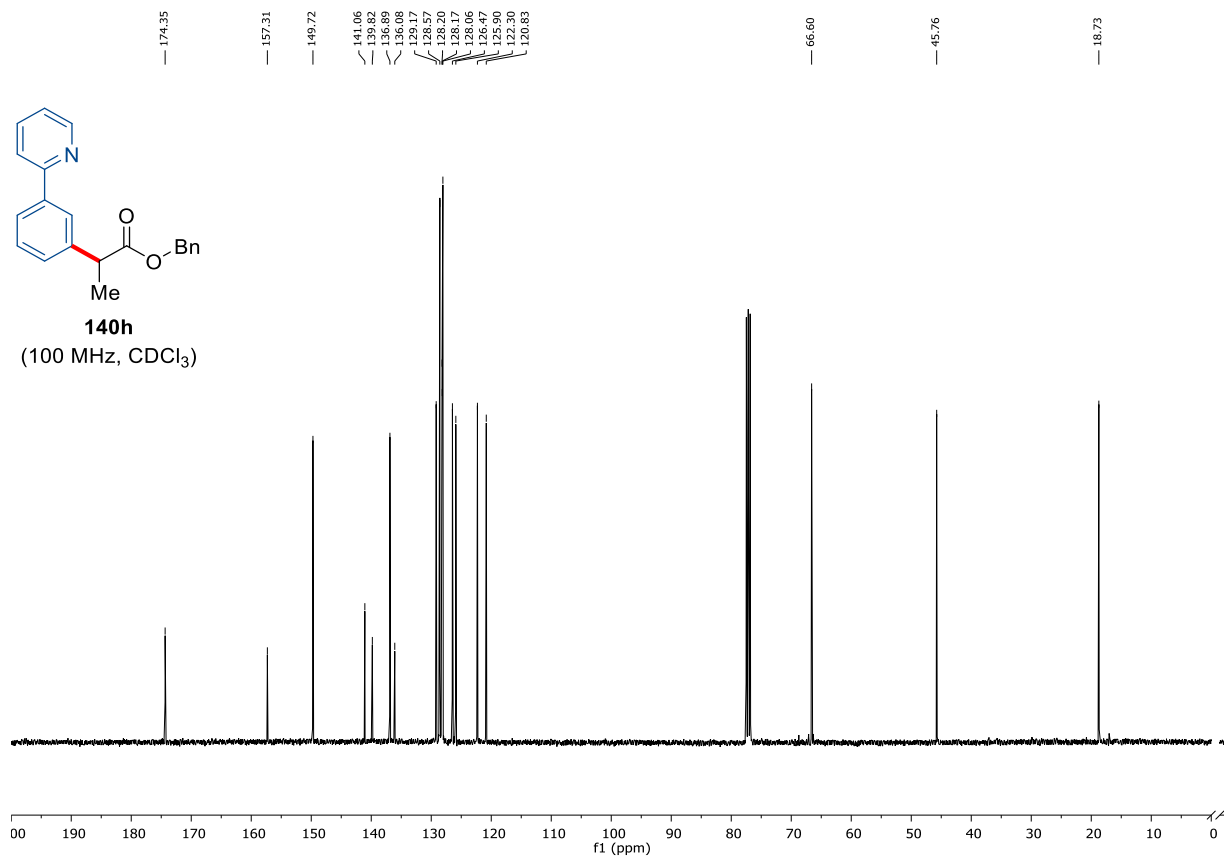
7. Appendix: NMR-Spectra and HPLC Chromatograms



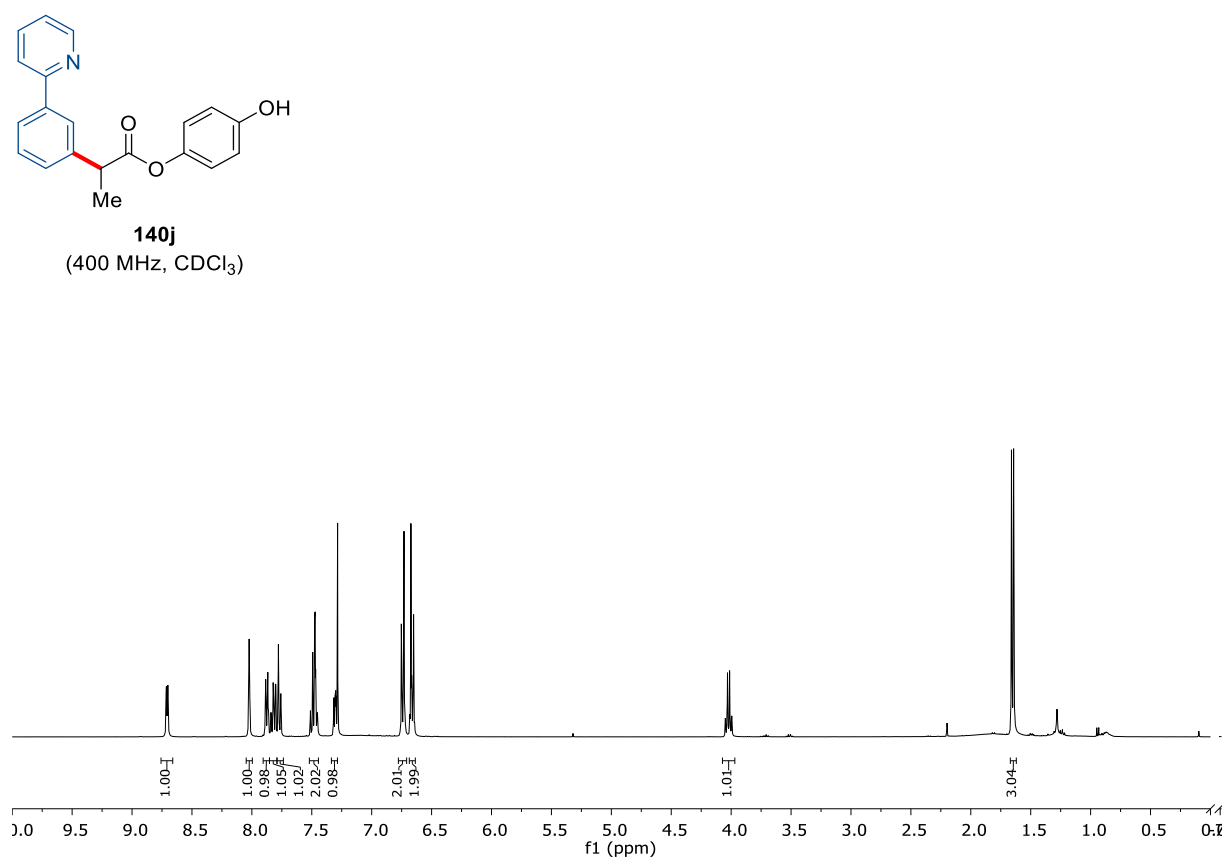
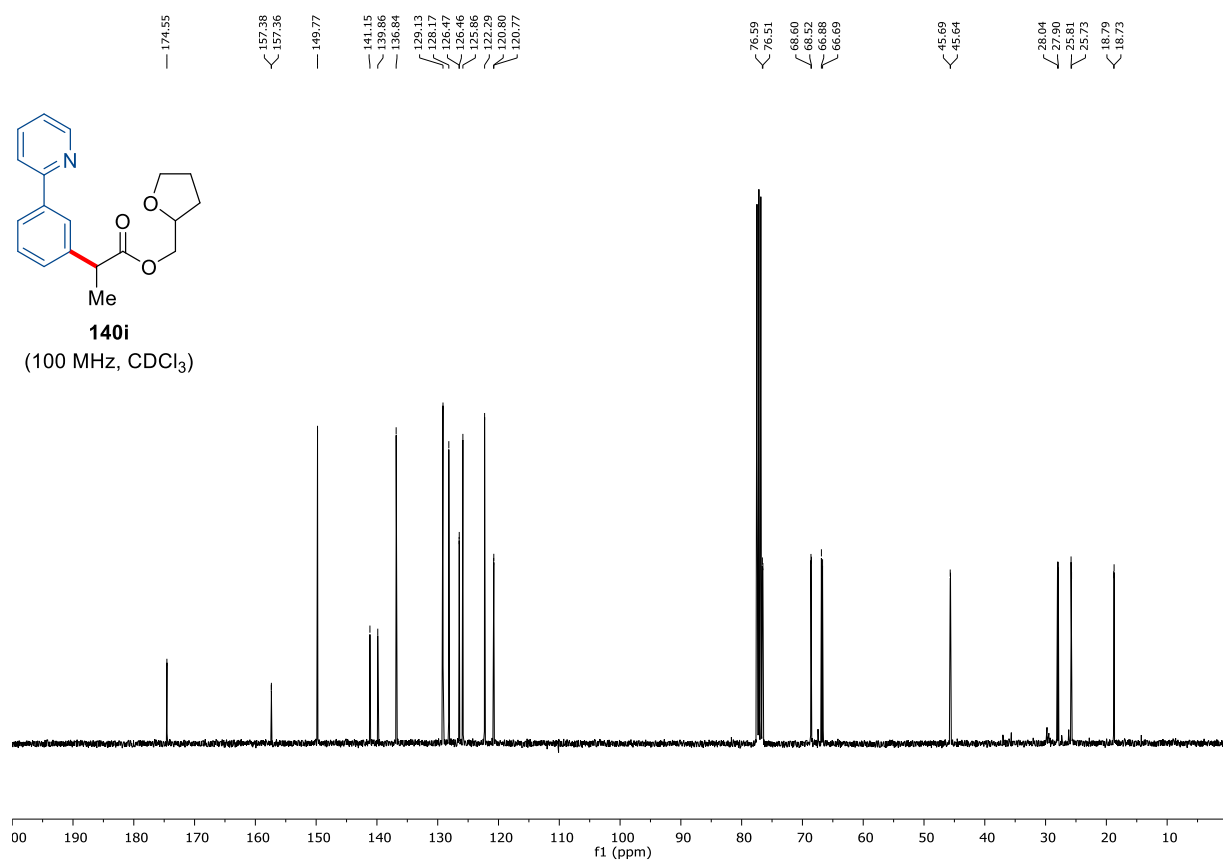


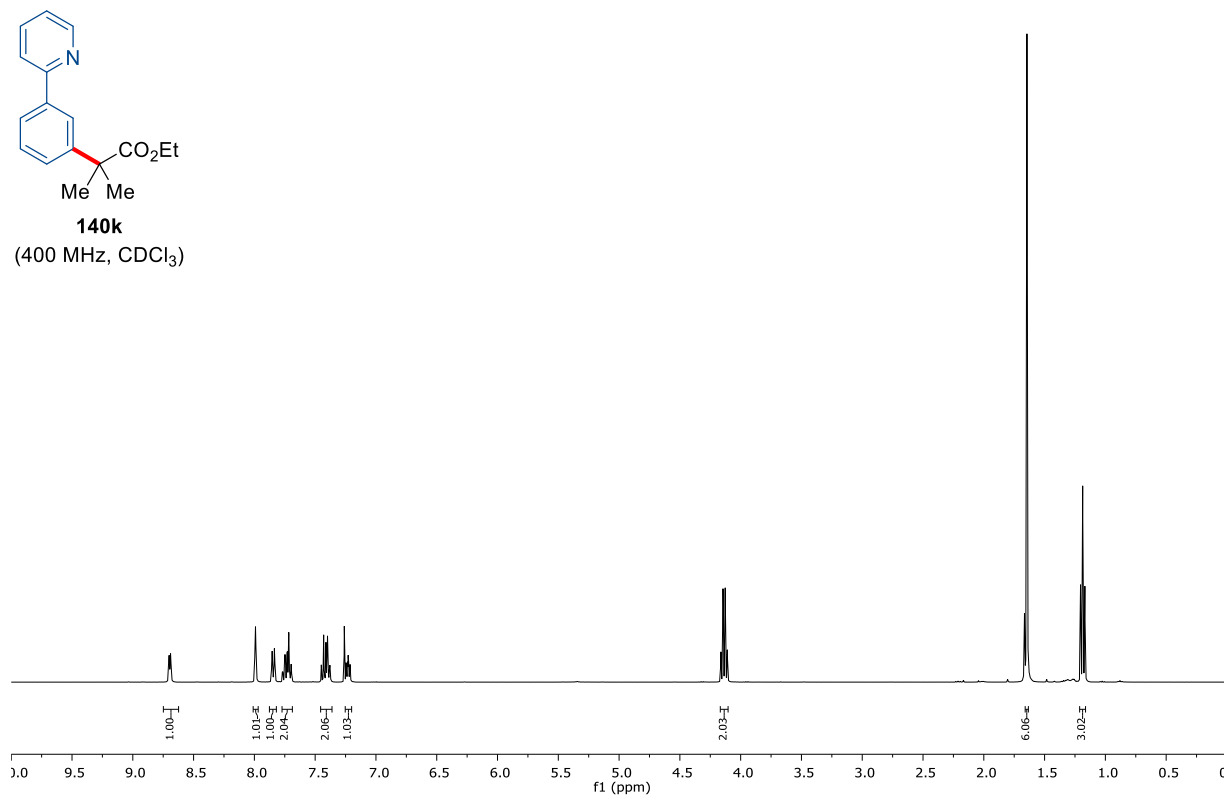
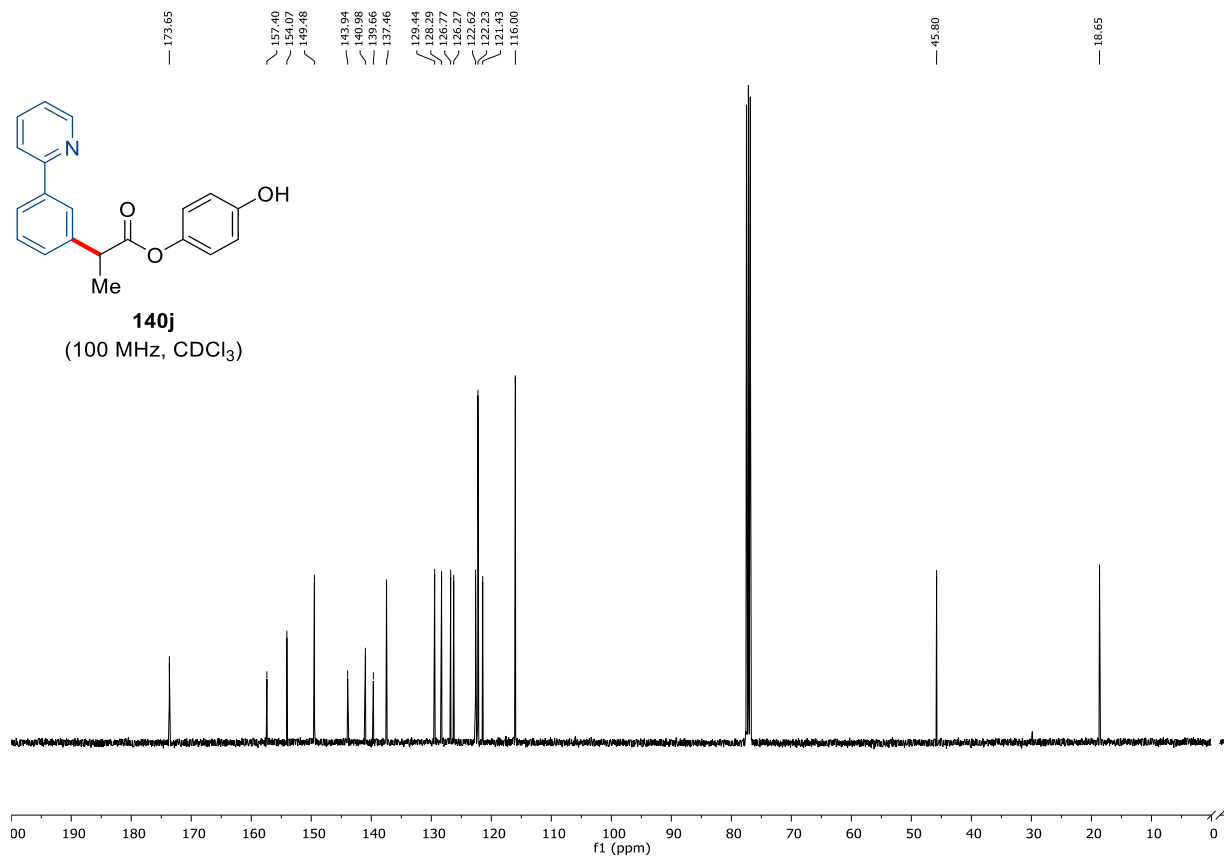
7. Appendix: NMR-Spectra and HPLC Chromatograms



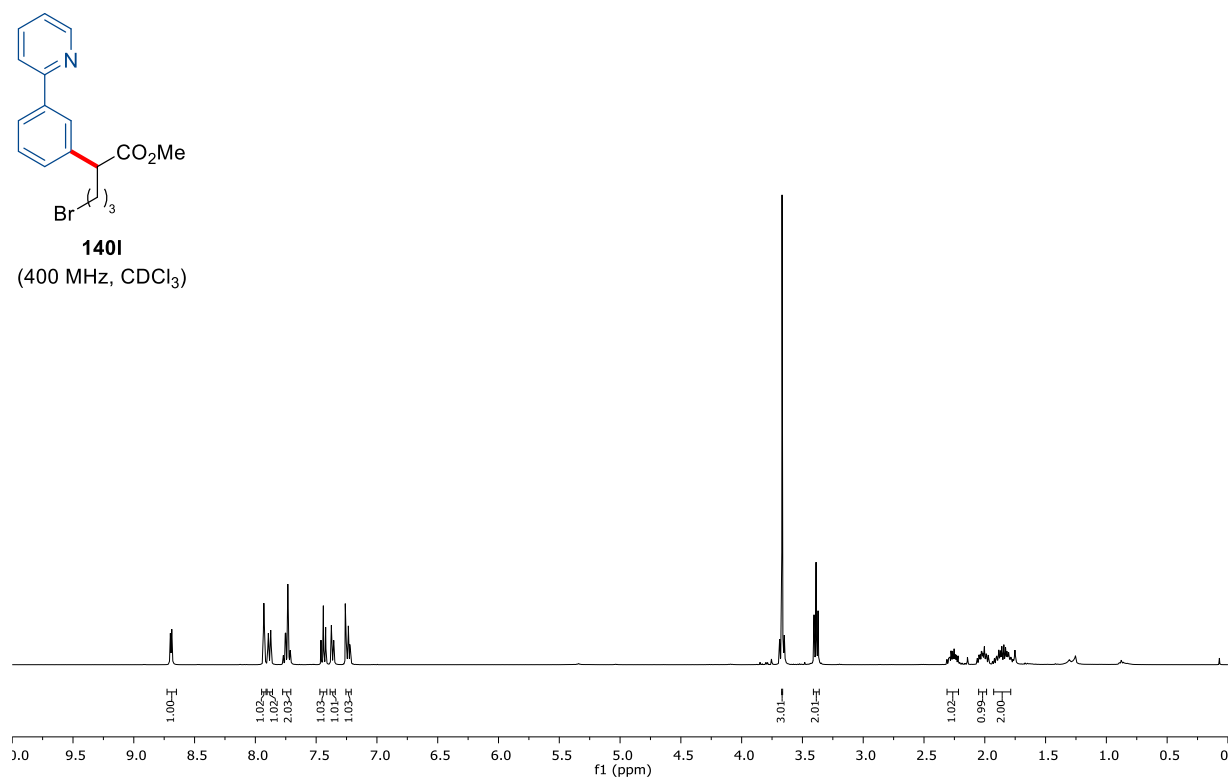
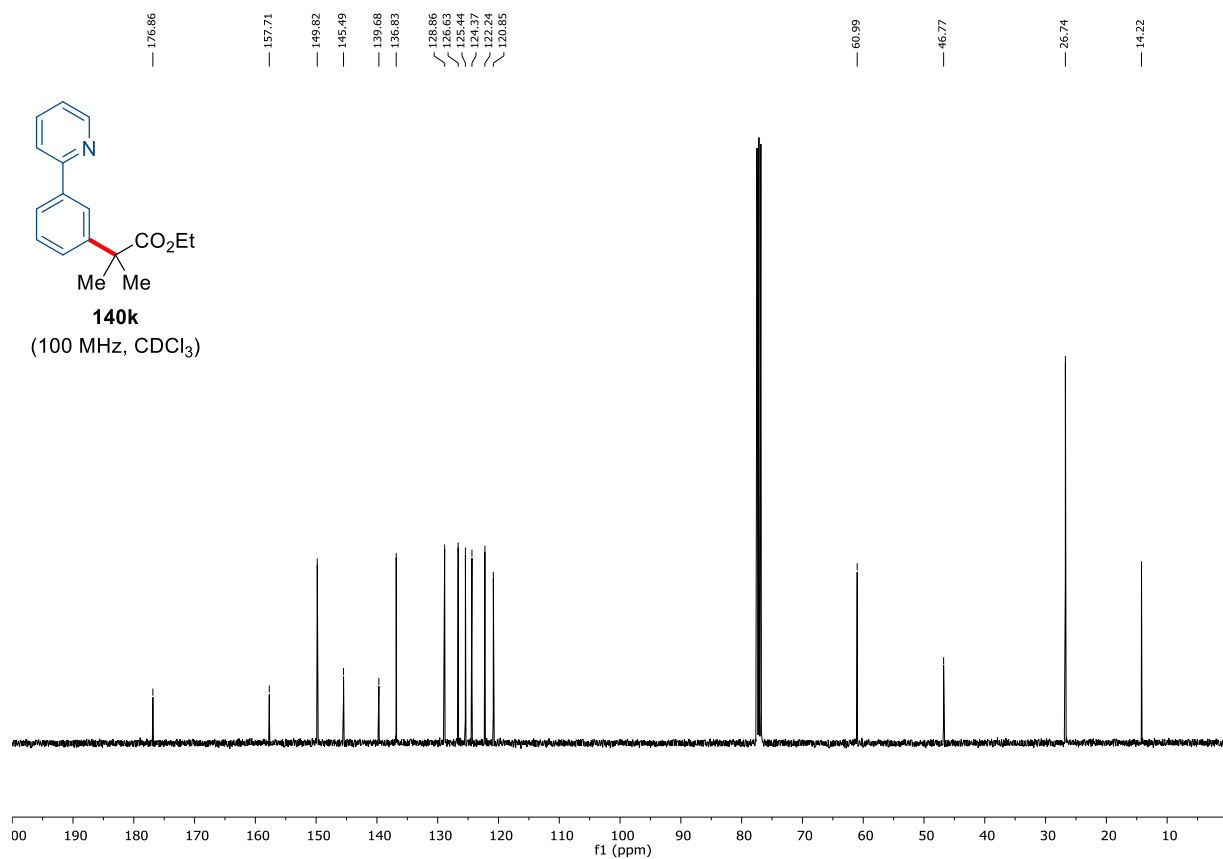


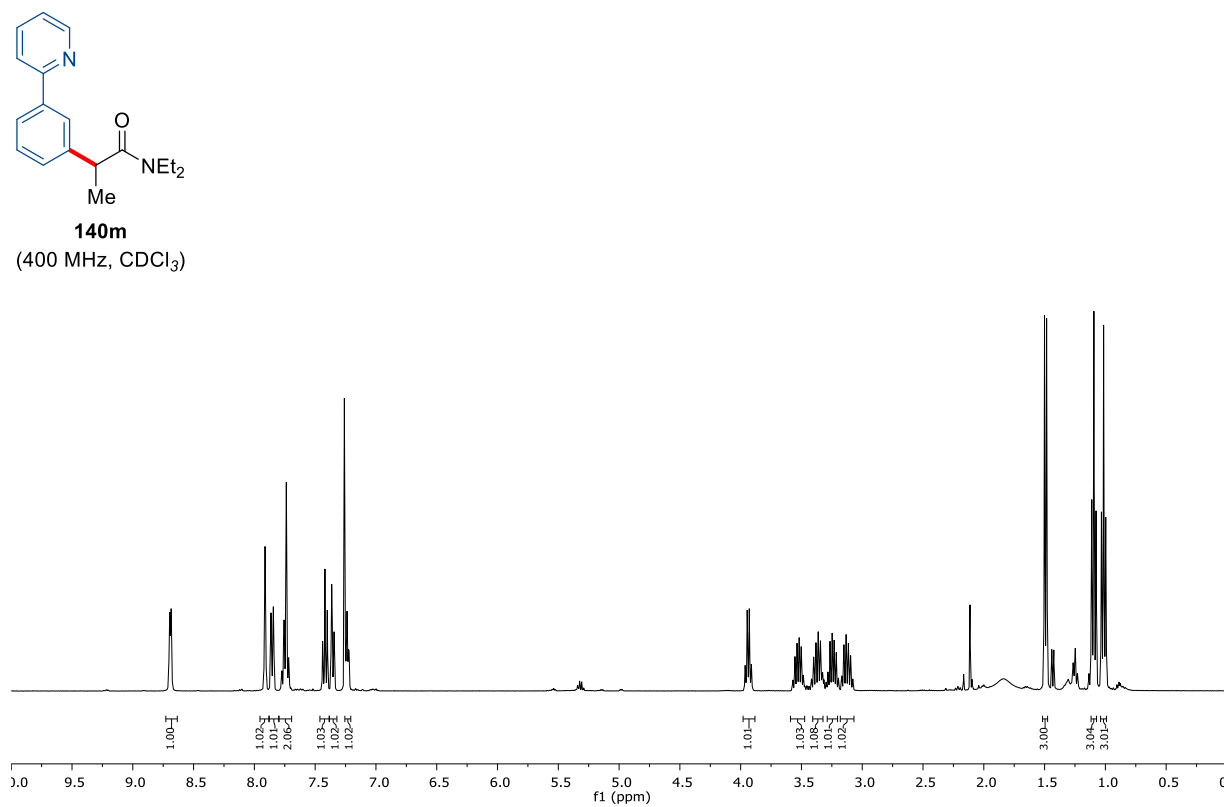
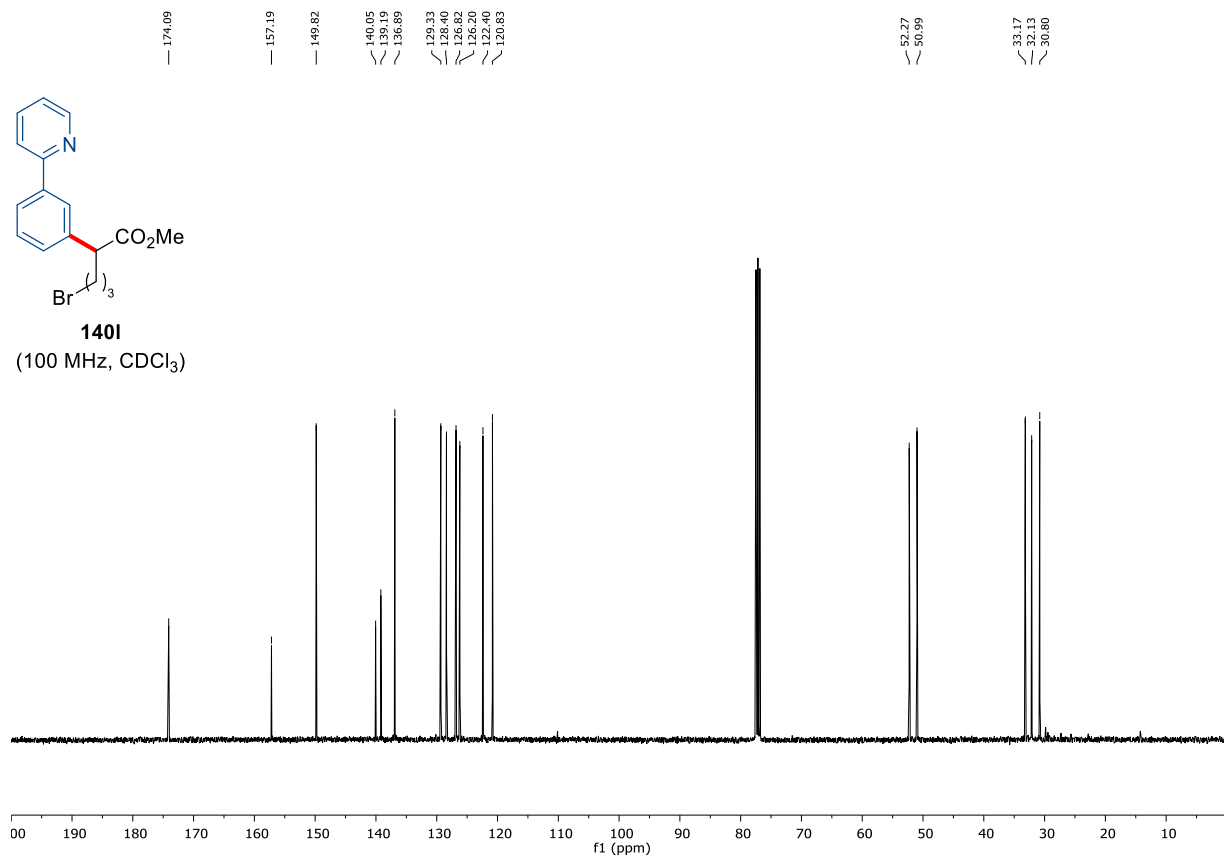
7. Appendix: NMR-Spectra and HPLC Chromatograms



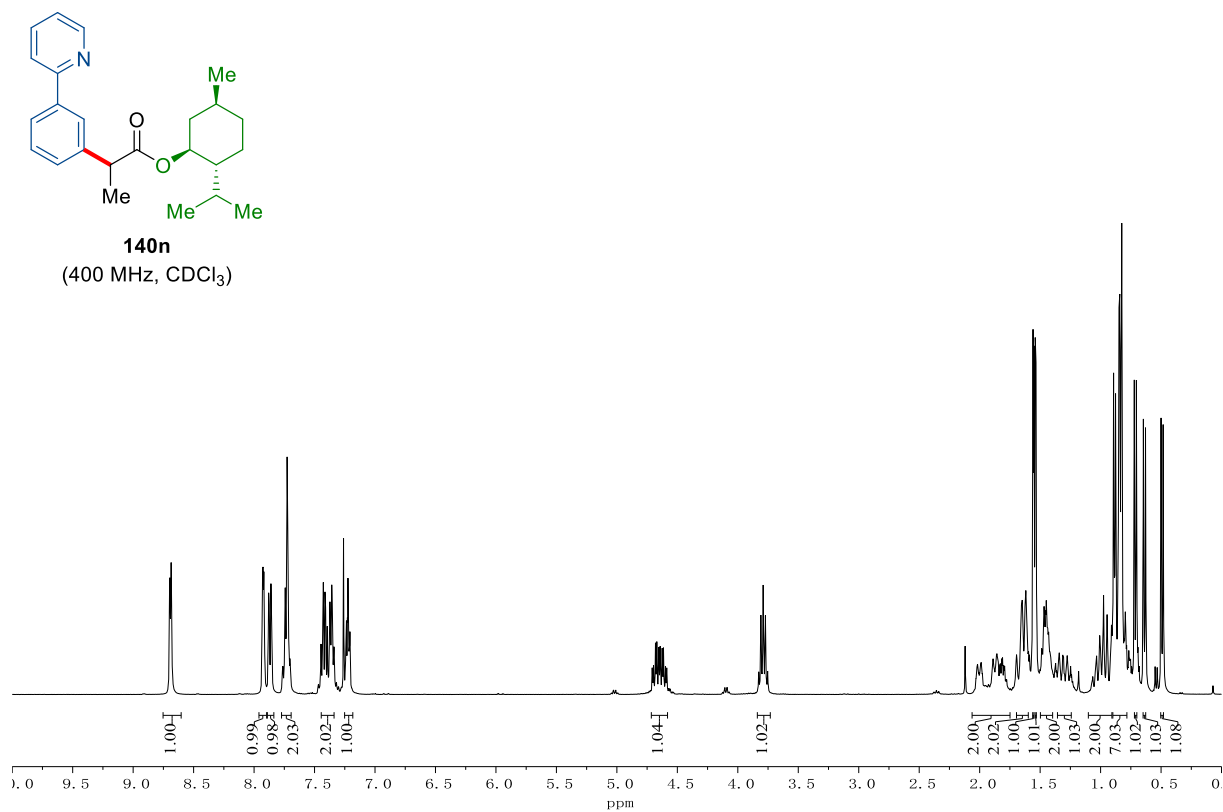
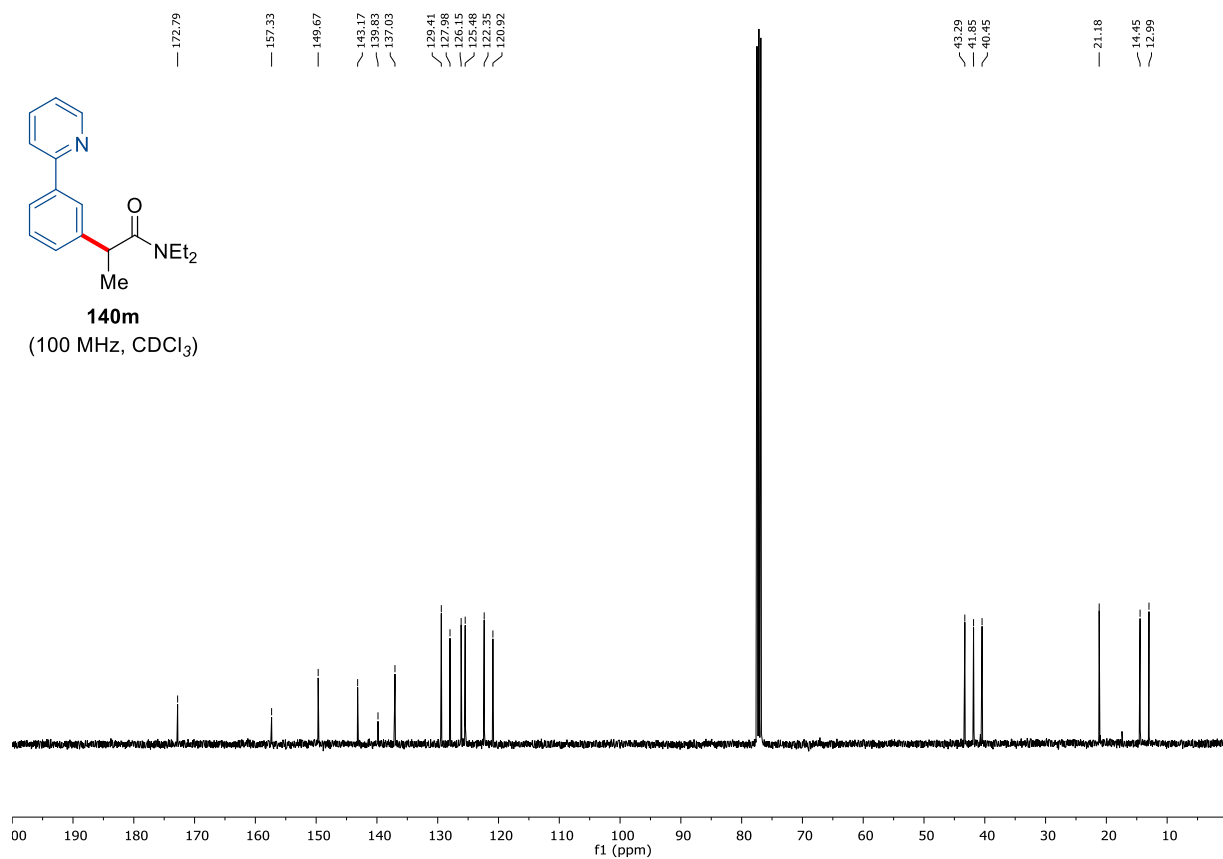


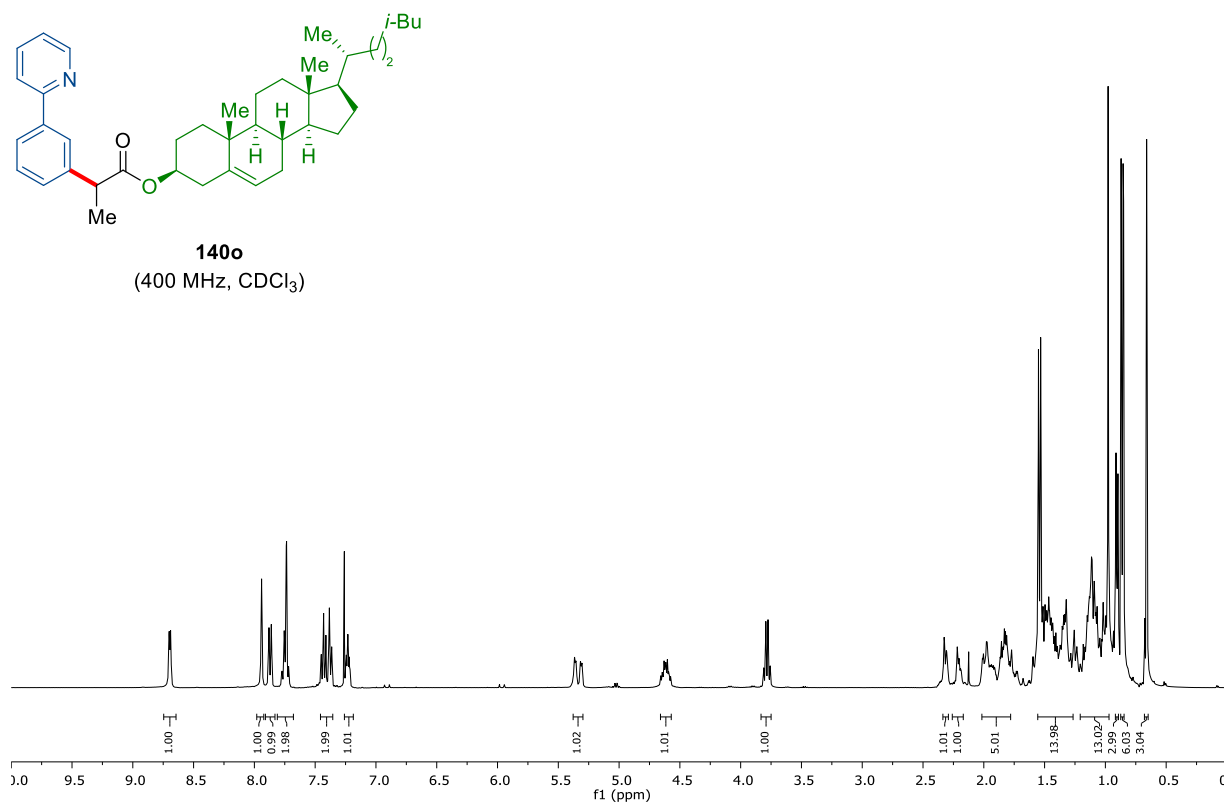
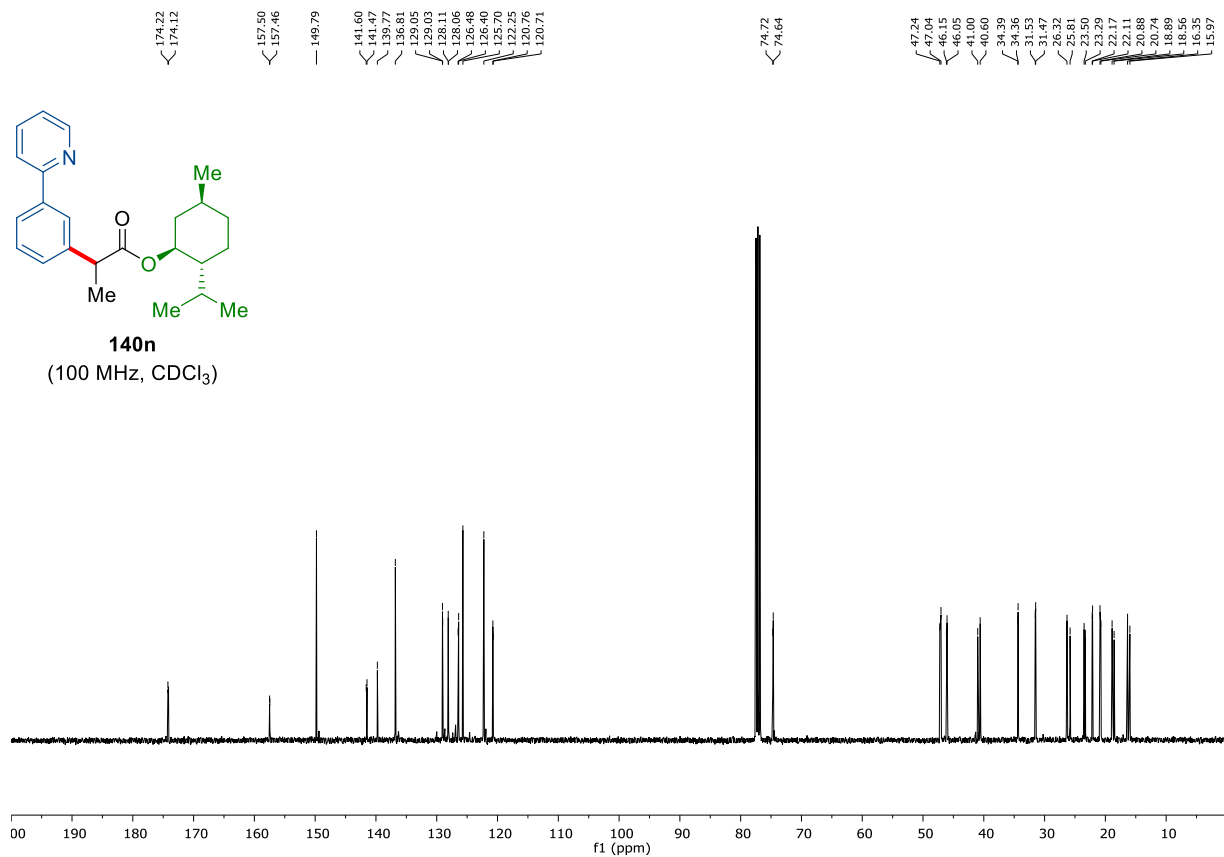
7. Appendix: NMR-Spectra and HPLC Chromatograms



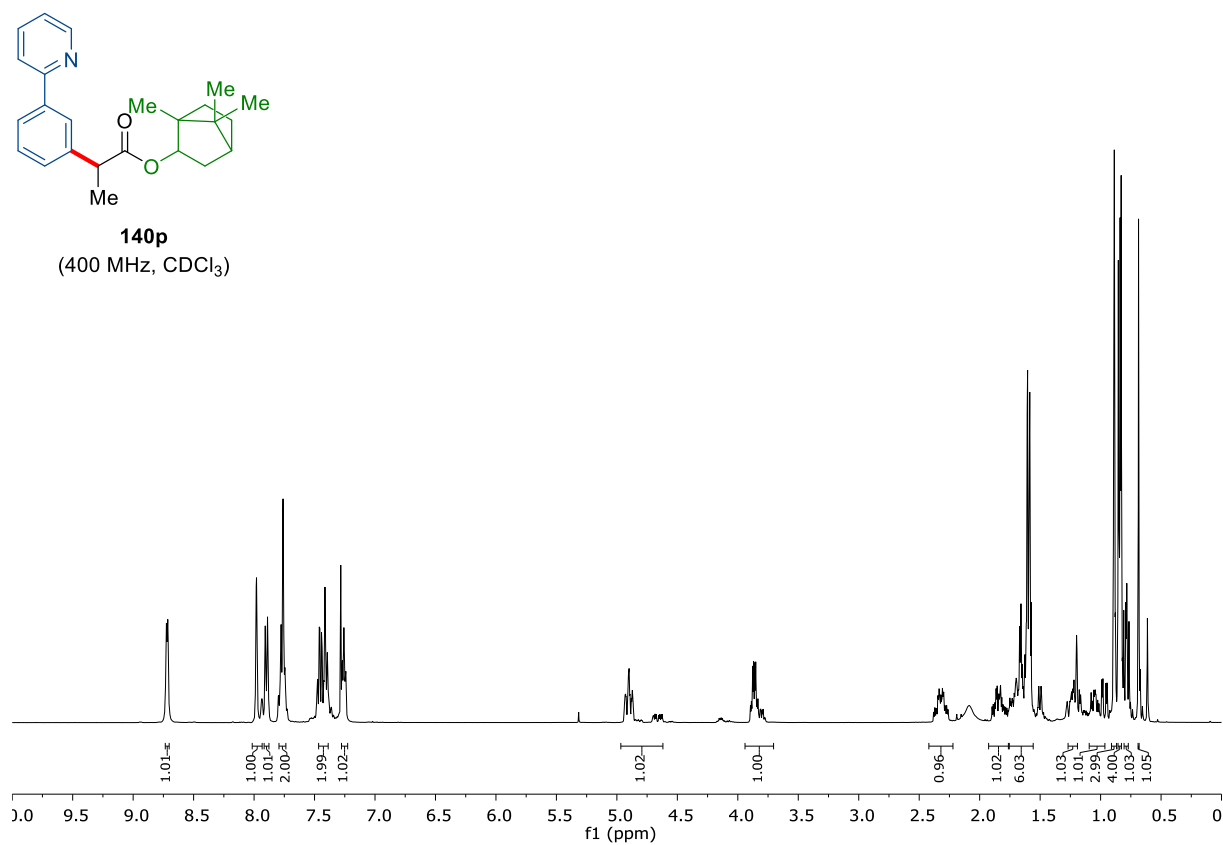
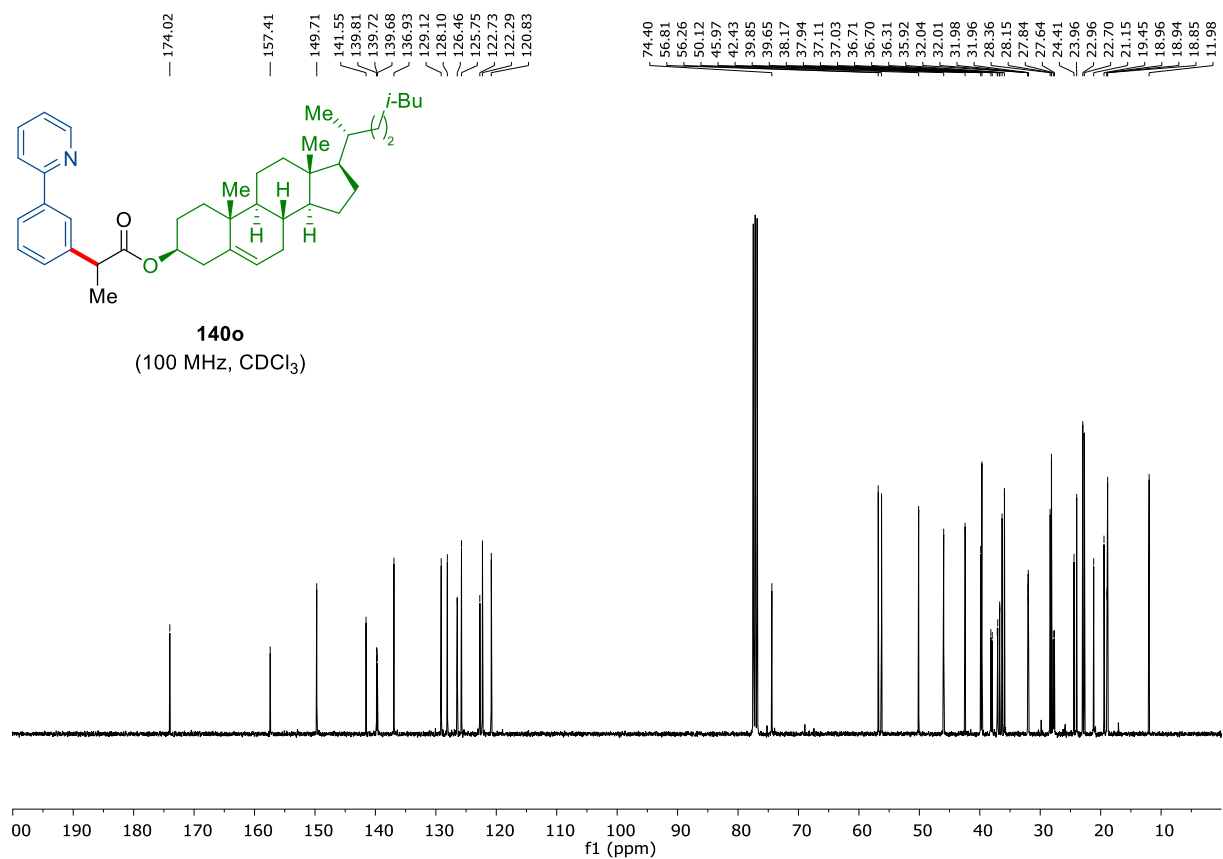


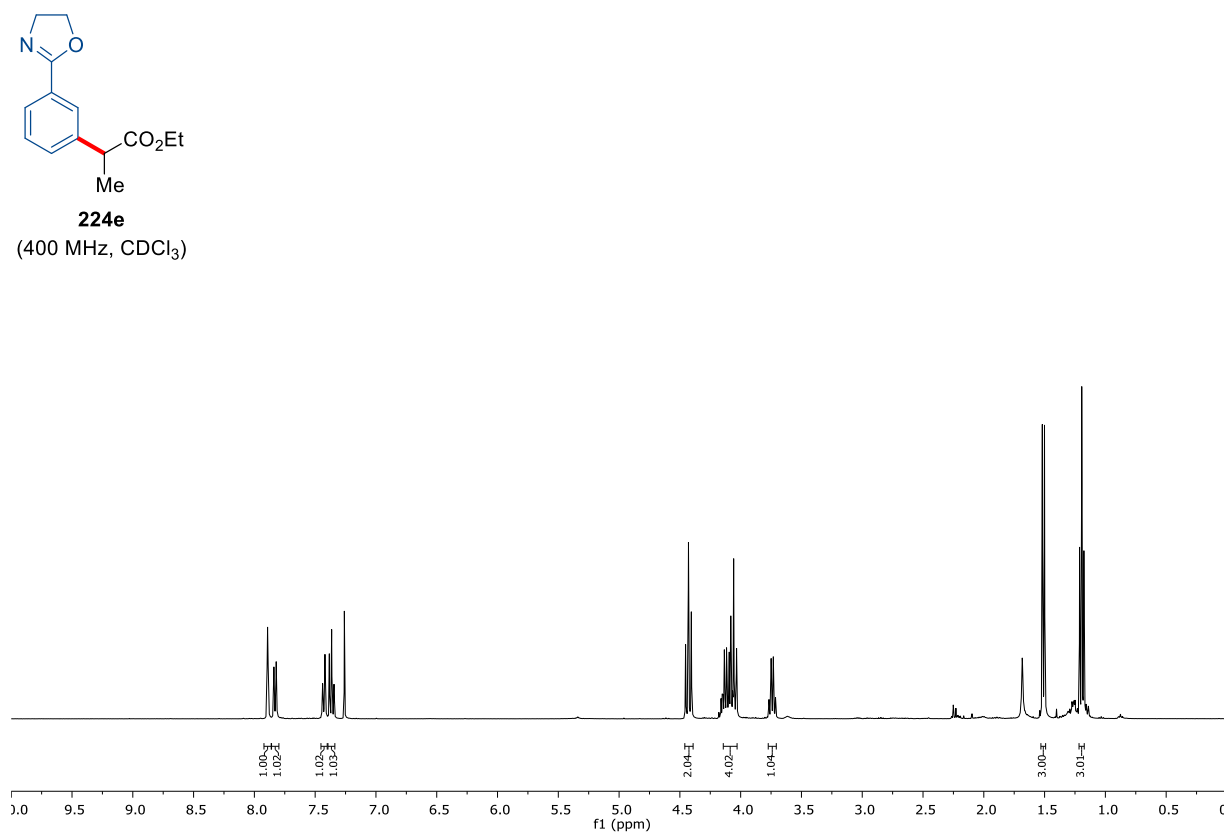
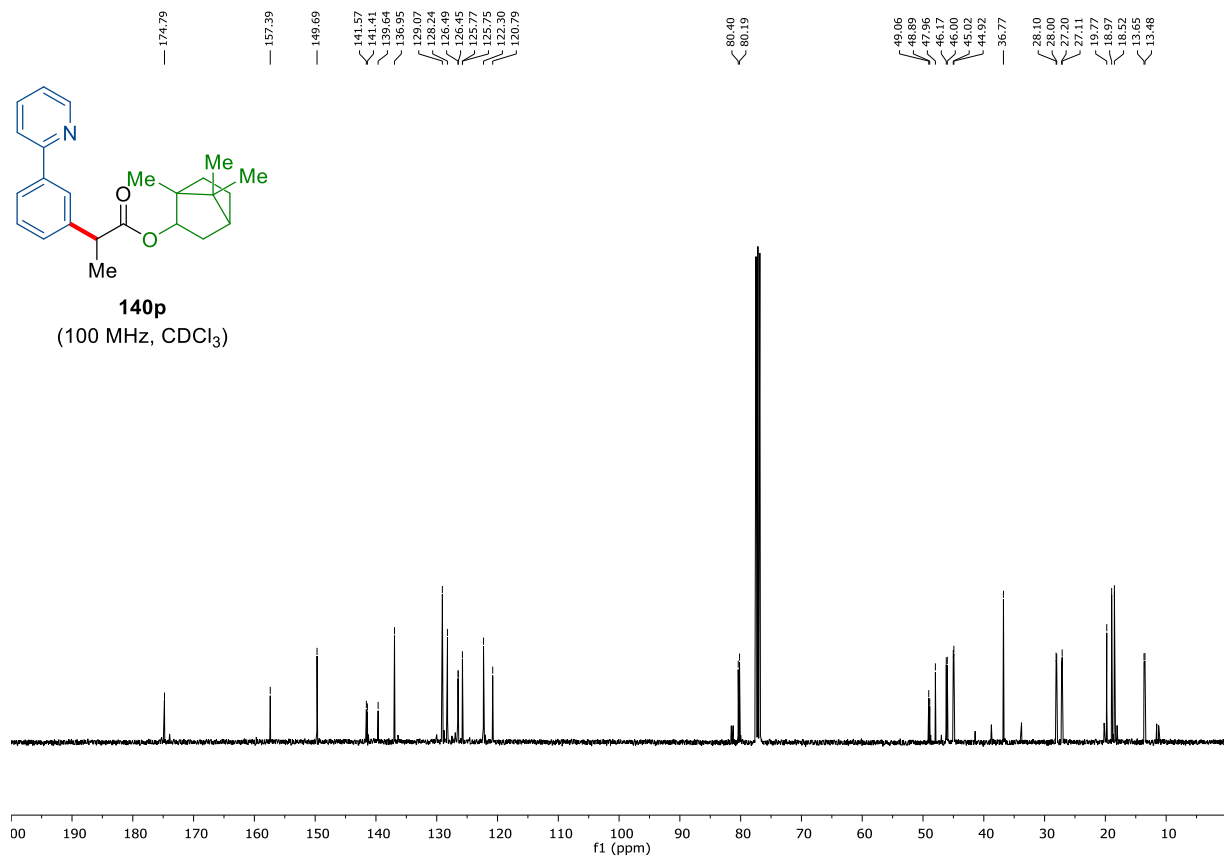
7. Appendix: NMR-Spectra and HPLC Chromatograms



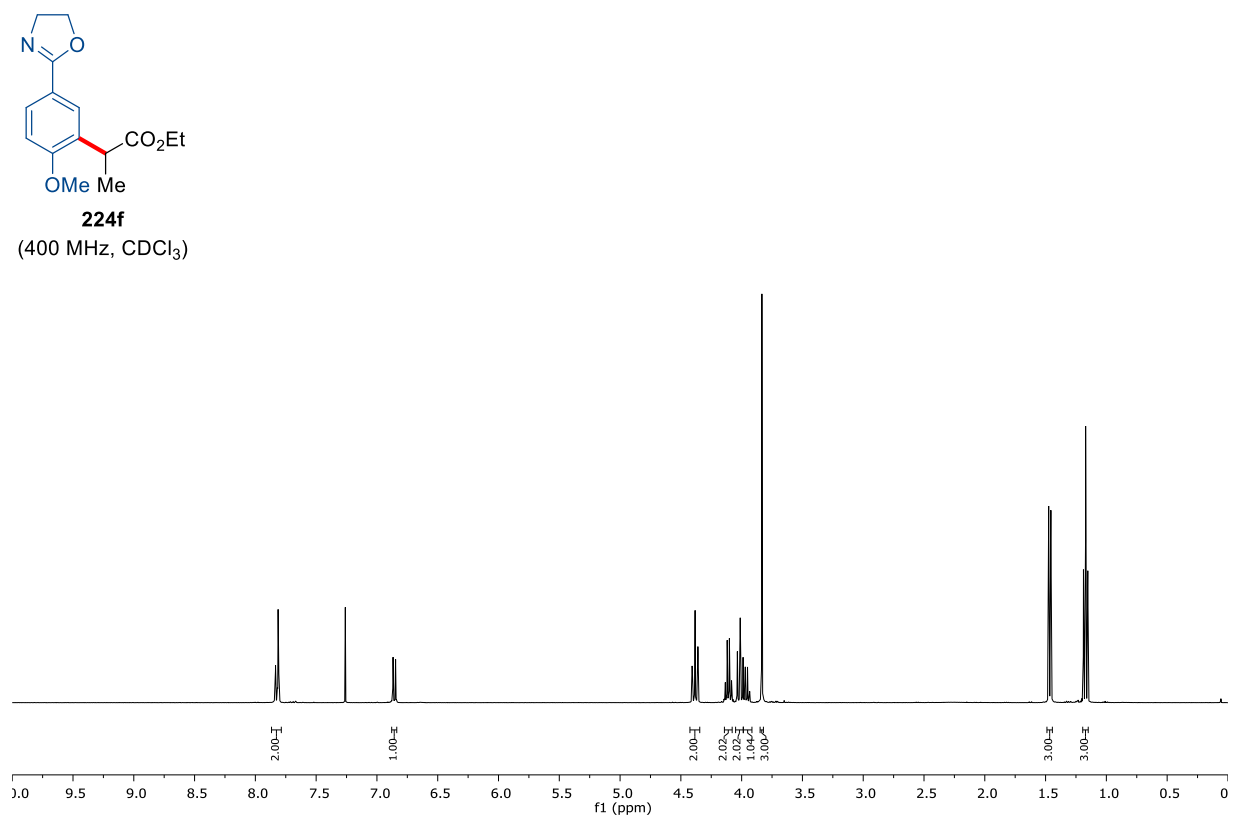
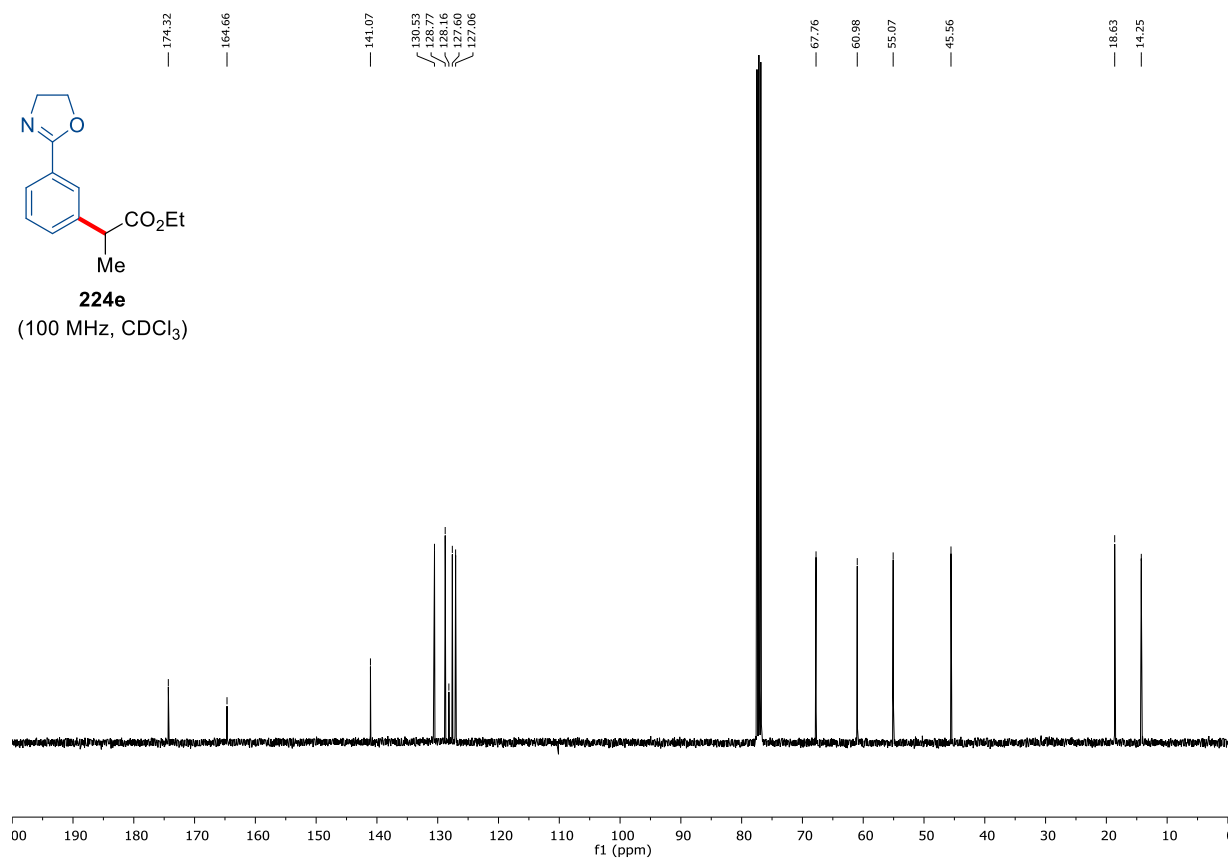


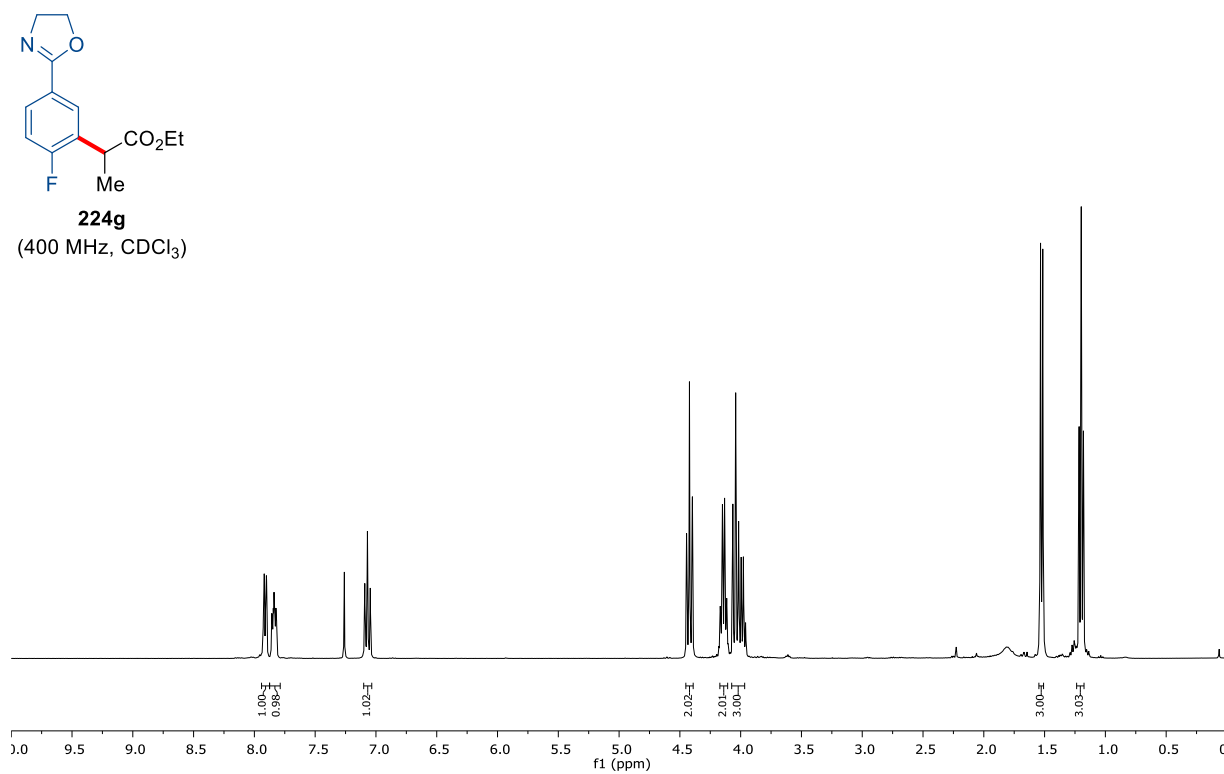
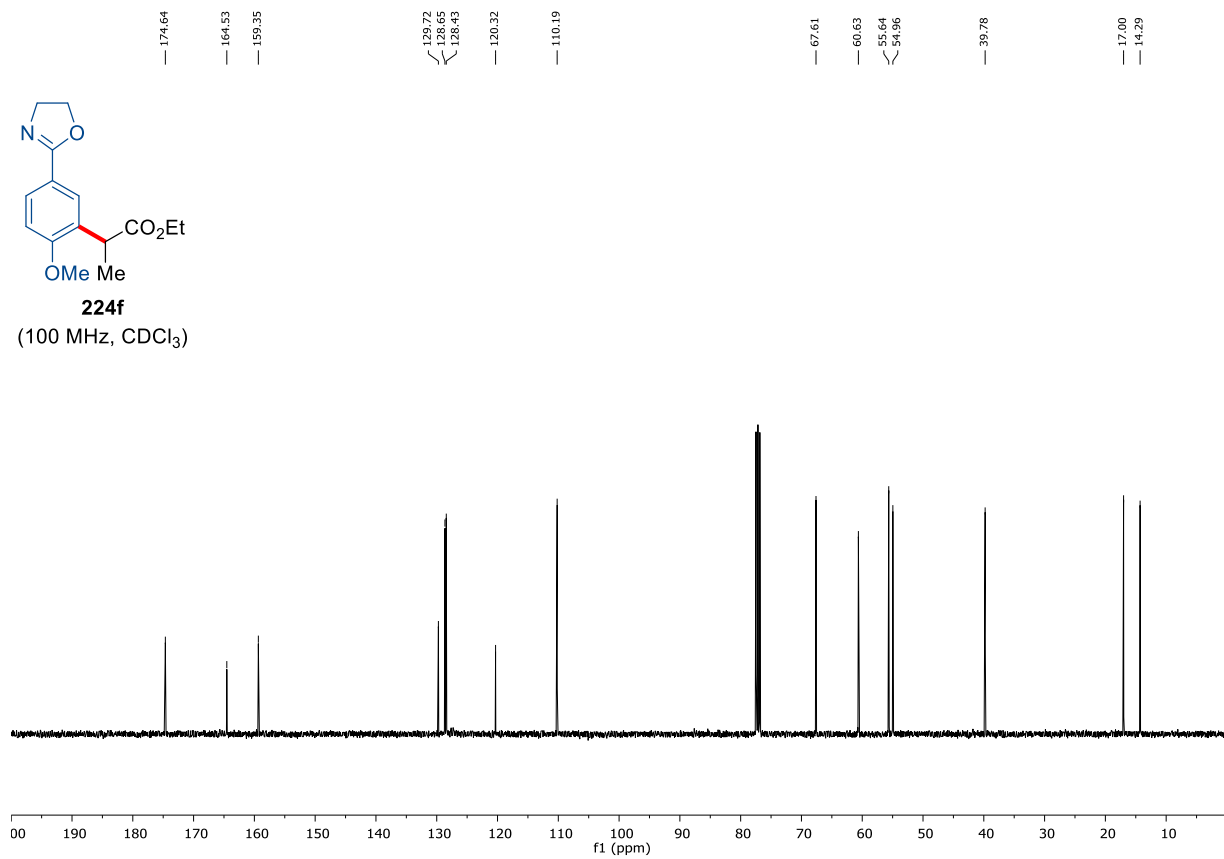
7. Appendix: NMR-Spectra and HPLC Chromatograms



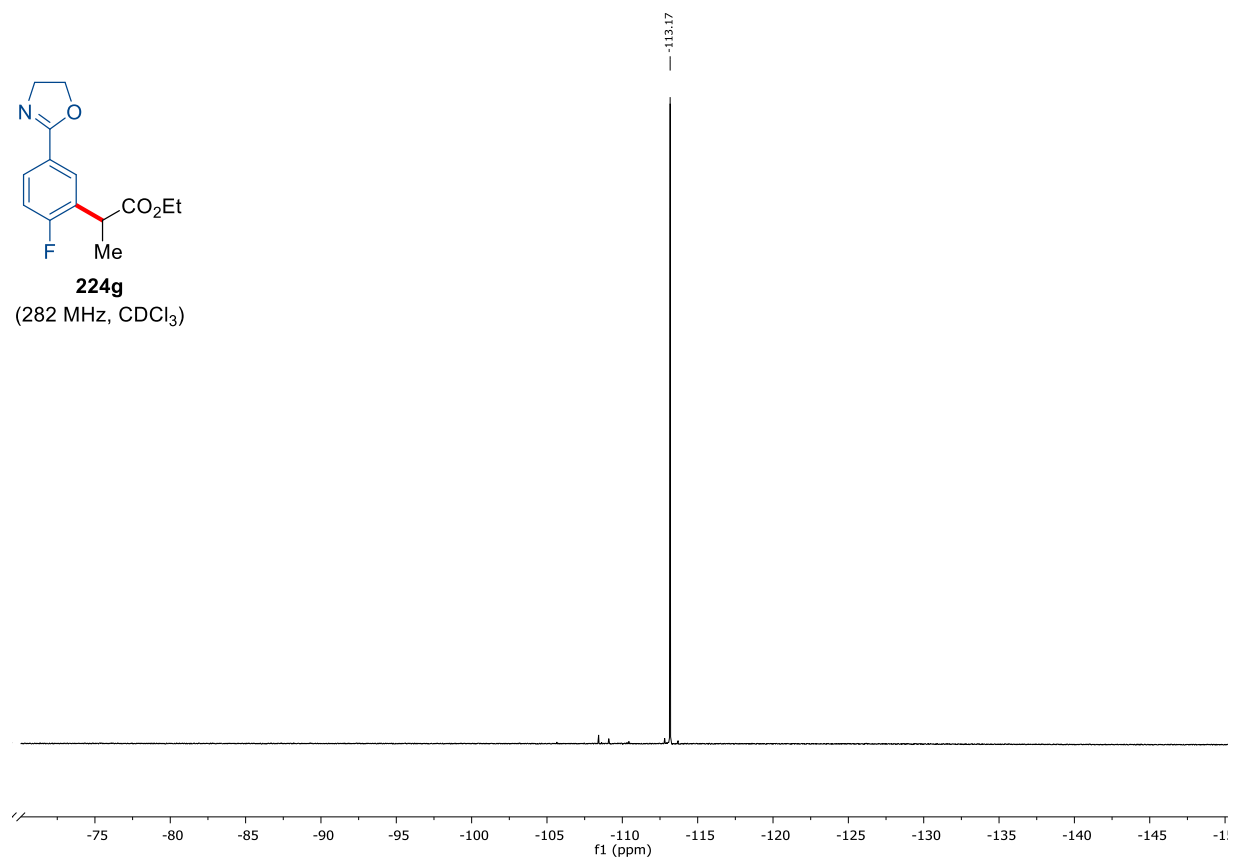
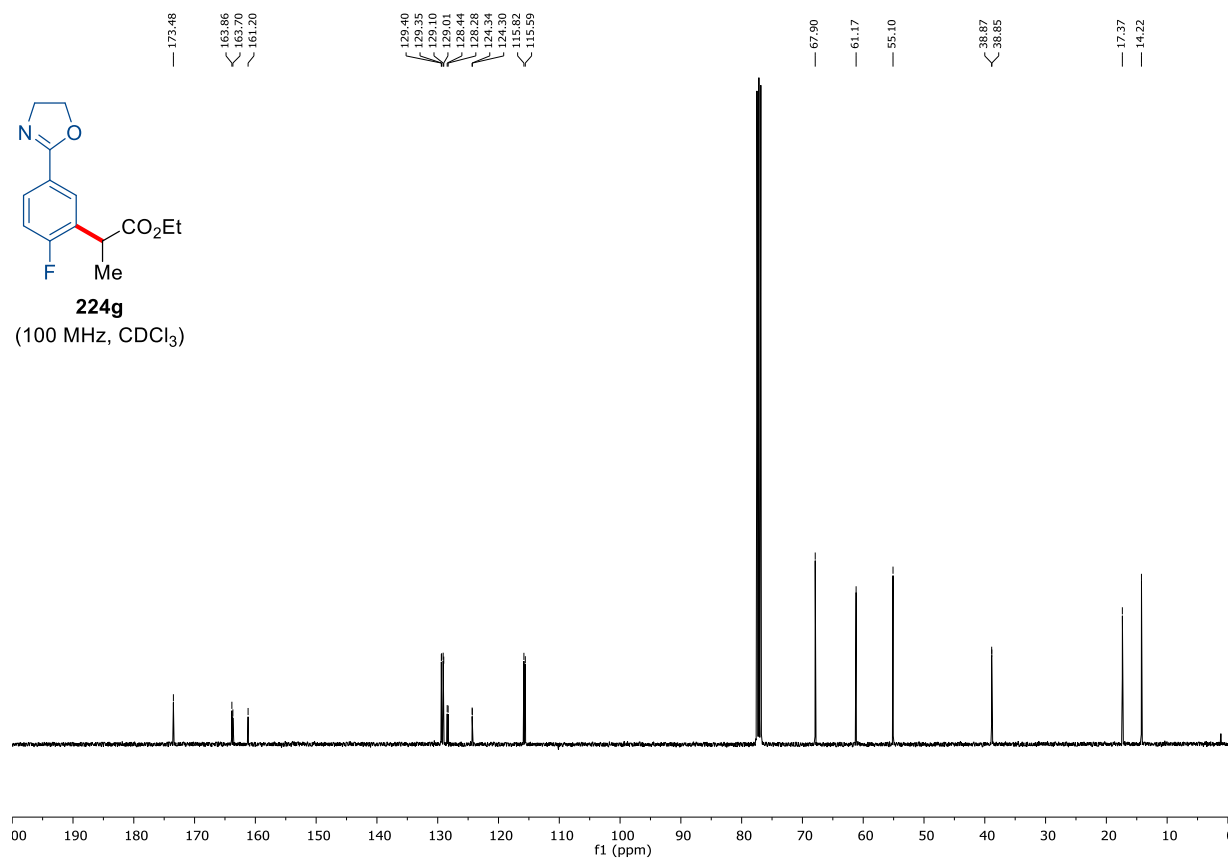


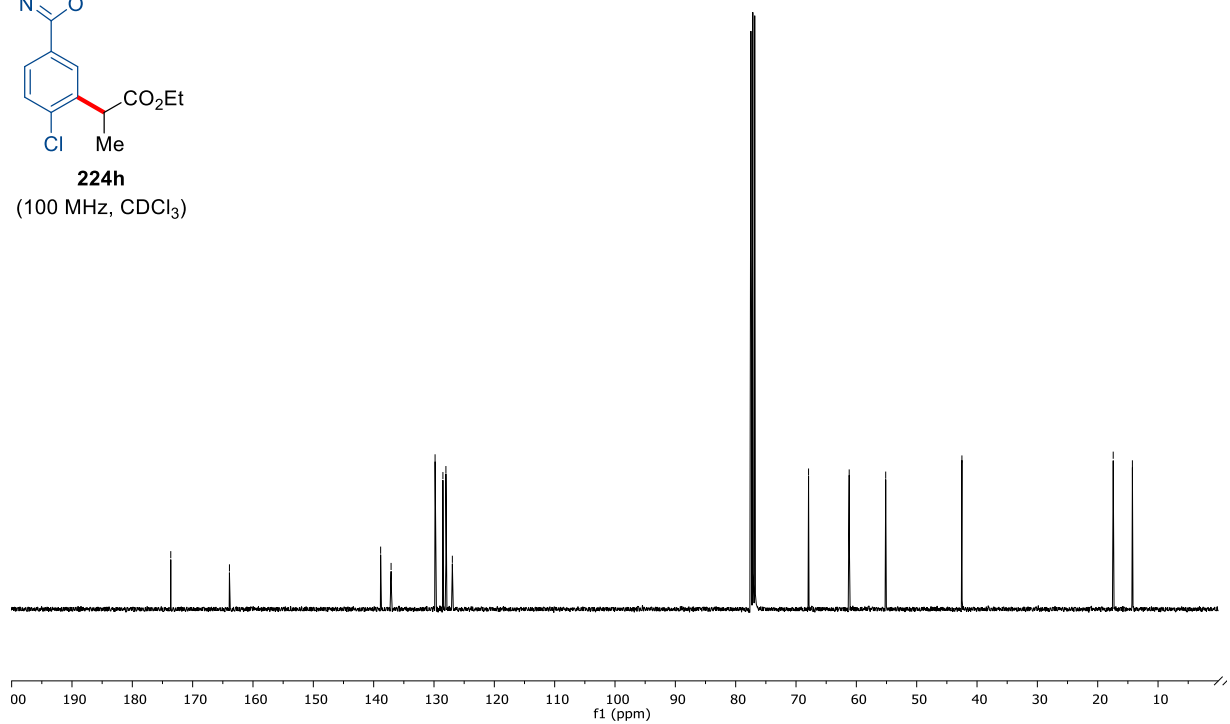
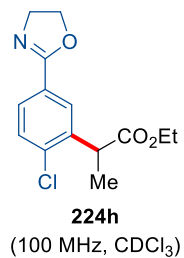
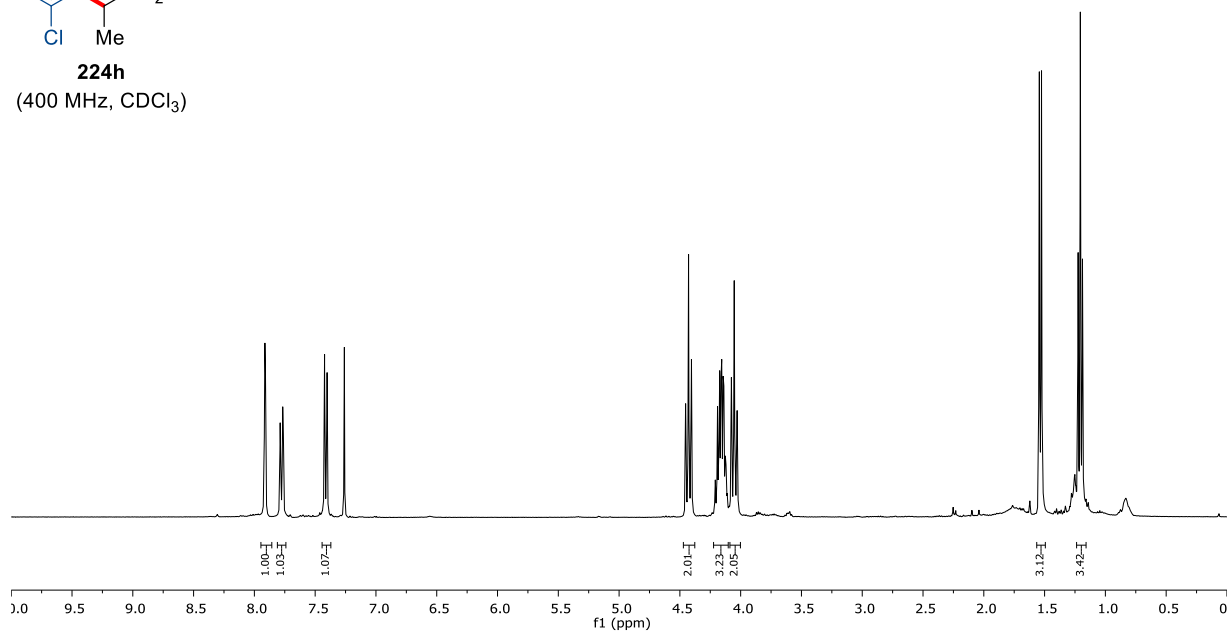
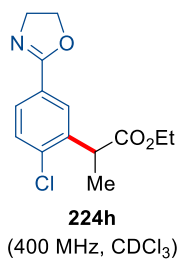
7. Appendix: NMR-Spectra and HPLC Chromatograms



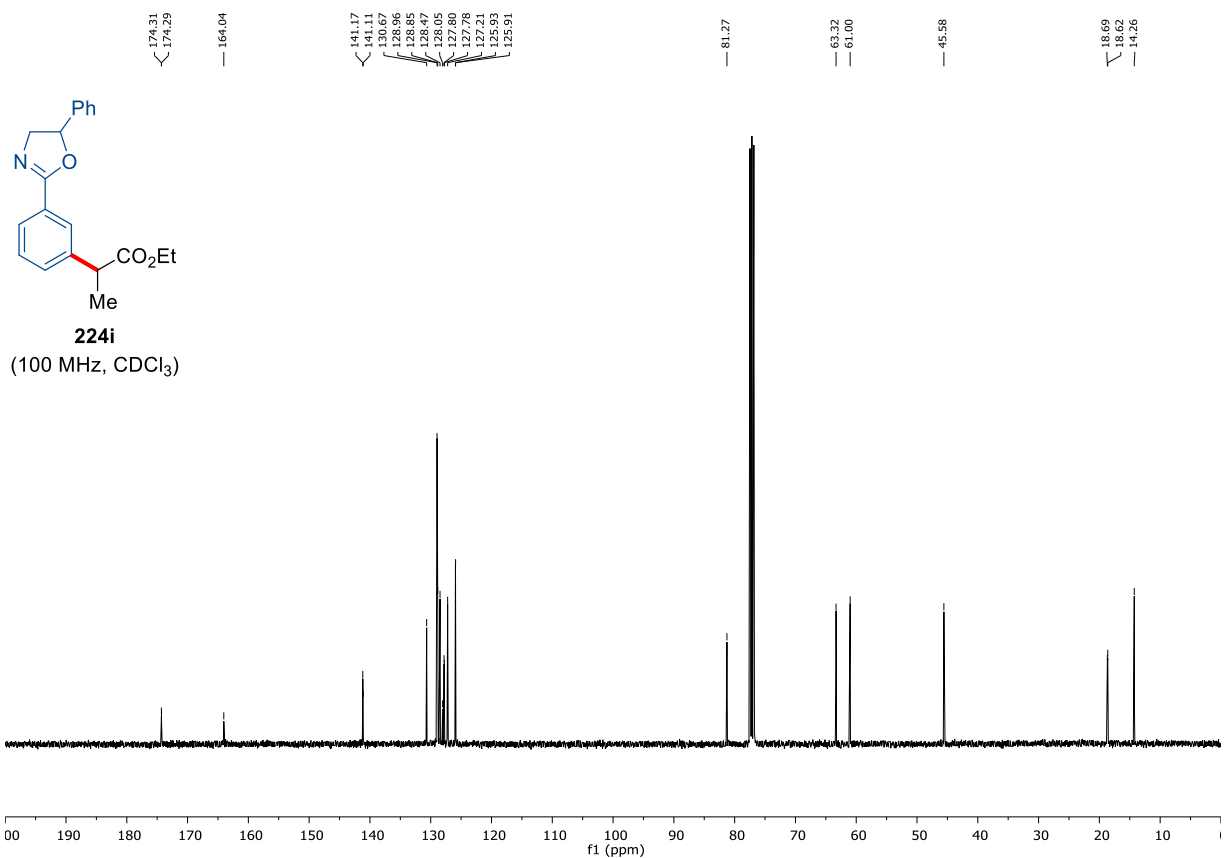
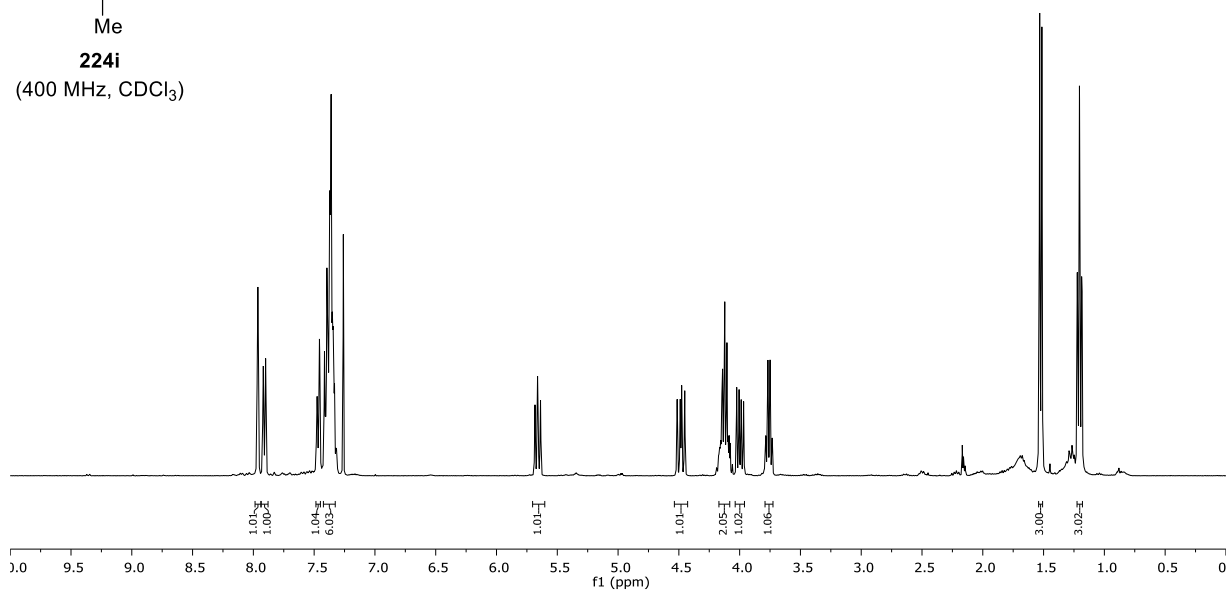
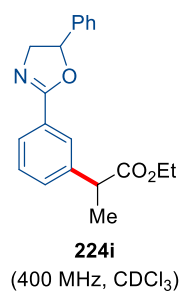


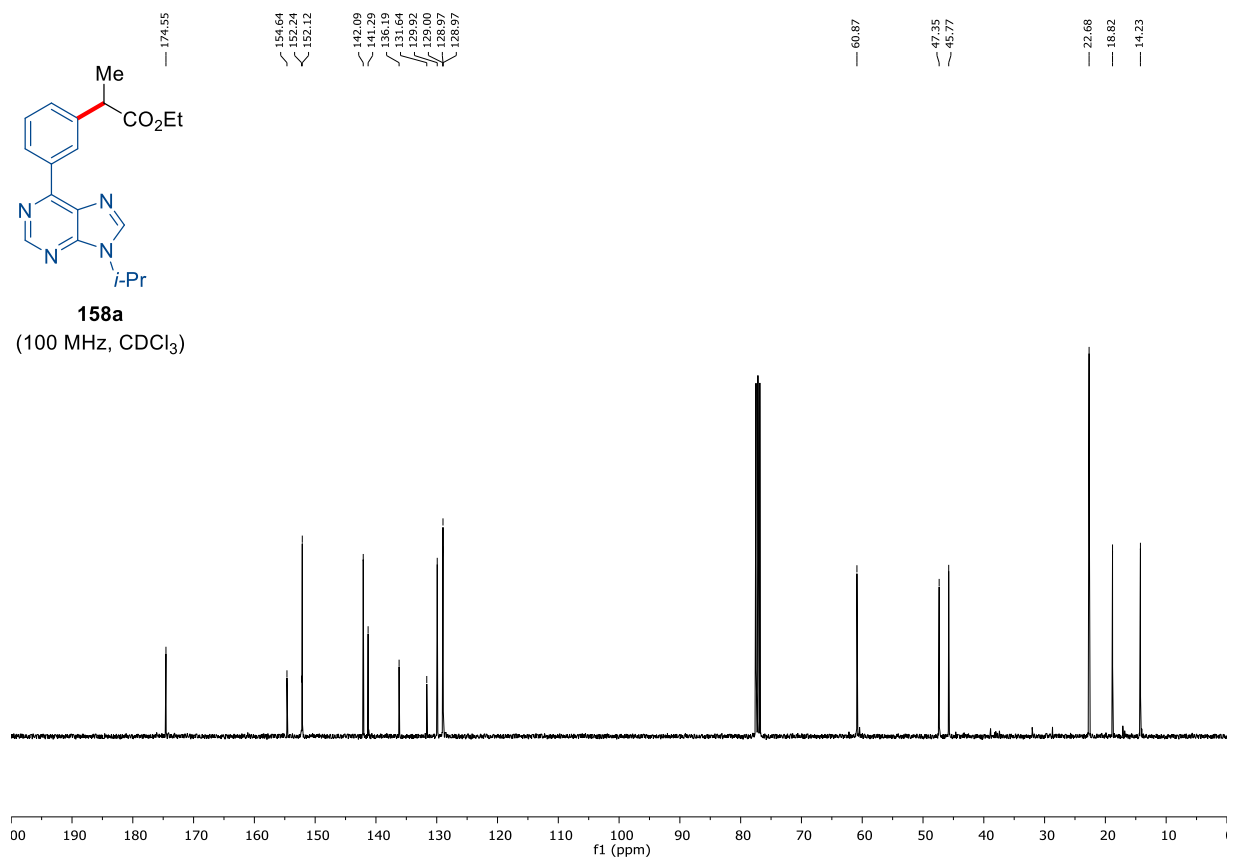
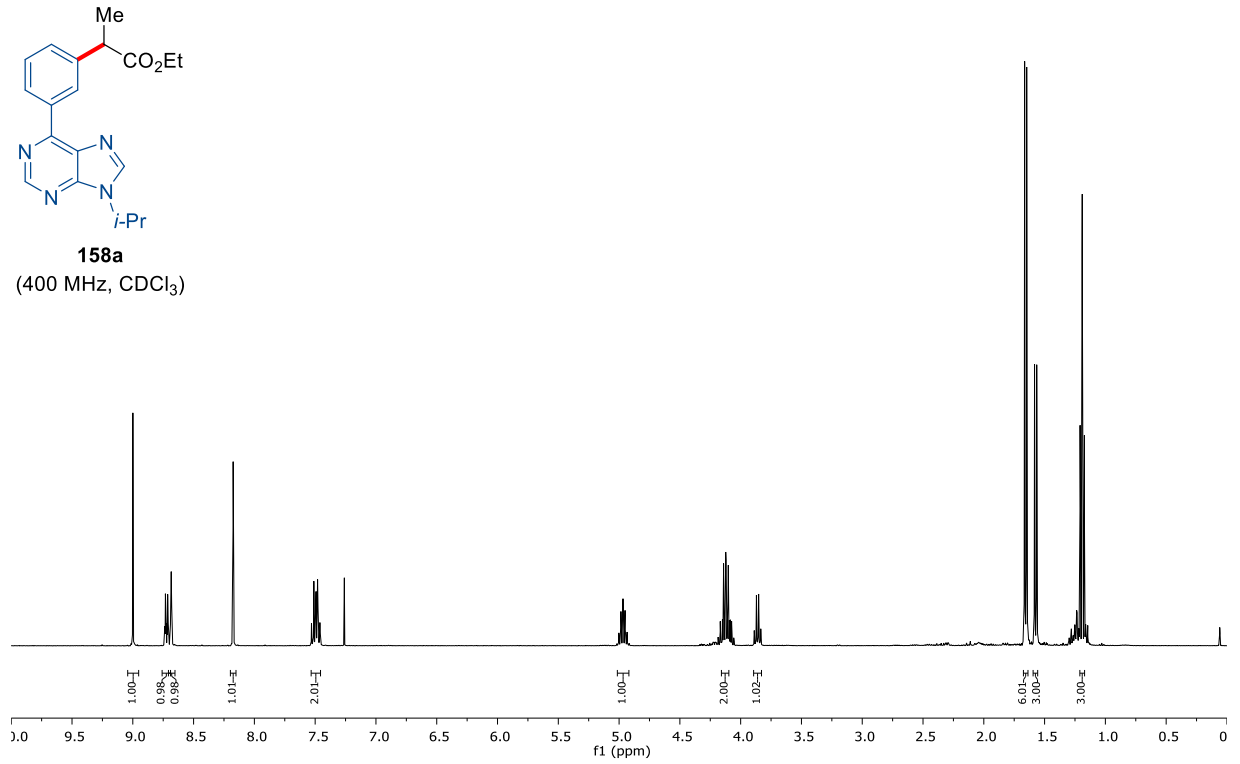
7. Appendix: NMR-Spectra and HPLC Chromatograms



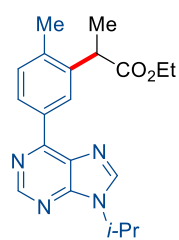


7. Appendix: NMR-Spectra and HPLC Chromatograms

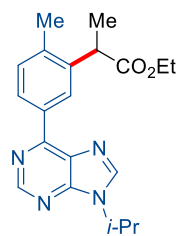
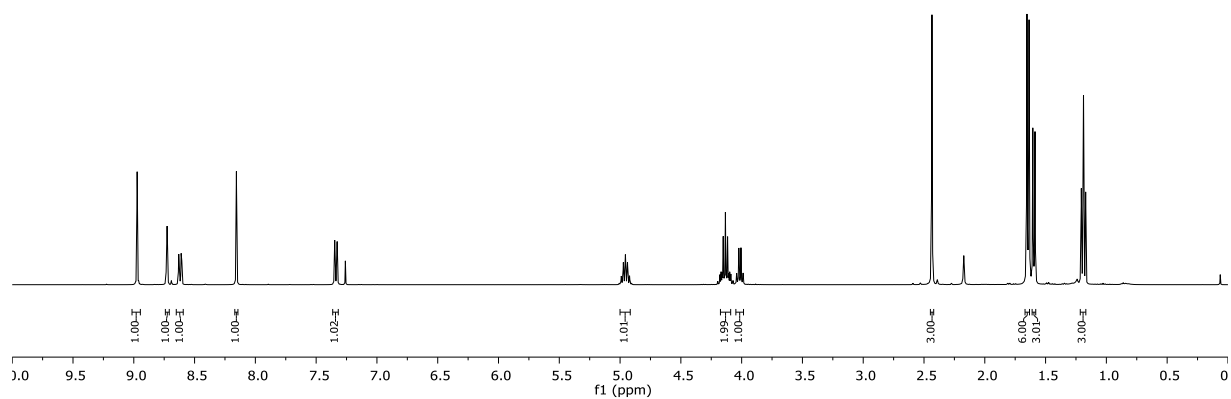




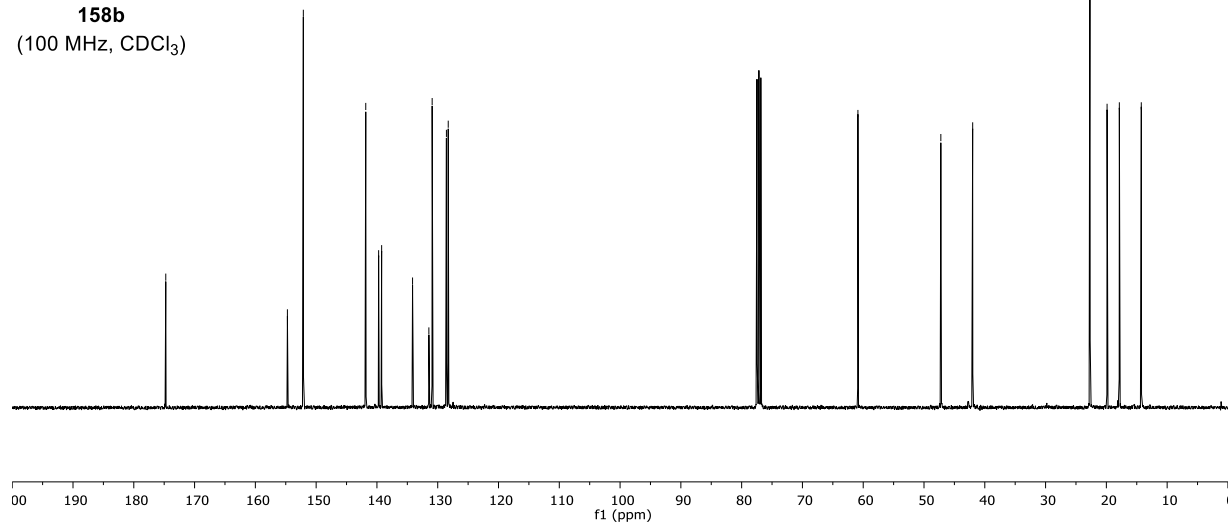
7. Appendix: NMR-Spectra and HPLC Chromatograms

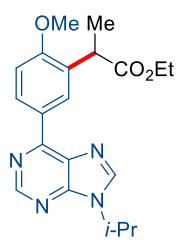


158b
(400 MHz, CDCl₃)

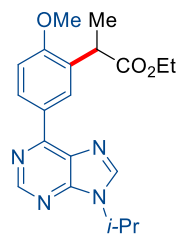
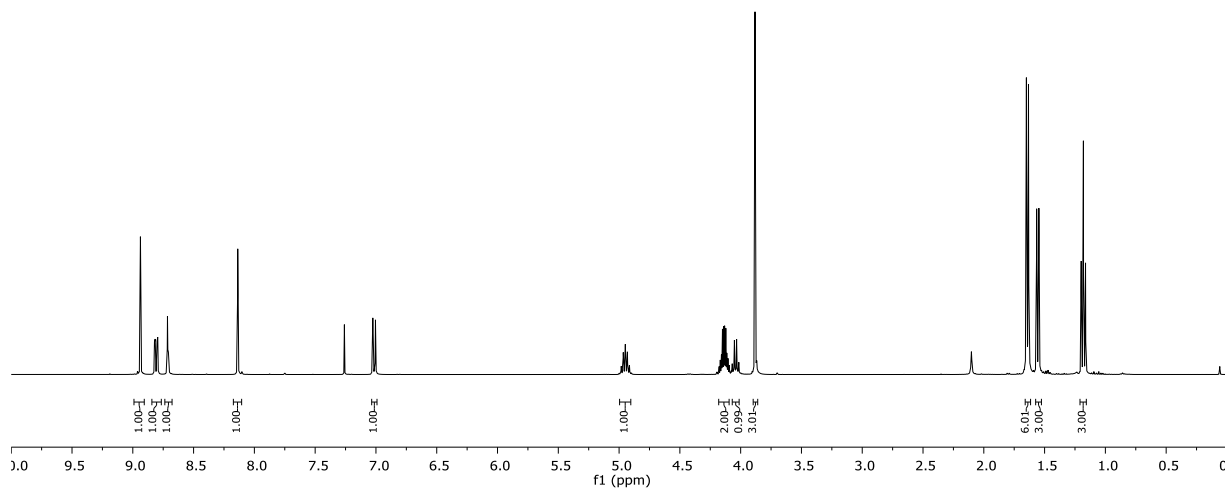


158b
(100 MHz, CDCl₃)

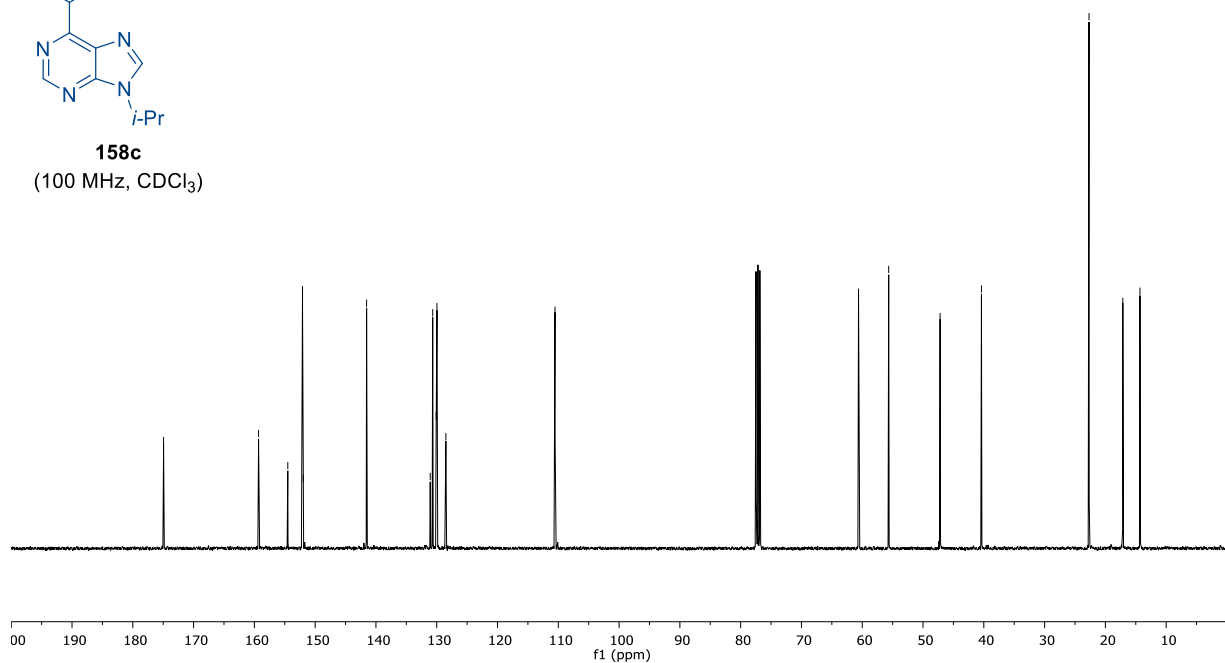




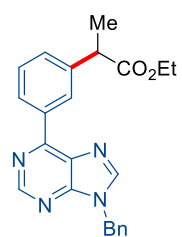
158c
(400 MHz, CDCl₃)



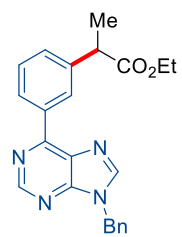
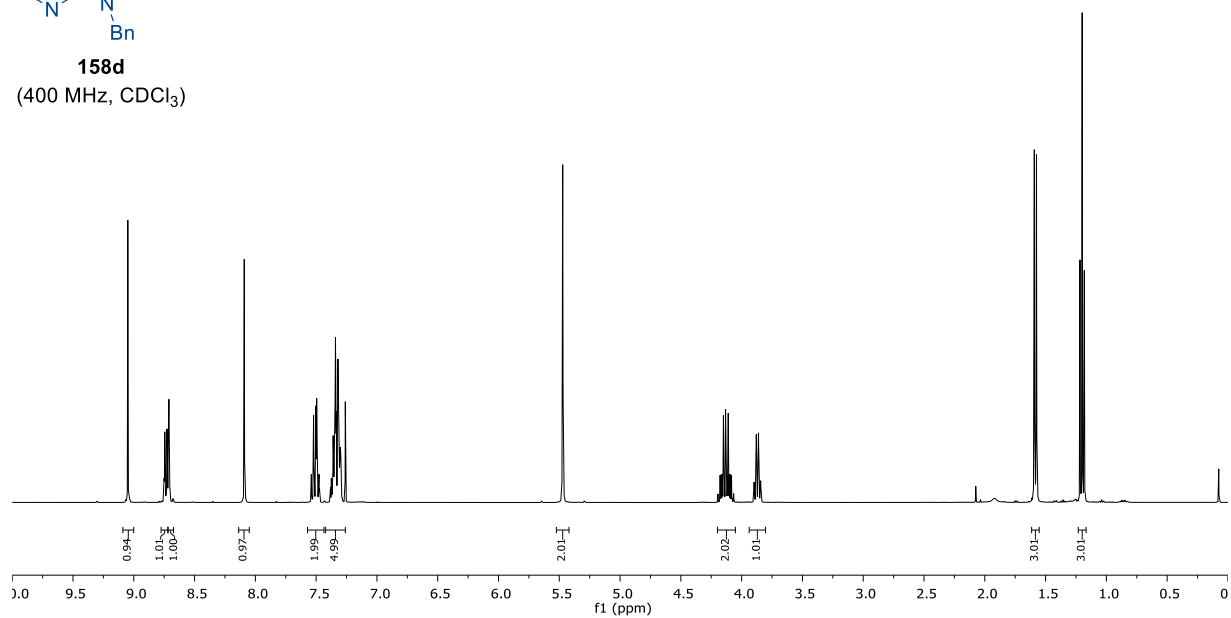
158c
(100 MHz, CDCl₃)



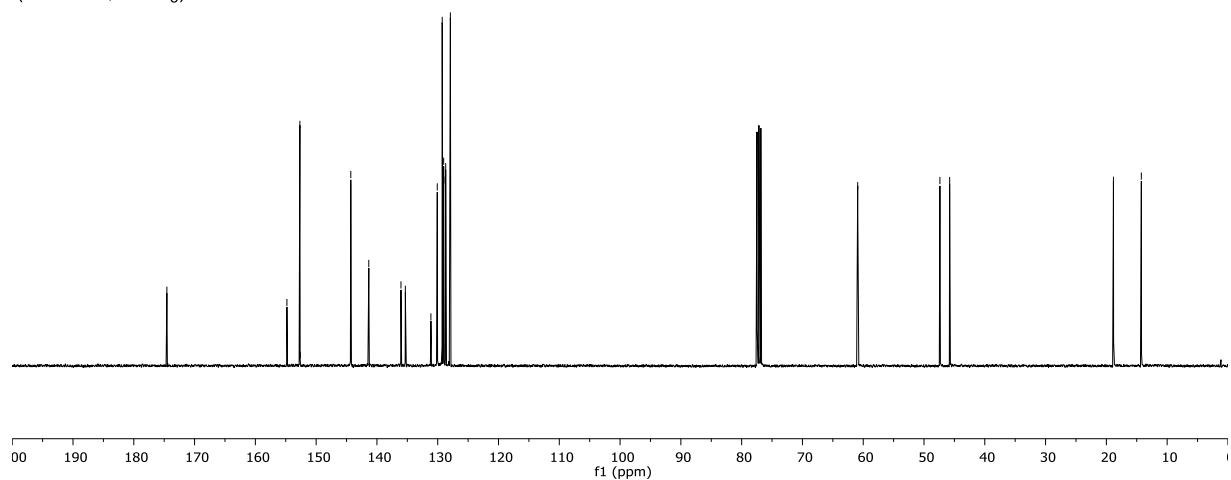
7. Appendix: NMR-Spectra and HPLC Chromatograms

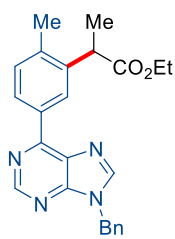


158d
(400 MHz, CDCl₃)

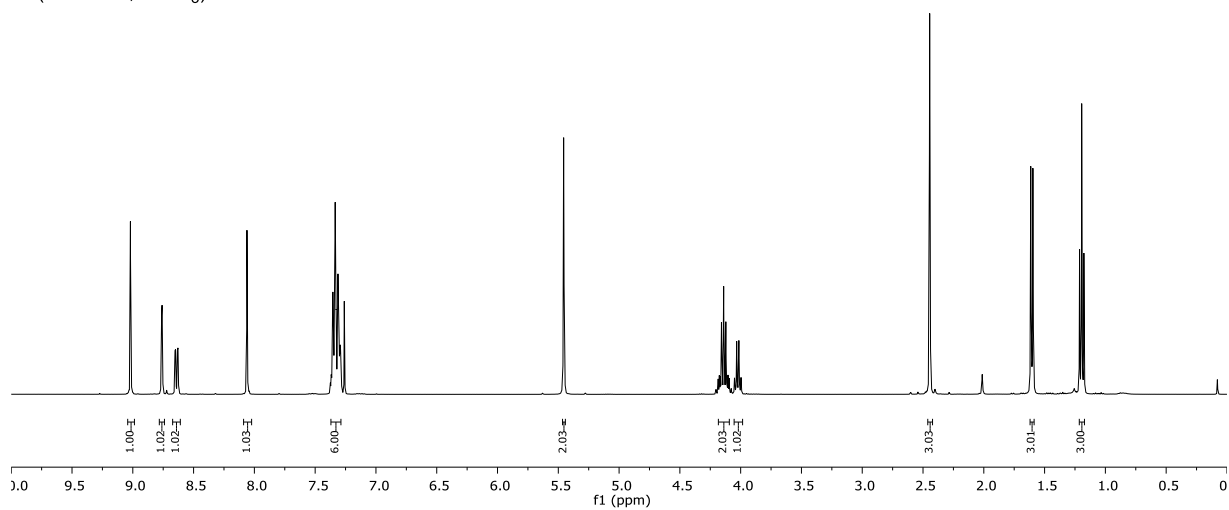


158d
(100 MHz, CDCl₃)

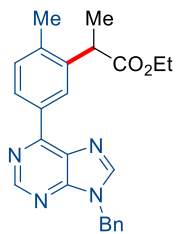




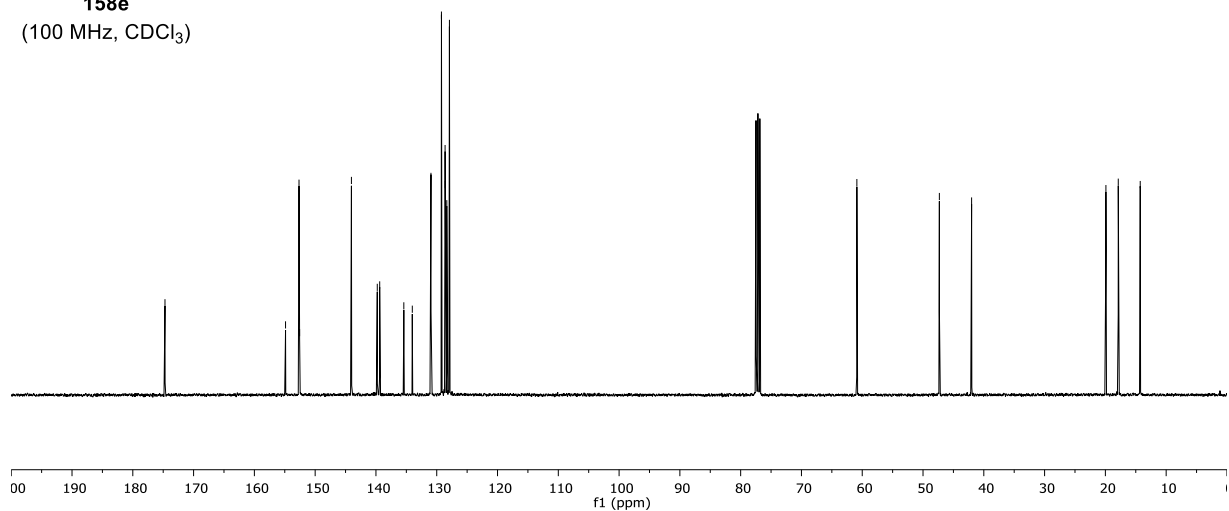
158e
(400 MHz, CDCl₃)



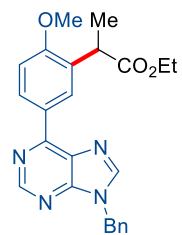
174.71
154.87
152.66
152.56
144.03
143.28
139.38
135.41
134.02
130.95
129.22
128.62
128.61
128.54
127.91
60.88
47.31
42.01
19.91
18.99
14.27



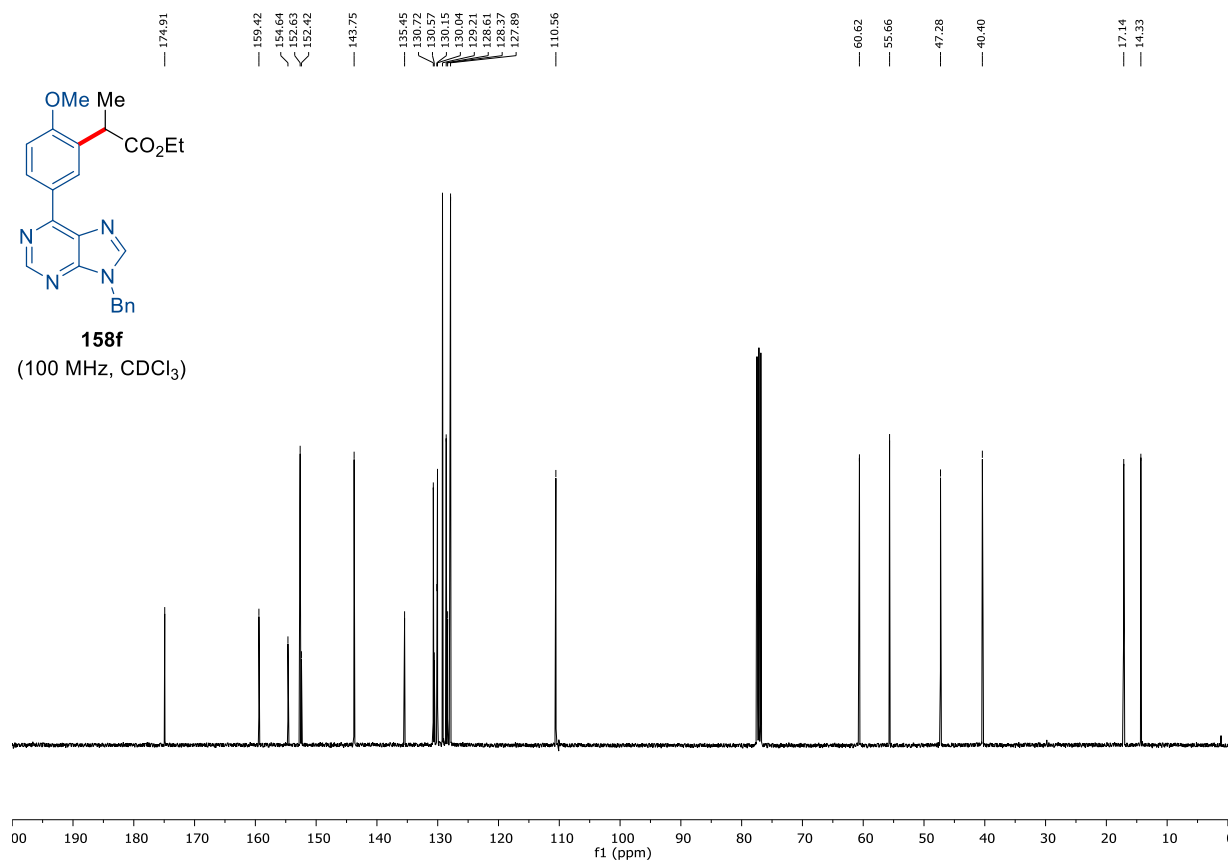
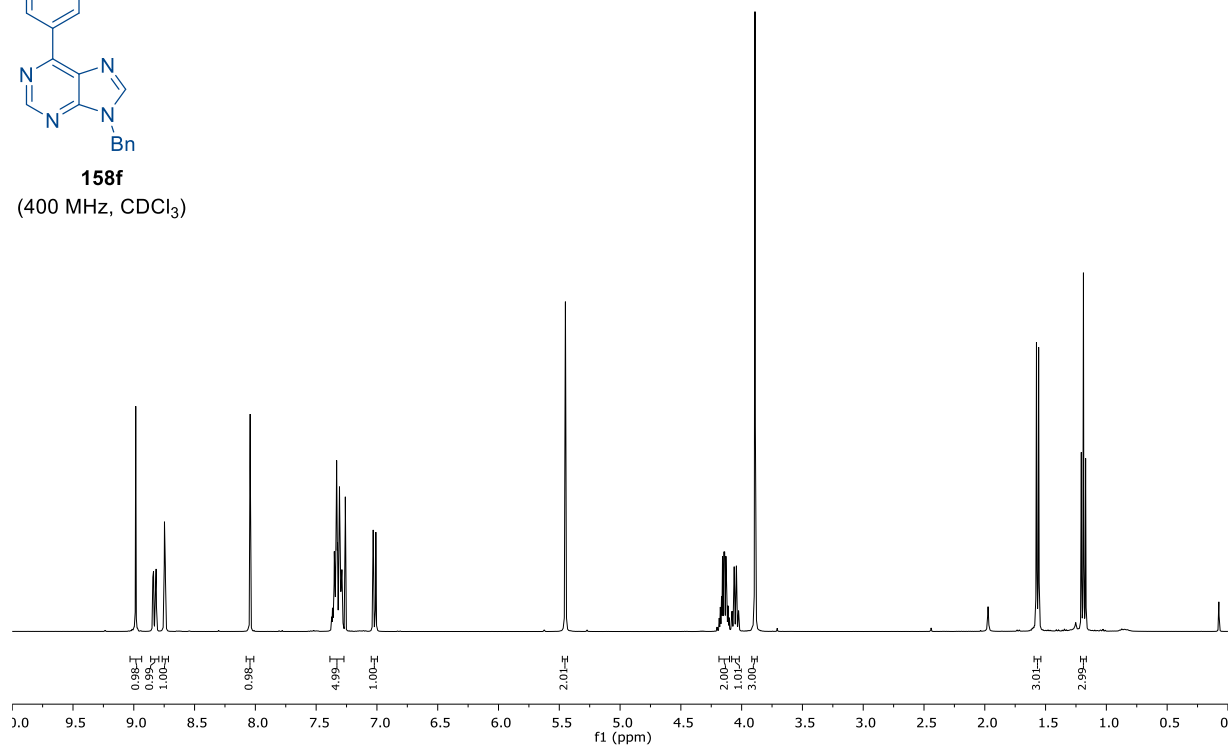
158e
(100 MHz, CDCl₃)



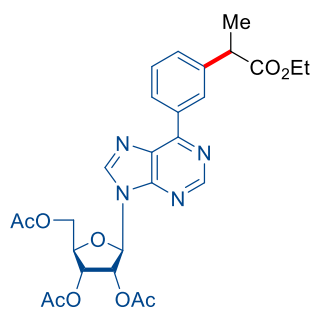
7. Appendix: NMR-Spectra and HPLC Chromatograms



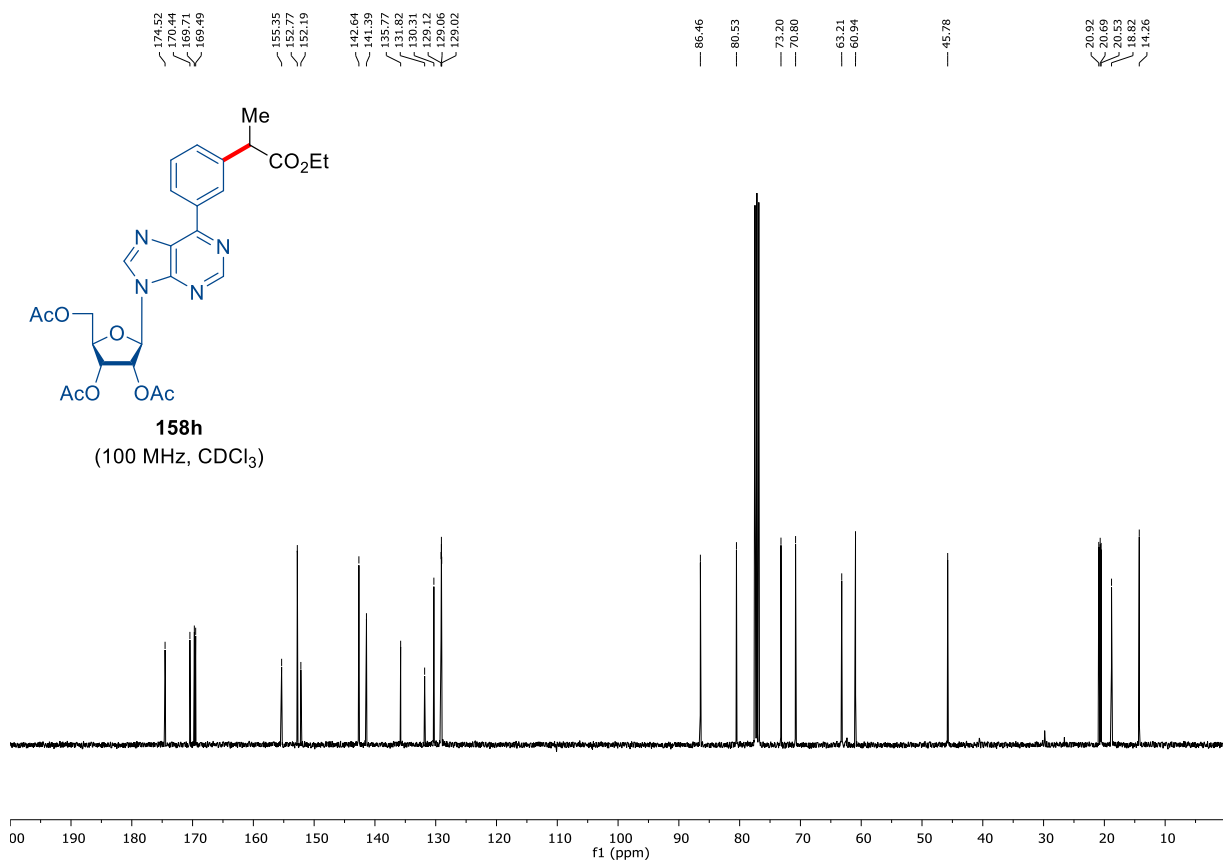
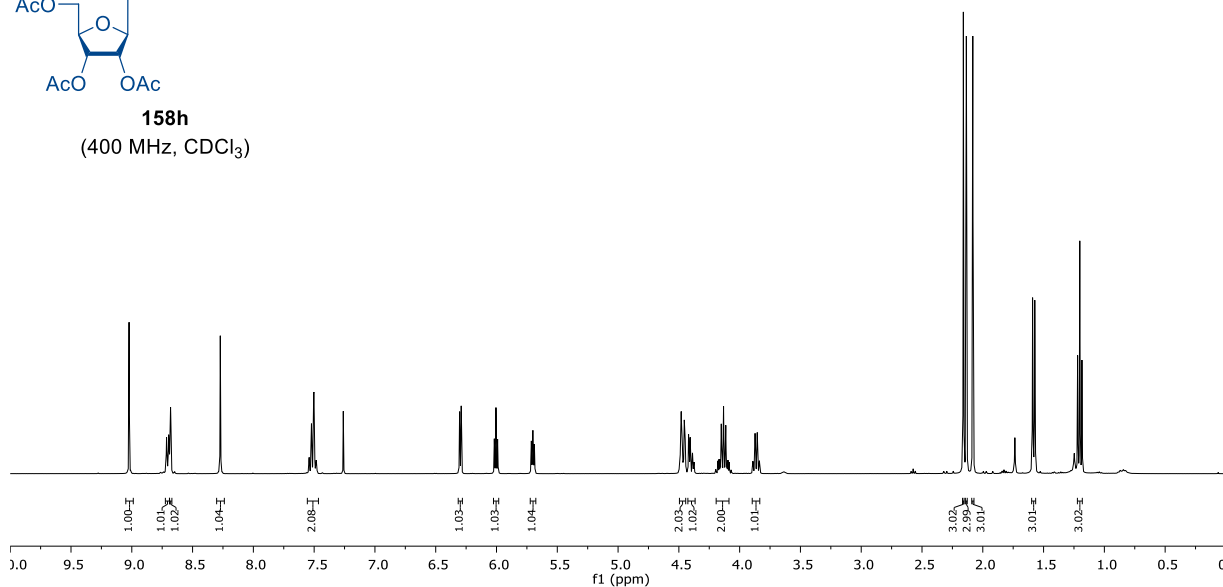
158f
(400 MHz, CDCl₃)

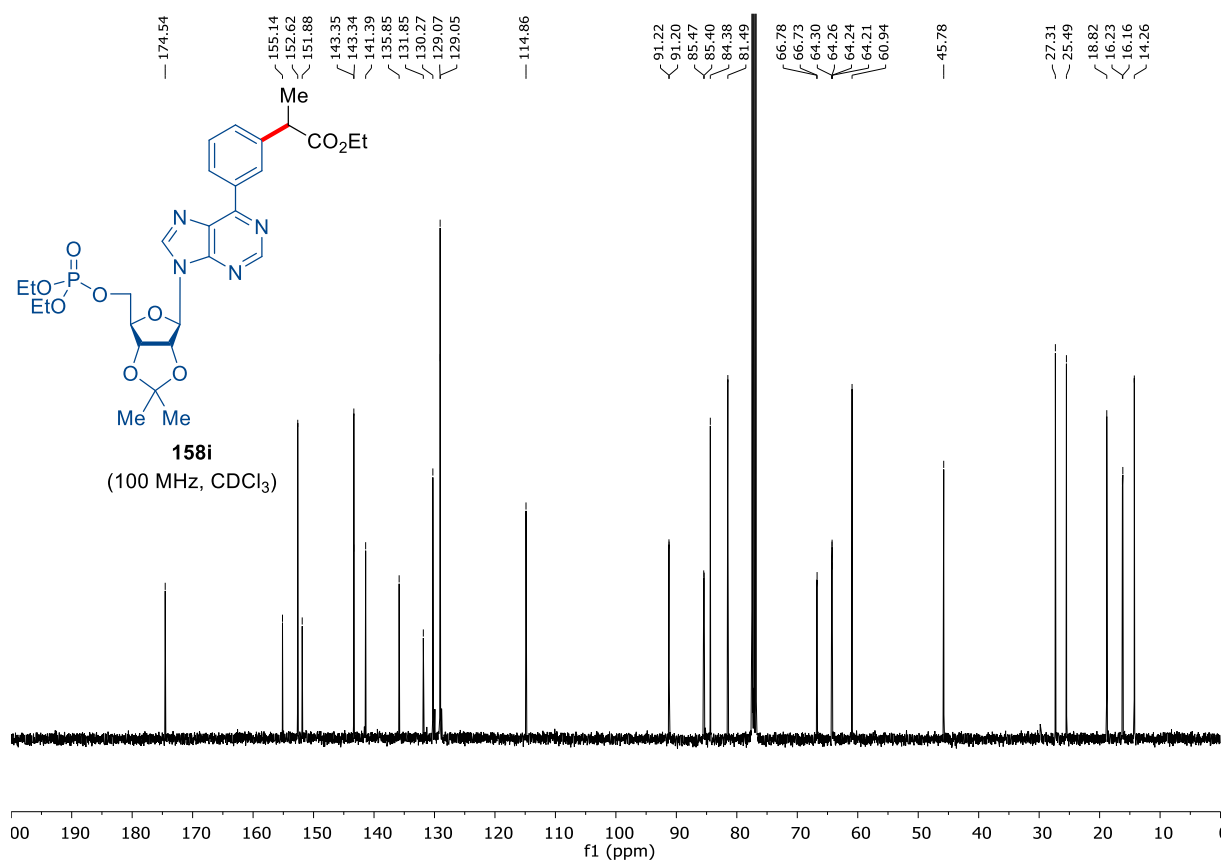
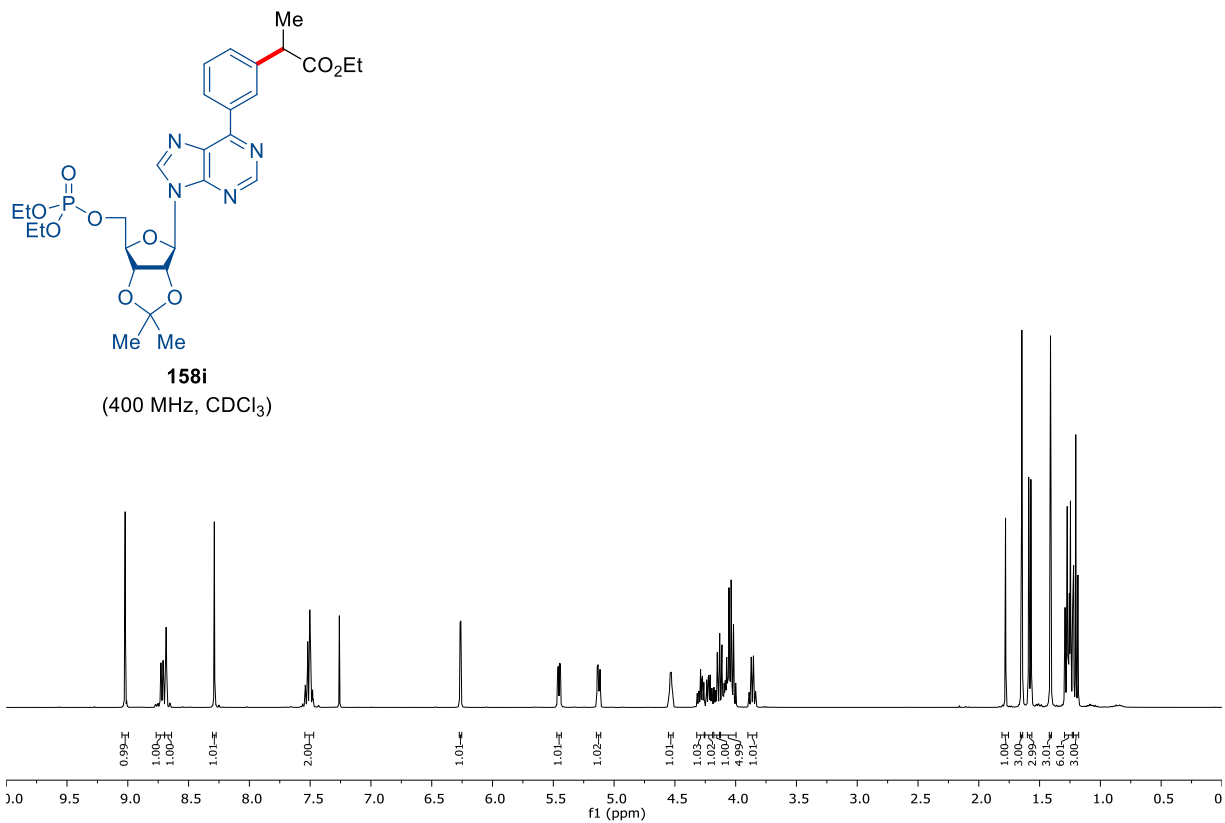


7. Appendix: NMR-Spectra and HPLC Chromatograms

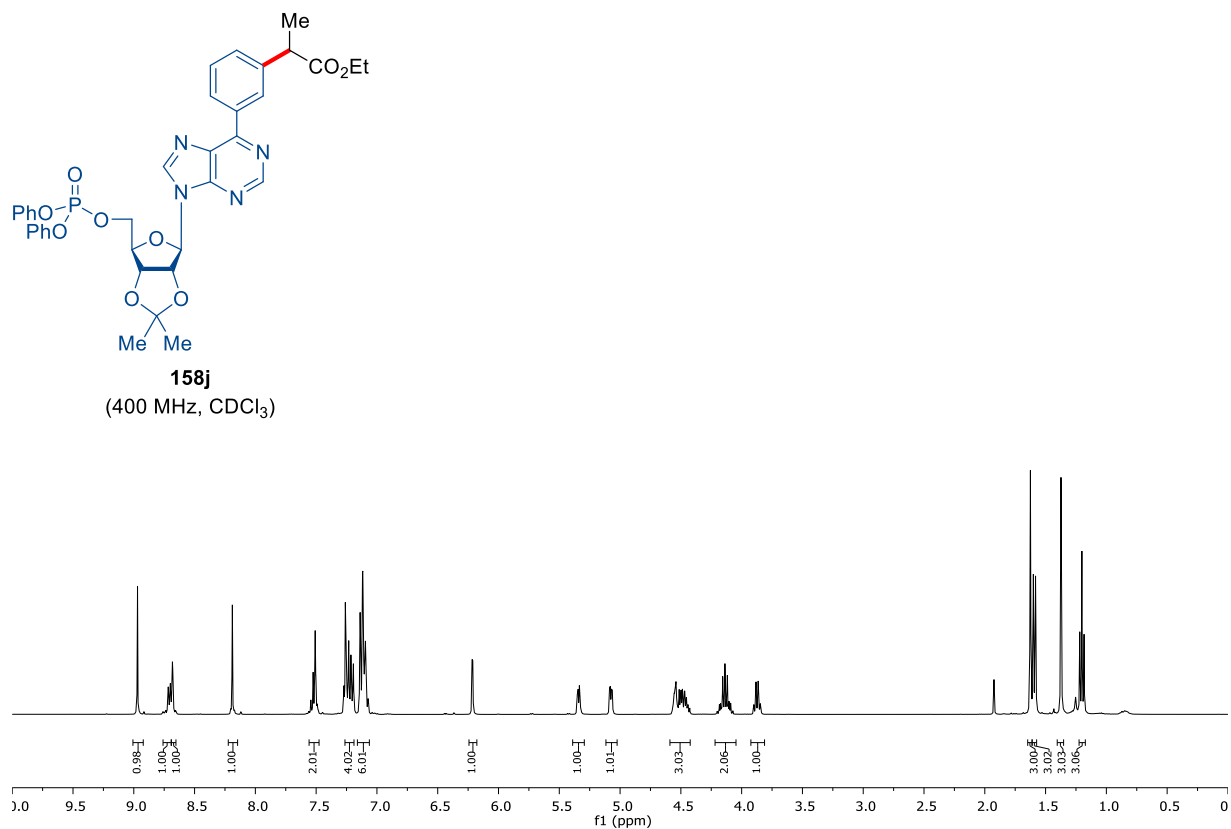
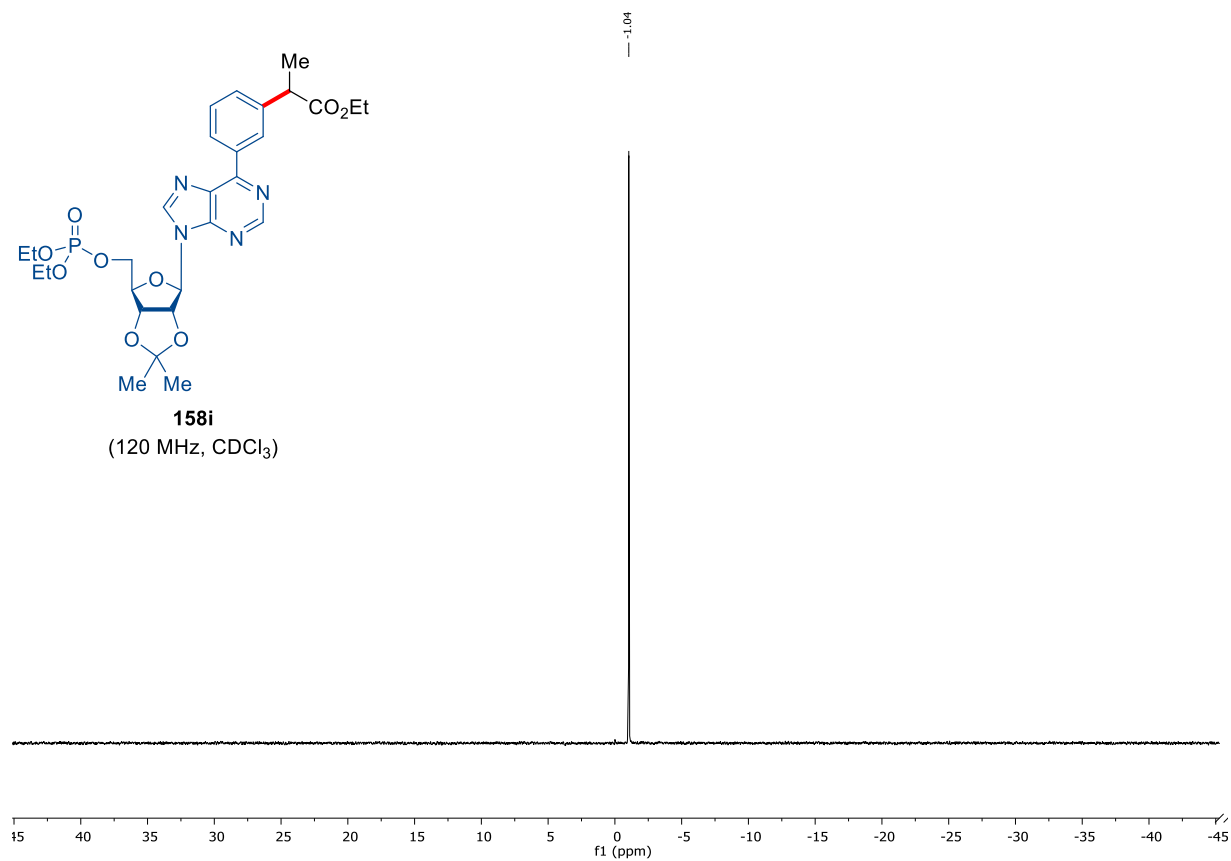


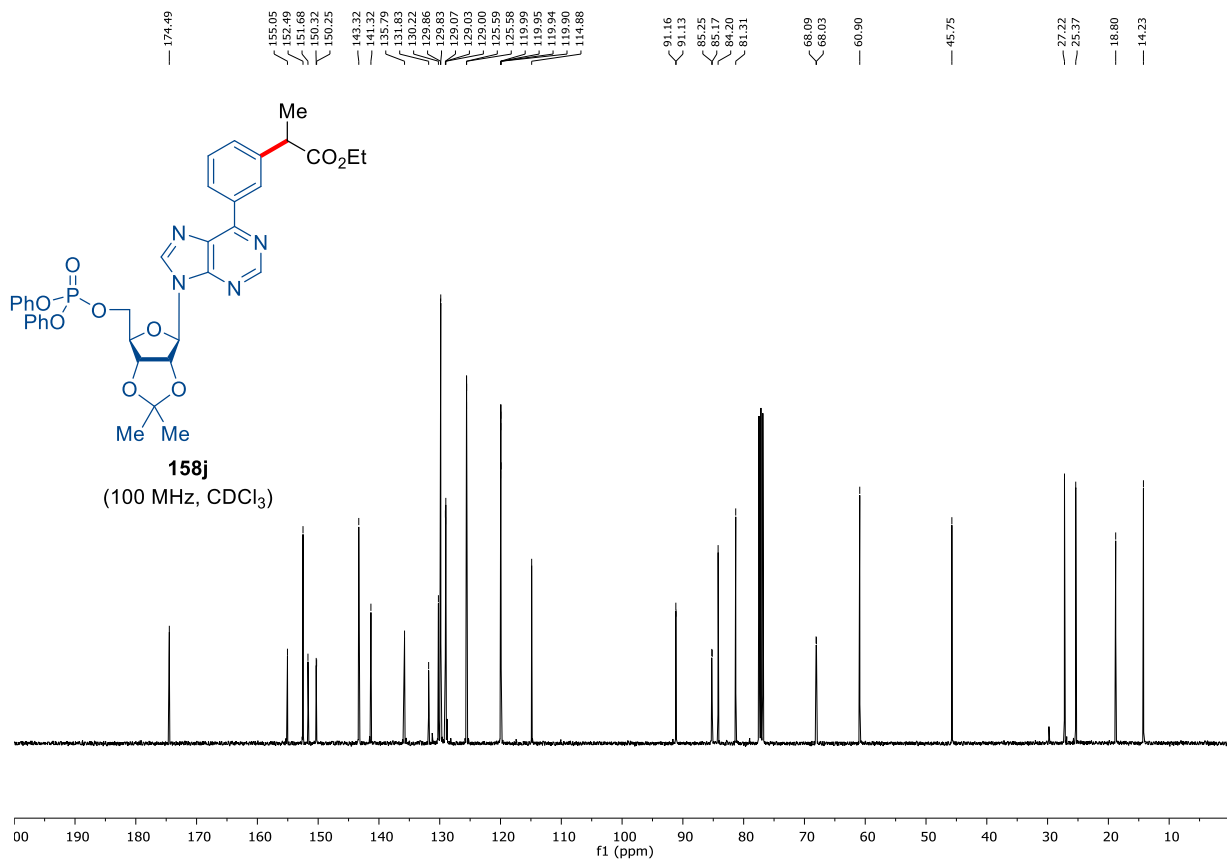
158h
(400 MHz, CDCl₃)



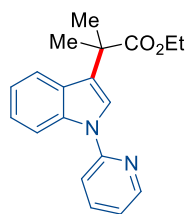


7. Appendix: NMR-Spectra and HPLC Chromatograms

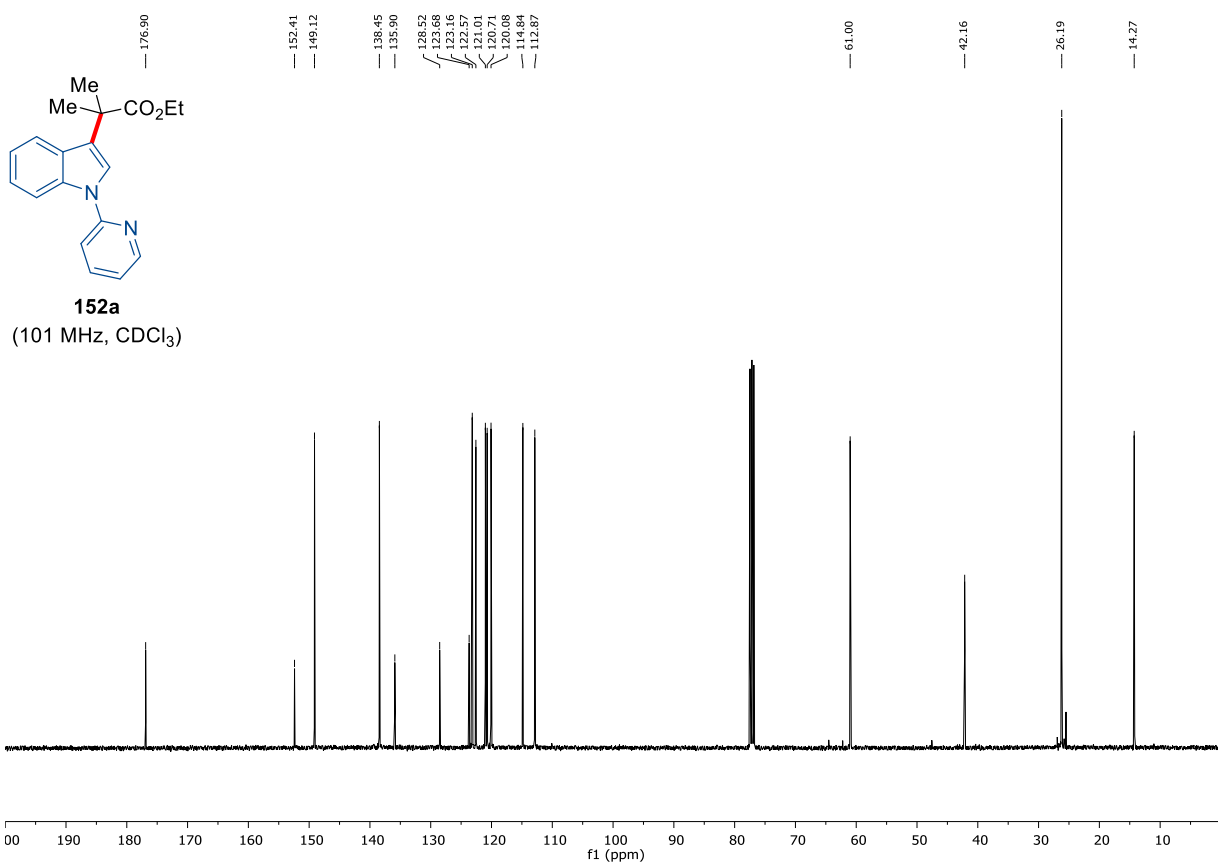
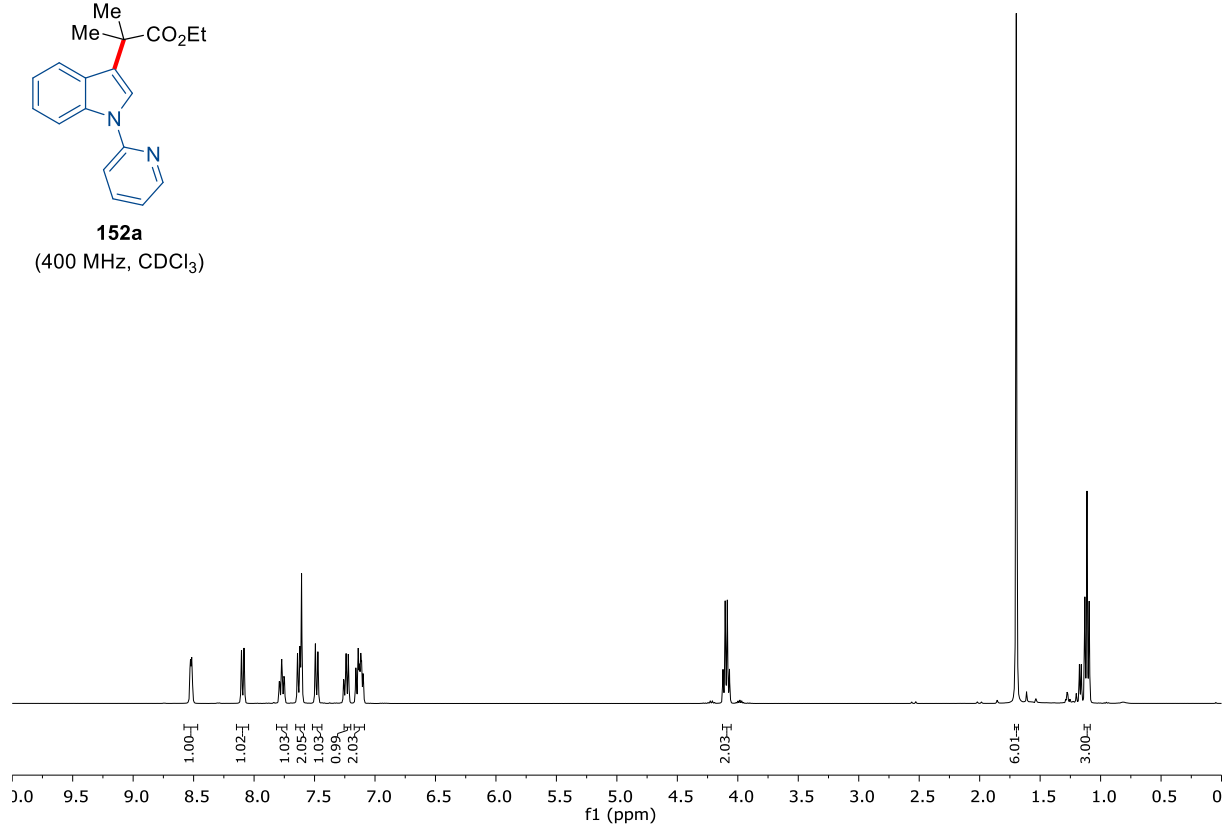


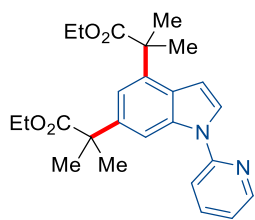


7. Appendix: NMR-Spectra and HPLC Chromatograms

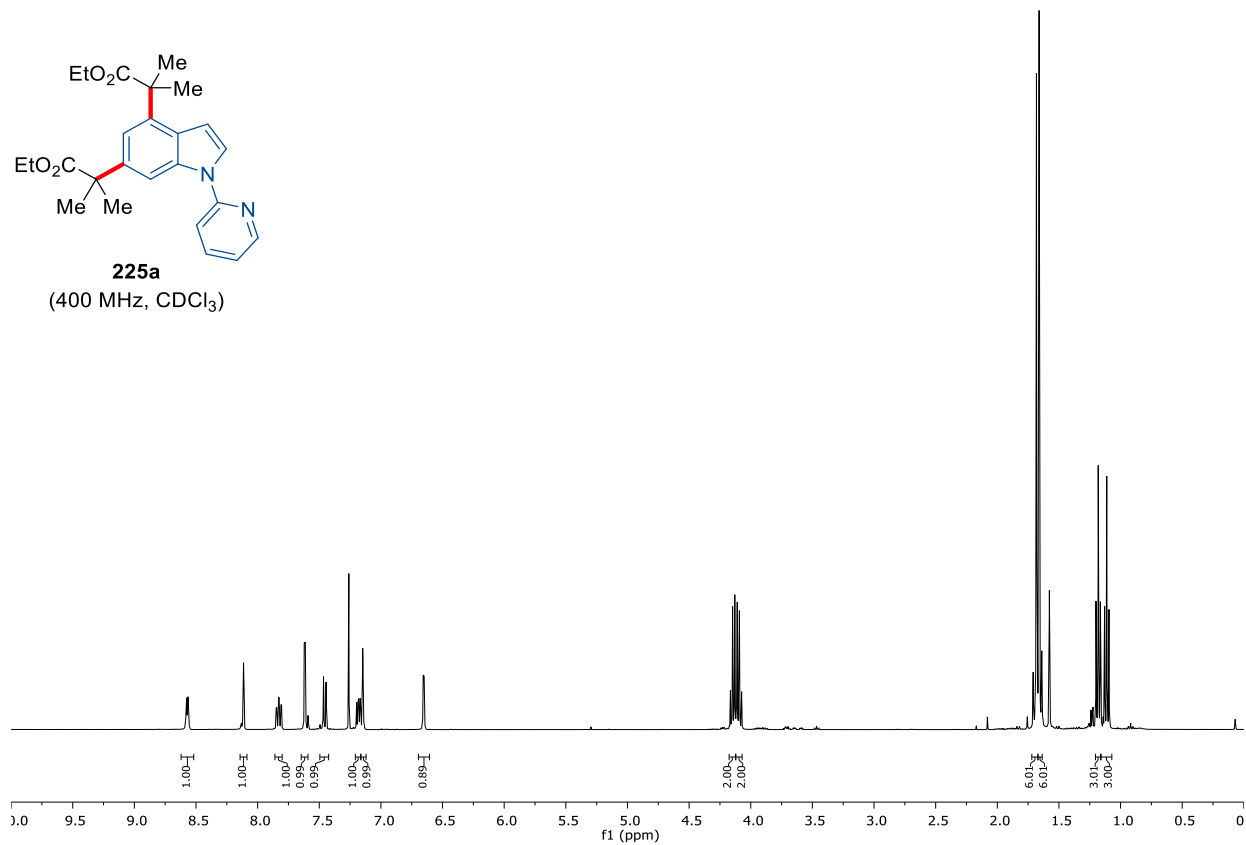


152a
(400 MHz, CDCl₃)

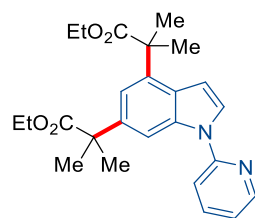




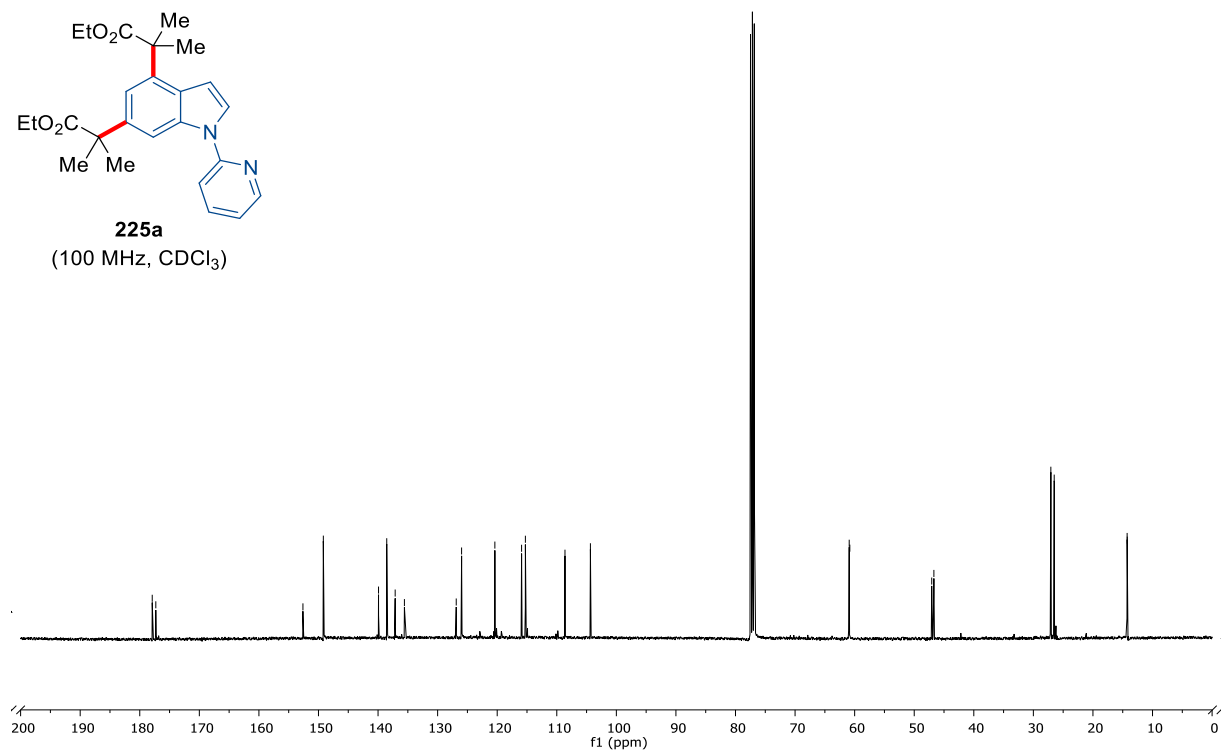
225a
(400 MHz, CDCl₃)



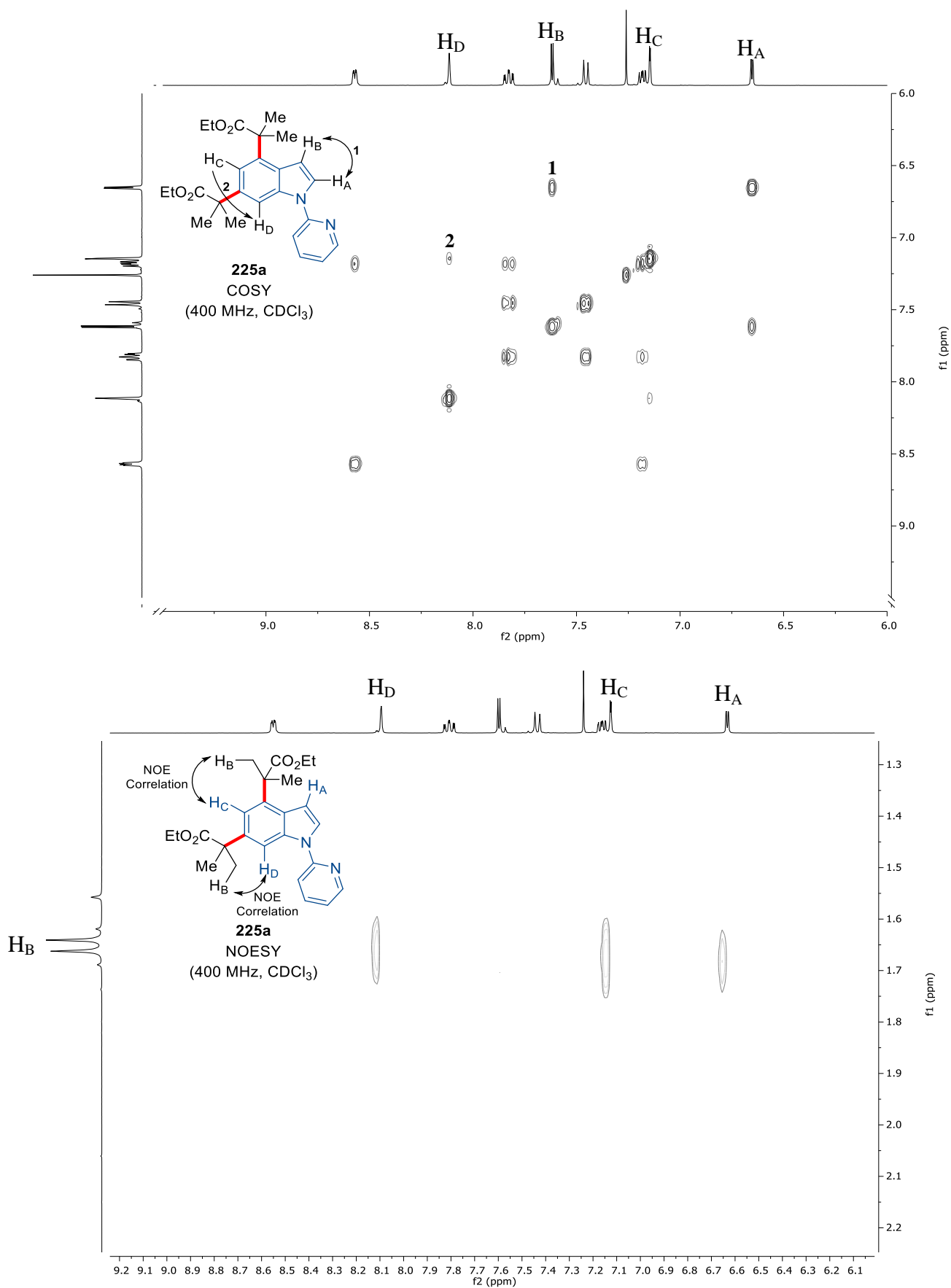
177.91
 177.31
 152.61
 149.19
 139.92
 138.54
 137.13
 135.58
 126.88
 125.98
 120.39
 115.91
 115.27
 106.62
 104.35
 60.91
 60.81
 47.06
 46.70
 27.07
 26.50
 14.26
 14.24

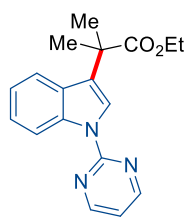


225a
(100 MHz, CDCl₃)

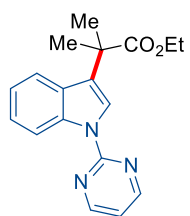
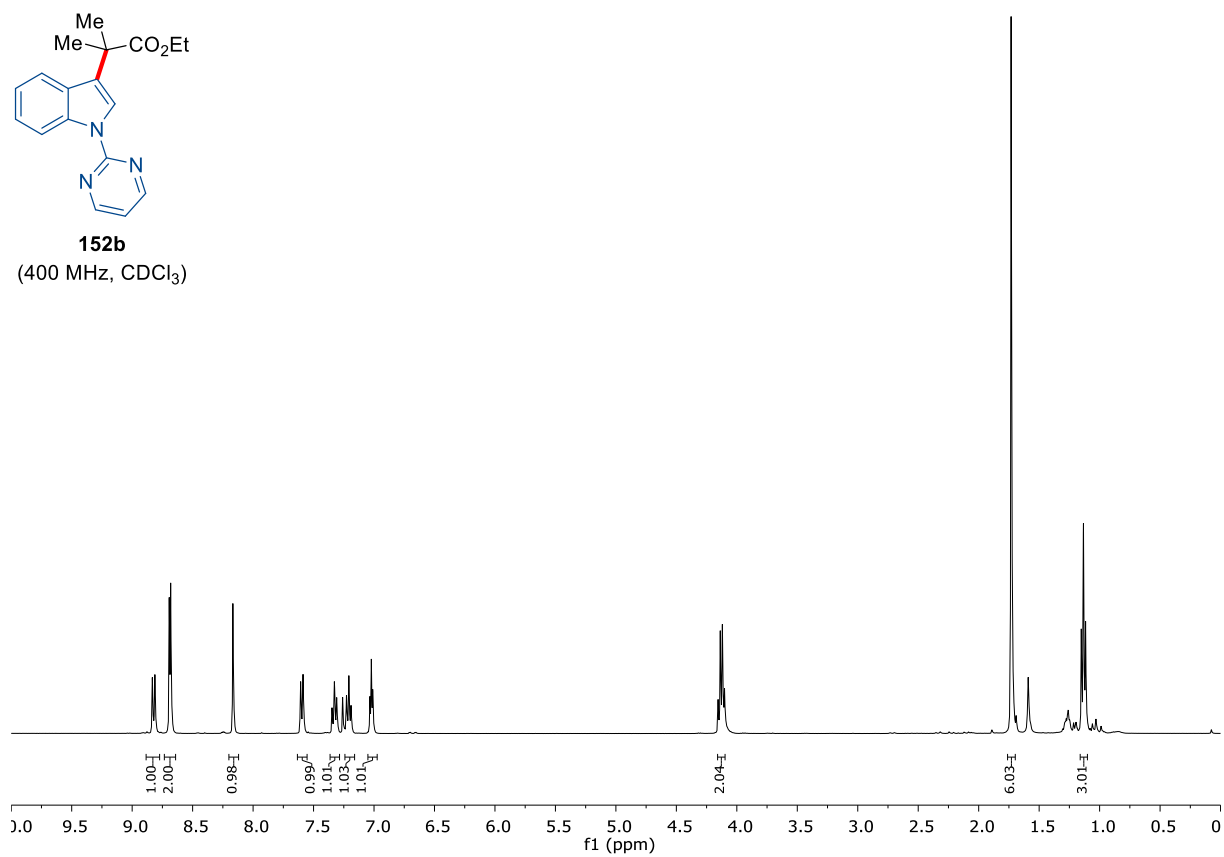


7. Appendix: NMR-Spectra and HPLC Chromatograms

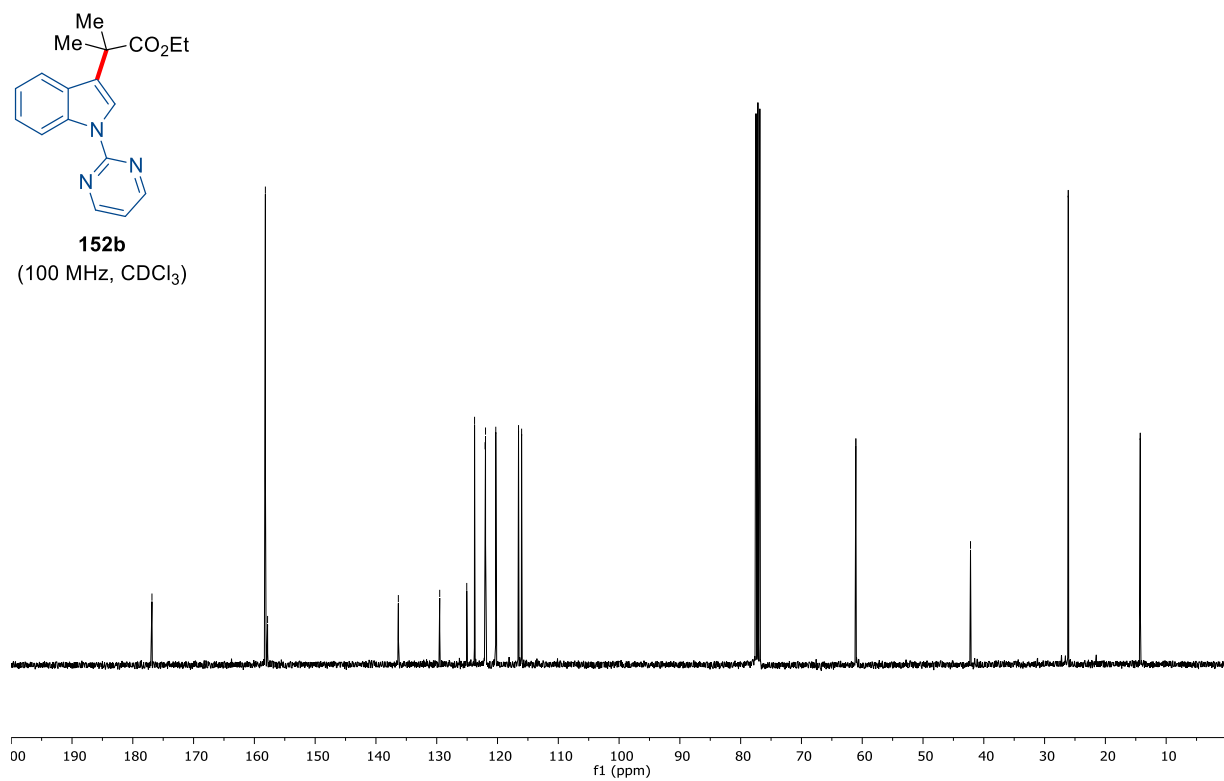




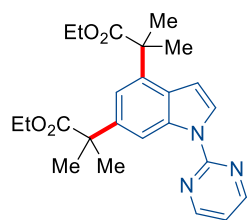
152b
(400 MHz, CDCl₃)



152b
(100 MHz, CDCl₃)

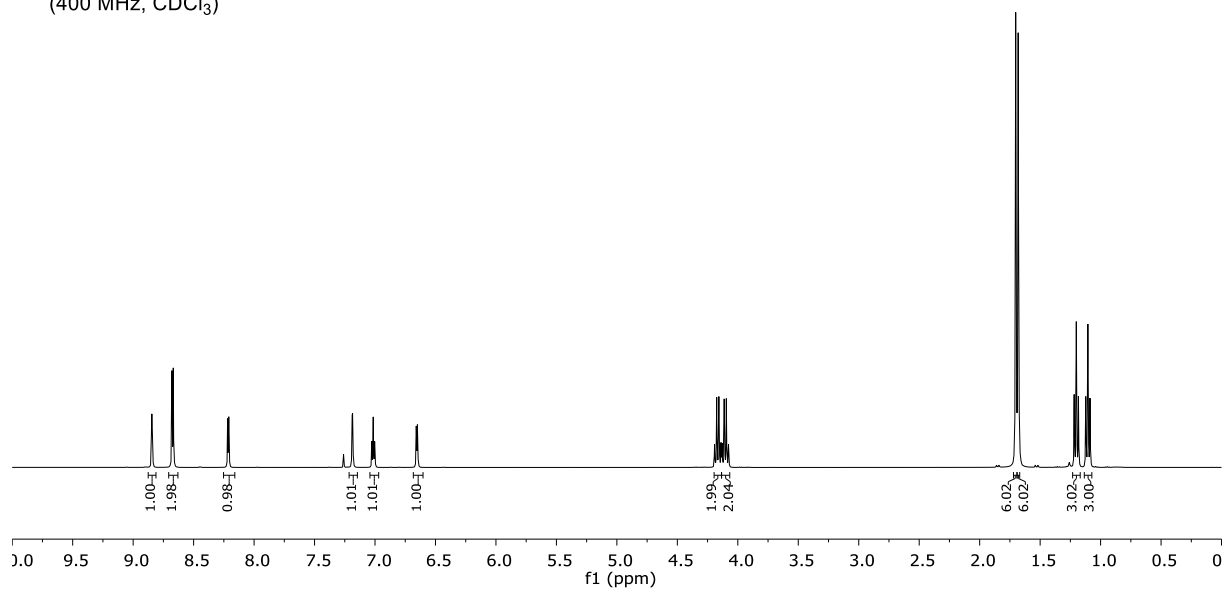


7. Appendix: NMR-Spectra and HPLC Chromatograms



225b

(400 MHz, CDCl₃)



177.88
177.36

158.17
157.84

140.50
136.77
135.90

127.84
125.73

116.59
116.27
112.18

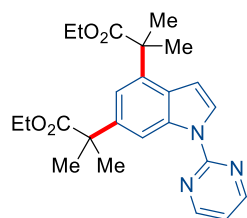
105.59

60.91
60.78

47.20
46.61

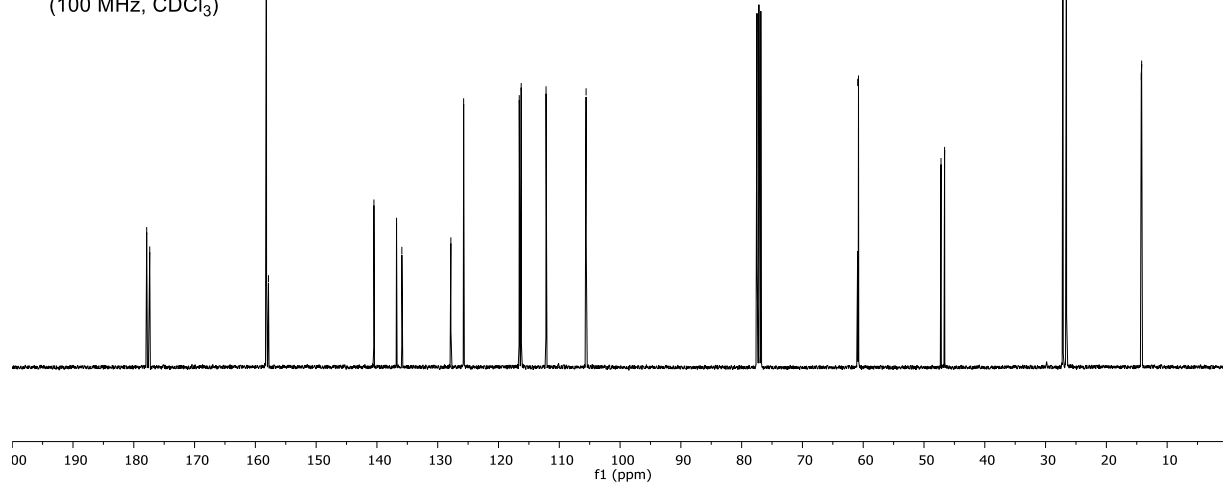
27.15
26.57

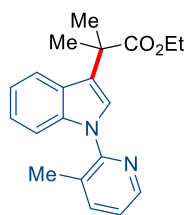
14.25
14.20



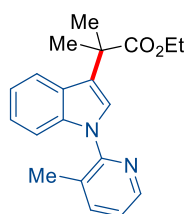
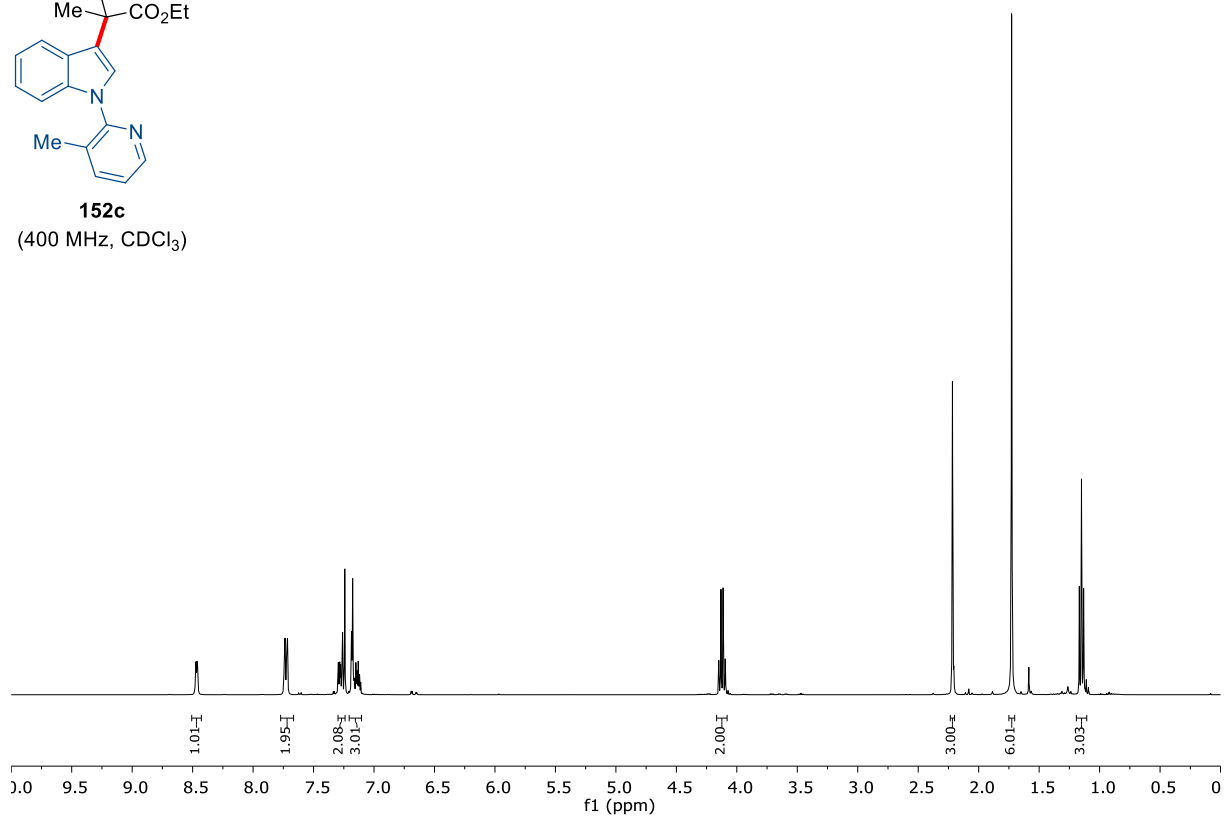
225b

(100 MHz, CDCl₃)

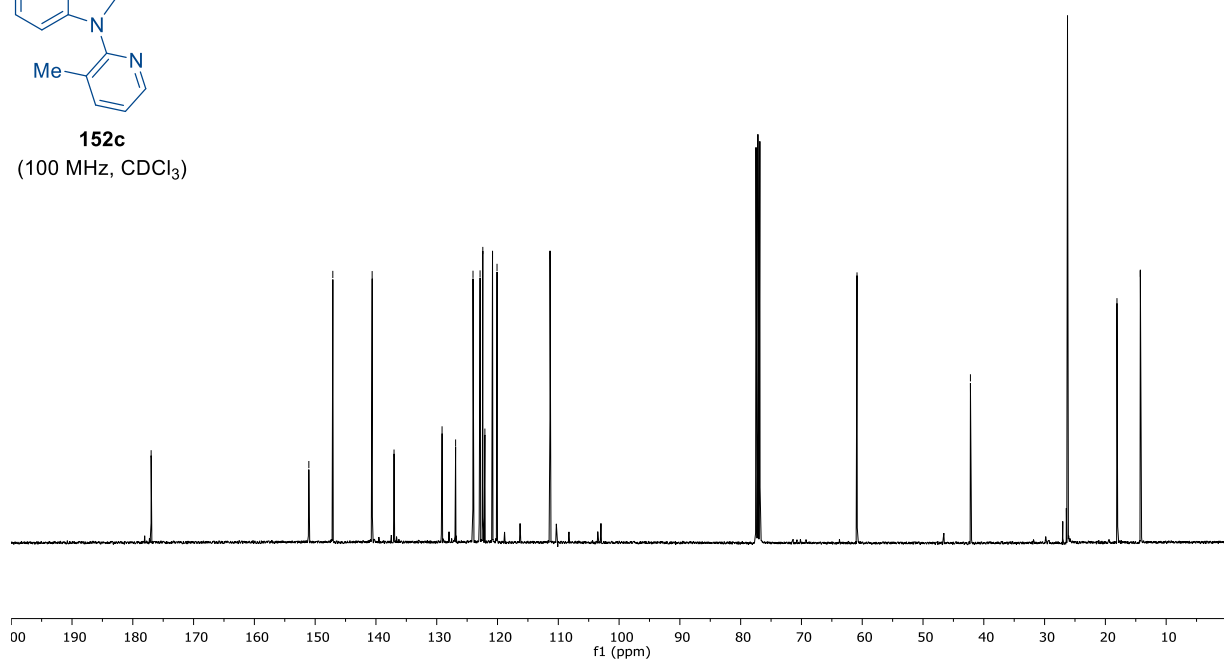




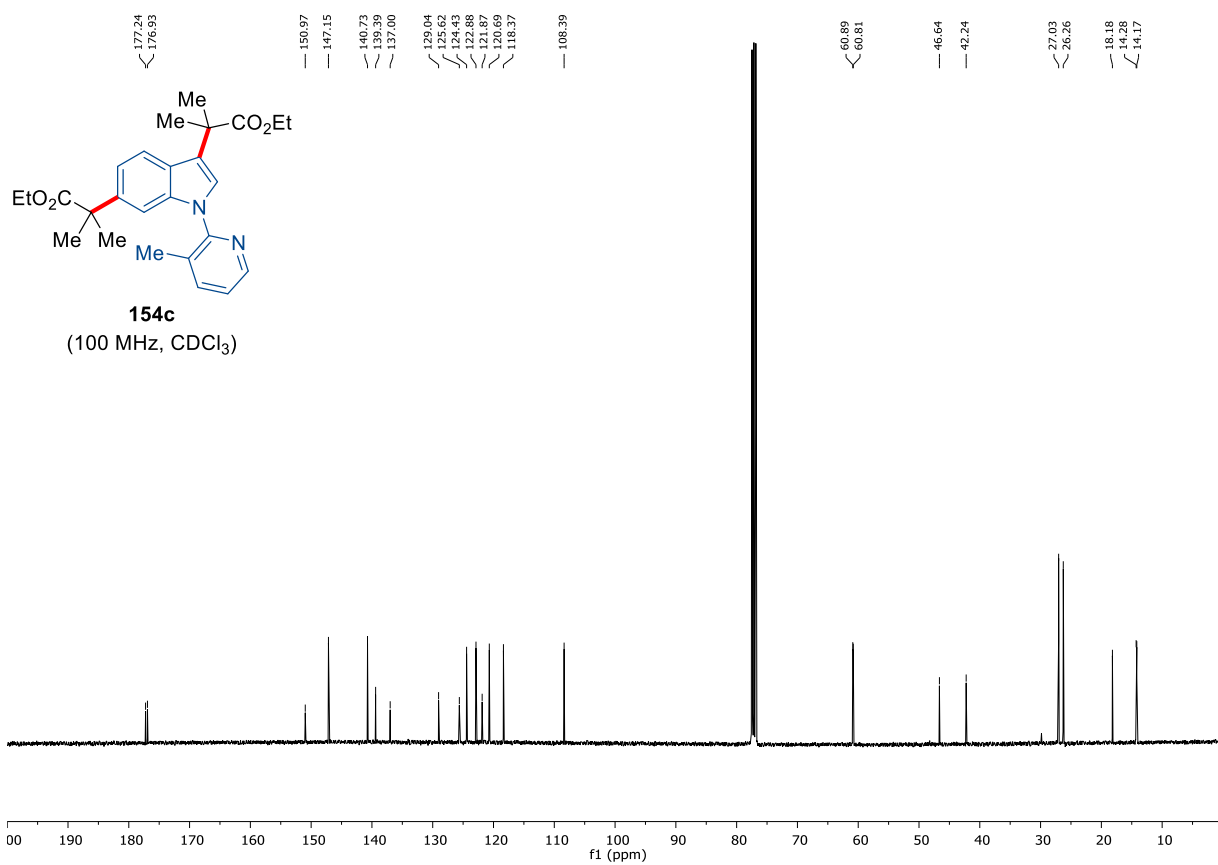
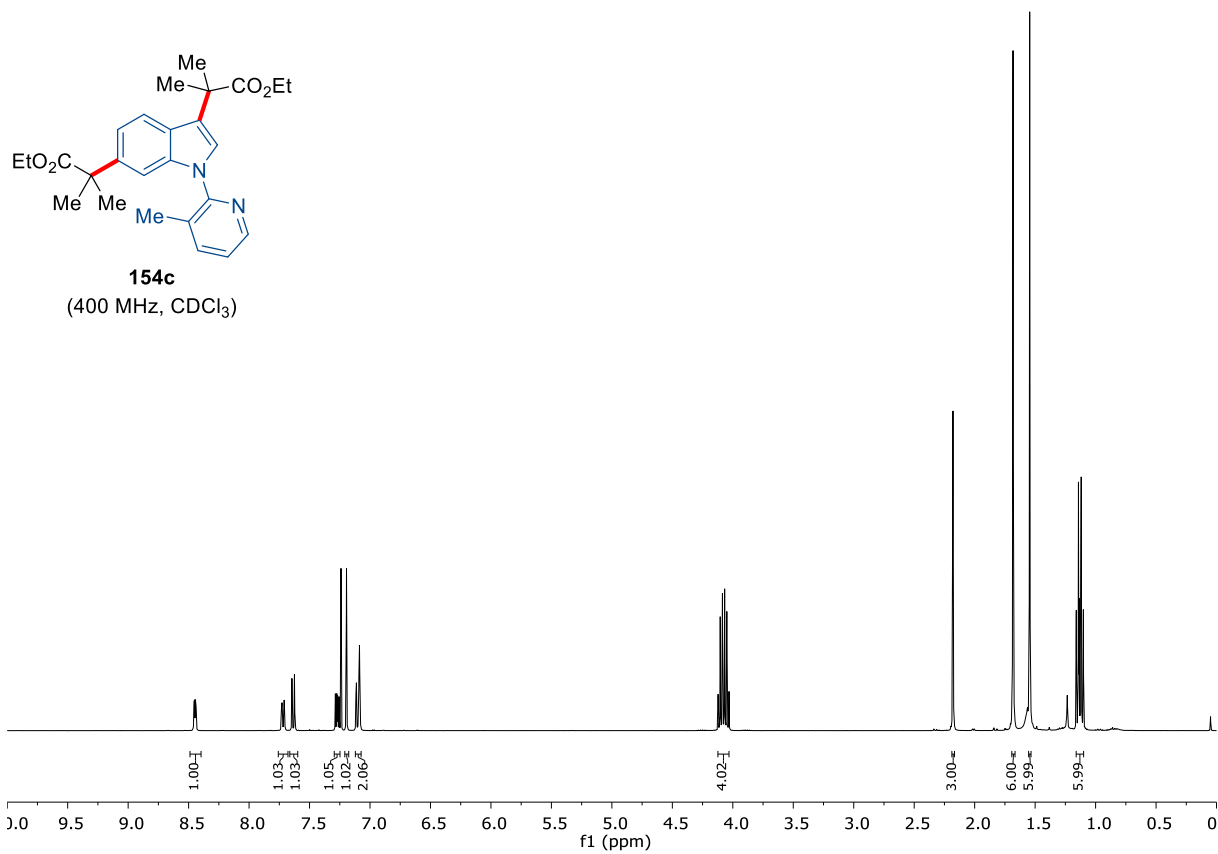
152c
(400 MHz, CDCl₃)

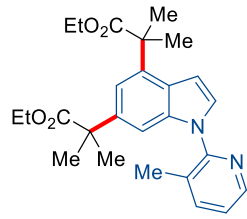


152c
(100 MHz, CDCl₃)

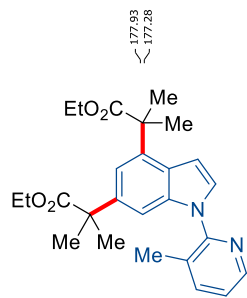
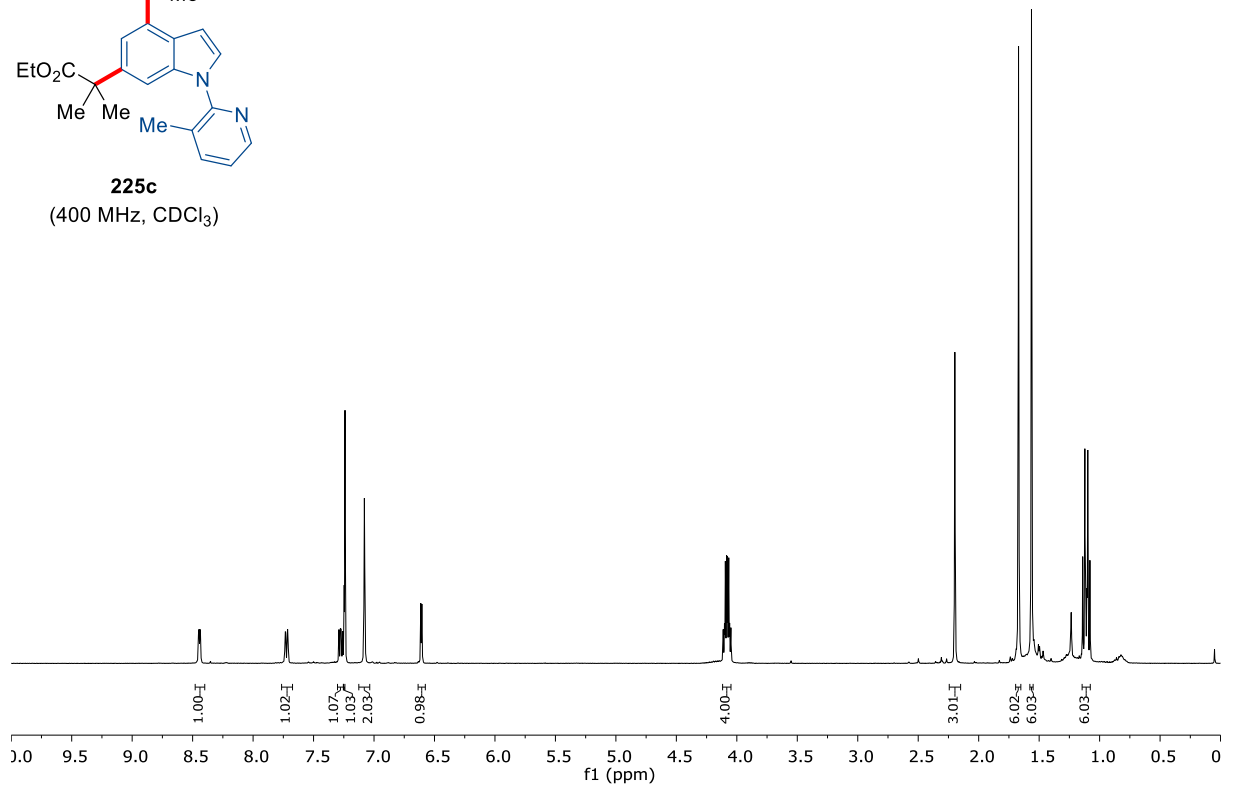


7. Appendix: NMR-Spectra and HPLC Chromatograms

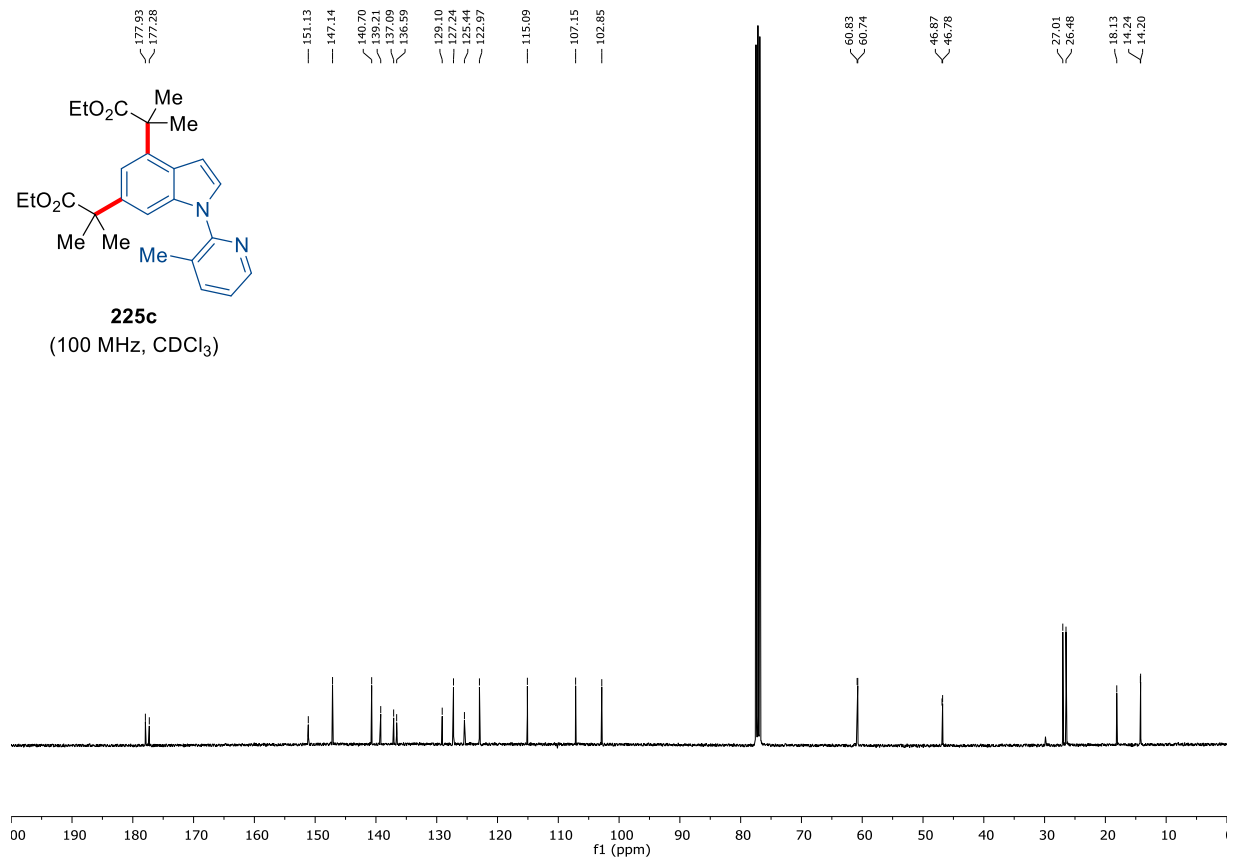




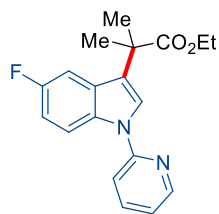
225c
(400 MHz, CDCl₃)



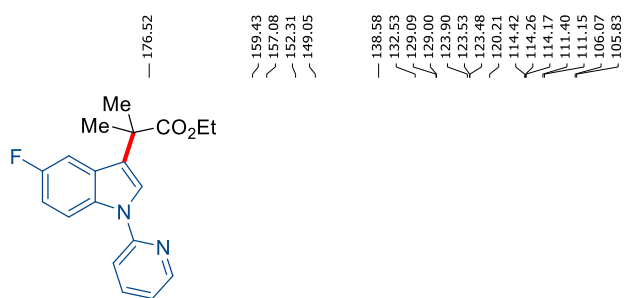
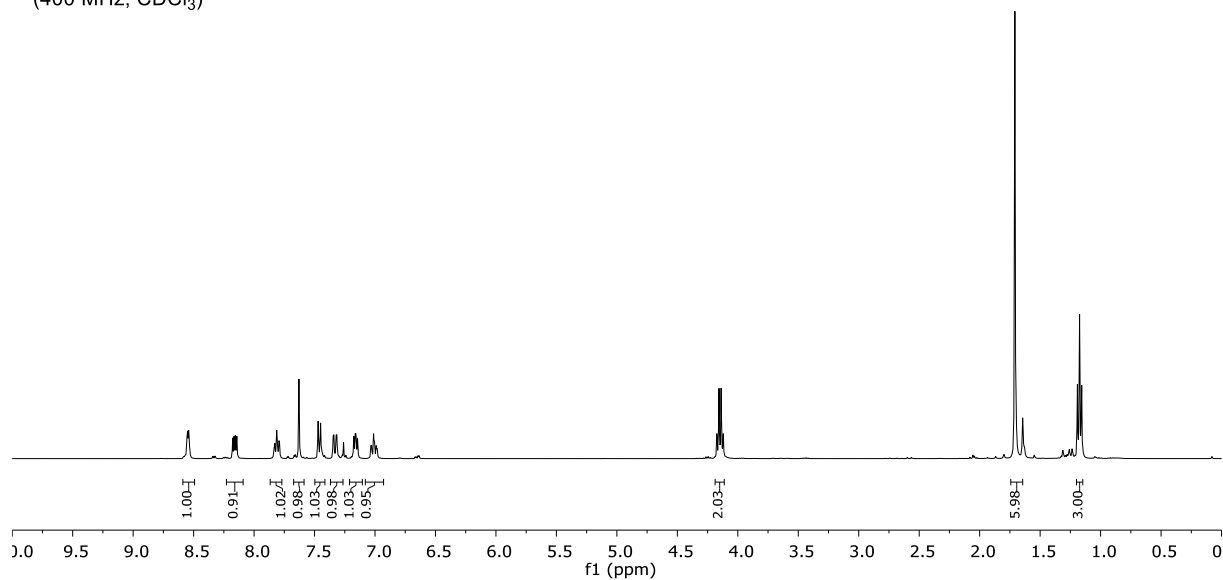
225c
(100 MHz, CDCl₃)



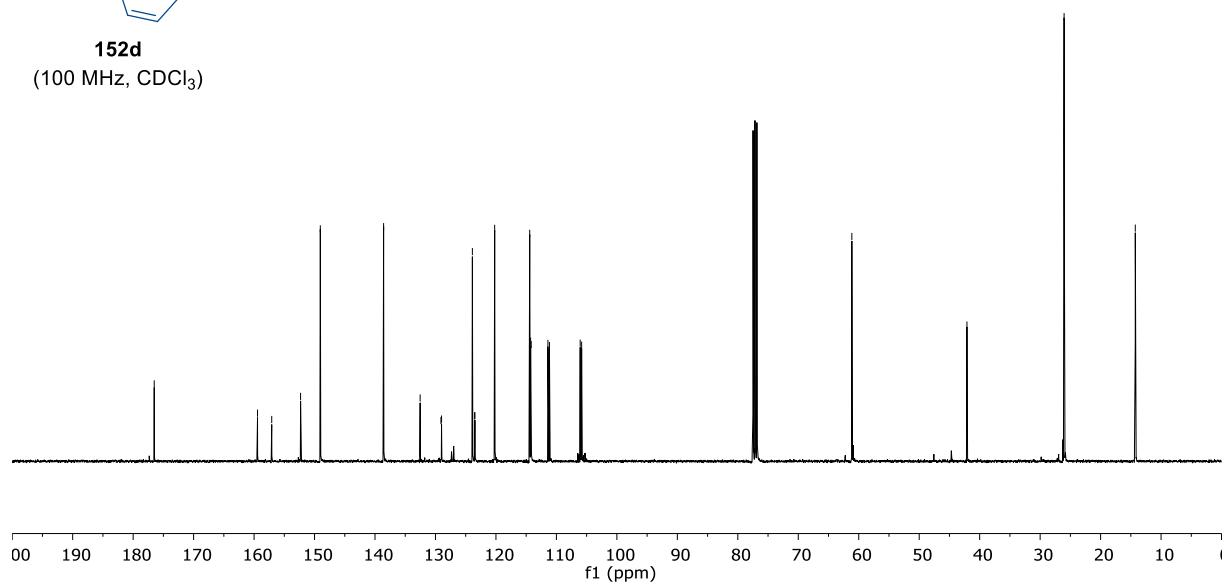
7. Appendix: NMR-Spectra and HPLC Chromatograms

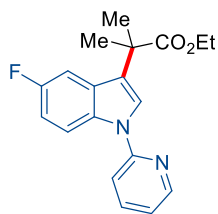


152d
(400 MHz, CDCl₃)

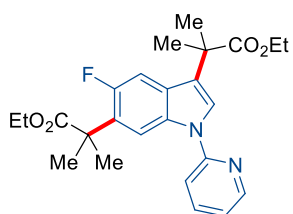
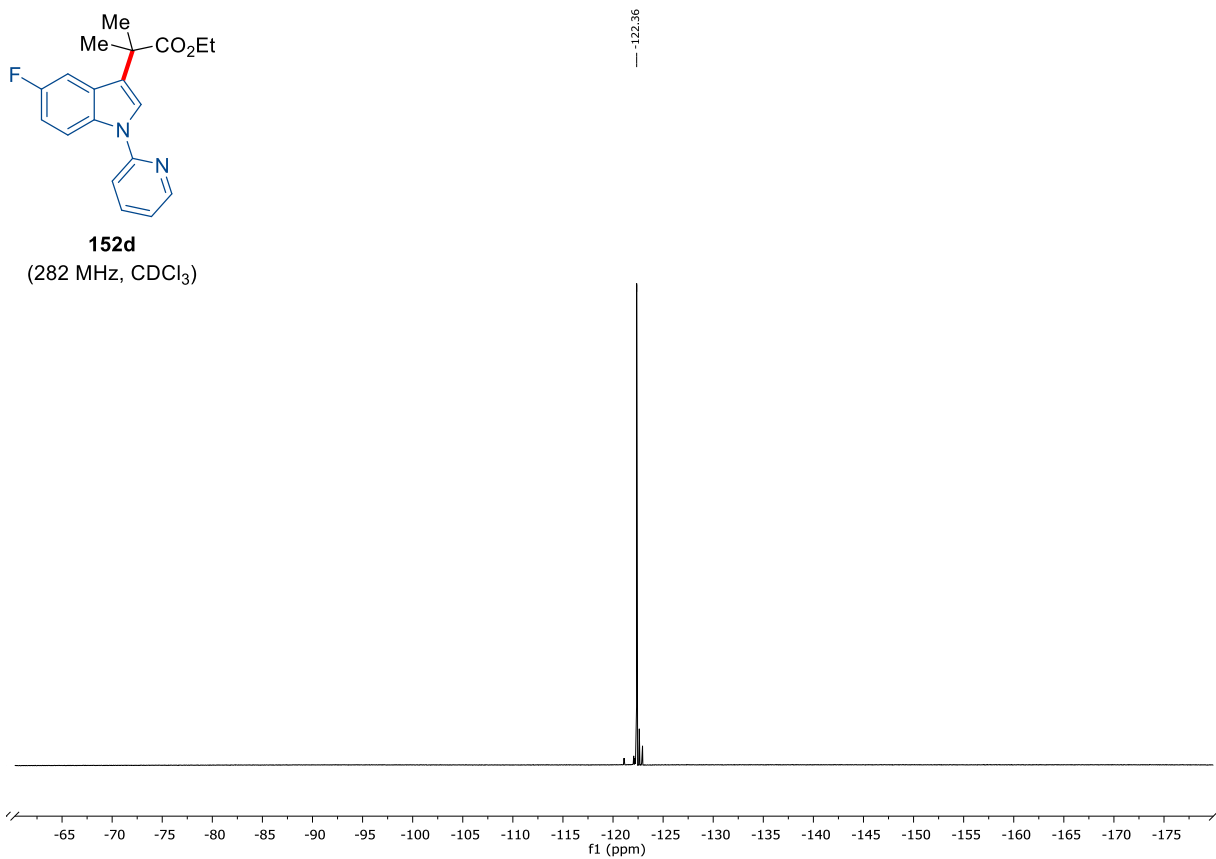


152d
(100 MHz, CDCl₃)

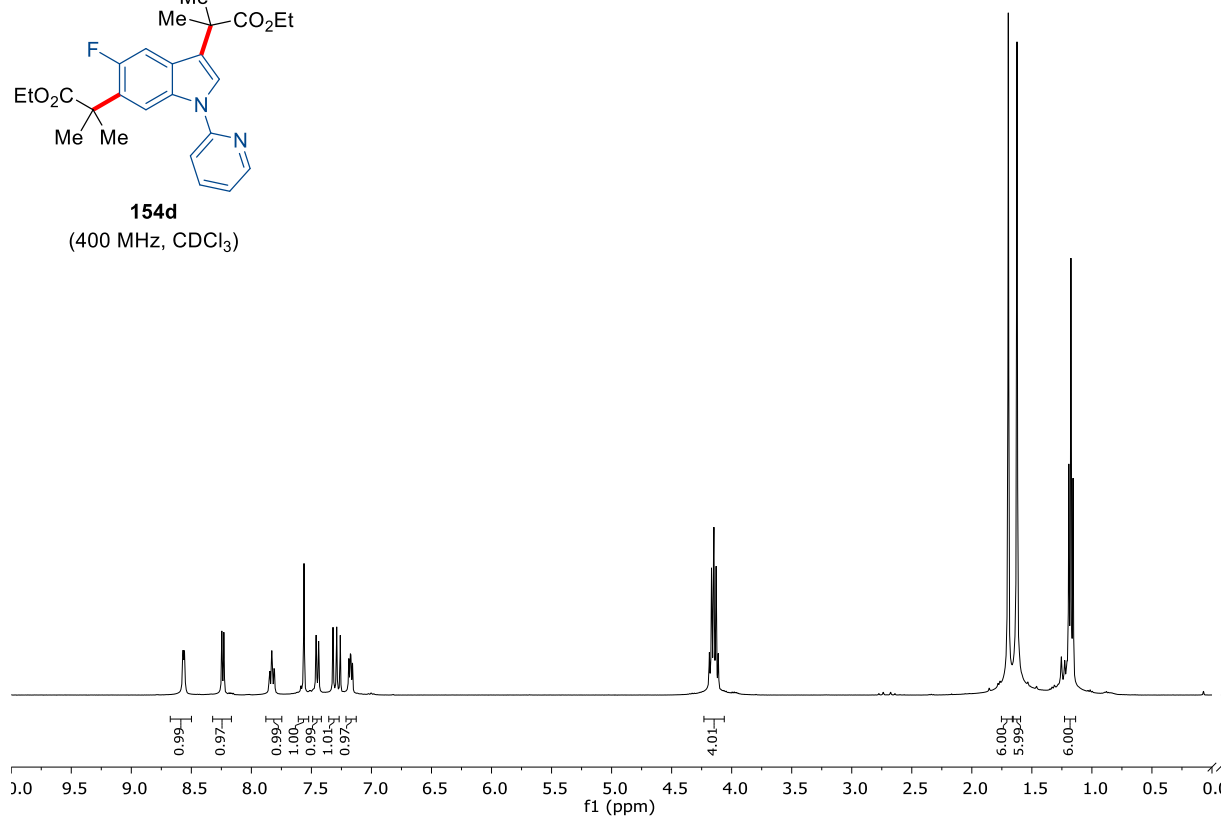




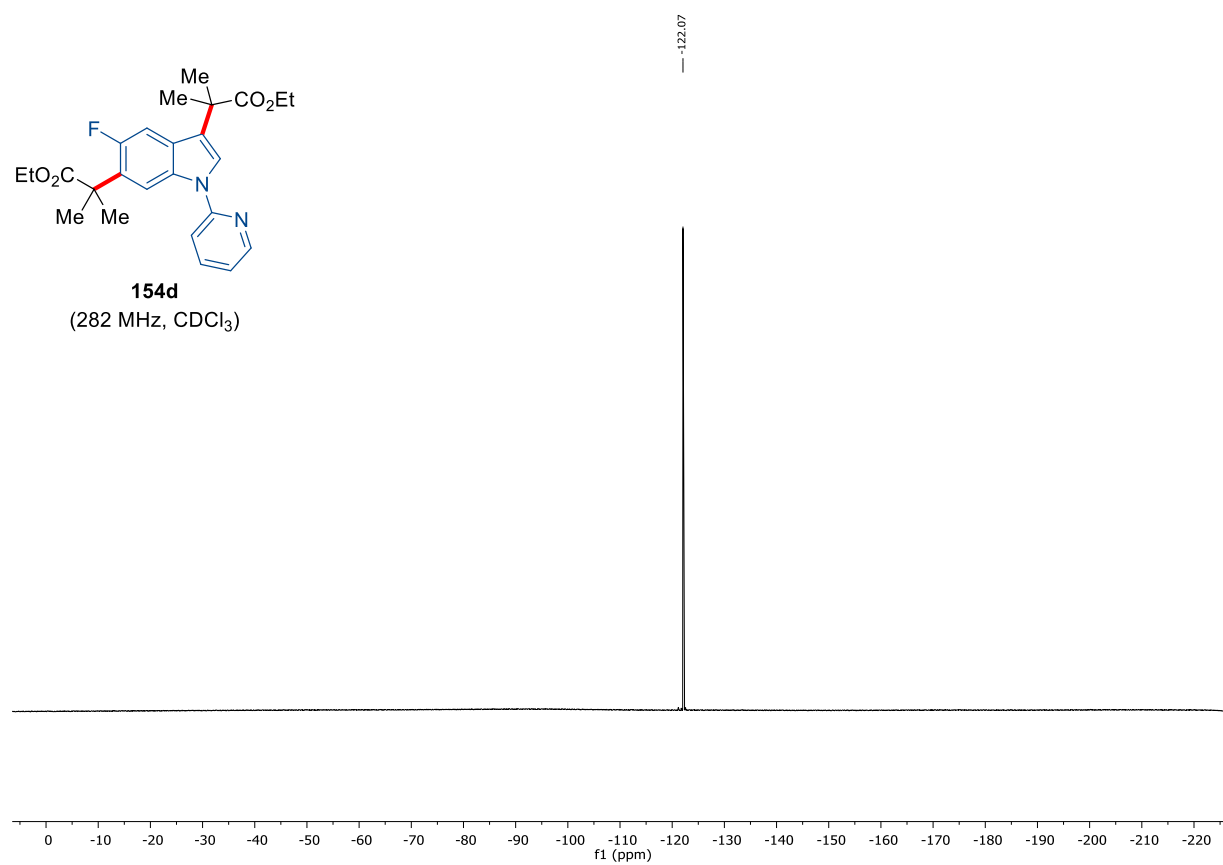
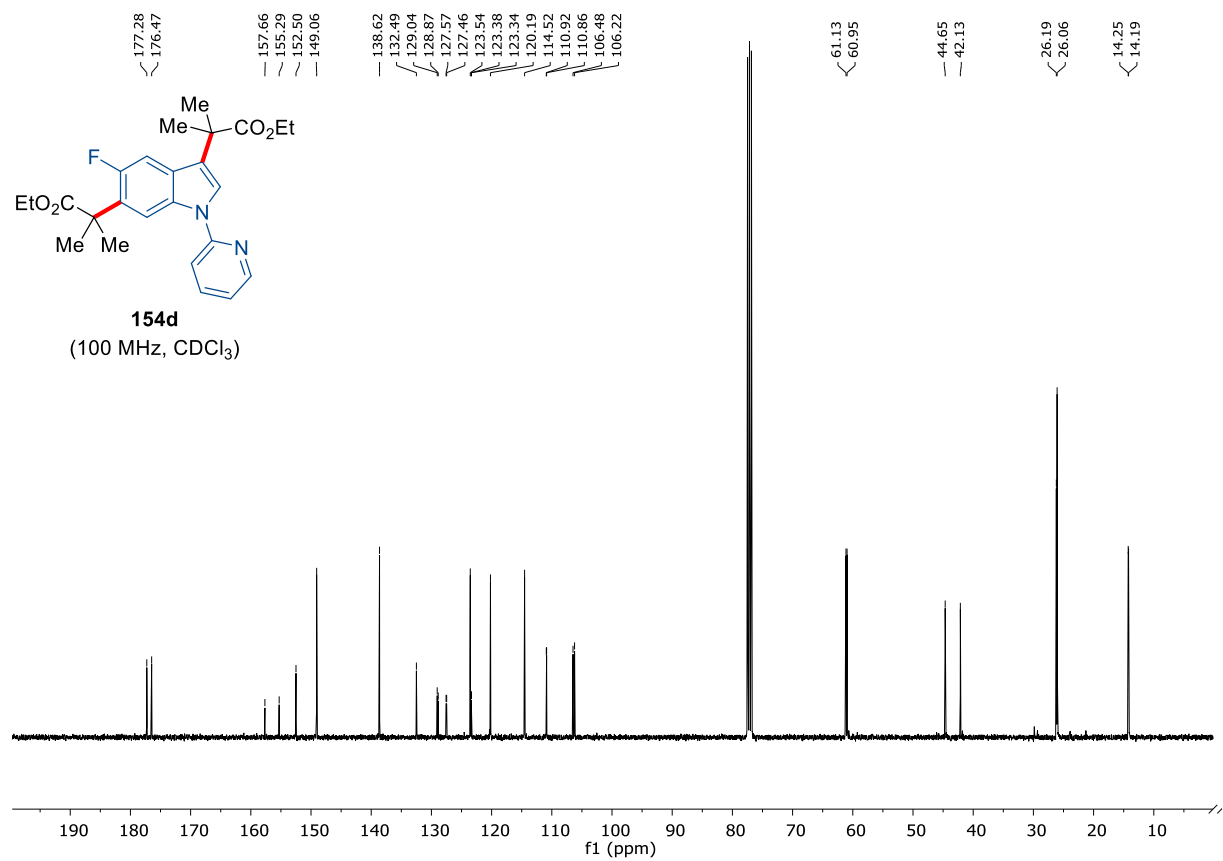
152d
(282 MHz, CDCl₃)

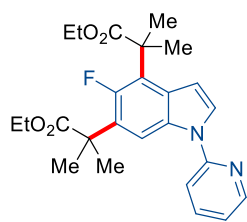


154d
(400 MHz, CDCl₃)

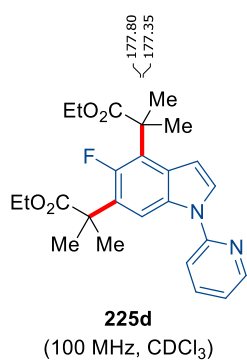
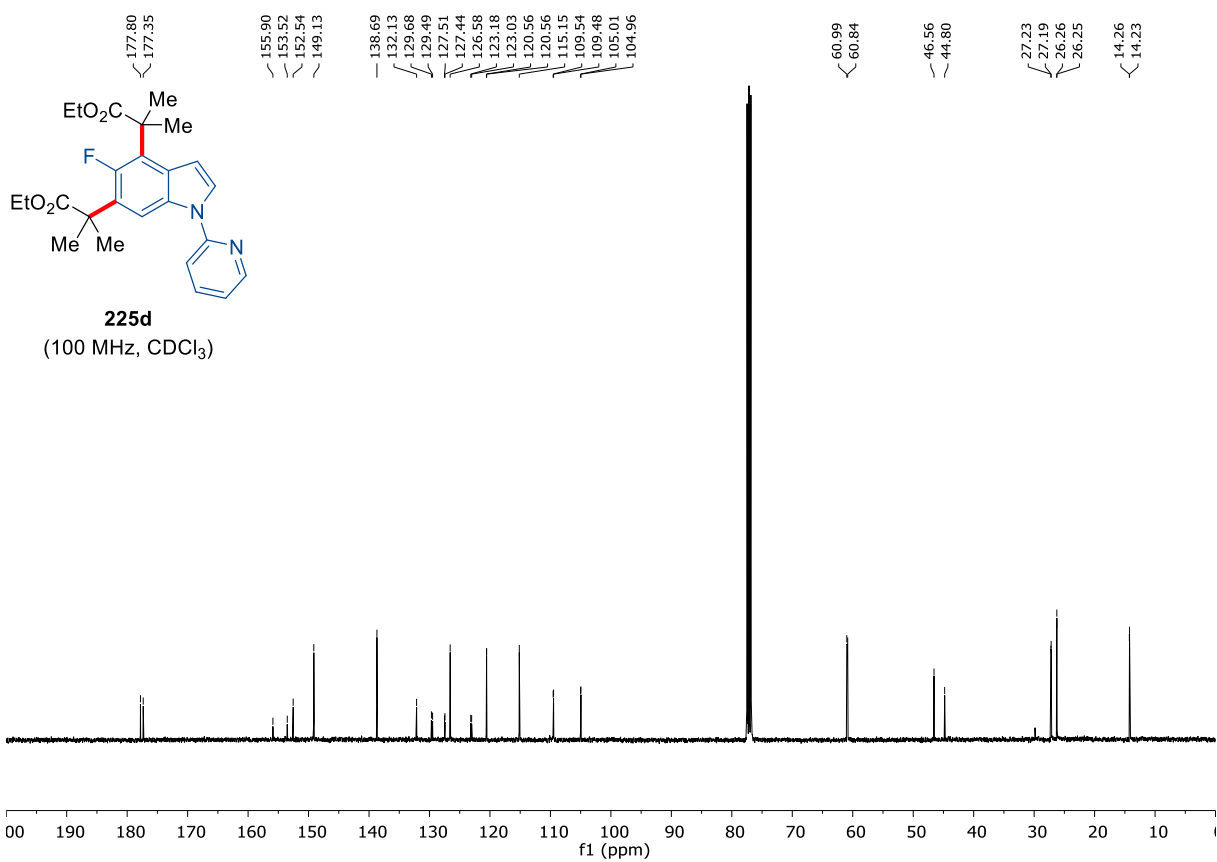
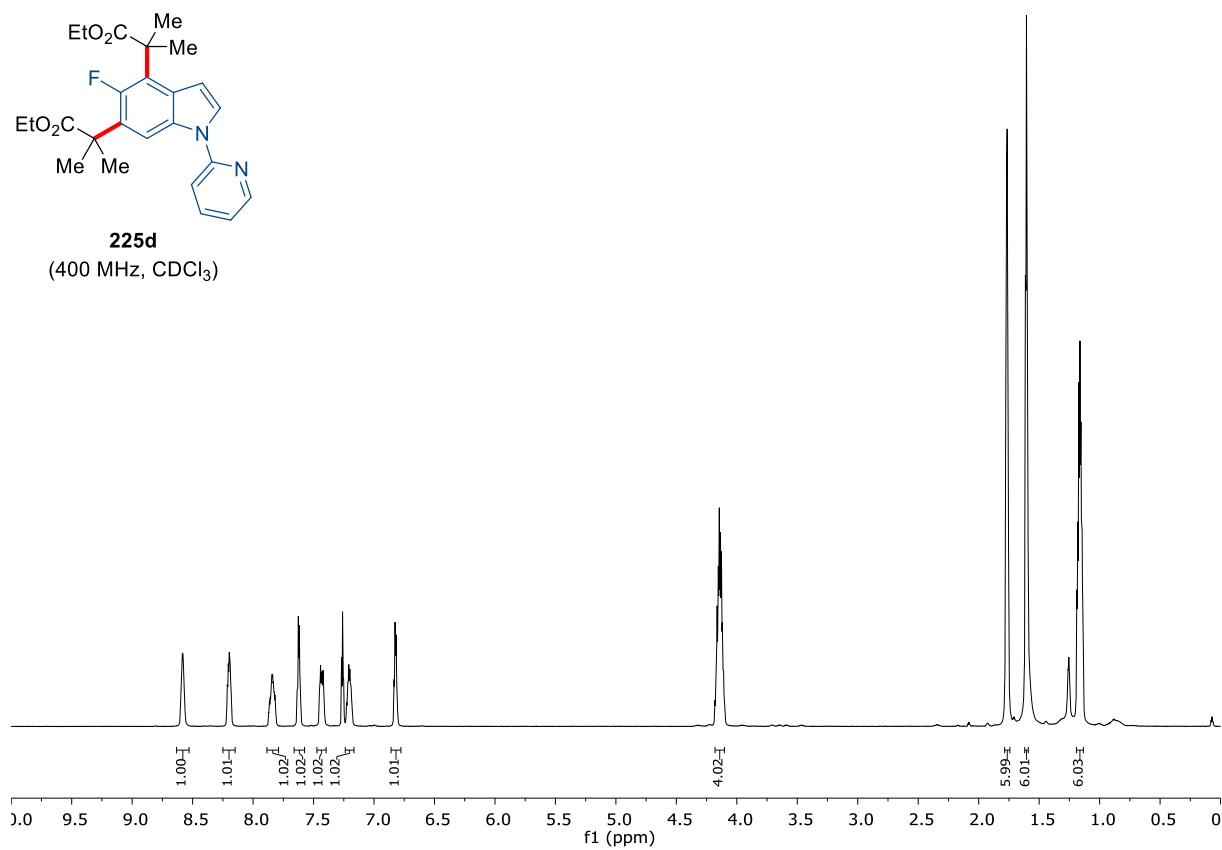


7. Appendix: NMR-Spectra and HPLC Chromatograms

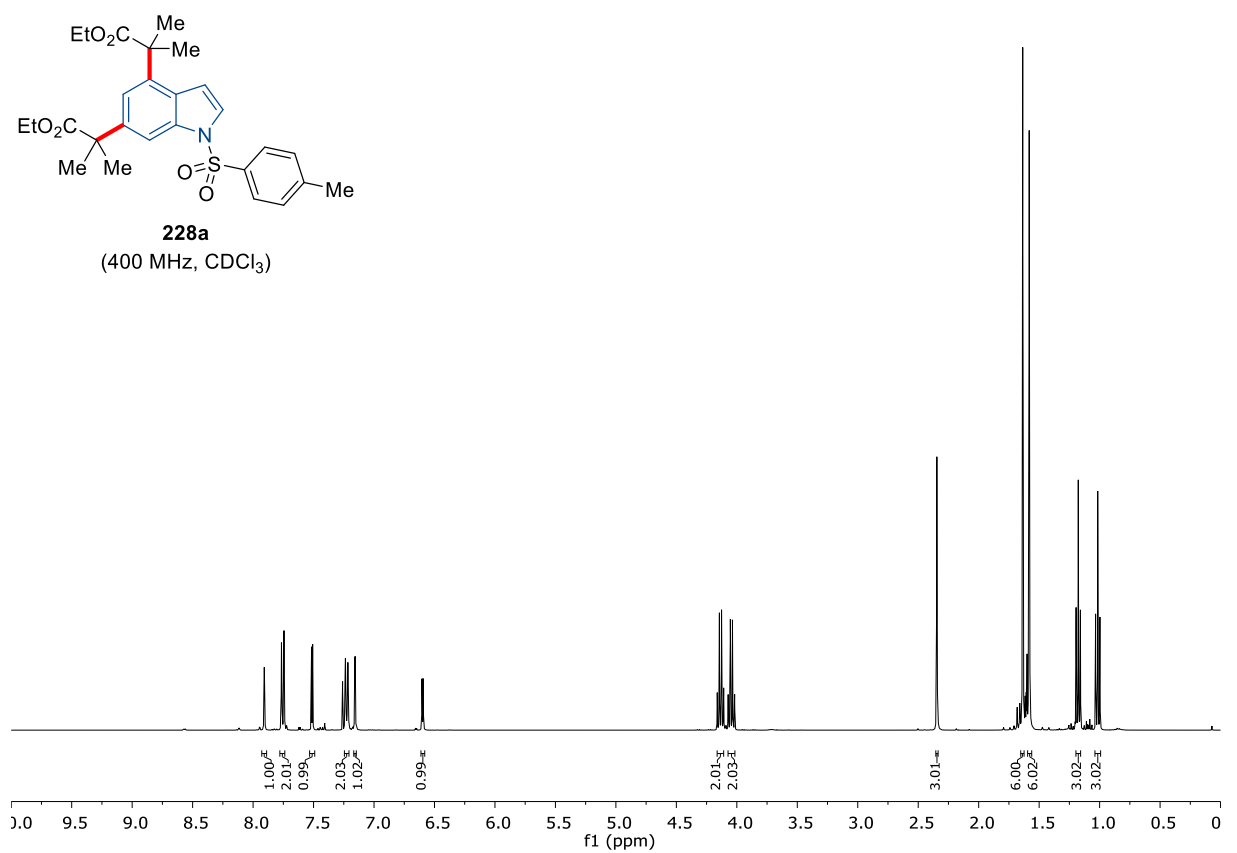
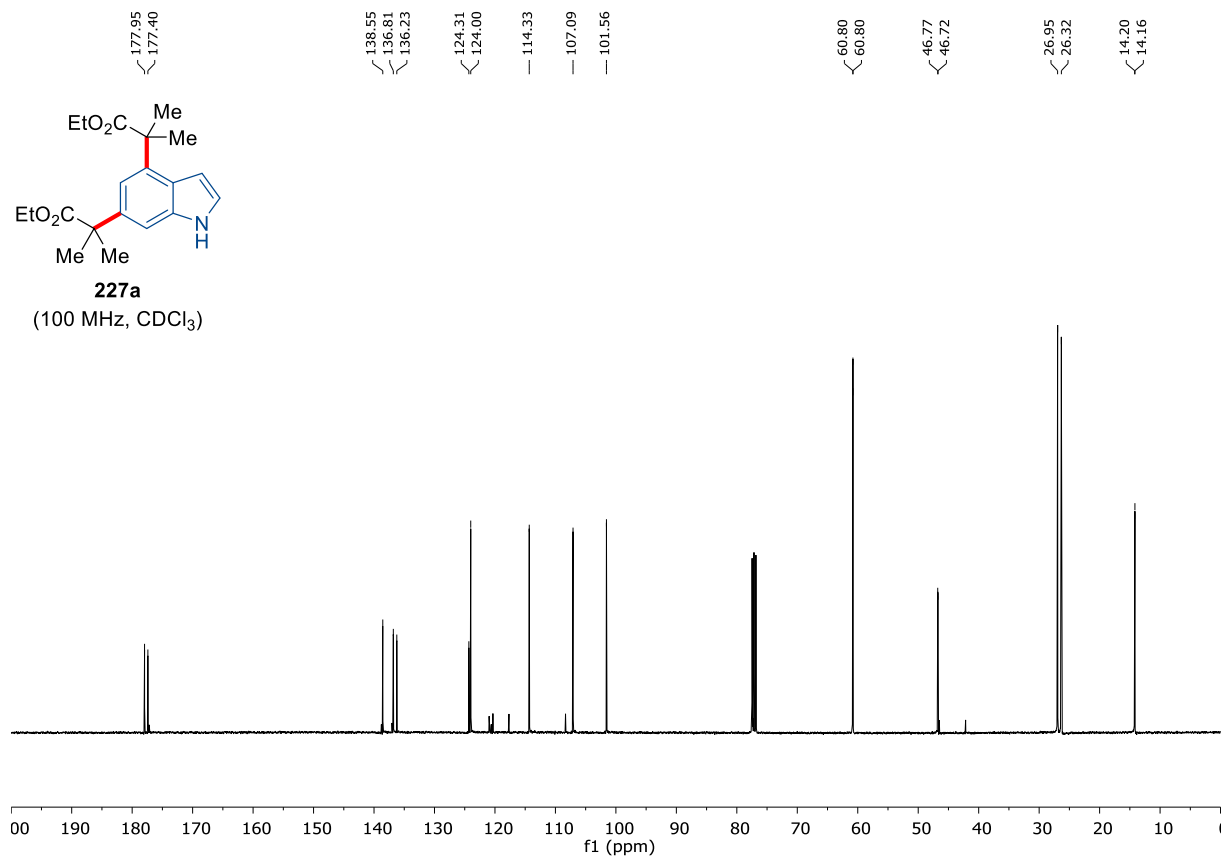




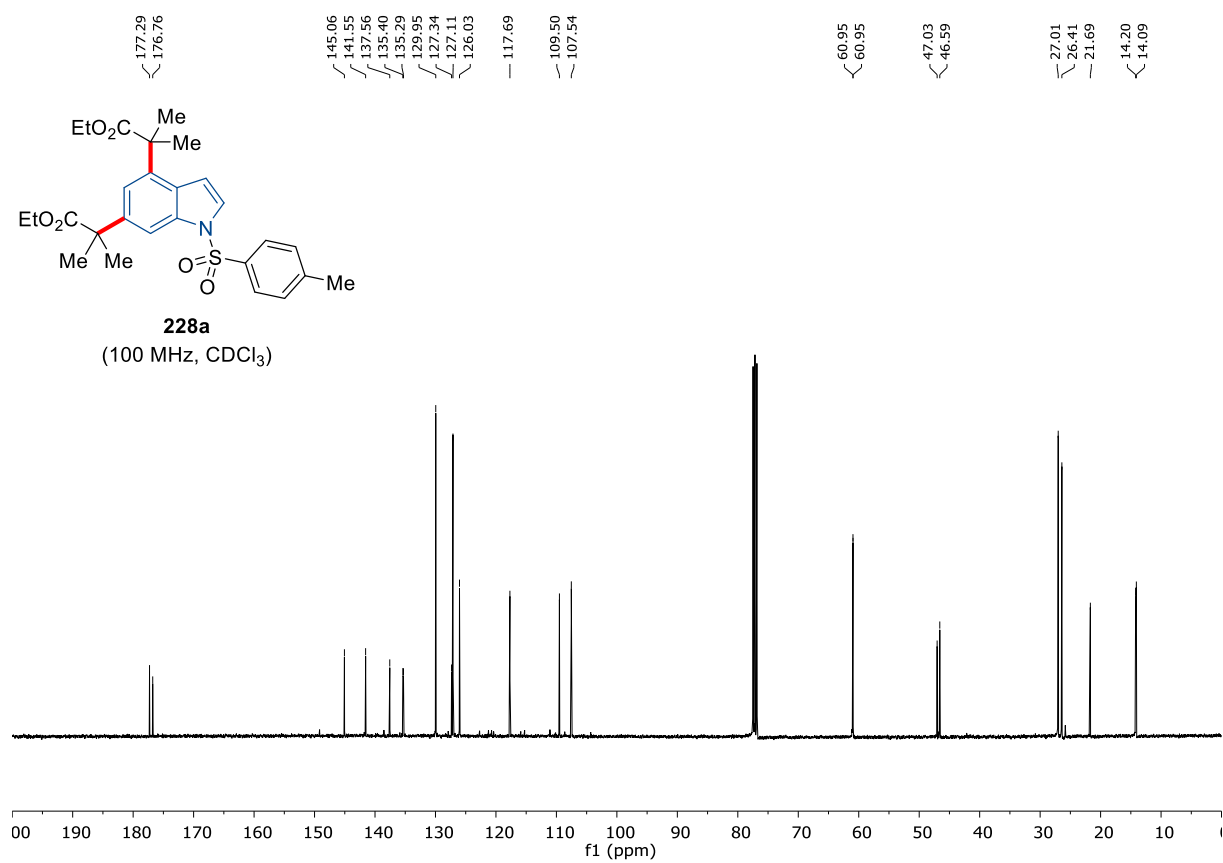
225d
(400 MHz, CDCl₃)



225d
(100 MHz, CDCl₃)



7. Appendix: NMR-Spectra and HPLC Chromatograms



Teaching Experience

04/2020–09/2020	Assistant for the practical course „Organisch-Chemisches Praktikum“
10/2019–03/2020	Assistant for the practical course „Angewandte Organische Synthese“
04/2019–09/2019	Assistant for the practical course „Organisch-Chemisches Praktikum“
10/2018–03/2019	Assistant for the practical course „Angewandte Organische Synthese“
04/2018–09/2018	Assistant for the practical course „Organisch-Chemisches Praktikum“
10/2017–03/2018	Assistant for the practical course „Organisch-Chemisches Praktikum“
10/2017–03/2018	Assistant within the FoLL Program (Research-Oriented Teaching and Learning)
04/2017–04/2017	Teaching assistant for the course „Einführung in die Organische Chemie“

Publications

12) I. Choi, V. Müller, Y. Wang, K. Xue, R. Kuniyil, L. B. Andreas, V. Karius, J. G. Alauzun, L. Ackermann, "Recyclable Ruthenium Catalyst for Distal meta-C–H Activation" *Chem. Eur. J.* **2020**, 26, 15290–15297.

11) V. Müller, D. Ghorai, L. Capdevila, A. M. Messinis, X. Ribas, L. Ackermann, "C–F Activation for C(sp²)–C(sp³) Cross-Coupling by a SPO-Nickel Complex" *Org. Lett.* **2020**, 22, 7034–7040.

10) I. Choi, V. Müller, G. Lole, R. Köhler, V. Karius, W. Viöl, C. Jooß, L. Ackermann, "Photo-Induced Heterogeneous C–H Arylation by Reusable Hybrid-Copper Catalyst" *Chem. Eur. J.* **2020**, 26, 3509–3514.

-
- 9) V. Müller, R. Weck, V. Derdau, L. Ackermann, "Ruthenium(II)-Catalyzed Hydrogen Isotope Exchange of Pharmaceutical Drugs by C–H Deuteration and C–H Tritiation" *ChemCatChem* **2020**, *12*, 100–104.
- 8) J. Loup, V. Müller, D. Ghorai, L. Ackermann, "Enantioselective Aluminum-Free Alkene Hydroarylations via C–H Activation by a Chiral Nickel/JoSPOphos Manifold" *Angew. Chem. Int. Ed.* **2019**, *58*, 1749–1753. '
- 7) E. Detmar, V. Müller, D. Zell, L. Ackermann, M. Breugst, "Cobalt-Catalyzed C–H Cyanations: Insights into the Reaction Mechanism and the Role of London Dispersion" *Beilstein J. Org. Chem.* **2018**, *14*, 1537–1545.
- 6) D. Zell, M. Bursch, V. Müller, S. Grimme, L. Ackermann, "Switch of C-H Activation Mechanism for Full Selectivity Control in Cobalt(III)-Catalyzed C-H Alkylations" *Angew. Chem. Int. Ed.* **2017**, *56*, 10378–10382.
- 5) D. Ghorai, V. Müller, H. Keil, D. Stalke, G. Zanoni, B. A. Tkachenko, Peter R. Schreiner, L. Ackermann, "Secondary Phosphine Oxide Preligand for Palladium-Catalyzed C-H (Hetero)Arylations: Efficient Access to Pybox Ligands" *Adv. Synth. Catal.* **2017**, *359*, 3137–3141.
- 4) D. Zell, V. Müller, U. Dhawa, M. Bursch, R. R. Presa, S. Grimme, L. Ackermann, "Mild Cobalt(III)-Catalyzed Allylative C-F/C-H Functionalizations at Room Temperature" *Chem. Eur. J.* **2017**, *23*, 12145–12148.
- 3) Y.-F. Liang, V. Müller, W. Liu, A. Münch, D. Stalke, L. Ackermann, "Methylenecyclopropane Annulation by Manganese(I)-Catalyzed Stereoselective C-H/C-C Activation" *Angew. Chem. Int. Ed.* **2017**, *56*, 9415–9419.
- 2) D. Zell, U. Dhawa, V. Müller, M. Bursch, S. Grimme, L. Ackermann, "C-F/C-H Functionalization by Manganese(I) Catalysis: Expedient (Per)Fluoro-Allylations and Alkenylations" *ACS Catal.* **2017**, *7*, 4209–4213.
- 1) D. Tonin, D. Zell, V. Müller, L. Ackermann, "Ruthenium(II)-Catalyzed C-H Methylation with Trifluoroborates" *Synthesis* **2017**, *49*, 127–134.

Conferences

07/2020	1 th Virtual International Symposium on C–H Activation, online via Zoom
07/2019	20th IUPAC International Symposium on Organometallic Catalysis Directed Towards Organic Synthesis, Heidelberg, Germany (Poster presentation)
12/2019	H-CCAT meeting, Dresden, Germany (Oral presentation)
06/2019	H-CCAT meeting, Reading, United Kingdom
09/2018	1 st H-CCAT Summer School, Perugia, Italy (Poster presentation)
09/2017	1 st ICASEC Summer School, Göttingen, Germany (Poster presentation)
08/2017	1 st CHAOS training school Tallinn, Estonia

Erklärung

Hiermit versichere ich, dass ich die vorliegende Dissertation im Zeitraum von Januar 2017 bis März 2021 am Institut für Organische und Biomolekulare Chemie der Georg-August-Universität Göttingen

auf Anregung und unter Anleitung von

Herrn Prof. Dr. Lutz Ackermann

selbstständig durchgeführt und keine anderen als die angegebenen Hilfsmittel und Quellen verwendet habe.

Göttingen, den 08.03.2021

.....

Valentin Müller